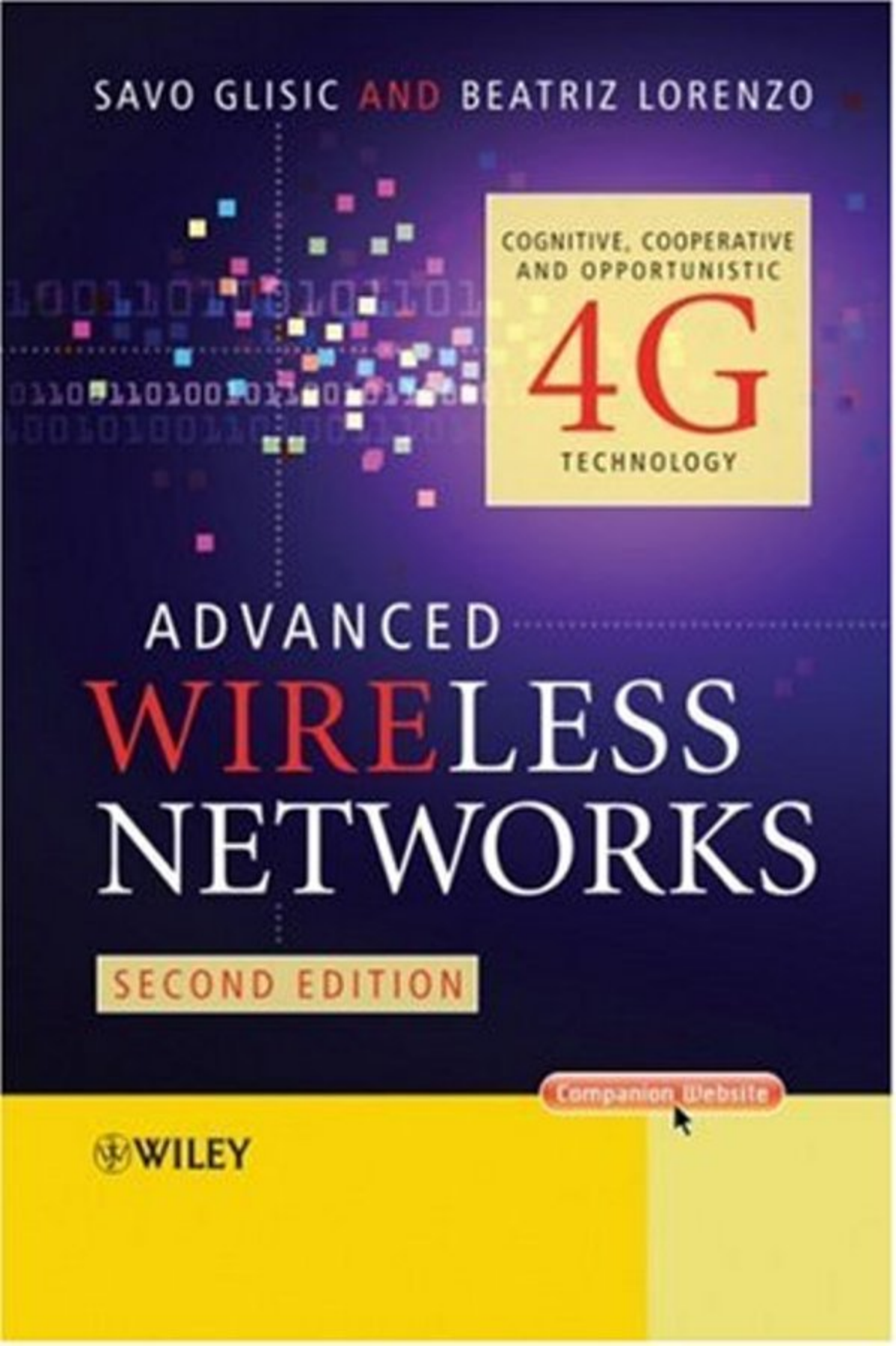
SAVO GLISIC AND BEATRIZ LORENZO
COGNITIVE, COOPERATIVE AND OPPORTUNISTIC
4G
TECHNOLOGY
ADVANCED
WIRELESS
NETWORKS
SECOND EDITION
Companion Website
WILEY

ADVANCED WIRELESS NETWORKS

Cognitive, Cooperative and Opportunistic 4G Technology

Second Edition

Savo Glisic
Beatriz Lorenzo
University of Oulu, Finland

A John Wiley and Sons, Ltd., Publication

ADVANCED WIRELESS NETWORKS

ADVANCED WIRELESS NETWORKS

Cognitive, Cooperative and Opportunistic 4G Technology

Second Edition

Savo Glisic
Beatriz Lorenzo
University of Oulu, Finland

A John Wiley and Sons, Ltd., Publication

This edition first published 2009

Registered office
John Wiley & Sons Ltd, The Atrium, Southern Gate, Chichester, West Sussex, PO19 8SQ, United Kingdom

Library of Congress Cataloging-in-Publication Data

Glisic, Savo G.
Advanced wireless networks : 4G technologies / Savo Glisic, Beatriz Lorenzo Veiga. – 2nd ed.
p. cm.
Includes bibliographical references and index.
ISBN 978-0-470-74250-1 (cloth)
1. Wireless communication systems. I. Veiga, Beatriz Lorenzo. II. Title.
TK5103.2.G553 2009
621.384—dc22

2009001817

A catalogue record for this book is available from the British Library.

ISBN 978-0-470-74250-1 (H/B)

Typeset in 9/11 Times by Laserwords Private Limited, Chennai, India
Printed in Singapore by Markono Print Media Pte Ltd

To our families

Contents

Preface to the Second Edition

Although the first edition of the book was not published long ago, a constant progress in research in the field of wireless networks has resulted in a significant accumulation of new results that urge the extension and modification of its content. The major additions in the book are the following new chapters: *Chapter 1: Fundamentals, Chapter 2: Opportunistic Communications, Chapter 3: Relaying and Mesh Networks, Chapter 4: Topology Control, Chapter 10: Network Optimization and Chapter 12: Cognitive Radio Resource Management.*

OPPORTUNISTIC COMMUNICATIONS

Multiuser diversity is a form of diversity inherent in a wireless network, provided by independent time-varying channels across the different users. The diversity benefit is exploited by tracking the channel fluctuations of the users and scheduling transmissions to users when their instantaneous channel quality is near the peak. The diversity gain increases with the dynamic range of the fluctuations and is thus limited in environments with little scattering and/or slow fading.

In such environments, the multiple transmit antennas can be used to induce large and fast channel fluctuations so that multiuser diversity can still be exploited. The scheme can be interpreted as opportunistic beamforming and true beamforming gains can be achieved when there are sufficient users, even though very limited channel feedback is needed. Furthermore, in a cellular system, the scheme plays an additional role of opportunistic nulling of the interference created on users of adjacent cells. This chapter discusses the design implications of implementing this scheme in a wireless system.

RELAYING AND MESH NETWORKS

In a wireless network with many source–destination pairs, cooperative transmission by relay nodes has the potential to improve the overall network performance. In a distributed multihop mesh/relay network (e.g. wireless ad hoc/sensor network, cellular multihop network), each node acts as a relay node to forward data packets from other nodes. These nodes are often energy-limited and also have limited buffer space. Therefore, efficient power-saving mechanisms (e.g. sleeping mechanisms) are

required so that the lifetime of these nodes can be extended while at the same time the quality of service (QoS) requirements (e.g. packet delay and packet loss rate) for the relayed packets can be satisfied. In Chapter 3, a queuing analytical framework is presented to study the tradeoffs between the energy saving and the QoS at a relay node as well as relaying strategies in cooperative cellular networks. In addition integrated cellular and *ad hoc* multicast, which increases multicast throughput through opportunistic use of *ad hoc* relays, is also discussed.

NETWORK TOPOLOGY CONTROL

Energy efficiency and network capacity are perhaps two of the most important issues in wireless *ad hoc* networks and sensor networks. Topology control algorithms have been proposed to maintain network connectivity while reducing energy consumption and improving network capacity.

The key idea to topology control is that, instead of transmitting with maximal power, nodes in a wireless multihop network collaboratively determine their transmission power and define the network topology by forming the proper neighbour relation under certain criteria. The topology control affects network spatial reuse and contention for the medium.

A number of topology control algorithms have been proposed to create a power-efficient network topology in wireless multihop networks with limited mobility. In Chapter 4, we summarize existing work in this field. Some of the algorithms require explicit propagation channel models, while others incur significant message exchanges. Their ability to maintain the topology in the case of mobility is also rather limited. The chapter will discuss the tradeoffs between these opposing requirements.

NETWORK OPTIMIZATION

Network protocols in layered architectures have traditionally been obtained on an *ad hoc* basis, and many of the recent crosslayer designs are also conducted through piecemeal approaches. Network protocol stacks may instead be systematically analyzed and designed as distributed solutions to some global optimization problems. Chapter 10 presents a survey of the recent efforts toward a systematic understanding of layering as optimization decomposition, where the overall communication network is modelled by a generalized network utility maximization problem, where each layer corresponds to a decomposed subproblem and the interfaces among layers are quantified as functions of the optimization variables coordinating the subproblems. There can be many alternative decompositions, leading to a choice of different layering architectures. This chapter will survey the current status of horizontal decomposition into distributed computation and vertical decomposition into functional modules such as congestion control, routing, scheduling, random access, power control and channel coding. Key results are summarized and open issues discussed. Through case studies, it is illustrated how layering as optimization decomposition provides a common language to modularization, a unifying, top-down approach to design protocol stacks and a mathematical theory of network architectures.

COGNITIVE RADIO RESOURCE MANAGEMENT

Network optimization, including radio resource management, discussed in Chapter 10, provides algorithms that optimize system performance defined by a given utility function. In Chapter 12, we present suboptimum solutions for resource management that include high level of cognition and cooperation to mitigate intercell interference. An important segment of this topic dealing with the

flexible spectra sharing is covered in another of our books on *Advanced Wireless Communications* focusing more on the physical layer, published by John Wiley & Sons, Ltd in 2007.

In addition to the new chapters, which represent about 40 % of the book, other chapters have been also updated with latest results.

Savo Glisic
Beatriz Lorenzo

1
Fundamentals

1.1 4G NETWORKS AND COMPOSITE RADIO ENVIRONMENT

In the wireless communications community we are witnessing more and more the existence of the *composite radio environment* (*CRE*) and as a consequence the need for *reconfigurability* concepts based on cognitive, cooperative and opportunistic algorithms.

The CRE assumes that different radio networks can be cooperating components in a heterogeneous wireless access infrastructure, through which network providers can more efficiently achieve the required capacity and quality of service (QoS) levels. Reconfigurability enables terminals and network elements dynamically to select and adapt to the most appropriate radio access technologies for handling conditions encountered in specific service area regions and time zones of the day. Both concepts pose new requirements on the management of wireless systems. Nowadays, a multiplicity of radio access technology (RAT) standards are used in wireless communications. As shown in Figure 1.1, these technologies can be roughly categorized into four sets:

- Cellular networks that include second-generation (2G) mobile systems, such as Global System for Mobile Communications (GSM) [1], and their evolutions, often called 2.5G systems, such as enhanced digital GSM evolution (EDGE), General Packet Radio Service (GPRS) [2] and IS 136 in the US. These systems are based on TDMA technology. Third-generation (3G) mobile networks, known as Universal Mobile Telecommunications Systems (UMTS) (WCDMA and cdma2000) [3] are based on CDMA technology that provides up to 2 Mbit/s. Long-term evolution (LTE) [4–12] of these systems is expected to evolve into a 4G system providing up to 100 Mbit/s on the uplink and up to 1 Gbit/s on the downlink. The solutions will be based on a combination of multicarrier and space–time signal formats. The network architectures include macro, micro and pico cellular networks and home (HAN) and personal area networks (PAN).
- Broadband radio access networks (BRANs) [13] or wireless local area networks (WLANs) [14] which are expected to provide up to 1 Gbit/s in 4G. These technologies are based on OFDMA and space–time coding.
- Digital video broadcasting (DVB) [15] and satellite communications.
- Ad hoc and sensor networks with emerging applications.

Advanced Wireless Technologies: Cognitive, Cooperative & Opportunistic 4G Technology Second Edition Savo G. Glisic

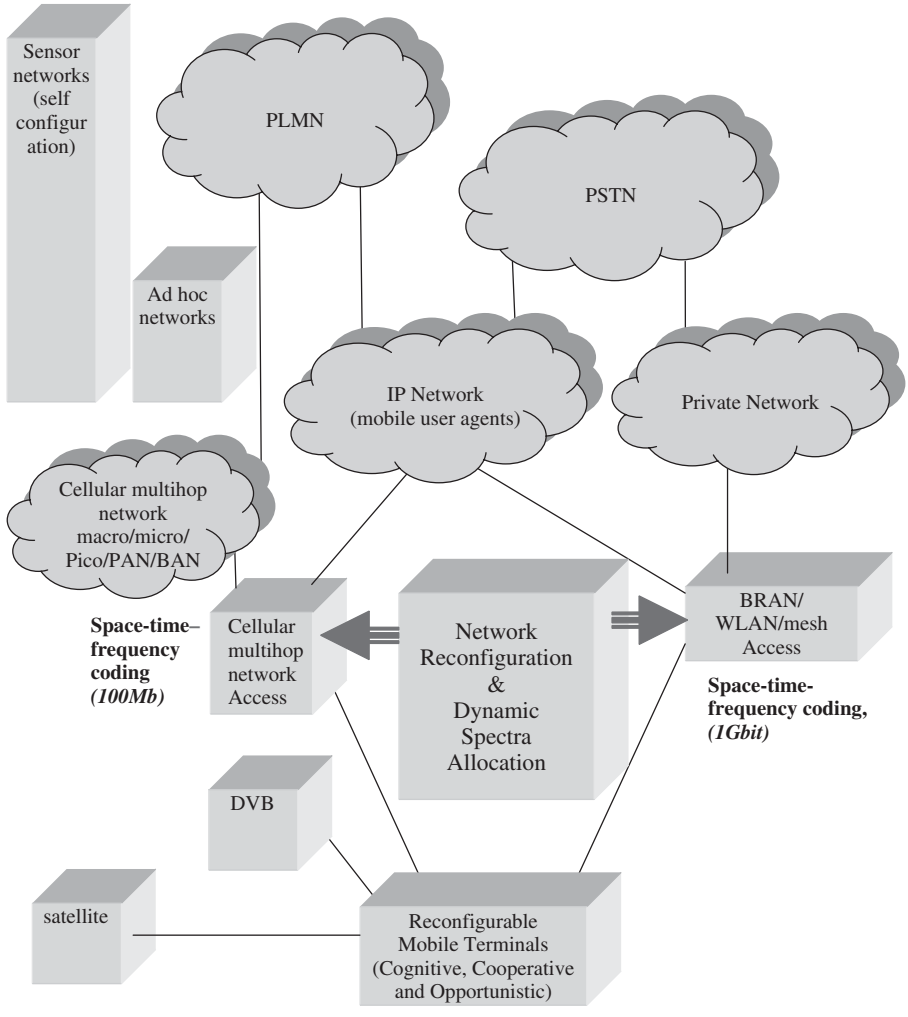

Figure 1.1 Composite radio environment in cognitive, cooperative and opportunistic 4G networks.

In order to increase the spectral efficiency further, besides the space–time frequency coding in the physical layer, the new paradigms like cognitive [16–20], cooperative [21–32] and opportunistic [33–38] solutions will be used.

Although 4G is open for new multiple access schemes, the CRE concept remains attractive for increasing the service provision efficiency and the exploitation possibilities of the available RATs. The main assumption is that the different radio networks, GPRS, UMTS, BRAN/WLAN, DVB and so on, can be components of a heterogeneous wireless access infrastructure. A network provider (NP) can own several components of the CR infrastructure (in other words, can own licenses for deploying and operating different RATs), and can also cooperate with affiliated NPs. In any case, an NP can rely on several alternate radio networks and technologies, for achieving the required capacity and QoS levels, in a cost-efficient manner. Users are directed to the most appropriate radio networks and technologies, at different service area regions and time zones of the day, based on profile requirements and network performance criteria. The various RATs are thus used in a

complementary manner rather than competing each other. Even nowadays a mobile handset can make a handoff between different RATs. The deployment of CRE systems can be facilitated by the *reconfigurability* concept, which is an evolution of a software-defined radio [39, 40]. The CRE requires terminals that are able to work with different RATs, and the existence of multiple radio networks offering alternate wireless access capabilities to service area regions. Reconfigurability supports the CRE concept by providing essential technologies that enable terminals and network elements dynamically (transparently and securely) to select and adapt to the set of RATs that are most appropriate for the conditions encountered in specific service area regions and time zones of the day. According to the reconfigurability concept, RAT selection is not restricted to those that are pre-installed in the network element. In fact, the required software components can be dynamically downloaded, installed and validated. This makes it different from the static paradigm regarding the capabilities of terminals and network elements.

The networks provide wireless access to IP (Internet protocols)-based applications and service continuity in the light of intrasystem mobility. Integration of the network segments in the CR infrastructure is achieved through the management system for the CRE (MS-CRE) component attached to each network. The management system in each network manages a specific radio technology; however, the platforms can cooperate. The fixed (core and backbone) network will consist of public and private segments based on IPv4- and IPv6-based infrastructures. A mobile IP (MIP) will enable the maintenance of IP-level connectivity regardless of the likely changes in the underlying radio technologies used that will be imposed by the CRE concept.

Figures 1.2 and 1.3 depict the architecture of a terminal that is capable of operating in a CRE context. The terminals include software and hardware components (layer 1 and 2 functionalities) for operating with different systems. The higher protocol layers, in accordance with their peer entities in the network, support continuous access to IP-based applications. Different protocol busters can further enhance the efficiency of the protocol stack. There is a need to provide the best possible IP performance over wireless links, including legacy systems. Within the performance implications of link characteristics (PILC) of the IETF group, the concept of a performance-enhancing proxy

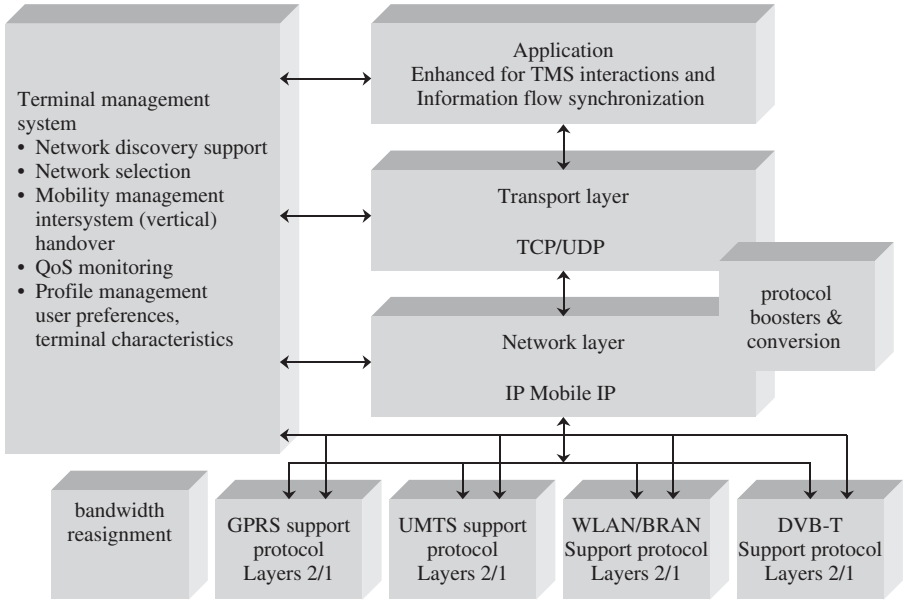

Figure 1.2 Architecture of a terminal that operates in a composite radio environment.

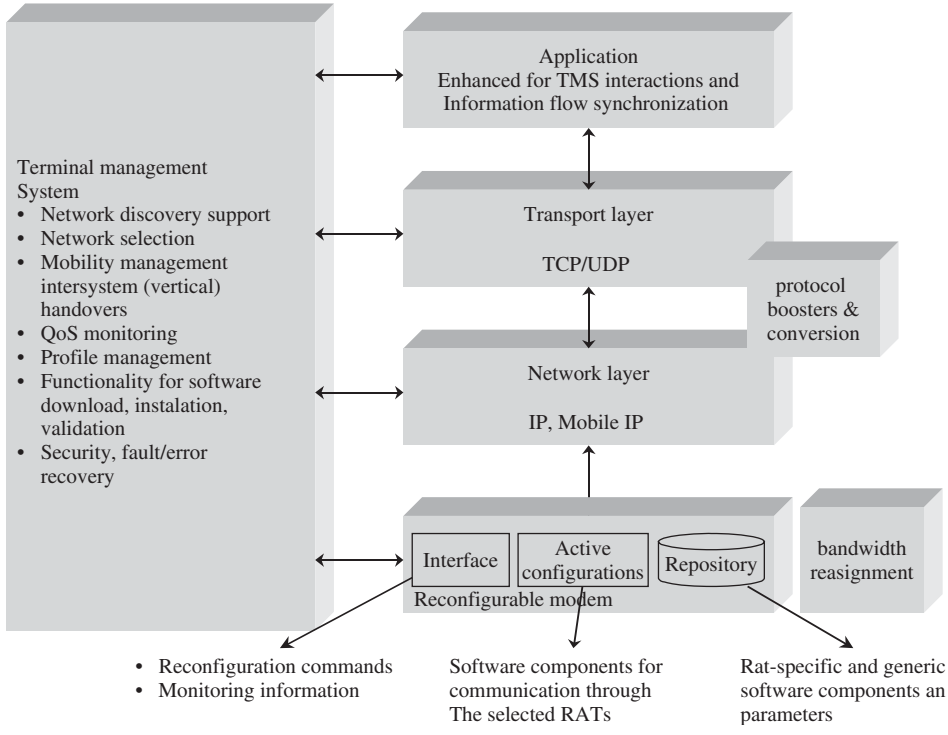

Figure 1.3 Architecture of a terminal that operates in the reconfigurability context.

(PEP) [41–44] has been chosen to refer to a set of methods used to improve the performance of Internet protocols on network paths where native TCP/IP performance is degraded due to characteristics of a link. Different types of PEPs, depending on their basic functioning, are also distinguished. Some of them try to compensate for the poor performance by modifying the protocols themselves. In contrast, a symmetric/asymmetric boosting approach, transparent to the upper layers, is often both more efficient and flexible.

A common framework to house a number of different protocol boosters provides high flexibility, as it may adapt to both the characteristics of the traffic being delivered and the particular conditions of the links. In this sense, a control plane for easing the required information sharing (cross-layer communication and configurability) is needed. Furthermore, another requirement comes from the appearance of multihop communications, as PEPs have been traditionally used over the last hop, so they should be adapted to the multihop scenario.

Most communications networks are subject to time and regional variations in traffic demands, which lead to variations in the degree to which the spectrum is utilized. Therefore, a service's radio spectrum can be underused at certain times or geographical areas, while another service may experience a shortage at the same time/place. Given the high economic value placed on the radio spectrum and the importance of spectrum efficiency, it is clear that wastage of radio spectrum must be avoided. These issues provide the motivation for a scheme called dynamic spectrum allocation (DSA), which aims to manage the spectrum utilized by a converged radio system and share it between participating radio networks over space and time to increase overall spectrum efficiency, as shown in Figures 1.4 and 1.5.

Composite radio systems and reconfigurability, discussed above, are potential enablers of DSA systems. Composite radio systems allow seamless delivery of services through the most appropriate

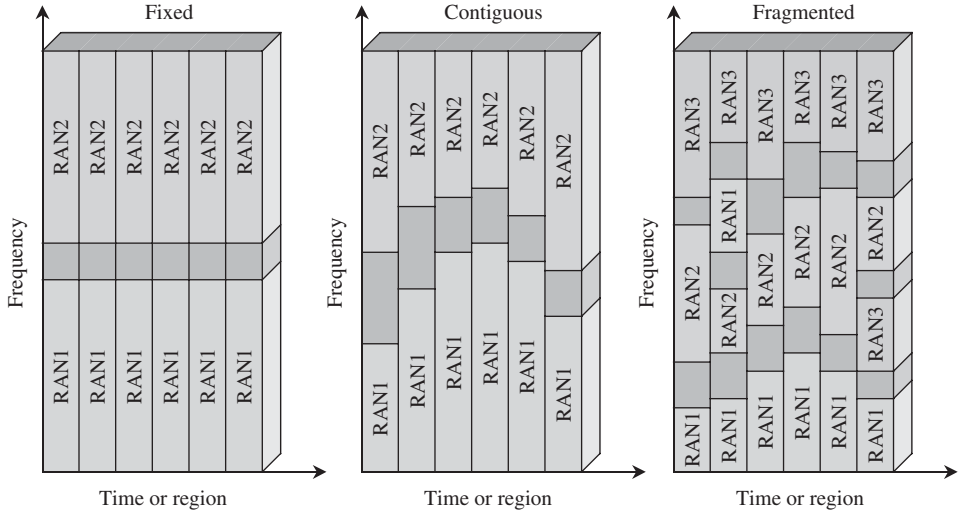

Figure 1.4 Fixed spectrum allocation compared to contiguous and fragmented DSA.

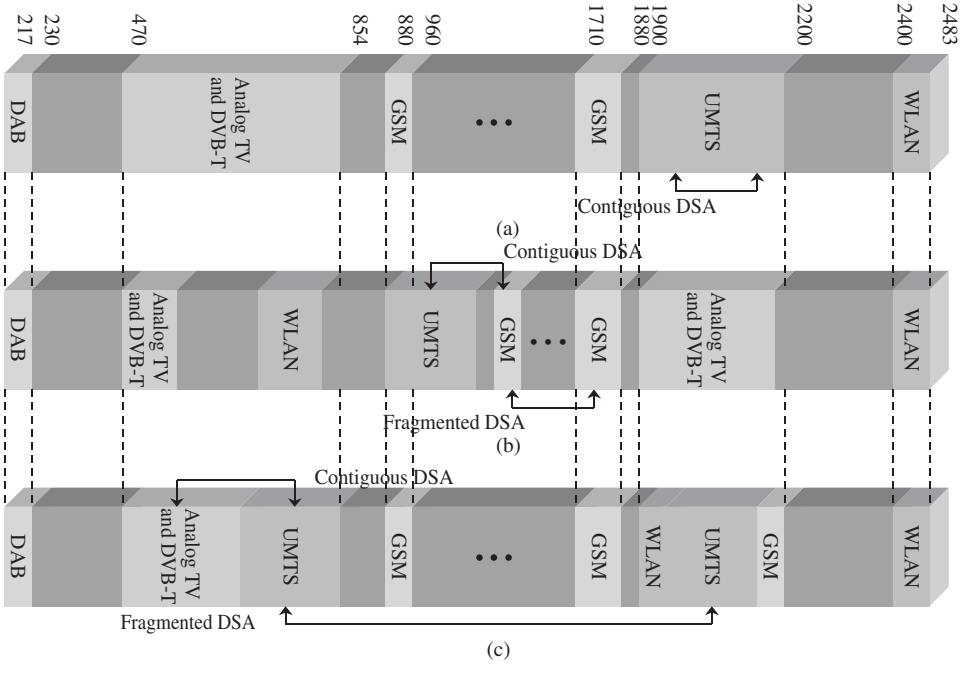

Figure 1.5 DSA operation configurations: (a) static (current spectrum allocations); (b) continuous DSA operations; (c) discrete DSA operations.

access network, and close network cooperation can facilitate the sharing not only of services but also of spectrum. Reconfigurability is also a very important issue, since with a DSA system a radio access network could potentially be allocated any frequency at any time in any location. It should be noted that the application layer is enhanced with the means to synchronize various information streams of the same application, which could be transported simultaneously over different RATs.

The terminal management system (TMS) is essential for providing functionality that exploits the CR environment. On the user/terminal side, the main focus is on the determination of the networks that provide, in a cost-efficient manner, the best QoS levels for the set of active applications. A first requirement is that the MS-CRE should exploit the capabilities of the CR infrastructure. This can be done in a reactive or proactive manner.

Reactively, the MS-CRE reacts to new service area conditions, such as the unexpected emergence of hot spots. Proactively, the management system can anticipate changes in the demand pattern. Such situations can be alleviated by using alternate components of the CR infrastructure to achieve the required capacity and QoS levels. The second requirement is that the MS-CRE should provide resource brokerage functionality to enable the cooperation of the networks of the CR infrastructure. Finally, parts of the MS-CRE should be capable of directing users to the most appropriate networks of the CR infrastructure, where they will obtain services efficiently in terms of cost and QoS. To achieve the above requirements the MS architecture shown in Figure 1.6 is required.

The architecture consists of three main logical entities:

- Monitoring, service-level information and resource brokerage (MSRB).
- Resource management strategies (RMS).
- Session managers (SMs).

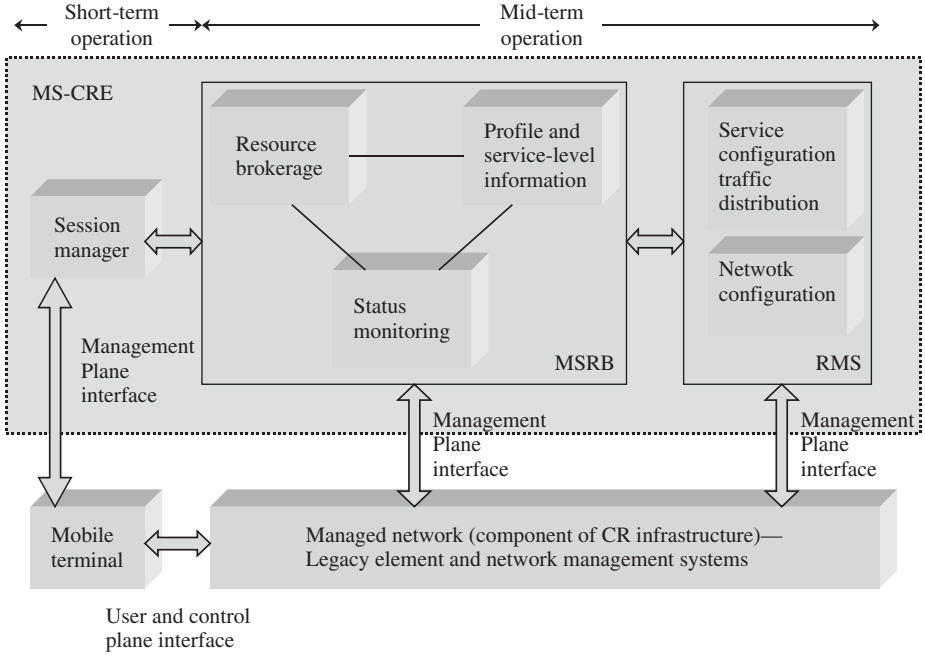

Figure 1.6 Architecture of the MS-CRE.

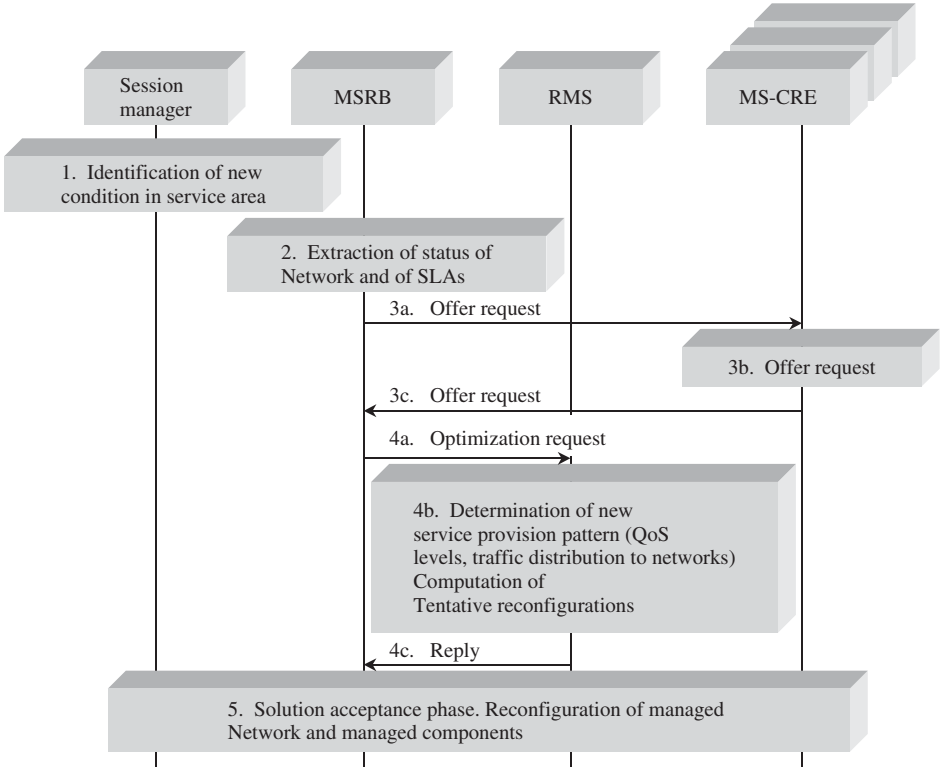

Figure 1.7 MS-CRE operation scenario.

The MSRB entity identifies the triggers (events) that should be handled by the MS-CRE and provides corresponding auxiliary (supporting) functionality. The RMS entity provides the necessary optimization functionality. The SM entity is in charge of interacting with the active subscribed users/terminals. The operation steps and *cooperation of the RMS components* are shown in Figures 1.7 and 1.8, respectively.

In order to gain an insight into the scope and range of possible reconfigurations, we review the network and protocol stack architectures of the basic CRE components as indicated in Figure 1.1.

1.2 PROTOCOL BOOSTERS

As pointed out in Figure 1.2, an element of the reconfiguration in 4G networks are protocol boosters. A protocol booster is a software or hardware module that transparently improves protocol performance. The booster can reside anywhere in the network or end systems, and may operate independently (one-element booster) or in cooperation with other protocol boosters (multielement booster). Protocol boosters provide an architectural alternative to existing protocol adaptation techniques, such as protocol conversion.

A protocol booster is a supporting agent that by itself is not a protocol. It may add, delete or delay protocol messages, but never originates, terminates or converts that protocol. A multielement protocol booster may define new protocol messages to exchange among themselves, but these protocols are originated and terminated by protocol booster elements, and are not visible or

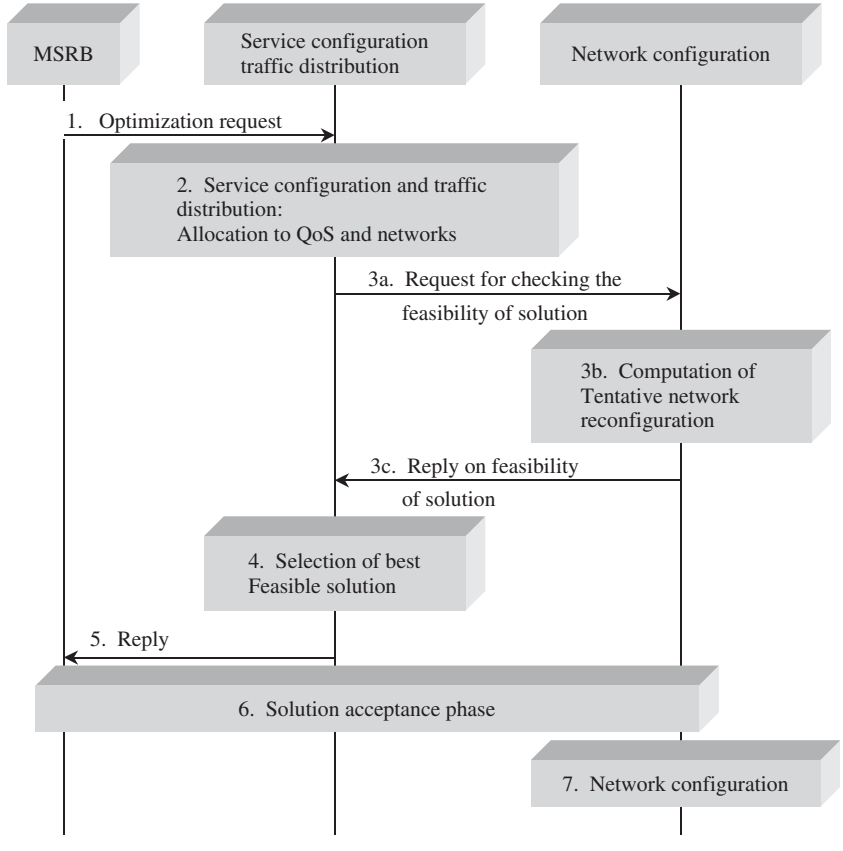

Figure 1.8 Cooperation of the RMS components.

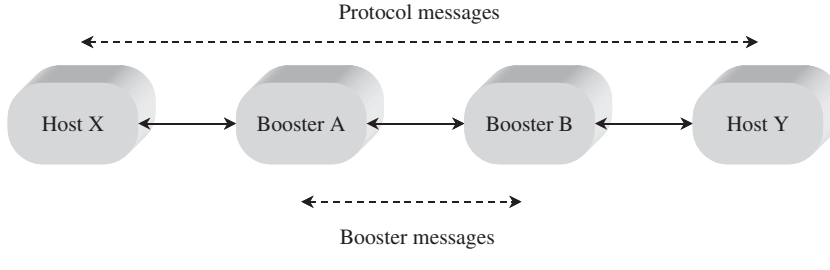

Figure 1.9 Two-element booster.

meaningful external to the booster. Figure 1.9 shows the information flow in a generic two-element booster. A protocol booster is transparent to the protocol being boosted. Thus, the elimination of a protocol booster will not prevent end-to-end communication, as would, for example, the removal of one end of a conversion (e.g. a TCP/IP header compression unit).

In what follows we will present examples of protocol busters.

1.2.1 One-element error detection booster for UDP

UDP has an optional 16-bit checksum field in the header. If it contains the value zero, it means that the checksum was not computed by the source. Computing this checksum may be wasteful on a reliable LAN. On the other hand, if errors are possible, the checksum greatly improves data integrity. A transmitter sending data does not compute a checksum for either local or remote destinations. For reliable local communication, this saves the checksum computation (at the source and destination). For wide-area communication, the single-element error detection booster computes the checksum and puts it into the UDP header. The booster could be located either in the source host (below the level of UDP) or in a gateway machine.

1.2.2 One-element ACK compression booster for TCP

On a system with asymmetric channel speeds, such as broadcast satellite, the forward (data) channel may be considerably faster than the return (ACK) channel. On such a system, many TCP ACKs may build up in a queue, increasing round-trip time and thus reducing the transmission rate for a given TCP window size. The nature of TCP's cumulative ACKs means that any ACK acknowledges at least as many bytes of data as any earlier ACK. Consequently, if several ACKs are in a queue, it is necessary to keep only the ACK that has arrived most recently. A simple ACK compression booster could ensure that only a single ACK exists in the queue for each TCP connection. (A more sophisticated ACK compression booster allows some duplicate ACKs to pass, allowing the TCP transmitter to get a better picture of network congestion.) The booster increases the protocol performance because it reduces the ACK latency and allows faster transmission for a given window size.

1.2.3 One-element congestion control booster for TCP

Congestion control reduces buffer overflow loss by reducing the transmission rate at the source when the network is congested. A TCP transmitter deduces information about network congestion by examining acknowledgments (ACKs) sent by the TCP receiver. If the transmitter sees several ACKs with the same sequence number, then it assumes that network congestion caused a loss of data messages. If congestion is noted in a subnet, then a congestion control booster could artificially produce duplicate ACKs. The TCP receiver would think that data messages have been lost because of congestion, and would reduce its window size, thus reducing the amount of data it injects into the network.

1.2.4 One-element ARQ booster for TCP

TCP uses ARQ to retransmit data unacknowledged by the receiver when a packet loss is suspected, such as after a retransmission timeout expires. If we assume the network of Figure 1.9 (except that Booster B does not exist), then an ARQ booster for TCP will: (a) cache packets from Host Y; (b) if it sees a duplicate acknowledgment arrive from Host X and it has the next packet in the cache; then it deletes the acknowledgment and retransmits the next packet (because a packet must have been lost between the booster and Host X); and (c) delete packets retransmitted from Host Y that have been acknowledged by Host X. The ARQ booster improves performance by shortening the retransmission path. A typical application would be if Host X were on a wireless network and the booster were on the interface between the wireless and wireline networks.

1.2.5 A forward erasure correction booster for IP or TCP

For many real-time and multicast applications, forward error correction coding is desirable. The two-element FZC booster uses a packet forward error correction code and erasure decoding. The FZC booster at the transmitter side of the network adds parity packets. The FZC booster at the receiver side removes the parity packets and regenerates missing data packets. The FZC booster can be applied between any two points in a network (including the end systems). If applied to an IP, then a sequence number booster adds sequence number information to the data packets before the first FZC booster. If applied to TCP (or any protocol with sequence number information), then the FZC booster can be more efficient because: (1) it does not need to add sequence numbers and (2) it could add new parity information on TCP retransmissions (rather than repeating the same parities). At the receiver side, the FZC booster could combine information from multiple TCP retransmissions for FZC decoding.

1.2.6 Two-element jitter control booster for IP

For real-time communication, we may be interested in bounding the amount of jitter that occurs in the network. A jitter control booster can be used to reduce jitter at the expense of increased latency. At the first booster element, timestamps are generated for each data message that passes. These

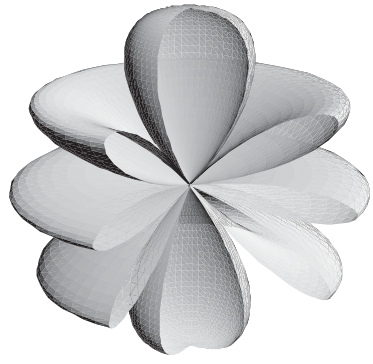

(a)

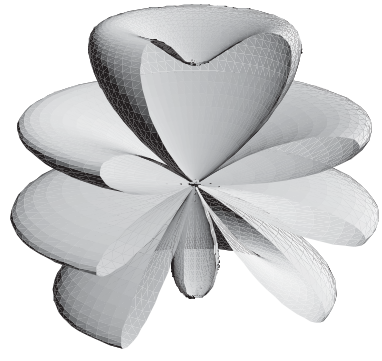

(b)

Figure 1.10 Three-dimensional amplitude patterns of a two-element uniform amplitude array for $d = 2\lambda$, directioned towards (a) $\theta_0 = 0^\circ$, (b) $\theta_0 = 60^\circ$.

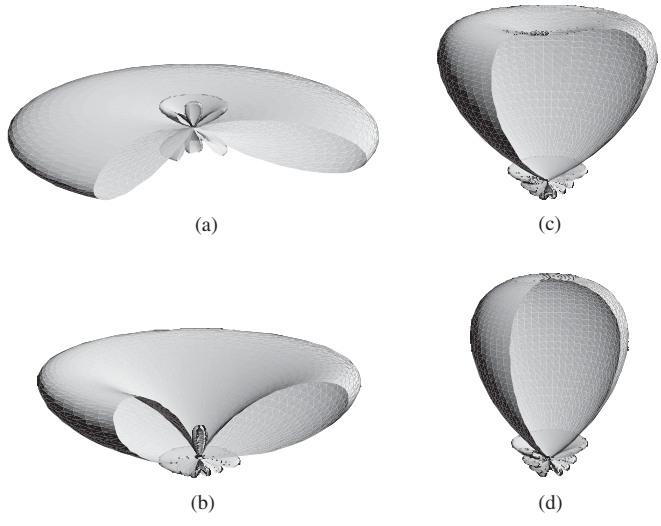

Figure 1.11 Three-dimensional amplitude patterns of a ten-element uniform amplitude array for $d = \lambda/4$, directioned towards (a) $\theta_0 = 0^\circ$, (b) $\theta_0 = 30^\circ$, (c) $\theta_0 = 60^\circ$, (d) $\theta_0 = 90^\circ$.

timestamps are transmitted to the second booster element, which delays messages and attempts to reproduce the intermessage interval that was measured by the first booster element.

1.2.7 Two-element selective ARQ booster for IP or TCP

For links with significant error rates using a selective ARQ protocol (with selective acknowledgment and selective retransmission) can significantly improve the efficiency compared to using TCP's ARQ (with cumulative acknowledgment and possibly go-back-N retransmission). The two-element ARQ booster uses a selective ARQ booster to supplement TCP by: (1) caching packets in the upstream booster, (2) sending negative acknowledgments when gaps are detected in the downstream booster and (3) selectively retransmitting the packets requested in the negative acknowledgments (if they are in the cache).

1.3 GREEN WIRELESS NETWORKS

4G wireless networks might be using a spatial notching (angle α) to suppress completely antenna radiation towards the user, as illustrated in Figures 1.10 and 1.11. These solutions will be referred to as 'green wireless networks' for obvious reasons.

In order to ensure the connectivity in the case when the antenna lobe is not directed towards the access point, a multihop communication, with the possibility of relaying, is required. In addition, to reduce the overall transmit power a cooperative transmit diversity, discussed in Section 19.4, and adaptive MAC protocol, discussed in Chapter 5 can be used.

REFERENCES

[1] M. Mouly and M.-B. Pautet, *The GSM System for Mobile Communications*, Palaiseau, France, 1992.

[2] R. Kalden, I. Meirick and M. Meyer, Wireless Internet access based on GPRS, *IEEE Pers. Commun.*, vol. 7, no. 2, April 2000, pp. 8–18.
[3] 3rd Generation Partnership Project (3GPP), http://www.3gpp.org.
[4] P. Mogensen, Wei Na, I. Z. Kovacs, F. Frederiksen, A. Pokhariyal, K. I. Pedersen, T. Kolding, K. Hugl and M. Kuusela, LTE capacity compared to the Shannon bound, in *Vehicular Technology Conf.*, 22–25 April 2007, pp. 1234–1238.
[5] H. Holma, A. Toskala, K. Ranta-aho, and J. Pirskanen, High-speed packet access evolution in 3GPP Release 7 [Topics in Radio Communications], *IEEE Commun. Mag.*, vol. 45, no. 12, December 2007, pp. 29–35.
[6] A. Hoikkanen, A techno-cconomic analysis of 3G long-term evolution for broadband access, in *Conf. on Telecommun. Techno-Economics*, 14–15 June 2007, pp. 1–7.
[7] A. Racz, A. Temesvary and N. Reider, Handover performance in 3GPP long term evolution (LTE) systems, in *Mobile and Wireless Commun. Summit, 16th IST*, 1–5 July 2007, pp. 1–5.
[8] M. Valkama, L. Anttila and M. Renfors, Some radio implementation challenges in 3G-LTE context, in *Signal Processing Advances in Wireless Commun., IEEE 8th Workshop on SPAWC 2007*, 17–20 June 2007, pp. 1–5.
[9] J. J. Sanchez, D. Morales-Jimenez, G. Gomez and J. T. Enbrambasaguas, Physical layer performance of long term evolution in cellular technology, in *16th IST Mobile and Wireless Commun. Summit*, 1–5 July 2007, pp. 1–5.
[10] J. Berkmann, C. Carbonelli, F. Dietrich, C. Drewes and Wen Xu, On 3G LTE terminal implementation – standards, algorithms, complexities and challenges, in *International Wireless Commun. and Mobile Computing Conf., IWCMC '08*, 6–8 August 2008, pp. 970–975.
[11] C. Spiegel, J. Berkmann, Zijian Bai, T. Scholand and C. Drewes, MIMO schemes in UTRA LTE, a comparison, in *IEEE Vehicular Technology Conf.*, 11–14 May 2008, pp. 2228–2232.
[12] S.-E. Elayoubi, O. Ben Haddada and B. Fourestie, Performance evaluation of frequency planning schemes in OFDMA-based networks, *IEEE Trans. Wireless Commun.*, vol. 7, no. 5, part 1, May 2008, pp. 1623–1633.
[13] J. Khun-Jush *et al*., HiperLAN2: broadband wireless communications at 5 GHz, *IEEE Commun. Mag.*, vol. 40, no. 6, June 2002, pp. 130–137.
[14] U. Varshney, The status and future of 802.11-based WLANs, *IEEE Comp.*, vol. 36, no. 6, June 2003, pp. 102–105.
[15] Digital Video Broadcasting (DVB), http://www.dvb.org, January 2002.
[16] V. Stavroulaki, P. Demestichas, A. Katidiotis and D. Petromanolakis, Evolution in equipment management concepts: from reconfigurable to cognitive wireless terminals, in *16th IST Mobile and Wireless Commun. Summit*, 1–5 July 2007, pp. 1–5.
[17] R. Muraleedharan and L. A. Osadciw, Increasing QoS and security in 4G networks using cognitive intelligence, in *IEEE Globecom Workshops*, 26–30 November 2007, pp. 1–6.
[18] I. F. Akyildiz, W.-Y. Lee, M. C. Vuran and S. Mohanty, Next generation/dynamic spectrum access/cognitive radio wireless networks: a survey, *Computer Networks J.*, Elsevier, vol. 50, September 2006, pp. 2127–2159.
[19] M. Muck, D. Bourse, K. Moessner, N. Alonistioti, P. Demestichas, E. Nicollet, E. Buracchini, D. Bateman, Z. Boufidis, E. Patouni, V. Stavroulaki, A. Trogolo and P. Goria, End-to-end reconfigurability in heterogeneous wireless systems – software and cognitive radio solutions enriched by policy- and context-based decision making, in *16th IST Mobile and Wireless Commun. Summit*, 1–5 July 2007, pp. 1–5.
[20] B. Aazhang, J. Lilleberg and G. Middleton, Spectrum sharing in a cellular system, in *2004 IEEE Eighth Int. Symp. on Spread Spectrum Techniques and Applications*, 30 August–2 September 2004, pp. 355–359.
[21] K. Doppler, A. Osseiran, M. Wodczak and P. Rost, On the integration of cooperative relaying into the WINNER system concept, in *16th IST Mobile and Wireless Commun. Summit*, 1–5 July 2007, pp. 1–5.

[22] Qian Zhang, Qing Chen, Fan Yang, Xuemin Shen and Zhisheng Niu, Cooperative and opportunistic transmission for wireless ad hoc networks, *IEEE Network*, vol. 21, no. 1, January–February 2007, pp. 14–20.
[23] M. Katz and F. H. P. Fitzek, Cooperative techniques and principles enabling future 4G wireless networks, in *EUROCON 2005*, *The Int. Conf. on Computer as a Tool*, vol. 1, 2005, pp. 21–24.
[24] H. Paloheimo, J. Manner, J. Nieminen and A. Yla-Jaaski, Challenges in packet scheduling in 4G wireless networks, in *2006 IEEE 17th Int. Symp. on Personal, Indoor and Mobile Radio Commun.*, September 2006, pp. 1–6.
[25] Carlos Leonel Flores Mayorga,, Francescantonio della Rosa, Satya Ardhy Wardana, Gianluca Simone,, Marie Claire Naima Raynal, Joao Figueiras and Simone Frattasi, Cooperative positioning techniques for mobile localization in 4G cellular networks, in *IEEE Int. Conf. on Pervasive Services*, 15–20 July 2007, pp. 39–44.
[26] D. Niyato and E. Hossain, A cooperative game framework for bandwidth allocation in 4G heterogeneous wireless networks, in 2006 *IEEE Int. Conf. on Commun.*, vol. 9, June 2006, pp. 4357–4362.
[27] M. Dohler, D.-E. Meddour, S.-M. Senouci and A. Saadani, Cooperation in 4G – hype or ripe?, in *IEEE Technology and Society Mag.*, vol. 27, no. 1, Spring 2008, pp. 13–17.
[28] S. Frattasi, M. Monti and R. Prasad, A cooperative localization scheme for 4G wireless communications, in *2006 IEEE Radio and Wireless Symp.*, 17–19 January 2006, pp. 287–290.
[29] C. Politis, T. Oda, S. Dixit, A. Schieder, H.-Y. Lach, M. I. Smirnov, S. Uskela and R. Tafazolli, Cooperative networks for the future wireless world, *IEEE Commun. Mag.*, vol. 42, no. 9, September 2004, pp. 70–79.
[30] V. Marques, R. L. Aguiar, C. Garcia, J. I. Moreno, C. Beaujean, E. Melin and M. Liebsch, An IP-based QoS architecture for 4G operator scenarios, *IEEE Wireless Commun.* [see also *IEEE Pers. Commun.*], vol. 10, no. 3, June 2003, pp. 54–62.
[31] Luan Huang, Kar Ann Chew and R. Tafazolli, Network selection for one-to-many services in 3G-broadcasting cooperative networks, in *2005 IEEE 61st Vehicular Technology Conf.*, vol. 5, 30 May–1 June 2005, pp. 2999–3003.
[32] S. M. S. Masajedian and H. Khoshbin, Cooperative location management method in next generation cellular networks, in *Ninth Int. Symp. on Computers and Communications, ISCC 2004*, vol. 1, 28 June–1 July 2004, pp. 525–530.
[33] S. Sorrentino and U. Spagnolini, A predictive opportunistic scheduler for 4G wireless systems, in *16th IST Mobile and Wireless Commun. Summit*, 1–5 July 2007, pp. 1–5.
[34] A. K. F. Khattab and K. M. F. Elsayed, Opportunistic scheduling of delay sensitive traffic in OFDMA-based wireless networks, in *Int. Symp. on a World of Wireless, Mobile and Multimedia Networks, WoWMoM 2006*, 26–29 June 2006, 10 pp.
[35] Yu Wu, Ji-bo Wei, Yong Xi, Byung-Seo Kim and Sung Won Kim, Opportunistic scheduling with statistical fairness guarantee in wireless networks, in *IEEE 18th Int. Symp. on Personal, Indoor and Mobile Radio Commun., PIMRC 2007*, 3–7 September 2007, pp. 1–5.
[36] S. Mangold, Zhun Zhong, K. Challapali and Chun-Ting Chou, Spectrum agile radio: radio resource measurements for opportunistic spectrum usage, in *IEEE Global Telecommun. Conf. 2004*, *GLOBECOM '04*, vol. 6, 29 November–3 December 2004, pp. 3467–3471.
[37] S. Sanayei, A. Nosratinia and N. Aldhahir, Opportunistic dynamic subchannel allocation in multiuser OFDM networks with limited feedback, in *IEEE Information Theory Workshop, 2004*, 24–29 October 2004, pp. 182–186.
[38] W. Ajib and D. Haccoun, An overview of scheduling algorithms in MIMO-based fourth-generation wireless systems, *IEEE Network*, vol. 19, no. 5, September–October 2005, pp. 43–48.
[39] S. Glisic, *Advanced Wireless Communications: 4G Cognitive and Cooperative Broadband Technology*, 2nd edition. John Wiley & Sons, Ltd: Chichester, London, 2007.

[40] J. Mitola III and G. Maguire Jr, Cognitive radio: making software radios more personal, *IEEE Pers. Commun.*, vol. 6, no. 4, August 1999, pp. 13–18.
[41] J. Border *et al*., Performance enhancing proxies intended to mitigate link-related degradations, RFC 3135, June 2001.
[42] D. C. Feldmeier *et al*., Protocol boosters, *IEEE J. Selected Areas Commun.*, vol. 16, no. 3, April 1998, pp. 437–444.
[43] M. García *et al*., An experimental study of snoop TCP performance over the IEEE 802.11b WLAN, in *5th Int. Symp. on Wireless Personal Multimedia Commun.*, vol. III, Honolulu, HA, October 2002, pp. 1068–1072.
[44] L. Muñoz *et al*., Optimizing Internet flows over IEEE 802.11b wireless local area networks: a performance enhancing proxy based on forward error correction, *IEEE Commun. Mag.*, vol. 39, no. 12, December 2001, pp. 60–67.

2

Opportunistic Communications

As pointed out in Chapter 1, opportunistic signaling will be used in 4G networks to increase further the spectral efficiency of these systems. In this chapter we discuss a number of different solutions that are based on that principle.

2.1 MULTIUSER DIVERSITY

Multiuser diversity is provided in wireless networks by independent time-varying channels across the different users. The diversity benefit is exploited by tracking the channel fluctuations of the users and scheduling transmissions to users when their instantaneous channel quality is highest. The diversity gain increases with the dynamic range of the fluctuations and is thus limited in environments with slow fading. In such environments, multiple-transmit antennas can be used to induce large and fast channel fluctuations so that multiuser diversity can be improved [1]. The scheme can be interpreted as *opportunistic beamforming* and beamforming gains can be achieved when there are sufficient users. In a cellular system, the scheme plays an additional role of *opportunistic nulling* of the interference created on users of adjacent cells.

Let us assume a simple model of the downlink of a cellular wireless communication system with a base station (transmitter) having a single antenna communicating with K users (receivers). The time-slotted block-fading channel model in baseband is given by

$$\mathbf{y}_k(t) = h_k(t)\mathbf{x}(t) + \mathbf{z}_k(t), \quad k = 1, 2, \ldots, K \tag{2.1}$$

In Equation (2.1), $\mathbf{x}(t) \in C^T$ is the vector of T transmitted symbols, $\mathbf{y}_k(t) \in C^T$ is the vector of T received symbols of user k, $h_k(t) \in C$ is the fading channel gain from the transmitter to receiver k and $\{\mathbf{z}_k(t)\}_t$ is an independent and identically distributed (i.i.d.) sequence of zero mean circular-symmetric Gaussian random vectors $CN(0,\ \sigma^2 I_T)$. Here we assume that the channel is constant over time slots of length T samples and that the transmit power level is $P = const$ at all times, i.e. $E[\|x(t)\|^2] = PT$.

Advanced Wireless Technologies: Cognitive, Cooperative & Opportunistic 4G Technology Second Edition Savo G. Glisic

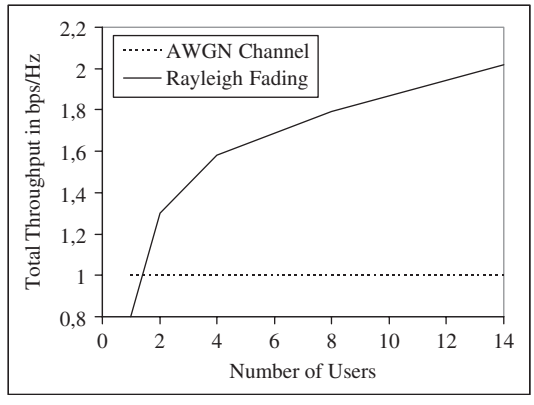

Figure 2.1 Sum capacity of two channels, Rayleigh fading and AWGN, with average SNR = 0 dB.

We can view this downlink channel as a set of parallel Gaussian channels, one for each fading state. The sum capacity of this channel, defined by the maximum achievable sum of long-term average data rates transmitted to all the users, can be achieved by a simple time division multiple access (TDMA) strategy: at each fading state, transmit to the user with the strongest channel [2].

The sum capacity of the downlink channel is presented in Figure 2.1, as a function of the number of users, for the case when users undergo independent Rayleigh fading with average received signal-to-noise ratio (SNR) = 0 dB.

One can see that the sum capacity increases with the number of users in the system. On the other hand, the sum capacity of a nonfaded downlink channel, where each user has a *fixed* additive white Gaussian noise (AWGN) channel with SNR = 0 dB, is constant irrespective of the number of users. In a system with many users with independently varying channels, it is likely that at any time there is a user with a channel much stronger than the average SNR. By transmitting to users with strong channels at all times, the overall spectral efficiency of the system can be made high, significantly higher than that of a nonfaded channel with the same average SNR.

In order to exploit such multiuser diversity it is necessary that:

- Each receiver should track its own channel SNR through, say, common downlink pilot, and feed back the instantaneous channel quality to the base station.
- The base station has the ability to schedule transmissions among the users as well as to adapt the data rate as a function of the instantaneous channel quality.

2.2 PROPORTIONAL FAIR SCHEDULING

The concept of multiuser diversity brings about two issues: fairness and delay. When users' fading *statistics* are the same, the strategy above maximizes not only the total capacity of the system but also the throughput of individual users. When the statistics are not symmetrical, the multiuser diversity concept provides maximum long-term average throughputs. In practice, there are latency requirements, in which case the average throughputs and limited delay is the performance metric of interest.

In the sequel the objective will be to address these issues while at the same time exploiting the multiuser diversity gain inherent in a system, with users having independent, fluctuating channel conditions. In a further discussion the feedback of the channel quality of user k in time slot t

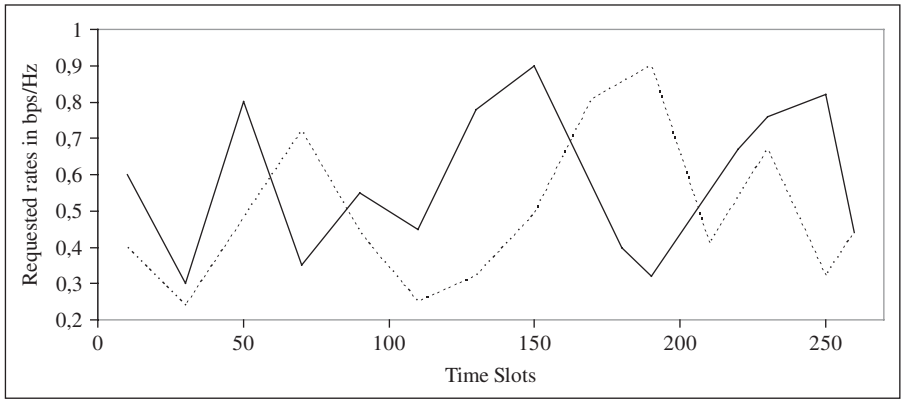

Figure 2.2 For symmetric channel statistics of users, the scheduling algorithm reduces to serving each user with the largest requested rate.

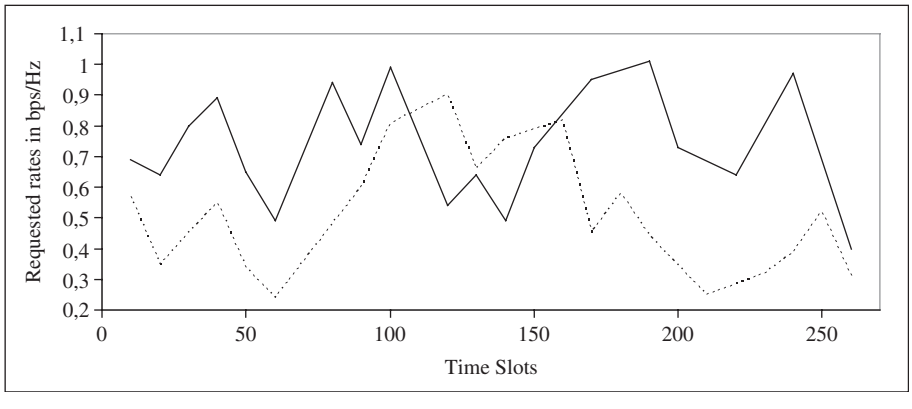

Figure 2.3 In general, with asymmetric user channel statistics, the scheduling algorithm serves each user when it is near its peak within the latency time scale t_c.

to the base station will be expressed in terms of a requested data rate $R_k(t)$. This is the data rate that the kth user's channel can support at the time. The scheduling algorithm keeps track of the average throughput $T_k(t)$ of each user in a past window of length t_c, and in time slot t the scheduling algorithm transmits to the user k^* with the largest $R_k(t)/T_k(t)$ among all active users in the system. The average throughputs $T_k(t)$ can be updated using an exponentially weighted low-pass filter

$$T_k(t+1) = \begin{cases} (1-1/t_c)T_k(t) + R_k(t)/t_c, & k = k^* \\ (1-1/t_c)T_k(t), & k \neq k^* \end{cases}. \tag{2.2}$$

The operation of the algorithm is illustrated in Figures 2.2 and 2.3. The sample paths of the requested data rates of two users are plotted as a function of time slots (each time slot is 1.67 ms). In Figure 2.2, the two users have identical fading *statistics*. If the scheduling time scale t_c is much larger than the correlation time scale of the fading dynamics, then by symmetry the throughput of each user $T_k(t)$ converges to the same quantity. The scheduling algorithm reduces to always

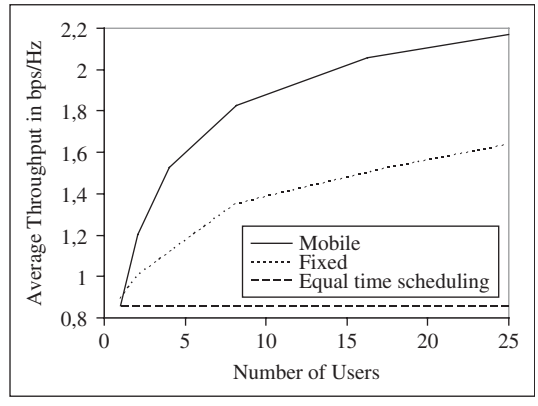

Figure 2.4 Multiuser diversity gain in fixed and mobile environments.

picking the user with the highest requested rate. Thus, each user is scheduled when its channel is good and at the same time the scheduling algorithm is perfectly fair in the long term. In Figure 2.3, one user's channel is much stronger than the other user's on the average, although both channels fluctuate due to multipath fading. Always picking the user with the highest requested rate means giving all the system resources to the statistically stronger user and would be unfair. Under the scheduling algorithm defined by Equation (2.2), users compete for resources not only based on their requested rates but after normalization by their respective average throughputs. The user with the statistically stronger channel will have a higher average throughput. Thus, the algorithm schedules a user when its instantaneous channel quality is high *relative* to its own average channel condition over the period t_c. In other words, data are transmitted to a user when the channel is *near its own peaks*. Multiuser diversity benefit can still be exploited because channels of different users fluctuate independently so that if there is a sufficient number of users in the system, there is likely to be a user near its peak at any one time.

The parameter t_c is tied to the latency time scale of the application. Peaks are defined with respect to this time scale. If the latency time scale is large, then the throughput is averaged over a longer time scale and the scheduler can afford to wait longer before scheduling a user when its channel hits a really high peak. The theoretical properties of this scheduling algorithm are further explored later in this chapter. It will be shown that this algorithm guarantees a fairness property called *proportional fairness*.

Figure 2.4 gives some insights into the issues involved in realizing multiuser diversity benefits in practice. The plot shows the total throughput of the downlink under the proportional fair scheduling algorithm in the following two simulated environments:

- *Fixed.* Users are static but there are movements of objects around them (2 Hz Rician, $\kappa \stackrel{\text{def}}{=} E_{\text{direct}}/E_{\text{specular}} = 5$).
- *Mobile.* Users move at walking speeds (3 km/h, Rayleigh).

The total throughput increases with the number of users in both the fixed and mobile environments, but the increase is more dramatic in the mobile case. While the channel fades in both cases, the dynamic range and the rate of the variations is larger in the mobile environment than in the fixed one. This means that over the latency time scale (1.67 s in these examples), the peaks of the channel fluctuations are likely to be higher in the mobile environment, and the peaks are what determines the performance of the scheduling algorithm. Thus, the inherent multiuser diversity is more limited in the fixed environment.

2.3 OPPORTUNISTIC BEAMFORMING

The effectiveness of multiuser diversity depends on the rate and dynamic range of channel fluctuations. In environments where the channel fluctuations are small, the multiuser diversity gain can be increased by *inducing* faster and larger fluctuations. In Reference [1] multiple-transmit antennas at the base station are used for these purposes, as illustrated in Figure 2.5.

For such a system with N transmit antennas at the base station, let $h_{nk}(t)$ be the complex channel gain from antenna n to the kth user in time slot t. In time slot t, the same block of symbols $\mathbf{x}(t)$ is transmitted from all of the antennas except that it is multiplied by a complex number $\sqrt{\alpha_n(t)}e^{j\theta_n(t)}$ at antenna n, for $n = 1, \ldots, N$, such that $\sum_{n=1}^{N} \alpha_n(t) = 1$, preserving the total transmit power. The received signal at user k is given by

$$\mathbf{y}_k(t) = \left(\sum_{n=1}^{N} \sqrt{\alpha_n(t)} e^{j\theta_n(t)} h_{nk}(t) \right) \mathbf{x}(t) + \mathbf{z}_k(t) \tag{2.3}$$

Thus, the overall channel gain seen by receiver k is now

$$h_k(t) := \sum_{n=1}^{N} \sqrt{\alpha_n(t)} e^{j\theta_n(t)} h_{nk}(t) \tag{2.4}$$

In Equation (2.4), the $\alpha_n(t)$ denote the fractions of power allocated to each of the transmit antennas and the $\theta_n(t)$ the phase shifts applied at each antenna to the signal. By varying over time $\alpha_n(t)$ from 0 to 1 and $\theta_n(t)$ from 0 to 2π, fluctuations in the overall channel can be induced even if the physical channel gains $h_{nk}(t)$ do not fluctuate much. Each receiver k reports back the value of

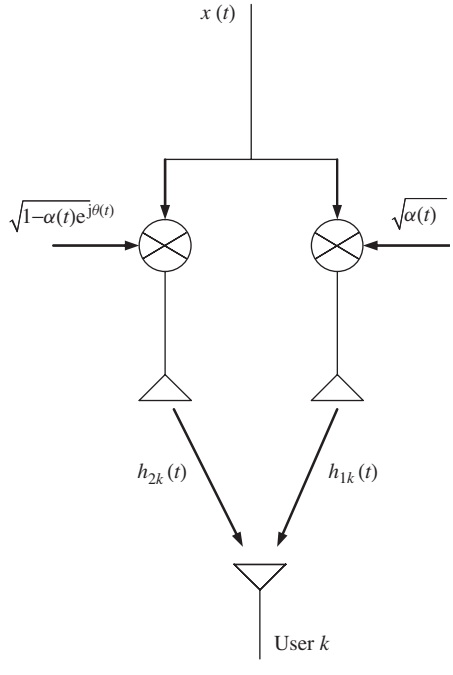

Figure 2.5 The same signal is transmitted over the two antennas with time-varying phase and powers.

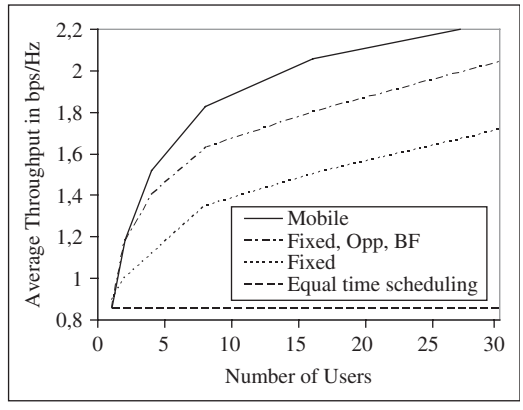

Figure 2.6 Amplification in multiuser diversity gain with opportunistic beamforming in a fixed environment.

$\mathrm{SNR}|h_k(t)|^2/\sigma^2$ of its own channel to the base station and the base station schedules transmissions to users accordingly.

The rate of variation of $\{\alpha_n(t)\}$ and $\{\theta_n(t)\}$ in time is a design parameter of the system. On one side it should be as fast as possible to provide full channel fluctuations within the latency time scale of interest. On the other hand, the variation should be slow enough to allow the channel to be reliably estimated by the users and the SNR information feedback. Further, the variation should be slow enough to ensure that the channel seen by the users does not change abruptly and thus maintains stability of the channel tracking loop.

To illustrate the performance of this scheme, we now consider the fixed environment of Figure 2.5 with two antennas of equal and constant (over time) power split and phase rotation over $[0, 2\pi]$ (with one complete rotation in 30 ms as in Reference [1]). Figure 2.6 plots the improved performance as a function of number of users. This improvement is due to the fact that the channel is changing faster and the dynamic range of variation is larger over the time scale of scheduling (1.67 s in this example).

2.4 OPPORTUNISTIC NULLING IN CELLULAR SYSTEMS

For wide-band cellular systems with full frequency reuse, it is important to consider the effect of intercell interference on the performance of the system, particularly in interference-limited scenarios. In a cellular system, the channel quality of a user is measured by the signal-to-interference plus noise ratio (SINR). In a fading environment, the energies in both the received signal and the received interference fluctuate over time. Since the multiuser diversity scheduling algorithm allocates resources based on the channel SINR (which depends on both the channel amplitude and the amplitude of the interference), it automatically exploits both the fluctuations in the energy of the received signal as well as that of the interference: the algorithm tries to schedule resource to a user whose instantaneous channel is good *and* the interference is weak. Thus, multiuser diversity naturally takes advantage of the time-varying interference to increase the spatial reuse of the network.

From this point of view, power and phase randomization at the base station transmit antennas plays an additional role: it increases not only the amount of fluctuations of the received signal

to the intended users within the cells, but also the amount of the fluctuations of the interference the base station causes in adjacent cells. Hence, opportunistic beamforming has a dual benefit in an interference-limited cellular system. In fact, opportunistic beamforming performs opportunistic nulling simultaneously, while randomization of power and phase in the transmitted signals from the antennas allows near-coherent beamforming to some user within the cell; it will create near nulls at some other user in adjacent cells. This in effect allows interference avoidance for that user if it is currently being scheduled.

In a slow flat fading scenario under power and phase randomization at all base stations, the received signal of a typical user being interfered by J adjacent base stations is given by

$$y(t) = h(t)x(t) + \sum_{j=1}^{J} g_j(t)u_j(t) + z(t) \tag{2.5}$$

where $x(t)$ is the signal of interest, $u_j(t)$ is the interference from the jth base station and $z(t)$ is additive Gaussian noise. All base stations have the same transmit power P and N transmit antennas and are performing power and phase randomization independently; $h(t)$ and $g_j(t)$ are the *overall* channel gains from the base stations

$$h(t) := \sum_{n=1}^{N} \sqrt{\alpha_n(t)}\mathrm{e}^{\mathrm{j}\theta_n(t)}h_n \tag{2.6}$$

$$g_j(t) := \sum_{n=1}^{N} \sqrt{\beta_{nj}(t)} = \mathrm{e}^{\mathrm{j}\phi_{nj}(t)}g_{nj} \tag{2.7}$$

where h_n and g_{nj} are the slow fading channel gains to the user from the nth transmit antenna of the base station of interest and the interfering base station j, respectively. Averaging over the signal $x(t)$ and the interference $u_j(t)$, the (time-varying) SINR of the user can be computed to be

$$SINR(t) = \frac{P|h(t)|^2}{P\sum_{j=1}^{J}|g_j(t)|^2 + \sigma^2} \tag{2.8}$$

The SINR varies because of both the variations of the overall gain from the base station of interest as well as those from the interfering base station. In a system with many other users, the proportional fair scheduler will serve this user while its SINR is at its peak $P\sum_{n=1}^{N}|h_n(t)|^2/\sigma^2$, i.e. when the received signal is the strongest and the interference is completely nulled out. Thus, the opportunistic nulling and beamforming technique has the potential to shift a user from a low-SNR interference-limited regime to a high-SNR noise-limited regime.

How close the performance of opportunistic beamforming and nulling in a finite-size system is to this asymptotic limit depends on the probability that the received signal is near beamformed *and* all the interference is near null. In the interference-limited regime when $P/\sigma^2 \gg 1$, the performance depends mainly on the probability of the latter event. This probability is larger when there are only one or two base stations contributing most of the interference, as is typically the case. In contrast, when there is interference from many base stations, interference averaging occurs and the probability that the *total* interference is near null is much smaller. Interference averaging, which is good for CDMA networks, is actually unfavorable for the opportunistic scheme described here, since it reduces the likelihood of the nulling of the interference and hence the likelihood of the peaks of the SINR.

In a typical cell, there will be a distribution of users, some closer to the base station and some closer to the cell boundaries. Users close to the base station are at high SNR and are noise-limited; the contribution of the intercell interference is relatively small. These users benefit

mainly from opportunistic beamforming (diversity gain plus a 3 dB power gain if there are two transmit antennas). Users close to the cell boundaries, on the other hand, are at low SNR and are interference-limited; the average interference power can be much larger than the background noise. These users benefit both from opportunistic beamforming and from opportunity nulling of intercell interference. Thus, the cell-edge users benefit more in this system than users in the interior. This is rather desirable from a system fairness point of view, as the cell-edge users tend to have poorer service. This feature is particularly important for a system without soft handoff (which is difficult to implement in a packet data scheduling system). To maximize the opportunistic nulling benefits, the transmit power at the base station should be set as large as possible, subject to regulatory and hardware constraints.

2.5 NETWORK COOPERATION AND OPPORTUNISTIC COMMUNICATIONS

In this section we consider a network architecture with B cooperating and $\overline{B}$ noncooperating base stations (BSs). The cluster of cooperating BSs cooperate to improve the capacity with fairness to the users in the network. The noncooperating BSs do not cooperate with BSs in this cluster and cause interference to the users, which cannot be mitigated. As an example, in Figure 2.7 [3], there are three BSs (marked with circles), which cooperate and provide service to the users in the shaded region. The other BSs cause interference to these users. In the sequel we focus only on the activities of the cooperating BSs.

During every time slot each coordinating BS selects one beam out of the set of L beams available to it and services one user. In this way, the cluster of B cooperating BSs supports B users simultaneously. The system operates in two steps. In the first step, each BS transmits a pilot signal using a certain beam and collects the SINR reports from the users. The BS then transmits these reports to a centralized unit which, in the second step, schedules users based on their current and past SINR reports for data packet transmission. This process is repeated for the entire time period over which data are transmitted. The number of users K being serviced during this time period is assumed constant.

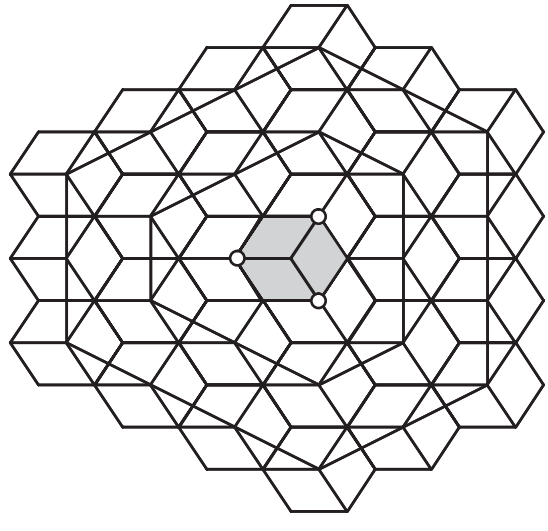

Figure 2.7 Three-base intercell coordination scenario.

In a given timeslot n during the first step, each BS transmits a pilot signal using one of the L beams. The received signal power at user i from the BS b on the lth beam is $S_i[n] = P_{(i,b)}|h_{(i,b,l)}[n]|^2$, where $h_{(i,b,l)}[n]$ is the channel gain from BS b to the user i on beam l and $P_{(i,b)}$ is the received signal power at the user i with the combined effect of path loss and shadowing.

The interference plus noise power is $IN_i[n] = I_i[n] + No_i[n]$, where $I(\cdot)$ is the interference power from the noncooperating BSs and $No(\cdot)$ is the thermal noise power. The user measures the received SINR, $\gamma_{(i,b,l)}[n] = S_i[n]/IN_i[n]$ and transmits this SINR value to the BS. The centralized scheduler collects the SINR reports from all the BSs and obtains the matrix $\mathbf{\Gamma}_{K\times B}$, where the (i, b)th element represents the SINR feedback by user i on the beam from BS b. In the second phase the centralized scheduler using these data opportunistically schedules B users on each of the B BSs, and each BS then transmits to the scheduled user. The data rate $R_{(i,b,l)}$, a BS b, provides a given user i on beam l and is calculated by

$$R_{(i,b,l)} = \log_2\left[1 + S_i[n] \Big/ \left(IN_i[n] + \sum_{\bar{b}\neq b}^{B} P_{(i,\bar{b})}\left|h_{(i,\bar{b},\bar{l})}[n]\right|^2\right)\right]$$
$$= \log_2\left[1 + \gamma_{(i,b,l)}[n] \Big/ \left(1 + \sum_{\bar{b}\neq b}^{B}\left(\gamma_{(i,\bar{b},\bar{l})}[n]\right)\right)\right] \tag{2.9}$$

In a scenario where the BSs cooperate and opportunistically beamform and schedule users the main steps are [3]:

(1) *Choose U users to serve: ($\|U\| = K_u$; $B < K_u < K$) using one of the following criteria:*
   a) *Select users that experience large inter-packet delay, $\mu_i[n]$.*
   b) *Select users who have low short-term throughput $T_i[n]$.*
   c) *Select users who have the largest $\mu_i[n]/T_i[n]$ ratio.*

(2) *The centralized scheduler using the user-base-beam selection algorithm described below selects, a subset of B users from the above chosen group of K_u users, and the corresponding BSs and beams on which they may be serviced. This algorithm generates a set of B triplets where the triplet (i_j, b_j, l_j) represents the case where user i_j is best served by BS b_j on the beam l_j, $j \in \{1 \cdots B\}$.*

(3) *Each BS generates the above assigned beam and collects the SINR reports from all the users. All the BSs transmit these reports to the centralized scheduler.*

(4) *The centralized scheduler using the $\mathbf{\Gamma}_{K\times B}$ SINR matrix and the short-term throughput vector $\mathbf{T}$ schedules B users for service.*

Steps 1,2 and 3 constitute the first phase of the system and step 4 constitutes the second phase.

In the *user-base-beam selection (UBBS) algorithm*, mentioned above, B users from the initially chosen set of K_u users and the indices of the BSs and the beams on which these users may be serviced are chosen. The beams must be chosen such that they least interfere with the B selected users. One possible approach to attain this objective is through the instantaneous system throughput, which is the sum of the achievable user rates. For $B = 3$ we state this formally as

$$\underset{i_1,i_2,i_3\in\{1\cdots K_u\},b_1,b_2,b_3\in\{1\cdots B\},l_1,l_2,l_3\in\{1\cdots L\}}{\arg\max} f(\mathbf{i}, \mathbf{b}, \mathbf{l}) \tag{2.10}$$

with $\mathbf{i} = \{i_1, i_2, i_3\}$, $\mathbf{b} = \{b_1, b_2, b_3\}$, $\mathbf{l} = \{l_1, l_2, l_3\}$ and $f(\cdot)$ is the sum of the rates of the three users. By using Equation (2.9) we have

$$f(\mathbf{i}, \mathbf{b}, \mathbf{l}) = \log_2 \left[\left(1 + \frac{\gamma_{(i_1,b_1,l_1)}}{1 + \gamma_{(i_1,b_2,l_2)} + \gamma_{(i_1,b_3,l_3)}} \right) \left(1 + \frac{\gamma_{(i_2,b_2,l_2)}}{1 + \gamma_{(i_2,b_1,l_1)} + \gamma_{(i_2,b_3,l_3)}} \right) \times \left(1 + \frac{\gamma_{(i_3,b_3,l_3)}}{1 + \gamma_{(i_3,b_1,l_1)} + \gamma_{(i_3,b_2,l_2)}} \right) \right]$$

In the absence of current SINRs, the short-term averaged SINRs $\tilde{\gamma}_{(i,b,l)}$ can be used instead of $\gamma_{(i,b,l)}$ in Equation (2.10). The short-term SINR is computed as

$$\tilde{\gamma}_{(i,b,l)}[n] = \frac{\sum_{t=0}^{n-1} \gamma_{(i,b,l)}[t] \delta(\theta_{(i,b)}[t], l) a^{n-t-1}}{\sum_{t=0}^{n-1} \delta(\theta_{(i,b)}[t], l) a^{n-t-1}} \tag{2.11}$$

where $\theta_{(i,b,l)}[t]$ represents the index of the beam on which user i was serviced by base station b at time instant t. Thus, this alternative criterion for selecting the set of triplets is stated as

$$\underset{i_1,i_2,i_3 \in \{1 \cdots K_u\}, b_1,b_2,b_3 \in \{1 \cdots B\}, l_1,l_2,l_3 \in \{1 \cdots L\}}{\arg\max} \tilde{f}(\mathbf{i}, \mathbf{b}, \mathbf{l}) \tag{2.12}$$

with $\tilde{f}(\mathbf{i}, \mathbf{b}, \mathbf{l})$ given by Equation (2.10) using $\tilde{\gamma}_{(i,b,l)}$ instead of $\gamma_{(i,b,l)}$.

The optimization of Equation (2.12) is practically infeasible when B and L are large. The following, computationally less intensive, modified UBBS algorithm was proposed in Reference [3] for scenarios where B and L are large.

A group of users U is initially chosen and arranged in order of preference for service using one of the criteria stated earlier. The main steps of this modified procedure are:

(1) *Choose the first user i_1 and obtain the BS and beam index $\{b_1, l_1\}$ on which the user i_1 experiences maximum throughput. Formally these indices are obtained as*

$$(b_1, l_1) = \underset{b \in \{1 \cdots B\}, l \in \{1 \cdots L\}}{\arg\max} \tilde{\gamma}_{(i,b,l)} \tag{2.13}$$

$$\kappa_1 = \tilde{\gamma}_{(i_1,b_1,l_1)} \tag{2.14}$$

(2) *Choose the second user i_2 from the remainder of the set $(U - i_1)$, and the indices for the beam and BS using the following criterion*:

$$\underset{b_2 \in \{1 \cdots B\}, l_2 \in \{1 \cdots L\}}{\arg\max} \tilde{f}_2(\mathbf{i}, \mathbf{b}, \mathbf{l}); \tag{2.15}$$

with $\mathbf{i} = \{i_1, i_2\}$ *and* $\mathbf{b} = \{b_1, b_2\}, \mathbf{l} = \{l_1, l_2\}$ *and*

$$\tilde{f}_2(\mathbf{i}, \mathbf{b}, \mathbf{l}) = \left(1 + \frac{\tilde{\gamma}_{(i_1,b_1,l_1)}}{1 + \tilde{\gamma}_{(i_1,b_2,l_2)}} \right) \times \left(1 + \frac{\tilde{\gamma}_{(i_2,b_2,l_2)}}{1 + \tilde{\gamma}_{(i_2,b_1,l_1)}} \right)$$

$$\kappa_2 = \tilde{f}_2^*(\mathbf{i}, \mathbf{b}, \mathbf{l})$$

In this way the newly chosen user i_2 causes minimal interference to user i_1 and vice versa. The terms κ_1, κ_2 represent the virtual SINR of the system as the system is loaded with users and BSs. We also use the constraint that $\kappa_2 > \kappa_1$ to ensure that the addition of a new user does not decrease the overall virtual SINR of the system. In the same way, the remaining set of users and the beams on which they are serviced by the BSs are chosen. When this constraint of increasing the virtual SINR of the system fails, the beams are chosen at random.

The scheduler obtains the terms $\gamma_{(i,b,l)}$, which are the SINR reports of the users from the BSs on the beams given by the UBBS algorithm. Then the rate $R_{(i,b,l)}$ that user i obtains from BS b using

beam l is computed. Using this information, B users are chosen whose weighted sum of rates is maximum, with the weights given by the reciprocal of the user's short-term throughputs $T[\cdot]$. This criterion is also computationally intensive, so the following alternative is considered. The users are ordered according to their weighted rates as $(R/T)_{i_1,b_1} \geq (R/T)_{i_2,b_2} \cdots \geq (R/T)_{i_K,b_k}$ and the first B users are chosen while maintaining the constraint that only one user is scheduled from a BS.

2.5.1 Performance example

We will illustrate the performance of the above methods for two different hexagonal cellular networks, as shown in Figures 2.7 and 2.8.

The number of coordinating BSs B in these two networks are 3 and 9 respectively. The hexagonal cells are divided into three 120° sectors and each of these sectors are covered by a BS with a smart antenna system. The BSs are located at the centre of each of the hexagonal cells and the users are distributed randomly in the shaded regions. The received signal at the user is modelled as in Section 2.5 to take into account path loss, shadow fading and correlated Rayleigh fading effects. The path loss is based on the Hata urban propagation model with a path loss coefficient of 3.5. A lognormal shadow fading process with zero mean and a standard deviation of 8 dB was used to characterize the variations in the signal due to environmental clutter. Two different correlated Rayleigh fading channels corresponding to Doppler rates with user velocities of 1 m/s and 8 m/s are analyzed. The antennas at the BSs consist of a uniform linear array (ULA) of antenna elements. Each of these elements is fed equal currents and only their phases are varied. Eleven such equispaced radiation patterns were generated using a four-element array. The normalized array factor considered in the simulations is $|A(\psi)| = |\sin(N\psi/2)/\sin(\psi/2)|/N$, where N is the number of antenna array elements and ψ is the azimuth in radians. The radiation pattern of each element is shown by the dashed line in Figure 2.9.

The interference terms due to the noncoordinating BSs were simulated by randomly generating beams from these BSs in their assigned sectors. The other system parameters used in the simulations are the same as in Reference [3]: cell radius 1 km, transmit base power 40 dBm, carrier frequency 2 GHz, sampling frequency 500 Hz, number of users per sector 20 and the forgetting factor a used in Equation (2.11) is 0.998.

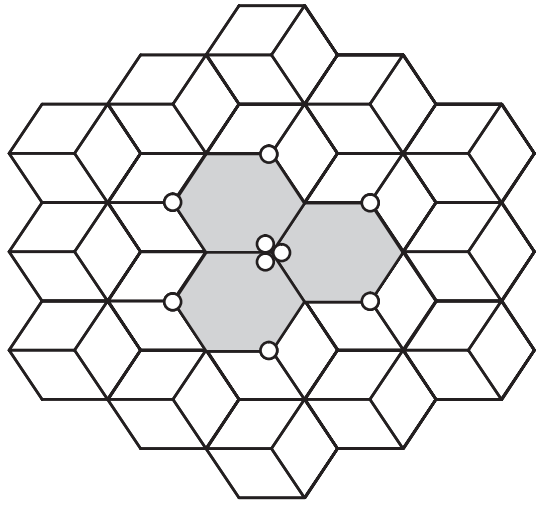

Figure 2.8 Nine-base intercell cooperation scenario.

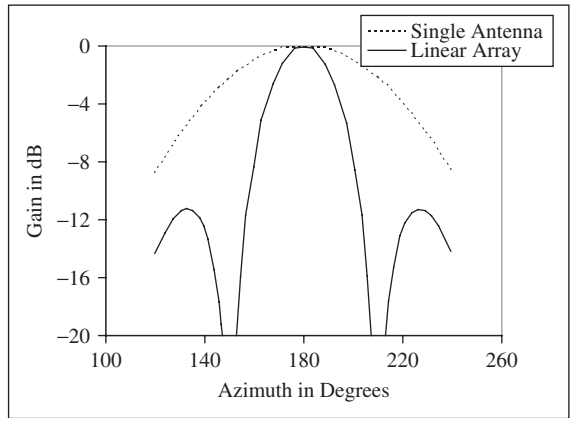

Figure 2.9 Single antenna and linear array antenna radiation pattern.

The following algorithms using methods described in Section 2.5 have been simulated for a comparative study.

(a) *In the case of 3 BS cooperation,* $K_u = 15$ *is chosen initially and using the USBBA the three sets of users and the indices of beams on which they are best serviced are obtained. In the case of cooperation with nine BSs, the modified USBBA is used to choose these set of indices, BSs and beams.*

(b) *In this case the beams are chosen randomly. The cooperation here is limited to choosing the users who are to be serviced by the BSs according to the PF (proportional fair) criterion.*

(b1) *This is the (b) algorithm where beams are sequentially chosen at each BS.*

(c) *In these methods, the users are randomly deployed in the sectors and are tied to the BSs to which they are geographically close. In these scenarios the BSs do not cooperate with the neighboring BSs either for generating beams or scheduling users. The BSs implement an independent algorithm (a) while in*

(c1) *an independent algorithm (b) is executed.*

(d) *In this method, the BSs have a single conventional* 120° *sectored antenna and the users are scheduled according to the PF algorithm. In our simulations, for a fair comparison between these methods and the above proposed methods, it was ensured that the BSs transmit at the same power in their respective sectors.*

In Figures 2.10 and 2.11, the interpacket delay is plotted versus the total system throughput statistics when user velocity $v = 1$ m/s in the three-BS and nine-BS coordination scenario.

In Figures 2.12 and 2.13, the tradeoff when $v = 8$ m/s is shown. For the three-BS coordination scenario with $v = 1$ m/s, simulation results show small gains in terms of throughput using the described algorithms. In the nine-BS coordination scenario the throughput and interpacket delay tradeoffs with (a) and (b1) are almost the same. Significant gains with $v = 8$ m/s are observed as expected due to the rapidly varying channel conditions. With $v = 8$ m/s, the throughput delay tradeoff patterns are similar to the case with $v = 1$ m/s.

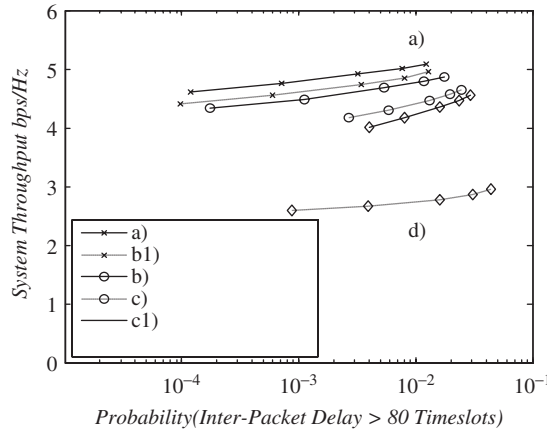

Figure 2.10 Base coordination, interpacket delay versus total system throughput statistics with user velocity of 1 m/s.

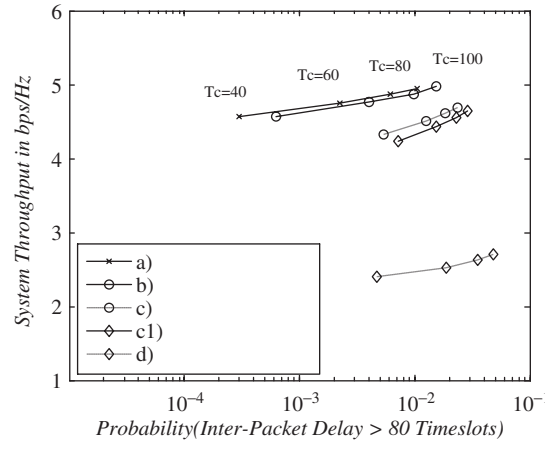

Figure 2.11 Nine-base coordination, interpacket delay versus total system throughput statistics with user velocity of 1 m/s.

2.6 MULTIUSER DIVERSITY IN WIRELESS AD HOC NETWORKS

In this section, we discuss a scheme to utilize the shared medium in IEEE 802.11-based *ad hoc* networks efficiently by taking advantage of multiuser diversity, distributed scheduling and adaptability. In a heterogeneous ad hoc network or a mesh network, some nodes may need to communicate with multiple one-hop nodes. The scheme allows such a node with a certain number of links to function as a clusterhead to coordinate multiuser communications locally. A CDF (cumulative distribution function)-based K-ary opportunistic splitting algorithm and a distributed stochastic scheduling algorithm are used to resolve intra- and intercluster collisions, respectively. Fairness is formulated and solved in terms of social optimality within and across clusters. Analytical and simulation results, which will be presented in this section, show that such a scheme can significantly improve communication efficiency while providing social fairness.

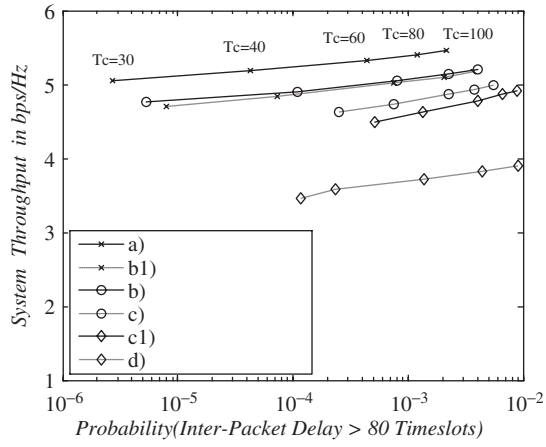

Figure 2.12 Three-base coordination, interpacket delay versus total system throughput statistics with user velocity of 8 m/s.

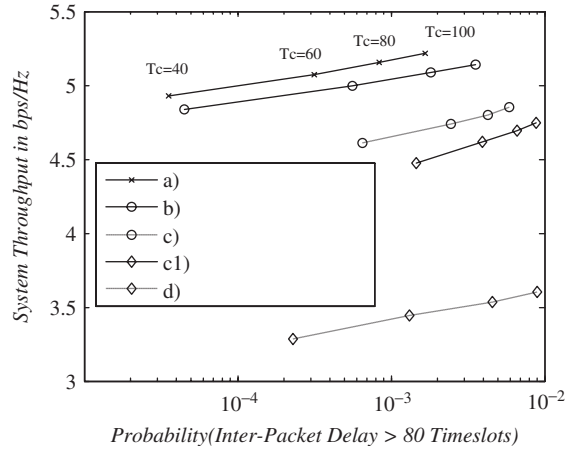

Figure 2.13 Nine-base coordination, interpacket delay versus total system throughput statistics with user velocity of 8 m/s.

The diversity techniques considered so far in this chapter may not be applicable in multihop ad hoc networks [4–22] because there is no base station to act as the central controller and no dedicated control channel to feed back the channel state in a timely fashion. In addition, in ad hoc networks, the medium access control is distributed and each node randomly accesses the shared medium without prior channel information.

Most of the work on diversity in *ad hoc* networks is limited to multipath diversity, as described in Chapter 10 on crosslayer optimization and References [16], [17], [18], [19] and [20], i.e. using multiple paths to opportunistically forward packets to enhance end-to-end reliability. Research on multi-output link diversity and multi-input link diversity is still open. The multi-output link diversity is the output multiuser diversity from one to many (from a node to multiple neighbors). A corresponding case of the multi-output link diversity in ad hoc networks is the downlink diversity in the cellular networks. Similarly, the multi-input link diversity is the input multiuser diversity

from many to one (from multiple neighbors to a node), which corresponds to uplink diversity in the cellular networks.

Having this in mind, in this section we present an 802.11-based MAC protocol that exploits these two kinds of multiuser diversity to improve channel and energy efficiency. The scheme is designed to work for multihop *ad hoc* networks, especially heterogeneous *ad hoc* networks and mesh networks, where multiple nodes need to communicate with a relatively powerful node in the distributed manner. Since opportunistic medium access may easily lead to unfairness, in this section the fairness is addressed in terms of social optimality.

The operation of the scheme is based on the following steps. Each node with a certain number of links is enabled to form a cluster and function as the clusterhead to coordinate multiuser communications locally. In each cycle of data transmissions, the clusterhead initiates medium access (with certain probability in a multicluster scenario to ensure intercluster fairness), and then the cluster members (which will be referred to as users in the following) make medium access decisions in a distributed way based on the observed instantaneous channel conditions. A CDF-based K-ary opportunistic splitting algorithm is used to guarantee that only the user with the best normalized instantaneous channel quality will win the channel. After successful collision resolution, a rate-adaptation technique is employed to achieve the highest reliable data rate for the selected user. In this way, the exploitation of link diversity is facilitated during the process of collision avoidance.

In some other works [12, 13], MAC enhancement is discussed to utilize output link diversity. The scheme discussed in this section [4] differs from that work in its throughput scaling and social optimality. Two papers mostly related to this approach are References [14] and [15]. They presented a channel-aware Aloha protocol and a binary opportunistic splitting algorithm, which is one of the first schemes that addresses the utilization of multiuser diversity in a distributed way. The solution presented in this section first of all targets the IEEE 802.11-based multihop *ad hoc* networks, the design of which is very different from that of Aloha-based single-hop networks. Second, the CDF-based binary opportunistic splitting algorithm is an extension to the weighted CDF-based K-ary opportunistic splitting algorithm so that general optimization goals can be achieved in a more efficient way. Third, a distributed intercluster collision resolution scheme is used to achieve the system-wide social optimality in multihop *ad hoc* networks.

This design is in line with the 802.11 (DCF mode) standard in that the scheme inherits similar mechanisms to probe the channel and avoid collisions and uses a similar idea to resolve collisions. Thus, the scheme can be easily incorporated into future 802.11 standards. Theoretical analysis and simulation results demonstrate that the scheme can significantly improve communication efficiency while providing social fairness and can significantly increase energy efficiency and throughput.

2.6.1 Multiple-output and multiple-input link diversity

The model of *ad hoc* networks used in this section is quite general. It includes homogeneous and heterogeneous ad hoc networks, and wireless mesh networks. In all these networks, the channel quality of a link is normally time-varying due to fading, shadowing, noise and interference. Different links usually experience independent instantaneous channel qualities. This phenomenon was referred to in the previous sections as the multiuser diversity. For example, in the case of ad hoc networks, as shown in Figure 2.14(a), node 1 is interfered by ongoing transmission of node 5 and the link of $0 \rightarrow 2$ suffers deep fading or shadowing.

The link of $0 \rightarrow 4$ has an instantaneous quality to support basic data rate transmission. The link quality of $0 \rightarrow 3$ happens to be 'on-peak'. Since only one of these links is allowed to communicate at a time, it is better for node 0 to transmit data to node 3 or 4 rather than node 1 or 2 at the current time. This is referred to as the multi-output link diversity. Similarly, the multi-input link diversity is demonstrated in the example shown in Figure 2.14(b).

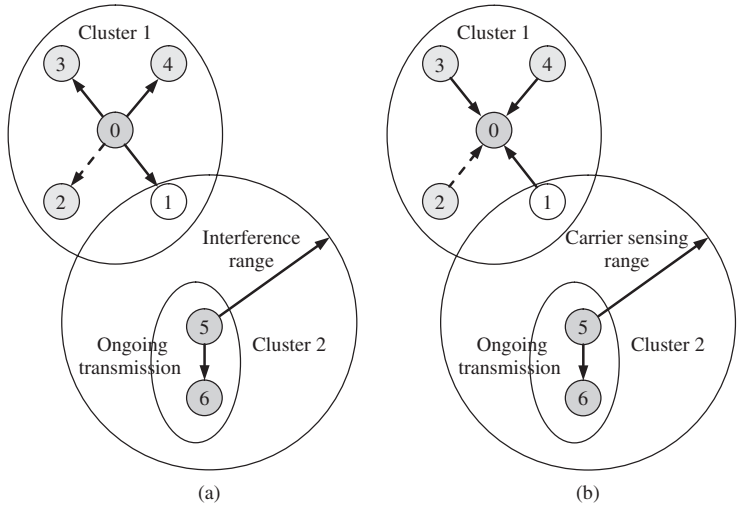

Figure 2.14 (a) An illustration of multi-output link diversity. (b) An illustration of multi-input link diversity.

2.6.2 Localized opportunistic transmission

If there is a global scheduler who knows the system-wide channel information and topology with little cost, the efficiency will be maximally exploited by considering both link quality and space reuse of all active links. In practice, global multiuser scheduling is impossible in multihop *ad hoc* networks, where no centralized scheduler is available and complete channel information and topology information are hard to obtain. It was shown that it is still interesting to utilize the multiuser diversity locally [12, 13].

Multiuser diversity gain can be significant without too many links in participation. Even two links can produce substantial diversity gain. Based on the above observation, we limit multiuser scheduling to a set of links with the same sending node or the same receiving node. Therefore, a node satisfying certain degree requirements can locally coordinate multiuser scheduling among its own input links or output links. The set of links with the same sending node or the same receiving node will be defined as a cluster and the common sending node or receiving node as the clusterhead and others as cluster members or users. Since multiple clusters may share the same medium, intercluster contention resolution is necessary. In the protocol discussed in this section, the clusterhead represents the whole cluster to resolve intercluster channel contention. If a clusterhead successfully captures the channel floor, it immediately coordinates the multiuser diversity-based transmission within the cluster for a certain period.

As illustrated in Figure 2.14, nodes 0–4 form one cluster and nodes 5–6 form another cluster. Node 0 coordinates the opportunistic transmissions to (from) nodes 1–4. Node 5 coordinates the transmission to node 6. Further details on the cluster formation and maintenance will be discussed in the next section.

One should notice that this link-layer diversity-driven clustering is very different from the network-layer clustering discussed later in Chapter 13 on *ad hoc* networks and, for example, in References [21], [22] and [23]. The network-layer clustering is designed to improve routing scalability and simplify network management; the dimension of network-layer clustering may be across several hops and the cost to establish and maintain such network clusters is one of the major design issues. The link-layer clustering is a logical organization to utilize multiuser diversity

locally, under which each cluster member is directly associated with a clusterhead, and neighboring clusters do not need to exchange information between each other.

The first challenge in this concept is the MAC design for multiuser diversity-based transmissions within a cluster. One straight approach is that the clusterhead schedules transmissions based on the channel and queue information collected from all users. Although this approach is feasible in cellular networks where dedicated control channels (one for each user) are available, the cost of collecting channel and queue information can be too high in single-channel ad hoc networks, especially when the number of users is large. Another approach is that each user makes a transmission decision in a distributed way based on its own instantaneous channel quality (known to each user by observation) and past channel quality distribution. The user with the higher normalized channel quality is granted higher priority, e.g. with a smaller IFS (interframe space) to access the medium. In this chapter, a MAC based on the latter approach will be designed since it does not require the collection of channel information from others, so that the overhead can be significantly reduced. Under this distributed approach, the challenge will be how to make the user with the highest normalized channel quality win the channel in a more efficient way.

The objective in utilizing multiuser diversity is to improve the system performance without sacrificing social fairness. Intracluster fairness and intercluster fairness will be used to characterize the fairness within and across clusters, respectively. The intracluster problem occurs when links in a cluster have different channel quality distributions.

Opportunistic medium access may easily lead to unfairness when the channel states of different users are statistically heterogeneous. For example, in the saturated scenario with two users, the user with a poor average SNR (signal-to-noise-plus-interference ratio) may be severely starved, while the one with a good average SNR may occupy the medium for most of the time. The intracluster problem becomes more complicated when links have different weights in terms of traffic and utility. The intercluster fairness problem always exists since intercluster channel contentions are normally location-dependent and clusters may carry different weights in terms of aggregate traffic and utility. The intercluster fairness problem is hard to solve because the traffic/topology/channel information of a cluster is normally unknown to another cluster. In this section, we will discuss both intracluster and intercluster fairness problem in terms of social optimality within and across clusters.

2.6.3 Multiuser diversity-driven clustering

When a node has more than one output link, it will form an output cluster so that each output link joins the output cluster. When a node has more than one input link that is not associated with an output cluster, it will form an input cluster so that each input link that is not associated with an output cluster joins the input cluster.

Each cluster has a unique cluster ID. The cluster ID is comprised of the MAC address of the clusterhead, the direction flag (1 indicates input, 0 indicates output) and a sequence number. Each cluster member is allocated a local user ID for identification within the cluster. The cluster ID and the local user ID are sent to the cluster member as a global identity. This process is called the association process.

After a cluster is created, the clusterhead periodically or reactively checks the connectivity of associated links. If a link is disconnected, the clusterhead removes the link from its cluster and returns the local user ID to the user ID pool. This is referred to as the deassociation process. Similarly, if a new link is established to be connected with the clusterhead, the clusterhead will allocate a new local user ID from the user ID pool to the new user and run the association process. Depending on the change of out-degree at the sender side and in-degree at the receiver side, a directed link may leave an input cluster to join an output cluster, and vice versa, by following the same rule as the cluster formation introduced earlier in this section.

2.6.3.1 Intracluster medium access and collision resolution

In each transmission cycle, the clusterhead initiates medium access, while cluster members make medium access decisions in a distributed way based on the observed instantaneous channel conditions. In the multi-output scenario, the clusterhead is the sender of data traffic, so sender-initiated medium access control (SI-MAC) is used. The handshake before data transmission in sender-initiated medium access control includes an RTS (request-to-send) and CTS (clear-to-send) in sequence. The unicast RTS can be extended to the multicast RTS and CTS enhanced with channel awareness capability so that the handshake can probe the channel among multiple users as well as avoiding or resolving collisions within and outside the cluster. In the multi-input scenario, the clusterhead is the receiver of data traffic, so the receiver-initiated medium access control (RI-MAC) [24, 25] is used. The handshake before data transmission in the receiver-initiated medium access control includes RTR (ready-to-receive), RTS and CTS in sequence. In Reference [4] multicast RTR and channel-aware RTS (followed by CTS) using multi-input link diversity as well as collision avoidance and resolution is discussed.

For the RI-MAC, it is better for the clusterhead to know the traffic information. In this section it is assumed that the clusterhead knows this information either by service level agreement on the flow level or the piggyback in the users' transmitted/received packets on the packet level. Related discussions can be found in References [24] and [25].

When the clusterhead has packets backlogged for several users (in the SI-MAC) or wants to receive packets from one of the backlogged users (in the RI-MAC), it will multicast RTS or RTR with the cluster ID to the chosen candidate users. To notify a user as to whether it is chosen or not, an array of n bits is included in the RTS or RTR, where n is the total number of cluster members. The ith bit in the array corresponds to the user whose user ID is equal to i. If a bit is marked as 1, this means that the corresponding user is chosen to compete for data reception or transmission; otherwise, it is not within the candidate list in the given transmission cycle. When all the users in the cluster are candidates for data reception or transmission, the clusterhead may send RTS or RTR in the manner of groupcast without using the bit array to notify individual users. The groupcast frames are similar, but without the bit marking the array.

The noise power included in the RTR frame indicates the noise plus interference power level at the clusterhead. Recall that, in the multi-input scenario, data traffic is transmitted from users to the clusterhead. It is the received SNR at the clusterhead that determines the achievable data rate. However, the medium access decisions are made in a distributed way by the users. Therefore, it is necessary that the users know the noise power level at the clusterhead.

Assuming that the instantaneous channel gains between two nodes are identical in either direction, a candidate user can derive the channel gain. From the derived channel gain and informed noise power level at the clusterhead, users can estimate the received SNR and make the appropriate MAC decision.

Since an RTS (RTR) has to be sent at the beginning of each cycle of data transmission for collision avoidance and channel probing and is normally sent at the basic rate in multirate ad hoc networks, the overhead of the RTS (RTR) is one of the major factors affecting the channel utilization ratio. With the clustering technique introduced above, the length of the RTS (RTR) is quite small and scalable to a very large group (one additional bit with one additional member). In addition, a large group may be partitioned into several smaller groups so that the scalability is still maintained.

Anyone except the candidate receivers who receive the multicast RTS (RTR) should tentatively keep silent to avoid possible collisions before the clusterhead receives the collision-free CTS (RTS). After a qualified user is selected and the transmission duration is determined and announced by the CTS, the sender will include the duration in the subheader of DATA. The subheader is referred to as the reservation subheader (RSH), which has already been employed in the MAC header of data packets in IEEE 802.11e. RSH is sent at the basic rate so that all overhearing nodes can decode.

Upon receiving a multicast RTS (RTR), each user checks the bit-marking array. If the corresponding bit is set to 1 and the observed instantaneous SNR is above the threshold indicated in the RTS (RTR) message, it is allowed to compete for the channel. For groupcast RTS (RTR), every user needs to evaluate the channel and prepare to compete for the channel if the observed channel condition is good enough.

If there is only one user who has the desired channel condition, the user captures the channel without a collision within the cluster. If there is no qualified user, the group head defers for a certain time and sends a multicast RTS (RTR) again. In case there is more than one qualified user, collisions may happen. Thus, a collision resolution scheme is required to find a qualified user. A scheme termed the CDF-based K-ary opportunistic splitting algorithm is discussed later. This scheme can quickly determine the user with the best normalized channel quality. The basic CDF-based K-ary splitting algorithm guarantees timeshare fairness among users and a generalized weighted CDF-based K-ary opportunistic splitting algorithm optimizes local system performance.

The basic principle and necessary procedures to utilize multi-input link diversity are similar to that of multi-output link diversity. Thus, in the following discussion, we will focus on the multi-output link diversity.

In each cycle of contention resolution plus data transmission, it is assumed that, once a user captures the shared medium, it is allowed to transmit data up to TXOP (transmission opportunity) within which a user can consecutively transmit data without contending for the channel. TXOP can be represented as the total transmission time T.

For low mobility, the channel is modelled as a block-fading channel and it is assumed that the noise plus interference power does not change much during one cycle, although it may change significantly when a user captures the channel in another cycle. Therefore, the SNR is stable in each cycle but may randomly change from one cycle to another. Let $h_i(t) = h_i =$ SNR of user i, which is considered to be independent for different users. If the large-scale path loss changes very slowly in comparison with the instantaneous channel gain and noise power, h_i can be considered ergodic during a sufficiently long system observation period.

In the multihop scenario, the interference may partly depend on which set of nodes are actually transmitting. In other words, the instantaneous interference each user gets is spatially correlated to some extent, even though fading effects make the interference power random. However, since a multihop intercluster collision is avoided and resolved based on carrier sensing, the interference can be kept low. The simulation results validate this assumption.

It is assumed that h_i is a random variable with the probability density function $f_{H_i}(n)$. In practice, each user may know the distribution of its own SNR but not those of other nodes. Similarly, each user can determine its own instantaneous SNR just at the beginning of each cycle of data transmission, but not those of other nodes. The instantaneous channel state can be measured during the handshake of the collision avoidance process. The long-term SNR distribution can be derived via the iterative approach. If SNRs required to support the lowest rate and the highest rate are $h_{\min}$ and $h_{\max}$, respectively, $h_{\min} + j/M(h_{\max} - h_{\min})(0 \le j \le M)$ is quantized channel quality, where $(h_{\max} - h_{\min})/M$ represents the quantization interval, k is the iteration index and P_j is the PMF (probability mass function) that the quantized channel quality equals $h_{\min} + j/M(h_{\max} - h_{\min})$; then P_j can be updated as

$$P_j^{k+1} = \begin{cases} (1 - \phi^k)P_m^k + \phi^k, & j = m \\ (1 - \phi^k)P_j^k, & j \neq m \end{cases}$$

where $\phi^k(0 \le \phi^k \le 1)$ is the step size to update the PMF. An appropriate step-size sequence to balance the convergence speed and smoothness (used also in the simulation presented later) is $\phi^k = 1/\min(k, 1000)$.

Rate adaptation is based on the instantaneous SNR h evaluated at the beginning of each cycle of data transmission. Once the data rate is set, it will not be changed during the whole data

transmission period. In the sequel, $R(h)$ will denote the rate at which a user can reliably transmit if the instantaneous SNR evaluated at the beginning of data transmission is h.

2.6.4 Opportunistic MAC with timeshare fairness

If channel quality of each user follows i.i.d. distribution, we can directly use the SNR value as the criterion for MAC in each cycle of data transmission. Timeshare fairness is naturally preserved due to the statistical properties of the SNR. However, it fails to guarantee timeshare fairness if the SNRs are heterogeneously distributed among users.

One possibility to guarantee timeshare fairness, while exploiting multiuser diversity, is to use the normalized channel quality as the threshold for MAC and as the criteria to determine who will win the channel access.

In the sequel we will use the complementary cumulative probability

$$p_i = F_{H_i}(h_i) = \int_{h_i}^{\infty} f_{H_i}(h)dh \text{ or } p_i = F_{H_i}(h_i) = \sum_{j=M(h_i-h_{\min})/(h_{\max}-h_{\min})}^{M} P_j$$

where P_j is the PMF and takes some $p(0 < p \leq 1)$ as the MAC threshold, which means that users with the instantaneous SNR higher than $F_{H_i}^{-1}(p)$ are allowed medium access. T*he lower p corresponds to the higher channel quality for medium access*, which limits the number of users involved in the competition for the channel. Considering $F_{H_i}(h_i)$ as a random variable, we easily find that $F_{H_i}(h_i)$ is i.i.d across users with the normalized uniform distribution. This means that each user has the same probability to access the medium for any medium access threshold p. In addition, the policy that the user with the lowest instantaneous $F_{H_i}(h_i)$ wins the channel will guarantee that each user has the same probability of capturing the channel. This scheme will be referred to as the *basic opportunistic medium access control* (BO-MAC).

The remaining question is how to design a distributed collision resolution algorithm to find the user with the best normalized instantaneous quality. In the following, we discuss a fast carrier sensing-based splitting algorithm, namely the K-ary opportunistic splitting algorithm, to resolve the collisions among the qualified users originally described in Reference [4]. The K-ary opportunistic splitting algorithm can be considered the extension of the binary-tree collision resolution algorithm introduced in Reference [15, 26].

2.6.5 CDF-based K-ary opportunistic splitting algorithm

When user i, with channel quality $h_i > F_{H_i}^{-1}(p)$, receives an RTS (ready to send) it is allowed to compete for the channel and transmit a CTS (clear-to-send) at the beginning of minislot $m_{1,i}$ if there is no transmission in the previous $m_{1,i} - 1$ minislots. Carrier sensing is used for detection of transmission of other users without the need to decode the transmitted packet. The carrier sensing range is usually more than twice the transmission range. In addition, CTS (as well as RTS) is applied with sufficient channel error coding and sent at the basic data rate. Therefore, even with fading, a large carrier sensing range still allows users in the same cluster to check if the channel is busy or not. The minislot used in this chapter for the performance example is *aSlotTime* (20 μs in 802.11b with DSSS), as defined in the 802.11 standard and also used in Reference [4].

The round of competition following the RTS is the first round of competition. If there are at least two users in the above process who send CTS simultaneously, it goes to the second round of competition. The users involved with collisions can detect collisions by observing that there is no data transmission one minislot after the CTS. Let $m_j (1 \leq m_j \leq K)$ denote the number of minislots at the beginning of which collisions occur in the jth round of competition.

User i will participate in the second round of competition if it participated in the first round of competition, i.e. had channel quality better than $F_{H_i}^{-1}(m_1 p/K)$. It will transmit CTS at the

beginning of minislot $m_{2,i}$ if there is no transmission in the previous $m_{2,i} - 1$ minislots after it detects collisions. In the jth($j \geq 3$) round of competition, user i involved with the $(j-1)$th round of competition, i.e. user i with channel quality better than $F_{H_i}^{-1}(\sum_{k=1}^{j-2}(m_k - 1)p/K^k + m_{j-1}p/K^{j-1})$, will participate in the competition again and transmit a CTS at the beginning of minislot $m_{j,i}$ if there is no data transmission in the previous $m_{j,i} - 1$ minislots after it detects collisions, where

$$m_{j,i} = \begin{cases} \left\lceil F_{H_i}(h_i)/(p/K) \right\rceil, & j = 1 \\ \left\lceil \left(F_{H_i}(h_i) - \sum_{k=1}^{j-1}(m_k - 1)\frac{p}{K^k} \right) /(p/K^j) \right\rceil, & j \geq 2 \end{cases} \tag{2.16}$$

An example of intracluster collision resolution with five users, medium access threshold $p = 0.8$ and $K = 4$ is shown in Figure 2.15 [4]. In the first round, those users with channel quality between 0 and 0.2 are expected to transmit CTS at the time SIFS (short interframe space) after receiving RTS. Those users with channel quality between 0.2 and 0.4 are expected to transmit CTS at the time *SIFS* + *aSlotTime* after receiving RTS and so on. Since no user is with channel quality less than 0.2, users 1 and 2 take the opportunity to transmit CTS at the time *SIFS* + *aSlotTime* after receiving RTS. User 3 and user 4 may transmit CTS at *SIFS* + 2 * *aSlotTime* and *SIFS* + 3 * *aSlotTime*, respectively, after receiving RTS, but observe that the channel is busy and, thus, they yield opportunity to user 1 and user 2.

User 5 is not qualified and thus will not prepare to transmit CTS. User 1 and user 2 detect collision and enter the second round of channel contention. Since the channel quality of user 1 falls between 0.2 and 0.25, user 1 transmits CTS at the beginning of the first minislot after detecting collision. User 2 may transmit CTS at the beginning of the second minislot if it observes that the channel stays idle after collision. Since user 1 has better quality and takes the opportunity, user 2 gives up. Now, the clusterhead receives collision-free CTS and starts DATA transmission.

When two of the best quality users, say user a and user b, have very close SNRs, which means that $|F_{H_a}(h_a) - F_{H_b}(h_b)| \to 0$, it may take a large number of competition rounds to resolve collisions. With the limitation of quantization in SNR distribution, it may be impossible to tell which one is better than the other. Besides, it is not worth finding the best one since not much SNR gain can be achieved even if the best one is found. The following algorithm can be used to resolve collisions after certain rounds, say α, of competition.

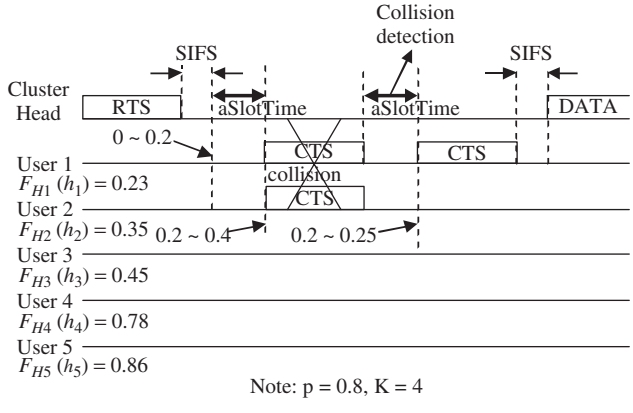

Figure 2.15 An example of an intracluster collision resolution. (Reproduced by permission of IEEE [4]).

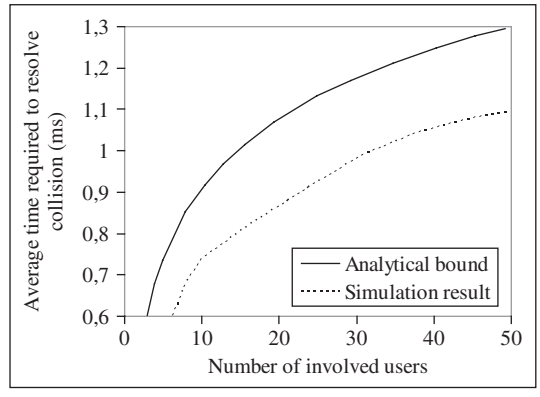

Figure 2.16 Average time required to resolve collision.

Table 2.1 Parameter setting

Parameter	Value
p_0	0.9
aSlotTime (μs)	20
T_{id} (μs)	20
T_{ini} (μs)	300
T_{crs} (μs)	300
T_{crf} (μs)	320

In the jth($j \geq \alpha$) round of competition, user i involved with the $(j-1)$th round of competition will randomly select a minislot, say $m_{i,j}$, among K minislots to transmit a CTS again after it detects collisions if there is no transmission in the previous $m_{i,j} - 1$ minislots in the jth(j $\geq \alpha$) round of competition.

In practice, the maximal number of rounds to resolve collisions should not be too large; otherwise, the channel condition may change significantly after a user wins out. For this reason the window size of opportunistic collision resolution, i.e. the total resolution time, should be limited to T_{ic}, which is a system parameter set by the clusterhead according to the number of backlogged users and channel coherence time. In practice, the average number of rounds of competition needed is very small, about $O(\log_K(n))$, where n is the number of qualified users.

If EX_n denotes the expected time required to resolve a collision with n involved users in SI-MAC by the carrier sense opportunistic splitting algorithm with K-dimensional trees, then we have [4] $EX_n \leq T_{ini} + \log_k(n)T_{crf} + (\log_k(n) + K/2)T_{id} + T_{crs}$ for any $K \geq 2$ and $n \geq 1$, where $T_{id} = aSlotTime$, $T_{ini} = RTS + SIFS$, $T_{crs} = CTS + SIFS$ and $T_{crf} = CTS + aSlotTime$.

Figure 2.16 shows the analytical bound and simulation result. The parameter settings for the simulation shown in Table 2.1 are the same as in Reference [4]. In addition, we use $B = 1$ MHz, $T = 6$ ms, $K = 4$, $\alpha = 4$, $T_{ic} = 2$ ms and $\xi = 10^6$.

The lower bound of the expected time, denoted by EX_n^Q, required to resolve a collision by the algorithm described in Reference [15] is $EX_n^Q \geq T_{ini} + \log_2(n)T_{crf}^Q + T_{crs}$ for any $n \geq 1$, where T_{crf}^Q denotes the round-trip time required for a user to transmit a small reservation packet and detect if a collision occurs. T_{crf}^Q is no less than T_{crf}. Since T_{crf} is normally tens of *aSlotTime*, it can be seen that the K-ary carrier sensing splitting algorithm reduces a lot of collision-resolution overhead when K is larger than 2.

2.6.6 Throughput

Let us assume that a user transmits data with fixed T after successfully capturing the medium. For simplicity it is assumed that the packet transmitted in T is pure data. Then the achievable throughput of user i, $S_B(p, n, i)$, and the total achievable throughput, $S_B(p, n)$, with n independent backlogged users and the medium access threshold p for the pure output-link scenario with the BO-MAC and the K-ary splitting tree algorithm, are [4]

$$S_B(p, n, i) \geq [R(p, n, i)T/n]/[T_0(p, n, K) + T] \tag{2.17}$$

and

$$S_B(p, n) \geq \left[\sum_{i=1}^{n} R(p, n, i)T/n\right]/[T_0(p, n, K) + T] \tag{2.18}$$

with timeshare fairness, where

$$R(p, n, i) = \sum_{k=1}^{n} \left(\binom{n}{k} p^k (1-p)^{n-k} \left(\int_0^p R\left(F_{H_i}^{-1}(t)\right)(k/p)(1-t/p)^{k-1}\, dt \right) \right) \tag{2.19}$$

$$\begin{aligned} T_o(p, n, K) = {} & (1-(1-p)^n)(T_{ini} + \log_k\{np/[1-(1-p)]\}T_{crf} \\ & + (\log_K\{np/[1-(1-p)^n] + K/2\}T_{id} + T_{crs}) \end{aligned} \tag{2.20}$$

$R(h)$ is the transmission rate when SNR is h, $T_{id} = aSlotTime$, $T_{ini} = RTS + SIFS$, $T_{crs} = CTS + SIFS$ and $T_{crf} = CTS + aSlotTime$.

2.6.7 Optimal opportunistic MAC

In the last section, the opportunistic medium access algorithm guarantees each user the same probability of accessing the channel. In other words, each user gains the same time fraction of T. A modification of the algorithm (MA or MO-MAC) can provide a different proportion of service time to different users. By adjusting the weight vector, we can obtain the desired rate vector that optimizes the local system performance.

If $\mathbf{w} = \{w_1, \ldots, w_k, \ldots, w_n\}$ denotes the weight vector, where $0 < w_i < 1(\forall i)$ and $\sum_{i=1,n} w_i = 1$, the MA is defined as [4]

$$i^* = \arg\max_i \left\{ \left[1 - F_{H_i}(h)\right]^{1/w_i} \right\} \tag{2.21}$$

The probability that user i is selected for transmission, given that $h_i = h$, is $\Pr\{i^* = i | h_i = h\} = [1 - F_{H_i}(h)]^{(1-w_i)/w_i}$ and the average probability that user i can win the channel is w_i. To prove these statements we start with

$$\begin{aligned} \Pr\{i^* = i | h_i = h\} &= \Pr\{[1 - F_{H_j}(h_j)]^{1/w_j} \leq [1 - F_{H_i}(h)]^{1/w_i},\ \forall j \neq i\} \\ &= \prod_{j \neq i} [1 - F_{H_i}(h)]^{w_j/w_i} = [1 - F_{H_i}(h)]^{(1-w_i)/w_i} \end{aligned} \tag{2.22}$$

and

$$\begin{aligned} \Pr\{i^* = i\} &= \int_0^\infty \Pr\{i^* = i | h_i = h\} f_{H_i}(h)\, dh \\ &= \int_0^\infty (1 - F_{H_i}(h))^{(1-w_i)/w_i} d(1 - F_{H_i}(h)) = w_i \end{aligned} \tag{2.23}$$

In the sequel, we discuss the modified opportunistic splitting algorithm (MOSA). The threshold $p$is now set to 1, which means each user is allowed to compete for the channel regardless of

its instantaneous channel condition. Similarly to the basic K-ary splitting algorithm discussed in Section 2.6.5, in the first round of channel competition, user i will transmit a CTS at the beginning of minislot $m'_{1,i}$ if there is no transmission in the previous $m'_{1,i} - 1$ minislots after receiving RTS. User i will participate in the jth($j \geq 2$) round of competition if it participated in the last round of competition and collided with others. It will transmit a CTS at the beginning of minislot $m'_{1,i}$ if there is no transmission in the previous $m'_{1,i} - 1$ minislots after it detects collisions. Parameter $m'_{1,i}$ is calculated as follows:

$$m^*_{j,i} = \begin{cases} \left\lceil K(1-(1-F_{H_i}(h_i))^{1/nw_i}) \right\rceil, & j = 1 \\ \left\lceil K^j \left(1-(1-F_{H_i}(h_i))^{1/nw_i} - \sum_{k=1}^{j-1}(m_k-1)/K^k\right) \right\rceil, & j \geq 2 \end{cases} \tag{2.24}$$

where n is the number of backlogged users. We note that, when each user has equal weight, i.e. $w_i = w_j (\forall i \neq j)$, the MOSA is reduced to the basic one given the medium access threshold $p = 1$. Generally speaking, the expected time to resolve collision in each cycle of data transmission will depend on the weight vector $\mathbf{w}$. However, it would be a good approximation if we used the upper bound of EX_n specified in Section 2.6.5 to characterize the expected time to resolve collision by the MOSA. If EX_n^+ denotes the upper bound of $EX_n$and the transmission opportunity time (TXOP) is T, then the service rate of user i is

$$\begin{aligned} S_E(n,i,w_i) &= \frac{T}{EX_n^+ + T}\int_0^\infty R(h)\Pr\{i^* = i | h_i = h\} f_{H_i}(h)\,dh \\ &= \frac{T}{EX_n^+ + T}\int_0^\infty R(h)(1-F_{H_i}(h))^{(1-w_i)/w_i} f_{H_i}(h)\,dh \end{aligned} \tag{2.25}$$

where $R(h)$ is the transmission rate when SNR is h. $S_E(n,i,w_i)$ is concave in w_i and can be optimized. To prove it we start with

$$\begin{aligned} S_E(n,i,w_i) &= \frac{T}{EX_n^+ + T}\int_0^\infty R(h)(1-F_{H_i}(h))^{(1-w_i)/w_i} f_{H_i}(h)\,dh \\ &= \frac{T}{EX_n^+ + T}\left(w_i R(\infty) - \int_0^\infty w_i (1-F_{H_i}(h))^{1/w_i} R'(h)\,dh\right) \end{aligned} \tag{2.26}$$

Since nonnegative weighted sums and integrals preserve concavity, it is sufficient to show that $f(w_i) \equiv -w_i a_i^{1/w_i}$ is concave in w_i, given $0 < w_i \leq 1$ and $0 \leq a_i \leq 1$. Since $f''(w_i) = -a^{1/w_i}(\log a)^2/w_i^3 \leq 0$, it completes the proof. To optimize the system performance by choosing an appropriate weight vector we define $U_i(x)$ as the utility function of user i in terms of average service rate x. Suppose it is strictly increasing, concave, differentiable and additive. The optimal weight vector can be achieved by solving the optimization problem

$$\text{Maximize } z = \sum_{i=1}^n U_i(S_E(n,i,w_i)) \tag{2.27}$$

$$\text{subject to } \sum_{i=1}^n w_i \leq 1 \text{ and } w_i \geq 0,\ \forall i \tag{2.28}$$

For analytical tools to solve the optimization problem (2.28) see Chapter 12.

2.6.8 Contention resolution between clusters

Within a cluster, as discussed in the previous sections, opportunistic splitting algorithms (OSA) can be used to resolve collisions among qualified users. For collision resolution between clusters,

an exponential backoff algorithm can still be used but may not provide system-wide fairness. In order to optimize system-wide performance, a persistent-based contention resolution algorithm was introduced in References [4] and [27] to resolve collision between clusters. The system-wide optimization problem is now formulated as

$$\begin{aligned} &\text{Maximize } Z = \sum_{j\in A}\sum_{i=1}^{n_j} U_i(r_j S_E(n_j, i, w_{ij})) \\ &\text{subject to } \quad \sum_{i=1}^{n_j} w_{ij} \le 1, \ \forall j \in A \\ &\sum_{j\in A_k} r_j \le 1, \ \forall k \in A; \quad w_{ij} \ge 0, \ r_j \ge 0, \ \forall i, j \end{aligned} \tag{2.29}$$

In Problem (2.29), j, k are indices of clusters, A is the set of all clusters, A_k is a subset of A, which includes cluster k plus the clusters who share the channel with cluster k, r_j is the channel allocation rate (i.e. time fraction) for j, n_j is the number of associated users (active directed links) in cluster j and w_{ij} is the weight for user i in cluster j.

Problem (2.29) can be solved using a convex optimization technique similar to that shown in Chapter 12, either in a centralized or a distributed way. Here we focus on fully distributed channel allocation. Each cluster is supposed to control its channel allocation rate, which is adjusted in response to the feedback of contention with neighboring clusters. The optimization function of each cluster is

$$\begin{aligned} &\text{Maximize } J(r_j) = \sum_{i=1}^{n_j} U_i(r_j S_E(n_j, i, w_{ij})) - \lambda(\theta_j) r_j \\ &\text{subject to } \quad \sum_{i=1}^{n_j} w_{ij} \le 1; \quad w_{ij} \ge 0, \ \forall (i, j) \end{aligned} \tag{2.30}$$

In Problem (2.30), θ_j is the perceived contention loss probability between cluster j and its neighbouring clusters. The higher r_j results in larger θ_j. Parameter $\lambda(\theta_j)$ is the price in terms of contention loss probability. The price function should be strictly increasing and convex in θ. The above problem can also be represented as

$$\text{Maximize } J(r_j) = \sum_{i=1}^{n_j} U_i(r_j S_E(n_j, i, w_{ij}^*(r_j))) - \lambda(\theta_j) r_j \tag{2.31}$$

where $w_{ij}^*(r_j)$ denotes the optimal w_{ij} given r_j. The optimal weight vector $\mathbf{w}_j^*$ is obtained by solving the following problem:

$$\begin{aligned} &\text{Maximize } z = \sum_{i=1}^{n_j} U_i(r_j S_E(n_j, i, w_{ij})) \\ &\text{subject to } \quad \sum_{i=1}^{n_j} w_{ij} \le 1; \ w_{ij} \ge 0, \ \forall (i, j) \end{aligned} \tag{2.32}$$

$\sum_{j\in A} J(r_j)$ is maximized when each individual cluster j maximizes its own objective function $J(r_j)$ [4]. As the price becomes large with the increase of contention loss probability, the fully distributed solution also converges to a channel allocation scheme that maximizes the aggregate utility over all the clusters.

The concave objective function $J(r_j)$ is maximized when $J'(r_j) = 0$, resulting in $\sum_{i=1}^{n_j} U_i'(r_j^* S_E(n_j, i, w_{ij}^*(r_j^*))) - \lambda(\theta_j^*) = 0$, where r_j^* is the optimal channel allocation rate of

cluster j and θ_j^* is the perceived contention loss probability when cluster j and its neighboring clusters access the medium with an optimal channel allocation rate.

A time-averaging stochastic approximation algorithm with feedback can be used to update the channel allocation rate:

$$r_j^{k+1} = \overline{r}_j^k + \xi v_k \left(\sum_{i=1}^{n_j} U_i' \left(\overline{r}_j^k S_E \left(n_j, i, w_{ij}^* \left(\overline{r}_j^k \right) \right) \right) - \lambda \left(\overline{\theta}_j^k \right) \right)$$

$$\overline{r}_j^k = (1 - \beta_k)\overline{r}_j^{k-1} + \beta_k r_j^k$$

$$\overline{\theta}_j^k = \begin{cases} (1 - \delta_k)\overline{\theta}_j^{k-1} + \delta_k, & \text{collision happens in cycle } k \\ (1 - \delta_k)\overline{\theta}_j^{k-1}, & \text{no collision in cycle } k \end{cases}$$

where ξ, v_k, β_k and δ_k are adjusting parameters. Using the standard methodology described in Reference [28], we can show that r_j^k converges to r_j^* with probability 1.

2.6.9 Performance examples

In this section, we take ξ as 10^6 and take v_k, β_k and δ_k as $1/k$ as in Reference [4] and show by simulations that the convergence speed is quick. The state diagram of a clusterhead is shown in Figure 2.17. At the initial state, k, r_j and θ_j are, respectively, set to 100, 1/6 and 0. However, the setting of initial values for r_j and θ_j is quite flexible. With r_j optimized iteratively, the statistical approximation algorithm guarantees that r_j converges to r_j^* with any initial state. The optimal

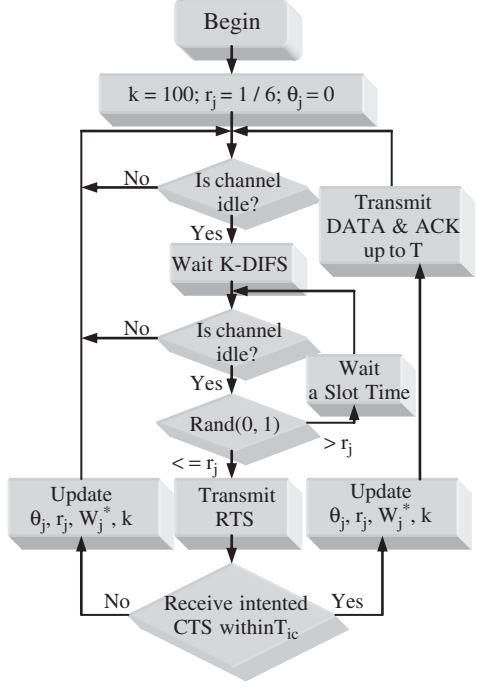

Figure 2.17 State diagram of clusterhead. (Reproduced by permission of IEEE [4]).

weight vector $\mathbf{w}_j^*$ will be derived iteratively by Problem (2.29) with updated r_j. K-DIFS (K-ary DCF interframe space) is equal to *aSlotTime*. T_{ic}, as defined earlier, denotes the window size for intracluster opportunistic collision resolution.

A local area *ad hoc* network with only one clusterhead is considered first. All the traffic is from the clusterhead to the users. The clusterhead can immediately initiate a new cycle of data transmission after the previous one completes. It is assumed that each packet can be correctly received once it is transmitted at the appropriate data rate and that ACK is not used. The protocol operation is set in this way to facilitate the comparative study on the channel efficiency of different schemes. The channel is modeled as Rayleigh fading. If h_i = SNR then we have $f_{H_i}(h) = \mathrm{e}^{-h/\overline{h}_i} \Big/ \overline{h}_i$, where $\overline{h}_i$ is the average SNR of user i. It is assumed that the link qualities at different nodes are i.i.d. The achievable data rate of each link is formulated as $R(h) = B \log_2[1 + \min(h,\ h_{\max})]$, where $h_{\max}$ is the upper bound related to T ($h_{\max}$ is set as 100).

The basic algorithm (BO-MAC) is compared with the round-robin scheduler and the ideal scheduler. The ideal scheduler has full knowledge of the channel information prior to scheduling so that it can target the best quality user without overhead. For the analytical results, the formula to calculate the throughput of BO-MAC has been introduced in the previous sections. The formula to calculate the throughput of the round-robin scheduler and the ideal scheduler are similar to that of BO-MAC and are omitted here.

The case with the homogeneous channel condition and $\overline{h}_i$ equal to 1 for each user is considered first.

Figure 2.18 shows one set of analytical and simulation results in which the medium access threshold for BO-MAC is 0.9. The simulation results are quite close to the analytical results. The BO-MAC performs much better than the round-robin scheduler (channel efficiency 0.8 and independent of the number of users) and can scale well with the number of backlogged users. The channel efficiency of the BO-MAC can approach approximately 90 % of that for the ideal scheduler when TXOP is T. When the medium access thresholds for BO-MAC are set with different values, the performance is affected. However, the throughput scaling effects and the relationship between the theoretical results and simulation results are also observed.

Heterogeneous channel conditions were considered in Reference [4]. Table 2.2 shows the channel condition and throughput result of each user. The simulation results match the analytical results very well. Almost every user of the BO-MAC scheme obtains twice the throughput of the round-robin scheme.

For general optimization [4] considers two cases. In the first case, the utility function of user i equals $U_i(x_i) = v_i \log(x_i)$, where x_i is the achievable throughput (bit/s). This kind of utility function will be used most often in Chapter 12. In the second case, the utility function of user i is equal to

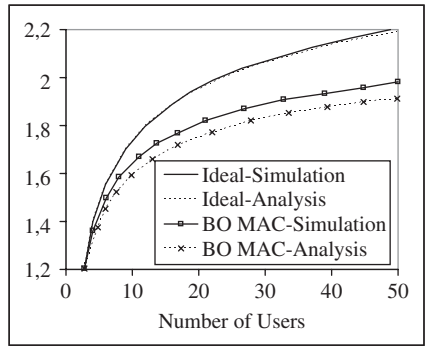

Figure 2.18 Channel efficiency with timeshare fairness.

Table 2.2 Throughput with timeshare fairness in the heterogeneous case (BO-MAC = OMAR). (Reproduced by permission of IEEE [4])

Flow ID	0	1	2	3	4	5	6	7	8	Total
$\overline{h}_i$	0.6	0.7	0.8	0.9	1.0	1.1	1.2	1.3	1.4	
Ideal-Anl (bit/s)	139323	153259	165952	177609	188388	198413	207785	216584	224876	1672189
Ideal-Sim (bit/s)	140834	154745	167252	177787	187636	197637	207066	216356	223877	1673190
OMAR-Anl (bit/s)	128551	141410	153121	163877	173822	183073	191720	199838	207490	1542902
OMAR-Sim (bit/s)	132708	146138	157953	168142	177599	187697	197382	206643	213307	1587569
RR-Anl (bit/s)	60516	67753	74529	80904	86929	92644	98082	103271	108235	772863
RR-Sim (bit/s)	59938	67820	73932	80858	86931	93228	98136	103030	108196	772069

$U_i(x_i) = v_i * x_i/1000$, where v_i is the assigning utility weight. As shown in Table 2.3, the higher the utility weight v_i, the higher the throughput and the higher the achieved utility. In the first case, even with $\log(\cdot)$ effects, the aggregate utility is still improved significantly in comparison with the round-robin scheme. For the second case, since the utility function is linear, the aggregate utility has been significantly improved.

In the case of multicluster without mobility we discuss the intercluster collision resolution. Global fairness is achieved by distributedly optimizing social optimality. Figure 2.19 shows the simulated topology.

There are three clusters with five, one and three directed link flows, respectively. Suppose that the traffic on each link flow is greedy. The utility function of each flow is $U_i(x_i) = v_i \log(x_i)$, where v_i is the utility weight and x_i is the throughput (bit/s). In the first cluster, the clusterhead node 6 coordinates the RI-MAC to exploit the multi-input link diversity. In cluster 3, node 7 coordinates the SI-MAC to exploit the multi-output link diversity. The channel model and achievable rate function are formulated in the same way as the single-cluster case.

The stochastic approximation algorithm is used to achieve the optimal channel allocation rate for each cluster in a distributed way. The pricing in terms of perceived collision probability is given by $\lambda(\theta) = 0.001\theta$. Figure 2.20 shows the convergence speed of the time-averaged stochastic approximation with feedback. It takes only about 200 cycles, i.e. 1.5 s, to reach stability. It was also found that the slope of the pricing function does not affect the convergence speed much as long as it is sufficiently large. The channel allocation rate of each cluster decreases (proportionally with each other) when the pricing increases to a very large value. However, the throughput and utility are not affected much. The reason is that each clusterhead persistently accesses medium at the channel allocation rate, minislot by minislot, whenever a channel is free. Having in mind the fact that the minislot is relatively short to the TXOP, the wasted time for collision resolution is small.

Throughput and utility are used to compare the performance gain with 802.11. Table 2.4, shows that the aggregate utility and aggregate throughput have been improved by 6 % and 54 %, respectively. In 802.11, the throughputs are equally shared. In BO-MAC (OMAR), more timeshares are given to the user with a higher utility function; thus the aggregate utility is increased. Furthermore, as BO-MAC exploits multiuser diversity, the throughput of each user has been increased.

For the analysis of a multicluster with mobility a heterogeneous *ad hoc* network as shown in Figure 2.21 is used. Each high-power (HP) node forms a cluster and functions as the clusterhead. Each low-power (LP) node associates with the nearest HP node. In the beginning, both HP nodes

Table 2.3 Case study of general optimization (BO-MAC = OMAR), (Reproduced by permission of IEEE [4])

	Flow ID	0	1	2	3	4	5	6	7	8	9	
Parameter	$\overline{h}_i$	1.0	1.0	1.0	1.0	1.0	1.0	1.0	1.0	1.0	1.0	Aggregate
	$\overline{v}_i$	1.0	1.1	1.2	1.3	1.4	1.5	1.6	1.7	1.8	1.9	
	OMAR (W^*)	0.071	0.078	0.084	0.091	0.097	0.103	0.110	0.116	0.122	0.128	1.0
case 1	OMAR-utility	11.7	13.0	14.2	15.5	16.8	18.0	19.3	20.6	21.9	23.2	174.0
	RR-utility	11.3	12.4	13.5	14.6	15.8	16.9	18.0	19.3	20.3	21.4	163.4
	OMAR (W^*)	0.014	0.027	0.043	0.063	0.084	0.106	0.130	0.153	0.178	0.202	1.0
case 2	OMAR-utility	29.8	58.1	94.8	145.1	197.8	256.5	321.4	388.7	461.2	536.6	2490.0
	RR-utility	78.2	86.1	93.0	102.2	109.8	116.8	126.5	132.9	140.0	148.8	1134.4

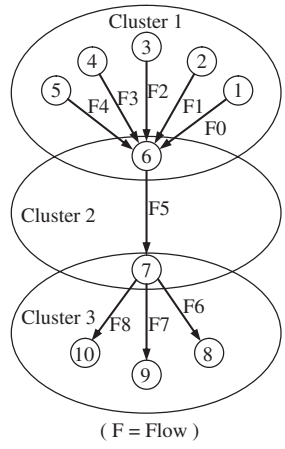

Figure 2.19 Multicluster topology.

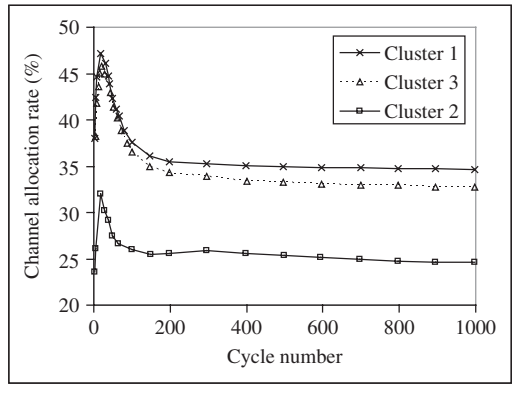

Figure 2.20 Convergence speed of the channel allocation rate with the stochastic approximation algorithm.

and LP nodes are evenly distributed over a $400\,m \times 600\,m$ area (but each LP node is away from the nearest HP node by 70 m). Later on, LP nodes move randomly, following the random-way point mobility model with minimal speed larger than 0.1 m/s. Each LP node estimates its SNR distribution iteratively, as discussed in Section 2.6.3. For simplicity, it is assumed that all the traffic is from HP nodes to associated LP nodes. The traffic of each link is saturated. The utility function of each link is $U_i(x_i) = \log(x_i)$, where x_i is the throughput (bit/s). Under this utility function, each user can obtain equal opportunity to access the channel in a cluster; i.e. timeshare fairness within a cluster can be achieved by BO-MAC. For 802.11, round-robin scheduling is used to guarantee the timeshare fairness among the output links. The achievable data rate, in terms of the distance d and the fading factor h, is

$$R(d, h) = B \log_2\{1 + [250/\max(25,\ d)]^4\ [\min(h,\ h_{\max})/156]\}$$

where h follows the Rayleigh distribution with expectation 1 and $h_{\max}$ is equal to 100. The simulation time of each scene is 2000 s. The result of each scenario is averaged over 10 simulation results.

Table 2.4 Optimal intercluster collision resolution. (Reproduced by permission of IEEE [4])

Flow ID	0	1	2	3	4	5	6	7	8	
$\overline{h}_i$	1.0	1.0	1.0	1.0	1.0	1.0	1.0	1.0	1.0	Aggregate
$\overline{v}_i$	1.0	1.0	1.0	1.0	1.0	5.0	2.0	2.0	2.0	
OMAR-throughput	111665	111229	116085	113279	110363	172492	137754	145348	145591	1163807
OMAR-utility	11.6	11.6	11.7	11.6	11.6	60.3	23.7	23.8	23.8	189.7
802.11-throughput	108151	108150	108151	108152	108150	108151	36050	36051	36050	757057
802.11-utility	11.6	11.6	11.6	11.6	11.6	57.9	21.0	21.0	21.0	178.9

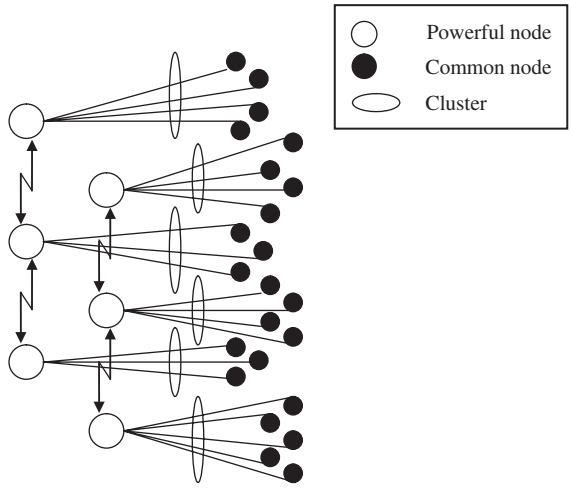

Figure 2.21 The simulated heterogeneous *ad hoc* network.

The total number of nodes is varied from six to 60 such that the average number of users in each cluster is varied from one to 10. Each LP node moves at the average speed of 1 m/s. As shown in Fig. 2.22(a), the aggregate throughput can be significantly improved by utilizing multiuser diversity even though the number of users in each cluster is small, e.g. two. The performance gain steadily increases as the number of users increases. When the average number of users in each cluster is 10, the throughput by BO-MAC is about twice that of 802.11.

For the mobility study the average number of users in each cluster is five. As shown in Figure 2.22(b), both BO-MAC and 802.11 increase throughput as the average speed increases. This should be expected. In the beginning, each node is put 70 m away from the nearest HP node. Later on, some nodes get much closer to the associated HP node even though some nodes become further away. However, no matter how far away, each link is in a cluster and gets a similar opportunity to access the channel. The aggregate throughput will increase as the speed increases from 0.5 m/s to 5 m/s. It is worthy to note that the performance gain of BO-MAC over 802.11 is affected when speed increases, mainly due to increasing clustering overhead and the channel estimation error. However, the performance gain of BO-MAC over 802.11 is still substantial.

BO-MAC achieves higher aggregate throughput without sacrifice of individual fairness. Figure 2.22© shows the throughput of each user in the scenario with 30 LP nodes moving at 1 m/s on average. Users are sorted according to throughput. Each user of BO-MAC achieves much higher throughput than that under 802.11. The reason that some nodes get higher throughput than others under the same scheme is mainly because of their shorter distances to HP nodes after they randomly move.

2.7 MOBILITY-ASSISTED OPPORTUNISTIC SCHEDULING (MAOS)

In this section we present optimal (OOSA) and suboptimal (SOOSA) opportunistic scheduling algorithms that combine channel fluctuation and user mobility information in their decision rules. The algorithms are based on the opportunistic scheduling framework with dynamic constraints for fairness. These fairness constraints adapt according to the user mobility. The adaptation of constraints in the algorithms implicitly results in giving priority to the users that are in the most favourable locations. The optimal algorithm precomputes constraint values according to a known

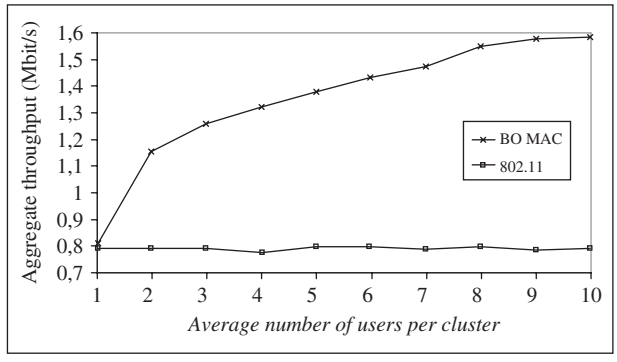

(a)

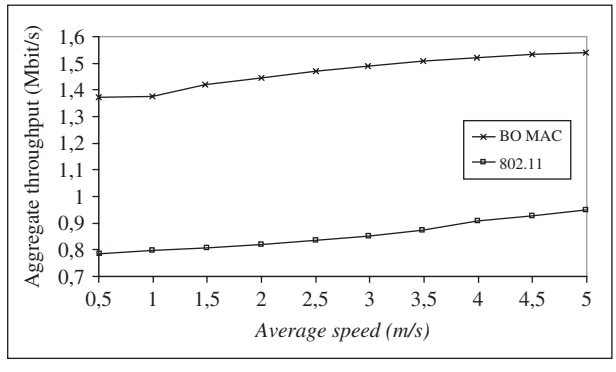

(b)

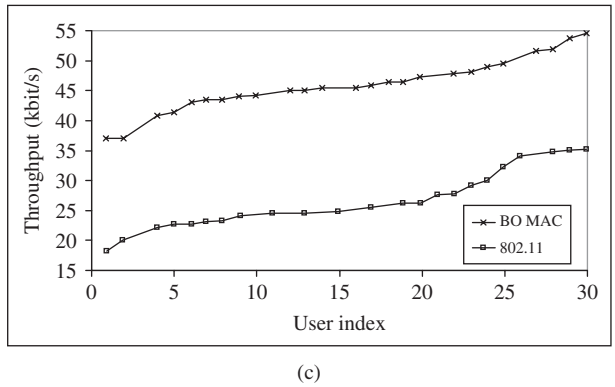

(c)

Figure 2.22 (a) Throughput versus node density. (b) Throughput versus node mobility. (c) Throughput fairness.

mobility model. The suboptimal algorithm relies on the future prediction of the user mobility locations in time.

Let us assume that there are N users in a cell with the feasible data rate vector at a generic scheduling timeslot $\mathbf{R} = (R_1, \ldots, R_N)$ (the rate at which user i can be served if scheduled). It is also assumed that $E(R_i \mathbf{1}_{\{Q(\mathbf{R})\}})$ is the average scheduled data rate of user i achieved by the

scheduling policy Q, where $\mathbf{1}_{\{\}}$ is the indicator function. The overall *system data rate* is $E(R_{Q(\mathbf{R})}) = \sum_{i=1}^{N} E(R_i \mathbf{1}_{\{Q(\mathbf{R})=i\}})$.

The *temporal* fairness measure considers time as a resource and shares it among multiple users according to the given fairness constraints. In other words, if $P\{Q(\mathbf{R}) = i\}$ is the probability of scheduling user i by policy Q and r_l is the long-term minimum temporal requirement for user i, where $r_i \geq 0$, $\varepsilon = \sum_{i=1}^{N} r_i \leq 1$, then the LCS (Liu, Chong, Shroff) algorithm [29] solves the following stochastic optimization problem:

$$\begin{aligned} &\max_{Q} \ E(R_{Q(\mathbf{R})}), \\ &\text{subject to } P\{Q(\mathbf{R}) = i\} \geq r_i, \ i = 1, 2, .., N \end{aligned} \tag{2.33}$$

The LCS algorithm defines the optimal policy as

$$Q^*(\mathbf{R}) = \arg\max_i (R_i + v_i^*) \tag{2.33a}$$

where v_i^* are given Lagrange multipliers that satisfy the constraints in problem (2.33). The algorithm has a polynomial complexity of $O(N)$.

As an illustration let us assume that there are 10 users sharing a single channel with fairness constraints given as $r_i = 1/12$. These constraints mean that each user expects an allocation of at least 8.33 % of the time slots for itself. This is an average fairness measure and considers only a fraction of the total time. In other words, the position of the allocated time slots or their order is not important.

2.7.1 Mobility models

For the mobility, a finite-state semi-Markov model is used. The model divides cell geography into a set of nonoverlapping topological spaces $S = \{1, \ldots, M\}$ called *mobility states*. The model can, for example, represent regular concentric rings [30] or irregular cell areas depending on the accessibility and geography of the cell. The rings or spaces are characterized by the average SINR, $\rho(m)$, where $m \in S$. The average SINR depends on y_m (the distance between BS and mobility state m). User mobility among these states follows a semi-Markov process with (known) dwell times with distribution function $P_d(m)$ and mean $\overline{d}(m)$. The stationary distribution of the underlying process is found as follows [31]:

$$\pi(m) = \frac{\pi^e(m)\overline{d}(m)}{\Sigma_{m' \in S}\pi^e(m')\overline{d}(m')} \tag{2.34}$$

where $\pi^e(m)$ is the stationary distribution of the embedded Markov chain. The SINR is a function of path loss, interference and fading processes. Path loss is a function of the distance from the BS and interference is a function of the distance from the neighboring cells. Because our mobility model allows user mobility over large areas, the average SINR will change over time, resulting in a nonstationary channel model. To cope with the nonstationarity and to have a simpler model that allows analysis, we employ a piecewise stationary channel model and assume that the path loss and interference remains constant within a mobility state.

Let mobility state m be at distance y_m from the BS. By using a simple propagation model, the path loss at distance y_m from the BS is given as

$$\Gamma(m) = \begin{cases} 1; \ y_m \leq y_0 \\ (y_0/y_m)^{\alpha}; \ y_m > y_0 \end{cases} \tag{2.35}$$

In Equation (2.35), y_0 is the maximum distance from the BS up to where full transmitted power P_t is received and α is the path loss exponent. In the network where the central cell is surrounded

by six interfering cells the interference from the neighboring cells is approximated as [30]

$$I(m) = P_I \times \left\{ \Gamma\ (2Y - y_m) + 2\Gamma \left[\sqrt{(Y - y_m)^2 + 3Y^2} \right] + 2\Gamma \left[\sqrt{(Y + y_m)^2 + 3Y^2} \right] + \Gamma\ (2Y + y_m) \right\} \tag{2.36}$$

where P_I is the transmit power of the interfering cell and Y is the cell radius. For small-scale fading, a flat fading channel is assumed, valid for systems where, the feed back delay is relatively short compared to the fading frequency.

If user l is in mobility state m at a generic time slot then the received SINR is given as [30]:

$$Z_l(m) = \zeta_l \frac{P_t \times \Gamma(m)}{\eta + I(m)}, \tag{2.37}$$

where ζ_l is the time-dependent fading process, P_t is the transmitted power, $\Gamma(m)$ and $I(m)$ are the path loss and interference experienced by the user and η is the background noise. The fading processes ζ_l are independent and identically distributed (i.i.d.) (exponentially distributed stationary process with unit mean). Therefore, Z is also an exponentially distributed random process with mean $\rho(m) = P_t \times \Gamma(m)/[\eta + I(m)]$ and, for $z \geq 0$, its distributions are given as $p_Z(z, m) = \mathrm{e}^{-z/\rho(m)}/\rho(m)$. If $H = \{Z_0, Z_1, \ldots, Z_{H-1}\}$ represents the set of discrete SINR levels in ascending order, the fading channel takes level h if the received SINR falls in the interval $[Z_h, Z_{h+1})$ and the corresponding steady-state probability of level h in mobility state m is

$$p(h, m) = \int_{Z_h}^{Z_{h+1}} p_Z(z, m)\mathrm{d}z = \mathrm{e}^{-z_h/p(m)} - \mathrm{e}^{-z_{h+1}/\rho(m)} \tag{2.38}$$

The state transition probabilities are computed according to the procedure given in References [32] and [33]. The physical layer coding and modulation schemes map fading levels to corresponding data rates.

The overall system model employs a hierarchical time scale with two levels. The *mobility slot* operates on a wider timeslot. This timeslot allows the algorithm to take advantage of the slow time path loss variations in the feasible data rate. At the mobility slot level, the fast time-fading variations in the feasible rate can be represented by their expected values. The *scheduling slot* handles scheduling decisions and has a narrower timeslot. The scheduling slot allows the algorithm to benefit from the fast time-fading fluctuations. At the scheduling slot, the slow time path loss variations can be modelled as a constant path loss experienced at the centre of the corresponding mobility state. The presence of two time scales helps to accommodate user mobility, which evolves relatively slowly compared to the scheduling decisions.

2.7.2 Optimal MAOS algorithm

At the time scale of user mobility, the fading experienced by a user in a mobility state can be abstracted by the corresponding expected feasible rate. In order to improve the system data rate, it is imperative to give preference to users when they are in the most favorable locations, i.e. having high expected feasible rates. Since the algorithm considers time as a resource to be allocated, if time fractions are distributed such that they *maximize their product with the expected feasible rates* of the corresponding users for all aggregate mobility states, then the algorithm can achieve its stated objectives of improving the system data rate. Therefore, this stage of the MAOS algorithm determines *optimum time fractions* that maximize the expected feasible rates of the users under the constraints of providing fairness and preventing starvation.

For N users and M mobility states per user, the set of possible aggregate states is an N-dimensional space given by $S = S_1 \times \cdots \times S_N$, where $\times$ denotes the Cartesian product and

S_l is the state space of user l defined earlier. Therefore, the aggregate mobility model contains M^N states ($|S| = M^N$), and a state is identified by a vector $\mathbf{m} = (m_1, \ldots, m_N)$ at a generic mobility slot. Assuming independence among users, the stationary distribution of state $\mathbf{m} \in S$ equates to the product of the individual stationary distributions, $P(\mathbf{m}) = \prod_{l=1}^{N} \pi(m_l)$. In the sequel, we assume that the scheduler knows the above mobility model, expected feasible rates $R(\mathbf{m}, l) \forall \mathbf{m}$ and l, and can track the user state accurately.

The MAOS algorithm first computes the optimal time-fraction allocations for every mobility state $\mathbf{m}$ that maximizes its product with the expected feasible rate summed over all states and for all users. If r_l is the long-term minimum temporal requirement for user l and $\varepsilon = \sum_{l=1}^{N} r_l \leq 1$, the MAOS algorithm solves the following linear program (LP):

$$\max \sum_{\mathbf{m} \in S} \sum_{i=1}^{N} \mathbf{R}(\mathbf{m}, i) r(\mathbf{m}, i) \tag{2.39a}$$

$$\text{subject to } \sum_{i=1}^{N} r(\mathbf{m}, i) \leq P(\mathbf{m}), \ \forall \mathbf{m} \in S \tag{2.39b}$$

$$\sum_{\mathbf{m} \in S} r(\mathbf{m}, i) = r_i, \ i = 1, \ \ldots, \ N \tag{2.39c}$$

$$r(\mathbf{m}, i) \geq \frac{\theta r_i}{|S|}, \ \forall \mathbf{m} \in S, \forall i \text{ and } 0 \leq \theta \leq \theta_{\max} \tag{2.39d}$$

where $r(\mathbf{m}, i)$ are optimization variables and θ is a parameter.

LP (2.39) maximizes the weighted sum of the expected feasible rate and complies with the stationary distribution of user mobility (2.39b), satisfies long-term temporal fairness constraints (2.39c) and prevents long-term starvation (2.39d). The time fraction r_i behaves as a resource and the above LP optimally distributes it among all mobility states accessible to the user i.

With $\theta > 0$ in (2.39d) the long-term starvation of users is prevented. With $\theta = 0$, the resulting solution of (2.39) is a greedy solution where users are denied access in mobility states with weak channels. This denial results in the starvation of such users. Therefore, $\theta > 0$ guarantees that a minimum fraction of r_l, distributed over all mobility states, is assigned to every user, even in mobility states with bad channels. In this way, the MAOS algorithm avoids long-term starvation. For the feasibility of LP, θ is upper bounded by $\theta_{\max} = \min_{\mathbf{m}}(P(\mathbf{m}))|S|/\varepsilon$.

If $r^*(\mathbf{m}, i)$ maximizes the objective function (2.39a) it is still only a fraction of r_i because of the construction of LP (2.39). When $\varepsilon = 1$, then r_i behaves like the probability of allocation of user i. The resulting $r^*(\mathbf{m}, i)$ is the joint probability of two events: user $i's$ allocation and the occurrence of mobility state $\mathbf{m}$. Thus, user $i's$ allocation probability given mobility state $\mathbf{m}$ can be found by dividing $r^*(\mathbf{m}, i)$ by the corresponding probability of the state. For a more general case when $\varepsilon < 1$ and considering the feasibility of the constraint (2.39b), the resulting allocation probability, called the *normalized time fraction* $\hat{r}(.)$, is

$$\hat{r}(\mathbf{m}, i) = \varepsilon r^*(\mathbf{m}, i) / \sum_{i=1}^{N} r^*(\mathbf{m}, i), \quad \forall \mathbf{m} \in S \tag{2.40}$$

The algorithm gains also from the fast time-fading fluctuations in the feasible data rate. For this purpose, it uses the LCS methodology for the normalized time fractions found in the first stage. It maximizes the expectation of the scheduled (system data) rate for each mobility state and satisfies the respective time-fraction allocation. For this objective, the algorithm solves the following stochastic optimization problem after modifying problem (2.33):

$$\begin{aligned} &\max_{Q} E(R_{Q(\mathbf{R}(\mathbf{m}))}) \\ &\text{subject to } P\{Q(\mathbf{R}(\mathbf{m})) = i\} \geq \hat{r}(\mathbf{m}, i), \ i = 1, 2, .., N \end{aligned} \tag{2.41}$$

The problem has dynamic constraint values that are functions of $\mathbf{m}$. The optimal scheduling policy is found by adapting the solution (2.33a) for state $\mathbf{m}$:

$$Q^*(\mathbf{R}) = \arg\max_i [R_i + v_i^*(\mathbf{m})] \tag{2.41a}$$

In Equation (2.41a), $v_i^*(\mathbf{m})$ is the given Lagrange multiplier that satisfies the corresponding constraint in problem (2.41). Therefore, MAOS can be considered as a piecewise LCS algorithm, i.e. one for every $\mathbf{m}$ state.

2.7.3 Suboptimum MAOS algorithm

The optimal MAOS algorithm has exponential complexity in the number of users because it precomputes time fractions for all aggregate mobility states. The first stage of the suboptimum MAOS finds $\hat{r}(t+\Delta, i), \forall i$ and $\Delta = 1, \ldots, \tau$, as a solution to the following LP:

$$\max \sum_{\Delta=1}^{\tau} \sum_{i=1}^{N} \overline{R}(t+\Delta, i) r(t+\Delta, i) \tag{2.41b}$$

$$\text{subject to } \sum_{i=1}^{N} r(t+\Delta, i) = \varepsilon, \ \forall \Delta \tag{2.41c}$$

$$\frac{1}{\tau} \sum_{\Delta=1}^{\tau} r(t+\Delta, i) = r_i, \quad i = 1, \ldots, N, \tag{2.41d}$$

where $\overline{R}(t+\Delta, i)$ is the average feasible data rate of user i at the $t+\Delta$ (mobility) timeslot in the future in accordance with the predicted mobility state. The constraint (2.41b) ensures that, for every Δ, the time fraction resource ε is distributed among users, and constraint (2.41c) makes sure that, for every τ, the assigned fraction satisfies the long-term fairness requirement. LP (2.41) is solved after every τ mobility slot.

If $\hat{r}(t+\Delta, i)$ maximize the objective function (2.41) in the second stage, these values are used to modify and solve problem (2.33). The resulting stochastic optimization problem maximizes the expectation of the scheduled (system data) rate and satisfies the new fairness constraints

$$\begin{aligned} &\max_Q E(R_{Q(\mathbf{R}(t+\Delta))}) \\ &\text{subject to } P\{Q(\mathbf{R}(t+\Delta)) = i\} \geq \hat{r}(t+\Delta, i) \\ &i = 1, \ 2, \ \ldots, \ N, \ \Delta = 1, \ \ldots, \ \tau \end{aligned} \tag{2.42}$$

Parameter $\hat{r}(t+\Delta, i)$ changes only when a user makes a transition to a new mobility state. After that transition, it remains constant for several mobility timeslots until the next transition. LP (2.41) can be modified by lower bounding $r(t+\Delta, .)$ like (2.39d) in order to avoid possible long-term starvation.

The solution of problem (2.42) is a modified LCS policy that selects a user at every (scheduling) timeslot according to

$$Q^*(\mathrm{P}) = \arg\max_i [R_i + v_i^*(t+\Delta)] \tag{2.42a}$$

In Equation (2.43),$v_I^*(t+\Delta)$ is the Lagrange multiplier for the constraint active at (mobility) time $t+\Delta$. The resulting subopimum MAOS algorithm has a complexity of $O(N\tau)$.

2.7.4 Mobility estimation and prediction

The optimal MAOS algorithm only needs to estimate the current mobility state of every user. This is not difficult because the mobility model considers a large area within a cell as a state.

A user anywhere in that area is considered to be in that state. Monitoring the respective radio signal strength or alternative technologies, like the angle of arrival (*AoA*) and time delay of arrival (*TDoA*), may be used for location estimation [34, 35]. The presence of two time scales helps in reducing the errors in the estimation process.

The suboptimum MAOS algorithm also needs to predict the mobility state in the future. An alternative technique is suggested in Reference [4]. Straight-line movement on highways mostly follows deterministic mobility with constant speed and velocity [36–38]. Therefore, the future trajectory can be accurately predicted. For stochastic user mobility, the approximate MAOS algorithm can employ a hierarchical mobility model. The higher layer of this model will have a discrete-state space like the one presented in this section. The lower layer of the model will have a continuous-state space modelled by some linear dynamical system. This continuous-state-space model will help to monitor not only the state but also the fine-grain location information in the form of coordinates, velocity and acceleration [37, 38]. The fine-grain mobility information will help in predicting the future discrete states to be visited by a user. For example, Reference [37] showed a fairly accurate prediction of the next state several seconds ahead of time. With the help of fingerprinting of the road network, the future prediction of mobility states can be further improved.

2.7.5 Estimation of Lagrange multipliers

Both the optimal and suboptimal MAOS algorithms use a stochastic approximation technique for the estimation of Lagrange multipliers. The optimal MAOS sets the initial value of $v(.) = 0 \forall i$ and $\mathbf{m}$ and maintains a database for every mobility state $\mathbf{m}$, where it holds the most recent estimated values of $v(.)$ and supporting parameters used in its computation. Whenever the system enters into mobility state $\mathbf{m}$, the algorithm retrieves the stored values from the database. As long as the system remains in state $\mathbf{m}$, it updates the values of $v(.)$ for every scheduling slot $k+1$ as (see Chapter 12 and Reference [29])

$$v_i^{k+1}(\mathbf{m}) = \max[(v_i^k(\mathbf{m}) - \delta\ (1_{\{Q^k(\mathbf{R}(\mathbf{m})=i)\}} - \hat{r}(\mathbf{m}, i)), 0)] \tag{2.43}$$

A small constant δ is used as the step size because the corresponding LCS algorithm, being indifferent to the user mobility information, views the piecewise stationary channel as a nonstationary process. For nonstationary processes, the stochastic approximation technique recommends a constant step size [29]. The presence of a database to store the values of $v(.)$ and supporting parameters for future use and the difference in time scales between mobility transitions and scheduling decisions guarantees the saturation of Equation (2.43).

The suboptimum MAOS cannot store the values of $v(.)$into a database because it lacks the complete knowledge of the state space. Therefore, whenever a new state is visited, the algorithm resets $v(.)$ and the supporting parameters. Then it uses an expression similar to (2.43) for subsequent scheduling and mobility slots until the next mobility transition. The time scale difference between mobility transitions and scheduling may allow the suboptimum MAOS to achieve saturation.

2.7.6 Performance examples

In Reference [39] a performance example for MAOS is presented for a hexagonal cell that has a maximum coverage distance of 5 km from the central BS to a mobile user. The service area is divided into two concentric rings ($m = \{1, 2\}$). The innermost ring covers an area of up to 3 km from the BS. The BS's maximum output power is 15 W and 80 % of this power is used for the shared data channel. The system provides a data service with feasible data rates of {2457.6, 1843.2, 1228.8, 921.6, 614.4, 307.2, 204.8, 153.6, 102.6, 76.8, 38.4} Kbps and corresponding SINRs of {9.5, 7.2, 3.0, 1.3, −1.0, −4.0, −5.7, −6.5, −8.5, −9.5, −12.5}dB. The parameter $\rho(m)$, defined in Section 2.7.1, at the centre of the rings is found from the path loss model for $\alpha = 4$, $y_0 = 1$ km, and

$\eta = 1$ W. The steady-state channel distribution is determined using Equation (2.38) for a speed of 60 km/h. The resulting expected feasible rate values are 1438 Kbps in the inner ring and 116 Kbps in the outer ring. The scheduling decisions are made at every 1.67 ms.

For the two concentric rings, the coarse-grained mobility model is learned through the simulation of a user following a fine-grained mobility model. For our simulation, random-walk mobility is considered with a constant speed of 60 km/h to model fine-grained user movement. Travel intervals are randomly distributed between 8 to 12 minutes. After completing one travel interval, the user selects a new direction randomly from 0 to 2π. When the user moves out of the service area, it wraps around and re-enters the service area. Mobility slots are of one second duration. The choice of identical mobility and channel distributions is only for ease of simulation. The algorithm can handle nonidentical cases too. Half of the users require (minimum) fairness requirements of $\varepsilon/6$ and the other half expect at least an $\varepsilon/12$ fraction. In Equation (2.43), $\delta = 0.05$ is used.

Figure 2.23(a) compares the average data rates achieved by eight users under the MR, LCS and MAOS algorithms. Because the first four users have higher fairness requirements, their data rates are higher than the remaining four users. On the other hand, LCS suffers performance losses in order to support constant fairness constraints. These constant fairness constraints force the LCS algorithm to schedule users when they are in an unfavorable location. Although the channel information is considered in scheduling, this information only allows it to benefit from the fast time fading while slow time path loss variations remain untapped. Thus, LCS ends up satisfying fairness constraints for users when they have weak channels.

The performance improvements seen in the case of MAOS have been achieved without sacrificing the long-term fairness requirements, as shown in Figure 2.23(b). This figure compares the temporal fairness requirements for all users to their actual allocations performed by the scheduling algorithms. The MR algorithm, which is a greedy algorithm without any regard to fairness, failed to support the required fairness measure. It gave equal access to all users, not because of any conscious decision on the part of the algorithm, but because of identical mobility and channel distributions used in the simulation. The MAOS and LCS are able to satisfy the minimum fairness requirements of $r_{1,\ldots,4} = \varepsilon/6$ and $r_{5,\ldots,8} = \varepsilon/12$.

2.8 OPPORTUNISTIC AND COOPERATIVE COGNITIVE WIRELESS NETWORKS

Cognitive wireless networks benefit from context awareness, which is integrated in the decision-making process in different layers. In this section, we discuss a system where the MAC layer transmission permission probability is modified, for elastic traffic users, in such a way as to discourage the transmissions from/to the users at the border of the cell where transmissions cause significant interference in adjacent cells. This will be referred to as spatial traffic shaping. By using the absorbing Markov chain theory, we provide, for such a concept, analytical models to analyze system performance, mainly the probability of successful channel assignment and message delivery delay. The analysis shows that in the cellular network, with the channel spatial reuse factor equal to one, the probability of successful channel assignment close to one can be achieved with an acceptable message delivery delay.

2.8.1 The system model

We assume that the beamforming has generated M spatial channels that can be reused across each cell. Within each spatial channel, N additional channels are generated by using either a timeslot (TDMA), frequency beam (OFDM) or code (CDMA). In the sequel we model adjacent cell interference for the case when the cochannel adjacent cell interference is caused by one interfering user (TDMA or OFDMA system) or users located in a relatively small area (CDMA). In this section we focus on the downlink although extension to the uplink is straightforward [42].

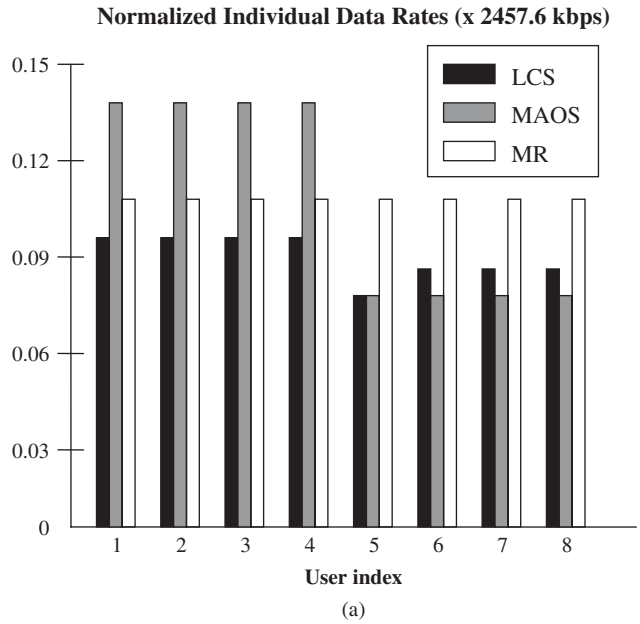

(a)

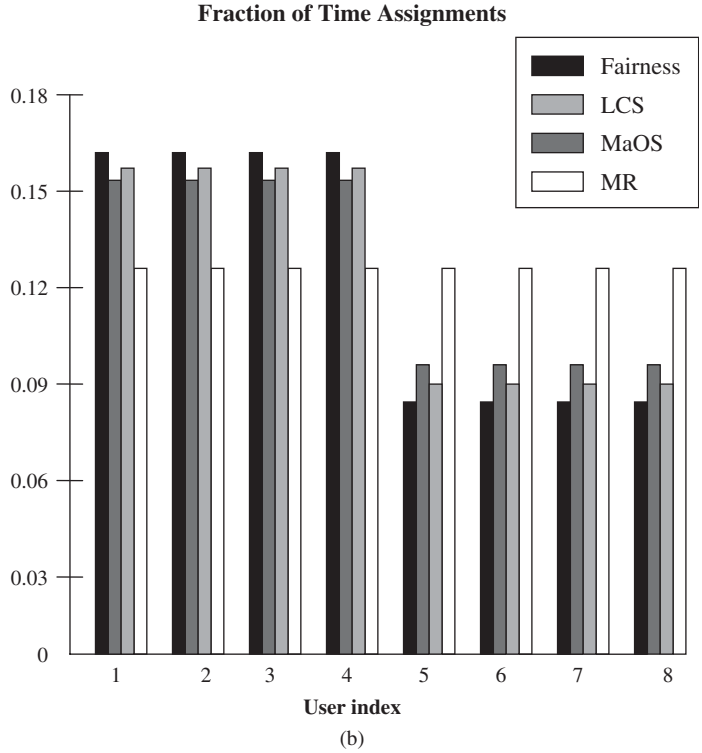

(b)

Figure 2.23 Comparison of MAOS with the LCS and MR algorithms: (a) individual data rates for $\varepsilon = 0.99$ and (b) fairness. (Reproduced by permission of IEEE [40]).

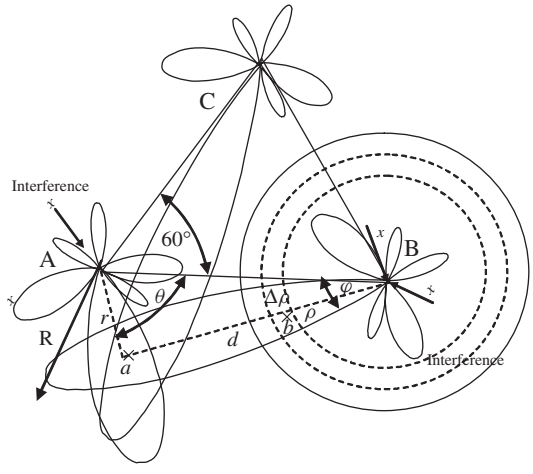

Figure 2.24 Size 3 cell cluster scenario.

2.8.1.1 Signal to adjacent cell interference ratio

Suppose mobile stations a and b are in two adjacent cells, as shown in Figure 2.24. Different simplified models for a signal-to-adjacent cell interference ratio are used for specific sets of assumptions.

(1) *Assuming no power control and no fading, with the same transmit power P.* Let $I(b \to a)$ represent the interference power level at location a of the signal transmitted to station b, by base B. This power is defined by the set of equations

$$\frac{P}{r_a^\alpha} = p_a,\ \frac{P}{r_b^\alpha} = p_b,\ I(b \to a) = \frac{P}{(r_b + d)^\alpha}$$
$$SIR = \frac{p_a}{I(b \to a)} = y = \frac{P(r_b + d)^\alpha}{r_a^\alpha P} = \left(\frac{r_b + d}{r_a}\right)^\alpha \tag{2.44}$$

where α is the propagation constant, P is the base station transmit power and p_a and p_b are the useful signal powers received at the locations a and b transmitted from their base stations A and B, respectively. From the geometry shown in Figure 2.24 we also have

$$\begin{aligned} &r_a/R = g \\ &(2R - r_a\cos\theta)^2 + (r_a\sin\theta)^2 = (d + r_b)^2 \\ &(2R/r_a - \cos\theta)^2 + (\sin\theta)^2 = \left(\frac{d + r_b}{r_a}\right)^2 \\ &y_1 = \left[(2/g - \cos\theta)^2 + (\sin\theta)^2\right]^{\alpha/2} \\ &i_1 = 1/y_1 \end{aligned} \tag{2.44a}$$

(2) *Assuming no power control in the presence of the fading.* If ξ represents Rayleigh fading, β lognormal shadowing and α the propagation constant, the previous relation becomes

$$\frac{\xi_a\beta_a P}{r_a^\alpha} = p_a;\ \frac{\xi_b\beta_b P}{r_b^\alpha} = p_b;\ I(b \to a) = \frac{\xi_{b+d}\beta_{b+d} P}{(r_b + d)^\alpha}$$
$$SIR = y = \frac{\xi_a\beta_a P(r_b + d)^\alpha}{r_a^\alpha P\xi_{b+d}\beta_{b+d}} = \frac{\xi_a\beta_a}{\xi_{b+d}\beta_{b+d}}\left(\frac{r_b + d}{r_a}\right)^\alpha$$

$$
\begin{aligned}
& r_a/R = g \\
& (2R - r_a\cos\theta)^2 + (r_a\sin\theta)^2 = (d + r_b)^2 \\
& (2R/r_a - \cos\theta)^2 + (\sin\theta)^2 = \left(\frac{d + r_b}{r_a}\right)^2 \\
& y_2 = \frac{\xi_a\beta_a}{\xi_{b+d}\beta_{b+d}}\left[(2/g - \cos\theta)^2 + (\sin\theta)^2\right]^{\alpha/2} \\
& i_2 = 1/y_2
\end{aligned}
\tag{2.45}
$$

(3) *Power control, arbitrary user location and no fading.* In this case the received signal power P is constant and we have

$$
\begin{aligned}
& \frac{P_a}{r_a^\alpha} = P,\ \ \frac{P_b}{r_b^\alpha} = P,\ \ I(b \to a) = \frac{P_b}{(r_b + d)^\alpha} \\
& SIR = y_5 = \frac{P(r_b + d)^\alpha}{P_b} = \left(\frac{r_b + d}{r_b}\right)^\alpha = \left(\frac{r_b/R + d/R}{r_b/R}\right)^\alpha = \left(\frac{h + d/R}{h}\right)^\alpha \\
& h = r_b/R \\
& a \Rightarrow (x, y) \Rightarrow (r, \theta) \\
& (2R - x)^2 + y^2 = (d + r_b)^2 \\
& d = -r_b + \sqrt{(2R - x)^2 + y^2} \\
& x = r\cos\theta \\
& r^2 = x^2 + y^2 \\
& d = -r_b + \sqrt{(2R - r\cos\theta)^2 + y^2} \\
& d = -r_b + \sqrt{4R^2 - 4Rr\cos\theta + r^2} \\
& d = -r_b + R\sqrt{4 - 4(r/R)\cos\theta + (r/R)^2} \\
& d/R = -h + \sqrt{4 - 4g\cos\theta + g^2} \\
& SIR = \left(\frac{d/R + h}{h}\right)^\alpha \\
& d/R = -1 + g + \sqrt{4 - 4g\cos\theta + g^2} \\
& g, h \in [0, 1] \quad \text{arbitrary independent values}
\end{aligned}
\tag{2.46}
$$

In the case of a size 3 cluster scenario (cells A, B and C), as shown in Figure 2.24, the angle between directions $\overline{AB}$ and $\overline{AC}$ is $\varphi = 60^\circ$. If the distance is calculated for cells A and B by using (1) then for cells A and C we use (1) with $\theta_1 = \theta + \varphi = \theta + 60^\circ$.

The extension of the previous two models to the case with power control, arbitrary user location and channel with fading is straightforward.

(4) *sir* (*snir*) *control.* In order to keep the equations simple and representative we will ignore the presence of Gaussian noise in the *snir* control loop and focus our attention on *sir* only. In the case when θ is such that the users a and b mutually interfere with each other the above equations become

$$
\begin{aligned}
& P_a/r_a^\alpha = p_a,\ \ P_b/r_b^\alpha = p_b,\ \ I(b \to a) = P_b/(r_b + d)^\alpha,\ \ I(a \to b) = P_a/(r_a + d)^\alpha \\
& sir(a) = p_a/I(b \to a) = P_a(r_b + d)^\alpha/P_b r_a^\alpha = \frac{P_a}{P_b}\left(\frac{r_b + d}{r_a}\right)^\alpha \\
& sir(b) = p_a/I(a \to b) = P_b(r_a + d)^\alpha/P_a r_b^\alpha = \frac{P_b}{P_a}\left(\frac{r_a + d}{r_b}\right)^\alpha
\end{aligned}
\tag{2.47}
$$

If the required *sir* is Y, we have $sir(a) = sir(b) \to Y$ and the question is whether or not we can guarantee this value across the entire network for all mutual positions of the terminals given that $P_a,\ P_b \le P_{\max}$. This can also be defined in terms of an equivalent power constraint $P_{\min} \le P_a,\ \ P_b \le P_{\max}$ or equivalently the power ratio $P_r = P_a/P_b;\ \ P_{r\,\min} \le P_r \le P_{r\,\max}$. With d defined in the previous discussions we have to find solutions where the above conditions are satisfied.
From the required *sir* we have

$$P_r \left(\frac{r_b + d}{r_a}\right)^{\alpha} \ge Y \to P_r \ge Y \left(\frac{r_b + d}{r_a}\right)^{-\alpha}$$

$$P_r^{-1} \left(\frac{r_a + d}{r_b}\right)^{\alpha} \ge Y \to P_r \le Y^{-1} \left(\frac{r_a + d}{r_b}\right)^{\alpha} \tag{2.48}$$

This should be within the limits $P_r = P_a/P_b;\ \ P_{r\,\min} \le P_r \le P_{r\,\max}$. In the case when only one user interferes with the other (as in Figure 2.24) the simplification of the above discussion is straightforward.

2.8.2 The outage probability

The outage probability is

$$P_{out}(x,\theta) = P(i > \varepsilon) = 1 - P(i < \varepsilon) = 1 - P\left(\frac{\xi_{b+d}\beta_{b+d}}{\xi_b\beta_b} i_0(x,\theta) < \varepsilon\right) \tag{2.49}$$

In general there will be a correlation between the spatial samples of ξ_{b+d} and ξ_b as well as between β_{b+d} and β_b. The amount of correlation will depend on both the beam width and the mutual distance d between interfering users. Both larger distance and larger beamwidth will result in less correlation. Although the modeling of the channel resemblance (correlation) for the two interfering users is outside the scope of this book we can make some suggestions that can be used in further evaluation of the protocols. For a very narrow beam we can use the approximation $\xi_{b+d} = \xi_b\xi_d$ and for $d \to 0$, $\xi_{b+d} \to \xi_b$. For larger beamwidths we can use the approximation $\xi_{b+d} = (1-\rho)\xi_{-b} + \rho\xi_b$, where ξ_{-b} represents the portion of the signal received in point $b+d$ not seen by point b, and the resemblance factor ρ can be represented as $\rho(\varphi, d) = (1 - d/d_0)(1 - \varphi/\varphi_0)$. For a precise analysis of the P_{out} we need joint probability distribution functions of ξ_{b+d} and ξ_b. However, for a relatively wide beam and d large enough (e.g. $d = R$ for the CD protocol described in Chapter 12) we can assume that the fading at two mutually interfering terminal locations is independent. In this case, if β is lognormal variable with zero mean and variance σ then in this calculus we can use the fact that $\beta = \beta_{b+d}/\beta_b = 10^{n_{b+d}-n_b} = 10^n$ is also lognormal variable with zero mean and variance $\sqrt{2}\sigma$. Therefore, we have

$$P_{out}(x,\theta) = P(i > \varepsilon) = 1 - P(i < \varepsilon) = 1 - P\left(\beta\frac{\xi_{b+d}}{\xi_b} i_0(x,\theta) < \varepsilon\right)$$

$$= 1 - \int_0^{\infty} P(\beta)d\beta \int_0^{\infty} P(\xi_{b+d})d\xi_{b+d} \int_{i_0\beta\xi_{b+d}/\varepsilon}^{\infty} P(\xi_b)d\xi_b \tag{2.49a}$$

In the sequel we use the notation $S(k^{\Uparrow})$ for the set of all possible combinations of k channels where $i > \varepsilon$ and $S(k^{\Downarrow})$ for the set of all possible complementary combinations of $N - k$ channels where $i < \varepsilon$. For each element with index s in $S(k^{\Downarrow})$ there is one corresponding element in $S(k^{\Downarrow})$.

The probability of having k channels with $i > \varepsilon$ can be presented as

$$p_{out}(k) = \sum_{s} \prod_{i \in s \in S(k\Uparrow)} p_{out}^{(i)} \prod_{j \in s \in S(k\Downarrow)} (1 - p_{out}^{(j)}) \tag{2.50}$$

where $p_{out}^{(i)}$ is the channel outage probability given by Equation (2.49).

2.8.3 Cellular traffic shaping

Cognition may help to stimulate users to transmit from the locations where they induce minimum interference to other users in the network, especially to reduce intercell interference. The conventional approach for service pricing so far includes only charging the user based on the required bit rate, with additional possible requirements on delay, without taking into account how much the user was interfering with others and so reducing the overall available capacity for others. An introduction of an effective network usage parameter may stimulate the user, having delayed elastic traffic, to transmit/receive from/at the positions that are preferable.

Storing the message and waiting for such a position may be a way to go. For the theoretical modeling of such systems game theory may offer interesting solutions. This will be further elaborated later.

For illustration purposes suppose that there is effectively one cochannel interfering signal sent to the user in the adjacent cell per beam. We consider two scenarios:

(1) *Unregulated traffic*. In this case the user is charged based on a bandwidth independent of its location in the cell. Therefore, its position in the moment of transmission/reception is uniformly distributed within the cell of radius $R = 1$.

(2) *Spatially regulated traffic.* In this case users are encouraged to transmit/receive at the position closer to the BS (further away from the cell border where they produce a lot of interference) by using the cost function $c = r$, where r is the normalized distance from the BS. Based on this we assume that a rational user will transmit with probability

$$f(r) = 1 - r \tag{2.51}$$

given that it has traffic to transmit. The number of additional options for $f(r)$ will also be discussed.

This protocol will be referred to as position aware multiple access (PAMA) as a part of a more general class of protocols that will be referred to as context aware multiple access (CAMA).

CAMA may include additional cognition when calculating transmission probabilities $f(r)$. The most relevant information would be the terminal speed. If the terminal is static there would not be a possibility to postpone the transmission because there would be no chance that the terminal would assume a more preferable position in the near future. If v_{MAX} is the maximum speed of the terminal a possible modification of the transmission probability could be

$$f(r, v) = (1 - v/v_{MAX}) + (v/v_{MAX}) f(r) \tag{2.51a}$$

If more sophisticated cognition is available to provide information about the direction of terminal movement, then we can define direction D as

$$D = \frac{|\Delta\theta|}{\pi/2} = \frac{2|\Delta\theta|}{\pi} \tag{2.51b}$$

where $\Delta\theta$ is the angle between the direction mobile base and the terminal velocity vector. Now we can use the transmission probability as

$$f(r, v, \Delta\theta) = \begin{cases} 1; D > 1 \\ D + (1 - D) f(r, v); \ D < 1 \end{cases} \tag{2.51c}$$

An alternative definition of the directivity which is convenient to specify the Markov chain model appropriately is

$$D = \frac{q}{p + q + s} = q$$

where q can be estimated from the sojourn angle $\Delta\theta$ as $q = (360 - \Delta\theta)/360$. If q is represented as $q = kq'$, where k is an integer $0 \leq k \leq K_{\max}$, then the transmission probability function can be generated as

$$f(r, k) = (1 - r)^k \text{ or } f(r, k) = 1 - r^k$$

Parameter $K_{\max}$ is the design parameter and k is obtained from the observed value of $\Delta\theta$ in the optimization process. Depending on the type of service, the performance measure (pm) to be optimized may be either throughput S for data or message transmission delay τ for voice or a joint parameter $pm = S/\tau$. Parameter k is chosen to maximize pm as $k = \max_k \ pm$ and can be either pretabulated based on the results shown later or dynamically adjusted based on the observation of the pm. For delay constrained traffic we may use $f(r)$ as

$$f(r) = \begin{cases} f(r, v, \Delta\theta); \ \tau < \tau_{\max} \\ 1; \ \text{otherwise} \end{cases} \tag{2.51d}$$

where $\tau_{\max}$ is the maximum delay that can be tolerated. For fair scheduling we can use

$$f(r) = \begin{cases} \tau f(r, v, \Delta\theta); \ \tau < \tau_{\max} \\ 1; \ \text{otherwise} \end{cases} \tag{2.51e}$$

where users with longer starvations (time τ since the last transmission) are given higher priority. The above algorithms will be collectively referred to as traffic shaping multiple access (TSMA). When applied to multicarrier systems these protocols will be referred to as context aware broadband access (CABA).

2.8.4 User mobility modeling

For further analysis of the system we model user mobility by a Markov random walk model, shown in Figure 2.25(a), with states 0 and N modeled as reflective states (see below). The system is observed in discrete time intervals T seconds (packet or message length) apart and the state of a user represents its normalized distance r from the base station. In the mobility model we are not interested in the information on the angular position θ from Figure 2.24, because the decision on whether or not to transmit will depend only on r. On the other hand, the outcome of the transmission (success or collision) will also depend on θ and could be averaged out with respect to θ in the appropriate range. The state transition probabilities are given as

$$p = P(2\Delta > dr > \Delta), \ q = P(-2\Delta < dr < -\Delta), \ s = P(0 \leq |dr| \leq \Delta) \tag{2.52}$$

Suppose that the cell radius $R = 1$ is divided into $R/\Delta = N$ segments. Therefore the user movement across the cell is characterized by discrete state n, representing its current distance from the

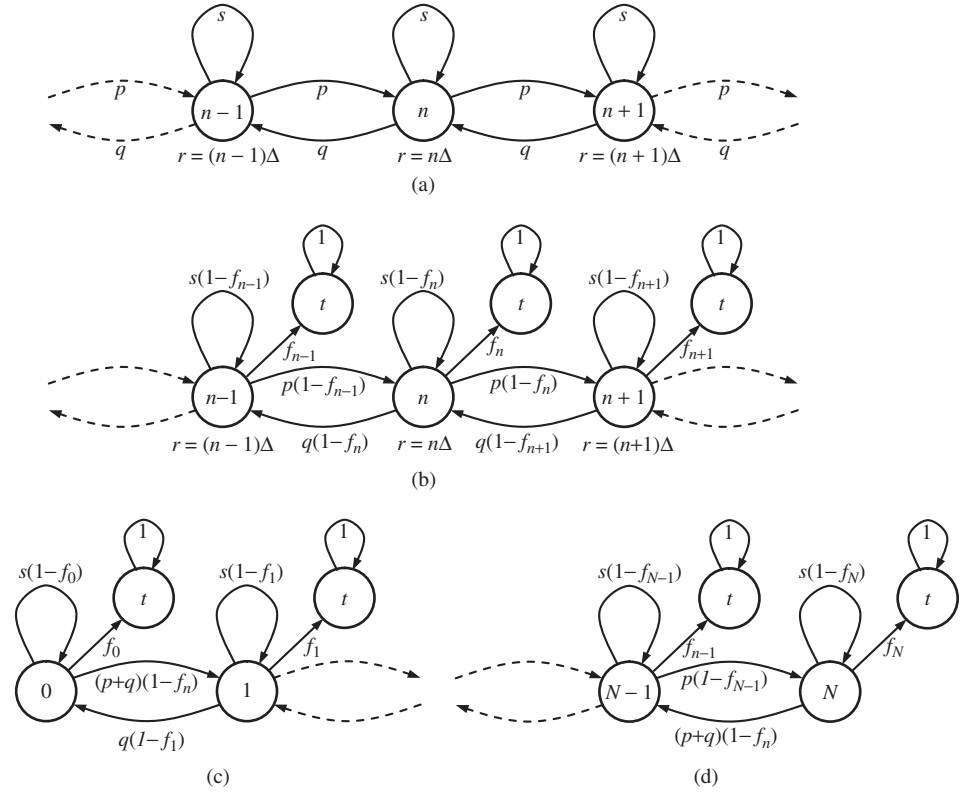

Figure 2.25 User mobility modeling: (a) reflecting Markov chain model; (b) to (d) absorbing Markov chain model.

base station $r = n\Delta$, the state transition probability $(N+1) \times (N+1)$ matrix $\mathbf{P}$ and initial state probability vector row $\mathbf{p}^{(0)}$, where

$$\begin{aligned} &\mathbf{P} = \|p_{ij}\| i, j = 0, 1, \ldots, N \\ &\mathbf{p}^{(0)} = (p_0^{(0)}, p_1^{(0)}, p_2^{(0)}, \ldots, p_N^{(0)}) \\ &\mathbf{p}^{(1)} = \mathbf{p}^{(0)}\mathbf{P} \\ &\mathbf{p}^{(k)} = \mathbf{p}^{(k-1)}\mathbf{P} = \mathbf{p}^{(0)}\mathbf{P}^k \end{aligned} \tag{2.53}$$

If we now introduce the row vector of transmission probabilities as

$$\mathbf{f} = (f_0, f_1, f_2, \ldots, f_N) \tag{2.54}$$

then the probability to transmit at instant $t_k = kT$ is given by recursion:

$$\begin{aligned} &p_t^{(0)} = \mathbf{p}^{(0)}\mathbf{f}^T \\ &p_t^{(1)} = (1 - p_t^{(0)})\mathbf{p}^{(1)}\mathbf{f}^T = (1 - \mathbf{p}^{(0)}\mathbf{f}^T)\mathbf{p}^{(0)}\mathbf{P}\mathbf{f}^T \\ &\vdots \\ &p_t^{(k)} = (1 - p_t^{(k-1)})\mathbf{p}^{(k)}\mathbf{f}^T = (1 - p_t^{(k-1)})\mathbf{p}^{(0)}\mathbf{P}^k\mathbf{f}^T \end{aligned} \tag{2.55}$$

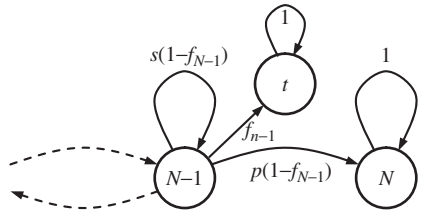

Figure 2.26 Handoff modeling.

The average transmission delay is given as

$$D = TE_k(kp_t^{(k)}) \tag{2.56}$$

We point out once again that for the above analysis states 0 and N are modeled as reflective states. For more information on mobility modeling see Reference [40].

2.8.5 Absorbing Markov chain system model

Although the above approach is straightforward it becomes impractical for producing numerical results. For this reason, in the sequel we present an alternative way to model the problem by using absorbing Markov chains, shown in Figure 2.25(b) to (d), where each state is also connected to an absorbing state t representing transmission.

The probability that the user leaves the cell (handoff) without transmission can be calculated by modeling state N and state t (transmission) as absorbing and state 0 as the reflecting state, with state transition probabilities defined as indicated in Figures 2.25 and 2.26. If $f_0 = 1$, state 0 also becomes the absorbing state:

$$\begin{aligned} &\mathbf{P} = \|p_{ij}\| \\ &p_{ij} \rightarrow p_{ij}(1 - f_i) \text{ for transient states} \\ &p_{it} = f_i \\ &p_{01} = (p + q)(1 - f_0) \\ &p_{NN-1} = 0 \end{aligned} \tag{2.57}$$

Next we reorganize the transmission matrix into $(N + 2) \times (N + 2)$ matrix of the form [41]

$$\mathbf{P}^* = \begin{bmatrix} \mathbf{I} & \mathbf{0} \\ \mathbf{R} & \mathbf{Q} \end{bmatrix} \tag{2.58}$$

where $\mathbf{I}$ is a 2×2 diagonal unitary matrix, $\mathbf{0}$ is **a** $2 \times N$ all-zero matrix, $\mathbf{R}$ is an $N \times 2$ matrix of transition probabilities from transient states to absorbing state t and $\mathbf{Q}$ is an $N \times N$ matrix of transition probabilities between the transient states. By using the notation $\mathbf{N} = (\mathbf{I} - \mathbf{Q})^{-1}$, the mean time for the process to reach any absorbing state starting from transient state i is [41]

$$\boldsymbol{\tau} = (\tau_0, \tau_1, \ldots, \tau_{N-1})^T = T(\mathbf{I} - \mathbf{Q})^{-1}\mathbf{1} = T\mathbf{N}\mathbf{1} \tag{2.59}$$

and if the dwell time $T_i = T$ for each state i is the same otherwise, then

$$\begin{aligned} &\boldsymbol{\tau} = (\tau_0, \tau_1, \ldots, \tau_{N-1})^T = (\mathbf{I} - \mathbf{Q})^{-1}\boldsymbol{\eta} = \mathbf{N}\boldsymbol{\eta} \\ &\boldsymbol{\eta} = \text{column vec } \{T_i\} \end{aligned} \tag{2.59a}$$

where $\mathbf{1}$ is an $N \times 1$ column vector of all once. In general, the variance of that time is

$$\text{var } \boldsymbol{\tau} = 2(\mathbf{I}-\mathbf{Q})^{-1}\mathbf{T}\mathbf{Q}(\mathbf{I}-\mathbf{Q})^{-1}\boldsymbol{\eta} + (\mathbf{I}-\mathbf{Q})^{-1}(\boldsymbol{\eta}_{sq}) - ((\mathbf{I}-\mathbf{Q})^{-1}\boldsymbol{\eta})_{sq}$$
$$\mathbf{T} = \text{diag matrix } \{T_i\} \tag{2.60}$$

and if the dwell times for each state is the same then

$$\text{var } \boldsymbol{\tau} = [(2\mathbf{N}-\mathbf{I})\mathbf{N}\mathbf{1} - (\mathbf{N}\mathbf{1})_{sq}]T^2$$
$$(\mathbf{N}\mathbf{1})_{sq} = \text{square of each component of } \mathbf{N}\mathbf{1} \tag{2.61}$$

The average time to reach absorbing state is

$$\tau_a = \mathbf{f}\boldsymbol{\tau} \tag{2.62}$$

where $\mathbf{f}$ is a row and $\boldsymbol{\tau}$ is a column vector. The probability that the Markov process starting in a transient state i ends up in an absorbing state j is b_{ij} where

$$B = [b_{ij}] = (\mathbf{I}-\mathbf{Q})^{-1}\mathbf{R} \tag{2.63}$$

The average probabilities of handoff and transmission from the cell are given as

$$\mathbf{a} = (a_1, a_2) = (p_h, p_t) = \mathbf{p}^{(0)}\mathbf{B} \tag{2.64}$$

If we are not interested from which cell the information is transmitted then state N should be modeled as a reflective state and only state t would be an absorbing state. By modifying the equations accordingly the average time to transmit or average waiting time would be calculated in the same way with the new model, and vector $\mathbf{a}$ would have only one element.

2.8.6 Throughput analysis

In general the amount of interference between the users will depend on their mutual distance. Therefore, for the analysis of the throughput we need to model joint mobility of the two interfering users belonging to two different cells. The model is based on a two-dimensional random walk process with states (i, j) representing the joint distance (r_a, r_b) of the two users with respect to their corresponding BSs. As explained earlier, only distance from the base station has an impact on the decision to transmit. For a given transmission the performance (success or collision) will depend on angle θ, shown in Figure 2.24, and performance could be averaged with respect to this parameter.

2.8.6.1 Low-mobility (or wide-beam) model

In this case we assume that during the transmission waiting period the two interfering users do not leave the interfering area. The walk of the process along $I(i)$ and $J(j)$ axes is independent and both of these walks can be represented by the model from Figure 2.25 with separate t states; call them $t(I)$ and $t(J)$. The state transition probabilities now have the form

$$p_{i_1 i_2, j_1 j_2} = P((i_1, j_1) \Rightarrow (i_2, j_2)) \tag{2.65}$$

which is the probability that the process moves from state (i_1, j_1) to the state (i_2, j_2) and the matrix $\mathbf{P}$ has the form

$$\mathbf{P} = \| p_{i_1 i_2, j_1 j_2} \|. \tag{2.66}$$

To analyze the throughput, states $t(I)$ and $t(J)$ should be converted into states S (successful transmission) if only one user was transmitting. An additional state C (collision) will be introduced

to represent the event when both users transmit simultaneously, producing a collision, which happens with probability $P_{out}(i, j)$. These probabilities can be represented as

$$p_{i_1 i_2, j_1 j_2} = \begin{cases} s(1-f_{i_1})s(1-f_{j_1});\ i_1 = i_2;\ j_1 = j_2 \\ s(1-f_{i_1})p(1-f_{j_1});\ i_1 = i_2;\ j_2 = j_1 + 1 \\ s(1-f_{i_1})q(1-f_{j_1});\ i_1 = i_2;\ j_2 = j_1 - 1 \\ s(1-f_{i_1})f_{j_1} = p_{i_1 i_2, j_1 s}\ (state\ S);\ i_1 = i_2;\ j_2 = t(J) \\ \\ p(1-f_{i_1})s(1-f_{j_1});\ i_1 = i_2 + 1;\ j_1 = j_2 \\ p(1-f_{i_1})p(1-f_{j_1});\ i_1 = i_2 + 1;\ j_2 = j_1 + 1 \\ p(1-f_{i_1})q(1-f_{j_1});\ i_1 = i_2 + 1;\ j_2 = j_1 - 1 \\ p(1-f_{i_1})f_{j_1} = p_{i_1 i_2, j_1 s}\ (state\ S);\ i_1 = i_2 + 1;\ j_2 = t(J) \\ \\ q(1-f_{i_1})s(1-f_{j_1});\ i_1 = i_2 - 1;\ j_1 = j_2 \\ q(1-f_{i_1})p(1-f_{j_1});\ i_1 = i_2 - 1;\ j_2 = j_1 + 1 \\ q(1-f_{i_1})q(1-f_{j_1});\ i_1 = i_2 - 1;\ j_2 = j_1 - 1 \\ q(1-f_{i_1})f_{j_1} = p_{i_1 i_2, j_1 s}\ (state\ S);\ i_1 = i_2 - 1;\ j_2 = t(J) \\ \\ f_{i_1}s(1-f_{j_1}) = p_{i_1 s, j_1 j_2};\ i_1 = t(I);\ j_1 = j_2 \\ f_{i_1}p(1-f_{j_1}) = p_{i_1 s, j_1 j_2};\ i_1 = t(I);\ j_2 = j_1 + 1 \\ f_{i_1}q(1-f_{j_1}) = p_{i_1 s, j_1 j_2};\ i_1 = t(I);\ j_2 = j_1 - 1 \\ f_{i_1}f_{j_1}(1 - P_{out}(i_1, j_1)) = p_{i_1 s, j_1 s}\ (state\ S);\ \ i_1 = t(I);\ j_2 = t(J) \\ f_{i_1}f_{j_1}P_{out}(i_1, j_1) = p_{i_1 c, j_1 c}\ (state\ C);\ i_1 = t(I);\ j_2 = t(J) \end{cases} \tag{2.67}$$

By modeling states S and C as absorbing states we can calculate the probability of successful transmission and throughput by using Equation (2.61). In the case of cell cooperation, only the states with mutual distance R would exist and matrix $\mathbf{P}$ should be modified accordingly. The rest of the analysis is the same.

The model can be further elaborated by having states C_{ij} and S_{ij} from each state (i, j) and transitions back to state (i, j). For low mobility the transitions would be with probability one to state (i, j) and for high mobility with equal probability $1/N$ to any other state. Any other mobility can be included to make more probable transitions closer to (i, j). Now the steady-state solutions of the system would give the steady-state probabilities of being in state S_{ij}.

More precisely, S_{ij} represents the throughput of a user in state i given that the interfering user is in state j. Similarly,

$$S_i = \sum_j S_{ij} \tag{2.68}$$

represents the average throughput of a user in state i and

$$S = \sum_i S_i = \sum_i \sum_j S_{ij} \tag{2.69}$$

represents the average throughput of the user.

The modified function $f(r, v)$, defined by Equation (2.51a) can be directly included in the model in Figure 2.25. Modifications that include directivity defined by (2.51b) and (2.51c) can be included by additionally modifying probabilities p, q and s accordingly, as discussed in the derivation of (2.51c). To include modifications defined by (2.51d) and (2.51e) the model has to be extended into the two-dimensional Markov model (τ, r), which also includes state dependency on the discrete value of τ, representing the number of times the message transmission has been postponed from/to the terminal, as shown in Figure 2.27.

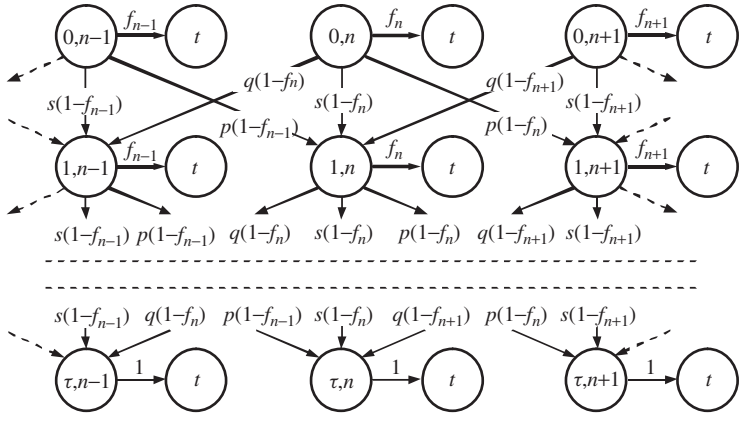

Figure 2.27 Two-dimensional Markov model of the opportunistic scheduling with delay constrained.

2.8.6.2 High-mobility (or narrow-beam) model

Due to higher mobility (or narrow beams), during the transmission waiting period the two users may leave the interfering area and interact with different users as interferers. The new interferer may have any position with respect to the reference user, which can be modeled by allowing the second user to transfer to any state with the same probability. It may also happen that in the new situation the reference user will not be jammed due to angular isolation. In a cognitive system this information may be available and the BS is free to transmit to the user at this moment so that $f(r)$ becomes one. A number of additional models are also possible, but due to the limited space we cannot go into further details.

2.8.6.3 Performance measure and system utility function

The concept discussed so far requires criteria for optimal transmission probability f_n. In this section we use the utility function to optimize location dependent f_n. One should be aware that we use the utility function only as a performance measure and do not use utility function decomposition techniques to implement and optimize the MAC protocol, as discussed later in Chapter 10. The utility function can be defined as

$$\begin{aligned} U_n &= (1 - 2P_{out}(n))f_n \\ U &= \sum_n U_n \\ f_n &= \max_{f_n} U \\ f_n &\in \Im = \{f_n(k)\} \end{aligned} \tag{2.70}$$

The set of feasible values for function $f_n \in \Im = \{f_n(k)\}$ can be generated from the function $f_n \rightarrow f_n(k) \rightarrow f(r,k) = f(n\Delta r, k) = (1-r)^k = (1-n\Delta r)^k$; $k = 1, 2, .., K_{\max}$, and $r \leq 1$, as discussed in Section 2.3. The first term $[1 - 2P_{out}(n)] \in [0, 1]$ in the expression for the utility function tries to minimize the errors. The second term is the transmission probability. Increasing f_n would increase U, but at the same time would increase the outage probability, which would tend to reduce U.

The previous expression does not include the delay. The delay D can be included in the optimization process in two ways:

$$\begin{aligned}&(1)\ \ f_n = \max_{f_n}(\alpha U - \beta D);\ f_n \in \Im = \{f_n\}\\ &(2)\ \ f_n = \max_{f_n} U;\ f_n \in \Im = \{f_n\}\\ &\text{subject to } D \le D_{\max}\end{aligned} \tag{2.71}$$

An alternative approach would be to define the utility function in state n as

$$\begin{aligned}&U_n = S_n\\ &U = S\\ &f_n = \max_{f_n} U;\ f_n \in \Im = \{f_n\}\end{aligned} \tag{2.72}$$

where S_n and S are given by Equations (2.68) and (2.69) with $i \to n$.

2.8.7 Collision resolution

2.8.7.1 Joint master/slave base MAC protocol

The network controller allocates the status M (master) or S (slave) *to the bases*. After the first transmission the neighboring cells find out the channels with collision, say k out of N. In the next transmission M basis use all channels and S basis only $N - k$ with no collision. The cognition is used to allocate M and S status, which may alternate depending on traffic. The average intercell throughput is

$$S = (2N - k)/(2N) = 1 - k/(2N) \tag{2.73}$$

2.8.7.2 Joint master/slave mobile MAC protocol

The terminals are classified as M (master with lower processing capabilities, e.g. a phone) or S (slave with higher processing capabilities, e.g. a PC). After the first transmission the neighboring cells find out the channels with collision, say k out of N. In the next transmission M terminals use the channels with no collisions and S terminals use the channels with collision and have to engage sp (signal processing)–separability (interference cancellation). The throughput now is 1.

2.8.8 Opportunistic transmission with intercell interference awareness

The concept discussed so far will achieve high probability of successful transmission per user when transmission occurs. Unfortunately the overall throughput (channel allocation efficiency per user) will be relatively low because of a significant percentage of time the user might have to wait to move into the position where the opportunity will arise to transmit with such high probability of success. From the network point of view (social optimum) it would be of interest to constantly use the resource so that a channel is always allocated to the user who has an opportunity to transmit. Therefore, in this section we consider a pure opportunistic approach where the access point allocates with equal probability $1/m$ channel to one out of m users who is in the *opportunity zone.* Suppose that we have k candidates for a channel allocation. We use a nonabsorbing Markov chain model from Figure 2.25(a) to represent individual user mobility where both state N and state 0 are reflecting states. For such a model we find steady state probabilities p_n. We define the *opportunistic zone* as a set of states around state $n = 0$ for which SIR is acceptable (no collision).

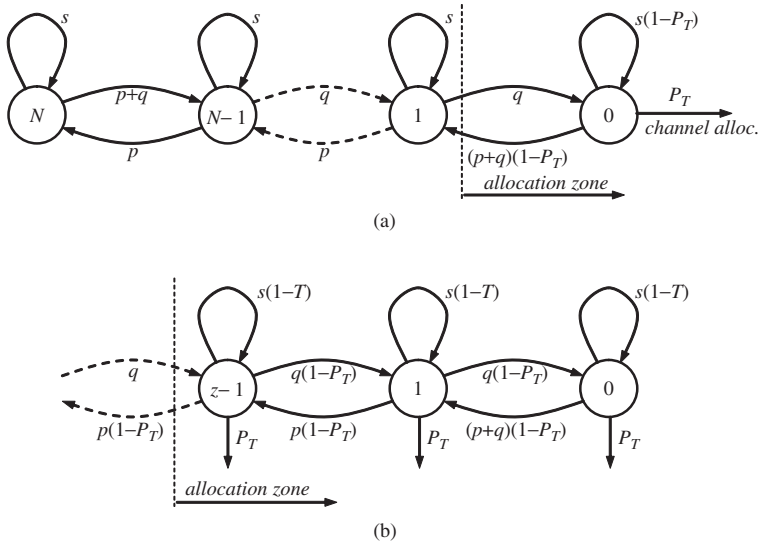

Figure 2.28 Model for message delivery time analysis: (a) z = 1; (b) allocation zone for z > 1.

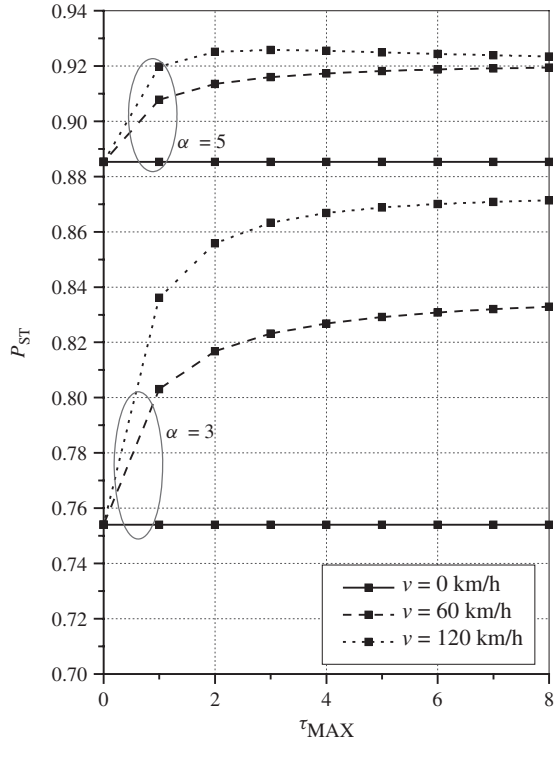

Figure 2.29 Probability of successful transmission as a function of maximum allowed transmission delay τ_{MAX}, $s = 0.5$, $p = q = (1 - s)/2$, $N = 4$, $\sigma_{\beta b} = 8$ dB, $\sigma_{b+d} = \sigma_b = 1$, $\varepsilon = 0.1$, $\theta = 45^{\circ}$, $v_{\max} = 120$ km/h.

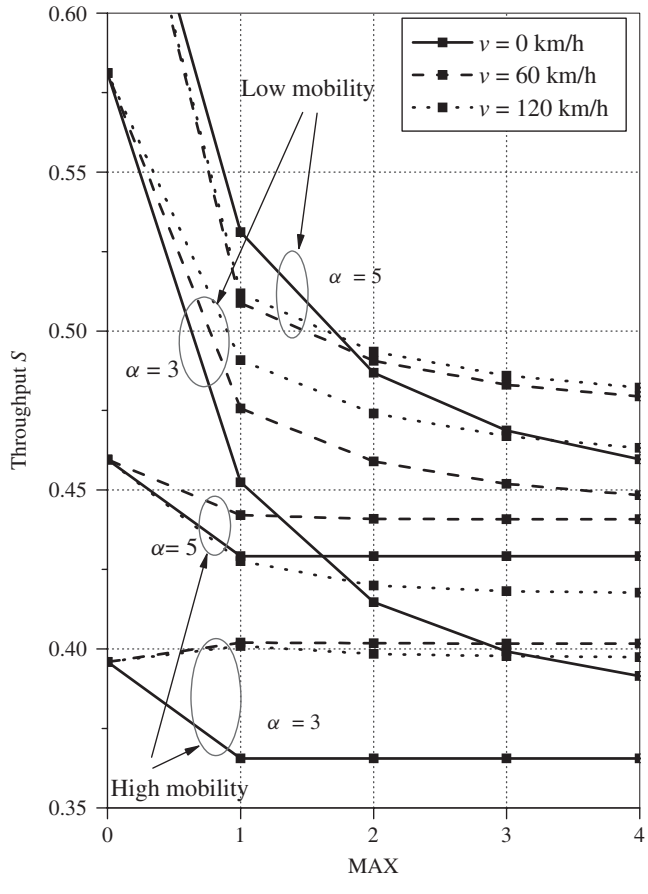

Figure 2.30 Average throughput as a function of maximum allowed transmission delay τ_{MAX}, $s = 0.5$, $p = q = (1 - s)/2$, $N = 4$, $\sigma_{\beta b} = 8\,\text{dB}$, $\sigma_{b+d} = \sigma_b = 1$, $\varepsilon = 0.1$, $\theta = 45^\circ$, $v_{\max} = 120\,\text{km/h}$.

Suppose that the size of the opportunity zone includes z states from the graph in Figure 2.25(a) including state $n = 0$. So the probability that a user is in the opportunity zone is

$$p(z) = \sum_{n=0}^{z-1} p_n \tag{2.74}$$

The probability of channel assignment is the probability that the opportunity zone is not empty, resulting in

$$P_S = 1 - [1 - p(z)]^k \tag{2.75}$$

For larger z, P_S is larger but the channels in the zone are of lower quality, which is equivalent to having less capacity per channel. Larger k will also increase S, but larger k will result in lower probability that the user will be chosen by the access point, which means longer delays in message delivery per user. To analyse the message delivery delay we use, for $z = 1$, the graph

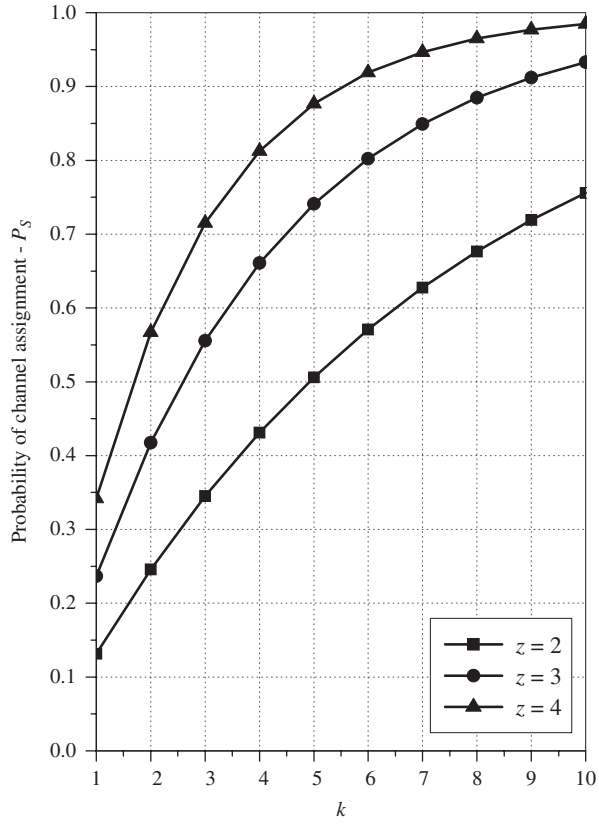

Figure 2.31 Probability of channel assignment as a function of number of users, $s = 0.5$, $p = q = (1 - s)/2$, $N = 10$.

from Figure 2.28, where

$$P_T = \sum_{m=1}^{k} \frac{1}{m} b_m$$
$$b_m = \binom{k}{m} p^m(z)[1 - p(z)]^{k-m} \tag{2.76}$$

Generalization may be obtained either by dimensioning the radius $\rho = \Delta$ of the zone in such a way that the level of intercell interference (ICI) is acceptable within the zone and not out of the zone or by including more states within the zone where transitions from state $n = 0$ will be copied z times, as in Figure 2.28(b). Now the average delivery time will be equal to the time for the process from Figure 2.28 to reach the absorbing state.

2.8.9 Performance examples

As an illustration of the proposed protocols performance, in this section we present some numerical results.

The probability of the successful transmission P_{ST} as a function of maximum allowed transmission delay τ_{MAX} is shown in Figure 2.29. The system is modeled with a Markov chain with three

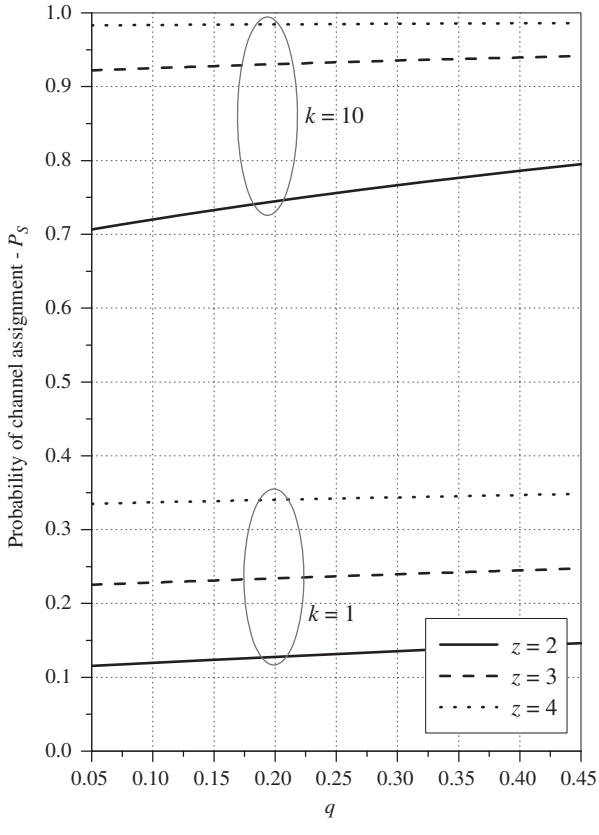

Figure 2.32 Probability of channel assignment as a function of transition probability q, $p = q$, $s = 1 - 2q$, $N = 10$.

absorbing states: successful transmission, collision and handoff. One can see that the higher τ_{MAX} and the higher mobile unit velocity v, the higher is the probability of a successful transmission since there is a higher probability for the user to get into position with a lower level of intercell interference. It should be noted that the case of $v = 0$ km/h leads to the probability of transmission $f = 1$, which represents the case of unregulated traffic. The improvement of the proposed traffic shaping is higher for lower values of propagation constant α.

Figure 2.30 shows the throughput as a function of τ_{MAX}. Higher τ_{MAX} leads to the higher probability of successful transmission, but users spend more time in waiting for the good opportunity to transmit, which results in lower overall throughput.

As already stated, in order to improve the throughput it would be of interest to constantly use the resource so that a channel is always allocated to the user who has the opportunity to transmit. The probability of channel assignment P_S as a function of the size of the opportunity zone z and the number of users k is shown in Figure 2.31. For larger z, P_S is larger, but the channels in the zone are of lower quality, which is equivalent to having less capacity per channel. Larger k will also increase P_S, but larger k will result in a lower probability that a specific user will be chosen by the access point, which means longer delays in message delivery per user.

The influence of transition probability q (transition probability towards the base station) on P_S is shown in Figure 2.32. It can be seen that the transition probability has a greater influence for higher numbers of users and for a lower width of the opportunity zone.

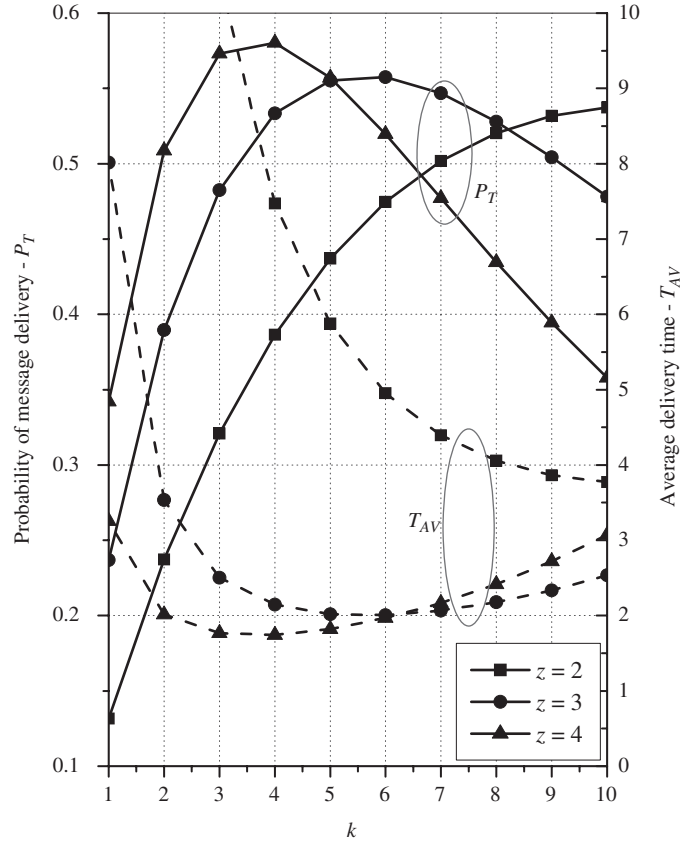

Figure 2.33 Probability of message delivery and average delivery time as a function of number of users, $s = 0.5$, $p = q = (1 - s)/2$, $N = 10$.

Figure 2.33 illustrates the average probability of message delivery P_T and the average normalized delivery time T_{AV}. The normalization is performed with respect to the time needed for the process to change state. In our models this time is fixed and equal to the message length. Therefore T_{AV} represents the number of times the message transmission from/to the terminal has been postponed. For lower number of users, both parameters improve (P_T is higher and T_{AV} is lower). After that, there is an optimum, which depends on the opportunity zone width. Finally, for high numbers of users P_T decreases and T_{AV} increases.

REFERENCES

[1] P. Viswanath, D. Tse and R. Laroia, Opportunistic beamforming using dumb antennas, *IEEE Trans. Information Theory*, vol. 48, no. 6, June 2002, pp. 1277–1294.

[2] D. N. C. Tse, Optimal power allocation over parallel Gaussian channels, in *Proc. Int. Symp. Information Theory*, Ulm, Germany, June 1997.

[3] M. Vemula, D. Avidort, J. Lingt and C. Papadias, Inter-cell coordination, opportunistic beamforming and scheduling, *ICC'06*, vol. 12, June 2006, pp. 5319–5324.

[4] J. Wang, H. Zhai, Y. Fang, J. M. Shea and D. Wu, OMAR: utilizing multiuser diversity in wireless ad hoc networks, *IEEE Trans. Mobile Computing*, vol. 5, no. 12, December 2006, pp. 1764–1779.
[5] T. Hou and T. Tsai, An access-based clustering protocol for multihop wireless ad hoc networks, *IEEE J. Selected Areas Commun.*, vol. 19, no. 7, July 2001.
[6] B. Sadeghi, V. Kanodia, A. Sabharwal and E. Knightly, Opportunistic medium access for multirate ad hoc networks, in *Proc. MobiCom '02*, 2002.
[7] R. Knopp and P. A. Humblet, Information capacity and power control in single-cell multiuser communications, in *Proc. Int. Conf. Commun.*, 1995.
[8] D. Tse and S. Hanly, Multi-access fading channels: Part I: polymatroid structure, optimal resource allocation and throughput capacities, *IEEE Trans. Information Theory*, vol. 44, no. 7, November 1998, pp. 2796–2815.
[9] P. Bender, P. Black, M. Grob, R. Padovani, N. Sindhushayana and A. Viterbi, CDMA/HDR: a bandwidth efficient high speed wireless data service for nomadic users, *IEEE Commun. Mag.*, vol. 38, no. 7, July 2000, pp. 70–77.
[10] M. Hu and J. Zhang, Opportunistic multi-access: multiuser diversity, real-aided opportunistic scheduling, and traffic-aided admission control, *J. Special Topics in Mobile Networking and Applications*, vol. 9, 2004, pp. 435–444.
[11] D. Park, H. Seo, H. Kwon and B. G. Lee, Wireless packet scheduling based on the cumulative distribution function of user transmission rates, *IEEE Trans. Commun.*, vol. 53, no. 11, 2005, pp. 1919–1929.
[12] J. Wang, H. Zhai and Y. Fang, Opportunistic packet scheduling and media access control for wireless LANs and multi-hop ad hoc networks, in *Proc. IEEE Wireless Commun. and Networking Conf. (WCNC '04)*, March 2004.
[13] J. Wang, H. Zhai, Y. Fang and M. C. Yuang, Opportunistic media access control and rate adaptation for wireless ad hoc networks, in *Proc. IEEE Commun. Conf. (ICC '04)*, June 2004.
[14] X. Qin and R. Berry, Exploiting multiuser diversity for medium access control in wireless networks, in *Proc. INFOCOM '03*, 2003.
[15] X. Qin and R. Berry, Opportunistic splitting algorithms for wireless networks, in *Proc. INFOCOM '04*, 2004.
[16] P. Larsson, Selection diversity forwarding in a multihop packet radio network with fading channel and capture, *Mobile Computing and Commun. Rev.*, vol. 5, no. 4, 2001, pp. 47–54.
[17] S. Biswas and R. Morris, Opportunistic routing in multi-hop wireless networks, in *Proc. Second Workshop Hot Topics in Networks (HotNets II)*, November 2003.
[18] R. R. Choudhury and N. H. Vaidya, MAC-layer anycasting in wireless ad hoc networks, in *Proc. Second Workshop Hot Topics in Networks (HotNets II)*, November 2003.
[19] S. Jain, Y. Lv and S. R. Das, Exploiting path diversity in the link layer in wireless ad hoc networks, Technical Report, WINGS Lab, July 2003.
[20] J. Wang, H. Zhai, W. Liu and Y. Fang, Reliable and efficient packet forwarding by utilizing path diversity in wireless ad hoc networks, in *Proc. IEEE Military Commun. Conf. (Milcom '04)*, November 2004.
[21] C.-C. Chiang, G. Pei, M. Gerla and T.-W. Chen, Scalable routing strategies for ad hoc wireless networks, *IEEE J. Selected Areas Commun.*, vol. 17, 1999, pp. 1369–1379.
[22] A. B. McDonald and T. F. Znati, A mobility-based framework for adaptive clustering in wireless ad hoc networks, *IEEE J. Selected Areas Commun.*, vol. 17, no. 8, August 1999.
[23] T. Hou and T. Tsai, An access-based clustering protocol for multihop wireless ad hoc networks, *IEEE J. Selected Areas Commun.*, vol. 19, no. 7, July 2001.
[24] J. J. Garcia-Luna-Aceves and A. Tzamaloukas, Receiver-initiated collision-avoidance in wireless networks, in *ACM Wireless Networks*, Special Issue on selected papers from MobiCom '99, vol. 8, no. 2/3, 2002, pp. 249–263.

[25] Y. Wang and J. J. Garcia-Luna-Aceves, A new hybrid channel access scheme for ad hoc networks, *ACM Baltzer Wireless Networks J.*, vol. 10, no. 4, July 2004.
[26] X. Liu, E. K. P. Chong and N. B. Shroff, Opportunistic transmission scheduling with resource-sharing constraints in wireless networks, *IEEE J. Selected Areas Commun.*, vol. 19, no. 10, October 2001, pp. 2053–2064.
[27] S. Hussain Ali, V. Krishnamurthy and C. M. Leung, Optimal and approximate mobility-assisted opportunistic scheduling in cellular networks, *IEEE Trans. Mobile Computing*, Vol. 6, No. 6, June 2007, p. 633.
[28] H. Kushner and G. Yin, *Stochastic Approximation Algorithms and Applications*. Springer-Verlag, 1997.
[29] X. Liu, E. K. P. Chong and N. B. Shroff, A framework for opportunistic scheduling in wireless networks, *Computer Networks*, vol. 41, no. 4, March 2003, pp. 451–474.
[30] T. Bonald and A. Proutiere, Wireless downlink data channels: user performance and cell dimensioning, in *Proc. MobiCom*, September 2003, pp. 339–352.
[31] I. Medhi, *Stochastic Models in Queueing Theory*. Academic Press, 1991.
[32] H. S. Wang and N. Moayeri, Finite-state Markov channel – A useful model for radio communication channels, *IEEE Trans. Vehicular Technology*, vol. 44, no. 1, February 1995, pp. 163–171.
[33] Q. Liu, S. Zhou and G. B. Giannakis, Queuing with adaptive modulation and coding over wireless links: cross-layer analysis and design, *IEEE Trans. Wireless Commun.*, vol. 4, no. 3, May 2005, pp. 1142–1153.
[34] S. Glisic, *Advanced Wireless Communications*, 2nd Edition. John Wiley and Sons, Ltd: London, 2007.
[35] Y. Zhao, Standardization of mobile phone positioning for 3G systems, *IEEE Commun. Mag.*, vol. 40, no. 7, July 2002, pp. 108–116.
[36] D. Hong and S. S. Rappaport, Traffic model and performance analysis for cellular mobile radio telephone systems with prioritized and nonprioritized handoff procedures, *IEEE Trans. Vehicular Technology*, vol. 35, no. 3, August 1986, pp. 77–92.
[37] T. Liu, P. Bahl and I. Chlamtac, Mobility modeling, location tracking and trajectory prediction in wireless ATM networks, *IEEE J. Selected Areas Commun.*, vol. 16, no. 6, August 1998, pp. 922–936.
[38] Z. R. Zaidi and B. L. Mark, Real-time mobility tracking algorithms for cellular networks based on Kalman filtering, *IEEE Trans. Mobile Computing*, vol. 4, no. 2, March/April 2005, pp. 195–208.
[39] S. H. Ali, V. Krishnamurty and V. Leung, Optimal and approximate mobility-assisted opportunistic scheduling in cellular networks, *IEEE Trans. Mobile Computing*, vol. 6, no. 6, June 2007, pp. 633–648.
[40] T. Camp, I. Boleng and V. Davies, A survey of mobility models for ad hoc network research, *Wireless Commun. and Mobile Computing (WCMC)*, Special Issue on Mobile Ad Hoc Networking, vol. 2, no. 5, 2002, pp. 483–502.
[41] J. G. Kemeny and J. L. Snell, *Finite Markov Chains*. Springer Verlag: New York, 1976.
[42] N. Milosevic, B. Lorenzo, B. Nikolic and S. Glisic, Opportunistic scheduling with spatial traffic shaping, in preparation.

3

Relaying and Mesh Networks

3.1 RELAYING STRATEGIES IN COOPERATIVE CELLULAR NETWORKS

In a wireless network with many source–destination pairs, cooperative transmission by relay nodes has the potential to improve the overall network performance. When a relay or a group of relays are physically located between the source and the destination, the relays may facilitate transmission by first decoding the transmitted codeword and then forwarding the decoded codeword to the destination. This strategy is known as decode-and-forward (DF). Alternatively, a relay may simply amplify its received signal and employ a so-called amplify-and-forward (AF) strategy. In both cases, the use of relay has been shown to improve the overall transmission rates [1] and/or the diversity [2–7] of the wireless network or some other performance measure [8–40].

This section focuses on physical layer relaying strategies where the source and the relay transmit in the same frequency, but in two different timeslots, so that at each frequency tone, the destination receives and processes data sent by the source and the relay in both timeslots. Both DF and AF strategies are considered.

We will use a utility maximization framework in which each data stream has an associated utility function, and the objective is to maximize the sum utility in the network. This network utility maximization framework has been recently applied to many physical-layer design problems as well as in crosslayer optimization, discussed in Chapter 10. A utility function is a concave and increasing function of data rates that reflects user satisfaction. The choice of utility function depends on the underlying application (e.g. data, voice, video). By maximizing the sum utility, a network operator maintains a balance between competing resource demands by different users in a network.

3.1.1 The system model

In this section it is assumed that the base station dictates when and how the user nodes may cooperate, which is realistic in a cellular environment with centralized control. The distributed algorithms will be discussed in the next section. The cooperative cellular network of interest is shown in Figure 3.1. The network consists of a base station and K user nodes, all of which are equipped with

Advanced Wireless Technologies: Cognitive, Cooperative & Opportunistic 4G Technology Second Edition Savo G. Glisic

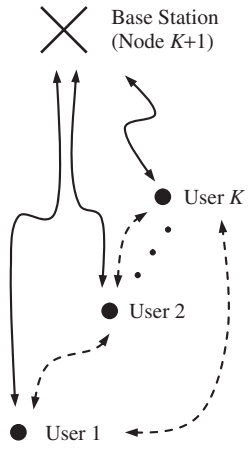

Figure 3.1 A cooperative cellular network with a base station and K users.

a single antenna. In the sequel $\mathcal{K} = \{1, 2, \ldots, K\}$ will denote the set of user nodes, the base station will be considered as node $K + 1$ and $\mathcal{K}_+ = \{1, 2, \ldots, K + 1\}$ will denote the extended set of nodes. Each of the K user nodes has both downstream and upstream communications with the base station. If (s, d) is a source–destination pair, or data stream, then the set of all data streams $\mathcal{M}$ is

$$\{(1, K + 1), (2, K + 1), \ldots, (K, K + 1), (K + 1, 1), (K + 1, 2), \ldots, (K + 1, K)\}$$

Set $\mathcal{M}$ has $2K$ elements.

The model assumes that the cooperative network employs an OFDMA physical layer with the set of tones $\mathcal{N} = \{1, \ldots, N\}$, where the OFDM frames are synchronized throughout the network, so that cooperative transmission takes place in a tone-by-tone basis and transmissions in different frequency tones do not interfere with each other. The wireless channel is modelled as a frequency-selective fading channel with uncorrelated fading between tones.

The network operates in a slow fading environment, so that channel estimation is possible and full channel side-information (CSI) is available at the base station. With suitable modifications, the optimization framework is also applicable to a frequency–flat fading environment if rate adaptation across fading states is possible.

It is assumed that only one data stream can be active in each tone and each of the $2K$ data streams can use more than one frequency tone. The active stream in each tone can use at most one relay (where the relay node can be any one of the other $K - 1$ user nodes), as illustrated in Figure 3.2.

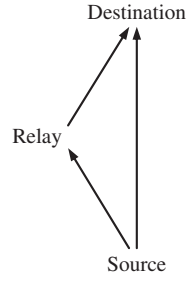

Figure 3.2 A single-relay channel.

The source-relay, source-destination and relay-destination links all use the same frequency tone. The upstream and downstream transmissions take place simultaneously in the network, so that the base station is both a source and a destination (but in different tones). The base station can never be a relay. On the other hand, all user nodes in the network can simultaneously be a source, a relay and a destination (again in different tones). The main challenge in designing such a network is to *allocate power and bandwidth optimally across all frequency tones and across all nodes*. If $\boldsymbol{P}$ is a $(K+1) \times N$ matrix such that $P(i,n)$ denotes the power expended by node i in tone n ($i \in \mathcal{K}_+, n \in \mathcal{N}$) then, because only one data stream is active in each tone and only the source and the relay may transmit, the column vector $P(:,n)$ ($n \in \mathcal{N}$) has at most two nonzero entries. Similarly, if $\boldsymbol{R}$ is a $2K \times N$ matrix with $R(m,n)$ denoting the data rate of stream m in tone $n (m \in \mathcal{M}, n \in \mathcal{N})$ then, since only one stream can be active in each tone, the column vector $R(;,n)$ ($n \in \mathcal{N}$) has at most one nonzero entry. Power and rate are related by the achievable rate region, denoted as $\boldsymbol{R} \in \mathcal{C}(\boldsymbol{P})$. The achievable rate region is the set of all possible rates achievable at a given power level. It implicitly accounts for the best possible use of relay strategies.

By definition, for $\mathbf{1} = (1, 1, \ldots 1)^{\mathrm{T}}$, $(\boldsymbol{P}1)_i$ ($i \in \mathcal{K}_+$), which is the row sum of $\boldsymbol{P}$, is the total power expended at node i, summing across all tones. Each node has a separate power constraint, $\mathbf{p}^{\max} = [p_1^{\max}, p_2^{\max}, \ldots, p_{K+1}^{\max}]^{\mathrm{T}}$, where $p_i^{\max}$ is the individual power constraint for node i. Similarly, $(\boldsymbol{R}\mathbf{1})_m (m \in \mathcal{M})$, which is the row sum of $\boldsymbol{R}$, gives the total data rate of stream m, summing across all tones.

3.1.2 System optimization

If U_m is the utility function of data stream m, which depends on the achievable rate of stream m, i.e. $(\boldsymbol{R}\mathbf{1})_m$, the objective of the optimization problem is to choose the active data stream optimally and allocate power in each tone, while at the same time selecting the best relay node and the best relay strategy, in order to maximize the network sum utility. In other words, the optimization problem is defined formally as

$$\begin{aligned} &\max_{\boldsymbol{P},\boldsymbol{R}} \sum_{m \in \mathcal{M}} U_m((\boldsymbol{R}\mathbf{1})_m) \\ &\text{subject to } \boldsymbol{P}\mathbf{1} \preceq \boldsymbol{p}^{\max}, \ \boldsymbol{R} \in \mathcal{C}(\boldsymbol{P}) \end{aligned} \tag{3.1}$$

The model assumes a slow-fading environment with full channel state information (CSI) in which adaptive power and bit loading may be implemented in a centralized fashion. In a practical system, channel estimation needs to be done at the receivers and fed back to the base station, which then must solve the above optimization problem and inform all users of the appropriate power levels and cooperative strategies. Finding the optimal solution of problem (3.1) involves a search over all possible power and bandwidth allocations and over all possible relays and relay strategies.

The optimization problem (3.1) has a zero duality gap in the limit as the number of OFDM tones goes to infinity [1]. The zero duality gap result enables convex optimization techniques to be used for solving the utility maximization problem (3.1). The rest of this section develops a Lagrangian dual decomposition approach to solve (3.1). For these purposes we first introduce a new variable

$$t = \left[t_{(1,K+1)}, t_{(2,K+1)}, \ldots, t_{(K,K+1)}, t_{(K+1,1)}, t_{(K+1,2)}, \ldots, t_{(K+1,K)}\right]^{\mathrm{T}}$$

and rewrite (3.1) as

$$\begin{aligned} &\max_{\boldsymbol{P},\boldsymbol{R},\boldsymbol{t}} \sum_{m \in \mathcal{M}} U_m(t_m) \\ &\text{subject to } \boldsymbol{P}\mathbf{1} \preceq \boldsymbol{p}^{\max}, \quad \boldsymbol{R}\mathbf{1} \succeq \boldsymbol{t}, \quad \boldsymbol{R} \in \mathcal{C}(\boldsymbol{P}) \end{aligned} \tag{3.2}$$

By relaxing the constraint $\boldsymbol{R}\mathbf{1} \succeq t$, the Lagrangian becomes

$$\begin{aligned} L(\boldsymbol{P},\boldsymbol{R},\boldsymbol{t},\lambda) &= \sum_{m\in\mathcal{M}} U_m(t_m) + \lambda^{\mathrm{T}}(\boldsymbol{R}\mathbf{1} - \mathbf{t}) \\ &= \sum_{m\in\mathcal{M}} \left\{ U_m(t_m) + \lambda_m \left[\sum_{n\in\mathcal{N}} R(m,n) - t_m \right] \right\} \end{aligned} \tag{3.3}$$

In (3.3), $\lambda = [\lambda_{(1,K+1)}, \lambda_{(2,K+1)}, \ldots, \lambda_{(K,K+1)}, \lambda_{(K+1,1)}, \lambda_{(K+1,2)}, \ldots, \lambda_{(K+1,K)}]^{\mathrm{T}}$, with each element $\lambda_m (m \in \mathcal{M})$ being a dual variable corresponding to stream m. The dual function

$$g(\lambda) = \begin{cases} \max\limits_{\boldsymbol{P},\boldsymbol{R},\boldsymbol{t}} & L(\boldsymbol{P},\boldsymbol{R},\boldsymbol{t},\lambda) \\ \text{subject to} & \boldsymbol{P}\mathbf{1} \preceq p^{\max}, \quad \boldsymbol{R} \in \mathcal{C}(\boldsymbol{P}) \end{cases} \tag{3.4}$$

consists of application-layer variable $\mathbf{t}$ and physical layer variables $\boldsymbol{P}$ and $\boldsymbol{R}$. Function $g(\lambda)$ can be separated into two maximization subproblems, a utility maximization problem, corresponding to a rate adaptation problem in the application layer,

$$g_{appl}(\lambda) = \max_{t} \sum_{m\in\mathcal{M}} (U_m(t_m) - \lambda_m t_m) \tag{3.5}$$

and a joint relay strategy and relay node selection and power and bandwidth allocation problem in the physical layer,

$$g_{phy}(\lambda) = \begin{cases} \max\limits_{\boldsymbol{P},\boldsymbol{R}} & \sum\limits_{m\in\mathcal{M}} \lambda_m \sum\limits_{n\in\mathcal{N}} R(m,n) \\ \text{subject to} & \boldsymbol{P}\mathbf{1} \preceq p^{\max}, \quad \boldsymbol{R} \in \mathcal{C}(\boldsymbol{P}) \end{cases} \tag{3.6}$$

Equations (3.2) to (3.6) define a layered approach to the sum utility maximization problem. The interaction between the layers is controlled through the use of the dual variable λ as a set of weighting factors, which centrally coordinates the application layer demand and physical layer supply of rates. The dual variable λ has a pricing interpretation: $\lambda_m (m \in \mathcal{M})$ represents the amount of money per unit of bit rate. As a supplier of data rates, the physical layer attempts to maximize the total revenues by adaptively allocating power and bandwidth and selecting the best choice of relay and relaying scheme in each tone. A higher value of λ_m induces the physical layer to allocate more resources to the corresponding data stream. As a consumer of data rates, the application layer aims to maximize the sum utility discounted by the total cost of data rates. A higher value of λ_m indicates that the cost of rate for the corresponding data stream is high, thus inducing the application layer to lower traffic demand. Finally, because the sum utility maximization problem (3.2) has a zero duality gap, it can be solved by minimizing the dual objective:

$$\begin{aligned} &\min_{\lambda} g(\lambda) \\ &\text{subject to } \lambda \succeq 0 \end{aligned} \tag{3.7}$$

This dual problem can be solved by updating λ using a subgradient method (see Chapter 10 and Reference [41]) as follows:

(1) *Initialize* $\lambda^{(0)}$.

(2) *Given* $\lambda^{(l)}$, *solve the two subproblems (3.5) and (3.6) separately to obtain the optimal values* $\mathbf{t}^*, \mathbf{P}^*$ *and* $\mathbf{R}^*$.

(3) *Perform a subgradient update for* λ *(see Chapter 10):*

$$\boldsymbol{\lambda}^{(l+1)} = \left[\boldsymbol{\lambda}^{(l)} + (\mathbf{v}^{(l)})^{\mathrm{T}}(\mathbf{t}^{*} - \mathbf{R}^{*}\mathbf{1})\right]^{+} \tag{3.8}$$

(4) *Return to step 2 until convergence.*

The convergency is guaranteed if the step sizes $v^{(l)}$ are chosen following a diminishing step size rule [42]. With the optimal dual variables, the optimal primal variables can then be found easily.

The physical layer joint relay strategy and relay node selection and resource allocation problem can be solved efficiently by introducing another set of pricing variables that accounts for the cost of power. This second decomposition at the physical layer, together with the first decomposition described in the previous discussion, solves the overall utility maximization problem globally and efficiently.

3.1.2.1 Application layer subproblem

Finding the optimal solution of $g_{appl}(\lambda)$ as described in problem (3.5) is straightforward. Problem (3.5) can be solved by maximizing each of the summation terms separately. This means that the system searches for the optimal user traffic demand t_m^* independently for each stream m, balancing the stream's utility with the cost of rate. Since U_m is a concave function of t_m, $(U_m(t_m) - \lambda_m t_m)$ is also a concave function of $t_m (m \in \mathcal{M})$ and t_m^* can be found by taking the derivative of $(U_m(t_m) - \lambda_m t_m)$ with respect to t_m and setting it to zero.

Many different choices of utility functions are possible depending on the application. As an example for a given data rate t (in Mbps), we use the utility function as in Reference [1]:

$$U(t) = \begin{cases} a(1 - \mathrm{e}^{-bt}), & \text{if } t \geq 0, \\ -\infty, & \text{if } t < 0 \end{cases} \tag{3.9}$$

where a and b are strictly positive real numbers, as shown in Figure 3.3.

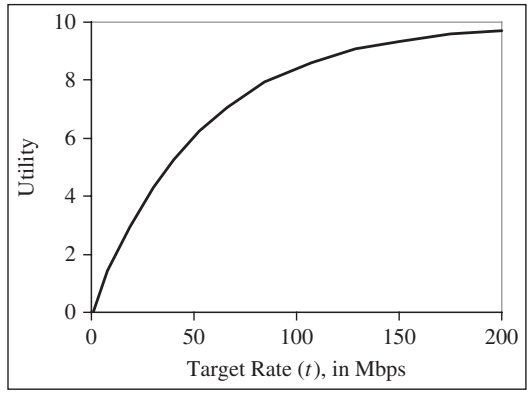

Figure 3.3 An example of a utility function $U(t) = 10(1 - \mathrm{e}^{-1.8421\times10^{-8}t})$. (Reproduced by permission of IEEE © 2007 from Ng and Yu [1]).

In the application layer subproblem, the per-stream maximization is of the form $(U(t) - \lambda t)$, where λ is a constant, resulting in

$$t^* = \max\left(0, -\frac{1}{b}\ln\frac{\lambda}{ab}\right) \tag{3.10}$$

representing the value of t that maximizes $(U(t) - \lambda t)$.

3.1.2.2 Physical layer subproblem

Finding the optimal $\boldsymbol{R}$ involves selecting the best data stream, power allocation, relay node and relaying strategy in each tone. However, the per-node power constraint implies coupling across tones. This section introduces a second decomposition step that relaxes the power constraint. This removes the coupling across tones, resulting in a procedure that is linear in the number of tones. The main technique here is similar to the weighted sum-rate maximization problem considered in Reference [43].

The main step is to relax the power constraint $\boldsymbol{P}1 \prec p^{\max}$ by introducing prices into the objective function of Equation (3.6):

$$\begin{aligned} Q &= \sum_{m\in\mathcal{M}} \lambda_m \sum_{n\in\mathcal{N}} R(m,n) + \mu^{\mathrm{T}}(p^{\max} - \boldsymbol{P}1) \\ &= \sum_{m\in\mathcal{M}} \lambda_m \sum_{n\in\mathcal{N}} R(m,n) + \sum_{i\in\mathcal{K}} \mu_i \left(p_i^{\max} - \sum_{n\in\mathcal{N}} P(i,n)\right) \end{aligned} \tag{3.11}$$

In Equation (3.11), $\mu = [\mu_1, \mu_2, \ldots, \mu_{K+1}]^{\mathrm{T}}$ is a vector dual variable. The dual function of the physical layer subproblem

$$q(\mu) = \begin{cases} \max\limits_{\boldsymbol{P},\boldsymbol{R}} & Q(\boldsymbol{P},\boldsymbol{R},\boldsymbol{\lambda},\boldsymbol{\mu}) \\ \text{subject to} & \boldsymbol{R} \in \mathcal{C}(\boldsymbol{P}) \end{cases} \tag{3.12}$$

can now be decoupled into N per-tone maximization subproblems

$$\begin{aligned} &\max_{\boldsymbol{P}(:,n),\boldsymbol{R}(:,n)} \sum_{m\in\mathcal{M}} \lambda_m R(m,n) - \sum_{i\in\mathcal{K}_+} \mu_i P(i,n) \\ &\text{subject to} \quad R(:,n) \in \mathcal{C}(P(:,n)) \end{aligned} \tag{3.13}$$

There is only one active stream in each tone, and only the source $\mathcal{S}$ and relay $\mathcal{R}$ expend power. Therefore, problem (3.13) can also be written as

$$\begin{aligned} &\max \quad \lambda_m R(m,n) - \left[\mu_{\mathcal{S}} P(\mathcal{S},n) + \mu_{\mathcal{R}} P(\mathcal{R},n)\right] \\ &\text{subject to} \quad R(:,n) \in \mathcal{C}(P(:,n)) \end{aligned} \tag{3.14}$$

In problem (3.14) the maximization is over m, choice of $\mathcal{R}$, $R(m,n)$, $P(\mathcal{S},n)$ and $P(\mathcal{R},n)$. The relaxation of $\boldsymbol{P}1 \preceq \mathbf{p}^{\max}$ removes the per-node power constraint. The per-tone problem (3.14) is easier to solve than the original physical layer subproblem.

The physical layer subproblem is decoupled across tones and the computational complexity becomes linear in the number of tones N. Again, using a pricing interpretation, $\mu_i (i \in \mathcal{K}_+)$ represents the amount of money per unit of power at node i. A higher value of μ_i discourages node i from expending power, while a lower value of μ_i does the opposite. Thus, the physical layer subproblem tries to maximize total revenue of data rates discounted by the cost of power. Together, λ and μ act as a set of weighting factors to determine centrally the optimal resource allocations and relay strategy at each tone.

A critical requirement for the decomposition of the physical layer subproblems into N per-tone subproblems is its convexity structure. The physical layer subproblem (3.6) can always be made a convex function of $\mathbf{p}^{\max}$ if time or frequency sharing can be implemented. Therefore, the physical layer subproblem also has a zero duality gap, and it can be solved optimally via the dual problem

$$\min_{\mu} q(\mu) \quad \text{subject to} \quad \mu \rightarrow \succeq 0 \tag{3.15}$$

Again, a subgradient approach with appropriate step sizes $\varepsilon^{(l)}$ may be used to solve the dual problem.

(1) *Initialize* $\mu^{(0)}$.

(2) *Given* $\mu^{(l)}$, *solve the* N *per-tone maximization problems (3.14) separately; then combine the results to obtain* P^* *and* R^*.

(3) *Perform subgradient updates for* μ:

$$\mu^{(l+1)} = [\mu^{(l)} + (\varepsilon^{(l)})^{\mathrm{T}}(P^*1 - p^{\max})]^+ \tag{3.16}$$

(4) *Return to step 2 until convergence.*

3.1.3 Relay strategy selection optimization

The previous discussion shows that in a cooperative cellular network employing OFDMA for each tone $n(n \in \mathcal{N})$ the per-tone problem is a maximization of $\lambda_m R(m,n) - \mu_{\mathcal{S}} P(\mathcal{S},n) - \mu_{\mathcal{R}} P(\mathcal{R},n)$, where λ_m, $\mu_{\mathcal{S}}$ and $\mu_{\mathcal{R}}$ are fixed dual variables. In this section we show that this per-tone maximization problem can be solved efficiently via an exhaustive search. $R(m,n)$ can be considered as the optimizing variable and $P(\mathcal{S},n)$ and $P(\mathcal{R},n)$ can be expressed as functions of $R(m,n)$. As any practical system has a finite constellation, bit rate is always discrete. As a result, the per-tone problem can be solved by an exhaustive search over a finite set defined by:

(a) *Active data stream:* $m(m \in \mathcal{M})$ *(which also implicitly determines* $\mathcal{S}$ *and* $\mathcal{D}$*).*

(b) *Relay node:* $\mathcal{R}(\mathcal{R} \in \mathcal{K}, \mathcal{R} \neq \mathcal{S}$ or $\mathcal{D})$.

(c) *Relaying strategy:* {*channel, decode-and-forward, amplify-and-forward*}.

(d) *Bit rate:* $R(m,n)$.

The size of the search set is the product of the number of data streams, potential relays, relay strategies and possible bit rates. An exhaustive search over such a discrete set is often feasible for a practical network. However, expressing $P(\mathcal{S},n)$ and $P(\mathcal{R},n)$ as functions of $R(m,n)$ for each relay strategy might involve some details. This is because, with the participation of a relay, an entire range of power allocations at the source and at the relay is possible to achieve a fixed bit rate. In this section we show that by using an extra optimization step, which accounts for the pricing structure of the power availability, the optimal power allocations at both the source and the relay can be readily found [1]. Two-timeslot implementation of DF and AF strategies will be assumed.

Subscripts 1 and 2 are used to denote the first and the second timeslot respectively. Let $x_{\mathcal{S}1}$ be the symbol sent by $\mathcal{S}$, $y_{\mathcal{D}1}$ and $y_{\mathcal{D}2}$ be the received symbols at $\mathcal{D}$ and $y_{\mathcal{R}1}$ be the received symbol at $\mathcal{R}$. We assume that all nodes have one antenna each. The complex channel gains from $\mathcal{S}$ to $\mathcal{D}$, $\mathcal{S}$ to $\mathcal{R}$ and $\mathcal{R}$ to $\mathcal{D}$ are denoted by $h_{\mathcal{SD}}$, $h_{\mathcal{SR}}$ and $h_{\mathcal{RD}}$, respectively. The channel gains are assumed to be identical in both timeslots. Moreover, $n_{\mathcal{D}1}$, $n_{\mathcal{D}2}$ and $n_{\mathcal{R}1}$ are circularly symmetric complex Gaussian noises. A circularly symmetric complex Gaussian random variable $Z = X + jY \sim \mathcal{CN}(0, \sigma^2)$ has its real and imaginary components independent and identically distributed (i.i.d.) as normal random variables: $X, Y \sim \mathcal{N}(0, \sigma^2/2)$.

3.1.3.1 Direct channel (DC)

In the DC, the source ($\mathcal{S}$) transmits directly to the destination ($\mathcal{D}$). The channel can be modelled as

$$y_{\mathcal{D}} = \sqrt{P(\mathcal{S}, n)} h_{\mathcal{SD}}\, x_{\mathcal{S}} + n_{\mathcal{D}} \tag{3.17}$$

The achievable rate of the DC is

$$R(m, n) \leq I(x_{\mathcal{S}}; y_{\mathcal{D}}) = \log_2 \left[1 + \frac{P(\mathcal{S}, n)|h_{\mathcal{SD}}|^2}{\Gamma N_o W} \right] \tag{3.18}$$

where Γ is the gap to capacity. For discrete bit loading,

$$P^*(\mathcal{S}, n) = \left(2^{R_{(m,n)}} - 1\right) \frac{\Gamma N_o W}{|h_{\mathcal{SD}}|^2} \tag{3.19}$$

3.1.3.2 Decode-and-forward (DF)

The DF relay channel is shown in Figure 3.4. In the first timeslot, $\mathcal{R}$ attempts to decode $x_{\mathcal{S}1}$. Assuming that decoding is successful, $\mathcal{R}$ transmits $x_{\mathcal{S}1}$ in the second timeslot with power $P(\mathcal{R}, n)$. The channel equations are

$$\begin{aligned} y_{\mathcal{D}1} &= \sqrt{P(\mathcal{S}, n)} h_{\mathcal{SD}}\, x_{\mathcal{S}1} + n_{\mathcal{D}1} \\ y_{\mathcal{R}1} &= \sqrt{P(\mathcal{S}, n)} h_{\mathcal{SR}}\, x_{\mathcal{S}1} + n_{\mathcal{R}1},\ y_{\mathcal{D}2} = \sqrt{P(\mathcal{R}, n)} h_{\mathcal{RD}}\, x_{\mathcal{S}1} + n_{\mathcal{D}2} \end{aligned} \tag{3.20}$$

Successful decoding of $x_{\mathcal{S}1}$ at $\mathcal{R}$ requires

$$R(m, n) \leq I(x_{\mathcal{S}1}; y_{\mathcal{R}1}) = \log_2 \left[1 + \frac{P(\mathcal{S}, n)|h_{\mathcal{SR}}|^2}{\Gamma N_o W} \right] \tag{3.21}$$

or, equivalently,

$$P(\mathcal{S}, n) \geq \left(2^{R_{(m,n)}} - 1\right) \frac{\Gamma N_o W}{|h_{\mathcal{SR}}|^2} \tag{3.21a}$$

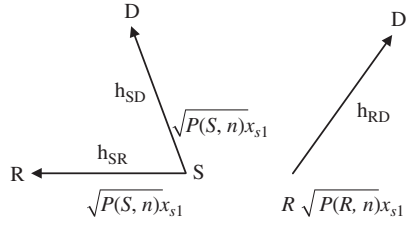

Figure 3.4 The DF relay channel, where the first timeslot is shown on the left and the second timeslot is shown on the right.

Successful decoding at $\mathcal{D}$ requires

$$\begin{aligned} R(m,n) &\le I(x_{\mathcal{S}1}\,; y_{\mathcal{D}1}, y_{\mathcal{D}2}) \\ &= \log_2\left[1 + \frac{P(\mathcal{S},n)|h_{\mathcal{S}\mathcal{D}}|^2 + P(\mathcal{R},n)|h_{\mathcal{R}\mathcal{D}}|^2}{\Gamma N_o W}\right] \end{aligned} \tag{3.22}$$

Since $\mathcal{D}$ receives two scaled and noisy versions of $x_{\mathcal{S}1}$ across two timeslots a maximum-ratio combining formula is used to derive Equation (3.22), where the achievable rate of a 2×1 channel $\mathbf{y} = \psi x + \boldsymbol{n}$ with $\mathbf{y} = [y_1, y_2]^T$, $\psi = [\psi_1, \psi_2]^T$, $\mathbf{n} \sim \mathcal{CN}(0, K_N)$,

$$K_N = \begin{bmatrix} \sigma_1^2 & 0 \\ 0 & \sigma_2^2 \end{bmatrix}$$

is

$$C = \log_2\left|\frac{1}{\Gamma}\psi\psi^H + K_N\right| - \log_2|K_N| = \log_2\left[1 + \frac{1}{\Gamma}\left(\frac{|\psi_1|^2}{\sigma_1^2} + \frac{|\psi_2|^2}{\sigma_2^2}\right)\right]$$

In order for DF to work, the achievable rate of $x_{\mathcal{S}1}$ at $\mathcal{R}$ has to be higher than at $\mathcal{D}$. This means that the expression on the right-hand side of Equation (3.21) has to be greater than or equal to that of Equation (3.22). Notice that this can happen only if $|h_{\mathcal{S}\mathcal{R}}| > |h_{\mathcal{S}\mathcal{D}}|$, which is intuitive. From Equation (3.22), the minimum $P(\mathcal{R}, n)$ is

$$P^*(\mathcal{R},n) = \frac{(2^{R(m,n)} - 1)\Gamma N_o W - P(\mathcal{S},n)|h_{\mathcal{S}\mathcal{D}}|^2}{|h_{\mathcal{R}\mathcal{D}}|^2} \tag{3.23}$$

If $P^*(\mathcal{R}, n) \le 0$, then DF is not a suitable relaying scheme.

Now it remains to optimize $P(\mathcal{S}, n)$, which is not straightforward since at a fixed rate $R(m, n)$, decreasing $P(\mathcal{S}, n)$ would increase $P^*(\mathcal{R}, n)$. Recall that the objective of the per-tone optimization problem for each tone n as expressed in (3.14) is

$$\max_{P(\mathcal{S},n)} \lambda_m R(m,n) - \mu_{\mathcal{S}} P(\mathcal{S},n) - \mu_{\mathcal{R}} P^*(\mathcal{R},n) \tag{3.24}$$

From Equation (3.23), $P^*(\mathcal{R}, n)$ may be obtained as a function of $P(\mathcal{S}, n)$, so that the objective of the per-tone optimization problem (3.24) is a function of $P(\mathcal{S}, n)$ only. Since problem (3.24) is now unconstrained, it can be solved by taking the first-order derivative of its objective function (called f below):

$$\frac{\mathrm{d}f}{\mathrm{d}P(\mathcal{S},n)} = -\mu_{\mathcal{S}} + \mu_{\mathcal{R}}\frac{|h_{\mathcal{S}\mathcal{D}}|^2}{|h_{\mathcal{R}\mathcal{D}}|^2} \tag{3.25}$$

Since f is a linear function of $P(\mathcal{S}, n)$, the derivative is a constant and if $\mathrm{d}f/\mathrm{d}P(\mathcal{S}, n) > 0$, then $P(\mathcal{S}, n)$ should be maximized. However, from Equation (3.23), the maximizing $P(\mathcal{S}, n)$ makes $P^*(\mathcal{R}, n) = 0$, which means that DF is unnecessary. On the other hand, if $\mathrm{d}f/\mathrm{d}P(\mathcal{S}, n) \le 0$, then $P^*(\mathcal{S}, n)$ should be minimized. This means that the expression for $P(\mathcal{S}, n)$, i.e. Equation (3.21a), should be satisfied with equality. Note that, by Equation (3.23), such a $P^*(\mathcal{S}, n)$ guarantees that $P^*(\mathcal{R}, n)$ is positive. In summary, optimal power allocation for a fixed $R(m, n)$ in the DF relay mode includes:

(1) *If* $|h_{SR}| <= |h_{\mathcal{S}\mathcal{D}}|$, *set* $P^*(\mathcal{S}, n) = P^*(\mathcal{R}, n) = \infty$.

(2) *Else if* $-\mu_{\mathcal{S}} + \mu_{\mathcal{R}}\frac{|h_{\mathcal{S}\mathcal{D}}|^2}{|h_{\mathcal{R}\mathcal{D}}|^2} > 0$, *then set* $P^*(\mathcal{S}, n) = P^*(\mathcal{R}, n) = \infty$.

(3) *Else set* $P^*(\mathcal{S}, n)$ *and* $P^*(\mathcal{R}, n)$ *according to Equations (3.21a) and (3.23), respectively, with equality.*

(4) *Divide* $R(m, n)$, $P^*(\mathcal{S}, n)$ *and* $P^*(\mathcal{R}, n)$ *by 2 since communication takes place in two timeslots.*

3.1.3.3 Amplify-and-forward (AF)

The AF relay channel is shown in Figure 3.5. The relay $\mathcal{R}$ receives $x_{\mathcal{S}1}$ in the first timeslot and transmits an amplified version of $x_{\mathcal{S}1}$ in the second timeslot with power $P(\mathcal{R}, n)$. The channel equations are

$$\begin{aligned} y_{\mathcal{D}1} &= \sqrt{P(\mathcal{S}, n)} h_{\mathcal{S}\mathcal{D}}\, x_{\mathcal{S}1} + n_{\mathcal{D}1},\; y_{\mathcal{R}1} = \sqrt{P(\mathcal{S}, n)} h_{\mathcal{S}\mathcal{R}}\, x_{\mathcal{S}1} + n_{\mathcal{R}1} \\ y_{\mathcal{D}2} &= \beta y_{\mathcal{R}1} h_{\mathcal{R}\mathcal{D}} + n_{\mathcal{D}2} \end{aligned} \tag{3.26}$$

where

$$\beta = \sqrt{\frac{P(\mathcal{R}, n)}{P(\mathcal{S}, n)|h_{\mathcal{S}\mathcal{R}}|^2 + N_o W}} \tag{3.27}$$

is the power amplification factor at $\mathcal{R}$. The AF scheme is a suitable choice when the relay does not have a sufficiently large SNR to decode the transmitted symbol. However, the AF scheme suffers from noise amplification.

In order for the destination $\mathcal{D}$ to decode the signal $x_{\mathcal{S}1}$, which is sent across two timeslots, we must have

$$\begin{aligned} R(m, n) &\le I(x_{\mathcal{S}1}; y_{\mathcal{D}1}, y_{\mathcal{D}2}) \\ &= \log_2 \left\{ 1 + \frac{1}{\Gamma} \left[\frac{P(\mathcal{S}, n)|h_{\mathcal{S}\mathcal{D}}|^2}{N_o W} + \frac{\dfrac{P(\mathcal{R}, n) P(\mathcal{S}, n)|h_{\mathcal{R}\mathcal{D}}|^2 |h_{\mathcal{S}\mathcal{R}}|^2}{P(\mathcal{S}, n)|h_{\mathcal{S}\mathcal{R}}|^2 + N_o W}}{N_o W \left(1 + \dfrac{P(\mathcal{R}, n)|h_{\mathcal{R}\mathcal{D}}|^2}{P(\mathcal{S}, n)|h_{\mathcal{S}\mathcal{R}}|^2 + N_o W} \right)} \right] \right\} \end{aligned} \tag{3.28}$$

The variables of Equation (3.28) are $P(\mathcal{S}, n)$ and $P(\mathcal{R}, n)$. From (3.28) we have

$$P^*(\mathcal{R}, n) = \frac{\left[c_1 P(\mathcal{S}, n) + c_2 \right] \left[c_3 P(\mathcal{S}, n) + c_4 \right]}{c_5 P(\mathcal{S}, n) + c_6} \tag{3.29}$$

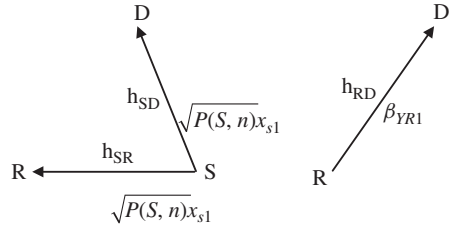

Figure 3.5 The AF relay channel: the first timeslot is shown on the left and the second on the right.

where $c_1 = |h_{\mathcal{SD}}|^2$, $c_2 = -(2^{R(m,n)} - 1)\Gamma N_o W$, $c_3 = |h_{\mathcal{SR}}|^2$, $c_4 = N_o W$, $c_5 = |h_{\mathcal{RD}}|^2(-|h_{\mathcal{SD}}|^2 - |h_{\mathcal{SR}}|^2)$ and $c_6 = (2^{R_{(m,n)}} - 1)\Gamma N_o W|h_{\mathcal{RD}}|^2$. Since $[c_3 P(\mathcal{S}, n) + c_4] > 0$, to ensure $P^*(\mathcal{S}, n) > 0$, the terms $[c_1 P(\mathcal{S}, n) + c_2]$ and $[c_5 P(\mathcal{S}, n) + c_6]$ must either be both greater than zero or both less than zero. A valid solution is obtained only when both terms are less than zero, leading to a feasible region for $P(\mathcal{S}, n)$ as

$$P_{\min}(\mathcal{S}, n) < P(\mathcal{S}, n) < P_{\max}(\mathcal{S}, n) \tag{3.30}$$

where

$$P_{\min}(\mathcal{S}, n) = \frac{(2^{R_{(m,n)}} - 1)\Gamma N_o W}{|h_{\mathcal{SD}}|^2 + |h_{\mathcal{SR}}|^2} \text{ and } P_{\max}(\mathcal{S}, n) = \frac{(2^{R_{(m,n)}-1})\Gamma N_o W}{|h_{\mathcal{SD}}|^2}$$

Equation (3.30) contains strict inequalities because if $P(\mathcal{S}, n)$ is equal to $P_{\min}(\mathcal{S}, n)$, then $P^*(\mathcal{R}, n)$ will be equal to infinity. On the other hand, $P(\mathcal{S}, n)$ cannot be equal to $P_{\max}(\mathcal{S}, n)$ either, because this implies $P^*(\mathcal{S}, n) = 0$, making AF relaying unnecessary.

To choose the optimal power allocations for a fixed $R(m, n)$, similar to the analysis in the DF mode, the per-tone objective is as expressed in problem (3.14):

$$f = \max_{P(\mathcal{S},n)} \lambda_m R(m, n) - \mu_{\mathcal{S}} P(\mathcal{S}, n) - \mu_{\mathcal{R}} P^*(\mathcal{R}, n) \tag{3.31}$$

To show that f is a concave function of $P(\mathcal{S}, n)$ compute

$$\frac{\mathrm{d}f}{\mathrm{d}P(\mathcal{S}, n)} = -\mu_{\mathcal{S}} - \mu_{\mathcal{R}} \frac{\mathrm{d}P^*(\mathcal{R}, n)}{\mathrm{d}P(\mathcal{S}, n)} \tag{3.31a}$$

$$\frac{\mathrm{d}^2 f}{\mathrm{d}P(\mathcal{S}, n)^2} = -\mu_{\mathcal{R}} \frac{\mathrm{d}^2 P^*(\mathcal{R}, n)}{\mathrm{d}P(\mathcal{S}, n)^2} \tag{3.31b}$$

It can be verified by algebra that for $P(\mathcal{S}, n)$ within the feasible region of Equation (3.30), $\mathrm{d}P^*(\mathcal{R}, n)/\mathrm{d}P(\mathcal{S}, n) < 0$ and $d^2 P^*(\mathcal{R}, n)/\mathrm{d}P(\mathcal{S}, n)^2 > 0$. Using the results in Equations (3.31a) and (3.31b) shows that within the feasible region of $P(\mathcal{S}, n)$, $\mathrm{d}^2 f/\mathrm{d}P(\mathcal{S}, n)^2 < 0$, thereby proving the concavity of f.

The concavity of f and the observation that f is continuous ensure that there is a unique optimal value of f within the feasible region of $P(\mathcal{S}, n)$. The optimal value can be found by finding the root of $\mathrm{d}f/\mathrm{d}P(\mathcal{S}, n)$. This can be done with a root-finding method such as Newton's method. An example of f as a function of $P(\mathcal{S}, n)$ is shown in Figure 3.6, as used in Reference [1].

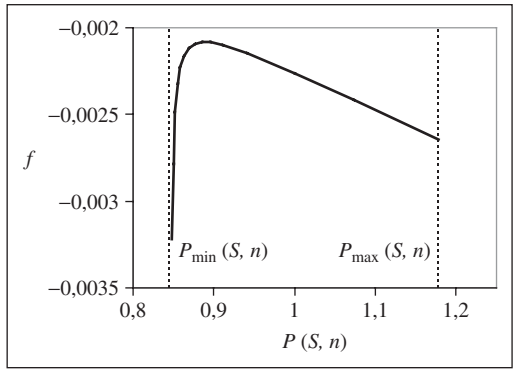

Figure 3.6 An example of f as a function of $P(\mathcal{S}, n)$ for the AF relay channel (there is a unique maximum value of f).

In summary, optimal power allocation for a fixed $R(m, n)$ in the AF relay mode consists of:

(1) *Solve the equation* $\mathrm{d}f/\mathrm{d}P(\mathcal{S}, n) = 0$ *to obtain* $P^*(\mathcal{S}, n)$, *using either bisection or Newton's method, within the feasible region of* $P(\mathcal{S}, n)$ *in Equation (3.30).*

(2) *Set* $P^*(\mathcal{R}, n)$ *according to Equation (3.29).*

(3) *Divide* $R(m, n)$, $P^*(\mathcal{S}, n)$ *and* $P^*(\mathcal{R}, n)$ *by 2.*

3.1.4 Performance example

This section presents some simulation results for the algorithm, which solves the utility maximization problem that uses physical layer relaying (3.2). The simulation parameters are the same as in Reference [1]. A network with a base station and $K = 4$ user nodes is simulated. The total system bandwidth is set to be 80 MHz and the number of OFDM tones is $N = 256$. This corresponds to a tone width $W = 312.5$ kHz. The channel gain between two nodes at each tone can be decomposed into a small-scale Rayleigh fading component and a large-scale path loss component with a path loss exponent of 4. To simulate a frequency-selective environment, small-scale fading is i.i.d. across tones. The gap to capacity Γ is set to 1, which corresponds to perfect coding. The type of utility function chosen is as described in Figure 3.3 with parameters $a = 10$ and $c = 125$ Mbps for downstream communications and $a = 1$ and $c = 12.5$ Mbps for upstream communications. Figure 3.7 shows the location of different nodes and describes the allowable transmissions in each link. In this example, both nodes 1 and 2 can potentially help the transmissions of nodes 3 and 4 by acting as relays.

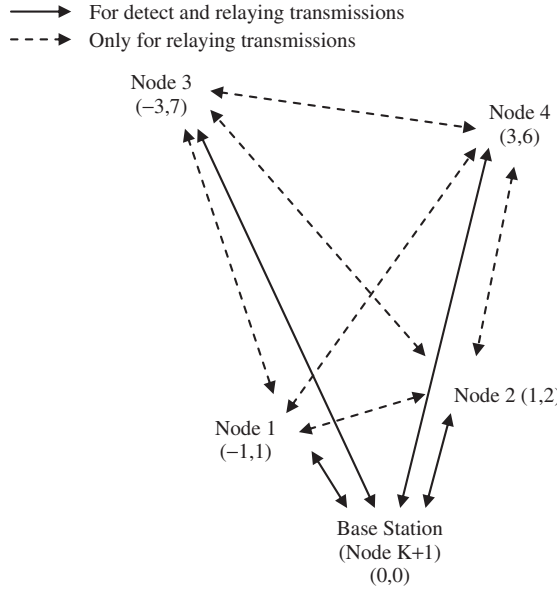

Figure 3.7 Topology of a cooperative network with four user nodes.

Table 3.1 Rates (Mbps) of various data streams in the four-user network

Stream	No relay	Relay	Percentage change
$(K+1,1)$	152	148	−2.9 %
$(K+1,2)$	135	129	−4.1 %
$(K+1,3)$	46	71	53.0 %
$(K+1,4)$	54	80	48.8 %
$(1,K+1)$	18	16	−11.7 %
$(2,K+1)$	18	16	−13.3 %
$(3,K+1)$	12	14	16.0 %
$(4,K+1)$	14	13	−5.0 %

Table 3.2 Percentage of power expended as a relay in the four-user network

Node	Percentage of power expended as a relay
1	94.9 %
2	92.2 %
3	0 %
4	0 %

The optimization algorithm selects the best relay in accordance with channel realizations and the availability of power and bandwidth. The power constraints of all nodes are such that $p_i^{\max}/N_o W = 20\,\text{dB} (i \in \mathcal{K}_+)$. This corresponds to a medium-SNR environment.

Using the optimization algorithm, it is found that by allowing relaying, the maximized sum utility increases from 34 to 37, which again quantifies the merit of cooperative relaying. Note that each source–destination pair selects both the best relay and the best relay strategy in each frequency tone. This is done in a globally optimal way. Table 3.1 shows the rates of various data streams with and without relaying. Again, as downstream is preferred by virtue of the choice of the utility function, both streams $(K+1, 3)$ and $(K+1, 4)$ benefit tremendously from relaying. In fact, in the optimal solution, only streams $(K+1, 3)$ and $(K+1, 4)$ use relays. For both of these streams, node 1 or node 2 act as the relay, depending on the tone. This result illustrates that there is negligible performance loss (in this case, there is no loss at all) if we restrict attention to relays located roughly between the source and the destination. In Table 3.2, we see that nodes 1 and 2 expend over 90 % of their power to act as a relay. These results illustrate that in a system with optimal allocations of bandwidth and power that truly maximizes the sum utility, nodes 1 and 2 would sacrifice their own data rates for the benefits of nodes 3 and 4.

3.2 MESH/RELAY NETWORKS

In a distributed multihop mesh/relay network (e.g. wireless ad hoc/sensor network, cellular multihop network), each node acts as a relay node to forward data packets from other nodes. These nodes are often energy-limited and also have limited buffer space. Therefore, efficient power-saving mechanisms (e.g. sleeping mechanisms) are required so that the lifetime of these nodes can be extended while at the same time the quality of service (QoS) requirements (e.g. packet delay

and packet loss rate) for the relayed packets can be satisfied. In this section, we present a queuing analytical framework to study the tradeoffs between the energy saving and the QoS at a relay node.

A major issue in distributed mobile computing is to design efficient mechanisms for minimizing energy consumption in the wireless terminals [44–72]. A common way to minimize energy consumption in a node is to allow the node to go to the sleep mode in which the node does not transmit and, therefore, it does not use a significant amount of battery power. A tradeoff exists between the node energy saving and the network performance in terms of waiting time for the relayed packets and packet loss rate (due to buffer overflow) at a relay node.

In this section, we present a queuing analytical model that enables us to explore this tradeoff and to investigate the QoS performance as the node dynamics (due to the sleeping and wakeup mechanism) varies [44]. We consider a wireless relay network with stationary nodes where each node is described by two operational modes: the active mode and the sleep mode. In the active mode, a node is fully operational and is able to transmit/receive data, while in the sleep mode it does not take part in any data transmission activity but it can receive packets when the transmitter circuitry is turned off.

At each node, two separate queues are maintained: one for data packets relayed from other nodes and the other for the node's own packets. During transmission, the node prioritizes the relayed packets over its own packets and packets from each queue are served on a first-in first-out (FIFO) basis.

We model the queuing dynamics at a node by using the theory of discrete-time Markov chains, where time is divided into slots. The server process (i.e. the MAC/PHY protocol) goes into the sleep mode either after both the queues have been served exhaustively or a predefined number of packets have been served. A nonpreemptive service model is assumed where the low-priority queue in service would not be interrupted by new packet arrivals at the high-priority queue.

Queuing analysis in this section provides queue length and waiting time distributions for high-priority packets as well as packet loss probability in the case of a finite queue length. Also, the probability of the server being in the sleep mode (vacation) is computed which provides a measure for energy saving.

3.2.1 The system model

3.2.1.1 Phase-type distribution

For an $n+1 (n \leq \infty)$ state absorbing Markov chain with the set of states $\varepsilon = [0, 1, 2, \ldots, n]$ let the state transition matrix be P, where

$$P = \begin{bmatrix} 1 & 0 \\ T^0 & T \end{bmatrix} \tag{3.32}$$

The matrix T is an $n \times n$ transition matrix corresponding to the transitions within the transient states, with $0 \leq T_{ij} \leq 1$ and the sum of at least one row of T being strictly less than 1. The column vector T^0 is given as $T^0 = e - Te$, where e is a column vector of ones with the appropriate dimension. For $\alpha = [\alpha_1, \alpha_2, \ldots, \alpha_n]$, where α_i is the probability that the Markov chain starts from state i, we have $\alpha_0 + \alpha e = 1$. If time to absorption for this Markov chain is denoted as τ, then $\text{Prob}(\tau = i) = p_i = \alpha T^{i-1} T^0, i \geq 1$ and $p_0 = \alpha_0$. The time to absorption in such a Markov chain is said to have a phase-type distribution [73].

A node in a distributed mesh/relay network is modelled as a discrete-time queuing system. Packet arrivals at a node are modelled by a discrete Markovian arrival process (D-MAP). In this model relayed packets and own packets will be referred to as type 1 and type 2 packets, respectively. A state of the process represents the number of the packets in the queue and MAP is described by four substochastic matrices D_0, D_{11}, D_{12} and D_2, with $D_1 = D_{11} + D_{12}$ and $D = D_0 + D_1 + D_2$,

where D is stochastic. The element $(D_0)_{ij}$ represents the probability of a transition from phase i to phase j with no arrival, $(D_{11})_{ij}$ represents a transition with an arrival of a type 1 packet, $(D_{12})_{ij}$ represents a transition with an arrival of a type 2 packet and $(D_2)_{ij}$ represents a transition with two arrivals (one of each type). The arrival rate λ_i for a type i packet ($i = 1, 2$) is given as $\lambda_i = \psi(D_{11} + D_2)$, where ψ is the solution of $\psi = \psi D$ and $\psi e = 1$ (e is a column vector of 1 s with appropriate dimension).

The D-MAP is an extension of the Markov modulated Bernoulli process (MMBP). In the MMBP, a Bernoulli arrival is modulated by a discrete-time Markov chain. A Markovian arrival process works in a similar manner, but arrivals may also occur when the Markov process jumps from one state to another. The Bernoulli process is a special type of D-MAP. We consider one special case of this arrival process where there are two independent discrete arrival streams described by the matrices $D_0(i), D_1(i), i = 1, 2$. In such a case,

$$D_0 = D_0(1) \otimes D_0(2),\ D_{11} = D_1(1) \otimes D_0(2),\ D_{12} = D_0(1) \otimes D_1(2) \text{ and}$$
$$D_2 = D_1(1) \otimes D_1(2)$$

where $\otimes$ is the Kronecker product.

The service process is determined by the MAC/PHY protocol activity (i.e. the active mode and the sleep mode) and the corresponding mechanisms (e.g. channel access mechanism, handshaking protocols, etc.). The type 1 and type 2 packets are stored in two separate queues (Figure 3.8). In the active mode, the service process prioritizes type 1 packets over type 2 packets. We study the nonpreemptive priority case. Packets from each queue are served on a FIFO basis.

The service time follows a discrete phase-type distribution represented by $(\beta(i), S(i)), i = 1, 2$ for packet type i. In this representation, $\beta(i)$ is a row vector, $S(i)$ is a substochastic matrix and $S^0(i) = e - S(i)e$.

For the service process, the distribution of time spent in vacation (i.e. in the sleep mode) is also assumed to phase-type with parameters (v, V). To make the system more energy efficient, we assume a multiple vacation model; i.e. upon going from the vacation to the active mode, if the server finds the queues empty, it returns to the vacation mode.

Along the lines presented in [44], we consider two types of vacation systems: the standard exhaustive vacation system and the number-limited (NL) exhaustive vacation system. In the first case, the server goes to the sleep mode after serving all packets from both of the queues. In the second case, the server process goes to the sleep mode after it has served M packets or the queues have become empty, whichever occurs first.

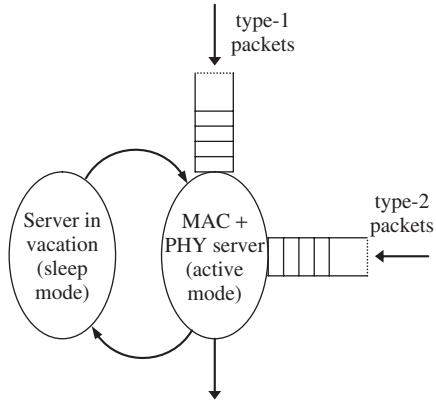

Figure 3.8 Queueing model at a node: MAC/PHY layer as the server.

3.2.2 Exhaustive sleep

In this case, the server goes to the sleep mode when the queues are empty. Consider the following state space:

$$\begin{aligned}
\Omega_0^v &= (0, 0, j, l) \\
\Omega_0^s &= (0, i_2, j, k_2), i_2 \geq 1 \\
\Omega^v &= (i_1, i_2, j, l), (i_1 + i_2) \geq 1 \\
\Omega_1^s &= (i_1, i_2, j, k_1), i_1 \geq 1; i_2 \geq 0 \\
\Omega_2^s &= (i_1, i_2 + 1, j, k_2), i_1 \geq 1; i_2 \geq 0
\end{aligned} \tag{3.33}$$

Here, Ω_0^v represents the vacation (i.e. sleep mode) while the queues are empty with the arrival process in phase j and the vacation process in phase l. In Ω_0^s, there are only type 2 packets in the system with the arrival process in phase j and a type 2 packet is being served while the service process is in phase k_2. In states Ω^v, Ω_1^s and Ω_2^s, there is at least one type 1 packet in the system. In Ω^v, the server is in vacation (i.e. sleep mode), while the phases of arrival and vacation processes are j and l, respectively. Ω_1^s and Ω_2^s represent the system in service, while in Ω_1^s the packet in the server is of type 1 with k_1 as the phase of service and in Ω_2^s the packet in the server is of type 2 with k_2 as the phase of service. The state space for the system is

$$\Omega = \Omega_0^v \cup \Omega_0^s \cup \Omega^v \cup \Omega_1^s \cup \Omega_2^s$$

The transition matrix P describing this Markov chain has the following form:

$$P = \begin{bmatrix}
B_{00} & B_{01} & & & & \\
B_{10} & A_1 & A_0 & & & \\
 & A_2 & A_1 & A_0 & & \\
 & & A_2 & A_1 & A_0 & \\
 & & & \ddots & \ddots & \ddots
\end{bmatrix} \tag{3.34}$$

All the blocks B_{00}, B_{01}, B_{10}, B_{11}, A_0, A_1, A_2 are of infinite dimensions and are given as [44]

$$B_{00} = \begin{bmatrix}
B_{00}^{00} & B_{00}^{01} & & & & \\
B_{00}^{10} & B_{00}^{1} & B_{00}^{0} & & & \\
 & B_{00}^{2} & B_{00}^{1} & B_{00}^{0} & & \\
 & & B_{00}^{2} & B_{00}^{1} & B_{00}^{0} & \\
 & & & \ddots & \ddots & \ddots
\end{bmatrix}$$

$$B_{00}^{00} = D_0, \quad B_{00}^{01} = [D_{12} \otimes V \quad D_{12} \otimes V^0 \beta(2)]$$

$$B_{00}^{10} = \begin{bmatrix} 0 \\ D_0 \otimes S^0(2) v \end{bmatrix}, \quad B_{00}^{0} = \begin{bmatrix} D_{12} \otimes V & D_{12} \otimes V^0 \beta(2) \\ 0 & D_{12} \otimes S(2) \end{bmatrix}$$

$$B_{00}^{1} = \begin{bmatrix} D_0 \otimes V & D_0 \otimes V^0 \beta(2) \\ 0 & D_0 \otimes S(2) + D_{12} \otimes S^0(2) \beta(2) \end{bmatrix}$$

$$B_{00}^{2} = \begin{bmatrix} 0 & 0 \\ 0 & D_0 \otimes S^0(2) \beta(2) \end{bmatrix}$$

$$B_{01} = \begin{bmatrix}
B_{01}^{00} & B_{01}^{01} & & & \\
B_{01}^{2} & B_{01}^{1} & B_{01}^{0} & & \\
 & B_{01}^{2} & B_{01}^{1} & B_{01}^{0} & \\
 & & \ddots & \ddots & \ddots
\end{bmatrix}$$

$$B_{01}^{00} = \begin{bmatrix} D_{11} \otimes V & D_{11} \otimes V^0\beta(1) & 0 \end{bmatrix}$$

$$B_{01}^{01} = \begin{bmatrix} D_2 \otimes V & D_2 \otimes V^0\beta(1) & 0 \end{bmatrix} \quad B_{01}^{0} = \begin{bmatrix} D_2 \otimes V & D_2 \otimes V^0\beta(1) & 0 \\ 0 & 0 & 0 \end{bmatrix}$$

$$B_{01}^{2} = \begin{bmatrix} 0 & 0 & 0 \\ 0 & D_{11} \otimes S^0(2)\beta(1) & D_{11} \otimes S(2) \end{bmatrix}$$

$$B_{01}^{1} = \begin{bmatrix} D_{11} \otimes V & D_{11} \otimes V^0\beta(1) & 0 \\ 0 & D_2 \otimes S^0(2)\beta(1) & D_2 \otimes S(2) \end{bmatrix}$$

$$B_{10} = \begin{bmatrix} B_{10}^{00} & B_{10}^{0} & & \\ & B_{10}^{1} & B_{10}^{0} & \\ & & B_{10}^{1} & B_{10}^{0} \\ & & & \ddots & \ddots \end{bmatrix}$$

$$B_{10}^{00} = \begin{bmatrix} 0 \\ D_0 \otimes S^0(1)v \\ 0 \end{bmatrix}, \quad B_{10}^{0} = \begin{bmatrix} 0 & 0 \\ 0 & D_{12} \otimes S^0(1)\beta(2) \\ 0 & 0 \end{bmatrix}$$

$$B_{10}^{1} = \begin{bmatrix} 0 & 0 \\ 0 & D_0 \otimes S^0(1)\beta(2) \\ 0 & 0 \end{bmatrix}$$

$$A_0 = \begin{bmatrix} A_0^1 & A_0^0 & \\ & A_0^1 & A_0^0 \\ & & \ddots & \ddots \end{bmatrix}$$

$$A_0^0 = \begin{bmatrix} D_2 \otimes V & D_2 \otimes V^0\beta(1) & 0 \\ 0 & D_2 \otimes S(1) & 0 \\ 0 & D_2 \otimes S^0(2)\beta(1) & D_2 \otimes S(2) \end{bmatrix}$$

$$A_0^1 = \begin{bmatrix} D_{11} \otimes V & D_{11} \otimes V^0\beta(1) & 0 \\ 0 & D_{11} \otimes S(1) & 0 \\ 0 & D_{11} \otimes S^0(2)\beta(1) & D_{11} \otimes S(2) \end{bmatrix}$$

$$A_1 = \begin{bmatrix} A_1^1 & A_1^0 & \\ & A_1^1 & A_1^0 \\ & & \ddots & \ddots \end{bmatrix}$$

$$A_1^0 = \begin{bmatrix} D_{12} \otimes V & D_{12} \otimes V^0\beta(1) & 0 \\ 0 & D_{12} \otimes S(1) + D_2 \otimes S^0(1)\beta(1) & 0 \\ 0 & D_{12} \otimes S^0(2)\beta(1) & D_{12} \otimes S(2) \end{bmatrix}$$

$$A_1^1 = \begin{bmatrix} D_0 \otimes V & D_0 \otimes V^0\beta(1) & 0 \\ 0 & D_0 \otimes S(1) + D_{11} \otimes S^0(1)\beta(1) & 0 \\ 0 & D_0 \otimes S^0(2)\beta(1) & D_0 \otimes S(2) \end{bmatrix}$$

$$A_2 = \begin{bmatrix} A_2^1 & A_2^0 & \\ & A_2^1 & A_2^0 \\ & & \ddots & \ddots \end{bmatrix}$$

$$A_2^0 = \begin{bmatrix} 0 & 0 & 0 \\ 0 & D_{12} \otimes S^0(1)\beta(1) & 0 \\ 0 & 0 & 0 \end{bmatrix}$$

$$A_2^1 = \begin{bmatrix} 0 & 0 & 0 \\ 0 & D_0 \otimes S^0(1)\beta(1) & 0 \\ 0 & 0 & 0 \end{bmatrix}$$

The matrix P is of the quasi-birth–death (QBD) type while its blocks are of infinite dimension. The first step in analyzing the system using the matrix-geometric method [73] is to determine the matrix R which is the minimal nonnegative solution to the following matrix quadratic equation:

$$R = A_0 + RA_1 + R^2 A_2$$

For the QBD case, the matrix R has the following form [68]:

$$R = \begin{bmatrix} R_0 & R_1 & R_2 & R_3 & R_4 & \cdots \\ & R_0 & R_1 & R_2 & R_3 & \cdots \\ & & R_0 & R_1 & R_2 & \cdots \\ & & & \ddots & \ddots & \ddots \end{bmatrix}$$

and the blocks of matrices $R_i (i \geq 0)$ are given as follows:

$$\begin{aligned} R_0 &= A_0^1 + R_0 A_1^1 + R_0^2 A_2^1 \\ R_1 &= A_0^0 + R_0 A_1^0 + R_1 A_1^1 + R_0^2 A_2^0 + (R_0 R_1 + R_1 R_0) A_2^1 \\ R_j &= R_{j-1} A_1^0 + R_j A_1^1 + \sum_{k=0}^{j-1} R_{j-k-1} R_k A_2^0 + \sum_{k=0}^{j} R_{j-k} R_k A_2^1 \end{aligned}$$

The matrix blocks $R_i (i \geq 0)$ can be further partitioned as follows:

$$R_i = \begin{bmatrix} R_i(vv) & R_i(vs_1) & 0 \\ 0 & R_i(s_1 s_1) & 0 \\ 0 & R_i(s_2 s_1) & R_i(s_2 s_2) \end{bmatrix}$$

Since $(R_{k+1})_{ij} \leq (R_k)_{ij}$ $(\forall k \geq 1, \forall i, j)$ [68], we can compute $R_0, R_1, \ldots$ recursively up to the point of truncation. If $x = [x_0 x_1 x_2 \cdots]$ is the steady-state probability vector corresponding to P, where $x = xP$, and $xe = 1$, it can be shown that [44] $x_{i+1} = x_i R, i \geq 1$ where

$$x_i = [x_{i0} x_{i1} x_{i2} \cdots], i \geq 0, x_{ij} = [x_{ij}^v x_{ij}^s(1) x_{i,j+1}^s(2)], i \geq 1, j \geq 0$$

Then

$$\begin{aligned} x_{i+1,j}^v &= \sum_{k=0}^{j} x_{i,j-k}^v R_k(vv) \\ x_{i+1,j}^s(1) &= \sum_{k=0}^{j} \left[x_{i,j-k}^v R_k(vs_1) + x_{i,j-k}^s(1) R_k(s_1 s_1) + x_{i,j-k+1}^s(2) R_k(s_2 s_1) \right], \ i \geq 1, j \geq 0 \\ x_{i+1,j+1}^s(2) &= \sum_{k=0}^{i} x_{i,j-k+1}^s(2) R_{j-k}(s_2 s_2), i \geq 1, j \geq 0 \end{aligned}$$

$[x_0 \ x_1]$ can be calculated as follows:

$$\begin{aligned} &[x_0 \quad x_1] = [x_0 \quad x_1] \begin{bmatrix} B_{00} & B_{01} \\ B_{10} & A_1 + RA_2 \end{bmatrix} \\ &x_1 = x_0 B_{01} + x_1 (A_1 + RA_2), \text{ which implies} \\ &x_1 = x_0 B_{01} (I - A_1 - RA_2)^{-1} \end{aligned} \tag{3.35}$$

The vector x_0 is then normalized by

$$x_0 e + x_0 \left[B_{01}(I - A_1 - RA_2)^{-1}(I - R)^{-1} \right] e = 1 \tag{3.36}$$

The inverses of the matrices in Equations (3.35) and (3.36) exist and can be calculated recursively since they are both upper triangular with the following form:

$$U = \begin{bmatrix} U_0 & U_1 & U_2 & U_3 & U_4 & \cdots \\ & U_0 & U_1 & U_2 & U_3 & \cdots \\ & & U_0 & U_1 & U_2 & \cdots \\ & & & U_0 & U_1 & \cdots \\ & & & & \ddots & \ddots \\ & & & & & \ddots \end{bmatrix}$$

If V denotes the inverse of matrix U, then V is given as

$$V = \begin{bmatrix} V_0 & V_1 & V_2 & V_3 & V_4 & \cdots \\ & V_0 & V_1 & V_2 & V_3 & \cdots \\ & & V_0 & V_1 & V_2 & \cdots \\ & & & V_0 & V_1 & \cdots \\ & & & & \ddots & \ddots \\ & & & & & \ddots \end{bmatrix}$$

where $V_0 = U_0^{-1}$ and $V_n = -U_0^{-1} \sum_{j=0}^{n-1} U_{n-j} V_j, n \geq 1$.

To calculate x_0, we have the following equation in addition to the normalization equation:

$$x_0 = x_0 B_{00} + x_1 B_{10} = x_0 B_{00} + x_0 B_{01}(I - A_1 - RA_2)^{-1} B_{10}$$

This equation has the following structure:

$$x_0 = x_0 \begin{bmatrix} F_0 & F_1 & F_2 & F_3 & F_4 & \cdots \\ J_0 & H_1 & H_2 & H_3 & H_4 & \cdots \\ & H_0 & H_1 & H_2 & H_3 & \cdots \\ & & \ddots & \ddots & \ddots & \ddots \end{bmatrix}$$

where

$$\bar{F}_v = \sum_{i=v}^{\infty} F_i G^{i-v} \text{ and } \bar{H}_v = \sum_{i=v}^{\infty} H_i G^{i-v}, v \geq 0$$

and G is the minimal nonnegative solution of the nonlinear matrix equation

$$G = \sum_{i=0}^{\infty} A_i G^i$$

The vectors x_i, $i \geq 1$, are given by the following recursion formula [74]:

$$x_i = \left[x_0 \bar{F}_i + \sum_{j=1}^{i-1} x_j \bar{H}_{i+1-j} \right] (I - \bar{H}_1)^{-1}, i \geq 1 \tag{3.37}$$

The computation of Equation (3.37) can be performed efficiently by noting that as $i \to \infty$, $\bar{F}_i$, $\bar{H}_i \to \infty$. Therefore, one may choose a large index i, set $\bar{F}_i = \bar{H}_i = 0$ and compute the other required matrices to compute the following backward recursion: $\bar{F}_k = F_k + \bar{F}_{k+1} G$ and $\bar{H}_k = H_k + \bar{H}_{k+1} G$. The equations $G = H_0 + \bar{H}_1 G$ and $K = F_0 + \bar{F}_1 G$ can be used to confirm that the truncation index has been chosen to be a sufficiently large value.

If q_i is the probability that there are i high-priority (i.e. type 1) packets in the system, then we have $q_i = x_i e$ and *the mean number of high-priority packets in the system* is

$$L = x_1(I - R)^{-2}e \tag{3.38}$$

The *energy saving factor* is defined as the probability that the server is in the sleep mode and is given by

$$S = \sum_{i=0}^{\infty} x_i^v \tag{3.39}$$

Having the steady-state probability vector x_i for a maximum queue length of L packets for high-priority packets, the *probability of packet loss* (p_l) can be found as

$$p_l = \sum_{i=L+1}^{\infty} x_i \tag{3.40}$$

The *distribution of waiting time* (or *access delay*) is defined as the time required for a packet to arrive at the head of the queue since its arrival into the queue. The distribution of access delay for high-priority packets is obtained by using the concept of an absorbing Markov chain. The absorbing state in this case is the state where the target packet arrives at the head of the queue. This is the point where the target packet is ready to be transmitted.

We first find out the state probability vectors $z_{ij}^s(j+1)(i \geq 1,\ j = 0, 1)$ representing the probability of an arriving high-priority packet finding i high-priority (i.e. type 1) packets ahead of it and a type $(j+1)$ packet in processing. Let z_{ij}^v denote the same probability as above except that upon arrival the packet finds the server in the sleep mode. Also, z_{01}^s denotes the probability of having no type 1 packet and at least one type 2 packet in the system and z_{00}^s denotes the probability of having the system empty. Parameter z_0^v denotes the probability for a type 1 packet, upon its arrival, to find the system empty and the server on vacation. With this notation we then have [44]

$$\begin{aligned}
z_0^v &= \lambda_1^{-1} x_{00} \left[(D_{11} + D_2) \otimes \left(V + V^0 v\right)\right] \\
&\quad + \lambda_1^{-1} \sum_{j=1}^{\infty} x_{0j}^v \left[(D_{11} + D_2) \otimes \left(V + V^0 v\right)\right] \\
z_{00}^s &= \lambda_1^{-1} \sum_{j=1}^{\infty} x_{0j}^s \left[(D_{11} + D_2) \otimes S^0(2)\right] \\
&\quad + \lambda_1^{-1} \sum_{j=0}^{\infty} x_{1j}^s(1) \left[(D_{11} + D_2) \otimes S^0(1)\right] \\
z_{01}^s &= \lambda_1^{-1} \sum_{j=1}^{\infty} x_{0j}^s \left[(D_{11} + D_2) \otimes S(2)\right] \\
z_{i0}^v &= \lambda_1^{-1} \sum_{j=0}^{\infty} x_{ij}^v \left[(D_{11} + D_2) \otimes V\right] \\
z_{i0}^s(1) &= \lambda_1^{-1} \sum_{j=0}^{\infty} x_{ij}^s(1) \left[(D_{11} + D_2) \otimes S(1)\right] \\
&\quad + \lambda_1^{-1} \sum_{j=0}^{\infty} x_{i,j+1}^s(2) \left[(D_{11} + D_2) \otimes S^0(2)\beta(1)\right]
\end{aligned}$$

$$+\lambda_1^{-1}\sum_{j=0}^{\infty} x_{i+1,j}^s(1)\left[(D_{11}+D_2)\otimes S^0(1)\beta(1)\right]$$

$$+\lambda_1^{-1}\sum_{j=0}^{\infty} x_{ij}^s\left[(D_{11}+D_2)\otimes V^0\beta(1)\right]$$

$$z_{i1}^s(2)=\lambda_1^{-1}\sum_{j=1}^{\infty} x_{ij}^s(2)\left[(D_{11}+D_2)\otimes S(2)\right]$$

$$z_0=\left[z_0^v\ z_{00}^s\ z_{01}^s\right],\quad z_i=\left[z_{i0}^v\ z_{i0}^s(1)\ z_{i1}^s(2)\right],\ i\geq 1$$

$$z=[z_0\ z_1\ \cdots]$$

The distribution of access delay for the high-priority packet as the time to absorption for a Markov chain is obtained with the following transition matrix:

$$\tilde{P}=\begin{bmatrix}\tilde{B}_{00} & & & \\ \tilde{B}_{10} & \tilde{A}_1 & & \\ & \tilde{A}_2 & \tilde{A}_2 & \\ & & \ddots & \ddots\end{bmatrix}$$

where

$$\tilde{B}_{00}=\begin{bmatrix}V & V^0 & 0\\ 0 & I & 0\\ 0 & I\otimes S^0(2) & I\otimes S(2)\end{bmatrix}$$

$$\tilde{B}_{10}=\begin{bmatrix}0 & 0 & 0\\ 0 & I\otimes S^0(1) & 0\\ 0 & 0 & 0\end{bmatrix}$$

$$\tilde{A}_1=\begin{bmatrix}I\otimes V & I\otimes V^0\beta(1) & 0\\ 0 & I\otimes S(1) & 0\\ 0 & I\otimes S^0(2)\beta(1) & I\otimes S(2)\end{bmatrix}$$

$$\tilde{A}_2=\begin{bmatrix}0 & 0 & 0\\ 0 & I\otimes S^0(1)\beta(1) & 0\\ 0 & 0 & 0\end{bmatrix}$$

Then,

$$z^{n+1}=z^n\tilde{P}$$

with

$$\begin{aligned}
z_0 &= z_0\tilde{B}_{00}+z_1\tilde{B}_{10}\\
z_i &= z_i\tilde{A}_1+z_{i+1}\tilde{A}_2\\
z_0^v &= z_0^vV\\
z_{00}^s &= z_{00}^s+z_{01}^s\left[I\otimes S^0(2)\right]+z_{10}^s\left[I\otimes S^0(1)\right]+z_0^vV^0\\
z_{01}^s &= z_{01}^s\left[I\otimes S(2)\right]\\
z_{i0}^v &= z_{i0}^v(I\otimes V)\\
z_{i0}^s(1) &= z_{i0}^v\left[I\otimes V^0\beta(1)\right]+z_{i0}^s(1)\left[I\otimes S(1)\right]\\
&\quad +z_{i1}^s(2)\left[I\otimes S^0(2)\beta(1)\right]+z_{i+1,0}^s(1)\left[I\otimes S^0(1)\beta(1)\right]\\
z_{i1}^s(2) &= z_{i1}^s(2)\left[I\otimes S(2)\right]
\end{aligned}$$

If W_T is the probability that the access delay of a high-priority packet is less than or equal to T, then

$$W_T = z_o^{\mathrm{T}}\mathrm{e} \tag{3.41}$$

For more details on analytical models for the number-limited exhaustive case see Reference [44].

3.2.3 Practical applications

With the slotted S-ALOHA protocol, when a node is in the active mode and there are packets available in the transmission queue, a packet successfully departs the queue with probability p (which is given by the probability of channel access multiplied by the probability of successful transmission in the presence of collision). Therefore, the service time distribution of packets can be considered to be geometric, which is a special case of phase-type distribution having one phase with $\beta = 1$, $S = 1 - \mu$ and $S^0 = \mu$, where $\mu = p$. Also, a prioritized access scheme based on S-ALOHA is obtained if we assume different probability of access (probability of service) for packets with different priorities.

For energy saving, a node goes to the sleep mode occasionally and it returns to the active mode with probability γ. To model this sleep and wakeup dynamics a one-phase PH distribution can be considered with $V = 1 - \gamma$ and $V^0 = \gamma$. We refer to μ and γ as the probability of service and the probability of wakeup, respectively. Moreover, we assume that the probability of service is the same for both type 1 and type 2 packets unless it is explicitly stated.

IEEE 802.11 DCF consists of two main mechanisms: contention window adjustment and backoff mechanisms. Once a station (STA) is turned on, it sets the contention window to the minimum value ($W_{\min}$). The contention window is doubled for every transmission failure until it reaches the maximum value ($W_{\max}$). If the transmission is successful, the contention window is reset to $W_{\min}$. After a window adjustment, an STA waits for a distributed interframe space (DIFS) period of time and calculates a backoff value from $U(0, W)$, where $U(a, b)$ generates a random variable uniformly distributed between a and b, and W is the current contention window. After this point, the backoff value is decreased by one every idle timeslot. When the channel becomes busy, the backoff value is frozen until the channel becomes idle again for the DIFS period of time. After that, the STA starts decreasing the backoff value by one for each subsequent idle timeslot. When the backoff value is zero, the STA can transmit data in the next timeslot.

Setting up a phase-type service process with two phases (one for the case when the server is in backoff mode and the other for the case when the server is in busy mode) enables us to model the IEEE 802.11 DCF MAC protocol. The backoff mode ends when the backoff counter expires, and depending on the stage of the backoff and the probability of backoff counter expiration is given as follows [75]:

$$Pr(BC = 1) = \sum_{k=2}^{m-1} \frac{p^k}{2^k CW_{\min}} + \frac{p^m}{CW_{\max}}$$

where p is the probability of collision and $m = \log_2(CW_{\max}/CW_{\min})$.

On the other hand, a node goes to the backoff mode (from the busy mode) when a collision occurs (with probability p). We assume that the packet collision process follows a Bernoulli process (as in Reference [76]) and that the packet collision probability is constant and independent of the number of retransmissions already suffered. This assumption was extended to the finite load case in Reference [80]. Therefore, a phase-type distribution for the service process can be set up as follows:

$$S = \begin{bmatrix} 1 - Pr(BC = 1) & Pr(BC = 1) \\ p & 0 \end{bmatrix}, \quad S^0 = \begin{bmatrix} 0 \\ 1 - p \end{bmatrix}$$

Similar to the S-ALOHA case, a one-phase PH distribution can be assumed for the vacation process to model the sleep and wakeup dynamics in a node. For a given arrival probability and given QoS requirements, the wakeup probability and the service probability at a node are the tuning parameters to control the node's behavior dynamically, where the service probability can be tuned by changing the MAC/PHY layer access control and error control parameters. Having a high probability of service may not guarantee the required QoS when the wakeup probability is low.

We can use the presented analytical model to obtain the optimal system parameter settings. For example, if we want to maximize the battery lifetime, the wakeup probability γ should be minimized while maintaining the packet loss rate (p_l) below a target threshold p_l^{tar}. We can then formulate an optimization problem as

$$\text{Minimize}|p_l(\gamma) - p_l^{tar}| \tag{3.42}$$

With this formulation, the decision variable is γ. Similar formulations can be developed under constraints on packet delay and packet loss probability (or a combination of these QoS metrics) as well. The algorithm presented in Reference [33] can be used to find the minima of (3.42) and the corresponding optimal value $\bar{\gamma}$. Starting at a given initial interval a_1 and $b_1(a_1 < b_1)$, the algorithm below proceeds by evaluating the function $f(x) = |p_l(x) - p_l^{tar}|$.

Algorithm $(inputs : a_1, b_1, tol)$

$$b_1 \leftarrow a_1 + (1-\tau)(b_1 - a_1),\ F_b \leftarrow f(b_1)$$
$$d_1 \leftarrow b_1 - (1-\tau)(b_1 - a_1),\ F_d \leftarrow f(d_1)$$
$$\tilde{\gamma} \leftarrow b_1$$

repeat
if $F_b < F_d$ then

$$\begin{cases} \bar{\gamma} \leftarrow b_k \\ a_{k+1} \leftarrow a_k, b_{k+1} \leftarrow d_k, d_{k+1} \leftarrow b_k \\ b_{k+1} \leftarrow a_{k+1} + (1-\tau)(b_{k+1} - a_{k+1}) \\ F_d \leftarrow F_b, F_b \leftarrow f(b_{k+1}) \end{cases}$$

else

$$\begin{cases} \bar{\gamma} \leftarrow d_k \\ a_{k+1} \leftarrow b_k, b_{k+1} \leftarrow b_k, b_{k+1} \leftarrow d_k \\ d_{k+1} \leftarrow b_{k+1}(1-\tau)(b_{k+1} - a_{k+1}) \\ F_b \leftarrow F_d, F_d \leftarrow f(d_{k+1}) \end{cases}$$

until $b_{k+1} - a_{k+1} < tol$
return $\bar{\gamma}$

3.2.4 Performance example

We analyze the queue length and the delay distribution as well as the probability of loss (for finite queues) for high-priority packets with the same system assumptions as in Reference [44]. For packet arrival, we assume a Bernoulli process that is a special case of MAP with α as the probability of arrival. The probability of arrival for a high-priority packet is α_1 and the probability of arrival for a low-priority packet is α_2. Then the matrices D_0, D_{11}, D_{12} and D_2 become scalars and are given as follows:

$$D_0 = (1-\alpha_1)(1-\alpha_2) = d_0$$
$$D_2 = \alpha_1\alpha_2 = d_2$$

$$D_{11} = \alpha_1(1 - \alpha_2) = d_{11}$$
$$D_{12} = (1 - \alpha_1)\alpha_2 = d_{12}$$

Note that, for numerical analysis, we can obtain the performance measures after the R matrix and the boundary values $[x_0, x_1]$ have been computed. To compute the delay distribution for a packet, we need to first compute the probability distribution corresponding to the system states (given as the z vector) upon arrival of a packet in the system. For the 802.11 DCF MAC protocol, we assume the same set of parameters as specified in Reference [77]. Each node operates under the nonsaturation condition and we obtain the probability of collision from References [78] to [80].

Figures 3.9, 3.10 and 3.11 show the effect of wakeup probability on the queue length distribution, access delay, energy-saving factor and probability of packet loss in the slotted ALOHA.

The simulation results are plotted against the numerical results obtained from the analysis. It is evident that the simulation results follow the numerical results very closely, which validates the accuracy of the analytical model.

The probability of packet arrival and the probability of service (in Figures 3.9, 3.10 and 3.11) are assumed to be 0.2 and 0.9, respectively, for both types of packets. Figure 3.9(a) shows the energy-saving factor as a function of wakeup probability for both the standard (exhaustive vacation)

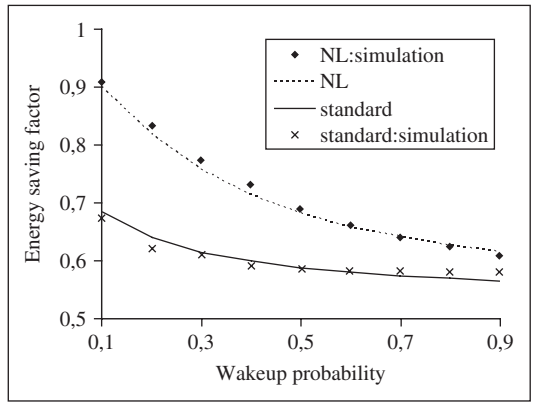

(a)

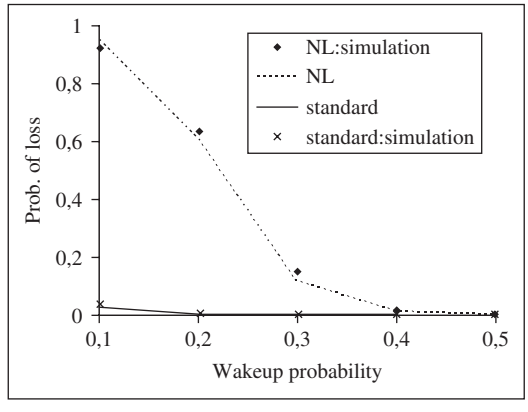

(b)

Figure 3.9 Effect of wakeup probability on the energy saving factor and packet loss rate.

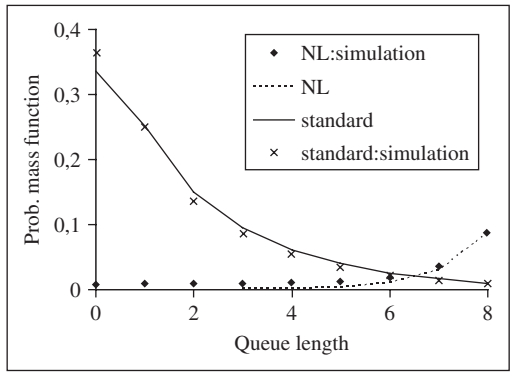

(a)

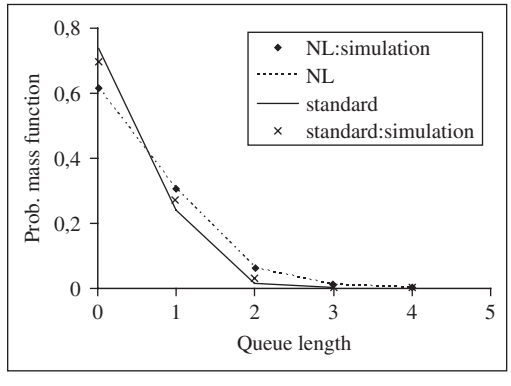

(b)

Figure 3.10 Effect of wakeup probability on queue length distribution.

and the number-limited (NL) service cases. Note that the wakeup probability can be chosen as a function of the battery level in the node.

Although the number-limited strategy is more energy efficient, the probability of packet loss is more severe in this case when the wakeup probability is low. From Figure 3.10, we observe that with the number-limited service, it is more probable that the queue length will be larger than that for the standard exhaustive case. Also, the queue length distribution for the number-limited case approaches that for the standard case when the wakeup probability becomes higher. However, the distributions differ significantly when the wakeup probability is small.

Figure 3.11 clearly shows the difference in the access delay performance for the two different service strategies. Specifically, with a small wakeup probability, the access delay is much higher in the number-limited case compared to that in the standard exhaustive service case.

3.3 OPPORTUNISTIC *AD HOC* RELAYING FOR MULTICAST

Multicast throughput decreases with the increase in multicast group size, since a conservative strategy for the base station is to use the lowest data rate of all the receivers so that the receiver with the worst downlink channel condition can decode the transmission correctly. For more details see Chapter 19. In this section we discuss integrated cellular and *ad hoc* multicast (ICAM), which

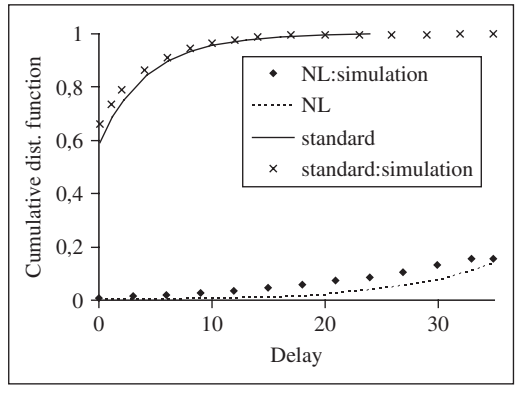

(a)

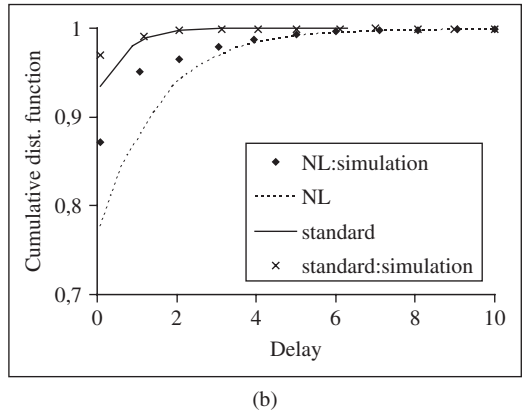

(b)

Figure 3.11 Effect of wakeup probability on the distribution of access delay.

increases multicast throughput through opportunistic use of *ad hoc* relays [81]. In ICAM, a base station delivers packets to proxy mobile devices with better channel quality. The proxy then forwards the packets to the receivers through an IEEE 802.11-based ad hoc network.

3.3.1 The system model

The downlink channel of a mobile client is modelled with both slow and fast fading. Slow fading is modelled as a function of the client's distance from the base station. Fast fading is modelled by Jakes' Rayleigh fading. The combined E_c/N_t for both slow and fast fading is then mapped to a table of supported data rate. Figure 3.12 presents the average rate over a long time period for clients with different distances from the base station.

A general proximity-based interference model for the IEEE 802.11-based multihop wireless network is assumed. In this model, the transmission of a node u does not cause interference to the transmission of a node x if their distance is greater than R_I, where R_I is the maximal interference range. We assume that R_I is $q \times R_t$, where R_t is the transmission range of each node and $q \geq 1$. It is assumed that the hop distance between a proxy and any of its receivers is upper-bounded by a small number h.

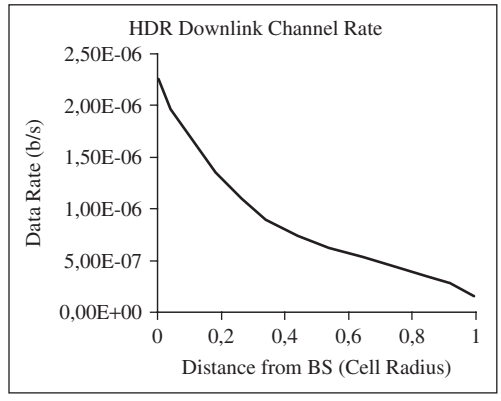

Figure 3.12 Downlink average channel rate.

The simulation study shows that, for a 500 m radius cell, using a proxy beyond a $h = 4$ hop neighborhood of the multicast receiver does not further increase throughput. It will also be assumed that there is a minimal separation of distance sR_t between any pair of transmitters where $s > 0$, as well as the base station knowledge of the location of each node.

3.3.2 Proxy discovery and route interference

In this section, we present an algorithm that discovers proxies and establishes multicast routing entries for the distribution of packets from proxies to multicast receivers and discuss the issue of multihop wireless channel interference that limits the performance gain of the greedy *ad hoc* relay.

The proxy discovery is initiated from a multicast receiver by broadcasting an RTREQ message within a certain range. The RTREQ message carries the multicast receiver's average downlink channel rate, the multicast group ID and a sequence number that is increased by one every time the multicast receiver initiates a new round of proxy discovery. The client then compares its own downlink channel rate with that included in the RTREQ message. It further processes the RTREQ message only if its own downlink channel rate is higher. The client then writes his or her own channel rate into RTREQ and forwards a copy of the RTREQ message to the base station. Finally, the client decreases the TTL of RTREQ by one. If the TTL is still positive, the client attaches the identifier into the relay path in the RTREQ message and further broadcasts the updated RTREQ.

The RTREQ message is propagated greedily along paths of clients with increasing downlink rates. The algorithm only allows these nodes with higher average downlink channel rates to report to the base station since other nodes with lower downlink channel rates are unlikely to have high instantaneous downlink channel rates to serve as proxies. There are no route reply messages in the system from proxies back to the multicast receiver. Candidate proxies send the entire relay path (in RTREQ) to the base station. The base station collects and maintains topology and channel information for relay and makes decisions in selecting proxies. If no proxy information has been established yet, the base station will simply default to multicast.

The base station extracts the relay path from RTREQ messages and constructs/updates the partial *ad hoc* network topology around the multicast receiver. The partial topology includes all the greedy relay paths for a multicast receiver. With such topology available, at each timeslot t the base station calculates for each multicast receiver v the highest downlink data rate possible through its potential proxy clients, i.e. $p(v)^t$. The base station then sets the actual downlink broadcast data rate to $\min_{v \in R} p(v)^t$ for correct reception at all multicast receivers or their proxies.

For each multicast receiver there may exist multiple potential proxy clients whose downlink channel rates are higher than $\min_{v \in R} p(v)^t$. The base station ranks each relay client according to the total number of multicast receivers reachable from the relay client in h hops. Relay clients that are connected to more multicast receivers will be chosen as proxies with higher priority. In this way, the base station merges the paths to different multicast receivers opportunistically to save the relay overhead on the IEEE 802.11 *ad hoc* network, since for each common link among different receiver relay paths, we only send one copy of the packet. A relay path breaks when the proxy, relay or the multicast receiver moves out of range. When the next-hop relay client is not reachable, the IEEE 802.11b MAC layer calls a callback function to inform the relay client of such failures. In the case of unicast, link failure is detected by failure to receive CTSs or ACKs; in the case of a broadcast, failure is detected by the lack of heartbeat messages. The relay client then reports this routing failure to the base station using the uplink. The routing failure message deletes the broken wireless link from the topology maintained at the base station and initiates the recomputation of the proxies. In addition, the relay client also sends out 'prune' messages one-hop upstream to notify its upstream node of the unreachability of the multicast receivers included in the destination header of the multicast packet. Similar approaches apply when an existing multicast node leaves or a new node joins the multicast group.

In many situations the greedy *ad hoc* relay significantly improves the multicast throughput by as much as 400–600 %. We now discuss why, in some situations, the greedy *ad hoc* relay does not perform well.

The primary goal of the greedy *ad hoc* relay strategy is to choose the proxy with the best downlink channel rate. However, since the offered load to the *ad hoc* network equals to the data rate of the downlink 'magnified' by a factor of the number of multicast receivers, it turns out that in some situations the offered load can be higher than the capacity of the *ad hoc* relay paths. We use the simple example shown in Figure 3.13 to illustrate this problem.

In Figure 3.13, two multicast receivers, i.e. clients v_2 and v_3, belong to a multicast group. For each multicast receiver, there are two alternative relay paths, as shown in the figure by solid and dot lines. Clients v_{14} and v_{15} are located closer to the base station and their average downlink channel rates are higher than those of clients v_8 and v_9. The greedy algorithm will discover client v_{14} and v_{15} in pursuit of the proxy with the highest downlink data rate.

However, because the two relay paths, i.e. $v_{14} \rightarrow v_{12} \rightarrow v_{10} \rightarrow v_2$ and $v_{15} \rightarrow v_{13} \rightarrow v_{11} \rightarrow v_3$, interfere with each other, at any given time only one path can transmit and receive packets. On the other hand, although clients v_8 and v_9 have slightly lower downlink channel rates than those of clients v_{14} and v_{15}, relaying through $v_8 \rightarrow v_6 \rightarrow v_4 \rightarrow v_2$ and $v_9 \rightarrow v_7 \rightarrow v_5 \rightarrow v_3$ results in higher throughput because these two paths are out of their interference range and they can transmit

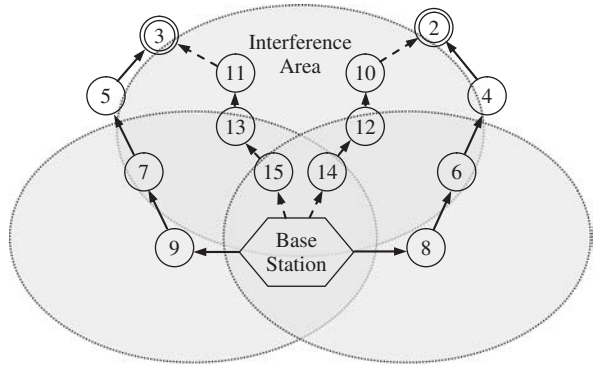

Figure 3.13 Greedy *ad hoc* relay versus optimal relay.

and receive concurrently. The reason for the greedy *ad hoc* relay's suboptimal performance is that greedily maximizing the throughput for each individual multicast receiver does not yield globally optimal throughput due to interference in the *ad hoc* network. Explicit consideration of the wireless interference among different relay paths is necessary.

3.3.3 Near-optimal multicast and approximations

In the problem definition the notation summarized in Table 3.3 [81] will be used. An *ad hoc* network is represented as a graph $G = (V, E)$ where V is the set of (n) nodes and E the set of (m) links. If $(u, v) \in E$, then node u and v are at most R_t apart. The set $R \subseteq V$ is the set of receivers of a given multicast group. The average downlink rate of node $v \in V$ is $r_v \geq 0$. A receiver $v \in R$ may receive data either directly from the base station at rate r_v or through a proxy. The *ad hoc* relay subnetwork for a given multicast group is graph $G' = (V', E')$, where $(u, v) \in E'$ iff $u, v \in V'$ and $(u, v) \in E$. For example, one relay subnetwork for multicast in Figure 3.13 consists of the node set

$$V' = \{v_8, v_6, v_4, v_2, v_9, v_7, v_5, v_3\}$$

and the link set

$$E' = \{(v_8, v_6), (v_6, v_4), (v_4, v_2), (v_9, v_7), (v_7, v_5), (v_5, v_3)\}$$

The relay subnetwork G' is composed of a collection of directed trees F (forest) spanning node set V'. Along each tree $T \in F$, data (received from the base station) is multicasted from the root (proxy) to all the receivers in T.

Receivers in $R - R_{3G}$ receive data at the rate of $\max\{r_v, r_v^a\}$, where r_v^a is the rate at which data are received through the *ad hoc* relay subnetwork G'. For a given G', we denote $\max\{r_v, r_v^a\}$ as $r_v(G')$. We denote by $I = (V, A)$ the interference graph for the *ad hoc* network. Thus, two *ad hoc* nodes u and v interfere with each other iff$(u, v) \in A$. For unicast transmissions, each node in the interference graph will represent an edge in G and $(u, v) \notin A$ if u and v are at least qR_t apart for some fixed constant q. Given $G' = (V', E')$, let $k(G')$ denote the minimum number of

Table 3.3 Notation summary. (Reproduced by permission of IEEE ©2006 from Bhatia *et al*. [81])

$G = (V, E)$	Connectivity graph of the *ad-hoc* network
$I = (V, A)$	Interference graph of the *ad-hoc* network
R_t	Transmission range of each node $v \in V$
R_I	The maximum interference range $R_I = qR_t$
r_v	The 3G downlink channel rate of $v \in V$
$p(v)$	The 3G downlink channel rate of the proxy of node of $v \in V$
r_v^a	The data rate of v through the *ad-hoc* relay network, $r_v^a = \min\{f/k(G'), p(v)\}$
$r(G)$	The optimal multicast rate
f	The channel rate of 802.11 *ad-hoc* network
$k(G')$	Minimal number of colors needed to color G' a subgraph of I
k_C	Minimal number of colors needed to color the best relay network for receivers in cell $C \in \Gamma$
R	The set of multicast receivers in the multicast group
R_{3G}	A subset of R that receive the multicast data directly frog 3G base station and are not selected in *ad-hoc* relay subnetwork
R_C	A subset of R that are in cell $C \in \Gamma$
Γ	The number of grid cells under a base station
$G'_C = (V'_C, E'_C)$	The optimal multicast relay subnetwork for cell $C \in \Gamma$
$G_0 = (V_0, E_0)$	The *ad-hoc* relay network output by algorithm ALGO

colors required to color the nodes in V' such that two nodes $u, v \in V'$ have the same color if $(u, v) \notin A$. For unicast transmissions, $k(G')$ denotes the minimum number of colors required to color the edges in E'. Therefore, the best multicast rate that can be achieved in G' is at most $f/k(G')$. To be precise, only nonleaf nodes need to be colored since the leaf nodes (receivers) do not participate in transmissions. The results presented here, although applicable to this more precise model, are more involved and hence for ease of presentation we will use the model where all leaf receivers, except R_{3G}, are colored.

As stated earlier, we make the assumption that the best proxy for receiver v is no more than h hops away for some small value h, e.g. $h = 4$. For receiver $v \in R - R_{3G}$, let $p(v)$ be the rate of the 3G proxy for v. Then, $r_v^a = \min[f/k(G'), p(v)]$. Hence, the multicast rate for v in G' is $r_v(G') = \max\{r_v, \min[f/k(G'), p(v)]\}$. With notation $r(G') = \min_{v \in R} r_v(G')$, the ICAM problem is to compute G' such that the multicast rate $r(G')$ for its associated ad hoc subnetwork G' is maximized. The ICAM problem is NP hard [81, 82] and acceptable approximations are needed.

The polynomial–time approximation algorithm [81] leverages the property so that for each multicast receiver the best proxy can be at most h hops away. The algorithm performs localized proxy search and constructs the optimal multicast trees for the receivers within a certain locality. All local optimal multicast trees are then combined to form the global multicast forest. The approximation algorithm ALGO is formally represented as in Reference [81].

Algorithm ALGO for computing a multicast relay forest

computeMcastForest()

(1) Divide the 3G base station coverage area into a grid of cell size $(2h + q + \varepsilon)R_t \times (2h + q + \varepsilon)R_t$

(2) For each grid cell $C \in \Gamma // \Gamma$: the set of grid cells

(3) $V'_C = \text{computeOptCellForest}(C)$

(4) //Merge for solution of each cell

(5) $V_0 = \cup_{C \in \Gamma} V'_C$

(6) $R_{3G} = R \bigcap (V - V_0)$

It first divides the coverage area of a base station into a two-dimensional grid of $(2h + q + \varepsilon)R_t \times (2h + q + \varepsilon)R_t$ cells, where $\varepsilon > 0$. ALGO then computes a solution for each cell of the grid Γ that contains at least one receiver. In other words, ALGO computes the optimal solution for ICAM when restricted only to the receivers $R_C \subseteq R$ in a cell $C \in \Gamma$. Finally, ALGO merges these solutions for all cells to compute a feasible solution to the original instance of the problem.

Let C be a cell with at least one receiver ($|R_C| > 0$) and $V_C \subseteq V$ be the set of all nodes that are at most h hops from at least one receiver in R_C. Note that in any optimal solution the set of proxies for the receivers in R_C and any intermediate relay nodes must be in V_C. Algorithm ALGO computes the optimal solution for a cell C as follows:

Algorithm for computing optimal multicast relay forest in one grid cell

computeOptCellForest(C)

(1) Enumerate all subsets V'_C of $V_C // V_C$ is the set of // nodes that are within h hops from receiving in C

(2) For each $v \in V'_C$

(3) $p(v) =$ findBestProxy(v);

(4) rm = computeMinProxyRate();

(5) $k(G'_C)$ minColor (V'_C)

(6) $rate =$ min (rm, $f/k(G'_C)$)

(7) Output the subset V'_C with maximal *rate*

ALGO enumerates all subsets V'_C of nodes in V_C. For a given subset V'_C, let G'_C be its associated ad hoc relay subnetwork. It computes the minimum number of colors $k(G'_C)$ needed to color the vertexes of G'_C based on the interference graph I. Algorithm ALGO then computes the best proxy $p(v)$ in G'_C for every receiver $v \in V'_C$, as described before. Note that all this information is sufficient to compute $r_v(G'_C)$ for every receiver $v \in V'_C$. The $r_v(G'_C)$ of all receivers $v \in R_C$ that are not in V'_C is $r_v(G'_C) = r_v$. Taking the minimum of $r_v(G'_C)$ for all receivers $v \in R_C$, ALGO is able to compute the multicast rate $r(G'_C)$ for the *ad hoc* relay subnetwork for the receivers in R_C. ALGO then selects the subset $V'_C \subseteq V_C$, whose associated *ad hoc* relay subnetwork has the highest rate, to generate the optimal multicast strategy for the receivers R_C in cell C. All this can be done in constant time [81]. Finally, ALGO outputs the union of the subnetworks computed for each grid cell, i.e. $V_0 = \cup_{C \in \Gamma} V'_C \subseteq V$ as the solution for the original problem instance. The set of receivers R_{3G} that receive directly from the 3G base station is $R \cap (V - V_0)$.

It can be shown [81] that ALGO has the following properties: (a) it runs in polynomial time, (b) the number of nodes in any set $V_C \subseteq V$ for a cell C is bounded by a constant, (c) the optimal multicast rate for the original problem instance is at most $f/\max_{C \in \Gamma} k_C$, (d) the graph $G_0 = (V_0, E_0)$ induced by the node set V_0 can be colored with at most $4 \max_{C \in \Gamma} k_C$ four colors and (e) ALGO is a four-approximation for ICAM.

3.3.4 Performance examples

In this section, we present some performance examples of the greedy and the near-optimal relay with the same parameters as in Reference [81]. As an example, 65 mobile nodes are randomly placed in a 3G HDR cell with a maximum moving speed of 15 m/s. Figures 3.14 to 3.25 show the simulation results.

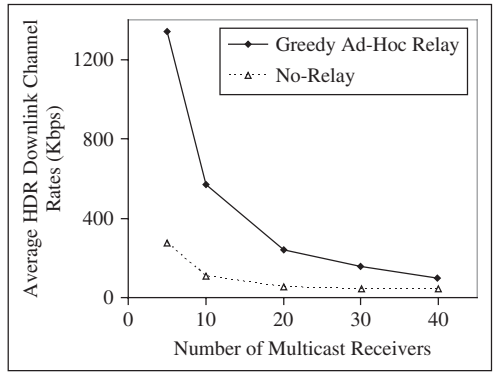

Figure 3.14 Average downlink channel rates versus number of multicast receivers.

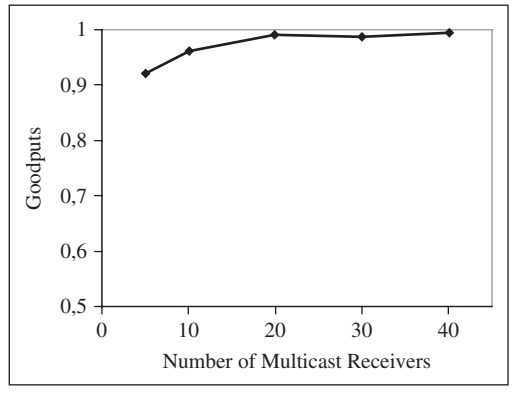

Figure 3.15 Goodputs versus number of multicast receivers.

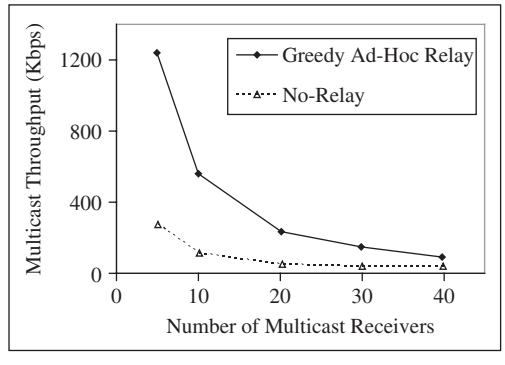

Figure 3.16 Throughput versus number of multicast receivers.

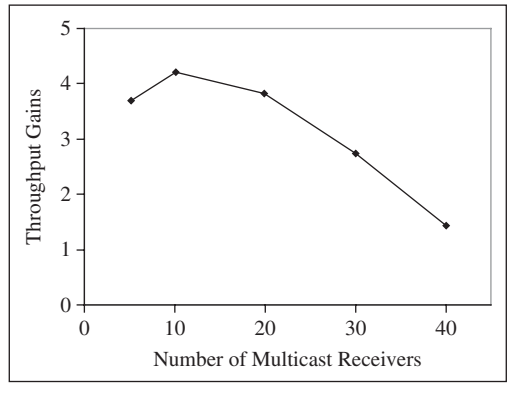

Figure 3.17 Throughput gains versus number of multicast receivers.

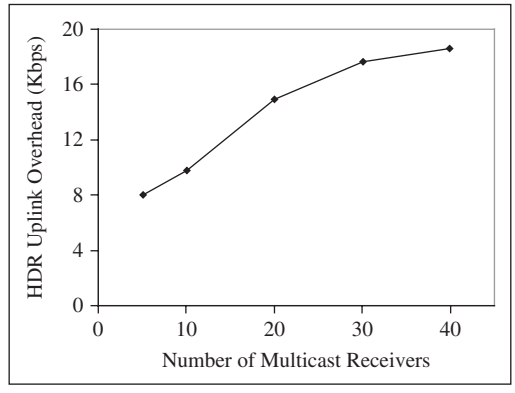

Figure 3.18 Uplink overhead versus number of multicast receivers.

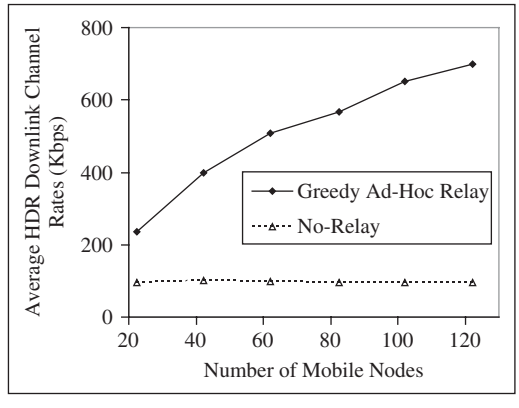

Figure 3.19 Average downlink channel rates versus number of mobile nodes.

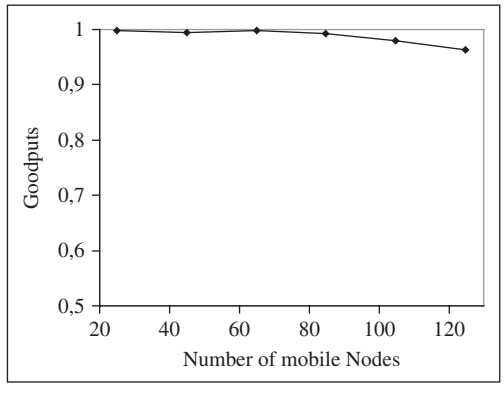

Figure 3.20 Goodputs versus number of mobile nodes.

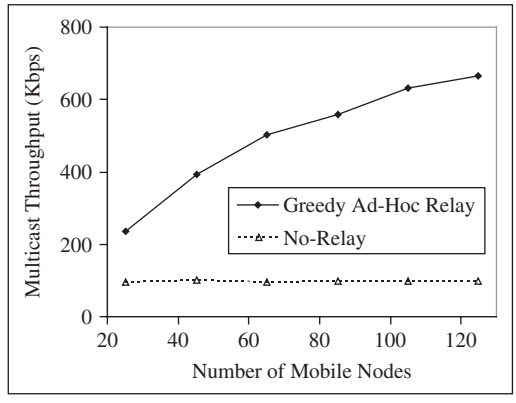

Figure 3.21 Throughput versus number of mobile nodes.

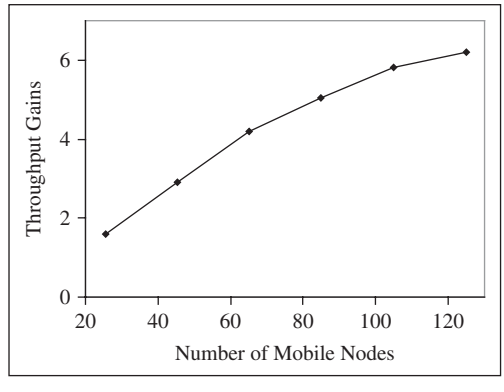

Figure 3.22 Throughput gains versus number of mobile nodes.

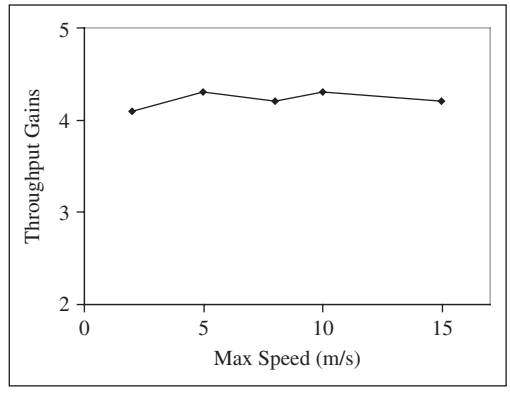

Figure 3.23 Throughput gains versus number of mobile nodes.

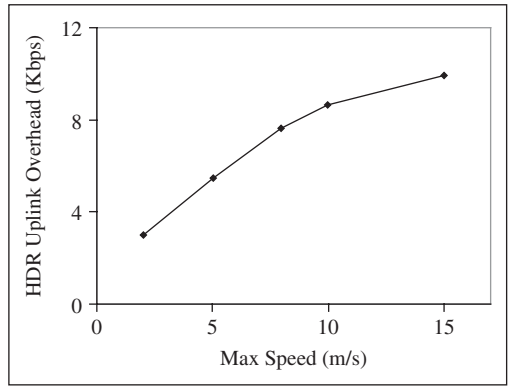

Figure 3.24 Uplink overhead versus maximum speed.

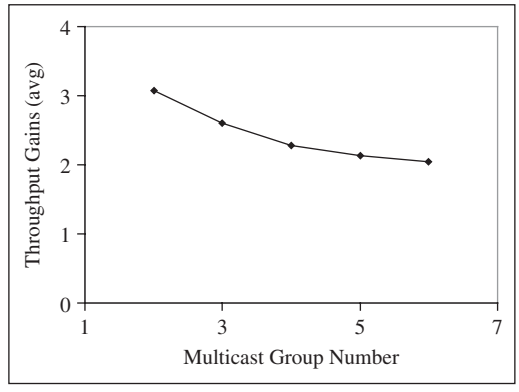

Figure 3.25 Throughput gains versus multicast group number.

It can see from these figures that relaying provides improved performance of the system. For more information on this topic see References [81] to [102].

REFERENCES

[1] Truman Chiu-Yam Ng and Wei Yu, Joint optimization of relay strategies and resource allocations in cooperative cellular networks, *IEEE J. Selected Areas Commun.*, vol. 25, no. 2, February 2007, p. 328.

[2] A. Nosratinia, T. E. Hunter and A. Hedayat, Cooperative communication in wireless networks, *IEEE Commun. Mag.*, vol. 42, no. 10, October 2004, pp. 74–80.

[3] J. N. Laneman and G. W. Wornell, Distributed space – time coded protocols for exploiting cooperative diversity in wireless networks, *IEEE Trans. Information Theory*, vol. 49, no. 10, October 2003, pp. 2415–2425.

[4] J. N. Laneman, D. N. C. Tse and G.W. Wornell, Cooperative diversity in wireless networks: efficient protocols and outage behavior, *IEEE Trans. Information Theory*, vol. 50, no. 12, December 2004, pp. 3062–3080.

[5] A. Sendonaris, E. Erkip and B. Aazhang, User cooperation diversity – Part I: system description, *IEEE Trans. Commun.*, vol. 51, no. 11, November 2003, pp. 1927–1938.
[6] A. Sendonaris, E. Erkip and B. Aazhang, User cooperation diversity – Part II: implementation aspects and performance analysis, *IEEE Trans. Commun.*, vol. 51, no. 11, November 2003, pp. 1939–1948.
[7] A. Stefanov and E. Erkip, Cooperative coding for wireless networks, *IEEE Trans. Commun.*, vol. 52, no. 9, September 2004, pp. 1470–1476.
[8] R. Pabst, B. Walke, D. Schultz, P. Herhold, H. Yanikomeroglu, S. Mukherjee, H. Viswanathan, M. Lott, W. Zirwas, M. Dohler, H. Aghvami, D. Falconer and G. Fettweis, Relay-based deployment concepts for wireless and mobile broadband radio, *IEEE Commun. Mag.*, vol. 42, no. 9, September 2004, pp. 80–89.
[9] H. Viswanathan and S. Mukherjee, Performance of cellular networks with relays and centralized scheduling, *IEEE Trans. Wireless Commun.*, vol. 4, no. 5, September 2005, pp. 2318–2328.
[10] J. Cho and Z. J. Haas, On the throughput enhancement of the downstream channel in cellular radio networks through multihop relaying, *IEEE J. Selected Areas Commun.*, vol. 22, no. 7, September 2004, pp. 1206–1219.
[11] H.-Y. Hsieh and R. Sivakumar, On using peer-to-peer communication in cellular wireless data networks, *IEEE Trans. Mobile Comput.*, vol. 3, no. 1, January 2004, pp. 57–72.
[12] T. M. Cover and A. A. E. Gamal, Capacity theorems for the relay channel, *IEEE Trans. Information Theory*, vol. 25, no. 5, September 1979, pp. 572–584.
[13] V. Sreng, H. Yanikomeroglu and D. Falconer, Relay selection strategies in cellular networks with peer-to-peer relaying, in *Proc. 58th IEEE Vehicle Technol. Conf. (VTC 2003-Fall)*, vol.3, orlando, FL, 6–9 October 2003, pp. 1949–1953.
[14] M. Yu and J. Li, Is amplify-and-forward practically better than decode-and-forward or vice versa, in *Proc. IEEE Int. Conf. Acoustics*, *Speech, and Signal Processing (ICASSP)*, vol. 3, March 2005, pp. 365–368.
[15] B. Can, H. Yomo and E. D. Carvalho, A novel hybrid forwarding scheme for OFDM based cooperative relay networks, in *Proc. IEEE Int. Conf. Commun. (ICC)*, 2006.
[16] M. A. Khojastepour, A. Sabharwal and B. Aazhang, On the capacity of 'cheap' relay networks, in *Proc. 37th Annual Conf. Information Sciences and Systems (CISS)*, 2003, pp. 12–14.
[17] M. A. Khojastepour, A Sabharwal and B. Aazhang, On the capacity of Gaussian 'cheap' relay channel, in *Proc. IEEE Global Telecommun. Conf. (GLOBECOM)*, 2003, pp. 1776–1780.
[18] A. Wittneben and B. Rankov, Impact of cooperative relays on the capacity of rank-deficient MIMO channels, in *Proc. 12th IST Summit on Mobile Wireless Commun.*, 2003, pp. 421–425.
[19] M. Dohler, A. Gkelias and H. Aghvami, A resource allocation strategy for distributed MIMO multi-hop communication systems, *IEEE Commun. Lett.*, vol. 8, no. 2, February 2004, pp. 99–101.
[20] J. Luo, R. S. Blum, L. Cimini, L. Greenstein and A. Haimovich, Power allocation in a transmit diversity system with mean channel gain information, *IEEE Commun. Lett.*, vol. 9, no. 7, July 2005, pp. 616–618.
[21] A. Host-Madsen and J. Zhang, Capacity bounds and power allocation for wireless relay channels, *IEEE Trans. Information Theory*, vol. 51, no. 6, June 2005, pp. 2020–2040.
[22] M. O. Hasna and M.-S. Alouini, Optimal power allocation for relayed transmissions over Rayleigh-fading channels, *IEEE Trans. Wireless Commun.*, vol. 3, no. 6, November 2004, pp. 1999–2004.
[23] I. Maric and R. D. Yates, Bandwidth and power allocation for cooperative strategies in Gaussian relay networks, in *Proc. 38th Asilomar Conf. Signals, Systems and Computers*, vol. 2, 7–10 November 2004, pp. 1907–1911.

[24] J. Adeane, M. R. D. Rodrigues and I. J. Wassell, Centralised and distributed power allocation algorithms in cooperative networks, in *Proc. IEEE 6th Workshop on Signal Processing Advances in Wireless Commun. (SPAWC)*, 2005, pp. 333–337.

[25] X. Deng and A. M. Haimovich, Power allocation for cooperative relaying in wireless networks, *IEEE Commun. Lett.*, vol. 9, no. 11, November 2005, pp. 994–996.

[26] A. Reznik, S. R. Kulkarni and S. Verdú, Degraded Gaussian multirelay channel: capacity and optimal power allocation, *IEEE Trans. Information Theory*, vol. 50, no. 12, December 2004, pp. 3037–3046.

[27] M. Chen, S. Serbetli and A. Yener, Distributed power allocation for parallel relay networks, in *Proc. IEEE Global Telecommun. Conf. (GLOBECOM)*, vol. 3, November 2005, pp. 1177–1181.

[28] E. G. Larsson and Y. Cao, Collaborative transmit diversity with adaptive radio resource and power allocation, *IEEE Commun. Lett.*, vol. 9, no. 6, June 2005, pp. 511–513.

[29] S. Serbetli and A. Yener, Optimal power allocation for relay assisted F/TDMA *ad hoc* networks, in *Proc. Int. Conf. Wireless Networks*, *Commun. and Mobile Comput.*, vol. 2, Montreal, Canada, 13–16 June 2005, pp. 1319–1324.

[30] Y. Liang and V. V. Veeravalli, Resource allocation for wireless relay channels, in *Proc. 38th Asilomar Conf. Signals, Systems and Computers*, vol. 2, 7–10 November 2004, pp. 1902–1906.

[31] Y. Liang and V. V. Veeravalli, Gaussian orthogonal relay channels: optimal resource allocation and capacity, *IEEE Trans. Information Theory*, vol. 51, no. 9, September 2005, pp. 3284–3289.

[32] G.-D. Yu, Z.-Y. Zhang, Y. Chen, S. Chen and P.-L. Qiu, Power allocation for non-regenerative OFDM relaying channels, in *Proc. Int. Conf. Wireless Commun., Networking and Mobile Comput. (WCNC)*, vol. 1, 2005, pp. 185–188.

[33] K. Lee and A. Yener, On the achievable rate of three-node cognitive hybrid wireless networks, in *Proc. Int. Conf. Wireless Networks, Commun. and Mobile Comput.*, vol. 2, 2005, pp. 1313–1318.

[34] K. Chen, Z. Yang, C. Wagener and K. Nahrstedt, Market models and pricing mechanisms in a multihop wireless hotspot network, in *Proc. Second Annual Int. Conf. Mobile and Ubiquitous Systems: Networking and Services (MobiQuitous)*, 2005, pp. 73–82.

[35] O. Ileri, S.-C. Mau and N. Mandayam, Pricing for enabling forwarding in self-configuring *ad hoc* networks, *IEEE J. Selected Areas Commun.*, vol. 23, no. 1, January 2005, pp. 151–162.

[36] F. P. Kelly, A. Maulloo and D. Tan, Rate control for communication networks: shadow prices, proportional fairness and stability, *J. Ops Res. Soc.*, vol. 49, no. 3, 1998, pp. 237–252.

[37] G. Song and Y. G. Li, Cross-layer optimization for OFDM wireless networks – Part I: theoretical framework, *IEEE Trans. Wireless Commun.*, vol. 4, no. 2, March 2005, pp. 614–624.

[38] G. Song and Y. G. Li, Cross-layer optimization for OFDM wireless networks – Part II: algorithm development, *IEEE Trans. Wireless Commun.*, vol. 4, no. 2, March 2005, pp. 625–634.

[39] W. Yu and R. Lui, Dual methods for nonconvex spectrum optimization of multicarrier systems, *IEEE Trans. Commun.*, vol. 54, no. 7, July 2006, pp. 1310–1322.

[40] R. U. Nabar, H. Bölcskei, and F. W. Kneubühler, Fading relay channels: performance limits and space–time signal design, *IEEE J. Selected Areas Commun.*, vol. 22, no. 6, August 2004, pp. 1099–1109.

[41] N. Z. Shor, *Minimization Methods for Non-differentiable Functions*. Springer, 1985.

[42] S. Boyd, L. Xiao and A. Mutapcic, *Subgradient methods*, Lecture notes of EE392o, Stanford University, Autumn Quarter 2003–2004.
[43] R. Cendrillon, W. Yu, M. Moonen, J. Verlinden and T. Bostoen, Optimal spectrum balancing for digital subscriber lines, *IEEE Trans. Commun.*, vol. 54, no. 5, May 2006, pp. 922–933.
[44] A. Fallahi, E. Hossain and A. Alfa, QoS and energy trade off in distributed energy-limited mesh/relay networks: a queuing analysis, *IEEE Trans. Parallel and Distributed Systems*, vol. 17, no. 6, June 2006, p. 576.
[45] R. Bruno, M. Conti and E. Gregori, Mesh networks: commodity multihop *ad hoc* networks, *IEEE Commun. Mag.*, vol. 43, no. 3, March 2005, pp. 123–131.
[46] C. E. Jones, K. M. Sivalingam, P. Agrawal and J. C. Chen, A survey of energy efficient network protocols for wireless networks, *Wireless Networks*, vol. 7, no. 4, 2001, pp. 343–358.
[47] P. Lettieri and M. Srivastava, Advances in wireless terminals, *IEEE Personal Commun.*, February 1999, pp. 6–19.
[48] S. Sheng, A. Chandrakasan and R.W. Brodersen, A portable multimedia terminal, *IEEE Commun. Mag.*, vol. 30, no. 12, December 1992, pp. 64–75.
[49] R. Zheng, J. C. Hou and L. Sha, Performance analysis of power management policies in wireless networks, *IEEE Trans. Wireless Commun.* (to appear).
[50] C. Schurgers, V. Tsiatsis, S. Ganeriwal and M. Srivastava, Optimizing sensor networks in the energy–latency–density design space, *IEEE Trans. Mobile Comput.*, vol. 1, no. 1, January/March 2002, pp. 70–80.
[51] M. J. Miller and N. H. Vaidya, A MAC protocol to reduce sensor network energy consumption using a wakeup radio, *IEEE Trans. Mobile Comput.*, vol. 4, no. 3, May/June 2005, pp. 228–242.
[52] X. Yang and N. H. Vaidya, A wakeup scheme for sensor networks: achieving balance between energy saving and end-to-end delay, in *Proc. IEEE Real-Time and Embedded Technology and Applications Symp. (RTAS)*, May 2004.
[53] W. Ye, J. Heidemann and D. Estrin, Medium access control with coordinated adaptive sleeping for wireless sensor networks, *IEEE/ACM Trans. Networking*, vol. 12, no. 3, June 2004, pp. 493–506.
[54] A. Sinha and A. P. Chandrakasan, Dynamic power management in wireless sensor networks, *IEEE Design and Test of Computers Mag.*, vol. 18, no. 2, March/April 2001, pp. 62–74.
[55] K. Sohrabi, J. Gao, V. Ailawadhi and G. Pottie, A self organizing wireless sensor network, in *Proc. 1999 Allerton Conf. Commun., Control, and Comput.*, October 1999.
[56] F. J. Block and C. W. Baum, Energy-efficient self-organizing communications protocols for wireless sensor networks, in *Proc. IEEE Military Commun. Conf. 2001 (MILCOM '01)*, October 2001.
[57] C.-F. Chiasserini and M. Garetto, Modeling the performance of wireless sensor networks, in *Proc. IEEE INFOCOM '04*, 2004.
[58] S. Singh and C. S. Raghavendra, PAMAS: power aware multi-access protocol with signaling for ad hoc networks, *ACM Computer Commun. Rev.*, July 1998, pp. 5–26.
[59] F. Zhang, T. D. Todd, D. Zhao and V. Kezys, Power saving access points for IEEE 802.11 wireless network infrastructure, *IEEE Trans. Mobile Comput.* (to appear).
[60] E. Shih, S. Cho, N. Ickes, R. Min, A. Sinha, A. Wang and A. Chandrakasan, Physical layer driven protocol and algorithm design for energy-efficient wireless sensor networks, in *Proc. 2001 ACM MOBICOM*, July 2001, pp. 272–286.
[61] A. S. Alfa, Vacation models in discrete time, *Queueing Systems*, vol. 44, 2003, pp. 5–30.
[62] G. L. Choudhury and S. S. Rappaport, Priority access schemes using CSMA-CD, *IEEE Trans. Commun.*, vol. 33, July 1985, pp. 620–626.
[63] D. Chen and P. K. Varshney, QoS support in wireless sensor networks: a survey, in *Proc. 2004 Int. Conf. Wireless Networks (ICWN '04)*, June 2004.

[64] M. Younis, K. Akayya, M. Eltowiessy and A. Wadaa, On handling QoS traffic in wireless sensor networks, in *Proc. 37th Hawaii Int. Conf. System Sciences (HICSS-37)*, January 2004.
[65] Q. Gao, K. J. Blow, D. J. Holding and I. Marshall, Analysis of energy conservation in sensor networks, *Wireless Networks*, vol. 11, no. 6, November 2005, pp. 787–794.
[66] A. F. Mini, B. Nath and A. A. F. Loureiro, A probabilistic approach to predict the energy consumption in wireless sensor networks, in *Proc. IV Workshop Comunicao sem Fio e Computao Mvel*, October 2002.
[67] J. Misic and V. B. Misic, Duty cycle management in sensor networks based on 802.15.4 beacon enabled MAC, *Ad Hoc and Sensor Wireless Networks J.*, vol. 1, no. 1, Old City Publishing, 2005.
[68] A. S. Alfa, Matrix-geometric solution of discrete time MAP/PH/1 priority ueue, *Naval Res. Logistics*, vol. 45, 1998, pp. 23–50.
[69] N. Akar, N. C. Oguz and K. Sohraby, Matrix-geometric solutions of M/G/1-type Markov chains: a unifying generalized state-space approach, *IEEE J. Selected Areas Commun.*, vol. 16, no. 5, June 1998.
[70] R. Mukhtar, S. Hanly, M. Zukherman and F. Cameron, A model for the performance evaluation of packet transmissions using type-II hybrid ARQ over a correlated error channel, *Wireless Networks*, vol. 10, no. 1, 2004, pp. 7–16.
[71] U. Vornefeld, Analytical performance evaluation of mobile Internet access via GPRS networks, in *Proc. Conf. European Wireless* 2002, February 2002.
[72] M. F. Neuts, A versatile Markovian point process, *J. Applied Probability*, vol. 16, 1979, pp. 764–779.
[73] M. F. Neuts, *Matrix-Geometric Solutions in Stochastic Models*. John Hopkins University Press: Baltimore, MD, 1981.
[74] V. Ramaswami, A stable recursion for the steady state vector in Markov chains of M/G/1 type, *Commun. Statistic–Stochastic Models*, vol. 4, 1988, pp. 183–263.
[75] O. Tickoo and B. Sikdar, A queueing model for finite load IEEE 802.11 random access MAC, in *Proc. IEEE ICC'04*, 2004.
[76] G. Bianchi, Performance analysis of the IEEE 802.11 distributed coordination function, *IEEE J. Selected Areas Commun.*, vol. 18, no. 3, March 2000.
[77] W. H. Press, S. A. Teukolsky, W. T. Vetterling and B. P. Flannery, *Numerical Recipes in C: The Art of Scientific Computing*. Cambridge University Press, 1988.
[78] *IEEE 802.11 Wireless LAN Medium Access Control (MAC) and Physical Layer (PHY) Specifications*. IEEE Std., 1999.
[79] F. A. Tobagi, Carrier sense multiple access with message-based priority functions, *IEEE Trans. Commun.*, vol. 30, no. 1, pp. 185–200, January 1982.
[80] G. Cantieni, Q. Ni, C. Barakat and T. Turletti, Performance analysis under finite load and improvements for multirate 802.11, *Computer Commun. J.*, vol. 28, no. 10, pp. 1095–1109, June 2005.
[81] R. Bhatia, L. Li, H. Luo and R. Ramjee, ICAM: integrated cellular and ad hoc multicast, *IEEE Trans. Mobile Comput.*, vol. 5, no. 8, August 2006, p. 1004.
[82] R. Bhatia, L. E. Li, H. Luo and R. Ramjee, IICAM: integrated cellular *ad hoc* multicast, Technical Report, Computer Science Department, University of Illinois at Urbana-Champaign, November 2004.
[83] 3G Today, http://www.3gtoday.com/, 2004.
[84] *1xEV: 1x EVolution IS-856 TIA/EIA Standard – Airlink overview*, QUALCOMM Inc., White paper, November 2001.
[85] H. Luo, R. Ramjee, P. Sinha, L. E. Li and S. Lu, UCAN: a unified cellular and *ad hoc* network architecture, in *Proc. ACM MOBICOM Conf.*, 2003, pp. 353–367.
[86] H. Wu, C. Qiao, S. De and O. Tonguz, An integrated cellular and *ad hoc* relaying system: iCAR, *IEEE J. Selected Areas Commun.*, vol. 19, October 2001, pp. 2105–2115.

[87] M. S. Corson and S. G. Batsell, A reservation-based multicast (RBM) routing protocol for mobile networks: initial route construction phase, *Wireless Networks*, vol. 1, December 1995, pp. 427–450.
[88] L. Ji and M. S. Corson, A lightweight adaptive multicast algorithm, in *Proc. IEEE GLOBECOM Conf.*, 1998, pp. 1036–1042.
[89] E. Bommaiah, M. Liu, A. McAuley and R. Talpade, AMRoute: *ad hoc* multicast routing protocol, Internet Draft, draft-talpademanet-amroute-00.txt, 1998.
[90] C. Wu, Y. C. Tay and C.-K. Toh, *Ad hoc* multicast routing protocol utilizing increasing ID-Numbers (AMRIS) functional specification, Internet Draft, draft-ietf-manet-amris-spec-00.txt, 1998.
[91] E. M. Royer and E. E. Perkins, Multicast operation of the *ad hoc* on-demand distance vector routing protocol, in *Proc. ACM MOBICOM Conf.*, 1999, pp. 207–218.
[92] J. J. Garcia-Luna-Aceves and E. L. Madruga, The core-assisted mesh protocol, *IEEE J. Selected Areas Commun.*, vol. 17, August 1999, pp. 1380–1384.
[93] S.-J. Lee, W. Su and M. Gerla, On-demand multicast routing protocol in multihop wireless mobile networks, *Mobile Networks and Applications*, vol. 7, 2002, pp. 441–453.
[94] P. Agashe, R. Rezaiifar and P. Bender, CDMA2000 high rate broadcast packet data air interface design, *IEEE Commun. Mag.*, February 2004, pp. 83–89.
[95] W. C. Jakes, *Microwave Mobile Communication*. John Wiley & Sons, Ltd, 1974.
[96] P. Bender, P. Black, M. Grob, R. Padovani, N. Sindhushayana and A. Viterbi, CDMA/HDR: a bandwidth-efficient high-speed wireless data service for nomadic users, *IEEE Commun. Mag.*, vol. 38, July 2000, pp. 70–77.
[97] J. Li, C. Blake, D. S. J. De Couto, H. Lee and R. Morris, Capacity of *ad hoc* wireless networks, in *Proc. ACM MOBICOM Conf.*, 2001, pp. 61–69.
[98] T. He, C. Huang, B. M. Blum, J. A. Stankovic and T. Abdelzaher, Range-free localization schemes for large scale sensor networks, in *Proc. ACM MOBICOM Conf.*, 2003, pp. 81–95.
[99] A. Rao, C. Papadimitriou, S. Shenker and I. Stoica, Geographic routing without location information, in *Proc. ACM MOBICOM Conf.*, 2003, pp. 96–108.
[100] S. Marti, T. Giuli, K. Lai and M. Baker, Mitigating routing misbehavior in mobile *ad hoc* networks, in *Proc. ACM MOBICOM Conf.*, 2000, pp. 255–265.
[101] H. Bodlaender, Dynamic programming on graphs of bounded treewidth, in *Proc. 15th Int. Colloq. Automata, Languages and Programming*, 1988, pp. 631–643.
[102] J. Yoon, M. Liu and B. Noble, Random waypoint considered harmful, *Proc. IEEE INFOCOM Conf.*, 2003, pp. 1312–1321.

4

Topology Control

Topology control algorithms are used to maintain network connectivity while reducing energy consumption and improving network capacity. The key idea to topology control is that, instead of transmitting with the maximal power, nodes in a wireless multihop network collaboratively determine their transmission power and define the network topology by forming the proper neighbor relation under certain criteria. The importance of topology control lies in the fact that it critically affects the system performance in several ways. For one, it affects network spatial reuse and, hence, the traffic-carrying capacity. Choosing too high power level results in excessive interference, while choosing too low power level may result in a disconnected network. Topology control also affects energy usage of communication, and thus impacts on the battery life, a critical resource in many mobile applications. In addition, topology control also impacts on contention for the medium. Collisions can be mitigated by choosing the smallest transmission power subject to maintaining network connectivity. For these reasons, the subject has been recently extensively studied [1–23].

In Reference [10], Rodoplu and Meng (*R&M*) defined *relay region* and *enclosure* for the purpose of power and topology control. For any node i that intends to transmit to node j, node j is said to lie in the *relay region* of a third node r, if node i will consume less power when it chooses to relay through node r instead of transmitting directly to node j. The *enclosure* of node i is then defined as the union of the complement of relay regions of all the nodes that node i can reach by using its maximal transmission power. A two-phase distributed protocol was then devised to find the minimum power topology for a static network. In the first phase, each node i executes a local search to find the enclosure graph. This is done by examining neighbor nodes, which a node can reach by using its maximal power and keeping only those that do not lie in the relay regions of previously found nodes. In the second phase, each node runs the distributed Bellman–Ford shortest-path algorithm (see Chapters 7 and 13) upon the enclosure graph, using the power consumption as the cost metric. It is shown that the network is strongly connected if every node maintains links with the nodes in its enclosure and the resulting topology is a minimum power topology. To deal with limited mobility, each node periodically executes the distributed protocol to find the enclosure graph. This algorithm assumes that there is only one data sink (destination) in the network, which may not be the case in practice. Also, an explicit propagation channel model is needed to compute the relay region.

Two centralized algorithms, *CONNECT* and *BICONNAUGMENT*, are presented in Reference [9] to minimize the maximal power used per node while maintaining the (bi)connectivity

Advanced Wireless Technologies: Cognitive, Cooperative & Opportunistic 4G Technology Second Edition Savo G. Glisic

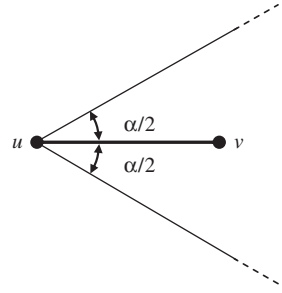

Figure 4.1 Definition of $cone(u, \alpha, v)$.

of the network. Both algorithms are greedy and iteratively merge different components until only one remains. They introduced two distributed heuristics for mobile networks. In *LINT*, each node is configured with three parameters – the 'desired' node degree d_d, a high threshold d_h on the node degree and a low threshold d_l. Every node will periodically check the number of active neighbors and change its power level accordingly, so that the node degree is kept within the thresholds. *LILT* further improves *LINT* by overriding the high threshold when the topology change indicated by the routing update results in undesirable connectivity. Both centralized algorithms require global information, and thus cannot be directly deployed in the case of mobility, and the proposed distributed heuristics may not preserve the network connectivity.

The approaches implemented in the network layer, *COMPOW* [5] and *CLUSTERPOW* [8], are based on the idea that if each node uses the smallest common power required to maintain network connectivity, the traffic-carrying capacity of the entire network is maximized, the battery life is extended and the MAC-level contention is mitigated. Each node runs several routing daemons in parallel, one for each power level. Each routing daemon maintains its own routing table by exchanging control messages at the specified power level. By comparing the entries in different routing tables, each node can determine the smallest common power that ensures the maximal number of nodes are connected. The major drawback of these two approaches is their significant message overhead, since every node has to run multiple routing daemons, each of which has to exchange link state information with the counterparts at other nodes.

Cone-based topology control ($CBTC(\alpha)$) is a two-phase algorithm in which each node finds the minimal power p such that transmitting with the power p ensures that the node can reach some node in every cone of degree α. A definition of $cone(u, \alpha, v)$ is given in Figure 4.1.

The algorithm has been proved to preserve network connectivity if $\alpha < 5\pi/6$ [7]. Several optimization methods (which are applied after the topology is derived under the base algorithm) are also discussed to reduce the transmitting power further. An event-driven strategy is proposed to reconfigure the network topology in the case of mobility. Each node is notified when any neighbor *leaves*/*joins* the neighborhood *and*/*or* the angle changes. The mechanism used to realize this requires the state to be kept at, and message exchanges among, neighboring nodes. The node then determines whether it needs to rerun the topology control algorithm.

Instead of adjusting the transmission power of individual devices, there also exist other approaches to generate power-efficient topology. By following a probabilistic approach, the suitable common transmission range which preserves network connectivity was derived in Reference [6] and the lower and upper bounds on the probability of connectedness were established. A 'backbone protocol' is proposed in Reference [11], to manage large wireless ad hoc networks, in which a small subset of nodes is selected to construct the backbone. In Reference [12], a method of calculating the power-aware connected dominating sets was proposed to establish an underlying topology for the network.

4.1 LOCAL MINIMUM SPANNING TREE (LMST) TOPOLOGY CONTROL

In this section, we discuss a minimum spanning tree (MST)-based topology control algorithm, called a *local minimum spanning tree* (LMST), for multihop wireless networks with limited mobility [23]. The topology is constructed in such a way that each node builds its local MST independently (with the use of information locally collected) and keeps only one-hop on-tree nodes as neighbors. The MST design is discussed in Chapters 7 and 13. The topology constructed under LMST preserves the network connectivity. The degree of any node in the resulting topology is bounded by 6 and the resulting topology can be converted into one with only bidirectional links (after removal of unidirectional links). The bounded node degree is desirable because a small node degree reduces the MAC-level contention and interference. The capability of forming a topology that consists of only bidirectional links is important for link level acknowledgments and packet *transmissions/retransmissions* over the unreliable wireless medium. Bidirectional links are also important for floor acquisition mechanisms such as *RTS/CTS* (ready-to-send/clear-to-send) in IEEE 802.11.

4.1.1 Basics of MST topology control

In general, the following guidelines are essential to effective topology control algorithms: (1) The network connectivity should be preserved with the use of minimal possible power. This is the most important objective of topology control. (2) The algorithm should be distributed. This is due to the fact that there is, in general, no central authority in a wireless multihop network and thus each node has to make its decision based on the information collected from the network. (3) To be less susceptible to the impact of mobility, the algorithm should depend only on the information collected locally, e.g. within one hop. Algorithms that depend only on local information also incur less message overhead/delay in the process of collecting information. (4) It is desirable that in the topology derived under the algorithm, all links are bidirectional. Bidirectional links ensure existence of reverse paths and facilitate link-level acknowledgment and proper operation of the *RTS/CTS* mechanism. (5) It is also desirable that the node degree in the derived topology is small. A small node degree helps to mitigate the well-known hidden and exposed terminal problems, as there will be fewer nodes that have to be silenced in a communication activity.

In the discussion of the *LMST algorithm*, the following terminology will be used. The network topology constructed under the common transmission range $d_{\max}$ will be denoted as an undirected simple graph $G = (V, E)$ in the plane, where V is the set of nodes in the network and $E = \{(u, v) : d(u, v) \leq d_{\max}, u, v \in V\}$ is the set of edges of G. A unique id ($id(v_i) = i$) is assigned to each node. We also define the *visible neighborhood* ($NV_u(G)$) of node u as the set of nodes that node u can reach by using the maximal transmission power, i.e. $NV_u(G) = \{v \in V(G) : d(u, v) \leq d_{\max}\}$. For each node $u \in V(G)$, let $G_u = (V_u, E_u)$ be the induced subgraph of G such that $V_u = NV_u$.

The LMST algorithm is composed of the following three phases: (1) *information collection*, (2) *topology construction* and (3) *determination of transmission power*, and an optional optimization phase: (4) *construction of topology with only bidirectional edges*.

It is assumed that the propagation channel is symmetric and obstacle-free and that each node is equipped with the ability to gather its location information.

4.1.1.1 Information collection

The information needed by each node u in the topology construction process is the information of all nodes in $NV_u(G)$. This can be achieved if each node broadcasts periodically a '*hello*' message using its maximal transmission power. The information contained in a '*hello*' message should include the node id and the position of the node. Those periodic messages can be sent either in

the data channel or in a separate control channel. The '*hello*' messages can be combined with those already employed in most ad hoc routing protocols. In addition, each node can piggyback its location information in data packets to reduce the number of '*hello*' exchanges. The time interval between two broadcasts of '*hello*' messages depends on the level of node mobility.

4.1.1.2 Topology construction

After obtaining the information of the visible neighborhood $NV_u(G)$, each node u builds its local MST $T_u = (V(T_u), E(T_u))$ of G_u, which spans all the nodes within its neighborhood. The time complexity varies from $O(e \log v)$ (the original Prim's algorithm; see Chapters 7 and 13 and Reference [15]) to almost linear of e (the optimal algorithm [16]), where e is the number of edges and v is the number of vertices.

To build a power efficient MST, the weight of an edge should be the transmission power between the two nodes. As power consumption is, in general, of the form $c \cdot d^r$, $r \geq 2$, i.e. a strictly increasing function of the Euclidean distance, it suffices to use the Euclidean distance as the weight function. The same MST will result. The MST may not be unique if multiple edges exist with the same weight. As the uniqueness is necessary for the proof of connectivity, we refine the weight function as follows. Given two edges (u_1, v_1) and (u_2, v_2), the *weight function* $d' : E \mapsto R$ is defined as:

$$
\begin{aligned}
&d'(u_1, v_1) > d'(u_2, v_2) \Leftrightarrow d(u_1, v_1) > d(u_2, v_2) \\
&\text{or } (d(u_1, v_1) = d(u_2, v_2) \\
&\&\& \max\{id(u_1), id(v_1)\} > \max\{id(u_2), id(v_2)\}) \\
&\text{or } (d(u_1, v_1) = d(u_2, v_2) \\
&\&\& \max\{id(u_1), id(v_1)\} = \max\{id(u_2), id(v_2)\} \\
&\&\& \min\{id(u_1), id(v_1)\} > \min\{id(u_2), id(v_2)\})
\end{aligned}
$$

The weight function d' guarantees that the local MST T_u constructed by node u is unique. After node u builds the MST, it will determine its neighbors. To facilitate discussion, we define the *neighbor relation* and the *neighbor set*. Node v is a neighbor of node $u's$ ($u \rightarrow v$) if and only if $(u, v) \in E(T_u)$ and $u \leftrightarrow v$ if and only if $u \rightarrow v$ and $v \rightarrow u$. That is, node v is a neighbor of node $u's$ if and only if node v is on node $u's$ local MST, T_u, and is 'one hop' away from node u. The *neighbor set* $N(u)$ of node u is $N(u) = \{v \in V(G_u) : u \rightarrow v\}$.

The neighbour relation defined above is not symmetric, i.e. $u \rightarrow v$ does not automatically imply $v \rightarrow u$. An illustration is given in Figure 4.2. There are altogether six nodes, $V = \{u, v, w_1, w_2, w_3, w_4\}$, where $d(u, v) = d < d_{\max}$, $d(u, w_4) < d_{\max}$, $d(u, w_i) > d_{\max}$, $i = 1, 2, 3, 0$ and $d(v, w_j) < d_{\max}$, $j = 1, 2, 3, 4$. Since $NV_u = \{u, v, w_4\}$, it can be obtained from T_u that $u \rightarrow v$ and $u \rightarrow w_4$. Also $VN_v = \{u, v, w_1, w_2, w_3, w_4\}$ and, hence, $v \rightarrow w_1$. Here we have $u \rightarrow v$ but $v \searrow u$, where $\searrow = no \rightarrow$ stands for negation of $\rightarrow$.

The network topology under LMST is all the nodes in V and their individually perceived neighbor relations. Note that the topology is *not* a simple superposition of all local MSTs. *The topology,* G_0, derived under LMST is a directed graph $G_0 = (V_0, E_0)$, where $V_0 = V$, $E_0 = \{(u, v) : u \rightarrow v, u, v \in V(G)\}$.

4.1.1.3 Transmission power optimization

Assume that the maximal transmission power is known and is the same to all nodes. By measuring the receiving power of '*hello*' messages, each node can determine the specific power

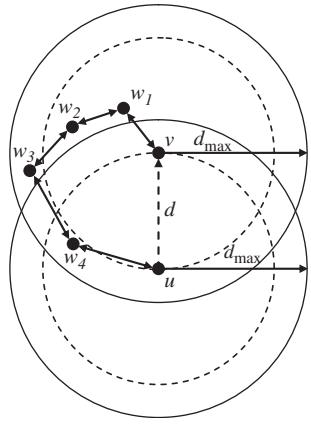

Figure 4.2 An example that links in the topology derived under LMST may be unidirectional.

levels it needs to reach each of its neighbours. In the *free space* propagation model, we have $P_r = P_t G_t G_r \lambda^2 / [(4\pi d)^2 L]$, where the power used to transmit packets is P_t, the power received is P_r, G_t is the antenna gain of the transmitter, G_r is the antenna gain of the receiver, λ is the wavelength, d is the distance between the antenna of the transmitter and that of the receiver and L is the system loss.

In the *two-ray ground* propagation model, the relation between P_t and P_r is $P_r = P_t G_t G_r h_t^2 h_r^2 / (d^4 L)$, where h_t is the antenna height of the transmitter and h_r is the antenna height of the receiver.

In general, the relation between P_t and P_r is of the form $P_r = P_t \cdot G$, where G is a function of $G_t, G_r, h_t, h_r, \lambda, d, \alpha, L$ and is time-invariant if all the above parameters are time-invariant. At the information collection stage, each node broadcasts its position using the maximal transmission power $P_{\max}$. When node A receives the position information from node B, it measures the receiving power P_r and obtains $G = P_r / P_{\max}$. Henceforth node A needs to transmit using at least $P_{th} \cdot G = P_{th} P_r / P_{\max}$ so that node B can receive messages, where P_{th} is the power threshold that receives the message correctly. A broadcast to all neighbors requires a power level that can reach the farthest neighbor. The radius, r_u, of node u is defined as the Euclidean distance between node u and its farthest neighbor, i.e. $r_u = \max\{d(u, v) : v \in N(u)\}$.

4.1.1.4 Topology with exclusively bidirectional edges

Some links in G_0 may be unidirectional. It is desirable to obtain network topologies consisting of only bidirectional edges. There are two possible solutions: (1) to enforce all the unidirectional links in G_0 to become bidirectional or (2) to delete all the unidirectional links in G_0. We term the two new topologies G_0^+ and G_0^-, respectively. The topology G_0^+ is a undirected graph $G_0^+ = (V_0^+, E_0^+)$, where $V_0^+ = V_0$, $E_0^+ = \{(u, v) : (u, v) \in E(G_0)$ or $(v, u) \in E(G_0)\}$. The topology G_0^- is a undirected graph $G_0^- = (V_0^-, E_0^-)$, where $V_0^- = V_0$, $E_0^- = \{(u, v) : (u, v) \in E(G_0)$ and $(v, u) \in E(G_0)\}$.

To convert G_0 into either G_0^+ or G_0^-, every node u may probe each of its neighbors in the neighbor set $N(u)$ to find out whether or not the corresponding edge is unidirectional and, in the case of a unidirectional edge, either deletes the edge (G_0^-) or notifies its neighbor to add the reverse edge (G_0^+). It was proven in Reference [23] that both topologies preserve the desirable properties of G_0. A tradeoff exists between the two choices: the latter gives a comparatively simpler topology and, hence, is more efficient in terms of spatial reuse, while the former allows more routing redundancy.

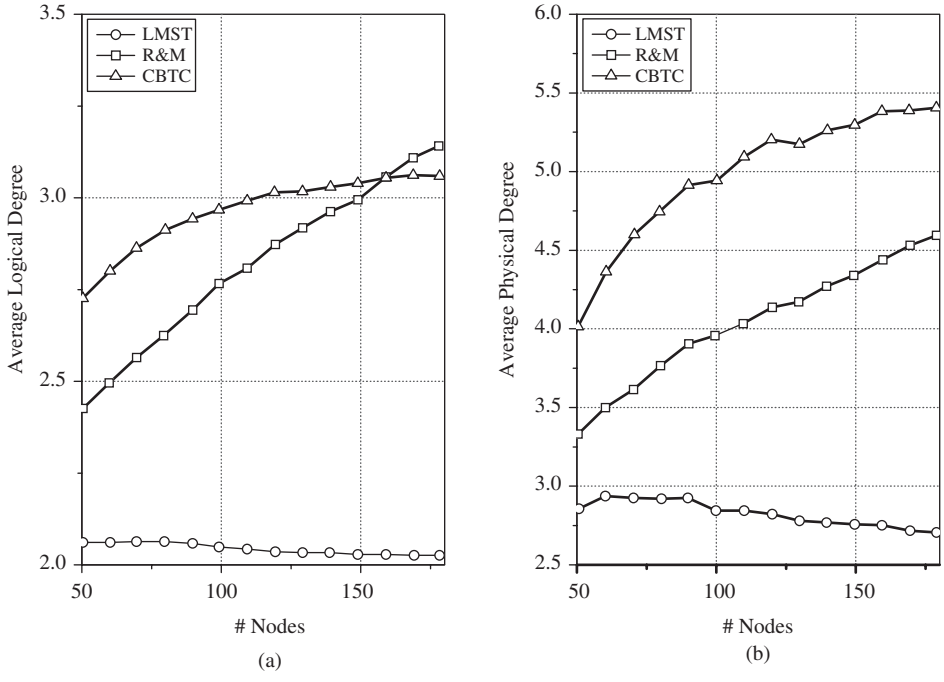

Figure 4.3 Performance comparisons (w.r.t. degree, radius and average length of links) among different algorithms: (a) average logical degree, (b) average physical degree.

4.1.2 Performance examples

All simulations in this section were carried out in *J-Sim*, a component-based, compositional network simulator written in Java (www.j-sim.org). Nodes are randomly distributed in a $1000 \times 1000\,\text{m}^2$ region. The transmission range of each node is $d_{\max} = 250\,\text{m}$. In the simulation, we vary the number of nodes in the region from 50 to 180. The average logical and physical node degrees for the topologies generated by R&M, CBTC and LMST are shown in Figure 4.3. Both the average logical and physical node degrees derived under R&M and CBTC increase with the increase of spatial density, while that under LMST remains constant. The physical topology consists of the nodes and links in the network. On a network physical topology, we can set up paths between pairs of nodes, where a path represents a direct connection without any intermediate electronics. The set of paths along with the nodes constitutes the logical topology.

The average radius and the average link length for the topologies derived using the maximal transmission power, R&M, CBTC and LMST with link removal are shown, respectively, in Figure 4.4(a) and (b). LMST outperforms the others in both cases.

4.2 JOINT TOPOLOGY CONTROL, RESOURCE ALLOCATION AND ROUTING

The joint topology control and routing (JTCR) protocol jointly coordinates the transmission power at each node, the channel selection on each wireless interface and the route selection among interfaces based on the traffic information that is measured and exchanged among two-hop neighbor nodes.

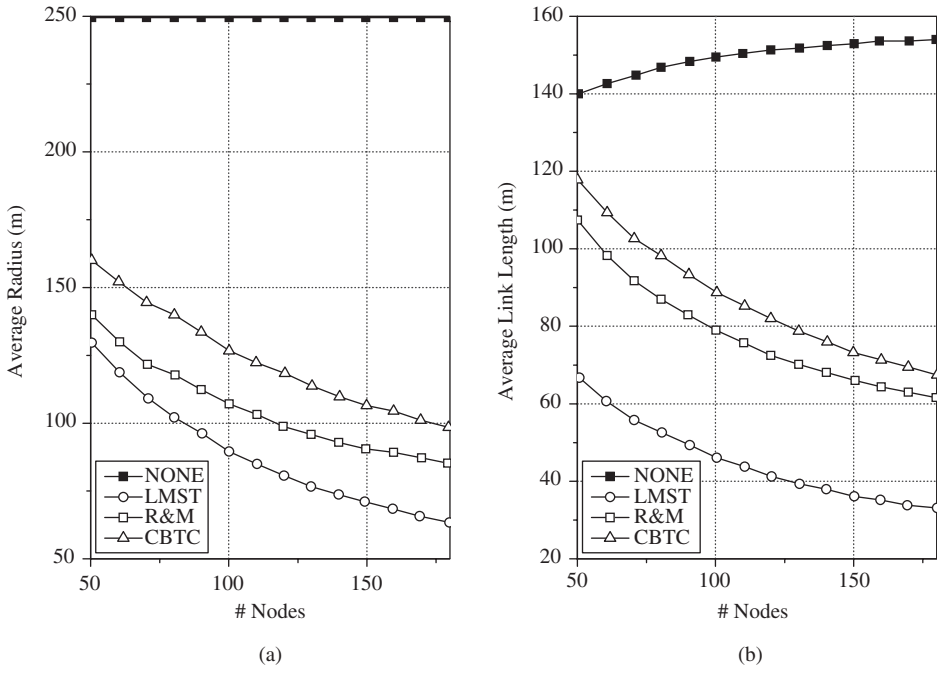

Figure 4.4 Performance comparisons (w.r.t. radius and average length of links) among different algorithms (NONE indicates the case where no topology control is employed): (a) average radius, (b) average link length.

Some systems, like standard IEEE 802.11, offer multiple orthogonal channels that can simultaneously work within a neighborhood. At the same time, the price for commodity 802.11 radios is rapidly diminishing. These make it natural to consider the use of multiple inexpensive radios at a single node, where each radio is designed to be capable of switching over multiple orthogonal channels. By allowing multiple simultaneous transmissions within a neighborhood, the cochannel interference is alleviated. As a result, it is expected that higher system throughput can be achieved.

The problem is illustrated on a network topology composed of ten wireless nodes ($N_1 - N_{10}$), as shown in Figure 4.5(a).The distance of neighboring nodes along the hexagon is 50 m. Each node is equipped with two radios, and each radio has two transmission power levels, which result in transmission ranges of 90 and 60 m, respectively. For simplicity, we assume that the interference range of each radio is almost equal to its transmission range in this specific scenario. There are, in total, four orthogonal channels available. Assume that, initially, the first channel is assigned to the first radio, whereas the second channel is assigned to the second radio for all the nodes.

Suppose that we tune the transmission power of each radio to the range of 90 m. Then, the network topology is as illustrated in Figure 4.5(a). Similarly, the network topology with a transmission range of 60 m is illustrated in Figure 4.5(b). Each neighboring node pair has two virtual links that are tuned on channels 1 and 2, respectively. For simplicity, we assume that all the links are free of transmission error and the raw capacity of each link is B Mb/s.

As shown in Figure 4.5(c), there are four flows, which are named flow 1 (from node N_1 to node N_4), flow 2 (from node N_1 to node N_5), flow 3 (from node N_7 to node N_{10}) and flow 4 (from node N_6 to node N_7). Here, each node in the figure is composed of two small circles – the black one and the white one – which denote the two radios. The route chosen in a multiradio network

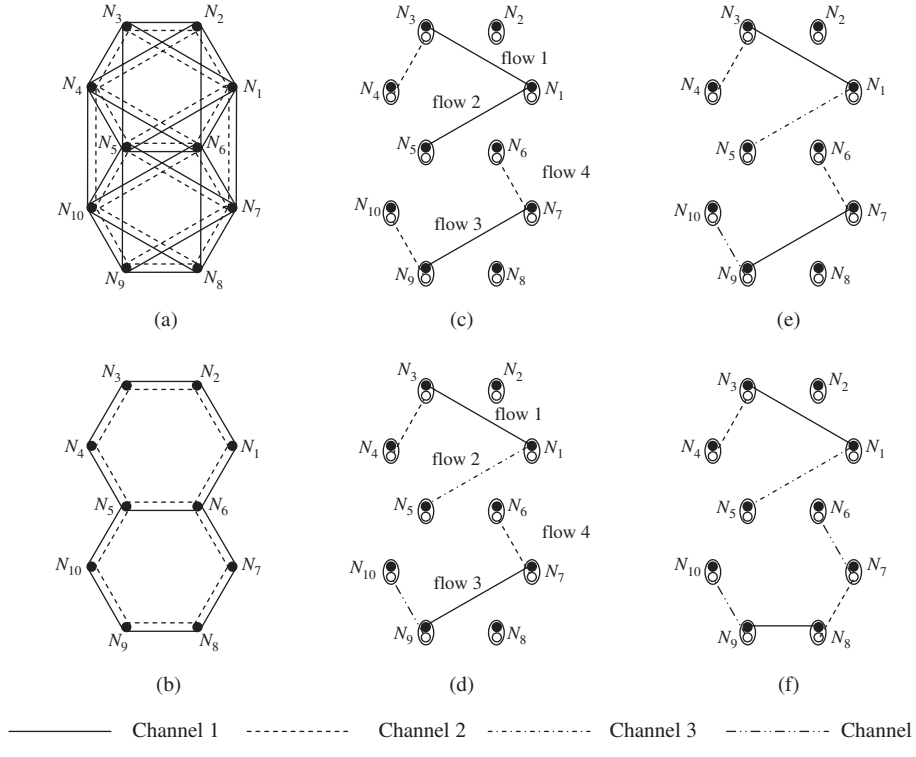

Figure 4.5 Illustration of joint topology control and routing.

should satisfy higher channel diversity in route path and lower packet loss rate properties. In a multiradio network, the route (path) for a flow will be defined as a sequence of node ID and radio interface pair instead of the node ID only. We utilize $N_l(j) \xrightarrow{k}$ to present the route for flows, where N_l denotes the node ID, j denotes the traffic outgoing radio interface number and k denotes the channel utilized on that link. In this way, the potential routes for the four flows may be

$$N_1(1) \xrightarrow{1} N_3(2) \xrightarrow{2} N_4,\ N_1(1) \xrightarrow{1} N_5,\ N_7(1) \xrightarrow{1} N_9(2) \xrightarrow{2} N_{10} \text{ and } N_6(2) \xrightarrow{2} N_7 \tag{4.1}$$

respectively, as illustrated in Figure 4.5(c). In this configuration, on both channels 1 and 2, there are three cochannel links that interfere with each other. Assuming that all four flows transmit a packet at the peak link data rate, the aggregated network throughput of the four flows is about

$$T = \{B \times (1/3) + B \times (1/3) + B \times (1/3) + B \times (1/3)\}/2B = 2/3 = 16/24 \tag{4.2}$$

since each flow can only occupy a one-third fraction of channel access time and the overall bandwidth of $2B$ is used.

Then, with the above-selected routes, we apply channel assignment with the hope to improve the network performance. After switching the overloaded channel into a less used one, both nodes N_1 and N_5 have one radio tuned from channel 1 to channel 3 and nodes N_9 and N_{10} have one radio tuned from channel 2 to channel 4. As shown in Figure 4.5(d), the cochannel interference on channels 1 and 2 is alleviated in that the number of interfering links is reduced from three to

two. Now, the aggregated network throughput for the four flows is

$$T = \{B \times (1/2) + B + B \times (1/2) + B \times (1/2)\}/4B = 5/8 = 15/24 \tag{4.3}$$

We can see that although the bandwidth has been doubled the throughput has not been increased since there are still two interfering links on channel 1 ($l^1_{N_1N_3}, l^1_{N_7N_9}$) and channel 2 ($l^2_{N_3N_4}, l^2_{N_6N_7}$), respectively. The notation $l^c_{N_lN_x}$ is utilized to denote the link between nodes N_l and N_x on channel c.

With the same route and channel assignment, we now check whether power control can be utilized to improve the network performance. As shown in Figure 4.5(e), we lower the transmission power level of the second radio on nodes N_3, N_4, N_6 and N_7 so that the transmission ranges of those radios are reduced from 90 to 60 m. Now, the previously conflicting links $l^2_{N_3N_4}$ and $l^2_{N_6N_7}$ can concurrently transmit. Through simple power control, the aggregated throughput is

$$T = \{B \times (1/2) + B + B + B \times (1/2)\}/4B = 3/4 = 18/24 \tag{4.4}$$

Based on the same logic, the ideal adjustment for the network, as illustrated in Figure 4.5(f), is to reduce the transmission power of nodes N_7, N_9, N_6 and N_{10} to the transmission range of 60 m. The routing path for flow 3 changes to $N_7(2) \xrightarrow{2} N_8(1) \xrightarrow{1} N_9(2) \xrightarrow{4} N_{10}$. The channels of nodes N_6 and N_7 are switched from channel 1 to channel 4. In this way, all the links may concurrently transmit. The aggregate throughput can reach

$$T = \{B + B + B + B\}/4B = 1 \tag{4.5}$$

The above example demonstrates that considering only channel assignment and routing does not give the best performance. To reduce the cochannel interference fully and consequently achieve higher gain of network performance, the topology control and routing should be jointly considered to exploit not only channel diversity but also spatial reusability.

4.2.1 JTCR algorithm

The system model presented in this section is based on Reference [24]. As in the previous section, we model the wireless mesh network as an undirected graph $G = (V, E)$. Set V represents wireless nodes, whereas set E represents the virtual links set between nodes. We assume that there are L orthogonal channels available in the system denoted by $c_1, c_2, \ldots, c_L$. A total of K types of radios are assumed to be available in the network, which relate to K channel sets $cs_1, cs_2, \ldots, cs_K$. For each channel set, we have $cs_k \subseteq \{c_l, l = 1, \ldots, L\}$. A different radio is capable of selecting a working channel from the related channel set. Each node $u \in V$ is equipped with one or more radio interfaces represented by $I(u)$, where $1 \leq I(u) \leq K$. Thus, each wireless node u is associated with an ordered set $A(u) \subseteq \{1, 2, \ldots, L\}$ of $I(u)$ distinct channels.

It is assumed that a node can adjust the transmission power of each radio within a number of power levels $\{P_1, P_2, \ldots, P_{\max}\}$. Different power levels result in different transmission ranges $\{R_1, R_2, \ldots, R_{\max}\}$. Note that the power control is based on a per radio scheme; i.e. the transmission power of different radios on a node can be tuned to distinct power levels.

The traffic demands are assumed as M end-to-end flows, denoted as $f_m = (s_m, d_m)$, where $s_m, d_m \in V$ and $m = 1, 2, \ldots, M$; s_m and d_m, respectively, denote the source and destination node of flow f_m. If the achieved throughput at the destination is t_m, then the overall throughput of a network is defined as $T = \sum_{1 \leq m \leq M} t_m$. The objective is to adjust the channel assignment, the power level of each radio and the route for flows in such a way that the network throughput is maximized.

Two nodes will be able to communicate if they have a common channel that is assigned to their radio interfaces and are located within communication range of each other. In the sequel $A(c)$ denotes the common working channels among $A(u)$ and $A(v)$, $R^{p,c}_T$ the transmission range of

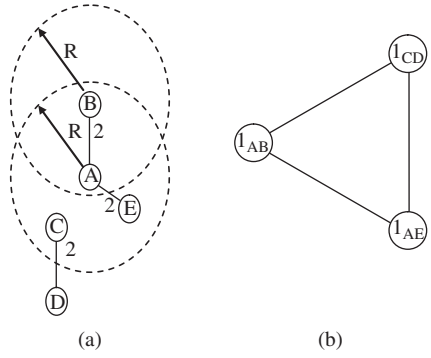

Figure 4.6 Cochannel interference and conflict graph: (a) network topology on channel 2, (b) conflict graph on channel 2.

their radio, which resides on the common channel c with the power level tuned on p, and $d_{u,v}$ the distance between the nodes u and v. An edge $e(u, v; c) \in E$ if and only if $d_{u,v} \leq R_T^{p,c}$, $A(c) \neq \emptyset$ and $c \in A(c)$.

The success of a transmission depends on the amount of multiple-access interference in neighborhood area. We use $R_I^{p,c}$ to denote the interference range (which is typically Q times $R_T^{p,c}$, $Q \geq 1$) associated with each radio tuned on channel c with power level p. If u, v, x, y are wireless nodes and links $e(u, v; c) \in E, e'(x, y; c) \in E$ exist, and if nodes x or y are within the interference range of u or v, then transmission on link e interferes with that of link e'. This definition of the cochannel interference also includes the cases where the two links share a common node. As shown in Figure 4.6(a), links $(A, B; 2)$, $(A, E; 2)$ and $(C, D; 2)$ interfere with each other on channel 2. Such a cochannel interference is represented using a conflict graph. The conflict graph of channel c, corresponding to link $e(u, v; c) \in E$ between nodes u and v on a specific channel c, contains a node (denoted by l_{uv}). We place an edge between two nodes (e.g. l_{uv} and l_{xy}) in the conflict graph if the links $(u, v; c)$ and $(x, y; c)$ in the network interfere. Figure 4.6(b) shows the contention graph on channel 2 for the network topology of Figure 4.6(a).

For the problem formulation we use:

set of parameters

> V, *set of* n *nodes;* L, *orthogonal channels available;* B, *bandwidth of each channel;* $I(u)$, *radio interfaces used by node* u; $\{P_1, P_2, \ldots, P_{\max}\}$, *power levels for each radio;* f_m, *traffic demand for each node pair* (s_m, d_m).

and set of variables

> $e_{u,v;c}$, *Boolean variables;* $e_{u,v;c} = 1$ *if there is a link from node* u *to node* v *on channel* c; *otherwise,* $e_{u,v;c} = 0$; $e_{u,v;c}^{s_m,d_m}$, *Boolean variables;* $e_{u,v;c}^{s_m,d_m} = 1$ *if the route from* s_m *to* d_m *goes through the link* $(u, v; c)$; *otherwise,* $e_{u,v;c}^{s_m,d_m} = 0$; $t_{u,v;C}$, *traffic load per unit time that was sent from node* u *and achieved at node* v *on channel* c. *In other words,* t_m *denotes the achieved throughput at the destination for traffic flow* f_m.

The optimization process is defined as

$$\max \sum_{1 \leq m \leq M} t_m \tag{4.6}$$

with respect to

(1) *Transmission power level* P_u^i *for the* i*th radio of node* $u, 1 \le i \le I(u), \forall u \in V$.

(2) *Channel assignment scheme* $A(u)$ *for node* u, $\forall u \in V$.

(3) *Delivery route* $e_{u,v;c}^{s_m,d_m}$ *for flows*, $\forall u$, $v \in V$.

subject to constraints

– Topology constraints

$$e_{u,v;c} = e_{v,u;c}, \ \forall u, \ v \in V \tag{4.7}$$

– Power constraints

$$R_T^{p,c}(u) \ge d_{u,v} * e_{u,v;C}, \ \forall u, \ v \in V \tag{4.8}$$

– Bandwidth constraints

$$\sum_{1 \le m \le M} \sum_{i or j \in D(u R_I^{pc})} (e_{i,j;c}^{s_m,d_m} * t_{i,j;c} + e_{j,i;c}^{s_m,d_m} * t_{j,i;c}) \le B, \ \forall u \in V \tag{4.9}$$

where $D(u, R_I^{p,c})$ denotes the set of nodes that are located within the interference range of node u on channel c.

– Route constraints

$$e_{u,v;c}^{s_m,d_m} \le e_{u,v;C}, \ \forall u, \ v \in V \tag{4.10}$$

– Radio constraints

$$\|\{c | e_{u,v;C} = 1, 1 \le c \le L, \forall v \in V\}\| \le I(u), \ \forall u \in V \tag{4.11}$$

Constraint (4.7) ensures that each edge in the network corresponds to two directed links. Constraint (4.8) determines the allowable transmission power level for a radio on channel c. Constraint (4.9) ensures that the total transmission and reception of packets at a node's interference range on channel c do not exceed the bandwidth capacity of this channel. The two terms of inequality (4.10) represent all the ingoing and outgoing traffics, respectively, on cochannel links that are within node $u's$ interference range. Constraints (4.10) ensure the validity of the route for each node pair. Only single-path routing is considered. Multipath routing is beyond the scope of this section. Constraints (4.11) ensure that node u, who has $I(u)$ radios, can be assigned at most $I(u)$ channels from $1 \le c \le L$.

Pseudo code for the implementation of the algorithm (4.6 to 4.11) can be found in Reference [24] along with performance results. The discussion on the logic behind the expectations of performance improvements is given in Section 4.2 and further elaboration is omitted. For more detail on the subject of channel assignment, routing and topology control in mesh networks see References [25] to [47].

4.3 FAULT-TOLERANT TOPOLOGY

In this section we discuss power assignments of wireless devices that minimize power while maintaining k-fault tolerance/connectivity. Specifically, it is required that all links established by

this power setting be symmetric and form a k-vertex connected subgraph of the network graph. A *k-vertex connected* graph has k vertex-disjoint paths between every pair of vertices or, equivalently, remains connected when any set of utmost $k-1$ vertices is removed. Such a subgraph is said to be k-fault tolerant. This problem is known to be *NP*-hard so we discuss the approximation algorithms.

4.3.1 The system model

In this section a wireless network will be modelled as a graph $G(V, E)$, where V is the set of mobile devices and $E \subseteq V^2$ is the set of pairs of devices between which communication is possible. As maximal transmission ranges and environmental conditions may impose constraints on possible pairs of communicating nodes, E does not necessarily equal V^2. In general, this graph may be directed, but our symmetric link constraint allows us to eliminate all *uni*-directional edges. Typically, an edge (i, j) is assigned a distance $d(i, j)$, representing the distances between devices i and j, and cost $p(i, j)$, representing the power setting i and j must use to transmit to each other.

A *range assignment* R is an assignment of power settings $R(i)$ to devices i. A subgraph $H = (V, E')$, where $E' \subseteq E$ of the network graph $G = (V, E)$, defines a range assignment $R_{E'}$, where

$$R_{E'}(i) = \max_{\{j|(i,j)\in E'\}} p(i, j) \tag{4.12}$$

The *power cost* of graph $G = (V, E)$ with edge costs $p(i, j)$ is

$$P(G) = \sum_{i\in V;\{j|(i,j)\in E\}} \max\ p(i, j) \tag{4.13}$$

The *normal cost* of graph $G = (V, E)$ with edge costs $p(i, j)$ is

$$C(G) = \sum_{(i,j)\in E} p(i, j) \tag{4.14}$$

Using these definitions, we can define the undirected minimum power k-vertex connected subgraph problem.

An *undirected minimum power k-vertex connected subgraph* (k-*UPVCS*) of a graph $G = (V, E)$ is a k-vertex connected subgraph $H = (V, F)$, $F \subseteq E$, such that $P(H) \leq P(H')$ for any k-vertex connected subgraph $H' = (V, F')$, $F' \subseteq E$. This problem is closely related to the standard k-vertex connected subgraph problem which corresponds to k-fault tolerance in wired networks.

An *undirected minimum cost k-vertex connected subgraph* (k-*UCVCS*) of a graph $G = (V, E)$ is a k-vertex connected subgraph $H = (V, F)$, $F \subseteq E$, such that $C(H) \leq C(H')$ for any k-vertex connected subgraph $H' = (V, F')$, $F' \subseteq E$.

When k is not specified, it is understood that $k = 1$. Both the k-UPVCS and k-UCVCS problems are *NP*-hard, and thus it is of practical interest to find approximations for these problems. An *α-approximation algorithm* is a polynomial time algorithm whose solution cost is at most α times the optimal solution cost.

4.3.2 Fault-tolerant topology design

As the k-UPVCS problem is *NP*-hard, an exact solution is infeasible. One line of work has focused on approximate solutions. Approximations are often obtained via a linear programming representation of the problem. However, we show that for the k-UPVCS problem, a linear programming approach is unlikely to yield a good approximation in the worst case. Another line of work has focused on providing heuristics, which work well in practice. However, heuristics do not have provably good solutions, and in fact we can show that, in the worst case, the current k-UPVCS heuristics perform poorly.

The results in this section make claims about the worst-case performance of the proposed algorithms. This does not imply poor behavior on average or in typical situations.

The *linear programming approach* has been used to derive many approximation algorithms [48–87]. In this section, as in Chapter 19, we will use the notation: $f = O(g)$ if $\limsup_{n\to+\infty}(f(n)/g(n)) < +\infty$; $f = \Omega(g)$ if $g = O(f)$; $f = \Theta(g)$ if $f = O(g)$ as well as $g = O(f)$. The best known k-UCVCS approximation algorithm (an $O(\log k)$-approximation algorithm by Cheriyan *et al*. [57]) is such an example. In these algorithms, the problem is formulated as an integer program. Then the fractional solution of the linear programming relaxation is rounded to an integral solution and its value is used as a lower bound in the analysis. The integrality gap of linear programming formulation, i.e. the ratio between the optimal values of the integral and fractional solutions, is a lower bound on the achievable approximation factor. One might hope for a linear-programming-based approximation algorithm for k-UPVCS with performance similar to that of k-UCVCS. Reference [48] shows that the natural linear programming formulation for the k-UPVCS problem has an integrality gap of $\Omega(n/k)$, implying that there is no approximation algorithm based on this linear program with an approximation factor better than $\Omega(n/k)$.

We now discuss a natural linear programming formulation of this problem introduced by Cheriyan *et al*. [57]. Let us assign a zero–one variable x_e to each edge e indicating whether edge e is in the k-connected subgraph $G' = (V, E')$ of the input graph $G = (V, E)$. The cost of subgraph G' is $\sum_{v\in V} p_v$, where p_v is the maximum power of all edges adjacent to v in G', i.e. $p_v \geq p(u, v)x_{(u,v)}$ for all $(u, v) \in E$. To guarantee that solutions to the integer program represent k-connected subgraphs, we introduce a constraint ensuring that there are k vertex-disjoint paths between every pair of vertices (in fact, every pair of sets). Define a *setpair* $S = (T, H)$ to be any pair of two disjoint nonempty subsets T and H of vertices. The idea is that any such pair of sets must have k vertex- disjoint paths between them in order for G to be k-vertex connected. Let $\delta(S) = \delta(T, H)$ be the set of all edges with one endpoint in T and the other in H. There are $n - |H \cup T|$ vertices outside H and T that can participate in paths between H and T. Thus, there are at most $n - |H \cup T|$ vertex-disjoint paths between H and T that leave $H \cup T$, and so there must be at least $k - (n - |H \cup T|)$ edges in $\delta(T, H)$. The setpair linear programming relaxation is as follows:

Minimize $\sum_{v\in V} p_v$

subject to $\sum_{e\in\delta(S)} x_e \geq \max\{0, k - (n - |H \cup T|)\}$

for all setpairs $S = (T, H)$

$$p_v \geq p(u, v)x_{vu} \tag{4.15}$$

for all $v \in V, (u, v) \in E$

$$0 \leq x_e \leq 1$$

for all $e \in E$.

The above discussion shows that these constraints are necessary for G' to be a k-connected subgraph. To see that they are also sufficient, we refer the reader to the result of Cheriyan *et al*. [48, 57]. If $n \geq 2k$, the integrality gap of the above linear programming is $\Omega(n/k)$. The proof can be found in Reference [48].

A *heuristic-based approach* for the k-UPVCS problem is also studied in the literature. One example is work by Bahramgiri *et al*. [50], where they show that the cone-based topology control

algorithm of Wattenhofer *et al*. [86, 74] for UPVCS can be extended to an algorithm for k-UPVCS. In the following, we describe this algorithm and then elaborate examples presented in Reference [48] that demonstrate that the approximation factor for this algorithm is at least $\Omega(n/k)$.

In the *cone-based topology control* (*CBTC*) algorithm, each node increases its power until the angle between its consecutive neighbors is less than some threshold. In the following, we present a brief description of this algorithm. For details of CBTC and how to implement it in a distributed fashion, we refer to Wattenhofer *et al*. [86, 74]. Node u sends a *'hello'* message to every other node v using power p. Upon receiving a *'hello'* message from node u, node v replies with an *Ack* message. After gathering the *Ack* messages, node u constructs the set of its neighbors, $N(u)$, along with a set of vectors indicating the direction of each neighbor. Node u increases its power until the angle between any pair of adjacent neighbours is at most α for some fixed α. Now, let $N_\alpha(u)$ be the final set of neighbors computed by anode u and $E_\alpha = \{(u, v) | v \in N_\alpha(u) \text{ and } u \in N_\alpha(v)\}$. Output graph $G_\alpha = (V, E_\alpha)$.

Wattenhofer *et al*. [86] have shown that for $\alpha \leq 2\pi/3$, the sub-graph G_α produced by this algorithm is connected if and only if G is connected. Li *et al*. [74] show that the theorem does not hold necessarily for $\alpha > 2\pi/3$ and they also extend the result to the directed case. Bahramgiri *et al*. [50] generalize the first result for k-connected subgraphs in the following way: for $\alpha \leq 2\pi/3k$, G_α is k-connected if and only if G is k-connected. They also show that the theorem does not hold necessarily for $\alpha > 2\pi/3k$ if k is even and $\alpha > 2\pi/3(k-1)$ if k is odd. Although this heuristic-based algorithm is very practical in a distributed mobile setting, it does not have a reasonable approximation guarantee. Reference [48] shows that this algorithm solution can be as much as n/k times the optimal one. Specifically, Reference [48] shows that there are examples for which the approximation factor of the CBTC algorithm for k-connectivity ($k \geq 1$) is at least $\Omega(n/k)$; i.e. the ratio between the power of the output of CBTC and the minimum power k-connected subgraph is $\Omega(n/k)$.

As an illustration Figure 4.7 shows an example when the network has eight nodes and compares the optimal 2-connected subgraph with the output of CBTC for $k = 2$. In the CBTC algorithm, each node increases its power until the angle between any two consecutive neighbors is at most $2\pi/3k$. As a result, each vertex is connected to vertices in each half of the cycle, which yields a regular graph of degree $n/2 - n/3k = \Omega(n)$. The power of each node is the length of the chord, which corresponds to the arc of length $1/2 - 1/3k$ of the perimeter. More precisely, the length of this chord is $2R \sin[(1/2 - 1/3k)\pi]$.

A feasible solution is to connect each vertex to $\lceil k/2 \rceil$ neighbours on each side. The resulting graph, a Harary graph, is k-connected. The power of each node is the length of the chord

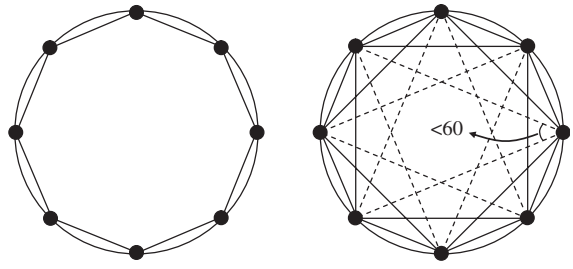

Figure 4.7 Illustration of the CBTC lower bound: (a) the optimum 2-connected subgraph; (b) the output of CBTC for $k = 2$ in which each node increases its power until the angle is less than $2\pi/(3 \times 2) = 60^\circ$ [48].

corresponding to the arc of length k/n of the perimeter. The length of this chord is $2R \sin(\lceil k/2 \rceil \pi/n)$. Thus, the ratio between the output of CBTC and the optimum solution is $\Omega(n/k)$ when n is large and k is small since $\sin(\lceil k/n \rceil \pi/n) \simeq \lceil k/n \rceil \pi/n$ and $\sin[(1/2 - 1/3k)\pi] = \Theta(1)$, i.e. constant. This example shows that the approximation factor of CBTC is at least $\Omega(n/k)$.

4.3.3 α-Approximation algorithms

A *global approximation* is based on the fact that the normal cost and power cost of graphs are closely related. In the sequel we show how a 2-approximation for the UPVCS problem can be obtained via a solution for the UCVCS, or minimum spanning tree, problem. For these purposes we need the following lemmas.

Lemma 1
For any graph G, $P(G) \leq 2C(G)$.

Proof. This follows straightforwardly from the following inequalities:

$$\begin{aligned} P(G) &= \sum_{v \in V} \max_{\{u|(u,v)\in E\}} \max p(u, v) \\ &\leq \max_{v \in V} \sum_{(u,v)\in E} p(u, v) = 2 \sum_{e \in E} p_e = 2C(G) \end{aligned} \tag{4.16}$$

□

Lemma 2
For any tree T, $C(T) \leq P(T)$.

Proof. Root T at an arbitrary vertex r. Note that the power of each node is at least the cost of its parent edge. The lemma follows. □

Lemma 3
For any graph G that can be written as a union of t forests, $C(G) \leq t\,P(G)$.

Proof. Write $G = \bigcup_{i=1}^{t} F_i$ for forests F_i. Then

$$C(G) \leq \sum_{i=1}^{t} C(F_i) \leq \sum_{i=1}^{t} P(F_i) \leq \sum_{i=1}^{t} P(G) = t\,P(G) \tag{4.17}$$

where the second inequality follows from Lemma 2 and the third follows since each forest is a subgraph of G. □

Using these lemmas, it can be shown that a k-UCVCS subgraph G_C is in fact a $2k$-approximation to a k-UPVCS subgraph G_P. Having in mind that an edge (u, v) of a k-vertex connected graph H is *critical* if $H - (u, v)$ is not k-vertex connected, graph G is *critically* k-vertex connected if and only if G is k-vertex connected and all edges of G are critical. We use the following theorem [83] to find a forest decomposition of a critical k-vertex connected graph.

Theorem 1
In a k-vertex connected graph, a cycle consisting of critical edges must be incident to at least one node of degree k.

Lemma 4
Any critical k-vertex connected graph, G, can be written as the union of k forests [48]. Based on Equation (4.17), we can now see that a k-UCVCS subgraph G_C is in fact a $2k$-approximation to a k-UPVCS subgraph G_P

$$P(G_C) \leq 2C(G_C) \leq 2C(G_P) \leq 2kP(G_P) \tag{4.18}$$

where the last inequality follows from the fact that there is a subgraph of G_P that is critically k-vertex connected which has the same power-cost as G_P.

Theorem 2
The power of a k-UCVCS subgraph is at most $2k$ times the power of a k-UPVCS subgraph.

It follows from Theorem 2 that an α-approximation algorithm for the k-UCVCS problem is a $2\alpha k$-approximation for the k-UPVCS problem. In general graphs, Cheriyan *et al.* [57] give a $\log k$-approximation algorithm for the k-UCVCS problem for general graphs with at least $6k^2$ vertices, implying an $O(k \log k)$-approximation algorithm for the k-UPVCS problem in such graphs. Kortsarz and Nutov [71] give a k-approximation algorithm with no assumption on the size of the graph, implying an $O(k^2)$ algorithm for the k-UPVCS problem in any graph. In geometric graphs, the triangle inequality on edge lengths implies that the edge costs satisfy a *weak* triangle inequality $c_{ik} \leq 2^{c-1} \cdot (q_j + c_{jk})$, where $2 \leq c \leq 4$ is the power attenuation exponent. A direct extension of the results in Khuller and Raghavachari [69] shows $\alpha = 2 + 2^c(k-1)/n$ for the k-UCVCS problem in these graphs, implying an $O(k)$-approximation for the k-UPVCS problem.

The approach described in this chapter for k-vertex connectivity can also be applied to obtain an $O(k)$-approximation for *k-edge connectivity*, another important concept in fault-tolerant network design. Graph G is k-edge connected if it remains connected after deleting any set of $k-1$ edges. Formally, we can define the *undirected minimum power k-edge connected subgraph* (k-UPECS) and the *undirected minimum cost k-edge connected subgraph* (k-UCECS) similar to the k-UPVCS problem and the k-UCVCS problem, respectively. It turns out that the k-UCECS problem is easier to approximate than the k-UCVCS problem. In fact, constant factor approximations are known even for general graphs [72, 67]. Work in Reference [72] first gives a 2-approximation for the k-UCECS problem. Later, work in Reference [19] uses an iterative rounding method to achieve a 2-approximation algorithm for this problem and its generalization. In this section, we design a $2\alpha k$-approximation for the k-UPECS problem from an α-approximation for the k-UCECS problem. As a result, a $4k$-approximation for the k-UPECS problem is obtained using 2-approximations for the k-UCECS problem [72, 67].The proof is the same as the proof for vertex connectivity except that we need to reprove Lemma 4 for critical k-edge connected graphs.

Lemma 5
Any critical k-edge connected graph, G, can be written as the union of k forests [48].

Reference [48] follows the k-approximation algorithm introduced in Reference [71] to approximate k-UCVCS subgraphs. The algorithm in Reference [71], which is referred to as *Algorithm Global k-UPVCS*, first finds a 2-approximation to the cheapest normal cost *k-outconnected subgraph* H rooted at an arbitrary vertex r using a subroutine which we refer to as $A(r, G)$. A k-outconnected subgraph rooted at r is a subgraph with k internal vertex-disjoint paths between r and every other vertex $v \in G$. They show that such a graph has a *cover* of size at most $k-2$, where a cover is a set of edges that can be added to a graph to make it k-connected. The algorithm computes a $k-2$ cover F' for H and finally replaces each edge $(u, v) \in F'$ by k vertex-disjoint paths from u to v with the cheapest (normal) cost. These paths can be found in polynomial time

Table 4.1 A formal description of algorithm Global k-UPVCS

Algorithm Global k-UPVCS ($G(V, E)$)
//choose arbitrary root r
$r \in V$
//find k-outconnected subgraph H
//and covering set F' *using subroutine* $A(r, G)$
$H, F' \leftarrow A(r, G)$
for $(u, v) \in F'$
//find k vertex disjoint paths F_{uv} *with the cheapest*
//(normal) cost from u *to* v *in* G
$F_{uv} \leftarrow k$ *vertex disjoint paths with cheapest cost*
end
//replace edges in cover by the sets of
//cheapest k vertex disjoint paths
for $(u, v) \in F'$
$H \leftarrow H \cup F_{uv}$
end
output $G_k = H$

Table 4.2 Improved approximation factor α of algorithm Global k-UPVCS for $k \leq 7$

k	2	3	4	5	6	7
α	8	16	20	24	32	36

via a min cost k-flow algorithm. Adding these k disjoint paths instead of each edge of the cover preserves k-connectivity. For a formal description of this algorithm, see Table 4.1.

Work in Reference [48] shows that this algorithm of Kortsarz and Nutov is in fact an $8(k-1)$-approximation for the k-UPVCS problem in general graphs. For the special cases of $k \in \{4, 5\}$ and $k \in \{6, 7\}$, Reference [71] shows that the covering set of a k-outconnected graph has size 1 and 2, respectively, implying better approximations in these cases. Table 4.2 lists the approximation factor of this algorithm for various k, taking into account these special cases. For the important case of $k = 2$, this algorithm yields an 8-approximation. Lloyd *et al*. [76] independently obtained a different 8-approximation algorithm for the 2-UPVCS problem.

Theorem 3
Algorithm Global k-UPVCS returns a k-vertex connected subgraph G_k whose power cost is at most $8(k-1)$ times the power of a k-UPVCS subgraph for $k \geq 2$ [48].

A *distributed approximation* will be discussed under the assumption that our graph is geometric (i.e. the edge lengths satisfy the triangle inequality) and the power attenuation exponent is uniform. In other words, the cost of an edge e of length r_e is r_e^c, $2 \leq c \leq 4$. This implies the following lemma.

Lemma 6

$$\text{If } x_0 \leq \sum_{i=1}^{k} x_i, \text{ then } x_0^c \leq k^{c-1} \sum_{i=1}^{k} x_i^c. \tag{4.19}$$

Table 4.3 A formal description of algorithm Distributed k-UPVCS for $k = 2$

```
Algorithm Distributed 2-UPVCS (G(V, E))
//compute the minimum spanning tree
T_MST ← Algorithm MST(G(V, E))
for node u ∈ T_MST
    //find neighbors of u
    N ← {v|(u, v) ∈ T_MST}
    //add arbitrary path connecting neighbors
    label vertices in N in an arbitrary order
    E ← E ∪ {(v_1, v_2), ..., (v_|N|−1, v_|N|)}
end
```

Proof. Dividing both sides of the inequality by k^c, we see that

$$\left(\frac{x_0}{k}\right)^c \leq \left(\frac{\sum_{i=1}^{k} x_i}{k}\right)^c \leq \left(\frac{\sum_{i=1}^{k} x_i^c}{k}\right) \tag{4.20}$$

by the convexity of the function $f(x) = x^c$. □

Corollary 1
In a geometric graph with edge lengths r_{ij}, the edge costs $p_{ij} = r_{ij}^c$ satisfy a weak triangle inequality:

$$\forall (i, j),\ (j, k),\ (i, k) \in E,\ p_{ik} \leq 2^{c-1} \cdot (p_{ij} + p_{jk}) \tag{4.21}$$

We start with an algorithm for the 2-UPVCS problem. As Theorem 4 below states, the algorithm uses only a constant factor more power than the optimal configuration. The algorithm uses as a subroutine *Algorithm MST*, an algorithm for computing the minimum spanning tree of the input graph. It then adds a path among the neighbors of each node in the returned tree. See Table 4.3 for a formal description.

After the computation of the minimum spanning tree, this algorithm is *distributed*; i.e. each node can compute its power setting with just a small number of messages to other nodes. Once the minimum spanning tree has been computed, each node just needs to know its neighbors and their neighbors in order to decide at what power to transmit. The minimum spanning tree itself can be computed by the distributed minimum spanning tree algorithm of Gallager *et al.* [64] with just $5n \log n + 2m$ messages, where $n = |V|$, the number of devices, and $m = |E|$, the number of valid communication links. The number of required messages can be reduced by finding an approximate minimum spanning tree, although this will affect the approximation factor of the resulting algorithm. Since we only need $O(n)$ messages once we have the minimum spanning tree, the overall number of messages is $O(n \log n + m)$.

Theorem 4
For any geometric graph G, algorithm Distributed 2-UPVCS returns a 2-vertex *connected* subgraph G_2 whose power $P(G_2)$ is a $2(4 \times 2^{c-1} + 1)$-approximation of the power of a 2-UPVCS subgraph [48].

It is not straightforward to generalize this algorithm for $k \geq 3$. The main difficulty arises from the fact that the tree itself is just 1-connected. Thus the neighbor sets of vertices as defined by the tree can be too localized. In order to make the output graph k-connected, an additional step in the algorithm is needed that *adds* neighbors to guarantee a good intersection of neighbor sets

Table 4.4 A formal description of algorithm k-UCVCS

```
Algorithm Distributed k-UPVCS (G(V, E))
//compute the minimum spanning tree
T_MST ← Algorithm MST(G(V, E))
Root T_MST at an arbitrary vertex r
Perform a depth first search, labeling each node the first and the last
time it is visited (the first node, i.e. r, has labels 0 and 2n − 1)
//add neighbors to each vertex
G_k ← (V, ∅)
for each node v_x ∈ T_MST
   Add edges (v_x, v_j) to G_k for i + 1 ≤ j ≤ i + 2k
   where indices are computed mod 2n
   N_i ← {v_{i+1}, ..., v_{i+2k}} ∪ {u' : (v_i, u) ∈ T_MST}
end
//add a Harary graph among neighbors of vertices
for each node v ∈ G_k
   Consider an arbitrary cyclic ordering σ(N_i) of vertices in N_i
   for each u ∈ N_i
Add to G_k edges (u, v) for each of
the ⌈k/2⌉ vertices before and after u in σ(N_i)
   end
end
```

throughout the graph. We would like to add these neighbors without incurring too much cost. We will bound the additional cost in a manner similar to the bound argument for $P(F)$; namely, we will charge the additional cost to the edges of T_{MST}. However, we must be careful to charge each edge only a small number of times in order to get a good approximation factor. We can accomplish this by using the extended family of a vertex as its additional neighbors.

A cyclic ordering of the vertices is created as follows: root T_{MST} at an arbitrary node r and let r be the first node in the ordering, i.e. $r = v_0$. Perform a depth first search of T_{MST} from vertex r, adding each element v to the ordering both when the search enters the subtree routed at v and when it leaves the subtree routed at v. Hence, each element appears in the ordering twice, and $r = v_0 = v_{2n-1}$. Suppose the ith vertex v_i in this ordering has just $j < k$ neighbors. Then we augment the neighborhood by adding edges from v_i to the $2k - j$ vertices that follow v_i in the ordering, i.e. $v_{i+1}, \ldots, v_{i+2k-j}$ (so as long as k is constant, this step is locally distributed). Now all vertices have at least k neighbors. For each vertex v, we add the following k-connected graph (a *Harary graph*) to its neighbors N: form an arbitrary cycle C among the vertices in N; connect each vertex $u \in C$ to the first $\lceil k/2 \rceil$ vertices on each side of u. Repeating this procedure for every vertex will make the entire graph k-connected. See Table 4.4 for a formal description.

The algorithm is based on a distributed minimum spanning tree algorithm, which can be computed with $O(n \log n + m)$ messages. After the computation of the minimum spanning tree, the remainder of the algorithm is locally distributed. Even the neighbor addition step must query at most $O(k)$ neighbors, which are at most a distance of $O(k)$ from the original vertex. Therefore, these remaining steps use just $O(k^2 n)$ messages and the total message complexity of the algorithm is $O(n \log n + m + k^2 n)$.

Theorem 5

For any geometric graph G, algorithm Distributed k-UPVCS is a distributed algorithm that outputs a k-vertex connected subgraph whose power is an $O(k^{2c+2})$-approximation of the power of a k-UPVCS subgraph [48].

Table 4.5 Expended energy ratio $c = 2$ for 2-UPVCS ($k = 2$)

Density	Degree	Cone–based topology control EER	Distributed k-UPVCS EER	Global k-UPVCS EER
6	15.56	90	31	15
10	21.62	89	18	11
14	34.02	74	13	72
18	38.72	62	10	61
22	45.24	63	90	45
26	51.26	60	78	44
30	54.56	58	70	36

Table 4.6 Expended energy ratio $c = 2$ for 2-UPVCS ($k = 3$)

Density	Degree	Cone–based topology control EER	Distributed k-UPVCS EER	Global k-UPVCS EER
6	15.56	99	35	20
10	21.62	99	25	17
14	34.02	90	15	11
18	38.72	81	13	85
22	45.24	84	10	64
26	51.26	80	85	66
30	54.56	75	83	53

4.3.4 Performance examples

For performance illustrations we generate random networks, each with 100 nodes. The maximum possible power at each node is fixed at $E_{\max} = (250)^2$ and the *power attenuation exponent* $c = 2$, as in Reference [48], which implies a maximum communication radius R of 250 meters. We assume the MAC layer is ideal. These networks are similar to the sample networks used by Wattenhofer *et al*. [86] and Cartigny *et al*. [56].

As a performance measure, we compute the average expended energy ratio (EER) of each algorithm for these random networks:

$$EER = \frac{\text{Average}}{E_{\max}} \text{ Power} \times 100 \tag{4.22}$$

This measure compares the average power of a node in the network to the maximum power of a node in the network; the objective is to keep this ratio small. The results are shown in Tables 4.5 and 4.6. A significant improvement of the system performance with the k-UPVCS algorithm is evident. For more details on this subject see References [48] to [87].

4.4 TOPOLOGY CONTROL IN DIRECTED GRAPHS

This section introduces the problem of fault-tolerant topology control for all-to-one and one-to-all communication in static wireless networks with asymmetric wireless links represented by a directed graph. The results are used to model sensor networks and multicast transmission respectively.

4.4.1 The system model

We assume that a wireless network consists of N nodes, each of which is equipped with an omnidirectional antenna with a maximal transmission range of r_{max}. The power required for a node to attain a transmission range of r is Cr^{α}, where C is a constant and α is the power attenuation exponent (between two and four). For any two nodes u and v, there exists a link from u to v if the distance $d(u, v) \leq r_u$, where r_u is the transmission range for node u, determined by its power level. If the links are asymmetric, the existence of a link from u to v does not guarantee the existence of a link from v to u. In this section, we consider asymmetric links and assume that the wireless network is static (the nodes in the network are stationary).

Given the coordination of the nodes in the plane and the transmission power of the nodes, the network can be mapped into a *cost graph* $G = (V, E, c)$, where V denotes the set of wireless nodes, E denotes the set of wireless links induced by the transmission power and the weight c for a given edge (u, v) is computed as $Cd(u, v)^{\alpha}$, where d is the distance. By this mapping, an asymmetric wireless network is represented by a directed graph.

In a multicast wireless network, for a node to send data to multiple nodes in its transmission range, instead of sending data multiple times, it only needs to send it once, and all nodes in its transmission range can receive the same data. In these networks the power and link weight are defined as follows. Given a cost graph $G = (V, E, c)$, let $p(u)$ be the power assignment of node u, $w(uv)$ be the cost of an edge uv, $c(G)$ be the weight of G and $p(G)$ be the power of G. Then we have $p(u) = \max_{uv \in E} w(uv)$, $c(G) = \sum_{e \in E} w(e)$ and $p(G) = \sum_{v \in V} p(v)$.

Traditional problems in graph theory are link based, with the goal of minimizing total weight. However, wireless networks call for node-based algorithms to minimize the total power consumption. In the following, we give formal definitions for the all-to-one and one-to-all fault-tolerant problem.

4.4.1.1 All-to-one k-fault-tolerant problem

Given the cost graph of a network and root node r, find the power assignment of each node such that there exist k node-disjoint paths from every other node to r in the induced spanning subgraph and the total node power assignment is minimized. This is also called the minimum power k-inconnectivity problem.

4.4.1.2 One-to-all k-fault-tolerant problem

Given the cost graph of a network and root node r, find the power assignment of each node such that there exist k node-disjoint paths from r to every other node in the induced spanning subgraph and the total node power assignment is minimized. This is also called the minimum power k-outconnectivity problem.

4.4.1.3 Concurrent all-to-one and one-to-all k-fault-tolerant problem

Given the cost graph of a network and root node r, find the power assignment of each node such that the induced spanning subgraph is both k-inconnected and k-outconnected and the total node power assignment is minimized. This is also called the minimum power k-bothconnectivity problem.

4.4.2 Minimum-weight-based algorithms

The *minimum weight* (MW) algorithms construct a minimum weight spanning subgraph that satisfies a certain connectivity constraint. In this section we present three algorithms called

MW-IN, MW-OUT and Minimum Weight k-bothconnected (MW-BOTH) for minimum power k-inconnectivity, minimum power k-outconnectivity and minimum power k-bothconnectivity problems, respectively [88].

All three algorithms use an algorithm proposed by Frank and Tardos (FT) [89], which for a given $D = (V, E, c)$ define $x : E \to \{0, 1\}$ as follows:

$$x(e) = \begin{cases} 1 & \text{if } e \in MW - OUT \text{ subgraph} \\ 0 & \text{otherwise} \end{cases} \tag{4.23}$$

Let $O(A)$ be the set of all incoming edges to node set A, where $A \subseteq V - r$. Let $O_x(A) = \sum_{uv \in O(A)} x(uv)$.

The minimum weight k-outconnectivity problem has the following LP relaxation:

$$\begin{aligned} &\text{Minimize } cx \\ &\text{subject to } O_x(A) \geq k \text{ for any } A \subseteq V - r \\ &\qquad 0 \leq x \leq 1 \end{aligned} \tag{4.24}$$

If we define $p : 2^V \to Z \cup \{-\infty\}$ as [90]

$$p(A) = \begin{cases} k & kA \subseteq V - r \text{ and } A \neq \emptyset \\ 0 & \text{if } A = \emptyset \\ -\infty & \text{otherwise} \end{cases} \tag{4.25}$$

problem (4.24) becomes

$$\begin{aligned} &\text{Minimize } cx \\ &\text{subject to } O_x(A) \geq p(A) \text{ for any } A \subseteq V - r \\ &\qquad 0 \leq x \leq 1 \end{aligned} \tag{4.26}$$

This problem is an intersecting supermodular flow problem, and the integer solution is the optimal one [90]. Since the integer value of x can only be 0 or 1, by solving this *LP* we can get the solution for the minimum weight k-outconnected problem.

MW-IN is designed based on the following observation. If we first reverse the direction of edges of a given graph D to produce a new graph D', then construct the minimum weight k-outconnected subgraph S' of D' and then reverse the edge of S', we get a minimum weight k-inconnected subgraph S of the original graph D.

If the algorithm constructing a minimum weight k-outconnected subgraph by problem (4.26) is denoted as *FT*, then *MW-IN*(D, k, r) constructs a k-inconnected subgraph as follows:

(a) *Construct D' by reversing the direction of each edge in D and keep the weight of each edge the same.*

(b) $S' = FT(D', k, r)$.

(c) *Reverse the direction of each edge in S' to get S, where S is the k-inconnected spanning subgraph rooted at r.*

The design of *MW-OUT* and *MW-BOTH* is similar. *MW-OUT* is the same as *FT*. MW-BOTH first applies MW-IN on D, then applies MW-OUT on D and finally joins the output of MW-IN

and MW-OUT. Note that the output of MW-BOTH does not necessarily have the minimum weight.

The dominating step of MW algorithms is the step to apply the FT algorithm. Thus, the time complexity of MW algorithms is the same as that of the FT algorithm, which is $O(n^9 \log n)$, where n is the node size.

In the sequel, Theorems 6 to 8 give the approximation ratios of MW-IN, MW-OUT and MW-BOTH, respectively. The formal proofs for the theorems can be found in Reference [88].

Theorem 6
If $D_{MW\text{-}IN}$ is the output of algorithm MW-IN and $D_{popt-in}$ is a k-inconnected subgraph with optimal power, then $p(D_{MW-IN}) \leq kp(D_{popt-in})$.

Theorem 7
If D_{MW-OUT} is the output of the algorithm MW-OUT and $D_{popt-out}$ is the k-outconnected subgraph with optimal power, then $p(D_{MW-OUT}) \leq \Delta^- p(D_{popt-out})$, where Δ^- is the minimum maximum out-degree of any critically k-outconnected subgraph of $D_{popt-out}$.

Theorem 8
If $D_{MW\text{-}BOTH}$ is the output of algorithm MW-BOTH and D_{popt} is the k-bothconnected subgraph with optimal power, then $p(D_{MW-BOTH}) \leq (k + \Delta^-)p(D_{popt})$.

4.4.3 Augmentation-based algorithms

The *augmentation-based* (*AB*) approach is based on the idea to first construct a graph that consumes small total power and then augment it to satisfy a certain connectivity requirement. In this section, we present three algorithms called AB-IN, AB-OUT and augmentation-based k-bothconnected (AB-BOTH) for minimum power k-inconnectivity, minimum power k-outconnectivity and minimum power k-bothconnectivity, respectively, as proposed in Reference [88]. For these purposes we need to introduce the definitions of the i nearest *outgoing*/*incoming* neighbor graph and k-outconnected/k-inconnected augmentation. Given $G = (V, E)$, the i nearest outgoing neighbor graph $D_i^- = (V, E')$ is constructed as follows. For each $v \in V$, sort its outgoing edges in nondecreasing order by weight and then choose the first i edges in E'. The i nearest incoming neighbor graph D_i^+ can be defined accordingly. Also, given $D = (V, E)$ and its subgraph, H, F is called the k-outconnected augmentation to H if $H \cup F$ is the k-outconnected spanning subgraph of D. The k-inconnected augmentation can be defined accordingly.

The *AB-IN algorithm* is designed based on the observation that for any k-inconnected subgraph, the out-degree of each vertex is at least k. Since the power of a node is the maximum weight of all out-edges incident to this node, the power assignment for a node in any k-inconnected subgraph is at least the weight of the edge whose weight is the kth smallest among all edges. This power assignment causes all the edges with a weight less than the kth smallest weight to appear in any k-inconnected subgraph, including the one with minimum power. Because these are the *free* edges, we want to use as many such edges as possible. Hence, the main idea of AB-IN is to first construct a $(k-1)$-nearest outgoing neighbor graph, then augment it to be k-inconnected by setting the weight of edges in the nearest neighbor graph to zero and apply algorithm MW-IN to find the optimal weight k-inconnected subgraph. AB-IN is similar to the algorithm proposed by Jia *et al*. [91]. The main differences are that (1) AB-IN handles directed graphs, whereas [91] deals with undirected graphs, and (2) AB-IN constructs a k-inconnected subgraph, whereas the Reference [91] goal is to

construct a k-vertex connected subgraph, i.e. there exist k vertex-disjoint paths between any pair of vertices. Formally AB-IN can be represented as [88]:

Augmentation-based k-inconnected AB-IN (D, k, r)

- *Input:* (D, k, r) *where* $D = (V, E, c)$ *is a directed graph of network topology and* r *is the root.*
- *Output: a spanning subgraph that is* k*-inconnected to* r.
- *Construct* $(k-1)$*-nearest neighbor graph* D_{k-1}^{-}.
- *Construct* D' *from* D *by setting the weight of edges in* D_{k-1}^{-} *to zero.*
- *Reverse the direction of each edge in* D'.
- $H' = FT(D', k, r)$
- *Reverse the direction of each edge in* H'. *The new graph will be referred to as* H. H *is a spanning subgraph that is* k*-inconnected to* r.

AB-OUT gives a k-outconnected subgraph by first constructing a $(k-1)$-nearest incoming neighbor graph D_{k-1}^{+} and then augmenting it to be k-outconnected. Since a k-bothconnected subgraph is also a k-inconnected subgraph, the main idea of AB-BOTH is first to construct a k-inconnected subgraph and then augment it to be k-outconnected as well. The AB-BOTH algorithm can be formally presented as [88]:

Augmentation-based k-bothconnected AB-BOTH (D, k, r)

- *Input:* (D, k, r), *where* $G = (V, E, c)$ *is a directed graph of network topology and* r *is the root.*
- *Output: a spanning subgraph where there exist* k*-vertex disjoint paths between every vertex in* $V - r$ *and* r.
- $H = AB - IN(D, k, r)$
- *Construct* D' *from* D *by setting the weight of edges in* H *to zero.*
- $S = FT(D', k, r)$
- *Output* $H \cup S$, *which is a spanning subgraph that is both* k*-outconnected from* r *and* k*-inconnected to* r.

The dominating step of AB algorithms is the step to apply the FT algorithm. Thus, the time complexity of AB algorithms is the same as that of the FT algorithm, which is $O(n^9 \log n)$, where n is the node size. Figure 4.8 gives an example illustrating the six algorithms of the two approaches for $k = 2$.

Theorems 9 to 11, proven in Reference [88], give the approximation ratios of these three algorithms.

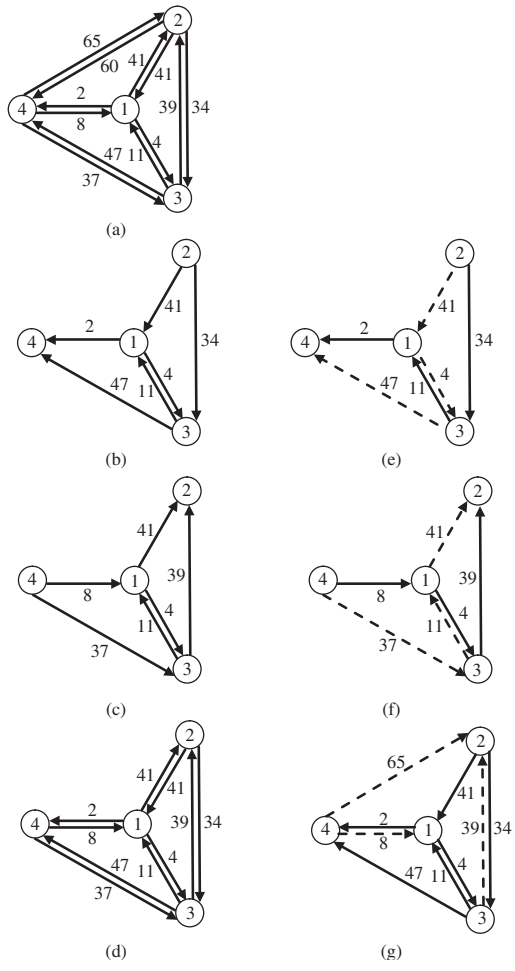

Figure 4.8 An example illustrating the MW and AB algorithms. (a) The original topology, where node 4 is the root node. (b), (c) and (d) The 2-inconnected, 2-outconnected and 2-bothconnected subgraphs constructed by MW-IN, MW-OUT and MW-BOTH, respectively. (e), (f) and (g) The outputs from AB-IN, AB-OUT and AB-BOTH, respectively. (e) The solid line is the first nearest outgoing neighbor graph and the dashed line is its 2-inconnected augmentation. (f) The solid line is the first nearest incoming neighbor graph and the dashed line is its 2-outconnected augmentation. (g) The solid line is the 2-inconnected subgraph in (e) and the dashed line is its 2-outconnected augmentation.

Theorem 9
If $D_{AB\text{-}IN}$ is the output of AB-IN, then $p(D_{AB-IN}) \leq (k+1)p(D_{popt\text{-}in})$.

Theorem 10
If $D_{AB\text{-}OUT}$ is the output of algorithm AB-OUT and $D_{popt\text{-}out}$ is the k-outconnected subgraph with optimal power, then $p(D_{AB-OUT}) \leq 2\Delta^- p(D_{popt-out})$, where Δ^- is the maximum out-degree of $D_{popt-out}$.

Theorem 11
If $D_{AB\text{-}BOTH}$ is the output of algorithm AB-BOTH and D_{popt} is the k-bothconnected subgraph with optimal power, then $p(D_{AB-BOTH}) \leq (1 + k + \Delta^{-})p(D_{popt})$.

4.4.4 Performance examples

To set up the simulation environment, we randomly generate various numbers of nodes in a fixed area and construct a complete cost graph from these nodes by setting the weight of each edge uv as $Cd^2(uv)$, where C is randomly chosen between 0.5 and 1.5 as in Reference [88]. For each node size, we run the simulation 100 times.

Figure 4.9 shows a comparison of the total power consumption for both approaches. Over 100 runs for each node size, we calculate the percentage of times when the MW approach outperforms the AB approach, as illustrated by the solid line with the triangle, the percentage of times when the AB approach outperforms the MW approach, as illustrated by the dashed line with the diamond, and the percentage of times when both approaches use the same power, as illustrated by the dotted line with the rectangle. For more information on the subject see References [88] to [115].

4.5 ADJUSTABLE TOPOLOGY CONTROL

In wireless ad hoc networks, constructing and maintaining a topology with lower node degrees is usually intended to mitigate excessive traffic load on wireless nodes. However, keeping lower node degrees often prevents nodes from choosing better routes that consume less energy. In this section a structure that has the flexibility to be adjusted between the two objectives through a single parameter is presented.

More generally, in this section we have an objective to control the topology with the following goals:

(1) *Symmetry.* The MAC layer's ACK is hard to implement when some links are not bidirectional. Besides, asymmetric links in topology would also cause inconsistent routing qualities at two ends.

(2) *Connectivity.* Two nodes u and v are strongly connected if there is a directed path from u to v and vice versa.

(3) *Energy efficiency.* Due to the severe path loss in radio carriers, transmitting with large ranges would exponentially run out of node energy. Therefore, relaying messages through multiple hops with shorter ranges could usually consume less energy. How to choose the links between nodes for relaying is a critical point in this goal.

(4) *Sparseness.* Numerous distributed and localized routing protocols are based on flooding, but this may burden networks with unavoidable redundant messages. Thus, keeping a sparse topology would be an ingenious way to shrink the expenditure from network operations.

(5) *Maximum node degree.* For some nodes with overly large degrees, the network flows will concentrate on them and rapidly draw out their energy. Besides, a larger node degree means tighter dependency among nodes, which is not expected when wireless nodes move frequently. Therefore, the maximum node degree over a topology should be bounded from above by some constant.

(6) *Planarity.* A graph is planar if it has no crossed links inside. It is helpful for many geometric problems. For example, the shortest path (least energy unicast route) can be quickly found in

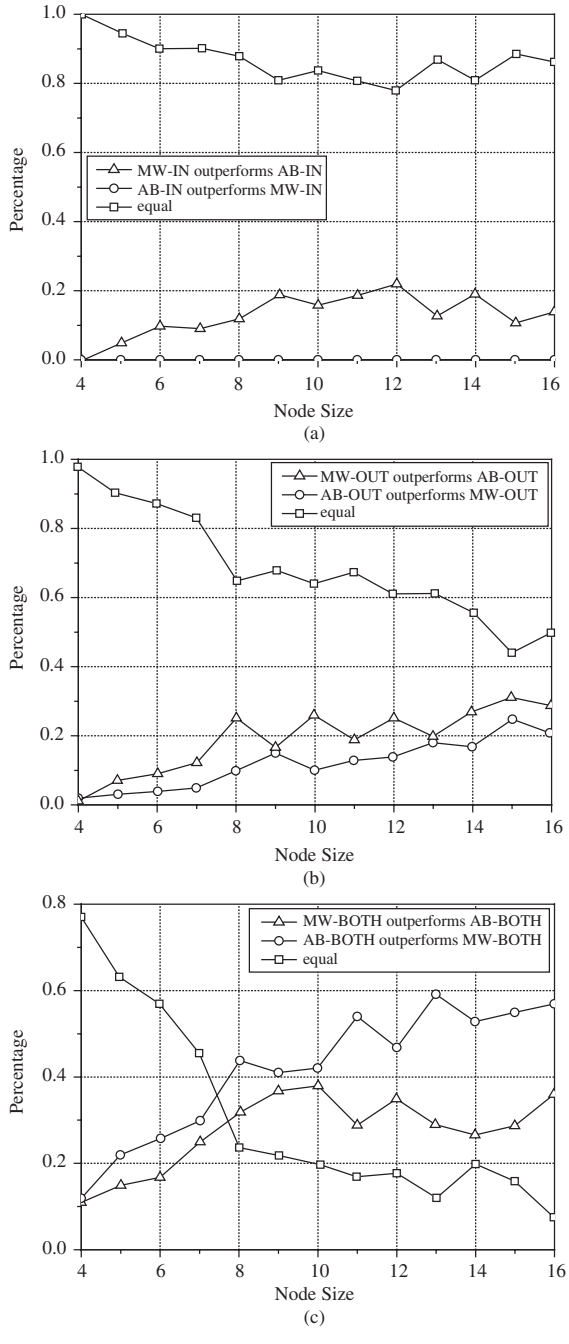

Figure 4.9 Total power consumption of the MW approach versus the power of the AB approach. (a) The power consumption of MW-IN versus the power consumption of AB-IN. (b) The power consumption of MW-OUT versus the power consumption of AB-OUT. (c) The power consumption of MW-BOTH versus the power consumption of AB-BOTH. (Reproduced by permission of IEEE (c) 2008 from Wang *et al*. [88]).

linear time when the underlying topology is planar. Besides, in many position-based routing algorithms, the successful delivery can be guaranteed only if the underlying topology is planar.

(7) *Localized approach.* In wireless ad hoc networks, due to the absence of a central arbitrator and the limited sensing range, centralized approaches are rarely attainable. Therefore, a variety of distributed approaches were proposed. A distributed protocol passes messages hop-by-hop. However, this may cause considerable overhead through the entire network. Therefore, a localized approach is more preferred.

4.5.1 The system model

The wireless ad hoc network discussed in this section consists of a set V of n wireless nodes distributed on a two-dimensional plane $\Re^2$. Each node has an omnidirectional antenna and can change its transmission range by adjusting the transmitting power at any level. The maximum transmission ranges are equal among all nodes so that we can normalize the maximum transmission ranges of all nodes to be 1. Each node u can obtain its position $P(u)$ and a unique $id(u)$.

This is modeled as a unit disk graph, $UDG(V)$, where an edge uv exists if and only if the Euclidean distance between u and v, denoted as $\|uv\|$, is atmost 1. The least power required to transmit directly between u and v is modeled as $\|uv\|^\alpha$, where α is the attenuation factor. To measure the power efficiency of a topology, Li *et al.* [116] defined the power stretch factor. If $\pi(u, v) = v_0 v_1 \cdots v_{h-1} v_h$ is a unicast path connecting nodes u and v, where $v_0 = u$ and $v_h = v$, the total transmission power consumed by path $\pi(u, v)$ is defined as

$$p(\pi(u, v)) = \sum_{x=1}^{h} \|v_{x-1} v_x\|^\alpha \tag{4.27}$$

If $\pi^*_{G(V)}(u, v)$ is the least-energy path connecting u and v in graph $G(V)$, for a subgraph $G'(V)$ in $UDG(V)$ the power stretch factor with respect to $UDG(V)$ is defined as

$$\rho(G(V)) = \max_{u,v \in V} \frac{p(\pi^*_{G'(V)}(u, v))}{p(\pi^*_{UDG(V)}(u, v))} \tag{4.28}$$

The maximum node degree of graph $G(V)$ is defined as

$$d_{\max}(G(V)) = \max_{u \in V} d_{G(V)}(u) \tag{4.29}$$

where $d_{G(V)}(u)$ is the degree of node u in graph $G(V)$.

In the sequel we will use the following terminology:

(a) An algorithm is purely localized if all its operations depend only on the inherent information (like position and id) in nodes, available before any execution of the algorithm.

(b) A structure is purely localizable if it can be constrained by a purely localized algorithm.

Many localizable structures, used to control the network topology, have been proposed in the literature [116–119], but only a few of them are purely localizable. In the following, we discuss some of them.

(1) The *constrained relative neighborhood graph* [120], denoted by $RNG(V)$, has an edge uv if and only if $\|uv\| \leq 1$ and the intersection of two open disks centered at u, v with radius $\|uv\|$ contain no node $w \in V$ (see Figure 4.10(a)). An open disk centered at point x with radius d is the collection of points with distance less that d from $P(x)$.

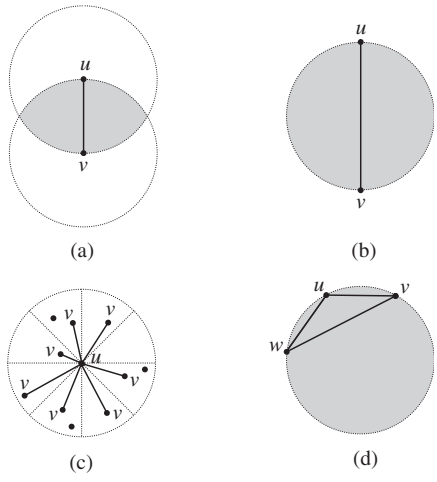

Figure 4.10 (a) $RNG(V)$, (b) $GG(V)$, (c) $YG_k(V)$, $k = 8$, (d) $UDel(V)$.

(2) The *constrained Gabriel graph* [121], denoted by $GG(V)$, has an edge uv if and only if $\|uv\| \leq 1$ and the open disk using $\|uv\|$ as diameter contain no node $w \in V$ (see Figure 4.10(b)).

(3) The *constrained Yao graph* [122] with a parameter $k \geq 6$, denoted *by* $YG'_k(V) \rightarrow$, is constructed as follows. For each node u, define k equal cones by k equal separated rays originated at u. At each cone, a directed edge uv exists if $\|uv\| \leq 1$ and the cone contains no vertex $w \in V$ such that $\|uw\| < \|uv\|$. Ties are broken arbitrarily. $YG_k(V)$ is denoted as the underlying undirected graph of $YG'_k(V)_i$ (see Figure 4.10(c)).

(4) A *Delaunay triangulation*, denoted by $Del(V)$, is a triangulation of V in which the interior of the circumcircle of each $\triangle uvw$ contains no node $w \in V$. The unit Delaunay triangulation, denoted by $UDel(V)$, has all edges of $Del(V)$ except those longer than 1 [118, 123] (see Figure 4.10(d)).

It was shown in Reference [122] that in a set V of nodes on $\Re^2$, with no node having two or more neighbors at exactly the same distance, $d_{\max}(RNG(V)) \leq 6$.

The constrained Gabriel graph $GG(V)$ has the least power stretch factor 1 in comparison with the unbounded power stretch factor $n-1$ of $RNG(V)$ [116]. At the same time, $d_{\max}(GG(V))$ could be as large as $n-1$. An extended structure, the enclosure graph [10, 117, 124], denoted by $EG(V)$, is generalized from $GG(V)$. It can always result in a subgraph of $GG(V)$ [117]. Even so, its maximum node degree is still unbounded [125].

For tradeoff between the maximum node degree and the power stretch factor, an adjustable structure having the flexibility to be adjusted between the two objectives is more attractive. $YG'_k(V)$ is such a structure. It can be adjusted through a parameter k such that, for any given k, the maximum out-degree is at most k and the power stretch factor is at most $1/[1-(2\sin\pi/k)^\alpha]$ [116]. It is said that an objective $f(.)$ of an adjustable structure $S_k(V)$ with parameter k is partially bounded if there is at least one k_0 such that $f(S_{k_0}(V))$ is bounded. In accordance with this definition, the maximum out-degree and power stretch factor of $YG'_k(V)$ are partially bounded since, for some ranges of k, k and $1/[1-(2\sin\pi/k)^\alpha]$ are constants. The asymmetric edges of $YG'_k(V)$ may lead to large in-degrees even when k is very small [116]. Therefore, $d_{\max}(YG_k(V))$ can be neither bounded nor partially bounded. To improve this, an extension of $\rightarrow YG'_k(V)$, named Yao and Sink, was

proposed [116, 126, 127]. It can limit the maximum node degree in $(k+1)^2 - 1$ and result in symmetric edges. In this structure, the neighbors of some nodes should be recursively determined by one another so that they cannot be purely localizable.

The unit Delaunay triangulation $UDel(V)$ has a bounded power stretch factor. At the same time, neither $Del(V)$ nor $UDel(V)$ can be computed locally. Li *et al*. [118] suggested a localized version of the Delaunay graph, referred to as $LDel^{(h)}(V)$, where h means that each node uses at most k-hop information. The power stretch factor of $LDel^{(k)}(V)$ is bounded for all $k \geq 1$. Unfortunately, its maximum node degree is not bounded for any h.

These structures were studied in References [117] and [129] to [131], and included EMST(V), the Euclidean minimum spanning tree of $UDG(V)$.

From the above works, we know that EMST(V) is connected if $UDG(V)$ is itself a connected component of V. Therefore, when $UDG(V)$ is connected, all graphs containing EMST(V) are connected. In other words, $RNG(V)$, $GG(V)$, $EG(V)$, $UDel(V)$, $LDel^{(k)}(V)$ and $YG_k(V)$ are all connected. The connectivity of $XTC(X)$ [122] was proven in a different way [10]. $LDel^{(k)}(V)$ is planar for any $k \geq 2$ [118]. Therefore, all subgraphs of $LDel^{(2)}(V)$ that include $UDel(V)$, $GG(V)$, $EG(V)$, $RNG(V)$, $XTC(V)$ and EMST(V) are planar. On the other hand, $YG'_k(V)$ and $LDel^{(1)}(V)$ are not planar [116, 118].

From the discussion, we can see that none of the above structures can simultaneously bound or even partially bound the two objectives, the power stretch factor and the maximum node degree. The r-neighborhood graph [132] fills this gap. This structure is adjustable and can always result in a connected planar graph with symmetric edges.

4.5.2 The r-neighborhood graph [132]

First, we define a region on $\Re^2$. Let x be any point on $\Re^2$, and the open disk and circle centered at $P(x)$ with radius d are denoted as $D(x, d)$ and $C(x, d)$, respectively. The region is defined as follows. Given a node pair (u, v) on $\Re^2$, the r-neighborhood region of (u, v), denoted as $NR_r(u, v)$, is $NR_r(u, v) = D(u, \|uv\|) \cap D(v, \|uv\|) \cap D(m_{uv}, l_{uv})$, where m_{uv} is the middle point on uv, $l_{uv} = (\|uv\|/2)(1 + 2r^2)^{1/2}$ and $0 \leq r \leq 1$.

In Figure 4.11, the shaded region intersected by the three open disks represents an example of the r-neighborhood region. This region is equivalent to the following point set: $NR_r(u, v) = \{P(x) \in R^2 \| ux\| < \|uv\|, \|vx\| < \|uv\|, \|mx\| < l\}$. For any node w located on $NR_r(u, v)$, this region limits the power consumed by path uwv. This property is formally expressed as follows. Given two nodes u and v on $\Re^2$, for any node w then [132]

$$\begin{array}{l} P(w) \in NR_r(u, v) \\ p(uwv) < \|uv\|^\alpha (1 + r^\alpha) \end{array} \text{ for all } \alpha \geq 2 \tag{4.30}$$

Equation (4.30) explains why we call such a plane a neighbourhood region. For any node w located in the region $NR_r(u, v)$, it should be an alternative neighbor for u with respect to v in the sense that the power required for relaying from u to v through w is no greater than $1 + r^\alpha$ times the power required for direct transmission. Based on this region, the structure is defined as follows. Given a set V of nodes on $\Re^2$, the r-neighborhood graph of V, denoted as $NG_r(V)$, has an edge uv if and only if $\|uv\| \leq 1$ and $NR_r(u, v)$ contains no node $w \in V$, where $0 \leq r \leq 1$.

If edge uv is not in $UDG(V)$ or a node w is inside $NR_r(u, v)$, there is no direct link connecting u and v in $NG_r(V)$, which means that all transmissions between u and v should be relayed through some other node(s) in $NG_r(V)$. Now, before we explore the desired properties in this structure we will discuss the following relations. For any set V of nodes on $\Re^2$, we find that $RNG(V) \subseteq NG_r(V) \subseteq GG(V)$, for all $0 \leq r \leq 1$ [132]. As $r = 0, NR_0(u, v) \equiv D(m, \|uv\|/2)$, we have the disk defining $GG(V)$ and as $r = 1, NR_1(u, v) \equiv D(m, \|uv\|)$, we have the disk defining $RNG(V)$. Therefore, $GG(V) \equiv NG_0(V)$ and $RNG(V) \equiv NG_1(V)$ and so we can conclude that the

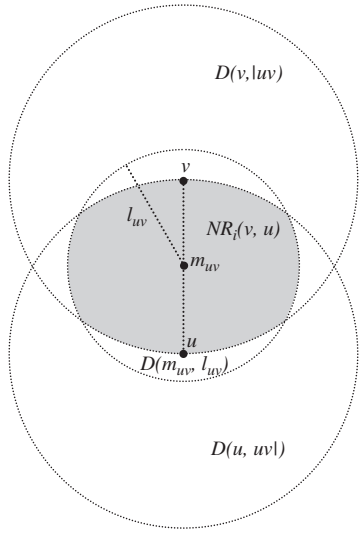

Figure 4.11 The r-neighborhood region of nodes u and v.

r-neighborhood graph is a generalized structure of both the restricted Gabriel graph and the restricted relative neighborhood graph.

Since a subgraph of a planar graph is always planar and a supergraph of a connected graph is always connected, with the planarity of $GG(V)$ and connectivity of $RNG(V)$ we can see that for any set V of nodes on $\Re^2$, $NR_r(V)$ is planar, for all $0 \leq r \leq 1$, and if the underlying $UDG(V)$ is connected, $NR_r(V)$ is connected, for all $0 \leq r \leq 1$.

The energy efficiency and node degree of $NR_r(V)$ was described in Reference [132], where it was shown that the upper bound of $\rho(NG_r(V))$ is increased by r and the upper bound of $d_{\max}(NG_r(V))$ is decreased by r. In other words, the r-neighborhood graph is adjustable to the two objectives through the parameter r. More specifically, we have:

(1) For any set V of n nodes on $\Re$ for all $0 \leq r \leq 1$ and $\alpha \geq 2$, $\rho(NG_r(V)) \leq 1 + r^{\alpha}(n-2) = F(r)$.

(2) For any set V of nodes on $\Re^2$ with the assumption that there is no node in V having two or more neighbors at exactly the same distance, for all $0 \leq r \leq 1$, $d_{\max}(NG_r(V)) \leq |\pi / \sin^{-1}(r/2)|$.

For more details on the subject see References [116] to [130] and [132] to [148].

4.6 SELF-CONFIGURING TOPOLOGIES

The large number of nodes deployed in sensor networks may preclude manual configuration, and the environmental dynamics may preclude design-time preconfiguration. Therefore, nodes will have to self-configure to establish a topology that provides communication under stringent energy constraints. Self-configuring topology (SCT) is based on the notion that, as density increases, only a subset of the nodes are necessary to establish a routing forwarding backbone. In SCT, each node assesses its connectivity and adapts its participation in the multihop network topology based on the measured operating region.

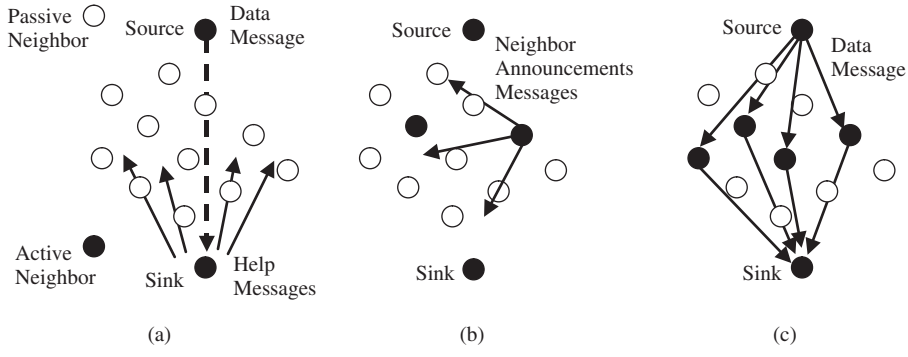

Figure 4.12 Network self-configuration example: (a) communication hole, (b) transition, (c) final state.

SCT adaptively elects 'active' nodes from all nodes in the network. Active nodes stay awake all the time and perform multihop packet routing, while the rest of the nodes remain 'passive' and periodically check if they should become active. Figure 4.12 shows a simplified schematic for SCT during initialization in a high-density region of a simple sensor network for data gathering.

For the sake of clarity, formation of only the two-hop network is shown. The extention to networks of larger sizes is straightforward. Initially, only some nodes are active. The other nodes remain passively listening to packets but not transmitting (see Figure 4.12(a)). The source starts transmitting data packets toward the sink. Because the sink is at the limit of the radio range, it gets very high packet loss from the source. The sink then starts sending help messages to signal neighbors that are in listen-only mode (*passive neighbors*) to join the network.

When a neighbour receives a *help message*, it may decide to join the network (see Figure 4.12(b)).When a node joins the network, it starts transmitting and receiving packets, i.e. it becomes an *active neighbor*. As soon as a node decides to join the network, it signals the existence of a new active neighbor to other passive neighbors by sending a *neighbour announcement message*. This situation continues until the number of active nodes stabilizes on a certain value and the cycle stops (see Figure 4.12(c)). When the process completes, the group of newly active neighbors that have joined the network make the delivery of data from the source to the sink more reliable. The process will restart when some future network event (e.g. node failure) or environmental effect (e.g. new obstacle) causes packet loss again.

In SCT, nodes are in one of four states: *sleep, passive, test* and *active*. Figure 4.13 shows a state transition diagram.

Initially, a random timer turns on the nodes to avoid synchronization. When a node starts, it initializes in the *test state*. Nodes in the *test state* exchange data and routing control messages. In addition, when a node enters the *test state*, it sets up a timer T_t and sends *neighbor announcement messages*. When T_t expires, the node enters the *active state*. If, before T_t expires, the number of active neighbors is above the *neighbor threshold* (*NT*) or if the average *data loss rate* (*DL*) is higher than the average loss before entering in the *test state*, then the node moves into the *passive state*. If multiple nodes make a transition to the *test state*, then we use the node ID in the announcement message as a tiebreaking mechanism (higher IDs win). The intuition behind the *test state* is to probe the network to see if the addition of a new node may actually improve connectivity.

When a node enters the *passive state*, it sets up a timer T_p and sends *new passive node announcement messages*. This information is used by active nodes to make an estimate of the total density of nodes in the neighborhood. Active nodes transmit this density estimate to any new passive node in the neighborhood. When T_p expires, the node enters the sleep state. If, before T_p

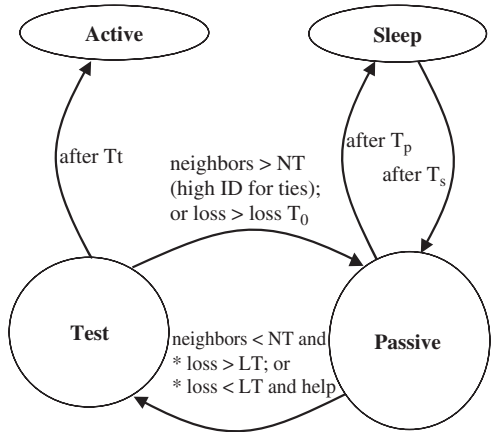

Figure 4.13 STC state transition.

expires, the number of neighbors is below *NT* and either the *DL* is higher than the *loss threshold* (*LT*) or *DL* is below the *loss threshold* but the node received a *help message* from an active neighbour, it makes a transition to the *test state*. While in the *passive state*, nodes have their radio on and are able to overhear *all* packets transmitted by their active neighbors. No routing or data packets are forwarded in this state since this is a listen-only state. The intuition behind the *passive state* is to gather information regarding the state of the network without causing interference with the other nodes. Nodes in the *passive* and *test states* continuously update the number of active neighbors and data loss rate values. Energy is still consumed in the *passive state* since the radio is still on when not receiving packets. A node that enters the *sleep state* turns the radio off, sets a timer T_s and goes to sleep. When T_s expires, the node moves into the *passive state*. Finally, a node in the *active state* continues forwarding data and routing packets until it runs out of energy. If the *data loss rate* is greater than the *LT*, the active node sends *help messages*.

4.6.1 SCT performance

We characterize the system performance by the following parameters:

(1) The *one-hop delivery rate* measures the percentage of packets received by any node in the network. When all the nodes are turned on – we call this the *active* case – the packet reception includes all nodes. In the SCT case, it includes all nodes but the ones in the sleep state. This metric indicates the effective one-hop bandwidth available to the nodes in the sensor network.

(2) The *end-to-end delivery rate* is the ratio of the number of distinct packets received by the destination to the number originally sent by the source. It provides an idea of the quality of the paths in the network and the effective multihop bandwidth. A similar metric has been used in ad hoc routing.

(3) *Energy savings* is the ratio of the energy consumed by the active case to the energy consumed by the SCT case. This metric defines the amount of energy savings and network lifetime we gain by using the SCT algorithm.

(4) *Average per-hop latency* measures the average delay in packet forwarding in a multihop network. It provides an estimate of the end-to-end delay in packet forwarding.

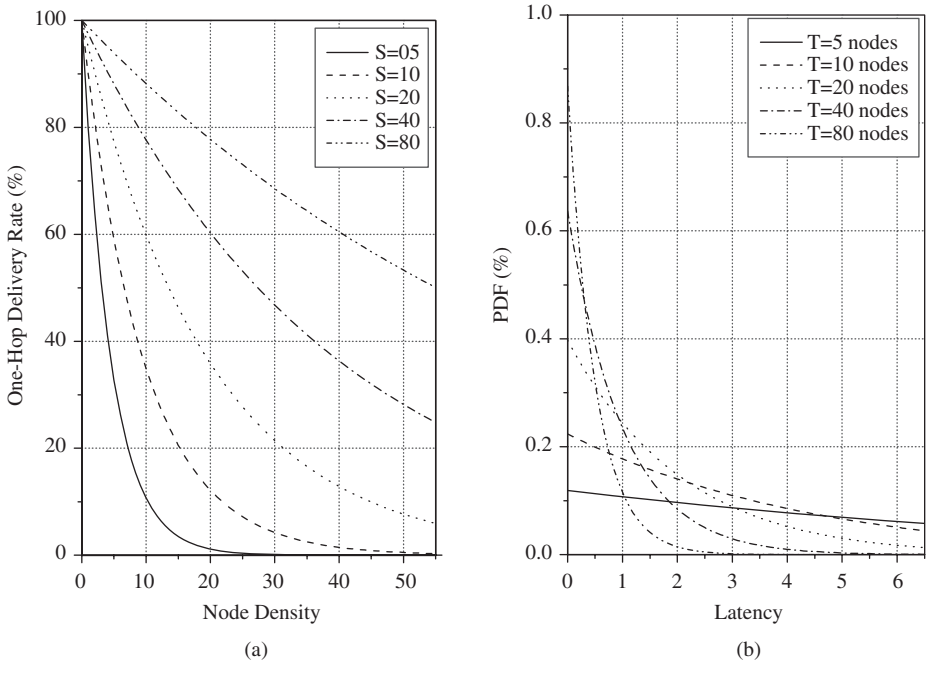

Figure 4.14 (a) The expected one-hop delivery rate as a function of density. The larger the randomization period, the better the one-hop delivery rate for any given density. (b) The probability distribution of the one-hop latency. The larger the density, the smaller the probability of a large latency.

For an analysis of these parameters we assume that nodes are randomly distributed in an area A and have an average degree of connectivity of n. Further, we assume that packets are propagated using flooding with a random backoff upon packet reception. This random component is chosen from a discrete pool of S slots with a uniform probability distribution. Thus, the probability of successfully transmitting a packet with no collisions when there are T potential forwarding nodes in the vicinity is given by

$$P(\text{success}) = [(S-1)/S]^T \tag{4.31}$$

Figure 4.14(a) shows the analytical relation between the expected one-hop delivery rate versus the density of nodes for different S values.

The relationship between the hop-by-hop latency introduced by the randomization and the density of nodes can be analyzed similarly. The average latency experienced per hop is related to the number of random slots S and the total number of active nodes T. After reception of a message to be forwarded toward the destination, each of the T active nodes picks a random slot, say $S_1, S_2, \ldots, S_T$. The mean number of all the random slots chosen will tend to be $S/2$, since it is a uniform probability distribution. Assuming no collision losses, i.e. $\forall i \neq j \in 1, 2, \ldots, T \Rightarrow S_i \neq S_j$, the hop-by-hop latency is determined by the first message to be forwarded. The delay δ is then $\delta = \min(S_1, S_2, \ldots, S_T)$. We want to find $P(\delta)$, the probability distribution of the smaller random timeslot picked by T nodes. We define:

$$\begin{aligned} &Q(y) = Prob\{\min(S_1, S_2, \ldots, S_T) > y\} \\ &\min(S_1, S_2, \ldots, S_T) > y \Leftrightarrow \min(S_1, S_2, \ldots, S_T) \end{aligned} \tag{4.32}$$

This happens with probability

$$\begin{aligned} &\{(S-y)/S\}^T \\ &\text{therefore } \; Q(y) = (1-y/S)^T \end{aligned} \tag{4.33}$$

$P(\delta)$ as defined above is

$$P(\delta) = Q(\delta) - Q(\delta+1) = \left(1 - \frac{\delta}{S}\right)^T - \left(1 - \frac{\delta+1}{S}\right)^T \tag{4.34}$$

Figure 14.4(b) shows the $P(\delta)$ distribution for different values of T and $S = 20$. When the system is not running SCT, all the nodes have their radios on, consuming I (*idle)* power. When the system is running SCT, NT nodes have their radios on, while the rest alternate between sleeping and listening. The energy savings (ES) are

$$ES = \frac{n \times I}{NT \times I + (n - NT) \times I \frac{T_p}{T_p + T_s} + (n - NT) P_{\text{sleep}} \frac{T_s}{T_p + T_s}} \tag{4.35}$$

The numerator represents the power consumed by all the nodes when not running SCT. The denominator represents the power consumed by all nodes running SCT. The first term in the denominator indicates the power consumed by the NT nodes selected by SCT to have their radios on. The second term in the denominator indicates the energy of nonactive nodes when in the passive state and the third term indicates the energy consumed while in the sleep state. We define α to be the ratio of the passive timer T_p to the sleep timer T_s and β to be the ratio of the radio's sleep mode to the idle mode power consumption, so that Equation (4.35) becomes

$$ES = \frac{n}{NT + (n - NT)\frac{\alpha+\beta}{\alpha+1}} \tag{4.36}$$

and the upper bound of the energy savings as we increase density is $\lim_{n\to\infty} ES = (\alpha+1)/(\alpha+\beta)$. Figure 4.15 shows the energy savings versus the density of nodes for a fixed value of β.

For more information on the subject see References [131] and [149] to [157].

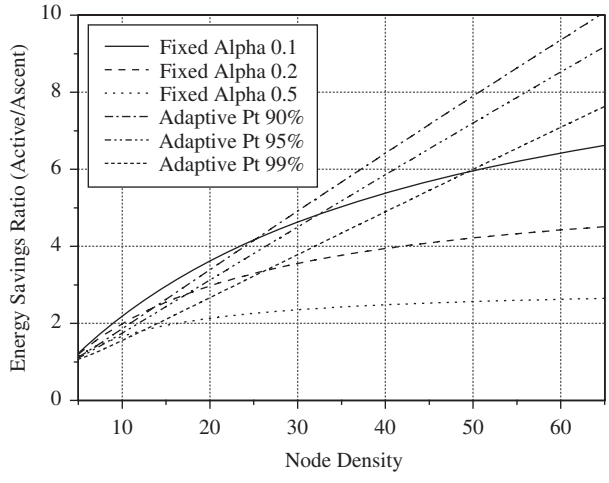

Figure 4.15 Energy savings as a function of density for SCT fixed and adaptive state timers. Fixed state timers converge asymptotically to a particular maximum value when increasing density. On the other hand, adaptive state timers do not present this asymptotic limit and the energy savings increase linearly as a function of density.

REFERENCES

[1] N. Li, J. C. Hou and L. Sha, Design and analysis of an MST-based topology control algorithm, in *Proc. IEEE INFOCOM*, San Francisco, CA, April 2003, pp. 1702–1712.

[2] C. E. Jones, K. M. Sivalingam, P. Agrawal and J. C. Chen, A survey of energy efficient network protocols for wireless networks, *Wireless Networks*, vol. 7, no. 4, August 2001, pp. 343–358.

[3] D. A. Maltz, J. Broch, J. Jetcheva and D. Johnson, The effects of on-demand behavior in routing protocols for multihop wireless ad hoc networks, *IEEE J. Selected Areas Commun.*, vol. 17, no. 8, August 1999, pp. 1439–1453.

[4] P. Gupta and P. R. Kumar, The capacity of wireless networks, *IEEE Trans. Information Theory*, vol. 46, no. 2, March 2000, pp. 388–404.

[5] S. Narayanaswamy, V. Kawadia, R. S. Sreenivas and P. R. Kumar, Power control in ad hoc networks: theory, architecture, algorithm and implementation of the COMPOW protocol, in *Proc. Eur. Wireless, Next Generation Wireless Networks*: *Technologies, Protocols*, *Services and Applications*, Florence, Italy, February 2002, pp. 156–162.

[6] P. Santi, D. M. Blough and F. Vainstein, A probabilistic analysis for the range assignment problem in ad hoc networks, in *Proc. ACM Symp. Mobile Ad Hoc Networking and Computing* (*MOBIHOC*), Long Beach, CA, August 2000, pp. 212–220.

[7] L. Li, J. Y. Halpem, P. Bahl, Y.-M. Wang and R. Wattenhofer, Analysis of a cone-based distributed topology control algorithm for wireless multihop networks, in *Proc. ACM Symp. Principles of Distributed Computing* (*PODC*), Newport, RI, August 2001, pp. 264–273.

[8] V. Kawadia and P. Kumar, Power control and clustering in ad hoc networks, in *Proc. IEEE INFOCOM*, San Francisco, CA, April 2003, pp. 459–469.

[9] R. Ramanathan and R. Rosales-Hain, Topology control of multihop wireless networks using transmit power adjustment, in *Proc. IEEE INFOCOM*, Tel Aviv, Israel, March 2000, pp. 404–413.

[10] V. Rodoplu and T. H. Meng, Minimum energy mobile wireless networks, *IEEE J. Selected Areas Commun.*, vol. 17, no. 8, August 1999, pp. 1333–1344.

[11] S. Basagni, D. Turgut and S. K. Das, Mobility-adaptive protocols for managing large ad hoc networks, in *Proc. IEEE Int. Conf. Commun. (ICC)*, Helsinki, Finland, June 2001, pp. 1539–1543.

[12] M. G. J. Wu and I. Stojmenovic, On calculating power-aware connected dominating sets for efficient routing in ad hoc wireless networks, in *Proc. Int. Conf. Parallel Processing*, Vancouver, BC, Canada, August 2002, pp. 346–354.

[13] T. He, C. Huang, B. M. Blum, J. A. Stankovic and T. Abdelzaher, Range-free localization schemes for large scale sensor networks, in *Proc. ACM Int. Conf. Mobile Computing and Networking* (*MOBICOM*), San Diego, CA, September 2003, pp. 81–95.

[14] C. Kee, H. Jun, D. Yun, B. Kim, Y. Kim, B. W. Parkinson, T. Langenstein, S. Pullen and J. Lee, Development of indoor navigation system using asynchronous pseudolites, in *Proc. 13th Int. Technical Meeting of the Satellite Division of the Institute of Navigation* (*ION GPS*), Salt Lake City, UT, September 2000, pp. 1038–1045.

[15] R. Prim, Shortest connection networks and some generalizations, *Bell Syst. Tech. J.*, vol. 36, 1957, pp. 1389–1957.

[16] S. Pettie and V. Ramachandran, An optimal minimum spanning tree algorithm, *J. ACM*, vol. 49, no. 1, 2002, pp. 16–34.

[17] C. Monma and S. Suri, Transitions in geometric minimum spanning trees, in *Proc. ACM Symp. Computational Geometry*, North Conway, NH, 1991, pp. 239–249.

[18] I. Chlamtac and A. Farago, Making transmission schedules immune to topology changes in multihop packet radio networks, *IEEE/ACM Trans. Networking*, vol. 2, no. 1, February 1994, pp. 23–29.

[19] J. H. Ju and V. O. K. Li, An optimal topology-transparent scheduling method in multihop packet radio networks, *IEEE/ACM Trans. Networking*, vol. 6, no. 3, June 1998, pp. 298–306.

[20] D. M. Blough, G. Resta and P. Santi, A statistical analysis of the long-run node spatial distribution in mobile ad hoc networks, in *Proc. Int. Workshop on Modeling Analysis and Simulation of Wireless and Mobile Systems* (*MSWiMS*), Atlanta, GA, September 2002, pp. 30–37.

[21] N. Li, J. C. Hou and L. Sha, (2003) *Design and analysis of an MST-based topology control algorithm* Department of Computer Science, University of Illinois at Urbana-Champaign, IL [online], Available: http://www.students.uiuc.*edu*/∼*nli*/*papers*/*main*$_{-tech.pdf}$.

[22] N. Li and J. C. Hou, Topology control in heterogeneous wireless networks: problems and solutions, in *Proc. IEEE INFOCOM*, Hong Kong, March 2004, pp. 232–243.

[23] N. Li, J. C. Hou and L. Sha, Design and analysis of an MST-based topology control algorithm, *IEEE Trans. Wireless Commun.*, vol. 4, no. 3, May 2005, p. 1195.

[24] L. Chen, Q. Zhang, M. Li and W. Jia, Joint topology control and routing in IEEE 802.11-based multiradio multichannel mesh networks, *IEEE Trans. Vehicular Technol.*, vol. 56, no. 5, September 2007, p. 3123.

[25] R. Bruno, M. Conti and E. Gregori, Mesh networks: commodity multihop ad hoc networks, *IEEE Commun. Mag.*, vol. 43, no. 3, March 2005, pp. 123–131.

[26] IEEE 802.11 Working Group, *Wireless LAN Medium Access Control* (*MAC*) *and Physical Layer* (*PHY*) *Specifications*, 1997.

[27] IEEE 802.l la Working Group, *Wireless LAN Medium Access Control* (*MAC*) *and Physical Layer* (*PHY*) *Specifications – Amendment 1*: *High-Speed Physical Layer in the 5 GHz Band*, 1999.

[28] A. Raniwala, K. Gopalan and T. Chiueh, Centralized channel assignment and routing algorithms for multi-channel wireless mesh networks, *ACM SIGMOBILE Mobile Comput. Commun. Rev.*, vol. 8, no. 2, April 2004, pp. 50–65.

[29] J. Tang, G. Xue and W. Zhang, Interference aware topology control and QoS routing in multi-channel wireless mesh networks, in *Proc. Mobihoc*, 2005, pp. 68–77.

[30] M. Marina and S. Das, A topology control approach for utilizing multiple channels in multi-radio wireless mesh networks, in *Proc. Broadnets*, vol. 1, 2005, pp. 381–390.

[31] R. Draves, J. Padhye and B. Zill, Routing in multi-radio, multi-hop wireless mesh networks, in *Proc. Mobicom*, 2004, pp. 114–128.

[32] P. Kyasanur and N. Vaidya, Routing and link layer protocols for multi-channel multi-interface *ad hoc* wireless networks, *ACM SIGMOBILE Mobile Comput. Commun. Rev.*, vol. 10, no. 1, January 2005, pp. 31–43.

[33] A. Raniwala and T. Chiueh, Architecture and algorithms for an IEEE 802.11-based multi-channel wireless mesh network, in *Proc. Infocom*, vol. 3, 2005, pp. 2223–2234.

[34] H. Wu, F. Yang, K. Tan, J. Chen, Q. Zhang and Z. Zhang, Distributed channel assignment and routing in multi-radio multi-channel multi-hop wireless networks, *IEEE J. Selected Areas Commun.*, *Special Issue on Multi-hop Wireless Mesh Networks*, vol. 24, no. 11, November 2006, pp. 1972–1983.

[35] M. Alicherry, R. Bhatia and L. Li, Joint channel assignment and routing for throughput optimization in multi-radio wireless mesh networks, in *Proc. Mobicom*, 2005, pp. 58–72.

[36] D. De Couto, D. Aguayo, J. Bicket and R. Morris, High throughput path metric for multi-hop wireless routing, in *Proc. Mobicom*, 2003, pp. 134–146.

[37] V. Shah and S. Krishnamurthy, Handling asymmetry in power heterogeneous *ad hoc* networks: a cross layer approach, in *Proc. ICDCS*, June 2005, pp. 749–759.

[38] D. Johnson, D. Maltz and J. Broch, *DSR*. The dynamic source routing protocol for multi-hop wireless *ad hoc* networks, 2004, IETF Manet Working Group, Draft 10.

[39] W. Fang, N. Seddigh and B. Nandy, A time sliding window three colour marker (TSWTCM), June 2000, RFC 2859.

[40] R. L. Cruz and A. V. Santhanam, Optimal routing, link scheduling and power control in multi-hop wireless networks, in *Proc. Infocom*, vol. 1, 2003, pp. 702–711.
[41] M. Kodialam and T. Nandagopal, Characterizing achievable rates in multi-hop wireless networks: the joint routing and scheduling problem, in *Proc. Mobicom*, 2003, pp. 42–54.
[42] M. Kodialam and T. Nandagopal, Characterizing the capacity region in multi-radio multi-channel wireless mesh networks, in *Proc. Mobicom*, 2005, pp. 73–87.
[43] W. Song, Y. Wang, X. Li and O. Frieder, "Localized algorithms for energy efficient topology in wireless *ad hoc* networks," in *Proc. Mobihoc*, vol. 10, no. 6, December 2004, pp. 911–923.
[44] M. Burkhart, P. Rickenbach, R. Wattenhofer and A. Zollinger, Does topology control reduce interference?, in *Proc. Mobihoc*, 2004, pp. 9–19.
[45] C. Yu, B. Lee and H. Youn, Energy efficient routing protocols for mobile *ad hoc* networks, *Wireless Commun. Mobile Comput.*, vol. 3, no. 8, December 2003, pp. 959–973.
[46] P. Bergamo, A. Giovanardi *et al*., Distributed power control for energy efficient routing in *ad hoc* networks *Wireless Networks*, vol. 10, no. 1, 2004, pp. 29–42.
[47] Y. Wu, P. Chou, Q. Zhang, K. Jain, W. Zhu and S. Kung, Network planning in wireless *ad hoc* networks: a cross-layer approach, *IEEE J. Selected Areas Commun.*, vol. 23, no. 1, January 2005, pp. 136–150.
[48] M. Hajiaghayi, N. Immorlica and V. Mirrokni, Power optimization in fault-tolerant topology control algorithms for wireless multi-hop networks, *IEEE/ACM Trans. Networking*, vol. 15, no. 6, December 2007, p. 1345
[49] E. Althaus, G. Calinescu, I. Mandoiu, S. Prasad, N. Tchervenski and A. Zelikovsky, Power efficient range assignment in *ad-hoc* wireless networks, in *Proc. IEEE Wireless Commun. and Networking Conf.* (*WCNC*), 2003.
[50] M. Bahramgiri, M. Hajiaghayi and V. S. Mirrokni, Fault-tolerant and 3-dimensional distributed topology control algorithms for wireless multi-hop networks, *Wireless Networks*, 2002, pp. 392–398; see also in *Proc. 11th IEEE Int. Conf. Computer Commun. and Networks* (*ICCCN*).
[51] M. A. Bassiouni and C. Fang, Dynamic channel allocation for linear macrocellular topology, in *Proc. 13th ACM Symp. Applied Computing* (*SAC*), 1998, pp. 382–388.
[52] D. M. Blough, M. Leoncini, G. Resta and P. Santi, On the symmetric range assignment problem in wireless *ad hoc* networks, in *Proc. 2nd IFIP Int. Conf. Theoretical Computer Science* (*TCS*), 2002, pp. 71–82.
[53] D. M. Blough, M. Leoncini, G. Resta and P. Santi, The K-neigh protocol for symmetric topology control in *ad hoc* networks, in *Proc. ACM Int. Symp. Mobile Ad Hoc Networking and Computing* (*MobiHoc*), June 2003.
[54] J. L. Bredin, E. D. Demaine, M. T. Hajiaghayi and D. Rus, Deploying sensor networks with guaranteed capacity and fault tolerance, in *Proc. th ACM Int. Symp. Mobile Ad Hoc Networking and Computing* (*MobiHoc*), 2005, pp. 309–319.
[55] G. Calinescu, I. L. Mandoiu and A. Zelikovsky, Symmetric connectivity with minimum power consumption in radio networks, in *Proc. 7th IFIP World Computer Congr.*, 2002, pp. 119–130.
[56] J. Cartigny, D. Simplot and I. Stojmenovic, Localized minimum-energy broadcasting in *ad hoc* networks, in *Proc. IEEE INFOCOM*, 2003.
[57] J. Cheriyan, S. Vempala and A. Vetta, Approximation algorithms for minimum-cost k-vertex connected subgraphs, in *Proc. 34th ACM Symp. Theory of Computing (STOC)*, 2002, pp. 306–312.
[58] A. Clementi, P. Crescenzi, P. Penna, G. Rossi and P. Vocca, A worst-case analysis of an MST based heuristic on construct energy-efficient broadcast trees in wireless networks, in *Proc. 18th Annual Symp. Theoretical Aspects of Computer Science* (*STACS*), 2001, pp. 121–131.

[59] A. Clementi, A. Ferreira, P. Penna, S. Perennes and R. Silvestri, The minimum range assignment problem on linear radio networks, in *Proc. Annual European Symp. Algorithms* (*ESA*), 2000, pp. 143–154.

[60] A. E. F. Clementi, G. Huiban, P. Penna, G. Rossi and Y. C. Verhoeven, Some recent theoretical advances and open questions on energy consumption in *ad-hoc* wireless networks, in *Proc. 3rd Workshop on Approximation and Randomization Algorithms in Commun. Networks* (*ARACNE*), 2002, pp. 23–38.

[61] A. E. F. Clementi, P. Penna and R. Silvestri, Hardness results for the power range assignment problem in packet radio networks, in *Proc. 2nd Int. Workshop on Approximation Algorithms for Combinatorial Optimization Problems* (*APPROX*), 1999, pp. 197–208.

[62] A. Frank, Augmenting graphs to meet edge-connectivity requirements, *SIAM J. Discrete Math.*, vol. 5, no. 1, 1992, pp. 25–53.

[63] A. Frank and E. Tardos, An application of submodular flows, *Linear Algebra Applications*, vol. 114/115, 1989, pp. 329–348.

[64] R. Gallager, P. Humbler and P. Spira, A distributed algorithm for minimum-weight spanning trees, *ACM Trans. Programming Language Systems*, vol. 5, 1983, pp. 66–77.

[65] M. T. Hajiaghyi, G. Kortsarz, V. S. Mirrokni and Z. Nutov, Power optimization for connectivity problems, in *Proc. 11th Int. Integer Programming and Combinatorial Optimization Conf.* (*IPCO*), 2005, pp. 349–361.

[66] G. Kortsarz, V. S. Mirrokni, Z. Nutov and E. Tsanko, Power optimization for network design problems (submitted for publication).

[67] K. Jain, A factor 2 approximation for the generalized Steiner network problem, *Combinatorica*, vol. 21, no. 1, 2001, pp. 39–60.

[68] X. Jia, D. Kim, S. Makki, P. Wan and C. Yi, Power assignment for k-connectivity in wireless *ad hoc* networks, *J. Combinatorial Optimization*, vol. 9, no. 2, 2005, pp. 213–222.

[69] S. Khuller and B. Raghavachari, Improved approximation algorithms for uniform connectivity problems, *J. Algorithms*, vol. 21, no. 2, 1996, pp. 434–450.

[70] L. M. Kirousis, E. Kranakis, D. Krizanc and A. Pelc, Power consumption in packet radio networks, *Theoret. Comput. Sci.*, vol. 243, no. 1–2, 2000, pp. 289–305.

[71] G. Kortsarz and Z. Nutov, Approximating node connectivity problems via set covers, in *Proc. 3rd Int. Workshop on Approximation Algorithms for Combinatorial Optimization* (*APPROX*), 2000, pp. 194–205.

[72] S. Khuller and U. Vishkin, Biconnectivity approximations and graph carvings, in *Proc. 24th ACM Symp. Theory of Computing* (*STOC*), 1992, pp. 759–770.

[73] N. Li and J. C. Hou, FLSS: a fault-tolerant topology control algorithm for wireless networks, in *Proc. 10th Annual Int. Conf. Mobile Computing and Networking* (*MOBICOM*), 2004, pp. 275–286.

[74] L. Li, J. Halpem, V. Bahl, Y. M. Wang and R. Wattenhofer, Analysis of a cone-based distributed topology control algorithm for wireless multi-hop networks, in *Proc. ACM Symp. Principle of Distributed Computing* (*PODC*), 2001, pp. 264–273.

[75] W. Liang, Constructing minimum-energy broadcast trees in wireless *ad hoc* networks, in *Proc. 3rd ACM Int. Symp. Mobile Ad Hoc Networking and Computing* (*MobiHoc*), 2002.

[76] E. Lloyd, R. Liu, M. Marathe, R. Ramanathan and S. Ravi, Algorithmic aspects of topology control problems for *ad hoc* networks, in *Proc. 3rd ACM Int. Symp. Mobile Ad Hoc Networking and Computing* (*MobiHoc*), 2002.

[77] X. Li, W. Song and Y. Wang, Efficient topology control for wireless *ad hoc* networks with non-uniform transmission ranges, *Wireless Networks*, vol. 11, no. 3, May 2005.

[78] X. Li, Y. Wang and W. Song, Applications of k-local MST for topology control and broadcasting in wireless *ad hoc* networks, *IEEE Trans. Parallel Distributed Systems*, vol. 15, no. 12, 2004, pp. 1057–1069.

[79] X. Li, Y. Wang, P. Wan and C. Yi, Robust deployment and fault tolerant topology control for wireless *ad hoc* networks, in *Proc. ACM Int. Symp. Mobile Ad Hoc Networking and Computing* (*MobiHoc*), June 2003.
[80] R. Mathar and J. Mattfeldt, Optimal transmission ranges for mobile communication ln linear multihop packet radio networks, *Wireless Networks*, vol. 2, 1996, pp. 329–342.
[81] R. Ramanathan and R. Rosales-Hain, Topology control of multihop radio networks using transmit power adjustment, in *Proc. IEEE lNFOCOM*, 2000, pp. 404–413.
[82] V. Rodoplu and T. H. Meng, Minimum energy mobile wireless networks, *IEEE J. Selected Areas Commun.*, vol. 17, no. 8, pp. 1633–1639, August 1999.
[83] W. Mader, "Ecken vom grad n in minimalen n-fach zusammen-hangenden graphen," *Arch. Math. (Basel)*, vol. 23, 1972, pp. 219–224.
[84] P. Wan, A. Calinescu, X. Li and O. Frieder, Minimum energy broadcast routing in static *ad hoc* wireless networks, in *Proc. IEEE lNFOCOM*, 2001, pp. 607–617.
[85] Y. Wang and X. Y. Li, Minimum power assignment in wireless *ad hoc* networks with spanner property, in *Proc. IEEE Workshop on High Performance Switching and Routing*, 2004.
[86] R. Wattenhofer, L. Li, V. Bahl and Y. M. Wang, Distributed topology control for power efficient operation in multihop wireless *ad hoc* networks, in *Proc. IEEE INFOCOM*, 2001, pp. 1388–1397.
[87] H. Zhang and J. Hou, On the critical total power for asymptotic k-connectivity in wireless networks, in *Proc. IEEE INFOCOM*, 2005.
[88] F. Wang, M. Thai, Y. Li, X. Cheng and D. Du, Fault-tolerant topology control for all-to-one and one-to-all communication in wireless networks, *IEEE Trans. Mobile Comput.*, vol. 7, no. 3, March 2008, p. 322.
[89] A. Frank and E. Tardos, An application of submodular flows, *Linear Algebra and Its Applications*, vols 114/115, 1989, pp. 329–348.
[90] J. Edmonds and R. Giles, A min-max relation for submodular functions on graphs, *Ann. Discrete Math.*, vol. 1, 1977, pp. 185–204.
[91] X. Jia, D. Kim, P. Wan and C. Yi, Power assignment for K – connectivity in wireless ad hoc networks, in *Proc. IEEE INFOCOM*, 2005.
[92] I. F. Akyildiz, W. Su, S. Yogesh and E. Cayirci, A survey on sensor networks, *IEEE Commun. Mag.*, vol. 40, no. 8, 2002, pp. 102–114.
[93] R. Rajaraman, Topology control and routing in *ad hoc* networks: a survey, *SIGACT News*, vol. 33, no. 2, 2002, pp. 60–73.
[94] F. Wang, K. Xu, M. Thai and D.-Z. Du, Fault Tolerant topology control for one-to-all communications in symmetric wireless networks, *Int. J. Sensor Networks*, Special Issue on *Theoretical and Algorithmic Aspects in Sensor Networks*, vol. 2, no. 3/4, 2007, pp. 163–168.
[95] M. Hajiaghayi, N. Immorlica and V.S. Mirrokni, Power optimization in fault-tolerant topology control algorithms for wireless multi-hop networks, in *Proc. ACM MobiCom*, 2003.
[96] N. Li and I. C. Hou, FLSS: a fault-tolerant topology control algorithm for wireless networks, in *Proc. ACM MobiCom*, 2004.
[97] A. Srinivas and E. Modiano, Minimum energy disjoint path routing in wireless *ad-hoc* networks, in *Proc. ACM MobiCom*, 2003.
[98] J. E. Wieselthier, G. D. Nguyen and A. Ephremides, On the construction of energy-efficient broadcast and multicast trees in wireless networks, in *Proc. IEEE INFOCOM*, 2000.
[99] O. Egecioglu and T. F. Gonzalez, Minimum-energy broadcast in simple graphs with limited node power, in *Proc. IASTE D Int. Conf. Parallel and Distributed Computing and Systems* (*PDCS'*01), 2001.
[100] M. Cagalj, J.-P. Hubaux and C. Enz, Minimum-energy broadcast in all-wireless networks: NP-completeness and distribution issues, in *Proc. ACM MobiHoc*, 2002.
[101] D. Li, X. Jia and H. Liu, Energy efficient broadcast routing in static *ad hoc* wireless networks, *IEEE Trans. Mobile Comput.*, vol. 3, 2004.

[102] M. Bahramgiri, M. Hajiaghayi and V. Mirrokni, Fault-tolerant and 3-dimensional distributed topology control algorithms in wireless multi-hop networks, in *Proc. 11th IEEE Int. Conf. Computer Commun. and Networks* (*ICCCN*), 2002.

[103] E. L. Lloyd, R. Liu, M. V. Marathe, R. Ramanathan and S. S. Ravi, Algorithmic aspects of topology control problems for *ad hoc* networks, in *Proc. ACM MobiHoc*, 2002.

[104] E. L. Lloyd, R. Liu, M. V. Marathe, R. Ramanathan and S. S. Ravi, Algorithmic aspects of topology control problems for *ad hoc* networks, *Mobile Network Applications*, vol. 10, no. 1–2, 2005, pp. 19–34.

[105] G. Calinescu and P.-J. Wan, Range assignment for high connectivity in wireless *ad hoc* networks, in *Proc. Second Int. Conf. Ad-Hoc Networks and Wireless* (*ADHOC-NOW*), 2003.

[106] S. Khuller and B. Raghavachari, Improved approximation algorithms for uniform connectivity problems, *Proc. 27th Annual ACM Symp. Theory of Computing* (*STOC*), 1995.

[107] R. Wattenhofer, L. Li, P. Bahl and Y.-M. Wang, Distributed topology control for wireless multihop *ad-hoc* networks, in *Proc. IEEE INFOCOM*, 2001.

[108] L. Li, J. Y. Halpern, P. Bahl, Y.-M. Wang and R. Wattenhofer, Analysis of a cone-based distributed topology control algorithm for wireless multi-hop networks, in *Proc. 20th Annual ACM Symp. Principles of Distributed Computing* (*PODC′*01), 2001.

[109] R. Ramanathan and R. Hain, Topology control of multihop wireless networks using transmit power adjustment, in *Proc. IEEE INFOCOM*, 2000.

[110] J. W. Suurballe, Disjoint paths in a network, *Networks*, 1974, pp. 125–145.

[111] H. N. Gabow, A representation for crossing set families with applications to submodular flow problems, in *Proc. Fourth Annual ACM/SIGACT-SIAM Symp. Discrete Algorithms* (*SODA′*93), 1993.

[112] L. K. Fleischer, S. Iwata and S. T. McCormick, A faster capacity scaling algorithm for minimum cost submodular flow, *Math. Programming*, vol. 92, 2002, pp. 119–139.

[113] J. Cheriyan, T. Jord and Z. Nutov, Approximating K-out-connected subgraph problems, in *Proc. Int. Workshop on Approximation Algorithms for Combinatorial Optimization* (*APPROX*), 1998, pp. 77–88.

[114] Y. Li, X. Cheng and W. Wu, Optimal topology control for balanced energy consumption in wireless networks, *J. Parallel Distributed Computing*, vol. 65, no. 2, 2005, pp. 124–131.

[115] N. Lynch, *Distributed Algorithms*. Morgan Kaufmann, 1996.

[116] X. Y. Li, P. J. Wan and Y. Wang, Power, efficient and sparse spanner for wireless *ad hoc* networks, in *Proc. IEEE Int. Conf. Computer Commun. and Networks*, 2001, pp. 564–567.

[117] X. Y. Li and P. J. Wan, Constructing minimum energy mobile wireless networks, *ACM SIGMOBILE Mobile Comput. and Commun. Rev.*, vol. 5, 2001, pp. 55–67.

[118] X. Y. Li, G. Calinescu, P. J. Wan and Y. Wang, Localized Delaunay triangulation with application in *ad hoc* wireless networks, *IEEE Trans. Parallel and Distributed Systems*, vol. 14, no. 10, October 2003, pp. 1035–1047.

[119] P. Bose, P. Morin, I. Stojmenovič and J. Urrutia, Routing with guaranteed delivery in *ad hoc* networks," *ACM/Kluwer Wireless Networks*, vol. 7, no. 6, 2001, pp. 609–616.

[120] G. T. Toussaint, The relative neighborhood graph of a finite planar set, *Pattern Recognition*, vol. 12, no. 4, 1980, pp. 261–268.

[121] K. R. Gabriel and R. R. Sokal, A new statistical approach to geographic variation analysis, *Systematic Zoology*, vol. 18, 1969, pp. 259–278.

[122] A. C. C. Yao, On constructing minimum spanning trees in k-dimensional spaces and related problems, *SIAM J. Comput.*, vol. 11, 1982, pp. 721–736.

[123] J. Geo, L. J. Guibas, J. Hershburger, L. Zhang and A. Zhu, Geometric spanner for routing in mobile networks, in *Proc. ACM MobiHoc*, 2001.

[124] W. H. Lee and T. H. Meng, A lower power GPS receiver architecture, in *Proc. Global Telecommun. Conf.*, vol. 11, 1999, pp. 153–157.

[125] L. Li and J. Y. Halpern, Minimum-energy mobile wireless networks revisited, in *Proc. IEEE Int. Conf. Commun.* (*ICC*(1)), 2001.
[126] X. Y. Li, P. J. Wan, Y. Wang and O. Frieder, Sparse power efficient topology for wireless networks, in *Proc. 3th Annual Hawaii Int. Conf. System Sciences* (*HICSS*), vol. 9, 2002.
[127] W. Wang, X. Y. Li, K. Moaveninejad, Y. Wang and W. Z. Song, The spanning ratios of beta-skeleton, in *Proc. Canadian Conf. Computational Geometry* (*CCCG*), 2003.
[128] H. N. Gabow, J. L. Bently and R. E. Tarjan, Scaling and related techniques for geometry problems, in *Proc. ACM Symp. Theory of Computing*, 1984, pp. 135–143.
[129] J. Katajainen, The region approach for computing relative neighborhood graphs in the LP metric, *Computing*, vol. 40, 1988, pp. 147–161.
[130] F. P. Preparata and M. I. Shamos, *Computational Geometry – An Introduction*. Springer-Verlag, 1985.
[131] A. Cerpa and D. Estrin, ASCENT: adaptive self-configuring sensor networks topologies, *IEEE Trans. Mobile Comput.*, vol. 3, no. 3, July–September 2004, p. 272.
[132] A. Jeng and R. Jan, The r-neighborhood graph: an adjustable structure for topology control in wireless *ad hoc* networks, *IEEE Trans. Parallel and Distributed Systems*, vol. 18, no. 4, April 2007, p. 536.
[133] P. Bose, J. Gudmundsson and P. Morin, Ordered theta graphs, in *Proc. Canadian Conf. Computational Geometry*, 2002.
[134] P. Bose, L. Devroye, W. Evans and D. Kirkpatrick, On the spanning ratio of Gabriel graphs and beta-skeletons, *SIAM J. Discrete Math.*, vol. 20, no. 2, 2004, pp. 412–427.
[135] I. Chlamtac, M. Conti and J. N. Liu, Mobile *ad hoc* networking: imperatives and challenges, *Ad Hoc Networks*, vol. 1, 2003, pp. 13–64.
[136] L. Feeney, An energy-consumption model for performance analysis of routing protocols for mobile *ad hoc* networks, *ACM J. Mobile Networks and Applications*, vol. 3, no. 6, 2001, pp. 239–249.
[137] A. A. K. Jeng and R. H. Jan, An adjustable structure for topology control in wireless *ad hoc* network, in *Proc. 2005 Int. Conf. Wireless Network Commun. and Mobile Comput.*, 2005.
[138] B. Karp and H. T. Kung, GPSR: greedy perimeter stateless routing for wireless networks, in *Proc. MobiCom*, 2000.
[139] P. Klein, S. Rao, M. Rauch and S. Subramanian, Faster shortest-path algorithms for planar graph, in *Proc. Symp. Theory of Computing*, 1994.
[140] L. A. Latiff and N. Fisal, Routing protocols in wireless mobile *ad hoc* networks – A review, *Communications*, vol. 2, 2003, pp. 600–604.
[141] X. Y. Li and Y. Wang, Efficient construction of low weight bounded degree planar spanner, *Int. J. Computational Geometry and Applications*, vol. 14, no. 1–2, 2004, pp. 69–84.
[142] R. Prakash, Unidirectional links prove costly in wireless *ad- hoc* networks, in *Proc. Third Int. Workshop on Discrete Algorithms and Methods for Mobile Comput. and Commun.* (*DIAL-M*), 1999.
[143] R. Rajaraman, Topology control and routing and *ad hoc* network: a survey, *ACM SIAM J.*, vol. 33, no. 2, 2002.
[144] W. Z. Song, Y. Wang and X. Y. Li, Energy efficiency: localized algorithms for energy efficient topology in wireless *ad hoc* networks, in *Proc. Fifth ACM Int. Symp. Mobile Ad Hoc Networking and Comput.*, 2004.
[145] I. Stojmenovic and S. Datta, Power and cost aware localized routing with guaranteed delivery in wireless networks, *Wireless Commun. and Mobile Comput.*, vol. 4, no. 2, 2004, pp. 175–188.
[146] I. Stojmenovic and X. Lin, Power-aware localized routing in wireless networks, *IEEE Trans. Parallel and Distributed Systems*, vol. 12, no. 11, 2001, pp. 1122–1133.

[147] Y. Wang and X. Y. Li, Localized construction of bounded degree planar spanner for wireless *ad hoc* networks, in *Proc. 2003 Joint Workshop on Foundations of Mobile Comput.*, 2003, pp. 59–68.

[148] R. Wattenhofer and A. Zollinger, XTC: a practical topology control for *ad-hoc* networks, in *Proc. 18th Parallel and Distributed Processing Symp.*, 2004, pp. 26–30.

[149] K. Sohrabi and G. Pottie, Performance of a novel self-organization protocol for wireless *ad hoc* sensor networks, in *Proc. IEEE Vehicular Technol.*, September 2000.

[150] H. Gupta, Zongheng Zhou, S. R. Das and Q. Gu, Connected sensor cover: self-organization of sensor networks for efficient query execution, *IEEE/ACM Trans. Networking*, vol. 14, no. 1, February 2006, pp. 55–67.

[151] A. Karnik and A. Kumar, Distributed optimal self-organization in *ad hoc* wireless sensor networks, *IEEE/ACM Trans. Networking*, vol. 15, no. 5, October 2007, pp. 1035–1045.

[152] P. K. Biswas and S. Phoha, Self-organizing sensor networks for integrated target surveillance, *IEEE Trans. Computers*, vol. 55, no. 8, August 2006, pp. 1033–1047.

[153] Kian Hsiang Low, W. K. Leow and M. H. Ang Jr, Autonomic mobile sensor network with self-coordinated task allocation and execution, *IEEE Trans. Systems, Man, and Cybernetics, Part C: Applications and Reviews*, vol. 36, no. 3, May 2006, pp. 315–327.

[154] Yao-Chung Chang, Zhi-Sheng Lin and Jiann-Liang Chen, Cluster based self-organization management protocols for wireless sensor networks, *IEEE Trans. Consumer Electronics*, vol. 52, no. 1, February 2006, pp. 75–80.

[155] Fang Liu, Xiuzhen Cheng, Liran Ma and Kai Xing, SBK: a self-configuring framework for bootstrapping keys in sensor networks, *IEEE Trans. Mobile Comput.*, vol. 7, no. 7, July 2008, pp. 858–868.

[156] Fang Liu and Xiuzhen Cheng, LKE: a self-configuring scheme for location-aware key establishment in wireless sensor networks, *IEEE Trans. Wireless Communications*, vol. 7, no. 1, January 2008, pp. 224–232.

[157] A. V. Konstantinou, D. Florissi and Y. Yemini, Towards self-configuring networks, in *Proc. DARPA Active Networks Conf. and Exposition*, 29–30 May 2002, pp. 143–156.

5

Adaptive Medium Access Control

5.1 WLAN ENHANCED DISTRIBUTED COORDINATION FUNCTION

The last few years have witnessed an explosive growth in 802.11 WLAN [1]. Unfortunately, the current 802.11 MAC does not possess any effective service differentiation capability, because it treats all the upper-layer traffic in the same fashion. Hence, a special working group, IEEE 802.11e [2–12], was established to enhance the 802.11 MAC to meet QoS requirements for a wide variety of applications. The 802.11e EDCF (extended distributed coordination function) is an extension of the basic DCF mechanism of current 802.11 (Chapter 1). Unlike DCF, EDCF is not a separate coordination function, but a part of a single coordination function of 802.11e called the hybrid coordination function (HCF). The HCF combines both DCF and PCF (point coordination function) from the current 802.11 specification with new QoS specific enhancements. It uses EDCF and a polling mechanism for contention-based and contention-free channel access, respectively. In EDCF, each station can have multiple queues that buffer packets of different priorities. Each frame from the upper layers bears a priority value which is passed down to the MAC layer. Up to eight priorities are supported in a 802.11e station and they are mapped into four different access categories (AC) at the MAC layer [3]. A set of EDCF parameters, namely the arbitration interframe space (AIFS[AC]), minimum contention window size (CWMin[AC]) and maximum contention window size (CWMax[AC]), is associated with each access category to differentiate the channel access. $AIFS[AC]$ is the number of time slots a packet of a given AC has to wait after the end of a time interval equal to a short interframe spacing (SIFS) duration before it can start the backoff process or transmit. After $i (i \geq 0)$ collisions, the *backoff counter* in 802.11e is selected uniformly from $[1, 2^i \times CWMin[AC]]$, until it reaches the *backoff stage* i such that $2^i \times CWMin[AC] = CWMax[AC]$. At that point, the packet will still be retransmitted, if a collision occurs, until the total number of retransmissions equals the maximum number of allowable retransmissions ($RetryLimit[AC]$) specified in IST WSI [13], with the backoff counters always chosen from the range $[1, CWMax[AC]]$. Since multiple priorities

Advanced Wireless Technologies: Cognitive, Cooperative & Opportunistic 4G Technology Second Edition Savo G. Glisic

exist within a single station, it is likely that they will collide with each other when their back-off counters decrement to zero simultaneously. This phenomenon is called an *internal collision* in 802.11e and is resolved by letting the highest priority involved in the collision win the contention. Of course, it is still possible for this winning priority to collide with packets from other station(s).

Performance example – the basic parameters used in simulation are:

Packet payload size 8184 bits at 11 Mbps
MAC header 272 bits at 11 Mbps
PHY header 192 bits at 1 Mbps
ACK 112 bits + PHY header
Propagation delay 1 μs
Slot time 20 μs
SIFS 10 μs

The QoS parameters, i.e. *CWMin*[*AC*], *CWMax*[*AC*] and *AIFS*[*AC*], used in the following discussion are similar to the values specified by IEEE 802.11e Working Group for voice and video traffic [12].

Simulation with the same parameters is also presented for example, in Tao and Panwar [14]. In Figure 5.1, each station contains two priorities, which are only differentiated by the internal collision resolution algorithm discussed before. As expected, internal collision resolution by itself can provide some differentiation for channel access between different priorities.

The two priorities in each station are further differentiated by *AIFS* and *CWMin/CWMax* in Figures 5.2 and 5.3, respectively. It can be seen that *AIFS* may have a more marked effect on service differentiation than *CWMin/CWMax* alone. When all QoS mechanisms in 802.11e EDCF are enabled, the resulting throughput is shown in Figure 5.4. Comparing Figure 5.4 with Figure 5.2, we find that the QoS differentiation effect of *AIFS* is almost identical to the aggregate impact of *AIFS* plus *CWMin/CWMax*.

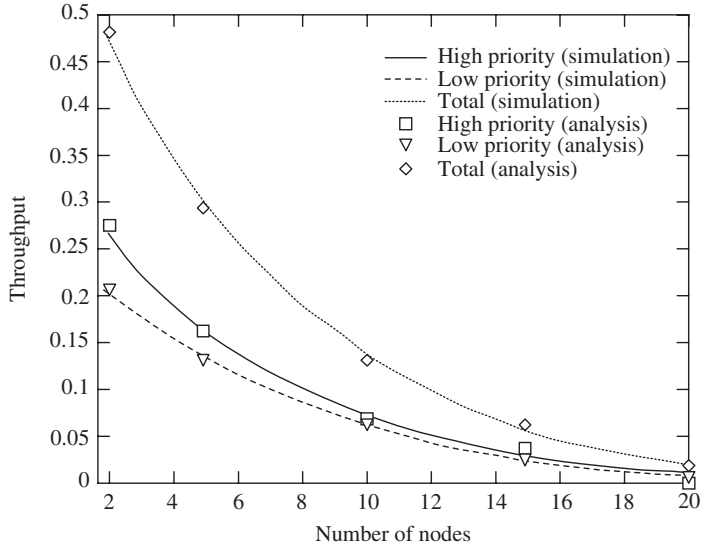

Figure 5.1 Two priorities differentiated only by internal collision resolution: CWMin/Max[0] = 8/16, CWMin/Max[1] = 8/16, AIFS[0] = 2, AIFS[1] = 2.

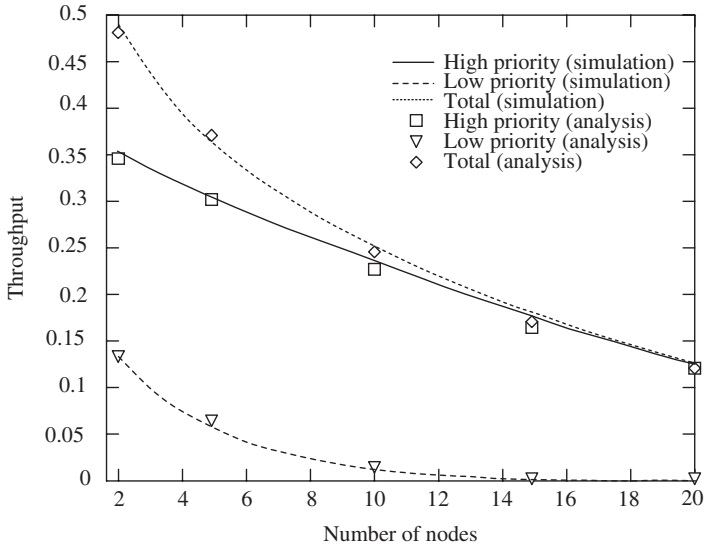

Figure 5.2 Two priorities with different AIFS values: CWMin/Max[0] = 8/16, CWMin/Max[1] = 8/16, AIFS[0] = 2, AIFS[1] = 3.

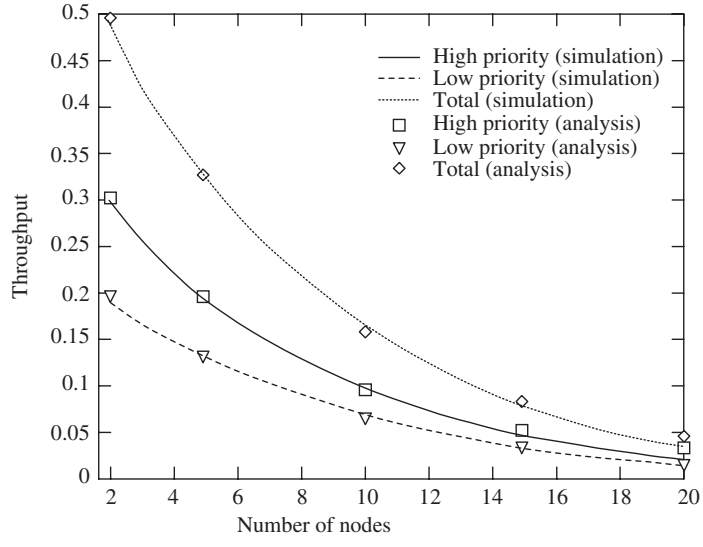

Figure 5.3 Two priorities with different CWMin and CWMax. AIFS[0] = 2, AIFS[1] = 2, CWMin/Max[0] = 8/16, CWMin/Max[1] = 10/20.

All the figures reveal that, as the number of stations in the network grows, the throughput for each priority as well as the total throughput drop fairly fast, especially when the QoS-specific parameters are small. Under heavy load assumption, the throughput for low priority often decreases to almost zero before the number of stations reaches 10. For this region, the high priority traffic dominates.

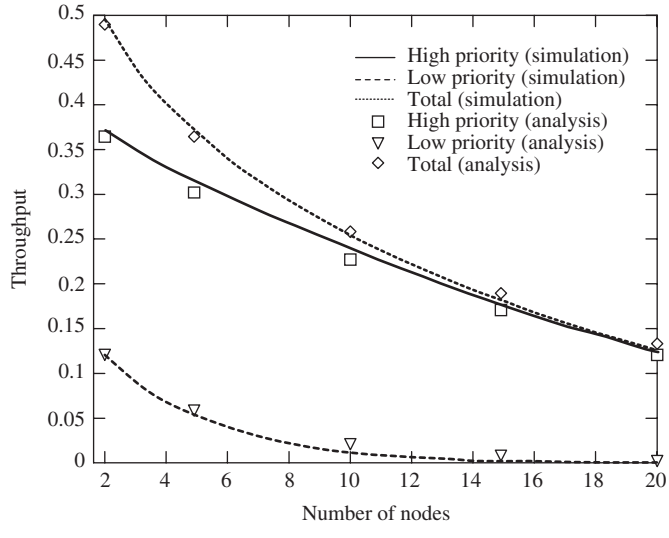

Figure 5.4 Two priorities with different CWMin, CWMax and AIFS: AIFS[0] = 2, AIFS[1] = 3, CWMin/Max[0] = 8/16, CWMin/Max[1] = 10/20.

5.2 ADAPTIVE MAC FOR WLAN WITH ADAPTIVE ANTENNAS

Smart antennas (or adaptive array antennas) have some unique properties that enable us to achieve high throughputs in *ad hoc* network scenarios. A transmitter equipped with a smart antenna can form a directed beam towards its receiver and a receiver can similarly form a directed beam towards the sender, resulting in very high gain. A receiver can also identify the direction of multiple simultaneous transmitters by running DOA algorithms and use this information to determine the directions in which it should place the *nulls*. Placing nulls effectively cancels out the impact of interfering transmitters. In this paper we present a simple 802.11b-based MAC protocol called Smart-802.11b that explicitly uses these three properties of smart antennas (beamforming, DOA and nulling) to achieve high throughputs. The two protocols are called *Smart-Aloha* [15, 16] and *Smart-802.11b* and, as the name implies, these two protocols are modifications to the well-known Aloha and 802.11b protocols. In both cases, functionality at the MAC layer is added to allow it to directly control the antenna: *the MAC layer controls the direction of the beam and the direction of the nulls*. In addition, the antenna provides the MAC layer with DOA information for all transmissions it can hear along with signal strength information. The main results are that these protocols show a very high throughput while maintaining fairness. Table 5.1 summarizes the main throughput results of the MAC protocols designed for directional antenna equipped nodes [15–26].

5.2.1 Description of the protocols

Consider the case when a node a needs to transmit a packet to node b which is its one-hop neighbor. It is assumed that a knows the angular direction of b and it can therefore form a beam in the direction of b. However, to maximize SINR, b should also form a beam towards a and form nulls in the direction of all other transmitters. In order to do this, b needs to know two things – first, that a is attempting to transmit to it, and second, the angular direction of all the other transmitters that interfere at b. The two protocols discussed in this section answer these two questions somewhat differently.

Table 5.1 Performance of MAC protocols using adaptive antennas. (Reproduced by permission of IEEE [27].)

Prior work	Characteristics of simulation experiments	Maximum throughput					
[17]	Switched beam antenna 45° beamwidth, 10 dB gain, 250 m range for omni, 900 m directional 4CBR sources, 75 kbps to 2 Mbps each	Random topology ($N = 25.4$ hops)			Mesh topology		
		MMAC	DMAC	802.11	MMAC	DMAC	802.11
		1000 kbps (5×)	400 (2×)	200 (1×)	800 (4×)	300 (1.5×)	200 (1×)
[18]	Multi-beam antenna (1, 2, 4, beams each) 30° beamwidth, 2 Mbps channel slotted (8 ms slot), 16 kbit packet (throughput converted to bps from pkts/slot/net)	Fully connected (20 nodes)			Multi-hop (100 nodes, 5 hops)		
		1 beam	2	4	1	2	4
		12 Mbps	30	60	60	150	300
		(Max over ROMA, UxDMA)					
[19]	Adaptive antenna: 4 × 4, 8 × 8 planar arrays, TDMA-802.11, 1-hop	4 × 4			8×8		
		(55 nodes)					
		8 pkts/packet time			9 pkts/packet time		
[20]	Switched beam, 60° beamwidth	Proposed		DRTS/DCTS		CSMA/CA	
		(50 nodes)					
		3.5 Mbps		2.5		2	

(*continued overleaf*)

Table 5.1 *(continued)*

Prior work	Characteristics of simulation experiments	Maximum Throughput					
[21]	Circular adaptive antenna array, beamwidth 64°, 8 dB gain (improvement over 802.11)	25 nodes (grid)			225 nodes (grid)		
		No PC	Global PC	Local PC	No PC	Global PC	Local PC
		(PC, power control)					
		1.3×	1.7×	2.1×	2.6×	4.75×	5.25×
[22]	Ideal adaptive antenna 20 nodes, no nulling (improvement over omni case) Packet transmission is directional at sender/receiver	*Protocol*		*Beamwidth* (20 nodes, degree = 7.5)			
		O, omnidirectional					
		D, directional		90°	60°	30°	10°
		ORTS/DCTS		35 %	57 %	100 %	142 %
		DRTS/DCTS		64 %	107 %	143 %	186 %
		DRTS/OCTS		28 %	43 %	n/a	57 %
		ORTS/OCTS		29 %	50 %	86 %	121 %
		STDMA		n/a	400 %	n/a	400 %
[23]		No mobility					
	Six-element circular antenna array (10 fixed patterns, no adaptation) 45° beamwidth, 100 nodes, 1500 m^2 2-ray propagation model, no nulling	Omni		RX directional TX omnidirectional		DVCS	DVCS-Ideal TX, RX directional
		400 kbps		800 kbps		1.4 Mbps	2.2 Mbps

Smart-Aloha is a slightly modified version of the standard *Slotted-Aloha* protocol. To transmit a packet, a transmitter forms a beam towards its receiver and begins transmission. However, it prefaces its packet transmission with the transmission of a short (8 byte) *pure tone* (this is a simple sinusoid). Idle nodes remain in an omnidirectional mode and receive a complex sum of all such tones (note that the tones are identical for all nodes and thus we cannot identify the nodes based on the tone) and run a DOA algorithm to identify the direction and strength of the various signals. An idle node then beamforms in the direction of the maximum received signal strength and forms nulls in other directions, and receives the transmitted packet. If the receiver node was the intended destination for the packet, it immediately sends an ACK using the already formed directed beam. On the other hand, if the packet was intended for some other node, then the receiver discards it.

A sender waits for an ACK immediately after transmission of the packet and if it does not receive the ACK, it enters backoff in the standard way. Thus, the Smart-Aloha protocol follows a *Tone/Packet/Ack* sequence. The intuition behind the receiver beamforming in the direction of the maximum signal is that, because of the directivity of the antenna, there is a high probability that it is the intended recipient for the packet. However, in some cases, as in Figure 5.5, the receiver d incorrectly beamforms towards a because a's signal is stronger than b's. While this is not a serious problem in most cases, we can envision scenarios where the $b \rightarrow d$ transmission gets starved due to a large volume of $a \rightarrow c$ traffic. A possible optimization is a *single-entry cache* scheme which works as follows:

- If a node beamforms incorrectly in a given timeslot, it remembers that *direction* in a single-entry cache.
- In the next slot, if the maximum signal strength is again in the direction recorded in the single-entry cache, then the node ignores that direction and beamforms towards the second strongest signal. If the node receives a packet correctly (i.e. it was the intended recipient), it does not change the cache. If it receives a packet incorrectly, it updates the cache with this new direction.
- If there is no packet in a slot from the direction recorded in the cache, the cache is reset.

The *Smart-802.11b* protocol is based on the 802.11b standard. As in the case of the Smart-Aloha protocol, transmitters beamform towards their receivers and transmit a short *sender-tone* to initiate communication. However, unlike Smart-Aloha, the transmitter does not immediately follow the tone with a packet. Instead, it waits for a *receiver-tone* and only then transmits its packet. After transmission of a packet, it waits for the receipt of an ACK. If there is no ACK, it enters backoff as in 802.11b. Figure 5.6 presents a state diagram of tone-based protocol. The behavior of the protocol in various states can be summarized as follows.

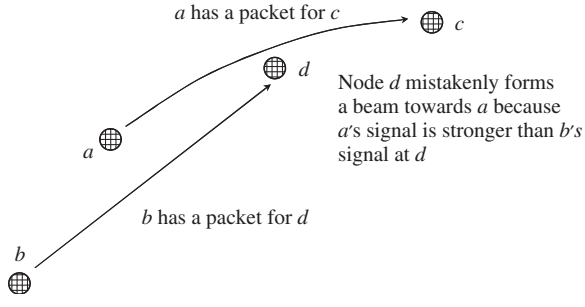

Figure 5.5 False beamforming. (Reproduced by permission of IEEE [27].)

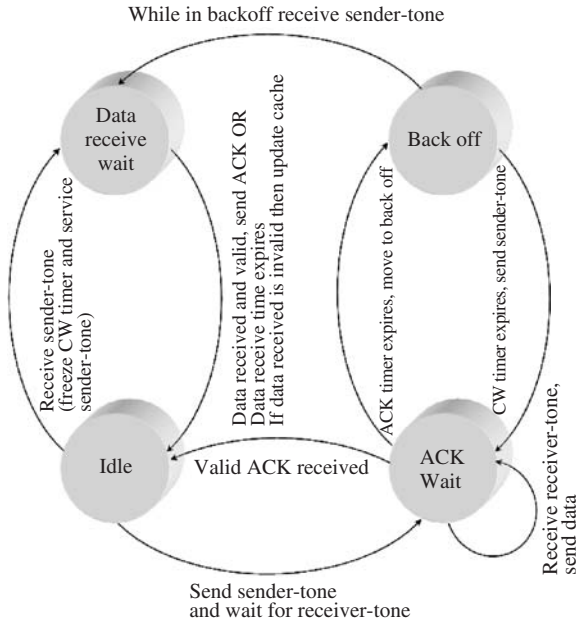

Figure 5.6 State diagram of the Smart-802.11b protocol.

5.2.1.1 Idle

In case a node has no packet to send, it will remain in the idle state and set its antenna to operate in the omnidirectional mode. If it receives a sender-tone from some other node, it will move into the data receive wait state. On the other hand, if it wishes to send data, it will beamform in the direction of the receiver. It chooses a random number [0–CW] and sets the CW (contention window) timer 1. When the CW timer expires, it sends a sender-tone in the direction of the receiver and moves to the ACK wait state. If, before the CW timer expires, the node receives a sender-tone from another node, it will freeze its CW timer and move to data receive wait state.

5.2.1.2 Data receive wait

A node will move to this state in the event it receives a sender-tone. The node will beamform towards the sender and then randomly defer transmitting the receiver-tone by choosing a random waiting period of $[0–32] \times 20\,\mu s$. The reason for deferring the reply is to minimize the chance of several receiver-tones colliding at sender 2. After transmitting a receiver-tone, the node remains in this state for 2τ (twice the maximum propagation delay + tone transmission time). If it does not hear a transmission, it returns to the idle state. If it hears the start of a transmission, it remains in this state and receives the packet. It then discards the packet if the packet was meant for some other node If, however, the packet was meant for it, then it sends an ACK.

5.2.1.3 Ack wait

If the sender node receives a receiver-tone before the tone RTT timer goes off (which is twice the tone transmission time plus propagation delay), it will transmit the data packet. Reception of a valid ACK will move the node to the idle state, and if packets are there in the queue then it

will schedule the one at the head of the queue. The node will move to the backoff state under two conditions: (1) a receiver-tone did not arrive; (2) an ACK was not received following transmission of the data packet.

5.2.1.4 Backoff

The node computes a random backoff interval (as in 802.11) and remains in backoff for this time period (it also resets its antenna to omnidirectional mode). If, however, a sender-tone is received, it freezes the backoff timer and enters the data receive wait state. If the node is in backoff, upon expiration of the timer, it retransmits the sender-tone, increments the retransmit counter and enters the ACK wait state. A packet is discarded after the retransmit counter exceeds Max Retransmit = 7, as in the IEEE 802.11 standard.

The reception of a data packet by a node may be interfered with by transmissions of sender-tones, receiver-tones or other data packets (since the protocol does not take care of hidden terminals). A node engaged in receiving a data packet can dynamically form nulls towards new interferers, but this process takes some time (*we model this time as the length of a sender-tone*). Thus, the data packet will have errors due to this interference. This error is mitigated by relying on FEC codes as used in IEEE 802.11e, where (224, 208) shortened RS codes are used. In 802.11e, an MAC packet is split into blocks of 208 octets and each block is separately coded using an RS encoder. A (48, 32) RS code, which is also a shortened RS code, is used for the MAC header, and CRC-32 is used for the FCS.

Performance example – the simulation parameters are:

Background noise + ambient noise = 143 dB
Propagation model free space
Bandwidth 1000 kHz
Min frequency 2402 MHz
Data rate 2000 kbps
Carrier sensing threshold + 3 dB
Minimum SINR 9 dB
Bit error based on BPSK modulation curve
Maximum radio range 250 m
Packet size 16 kb
Simulation time 200 s
Single hop: number of nodes 20, area 100 × 100 m
Multihop: number of nodes 100, area 1500 × 1500

The existing 802.11b implementation in OPNET is modified to create Smart-802.11b. The modifications included adding the two tones (sender and receiver) as well as changing the FEC to the 802.11e specification.

The performance of the protocol is presented for a single-hop case with 20 nodes and a five-hop case with 100 nodes using of 16 KB packets. The 16 antenna elements (for an effective beamwidth of 400) were used. Figure 5.7 presents the aggregate one-hop throughput as a function of arrival rate for the one-hop case. One can see that 802.11b achieves a maximum throughput of 1 Mbps while Smart-802.11b achieves a high of 8.5 Mbps and Smart-Aloha achieves a high of approximately 10.5 Mbps. In fact, the throughput of Smart-802.11b and Smart-Aloha increases with arrival rate because of good spatial reuse of the channel. Figure 5.8 plots the aggregate throughput of the protocol for the 100-node five-hop case; 802.11b reaches a maximum throughput of well below 0.5 Mbs while Smart- 802.11b reaches a maximum of 50 Mbs and Smart-Aloha reaches a maximum throughput of 60 Mbs. Again, the better spatial reuse of the channel given the directivity of the antenna is the reason for this performance improvement.

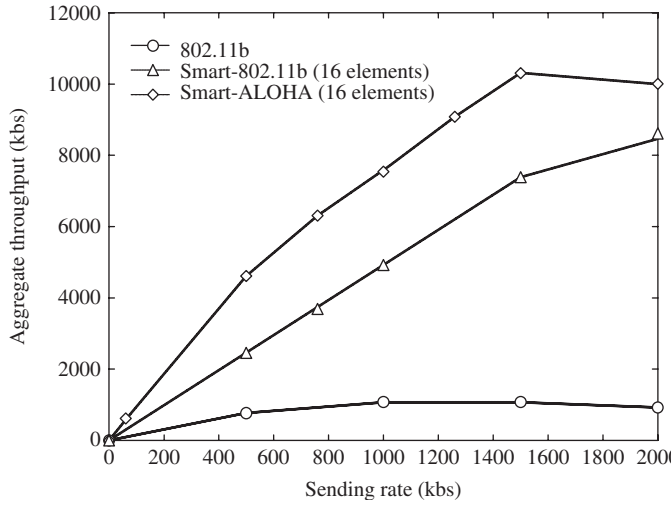

Figure 5.7 Single-hop case with 20 nodes. (Reproduced by permission of IEEE [27].)

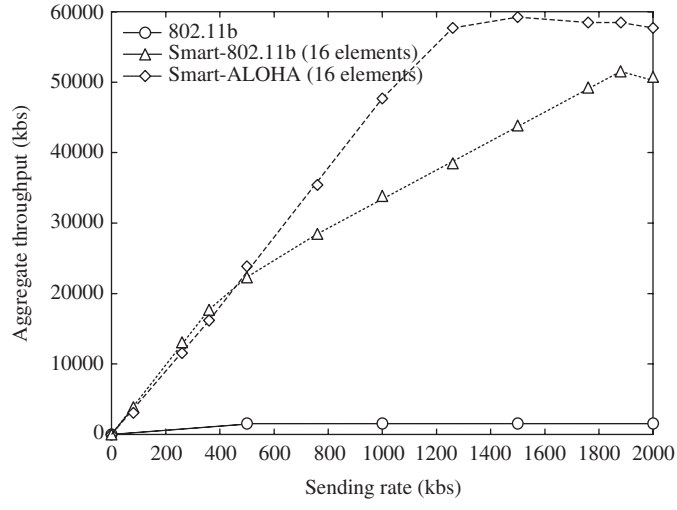

Figure 5.8 Five-hop case with 100 nodes. (Reproduced by permission of IEEE [27].)

5.3 MAC FOR WIRELESS SENSOR NETWORKS

This section discusses an MAC protocol designed for wireless sensor networks (S-MAC). As will be discussed in Chapter 14, wireless sensor networks use battery-operated computing and sensing devices. A network of these devices will collaborate for a common application such as environmental monitoring. Sensor networks are expected to be deployed in an *ad hoc* fashion, with nodes remaining largely inactive for long time, but becoming suddenly active when something is detected. These characteristics of sensor networks and applications motivate an MAC that is different from traditional wireless MACs such as IEEE 802.11, described in previous sections, in several

ways. Energy conservation and self-configuration are primary goals, while per-node fairness and latency are less important. S-MAC uses a few novel techniques to reduce energy consumption and support self-configuration. It enables low-duty-cycle operation in a multihop network. Nodes form *virtual clusters* based on common sleep schedules to reduce control overhead and enable traffic-adaptive wake-up. S-MAC uses in-channel signaling to avoid overhearing unnecessary traffic. Finally, S-MAC applies *message passing* to reduce contention latency for applications that require in-network data processing.

Woo and Culler [28] examined different configurations of carrier sense multiple access (CSMA) and proposed an adaptive rate control mechanism, whose main goal is to achieve fair bandwidth allocation to all nodes in a multihop network. There is also some work on the low-duty-cycle operation of nodes, which are closely related to S-MAC. The first example is Piconet [29], which is an architecture designed for low-power *ad hoc* wireless networks. Piconet also puts nodes into periodic sleep for energy conservation. However, there is no coordination and synchronization among nodes about their sleep and listen time. The scheme to enable the communications among neighboring nodes is to let a node broadcast its address when it wakes up from sleeping. If a sender wants to talk to a neighbor, it must keep listening until it receives the neighbor's broadcast. In contrast, S-MAC tries to coordinate and synchronize neighbors' sleep schedules to reduce latency and control overhead.

Perhaps the power-save (PS) mode in IEEE 802.11 DCF is the most related work to the low-duty-cycle operation in S-MAC. Nodes in PS mode periodically listen and sleep, just like that in S-MAC. The sleep schedules of all nodes in the network are synchronized together. The main difference from S-MAC is that the PS mode in 802.11 is designed for a single-hop network, where all nodes can hear each other, simplifying the synchronization.

As observed by Woo and Culler [28], in multihop operation, the 802.11 PS mode may have problems in clock synchronization, neighbor discovery and network partitioning. In fact, the 802.11 MAC in general is designed for a single-hop network, and there are questions about its performance in multihop networks [30]. In comparison, S-MAC is designed for multihop networks, and does not assume that all nodes are synchronized together. Finally, although 802.11 defines PS mode, it provides very limited policy about *when* to sleep, whereas in S-MAC, a complete system is defined. Tseng *et al.* [31] proposed three sleep schemes to improve the PS mode in the IEEE 802.11 for its operation in multihop networks. Among them the one named periodically fully awake interval is the closest to the scheme of periodic listen and sleep in S-MAC. However, their scheme does not synchronize the sleep schedules of any neighboring nodes. The control overhead and latency can be large. For example, to send a broadcast packet, the sender has to explicitly wake up each individual neighbor before it sends out the actual packet. Without synchronization, each node has to send beacons more frequently to prevent long-term clock drift.

5.3.1 S-MAC protocol design

S-MAC includes approaches to reducing energy consumption from all the sources of energy waste such as: (a) idle listening; (b) collision; and (c) overhearing and control overhead. Before describing the components in S-MAC, we first summarize assumptions about the wireless sensor network and its applications.

Sensor networks will consist of large numbers of nodes to take advantage of short-range, multihop communications to conserve energy (see Chapter 14). Most communications will occur between nodes as peers, rather than to a single base station. In-network processing is critical to network lifetime, and implies that data will be processed as whole messages in a store-and-forward fashion. Packet or fragment-level interleaving from multiple sources only increases overall latency. Finally, we expect that applications will have long idle periods and can tolerate latency on the order of network messaging time.

5.3.2 Periodic listen and sleep

As stated above, in many sensor network applications, nodes are idle for a long time if no sensing event happens. Given the fact that the data rate is very low during this period, it is not necessary to keep nodes listening all the time. S-MAC reduces the listen time by putting nodes into periodic sleep state. Each node sleeps for some time, and then wakes up and listens to see if any other node wants to talk to it. During sleeping, the node turns off its radio, and sets a timer (alarm clock) to wake itself later.

A complete cycle of listen and sleep is called a *frame*. The listen interval is normally fixed according to physical-layer and MAC-layer parameters, such as the radio bandwidth and the contention window size. The *duty cycle* is defined as the ratio of the listen interval to the frame length. The sleep interval can be changed according to different application requirements, which actually changes the duty cycle. For simplicity, these values are the same for all nodes. All nodes are free to choose their own listen/sleep schedules. However, to reduce control overhead, we prefer neighboring nodes to synchronize together. That is, they listen at the same time and go to sleep at the same time. It should be noticed that not all neighboring nodes can synchronize together in a multihop network. Two neighboring nodes A and B may have different schedules if they must synchronize with different nodes, C, and D, respectively, as shown in Figure 5.9.

Nodes exchange their schedules by periodically broadcasting a SYNC packet to their immediate neighbors. A node talks to its neighbors at their scheduled listen time, thus ensuring that all neighboring nodes can communicate even if they have different schedules. In Figure 5.9, for example, if node A wants to talk to node B, it waits until B is listening. The period for a node to send a SYNC packet is called the *synchronization period*. One characteristic of S-MAC is that it forms nodes into a flat, peer-to-peer topology. Unlike clustering protocols, S-MAC does not require coordination through cluster heads. Instead, nodes form virtual clusters around common schedules, but communicate directly with peers. One advantage of this loose coordination is that it can be more robust to topology change than cluster-based approaches. The downside of the scheme is the increased latency due to the periodic sleeping. Furthermore, the delay can accumulate on each hop. Later on, a technique that is able to significantly reduce such latency will be presented.

5.3.3 Collision avoidance

If multiple neighbors want to talk to a node at the same time, they will try to send when the node starts listening. In this case, they need to contend for the medium. Among contention protocols, the 802.11 does a very good job on collision avoidance. S-MAC follows similar procedures, including virtual and physical carrier sense, and the RTS/CTS (request to send/clear to send) exchange for the hidden terminal problem [32]. There is a duration field in each transmitted packet that indicates how long the remaining transmission will be. If a node receives a packet destined to another node, it knows how long to keep silent from this field. The node records this value in a variable called the network allocation vector (NAV) [33] and sets a timer for it. Every time the timer fires, the node decrements its NAV until it reaches zero. Before initiating a transmission, a node first looks at its NAV. If its value is not zero, the node determines that the medium is busy. This is called ‘virtual carrier sense’. Physical carrier sense is performed at the physical layer by listening to the channel for possible transmissions. Carrier senses time is randomized within a contention window

Figure 5.9 Neighboring nodes A and B have different schedules. They synchronize with nodes C and D respectively.

to avoid collisions and starvations. The medium is determined as free if both virtual and physical carrier senses indicates that it is free.

All senders perform carrier sense before initiating a transmission. If a node fails to get the medium, it goes to sleep and wakes up when the receiver is free and listening again. Broadcast packets are sent without using RTS/CTS. Unicast packets follow the sequence of RTS/CTS/DATA/ACK between the sender and the receiver. After the successful exchange of RTS and CTS, the two nodes will use their normal sleep time for data packet transmission. They do not follow their sleep schedules until they finish the transmission. With the low-duty-cycle operation and the contention mechanism during each listen interval, S-MAC effectively addresses the energy waste due to idle listening and collisions. In the next section, details of the periodic sleep coordinated among neighboring nodes will be presented. Two techniques will be presented that further reduce the energy waste due to overhearing and control overhead.

5.3.4 Coordinated sleeping

Periodic sleeping effectively reduces energy waste on idle listening. In S-MAC, nodes coordinate their sleep schedules rather than randomly sleep on their own. This section details the procedures that all nodes follow to set-up and maintain their schedules. It also presents a technique to reduce latency due to the periodic sleep on each node.

5.3.5 Choosing and maintaining schedules

Before each node starts its periodic listen and sleep, it needs to choose a schedule and exchange it with its neighbors. Each node maintains a *schedule table* that stores the schedules of all its known neighbors. It follows the steps below to choose its schedule and establish its schedule table.

(1) A node first listens for a fixed amount of time, which is at least the synchronization period. If it does not hear a schedule from another node, it immediately chooses its own schedule and starts to follow it. Meanwhile, the node tries to announce the schedule by broadcasting a SYNC packet. Broadcasting a SYNC packet follows the normal contention procedure. The randomized carrier sense time reduces the chance of collisions on SYNC packets.

(2) If the node receives a schedule from a neighbor before choosing or announcing its own schedule, it follows that schedule by setting its schedule to be the same. Then the node will try to announce its schedule at its next scheduled listen time.

(3) There are two cases where a node receives a different schedule after it chooses and announces its own schedule. If the node has no other neighbors, it will discard its current schedule and follow the new one. If the node already follows a schedule with one or more neighbors, it adopts both schedules by waking up at the listen intervals of the two schedules.

To illustrate this algorithm, consider a network where all nodes can hear each other. The node that starts first will pick up a schedule first, and its broadcast will synchronize all its peers on its schedule. If two or more nodes start first at the same time, they will finish initial listening at the same time, and will choose the same schedule independently. No matter which node sends out its SYNC packet first (wins the contention), it will synchronize the rest of the nodes.

However, two nodes may independently assign schedules if they cannot hear each other in a multihop network. In this case, those nodes on the border of two schedules will adopt both. For example, nodes A and B in Figure 5.9 will wake up at the listen time of both schedules. In this way, when a border node sends a broadcast packet, it only needs to send it once. The disadvantage is that these border nodes have less time to sleep and consume more energy than others.

Another option is to let a border node adopt only one schedule – the one it receives first. Since it knows that some other neighbors follow another schedule, it can still talk to them. However, for broadcasting, it needs to send twice to the two different schedules. The advantage is that the border nodes have the same simple pattern of periodic listen and sleep as other nodes.

It is expected that nodes only rarely see multiple schedules, since each node tries to follow an existing schedule before choosing an independent one. However, a new node may still fail to discover an existing neighbor for several reasons. The SYNC packet from the neighbor could be corrupted by collisions or interference. The neighbor may have delayed sending a SYNC packet due to the busy medium. If the new node is on the border of two schedules, it may only discover the first one if the two schedules do not overlap.

To prevent the case that two neighbors miss each other forever when they follow completely different schedules, S-MAC introduces periodic neighbor discovery, i.e. each node periodically listens for the whole synchronization period. The frequency with which a node performs neighbor discovery depends on the number of neighbors it has. If a node does not have any neighbors, it performs neighbor discovery more aggressively than in the case where it has many neighbors. Since the energy cost is high during the neighbor discovery, it should not be performed too often. In a typical implementation, the synchronization period is 10 s, and a node performs neighbor discovery every 2 min if it has at least one neighbor.

5.3.6 Maintaining synchronization

Since neighboring nodes coordinate their sleep schedules, the clock drift on each node can cause synchronization errors. Two techniques can be used to make it robust to such errors: (1) all exchanged timestamps are relative rather than absolute; and (2) the listen period is significantly longer than clock drift rates. For example, the listen time of 0.5 s is more than 10 times longer than typical clock drift rates. Compared with TDMA schemes with very short time slots, S-MAC requires much looser time synchronization. Although the long listen time can tolerate fairly large clock drift, neighboring nodes still need to periodically update each other with their schedules to prevent long-term clock drift. The synchronization period can be quite long. The measurements show that the clock drift between two nodes does not exceed 0.2 ms/s.

As mentioned earlier, schedule updating is accomplished by sending a SYNC packet. The SYNC packet is very short, and includes the address of the sender and the time of its next sleep. The next sleep time is relative to the moment that the sender starts transmitting the SYNC packet. When a receiver gets the time from the SYNC packet, it subtracts the packet transmission time and uses the new value to adjust its timer. In order for a node to receive both SYNC packets and data packets, its listen interval is divided into two parts. The first one is for SYNC packets, and the second one is for data packets, as shown in Figure 5.10. Each part has a contention window with many time slots for senders to perform carrier sense. For example, if a sender wants to send a SYNC packet, it starts carrier sense when the receiver begins listening. It randomly selects a time slot to finish its carrier sense. If it has not detected any transmission by the end of that time slot, it wins the contention and starts sending its SYNC packet. The same procedure is followed when sending data packets.

Figure 5.10 shows the timing relationship of three possible situations that a sender transmits to a receiver. Sender 1 only sends a SYNC packet. Sender 2 only sends a unicast data packet. Sender 3 sends both a SYNC and a data packet.

5.3.7 Adaptive listening

The scheme of periodic listen and sleep is able to significantly reduce the time spent on idle listening when traffic load is light. However, when a sensing event indeed happens, it is desirable

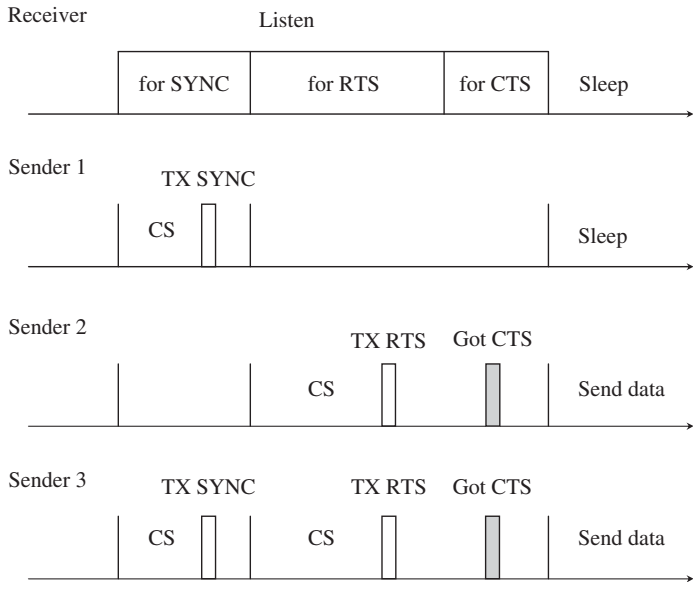

Figure 5.10 Timing relationship between a receiver and different senders. CS stands for carrier sense.

that the sensing data can be passed through the network without too much delay. When each node strictly follows its sleep schedule, there is a potential delay on each hop, whose average value is proportional to the length of the frame. For this reason, a mechanism is introduced to switch the nodes from the low-duty-cycle mode to a more active mode in this case.

S-MAC uses an important technique, called *adaptive listen*, to improve the latency caused by the periodic sleep of each node in a multihop network. The basic idea is to let the node that overhears its neighbor's transmissions [ideally only request to send (RTS) or clear to send (CTS)] wake up for a short period of time at the end of the transmission. In this way, if the node is the next-hop node, its neighbor is able to immediately pass the data to it instead of waiting for its scheduled listen time. If the node does not receive anything during the adaptive listening, it will go back to sleep until its next scheduled listen time.

Let us look at the timing diagram in Figure 5.10 again. If the next-hop node is a neighbor of the sender, it will receive the RTS packet. If it is only a neighbor of the receiver, it will receive the CTS packet from the receiver. Thus, both the neighbors of the sender and receiver will learn about how long the transmission is from the duration field in the RTS and CTS packets. So they are able to adaptively wake up when the transmission is over.

The interval of the adaptive listening does not include the time for the SYNC packet as in the normal listen interval (see Figure 5.10). SYNC packets are only sent at scheduled listen time to ensure all neighbors can receive it. To give the priority to the SYNC packet, adaptive listen and transmission are not performed if the duration from the time the previous transmission is finished to the normally scheduled listen time is shorter than the adaptive listen interval.

One should note that not all next-hop nodes can overhear a packet from the previous transmission, especially when the previous transmission starts adaptively, i.e. not at the scheduled listen time. Therefore, if a sender starts a transmission by sending out an RTS packet during the adaptive listening, it might not get a CTS reply. In this case, it just goes back to sleep and will try again at the next normal listen time.

5.3.8 Overhearing avoidance and message passing

Collision avoidance is a basic task of MAC protocols. S-MAC adopts a contention-based scheme. It is common that any packet transmitted by a node is received by all its neighbors even though only one of them is the intended receiver. Overhearing makes contention-based protocols less efficient in energy than TDMA protocols.

5.3.9 Overhearing avoidance

In 802.11 each node keeps listening to all transmissions from its neighbors in order to perform effective virtual carrier sense. As a result, each node overhears many packets that are not directed to itself. It is a significant waste of energy, especially when node density is high and traffic load is heavy. S-MAC tries to avoid overhearing by letting interfering nodes go to sleep after they hear an RTS or CTS packet. Since DATA packets are normally much longer than control packets, the approach prevents neighboring nodes from overhearing long DATA packets and following ACKs. The question is which nodes should sleep when there is an active transmission in progress.

In Figure 5.11, nodes A, B, C, D, E and F form a multihop network where each node can only hear the transmissions from its immediate neighbors. Suppose node A is currently transmitting a data packet to B. Which of the remaining nodes should go to sleep during this transmission? Remember that collision happens at the receiver.

It is clear that node D should sleep since its transmission interferes with B's reception. Nodes E and F do not produce interference, so they do not need to sleep. Should node C go to sleep? C is two hops away from B, and its transmission does not interfere with B's reception, so it is free to transmit to its other neighbors, like E. However, C is unable to get any reply from E, e.g. CTS or data, because E's transmission collides with A's transmission at node C. So C's transmission is simply a waste of energy. Moreover, after A sends to B, it may wait for an ACK from B, and C's transmission may corrupt the ACK packet. In summary, *all immediate neighbors of both the sender and receiver should sleep after they hear the RTS or CTS until the current transmission is over, as indicated in Figure 5.11.* Each node maintains the NAV to indicate the activity in its neighborhood. When a node receives a packet destined to other nodes, it updates its NAV using the duration field in the packet.

A nonzero NAV value indicates that there is an active transmission in its neighborhood. The NAV value decrements every time when the NAV timer fires. Thus, a node should sleep to avoid overhearing if its NAV is not zero. It can wake up when its NAV becomes zero. We also note that in some cases overhearing is indeed desirable. Some algorithms may rely on overhearing to gather neighborhood information for network monitoring, reliable routing or distributed queries. If desired, S-MAC can be configured to allow application-specific overhearing to occur. However, it is suggested that algorithms without requiring overhearing may be a better match to energy-limited networks. For example, S-MAC uses explicit data acknowledgments rather than implicit ones [28].

5.3.10 Message passing

A *message* is the collection of meaningful, interrelated units of data. The receiver usually needs to obtain all the data units before it can perform in-network data processing or aggregation. The disadvantages of transmitting a long message as a single packet is the high cost of re-transmitting

Figure 5.11 Which nodes should sleep when node A is transmitting to B?

the long packet if only a few bits have been corrupted in the first transmission. However, if we fragment the long message into many independent small packets, we have to pay the penalty of large control overhead and longer delay. This is so because the RTS and CTS packets are used in contention for each independent packet. A possibility is to fragment the long message into many small fragments, and transmit them in a burst. Only one RTS and one CTS are used. They reserve the medium for transmitting all the fragments. Every time a data fragment is transmitted, the sender waits for an ACK from the receiver. If it fails to receive the ACK, it will extend the reserved transmission time for one more fragment, and re-transmit the current fragment immediately. As before, all packets have the duration field, which is now the time needed for transmitting all the remaining data fragments and ACK packets. If a neighboring node hears an RTS or CTS packet, it will go to sleep for the time that is needed to transmit all the fragments. Each data fragment or ACK also has the duration field. In this way, if a node wakes up or a new node joins in the middle of a transmission, it can properly go to sleep whether it is the neighbor of the sender or the receiver. If the sender extends the transmission time due to fragment losses or errors, the sleeping neighbors will not be aware of the extension immediately. However, they will learn it from the extended fragments or ACKs when they wake up.

The purpose of using ACK after each data fragment is to prevent the hidden terminal problem in the case that a neighboring node wakes up or a new node joins in the middle. If the node is only the neighbor of the receiver but not the sender, it will not hear the data fragments being sent by the sender. If the receiver does not send ACKs frequently, the new node may mistakenly infer from its carrier sense that the medium is clear. If it starts transmitting, the current transmission will be corrupted at the receiver.

It is worth noting that IEEE 802.11 also has fragmentation support. In 802.11 the RTS and CTS only reserve the medium for the first data fragment and the first ACK. The first fragment and ACK then reserve the medium for the second fragment and ACK, and so forth. For each neighboring node, after it receives a fragment or an ACK, it knows that there is one more fragment to be sent. So it has to keep listening until all the fragments are sent. Again, for energy-constrained nodes, overhearing by all neighbors wastes a lot of energy.

The 802.11 protocol is designed to promote fairness. If the sender fails to get an ACK for any fragment, it must give up the transmission and re-contend for the medium so that other nodes have a chance to transmit. This approach can cause a long delay if the receiver really needs the entire message to start processing. In contrast, message passing extends the transmission time and re-transmits the current fragment. It has less contention and a small latency. S-MAC sets a limit on how many extensions can be made for each message where the receiver is really dead or the connection lost during the transmission. However, for sensor networks, application-level performance is the goal as opposed to per-node fairness.

5.3.10.1 Performance examples

In Ye *et al.* [34], The simulation results are obtained for the system with the following set of parameters:

Radio bandwidth	20 kbs
Channel coding	Manchester
Control packet length	10 bytes
Data packet length	up to 250 bytes
MAC header length	8 bytes
Duty cycle	1–99 %
Duration of listen interval	115 ms
Contention window for SYNC	15 slots
Contention window for data	31 slots

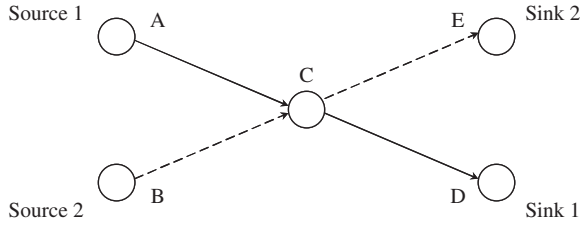

Figure 5.12 Two-hop network with two sources and two sinks.

The modulation scheme is the amplitude shift keying (ASK). The power consumptions of the radio in receiving, transmitting and sleep modes are 14.4 mW, 36 mW and 15 W, respectively. The topology is a two-hop network with two sources and two sinks, as shown in Figure 5.12. Packets from source A flow through node C and end at sink D, while those from B also pass through C but end at E. The traffic load is changed by varying the inter-arrival period of messages. If the message inter-arrival period is 5 s, a message is generated every 5 s by each source node. In this experiment, the message inter-arrival period varies from 1 to 10 s.

For the highest rate with a 1 s inter-arrival time, the wireless channel is nearly fully utilized due to its low bandwidth. For each traffic pattern, 10 independent tests are done when using different MAC protocols. In each test, each source periodically generates 10 messages, which in turn is fragmented into 10 small data packets (40 bytes each). Thus, in each experiment, there are 200 data packets to be passed from their sources to their sinks. The energy consumption of the radio on each node to pass the fixed amount of data is measured. The actual time to finish the transmission is different for each MAC module. In the 802.11-like MAC, the fragments of a message are sent in a burst, i.e. RTS and CTS are only used for the first fragment.

The 802.11-like MAC without fragmentation, which treats each fragment as an independent packet and uses RTS/CTS for each of them, is not measured, since it is obvious that this MAC consumes much more energy than the one with fragmentation. In S-MAC message passing is used, and fragments of a message are always transmitted in a burst. In the S-MAC module with periodic sleep, each node is configured to operate in the 50 % duty cycle.

Figure 5.13 shows the average energy consumption on the source nodes A and B. The traffic is heavy when the message inter-arrival time is less than 4 s. In this case, 802.11 MAC uses more than twice the energy used by S-MAC. Since idle listening rarely happens, energy savings from periodic sleeping is very limited. S-MAC achieves energy savings mainly by avoiding overhearing and efficiently transmitting long messages. When the message inter-arrival period is larger than 4 s, traffic load becomes light. In this case, the complete S-MAC protocol has the best energy performance, and far outperforms 802.11 MAC. Message passing with overhearing avoidance also performs better than 802.11 MAC. However, as shown in the figure, when idle listening dominates the total energy consumption, the periodic sleep plays a key role in energy savings.

Compared with 802.11, message passing with overhearing avoidance saves almost the same amount of energy under all traffic conditions. This result is due to overhearing avoidance among neighboring nodes A, B and C. The number of packets sent by each of them is the same in all traffic conditions.

5.4 MAC FOR *AD HOC* NETWORKS

A key component in the development of single channel *ad hoc* wireless networks is the MAC protocol with which nodes share a common radio channel. Of necessity, such a protocol has to be distributed. It should provide an efficient use of the available bandwidth while satisfying the

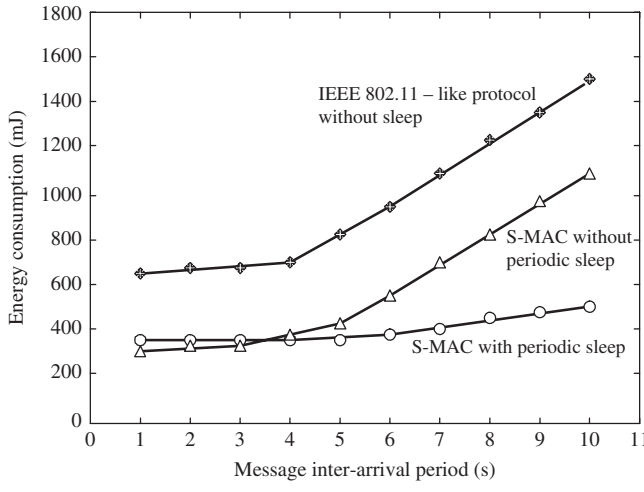

Figure 5.13 Mean energy consumption on radios in each source node. (Reproduced by permission of IEEE [34].)

QoS requirements of both data and real-time applications. CSMA is one of the most pervasive MAC schemes in *ad hoc* wireless networks. CSMA is a simple distributed protocol whereby nodes regulate their packet transmission attempts based only on their local perception of the state, idle or busy, of the common radio channel.

Packet collisions are intrinsic to CSMA. They occur because each node has only a delayed perception of the other nodes' activity. They also happen due to hidden nodes: two transmitting nodes outside the sensing range of each other may interfere at a common receiver. Many types of CSMA exist, but invariably the nodes that participate in a collision schedule the retransmission of their packets to a random time in the future, in the hope of avoiding another collision. This strategy, however, does not provide QoS guarantees for real-time traffic support.

MAC schemes for *ad hoc* wireless networks have been proposed, aimed either at improving the throughput over that of CSMA or at providing QoS guarantees for real-time traffic support. Among the first group of schemes is the multiple access collision avoidance protocol (MACA) [35], which forms the basis of several other schemes. With MACA, a source with a packet ready for transmission first sends a request-to-send (RTS) minipacket, which if successful elicits a clear-to-send (CTS) minipacket from the destination. Upon reception of the CTS minipacket, the source sends its data packet. In environments without hidden nodes, MACA may improve the throughput of the network over that attained with CSMA because collisions involve only short RTS minipackets rather than normal data packets as in CSMA. MACA also alleviates the hidden nodes problem because the CTS sent by the destination serves to inhibit the nodes in its neighborhood, i.e. exactly those nodes that may interfere with the ensuing packet transmission from source to destination. The floor acquisition multiple access (FAMA) class of protocols [36] includes several variants of MACA, one of which is immune to hidden nodes [37]. These protocols, however, have not been designed for QoS: control minipackets are subject to collisions, and their retransmissions are randomly scheduled.

The group allocation multiple access (GAMA) [38, 39] is an attempt to provide QoS guarantees to real-time traffic in a distributed wireless environment. In GAMA, there is a contention period where nodes use an RTS–CTS dialog to explicitly reserve bandwidth in the ensuing contention-free period. A packet transmitted in the contention-free period may maintain the reservation for the next cycle. The scheme is asynchronous and developed for wireless networks where all nodes

can sense, and indeed receive, the communications from their peers. MACA/packet reservation (MACA/PR) [40] is a protocol similar to GAMA, but an acknowledgment follows every packet sent in contention-free periods to inform the nodes in the neighborhood of the receiver whether or not another packet is expected in the next contention-free cycle. These schemes deviate from pure carrier sensing methods in that every node has to construct channel-state information based on reservation requests carried in packets sent onto the channel.

In this section, we elaborate on the black-burst (BB) contention mechanism presented in Sobrinho and Krishnakumar [41]. With this mechanism, real-time nodes contend for access to the common radio channel with pulses of energy, BBs, the lengths of which are proportional to the time that the nodes have been waiting for the channel to become idle. The scheme is distributed and is based only on carrier sensing. It gives priority access to real-time traffic and ensures collision-free transmission of real-time packets. When operated in an *ad hoc* wireless LAN, it further guarantees bounded real-time delays. In addition, the BB contention scheme can be overlaid on current CSMA implementations, notably that of IEEE 802.11 standard for wireless LANs, with only minor modifications required to the real-time transceivers: the random retransmission scheme is turned off, and in substitution, the possibility of sending BBs is provided.

5.4.1 Carrier sense wireless networks

Carrier sense wireless networks are designed in such a way that the distance from which a node can sense the carrier from a given transmitter is different and typically larger than the distance from which receivers are willing to accept a packet from that same transmitter. In addition, the carrier from a transmitter can usually be sensed at a range beyond the range at which the transmitter may cause interference. To account for these differences, a wireless network is modeled as a set of nodes N, interconnected by links of three different types. Node i has a communication link with node j, if and only if in the course of time, it has packets to send to node j. Node i has an interfering link with node j if and only if any packet transmission with destination j that overlaps in time at j with a transmission from i is lost.

The lost packets are said to have collided with the transmission from i. Finally, node i has a sensing link with node j, if and only if a transmission by node i prevents node j from starting a new transmission, i.e. node i inhibits node j. The communication, interference and sensing graphs are denoted by $G_C = (N, L_C)$, $G_I = (N, L_I)$, and $G_S = (N, L_S)$, respectively, where, L_C, L_I and L_S are the edge sets (the links). The communication graph is a directed graph, whereas the interfering and sensing graphs are undirected. We assume that if node i has a communication link with node j, then i and j also have an interfering link between them. Similarly, an interfering link is also a sensing link, but not conversely. That is, $L_I \subset L_S$: G_I is a spanning subgraph of G_S. Any node has an interfering and sensing link with itself, since whenever a node transmits, it cannot simultaneously receive or start another transmission. As an example in the wireless network of Figure 5.14, node 9 has a communication link with node 10, and thus these nodes have both an interfering and a sensing link between them. Nodes 10 and 13 have an interfering link, and thus they also have a sensing link between them. Finally, nodes 9 and 13 have only a sensing link between them. The links from a node to itself are not explicitly represented.

A path delay is associated with each sensing link to account for the propagation delay separating the nodes, the turn-around (round trip) time of the wireless transceivers, and the sensing delay. The path delay of link ij is denoted by τ_{ij}. Since the sensing graph is undirected, $\tau_{ij} = \tau_{ji}$. The path delays further satisfy the two conditions $\tau_{ij} > 0$ and $\tau_{ik} + \tau_{kj} > \tau_{ij}$, for $ik, kj, ij \in L_S$.

Let $\tau = \max(\tau_{ij})$. The sets $N_I(i)$ and $N_S(i)$ represent the nodes that are neighbors of i, i included, in the interfering and sensing graphs, respectively. In Figure 5.14, $N_I(10) = \{9, 10, 11, 12, 13\}$ and $N_S(9) = \{7, 8, 9, 10, 11, 12, 13\}$. For communication link ij, the set of nodes which are interfering neighbors of j but are not sensing neighbors of i, i.e. the set, $N_I(j) \cap [N - N_S(i)]$, is the set of nodes hidden from ij. A node in this set will not sense an ongoing packet transmission from i

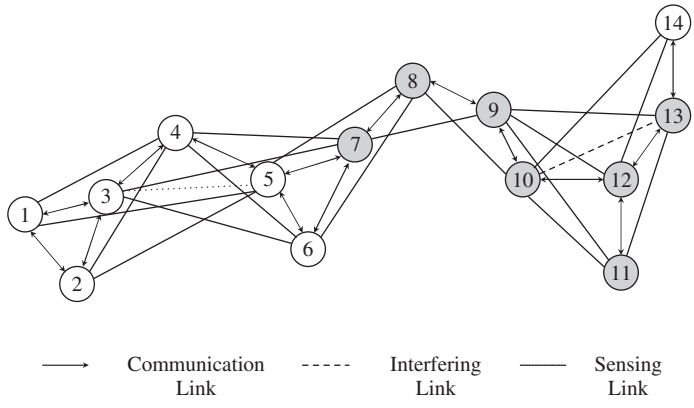

Figure 5.14 A wireless network without hidden nodes. The shaded nodes form the set N_S (9).

to j and may initiate its own packet transmission that will collide at j. In a wireless network without hidden nodes, we have $N_{\mathrm{I}}(j) \subset N_{\mathrm{S}}(i)$ for every $ij \in L_{\mathrm{C}}$. The network of Figure 5.14 does not have hidden nodes. Nevertheless, the common radio channel can be reused in space. For example, a packet transmission from node 9 to node 8 can coexist in time without collisions with a packet transmission from node 5 to node 7. We use the term 'wireless LAN' for wireless networks in which $G_{\mathrm{I}} = G_{\mathrm{S}}$ forms a complete graph. In a wireless LAN, all nodes can sense each other's transmissions. The CSMA/CA protocol of the IEEE 802.11 standard defines three interframe spacings, $t_{\mathrm{short}}, t_{\mathrm{med}}, t_{\mathrm{med}} \geq 2\tau + t_{\mathrm{short}}$ and $t_{\mathrm{long}}, t_{\mathrm{long}} \geq 2\tau + t_{\mathrm{med}}$. If a node with a packet that is ready for transmission has perceived that the channel is idle during a long interframe spacing of length t_{long}, the node immediately starts the transmission of the packet. Otherwise, it waits until that condition is satisfied and enters into backoff.

Likewise, a node whose packet has experienced c consecutive collisions enters into backoff. In this mode, the node chooses a random number of slots s uniformly distributed between zero and min $\{32 \times 2^c - 1{,}255\}$ and sets a timer with an initial value $s \times t_{\mathrm{slot}}$ units of time, where t_{slot}, $t_{\mathrm{slot}} \geq 2\tau$, is the length of a slot. The timer counts down only while the channel has been perceived idle for more than t_{long} units of time – it is frozen during a medium busy condition – and the packet is (re)transmitted as soon as the timer reaches zero. A node learns of the success or failure of its transmission through a positive acknowledgment scheme; the recipient of a correctly received packet sends back an acknowledgment minipacket within an interval of time of length t_{short}.

BB contention is a MAC mechanism developed to provide QoS guarantees to real-time traffic over carrier sense wireless networks. The real-time applications considered are those like voice and video that require more or less periodic access to the common radio channel during long periods of time denominated sessions. The main performance requirement for these applications is bounded end-to-end delay, which implies a bounded packet delay at the MAC layer. This is the goal of BB contention. Real-time nodes contend for access to the channel after a medium interframe spacing of length t_{med}, rather than after the long interframe spacing of length t_{long} used by data nodes. Thus, real-time nodes as a group have priority over data nodes.

Instead of sending their packets when the channel becomes idle for t_{med}, real-time nodes first sort their access rights by jamming the channel with pulses of energy, denominated BBs. The length of a BB transmitted by a real-time node is an increasing function of the contention delay experienced by the node, measured from the instant when an attempt to access the channel has been scheduled until the channel becomes idle for t_{med}, i.e. until the node starts the transmission of its BB. To account for the path delays in the network, BBs are formed by an integral number of black slots,

each of length t_{bslot}, with t_{bslot} not smaller than the maximum round-trip path delay 2τ. Now, we would like the BBs sent by distinct real-time nodes when the channel becomes idle for t_{med} to differ by at least one black slot. To this end, we assume that every real-time packet transmission lasts at least a certain time t_{pkt} and that real-time nodes only schedule their next transmission attempts – to a time t_{sch} in the future – when they start a packet transmission. If a node starts a packet transmission at time u and that transmission is successful, that means that no other real-time node started a packet transmission during an interval of length $2t_{\text{pkt}}$ around time u. Therefore, the next scheduled attempt made by the node in question is also staggered in time by t_{pkt} from the scheduled access attempts made by the other nodes. Counting the number of black slots to be sent in a BB in units of t_{pkt}, we obtain the desired property that distinct nodes contend with BBs comprising different numbers of black slots. Following each BB transmission, a node senses the channel for an observation interval of length t_{obs} to determine without ambiguity whether its BB was the longest of the contending BBs. The winning node will transmit its real-time packet successfully and schedule the next transmission attempt. On the other hand, the nodes that lost the BB contention wait for the channel to once again become idle for t_{med}, at which time they send new longer BBs. In conclusion, once the first real-time packet of a session is successfully transmitted, the mechanism ensures that succeeding real-time packets are also transmitted without collisions. In the end, real-time nodes appear to access a dynamic time division multiplexing (TDM) transmission structure without explicit slot assignments or slot synchronization. In the sequel a detailed description of the access rules followed by every real-time node is presented. Every real-time packet lasts for at least a certain amount of time $t_{\text{pkt}} \geq 2\tau$, when transmitted on the channel. At the beginning of a session, a real-time node uses conventional CSMA/CA rules, possibly with a more expedited retransmission algorithm, to convey its first packet until it is successful. Subsequent packets are transmitted according to the mechanisms, described below, until the session is dropped.

Whenever a real-time node transmits a packet, it further schedules its next transmission attempt to a time t_{sch} in the future, where t_{sch} is the same for all nodes. Suppose, then, that a real-time node has scheduled an access attempt for the present time. If the channel has been idle during the past medium interframe interval of length t_{med}, the node starts the transmission of a BB. Otherwise, it waits until the channel becomes idle for t_{med} and only then starts the transmission of its BB. The length b of the BB sent by the node is a direct function of the contention delay it incurred, d_{cont}:

$$b(d_{\text{cont}}) = \left(1 + \left\lfloor \frac{d_{\text{cont}}}{t_{\text{unit}}} \right\rfloor\right) t_{\text{bslot}}$$

where t_{bslot} is the length of a black slot, the parameter t_{unit} is the unit of time used to convert contention delays into an integral number of black slots, and $\lfloor x \rfloor$ is the floor of x, i.e. the largest integer not larger than x. Correct operation of the scheme requires that $t_{\text{unit}} \leq t_{\text{pkt}}$. After exhausting its BB transmission, the node waits for an observation interval t_{obs}, the length of which has to satisfy $t_{\text{obs}} \leq t_{\text{bslot}}$ and $t_{\text{obs}} \leq t_{\text{med}}$, to see if any other node transmitted a longer BB, implying that it would have been waiting longer for access to the channel. If the channel is perceived idle after t_{obs}, then the node (successfully) transmits its packet. On the other hand, if the channel is busy during the observation interval, the node waits again for the channel to be idle for t_{med} and repeats the algorithm.

The start of packet transmissions from different nodes is shifted in time by at least t_{pkt}. Since it is only when a node initiates the transmission of a packet that it schedules its next transmission attempt to a time t_{sch} in the future, the contention delays of different nodes will likewise differ by at least t_{pkt}. Therefore, taking $t_{\text{unit}} \leq t_{\text{pkt}}$, the BBs of different nodes differ by at least one black slot, and thus every BB contention period produces a unique winner. That winner is the node that has been waiting the longest for access to the channel. The observation interval t_{obs} cannot last longer than the black slot time, i.e. $t_{\text{obs}} \leq t_{\text{bslot}}$, so that a node always recognizes when its BB is shorter than that of another contending node. It also has to be shorter than the medium interframe spacing, i.e. $t_{\text{obs}} \leq t_{\text{med}}$, to prevent real-time nodes from sending BBs by the time that a real-time packet

transmission is expected. Overall, the BB contention scheme gives priority to real-time traffic, enforces a round-robin discipline among real-time nodes, and results in bounded access delays to real-time packets.

BB contention can also be used to support real-time sessions with different bandwidth requirements, which might be useful for multimedia traffic. On the one hand, distinct real-time sessions may have the corresponding nodes send packets of different sizes when they acquire access rights to the channel. On the other hand, the BB mechanism can be enhanced to accommodate real-time sessions with different scheduling intervals as long as the set of values allowed for the scheduling interval t_{sch} is finite and small. In the latter case, BB contention proceeds in two phases. Real-time nodes first sort their access rights based on contention delays as before. However, it is now possible for two nodes with different scheduling intervals to compute BBs with the same number of black slots. Hence, after this first phase, a real-time node contends again with a new BB, the length of which univocally identifies the scheduling interval being used by the node.

5.4.2 Interaction with upper layers

5.4.2.1 Operation with feedback

If a real-time node were alone in the network, two consecutive real-time packet transmissions belonging to the same session would be separated in time by exactly t_{acc}, $t_{\text{acc}} = t_{\text{sch}} + t_{\text{bslot}} + t_{\text{obs}}$. The access delays measure the deviation from this ideal situation. Specifically, an access delay is the time that elapses from the moment an access attempt occurs until the node is able to transmit the corresponding real-time packet, corrected for $t_{\text{bslot}} + t_{\text{obs}}$. For $n \geq 2$, the nth access delay associated with a session is denoted by $d^{(n)}$ and is given by $d^{(n)} = (u^{(n)} - u^{(n-1)} - t_{\text{acc}})$, where $u^{(n)}$ is the instant of time when the node started the transmission of its nth packet. Given the maximum length of data packets, the rate of real-time sessions and number of real-time nodes, the BB mechanism guarantees that the access delays are bounded and usually by a very small value $d_{\max}$.

When a node is the source node of a session, the contents of its real-time packets can reflect the access delays incurred in contending for access to the channel. Typically, a real-time application generates blocks of information bits at regular intervals of time, of length much smaller than t_{acc}. The block delay is the time interval that elapses from the moment an information block is made available by the application until it is successfully transmitted at the MAC layer (corrected for $t_{\text{bslot}} + t_{\text{obs}}$ and neglecting processing delays). The relation between access and block delays depends on how the application blocks of information are packetized for transmission at the MAC layer. One possibility is to have the MAC layer convey in a packet all the information blocks generated up to the instant when the node is about to start a packet transmission. The length of a real-time packet would thus grow with the access delay incurred by the node. The block delay of the oldest block conveyed in the packet would consist of t_{acc}, plus the corresponding access delay: the block delay would never exceed $t_{\text{acc}} + d_{\max}$. In general, however, it is not feasible to assemble a packet at the time that its transmission should start, and further, the MAC layer usually contains a single buffer that we must ensure is filled with a packet by the time access to the channel is granted.

For a realistic alternative within the spirit of this section, consider a simplified communication architecture in which a real-time application puts its generated blocks of information into an application buffer. Whenever the node successfully transmits a packet it signals the application, which will assemble the next packet with all the blocks of information currently queued at the application buffer, plus the blocks that will be generated during the next interaccess interval of length t_{acc}. At this later time, the packet is delivered to the MAC layer for transmission. With this procedure, the MAC layer always has a packet ready for transmission by the time it acquires undisputed access to the channel. When a node transmits its nth packet at time $u^{(n)}$, it leaves in the application buffer the blocks of information generated during the previous $d^{(n)}$ units of time;

they will be part of the contents of the $(n + 1)$th packet. The latter packet further incurs an access delay of $d^{(n+1)}$ at the MAC layer. Therefore, the block delay of the oldest block conveyed in the $(n + 1)$th packet is not greater than $(d_n + t_{acc} + d_{n+1})$: the block delay during a session never exceeds $(t_{acc} + 2d_{max})$.

5.4.2.2 Operation without feedback

In the previous section, the contents of a real-time packet depended on the access delays incurred by a node. There is a direct coupling between the MAC layer and the real-time application. A simpler communication architecture may be desired in which already assembled packets are passed onto the MAC layer for transmission one by one. This is also the situation encountered when a node is simply relaying real-time packets arriving from a distant source.

Suppose that real-time packets are presented to the MAC layer periodically, one every t_{rdy} units of time. The packet delay is the time that elapses from the moment a packet is available for transmission until it is successfully transmitted at the MAC layer (corrected for $t_{bslot} + t_{obs}$). The packet delay of the nth packet $\omega^{(n)}$ is given by $\omega^{(n)} = (u^{(n)} - t^{(n)} - t_{bslot} - t_{obs})$, where $t^{(n)}$ is the instant of time when the nth packet becomes ready for transmission, $t^{(n)} = t^{(1)} + (n - 1)t_{rdy}$.

Clearly, we should not choose $t_{sch} + t_{bslot} + t_{obs} = t_{rdy}$. If that choice was made, the instants when the node accesses the channel would start drifting in relation to the arrival times of new packets, and the node would not keep up with the packet arrival rate. Indeed, the packet delay of the nth packet would be

$$\omega^{(n)} = \omega^{(1)} + \sum_{i=2}^{n} d^{(i)}$$

which would grow monotonically with the number of packets already transmitted.

Consider instead a preventive approach whereby a real-time node schedules its next transmission attempt short of the inter-arrival time for packets t_{rdy}. Specifically, when a real-time node transmits a packet, it schedules the next transmission attempt to time t_{sch} in the future, now with $t_{sch} = t_{rdy} - t_{bslot} - t_{obs} - \delta$, where δ, $\delta > 0$, is called the slack time. At a scheduled access attempt, a real-time node will only start contending for access to the channel if a real-time packet is available for transmission. Otherwise, it waits for a ready packet and only then starts to contend for access to the channel. The correctness of the BB contention mechanism is preserved as long as the contention delays used to compute the lengths of BBs are always counted from the scheduled access attempts up to the time when the channel becomes idle for t_{med}.

REFERENCES

[1] *IEEE Std 802.11–1999, Part 11: Wireless LAN Medium Access Control (MAC) and Physical Layer (PHY) Specifications, Reference number ISO/IEC 8802-11:1999 (E)*, IEEE Std 802.11, 1999.

[2] *IEEE 802.11 Wireless Local Area Networks*; http://grouper.ieee.org/groups/802/11/.

[3] *IEEE 802.11e/D4.0, Draft Supplement to Part 11: Wireless Medium Access Control (MAC) and Physical Layer (PHY) Specifications: Medium Access Control (MAC) Enhancements for Quality of Service (QoS)*, November 2002.

[4] S. Choi, J. Prado, S. Shankar and S. Mangold, IEEE 802.11e Contention-Based Channel Access (EDCF) Performance Evaluation, in *Proc. IEEE ICC 2003*, Anchorage, AK, May 2003.

[5] P. Garg, R. Doshi, R. Greene, M. Baker, M. Malek and X. Cheng, Using IEEE 802.11e MAC for QoS over wireless, in *Proc. IEEE Int. Performance Computing and Communications Conf.*, Phoenix, AZ, April 2003.
[6] A. Banchs, X. Perez-Costa, and D. Qiao, Providing throughput guarantees in IEEE 802.11e wireless LANs, in *Proc. 18th Int. Teletraffic Congr. (ITC-18)*, Berlin, September 2003.
[7] Y. Xiao, Enhanced DCF of IEEE 802.11e to Support QoS, in *Proc. IEEE WCNC 2003*, New Orleans, LA, March 2003.
[8] S. Mangold, G. Hiertz and B. Walke, IEEE 802.11e wireless LAN – resource sharing with contention based medium access, in *IEEE PIMRC 2003*, Beijing, September 2003.
[9] G. Bianchi, Performance analysis of the IEEE 802.11 distributed coordination function, *IEEE JSAC*, vol. 18, no. 3, 2000, pp. 535–547.
[10] *IEEE Std 802.11b-1999, Supplement to Part 11: Wireless Medium Access Control (MAC) and Physical Layer (PHY) Specifications: Higher-Speed Physical Layer Extension in the 2.4 GHz Band*, September 1999.
[11] Z. Hadzi-Velkov and B. Spasenovski, Saturation throughput-delay analysis of IEEE 802.11 DCF in fading channel, in *Proc. IEEE ICC 2003*, Anchorage, AK, May 2003.
[12] S. Mangold, S. Choi, G. Hiertz, O. Klein and B. Walke, Analysis of IEEE 802.11e for QoS support in wireless LANs, *IEEE Wireless Commun.*, vol. 10, no. 6, 2003, pp. 40–50.
[13] IST WSI, *The Book of Visions 2000: Visions of the Wireless World*, *Version 1.0*, 2000.
[14] Z. Tao and S. Panwar, An analytical model for the IEEE 802.11e enhanced distributed coordination function, *IEEE Int. Conf. Communications*, vol. 7, 20–24 June 2004, pp. 4111–4117.
[15] H. Singh and S. Singh, Doa-aloha: slotted aloha for *ad hoc* networking using smart antennas, in *IEEE VTC Fall'03*, 6–9 October 2003.
[16] H. Singh and S. Singh, A MAC protocol based on adaptive beamforming for *ad hoc* networks, in *IEEE Pimrc'03*, 7–10 September 2003.
[17] R.R. Choudhury, X. Yang, R. Ramanathan and N.H. Vaidya, Using directional antennas for medium access control in *ad hoc* networks, in *ACM/SIGMOBILE MobiCom 2002*, 23–28 September 2002.
[18] L. Bao and J.J. Garcia-Luna-Aceves, Transmission scheduling in *ad hoc* networks with directional antennas, in *ACM/SIGMOBILE MobiCom 2002*, 23–28 September 2002.
[19] S. Bellofiore, J. Foutz, R. Govindarajula, I. Bahceci, C.A. Balanis, A.S. Spanias, J.M. Capone and T.M. Duman, Smart antenna system analysis, integration, and performance for mobile ad-hoc networks (manets), *IEEE Trans. Antennas and Propagation*, vol. 50, no. 5, 2002, pp. 571–581.
[20] T. ElBatt and B. Ryu, On the channel reservation schemes for *ad hoc* networks utilizing directional antennas, in *WPMC'02*, 2002.
[21] N. Fahmy, T.D. Todd and V. Kezys, *Ad hoc* networks with smart antennas using 802.11-based protocols, in *IEEE ICC'02*, 2002.
[22] G.M. Sanchez, Multiple access protocols with smart antennas n multihop *ad hoc* rural-area networks, M.S. thesis, Royal Institute of Technology, Sweeden, Radio Communication Systems Laboratory, Department of Signals, Sensors and Sytems, June 2002.
[23] R. Bagrodia, M. Takai, J. Martin and A. Ren, Directional virtual carrier sensing for directional antennas in mobile *ad hoc* networks, in *ACM/SIGMOBILE MobiHoc 2002*, October 2002.
[24] T. Nandagopal, T.-E. Kim, X. Gao and V. Bharghavan, Achieving MAC layer fairness in wireless packet networks, in *ACM MOBICOM'00*, August 2000, pp. 87–98.
[25] B. Bensaou, Y. Wang and C.C. Ko, Fair medium access in 802.11 based wireless *ad-hoc* networks, in *ACM MOBIHOC'00*, August 2000, pp. 99–106.
[26] V. Bharghavan, A. Demers, S. Shenker and L. Zhang, Macaw: a media access protocol for wireless lans, in *ACM SIGCOMM'94*, August 1994, pp. 212–225.

[27] H. Singh and S. Singh, Smart-802.11b MAC protocol for use with smart antennas, in *IEEE Int. Conf. Communications*, vol. 6, 20–24 June 2004, pp. 3684–3688.
[28] A. Woo and D. Culler, A transmission control scheme for media access in sensor networks, in *Proc. ACM/IEEE Int. Conf. Mobile Computing and Networking*, Rome, July 2001, pp. 221–235.
[29] F. Bennett, D. Clarke, J.B. Evans, A. Hopper, A. Jones and D. Leask, Piconet: embedded mobile networking, *IEEE Person Commun. Mag.*, vol. 4, 1997, pp. 8–15.
[30] S. Xu and T. Saadawi, Does the IEEE 802.11 MAC protocol work well in multihop wireless *ad hoc* networks?, *IEEE Commun. Mag.*, vol. 36, 2001, pp. 130–137.
[31] Y.-C. Tseng, C.-S. Hsu and T.-Y. Hsieh, Power-saving protocols for IEEE 802.11-based multi-hop ad hoc networks, in *Proc. IEEE INFOCOM*, New York, June 2002, pp. 200–209.
[32] V. Bharghavan, A. Demers, S. Shenker and L. Zhang, MACAW: a media access protocol for wireless lans, in *Proc. ACM SIGCOMM*, London, Septembar 1994, pp. 212–225.
[33] *Wireless LAN Medium Access Control (MAC) and Physical Layer (PHY) Specification*, IEEE Std 802.11, 1999.
[34] W. Ye, J. Heidemann and D. Estrin, Medium access control with coordinated adaptive sleeping for wireless sensor networks, *IEEE/ACM Trans. Networking*, vol. 12, no. 3, June 2004, pp. 493–506.
[35] P. Karn, MACA – A new channel access method for packet radio, in *Proc. ARRL/CRRL Amateur Radio Ninth Computer Networking Conf.*, ARRL, 1990, pp. 134–140.
[36] C. Fullmer and J. Garcia-Luna-Aceves, Floor acquisition multiple access (FAMA) for packet-radio networks, in *Proc. SIGCOMM'95*, Cambridge, MA, 1995, pp. 262–273.
[37] C. Fullmer and J. Garcia-Luna-Aceves, Solutions to hidden terminal problems in wireless networks, in *Proc. SIGCOMM'97*, vol. 2, Cannes, 1997, pp. 39–49.
[38] A. Muir and J. Garcia-Luna-Aceves, Supporting real-time multimedia traffic in a wireless LAN, in *Proc. SPIE Multimedia Computing and Networking 1997*, San Jose, CA, 1997, pp. 41–54.
[39] R. Garces and J. Garcia-Luna-Aceves, Collision avoidance and resolution multiple access with transmission groups, in *Proc. IEEE INFOCOM'97*, Kobe, 1997, pp. 134–142.
[40] C. Lin and M. Gerla, Asynchronous multimedia multihop wireless networks, in *Proc. IEEE INFOCOM'97*, Kobe, 1997, pp. 118–125.
[41] J.L. Sobrinho and A.S. Krishnakumar, Real-time traffic over the IEEE 802.11 medium access control layer, *Bell Labs Tech. J.*, vol. 1, 1996, pp. 172–187.

6

Teletraffic Modeling and Analysis

Traditional traffic models have been developed for wireline networks. These models predict the aggregate traffic going through telephone switches. Queueing theory is the tool which has been traditionally used in the analysis of such systems. A summary of the main results from the queueing theory is included in Appendix A (please go to www.wiley.com/go/glisic). These traditional models do not include subscriber mobility or callee distributions and therefore need modifications to be applicable for modeling the traffic in wireless networks.

6.1 CHANNEL HOLDING TIME IN PCS NETWORKS

Channel holding (occupancy) time is an important quantity in teletraffic analysis of PCS networks. It corresponds to service time in conventional queueing theory. This quantity is needed to derive key network design parameters such as the new call blocking probability and the handoff call blocking probability [1]. The cell residence time is a nonnegative random variable, so a good distribution model for the random variable will be sufficient for characterizing the users' mobility. In this section we use, the *hyper-Erlang distribution model* [2] for such purposes.

The *hyper-Erlang* distribution has the following probability density function and Laplace transform:

$$f_{\text{he}}(t) = \sum_{i=1}^{M} \alpha_i \frac{(m_i\eta_i)^{m_i} t^{m_i-1}}{(m_i-1)!} \mathrm{e}^{-m_i\eta_i t}, \qquad t \geq 0$$

$$f^*_{\text{he}}(s) = \sum_{i=1}^{M} \alpha_i \left(\frac{m_i\eta_i}{s+m_i\eta_i}\right)^{m_i} \tag{6.1}$$

where $\alpha_i \geq 0$, and $\sum_{i=1}^{M} \alpha_i = 1$. $M, m_1, m_2, \ldots,$ m_M are nonnegative integers and $\eta_1, \eta_2, \ldots, \eta_M$ are positive numbers. These distribution functions provide sufficiently general models, i.e. hyper-Erlang distributions are universal approximations.

Advanced Wireless Technologies: Cognitive, Cooperative & Opportunistic 4G Technology Second Edition Savo G. Glisic

It can be shown [3] that for a given cumulative distribution function $G(t)$ of a nonnegative random variable we can choose a sequence of distribution functions $G_m(t)$, each of which corresponds to a mixture of Erlangdistributions, so that $\lim_{m\to\infty} G_m(t) = G(t)$ for all t at which $G(t)$ is continuous. $G_m(t)$ can be chosen as

$$G_m(t) = \sum_{k=1}^{\infty} \left[G\left(\frac{k}{m}\right) - G\left(\frac{k-1}{m}\right) \right] G_m^k(t), \qquad t \geq 0 \tag{6.2}$$

where $G_m^k(t)$ is the distribution function of an Erlang distribution with mean k/m and variance k/m^2 (the distribution of the sum of k exponential random variables each with mean $1/m$). If $g_m(t)$ and $g_m^*(s)$ are the density function and Laplace transform of $G_m(t)$, and $g_m^k(t)$ is the density function of $G_m^k(t)$ then we have

$$\begin{aligned} g_m(t) &= \sum_{k=1}^{\infty} \left[G\left(\frac{k}{m}\right) - G\left(\frac{k-1}{m}\right) \right] g_m^k(t) \\ g_m^*(s) &= \sum_{k=1}^{\infty} \left[G\left(\frac{k}{m}\right) - G\left(\frac{k-1}{m}\right) \right] \left(\frac{k/m}{s+k/m}\right)^k \end{aligned} \tag{6.3}$$

where the asterisk is used to denote the Laplace transformation.

The resulting distribution is called the 'mixed Erlang distribution'. Their coefficients can be determined from the experimental data. If a finite number of terms is used to approximate the distribution function, the resulting distribution approximates the hyper-Erlang distribution.

To illustate why the distribution $G_m(t)$ provides the universal approximation to general distribution models we show Erlang distribution

$$f_e(t) = \frac{(m\eta)^{mt^{m-1}}}{(m-1)!} e^{-m\eta t}, \qquad t \geq 0 \tag{6.4}$$

in Figure 6.1 by varying the shape parameter m (Appendix A; please go to www.wiley.com/go/glisic). We observe that, as the shape parameter m becomes sufficiently large, the density function approaches the Dirac δ function. Hence, $f_e(t)$ approaches the δ function as m is sufficiently large. From signal processing theory [4], we know that the δ function can be used to sample a function and reconstruct the function from the sampled data (the sampling theorem). We can replace the δ function by the Erlang density function with sufficiently large m, and the resulting approximation is exactly in the form of the hyper-Erlang distribution.

If the cell residence time t is modeled by the hyper-Erlang distribution as in Equation (6.1), its kth moment is given as

$$E\left[t^k\right] = (-1)^k f_{he}^{*(k)}(0) = \sum_{i=1}^{M} \alpha_i \frac{(m_i + k - 1)!}{(m_i - 1)!} (m_i \eta_i)^{-k} \tag{6.5}$$

The parameters α_i, m_i and η_i $(i = 1, 2, \ldots, M)$ can be found by fitting a number of moments from field data. Moreover, if the number of moments exceeds the number of variables, then the least-square method can be used to find the best fit to minimize the least-square error.

The channel holding time distribution depends on the mobility of users, which can be characterized by the cell residence time [1–30, 5–31]. In the sequel we use the following notation: t_c, call holding time (exponentially distributed with parameter μ); t_m, cell residence time; r_1, time between the instant a new call is initiated and the instant the new call moves out of the cell if the new call is not completed; $r_m (m > 1)$, residual life time distribution of call holding time when the call finishes m th handoff successfully; and t_{nh} and t_{hh}, the channel holding times for a new call and a handoff call, respectively. Then, from Figure 6.2, the channel holding time for a new call

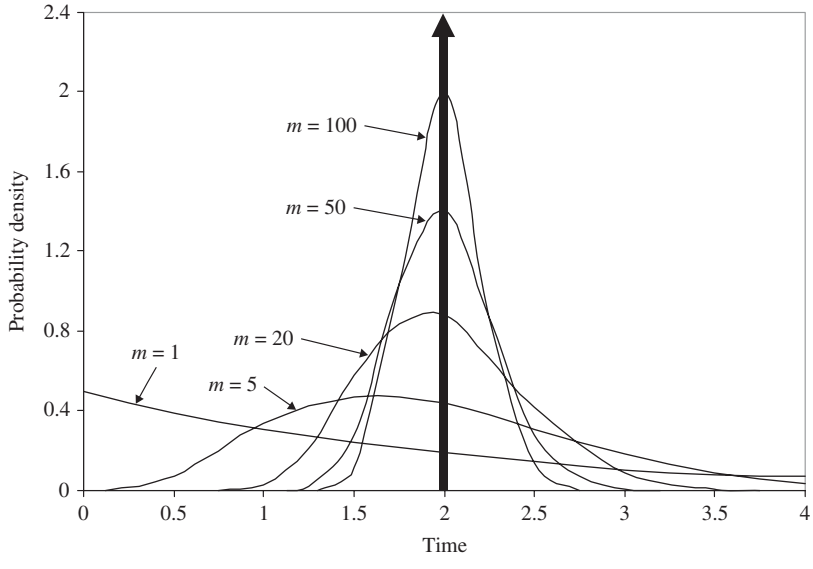

Figure 6.1 Probability density function for Erlang distribution.

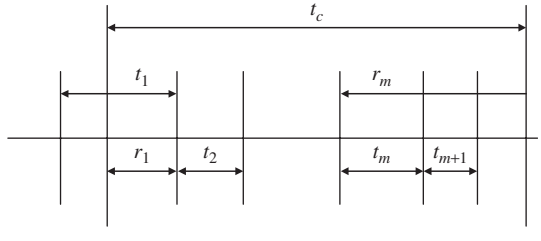

Figure 6.2 The call holding and cell residence times.

will be

$$t_{\text{nh}} = \min\{t_{\text{c}}, r_1\} \tag{6.6}$$

and the channel holding time for a handoff call is

$$t_{\text{hh}} = \min\{r_m, t_m\} \tag{6.7}$$

Let $t_{\text{c}}, t_m, r_1, t_{\text{hh}}$ and t_{nh} have density functions $f_{\text{c}}(t)$, $f(t)$, $f_{\text{r}}(t)$, $f_{\text{hh}}(t)$ and $f_{\text{nh}}(t)$ with their corresponding Laplace transforms $f_{\text{c}}^*(s)$, $f^*(s)$, $f_{\text{r}}^*(s)$, $f_{\text{hh}}^*(s)$ and $f_{\text{nh}}^*(s)$, respectively, and with cumulative distribution functions, $f_{\text{c}}(t)$, $F(t)$, $F_r(t)$, $F_{\text{hh}}(t)$ and $F_{\text{nh}}(t)$ respectively. From Equation (6.7) we obtain the probability

$$\begin{aligned}
\Pr(t_{\text{hh}} \le t) &= \Pr(r_m \le t \text{ or } t_m \le t) \\
&= \Pr(r_m \le t) + \Pr(t_m \le t) - \Pr(r_m \le t, t_m \le t) \\
&= \Pr(r_m \le t) + \Pr(t_m \le t) - \Pr(r_m \le t)\Pr(t_m \le t) \\
&= \Pr(t_{\text{c}} \le t) + \Pr(t_m \le t) - \Pr(t_{\text{c}} \le t)\Pr(t_m \le t)
\end{aligned} \tag{6.8}$$

which is based on the independency of r_m and t_m, and the memoryless property of the exponential distribution from which we have that the distribution of r_m has the same distribution as t_c. Differentiating Equation (6.8), gives

$$\begin{aligned} f_{hh}(t) &= f_c(t) + f(t) - f_c(t)\Pr(t_m \le t) - \Pr(t_c \le t) f(t) \\ &= f_c(t)\int_t^\infty f(\tau)\,d\tau + f(t)\int_t^\infty f_c(\tau)\,d\tau \end{aligned} \tag{6.9}$$

and

$$\begin{aligned} f_{hh}^*(s) &= f^*(s) + f_c^*(s) - \int_0^\infty e^{-st} f(t)\int_o^t f_c(\tau)\,d\tau\,dt - \int_0^\infty e^{-st} f_c(t)\int_o^t f(\tau)\,d\tau\,dt \\ f_{hh}^*(s) &= f^*(s) + f_c^*(s) - \mu\int_0^\infty e^{-(s+\mu)t}\int_o^t f(\tau)\,d\tau\,dt - \int_0^\infty e^{-st}(1-e^{-\mu t})\,f(t)\,dt \\ &= \frac{\mu}{s+\mu} + \frac{s}{s+\mu} f^*(s+\mu) \end{aligned} \tag{6.10}$$

From the above equations, we obtain the expected handoff call channel holding time as

$$E[t_{hh}] = -f_{hh}^{*'}(0) = \frac{1}{\mu}[1 - f^*(\mu)] \tag{6.11}$$

where $f_{hh}^{*'}$ is the first derivative of the function. Starting from Equation (6.6) and using a similar argument, we obtain

$$\begin{aligned} f_{nh}(t) &= f_c(t)\int_t^\infty f_r(\tau)\,d\tau + f_r(t)\int_t^\infty f_c(\tau)\,d\tau \\ f_{nh}^*(s) &= \frac{\mu}{s+\mu} + \frac{s}{s+\mu} f_r^*(s+\mu) \\ E[t_{nh}] &= -f_{nh}^{*(1)}(0) = \frac{1}{\mu}\Big[1 - f_r^*(\mu)\Big]. \end{aligned} \tag{6.12}$$

We need to consider the channel holding time distribution for any call (either new call or handoff call), i.e. the channel holding time for the merged traffic of new calls and handoff calls. We will simply call this the channel holding time, using no modifiers such as new call or handoff call. If t_h is the channel holding time and λ_h the handoff call arrival rate, and λ is the new call arrival rate then, $t_h = t_{nh}$ with probability $\lambda(\lambda + \lambda_h)$ and $t_h = t_{hh}$ with probability $\lambda_h(\lambda + \lambda_h)$. Let $f_h(t)$ and $f_h^*(s)$ be its density function and the corresponding Laplace transform. It is easy to obtain

$$\begin{aligned} f_h(t) &= \frac{\lambda}{\lambda+\lambda_h} f_{nh}(t) + \frac{\lambda_h}{\lambda+\lambda_h} f_{hh}(t) \\ f_h^*(s) &= \frac{\lambda}{\lambda+\lambda_h} f_{nh}^*(s) + \frac{\lambda_h}{\lambda+\lambda_h} f_{hh}^*(s) \\ E[t_h] &= \frac{\lambda}{\mu(\lambda+\lambda_h)}\Big[1 - f_r^*(\mu)\Big] + \frac{\lambda_h}{\mu\lambda+\lambda_h)}\big[1 - f^*(\mu)\big] \end{aligned} \tag{6.13}$$

When the residual lifetime r_1 of t_1 is exponentially distributed with parameter μ_r, then its Laplace transform $f_r^*(s)$ is $\mu_r/(s+\mu_r)$. Using this in Equation (6.12), results in

$$f_{nh}^*(s) = \frac{\mu}{s+\mu} + \frac{\mu_r s}{(s+\mu)(s+\mu+\mu_r)} = \frac{\mu+\mu_r}{s+\mu+\mu_r} \tag{6.14}$$

which implies that the new call channel holding time is exponentially distributed with parameter $\mu + \mu_r$. Similarly, if the cell residence time t_i is exponentially distributed with parameter η, then the handoff call channel holding time is also exponentially distributed with parameter $\mu + \eta$. In

this case, the channel holding time is hyperexponentially distributed. If $\mu_r = \eta$, then the channel holding time [see Equation (6.12)] is exponentially distributed with parameter $\mu + \eta$. In fact, since r_1 is the residual life of t_1, from the Residual Life Theorem [21], we have

$$f_r^*(s) = \frac{\eta\left[1 - f^*(s)\right]}{s} = \frac{\eta}{s+\eta} = f^*(s) \tag{6.15}$$

Hence, the channel holding time is exponentially distributed with parameter $\mu + \eta$ when the cell residence time is exponentially distributed.

Simple results for the conditional distribution for channel holding time when the cell residence time is generally distributed are presented next. Let $f_{cnh}(t)$, $f_{chh}(t)$ and $f_{ch}(t)$ denote the conditional density functions for new call channel holding time, the handoff call channel holding time and the channel holding time, respectively, with Laplace transforms $f_{cnh}^*(s)$, $f_{chh}^*(s)$ and $f_{ch}^*(s)$, and with cumulative distribution functions and $F_{cnh}(t)$, $F_{chh}(t)$ and $F_{ch}(t)$. Let us start with the *conditional distribution* for the handoff call channel holding time. We have

$$\begin{aligned} F_{chh}(h) &= \Pr(t_{hh} \le h \mid r_m \le t_m) = \frac{\Pr(r_m \le h, r_m \le t_m)}{\Pr(r_m \le t_m)} = \frac{\int_0^h f_c(t) \int_t^\infty f(\tau)\,\mathrm{d}\tau\,\mathrm{d}t}{\Pr(r_m \le t_m)} \\ &= \frac{\int_0^h f_c(t)\,[1 - F(t)]\,\mathrm{d}t}{\Pr(r_m \le t_m)} \end{aligned} \tag{6.16}$$

Differentiation of both sides gives the conditional density function

$$f_{chh}(h) = \frac{f_c(h)\,[1 - F(h)]}{\Pr(r_m \le t_m)} \tag{6.17}$$

with

$$\begin{aligned} \Pr(r_m \le t_m) &= \int_0^\infty \int_0^t f(t) f_c(\tau)\,\mathrm{d}\tau\,\mathrm{d}t = \int_0^\infty f(t)\left[1 - \mathrm{e}^{\mu t}\right]\mathrm{d}t \\ &= 1 - \int_0^\infty f(t)\mathrm{e}^{-\mu t}\,\mathrm{d}t = 1 - f^*(\mu) \end{aligned} \tag{6.18}$$

Using this in Equation (6.16) results in

$$f_{chh}(h) = \frac{[1 - F(h)]\,\mu \mathrm{e}^{-\mu h}}{1 - f^*(\mu)} \tag{6.19}$$

and

$$f_{chh}^*(s) = \frac{\mu \int_0^\infty \mathrm{e}^{-(s+\mu)h}\,[1 - F(h)]\,\mathrm{d}h}{1 - f^*(\mu)} = \frac{\mu}{s+\mu} \cdot \frac{1 - f^*(s+\mu)}{1 - f^*(\mu)} \tag{6.20}$$

Similarly, we obtain

$$\begin{aligned} f_{cnh}(h) &= \frac{[1 - F_r(h)]\,\mu \mathrm{e}^{-\mu h}}{1 - f_r^*(\mu)} \\ f_{cnh}^*(s) &= \frac{\mu}{s+\mu} \cdot \frac{1 - f_r^*(s+\mu)}{1 - f_r^*(\mu)} \end{aligned} \tag{6.21}$$

The conditional *channel holding time* distribution $f_{ch}(t)$, $f_{ch}^*(s)$ is the average of the conditional *new call channel holding time* distribution and *handoff call channel holding time* distribution. In summary, we therefore have

$$f_{cnh}^*(s) = \frac{\mu}{s+\mu} \cdot \frac{1 - f_r^*(s+\mu)}{1 - f_r^*(\mu)}$$

$$f^*_{\text{chh}}(s) = \frac{\mu}{s+\mu}.\frac{1-f^*(s+\mu)}{1-f^*(\mu)} \tag{6.22}$$

$$f^*_{\text{ch}}(s) = \frac{\mu}{s+\mu}\left[\frac{\lambda}{\lambda+\lambda_{\text{h}}}.\frac{1-f_{\text{r}}^*(s+\mu)}{1-f_{\text{r}}^*(\mu)} + \frac{\lambda_{\text{h}}}{\lambda+\lambda_{\text{h}}}.\frac{1-f^*(s+\mu)}{1-f^*(\mu)}\right]$$

If T_{cnh}, T_{chh} and T_{ch} are the expected conditional new call channel holding time, the expected conditional handoff call channel holding time, and the expected conditional channel holding time, respectively, then we have

$$\begin{aligned} T_{\text{cnh}} &= \frac{1}{\mu} + \frac{f_{\text{r}}^{*'}(\mu)}{1-f_{\text{r}}^*(\mu)} \\ T_{\text{chh}} &= \frac{1}{\mu} + \frac{f^{*'}(\mu)}{1-f^*(\mu)} \\ T_{\text{ch}} &= \frac{1}{\mu} + \frac{\lambda}{\lambda+\lambda_{\text{h}}}.\frac{f_{\text{r}}^{*'}(\mu)}{1-f_{\text{r}}^*(\mu)} + \frac{\lambda_{\text{h}}}{\lambda+\lambda_{\text{h}}}\frac{f^{*'}(\mu)}{1-f^*(\mu)} \end{aligned} \tag{6.23}$$

In order to be able to use these results, we need to find the handoff call arrival rate λ_{h}. This parameter depends on the new call arrival rate, the new call blocking probability and the handoff call blocking probability. If p_{bn} and p_{bh} are the new call and handoff call blocking probabilities, respectively, and H is the number of handoffs for a call (its expectation $E[H]$ is also called handoff rate), then using a procedure similar to the one in Fang *et al.* [12] gives

$$E[H] = -(1-p_{\text{bn}}) \sum_{P\in\sigma_{\text{c}}} \operatorname*{Res}_{s=p} \frac{f_{\text{r}}^*(s)}{s\left[1-(1-p_{\text{bh}})f^*(s)\right]} f_{\text{c}}^*(-s) \tag{6.24}$$

where σ_{c} denotes the set of poles of $f_{\text{c}}^*(-s)$ in the right half of the complex plane and $\text{Res}_{s=p}$ denotes the residue at the pole $s=p$. Since t_{c} is exponentially distributed with parameter μ, hence $f_{\text{c}}^*(s) = \mu/(s+\mu)$, from the above we obtain

$$E[H] = \frac{(1-p_{\text{bn}})f_{\text{r}}^*(\mu)}{1-(1-p_{\text{bh}})f^*(\mu)} \tag{6.25}$$

Since each unblocked call initiates $E[H]$ handoff calls on average, the handoff call arrival rate can be obtained:

$$\lambda_{\text{h}} = \lambda E[H] = \frac{(1-p_{\text{bn}})\lambda f_{\text{r}}^*(\mu)}{1-(1-p_{\text{bh}})f^*(\mu)} \tag{6.26}$$

As long as $f_{\text{r}}^*(s)$ and $f^*(s)$ are proper rational functions, then the Laplace transforms of distribution functions of all channel holding times (either conditional or unconditional) are all rational functions. To find the corresponding density functions, we only need to find the inverse Laplace transforms. This can be accomplished by using the partial fractional expansion [32].

As an illustration, suppose that $g(s)$ is a proper rational function with poles $p_1, p_2, \ldots, p_k$ with multiplicities $n_1, n_2, \ldots, n_k$. Then $g(s)$ can be expanded as

$$g(s) = \sum_{i=1}^{k}\sum_{j=0}^{n_i} A_{ij}\frac{s^j}{(s+p_i)^{n_i}}$$

where the constants can be found easily by the formula

$$A_{ij} = \frac{\text{d}^j}{\text{d}s^j}\left[(s+p_i)^{n_i}g(s)\right]\Big|_{s=0}, j=0,1,\ldots,\ i, \quad i=1,2,\ldots,k$$

The inverse Laplace transform L^{-1} gives

$$L^{-1}\left[s^j f(s)\right] = \frac{\mathrm{d}^j}{\mathrm{d}t^j}\left\{L^{-1}\left[f(s)\right]\right\}, \; L^{-1}\left[1/(s+\beta)^h\right] = \frac{t^h}{h!}\mathrm{e}^{-\beta t}$$

and

$$L^{-1}\left[g(s)\right] = \sum_{i=1}^{k}\sum_{j=0}^{m_i} A_{ij}\frac{\mathrm{d}^j}{\mathrm{d}t^j}\left(\frac{t^j}{j!}\mathrm{e}^{-p_i t}\right)$$

At this stage it is useful to remember that the inverse Laplace transform of a rational function is in fact the impulse response of a linear system in which the rational function is the system transfer function of the resulting linear system [32] and the cumulative distribution function is the step response of the linear system. In Matlab, the commands *impulse* and *step* can be used to find the density function and the distribution function. When applying the hyper-Erlang distribution

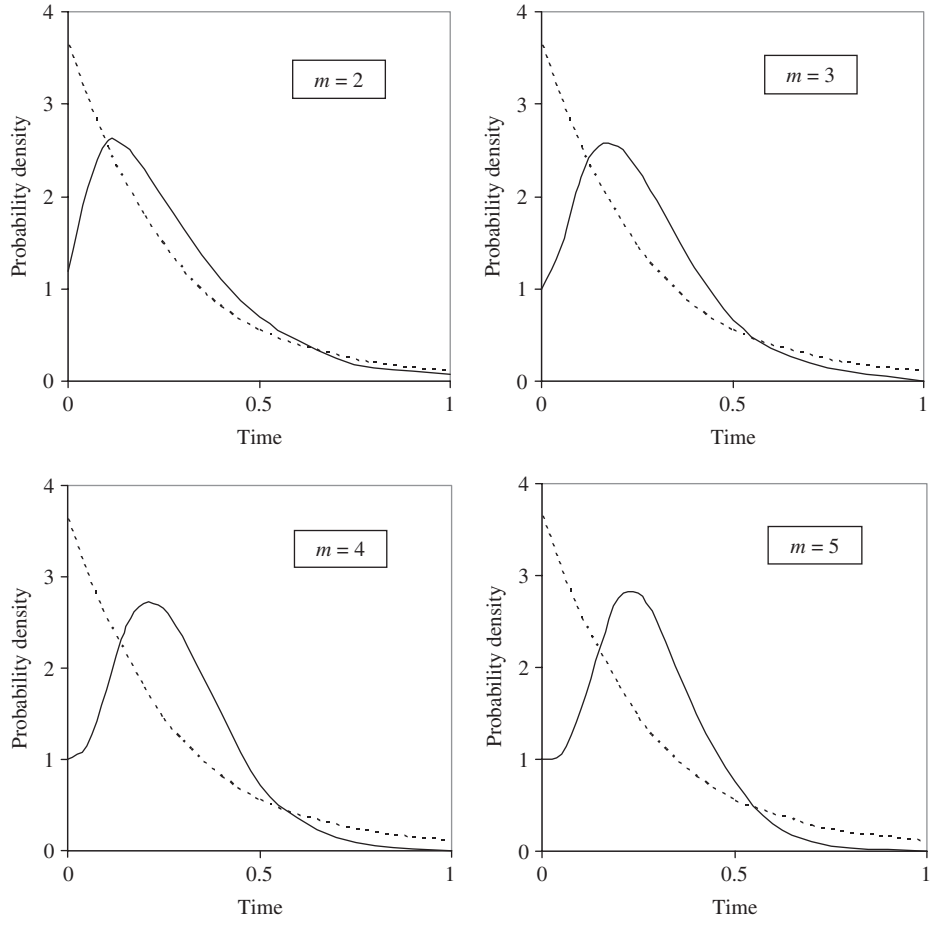

Figure 6.3 Probability density function of handoff call channel holding time (solid line) and its exponential fitting (dashed line) when cell residence time is Erlang distributed with parameter (m, η).

model for cell residence time, we can in fact reduce the computation further. Substituting $f^*(s)$ in Equation (6.10) with $f_{\text{he}}^*(s)$ given by Equation (6.1), gives

$$f_{\text{hh}}^*(s) = \sum_{i=1}^{M} \alpha_i \left[\frac{\mu}{s+\mu} + \frac{s}{s+\mu} \left(\frac{m_i \eta_i}{s + m_i \eta_i} \right)^{m_i} \right] = \sum_{i=1}^{M} \alpha_i f_{\text{e}}^*(s; m_i, \eta_i) \tag{6.27}$$

where $f_{\text{e}}^*(s; m_i, \eta_i)$ corresponds to the handoff call channel holding time when the cell residence time is Erlang distributed with parameters (m_i, η_i). Thus, the problem reduces to finding the algorithm for computing the channel holding time for the case when the cell residence time is Erlang distributed.

Performance examples: if the cell residence time is Erlang distributed we have

$$f(t) = \beta^m t^{m-1} \mathrm{e}^{-\beta t}/(m-1)!, \quad f^*(s) = \left[\beta/(s+\beta)\right]^m$$

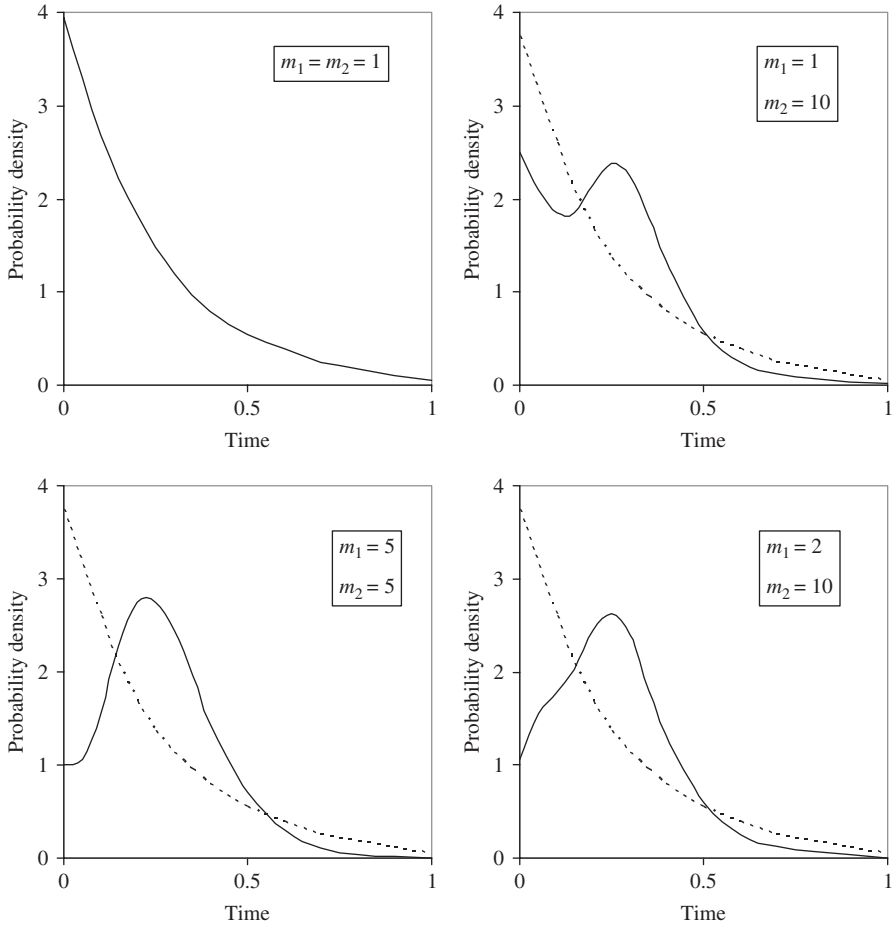

Figure 6.4 Probability density function of handoff call channel holding time (solid line) and its exponential fitting (dashed line) when cell residence time is hyper-Erlang distributed with parameter (m_1, m_2, η).

where $\beta = m\eta$ is the scale parameter and m is the shape parameter. The mean of this Erlang distribution is η and its variance is $1/(m\eta^2)$. When the mean η is fixed, varying the value m is equivalent to varying the variance and larger m means smaller variance and lesser spread of the cell residence time.

The handoff call channel holding time probability density functions with different variance of cell residence time distributed according to Erlang distribution with the same mean are shown in Figure 6.3. It can be seen that, when the cell residence time becomes less spread, the handoff call channel holding time shows severe mismatch to the exponential distribution.

In the simple case when the cell residence time is hyper-Erlang distributed with two terms,

$$f^*(s) = \alpha_1 \left(\frac{m_1\eta}{s+m_1\eta}\right)^{m_1} + \alpha_2 \left(\frac{m_2\eta}{s+m_2\eta}\right)^{m_2}$$

$$f^*_{\text{hh}}(s) = \alpha_1 \left\{\frac{\mu}{s+\mu} + \frac{s}{s+\mu}.\left(\frac{m_1\eta}{s+m_1\eta}\right)^{m_1}\right\} + \alpha_2 \left\{\frac{\mu}{s+\mu} + \frac{s}{s+\mu}.\left(\frac{m_2\eta}{s+m_2\eta}\right)^{m_2}\right\}$$

the results are shown in Figure 6.4. When m_1 and m_2 have different values, the variances of cell residence time are different and the handoff call channel holding time is no longer exponentially distributed.

REFERENCES

[1] D. Hong and S.S. Rappaport, Traffic model and performance analysis for cellular mobile radio telephone systems with prioritized and nonprioritized handoff procedures, *IEEE Trans. Vehicular Technol.*, vol. 35, no. 3, 1986, pp. 77–92.

[2] Y. Fang and I. Chlamtac, Teletraffic analysis and mobility modeling of PCS networks, *IEEE Trans. Commun.*, vol. 47, no. 7, 1999, pp. 1062–1072.

[3] F.P. Kelly, *Reversibility and Stochastic Networks*. Wiley: New York, 1979.

[4] J.G. Proakis, *Digital Communications*, 3rd edn. Prentice-Hall: Englewood Cliffs, NJ, 1995.

[5] V.A. Bolotin, Modeling call holding time distributions for CCS network design and performance analysis, *IEEE J. Select. Areas Commun.*, vol. 12, no. 3, 1994, pp. 433–438.

[6] F. Barcelo and J. Jordan, Channel holding time distribution in cellular telephony, in *Proc. 9th Int. Conf. Wireless Commun. (Wireless'97)*, Alta, Canada, July 9–11, 1997, vol. 1, pp. 125–134.

[7] E. Chlebus and W. Ludwin, Is handoff traffic really Poissonian?, *IEEE ICUPC'95*, Tokyo, 6–10, November, 1995, pp. 348–353.

[8] D.C. Cox, Wireless personal communications: What is it?, *IEEE Personal Commun. Mag.*, pp. 20–35, 1995.

[9] D.C. Cox, *Renewal Theory*. Wiley: New York, 1962.

[10] E. Del Re, R. Fantacci and G. Giambene, Handover and dynamic channel allocation techniques in mobile cellular networks, *IEEE Trans. Vehicular Technol.*, vol. 44, no. 2, 1995, pp. 229–237.

[11] E. Del Re, R. Fantacci and G. Giambene, Efficient dynamic channel allocation techniques with handover queueing for mobile satellite networks, *IEEE J. Selected Areas Commun.*, vol. 13, no. 2, 1995, pp. 397–405.

[12] Y. Fang, I. Chlamtac and Y.B. Lin, Channel occupancy times and handoff rate for mobile computing and PCS networks, *IEEE Trans. Comput.*, vol. 47, no. 6, 1998, pp. 679–692.

[13] Y. Fang, I. Chlamtac and Y.B. Lin, Modeling PCS networks under general call holding times and cell residence time distributions, *IEEE Trans. Networking*, vol. 5, 1997, pp. 893–906.

[14] Y. Fang, I. Chlamtac and Y.B. Lin, Call performance for a PCS network, *IEEE J. Select. Areas Commun.*, vol. 15, no. 7, 1997, pp. 1568–1581.

[15] E. Gelenbe and G. Pujolle, *Introduction to Queueing Networks*. Wiley: New York, 1987.

[16] R.A. Guerin, Channel occupancy time distribution in a cellular radio system, *IEEE Trans. Vehicular Tech.*, vol. 35, no. 3, 1987, pp. 89–99.
[17] B. Jabbari, Teletraffic aspects of evolving and next-generation wireless communication networks, *IEEE Commun. Mag.*, 1996, pp. 4–9.
[18] C. Jedrzycki and V.C.M. Leung, Probability distributions of channel holding time in cellular telephony systems, in *Proc. IEEE Vehicular Technology Conf.*, Atlanta, GA, May 1996, pp. 247–251.
[19] J. Jordan and F. Barcelo, Statistical modeling of channel occupancy in trunked PAMR systems, in *Proc. 15th Int. Teletraffic Conf. (ITC'15)*, V. Ramaswami and P.E. Wirth, Eds. Elsevier Science: Amsterdam, 1997, pp. 1169–1178.
[20] F.P. Kelly, Loss networks, *The Annals of Applied Probability*, vol. 1, no. 3, 1991, pp. 319–378.
[21] L. Kleinrock, *Queueing Systems: Theory*, vol. 1. Wiley: New York, 1975.
[22] W.R. LePage, *Complex Variables and the Laplace Transform for Engineers*. Dover: New York, 1980.
[23] Y.B. Lin, S. Mohan and A. Noerpel, Queueing priority channel assignment strategies for handoff and initial access for a PCS network, *IEEE Trans. Vehicular Technol.*, vol. 43, no. 3, 1994, pp. 704–712.
[24] S. Nanda, Teletraffic models for urban and suburban microcells: cell sizes and handoff rates, *IEEE Trans. Vehicular Technol.*, vol. 42, no. 4, 1993, pp. 673–682.
[25] A.R. Noerpel, Y.B. Lin, and H. Sherry, PACS: personal access communications system-A tutorial, *IEEE Personal Commun.*, vol. 3, no. 3, 1996, pp. 32–43.
[26] P. Orlik and S.S. Rappaport, A model for teletraffic performance and channel holding time characterization in wireless cellular communication with general session and dwell time distributions, *IEEE J. Select. Areas Commun.*, vol. 16, no. 5, 1998, pp. 788–803.
[27] P. Orlik and S.S. Rappaport, A model for teletraffic performance and channel holding time characterization in wireless cellular communication, in *Proc. Int. Conf. Universal Personal Commun. (ICUPC'97)*, San Diego, CA, October 1997, pp. 671–675.
[28] S. Tekinay and B. Jabbari, A measurement-based prioritization scheme for handovers in mobile cellular networks, *IEEE J. Select. Areas Commun.*, vol. 10, no. 8, 1992, pp. 1343–1350.
[29] C.H. Yoon and C.K. Un, Performance of personal portable radio telephone systems with and without guard channels, *IEEE J. Select. Areas Commun.*, vol. 11, no. 6, 1993, pp. 911–917.
[30] T.S. Yum and K.L. Yeung, Blocking and handoff performance analysis of directed retry in cellular mobile systems, *IEEE Trans. Vehicular Technol.*, vol. 44, no. 3, 1995, pp. 645–650.
[31] M.M. Zonoozi and P. Dassanayake, User mobility modeling and characterization of mobility patterns, *IEEE J. Select. Areas Commun.*, vol. 15, no. 7, 1997, pp. 1239–1252.
[32] T. Kailath, *Linear Systems*. Prentice-Hall: Englewood Cliffs, NJ, 1980.

7

Adaptive Network Layer

7.1 GRAPHS AND ROUTING PROTOCOLS

The most important function of the network layer is routing. A tool used in the design and analysis of routing protocols is graph theory. Networks can be represented by graphs where mobile nodes are vertices and communication links are edges. Routing protocols often use shortest path algorithms. In this section we provide a simple review of the most important principles in the field which provides a background to study the routing algorithms.

7.1.1 Elementary concepts

A graph $G(V, E)$ is two sets of objects, vertices (or nodes), set V, and edges, set E. A graph is represented by dots or circles (vertices) interconnected by lines (edges). The magnitude of graph G is characterized by number of vertices $|V|$ (called the order of G) and number of edges $|E|$, size G. The running times of algorithms are measured in terms of the order and size.

7.1.2 Directed graph

An edge $e \in E$ of a directed graph is represented as an ordered pair (u, v), where $u, v \in V$. Here u is the initial vertex and v is the terminal vertex. Also assume here that $u \neq v$. An example with

$$V = \{1, 2, 3, 4, 5, 6\}, |V| = 6$$
$$E = \{(1, 2), (2, 3), (2, 4), (4, 1), (4, 2), (4, 5), (4, 6)\}, |E| = 7$$

is shown in Figure 7.1.

Advanced Wireless Technologies: Cognitive, Cooperative & Opportunistic 4G Technology Second Edition Savo G. Glisic

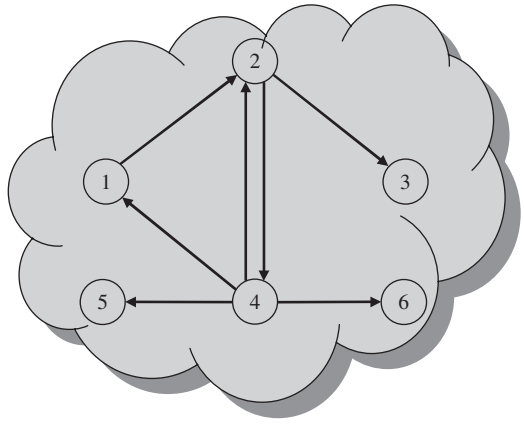

Figure 7.1 Directed graph.

7.1.3 Undirected graph

An edge $e \in E$ of an undirected graph is represented as an unordered pair $(u, v) = (v, u)$, where $u, v \in V$. Also assume that $u \neq v$. An example with

$$V = \{1, 2, 3, 4, 5, 6\}, |V| = 6$$
$$E = \{(1, 2), (2, 3), (2, 4), (4, 1), (4, 5)(4, 6)\}|E| = 6$$

is shown in Figure 7.2.

7.1.4 Degree of a vertex

Degree of a vertex in an undirected graph is the number of edges incident on it. In a directed graph, the *out degree* of a vertex is the number of edges leaving it and the *in degree* is the number of edges entering it. In Figure 7.2 the *degree* of vertex 2 is 3. In Figure 7.1 the *in degree* of vertex 2 is 2 and the *in degree* of vertex 4 is 1.

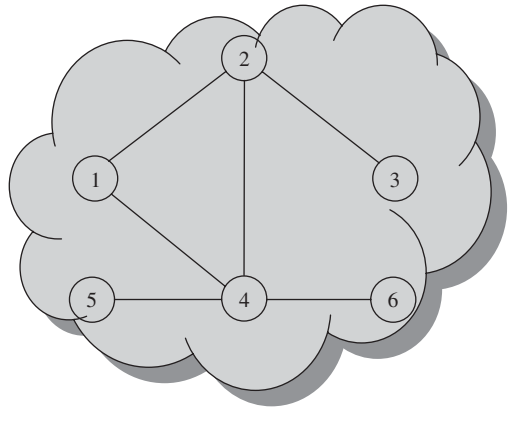

Figure 7.2 Undirected graph.

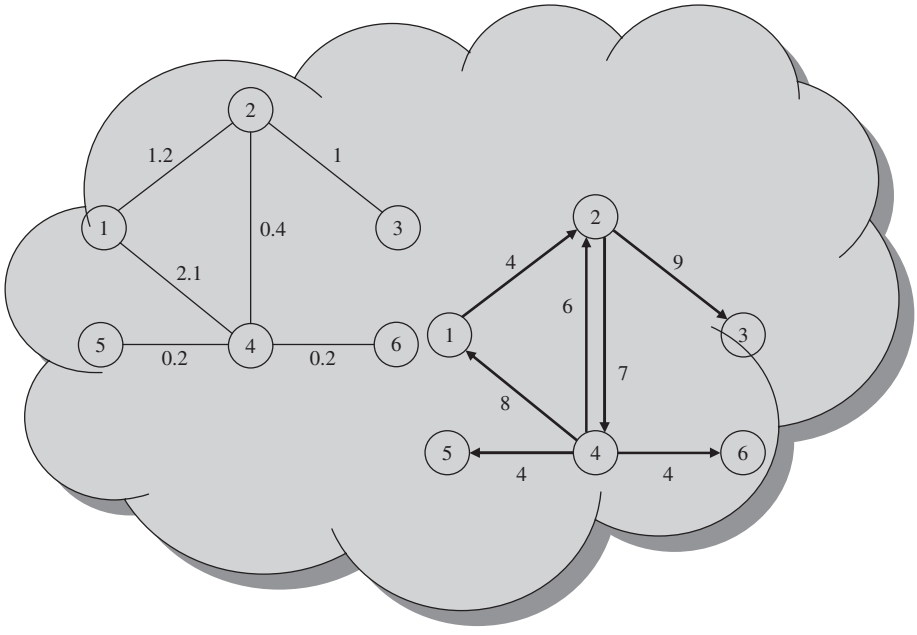

Figure 7.3 Weighted graphs.

7.1.5 Weighted graph

In a weighted graph each edge has an associated weight, usually given by a weight function $w : E \rightarrow R$. Weighted graphs from Figures 7.1 and 7.2 are shown in Figure 7.3. In the analysis of the routing problems, these weights represent the cost of using the link. Most of the time this cost would be delay that a packet would experience if using that link.

7.1.6 Walks and paths

A walk is a sequence of nodes $(v1, v2, \ldots, vL)$ such that $\{(v1, v2), (v2, v3), \ldots, (vL-1, vL)\} \subseteq E$, e.g. $(V2, V3, V6, V5, V3)$ in Figure 7.4. A *simple path* is a walk with no repeated nodes, e.g. $(V1, V4, V5, V6, V3)$. A *cycle* is a walk $(v1, v2, \ldots, vL)$ where $v1 = vL$ with no other nodes repeated and $L > 3$, e.g. $(V1, V2, V3, V5, V4, V1)$. A graph is called *cyclic* if it contains a cycle; otherwise it is called *acyclic*. A *complete graph* is an undirected/directed graph in which every pair of vertices is *adjacent*. An example is given in Figure 7.5. If (u, v) is an edge in a graph G, we say that vertex v is *adjacent* to vertex u.

7.1.7 Connected graphs

An undirected graph is connected if you can get from any node to any other by following a sequence of edges or any two nodes are connected by a path, as shown in Figure 7.6. A directed graph is *strongly connected* if there is a directed path from any node to any other node. A graph is *sparse* if $|E| \approx |V|$. A graph is *dense* if $|E| \approx |V|^2$.

A *bipartite graph* is an undirected graph $G = (V, E)$ in which V can be partitioned into two sets, $V1$ and $V2$, such that $(u, v) \in E$ implies either $u \in V1$ and $v \in V2$ or $v \in V1$ and $u \in V2$, see Figure 7.7.

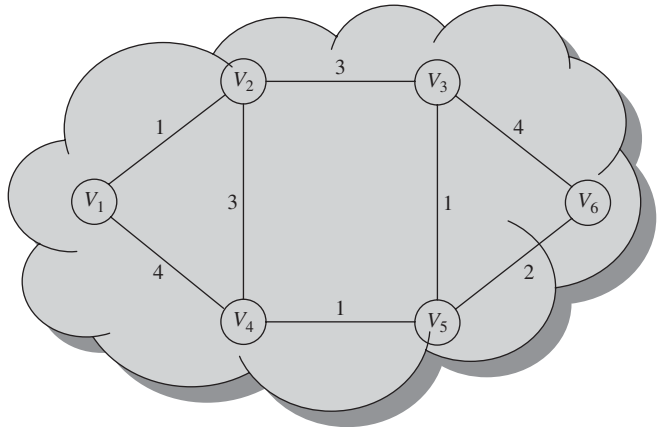

Figure 7.4 Illustration of a walk.

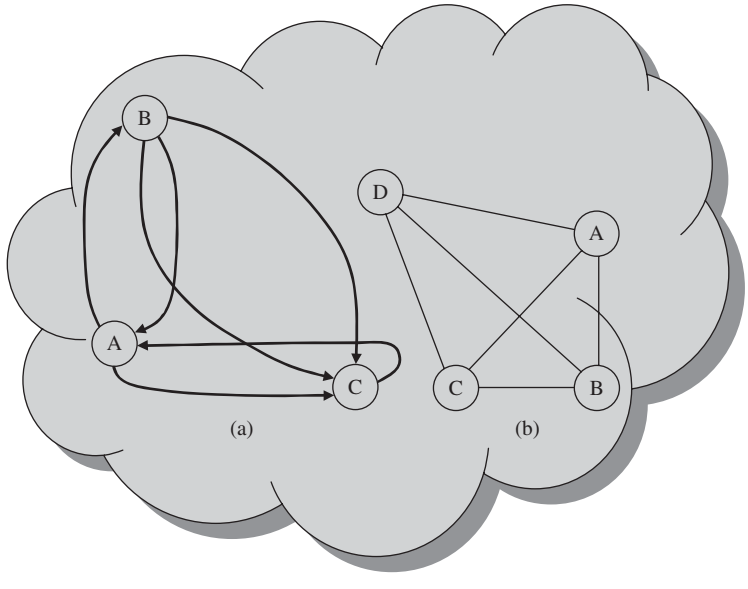

Figure 7.5 Complete graphs: (a) [V nodes and $V(V-1)$ edges] 3 nodes and 3×2 edges; (b) [V nodes and $V(V-1)/2$ edges] 4 nodes and $4 \times 3/2$ edges.

7.1.8 Trees

Let $G = (V, E)$ *be an undirected graph. The following statements are equivalent:*

(1) G is a tree;

(2) any two vertices in G are connected by unique simple path;

(3) G is connected, but if any edge is removed from E, the resulting graph is disconnected;

(4) G is connected, and $|E| = |V| - 1$;

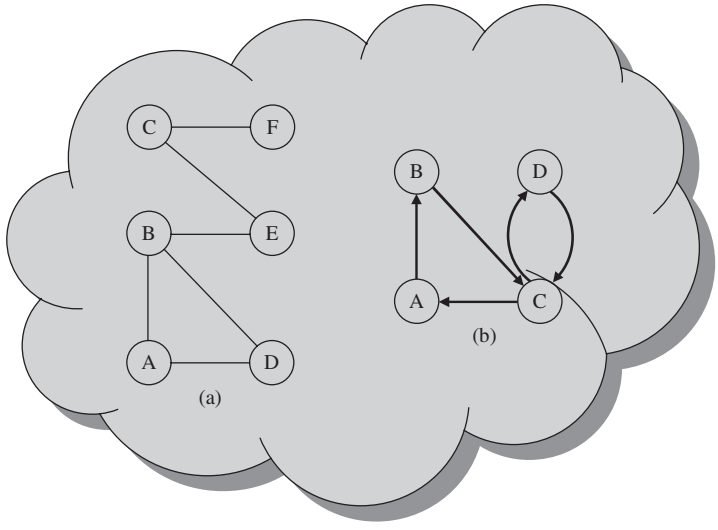

Figure 7.6 Connected graphs.

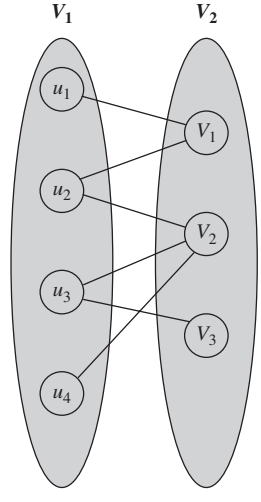

Figure 7.7 Bipartite graph.

(5) G is acyclic, and $|E| = |V| - 1$;

(6) G is acyclic, but if any edge is added to E, the resulting graph contains a cycle.

For an illustration see Figure 7.8.

7.1.9 Spanning tree

A tree (T) is said to span $G = (V, E)$ if $T = (V, E')$ and $E' \subseteq E$. For the graph shown Figure 7.4, two possible spanning trees are shown in Figure 7.9. Given connected graph G with real-valued

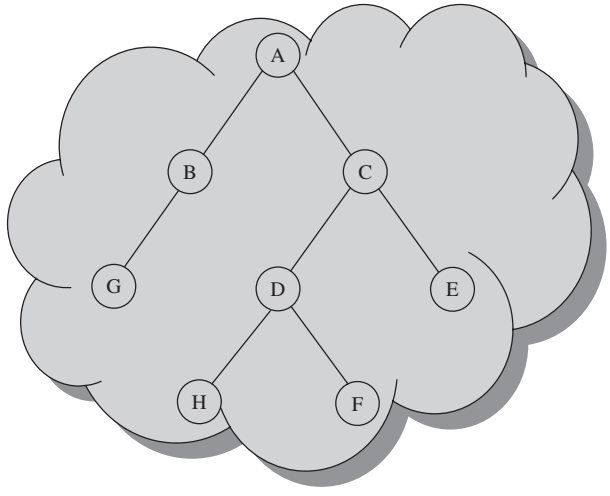

Figure 7.8 Tree.

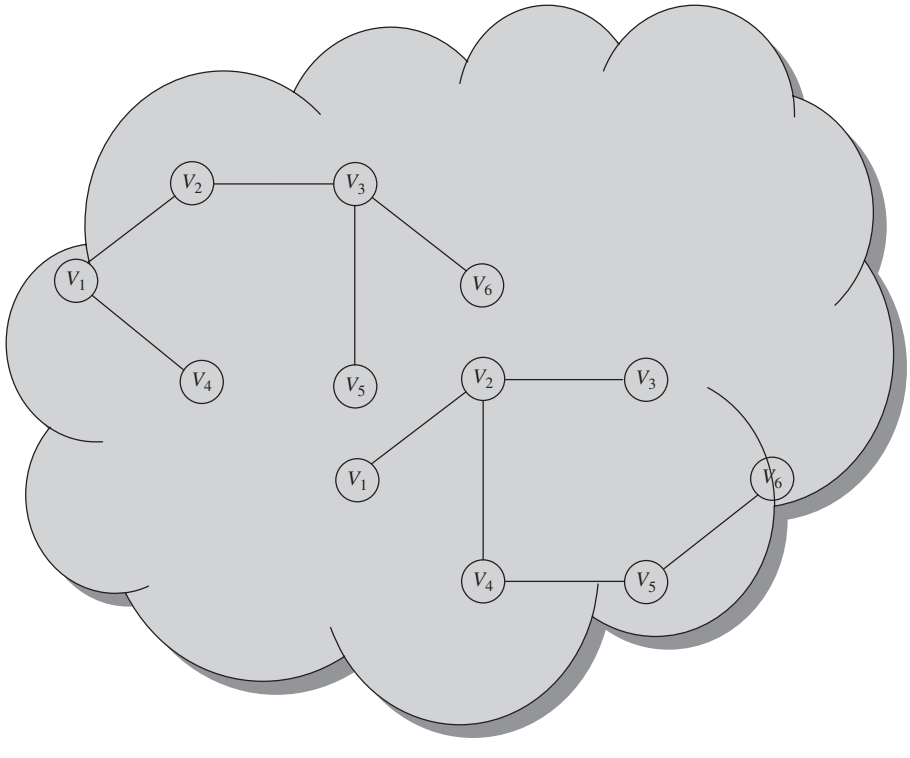

Figure 7.9 Spanning trees.

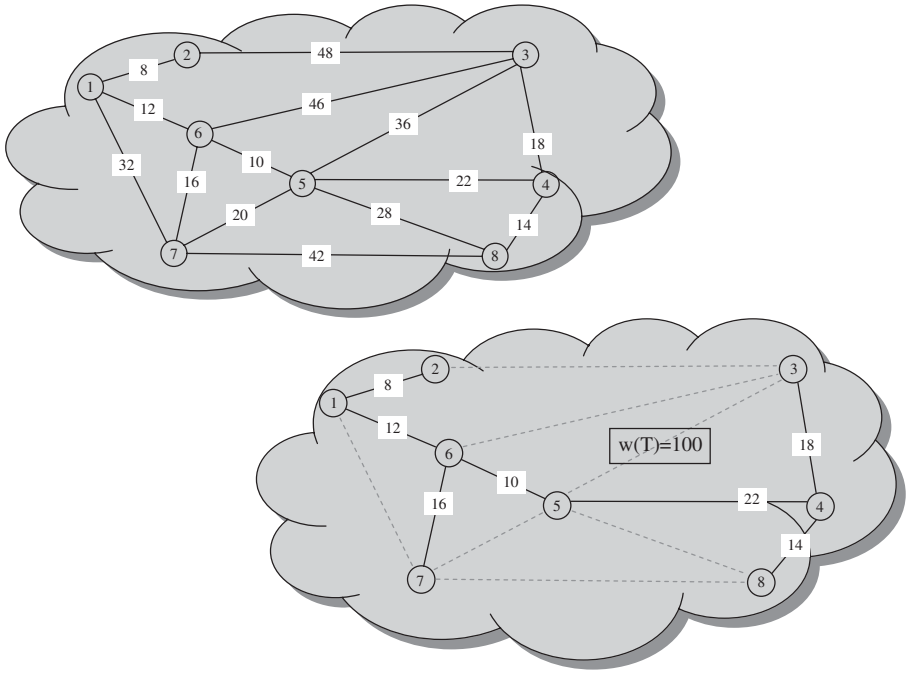

Figure 7.10 Minimum spanning tree.

edge weights ce, a minimum spanning tree (MST) is a spanning tree of G whose sum of edge weights is minimized as shown in Figure 7.10.

7.1.10 MST computation

7.1.10.1 Prim's algorithm

Select an arbitrary node as the initial tree (T). Augment T in an iterative fashion by adding the outgoing edge (u, v), (i.e. $u \in T$ and $v \in G - T$) with minimum cost (i.e. weight). The algorithm stops after $|V| - 1$ iterations. Computational complexity $= O(|V|^2)$. An illustration of the algorithm is given in Figure 7.11.

7.1.10.2 Kruskal's algorithm

Select the edge $e \in E$ of minimum weight $\rightarrow E' = \{e\}$. Continue to add the edge $e \in E - E'$ of minimum weight that, when added to E', does not form a cycle. Computational complexity $=$ $O(|E|x\log|E|)$. An illustration of the algorithm is given in Figure 7.12.

7.1.10.3 Distributed algorithms

For these algorithms each node does not need complete knowledge of the topology. The MST is created in a distributed manner. The algorithm starts with one or more fragments consisting of single nodes. Each fragment selects its minimum weight outgoing edge and, using control messaging fragments, coordinates to merge with a neighboring fragment over its minimum weight

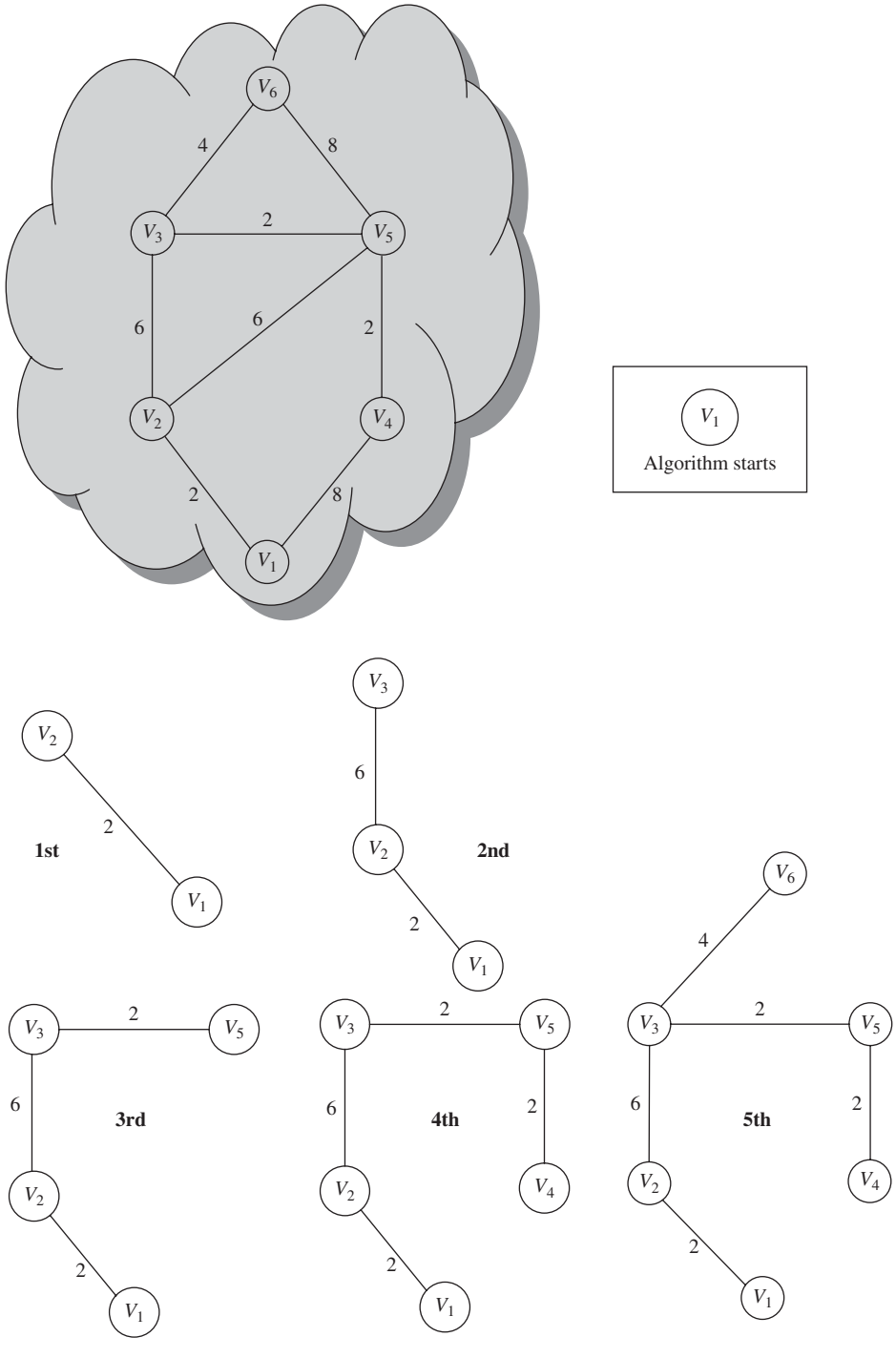

Figure 7.11 MST solution via Prim's algorithm.

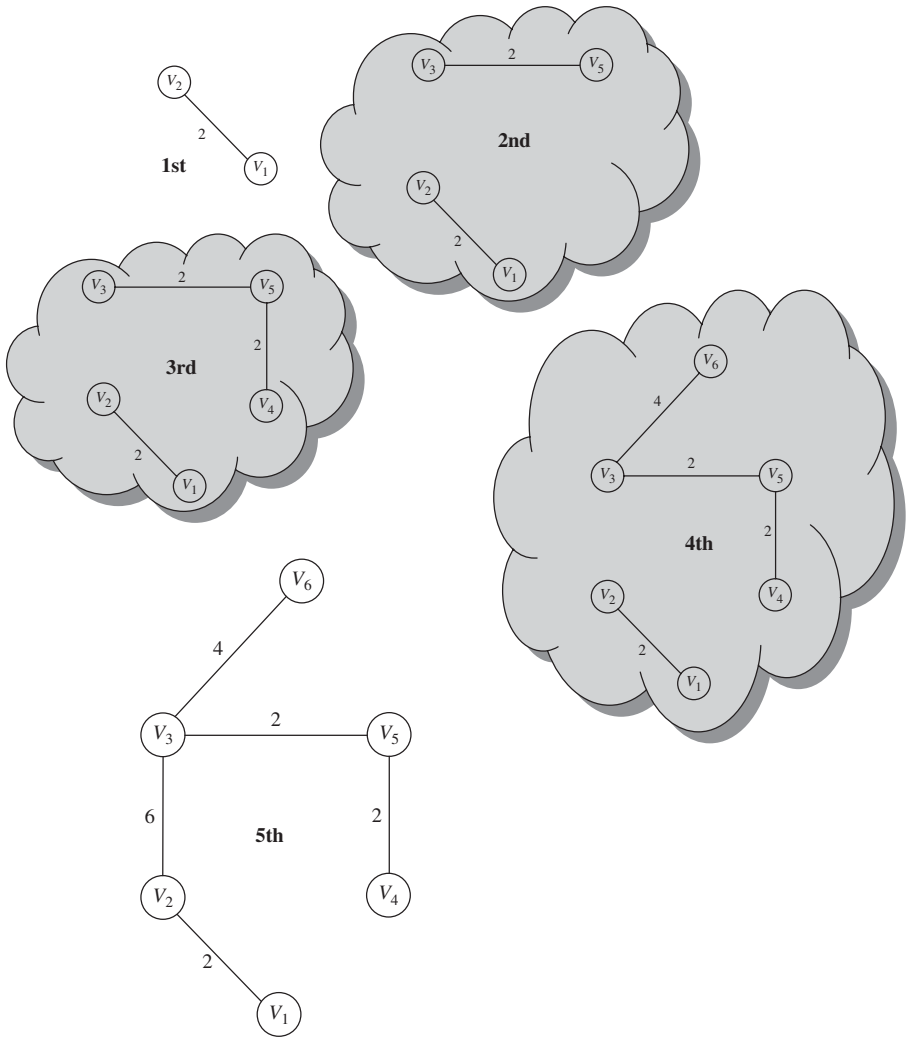

Figure 7.12 MST solution via Kruskal's algorithm.

outgoing edge. The algorithm can produce an MST in $O(|V|x|V|)$ time provided that the edge weights are unique. If these weights are not unique, the algorithm still works by using the nodes IDs to break ties between edges with equal weight. The algorithm requires $O((|V|x\log|V|) + |E|)$ message overhead. An illustration of the distributed algorithm is given in Figure 7.13.

7.1.11 Shortest path spanning tree

The shortest path spanning tree (SPST), T, is a spanning tree rooted at a particular node such that the $|V| - 1$ minimum weight paths from that node to each of the other network nodes are

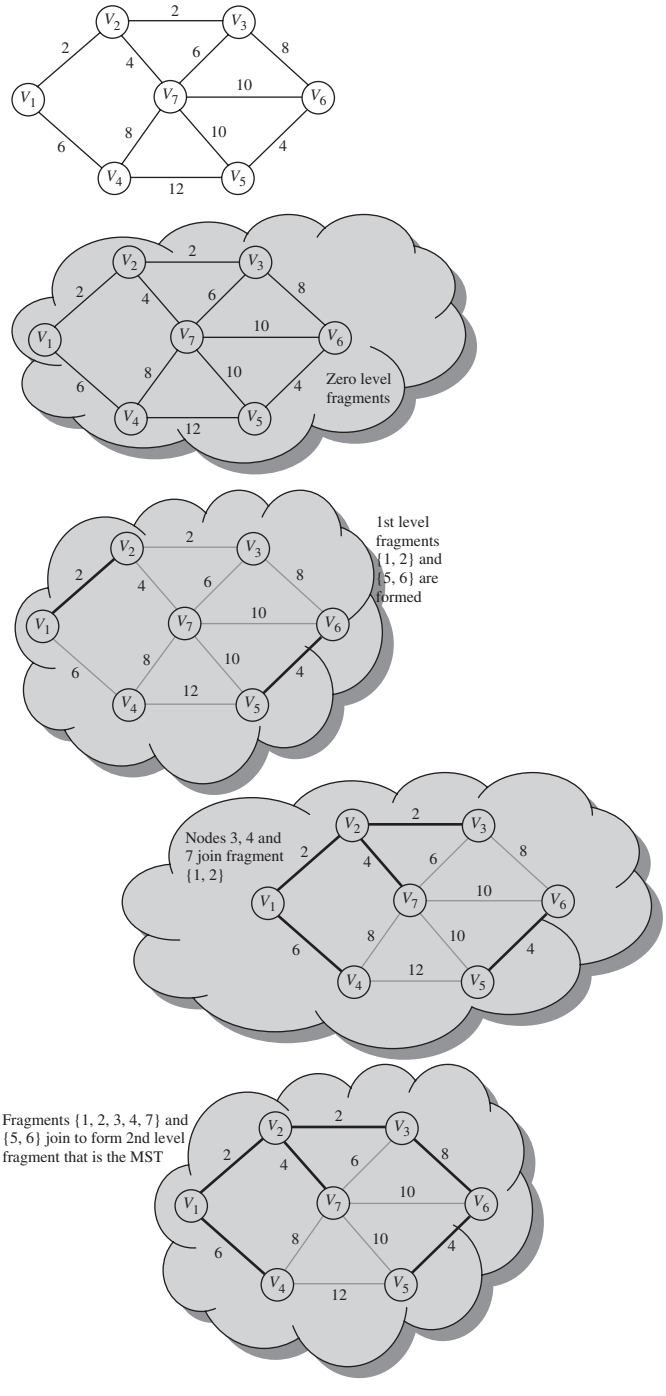

Figure 7.13 Example of the distributed algorithm.

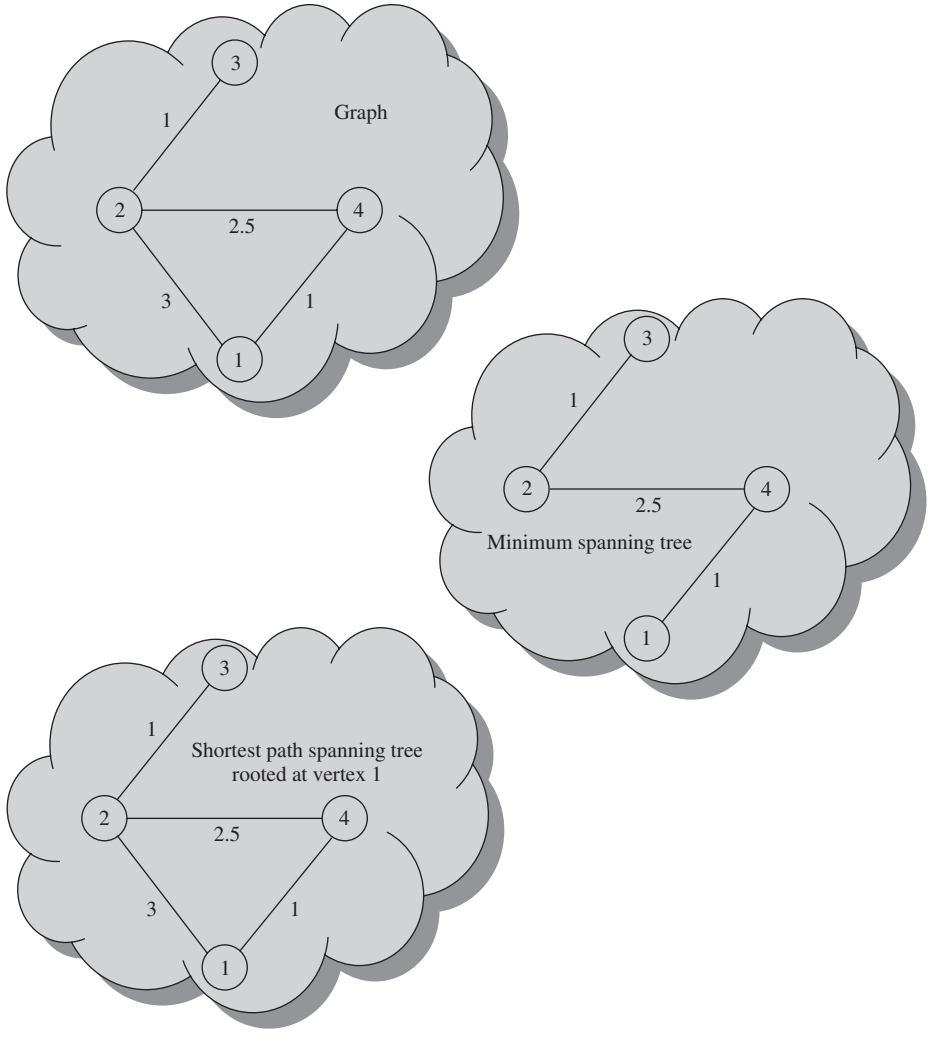

Figure 7.14 Examples of minimum spanning tree and shortest path spanning tree.

contained in T. An example of the shortest path spanning tree is shown in Figure 7.14. Note that the SPST is not the same as the MST.

SPST trees are used for unicast (one to one) and multicast (one to several) routing.

7.1.11.1 Shortest path algorithms

Let us assume nonnegative edge weights. Given a weighted graph (G, W) and a node s (*source*), a shortest path tree rooted at s is a tree T such that, for any other node $v \in G$, the path between s and v in T is a shortest path between the nodes. Examples of the algorithms that compute these shortest path trees are Dijkstra and Bellman–Ford algorithms as well as algorithms that find the shortest path between all pairs of nodes, e.g. Floyd–Marshall.

7.1.11.2 Dijkstra algorithm

For the source node s, the algorithm is described with the following steps:

$V' = \{s\}; U = V - \{s\};$
$E' = \phi;$
For $v \in U$ do
  $D_v = w(s, v);$
  $P_v = s;$
EndFor
While $U \neq \phi$ do
  Find $v \in U$ such that D_v is minimal;
  $V' = V' \cup \{v\}; U = U - \{v\};$
  $E' = E' \cup (P_v, v);$
  For $x \in U$ do
    If $D_v + w(v, x) < D_x$ then
      $D_x = D_v + w(v, x);$
      $P_x = v;$
  EndIf
  EndFor
  EndWhile

An example of the Dijkstra algorithm is given in Figure 7.15. It is assumed that $V1$ is s and D_v is the distance from node s to node v. If there is no edge connecting two nodes, x and $y \rightarrow w(x, y) = \infty$.

The algorithm terminates when all the nodes have been processed and their shortest distance to node 1 has been computed. Note that the tree computed is not a minimum weight spanning tree. A MST for the given graph is given in Figure 7.16.

7.1.11.3 Bellman–Ford algorithm

Find the shortest walk from a source node s to an arbitrary destination node v subject to the constraints that the walk consists of at most h hops and goes through node v only once. The algorithm is described by the following steps:

$D_v^{-1} = \infty \forall v \in V;$
$D_s^0 = 0$ and $D_v^0 = \infty \forall\ v \neq s, v \in V;$
$h = 0;$
Until $(D_v^h = D_v^{h-1} \forall v \in V)$ or $(h = |V|)$ do
  $h = h + 1;$
  For $v \in V$ do
    $D_v^{h+1} = \min\{D_u^h + w(u, v)\} u \in V;$
  EndFor
  EndUntil

An illustration for *Bellman–Ford Algorithm* is given in Figure 7.17(a).

7.1.11.4 Floyd–Warshall algorithm

The Floyd–Warshall algorithm finds the shortest path between all ordered pairs of nodes (s, v), $\{s, v\} v \in V$. Each iteration yields the path with the shortest weight between all pair of nodes

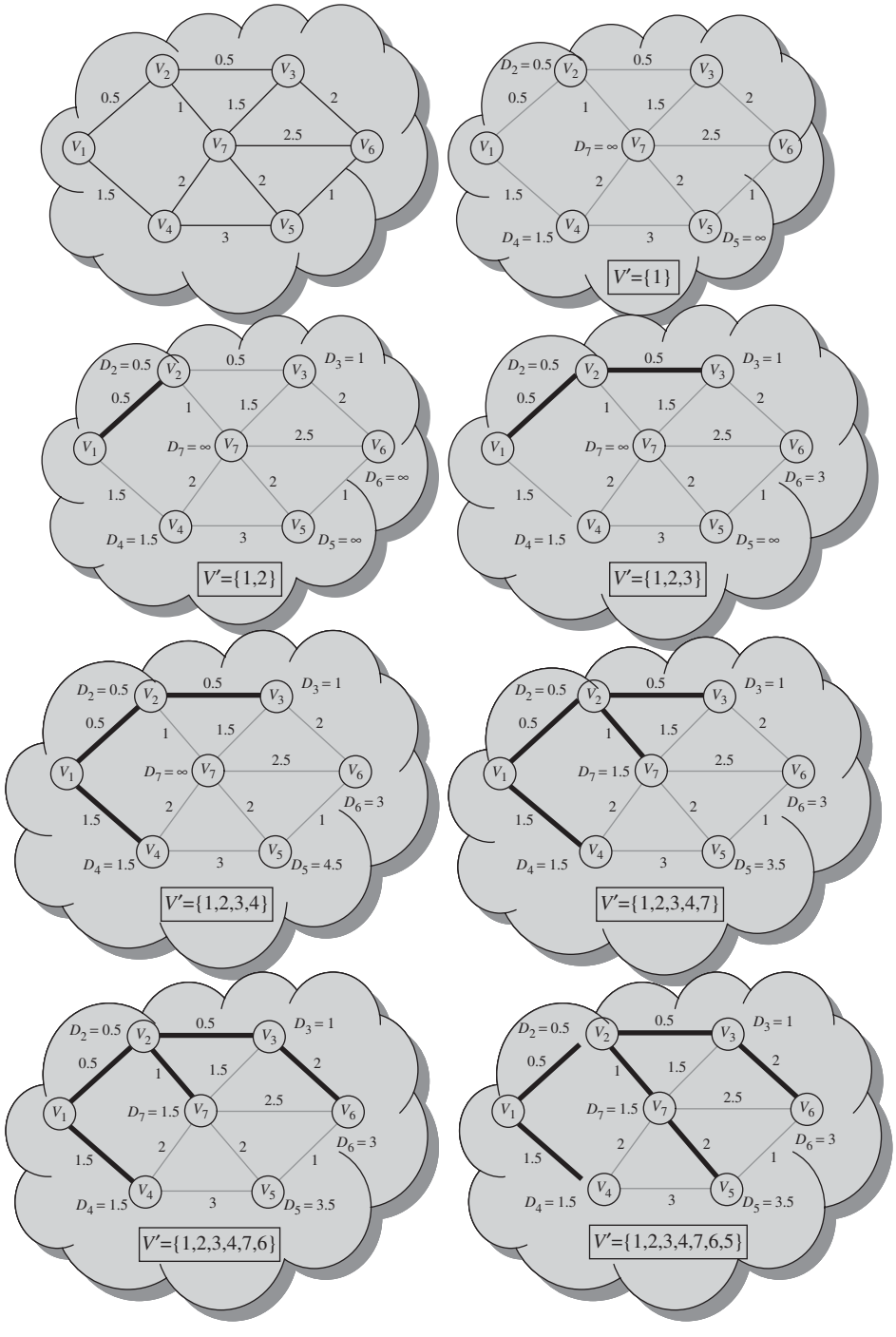

Figure 7.15 Example of Dijkstra algorithm.

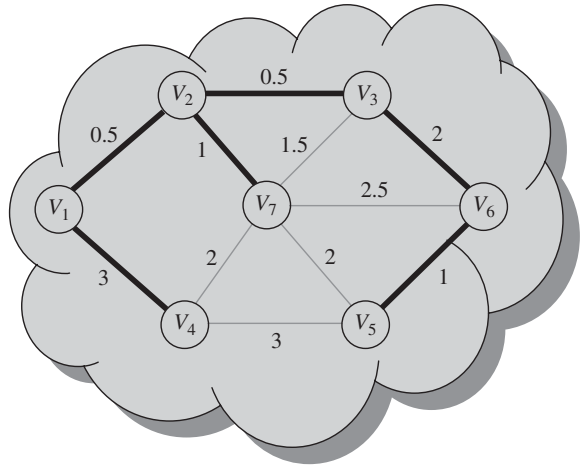

Figure 7.16 An MST for the basic graph in Figure 7.14.

under the constraint that only nodes $\{1, 2, \ldots n\}$, $n \in |V|$ can be used as intermediary nodes on the computed paths. The algorithm is defined by the following steps:

$D = W$; (W is the matrix representation of the edge weights)

For $u = 1$ to $|V|$do
For $s = 1$ to$|V|$do
For $v = 1$ to$|V|$do
$D_{s,v} = \min\{D_{s,v}, D_{s,u} + W_{u,v}\}$
EndFor
EndFor
EndFor

The algorithm completes in O($|V|^3$) time. An example of the Floyd–Warshall algorithm is given in Figure 7.17(b) with $D = W$ (W is the matrix representation of the edge weights).

7.1.11.5 Distributed asynchronous shortest path algorithms

In this case each node computes the path with the shortest weight to every network node. There is no centralized computation. The control messaging is also required for distributed computation, as for the distributed MST algorithm. Asynchronous means here that there is no requirement for inter-node synchronization for the computation performed at each node or for the exchange of messages between nodes.

7.1.11.6 Distributed Dijkstra algorithm

There is no need to change the algorithm. Each node floods periodically a control message throughout the network containing link state information. Transmission overhead is $O(|V|x|E|)$. The entire topology knowledge must be maintained at each node. Flooding of the link state information allows for timely dissemination of the topology as perceived by each node. Each node has typically accurate information to be able to compute the shortest paths.

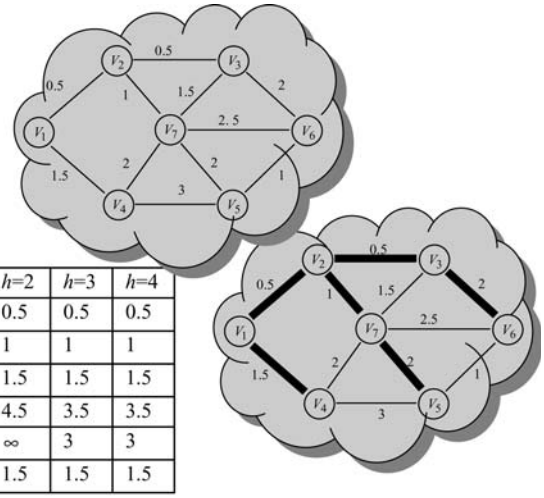

	h=1	h=2	h=3	h=4
D_2^h	0.5	0.5	0.5	0.5
D_3^h	∞	1	1	1
D_4^h	1.5	1.5	1.5	1.5
D_5^h	∞	4.5	3.5	3.5
D_6^h	∞	∞	3	3
D_7^h	∞	1.5	1.5	1.5

(a)

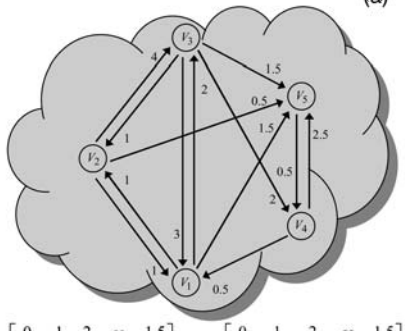

$$D_0 = \begin{bmatrix} 0 & 1 & 2 & \infty & 1.5 \\ 1 & 0 & 4 & \infty & 0.5 \\ 3 & 1 & 0 & 2 & 1.5 \\ 0.5 & \infty & \infty & 0 & 2.5 \\ \infty & \infty & \infty & 0.5 & 0 \end{bmatrix} \quad D_1 = \begin{bmatrix} 0 & 1 & 2 & \infty & 1.5 \\ 1 & 0 & 4 & \infty & 0.5 \\ 3 & 1 & 0 & 2 & 1.5 \\ 0.5 & 1.5 & 2.5 & 0 & 2 \\ \infty & \infty & \infty & 0.5 & 0 \end{bmatrix} \quad D_2 = \begin{bmatrix} 0 & 1 & 2 & \infty & .5 \\ 1 & 0 & 3 & \infty & 0.5 \\ 2 & 1 & 0 & 2 & 1.5 \\ 0.5 & 1.5 & 2.5 & 0 & 2 \\ \infty & \infty & \infty & 0.5 & 0 \end{bmatrix}$$

$$D_3 = \begin{bmatrix} 0 & 1 & 2 & 4 & 1.5 \\ 1 & 0 & 3 & 5 & 0.5 \\ 2 & 1 & 0 & 2 & 1.5 \\ 0.5 & 1.5 & 2.5 & 0 & 2 \\ \infty & \infty & \infty & 0.5 & 0 \end{bmatrix} \quad D_4 = \begin{bmatrix} 0 & 1 & 2 & 4 & 1.5 \\ 1 & 0 & 3 & 5 & 0.5 \\ 2 & 1 & 0 & 2 & 1.5 \\ 0.5 & 1.5 & 2.5 & 0 & 2 \\ 1 & 2 & 3 & 0.5 & 0 \end{bmatrix} \quad D_5 = \begin{bmatrix} 0 & 1 & 2 & 2 & 1.5 \\ 1 & 0 & 3 & 1 & 0.5 \\ 2 & 1 & 0 & 2 & 1.5 \\ 0.5 & 1.5 & 2.5 & 0 & 2 \\ 1 & 2 & 3 & 0.5 & 0 \end{bmatrix}$$

(b)

Figure 7.17(a) An illustration of the Bellman–Ford algorithm. An example of the Floyd–Warshall algorithm.

7.1.11.7 Distributed Bellman–Ford algorithm

Assume G contains only cycles of *nonnegative* weight. If $(u, v) \in E$ then so does (v, u). The updated equation is

$$D_{s,v} = \min_{u \in N(s)} \{w(s, u) + D_{u,v}\}, \forall v \in V - \{s\}$$

where $N(s)$ = neighbors of $s \rightarrow \forall u \in N(s)$, $(s, u) \in E$. Each node only needs to know the weights of the edges that are incident to it, the identity of all the network nodes and estimates (received from its neighbors) of the distances to all network nodes. The algorithm includes the following steps:

- each node s transmits to its neighbors its current distance vector $D_{s,V}$;
- likewise, each neighbor node $u \in N(s)$ transmits to s its distance vector $D_{u,V}$;
- node s updates $D_{s,v}, \forall\ v \in V - \{s\}$ in accordance with Equation (7.1);
- if any update changes a distance value then s sends the current version of $D_{s,v}$ to its neighbors;
- node s updates $D_{s,v}$ every time it receives a distance vector information from any of its neighbors;
- a periodic timer prompts node s to recompute $D_{s,V}$ or to transmit a copy of $D_{s,V}$ to each of its neighbors.

An example of distributed Bellman–Ford Algorithm is given in Figure 7.18.

7.1.11.8 Distance vector protocols

With this protocol each node maintains a routing table with entries{Destination, Next Hop, Distance (cost)}.

Nodes exchange routing table information with neighbors (a) whenever table changes; and (b) periodically. Upon reception of a routing table from a neighbor, a node updates its routing table if it finds a 'better' route. Entries in the routing table are deleted if they are too old, i.e. they are not 'refreshed' within a certain time interval by the reception of a routing table.

7.1.11.9 Link failure

A simple rerouting case is shown in Figure 7.19.

- F detects that link to G has failed;
- F sets a distance of ∞ to G and sends update to A;
- A sets a distance of ∞ to G since it uses F to reach G;
- A receives periodic update from C with 2-hop path to G (via D);
- A sets distance to G to 3 and sends update to F;
- F decides it can reach G in four hops via A.

A routing loop case is shown in Figure 7.20.

- The link from A to E fails;
- A advertises distance of ∞ to E;
- B and C had advertised a distance of 2 to E (prior to the link failure);
- upon reception of A's routing update, B decides it can reach E in three hops, and advertises this to A;
- A decides it can read E in four hops, and advertises this to C;
- C decides that it can reach E in five hops ...

Initial D_{sV}

s	A	B	C	D	E
A	0	3.5	∞	∞	0.5
B	3.5	0	0.5	∞	4
C	∞	0.5	0	1	∞
D	∞	∞	1	0	1
E	0.5	4	∞	1	0

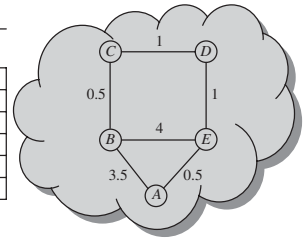

D_{sV}

s	A	B	C	D	E
A	0	3.5	∞	∞	0.5
B	3.5	0	0.5	∞	4
C	∞	0.5	0	1	∞
D	∞	∞	1	0	1
E	0.5	4	**2**	1	0

E receives D's routes and updates its s D_{sV}

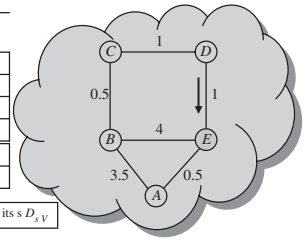

A receives B's routes and updates its D_{sV}

D_{sV}

s	A	B	C	D	E
A	0	3.5	**4**	∞	0.5
B	3.5	0	0.5	∞	4
C	∞	0.5	0	1	∞
D	∞	∞	1	0	1
E	0.5	4	**2**	1	0

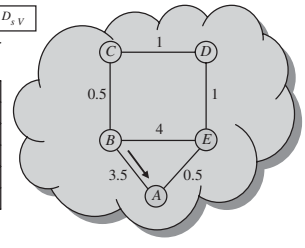

A receives E's routes and updates its D_{sV}

D_{sV}

s	A	B	C	D	E
A	0	3.5	**2.5**	**1.5**	0.5
B	3.5	0	0.5	∞	4
C	∞	0.5	0	1	∞
D	∞	∞	1	0	1
E	0.5	4	**2**	1	0

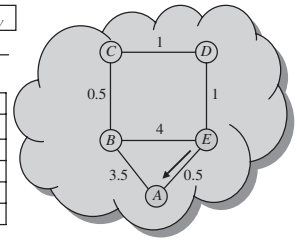

A's routing tables

Destination	Next hop	Distance
B	E	**3**
C	E	**2.5**
D	E	**1.5**
E	E	**0.5**

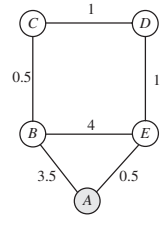

E's routing tables

Destination	Next hop	Distance
A	A	**0.5**
B	D	**2.5**
C	D	**2**
D	D	**1**

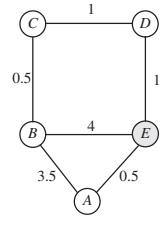

Figure 7.18 Distributed Bellman–Ford algorithm example.

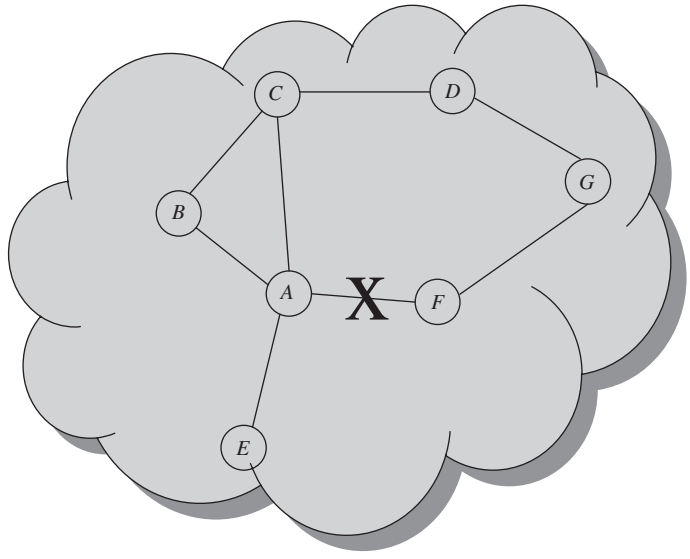

Figure 7.19 Simple rerouting case.

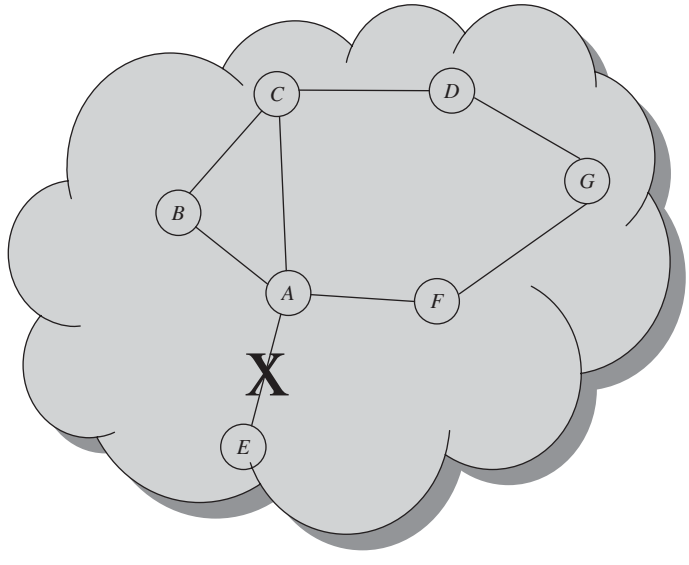

Figure 7.20 Routing loop case.

This behavior is called *count-to-infinity*. This problem is further elaborated in Figure 7.21. In the figure routing updates with distance to *A* are shown. When link from *A* to *B* fails, *B* can no longer reach *A* directly, but *C* advertises a distance of 2 to *A* and thus *B* now believes it can reach *A* via *C* and advertises it. This continues until the distance to *A* reaches infinity.

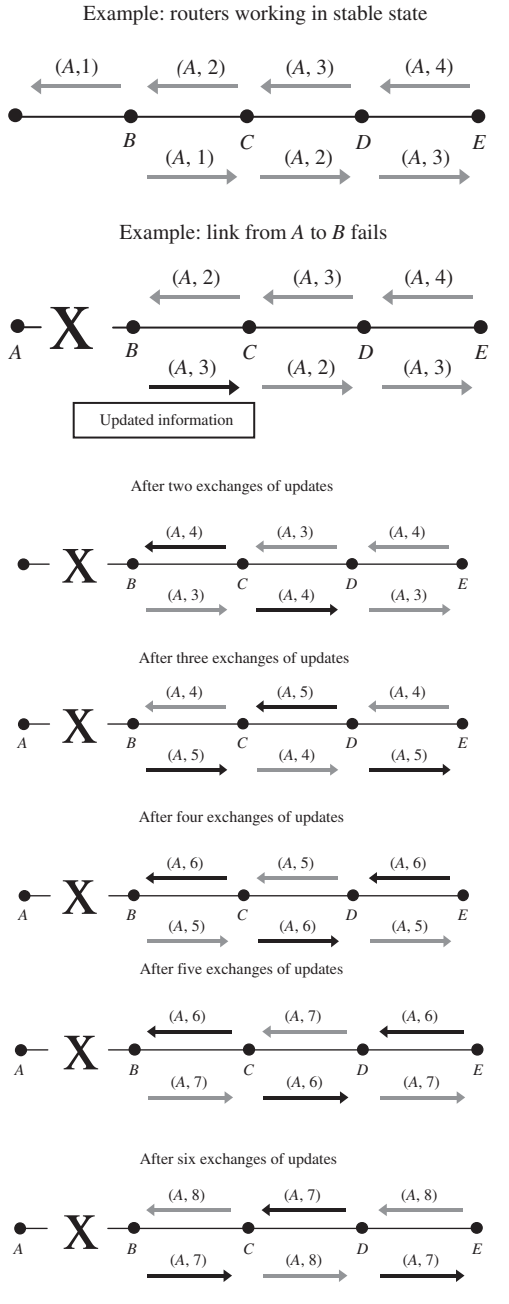

Figure 7.21 Count-to-infinity problem.

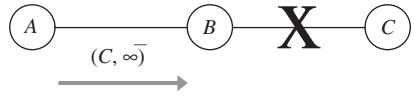

Figure 7.22 Split horizon algorithm.

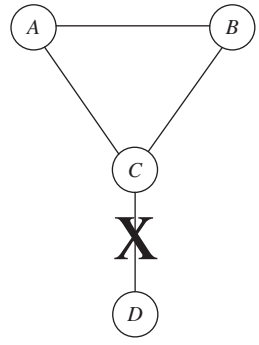

Figure 7.23 Example where split horizon fails.

7.1.11.10 Split horizon algorithm

Used to avoid (not always) the count-to-infinity problem. If A in Figure 7.22 routes to C via B, then A tells B that its distance to C is ∞. As result, B will not route to C via A if the link B to C fails. This works for two node loops, but not for loops with more than two nodes. An example where the split horizon fails is shown in Figure 7.23.

When link C to D breaks, C marks D as unreachable and reports that to A and B. Suppose A learns it first. A now thinks best path to D is through B. A reports D unreachable to B and a route of cost 3 to C. C thinks D is reachable through A at cost 4 and reports that to B. B reports a cost 5 to A who reports new cost to C, etc.

7.1.11.11 Routing information protocol

Routing information protocol (RIP) was originally distributed with BSD Unix and is widely used on the Internet (internal gateway protocol). RIP updates are exchanged in ordinary IP datagrams and RIP sets infinity to 16 hops (cost $\in$ [0–15]). RIP updates neighbors every 30 s, or when routing tables change.

7.2 GRAPH THEORY

The previous section summarized the basic relations and definitions in graph theory. A number of references that cover the graph theory in depth are available. The books [1–10] all discuss the various aspects of graph theory in general, not merely from a communication network point of view. Harary [7] has become a standard in this field. Buckley and Harary [3] provide a lot of material related to the hop distance and graph invariants defined in terms of distance properties, much of which may have applications in communications networks. Harary *et al.* [8] provide a comprehensive discussion of connectivity in directed networks. Capobianco and Molluzzo [4]

present a number of illuminative examples of relations holding among common graph invariants, such as node and edge connectivity, including counter examples which indicate the extent to which these results are best-possible.

Graph-theoretic algorithms are given good coverage in Tarjan [11] and in Evan [12, 13], but [14] is probably the best introduction to this subject. Additional references are [11–28]. Colbourn's book [18] is the only general text available at this time which covers network reliability. McHugh [22] includes a chapter on the implementation of graph algorithms for concurrent and parallel computation. Tenenbaum *et al*. [27, 28] discuss the implementation of some of these algorithms in the Pascal and C languages. See also References [19, 20] for more discussion of using data structures and graph algorithms in these computer languages. Christofides [17] discusses some important graph algorithms in much more detail, including the traveling salesman and Hamiltonian tour problems. A number of these works also treat some topics involved with flows in networks, a subject which we have not discussed so far but one which does have important applications to network connectivity, as discussed in Chapter 13 of this book (see also the article by Estahanian and Hakimi [21]).

References [29–40, 125, 126] discuss the efficiency and complexity of computer algorithms in general, not merely the graph-theoretic algorithms. Here the two books by Aho *et al*. [29, 30] and Knut's three volume series [36–38] are the best general references to the theory and practice of computer algorithms. Garey and Johnson [32] provide the best overall guide to NP-completeness and a compendium of many of those problems that were known to be NP-complete as of 1979. A problem is NP-hard if an algorithm for solving it can be translated into one for solving any other NP (nondeterministic polynomial time) problem. NP-hard therefore means 'at least as hard as any NP problem', although it might, in fact, be harder. There are now more than 1000 known NP-complete problems, many of them in graph theory, and dozens more are discovered every year, so this catalog has rapidly become out of date. As a result there is now an ongoing column on NP-complete problems by Johnson [35] which appears several times a year in the journal *Algorithms*. A number of these columns have discussed NP completeness for problems in communication networks and reliability. Hare [33] gives a very good and exceptionally readable overall account of the current state of the art in algorithmics and a good account of the problems that arise in designing and verifying algorithms for parallel processing. The book by Sedgewick [39] also comes in two other editions which give more details of the implementations of these algorithms in either Pascal or in C.

Problems concerning the statistical dependence of the network component failures are treated in References [41–48]. One should note that the assumption of independent failures can lead to either an overly pessimistic or an overly optimistic estimate of the true network reliability. The paper by Egeland and Huseby [41] gives some results as to how one might determine which of these is the case.

Most of the probabilistic measures of network connectivity lead to computability problems that are NP-hard, so there has been considerable effort in searching for restricted classes of networks for which there are reliability algorithms with a smaller order of complexity [49–59]. For example the papers by Boesch [52] and Pullen [58] consider only constant probability of edge failures. This may reduce the problem to one in graph enumeration, but this problem still has non-polynomial complexity. Similarly, the article by Bienstock [50] considers only planar networks, and he proves the existence of an algorithm whose complexity grows exponentially in the square root of p, rather than p itself. This is still very far from having polynomial growth, and to obtain that complexity even more drastic restrictions are necessary, as shown in the articles by Agrawal and Satayanarana [49] and by Politof and Satyanarayana [57]. Even very regular grid networks in the xy-plane yield NP-hard problems, as shown by the Clark and Colbourn article [54].

Owing to the computational intractability of the network reliability calculations for general probabilistic graphs, there are many papers devoted to the problem of obtaining bounds and approximations of the reliability [60–70]. For the same reason Monte Carlo simulations are also

used in this field [71–77]. The NCF (node connectivity factor) and the LCF (link connectivity factor) were introduced in References [78–84] as possible alternatives to the usual reliability measure. They are indicators of how close the network is to being totally disconnected. Unfortunately, the NCF at least is computationally difficult to compute and does not seem to be amenable to simplifying techniques such as factorization or edge reduction used by other methods. Thus it is not yet clear how useful a concept this will prove to be, although if these connectivity factors are available they can be used to identify the most vulnerable components of the network and to adapt the network so as to equalize the vulnerability over its components. References [85–98] are concerned with some aspects of graph connectivity other than the usual path-oriented one, primarily with those deriving from the notion of the diameter of a graph (i.e. the maximum node-to-node hop distance across the graph) or the average node-to-node hop distance. Of special interest here is the notion of leverage, as described in the papers of Bagga *et al*. [85], which is a general method of quantifying changes in graph invariants due to the loss of some network components.

A number of references [99–111] are concerned with a number of other graph invariants that have an obvious connection with the notions of vulnerability and survivability of communications networks. The main concepts here are those of dominance, independence and covering of a graph with respect to either a set of nodes or a set of edges of the underlying graph. These quantities have already been applied to problems involving networks used in scheduling and service facilities, although their applications and usefulness to communications networks remains to be determined. Also, the calculation of some of these quantities can be NP-hard (some in the deterministic sense, others from the probabilistic point of view). This is also an area of very active research.

7.3 ROUTING WITH TOPOLOGY AGGREGATION

The goal of QoS routing is to find a network path from a source node to a destination node which has sufficient resources to support the QoS requirements of a connection request. The execution time and the space requirement of a routing algorithm increase with the size of the network, which leads to the scalability problem. For very large networks, it is impractical to broadcast the whole topology to every node for the purpose of routing. In order to achieve scalable routing, large networks are structured hierarchically by grouping nodes into different domains [113, 114]. The internal topology of each domain is then aggregated to show only the cost of routing across the domain, that is, the cost of going from one *border node* (a node that connects to another domain) to another border node. This process is called *topology aggregation*. One typical way of storing the aggregated topology is for every node to keep detailed information about the domain that it belongs to, and aggregated information about the other domains.

Since the network after aggregation is represented by a simpler topology, most aggregation algorithms suffer from distortion, that is, the cost of going through the aggregated network deviates from the original value [115]. Nevertheless, Hao and Zegura [116] showed that topology aggregation reduces the routing overhead by orders of magnitude and does not always have a negative impact on routing performance. Some aggregation approaches have been proposed. Lee [117] presented algorithms that find a minimum distortion-free representation for an *undirected* network with either a single additive or a single bottleneck parameter. Examples of additive metrics are delay and cost, while an example of a bottleneck parameter is bandwidth. For an additive constraint, it may require $O(|B|^2)$ links to represent a domain in the distortion-free aggregation, where $|B|$ is the number of border nodes in the domain. Awerbuch and Shavitt [118] proposed an algorithm that aggregates *directed* networks with a single additive parameter using $O(|B|)$ links. The algorithm achieves bounded distortion with a worst-case distortion factor of $O(\sqrt{\rho}\log|B|)$, where ρ is the *network asymmetry constant*, defined as the maximum ratio between the QoS parameters of a pair of opposite directed links.

In this section, we discuss networks with two QoS parameters, *delay* and *bandwidth*. Some related work can be found in References [119]–[121]. Lee [117] presented an aggregation method that aggregates an undirected delay-bandwidth sensitive domain into a spanning tree among border nodes. Therefore, there is a unique path between each pair of border nodes after aggregation and the space complexity is $O(|B|)$. The paper showed that a spanning tree can provide a distortion-free aggregation for bandwidth, but not for delay. Iwata *et al.* [120] studied the problem of topology aggregation in networks of six different QoS parameters. The aggregated topology follows the ATM PNNI standard [113]. The authors proposed minimizing the distortion by using a linear programming approach. Both References [117] and [118] assumed certain precedence order among the parameters, so that, among several paths that go between the same pair of border nodes, one path can be selected as the 'best'. The state of a path in a delay-bandwidth sensitive network can be represented as a delay-bandwidth pair [121]. If there are several paths going across a domain, a single pair of values, which is a point on the delay-bandwidth plane, is not sufficient to capture the QoS parameters of all those paths [122].

Korkmaz and Krunz [121] was the first to use a curve on the delay-bandwidth plane to approximate the properties of multiple physical paths between two border nodes, without assuming any precedence among the parameters. A curve is defined by three values: the minimum delay, the maximum bandwidth, and the smallest stretch factor among all paths between two border nodes. The stretch factor of a path measures how much the delay and the bandwidth of the path deviate from the best delay and the best bandwidth of all paths. The curve provides better approximation than a single point, but this approach has several shortcomings. First, the paper did not provide a routing algorithm with polynomial complexity to *find* a feasible path based on the aggregated topology. Instead, it provided an algorithm to *check* if a given path is likely to be feasible. Essentially, the algorithm determined whether the point, defined by the delay/bandwidth requirement, is within the curve defined by the delay, bandwidth and stretch factor of the path. Second, although the paper provided an aggressive heuristic to find the stretch factor of an interdomain path, there are cases where only one QoS metric will contribute to the value, and the information about the other metric is lost. In this section, we discuss a way of representing the aggregated state in delay-bandwidth sensitive networks using line segments. The approach solves some problems in Korkmaz and Krunz [121] and other traditional approaches by introducing a specific QoS parameter representation, a specific aggregation algorithm and the corresponding routing protocol. The algorithm outperforms others due to smaller distortion.

7.4 NETWORK AND AGGREGATION MODELS

A large network consists of a set of domains and links that connect the domains. It is modeled as a directed graph, where link state can be asymmetric in two opposite directions. Figures 7.24 and 7.25 are examples of a network with four domains. There are two kinds of nodes in a domain. A node is called a *border node* if it connects to a node of another domain. A node is an *internal node* if it is not a border node. A domain is modeled as a tuple (V, B, E), where V is the set of nodes in the domain, $B \subseteq V$ is the set of border nodes, and E is the set of directed links among the nodes in V. The entire network is modeled as (G, L), where $G = \{g_i | g_i = (V_i, B_i, E_i), 1 \leq i \leq \eta\}$ is the set of domains, L is a set of links that connect border nodes of different domains, and η is the number of domains in G.

There are several aggregation models for large networks. In this section, we use the topology aggregation model proposed by the private network–network interface (PNNI) [113, 123]. One of the representative topologies in PNNI is the *star* topology. Other popular ones are *simple-node* and *mesh*. In a simple-node topology, a domain is collapsed into one virtual node. This offers the greatest reduction of information as the space complexity after aggregation is $O(1)$, but the

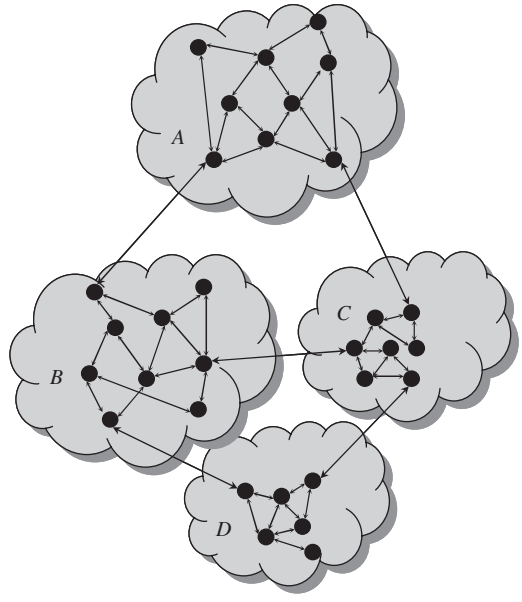

Figure 7.24 Network example.

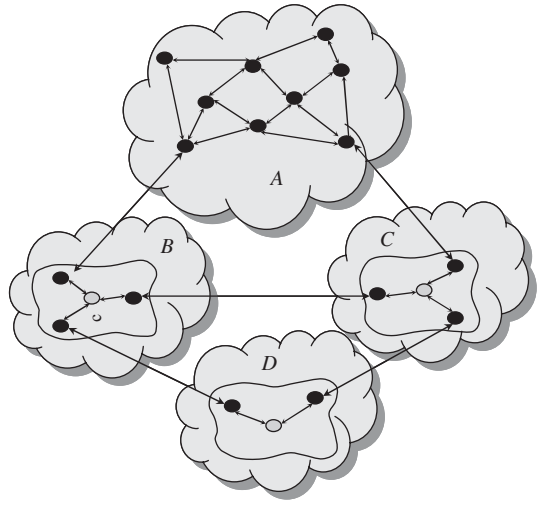

Figure 7.25 Aggregated network from Figure 7.24 with a complete view of domain A.

distortion is large. The mesh topology is a complete graph among the border nodes. The complexity of this topology is $O(|B|^2)$ and its distortion is much smaller. The star topology is a compromise between the above two. It has a space complexity of $O(|B|)$ and the distortion is between those of a simple node and a mesh. Guo and Matta [124] compare the performances of the above three aggregation methods.

It shows that the star topology outperforms the simple node and performs slightly worse than the mesh in a uniform network. Let us consider the domain in Figure 7.26(a), where nodes a, b, c and

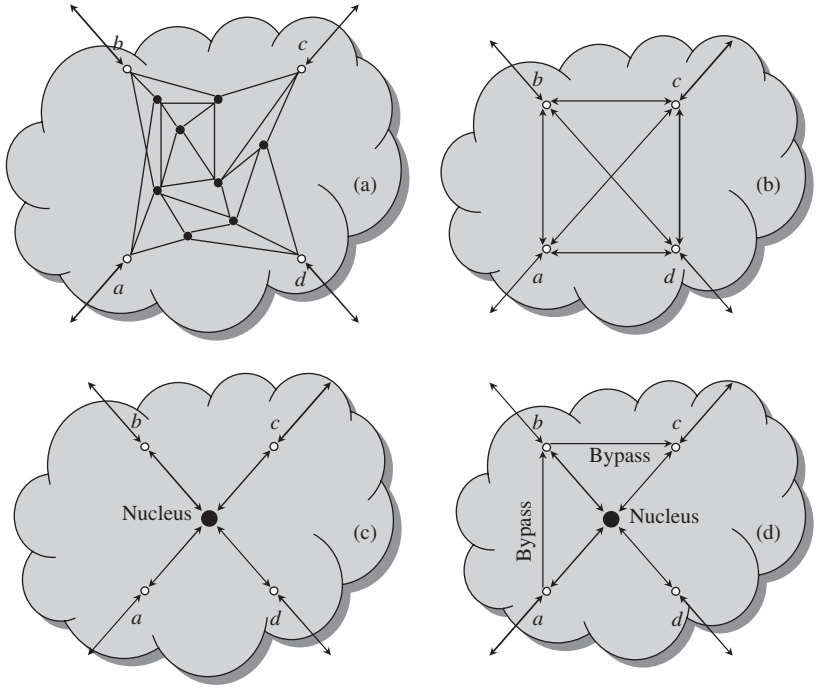

Figure 7.26 Topology aggregation. (a) Domain F. (b) Mesh of the borders. (c) Star representation. (d) Star representation with bypasses.

d are the border nodes. The mesh aggregation is shown in Figure 7.26(b), and the star aggregation is shown in Figure 7.26(c). In a star topology, the border nodes connect via links to a virtual *nucleus*. These links are called *spokes*. Each link is associated with some QoS parameters. To make the representation more flexible, PNNI also allows a limited number of links connected directly between border nodes. These links are called *bypasses*. Figure 7.26(d) is an example of a star with bypasses. We call the links in an aggregated topology *logical links* since they are not real.

After aggregation, a node in a domain sees all other nodes in the same domain, but only aggregated topologies of the other domains. For example, for the network in Figure 7.24, the aggregated view of the network stored at a node in domain A is shown in Figure 7.25. In such a view, the topology of domain A is exactly the same as the original one but the topologies of the other domains are now represented by border nodes, nuclei and spokes (without bypasses in this example). For a large network, this aggregated view is significantly smaller than the original topology and thus scalability is achieved. However, for the purpose of QoS routing, it is extremely important to develop solutions on how to represent the state information in this aggregated topology and how to control the information loss due to aggregation.

7.4.1 Line segment representation

In this section, we discuss a line-segment representation for the aggregated state information. Given the original topology and a (D, W) representing (delay, bandwidth) pair for each link, we shall first transform every domain to a mesh among the border nodes as an intermediate computation step, and then transform the mesh to a star with bypasses. The state information of a logical link in either the mesh or the final star is represented by line segments, which will be discussed in depth shortly.

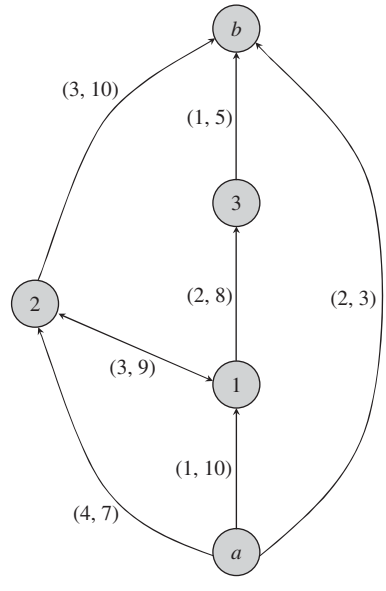

Figure 7.27 Multiple paths.

A mesh among the border nodes is a complete graph with logical links connecting each pair of border nodes [see Figure 7.26(b)]. A logical link may represent multiple physical paths. For example, in Figure 7.27, there are five paths going from border node a to border node b. One possible path is $a \rightarrow 1 \rightarrow 3 \rightarrow b$. The end-to-end QoS parameter of this path is (4, 5).We can find the parameters of all other paths and they are (7, 9), (10, 5), (2, 3), and (7, 7). *The equivalent delay is obtained as a sum of the delays on the path and equivalent bandwidth as a minimal value of the bandwidth among the individual segments.* When a logical link is used to represent all these paths, the QoS parameter of the link should be the 'best' parameter among the paths. However, the 'best' QoS parameter may not be defined since there does not exist an absolute order among those pairs. For example, parameter (2, 3) is better than parameter (7, 7) in terms of delay, but not in terms of bandwidth. Fortunately, a partial order can be developed.

By definition a point (x, y) is more representative than a point (x', y') if

- they are not the same, i.e. either $x \neq x'$ or $y \neq y'$; and
- $x \leq x'$ and $y \geq y'$.

Since the QoS parameter is a pair of values that represents a point on the delay-bandwidth plane, we often use *parameter*, *pair* and *point* interchangeably. In the previous example, (7, 9) is more representative than (10, 5) since $7 \leq 10$ and $9 \geq 5$.

Also, by definition, for a given set (S) of points on the delay-bandwidth plane, $(x, y) \in S$ is a representative of S if there does not exist any other point $(x', y') \in S$ which is more representative than (x, y). This means that $\forall(x', y') \in S$, $x < x'$ or $y > y'$. As an example let S be the set of the delay-bandwidth QoS pairs of the physical paths from a to b in Figure 7.27 [112]:

$$S = \{(4, 5), (7, 9), (10, 5), (2, 3), (7, 7)\}$$

Where (2, 3) is a representative of S, since its delay is less than all other points in S. The other representatives are (4, 5) and (7, 9). All QoS points in S on a delay-bandwidth plane are plotted in Figure 7.28. The shaded area defines the region of *supported services*, that is, any QoS request that

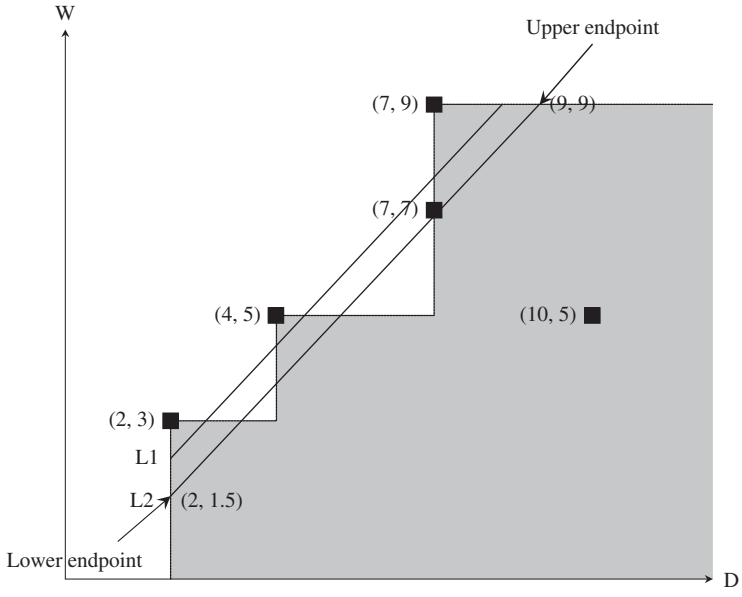

Figure 7.28 Representatives from example. (Reproduced by permission of IEEE [112].)

falls in that region can be supported by a physical path. The dotted line is a staircase rising from left to right. The representatives are points on the convex corners of the steps. The corresponding paths of the representatives are called nondominated paths or Pareto optimal paths in the literature. The size of S depends on how many physical paths there are between the pair of border nodes, which can be exponential. The number of representative points is $|E|$ in the worst case for a domain (V, B, E). That is because there are at most $|E|$ possible bandwidth values for the paths in the domain and thus the staircase can have at most $|E|$ convex corners.

For the purpose of scalability, it is desirable to reduce the memory space for storing the QoS parameter of a logical link to $O(1)$. Hence, we shall neither store all QoS points in S nor store all representative points. The traditional way to solve this problem is to keep only one QoS point per logical link. However, no matter which point we pick, much information is lost.

A possible solution for this problem is to use a line segment that approximates the staircase, e.g. L_1 or L_2 (Figure 7.28). Since every line segment can be defined unambiguously by two endpoints, the space needed for a logical link is $O(1)$. The line segment representation strikes a tradeoff between the accuracy in approximating the staircase and the overhead incurred.

After a line segment is chosen, all connection requests that fall under the line segment are accepted. However, it should be pointed out that not all requests under the line segment can actually be supported. For example, in Figure 7.28, if L_1 is selected to approximate the staircase, then the unshaded areas below L_1 represent connection requests that are accepted but not supported by any physical path. When a request is accepted but not supported, the routing process will detect it, and the request will eventually be rejected if a feasible path cannot be found (see the next section). On the other hand, when we reject the connection requests that are above the line segment, we may reject the supported QoS. For example, if a connection request is in the shaded region above L_1 in Figure 7.28, it is rejected although it can be served. Therefore, the choice of line segment depends on the strictness of the desired quality of the service. For instance, in Figure 7.28, both L_1 and L_2 are possible line segments. Using L_2 would probably reject more supported connection requests than L_1, while using L_1 would accept more unsupported requests than L_2. The least square method

is used to find a line segment, which takes linear time with respect to the number of representative points. This line segment minimizes the least-square error, i.e. the summation of the squares of the distances from the points to the line.

It was mentioned earlier that any line segment can be defined by two endpoints. Owing to the nature of the staircase, the line always has a nonnegative slope. The endpoint with smaller bandwidth is called the *lower endpoint*, while the other one is called the *upper endpoint*. So a line segment is denoted as [*lower endpoint*, *upper endpoint*]. For example, L_2 in Figure 7.28 is [(2, 1.5), (9, 9)]. We further denote the lower endpoint and the upper endpoint of a line segment l as $l.lp$ and $l.up$, respectively. The delay of a point p is $p.d$ and the bandwidth of a point p is $p.w$. Therefore, is $L_2.lp.d$ is 2 and $L_2.up.w$ is 9. Two operations for line segment parameters are defined. The first operation is the *joint* '+' and *disjoint* '−' operation, defined as

$$\begin{aligned}&[(a,\ b),(c,\ d)]+\left[(a',\ b'),(c',\ d')\right]=\\&\left[(a+a',\ \min(b,\ b')),(c+c',\ \min(d,\ d'))\right]\end{aligned} \tag{7.1}$$

$$\begin{aligned}&[(a,\ b),(c,\ d)]-\left[(a',\ b'),(c',\ d')\right]=\\&\left[(a-a',\ \min(b,\ b')),(c-c',\ \min(d,\ d'))\right]\end{aligned} \tag{7.2}$$

In other words, summing two segments results in a segment whose delay is the sum of the delays of the individuals segments and the bandwidth equals the minimum of the two bandwidths. If l_1, l_2 and l_3 are three line segments and they satisfy the following conditions:

$$\begin{aligned}&l_1.lp.d \geq l_2.lp.d \quad \text{and} \quad l_1.up.d \geq l_2.up.d\\&l_1.lp.w \leq l_2.lp.w \quad \text{and} \quad l_1.lp.w \leq l_2.lp.w\\&l_1 - l_2 = l_3\end{aligned} \tag{7.3}$$

then

$$l_1 = l_2 + l_3 \tag{7.4}$$

As an example let $l_1 = [(10, 4), (13, 7)]$ and $l_2 = [(6, 5), (11, 7)]$. One can see that for this example $l_1.lp.d \geq l_2.lp.d$, $l_1.up.d \geq l_2.up.d$, $l_1.lp.w \leq l_2.lp.w$ and $l_1.lp.w \leq l_2.lp.w$. and we have

$$\begin{aligned}l_1 - \ l_2 &= [(10,\ 4),(13,\ 7)]\ -[(6,\ 5),(11,\ 7)]\\&= [10-6,\ \min(4,\ 5),(13-11,\ \min(7,\ 7))]\\&= [(4,\ 4),(2,\ 7)]\end{aligned} \tag{7.5}$$

$$\begin{aligned}l_2 + l_3 &= l_2 + [(4,\ 4),(2,\ 7)] = [(6,\ 5),(11,\ 7)] + [(4,\ 4),(2,\ 7)]\\&= [6+4,\ \min(5,\ 4),\ (11+2,\ \min(7,\ 7))]\\&= [(10,\ 4),\ (13,\ 7)]\ = l_1\end{aligned} \tag{7.6}$$

7.4.2 QoS-aware topology aggregation

The topology aggregation algorithm consists of two phases: (1) find a line segment for each logical link in the mesh (complete graph) of the border nodes; and (2) construct a star topology with bypasses from the mesh.

7.4.3 Mesh formation

In this phase, representatives of the paths between each pair of border nodes are found. The representatives for each pair of border nodes can be obtained by running the Dijkstra's algorithm for

every link bandwidth value. The links in the domain are first sorted out by descending bandwidths. Let the largest bandwidth be $w_{\max}$. The algorithm starts by finding the smallest delay $d_{\max\_w}$ in a graph that consists of only links of bandwidth $w_{\max}$. The pair $(d_{\max\_w}, w_{\max})$ is a representative that has the largest bandwidth. The algorithm then inserts the links of the next largest bandwidth value (w') and finds the smallest delay d'. If $d < d_{\max\_w}$, (d', w') is another representative. The process ends after the smallest delays for all bandwidth values are identified. The detailed algorithm of finding the representatives can be found in References [125] and [126]. After the representatives are found, linear regression is used to find the line segment for each pair of border nodes.

7.4.4 Star formation

The next step is to aggregate the mesh into a star topology with bypasses. According to the recommendation of PNNI, a default parameter value to spokes can be set. There can be one or more spokes of the default parameter value but at most $3|B| - 1$ links can be of other values. As it is possible that all links in our aggregation are of different values, we shall put at most $3|B|$ links in the domain topology after aggregation.

Let i and j be two border nodes and n be the nucleus in the star representation. If there is no bypass between i and j, the only path from i to j is $i \rightarrow n \rightarrow j$ in the star. The goal in this phase is to find the QoS parameters of links $i \rightarrow n$ and $n \rightarrow j$, such that the line segment of $i \rightarrow n \rightarrow j$ in the star is the same as the line segment of $i \rightarrow n$ in the mesh. Basically, a single link in the mesh has to be 'split' into two links $i \rightarrow n$ and $n \rightarrow j$ in the star. There are three steps in this phase: (1) find the spokes from the border nodes to nucleus; (2) find the spokes from the nucleus to the border nodes; and (3) find the bypasses between border nodes.

7.4.4.1 Spokes incoming to the nucleus

In order to distinguish the line segments in the mesh from those in the star, superscript 'm' is used for mesh and 's' for star. For instance, let us consider a line segment from i to j. If it is in the mesh, it is denoted l_{ij}^{m}; if it is in the star, it is denoted l_{ij}^{s}.

In order to find spokes, we have to 'break' the line segments in the mesh. From the definition of the joint operation, we have a general idea what the 'broken' line segments look like. The endpoint delays of the spokes l_{in}^{s} and l_{nj}^{s} should be smaller than those of l_{ij}^{m}, while the endpoint bandwidths of the spokes should not be smaller than those of l_{ij}^{m}. The algorithm of finding spokes from border node to nucleus is based on these observations.

Recall that the lower endpoint and the upper endpoint of a line segment l are denoted $l.lp$ and $l.up$, respectively. Given a point p, its delay and bandwidth are denoted as $p.d$ and $p.w$, respectively. The algorithm that finds *spokes incoming to the nucleus* is defined as

$$l_{in}^{\mathrm{s}} = [(\min\_ld,\ \max\_lw), (\min\_ud,\ \max\_uw)] \tag{7.7}$$

where

$$\begin{aligned} \min\_ld &= \min_{j \in B, j \neq i} \left\{ l_{ij}^{\mathrm{m}}.lp.d \right\} \\ \min\_ud &= \min_{j \in B, j \neq i} \left\{ l_{ij}^{\mathrm{m}}.up.d \right\} \\ \max\_lw &= \max_{j \in B, j \neq i} \left\{ l_{ij}^{\mathrm{m}}.lp.w \right\} \\ \max\_uw &= \max_{j \in B, j \neq i} \left\{ l_{ij}^{\mathrm{m}}.up.w \right\} \end{aligned} \tag{7.8}$$

An example of the program calculating Equation (7.7) can be found in Lui *et al.* [112].

7.4.4.2 Spokes outgoing from the nucleus

Up to this point, we know the mesh, and we also know the set of spokes from borders to the nucleus, which is denoted $S_{b\to n}$. More specifically, we know l^{m}_{ij} as well as l^{s}_{in}, and we want to find l^{s}_{nj}, such that the result of joining l^{s}_{in} and l^{s}_{nj} is l^{m}_{ij}. Since $l^{\mathrm{m}}_{ij}.lp.d \geq l^{\mathrm{s}}_{in}.lp.d$, $l^{\mathrm{m}}_{ij}.up.d \geq l^{\mathrm{s}}_{in}.up.d$, $l^{\mathrm{m}}_{ij}.lp.w \leq l^{\mathrm{s}}_{in}.lp.w$, and $l^{\mathrm{m}}_{ij}.up.w \leq l^{\mathrm{s}}_{in}.up.w$, we can obtain l^{s}_{nj} by evaluating $l^{\mathrm{m}}_{ij} - l^{\mathrm{s}}_{in}$, according to Equation (7.3). However, for the same j, $l^{\mathrm{m}}_{ij} - l^{\mathrm{s}}_{in}$ may be different for different i. Since we can have at most one l^{s}_{nj}, we solve this problem by assigning l^{s}_{nj} the average of $l^{\mathrm{m}}_{ij} - l^{\mathrm{s}}_{in}$, for all $i \in B$, $i \neq j$.

7.4.4.3 Finding bypasses

Owing to the aggregation, $l^{\mathrm{s}}_{ij} = l^{\mathrm{s}}_{in} + l^{\mathrm{s}}_{nj}$ may no longer be the same as l^{m}_{ij} in the mesh. Some may deviate only a little, while others may be quite different. In order to make the aggregation more precise, bypasses are introduced, which are direct links between border nodes . When $l^{\mathrm{s}}_{in} + l^{\mathrm{s}}_{nj}$ deviates a lot from l^{m}_{ij}, a bypass between border nodes i and j is used, and the QoS parameters of the paths from i to j are defined by the bypass instead of $l^{\mathrm{s}}_{in} + l^{\mathrm{s}}_{nj}$. Since there are $2\,|B|$ spokes ($|B|$ outgoing from and $|B|$ incoming to the nucleus), $|B|$ bypasses can be used in the network according to the recommendation of the PNNI standard. Only bypasses between those $|B|$ pairs of border nodes that have the largest deviations are used.

7.4.5 Line-segment routing algorithm

In this segment the line-segment routing algorithm (LSRA) is presented. It is a QoS-based source routing algorithm, which integrates the line segment representation with Dijkstra's algorithm (DA) and the centralized bandwidth-delay routing algorithm (CBDRA) [125, 127]. DA is the fastest known algorithm for finding the least-delay paths. CBDRA first prunes all links that do not satisfy the bandwidth requirement and then applies DA to find the least-delay path. LSRA extends the idea to capitalize the additional information provided by the line segment representation.

Being a centralized routing protocol, LSRA requires that each node keeps the topology of its own domain and the *star-with-bypasses* aggregation of the other domains. As broadcasting takes a lot of time and bandwidth, it is desirable to keep the amount of broadcasted information small. This justifies why the aggregation is a star with bypasses of $O(|B|)$ space instead of a mesh of $O(|B|^2)$ space. Routing is performed at two levels: *interdomain routing* and *intradomain routing*. An interdomain routing path specifies the border nodes of the transit domains, and the intradomain routing finds the subpath within each transit domain. Accordingly, LSRA has two routing phases.

7.4.5.1 Interdomain routing

After obtaining the star-with-bypasses aggregation from the external domains, each node can see all nodes in its own domain and all border nodes of the other domains. There are five steps in the LSRA interdomain routing:

(1) *transform stars with bypasses to meshes* – since nuclei of stars are virtual, the actual routing paths should not include any nucleus;

(2) *prune logical links* – this step prunes the logical links that do not satisfy the bandwidth requirement;

(3) *determine the delays of logical links* – the delay value, supported by a line segment, is a function of the bandwidth requirement; this step determines the delay values of all logical links under the bandwidth requirement;

(4) *prune physical links* – this step prunes the physical links that do not satisfy the bandwidth requirement;

(5) *apply DA on the network* – this step uses DA to find a shortest-delay path to the destination domain.

7.4.5.2 Intradomain routing

After the interdomain routing, an interdomain path is determined. The source node knows how to traverse the nodes in its own domain to a border node, and how to traverse the border nodes of other domains to get to the destination domain. Because the source node does not have the detailed topology of any external domain, it does not know how to fill in the intradomain path segments across the external domains. Therefore, LSRA does the intradomain routing in a distributed fashion. A routing message is sent from the source to travel along the interdomain path. When a border node t of domain g receives the message and the next hop on the interdomain path is another border node t' of g, t locally computes the intradomain path going from itself to t' using CBDRA, since t has the complete knowledge about its own domain g. Node t inserts the intradomain path into the interdomain path that is carried by the message. Then the message is sent to t' along the intradomain path. The message also keeps track of the accumulated delay of the path that has been traversed so far, including the intradomain path segments. This accumulated delay is calculated from the actual link delays as the message travels. If the accumulated delay exceeds *req(d)* the message is forwarded back to the previous node to find an alternate path. This is called *crankback* [113]. If the message successfully reaches the destination node, a feasible path is found.

One should be aware that the expected path delay may be different from the actual path delay due to the network dynamics or the inaccuracy introduced by aggregation. If no intradomain path can be found without violating *req(d)*, the message is sent back to the source to reject the request.

7.4.5.3 Best point algorithm

In this case the best delay and the best bandwidth are used to represent a mesh link. For example, if the delay-bandwidth parameters between a border pair are (2, 3), (4, 4), and (5, 6), then (2, 6) is used to represent the QoS of the mesh link. This optimistic approach is aggressive by choosing the best delay and the best bandwidth that may come from different paths. It suffers from large crankback ratios defined in the sequel. A best point (BP) mesh can be aggregated to a BP star by taking the maximum bandwidth among the mesh links as the spoke bandwidth and by taking half of the average delay among the mesh links as the spoke delay.

7.4.5.4 Worst point

The worst delay and the worst bandwidth are used to represent a mesh link. That is, if the parameters are (2, 3), (4, 4) and (5, 6), then (5, 3) is used. As a result, this algorithm has low success ratios. The minimum bandwidth and average of half of the average delay are used for aggregating a worst point (WP) mesh to a WP star.

7.4.5.5 Modified Korkmaz–Krunz

This is a modified version of the algorithm presented in Korkmaz and Krunz [121], the MKK algorithm. Let us consider a set of delay-bandwidth parameters, which corresponds to a set of paths between two border nodes. The *stretch factor* of a parameter (d, w) is defined as $d/d_{\text{best}} + w_{\text{best}}/w$,

where d_{best} and w_{best} are the best delay and the best bandwidth among all parameters, respectively. Refer to the examples used previously for BP and WP, $d_{\text{best}} = 2$ and $w_{\text{best}} = 6$.

The stretch factor of (2, 3) is $2/2 + 6/3 = 3$, and the stretch factors of (4, 4) and (5, 6) are both 3.5. The smallest stretch factor is denoted as s_factor, which is 3 in the above case. The mesh link between the two border nodes is represented by a tuple (d_{best}, w_{best}, s_factor). The mesh link is likely to support a connection request [$req(d)$,$req(w)$], if, $d_{\text{best}} \leq req(d)$, $w_{\text{best}} \geq req(w)$ and $s\_factor \leq req(d)/d_{\text{best}} + w_{\text{best}}/req(w)$ [121].

The transformation from a mesh to a star, in the original KK algorithm, is defined as

$$\begin{aligned} s_{in}.d &= \frac{1}{b-1} \sum_{i=1, i\neq j}^{b} m_{ij}.d \\ s_{nj}.d &= \frac{1}{b-1} \sum_{i=1, i\neq j}^{b} m_{ij}.d \end{aligned} \tag{7.9}$$

where $m_{ij}.d$ is the delay of a mesh link from border node i to border node j, b is the number of border nodes, s_{in} is the delay of a spoke link from i to the nucleus, and s_{nj} is the delay of a spoke link from the nucleus to j.

The problem of this averaging approach is that the delay after transformation deviates a lot from the original delay, because the delay of $s_{in}.d + s_{nj}.d$ may be twice the delay of the mesh link $\left(m_{ij}.d\right)$. Therefore, the following modification is used (MKK):

$$\begin{aligned} s_{in}.d &= \frac{1}{2(b-1)} \sum_{i=1, i\neq j}^{b} m_{ij}.d \\ s_{nj}.d &= \frac{1}{2(b-1)} \sum_{i=1, i\neq j}^{b} m_{ij}.d \end{aligned} \tag{7.10}$$

7.4.6 Performance measure

In this kind of analysis the most often used performance measures are: *delay deviation* (DD), *success ratio* (SR) and *crankback ratio* (CBR).

7.4.6.1 Delay deviation

Owing to the distortion of aggregation, the delay between a source node and a destination domain, obtained using the method described in the previous sections, is not accurate. Delay deviation measures the difference between the real delay and the estimated delay, obtained by the aggregation. It is defined as

$$\text{DD} = \left| d_{\text{esp}} - d_{\text{asp}} \right| \tag{7.11}$$

where d_{esp} is the estimated delay of the shortest path and d_{asp} is the actual delay of the shortest path.

7.4.6.2 Success ratio

A feasible request may be rejected due to the imperfect approximation of the delay and bandwidth information during aggregation. The success ratio is used to measure quantitatively how well an

algorithm finds feasible paths and it is defined as

$$\text{SR} = \frac{\text{total number of acceptable feasible requests}}{\text{total number of feasible requests}} \tag{7.12}$$

The dividend represents all connection requests that are accepted by both interdomain routing and intradomain routing. The divider is the total number of *feasible* requests (not the total number of requests). Therefore, in simulation results, the success ratio measures the relative performance with respect to the optimal performance (accepting all feasible requests).

7.4.6.3 Crankback ratio

When an algorithm finds an interdomain path from the source node to the destination domain, it may overestimate the bandwidth or underestimate the delay and lead to crankbacks during intradomain routing. Crankback ratio measures how often that happens and is defined as

$$\text{CBR} = \frac{\text{total number requests crankbacked}}{\text{total number of requests accepted by interdomain routing}} \tag{7.13}$$

A good algorithm should have small crankback ratios, high success ratios and small delay deviations for different bandwidth and delay requirements.

7.4.7 Performance example

The *simulation environment* consists of the interdomain topology based on the power-law model [128, 129], and the intradomain topology based on the Waxman model [130]. The degree of a domain is defined as the total number of interdomain links adjacent to the border nodes of the domain. The simulation testbed and parameter configuration are set as follows: 10 % of the domains have a degree of one, and the degrees of the other domains follow the power law, i.e. the frequency f_{d} of a domain degree is proportional to the degree $d\,(\geq 2)$ raised to the power of a constant $O = -2.2$. In other words $f_{\text{d}} \propto d^{O}$. After each domain is assigned a degree according to the power law, a spanning tree is formed among the domains to ensure a connected graph. Additional links are inserted to fulfill the remaining degrees of every domain with the neighbors selected according to probabilities proportional to their respective unfulfilled degrees. The Waxman topology for the internal nodes of each domain is formed as follows: the nodes are randomly placed in a one-by-one square, and the probability of creating a link between node u and node v is $p\,(u, v) \propto \exp\left[-d\,(u, v)\,/\beta L\right]$.

In this expression $d(u, v)$ is the distance between u and v, $\beta = 0.6$, and L is the maximum distance between any two nodes. The average node degree is 4. The other simulation parameters are as follows: the number of domains in each topology is 200, the number of nodes in each domain is randomly selected between 10 and 40, the delay of a physical link is a random number between 2 and 10 units, and the bandwidth of a physical link is a random number between 1 and 5 units. For delay, a unit can be replaced by a certain number of milliseconds; for bandwidth, a unit can be replaced by a certain number of kilobytes (per second). Each data point is the average of 1000 randomly generated requests. More specifically, given a bandwidth requirement and/or a delay requirement, five topologies are randomly generated. On each topology, 200 requests are generated with the source and the destination randomly selected from the topology. LS, BP, WP and KK are run over these requests, respectively, and the average results give a set of data points in the figures. Simulations with the same set of parameters are presented for example in Liu *et al.* [112].

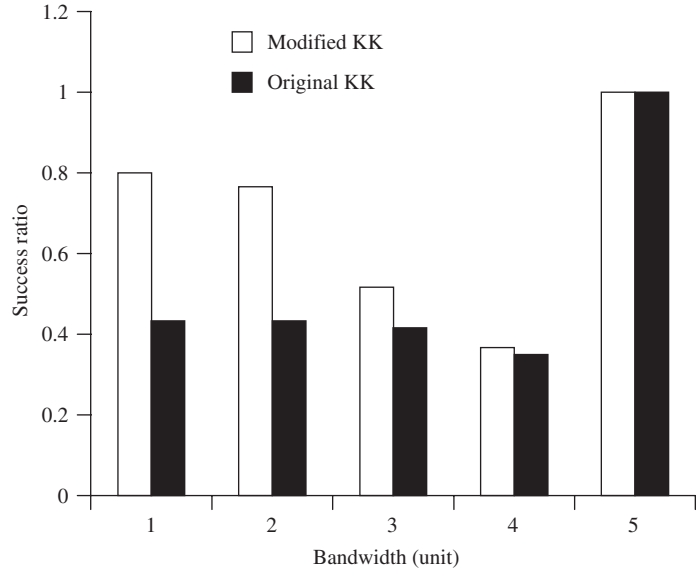

Figure 7.29 Success ratios of two aggregation schemes of the Korkmaz–Krunz method. (Reproduced by permission of IEEE [112].)

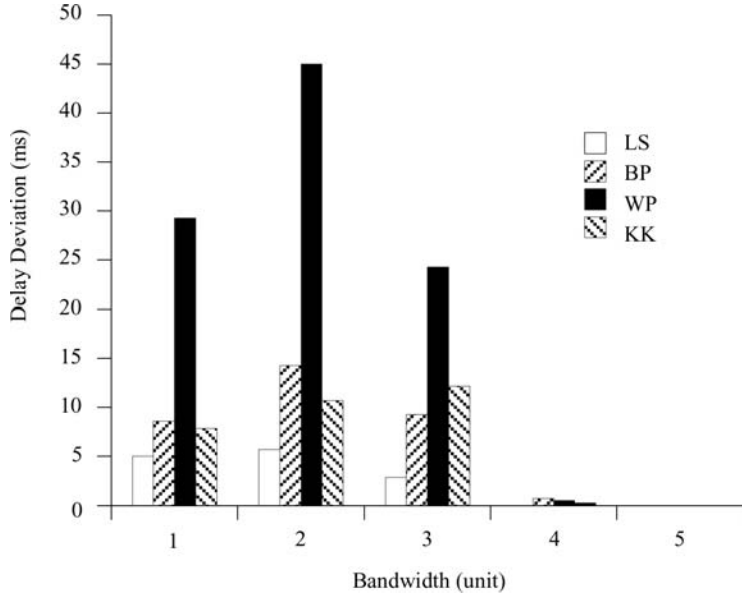

Figure 7.30 Delay deviation of different aggregation schemes. (Reproduced by permission of IEEE [112].)

The simulation results, using the described simulation environment, are shown in Figure 7.29. The horizontal axis is the bandwidth requirement. The results show that the modified algorithm (MKK) has better success ratios than the original algorithm. For CBR, the MKK algorithm is worse than the original KK algorithm, because the spoke delays in the modified KK are smaller than the spoke delays in the original KK. More optimistic estimation leaves more room for overestimation, which may lead to more crankbacks. However, as the crankback ratios of the modified KK are less than 5 % for all bandwidth values (Figure 7.31), it is believed that the performance improvement in success ratios outweighs the degradation of crankback ratios. As a result, the MKK algorithm is used in the rest of the section.

Figure 7.30 shows the delay deviations of LS, BP, WP, and KK. The horizontal axis presents the bandwidth requirement. For fairness, we count the paths of a request only when all four algorithms accept that request. Figure 7.30 shows that LS has smaller delay deviations than the other algorithms. That is because a line segment approximates the parameter staircase better than the other approaches, and thus gives more accurate information about the delay. The deviations are small when the bandwidth requirements are large (4), because the feasible paths are mostly short (within the same domain or between neighboring domains).

The success ratios are shown in Figure 7.31. It may be surprising that the success ratios are close to 1 when the bandwidth requirement is five units (maximum link capacity). Recall that our success ratio is defined relative to the number of feasible requests, not to the number of all requests. When the bandwidth request is large, there are few feasible requests. These feasible requests are mostly between nodes that are close to each other (in the same domain or neighboring domains),

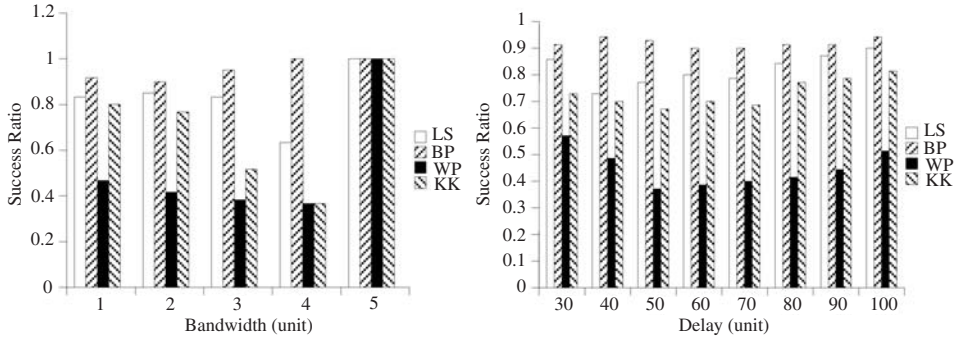

Figure 7.31 Success ratio vs bandwidth and delay. (Reproduced by permission of IEEE [112].)

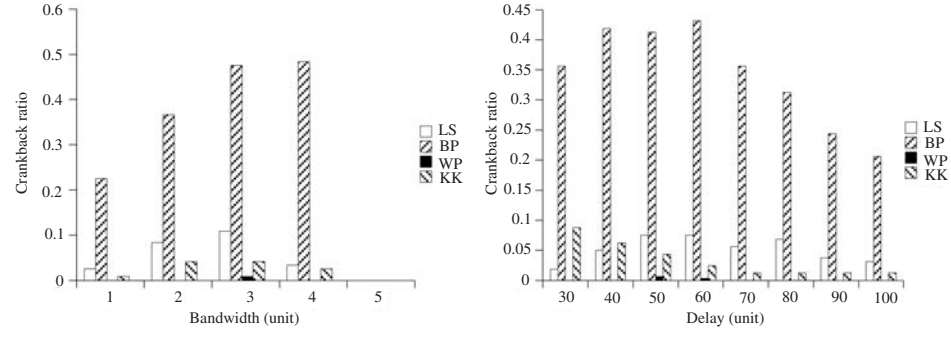

Figure 7.32 Crankback ratio vs bandwidth and delay. (Reproduced by permission of IEEE [112].)

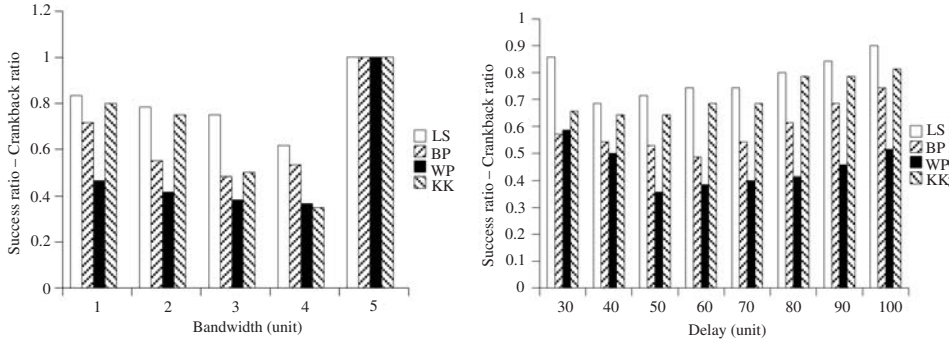

Figure 7.33 Success ratio–crankback ratio. (Reproduced by permission of IEEE [112].)

which makes the delay deviation small, as shown in Figure 7.30. That means it is less likely to reject a feasible request due to distortion. Therefore, the success ratio is high.

Figure 7.32 shows the crankback ratios of BP, WP, KK and LS. It is clear that BP has very high crankback ratios compared with other methods. On the contrary, as an aggregated WP topology tends to overestimate the real delay and underestimate the real bandwidth of the paths, WP has very small crankback ratios. Figure 7.33 compares *success ratio–crankback ratio*. BP does not perform well in this comparison due to its high crankback ratios. In contrast, LS has higher success ratios than WP and KK, and has reasonable crankback ratios. It outperforms all other schemes for different bandwidth and delay requirements by making a better tradeoff between success ratio and crankback ratio.

REFERENCES

[1] C. Berge, *Graphs*. North-Holland: New York, 1985.
[2] B. Bollobas, *Graph Theory: an Introductory Course*. Springer: New York, 1979.
[3] F. Buckley and F. Harary, *Distance in Graphs*. Addison-Wesley: Reading, MA, 1990.
[4] M. Capobianco and J.C. Molluzzo, *Examples and Counterexamples in Graph Theory*. North-Holland: New York, 1978.
[5] W.-K. Chen, *Theory of Nets. Flows in Networks*. Wiley: New York, 1990.
[6] N. Deo, *Graph Theory with Applications to Engineering and Computer Science*. Prentice Hall: Englewood Cliffs, NJ, 1974.
[7] F. Harary, *Graph Theory*. Addison-Wesley: Reading, MA, 1969.
[8] F. Harary, R.Z. Norman and D. Cartwright, *Structural Models: an Introduction to the Theory of Directed Graphs*. Wiley: New York, 1965.
[9] F. Harary and E.M. Palmer, *Graphical Enumeration*. Academic Press: New York, 1973.
[10] D.F. Robinson and L.R. Foulds, *Digraphs: Theory and Techniques*. Gordon and Breach: New York, 1980.
[11] R.E. Tarjan, *Data Structures and Network Algorithms*. SIAM: Philadelphia, PA, 1983.
[12] S. Even, *Graph Algorithms*. Computer Science Press: Rockville, MD, 1979.
[13] S. Even, *Algorithmic Combinatorics*. Macmillan: New York, 1973.
[14] A. Gibbons, *Algorithmic Graph Theory*. Cambridge University Press: Cambridge, 1985.
[15] L. Ammeraal, *Programs and Data Structures in C*. Wiley: New York, 1987.
[16] W. Arnsbury, *Data Structures: From Arrays to Priority Queues*. Wadsworth: Belmont, CA, 1985.

[17] N. Christofides, *Graph Theory: an Algorithmic Approach*. Academic Press: New York, 1975.
[18] C.J. Colbourn, *The Combinatorics of Network Reliability*. Oxford University Press: London, 1987.
[19] N. Dale and S.C. Lilly, *Pascal Plus Data Structures* (2nd edn). D. C. Heath: Lexington, MA, 1988.
[20] J. Esakov and T. Weiss, *Data Structures: an Advanced Approach Using C*. Prentice-Hall: Englewood Cliffs, NJ, 1989.
[21] A.H. Estahanian and S.L. Hakimi, On computing the connectivity of graphs and digraphs, *Networks*, vol. 14, 1984, pp. 355–366.
[22] J.A. McHugh, *Algorithmic Graph Theory*. Prentice Hall: Englcwood Cliffs, NJ, 1990.
[23] U. Manber, *Introduction to Algorithms*. Addison-Wesley: Reading, MA, 1989.
[24] E. Minieka, *Optimization Algorithms for Networks and Graphs*. Marcel Dekker: New York, 1978.
[25] C.H. Papadimitriou and K. Steiglitz, *Combinatorial Optimization: Algorithms and Complexity*. Prentice-Hall: Englewood Cliffs, NJ, 1982.
[26] M.N.S. Swarny and K. Thulasiraman. *Graphs, Networks, and Algorithms*. Wiley: New York, 1981.
[27] A.M. Tenenbaum and M.J. Augenstein, *Data Structures Using Pascal* (2nd edn). Prentice-Hall: Englewood Cliffs, NJ, 1986.
[28] A.M. Tenenbaum, Y. Langsarn, and M.J. Augenstein, *Data Structures Using C*. Prentice-Hall: Englewood Cliffs, NJ, 1990.
[29] A.V. Aho, J.E. Hopcroft, and J.D. Ullman, *The Design and Analysis of Computer Programs*. Addison-Wesley: Reading, MA, 1974.
[30] A.V. Aho, J.E. Hopcroft, and J.D. Ullrnan, *Data Structures and Algorithms*. Addison- Wesley: Reading, MA, 1983.
[31] T.H. Cormen, C.E. Leiserson, and R.L. Rivest, *Introduction to Algorithms*. MIT Press: Cambridge, MA, 1990.
[32] M.R. Garey and D.S. Johnson, *Computers and Intractibility. A Guide to the Theory of NP-Completeness*. Freeman: San Francisco, CA, 1979.
[33] D. Hare, *Algorithmics. The Spirit of Computing*. Addison-Wesley: Reading, MA, 1987.
[34] E. Horowitz and S. Sahni, *Fundamentals of Computer Algorithms*. Computer Science Press: Rockville, MD, 1978.
[35] D.S. Johnson, The NP-completeness column: an ongoing guide, *Algorithms* (this column appears several times per year).
[36] D.E. Knuth, *The Art of Computing: Vol. 1: Fundamental Algorithms* (2nd edn). Addison-Wesley: Reading, MA, 1973.
[37] D.E. Knuth, *The Art of Computing: Vol. 2: Scm inunierical Algorithms* (2nd edn). Addison-Wesley: Reading, MA, 1981.
[38] D.E. Knuth, *The Art of Computing: Vol. 3: Sorting and Searching*, Addison-Wesley: Reading, MA, 1973.
[39] R. Sedgewick, *Algorithms* (2nd edn). Addison-Wesley: Reading, MA, 1988.
[40] H.S. Wilf, *Algorithms and Complexity*. Prentice-Hall: Englewood Cliffs, NJ, 1986.
[41] T. Egeland and A.B. Huseby, On Dependence and Reliability Computation, *Networks*, vol. 21, 1991, pp. 521–546.
[42] H. Heffes and A. Kumar, Incorporating dependent node damage in deterministic connectivity analysis and synthesis of networks, *Networks*, vol. l6, l986, pp. Sl–65.
[43] Y.F. Lam and V. Li, On Network Reliability Calculations with Dependent Failures, in *Proc. IEEE 1983 Global Telecommunications Conf.* (GTC '83), San Diego, CA, November, 1977, pp. 1499–1503.
[44] Y.F. Lam and V. Li, Reliability modeling and analysis of communication networks with dependent failures, in Proc. *IEEE INFOCOM*, 3–7 June 1985, pp. 196–199.

[45] Y.F. Lam and V. Li, Reliability modeling and analysis of communication networks with dependent failures, *IEEE Trans. Commun.*, vol 34, 1986, pp. 82–84.
[46] K.V. Lee and V.O. K. Li, A path-based approach for analyzing reliability of systems with dependent failures and multinode components, *Proc. IEEE INFOCOM*, 1990, pp. 495–503.
[47] L.B. Page and J.E. Perry, A model for system reliability with common-cause failures, *IEEE Trans. Reliab.*, vol. 38, 1989, pp. 406–410.
[48] E. Zemel, Polynomial algorithms for estimation of network reliability, *Networks*, vol. 12, 1982, pp. 439–452.
[49] A. Agrawal and A. Satayanarana, An OIE time algorithm for computing the relaibility of a class of directed networks, *Op. Res.*, vol. 32, 1984, pp. 493–515.
[50] D. Bienstock, An algorithm for reliability analysis of planar graphs, *Networks*, vol. 16, 1986, pp. 411–422.
[51] F. Beichelt and P. Tittman, A generalized reduction method for the connectedness probability of stochastic networks, *IEEE Trans. Reliab.*, vol. 40, (1991), pp. 198–204.
[52] F.T. Boesch, On unreliability polynomials and graph connectivity in reliable network synthesis, *J. of Graph Theory*, vol. 10, 1988, pp. 339–352.
[53] A. Bobbio and A. Premoli, Fast algorithm for unavailibility and sensitivity analysis of series–parallel systems, *IEEE Trans. Reliab.*, vol. 31, 1982, pp. 359–361.
[54] B.N. Clark and C.L. Colbourn, Unit disk graphs, *Discrete Math.*, vol. 86, 1990, pp. 165–177.
[55] C.L. Colbourn, Network resiliance, *SIAM J. Algebra Discrete Math.*, vol. 8, 1987, pp. 404–409.
[56] W.H. Debany, P.K. Varshney and C.R.P. Hartman, Network reliability evaluation using probability expressions, *IEEE Trans. Reliab.*, vol. 35, 1986, pp. 161–166.
[57] T. Politof and A. Satyanarayana, A linear-time algorithm to compute the reliability of planar cube-free networks, *IEEE Trans. Reliab.*, vol. 39, 1990, pp. 557–563.
[58] K.W. Pullen, A random network model of message transmission, *Networks*, vol. 16, 1986, pp. 397–409.
[59] O.W.W. Yang, Terminal pair reliability of tree-type computer communication networks, in *Proc. IEEE 1991 Military Communications Conf. (MILCOM '91)*, vol. 3, November 1991, pp. 905–909.
[60] H.M. AboElFotoh and C.J. Colbourn, Computing 2-terminal reliability for radio-broadcast networks, *IEEE Trans. Reliab.*, vol. 38, 1989, pp. 538–555.
[61] M.O. Ball and J.S. Provan, Calculating bounds on reachability and connectedness in stochastic networks, *Networks*, vol. 13, 1983, pp. 253–278.
[62] M.O. Ball and J.S. Provan, Bounds on the reliabilty polynomial for shellable independence systems, *SIAM J. Algebra Discrete Math.*, vol. 3, 1981, pp. 166–181.
[63] T.B. Brecht and C.J. Colbourn, Improving reliabilty bounds in computer networks, *Networks*, vol. 16, 1986, pp. 369–380.
[64] T.B. Brecht and C.J. Colbourn, Multplicative improvements in network reliabilty bounds, *Networks*, vol. 19, 1989, pp. 521–529.
[65] T.B. Brecht and C.L. Colbourn, Lower bounds on two-terminal network reliability, *Discrete Appl. Math.*, vol. 21, 1988, pp. 185–198.
[66] C.J. Colbourn and A. Ramanathan, Bounds for all-terminal reliability by arc packing, *Ars Combinatorica*, vol. 23A, 1987, pp. 229–236.
[67] C.J. Colboum, Edge-packings of graphs and network reliability, *Discrete Math.*, vol. 72, 1988, pp. 49–61.
[68] C.J. Colbourn and D.D. Harms, Bounding all-terminal reliability in computer networks, *networks*, vol. 18, 1988, pp. 1–12.
[69] D. Torrieri, Algorithms for finding an optimal set of short disjoint paths in a communication network, in *Proc. IEEE 1991 Military Communications Cont. (MILCOM '91)*, vol. 1, November, 1991, pp. 11–15.

[70] D.K. Wagner, Disjoint (s, t)-cuts in a network, *Networks*, vol. 20, 1990, pp. 361–371.
[71] G.S. Fishman, A comparison of four Monte Carlo methods for estimating the probability of st-connectedness, *IEEE Trans. Reliab.*, vol. 35, 1986, pp. 145–154.
[72] G.S. Fishman, A Monte Carlo sampling plan for estimating network reliability, *Opns. Res.*, vol. 34, 1986, pp. 581–594.
[73] G.S. Fishman, Estimating the st-reliability function using importance and stratified sampling, *Opns. Res.*, vol. 37, 1989, pp. 462–473.
[74] G.S. Fishman, A Monte Carlo sampling plan for estimating reliability parameters and related functions, *Networks*, vol. 17, 1987, pp. 169–186.
[75] R.M. Karp and M.G. Luby, Monte-Carlo algorithms for enumeration and reliability problems, in *Proc. IEEE 24th Annual Symp. on Foundations of Computer Science*, 7–9 November 1983 Tuscon, AZ, pp. 56–64.
[76] P. Kubat, Estimation of reliability for communication/computer networks – simulation/analytic approach, *IEEE Trans. Commun.*, vol. 37, 1989, pp. 927–933.
[77] L.D. Nd and C.J. Colbourn, Combining Monte Carlo estimates and bounds for network reliability, *Networks*, vol. 20, 1990, pp. 277–298.
[78] K.T. Newport and M.A. Schroeder, Network survivability through connectivity optimization', in *Proc. 1987 IEEE Int. Conf. Communications*, vol. 1, 1987, pp. 471–477.
[79] K.T. Newport and P. Varshney, Design of communications networks under performance constraints, *IEEE Trans. Reliab.*, vol. 40, 1991, pp. 443–439.
[80] K.T. Newport and M.A. Schroeder, Techniques for evaluating the nodal survivability of large networks, in *Proc. IEEE 1990 Military Communications Conf. (MILCOM '90)*, Monterey, CA, 1990, pp. 1108–1113.
[81] K.T. Newport, M.A. Schroeder and G.M. Whittaker, A knowledge based approach to the computation of network nodal survivability, in *Proc. IEEE 1990 Military Communications Conf. (MILCOM '90)*, Monterey, CA, 1990, pp. 1114–1119.
[82] M.A. Schroeder and K.T. Newport, Tactical network survivability through connectivity optimization, in *Proc. 1987 Military Communications Conf. (MILCOM '87)*, Monterey, CA, vol. 2, 1987, pp. 590–597.
[83] G.M. Whittaker, A knowledge-based design aid for survivable tactical networks, in *Proc. the IEEE 1990 Military Communications Conf. (MILCOM '90)*, Monterey, CA, 1990, Section 53.5.
[84] M.A. Schroeder and K.T. Newport, Enhanced network survivability through balanced resource criticality, in *Proc. IEEE 1989 Military Communications Conf. (MILCOM '89)*, Boston, MA, 1989, Section 38.4.
[85] K.S. Bagga, L.W. Beineke, M.J. Lipman and R.E. Pippert, The concept of leverage in network vulnerability, in *Conf. Graph Theory*, Kalamazoo, MI, 1988, pp. 29–39.
[86] K.S. Bagga, L.W. Beineke, M.J. Lipman and R.E. Pippert, Explorations into graph vulnerability, in *Conf. Graph Theory*, Kalamazoo, MI, 1988, pp. 143–158.
[87] D. Bienstock and E. Gyori, Average distance in graphs with removed elements, *J. Graph Theory*, vol. 12, 1988, pp. 375–390.
[88] F.T. Boesch and I.T. Frisch, On the smallest disconnecting set in a graph, *IEEE Trans. Circuit Theory*, vol. 15, 1986, pp. 286–288.
[89] F. Buckley and M. Lewinter, A note on graphs with diameter preserving spanning trees, *J. Graph Theory*, vol. 12, 1988, pp. 525–528.
[90] F.R.K. Chung, The average distance and the independence number, *J. Graph Theory*, vol. 12, 1988, pp. 229–235.
[91] G. Exoo, On a measure of communication network vulnerability, *Networks*, vol. 12, 1982, pp. 405–409.
[92] O. Favaron, M. Kouider and M. Makeo, Edge-vulnerability and mean distance, *Networks*, vol. 19, 1989, pp. 493–509.

[93] F. Harary, F.T. Boesch and J.A. Kabell, Graphs as models of communication network vulnerability: connectivity and persistence, *Networks*, vol. 11, 1981, pp. 57–63.
[94] F. Haraty, Conditional connectivity, *Networks*, vol. 13, 1983, pp. 347–357.
[95] S.M. Lee, Design of e-invariant Networks, *Congressus Nurner*, vol. 65, 1988, pp. 105–102.
[96] O.R. Oellermann, Conditional graph connectivity relative to hereditary properties, *Networks*, vol. 21, 1991, pp. 245–255.
[97] J. Plesnik, On the sum of all distances in a graph or digraph, *J. Graph Theory*, vol. 8, 1984, pp. 1–21.
[98] A.A. Schoone, H.L. Bodlaender and J. van Leeuwer, Diameter increase caused by edge deletion, *J. Graph Theory*, vol. 11, 1987, pp. 409–427.
[99] M.O. Ball, J.S. Provan and D.R. Shier, Reliability covering problems, *Networks*, vol. 21, 1991, pp. 345–357.
[100] L. Caccetta, Vulnerability in communication networks, *Networks*, vol. 14, 1984, pp. 141–146.
[101] L.L. Doty, Extremal connectivity and vulnerability in graphs, *Networks*, vol. 19, 1989, pp. 73–78.
[102] T.J. Ferguson, J.H. Cozzens and C. Cho, SDI network connectivity optimization, in *Proc. the IEEE 1990 Military Communications Conf. (MILCOM '90)*, Monterey, CA, 1990, Sec. 53.1.
[103] J.F. Fink, M.S. Jacobson, L.F. Kinch and J. Roberts, The bondage number of a graph, *Discrete Math*, vol. 86, 1990, pp. 47–57.
[104] G. Gunther, Neighbor-connectedness in regular graphs, *Discrete Appl. Math.*, vol. 11, 1985, pp. 233–242.
[105] G. Gunther, B.L. Hartnell and R. Nowakowski, Neighbor-connected graphs and projective planes, *Networks*, vol. 17, 1987, pp. 241–247.
[106] P.L. Hammer, Cut-threshold graphs, *Discrete Appl. Math.*, vol. 30, 1991, pp. 163–179.
[107] A.M. Hobbs, Computing edge-toughness and fractional arboricity, *Contemp. Math., Am. Math. Soc.*, 1989, pp. 89–106.
[108] T.Z. Jiang, A new definition on survivability of communication networks, in *Proc. IEEE 1991 Military Communications Conf. (MJLCOM '91)*, vol. 3, November 1991, pp. 901–904.
[109] L.M. Lesniak and R.E. Pippert, On the edge-connectivity vector of a graph, *Networks*, vol. 19, 1989, pp. 667–671.
[110] Z. Miller and D. Pritikin, On the separation number of a graph, *Networks*, vol. 19, 1989, pp. 651–666.
[111] L. Wu and P.K. Varshney, On survivability measures for military networks, in *Proc. IEEE 1990 Military Communications Conf. (MILCOM '90)*, Monterey, CA, pp. 1120–1124.
[112] K.-S. Lui, K. Nahrstedt and S. Chen, Routing with topology aggregation in delay-bandwidth sensitive networks, *IEEE/ACM Trans. Networking*, vol. 12, No. 1, 2004, pp. 17–29.
[113] *Private Network-Network Interface Specification Version 1.0*, March 1996.
[114] Y. Rekhter and T. Li, A border gateway protocol 4 (BGP-4), Network Working Group, RFC 1771, 26–30 March 1995.
[115] R. Guerin and A. Orda, QoS-based routing in networks with inaccurate information: theory and algorithms, *IEEE/ACM Trans. Networking*, vol. 7, 1999, pp. 350–364.
[116] F. Hao and E.W. Zegura, On scalable QoS routing: performance evaluation of topology aggregation, in *Proc. IEEE INFOCOM*, 2000, pp. 147–156.
[117] W. Lee, Minimum equivalent subspanner algorithms for topology aggregation in ATM networks, in *Proc. 2nd Int. Conf. ATM (ICATM)*, 21–23 June 1999, pp. 351–359.
[118] B. Awerbuch and Y. Shavitt, Topology aggregation for directed graphs, *IEEE/ACM Trans. Networking*, vol. 9, 2001, pp. 82–90.
[119] W. Lee, Spanning tree method for link state aggregation in large communication networks, in *Proc. IEEE INFOCOM*, 2–6 April 1995, pp. 297–302.

[120] A. Iwata, H. Suzuki, R. Izmailow and B. Sengupta, QoS aggregation algorithms in hierarchical ATM networks, in *IEEE Int. Conf. Communications Conf. Rec.*, 7–11 June 1998, pp. 243–248.

[121] T. Korkmaz and M. Krunz, Source-oriented topology aggregation with multiple QoS parameters in hierarchical networks, *ACM Trans. Modeling Comput. Simulation*, vol. 10, no. 4, 2000, pp. 295–325.

[122] S. Chen and K. Nahrstedt, An overview of quality-of-service routing for the next generation high-speed networks: problems and solutions, *IEEE Network*, vol. 12, 1998, pp. 64–79.

[123] W. Lee, Topology aggregation for hierarchical routing in ATM networks, in *ACMSIGCOMM Comput. Commun. Rev.*, vol. 25, 1995, pp. 82–92.

[124] L. Guo and I. Matta, On state aggregation for scalable QoS routing, in *IEEE Proc. ATM Workshop*, May 1998, pp. 306–314.

[125] Z. Wang and J. Crowcroft, Bandwidth-delay based routing algorithms, in *Proc. IEEE GLOBECOM*, vol. 3, 26–29 May 1995, pp. 2129–2133.

[126] D. Bauer, J.N. Daigle, I. Iliadis and P. Scotton, Efficient frontier formulation for additive and restrictive metrics in hierarchical routing, in *IEEE Int. Conf. Communications Conf. Rec.*, vol. 3, June 2000, p. 1353.

[127] Z. Wang and J. Crowcroft, Quality-of-service routing for supporting multimedia applications, *IEEE J. Select. Areas Commun.*, vol. 14, 1996, pp. 1228–1234.

[128] M. Faloutsos, P. Faloutsos, and C. Faloutsos, On power-law relationships of the internet topology, in *Proc. ACM SIGCOMM*, 1999, pp. 251–262.

[129] C. Jin, Q. Chen, and S. Jamin, Inet-3.0: Internet Topology Generator, University of Michigan, Technical Report CSE-TR-456-02, 2002.

[130] B.M. Waxman, Routing of multipoint connections, *IEEE J. Select. Areas Commun.*, vol. 6, 1988, pp. 1617–1622.

[131] T.H. Cormen, C.E. Leiserson, and R.L. Rivest, *Introduction to Algorithms*. MIT Press: Cambridge, MA, 1990.

[132] M. Garey and D. Johnson, *Computers and Intractability: A Guide to the Theory of NP-Completeness*. Freeman: New York, 1979.

8

Effective Capacity

8.1 EFFECTIVE TRAFFIC SOURCE PARAMETERS

For efficient resource allocation for connections requiring QoS, reliable and accurate characterization of available effective capacity in the network [1–5, 7–21] and offered traffic [22–29] are needed. The ATM forum [1] has adopted an open-loop flow control mechanism for ATM networks known as usage parameter control (UPC). A UPC algorithm accepts a cell stream as input and determines whether or not each cell conforms to the parameters of the algorithm. Depending on the network policy, nonconforming cells are either dropped prior to entering the network or tagged as low priority. The UPC function acts as a *traffic policer* at the network access point. In contrast, a *traffic shaper* smoothes out the bitrate variations in a stream by delaying rather than dropping or tagging cells. A user can avoid possible cell loss at the network access point due to UPC by shaping its cell stream to conform to the negotiated UPC. All those actions will result in an *effective traffic source*. The UPC mechanisms proposed by the ATM Forum are variants of the leaky bucket algorithm. The leaky bucket is a simple means of shaping or policing a traffic stream and has desirable attributes in terms of network control [2–4].

A leaky bucket is parameterized by a leak rate μ and a bucket size B. It is convenient to describe the operation of the leaky bucket in terms of a fictitious $x/D/1/B$ queue for a deterministic input (D) served at constant rate μ with capacity B [2]. In this model, each cell arrival to the leaky bucket generates a corresponding customer arrival to the fictitious queue. At the time of a cell arrival, if the number of customers in the fictitious queue is less than B, the cell is said to be *conforming*, otherwise the cell is *nonconforming*. Nonconforming cells are either dropped or tagged as low priority cells.

A leaky bucket shaper parameterized by (μ, B) operates in a manner similar to the leaky bucket policer, except that nonconforming cells are delayed, rather than dropped or tagged. The operation of the leaky bucket shaper can be understood in terms of an $x/D/1$ queue. Upon arrival of a cell, if the number of customers in the fictitious queue is B or more, the cell is placed in an infinite capacity first-in, first-out (FIFO) buffer. Whenever a customer leaves the fictitious queue, a cell (if any) is removed and transmitted from the FIFO buffer.

The *dual leaky bucket* consists of two leaky buckets: a *peak rate* leaky bucket with parameters (λ_p, B_p) and a *sustainable rate* leaky bucket with parameters (λ_s, B_s), where $\lambda_p > \lambda_s$. A cell is

Advanced Wireless Technologies: Cognitive, Cooperative & Opportunistic 4G Technology Second Edition Savo G. Glisic

conforming with respect to the dual leaky bucket if and only if it is conforming with respect to both the peak and sustainable rate buckets. The sustainable rate λ_s represents the maximum long-run average rate for conforming cell streams. The peak rate λ_p specifies a minimum intercell spacing of $1/\lambda_p$ with burst tolerance B_p. In this section, we shall assume that $B_p = 1$, so that the intercell spacing of conforming streams is constrained to be at most $1/\lambda_p$. Values of $B_p > 1$ allow for cell delay variation (CDV) between the customer premises and the network access point.

The set $(\lambda_p, \lambda_s, B_s)$ constitutes a UPC descriptor that the user negotiates with the network. If the connection is accepted, the user applies a dual leaky bucket shaper to shape its cell stream according to the negotiated UPC. The dual leaky bucket limits the peak rate to λ_p, the long-term average rate to λ_s, and the maximum burst length (transmitted at peak rate) to $B_c = B_s\lambda_p/(\lambda_p - \lambda_s)$.

Deterministic traffic characterization is based on the queueing model of the leaky bucket [5]. Suppose that the cell stream is of finite length and that the peak rate λ_p is known. The cell stream is offered as input to a queue served at constant service rate μ. Let $B_{\max}(\mu)$ be the maximum number of cells observed in the system over the duration of the cell stream. The stream then can be characterized by the peak rate and the values $B_{\max}(\mu)$ for $0 < \mu < \lambda_p$ as

$$C_D = \left[\lambda_p, B_{\max}(\mu), 0 < \mu < \lambda_p\right] \tag{8.1}$$

Equation (8.1) can be interpreted as follows. For each μ, $0 < \mu < \lambda_p$, the cell stream passes through a leaky bucket parameterized by $[\mu, B_{\max}(\mu)]$ without being shaped, i.e. the cell stream conforms to the leaky bucket parameters $[\mu, B_{\max}(\mu)]$. The notation $B(C_D, \mu) = B_{\max}(\mu)$ is introduced to show that the choice of bucket size, for a given leak rate μ, depends on C_D. The characterization is *tight* in the following sense. If the cell stream conforms to a given set of leaky bucket parameters (μ, B'), then necessarily $B' \geq B(C_D, \mu)$. For a given leak rate μ^*, the minimum bucket size for conformance is $B^* \geq B(C_D, \mu^*)$.

Ideal statistical traffic characterization is based on assumption that the peak rate of the cell stream λ_p and the mean rate λ_m are known. Suppose that the cell stream is offered to a leaky bucket traffic shaper with leak rate μ, where $\lambda_m < \mu < \lambda_p$, and bucket size B.

The shaping probability is defined as the probability that an arbitrary arriving cell has to wait in the data buffer of the leaky bucket. In the $x/D/1$ queueing model of the leaky bucket, this event corresponds to a customer arrival to the fictitious queue when the number in the system exceeds B. If $B(\mu, \varepsilon)$ is defined as the minimum bucket size necessary to ensure that the shaping probability does not exceed ε, then

$$C_S(\varepsilon) = \left[\lambda_p, \lambda_m, (\mu, B(\mu, \varepsilon)), \lambda_m < \mu < \lambda_p\right] \tag{8.2}$$

represents statistical traffic characterization.

Approximate statistical traffic characterization is based on the assumption that the cell stream is offered to a queue with constant service rate μ, where $\lambda_m < \mu < \lambda_p$. If W is the steady-state waiting time, in the queue, for an arbitrary cell arriving in the queue, then the complementary waiting time distribution, can be approximated as (see Appendix A; please go to www.wiley.com/go/glisic):

$$P(W > t) \approx a(\mu)e^{-b(\mu)t}, \quad t \geq 0 \tag{8.3}$$

Two asymptotic approximations are of interest:

$$\begin{aligned} e^{bt} P(W > t) &\to a \ ; \ t \to \infty \\ t^{-1} \log P(W > t) &\to -b \ ; \ t \to \infty \end{aligned} \tag{8.4}$$

Also the following approximation is of interest, as suggested in Chang [6]: $a \approx bE(W)$.

In many cases, the approximation in Equation (8.3) with $a = 1$ tends to be conservative, i.e. the bound, $P(W > t) \leq e^{-bt}$, holds under certain conditions [6, 7]. The one-parameter approximation

$$P(W > t) \approx e^{-bt}, \quad t \geq 0 \tag{8.5}$$

is the basis for the theory of *effective bandwidths* that will be discussed below.

More extensive discussions of this class of approximations can be found in References [7, 8]. In this section Equation (8.3) is used as a reasonable approximation for an ATM cell stream modeled as a general Markovian source. Over the relatively short observation windows of interest (on the order of seconds), these approximations are fairly robust for a large class of real traffic sources, in particular, MPEG video sequences. Therefore, parameters $[a(\mu), b(\mu)]$ provide a statistical characterization of the cell stream when offered to a queue with a constant service rate μ. A more complete characterization of the cell stream records the values $[a(\mu), b(\mu)]$ for all μ in the range (λ_m, λ_p) as follows:

$$\hat{C}_S = \left\{\lambda_p, \lambda_m, [a(\mu), b(\mu)] : \lambda_m < \mu < \lambda_p\right\} \tag{8.6}$$

Values of $[a(\mu), b(\mu)]$ are chosen such that Equation (8.3) holds *approximately* for values of t in range of interest. Assuming that Equation (8.3) holds at equality, we have (see Chapter 6)

$$a(\mu)/b(\mu) = E[W] = \tau_r(\mu)E[S_a] + E[Q_a]/\mu \tag{8.7}$$

In Equation (8.7) S_a denotes the number of customers in service, Q_a the number of customers in queue seen by an arbitrary customer arrival, and $\tau_r(\mu)$ the average remaining service time for the customer in service as seen by an arriving customer conditional on there being a customer in service. Bearing in mind that

$$E[S_a] = P(W > 0) = a(\mu) \tag{8.8a}$$

and defining $q(\mu) = E[Q_a]$, Equation (8.7) gives

$$b(\mu) = \frac{\mu a(\mu)}{q(\mu) + \mu a(\mu)\tau_r(\mu)} \tag{8.8b}$$

The estimation of the above parameters is discussed later in this section. Once these parameters are obtained they are used in Equation (8.6) for statistical characterization of a cell stream. The next step is to map the characterization to a suitable UPC descriptor.

8.1.1 Effective traffic source

To avoid UPC violation at the network access point, typically a shaper is applied at the source to force the cell stream to conform to the negotiated UPC, resulting in an *effective traffic source*. If the user can tolerate a larger shaping delay, a UPC descriptor with smaller network cost can be chosen for the connection. So, the problem of selecting the UPC values for a cell stream can be formulated as:

$$\min_{\lambda_s, B_s} c\left(\lambda_p, \lambda_s, B_s\right) \text{ and } P(\textit{shaping}) \le \varepsilon \text{ and } \lambda_m \le \lambda_s \le \lambda_p \tag{8.9}$$

where parameters (λ_m, λ_p) are assumed to be known *a priori* or obtained through measurements. The *cost function c( )* is an increasing function of each argument and represents the cost to the network of accepting a call characterized by the UPC values $(\lambda_p, \lambda_s, B_s)$. The shaping probability *P(shaping)*, which depends on the cell stream characteristics, represents the probability that an arbitrary arriving cell will be delayed by the shaper.

In the case of an idealized traffic characterization $C_S(\varepsilon)$, defined by Equation (8.2), the values of $B(\mu, \varepsilon)$ *for* $\lambda_m < \mu < \lambda_p$ are recorded, where $B(\mu, \varepsilon)$ is the minimum bucket size that ensures a shaping probability less than ε for a leaky bucket with rate μ.

Alternatively, from the approximate statistical characterization, we can obtain an estimate $B(\hat{C}_s, \mu, \varepsilon)$ for this minimum bucket size. Substituting $B(\hat{C}_s, \mu, \varepsilon)$ in Equation (8.9), we have

$$\min_{\lambda_s} c[\lambda_p, \lambda_s, (B(\hat{C}_S, \lambda_s, \varepsilon)] \text{ and } \lambda_m \le \lambda_s \le \lambda_p \tag{8.9a}$$

8.1.2 Shaping probability

In a $x/D/1$ model of the (μ, B) leaky bucket shaper, an arriving cell is delayed *(shaped)* if and only if the number of customers seen in the fictitious queue is B or greater. Otherwise, the cell is transmitted immediately without delay. Suppose that the user wants to choose the UPC descriptor $(\lambda_p, \lambda_s, B_s)$ such that the probability that an arbitrary cell will be shaped is less than ε. For a fixed leak rate μ, we would like to determine the minimum bucket size $B(\mu, \varepsilon)$ required to ensure a shaping probability less than ε. On should remember that the shaping probability is an upper bound for the *violation probability*, i.e., the probability that an arriving cell is nonconforming, in the corresponding UPC policer. Let n_a be a random variable representing the number in the fictitious queue observed by an arbitrary cell arrival. Suppose that the number of customers in the fictitious queue upon cell arrival is given by $n = N$, where $N \geq 1$ is an integer. This means that the new customer sees $N - 1$ customers in the queue and one customer currently in service.

Therefore, the waiting time in the queue W' for this customer lies in the range $[(N-1)/\mu, N/\mu]$. Also we can say, if W' for this customer lies in this range, then $n = N$ at the arrival epoch. In other words $n = N \Leftrightarrow (N-1)/\mu < W' < N/\mu$ so $n \geq N \Leftrightarrow (N-1)/\mu < W'$.

Based on this we can write $P(n_a \geq B) = P[W > (B-1)/\mu]$. So by using Equation (8.3), the shaping probability can be expressed as

$$P(shaping) = P(n_a \geq B) \approx a(\mu)e^{-b(\mu)(B-1)/\mu}$$

From this relation, for $P(shaping) = \varepsilon$ we get

$$B(\hat{C}_s, \mu, \varepsilon) = [\mu/b(\mu)] \log[a(\mu)/\varepsilon] + 1 \tag{8.10}$$

8.1.3 Shaping delay

We can also specify the shaping constraint in terms of delay. Consider a cell stream passing through a leaky bucket traffic shaper with parameters (μ, B). Recall that the state counter n may be viewed as the number of customers in a fictitious $x/D/1$ queue. If W represents the waiting time in queue experienced by a given customer arriving in the fictitious queue served at rate μ, the *actual* delay experienced by the cell corresponding to the given fictitious customer can be expressed as

$$D = \max[0, W - (B-1)/\mu)] \tag{8.11}$$

Using Equation (8.3) and W from Equation (8.11) we have

$$\begin{aligned} P(D > D_{max}) &\approx a(\mu)e^{-b(\mu)D_{max}}e^{-b(\mu)(B-1)/\mu} \\ E[D] &\approx [a(\mu)/b(\mu)]e^{-b(\mu)(B-1)/\mu} \end{aligned} \tag{8.12}$$

Setting the expected delay equal to the target mean delay $\bar{D}$ gives B as

$$B(C_s, \mu, \bar{D}) = [\mu/b(\mu)] \log[a(\mu)/b(\mu)\bar{D}] + 1 \tag{8.13}$$

which will be referred to as *mean delay constraint curve*.

The *cost function* $c(\lambda_p, \lambda_s, B_s)$ represents the amount of resources that should be allocated to a cell characterized by the UPC parameters $(\lambda_p, \lambda_s, B_s)$. For a source with deterministic periodic on–off sample paths and a random offset, the lengths of the on and off periods are given by

$$T_{on} = B_s/(\lambda_p - \lambda_s) \text{ and } T_{off} = B_s/\lambda_s \tag{8.14}$$

Consider an on–off source model in which the source alternately transmits at rate r during an on-period and is silent during an off-period. The mean on-period and off period lengths are given by β^{-1} and α^{-1}, respectively. For mathematical tractability, Erlang-k distribution for on and off periods is assumed.

The *effective bandwidth* of a source is defined as the minimum capacity required to serve the traffic source so as to achieve a specified steady-state cell loss probability ε_{mux}, where the multiplexer or switch buffer size is denoted by B_{mux}. Using the result from Kobayashi and Ren [9], the effective bandwidth for this source model can be obtained as

$$c(eff) = r\alpha/(\alpha+\beta) + r^2\alpha\beta K/(\alpha+\beta)^3 \tag{8.15}$$

where $K = -\log \varepsilon_{\text{mux}}/(2kB_{\text{mux}})$. If we set the mean on and off periods as $\beta^{-1} = T_{\text{on}}$ and $\alpha^{-1} = T_{\text{off}}$, then by using Equation (8.14) in Equation (8.15), we have

$$c(eff) = \lambda_s + \lambda_s(\lambda_p - \lambda_s)KB_s/\lambda_p \tag{8.16}$$

Now, the following cost function for a UPC controlled source can be defined:

$$c(\lambda_p, \lambda_s, B_s) = \min[\lambda_p, c(eff)] = \min[\lambda_p, \lambda_s + \lambda_s\left(\lambda_p - \lambda_s\right)KB_s/\lambda_p] \tag{8.17}$$

The value for parameter K should be chosen such that $c(\lambda_p, \lambda_s, B_s)$ approximates the bandwidth allocation of the network CAC policy. The limiting behavior of the cost function with respect to K is

$$c(\lambda_p, \lambda_s, B_s) \to \lambda_s \text{ as } K \to 0 \quad \text{and} \quad c(\lambda_p, \lambda_s, B_s) \to \lambda_p \text{ as } K \to \infty$$

Real-time UPC estimation is based on observations of the cell stream over a time period T. The procedure consists of the following steps: (1) estimate the mean and peak cell rates; (2) choose a set of candidate sustainable rates; (3) obtain the characterization of the stream; (4) for each candidate sustainable rate, compute the minimum bucket size required to meet a user constraint on shaping delay; and (5) choose the candidate rate that minimizes the cost function.

The *peak and mean rates* can be estimated from observations of the cell stream over a window of length T. The interval is subdivided into smaller subintervals of equal length $T_s = T/M$. For example, in experiments with MPEG video sequences described in Mark and Ramamurthy [5], T_s was set equal to the frame period of 33 ms. If n is the total number of cell arrivals during T and n_i the number of cell arrivals in the ith subinterval, then the mean rate can be estimated as $\hat{\lambda}_m = n/T$. For some applications, the peak rate may be known *a priori.* Otherwise, the peak rate can be estimated by $\hat{\lambda}_p = \max\{n_i/T_s; 1 \le i \le M\}$.

Candidate rates $\mu_1, \ldots, \mu_N$ are chosen between the mean and peak rates. The simplest approach is to choose N and space the candidate rates at uniform spacing between the mean and peak rates. However, with a more judicious method of assignment, the set of candidate rates can be kept small, while still including rates close to the near-optimal sustainable rates. Suppose that a prior estimate of the operating sustainable rate, $\hat{\lambda}_s$, is available. In the absence of prior knowledge, one could assign $\hat{\lambda}_s = (\hat{\lambda}_m + \hat{\lambda}_p)/2$. The candidate rate μ_N is assigned equal to $\hat{\lambda}_s$. The remaining rates are grouped into a set of Nc *coarsely spaced rates* and N_f *finely spaced rates*, with $N = N_c + N_f + 1$ and with N_f even. The coarse rates $\mu_1, \ldots, \mu_{N_c}$ are assigned to be spaced uniformly over the interval $(\hat{\lambda}_s, \hat{\lambda}_p)$ as $\mu_i = \hat{\lambda}_m + i\Delta_c, i = 1, \ldots, N_c$, where Δ_c is defined as $\Delta_c = (\hat{\lambda}_p - \hat{\lambda}_m)/(N_c + 1)$. The remaining N_f fine rates are assigned in the neighborhood of $\hat{\lambda}_s$ as follows: $\mu_{j+N_c} = \hat{\lambda}_s + j\Delta_f$, $j = 1, \ldots, N_f/2$, and $\mu_{j+N_c} = \hat{\lambda}_s - (j - N_f/2)\Delta_f$, $j = N_f/2, \ldots, N_f$, where $\Delta_f = \Delta_c/(N_c + 1)$. Figure 8.1 shows an example of the choice of candidate rates example with $N = 8$, $N_c = 3$ and $N_f = 4$.

Measurement of traffic parameters is based on the bank of queues. The ith fictitious queue is implemented using a counter n_i that is decremented at the constant rate μ_i and incremented by 1 whenever a cell arrives [5]. For each rate μ_i, estimates of the queue parameters $\hat{a}(\mu_i)$ and $\hat{b}(\mu_i)$ are obtained. Each queue is sampled at the arrival epoch of an 'arbitrary' cell. This sampling is carried out by skipping a random number of N_j cells between the $(j\text{-}1)_{\text{st}}$ and jth sampled arrivals. Since all of the fictitious queues are sampled at the same arrival epochs, only one random number needs to be generated for all queues at a sampling epoch. Over an interval of length T, a number of

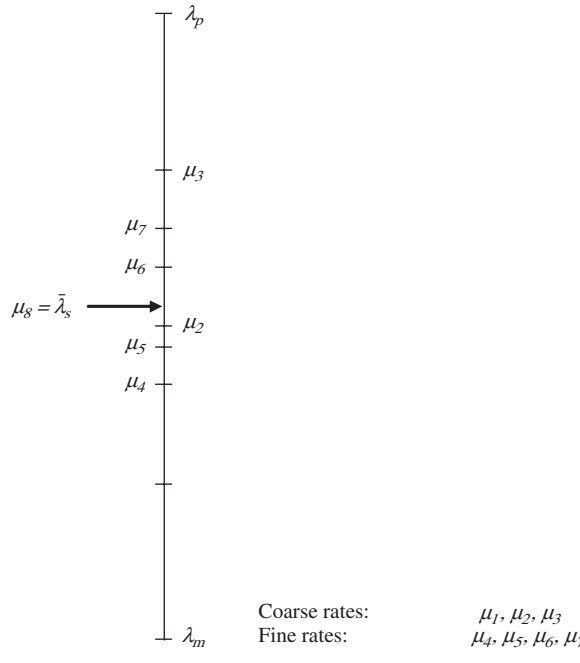

Figure 8.1 Example of candidate rate assignment.

samples, say M, are taken from the queues. At the jth sampling epoch, the following quantities are recorded for each queue: S_j, the number of customers in service (so $S_j \in \{0, 1\}$); Q_j, the number of customers in queue; and T_j, the remaining service time of the customer in service (if one is in service). After that the following sample means are computed:

$$\hat{a} = \sum_{j=1}^{M} S_j/M; \;\; \hat{q} = \sum_{j=1}^{M} Q_j/M; \;\; \hat{\tau}_r = \sum_{j=1}^{M} T_j/\hat{a}M$$

Parameter $\hat{b}$ is then computed by using Equation (8.8) as

$$\hat{b} = \frac{\mu\hat{a}}{\hat{q} + \mu\hat{a}\hat{\tau}_{\mathrm{r}}} \approx \frac{\mu\hat{a}}{\hat{q} + \hat{a}/2}$$

where $\hat{\tau}_{\mathrm{r}}$ is approximated by $\frac{1}{2}\mu$. The approximate statistical characterization is given by

$$\hat{C}_S = \left\{\hat{\lambda}_{\mathrm{p}}, \hat{\lambda}_{\mathrm{m}}\left[\hat{a}(\mu_i),\ \hat{b}(\mu_i)\right] : i = 1, \ldots, N\right\}$$

Mapping to a UPC Descriptor is focused on the case where the user specifies a maximum mean delay $\bar{D}$. The operating rate index is chosen to minimize the cost function defined in Equation (8.17):

$$i^* = \arg\min_{1 \le i \le N} c\left[\hat{\lambda}_{\mathrm{p}}, \mu_i, B_{\mathrm{s}}\left(\hat{C}_{\mathrm{S}}, \mu_i, \bar{D}\right)\right]$$

where $B_{\mathrm{s}}\left(\hat{C}_{\mathrm{S}}, \mu_i, \bar{D}\right)$ is defined in Equation (8.13) and represents the bucket size required to achieve a mean delay of $\bar{D}$ at a leak rate μ. Then the operating UPC descriptor is assigned as follows:

$$\lambda_{\mathrm{p}} = \hat{\lambda}_{\mathrm{p}}, \quad \lambda_{\mathrm{s}} = \mu_{i*}, \quad B_{\mathrm{s}} = B_{\mathrm{s}}\left(\hat{C}_{\mathrm{S}}, \mu_i, \bar{D}\right)$$

If the estimated mean and peak rates are close in value, the stream can be treated as a CBR stream. In this case, the UPC descriptor can simply be assigned according to the peak rate, i.e.

$$\lambda_p = \hat{\lambda}_p, \quad \lambda_s = \mu_{i*}, \quad B_s = 1$$

Some applications, such as video delivery, interactive multimedia sessions, etc., cannot be adequately characterized by a static set of parameters that are expected to hold for the entire session. The ability to renegotiate parameters during a session may be a viable way of efficiently supporting variable bit rate (VBR) traffic [5, 10] with real-time QoS constraints.

8.1.4 Performance example

In the MPEG standard for video compression, video is transmitted as a sequence of frames. For transmission over an ATM network, each MPEG frame must be segmented into ATM cells. In Mark and Ramamurthy [5], two modes of cell transmission over a frame interval are considered. In *nonsmooth mode*, the cells are transmitted at a constant rate λ_p starting at the beginning of the frame interval until the frame is fully transmitted. Then the source is silent until the beginning of the next frame interval. This results in an on–off type stream with correlated on and off periods. In *smooth mode*, the cells for the ith frame are transmitted at a constant rate $f(i)/\tau$ over the frame interval, where $f(i)$ is the total number of cells in the $i-$th frame and τ is the interframe period. Thus, buffering is done to smooth out the transmission of cells of each frame over the corresponding frame interval.

Figure 8.2 shows the characterization $\hat{C}_S$ obtained empirically for an MPEG video stream [5]. For this stream, the empirical mean and peak rates were determined to be 20 and 40.5 cells/ms, respectively. The two streams were offered to 19 queues running in parallel at the rates $\mu = 21, 22, \ldots, 39$ (cells/ms) and the corresponding values for $[a(\mu), b(\mu)]$ were obtained according to the procedure described above. In the nonsmooth mode, $a(\mu) \approx 1$ for all values of μ while for smooth mode, $a(\mu)$ monotonically decreases as μ increases from λ_m to λ_p. On the other hand the $b(\mu)$ curves for the nonsmooth and smooth modes are close for μ near to the extremes λ_m and λ_p. For values of μ closer to the center of the interval (λ_m, λ_p), the curve for smooth mode lies

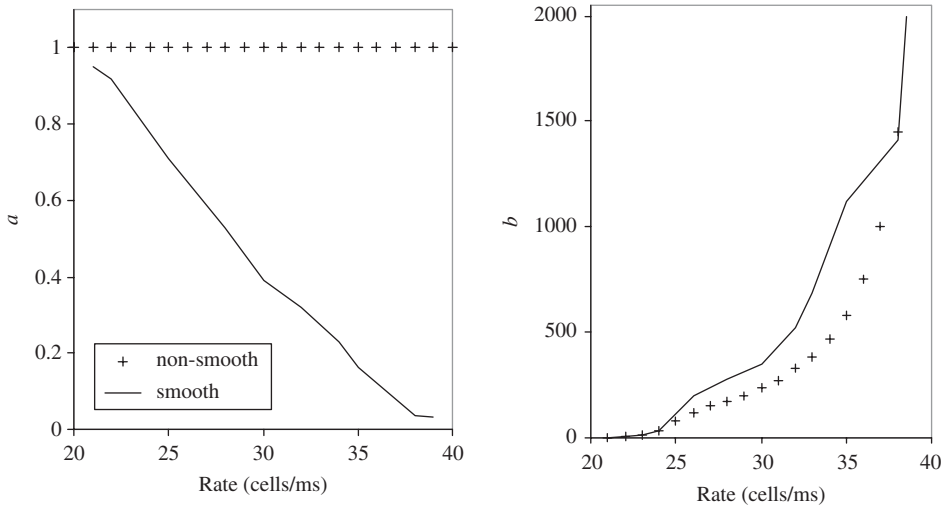

Figure 8.2 (a) a and (b) b parameters for MPEG.

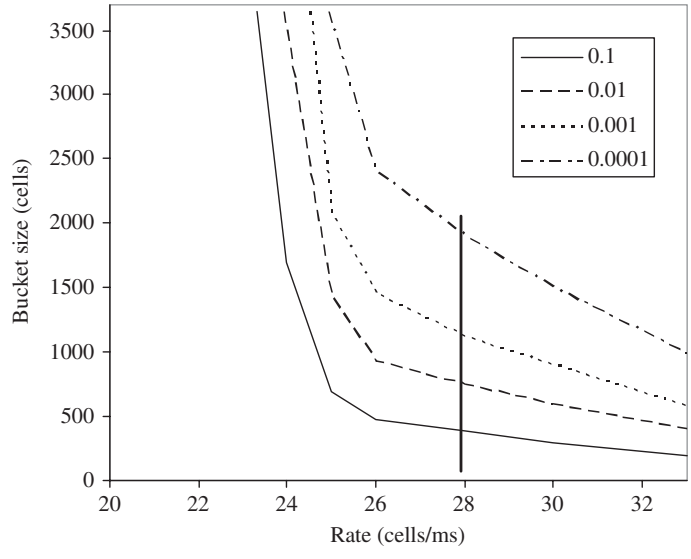

Figure 8.3 Shaping probability curves for nonsmooth mode.

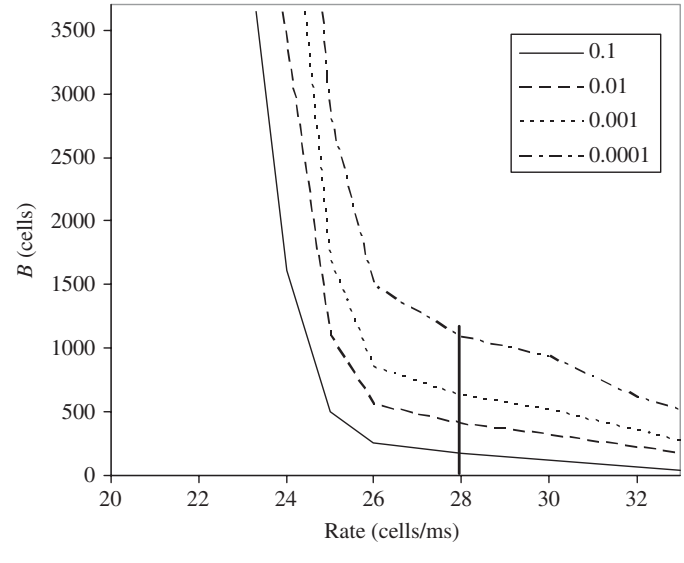

Figure 8.4 Shaping probability curves for smooth mode.

above the curve for nonsmooth mode. Thus, the characterization $\hat{C}_S$ captures the decrease in traffic burstiness due to intraframe smoothing.

Figures 8.3 and 8.4 demonstrate that, for example, the shaping probability of 0.00001 at cell rate of 28 can be achieved with $B = 1100$ in the case of *smooth mode* while nonsmooth mode would require $B = 2000$ for the same shaping probability. More interesting results on this issue can be found in Mark and Ramamurthy [5].

8.2 EFFECTIVE LINK LAYER CAPACITY

In the previous section we discussed the problem of effective characterization of the traffic source in terms of the parameters which are used to negotiate with the network a certain level of QoS. Similarly, on the network side, to enable the efficient support of quality of service (QoS) in 4G wireless networks, it is essential to model a wireless channel in terms of connection-level QoS metrics such as data rate, delay and delay-violation probability. The traditional wireless channel models, i.e. physical-layer channel models, do not explicitly characterize a wireless channel in terms of these QoS metrics. In this section, we discuss *a link-layer channel model* referred to as *effective capacity* (EC) [11]. In this approach, a wireless link is modeled by two EC functions, the probability of nonempty buffer and the QoS exponent of a connection. Then, a simple and efficient algorithm to estimate these EC functions is discussed. The advantage of the EC link-layer modeling and estimation is ease of translation into QoS guarantees, such as delay bounds and hence, efficiency in admission control and resource reservation.

Conventional channel models, directly characterize the fluctuations in the amplitude of a radio signal. These models will be referred to as *physical-layer channel* models, to distinguish them from the *link-layer channel* model discussed in this section. Physical-layer channel models provide a quick estimate of the physical-layer performance of wireless communications systems (e.g. symbol error rate vs SNR). However, physical-layer channel models cannot be easily translated into complex link-layer QoS guarantees for a connection, such as bounds on delay. The reason is that these complex QoS requirements need an analysis of the queueing behavior of the connection, which cannot be extracted from physical-layer models. Thus, it is hard to use physical-layer models in QoS support mechanisms, such as admission control and resource reservation.

For these reasons, it was proposed to move the channel model up the protocol stack from the physical layer to the link layer. The resulting model is referred to as EC link model because it captures a generalized link-level capacity notion of the fading channel. Figure 8.5 illustrates

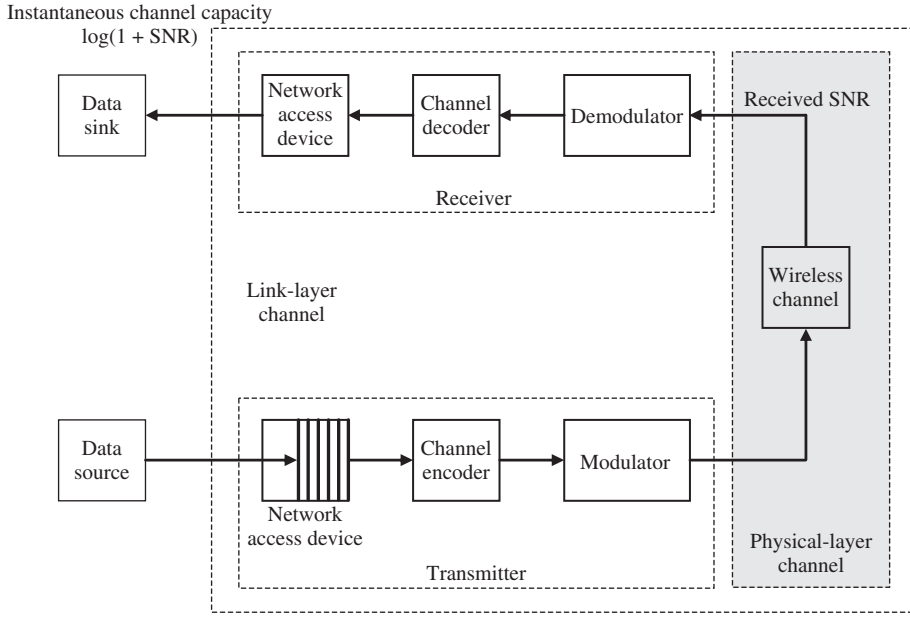

Figure 8.5 Packet-based wireless communication system.

the difference between the conventional physical-layer and link-layer model. For simplicity, the 'physical-layer channel' will be called the 'physical channel' and 'link-layer channel' will be referred to as the 'link'.

8.2.1 Link-layer channel model

4G wireless systems will need to handle increasingly diverse multimedia traffic, which are expected to be primarily packet-switched. The key difference between circuit switching and packet switching, from a link-layer design viewpoint, is that packet switching requires *queueing* analysis of the link. Thus, it becomes important to characterize the effect of the data traffic pattern, as well as the channel behavior, on the performance of the communication system.

QoS guarantees have been heavily researched in the *wired* networks [e.g. ATM and Internet protocol (IP) networks]. These guarantees rely on the queueing model shown in Figure 8.6 and studied in Chapter 6. This figure shows that the source traffic and the network service are matched using a first-in first-out buffer (queue). Thus, the queue prevents loss of packets that could occur when the source rate is more than the service rate, at the expense of increasing the delay. Queueing analysis, which is needed to design appropriate admission control and resource reservation algorithms, requires source *traffic characterization* and *service characterization*. The most widely used approach for traffic characterization is to require that the amount of data (i.e. bits as a function of time t) produced by a source conform to an upper bound, called the *traffic envelope*, $\Gamma(t)$. The service characterization for guaranteed service is a guarantee of a minimum service (i.e. bits communicated as a function of time) level, specified by a service curve $SC\ \Psi(t)$[12]. Functions $\Gamma(t)$ and $\Psi(t)$ are specified in terms of certain traffic and service parameters, respectively. Examples include the UPC parameters, discussed in the previous section, used in ATM for traffic characterization, and the traffic specification (T-SPEC) and the service specification (R-SPEC) fields used with the resource reservation protocol [12] in IP networks.

A traffic envelope $\Gamma(t)$ characterizes the source behavior in the following manner: over any window of size t, the amount of actual source traffic $A(t)$ does not exceed $\Gamma(t)$ (see Figure 8.7). For example, the UPC parameters, discussed in Section 8.1, specifies $\Gamma(t)$ by

$$\Gamma(t) = \min\left\{\lambda_{\mathrm{p}}^{(s)}t,\ \lambda_{\mathrm{s}}^{(s)}t + \sigma^{(s)}\right\} \tag{8.18}$$

where $\lambda_{\mathrm{p}}^{(s)}$ is the peak data rate, $\lambda_{\mathrm{s}}^{(s)}$ the sustainable rate, and $\sigma^{(s)} = B_{\mathrm{s}}$ the leaky-bucket size [12]. As shown in Figure 8.7, the curve $\Gamma(t)$ consists of two segments: the first segment has a slope equal to the peak source data rate $\lambda_{\mathrm{p}}^{(s)}$, while the second has a slope equal to the sustainable rate $\lambda_{\mathrm{s}}^{(s)}$, with

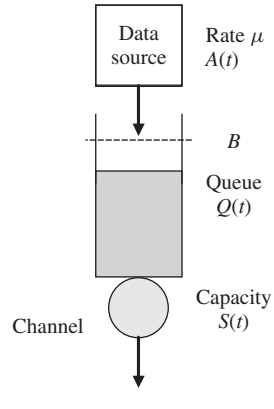

Figure 8.6 Queueing system model.

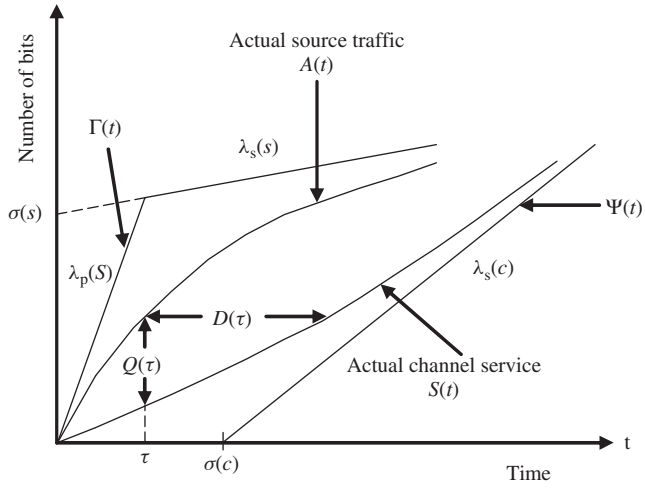

Figure 8.7 Traffic and service characterization. (Reproduced by permission of IEEE [11].)

$\lambda_s^{(s)} < \lambda_p^{(s)}$. $\sigma^{(s)}$ is the y-axis intercept of the second segment. $\Gamma(t)$ has the property that $A(t) \leq \Gamma(t)$ for any time t. Just as $\Gamma(t)$ upper bounds the source traffic, a network SC $\Psi(t)$ lower bounds the actual service $S(t)$ that a source will receive. $\Psi(t)$ has the property that $\Psi(t) \leq S(t)$ for any time t. Both $\Gamma(t)$ and $\Psi(t)$ are negotiated during the admission control and resource reservation phase. An example of a network SC is the R-SPEC curve used for guaranteed service in IP networks

$$\Psi(t) = \max\left[\lambda_s^{(c)}(t - \sigma^{(c)}), 0\right] = \left[\lambda_s^{(c)}(t - \sigma^{(c)})\right]^+ \tag{8.19}$$

where $\lambda_s^{(c)}$ is the constant service rate, and $\sigma^{(c)}$ the delay (due to propagation delay, link sharing, and so on). This curve is illustrated in Figure 8.7. $\Psi(t)$ consists of two segments; the horizontal segment indicates that no packet is being serviced due to propagation delay, etc., for a time interval equal to the delay $\sigma^{(c)}$, while the second segment has a slope equal to the service rate $\lambda_s^{(c)}$. In the figure, the horizontal difference between $A(t)$ and $S(t)$, denoted $D(\tau)$, is the delay experienced by a packet arriving at time τ, and the vertical difference between the two curves, denoted by $Q(\tau)$, is the queue length built up at time τ, due to packets that have not been served yet.

Providing QoS guarantees over wireless channels requires accurate models of their *time-varying capacity*, and effective utilization of these models for QoS support. The simplicity of the SCs discussed earlier motivates us to define the time-varying capacity of a wireless channel as in Equation (8.19). Specifically, we hope to lower bound the channel service using two parameters: the channel sustainable rate $\lambda_s^{(c)}$, and the maximum fade duration $\sigma^{(c)}$.

Parameters $\lambda_s^{(c)}$ and $\sigma^{(c)}$ are meant to be in a statistical sense. The maximum fade duration $\sigma^{(c)}$ is a parameter that relates the delay constraint to the channel service. It determines the probability $\sup_t \Pr\{S(t) < \Psi(t)\}$. We will see later that $\sigma^{(c)}$ is specified by the source with $\sigma^{(c)} = D_{\max}$, where D is the delay bound required by the source.

However, physical-layer wireless channel models do not explicitly characterize the channel in terms of such link-layer QoS metrics as data rate, delay and delay-violation probability. For this reason, we are forced to look for alternative channel models.

A problem that surfaces is that a wireless channel has a capacity that varies *randomly* with time. Thus, an attempt to provide a strict lower bound [i.e. the deterministic SC $\Psi(t)$, used in IP networks] will most likely result in extremely conservative guarantees. For example, in a Rayleigh or Ricean fading channel, the only lower bound that can be *deterministically* guaranteed is a capacity of zero. The capacity here is meant to be delay-limited capacity, which is the maximum

rate achievable with a prescribed delay bound (see Hanly and Tse [13] for details). This conservative guarantee is clearly useless in practice. Therefore, the concept of deterministic SC $\Psi(t)$ is extended to a *statistical* version, specified as the pair $\{\Psi(t),\ \varepsilon\}$. The statistical SC $\{\Psi(t),\ \varepsilon\}$ specifies that the service provided by the channel, denoted $\tilde{S}(t)$, will always satisfy the property that $\sup_t \Pr\left\{\tilde{S}(t) < \Psi(t)\right\} \leq \varepsilon$. In other words, ε is the probability that the wireless channel will not be able to support the pledged SC $\Psi(t)$, referred to as the outage probability. For most practical values of ε, a *nonzero* SC $\Psi(t)$ can be guaranteed.

8.2.2 Effective capacity model of wireless channels

From the previous discussion we can see that for the QoS control we need to calculate an SC $\Psi(t)$ such that, for a given $\varepsilon > 0$, the following probability bound on the channel service $\tilde{S}(t)$ is satisfied:

$$\sup_t \Pr\left\{\tilde{S}(t) < \Psi(t)\right\} \leq \varepsilon \text{ and } \Psi(t) = \left[\lambda_s^{(c)}(t - \sigma^{(c)})\right]^+ \tag{8.20}$$

The statistical SC specification requires that we relate its parameters $\{\lambda_s^{(c)}, \sigma^{(c)}, \varepsilon\}$ to the fading wireless channel, which at the first sight seems to be a hard problem. At this point, the idea that the SC $\Psi(t)$ is a *dual* of the traffic envelope $\Gamma(t)$ is used [11]. A number of papers exist on the so-called *theory of effective bandwidth* [14], which models the statistical behavior of *traffic*. In particular, the theory shows that the relation $\sup_t \Pr\{Q(t) \geq B\} \leq \varepsilon$ is satisfied for large B, by choosing two parameters (which are functions of the channel rate r) that depend on the actual data traffic, namely, the probability of nonempty buffer, and the effective bandwidth of the source. *Thus, a source model defined by these two functions fully characterizes the source from a QoS viewpoint*. The duality between Equation (8.20) and $\sup_t \Pr\{Q(t) \geq B\} \leq \varepsilon$ indicates that it may be possible to adapt the theory of effective bandwidth to SC characterization. This adaptation will point to a new channel model, which will be referred to as the *effective capacity (EC) link model*. Thus, the EC link model can be thought of as the dual of the effective bandwidth source model, which is commonly used in networking.

8.2.2.1 Effective bandwidth

The stochastic behavior of a source traffic can be modeled asymptotically by its effective bandwidth. Consider an arrival process $\{A(t), t \geq 0\}$, where $A(t)$ represents the amount of source data (in bits) over the time interval [0, t). Assume that the asymptotic *log-moment generating function* of $A(t)$, defined as

$$\Lambda(u) = \lim_{t\to\infty} \frac{1}{t} \log E\left[e^{uA(t)}\right] \tag{8.21}$$

exists for all $u \geq 0$. Then, the *effective bandwidth function* of $A(t)$ is defined as [11, 14]

$$\alpha(u) = \frac{\Lambda(u)}{u}, \qquad \forall u \geq 0. \tag{8.22}$$

This becomes more evident if we assume the constant traffic $A(t) = A$ so that Equation (8.21) gives

$$\Lambda(u) = \lim_{t\to\infty} \frac{1}{t} \log E\left[e^{uA(t)}\right] = \lim_{t\to\infty} \frac{1}{t} \log E\left[e^{uA}\right] = \lim_{t\to\infty} \frac{uA}{t} = u \lim_{t\to\infty} \frac{A}{t} = u\alpha(u) \tag{8.21a}$$

Consider now a queue of infinite buffer size served by a channel of *constant service rate r*, such as an AWGN channel. Owing to the possible mismatch between $A(t)$ and $S(t)$, the queue length

$Q(t)$ could be nonzero. As already discussed in Section 8.1 [analogous to Equation (8.5)] or by using the theory of large deviations [14] , it can be shown that the probability of $Q(t)$ exceeding a threshold B satisfies

$$\sup_t \Pr\{Q(t) \geq B\} \sim \mathrm{e}^{-\theta_B(r)B} \quad \text{as } B \to \infty \tag{8.23}$$

where $f(x) \approx g(x)$ means that $\lim_{x\to\infty} f(x)/g(x) = 1$. For smaller values of B, the following approximation, analogous to Equation (8.3), is more accurate [15]:

$$\sup_t \Pr\{Q(t) \geq B\} \approx \gamma(r)\mathrm{e}^{-\theta_B(r)B} \tag{8.24}$$

where both $\gamma(r)$ and $\theta_B(r)$ are functions of channel capacity r. According to the theory, $\gamma(r) = \Pr\{Q(t) \geq 0\}$ is the *probability that the buffer is nonempty* for randomly chosen time t, while the *QoS exponent* θ_B is the solution of $\alpha(\theta_B) = r$. Thus, the pair of functions $\{\gamma(r),\ \theta_B(r)\}$ model the source. Note that $\theta_B(r)$ is simply the inverse function corresponding to the effective bandwidth function $\alpha(u)$.

If the quantity of interest is the delay $D(t)$ experienced by a source packet arriving at time t, then with same reasoning the probability of $D(t)$ exceeding a delay bound $D_{\max}$ satisfies

$$\sup_t \Pr\{D(t) \geq D_{\max}\} \approx \gamma(r)\mathrm{e}^{-\theta(r)D_{\max}} \tag{8.25}$$

where $\theta(r) = \theta_B(r) \times r$ [16]. Thus, the key point is that for a source modeled by the pair $\{\gamma(r),\ \theta(r)\}$, which has a communication delay bound of $D_{\max}$, and can tolerate a delay-bound violation probability of at most ε, the effective bandwidth concept shows that the constant channel capacity should be at least r, where r is the solution to $\varepsilon = \gamma(r)\mathrm{e}^{-\theta(r)D_{\max}}$. In terms of the traffic envelope $\Gamma(t)$ (Figure 8.7), the slope $\lambda_s^{(s)} = r$ and $\sigma^{(s)} = rD_{\max}$.

In Section 8.1 a simple and efficient algorithm to estimate the source model functions $\gamma(r)$ and $\theta(r)$ was discussed. In the following section, we use the duality between traffic modeling $\{\gamma(r),\ \theta(r)\}$, and channel modeling to present an EC link model, specified by a pair of functions $\{\gamma^{(c)}(\mu),\ \theta^{(c)}(\mu)\}$. The intention is to use $\{\gamma^{(c)}(\mu),\ \theta^{(c)}(\mu)\}$ as the channel duals of the source functions $\{\gamma(r),\ \theta(r)\}$. Just as the constant *channel rate* r is used in source traffic modeling, we use the constant *source traffic rate* μ in modeling the channel. Furthermore, we adapt the source estimation algorithm from Section 8.1 to estimate the link model parameters $\{\gamma^{(c)}(\mu),\ \theta^{(c)}(\mu)\}$.

8.2.2.2 Effective capacity link model

Let $r(t)$ be the instantaneous channel capacity at time t. Define $\tilde{S}(t) = \int_0^t r(\tau)\,\mathrm{d}\tau$, which is the service provided by the channel. Note that the channel service $\tilde{S}(t)$ is different from the actual service $S(t)$ received by the source; $\tilde{S}(t)$ only depends on the instantaneous channel capacity and thus is independent of the arrival $A(t)$. Paralleling the development of Equation (8.21) and (8.22) we assume that

$$\Lambda^{(c)}(-u) = \lim_{t\to\infty} \frac{1}{t} \log E\left[\mathrm{e}^{-u\tilde{S}(t)}\right] \tag{8.26}$$

exists for all $u \geq 0$. This assumption is valid, for example, for a stationary Markov-fading process $r(t)$. Then, the *EC function* of $r(t)$ is defined as

$$\alpha^{(c)}(u) = \frac{-\Lambda^{(c)}(-u)}{u}, \qquad \forall u \geq 0 \tag{8.27}$$

Consider a queue of infinite buffer size supplied by a data source of *constant* data rate μ (see Figure 8.6). The theory of effective bandwidth can be easily adapted to this case. The difference

is that, whereas in the previous case the source rate was variable while the channel capacity was constant, now the source rate is constant while the channel capacity is variable. Similar to Equation (8.25), it can be shown that the probability of $D(t)$ exceeding a delay bound $D_{\max}$ satisfies

$$\sup_t \Pr\{D(t) \geq D_{\max}\} \approx \gamma^{(c)}(\mu)\mathrm{e}^{-\theta^{(c)}(\mu)D_{\max}} \tag{8.28}$$

where $\{\gamma^{(c)}(\mu),\ \theta^{(c)}(\mu)\}$ are functions of source rate μ. This approximation is accurate for large $D_{\max}$, but we will see later in the simulation results, that this approximation is also accurate even for smaller values of $D_{\max}$.

For a given source rate μ, $\gamma^{(c)}(\mu) = \Pr\{Q(t) \geq 0\}$ is again the *probability that the buffer is nonempty* at a randomly chosen time t, while the *QoS exponent* $\theta^{(c)}(\mu)$ is defined as $\theta(\mu) = \mu\alpha^{-1}(\mu)$, where $\alpha^{-1}(\cdot)$ is the inverse function of $\alpha^{(c)}(u)$. Thus, the pair of functions $\{\gamma^{(c)}(\mu),\ \theta^{(c)}(\mu)\}$ model the link.

So, if a link that is modeled by the pair $\{\gamma^{(c)}(\mu),\ \theta^{(c)}(\mu)\}$ is used, a source that requires a communication delay bound of $D_{\max}$, and can tolerate a delay-bound violation probability of at most ε, needs to limit its data rate to a maximum of μ, where μ is the solution to $\varepsilon = \gamma^{(c)}(\mu)\mathrm{e}^{-\theta^{(c)}(\mu)D_{\max}}$. In terms of the SC $\Psi(t)$ shown in Figure 8.7, the channel sustainable rate $\lambda_{\mathrm{s}}^{(c)} = \mu$ and $\sigma^{(c)} = D_{\max}$.

If the channel-fading process $r(t)$ is stationary and ergodic, then a simple algorithm to estimate the functions $\{\gamma^{(c)}(\mu),\ \theta^{(c)}(\mu)\}$ is similar to the one described in Section 8.1. Paralleling Equation (8.7) we have

$$\frac{\gamma^{(c)}(\mu)}{\theta^{(c)}(\mu)} = E[D(t)] = \tau_{\mathrm{s}}(\mu) + \frac{E[Q(t)]}{\mu} \tag{8.29}$$

$$\gamma^{(c)}(\mu) = \Pr\{D(t) > 0\} \tag{8.30}$$

where $\tau_{\mathrm{s}}(\mu)$ is the average remaining service time of a packet being served. Note that $\tau_{\mathrm{s}}(\mu)$ is zero for a fluid model (assuming infinitesimal packet size). Now, the delay $D(t)$ is the sum of the delay incurred due to the packet already in service, and the delay in waiting for the queue $Q(t)$ to clear which results in Equation (8.29), using Little's theorem. Substituting $D_{\max} = 0$ in Equation (8.28) results in Equation (8.30). As in Section 8.1, solving Equation (8.29) for $\theta^{(c)}(\mu)$ gives similarly to Equation (8.8a)

$$\theta^{(c)}(\mu) = \frac{\gamma^{(c)}(\mu) \times \mu}{\mu \times \tau_s(\mu) + E[Q(t)]} \tag{8.31}$$

According to Equation (8.30) and (8.31) , as in Section 8.1, the functions γ and θ can be estimated by estimating $\Pr\{D(t) > 0\}$, $\tau_{\mathrm{s}}(\mu)$, and $E[Q(t)]$. The latter can be estimated by taking a number of samples, say N, over an interval of length T, and recording the following quantities at the nth sampling epoch: S_n the indicator of whether a packets is in service ($S_n \in \{0,\ 1\}$), Q_n the number of bits in the queue (excluding the packet in service), and T_n the remaining service time of the packet in service (if there is one in service). Based on the same measurements, as in Section 8.1,

$$\hat{\gamma} = \sum_{n=1}^{N} S_n/N$$

$$\hat{q} = \sum_{n=1}^{N} Q_n/N$$

$$\hat{\tau}_{\mathrm{s}} = \sum_{n=1}^{N} T_n/N$$

are computed and then, from Equation (8.31), we have

$$\hat{\theta} = \frac{\hat{\gamma} \times \mu}{\mu \times \hat{\tau}_s + \hat{q}} \tag{8.32}$$

These parameters are used to predict the QoS by approximating Equation (8.28) with

$$\sup_t \Pr\{D(t) \geq D_{\max}\} \approx \hat{\gamma} e^{-\hat{\theta} D_{\max}} \tag{8.33}$$

If the ultimate objective of EC link modeling is to compute an appropriate SC $\Psi(t)$, then, given the delay-bound $D_{\max}$ and the target delay-bound violation probability ε of a connection, we can find $\Psi(t) = \{\sigma^{(c)}, \lambda_s^{(c)}\}$ by setting $\sigma^{(c)} = D_{\max}$, solving Equation (8.33) for μ and setting $\lambda_s^{(c)} = \mu$.

8.2.3 Physical layer vs link-layer channel model

In Jack's model of a Rayleigh flat-fading channel, the Doppler spectrum $S(f)$ is given as

$$S(f) = \frac{1.5}{\pi f_m \sqrt{1 - (F/f_m)^2}} \tag{8.34}$$

where f_m is the maximum Doppler frequency, f_c is the carrier frequency, and $F = f - f_c$. Below we show how to calculate the EC for this channel [11].

Denote a sequence of N measurements of the channel gain, spaced at a time interval δ apart, by $\mathbf{x} = [x_0,\ x_1, \cdots,\ x_{N-1}]$, where $\{x_n,\ n \in [0,\ N-1]\}$ are the complex-valued Gaussian distributed channel gains ($|x_n|$ are, therefore, Rayleigh distributed). For simplicity, the constant noise variance will be included in the definition of x_n. The measurement x_n is a realization of a random variable sequence denoted by X_n, which can be written as the vector $\mathbf{X} = [X_0, X_1, \cdots, X_{N-1}]$. The pdf of a random vector $\mathbf{X}$ for the Rayleigh-fading channel is

$$f_{\mathbf{X}}(\mathbf{X}) = \frac{1}{\pi^N \det(\mathbf{R})} e^{-\mathbf{x}\mathbf{R}^{-1}\mathbf{x}^H} \tag{8.35}$$

where $\mathbf{R}$ is the covariance matrix of the random vector $\mathbf{X}$, $\det(\mathbf{R})$ the determinant of matrix $\mathbf{R}$, and $\mathbf{x}^H$ the conjugate transpose (Hermitan) of $\mathbf{x}$. To calculate the EC, we start with

$$\begin{aligned} E[e^{-u\tilde{S}(t)}] &= E\left[\exp\left[-u\int_0^t r(\tau)\,d\tau\right]\right] \overset{(a)}{\approx} \int \exp\left\{-u\left[\sum_{n=0}^{N-1}\delta \times r(\tau_n)\right]\right\} f_{\mathbf{x}}(\mathbf{x})\,d\mathbf{x} \\ &\overset{(b)}{\approx} \int \exp\left\{-u\left[\sum_{n=0}^{N-1}\delta \log(1+|x_n|^2)\right]\right\} f_{\mathbf{x}}(\mathbf{x})\,d\mathbf{x} \\ &\overset{(c)}{\approx} \int \exp\left\{-u\left[\sum_{n=0}^{N-1}\delta \log(1+|x_n|^2)\right]\right\} \cdot \frac{1}{\pi^N \det(\mathbf{R})} e^{-\mathbf{x}\mathbf{R}^{-1}\mathbf{x}^H}\,d\mathbf{x} \end{aligned} \tag{8.36}$$

where (a) approximates the integral by a sum, (b) is the Shannon result for channel capacity (i.e. $\gamma(\tau_n) = \log(1 + |x_n|^2)$, and (c) is from Equation (8.35). This gives the EC, Equation (8.27), as

$$\alpha^{(c)}(u) = \frac{-1}{u} \lim_{t\to\infty} \log \int \exp\left\{-u\left[\sum_{n=0}^{N-1}\delta \log(1+|x_n|^2)\right]\right\} \cdot \frac{1}{\pi^N \det(\mathbf{R})} e^{-\mathbf{x}\mathbf{R}^{-1}\mathbf{x}^H}\,d\mathbf{x} \tag{8.37}$$

Using the approximation $(a)\ \log(1+|x_n|^2) \approx |x_n|^2$ for low SNR [11], Equation (8.37) can be further simplified as

$$\begin{aligned} E[\mathrm{e}^{-u\tilde{S}(t)}] &\overset{(a)}{\approx} \int \exp\left[-u\delta\left(\sum_{n=0}^{N-1}|x_n|^2\right)\right].\frac{1}{\pi^N \det(\mathbf{R})}\mathrm{e}^{-\mathbf{x}\mathbf{R}^{-1}\mathbf{x}^{\mathrm{H}}}\,\mathrm{d}\mathbf{x} \\ &\overset{(b)}{=} \int \mathrm{e}^{-u\delta||\mathbf{x}||^2}\frac{1}{\pi^N \det(\mathbf{R})}\mathrm{e}^{-\mathbf{x}\mathbf{R}^{-1}\mathbf{x}^{\mathrm{H}}}\,\mathrm{d}\mathbf{x} \overset{(b)}{=} \frac{1}{\pi^N \det(\mathbf{R})}\int \mathrm{e}^{-\mathbf{x}(\mathbf{R}^{-1}+u\delta\mathbf{I})\mathbf{x}^{\mathrm{H}}}\,\mathrm{d}\mathbf{x} \\ &= \frac{1}{\pi^N \det(\mathbf{R})}\times\pi^N \det\left[(\mathbf{R}^{-1}+u\delta\mathbf{I})^{-1}\right] = \frac{1}{\det(u\delta\mathbf{R}+\mathbf{I})} \end{aligned} \tag{8.38}$$

where approximation (b) is due to the definition of the norm of the vector $\mathbf{x}$, and (c) the relation $\|\mathrm{x}\|^2 = \mathbf{x}\mathbf{x}^{\mathrm{H}}$ ($\mathbf{I}$ is identity matrix). Reference [11] considers three cases of interest for Equation (8.38).

8.2.3.1 High mobility scenario

In the extreme high mobility (HM) case there is no correlation between the channel samples and we have $\mathbf{R} = r\mathbf{I}$, where $r = E\,|x_n|^2$ is the average channel capacity. From Equation (8.38), we have

$$E[\mathrm{e}^{-u\tilde{S}(t)}] \approx \frac{1}{\det(u\delta\mathbf{R}+\mathbf{I})} = \frac{1}{(ur\delta+1)^N} = \frac{1}{(urt/N+1)^N} \tag{8.39}$$

where $\delta = t/N$. As the number of samples $N \to \infty$, we have

$$\lim_{N\to\infty} E[\mathrm{e}^{-u\tilde{S}(t)}] \approx \lim_{N\to\infty}(urt/N+1)^{-N} = \mathrm{e}^{-urt} \tag{8.40}$$

Thus, in the limiting case, the Rayleigh-fading channel reduces to an AWGN channel. Note that this result would not apply at high SNRs because of the concavity of the $\log(\cdot)$ function.

8.2.3.2 Stationary scenario

In this case all the samples are fully correlated, $\mathbf{R} = [R_{ij}] = [r]$. In other words all elements of $\mathbf{R}$ are the same and Equation (8.38) now gives

$$E[\mathrm{e}^{-u\tilde{S}(t)}] \approx \frac{1}{\det(u\delta\mathbf{R}+\mathbf{I})} = \frac{1}{ur\delta N+1} = \frac{1}{ur\times\dfrac{t}{N}\times N+1} = \frac{1}{1+urt} \tag{8.41}$$

8.2.3.3 General case

Denote the eigenvalues of matrix $\mathbf{R}$ by $\{\lambda_n, n\in[0,N-1]\}$. Since $\mathbf{R}$ is symmetric, we have $\mathbf{R} = \mathbf{U}\mathbf{D}\mathbf{U}^{\mathrm{H}}$, where $\mathbf{U}$ is a unitary matrix, $\mathbf{U}^{\mathrm{H}}$ is its Hermitian, and the diagonal matrix $\mathbf{D} = \mathrm{diag}\,(\lambda_0, \lambda_1, \cdots, \lambda_{N-1})$. From Equation (8.38), we have

$$\begin{aligned} E[\mathrm{e}^{-u\tilde{S}(t)}] &\approx \frac{1}{\det(u\delta\mathbf{R}+\mathbf{I})} = \frac{1}{\det(u\delta\mathbf{U}\mathbf{D}\mathbf{U}^{\mathrm{H}}+\mathbf{U}\mathbf{U}^{\mathrm{H}})} \\ &= \frac{1}{\det[\mathbf{U}\,\mathrm{diag}\,(u\delta\lambda_0+1, u\delta\lambda_1+1, \ldots, u\delta\lambda_{N-1}+1)\mathbf{U}^{\mathrm{H}}]} \\ &= \frac{1}{\prod_n(u\delta\lambda_n+1)} = \exp\left[-\sum_n \log(u\delta\lambda_n+1)\right] \end{aligned} \tag{8.42}$$

We now use the calculated $E[e^{-u\tilde{S}(t)}]$ to get

$$\Lambda^{(c)}(-u) = \lim_{t\to\infty} \frac{1}{t} \log E[e^{-u\tilde{S}(t)}] \overset{(a)}{\approx} \lim_{t\to\infty} \frac{1}{t} \log \exp\left[-\sum_n \log(u\delta\lambda_n + 1)\right]$$
$$\overset{(b)}{=} \lim_{\Delta f\to 0} -\Delta f \sum_n \log\left(u\frac{\lambda_n}{B_w} + 1\right) \overset{(c)}{=} -\int \log(uS(f) + 1)\, \mathrm{d}f \tag{8.43}$$

where (a) follows from Equation (8.42), (b) follows from the fact that the frequency interval $\Delta f = 1/t$ and the bandwidth $B_\mathrm{w} = 1/\delta$, and (c) from the fact that the power spectral density $S(f) = \lambda_n/B_\mathrm{w}$ and that the limit of a sum becomes an integral. This gives the EC, Equation (8.27), as

$$\alpha^{(c)}(u) = \frac{\int \log(uS(f) + 1)\mathrm{d}f}{u} \tag{8.44}$$

Thus, the Doppler spectrum allows us to calculate $\alpha^{(c)}(u)$. The EC function, Equation (8.44), can be used to guarantee QoS using Equation (8.28).

One should keep in mind that the EC function, Equation (8.44), is valid only for a Rayleigh flat-fading channel, *at low SNR*. At high SNR, the EC for a Rayleigh-fading channel is specified by the complicated integral in Equation (8.37). To the best of our knowledge, a closed-form solution to Equation (8.37) does not exist. It is clear that a numerical calculation of EC is also very difficult, because the integral has a high dimension. Thus, it is difficult to extract QoS metrics from a physical-layer channel model, even for a Rayleigh flat-fading channel. The extraction may not even be possible for more general fading channels. In contrast, the EC link model that was described in this section can be easily translated into QoS metrics for a connection, and we have shown a simple estimation algorithm to estimate the EC model functions.

8.2.4 Performance examples

The discrete-time system depicted in Figure 8.8 is simulated. The data source generates packets at a *constant* rate μ which are first sent to the (infinite) buffer at the transmitter, whose queue length is Q_n, where n refers to the nth sample interval. The head-of-line packet in the queue is transmitted over the fading channel at data rate r_n. The fading channel has a random channel gain x_n (the noise variance is absorbed into x_n). We use a fluid model that is the size of a packet is infinitesimal. A perfect knowledge of the channel gain x_n (the SNR, really) at the transmitter side is assumed. Therefore, it can use rate-adaptive transmissions and strong channel coding to transmit packets without errors. Thus, the transmission rate r_n is equal to the instantaneous (time-varying) capacity of the fading channel, defined by the Shannon law, $r_n = B_\mathrm{c} \log_2(1 + |x_n|^2)$ where B_c is the channel bandwidth.

The average SNR is fixed in each simulation run. We define r_g as the capacity of an equivalent AWGN channel, which has the same average SNR, i.e. $r\mathrm{g} = B_\mathrm{c} \log_2(1 + \mathrm{SNR}_\mathrm{avg})$ where $\mathrm{SNR}_\mathrm{avg}$ is the average SNR, i.e. $E\,|x_n|^2$. Then, r_n/r_g relation

$$r_n = \frac{r_\mathrm{awgn} \log_2(1 + |x_n|^2)}{\log_2(1 + \mathrm{SNR}_\mathrm{avg})} \tag{8.45}$$

Simulation parameters as in Wu and Negi [11] were used. Channel samples x_n are generated by the following AR(1) (autoregressive) model: $x_n = kx_{n-1} + v_n$ where the modeling error v_n is zero-mean complex Gaussian with unit variance per dimension and is statistically independent of x_{n-1}. The coefficient k can be determined by the following procedure: (1) compute the coherence time T_c by $T_\mathrm{c} \approx 9/16\pi f_\mathrm{m}$, where the coherence time is defined as the time over which the time autocorrelation function of the fading process is above 0.5; (2) compute the coefficient k by

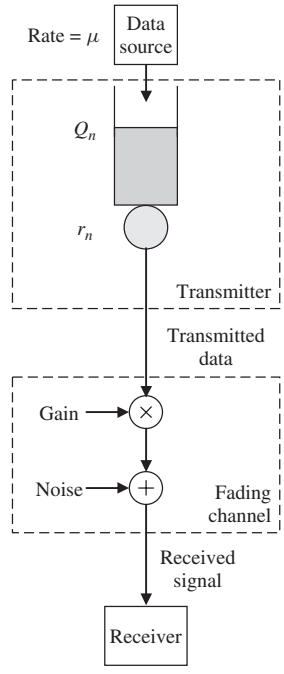

Figure 8.8 Queueing model used for simulations.

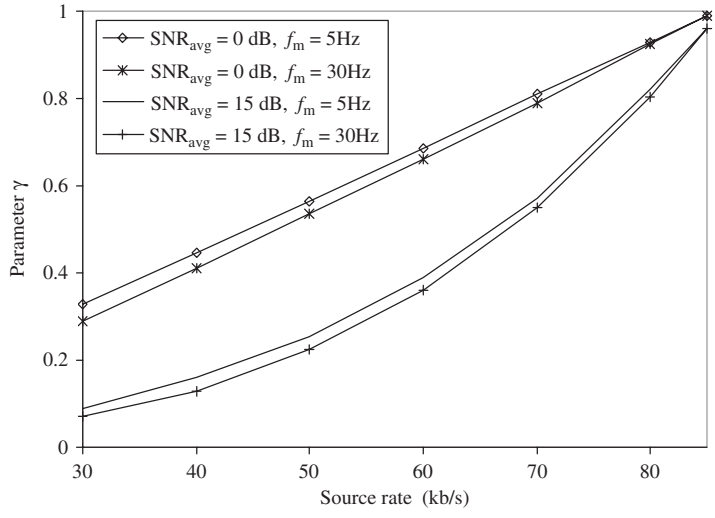

Figure 8.9 Estimated function $\hat{\gamma}(\mu)$ vs source rate μ.

$k = 0.5^{T_s/T_c}$ where T_s is the sampling interval. The other parameters are: $f_m = 5$–30 Hz, $r_g = 100$ kb/s, average SNR $= 0/15$ dB, $T_s = 1$ ms, bit rate $\mu = 30$–85 kb/s.

Figures 8.9 and 8.10 show the estimated EC functions $\hat{\gamma}(\mu)$ and $\hat{\theta}(\mu)$. As the source rate μ increases from 30 to 85 kb/s, $\hat{\gamma}(\mu)$ increases, indicating a higher buffer occupancy, while $\hat{\theta}(\mu)$ decreases, indicating a slower decay of the delay-violation probability. Thus, the delay-violation

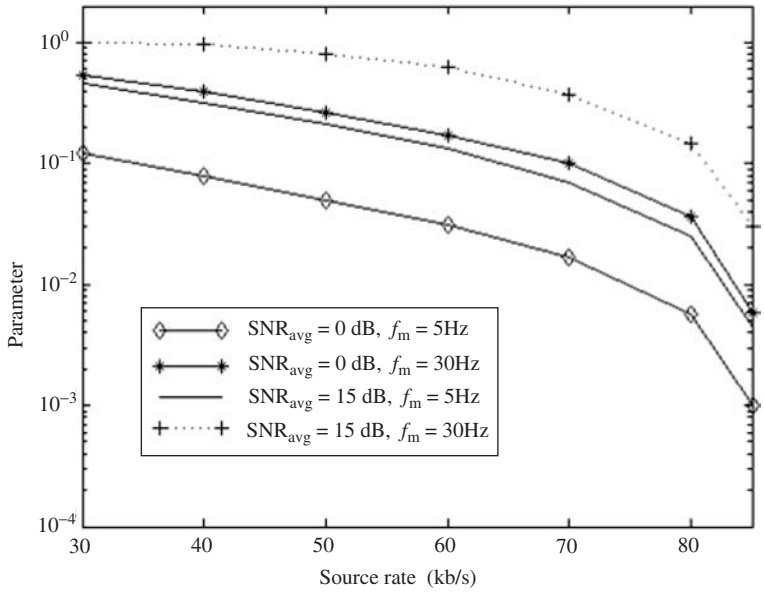

Figure 8.10 Estimated function $\hat{\theta}(\mu)$ vs source rate μ.

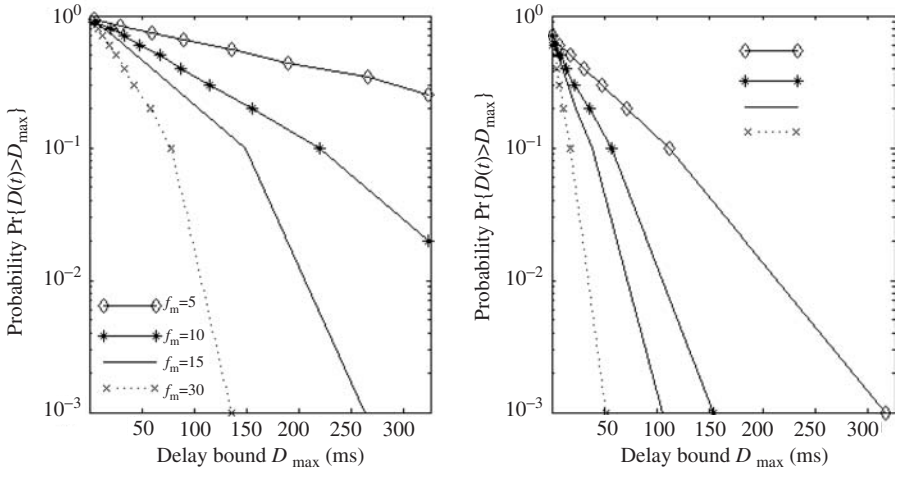

Figure 8.11 Actual delay-violation probability vs $D_{\max}$ for various Doppler rates. (a) Rayleigh fading and (b) Ricean fading $K = 3$.

probability is expected to increase with increasing source rate μ. From Figure 8.10, we also observe that SNR has a substantial impact on $\hat{\gamma}(\mu)$. This is because higher SNR results in larger channel capacity, which leads to smaller probability that a packet will be buffered, i.e. smaller $\hat{\gamma}(\mu)$. In contrast, Figure 8.9 shows that f_m has little effect on $\hat{\gamma}(\mu)$.

Figure 8.11 shows the actual delay-violation probability $\sup_t \Pr\{D(t) > D_{\max}\}$ vs the delay bound $D_{\max}$, for various Doppler rates. It can be seen that the actual delay-violation probability decreases exponentially with the delay bound $D_{\max}$, for all the cases. This justifies the use of an

exponential bound, Equation (8.33), in predicting QoS, thereby justifying the link model $\{\hat{\gamma}, \hat{\theta}\}$. The figure shows that delay-violation probability reduces with the Doppler rate. This is reasonable since the increase of the Doppler rate leads to the increase of time diversity, resulting in a larger decay rate $\hat{\theta}(\mu)$ of the delay-violation probability. More details on the topic can be found in References [11–17].

REFERENCES

[1] ATM Forum Technical Committee, *Traffic Management Specification, Version 4.0.* ATM Forum, 1996.

[2] A.I. Elwalid and D. Mitra, Analysis and design of rate-based congestion control of high speed networks – I: stochastic fluid models, access regulation, *Queueing Syst.*, vol. 9, 1991, pp. 29–63.

[3] J.S. Turner, New directions in communications (or which way to the information age?), *IEEE Commun. Mag.*, 1986, pp. 8–15.

[4] R.L. Cruz, A calculus for network delay, part I: network elements in isolation, *IEEE Trans. Inform. Theory*, vol. 37, 1991, pp. 114–131.

[5] B.L. Mark, and G. Ramamurthy, Real-time estimation and dynamic renegotiation of UPC parameters for arbitrary traffic sources in ATM networks, *IEEE/ACM Trans. Networking*, vol. 6, no. 6, 1998, pp. 811–828.

[6] C. Chang, Stability, queue length and delay of deterministic and stochastic queueing networks, *IEEE Trans. Automat. Contr.*, vol. 39, 1994, pp. 913–931.

[7] G.L. Choudhury, D.M. Lucantoni and W. Whitt, Squeezing the most out of ATM, *IEEE Trans. Commun.*, vol. 44, 1996, pp. 203–217.

[8] P.W. Glynn and W. Whitt, Logarithmic asymptotics for steadystate tail probabilities in a single-server queue, in *Studies in Applied Probability, Papers in Honor of Lajos Takacs*, J. Galambos and J. Gani, eds, Applied Probability Trust, 1994, pp. 131–156.

[9] H. Kobayashi and Q. Ren, A diffusion approximation analysis of an ATM statistical multiplexer with multiple types of traffic, part I: equilibrium state solutions, in *Proc. 1993 IEEE Int. Conf. Communications*, Geneva, May 1993, vol. 2, pp. 1047–1053.

[10] B.L. Mark and G. Ramamurthy, Joint source-channel control for realtime VBR over ATM via dynamic UPC renegotiation, in *Proc. IEEE Globecom'96*, London, November, 1996, pp. 1726–1731.

[11] D. Wu, and R. Negi, Effective capacity: a wireless link model for support of quality of service, *IEEE Trans. Wireless Commun.*, vol. 2, no. 4, 2003, pp. 630–643.

[12] R. Guerin and V. Peris, Quality-of-service in packet networks: Basic mechanisms and directions, *Comput. Networks, ISDN*, vol. 31, no. 3, 1999, pp. 169–179.

[13] S. Hanly and D. Tse, Multiaccess fading channels: Part II: Delay-limited capacities, *IEEE Trans. Inform. Theory*, vol. 44, 1998, pp. 2816–2831.

[14] C.-S. Chang and J.A. Thomas, Effective bandwidth in high-speed digital networks, *IEEE J. Select. Areas Commun.*, vol. 13, 1995, pp. 1091–1100.

[15] G.L. Choudhury, D.M. Lucantoni and W. Whitt, Squeezing the most out of ATM, *IEEE Trans. Commun.*, vol. 44, 1996, pp. 203–217.

[16] Z.-L. Zhang, End-to-end support for statistical quality-of-service guarantees in multimedia networks, Ph.D. dissertation, Department of Computer Science, University of Massachusetts, 1997.

[17] B. Jabbari, Teletraffic aspects of evolving and next-generation wireless communication networks, *IEEE Pers. Commun.*, vol. 3, 1996, pp. 4–9.

[18] S. Chong and S. Li, (σ; ρ)-characterization based connection control for guaranteed services in high speed networks, in *Proc. IEEE INFOCOM'95*, Boston, MA, April 1995, pp. 835–844.
[19] O. Yaron and M. Sidi, Performance and stability of communication networks via robust exponential bounds, *IEEE/ACM Trans. Networking*, vol. 1, 1993, pp. 372–385.
[20] T. Tedijanto and L. Gun, Effectiveness of dynamic bandwidth management in ATM networks, in *Proc. INFOCOM'93*, San Francisco, CA, March 1993, pp. 358–367.
[21] M. Grossglauser, S. Keshav, and D. Tse, RCBR: a simple and efficient service for multiple time-scale traffic, in *Proc. ACM SigCom'95*, Boston, MA, August 1995, pp. 219–230.
[22] D. Reininger, G. Ramamurthy and D. Raychaudhuri, VBR MPEG video coding with dynamic bandwidth renegotiation, in *Proc. ICC'95*, Seattle, WA, June 1995, pp. 1773–1777.
[23] J. Abate, G.L. Choudhury, and W. Whitt, Asymptotics for steady-state tail probabilities in structured Markov queueing models, *Stochastic Models*, vol. 10, 1994, pp. 99–143.
[24] D.P. Heyman and T.V. Lakshman, What are the implications of long-range dependence for VBR-video traffic engineering? *IEEE/ACM Trans. Networking*, vol. 4, 1996, pp. 301–317.
[25] W. Whitt, Tail probabilities with statistical multiplexing and effective bandwidths in multi-class queues, *Telecommun. Syst.*, vol. 2, 1993, pp. 71–107.
[26] D.E. Knuth, *The Art of Computer Programming, Volume 2: Seminumerical Algorithms*, *2nd edn. Addison-Wesley: Reading, MA, 1981.*
[27] A.I. Elwalid and D. Mitra, Effective bandwidth of general Markovian traffic sources and admission control of high speed networks, *IEEE/ACM Trans. Networking*, vol. 1, 1993, pp. 323–329.
[28] A.K. Parekh and R.G. Gallager, A generalized processor sharing approach to flow control in integrated services networks: The singlenode case, *IEEE/ACM Trans. Networking*, vol. 1, 1993, pp. 344–357.
[29] B.L. Mark and G. Ramamurthy, UPC-based traffic descriptors for ATM: How to determine, interpret and use them, *Telecommun. Syst.*, vol. 5, 1996, pp. 109–122.

9

Adaptive TCP Layer

9.1 INTRODUCTION

In this section we first discuss TCP performance independent of the type of network by considering the different possible characteristics of the connection path. We present the problems and the different possible solutions. This study permits us to understand the limitations of the actual solutions and the required modifications to let TCP cope with a heterogeneous Internet on an end-to-end basis. Then, in the rest of the chapter we focus on the specifics of TCP operation in wireless networks.

The TCP provides a reliable connection-oriented in-order service to many of today's Internet applications. Given the simple best-effort service provided by IP, TCP must cope with the different transmission media crossed by Internet traffic. This mission of TCP is becoming difficult with the increasing heterogeneity of the Internet. Highspeed links (optic fibers), long and variable delay paths (satellite links), lossy links (wireless networks) and asymmetric paths (hybrid satellite networks) are becoming widely embedded in the Internet. Many works have studied by experimentation [1], analytical modeling [2] and simulation [3, 4, 12, 17, 18] the performance of TCP in this new environment.

Most of these works have focused on a particular environment (satellite networks, mobile networks, etc.). They have revealed some problems in the operation of TCP. Long propagation delay and losses on a satellite link, handover and fading in a wireless network, bandwidth asymmetry in some media, and other phenomena have been shown to seriously affect the throughput of a TCP connection. A large number of solutions have been proposed. Some solutions suggest modifications to TCP to help it to cope with these new paths. Other solutions keep the protocol unchanged and hide the problem from TCP. In this section we consider the different characteristics of a path crossed by TCP traffic, focusing on bandwidth-delay product (BDP), RTT, noncongestion losses and bandwidth asymmetry. TCP is a reliable window-based ACK-clocked flow control protocol. It uses an additive-increase multiplicative-decrease strategy for changing its window as a function of network conditions. Starting from one packet, or a larger value as we will see later, the window is increased by one packet for every nonduplicate ACK until the source estimate of *network propagation time* (npt) is reached. By the propagation time of the network, sometimes called the *pipe size*, we mean the maximum number of packets that can be fit on the path, which is also

Advanced Wireless Technologies: Cognitive, Cooperative & Opportunistic 4G Technology Second Edition Savo G. Glisic

referred to as *network capacity*. This is the *slow start* (SS) phase, and the *npt* estimate is called the *SS threshold* (sst). SS aims to alleviate the burstiness of TCP while quickly filling the pipe. Once *sst* is reached, the source switches to a slower increase in the window by one packet for every window's worth of ACKs. This phase, called *congestion avoidance* (CA), aims to slowly probe the network for any extra bandwidth. The window increase is interrupted when a loss is detected. Two mechanisms are available for the detection of losses: the expiration of a retransmission timer (timeout) or the receipt of three duplicate ACKs (fast retransmit, FRXT). The source supposes that the network is in congestion and sets its estimate of the *sst* to half the current window.

Tahoe, the first version of TCP to implement congestion control, at this point sets the window to one packet and uses SS to reach the new *sst*. Slow starting after every loss detection deteriorates the performance given the low bandwidth utilization during SS. When the loss is detected via timeout, SS is unavoidable since the ACK clock has stopped and SS is required to smoothly fill the pipe. However, in the FRXT case, ACKs still arrive at the source and losses can be recovered without SS. This is the objective of the new versions of TCP (Reno, New Reno, SACK, etc.), discussed in this chapter, that call a fast recovery (FRCV) algorithm to retransmit the losses while maintaining enough packets in the network to preserve the ACK clock. Once losses are recovered, this algorithm ends and normal CA is called. If FRCV fails, the ACK stream stops, a timeout occurs, and the source resorts to SS as with Tahoe.

9.1.1 A large bandwidth-delay product

The increase in link speed, like in optic fibers, has led to paths of large BDP. The TCP window must be able to reach large values in order to efficiently use the available bandwidth. Large windows, up to 2^{30} bytes, are now possible. However, at large windows, congestion may lead to the loss of many packets from the same connection. Efficient FRCV is then required to correct many losses from the same window. Also, at large BDP, network buffers have an important impact on performance. These buffers must be well dimensioned and scale with the BDP. *Fast recovery* uses the information carried by ACKs to estimate the number of packets in flight while recovering from losses. New packets are sent if this number falls below the network capacity estimate. The objective is to preserve the ACK clock in order to avoid the timeout. The difference between the different versions of TCP is in the estimation of the number of packets in flight during FRCV. All these versions will be discussed later in more detail. *Reno* considers every duplicate ACK a signal that a packet has left the network. The problem of Reno is that it leaves FRCV when an ACK for the first loss in a window is received. This prohibits the source from detecting the other losses with FRXT. A long timeout is required to detect the other losses. *New Reno* overcomes this problem. The idea is to stay in FRCV until all the losses in the same window are recovered. Partial ACKs are used to detect multiple losses in the same window. This avoids timeout but cannot result in a recovery faster than one loss per RTT. The source needs to wait for the ACK of the retransmission to discover the next loss. Another problem of Reno and New Reno is that they rely on ACKs to estimate the number of packets in flight. ACKs can be lost on the return path, which results in an underestimation of the number of packets that have left the network, and thus an underutilization of the bandwidth during FRCV and, in the case of Reno, a possible failure of FRCV. More information is needed at the source to recover faster than one loss per RTT and to estimate more precisely the number of packets in the pipe. This information is provided by selective ACK (SACK), a TCP option containing the three blocks of contiguous data most recently received at the destination. Many algorithms have been proposed to use this information during FRCV. TCP-SACK may use ACKs to estimate the number of packets in the pipe and SACKs to retransmit more than one loss per RTT. This leads to an important improvement in performance when bursts of losses appear in the same window, but the recovery is always sensitive to the loss of ACKs. As a solution, forward ACK (FACK) may be used, which relies on SACK in estimating

the number of packets in the pipe. The number and identity of packets to transmit during FRCV is decoupled from the ACK clock, in contrast to TCP-SACK, where the identity is only decoupled.

9.1.2 Buffer size

SS results in bursts of packets sent at a rate exceeding the bottleneck bandwidth. When the receiver acknowledges every data packet, the rate of these bursts is equal to twice the bottleneck bandwidth. If network buffers are not well dimensioned, they will overflow early during SS before reaching the network capacity. This will result in an underestimation of the available bandwidth and a deterioration in TCP performance. Early losses during SS were first analyzed in Lakshman and Madhow [2]. The network is modeled with a single bottleneck node of bandwidth μ, buffer B, and two-way propagation delay T, as shown in Figure 9.1.

A long TCP-Tahoe connection is considered where the aim of *SS* is to reach quickly without losses *sst*, which is equal to half the pipe size $[(B + \mu T)/2]$. In the case of a receiver that acknowledges every data packet, they found that a buffer $B > BDP/3 = \mu T/3$ is required. Their analysis can be extended to an SS phase with a different threshold, mainly to that at the beginning of the connection, where *sst* is set to a default value. As an example, the threshold can be set at the beginning of the connection to the *BDP* in order to switch to *CA* before the occurrence of losses. This will not work if the buffer is smaller than half the *BDP* (half $\mu T/2$). In Barakat and Altman [5] the problem of early buffer overflow during SS for multiple routers was studied. It was shown that, due to the high rate at which packets are sent during SS, queues can build up in routers preceding the bottleneck as well. Buffers in these routers must also be well dimensioned, otherwise they overflow during SS and limit the performance even though they are faster than the bottleneck. With small buffers, losses during SS are not a signal of network congestion, but rather of transient congestion due to the bursty nature of SS traffic. Now in CA, packets are transmitted at approximately the bottleneck bandwidth. A loss occurs when the window reaches the pipe size. The source divides its window by two and starts a new cycle. To always get a throughput approximately equal to the bottleneck bandwidth, the window after reduction must be larger than the BDP. This requires a buffer B larger than the BDP. Note that we are talking about drop tail buffers, which start to drop incoming packets when the buffer is full. Active buffers such as *random early detection* (RED) [3] start to drop packets when the average queue length exceeds some threshold. When an RED buffer is crossed by a single connection, the threshold should be larger than the BDP to get good utilization. This contrasts one of the aims of RED: limiting the size of queues in network nodes in order to reduce end-to-end delay. For multiple connections, a lower threshold is sufficient given that a small number of connections reduce their windows upon congestion, in contrast to drop tail buffers, where often all the connections reduce their windows simultaneously.

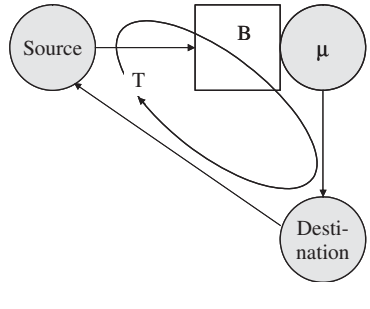

Figure 9.1 One-hop *TCP operation*.

9.1.3 Round-trip time

Long RTTs are becoming an issue with the introduction of satellite links into the Internet. A long RTT reduces the rate at which the window increases, which is a function of the number of ACKs received and does not account for the RTT. This poses many problems to the TCP. First, it increases the duration of SS, which is a transitory phase designed to quickly but smoothly fill the pipe. Given the low bandwidth utilization during SS, this deteriorates the performance of TCP transfers, particularly short ones (e.g. Web transfers). Second, it causes unfairness in the allocation of the bottleneck bandwidth. Many works have shown the bias of TCP against connections with long RTTs [2]. Small RTT connections increase their rates more quickly and grab most of the available bandwidth. The average throughput of a connection has been shown to vary as the inverse of T^{α}, where α is a factor between 1 and 2 [2].

Many solutions have been proposed to reduce the time taken by SS on long delay paths. These solutions can be divided into three categories: (1) change the window increase algorithm of TCP; (2) solve the problem at the application level; or (3) solve it inside the network. *On the TCP level* the first proposition was to use a larger window than one packet at the beginning of SS. An initial window of maximum four packets has been proposed. Another proposition, called *byte counting*, was to account for the number of bytes covered by an ACK while increasing the window rather than the number of ACKs. To avoid long bursts in the case of large gaps in the ACK stream, a limit on the maximum window increase has been proposed (*limited byte counting*). These solutions try to solve the problem while preserving the ACK clock. They result in an increase in TCP burstiness and an overload on network buffers. Another type of solution tries to solve the problem by introducing some kind of packet spacing (e.g. rate-based spacing). The source transmits directly at a large window without overloading the network. Once the large window is reached, the ACK clock takes over. This lets the source avoid a considerable part of SS. The problem can be solved at the application level without changing the TCP. A possible solution (e.g. XFTP), consists of establishing many parallel TCP connections for the same transfer. This accelerates the growth of the resultant window, but increases the aggressiveness of the transfer and hence the losses in the network. An adaptive mechanism has been proposed for XFTP to change the number of connections as a function of network congestion. Another solution has been proposed to accelerate the transfer of web pages. Instead of using an independent TCP connection to fetch every object in a page, the client establishes a persistent connection and asks the server to send all the objects on it (hypertext transfer protocol, HTTP). Only the first object suffers from the long SS phase; the remaining objects are transferred at a high rate. The low throughput during SS is compensated for by the long time remaining in CA.

The problem can be also solved inside the network rather than at hosts, which is worthwhile when a long delay link is located on the path. In order to decrease the RTT, the long delay link is eliminated from the feedback loop by acknowledging packets at the input of this link (A in Figure. 9.2). Packets are then transmitted on the long delay link using an optimized transport protocol (e.g. STP, described in Henderson and Katz [1]).

This transport protocol is tuned to quickly increase its transmission rate without the need for a long SS. Once arriving at the output (B), another TCP connection is used to transmit the packets to the destination. In a satellite environment, the long delay link may lead directly to the destination, so another TCP connection is not required. Because packets have already been acknowledged, any loss between the input of the link (A) and the destination must be locally retransmitted on behalf the source. Also, ACKs from the receiver must be discarded silently (at B) so as not to confuse the source. This approach is called *TCP spoofing*. The main gain in performance comes from not using SS on the long delay link. The window increases quickly, which improves performance, but spoofing still has many drawbacks. First, it breaks the end-to-end semantics of TCP; a packet is acknowledged before reaching its destination. Also, it does not work when encryption is accomplished at the IP layer, and it introduces a heavy overload

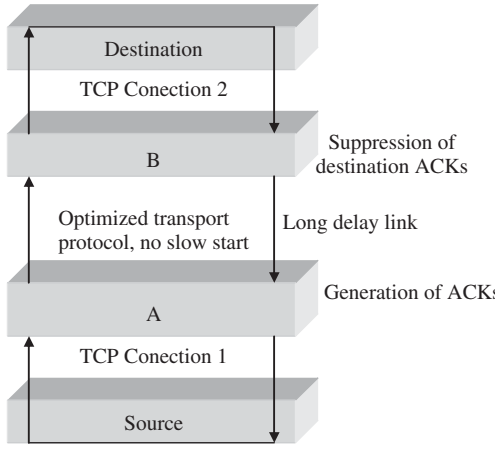

Figure 9.2 Spoofing: elimination of the long delay link from the feedback loop.

on network routers. Further, the transfer is vulnerable to path changes, and symmetric paths are required to be able to discard the ACKs before they reach the source. Spoofing can be seen as a particular solution to some long delay links. It is interesting when the long delay link is the last hop to the destination. This solution is often used in networks providing high-speed access to the Internet via geostationary earth orbit (GEO) satellite links.

9.1.4 Unfairness problem at the TCP layer

One way to solve the problem is action at the TCP level by accelerating the window growth for long RTT connections. An example of a TCP-level solution is, the *constant rate algorithm*. The window is increased in CA by a factor inversely proportional to $(RTT)^2$. The result is a constant increase rate of the throughput regardless of RTT, thus better fairness. The first problem in this proposition is the choice of the increase rate. Also, accelerating window growth while preserving the ACK clock results in large bursts for long RTT connections.

Inside the network, fairness is improved by isolating the different connections from each other. Given that congestion control in TCP is based on losses, isolation means that a congested node must manage its buffer to distribute drops on the different connections in such a way that they get the same throughput. Many buffer management policies have been proposed. Some of these policies, such as RED (random early detection) [3], drop incoming packets with a certain probability when the queue length or its average exceeds a certain threshold. This distributes losses on the different connections proportionally to their throughput without requiring any per-connection state. However, dropping packets in proportion to the throughput does not always lead to fairness, especially if the bottleneck is crossed by unresponsive traffic. With a first-in first-out (FIFO) scheduler, the connection share of the bandwidth is proportional to its share of the buffer. Better fairness requires control of the buffer occupancy of each connection. Another set of policies, known as Flow RED, try to improve fairness by sharing the buffer space fairly between active connections. This ensures that each connection has at least a certain number of places in the queue, which isolates connections sending at small rates from aggressive ones. This improves fairness, but at the same time increases buffer management overhead over a general drop policy such as RED.

The problem of fairness has additional dimensions. Solving the problem at the TCP level has the advantage of keeping routers simple, but it is not enough given the prevalence of non-TCP-friendly traffic. Some mechanisms in network nodes are required to protect conservative TCP flows

from aggressive ones. Network mechanisms are also required to ensure fairness at a level below or above TCP, say at the user or application level. A user (e.g. running XFTP) may be unfairly aggressive and establish many TCP connections in order to increase its share of the bandwidth. The packets generated by this user must be considered by the network as a single flow. This requires an aggregation in flows of TCP connections. The level of aggregation determines the level of fairness we want. Again this approach requires an additional effort.

9.1.5 Noncongestion losses

TCP considers the loss of packets as a result of network congestion and reduces its window consequently. This results in severe throughput deterioration when packets are lost for reasons other than congestion. In wireless communications noncongestion losses are mostly caused by transmission errors. A packet may be corrupted while crossing a poor-quality radio link. The solutions proposed to this problem can be divided into two main categories. The first consists in hiding the lossy parts of the Internet so that only congestion losses are detected at the source. The second type of solution consists of enhancing TCP with some mechanisms to help it to distinguish between different types of losses. When hiding noncongestion losses these losses are recovered locally without the intervention of the source. This can be accomplished at the link or TCP level. Two well known mechanisms are used *as link-level solutions* to improve the link quality: ARQ and FEC.

TCP-level solutions try to improve link quality by retransmitting packets at the TCP level rather than at the link level. A TCP agent in the router at the input of the lossy link keeps a copy of every data packet. It discards this copy when it sees the ACK of the packet, and it retransmits the packet on behalf of the source when it detects a loss. This technique has been proposed for terrestrial wireless networks where the delay is not so important as to require the use of FEC. The TCP agent is placed in the base station at the entry of the wireless network. Two possible implementations of this agent exist.

The first implementation, referred to as indirect TCP, consists of terminating the originating TCP connection at the entry of the lossy link. The agent acknowledges the packets and takes care of handing them to the destination. A TCP connection well tuned to a lossy environment (e.g. TCP-SACK) can be established across the lossy network. A different transport protocol can also be used. This solution breaks the end-to-end semantics of the Internet. Also, it causes difficulties during handover since a large state must be transferred between base stations. The second implementation (Snoop protocol) respects the end-to-end semantics. The intermediate agent does not terminate the TCP connection; it just keeps copies of data packets and does not generate any artificial ACK. Nonduplicate ACKs sent by the destination are forwarded to the source. Duplicate ACKs are stopped. A packet is retransmitted locally when three duplicate ACKs are received or a local timeout expires. This local timeout is set, of course, to a value less than that of the source. As in the link-level case, interference may happen between the source and agent mechanisms. In fact, this solution is no other than link-level recovery implemented at the TCP level. Again, because it hides all losses, congestion losses must not occur between the Snoop agent and the destination.

9.1.6 End-to-end solutions

The addition of some end-to-end mechanisms to improve TCP reaction to noncongestion losses should further improve performance. Two approaches exist in the literature. The first consists of explicitly informing the source of the occurrence of a noncongestion loss via an explicit loss notification (ELN) signal. The source reacts by retransmitting the lost packet without reducing its window. An identical signal has been proposed to halt congestion control at the source when a

disconnection appears due to handover in a cellular network. The difficulty with such a solution is that a packet corrupted at the link level is discarded before reaching TCP, and then it is difficult to get this information. The second approach is to improve the congestion control provided by TCP rather than recovery from noncongestion losses. We mention it here because it consists a step toward a solution to the problem of losses on an end-to-end basis.

The proposed solutions aim to decouple congestion detection from losses. With some additional mechanisms in the network or at the source, the congestion is detected and the throughput reduced before the overflow of network buffers. These examples, which will be discussed later in more detail, are the Vegas version of TCP [4] and the explicit congestion notification proposal. In Vegas, the RTT of the connection and the window size are used to compute the number of packets in network buffers. The window is decreased when this number exceeds a certain threshold. With ECN, an explicit signal is sent by the routers to indicate congestion to TCP sources rather than dropping packets. If all the sources, receivers and routers are compliant (according to Vegas or ECN), congestion losses will considerably decrease. The remaining losses could be considered to be caused mostly by problems other than congestion. Given that noncongestion losses require only retransmission without window reduction, the disappearance of congestion losses may lead to the definition at the source of a new congestion control algorithm which reacts less severely to losses. This ideal behaviour does ont exist in today's networks. In the absence of any feedback from the network as with Vegas, the congestion detection mechanism at the source may fail; here, congestion losses are unavoidable. If the source bases its congestion control on explicit information from the network as with ECN, some noncompliant routers will not provide the source with the required information, dropping packets instead. A reduction of the window is necessary in this case. For these reasons, these solutions still consider losses as congestion signals and reduce their windows consequently.

9.1.7 Bandwidth asymmetry

From the previous discussion we could see that TCP uses the ACK clock to predict what is happening inside the network. It assumes implicitly that the reverse channel has enough bandwidth to convey ACKs without being disturbed. This is almost true with the so-called symmetric networks where the forward and the reverse directions have the same bandwidth. However, some of today's networks (e.g. direct broadcast satellite, 4G cellular networks and asymmetric digital subscriber loop networks) tend to increase capacity in the forward direction, whereas a low-speed channel is used to carry ACKs back to the source. Even if ACKs are smaller in size than data packets, the reverse channel is unable to carry the high rate of ACKs. The result is congestion and losses on the ACK channel. This congestion increases the RTT of the connection and causes loss of ACKs. The increase in RTT reduces throughput and increases end-to-end delay. Also, it slows window growth, which further impairs performance when operating on a long delay path or in a lossy environment. The loss of ACKs disturbs one of the main functionalities of the ACK clock: smoothing the transmission. The window slides quickly upon receipt of an ACK covering multiple lost ACKs, and a burst of packets is sent, which may overwhelm the network buffers in the forward direction. Also, the loss of ACKs slows down the growth of the congestion window, which results in poor performance for long delay paths and lossy links. The proposed solutions to this problem can be divided into receiver-side solutions, which try to solve the problem by reducing the congestion on the return path, and source-side solutions, which try to reduce TCP burstiness. The first receiver-side solution is to compress the headers of TCP/IP packets on a slow channel to increase its capacity in terms of ACKs per unit of time (e.g. SLIP header compression). It profits from the fact that most of the information in a TCP/IP header does not change during the connection lifetime. The other solutions propose reducing the rate of ACKs to avoid congestion. The first proposition is to delay ACKs at the destination. An ACK is sent every d packets, and an

adaptive mechanism has been proposed to change d as a function of the congestion on the ACK path. Another option is to keep the destination unchanged and filters ACKs at the input of slow channel. When an ACK arrives, the buffer is scanned to see if another ACK (or a certain number of ACKs) of the same connection is buffered. If so, the new ACK is substituted for the old one. ACKs are filtered to match their rates to the rate of the reverse channel. Normally, in the absence of artificial filtering, ACKs are filtered sometime later when the buffer gets full. The advantage of this solution is that the filtering is accomplished before the increase in RTT. Solutions at the sender side which reduce the burstiness of TCP are also possible. Note that this problem is caused by the reliance of TCP on the ACK clock, and it cannot be completely solved without any kind of packet spacing.

First, a limit on the size of bursts sent by TCP is a possible solution. However, with systematic loss of ACKs, limiting the size of bursts limits the throughput of the connection. Second, it is possible to reconstruct the ACK clock at the output of the slow channel. When an ACK arrives at that point, all the missing ACKs are generated, spaced by a time interval derived from the average rate at which ACKs leave the slow channel. This reconstruction may contain a solution to this particular problem. However, the general problem of TCP burstiness upon loss of ACKs will still remain.

9.2 TCP OPERATION AND PERFORMANCE

The *TCP protocol* model will only include the data transfer part of the TCP. Details of the TCP protocol can be found in the various Internet requests for comments (RFCs; see also Stevens [6]). The versions of the TCP protocol that we model and analyze in this section all assume the same receiver process. The *TCP receiver* accepts packets out of sequence number order, buffers them in a TCP buffer, and delivers them to its TCP user in sequence. Since the receiver has a finite resequencing buffer, it advertises a maximum window size $W_{\max}$ at connection setup time, and the transmitter ensures that there is never more than this amount of unacknowledged data outstanding. We assume that the user application at the TCP receiver can accept packets as soon as the receiver can offer them in sequence and, hence, the receiver buffer constraint is always just $W_{\max}$. The receiver returns an ACK for every good packet that it receives. An ACK packet that acknowledges the first receipt of an error-free in-sequence packet will be called a *first* ACK. The ACKs are *cumulative*, i.e. an ACK carrying the sequence number n acknowledges all data up to, and including, the sequence number $n - 1$. If there is data in the resequencing buffer, the ACKs from the receiver will carry the *next expected* packet number, which is the first among the packets required to complete the sequence of packets in the sequencing buffer. Thus, if a packet is lost (after a long sequence of good packets), then the transmitter keeps getting ACKs with the sequence number of the first packet lost, if some packets transmitted after the lost packet do succeed in reaching the receiver. These are called *duplicate ACKs*.

9.2.1 The TCP transmitter

At all times t, the transmitter maintains the following variables for each connection:

(1) $A(t)$ the *lower window edge*. All data numbered up to and including $A(t) - 1$ has been transmitted and ACKed. $A(t)$ is nondecreasing; the receipt of an ACK with sequence number $n > A(t)$ causes $A(t)$ to jump to n.

(2) $W(t)$ the *congestion window*. The transmitter can send packets with the sequence numbers n, $A(t) \leq n < A(t) + W(t)$ where $W(t) \leq W_{\max}(t)$ and $W(t)$ increases or decreases as described below.

(3) $W_{\text{th}}(t)-$ the *slow-start threshold* controls the increments in $W(t)$ as described below.

9.2.2 Retransmission timeout

The transmitter measures the RTTs of *some* of the packets for which it has transmitted and received ACKs. These measurements are used to obtain a running estimate of the packet *RTT* on the connection. Each time a new packet is transmitted, the transmitter starts a timeout timer and *resets* the already running timeout timer, if any; i.e. there is a timeout only for the last transmitted packet. The timer is set for a *retransmission timeout* (RTO) value that is derived from the RTT estimation procedure. The TCP transmitter process measures time and sets timeouts only in multiples of a *timer granularity*. Further, there is a minimum timeout duration in most implementations. We will see in the analysis that *coarse timers* have a significant impact on TCP performance. For details on RTT estimation and the setting of RTO values, see Reference [6] or [8].

9.2.3 Window adaptation

The basic algorithm is common to all TCP versions [11]. The normal evolution of the processes $A(t)$, $W(t)$ and $W_{\text{th}}(t)$ is triggered by first ACKs (see definition above) and timeouts as follows.

(1) *Slow start:* if $W(t) < W_{\text{th}}(t)$, each first ACK increments $W(t)$ by one.

(2) *Congestion avoidance:* if $W(t) \geq W_{\text{th}}(t)$, each first ACK increments $W(t)$ by $1/W(t)$.

(3) *Timeout* at epoch t sets $W(t^+)$ to one, $W_{\text{th}}(t^+)$ to $\lceil (W(t)/2) \rceil$ and retransmissions begins from $A(t)$.

9.2.4 Packet loss recovery

If a packet is lost, $A(t)$ and $W(t)$ will continue to be incremented until the first ACK for the packet just before the lost packet is received. For a particular loss instance, let their final values be denoted by A and M, respectively; we will call M a *loss window*. Then the transmitter will continue to send packets up to the sequence number $A + M - 1$. If some of the packets sent after the lost packet get through, they will result in duplicate ACKs, all carrying the sequence number A. The last packet transmitted (i.e. $A + \mathrm{M} - 1$) will have an RTO associated with it. The TCP versions differ in the way they recover from loss. We provide some details here; later we will provide more detail on modeling these recovery procedures.

9.2.5 TCP-OldTahoe (timeout recovery)

The transmitter continues sending until packet number $A + M - 1$ and then waits for a coarse timeout.

9.2.6 TCP-Tahoe (fast retransmit [9])

A transmitter parameter K is used, a small positive integer; typically $K = 3$. If the transmitter receives the Kth duplicate ACK at time t (before the timer expires), then the transmitter behaves *as if* a timeout has occurred and begins retransmission, with $W(t^+)$ and $W_{\text{th}}(t^+)$ as given by the basic algorithm.

9.2.7 TCP-Reno fast retransmit, fast (but conservative) recovery [6]

Fast-retransmit is implemented, as in TCP-Tahoe, but the subsequent recovery phase is different. Suppose the Kth duplicate ACK is received at the epoch t_0. Loss recovery then starts. Bearing in

mind the definitions of A and M above, the transmitter sets

$$W(t_0^+) = \lceil M/2 \rceil + K \quad W_{\text{th}}(t_0^+) = \lceil M/2 \rceil \tag{9.1}$$

The addition of K takes care of the fact that more packets have successfully left the network. The Reno transmitter then retransmits *only* the packet with sequence number A. If only one packet is lost then this retransmission will produce an ACK for all of the other packets, whereas if more packets are lost we had better be sure that we are not really experiencing congestion loss. For the ith duplicate ACK received, at say t_{ack}, until recovery completes,

$$W(t_{\text{ack}}^+ i) = W(t_{\text{ack}} i) + 1 \tag{9.2}$$

Further details of the Reno recovery will be explained by using an example from Kumar [13], where $K = 3$. Suppose $A = 15$, $M = 16$ and packet 15 is lost. The transmitter continues sending packets 16, 17, 18, ..., 30; suppose packet 20 is also lost. The receiver returns ACKs (all asking for packet 15) for packets 16, 17, 18, 19, 21, 29 and 30. Note that the ACK for packet14 would have been the *first* ACK asking for packet 15. When the ACK for packet 18 is received (i.e. the third duplicate ACK), the transmitter sets

$$W(t_0^+) = \lceil M/2 \rceil + K = \lceil 16/2 \rceil + 3 = 11$$
$$W_{\text{th}}(t_0^+) = \lceil M/2 \rceil = \lceil 16/2 \rceil = 8$$

A is still 15; thus, packet 15 is retransmitted. Meanwhile, ACKs for packets 19, 21, ..., 30 are also received and based on Equation (9.2) W grows to $11 + 11 = 22$. Since $A = 15$, with $W = 22$, the transmitter is allowed to send packets 15–36; hence, retransmission of packet 15 is followed by transmission of packets 31–36. Receipt of packet 15 results in a first ACK asking for packet 20 (thus first-ACKing packets 15–19) and A jumps to 20. This is called a *partial ACK* since all of the packets transmitted in the original loss window were not ACKed.

If packets 31–36 succeed in getting through, then three duplicate ACKs asking for packet 20 are also obtained, and 20 is retransmitted. This results in a first ACK that covers all of the packets up to packet number 36. At this time t_1, the congestion window is reset as follows and a new transmission cycle starts:

$$W(t_1^+) = \lceil M/2 \rceil \quad W_{\text{th}}(t_1^+) = \lceil M/2 \rceil \tag{9.3}$$

Thus, Reno slowly recovers the lost packets and there is a chance that, owing to insufficient duplicate ACKs, the recovery stalls and a timeout has to be waited for. After a timeout, the basic timeout recovery algorithm is applied.

9.2.8 TCP-NewReno (fast retransmit, fast recovery [9])

When duplicate ACKs are received, the first lost packet is resent, but, unlike Reno, upon receipt of a partial ACK after the first retransmission, the next lost packet (as indicated by the partial ACK number) is retransmitted. Thus, after waiting for the first K duplicate ACKs, the remaining lost packets are recovered in as many RTTs. If less than K duplicate ACKs are received, then a timeout is inevitable. Consider the following example [13] to see the difference with Reno. Suppose that after a loss, $A = 7$ and $M = 8$, packets 7, 8, ..., 14 are sent, and packets 7, 8 and 11 are lost. The transmitter receives three duplicate ACKs for packets 9, 10 and 12 (asking for packet 7). A fast retransmit is done (the same as in Reno), i.e. $W = 4 + 3 = 7$, $W_{\text{th}} = 4$, and packet 7 is sent. The two ACK's for packets 13 and 14 cause W to become 9 [see Equation (9.2)]. Assuming that packet 7 now succeeds, its ACK (the first ACK asking for 8) would make A equal 8; the transmitter can now send packets 15 and 16 also. *NewReno* would now resend packet 8, whereas *Reno* would wait for three duplicate ACKs; these cannot come since only two more packets have been sent after

the retransmission of packet 7. Thus, in case of multiple losses, *Reno* has a higher probability of resorting to a coarse timeout.

9.2.9 Spurious retransmissions

Consider *TCP-OldTahoe*. The retransmission of the first lost packet may result in an ACK that acknowledges all of the packets until the next packet lost in the loss window. This would advance the lower window edge $A(t)$; the congestion window would be increased to two and the next lost packet and its successor would be transmitted, *even if this successor packet had gotten through in its first transmission*. Thus, some of the good packets in the loss window may be retransmitted when retransmission starts; this phenomenon can be seen in the sample path fragments shown in Fall and Floyd [9].

9.2.10 Modeling of TCP operation

The model from Figure.9.3, motivated by many experimental studies of TCP performance over wireless mobile links [7, 10, 13], is used the most often. In this section the additional issue of mobility is not considered [7]; hence, we refer to the wireless link as simply a 'lossy' link. We model only one direction of flow of packets from the LAN host (or base station in cellular system) to the mobile terminal. In this case propagation delays can be neglected. The transmission time of a TCP packet from the LAN host (respectively, the lossy link) is assumed to be exponentially distributed with mean λ^{-1} (respectively, μ^{-1}). By taking $\mu = 1$, time is normalized to the mean packet transmission time on the lossy link. During a bulk transfer over a TCP connection, we would expect that the packets would predominantly be of a fixed length. However, a MAC layer (or radio resource manager) will operate in these systems too. Thus, the randomness in packet transmission times in the model can be taken in to account for the variability in the time taken to transmit a head-of-the-line packet at the transmitter queues. The exponential assumption yields Markov processes and, hence, justifies the use of tools from Chapter 6. Performance analysis of TCP protocols under the above assumptions can be found in Kumar [13]. A sample result is shown in Figure 9.4.

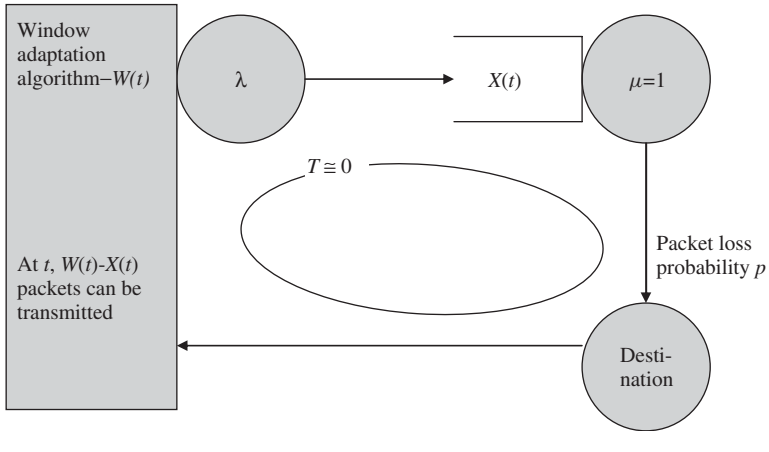

Figure 9.3 Model for the TCP connection. $X(t)$ is the number of TCP packets queued at the intermediate system (IS) at time t.

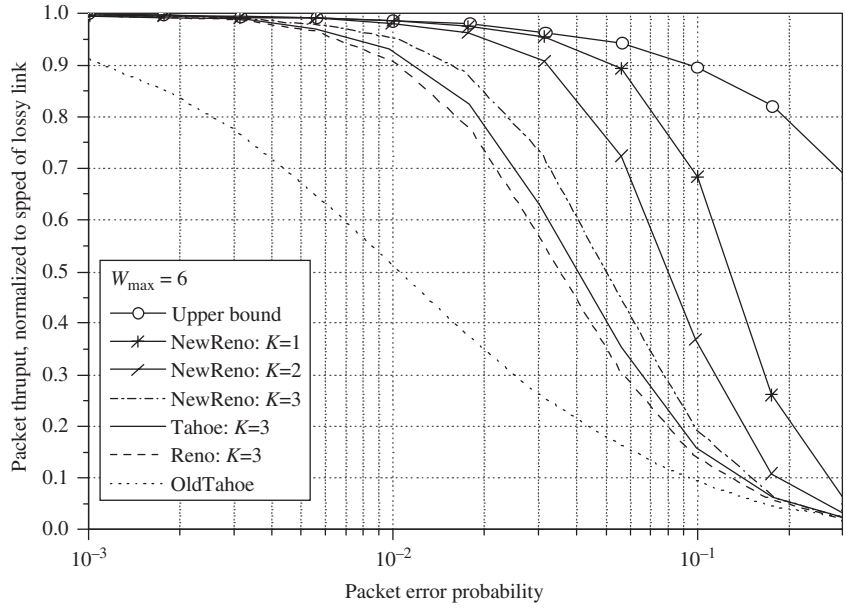

Figure 9.4 Throughput of versions of TCP vs packet-loss probability; $\lambda = 5\,\mu$; K is the fast-retransmit threshold. (Reproduced by permission of IEEE [13].)

9.3 TCP FOR MOBILE CELLULAR NETWORKS

Many papers have been written proposing methods for improving TCP performance over a wireless link [14–24]. Most of these papers have, however, concentrated on only one problem associated with wireless links, a perceived high BER over the wireless link. While a high BER has significant implications for protocol performance, other limitations of the wireless environment are equally or even more important than high BER. In this section we discuss the effects of periodic disconnections on TCP performance and present a protocol (M-TCP) that successfully deals with this problem. The protocol is also capable of on-the-fly data compression in the event that the wireless bandwidth available is very small. Finally, the protocol also maintains end-to-end TCP semantics.

If we use TCP without any modification in mobile networks, we experience a serious drop in the throughput of the connection. There are several reasons for such a drastic drop in TCP throughput.

(1) The wireless link might suffer from a high bit error rate. While this may be true in some cases, the bit error can be reduced by one or two orders of magnitude by the use of appropriate FEC codes and retransmission schemes at the link layer. However, let us assume for the sake of this discussion that the wireless link is susceptible to inordinately high bit error rates. Bit errors cause packets to become corrupted, which results in lost TCP data segments or acknowledgements. When acknowledgements do not arrive at the TCP sender within a short amount of time (the retransmit timeout or RTO which is a multiple of half a second), the sender retransmits the segment, exponentially backs off its retransmit timer for the next retransmission, and closes its congestion window to one segment. Repeated errors will ensure that the congestion window at the sender remains small, resulting in low throughput [15]. It is important to note that FEC may be used to combat high BER, but it will waste valuable wireless bandwidth when correction is not necessary.

(2) In a mobile environment, as a user moves between cells, there is a brief blackout period (or disconnection) while the mobile performs a handoff with the new access point. Disconnections may also be caused by physical obstacles in the environment that block radio signals, such as buildings. Disconnection periods can be of the order of several seconds, causing packet loss or delay in the transmission of acknowledgements of received packets. These disconnections result in lost data segments and lost ACKs which, in turn, result in the TCP sender timing out and closing its congestion window, thus greatly reducing the efficiency of the connection. Since these disconnections tend to be fairly lengthy, forward error correction schemes are ineffective.

(3) It is likely that, in order to provide high-bandwidth wireless connections, cell sizes in 4G systems will have to be reduced. Small cell sizes unfortunately result in small cell latencies that, in turn, cause frequent disconnections as a user roams. All the problems that result from disconnections, as we discussed above, occur more often here.

Another problem caused by small cell latencies and frequent disconnections is that of serial timeouts at the TCP sender. A serial timeout is a condition wherein multiple consecutive retransmissions of the same segment are transmitted to the mobile while it is disconnected. All these retransmissions are thus lost. Since the retransmission timer at the sender is doubled with each unsuccessful retransmission attempt (until it reaches 64 s), several consecutive failures can lead to inactivity lasting several minutes. Thus, even when the mobile is reconnected, no data is successfully transmitted for as long as 1 min. The serial timeouts at the TCP sender can prove to be even more harmful to overall throughput than losses due to bit errors or small congestion windows.

9.3.1 Improving TCP in mobile environments

In order to ensure that the TCP connection to a mobile is efficient, it is necessary to prevent the sender from shrinking its congestion window when packets are lost either due to bit-error or to disconnection. Furthermore, it is important to ensure that, when the mobile is reconnected, it begins receiving data immediately (rather than having to wait for the sender to timeout and retransmit). As we saw earlier, the sender may shrink its congestion window in response to a timeout (caused by lost packets either due to a high BER or disconnections) or in response to duplicate ACKs. As we already discussed in Section 9.1 some solutions attempt to keep the sender's congestion window open by introducing a host in the fixed network who 'spoofs' the sender into thinking everything is fine on the wireless link. Unfortunately, however, these solutions do not work under all scenarios of mobility. Specifically, they all perform poorly when faced with frequent or lengthy disconnections. Furthermore, some solutions fail to maintain end-to-end TCP semantics.

One proposed solution for losses caused by high BER is the Berkeley Snoop Module [16]. The snoop module resides at an intermediate host near the mobile user (typically the base station). It inspects the TCP header of TCP data packets and acknowledgements which pass through and buffers copies of the data packets. Using the information from the headers, the snoop module detects lost packets (a packet is assumed to be lost when duplicate acknowledgements are received) and performs local retransmissions to the mobile. The module also implements its own retransmission timer, similar to the TCP retransmission timeout, and performs retransmissions when an acknowledgement is not received within this interval. An improved version of the snoop module adds selective retransmissions from the intermediate node to the mobile. Another solution to the problem caused by high BER is the I-TCP [14] protocol (indirect-TCP). In the I-TCP protocol a TCP connection between a fixed host and a Mobile Host (MH) is split in two at the Mobile Support Station (MSS) or base station. Data sent to the MH is received and ACKed by the MSS before being delivered to the MH. Note that on the connection between the MSS and MH it is not necessary to use TCP, rather some protocol optimized for the wireless link could be used.

A solution that addresses the problem caused by short disconnections (where one or two segments only are lost) is presented in [21]. It, however, does not split the TCP connection. The solution is based on the following observation: during a handoff, since the MH cannot receive packets, unmodified TCP at the sender will think a congestion has occurred and will begin congestion control (reduce window size and retransmit) after a timeout. The timeout period is long and even though the MH may have completed the handoff it will have to wait for the full timeout period before it begins receiving packets from the sender. The fast retransmit idea presented in Caceres and Iftode [21] forces the MH to retransmit, in triplicate, the last old ACK as soon as it finishes a handoff. This forces the sender to reduce the congestion window to a half and retransmit one segment immediately.

9.3.2 Mobile TCP design

The implementation of M-TCP is influenced, to some degree, by the mobile network architecture. In this section we assume a three-level hierarchy. At the lowest level are the mobile hosts that communicate with MSS nodes in each cell. Several MSSs are controlled by a supervisor host (SH). The SH is connected to the wired network and it handles most of the routing and other protocol details for the mobile users. In addition it maintains connections for mobile users, handles flow-control and is responsible for maintaining the negotiated quality of service. These SHs thus serve the function of gateways.

The design of transport layer is influenced by a number of constraints unique to the mobile environment:

- Available bandwidth within a cell may change dynamically. This leads to difficulties in guaranteeing QoS parameters such as delay bounds and bandwidth guarantees.
- Mobile hosts frequently encounter extended periods of disconnection (due to handoff or physical interference with the signal), resulting in significant loss of data, causing poor TCP and UDP throughput.
- Mobile devices are battery powered and hence power is a scarce resource. Protocols designed for use on mobile platforms must therefore be tailored to be power-efficient.

All of these factors point towards using transport protocols which are optimized specifically for the wireless link. It is not reasonable, however, to assume that the entire installed network base will (or should) upgrade to these mobile-friendly protocols as they may never have occasion to communicate with a mobile user. Hence, the obvious solution is to split transport connections in two. The existing protocols may continue to be used on the fixed network, and the protocols optimized for the wireless environment may be used in the mobile subnetworks. In the following, all connections set up by an MH, where the other endpoint is either another MH or is a fixed host, are split at the SH. Thus, the service-provider sets up a connection with the SH assuming the SH is the other end-point of the connection. The SH sets up another connection to the MH. This allows us to address the problems listed above as follows:

- A bandwidth management module at the SH [19] assigns a fixed amount of bandwidth to each connection (this is recomputed periodically based on the changing needs of other MHs) and ensures that data is transmitted to all MHs at their assigned rate. This mechanism allows implementation of some limited form of QoS guarantees.
- In this architecture, the SH performs local error recovery to combat the efficiency problems resulting from loss over the wireless link.

- The SH tracks mobiles as they roam and uses this information to ensure that the number of duplicate packets transmitted to the mobile are kept small. Since every packet received by the MH has to be processed, consuming battery power, keeping the number of duplicates small reduces power consumption at the MH.

The goal in developing the M-TCP protocol is to provide a general solution to the problem of improving TCP's efficiency for mobile computing applications. Specifically, the following characteristics are desired:

(1) improve TCP performance for mobile clients; (2) maintain end-to-end TCP semantics; (3) be able to deal with the problems caused by lengthy disconnections or by frequent disconnections; (4) adapt to dynamically changing bandwidth over the already starved wireless link; (5) ensure that handoffs (as a mobile roams) are efficient

To this end we chose to use the split connection approach for implementing M-TCP because it fits in well with our general design philosophy articulated in the previous section and because it allows us to modify TCP on the mobile network to make it respond better to disconnections and low (or varying) wireless bandwidth.

So, every TCP connection is split in two at the SH. The TCP sender on the fixed network uses unmodified TCP to send data to the SH while the SH uses M- version of TCP for delivering data to the MH. Figure 9.5 illustrates the way in which a TCP connection is split. The TCP client at the SH (called SH-TCP) receives segments transmitted by the sender and passes these segments to the M-TCP client for delivery to the MH. ACKs received by M-TCP at the SH are forwarded to SH-TCP for delivery to the TCP sender. In the remainder of this section we discuss the behavior of SH-TCP and M-TCP in detail. Before doing so, however, we briefly discuss our assumptions regarding the mobile networking environment.

Wireless bandwidth will always be a precious resource and we therefore believe that it ought to be allocated to users based on their need. In this architecture, we use a bandwidth management module [19], that resides at the SH, to perform this task. This module determines the amount of bandwidth to be allocated to each connection within each cell (a discussion of the possible implementation of this module is given in Chapter 12). Thus, when a mobile opens a TCP connection, it is allocated a fixed amount of bandwidth (this amount may change periodically depending on the needs of other mobiles and the current status of this mobile's connection). What implication does this have for the design of TCP? Clearly, since the bandwidth allocated to the mobile is fixed, there is little reason to implement TCP's sophisticated congestion control mechanisms between the SH and MH. A second assumption we make in this development is that the BER visible at the transport layer will be small. This assumption is based on the fact that the physical layer will keep the BER over wireless channels, in a range close to 10^{-5}. Thus, it is necessary to design a TCP protocol that handles unremedied problems, disconnections and low bandwidth rather than a protocol that works well only in high BER environments.

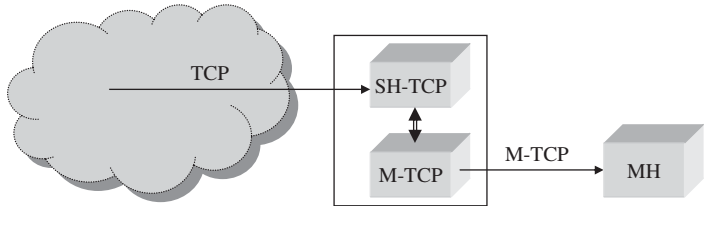

Figure 9.5 M-TCP connection.

9.3.3 The SH-TCP client

When SH-TCP receives a segment from the TCP sender, it passes the segment on to the M-TCP client. However, unlike I-TCP, it does not ACK this data until the MH does. SH-TCP is notified of MH ACKs by the M-TCP client running at the SH. It is easy to see that this behavior ensures that end-to-end TCP semantics are maintained. However, how do we ensure that the sender does not go into congestion control when ACKs do not arrive (because the MH was temporarily disconnected and did not receive the data, or could not send the ACKs)? The approach is to *choke* the TCP sender when the MH is disconnected, and allow the sender to transmit at full speed when the MH reconnects by manipulating the TCP sender's window. Specifically: let W denote the currently advertised receive window at SH-TCP. Say the window contains $w \leq W$ bytes. Assume that the MH has ACKed bytes up to $w' \leq w$. SH-TCP sends an ACK (or ACK) for bytes up to $w' - 1$ in the normal way. As and when the MH ACKs more data, more ACKs are generated but one last byte is always left unacknowledged.

Say the MH disconnects after having ACKed bytes up to w'. The M-TCP client assumes that the MH has been temporarily disconnected because it stops receiving ACKs for bytes transmitted after w'. M-TCP sends an indication of this fact to SH-TCP who then sends an ACK for the w'th byte to the sender. This ACK will also contain a TCP window size update that sets the sender's window size to zero. When the TCP sender receives the window update, it is forced into persist mode. While in this state, it will not suffer from retransmit timeouts and will not exponentially back off its retransmission timer, nor will it close its congestion window. RFC 1122 states that TCP clients go into persist mode when the window is shrunk to zero. However, in order to shrink the window to zero, the receiver must send a new ACK. To grow a window, however, an old ACK can be retransmitted. Note that as long as the SH-TCP sends ACKs for the persist packets sent by the TCP source, the state of the sender does not change no matter how long the disconnection period lasts.

If the MH has not disconnected but is in a cell with very little available bandwidth, SH-TCP still sends an ACK for byte w' with a window size set to 0. SH-TCP estimates the RTT to the TCP sender and estimates the RTO interval. It uses this information to preemptively shrink the sender's window before the sender goes into exponential backoff (to implement this scheme, a timer at the SR is maintained that is initialized to this estimated RTO value).

When an MH regains its connection, it sends a greeting packet to the SH. M-TCP is notified of this event and it passes on this information to SH-TCP which, in turn, sends an ACK to the sender and reopens its receive window (and hence the sender's transmit window). The window update allows the sender to leave persist mode and begin sending data again. Since the sender never timed out, it never performed congestion control or slow-start. Thus the sender can resume transmitting at full-speed! The sender will begin sending from byte $w + 1$ here, although possibly duplicating previous sends, so we do not want to shrink the window more often than necessary.

A potential problem with this protocol is the following: say the sender only sends data to the MH occasionally. Specifically, if the sender only needed to send bytes 0–50 to the MH, according to the above protocol, SH-TCP will ACK bytes up to 49 but will not ACK byte 50. This will cause the sender to timeout and retransmit this byte repeatedly. Eventually, after 12 retransmissions, will the TCP sender give up and quit? This is clearly an undesirable situation. This problem is handled by not allowing SH-TCP to shrink the sender's window if it believes that there will be no more new ACKs from the MH that will allow it to open up the sender's window again. Thus, when SH-TCP thinks that the sender will timeout (and if the MH is in a cell with plenty of available bandwidth), it simply ACKs the last byte. At this point, there will be no saved byte at SH-TCP to allow it to shrink the sender's window. Observe that this is not a problem because the sender did not really have any new segments to send to the MH. As and when the sender does transmit new data to the MH, SH-TCP reverts to its previously described behavior.

9.3.4 The M-TCP protocol

The goal in designing SH-TCP was to keep the TCP sender's congestion window open in the face of disconnection events at the MH. On the wireless side, on the other hand, the goal is to be able to recover quickly from losses due to disconnections, and to eliminate serial timeouts.

In designing M-TCP, a scheme similar to SH-TCP is used except that there is more design freedom since the protocol at both ends of M-TCP can be modified. M-TCP at the mobile receiver is very similar to standard TCP except that it responds to notifications of wireless link connectivity. When M-TCP at the MH is notified (by the communications hardware) that the connection to its MSS has been lost, it freezes all M-TCP timers. This essentially ensures that disconnections do not cause the MH's M-TCP to invoke congestion control. Observe that neither acknowledgements nor data are lost during a disconnection. When the connection is regained, M-TCP at the MH sends a specially marked ACK to M-TCP at the SH which contains the sequence number of the highest byte received thus far. It also unfreezes M-TCP timers to allow normal operation to resume.

At the SH we need to ensure that M-TCP monitors link connectivity and takes appropriate action either when a disconnection occurs or when a reconnection occurs. How does M-TCP determine that the MH has been disconnected? In the design M-TCP monitors the flow of ACKs from the MH in response to segments transmitted on the downlink. If it does not receive an ACK for some time, it automatically assumes that the MH has been disconnected. It then informs SH-TCP of this fact and SH-TCP reacts by putting the TCP sender in persist mode. M-TCP at the SH knows when the MH reconnects because M-TCP at the MH retransmits the last ACK, and marks it as a reconnection ACK, on being reconnected. M-TCP responds by informing SH-TCP who reopens the sender's transmit window. This behavior is based on the assumption that the bandwidth management module at the SH assigns bandwidth to each connection and regulates its usage so there is no need to invoke congestion control at the SH when ACKs are not received from the MH. M-TCP at the SH works as follows.

When a retransmit timeout occurs, rather than retransmit the segment and shrink the congestion window, we force M-TCP into persist mode. It is assumed that the absence of an ACK means that the mobile receiver has temporarily disconnected, hence retransmissions are futile until the MH notifies the SH that it has reconnected.

At first glance the implementation may appear to have a problem when operating in high BER environments. This is because a significant proportion of packet loss in such environments will be due to the high BER and not due to disconnections. In response to this observation the following arguments are used:

- It is believed that in most mobile environments link layer solutions will ensure that the bit error seen at the transport layer is small.
- Even if the mobile environment does have high BER, the M-TCP sender will come out of persist mode quickly and resume regular data transmissions. This is because, when in persist mode, M-TCP will send persist packets to the MH who will be forced to respond when it receives these packets. Typically, the persist packets are generated at increasing intervals starting at 5 s and doubling until the interval becomes 60 s. The interval could be changed to be equal to the RTT between the SH and the MH to ensure earlier recovery.

When the SH receives a specially marked reconnection ACK, it moves back out of persist mode and retransmits all packets greater than the ACKed byte as these must have been lost during the disconnection. If the SH misinterpreted a lengthy delay as a disconnection, the MH will eventually ACK the transmitted packets, which will also move the SH M-TCP out of persist but will not cause all packets to be retransmitted.

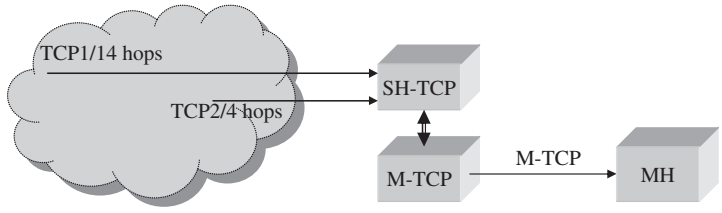

Figure 9.6 Experimental M-TCP connection setup.

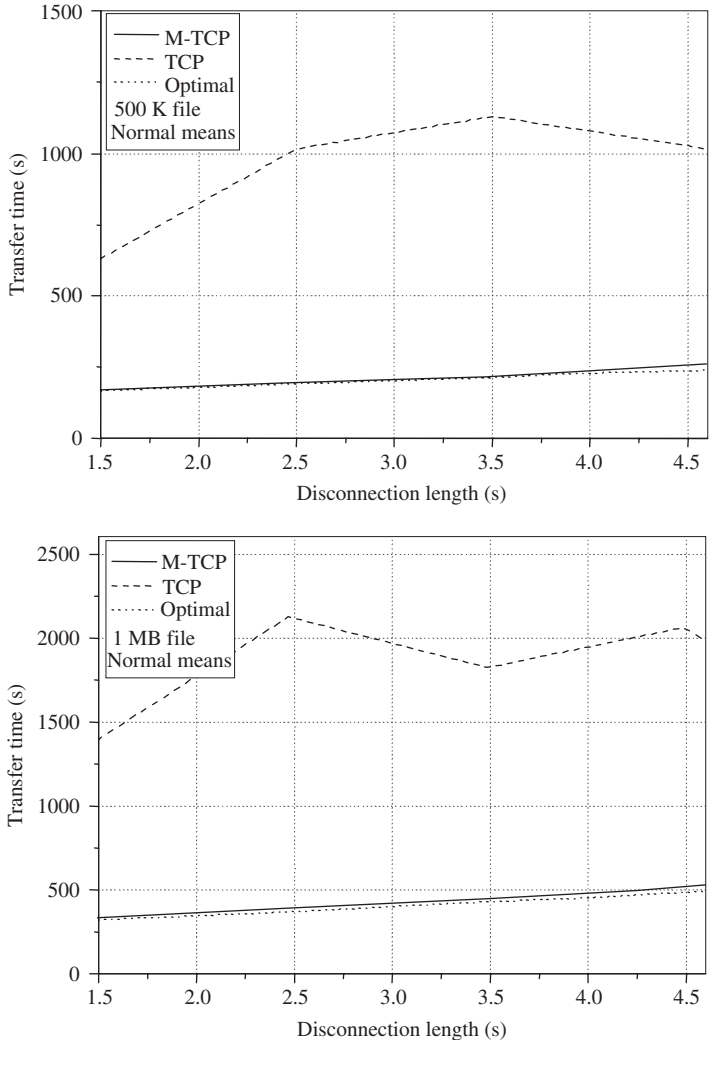

Figure 9.7 M-TCP/TCP vs disconnection length performance – 5 hops TCP connection.

9.3.5 Performance examples

Experimental/simulation set up is shown in Figure 9.6. The system parameters are used as in [20]. The wireless link has capacity of 32 kbit. File transfer times for 500 K and 1 MB files (respectively) vs disconnection length is given in Figures 9.7 and 9.8. Latency and disconnection length were normally distributed random variables and the TCP sender was five hops (Figure 9.7) and 15 hops (Figure 9.8) away. We can see that M-TCP offers better performance.

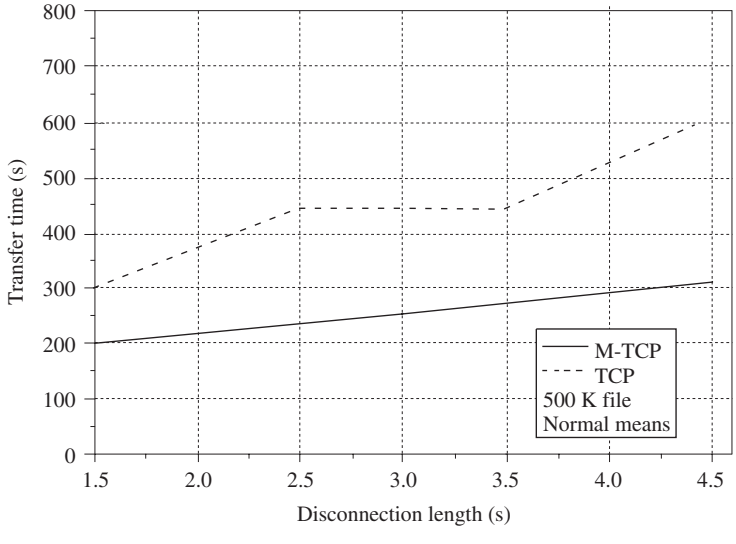

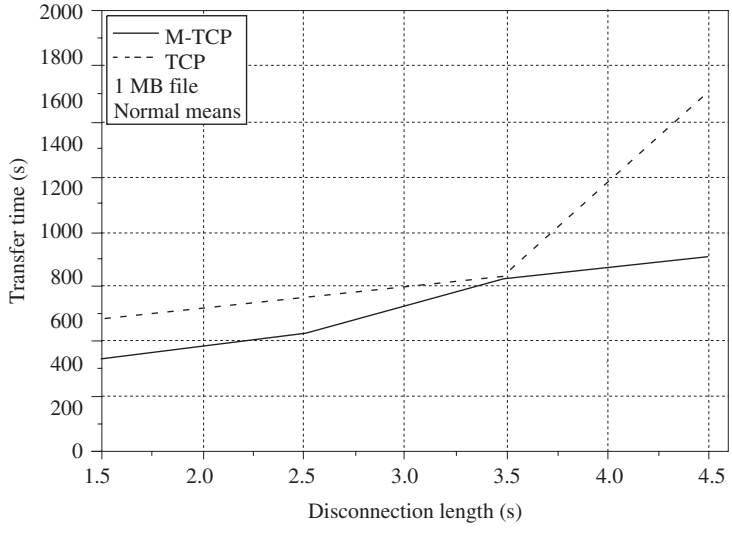

Figure 9.8 M-TCP/TCP vs disconnection length performance – 15 hops TCP connection.

9.4 RANDOM EARLY DETECTION GATEWAYS FOR CONGESTION AVOIDANCE

In this section we discuss *random early detection* gateways for congestion avoidance in packet-switched networks [25]. RED gateways are designed to accompany a transport-layer congestion control protocol. The gateway detects incipient congestion by computing the average queue size. The gateway could notify connections of congestion either by dropping packets arriving at the gateway or by setting a bit in packet headers. When the average queue size exceeds a preset threshold, the gateway drops or marks each arriving packet with a certain probability, where the exact probability is a function of the average queue size.

Prior to RED, *early random drop* gateways have been studied as a method for providing congestion avoidance at the gateway. The initial works proposed gateways to monitor the average queue size to detect incipient congestion and to randomly drop packets when congestion is detected. RED gateways differ from the earlier early random drop gateways in several respects: (1) the literate queue size is measured; (2) the gateway is not limited to dropping packets; and (3) the packet-marking probability is a function of the average queue size.

With an even earlier version called *random drop* gateways, when a packet arrives at the gateway and the queue is full, the gateway randomly chooses a packet from the gateway queue to drop. In the implementation of *early random drop* gateways, if the queue length exceeds a certain drop level, then the gateway drops each packet arriving at the gateway with a fixed drop probability p. Even then, it was stressed that, in future implementations, the drop level and drop probability should be adjusted dynamically depending on network traffic. With *drop tail* gateways, each congestion period introduces global synchronization in the network. When the queue overflows, packets are often dropped from several connections, and these connections decrease their windows at the same time. This results in a loss of throughput at the gateway.

9.4.1 The RED algorithm

The RED gateway calculates the average queue size W_q. The average queue size is compared with a minimum (W_q^-) and a maximum (W_q^+) threshold. When the average queue size is less than the minimum threshold, no packets are marked. When the average queue size is greater than the maximum threshold, every arriving packet is marked. If marked packets are, in fact, dropped or if all source nodes are cooperative, this ensures that the average queue size does not significantly exceed the maximum threshold. When the average queue size is between the minimum and maximum thresholds, each arriving packet is marked with probability p^0, where p^0 is a function of the average queue size Wq. Each time a packet is marked, the probability that a packet is marked from a particular connection is roughly proportional to that connection's share of the bandwidth at the gateway.

Thus, the RED gateway has two separate algorithms. The algorithm for computing the average queue size determines the degree of burstiness that will be allowed in the gateway queue. The algorithm for calculating the packet-marking probability determines how frequently the gateway marks packets, given the current level of congestion. The goal is for the gateway to mark packets at fairly evenly spaced intervals, in order to avoid biases and avoid global synchronization, and to mark packets sufficiently frequently to control the average queue size.

The gateway's calculations of the average queue size take into account the period when the queue is empty (the idle period) by estimating the number m of small packets that could have been transmitted by the gateway during the idle period. After the idle period, the gateway computes the average queue size as if m packets had arrived to an empty queue during that period. As W_q varies from W_q^- to W_q^+, the packet-marking probability p_b varies linearly from 0 to its maximum value P: $p_b \leftarrow P(W_q - W_q^-)/(W_q^+ - W_q^-)$. The final packet-marking probability p^a increases slowly

as the count c increases since the last marked packet: $p_b \leftarrow p_b/(1 - cp_b)$. This ensures that the gateway does not wait too long before marking a packet. The gateway marks each packet that arrives at the gateway when $Wq > W_q^+$.

9.4.2 Performance example

In this section we pay attention on the impact of traffic bursteness on the system performance. Bursty traffic at the gateway can result from an FTP connection with a long delay–bandwidth product but a small window; a window of traffic will be sent, and then there will be a delay until the ACK packets return and another window of data can be sent. Variable-bit rate video traffic and some forms of interactive traffic are other examples of bursty traffic seen by the gateway. This section shows that, unlike drop tail or random drop gateways. RED gateways do not have a bias against bursty traffic. For simulation FTP connections with infinite data, small windows and small RTT are used to model the less bursty traffic and FTP connections with smaller windows and longer RTT to model the more bursty traffic, as shown in Figure 9.9. Connections 1–4 have a maximum window of 12 packets, while connection 5 has a maximum window of eight packets. Because node 5 has a large RTT and a small window, node 5 packets often arrive at the gateway in a loose cluster. By this, we mean that, considering only node 5 packets, there is one long inter-arrival time and many smaller inter-arrival times. The same simulation scenario is used for example in Floyd and Jacobson [25].

Figure 9.10 shows the simulation results of the network in Figure 9.7 with drop tail, random drop and RED gateways, respectively. The simulations in Figure 9.10 (a) and (b) were run with the buffer size ranging from eight to 22 packets. The simulations in Figure 9.10 (c) were run many times with a minimum threshold ranging from three to 14 packets and a buffer size ranging from 12 to 56 packets.

For Figure 9.10 (a) and (b), the x-axis shows the buffer size, and the y-axis shows node 5's throughput as a percentage of the total throughput through the gateway. In these simulations, the concern is to examine the gateway's bias against bursty traffic.

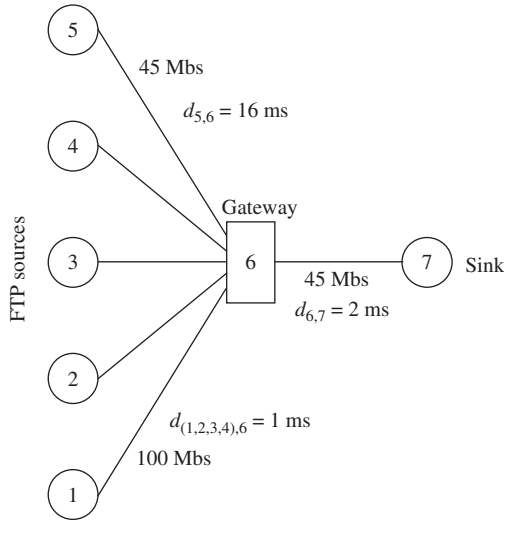

Figure 9.9 A simulation network with five FTP connections.

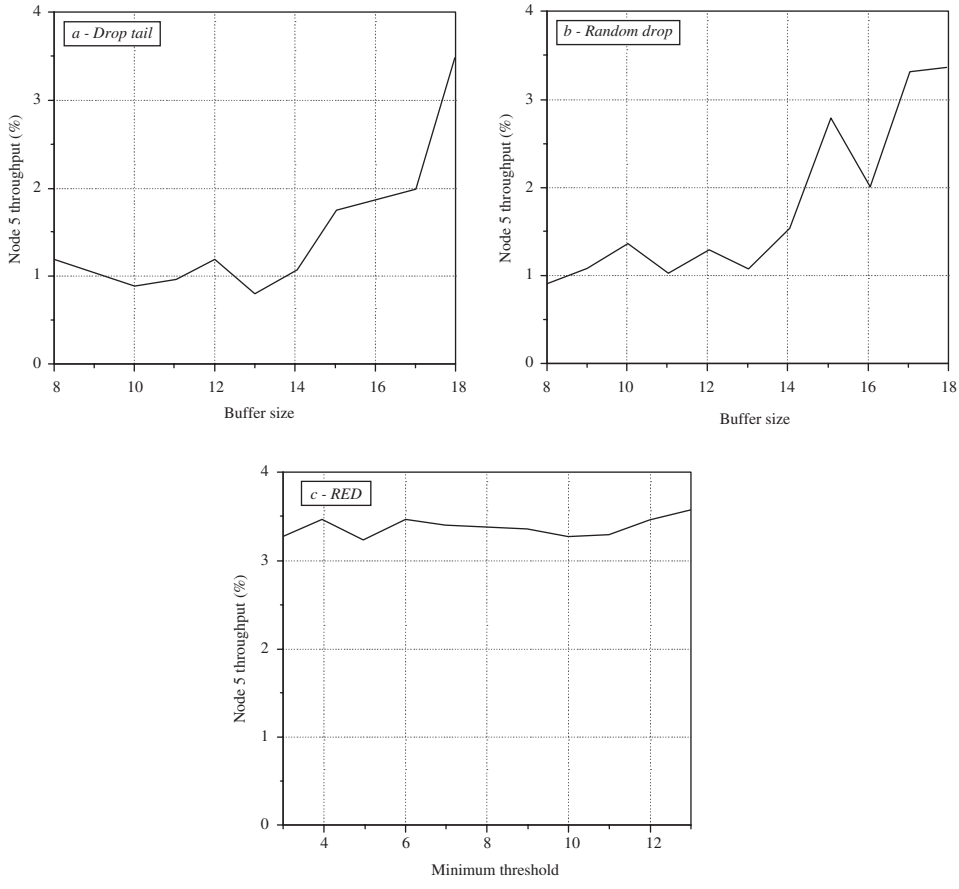

Figure 9.10 Performance of drop tail, random drop and RED gateways.

For the *drop tail gateway*, Figure 9.11(a) shows the average queue size (in packets) seen by arriving packets at the bottleneck gateway, and Figure 9.11(b) shows the average link utilization on the congested link. Because RED gateways are quite different from drop tail or random drop gateways, the gateways cannot be compared simply by comparing the maximum queue size. A fair comparison is between a drop tail gateway and an RED gateway that maintains the same average queue size. With drop tail or random drop gateways, the queue is more likely to overflow when the queue contains some packets from node 5. In this case, with either random drop or drop tail gateways, node 5 packets have a disproportionate probability of being dropped; the queue contents when the queue overflows are not representative of the average queue contents. Figure 9.10 (c) shows the result of simulations with RED gateways. The x-axis shows W_q^-, and the y-axis shows node 5's throughput. The throughput for node 5 is close to the maximum possible throughput given node 5's round trip time and maximum window. The parameters for the RED gateway are as follows: $W_q \leftarrow (1 - \omega_q) W_q + \omega_q W$ where ω_q represents the time constant of the low pass averaging filter and W is the current value of the queue, $\omega_q = 0.002$ and $P = 1/50$ were chosen. In addition $W_q^+ = 2W_q^-$, and the buffer size (which ranges from 12 to 56 packets) is $4W_q^-$.

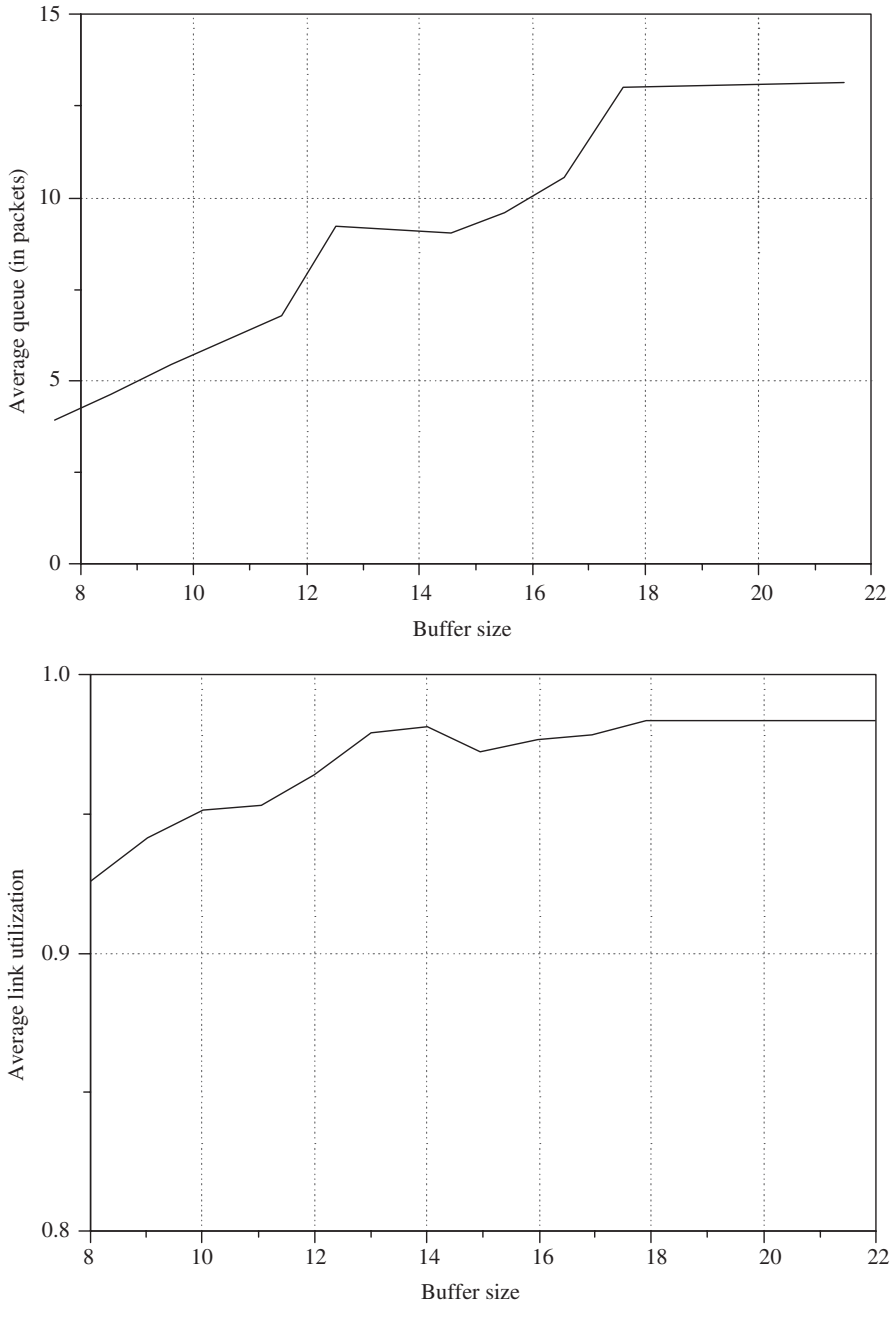

Figure 9.11 Drop tail gateway average queue length and link utilization.

9.5 TCP FOR MOBILE *AD HOC* NETWORKS

So far we have discussed in this chapter problems of TCP design when dealing with congestion, errors in the transmissions, and disconnections due to mobility and fading. Transport connections set up in wireless *ad hoc* networks are even further complicated by problems such as high bit error rates, frequent route changes, and partitions. If we run TCP over such connections, the throughput of the connection is observed to be extremely poor because TCP treats lost or delayed acknowledgments as congestion. In this section, we present an approach where a thin layer between Internet protocol and standard TCP is inserted that corrects these problems and maintains high end-to-end TCP throughput. This sublayer will be referred to as the *ad-hoc* TCP sublayer or A-TCP [26].

9.5.1 Effect of route recomputations

As we will see in Chapter 13, when an old route is no longer available, the network layer at the sender attempts to find a new route to the destination. In dynamic source routing (DSR) this is done via route discovery messages while in destination-sequenced distance-vectoring (DSDV) table exchanges are triggered that eventually result in a new route being found. It is possible that discovering a new route may take significantly longer than the RTO at the sender. As a result, the TCP sender times out, retransmits a packet, and invokes congestion control. Thus, when a new route is discovered, the throughput will continue to be small for some time because TCP at the sender grows its congestion window using the slow start and congestion avoidance algorithm. This is again undesirable behavior because the TCP connection will be very inefficient. If we imagine a network in which route computations are done frequently (due to high node mobility), the TCP connection will never get an opportunity to transmit at the maximum negotiated rate (i.e. the congestion window will always be significantly smaller than the advertised window size from the receiver).

9.5.2 Effect of network partitions

It is likely that the *ad hoc* network may periodically get partitioned for several seconds at a time. If the sender and the receiver of a TCP connection lie in different partitions, all the sender's packets get dropped by the network, resulting in the sender invoking congestion control. If the partition lasts for a significant amount of time (say, several times longer than the RTO), the situation gets even worse because of a phenomeon called *serial timeouts*. A serial timeout is a condition wherein multiple consecutive retransmissions of the same segment are transmitted to the receiver while it is disconnected from the sender. All these retransmissions are, thus, lost. Since the retransmission timer at the sender is doubled with each unsuccessful retransmission attempt (until it reaches 64 s), several consecutive failures can lead to inactivity lasting 1 or 2 *minutes*, even when the sender and receiver get reconnected.

9.5.3 Effect of multipath routing

As we will see in Chapter 13, some routing protocols, such as the temporally ordered routing algorithm (TORA) , maintain multiple routes between source destination pairs, the purpose of which is to minimize the frequency of route recomputation. Unfortunately, this sometimes results in a significant number of out-of-sequence packets arriving at the receiver. The effect of this is that the receiver generates duplicate ACKs which cause the sender (on receipt of three duplicate ACKs) to invoke congestion control.

The congestion window in TCP imposes an acceptable data rate for a particular connection based on congestion information that is derived from timeout events as well as from duplicate ACKs. In an *ad hoc* network, since routes change during the lifetime of a connection, we lose the

relationship between the congestion window (CWND) size and the tolerable data rate for the route. In other words, the CWND as computed for one route may be too large for a newer route, resulting in network congestion when the sender transmits at the full rate allowed by the old CWND.

9.5.4 ATCP sublayer

The ATCP sublayer utilizes network layer feedback (from intermediate hops) to put the TCP sender into either a persist state, congestion control state or retransmit state. So, when the network is partitioned, the TCP sender is put into persist mode so that it does not needlessly transmit and retransmit packets. On the other hand, when packets are lost due to error (as opposed to congestion), the TCP sender retransmits packets without invoking congestion control. Finally, when the network is truly congested, the TCP sender invokes congestion control normally.

We do not have to modify standard TCP itself when we want to maintain compatibility with the standard TCP/IP suite. Therefore, to implement this solution, we can insert a thin layer called ATCP (*ad hoc* TCP) between IP and TCP that listens to the network state information provided by ECN [27] messages and by ICMP 'destination unreachable' messages and then puts TCP at the sender into the appropriate state. Thus, on receipt of a 'destination unreachable' message, the TCP state at the sender is frozen (the sender enters the *persist* state) until a new route is found, ensuring that the sender does not invoke congestion control. Furthermore, the sender does not send packets into the network during the period when no route exists between the source and destination.

The ECN, which will be discussed later in more detail, is used as a mechanism by which the sender is notified of impending network congestion along the route followed by the TCP connection. On receipt of an ECN, the sender invokes congestion control without waiting for a timeout event (which may be caused, more often than not, due to lost packets). Thus, the benefits of A-TCP sublayer are:

- Standard TCP/IP is unmodified.
- ATCP is invisible to TCP and, therefore, nodes with and without ATCP can interoperate. The only drawback is that nodes without ATCP will see all the performance problems associated with running TCP over *ad hoc* networks.
- ATCP does not interfere with TCPs functioning in cases where the TCP connection is between a node in the wireline network and another in the wireless *ad hoc* network.

There are in the literature papers dealing with different aspects of TCP problem in *ad hoc* networks. Holland and Vaidya [28], for example, investigate the impact of link breakage on TCP performance in such networks. They use dynamic source routing (DSR), discussed in Chapter 13 (see also Johnson and Maltz [29]), as the underlying routing protocol (simulated in NS2). DSR is an on-demand routing protocol where a sender finds a route to the destination by flooding *route request* packets. DSR's performance is optimized by allowing intermediate nodes to respond to route request packets using cached routes. Unfortunately, if the cached information maintained at a intermediate node is stale, the time it takes to find a new route can be very long (several seconds). Thus, TCP running on top of DSR sees very poor throughput. The paper proposes the use of explicit link failure notification (ELFN) to improve TCP performance. Here, the TCP sender is notified that a link has failed, and it disables its retransmission timer and enters a stand-by mode. In stand-by mode, the TCP sender periodically sends a packet in its congestion window to the destination. When an ACK is received, TCP leaves the stand-by mode, restores its retransmission timers and resumes transmission as normal.

Chandran *et al*. [30] discusses a similar scheme for improving TCP performance in *ad hoc* networks in the presence of failures. Here, the router detecting a failed route generates a route failure notification (RFN) packet toward the source. The TCP source that receives this packet enters

a *snooze* state which is very similar to TCP's persist state. When the route is re-established, a route re-establishment notification (RRN) is sent to the source by any router on the previous route that detected the new route. This packet removes the source from the snooze state. In this method, the source continues using the old congestion window size for the new route. This is a problem because the congestion window size is route-specific (since it seeks to approximate the available bandwidth). Chandran *et al*. [30] also does not consider the effects of congestion, out-of-order packets and bit error.

9.5.5 ATCP protocol design

In this section we discuss the design of an ATCP that attempts to provide an integral solution to the problems of running TCP over multihop wireless networks. Such a protocol should have the following characteristics [26]:

(1) It should Improve TCP performance for connections set up in *ad hoc* wireless networks. As already discussed, TCP performance is affected by the problems of high BER and disconnections due to route recomputation or partition. In each of these cases, the TCP sender mistakenly invokes congestion control. A good protocol should provide only retransmissions for packets lost due to high BER, without shrinking the congestion window. Also, the sender should stop transmitting and resume when a new route has been found. As above, in the case of transient partition, the sender should stop transmitting until it is reconnected to the receiver. In the case of multipath routing when TCP at the sender receives duplicate ACKs, it should not invoke congestion control because multipath routing shuffles the order in which packets are received.

(2) It should maintain TCP's congestion control. If losses are caused due to network congestion, we want TCP to shrink its congestion window in response to losses and invoke slow start.

(3) It should have appropriate CWND. When there is a change in the route (e.g. a reconnection after a brief partition), the congestion window should be recomputed.

(4) It should maintain end-to-end TCP semantics in order to ensure that applications do not crash.

(5) It should be compatible with standard TCP because we cannot assume that all machines deployed in an *ad hoc* network will have ATCP installed.

The above functionalities are implemented within a separate sublayer, the ATCP, placed between the network and TCP layer in the protocol stack (TCP/ATCP/IP stack). This layer monitors the TCP state and the state of the network (based on ECN and ICMP messages) and takes appropriate action. Figure 9.12 illustrates ATCP's four possible states: *normal*, *congested*, *loss* and *disconnected*. When the TCP connection is initially established, ATCP at the sender is in the *normal* state.

In this state, ATCP does nothing and is invisible. Let us now examine ATCP's behavior under four circumstances.

9.5.5.1 Lossy channel

When the connection from the sender to the receiver is lossy, it is likely that some segments will not arrive at the receiver or may arrive *out-of-order*. Thus, the receiver may generate *duplicate* acknowledgment (ACKs) in response to out-of-sequence segments. When TCP receives three consecutive duplicate ACKs, it retransmits the appropriate segment and shrinks the congestion window. It is also possible that, due to lost ACKs, the TCP sender's RTO may expire, causing it to retransmit one segment and invoke congestion control.

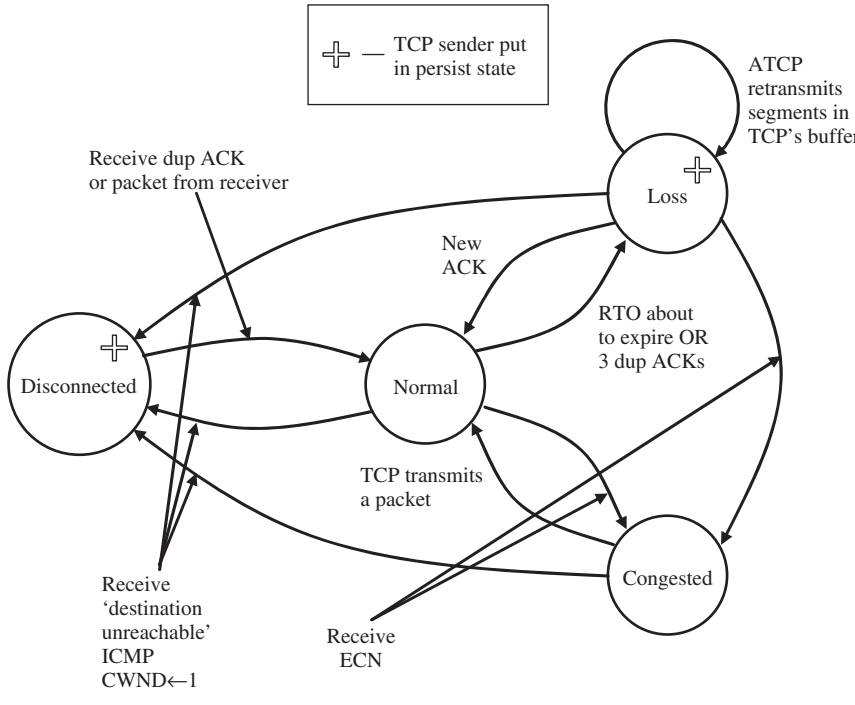

Figure 9.12 State transition diagram for ATCP at the sender.

ATCP in its *normal state* counts the number of duplicate ACKs received for any segment. When it sees that three duplicate ACKs have been received, it *does not forward* the third duplicate ACK but puts TCP in *persist mode*. Similarly, when ATCP sees that TCP's RTO is about to expire, it again puts TCP in *persist mode*. By doing this, we ensure that the TCP sender does not invoke congestion control because that is the wrong thing to do under these circumstances. After ATCP puts TCP in persist mode, ATCP enters the *loss state*. In the *loss state*, ATCP transmits the unacknowledged segments from TCP's send buffer. It maintains its own separate timers to retransmit these segments in the event that ACKs are not forthcoming. Eventually, when a *new* ACK arrives (i.e. an ACK for a previously unacknowledged segment), ATCP forwards that ACK to TCP, which also removes TCP from persist mode. ATCP then returns to its *normal state*.

9.5.5.2 Congested

When the network detects congestion, the ECN flag is set in ACK and data packets. Let us assume that ATCP receives this message when in its *normal state*. ATCP moves into its *congested state* and does nothing. It ignores any duplicate ACKs that arrive and it also ignores imminent RTO expiration events. In other words, ATCP does *not interfere* with TCP's normal congestion behavior. After TCP transmits a new segment, ATCP returns to its *normal state*.

9.5.5.3 Disconnected

Node mobility in *ad hoc* networks causes route recomputation or even temporary network partition. When this happens, we assume that the network generates an ICMP *destination unreachable*

message in response to a packet transmission. When ATCP receives this message, it puts the TCP sender into persist mode and itself enters the *disconnected state*. TCP periodically generates *probe packets* while in persist mode. When, eventually, the receiver is connected to the sender, it responds to these probe packets with a duplicate ACK (or a data packet). This removes TCP from persist mode and moves ATCP back into *normal state*. In order to ensure that TCP does not continue using the old CWND value, ATCP sets TCP's *CWND to one segment* at the time it puts TCP in persist state. The reason for doing this is to force TCP to probe the correct value of CWND to use for the new route.

9.5.5.4 Other transitions

When ATCP is in the *loss state*, reception of an ECN or an ICMP *source quench* message will move ATCP into *congested state* and ATCP removes TCP from its persist state. Similarly, reception of an ICMP *destination Unreachable* message moves ATCP from either the *loss state* or the *congested state* into the *disconnected state* and ATCP moves TCP into persist mode (if it was not already in that state).

9.5.5.5 Effect of lost messages

Note that due to the lossy environment, it is possible that an ECN may not arrive at the sender or, similarly, a *destination unreachable* message may be lost. If an ECN message is lost, the TCP sender will continue transmitting packets. However, every subsequent ACK will contain the ECN, thus ensuring that the sender will eventually receive the ECN, causing it to enter the congestion control state as it is supposed to. Likewise, if there is no route to the destination, the sender will eventually receive a retransmission of the *destination unreachable* message, causing TCP to be put into the persist state by ATCP. Thus, in all cases of lost messages, ATCP performs correctly. Further details on protocol implementation can be found in Liu and Singh [26].

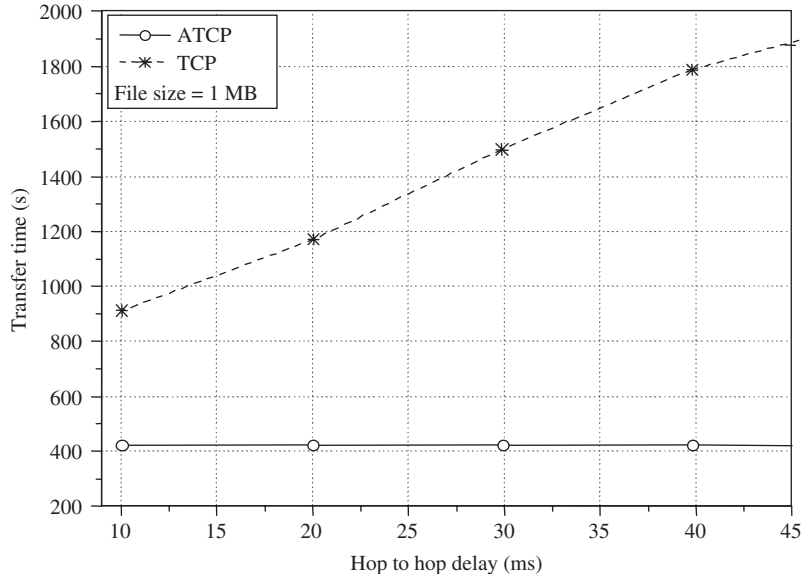

Figure 9.13 ATCP and TCP performance in the presence of bit error only.

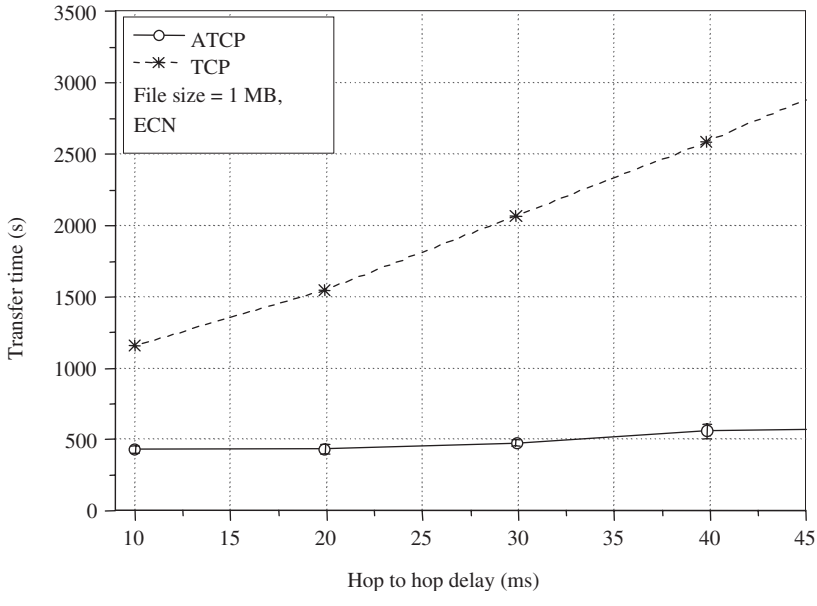

Figure 9.14 ATCP and TCP performance in the presence of bit error and congestion.

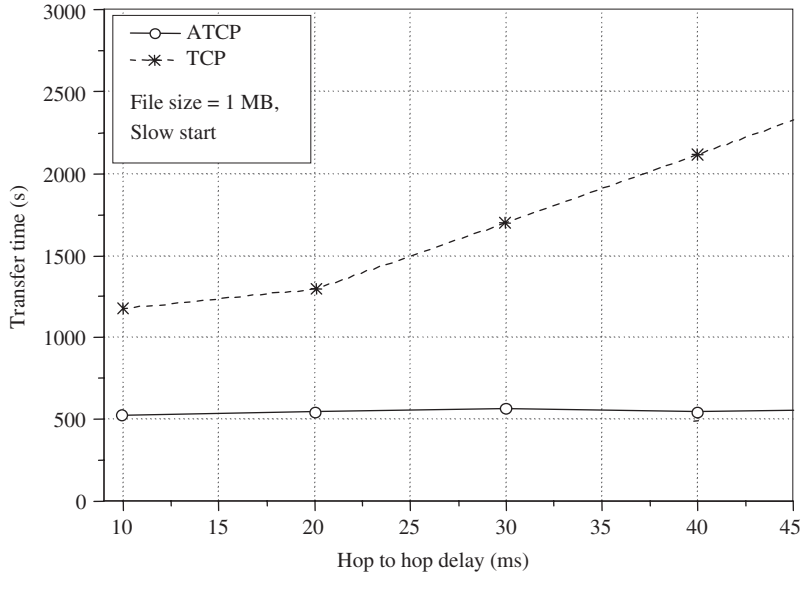

Figure 9.15 ATCP and TCP performance in the presence of bit error and partition.

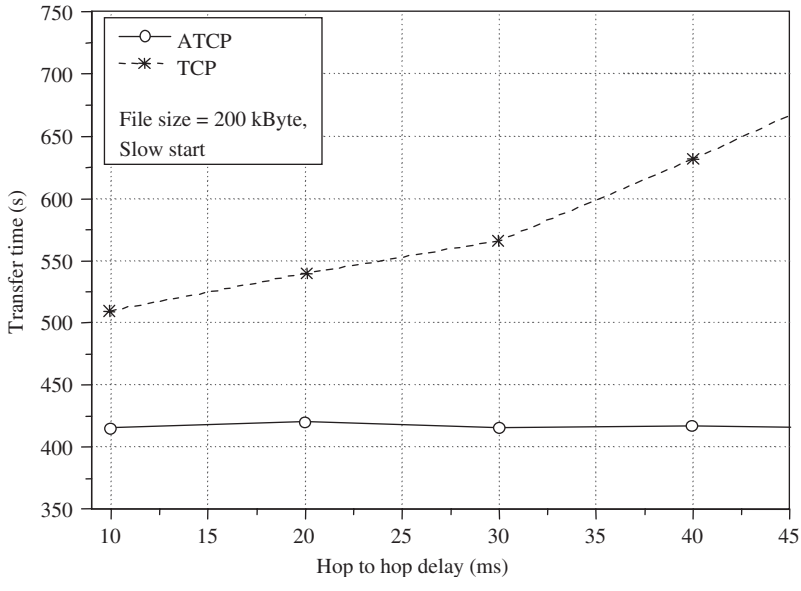

Figure 9.16 ATCP and TCP performance in the presence of bit error and larger partition.

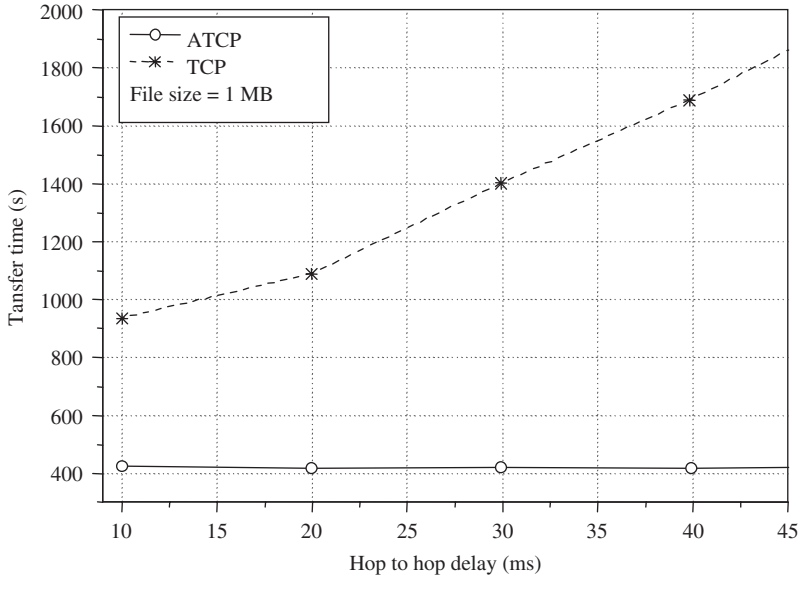

Figure 9.17 ATCP and TCP performance in the presence of bit error and packet reordering.

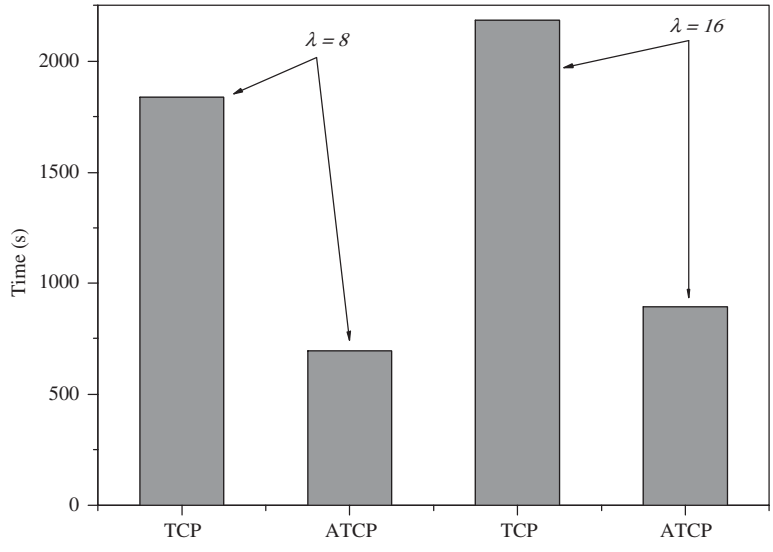

Figure 9.18 TCP and ATCP transfer time for 1 MB data in the general case.

9.5.6 Performance examples

An experimental testbed, for the evaluation of ATCP protocol, consisting of five Pentium PCs, each of which with two ethernet cards is described in Liu and Singh [26]. This gives a four-hop network where the traffic in each hop is isolated from the other hops. To model the lossy and low-bandwidth nature of the wireless links, in IP, a 32 kb/s channel is emulated over each hop. Performance examples are shown in Figures 9.13–18. A uniformly better performance of ATCP over standard TCP protocols is evident from all these examples.

REFERENCES

[1] T. Henderson and R.H. Katz, Transport protocols for Internet-compatible satellite networks, *IEEE JSAC*, vol. 17, no. 2, 1999, pp. 326–344.

[2] T.V. Lakshman and U. Madhow, The performance of TCP/IP for networks with high bandwidth–delay products and random loss, *IEEE/ACM Trans. Networking*, 1997, vol. 5, no. 3, pp. 336–350.

[3] S. Floyd and V. Jacobson, Random early detection gateways for congestion avoidance, *IEEE/ACM Trans*. *Networking*, vol. 1, no. 4, 1993, pp. 397–413.

[4] L. Brakmo and L. Peterson, TCP Vegas: end to end congestion avoidance on a global internet, *IEEE JSAC*, vol. 13, no. 8, 1995, pp. 1465–1480.

[5] C. Barakat and E. Altman, Analysis of TCP with several bottleneck nodes, *IEEE GLOBECOM*, 1999, pp. 1709–1713.

[6] W.R. Stevens, *TCP/IP Illustrated*, vol. 1. Reading, MA: Addison-Wesley, 1994.

[7] R. Caceres and L. Iftode, Improving the performance of reliable transport protocols in mobile computing environments, *IEEE J. Select. Areas Commun.*, vol. 13, 1995 pp. 850–857.

[8] A. Desimone, M.C. Chuah and O.C. Yue, Throughput performance of transport layer protocols over wireless LAN's, in *Proc. IEEE GLOBECOM'93*, December 1993, pp. 542–549.

[9] K. Fall and S. Floyd, *Comparisons of Tahoe, Reno, and Sack TCP* [Online], March 1996. Available FTP: ftp://ftp.ee.lbl.gov

[10] V.K. Joysula, R.B. Bunt and J.J. Harms, Measurements of TCP performance over wireless connections, in *Proc. WIRELESS'96, 8th Int. Conf. Wireless Communications*, Calgary, 8–10 July 1996, pp. 289–299.

[11] T.V. Lakshman and U. Madhow, The performance of TCP/IP for networks with high bandwidth–delay products and random loss, *IEEE Trans. Networking*, vol. 3, 1997, pp. 336–350.

[12] P.P. Mishra, D. Sanghi and S.K. Tripathi, TCP flow control in lossy networks: Analysis and enhancements, in *Computer Networks, Architecture and Applications*, IFIP Transactions C-13, S.V. Raghavan, G.V. Bochmann and G. Pujolle (eds). Amsterdam: Elsevier North-Holland, 1993, pp. 181–193.

[13] A. Kumar, Comparative performance analysis of versions of TCP in a local network with a lossy link, *IEEE/ACM Trans. Networking*, vol. 6, no. 4, 1998, pp. 485–498

[14] A. Bakre and B.R. Badrinath, I-TCP: indirect TCP for mobile hosts, in *Proc. 15th Int. Con. on Distributed Computing Systems*, Vancouver, June 1995, pp. 136–143.

[15] A. Bakre and B.R. Badrinath, Indirect transport layer protocols for mobile wireless environment, in *Mobile Computing*, T. Imielinski and H.F. Korth (eds). Kluwer Academic: Norwell, MA 1996, pp. 229–252.

[16] H. Balakrishnan, S. Seshan and Randy Katz, Improving reliable transport and handoff performance in cellular wireless networks, *Wireless Networks*, vol. 1, no. 4, 1995.

[17] H. Balakrishnan, V.N. Padmanabhan, S. Seshan and R. Katz, A comparison of mechanisms for improving TCP performance over wireless links, in *ACM SIGCOMM'*96, Palo Alto, CA, August 1996, pp. 256–269.

[18] B.R. Badrinath and T. Imielinski, Location management for networks with mobile users, in *Mobile Computing*, T. Imielinski and H.F. Korth (eds). Kluwer Academic: Norwell, MA 1996, pp. 129–152.

[19] K. Brown and S. Singh, A network architecture for mobile computing, in *Proc. IEEE INFOCOMM'96*, March 1996, pp. 1388–1396.

[20] K. Brown and S. Singh, M-UDP: UDP for mobile networks, *ACM Comput. Commun. Rev.*, vol. 26, no. 5, 1996, pp. 60–78.

[21] R. Caceres and L. Iftode, Improving the performance of reliable transport protocols in mobile computing environments, *IEEE Selected Areas in Commun.*, vol. 13, no. 5, 1994, pp. 850–857.

[22] R. Ghai and S. Singh, An architecture and communication protocol for picocellular networks, *IEEE Personal Commun. Mag.*, no. 3, 1994, pp. 36–46.

[23] K. Seal and S. Singh, Loss profiles: a quality of service measure in mobile computing, *J. Wireless Networks*, vol. 2, 1996, pp. 45–61.

[24] S. Singh, Quality of service guarantees in mobile computing, *J. Comput. Commun.*, vol. 19, no. 4, 1996, pp. 359–371.

[25] S. Floyd and V. Jacobson, Random early detection gateways for congestion avoidance, *IEEE/ACM Trans. Networking*, vol. 1, no. 4, 1993, pp. 397–413.

[26] J. Liu and S. Singh, ATCP: TCP for mobile *ad hoc* networks, *IEEE J. Selected Areas Commun.*, vol. 19, no. 7, 2001, pp. 1300–1315.

[27] http://www-nrg.ee.lbl.gov/ecn-arch/

[28] G. Holland and N. Vaidya, Analysis of TCP performance over mobile *ad hoc* networks, in *Proc. ACMMobile Communications Conf.*, Seattle, WA, 15–20 August 1999, pp. 219–230.

[29] D.B. Johnson and D.A. Maltz, Dynamic source routing in *ad hoc* wireless networks, in *Mobile Computing*, T. Imielinski and H. F. Korth (eds). Norwell, MA: Kluwer Academic, 1996, pp. 153–191.

[30] K. Chandran, S. Raghunathan, S. Venkatesan and R. Prakash, A feedback-based scheme for improving TCP performance in *ad hoc* wireless networks, in *Proc. 18th Int. Conf. Distributed Computing Systems*, Amsterdam, 26–29 May 1998, pp. 474–479.

10

Network Optimization Theory

10.1 INTRODUCTION

In the past, network protocols in layered architectures have been obtained on an *ad hoc* basis, and many of the recent crosslayer designs are also conducted through piecemeal approaches. It is only recently that network protocol stacks have instead been analyzed and designed as distributed solutions to some global optimization problems in the form of generalized network utility maximization (NUM), providing insight on what they optimize and on the structures of the network protocol stacks.

This chapter will present material required for understanding of layering as optimization decomposition where each layer corresponds to a decomposed subproblem, and the interfaces among layers are quantified as functions of the optimization variables coordinating the subproblems.

Decomposition theory provides the analytical tool for the design of modularized and distributed control of networks. This chapter will present results of horizontal decomposition into distributed computation and vertical decomposition into functional modules such as congestion control, routing, scheduling, random access, power control and channel coding. Key results from many recent works are summarized and open issues discussed. Through case studies, it is illustrated how layering as optimization decomposition provides a common framework for modularization, a way to deal with complex, networked interactions. The material presents a top-down approach to design protocol stacks and a mathematical theory of network architectures.

Convex optimization has become a computational tool of central importance in engineering, thanks to its ability to solve very large, practical engineering problems reliably and efficiently. Many communication problems can either be cast as or be converted into convex optimization problems, which greatly facilitate their analytic and numerical solutions. Furthermore, powerful numerical algorithms exist to solve the optimal solution of convex problems efficiently.For the basics in the area of convex optimization, the basics of convexity, Lagrange duality, distributed subgradient methods and other solution methods for convex optimization, the reader is referred to References [1] to [8].

Advanced Wireless Technologies: Cognitive, Cooperative & Opportunistic 4G Technology Second Edition Savo G. Glisic

10.2 LAYERING AS OPTIMIZATION DECOMPOSITION

Layered architectures form one of the most fundamental and influential structures of network design. It adopts a modularized and often distributed solution approach to network coordination and resource allocation. Each layer controls a subset of the decision variables and observes a subset of constant parameters and the variables from other layers. Intuitively, layered architectures enable a scalable, evolvable and implementable network design. Each layer in the protocol stack hides the complexity of the layer below and provides a service to the layer above.

Different layers iterate on different subsets of the decision variables using local information to achieve individual optimality. Taken together, these local algorithms attempt to achieve a global objective. Such a design process of modularization can be quantitatively understood through the mathematical language of *decomposition theory* for constrained optimization [9].

The framework of 'layering as optimization decomposition' exposes the interconnection between protocol layers and can be used to study rigorously the performance tradeoff in protocol layering, as different ways to modularize and distribute a centralized computation. Even though the design of a complex system will always be broken down into simpler modules, this theory will allow us systematically to carry out this layering process and explicitly trade off design objectives.

The network is modeled as a set L of links (scarce resources) with finite capacities $\mathbf{c} = (c_l, l \in L)$. They are shared by a set N of sources indexed by s. Each source s uses a set $L(s) \subseteq L$ of links. Let $S(l) = \{s \in N | l \in L(s)\}$ be the set of sources using link l. The sets $\{L(s)\}$ define an $L \times N$ routing matrix $R_{ls} = 1$, if $l \in L(s)$; i.e. source s uses link l and 0, otherwise.

The basic *NUM* problem has the following formulation:

$$\begin{aligned} &\text{Maximize} \sum_s U_s(x_s) \\ &\text{subject to } \mathbf{Rx} \leq \mathbf{c} \end{aligned} \tag{10.1}$$

where $U_s(x_s)$ are the utility functions. TCP variants have recently been reverse-engineered to show that they are implicitly solving this problem, where the source rate vector $\mathbf{x} \geq 0$ is the only set of optimization variables and the routing matrix $\mathbf{R}$ and link capacity vector $\mathbf{c}$ are both constants. One of the possible formulations of a generalized *NUM* for the entire protocol stack is

$$\begin{aligned} \text{Maximize } & \sum_s U_s(x_s, P_{e,s}) + \sum_j V_j(w_j) \\ \text{subject to } & \mathbf{Rx} \leq \mathbf{c}(\mathbf{w}, \mathbf{P}_e) \\ & \mathbf{x} \in C_1(\mathbf{P}_e), \mathbf{x} \in C_2(\mathbf{F}) \text{ or } \in \mathbf{\Pi}(\mathbf{w}) \\ & \mathbf{R} \in R, \mathbf{F} \in F, \mathbf{w} \in W \end{aligned} \tag{10.2}$$

Here, x_s denotes the rate for source s and w_j denotes the physical layer resource at network element j. The utility functions U_s and V_j may be any nonlinear, monotonic function. $\mathbf{R}$ is the routing matrix and $\mathbf{c}$ are the logical link capacities as functions of both physical layer resources $\mathbf{w}$ and the desired decoding error probabilities $\mathbf{P}_e$.

10.2.1 TCP congestion control

A congestion control algorithm consists of two components: a source algorithm that dynamically adjusts its rate $x_s(t)$ in response to prices $\lambda_l(t)$ in its path and a link algorithm that updates, implicitly or explicitly, its price $\lambda_l(t)$ and sends it back, implicitly or explicitly, to sources that use link l. On the current Internet, the source algorithm is carried out by TCP and the link algorithm is carried out by (active) queue management (AQM).

We now present a general model of congestion control algorithms and show that they can be interpreted as distributed algorithms to solve NUM (10.3) and its dual (10.4):

$$\begin{aligned} &\text{Maximize} \sum_s U_s(x_s) \\ &\text{subject to } \mathbf{Rx} \le \mathbf{c} \end{aligned} \tag{10.3}$$

and its Lagrangian dual problem:

$$\underset{\boldsymbol{\lambda}\ge 0}{\text{Minimize}}\ D(\boldsymbol{\lambda}) = \sum_s \max_{x_s \ge 0} \left[U_s(x_s) - x_s \sum_l R_{ls}\lambda_l \right] + \sum_l c_l \lambda_l \tag{10.4}$$

Let $y_l(t) = \sum_s R_{ls}x_s(t)$ be the aggregate source rate at link l and let $q_s(t) = \sum_l R_{ls}\lambda_l(t)$ be the end-to-end price for source s. In vector notation, $\mathbf{y}(t) = \mathbf{Rx}(t)$ and $\mathbf{q}(t) = \mathbf{R}^{\mathrm{T}}\boldsymbol{\lambda}(t)$, where $\mathbf{x}(t) = (x_s(t), s \in N)$ and $\mathbf{q}(t) = (q_s(t), s \in N)$ are in $\mathbf{R}_+^N$, and $\mathbf{y}(t) = (y_l(t), l \in L)$ and $\boldsymbol{\lambda}(t) = (\lambda_l(t), l \in L)$ are in $\mathbf{R}_+^L$.

The source rates $x_s(t)$ and link prices $\lambda_l(t)$ are updated in each period, based on local information. Source s can observe its own rate $x_s(t)$ and the end-to-end price $q_s(t)$ of its path, but not the vector $\boldsymbol{\lambda}(t)$, nor other components of $\mathbf{x}(t)$ or $\mathbf{q}(t)$. Similarly, link l can observe just local price $\lambda_l(t)$ and flow rate $y_l(t)$. The source rates $x_s(t)$ are updated according to

$$x_s(t+1) = F_s(x_s(t), q_s(t)) \tag{10.5}$$

In each period, the link congestion measure $\lambda_l(t)$ is adjusted based only on $\lambda_l(t)$ and $y_l(t)$, and possibly some internal (vector) variable $\mathbf{v}_l(t)$, such as the queue length at link l. This can be modeled by some functions $(G_l, \mathbf{H}_l)$: for all l,

$$\lambda_l(t+1) = G_l(y_l(t), \lambda_l(t),\ \mathbf{v}_l(t)) \tag{10.6}$$

$$\mathbf{v}_l(t+1) = \mathbf{H}_l(y_l(t), \lambda_l(t),\ \mathbf{v}_l(t)) \tag{10.7}$$

where G_l are nonnegative so that $\lambda_l(t) \ge 0$. Here, F_s model TCP algorithms (e.g. Reno or Vegas) and $(G_l, \mathbf{H}_l)$ model AQMs (e.g. RED, REM). We will often refer to AQMs by G_l, without explicit reference to the internal variable $\mathbf{v}_l(t)$ or its adaptation $\mathbf{H}_l$.

10.2.2 TCP Reno/RED

In the large majority of current TCP implementations the congestion control algorithm can be modelled as

$$F_s(t+1) = \left[x_s(t) + \frac{1}{T_s^2} - \frac{2}{3} q_s(t) x_s^2(t) \right]^+ \tag{10.8}$$

where T_s is the round-trip time (RTT) of source s, i.e. the time it takes for s to send a packet and receive its acknowledgment from the destination. Here we assume T_s is a constant even though in reality its value depends on the congestion level and is generally time-varying. The AQM mechanism of RED [10] maintains two internal variables, the instantaneous queue length $b_l(t)$ and the average queue length $r_l(t)$. These variables are updated as

$$b_l(t+1) = [b_l(t) + y_l(t) - c_l]^+ \tag{10.9}$$

$$r_l(t+1) = (1 - \omega_l) r_l(t) + \omega_l b_l(t) \tag{10.10}$$

where $\omega_l \in (0, 1)$. Then, random early detection (RED) protocol marks a packet with a probability $\lambda_l(t)$ that is a piecewise linear, increasing the function of $r_l(t)$ with constants $\rho_1, \rho_2, M_l, \bar{b}_1$

and $\underline{b}_l$:

$$\lambda_l(t) = \begin{cases} 0, & r_l(t) \le \underline{b}_l \\ \rho_1(r_l(t) - \underline{b}_l), & \underline{b}_l \le r_l(t) \le \overline{b}_l \\ \rho_2(r_l(t) - \overline{b}_l) + M_l, & \overline{b}_l \le r_l(t) \le 2\overline{b}_l \\ 1, & r_l(t) \ge 2\overline{b}_l \end{cases} \tag{10.11}$$

Equations (10.9) to (10.11) define the model $(\mathbf{G}, \mathbf{H})$ for RED.

10.2.3 TCP Vegas/Drop Tail

Vegas uses queuing delay as the congestion measure $\lambda_l(t) = b_l(t)/c_l$, where $b_l(t)$ is the queue length at time t. The update rule $G_l(y_l(t), \lambda_l(t))$ is given by (dividing both sides of (10.9) by c_l)

$$\lambda_l(t+1) = \left[\lambda_l(t) + \frac{y_l(t)}{c_l} - 1\right]^+ \tag{10.12}$$

AQM for Vegas does not involve any internal variable. The update rule $F_s(x_s(t), q_s(t))$ for the source rate is given by

$$x_s(t+1) = x_s(t) + \frac{1}{T_s^2(t)}\text{sgn}[\alpha_s d_s - x_s(t)q_s(t)] \tag{10.13}$$

where α_s is a parameter, d_s is the round-trip propagation delay of source s and $T_s(t) = d_s + q_s(t)$ is the RTT at time t.

For *FAST/DropTail*, if d_s is the round-trip propagation delay of source s, $\lambda_l(t)$ the queuing delay at link l at time t, $q_s(t) = \sum_l R_{ls}\lambda_l(t)$, the round-trip queuing delay, or in vector notation, $\mathbf{q}(t) = \mathbf{R}^{\mathrm{T}}\boldsymbol{\lambda}(t)$, then each source s adapts its window $W_s(t)$ periodically according to

$$W_s(t+1) = \gamma\left[\frac{d_s W_s(t)}{d_s + q_s(t)} + \alpha_s\right] + (1-\gamma)W_s(t) \tag{10.14}$$

where $\gamma \in (0, 1]$ and $\alpha_s > 0$ is a protocol parameter. The link queuing delay vector $\boldsymbol{\lambda}(t)$ is determined implicitly by the instantaneous window size in a static manner. Given $W_s(t) = W_s$ for all s, the link queuing delays $\lambda_l(t) = \lambda_l \ge 0$ for all l are given by

$$\sum_s R_{ls}\frac{W_s}{d_s + q_s(t)} \begin{cases} = c_l, & \text{if } \lambda_l(t) = 0 \\ \le c_l, & \text{if } \lambda_l(t) = 0 \end{cases} \tag{10.15}$$

where again $q_s(t) = \sum_l R_{ls}\lambda_l(t)$.

Hence, FAST is defined by the discrete-time model (10.14), (10.15) of window evolution. The sending rate is then defined as $x_s(t) := W_s(t)/[d_s(t) + q_s(t)]$. For more details see References [10] to [18].

10.2.4 Optimization of the MAC protocol

Consider an ad hoc network represented by a directed graph $G(V, E)$, e.g. as in Figure 10.1, where V is the set of nodes and E is the set of logical links. We define $L_{\text{out}}(n)$ as a set of outgoing links from node n, $L_{\text{in}}(n)$ as a set of incoming links to node n, t_l as the transmitter node of link l and r_l as the receiver node of link l.

In addition we define $N^l_{\text{to}}(l)$ as the set of nodes whose transmission causes interference to the receiver of link l, excluding the transmitter node of link l (i.e. t_l), and $L^l_{\text{from}}(n)$ as the set of links whose transmission suffers interference from the transmission of node n, excluding outgoing links from node n (i.e. $l \in L_{\text{out}}(n)$). Hence, if the transmitter of link l and a node in set $N^l_{\text{to}}(l)$ transmit

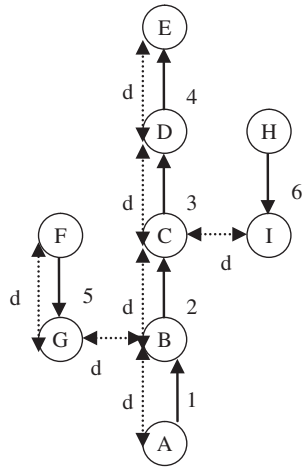

Figure 10.1 Logical topology graph of a network illustrating contention.

data simultaneously, the transmission of link l fails. If node n and the transmitter of link l in set $L^l_{\text{from}}(n)$ transmit data simultaneously, the transmission of link l also fails.

For contention resolution with a window-based exponential backoff (EB) protocol, each link l maintains its contention window size W_l, current window size CW_l, and minimum and maximum window sizes $W_l^{\min}$ and $W_l^{\max}$. After each transmission contention, window size and current window size are updated. If transmission is successful, the contention window size is reduced to the minimum window size (i.e. $W_l = W_l^{\min}$); otherwise it is doubled until reaching the maximum window size $W_l^{\max}$ (i.e. $W_l = \min\{2W_l, W_l^{\max}\}$). Then, the current window size CW_l is chosen to be a number between $(0, W_l)$ uniformly at random. It decreases in an over timeslot, and when it becomes zero, the link transmits data. In the IEEE 802 standard the window size is doubled after each transmission failure and the random across protocol in the distributed coordination function (DCF) is called the binary exponential backoff (BEB) protocol, which is a special case of EB protocols.

In this case each link l transmits data with a probability p_l, which is referred to as the persistence probability of link l. After each transmission attempt, if the transmission is successful without collisions then link l sets its persistence probability to be its maximum value $p_l^{\max}$. Otherwise, it multiplicatively reduces its persistence probability by a factor $\beta_l (0 < \beta_l < 1)$ until reaching its minimum value $p_l^{\min}$. This persistence probability node is a memoryless one that approximates the average behavior of the EB protocol.

Since in the window-based EB protocol the current window size CW_l of link l is randomly selected between $(0, W_l)$, when its window size is W_l, we may think that link l transmits data in a timeslot with an attempt probability $1/W_l$, which corresponds to the persistence probability p_l in the new model for the average behavior of the EB protocols. In the window-based protocol, after every transmission success, the attempt probability is set to be its maximum value (i.e. $1/W_l^{\min}$), which corresponds to $p_l^{\max}$ in our mode, and after every transmission failure, the attempt probability is set to be a fraction of its current value until it reaches its minimum value, which corresponds to reducing the persistence probability by a factor of $\beta = 0.5$ in BEB (and in general $\beta \in (0, 1)$ in EB) until reaching the minimum persistence probability $p_l^{\min}$. The update algorithm for the persistence probability can now be written as

$$p_l(t+1) = \max\{p_l^{\min}, p_l^{\max}\mathbf{1}_{\{T_l(t)=1\}}\mathbf{1}_{\{C_l(t)=0\}} + \beta_l p_l(t)\mathbf{1}_{\{T_l(t)=1\}}\mathbf{1}_{\{C_l(t)=1\}} + p_l(t)\mathbf{1}_{\{T_l(t)=0\}}\} \tag{10.16}$$

where $p_l(t)$ is a persistence probability of link l at timeslot t, $\mathbf{1}_a$ is an indicator function of event a, and $T_l(t)$ and $C_l(t)$ are the events that link l transmits data at timeslot t and that there is a collision to link $l's$ transmission given that link l transmits data at timeslot t, respectively. When $p_l^{\min} = 0$ for a given $\boldsymbol{p}$(t), we have

$$Prob\{T_l(t) = 1|\mathbf{p}(t)\} = p_l(t)$$

and

$$Prob\{C_l(t) = 1|\mathbf{p}(t)\} = 1 - \prod_{n \in L_{\text{to}}^I(l)} [1 - p_n(t)]$$

If $p_l(t)$ is the expected persistence probability we have

$$\begin{aligned} p_l(t+1) &= p_l^{\max} E\left\{\mathbf{1}_{\{T_l(t)=1\}}\mathbf{1}_{\{C_l(t)=0\}}|\mathbf{p}(t)\right\} + \beta_l E\left\{p_l(t)\mathbf{1}_{\{T_l(t)=1\}}\mathbf{1}_{\{C_l(t)=1\}}|\mathbf{p}(t)\right\} \\ &\quad + E\left\{p_l(t)\mathbf{1}_{\{T_l(t)=0\}}|\mathbf{p}(t)\right\} \\ &= p_l^{\max} p_l(t) \prod_{n \in L_{\text{to}}^I(l)} \left[1 - p_n(t)\right] + \beta_l p_l(t) p_l(t) \left\{1 - \prod_{n \in L_{\text{to}}^I(l)} \left[1 - p_n(t)\right]\right\} \\ &\quad + p_l(t)\left[1 - p_l(t)\right] \end{aligned} \tag{10.17}$$

In Equation (10.17), $E\{a|b\}$ is the expected value of a given b and $\mathbf{1}$ denotes the indicator function of probabilistic events.

We now consider a *game* in which each link l updates its persistence probability p_l to maximize its utility U_l based on strategies of the other links, i.e. $\mathbf{p}_{-l} = (p_1, \ldots, p_{l-1}, p_{l+1}, \ldots, p_{|E|})$. The game is formally defined as $G_{EB-MAC} = [E, \times_{l \in E} A_l, \{U_l\}_{l \in E}]$, where E is a set of players, i.e. links, $A_l = \{p_l | 0 \le p_l \le p_l^{\max}\}$ is an action set of player l and U_l is a utility function of player l to be determined through reverse engineering.

The expected net reward (expected reward minus expected cost) that the link can obtain from its transmission is given as

$$U_l(\mathbf{p}) = R(p_l)S(\mathbf{p}) - C(p_l)F(\mathbf{p}), \ \forall l \tag{10.18}$$

In Equation (10.18), $S(\mathbf{p}) = p_l \prod_{n \in L_{\text{to}}^I(l)} (1 - p_n)$ is the probability of transmission success, $F(\mathbf{p}) = p_l \prod_{n \in L_{\text{to}}^I(l)} (1 - p_n)$ is the probability of transmission failure, $R(p_l) \stackrel{\text{def}}{=} p_l((1/2)p_l^{\max} - (1/3)p_l)$ can be interpreted as the reward for transmission success and $C(p_l) \stackrel{\text{def}}{=} (1/3)(1 - \beta_l)p_l^2$ can be interpreted as the cost for transmission failure.

It can be shown that there exists a Nash equilibrium in the EB-MAC game $G_{EB-MAC} = [E, \times_{l \in E} A_l, \{U_l\}_{l \in E}]$, giving the optimal solution

$$p_l^* = \frac{p_l^{\max} \prod_{n \in L_{\text{to}}^I(l)} (1 - p_n^*)}{1 - \beta_l \left(1 - \prod_{n \in L_{\text{to}}^I(l)} (1 - p_n^*)\right)}, \forall l \tag{10.19}$$

Note that the expressions of $S(\mathbf{p})$ and $F(\mathbf{p})$ come directly from the definitions of success and failure probabilities, while the expressions of $R(p_l)$ and $C(p_l)$ are in fact derived in the proof by reverse-engineering the EB protocol description.

In the EB protocol there is no explicit message passing among links, and a link cannot obtain the exact information to calculate the gradient. For this reason each link may, instead of using an exact gradient as in (10.17), approximate it by using (10.16). It was shown in References [19] and [20] that the EB protocol described by (10.16) is a stochastic subgradient algorithm to maximize utility (10.18).

10.2.5 Utility optimal MAC protocol/social optimum

For illustration purposes, in the sequel we assume that if the distance between the receiver of one link and the transmitter of the other link is less than $2d$, there is interference between these two links. These relations are represented by a contention graph in Figures 10.2 and 10.3. Each vertex in the contention graph corresponds to a link in the network. There is an edge between the vertices if the corresponding links interfere with each other.

A maximum connected subgraph within a contention graph is called a clique. Therefore only one link at a time among the links in the same maximal clique in the contention graph can transmit data without collision. This is illustrated in Figure10.3.

The capacity of a clique is defined as the maximum value of the sum of time fractions such that each link in the clique can transmit data without collisions. A generalized NUM problem with capacity constraint C_{CL_l} at each maximal clique CL_i is formulated as follows:

$$\begin{aligned} &\text{Maximize } \sum_{l} U_l(x_l) \\ &\text{subject to } \sum_{l \in L(CL_i)} \frac{x_l}{c_l} \leq C_{CL_i} \forall i \end{aligned} \tag{10.20}$$

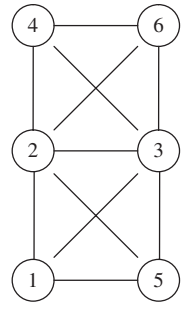

Figure 10.2 Contention graph derived from the logical topology graph shown in Figure 10.1.

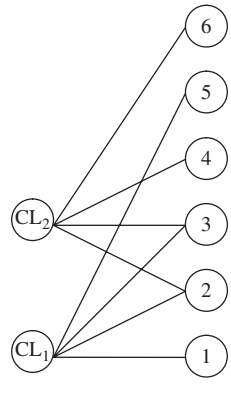

Figure 10.3 Bipartite graph between maximal cliques and links in the contention graph in Figure10.2.

This problem formulation essentially takes the same structure as the basic NUM (10.4) for TCP congestion control and can be solved following the same dual-decomposition algorithm. We refer to this as the deterministic approximation approach.

As an alternative approach consider a random-access-based MAC protocol in which each node n adjusts its own persistence probability and also the persistence probability of each of its outgoing links. Since persistent transmission decisions are made in a distributive way at each node we need to modify graph models based on logical links to graph models that incorporate nodes as well. If P^n is the transmission probability of node n and p_l is that of link l, the generalized NUM with variables $\{x_l\}, \{P^n\}, \{p_l\}$ is formulated as

$$\begin{aligned}
&\text{Maximize } U_l(x_l)\\
&\text{subject to } x_l = c_l p_l \prod_{k\in N^l_{\text{to}}(l)} (1-P^k), \forall l\\
&\qquad \sum_{\text{l}\in L_{\text{out}}(\text{n})} p_{\text{l}} = P^{\text{n}}, \forall n\\
&\qquad 0 \le P^{\text{n}} \le 1, \forall n\\
&\qquad 0 \le p_{\text{l}} \le 1, \forall l
\end{aligned} \tag{10.21}$$

The next step is to take a log change of variables and constants $x'_l = \log x_l$, $U'_l(x'_l) = U_l(e^{x'_l})$ and $c'_l = \log c_l$. This reformulation gives

$$\begin{aligned}
&\text{Maximize } \sum_{l\in L} U'_l(x'_l)\\
&\text{subject to } c'_l + \log p_l + \sum_{k\in N^l_{\text{to}}(l)} \log(1-P^k) - x'_l \ge 0, \forall l\\
&\qquad \sum_{l\in L_{\text{out}}(n)} p_l = P^n, \forall n\\
&\qquad 0 \le P^n \le 1, \forall n\\
&\qquad 0 \le p_l \le 1, \forall l
\end{aligned} \tag{10.22}$$

The problem is now separable but still may not be a convex optimization problem, since the objective $U'_l(x'_l)$ may not be a strictly concave function, even though $U_l(x_l)$ is a strictly concave function. The following condition guarantees its concavity:

$$\frac{\partial^2 U_l(x_l)}{\partial x_l^2} < -\frac{\partial U_l(x_l)}{x_l \partial x_l}$$

This condition states that the curvature (degree of concavity) of the utility function needs to be not just nonpositive but bounded away from zero by as much as $-(\partial U_l(x_l)/x_l \partial x_l)$; i.e. the application represented by this utility function must be elastic enough. In the sequel we summarize the utility optimal MAC algorithm.

Utility optimal random access protocol

Each node n constructs its local interference graph to obtain sets $L_{\text{out}}(n)$, $L_{\text{in}}(n)$, $L^I_{\text{from}}(n)$ and $N^I_{\text{to}}(l), \forall l \in L_{\text{out}}(n)$.
Each node n sets $t = 0, \lambda_l(1) = 1, \forall l \in L_{\text{out}}(n)$,

$$\begin{aligned}
P^n(1) &= |L_{\text{out}}(n)|/(|L_{\text{out}}(n)| + |L^I_{\text{from}}(n)|) \text{ and}\\
p_l(1) &= 1/(|L_{\text{out}}(n)| + |L^I_{\text{from}}(n)|), \forall l \in L_{\text{out}}(n)
\end{aligned}$$

For each node n,

(1) *Set* $t \leftarrow t+1$.

(2) *Inform* $\lambda_l(t)$ *to all nodes in* $N_{\text{to}}^I(l), \forall l \in L_{\text{out}}(n)$ *and* $P^n(t)$ *to* $t_l, \forall l \in L_{\text{from}}^I(n)$.

(3) *Set* $k_n(t) = \sum_{l \in L_{\text{out}}(n)} \lambda_l(t) + \sum_{k \in L_{\text{from}}^I(n)} \lambda_k(t)$ *and* $\beta(t) = 1/t$.

(4) *Solve the following problems to obtain* $P^n(t+1), x_l'(t+1), p_l(t+1)$ *and* $\lambda_l(t+1)$, $\forall l \in L_{\text{out}}(n)$:

$$P^n(t+1) = \begin{cases} \dfrac{\sum_{l \in L_{\text{out}}(n)} \lambda_l(t)}{\sum_{l \in L_{\text{out}}(n)} \lambda_l(t) + \sum_{k \in L_{\text{from}}^I} \lambda_k(t)}, & \text{if } k_n(t) = 0 \\ \dfrac{|L_{\text{out}}(n)|}{|L_{\text{out}}(n)| + |L_{\text{from}}^I(n)|}, & \text{if } k_n(t) = 0 \end{cases}$$

$$P_l(t+1) = \begin{cases} \dfrac{\lambda_l(t)}{\sum_{l \in L_{\text{out}}(n)} \lambda_l(t) + \sum_{k \in L_{\text{from}}^I(n)} \lambda_k(t)}, & \text{if } k_n(t) \neq 0 \\ \dfrac{1}{|L_{\text{out}}(n)| + |L_{\text{from}}^I(n)|}, & \text{if } k_n(t) = 0 \end{cases}$$

$$x_l'(t+1) = \underset{x_l'^{\min} \le x' \le x_l'^{\max}}{\arg\max} \{U_l'(x_l') - \lambda_l(t) x_l'\}$$

and

$$\lambda_l(t+1) = \left[\lambda_l(t) - \beta(t)(c_l' + \log p_l(t) + \sum_{k \in N_{\text{to}}^I(l)} \log(1 - p^k(t)) - x_l'(t) \right].$$

(5) *Set its persistence probability* $P^{n*} = P^n(t)$ *and the conditional persistence probability of each of its outgoing links* $q_l^* = p_l(t)/P^n(t)$.

(6) *Decide if it will transmit data with a probability* P^{n*}, *in which case it chooses to transmit on one of its outgoing links with a probability* $q_l^*, \forall l \in L_{\text{out}}(n)$.
while 1).

For a practical implementation it is important to be aware of the fact that the above algorithm is conducted at the transmitter of each node n to calculate P^n, and p_l, λ_l and x_l' for its outgoing link l. If we assume that two nodes within the interference range can communicate with each other, in the above algorithm each node requires information from nodes within a two-hop distance from it. To calculate P^n and p_l for its outgoing link l, node n needs λ_m from the transmitter node t_m of link m that is interfered from the transmission of node n (i.e. from $t_m, \forall m \in L_{\text{from}}^I(n)$). Note that t_m is within two hops from node n.

Alternatively, if λ_l and x_l' for each link l are calculated at its receiver node r_l instead of its transmits node t_l, a *modified version of the algorithm* can be devised in which each node requires information only with a one-hop distance.

For illustration we use an example where for each link l, $U_l(x_l)$ is given as [21]

$$U_l(x_l) = \frac{x_l^{(1-\alpha)} - x_l^{\min(1-\alpha)}}{x_l^{\max(1-\alpha)} - x_l^{\min(1-\alpha)}}$$

with $x_l^{\min} = 0.5$ and $x_l^{\max} = 5, \forall l$. The network utilities defined by (10.22) are shown in Figure 10.4. For more details see References [19], [20] and [22] to [26].

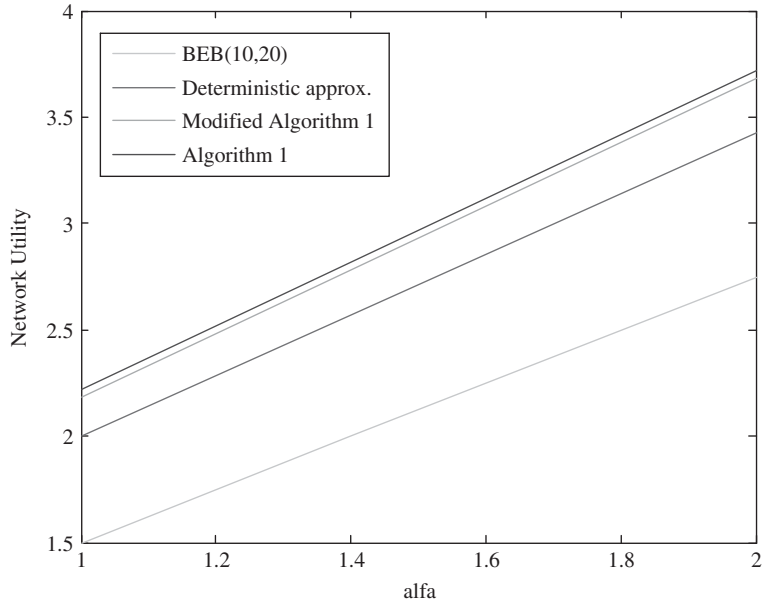

Figure 10.4 Comparison of network utilities in a numerical example.

10.3 CROSSLAYER OPTIMIZATION

10.3.1 Congestion control and routing

In this section we will discuss TCP/IP interaction. In the sequel we will use the following assumptions and notation:

(1) *There are* K^s *acyclic paths from source* s *to its destination, represented by an* $L \times K^s$ *0–1 matrix* $\mathbf{H}^s$, *where*

$$H^s_{lj} = \begin{cases} 1, & \text{if path } j \text{ of source } s \text{ uses link } l \\ 0, & \text{otherwise} \end{cases}$$

(2) $\mathcal{H}^s$ *is the set of all columns of* $\mathbf{H}^s$ *that represents all the available paths to* s.

(3) *The* $L \times K$ *matrix* $\mathbf{H} = [\mathbf{H}^1 \dots \mathbf{H}^N]$ *defines the physical topology of the network where* $K := \sum_s K^s$.

(4) $\mathbf{w}^s$ *is the* $K^s \times 1$ *vector where the* j*th entry represents the fraction of* i*'s flow on its* j*th path such that* $w^s_j \geq 0 \ \forall j$ and $\mathbf{1}^T \mathbf{w}^s = 1$, *where* $\mathbf{1}$ *is a vector of an appropriate dimension with the value 1 in every entry. We require* $w^s_j \in \{0, 1\}$ *for single path routing and allow* $w^s_j \in [0, 1]$ *for multipath routing.*

(5) $\mathbf{W}$ *is the* $K \times N$ *block-diagonal matrix collecting the vectors* $\mathbf{w}^s, s = 1, \dots, N$.

(6) W_n is the *the set of all such matrices for single path routing, defined as* $\{\mathbf{W}|\mathbf{W} = \text{diag}(\mathbf{w}^1, \ldots, \mathbf{w}^N) \in \{0, 1\}^{KxN}, \mathbf{1}^T\mathbf{w}^s = 1, \forall s\}$.

(7) W_m is the *corresponding set of matrices for multipath routing, defined as*

$$\{\mathbf{W}|\mathbf{W} = \text{diag}(\mathbf{w}^1, \ldots, \mathbf{w}^N) \in [0, 1]^{KxN}, \mathbf{1}^T\mathbf{w}^s = 1, \forall s\}.$$

H defines the set of acyclic paths available to each source and **W** defines how the sources load-balance across the paths. Their product defines an $L \times N$ routing matrix $\mathbf{R} = \mathbf{HW}$ that specifies the fraction of $s's$ flow at each link l. The set of all single-path routing matrices is

$$R_n = \{\mathbf{R}|\mathbf{R} = \mathbf{HW}, \mathbf{W} \in W_n\} \tag{10.23}$$

and the set of all multipath routing matrices is

$$R_m = \{\mathbf{R}|\mathbf{R} = \mathbf{HW}, \mathbf{W} \in W_m\} \tag{10.24}$$

The difference between single-path routing and multipath routing is the integer constraint on **W** and **R**. A single-path routing matrix in R_n is an 0–1 matrix

$$R_{ls} = \begin{cases} 1, & \text{if link l is in the path of source s,} \\ 0, & \text{otherwise} \end{cases}$$

while the multipath routing matrix in R_m is one whose entries are in the range [0,1]

$$R_{ls} = \begin{cases} >0, & \text{if link l is in the path of source s,} \\ 0, & \text{otherwise} \end{cases}$$

The path of source s is denoted by $\mathbf{r}^s = [R_{1s} \cdots R_{Ls}]^{\mathrm{T}}$, the sth column of the routing matrix **R**.

Let us first consider the situation where TCP-AQM operates at a faster time scale than a routing update. We assume for now a single path is selected for each source–destination pair that minimizes the sum of the link costs in the path, for some appropriate definition of the link cost.

Let $\mathbf{R}(t) \in R_n$ be the (single-path) routing in period t. Let the equilibrium rates $\mathbf{x}(t) = \mathbf{x}(\mathbf{R}(t))$ and prices $\boldsymbol{\lambda}(t) = \boldsymbol{\lambda}(\mathbf{R}(t))$ generated by TCP-AQM in period t, respectively, be the optimal primal and dual solutions, defined formally as

$$\mathbf{x}(t) = \arg\max_{\mathbf{x} \geq 0} \sum_s U_s(x_s) \text{ subject to } \mathbf{R}(t)\mathbf{x} \leq \mathbf{c} \tag{10.25}$$

$$\boldsymbol{\lambda}(t) = \arg\min_{\boldsymbol{\lambda} \geq 0} \sum_s \max_{x_s \geq 0} \left[U_s(x_s) - x_s \sum_l R_{ls}(t)\lambda_t \right] + \sum_l c_l \lambda_l \tag{10.26}$$

The link costs used in the routing decision in period t are the congestion prices $\lambda_l(t)$. Each source computes its new route $\mathbf{r}^s(t+1) \in H^s$ individually, which minimizes the total cost on its path

$$\mathbf{r}^s(t+1) = \arg\min_{\mathbf{r}^s \in H^s} \sum_l \lambda_l(t) r_l^s \tag{10.27}$$

$(\mathbf{R}^*, \mathbf{x}^*, \boldsymbol{\lambda}^*)$ is an equilibrium of *TCP/IP* if it is a fixed point of Equations (10.25) to (10.27); i.e. starting from routing $\mathbf{R}^*$ and associated $(\mathbf{x}^*, \boldsymbol{\lambda}^*)$, the above iterations yield $(\mathbf{R}^*, \mathbf{x}^*, \boldsymbol{\lambda}^*)$ in the subsequent periods.

We now characterize the condition under which *TCP/IP*, modeled by Equations (10.25) to (10.27), has an equilibrium. Consider the following generalized NUM:

$$\begin{aligned} &\underset{\mathbf{R}\in R_n}{\text{Maximize}} \left(\underset{\mathbf{x}\geq 0}{\text{Maximize}} \sum_s U_s(x_s) \right) \\ &\text{subject to } \mathbf{Rx} \leq \mathbf{c} \end{aligned} \tag{10.28}$$

and its Lagrange dual problem

$$\underset{\boldsymbol{\lambda}\geq 0}{\text{Minimize}} \sum_s \max_{x_s \geq 0} \left[U_s(x_s) - x_s \min_{\mathbf{r}^s \in H} \sum_l R_{ls}\lambda_t \right] + \sum_l c_l \lambda_l \tag{10.29}$$

where $\mathbf{r}^s$ is the sth column of $\mathbf{R}$ with $r_l^s = R_{ls}$. While Equation (10.25) maximizes utility over source rates only, problem (10.28) maximizes utility over both rates and routes. While Equation (10.25) is a convex optimization problem without a duality gap, problem (10.28) is nonconvex because the variable $\mathbf{R}$ is discrete, and generally has a duality gap. Since the maximization over $\mathbf{R}$ takes the form of minimum-cost routing with congestion prices $\boldsymbol{\lambda}$ generated by TCP-AQM as link costs, this suggests that *TCP/IP* might turn out to be a distributed algorithm that attempts to maximize utility, with a proper choice of link costs. This is true, provided that an equilibrium of *TCP/IP* actually exists.

It can be shown that an equilibrium $(\mathbf{R}^*, \mathbf{x}^*, \boldsymbol{\lambda}^*)$ of *TCP/IP* exists if and only if there is no duality gap between problems (10.28) and (10.29). In this case the equilibrium $(\mathbf{R}^*, \mathbf{x}^*, \boldsymbol{\lambda}^*)$ is a solution of (10.28) and (10.29).

Hence, one can regard the layering of TCP and IP as a decomposition of the NUM problem over source rates and routes into a distributed and decentralized algorithm, carried out on two different time scales, in the sense that an equilibrium of the *TCP/IP* iteration (10.25)–(10.27), if it exists, solves problems (10.28) and (10.29). However, an equilibrium may not exist. Even if it does, it may not be stable. The duality gap is a measure of 'cost for not splitting'. To elaborate, consider the Lagrangian

$$L(\mathbf{R}, \mathbf{x}, \boldsymbol{\lambda}) = \sum_s \left[U_s(x_s) - x_s \sum_l R_{ls}\lambda_l \right] + \sum_l c_l \lambda_l$$

The primal (10.21) and dual (10.22) can then be expressed as

$$V_{n\rho} = \max_{\mathbf{R}\in R_n,\ \mathbf{x}\geq 0} \min_{\boldsymbol{\lambda}\geq 0} L(\mathbf{R}, \mathbf{x}, \boldsymbol{\lambda}) \text{ and } V_{nd} = \min_{\boldsymbol{\lambda}\geq 0} \max_{\mathbf{R}\in R_n,\ \mathbf{x}\geq 0} L(\mathbf{R}, \mathbf{x}, \boldsymbol{\lambda}),$$

respectively. In the case of multipath routing we have

$$V_{m\rho} = \max_{\mathbf{R}\in R_m,\ \mathbf{x}\geq 0} \min_{\boldsymbol{\lambda}\geq 0} L(\mathbf{R}, \mathbf{x}, \boldsymbol{\lambda}) \text{ and } V_{md} = \min_{\boldsymbol{\lambda}\geq 0} \max_{\mathbf{R}\in R_m,\ \mathbf{x}\geq 0} L(\mathbf{R}, \mathbf{x}, \boldsymbol{\lambda}),$$

with $R_n \subseteq R_m$, $V_{n\rho} \leq V_{m\rho}$ and $V_{s\rho} \leq V_{sd} = V_{m\rho} = V_{md}$.

TCP/IP has an equilibrium exactly when there is no duality gap in the single-path utility maximization, i.e. when $V_{n\rho} = V_{nd}$. In this case, there is no penalty in not splitting the traffic; i.e. single-path routing performs as well as multipath routing, $V_{n\rho} = V_{m\rho}$. Multipath routing achieves a strictly higher utility $V_{m\rho}$ precisely when *TCP/IP* has no equilibrium, in which case the *TCP/IP* iteration (10.25)–(10.27) cannot converge, let alone solve the single-path utility maximization problem (10.28) or (10.29). In this case the problem (10.28) and its dual (10.29) do not characterize *TCP/IP*, but their gap measures the loss in utility in restricting routing to a single path and is of independent interest. Even though shortest-path routing is polynomial, the single-path utility maximization is NP-hard. For more details see References [27] to [32].

10.3.2 Congestion control and physical resource allocation

Consider a wireless multihop network with an established logical topology represented by $\mathbf{R}$ or equivalently $\{S(l)\}, \forall l$, where some nodes are sources of transmission and some nodes act as relay nodes. Based on the basic NUM of Equation (10.1), we observe that in an interference-limited wireless network, data rates attainable on wireless links are not fixed numbers $\mathbf{c}$ as in Equation (10.1), and can be written as functions of the transmit power vector $\mathbf{P}$ as $c_l(\mathbf{P}) = \log[1 + KSIR_l(\mathbf{P})]/T, \forall l$, where T is the symbol period, which will be assumed to be one unit, and constant $K = [-\phi_1/\log(\phi_2 BER)]$, with ϕ_1 and ϕ_2 being constants depending on the modulation and BER the required bit-error rate. The signal-to-interference ratio for link l is defined as $SIR_l(\mathbf{P}) = P_l G_{ll}/(\sum_{k\neq l} P_k G_{lk} + n_l)$ for a given set of path losses G_{lk}. The G_{lk} factors incorporate propagation loss, spreading gain and other normalization constants. Notice that G_{ll} is much larger that $G_{lk}, k \neq l$, and assuming that not too many close-by nodes transmit at the same time, KSIR is much larger that 1. In this high-SIR regime, c_l can be approximated as $\log[KSIR_l(\mathbf{P})]$.

With the above assumptions, the generalized NUM with 'elastic' link capacities becomes

$$\begin{aligned} &\text{Maximize} \sum_s U_s(x_s) \\ &\text{subject to} \sum_{s\in S(l)} x_s \leq c_l(\mathbf{P}), \forall l \\ &\mathbf{x}, \mathbf{P} \geq 0 \end{aligned} \tag{10.30}$$

where the optimization variables are both source rates $\mathbf{x}$ and transmit powers $\mathbf{P}$. The key difference from problem (10.4) is that each link capacity c_l is now a function of the new optimization variables: the transmit powers $\mathbf{P}$. The design space is enlarged from $\mathbf{x}$ to both $\mathbf{x}$ and $\mathbf{P}$, which are now coupled in problem (10.30). Linear flow constraints on $\mathbf{x}$ become nonlinear constraints on $(\mathbf{x}, \mathbf{P})$. In practice, problem (10.30) is also constrained by the maximum and minimum transmit powers allowed at each transmitter on link $l : P_{l,\min} \leq P_l \leq P_{l,\max}, \forall l$.

The major challenges are the two global dependencies in problem (10.30) Source rates $\mathbf{x}$ and link capacities $\mathbf{c}$ are globally coupled across the network, as reflected in the range of summation $\{s \in S(l)\}$ in the constraints in (10.30). In addition, each link capacity $c_l(\mathbf{P})$, in terms of the attainable data rate under a given power vector, is a global function of all the interfering powers.

In the sequel we focus on delay-based price and a TCP Vegas window update, and the corresponding logarithmic utility maximization over $(\mathbf{x}, \mathbf{P})$, where α_s is a constant parameter in TCP Vegas:

$$\begin{aligned} &\text{Maximize} \sum_s \alpha_s \log x_s \\ &\text{subject to} \sum_{s\in S(l)} x_s \leq c_l(\mathbf{P}), \forall l \\ &\mathbf{x}, \mathbf{P} \geq 0 \end{aligned} \tag{10.31}$$

During each time slot t, the following four updates are carried out simultaneously, until convergence:

(1) *At each intermediate node, a weighted queuing delay λ_l is implicitly updated where $\beta_1 > 0$ is a constant:*

$$\lambda_l(t+1) = \left\{\lambda_l(t) + \frac{\beta_1}{c_l(t)}\left[\sum_{s\in S(l)} x_s(t) - c_l(t)\right]\right\}^+ \tag{10.32}$$

(2) *At each source, total delay* D_s *is measured and used to update the TCP window size* w_s. *Consequently, the source rate* x_s *is updated*:

$$w_s(t+1) = \begin{cases} w_s(t) + \frac{1}{D_s(t)}, & \text{if } \dfrac{w_s(r)}{d_s} - \dfrac{w_s(r)}{D_s(t)} < \alpha_s \\ w_s(t) - \frac{1}{D_s(t)}, & \text{if } \dfrac{w_s(r)}{d_s} - \dfrac{w_s(r)}{D_s(t)} > \alpha_s \\ w_s(t), & \text{else} \end{cases}$$

$$x_s(t+1) = \frac{w_s(t+1)}{D_s(t)} \tag{10.33}$$

(3) *Each transmitter* j *calculates a message* $m_j(t) \in \mathbf{R}_+$ *based on locally measurable quantities and passes the message to all other transmitters by a flooding protocol*:

$$m_j(t) = \frac{\lambda_j(t) SIR_j(t)}{P_j(t) G_{jj}}$$

(4) *Each transmitter updates its power based on locally measurable quantities and the received messages, where* $\beta_2 > 0$ *is a constant*:

$$P_l(t+1) = P_l(t) + \frac{\beta_2 \lambda_l(t)}{P_l(t)} - \beta_2 \sum_{j \neq l} G_{lj} m_j(t) \tag{10.34}$$

With the minimum and maximum transmit power constraint $(P_{l,\min}, P_{l,\max})$ *on each transmitter, the update power is projected into the interval* $[P_{l,\min}, P_{l,\max}]$.

Step 2 is simply the TCP Vegas window update. Step 1 is a modified version of a queuing delay price update (and the original update is an approximation of step 1). Steps 3 and 4 describe a new power control using message passing. Taking in the current values of $\lambda_j(t) SIR_j(t) / P_j(t) G_{jj}$ as the messages from other transmitters indexed by j, the transmitter on link l adjusts its power level in the next timeslot by first increasing power directly proportional to the current price and inversely proportional to the current power level, and then decreasing power by a weighted sum of the messages from all other transmitters, where the weights are the path losses G_{lj}. Intuitively, if the local queuing delay is high, the transmit power should increase, with a more moderate increase when the current power level is already high. If queuing delays on other links are high, the transmit power should decrease in order to reduce interference on the links.

To compute m_j, the values of queuing delay λ_j, signal-to-interference ratio SIR_j and received power level $P_j G_{jj}$ can be directly measured by node j locally. This algorithm only uses the resulting message m_j but not the individual values of λ_j, SIR_j, P_j and G_{jj}. Each message is a real number to be explicitly passed. To conduct the power update, G_{lj} factors are assumed to be estimated through training sequences.

There is no need to change the existing TCP congestion control and queue management algorithms. All that is needed to achieve the joint and global optimum of problem (10.31) is to utilize the values of weighted queuing delay in designing the power control algorithm in the physical layer. It can be shown that for small enough constants β_1 and β_2, the algorithm defined by Equations (10.32), (10.33) and (10.34) converges to the global optimum of the joint congestion control and power control problem (10.31).

10.3.3 Congestion and contention control

The NUM problem for random-access-based MAC and TCP can be formulated as the following optimization over (**x, P, p**):

$$\begin{aligned}
&\text{Maximize } \sum_s U_s(x_s)\\
&\text{subject to } \sum_{s\in S(l)} x_s \le c_l p_l \prod_{k\in N_{\text{to}}^l(l)} (1-P^k), \forall l\\
&\qquad \sum_{l\in L_{\text{out}}(n)} p_l = P^n, \forall n\\
&\qquad x_s^{\min} \le x_s \le x_s^{\max}, \forall s\\
&\qquad 0 \le P^n \le 1, \ \forall n\\
&\qquad 0 \le p_l \le 1, \forall l
\end{aligned} \tag{10.35}$$

This is a convex optimization problem after a log change of variables $\{p_l, P^k\}$. Its solution can now be distributively carried out using either the penalty function approach or the dual-decomposition-based Lagrangian relaxation approach. Both have standard convergence properties but now producing different implications to the time scale of the *TCP/MAC* interaction. We start with the penalty function approach by defining

$$h_l(\mathbf{p}, \mathbf{x}') = \log\left(\sum_{s\in S(l)} e^{x_s'} - c_l' - \log p_l - \sum_{k\in N_{\text{to}}^l(l)} \log\left(1 - \sum_{m\in L_{\text{out}}(k)} p_m\right)\right)$$

and

$$w_n(\mathbf{p}) = \sum_{m\in L_{\text{out(n)}}} p_m - 1$$

Then problem (10.35) becomes

$$\begin{aligned}
&\text{Maximize } \sum_s U_s'(x_s')\\
&\text{subject to } h_l(\mathbf{p}, \mathbf{x}') \le 0, \forall l\\
&\qquad w_n(\mathbf{p}) \le 0, \forall n\\
&\qquad x_s'^{\min} \le x_s' \le x_s'^{\max}, \ \forall s\\
&\qquad 0 \le p_l \le 1, \forall l
\end{aligned} \tag{10.36}$$

Instead of solving problem (10.36) directly, we apply the penalty function method and consider the following problem:

$$\begin{aligned}
&\text{Maximize } V(\mathbf{p}, \mathbf{x}')\\
&\text{subject to } x_s'^{\min} \le x_s' \le x_s'^{\max}, \ \forall s\\
&\qquad 0 \le p_l \le 1, \forall l
\end{aligned} \tag{10.37}$$

where

$$V(\mathbf{p}, \mathbf{x}') = \sum_s U_s'(x_s') - \kappa \sum_l \max\{0, h_l(\mathbf{p}, \mathbf{x}')\} - \kappa \sum_n \max\{0, w_n(\mathbf{p})\}$$

and κ is a positive constant. We can easily show that

$$\frac{\partial V(\mathbf{p}, \mathbf{x}')}{\partial p_l} = \kappa \left(\frac{\varepsilon_l}{p_l} - \frac{\sum_{k \in L^l_{\text{from}}(t),} \varepsilon_k}{1 - \sum_{m \in L_{\text{out}}(r_I)} P_m} - \delta_{tl} \right)$$

and

$$\frac{\partial V(\mathbf{p}, \mathbf{x}')}{\partial x'_s} = \frac{\partial U'_s(x'_s)}{\partial x'_s} - \kappa e^{x'_s} \sum_{l \in L(s)} \frac{\varepsilon_l}{\sum_{k \in S(l)} e^{x'_k}}$$

where

$$\varepsilon_l = \begin{cases} 0, & \text{if } \sum_{n \in S(l)} e^{x'_n} \leq c_l p_l \prod_{k \in N^l_{\text{to}}(l)} \left(1 - \sum_{m \in L_{\text{out}}(k)} p_m\right) \\ 1 & \text{otherwise} \end{cases}$$

and

$$\delta_n = \begin{cases} 0, & \text{if } \sum\limits_{m \in L_{\text{out}}(n)} P_m \leq 1 \\ 1 & \text{otherwise} \end{cases}$$

Now, an iterative subgradient projection algorithm with iterations indexed by t that solves problem (10.37) is obtained:

On each local link, transmission is decided to take place with persistence probability

$$p'_l(t+1) = \left[p(t) + \alpha(t) \frac{\partial V(\mathbf{p}, \mathbf{x}')}{\partial p_l} |_{\mathbf{p}=\mathbf{p}(t), \mathbf{x}'=\mathbf{x}'(t)} \right]_0^1, \forall l \tag{10.38}$$

and concurrently at each source, the end-to-end rate is adjusted

$$x'_s(t+1) = \left[x'_s(t) + \alpha(t) \frac{\partial V(\mathbf{p}, \mathbf{x}')}{\partial_{x'_s}} |_{\mathbf{p}=\mathbf{p}(t), \mathbf{x}'=\mathbf{x}'(t)} \right]_{x'^{\min}_s}^{x'^{\max}_s}, \forall s \tag{10.39}$$

where $[a]_c^b = \max\{\min\{a, b\}, c\}$.

For practical implementation of Equations (10.38) and (10.39), each link l (or its transmission node t_l) updates its persistence probability $p_l(t)$ using (10.38) and, concurrently, each source updates its data rate $x_s(t)$ using (10.39). To calculate the subgradient each link needs information only from link $k, k \in L^l_{\text{from}}(t_l)$, i.e. from links whose transmissions are interfered from the transmission of link l and the links are in the neighborhood of link l. To calculate the subgradient each source needs information only from link $l, l \in L(s)$, i.e. from links on its routing path. Hence, to perform the algorithm, each source and link need only local information though limited message passing and the algorithm can be implemented in a distributed way. In particular, note that δ_n is calculated at the transmitter node of each link to update the persistence probability of that link and does not need to be passed among the nodes. There is no need explicitly to pass around the values of persistence probabilities, since their effects are included in $\{\varepsilon_l\}$. Quantities such as $\sum_{m \in L_{\text{out}}(t_l)} p_m$ and $\sum_{k \in S(l)} \exp(x'_k)$ can be measured locally by each node and each link.

To implement a dual-decomposition-based algorithm instead, we can decompose problem (10.35) into two problems, using a standard dual decomposition:

$$\text{Maximize} \sum_s U_s(x_s)$$

$$\text{subject to} \sum_{s \in S(l)} x_s \le y_l, \forall l$$
$$x_s^{\min} \le x_s \le x_s^{\max}, \forall s \tag{10.40}$$

where y_l is the average data rate of link l, and

$$\text{Maximize } \hat{U}(\mathbf{p})$$
$$\text{subject to} \sum_{m \in L_{\text{out}}(n)} p_m \le 1, \forall n$$
$$0 \le p_l \le 1, \ \forall l \tag{10.41}$$

where

$$\hat{U}(\mathbf{p}) = \max \left\{ \sum_s U_s(x_s) \Big| \sum_{s \in S(l)} x_s \le y_l(\mathbf{p}), \forall l \right.$$
$$y_l(\mathbf{p}) = c_l p_l \prod_{k \in N_{\text{to}}^I(l)} \left(1 - \sum_{m \in L_{\text{out}}(k)} P_m\right), \forall l,$$
$$\left. x_s^{\min} \le x_s \le x_s^{\max}, \forall s \right\}$$

For a given $\mathbf{y}$, problem (10.40) can be solved by dual decomposition and the distributed subgradient method just as before.

We now solve problem (10.41) by first adding a penalty function to the objective function of the problem:

$$\text{Maximize } \hat{V}(\mathbf{p})$$
$$\text{subject to } 0 \le p_l \le 1, \forall l \tag{10.42}$$

where $\hat{V}(\mathbf{p}) = \hat{U}(\mathbf{p}) - \kappa \max\{0, \sum_n (1 - \sum_{m \in L_{\text{out}}(n)} P_m)\}$ and κ is a positive constant. Since problem (10.42) is a convex problem with simple constraints, we can solve it by using a subgradient projection algorithm as

$$p_l(t+1) = \left[p(t) + \beta(t) \frac{\partial \hat{V}(\mathbf{p})}{\partial p_l}|_{\mathbf{p}=\mathbf{p}(t)} \right]_0^1, \forall l \tag{10.43}$$

where $\partial \hat{V}(\mathbf{p})/\partial p_l$ is a subgradient of $\hat{V}(\mathbf{p})$ with respect to p_l, where $\partial \hat{V}(\mathbf{p})/\partial p_l$ is obtained as

$$\frac{\partial \hat{V}(\mathbf{p})}{\partial p_l} = \lambda_l^*(t) c_l \prod_{k \in N_{\text{to}}^I(l)} \left(1 - \sum_{n \in L_{\text{out}}(k)} P_m\right) - \sum_{n \in L_{\text{from}}^I(t_l)} \lambda_n^*(t) c_n p_n$$
$$\times \prod_{k \in N_{\text{to}}^I(n), k \ne t_l} \left(1 - \sum_{m \in L_{\text{out}}(k)} P_m\right) - \kappa \delta_{tl} \tag{10.44}$$

with

$$\delta_n = \begin{cases} 0, & \text{if } \sum_{m \in L_{\text{out}}(n)} P_m \le 1 \\ 1, & \text{otherwise} \end{cases}$$

and $\boldsymbol{\lambda}^*(t)$ is the optimal dual solution to the dual problem of (10.40) with $\mathbf{y} = \mathbf{y}(\mathbf{p}(t))$. For more details see References [26] and [33] to [38].

10.3.4 Congestion control, routing and scheduling

Consider an *ad hoc* wireless network with a set N of nodes and a set L of logical links. A form of power control is assumed so that each logical link l has a fixed capacity c_l when it is active. The feasible rate region at the link layer is the convex hull of the corresponding rate vectors of independent sets of the conflict graph. For the feasible rate region $\mathbf{\Pi}$, the flow rate x_i^k generated at node i for destination k, when there is a queue for each destination k at each link (i, j), is the amount of capacity of link (i, j) allocated to the flows on that link for a final destination k, f_{ij}^k. Consider the following generalized NUM in variables $x_s \geq 0$, $f_{ij}^k \geq 0$:

$$\begin{aligned} &\text{Maximize } U_s(x_s) \\ &\text{subject to } x_i^k \leq \sum_{j:(i,j)\in L} f_{ij}^k - \sum_{j:(j,i)\in L} f_{ji}^k, \forall i, k \\ &\qquad \mathbf{f} \in \mathbf{\Pi} \end{aligned} \tag{10.45}$$

where x_s is an abbreviation for x_i^k. The first constraint is a flow balance equation: the flow originated from node i for final destination k plus the total capacity allocated for transit flows through node i for final destination k should be no more than the total capacity going out of node i for final destination k. The second constraint is on schedulability. The dual problem of (10.45) decomposes into minimizing the sum of the resulting values of the following two subproblems:

$$D_1(\boldsymbol{\lambda}) := \max_{x_s \geq 0} \sum_s (U_s(x_s) - x_s \lambda_s) \tag{10.46}$$

$$D_2(\boldsymbol{\lambda}) := \max_{f_{ij}^k \geq 0} \sum_{i,k} \lambda_i^k \sum_j (f_{ij}^k - f_{ji}^k)$$

$$\text{subject to } \mathbf{f} \in \mathbf{\Pi} \tag{10.47}$$

The first subproblem is congestion control, where λ_s is the congestion price locally at source $s = (i, k)$. The second subproblem corresponds to a joint problem of multipath routing and allocation of link capacities. Thus, by dual decomposition, the flow optimization problem decomposes into separate local optimization problems that interact through congestion prices.

The congestion control problem (10.46) admits a unique maximizer $x_s(\boldsymbol{\lambda}) = U_s^{-1}(\lambda_s)$. The joint routing and scheduling problem (10.47) is equivalent to $\sum_{i,j} \sum_k \max_{f_{ij}^k \geq 0} f_{ij}^k (\lambda_i^k - \lambda_j^k)$ subject to $\mathbf{f} \in \mathbf{\Pi}$.

Hence, an optimal schedule is to have $f_{ij}^k = c_{ij}$ if k maximizes $(\lambda_i^k - \lambda_j^k)$ and 0 otherwise. This motivates the following joint congestion control, scheduling and routing algorithm.

(1) *Congestion control: the source of flow s sets its rate as $x_s(\lambda) = U'^{-1}_s(\lambda_s)$.*

(2) *Scheduling:*
- *For each link (i, j), find destination k^* such that $k^* \in \arg\max_k (\lambda_i^k - \lambda_j^k)$ and define $w_{ij}^* := \lambda_i^{k^*} - \lambda_j^{k^*}$.*
- *Choose an $\tilde{\mathbf{f}} \in \arg\max_{\mathbf{f}\in\mathbf{\Pi}} \sum_{(i,j)\in L} w_{ij}^* f_{ij}$ such that $\tilde{\mathbf{f}}$ is an extreme point. Those links (i, j) with $\overline{f_{ij}} > 0$ will transmit and other links (i, j) (with $f_{ij} = 0$) will not.*

(3) *Routing: over link $(i, j) \in L$ with $\overline{f_{ij}} > 0$, send data for destination k^* at full link capacity c_{ij}.*

(4) *Price update: each node i updates the price on the queue for destination k according to*

$$\lambda_i^k(t+1) = \left\{ \lambda_i^k(t) + \beta \left[x_i^k(\boldsymbol{\lambda}(t)) - \sum_{j:(i,j)\in L} f_{ij}^k(\boldsymbol{\lambda}(t)) + \sum_{j:(j,i)\in L} f_{ji}^k(\boldsymbol{\lambda}(t)) \right] \right\}^+ \tag{10.48}$$

The w_{ij}^* values represent the maximum differential congestion price of destination k between nodes i and j. The above algorithm uses backpressure to perform optimal scheduling and hop-by-hop routing. This is an illustrating case study on the potential interactions between backpressure-based scheduling and dual decomposition for protocol stack design, where the 'pressures' are the congestion prices. For more details see References [39] to [45].

10.4 OPTIMIZATION PROBLEM DECOMPOSITION METHODS

We start with primal and dual decomposition for decoupling constraints, then consistency pricing for decoupling objective function and finally alternative decompositions.

10.4.1 Decoupling coupled constraints

As illustrated in Figure 10.5, primal decomposition methods have the interpretation that the master problem directly gives each subproblem an amount of resources that it can use; the role of the master problem is then to allocate the existing resources properly.

In computer engineering terminology, the master problem adapts the slicing of resources among competing demands. In dual decomposition methods, the master problem sets the price for the resources to each subproblem which has to decide the amount of resources to be used depending on the prices.

The role of the master problem is then to obtain the best pricing strategy. In many cases, it is preferable to solve the master problem distributively through message passing, which can be total or global, implicit or explicit.

In summary, the engineering mechanism realizing dual decomposition is pricing feedback while that realizing primal decomposition is adaptive slicing.

In general, the terminology of 'primal-dual' has a number of different meanings. For example, the 'primal-dual interior-point method' is a class of algorithms for centralized computation of an optimum for convex optimization and the 'primal-dual distributed algorithm' is sometimes used to describe any algorithm that solves the primal and dual problems simultaneously.

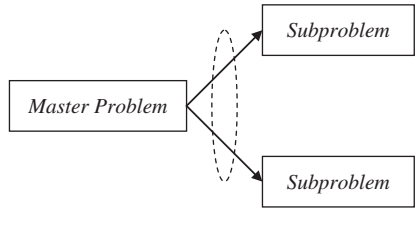

Figure 10.5 Schematic illustrating optimization problem decomposition.

In addition to this, 'primal-driven', dual-driven' and 'primal-dual-driven' terminology is used to differentiate when the update dynamic is carried out over the primal variables, or over the dual variables, or over both. Within the same terminology, 'penalty-function-based algorithms refer to those distributed algorithms obtained by moving the coupled constraints to the augmented objective function in the primal problem through a penalty.

This is in contrast to dual decomposition-based algorithms that are obtained through dual decomposition. In this section, primal and dual decomposition have yet a different set of meanings: decomposing coupling constraints through direct resource allocation and indirect pricing control, respectively.

A given decomposition method may lead to more than one distributed algorithm. Primal and dual decomposition leverage decomposability structures in a given optimization problem to turn it into subproblems coordinated by a master problem. Different distributed algorithms may then be developed based on the same decomposition, e.g. depending on the choice of update method (e.g. gradient or cutting plane or ellipsoid method), the ordering of variable updates (Jacobi or Gauss–Siedel) and the time scale of nested loops.

10.4.2 Dual decomposition of the basic NUM

In this section we illustrate how the dual decomposition approach can be applied to the basic NUM problem to produce the standard dual-decomposition-based distributed algorithm. Assume that the utility functions are concave, and possibly linear functions. The Lagrange dual problem of (10.1) is formed as

$$L(\mathbf{x},\boldsymbol{\lambda}) = \sum_s U_s(x_s) + \sum_l \lambda_l \left(c_l - \sum_{s \in S(l)} x_s \right)$$

where $\lambda_l \geq 0$ is the Lagrange multiplier (i.e. link price) associated with the linear flow constraint on link l. Additivity of total utility and linearity of flow constraints lead to a Lagrangian dual decomposition into individual source terms:

$$L(\mathbf{x},\boldsymbol{\lambda}) = \sum_s \left[U_s(x_s) - \left(\sum_{l \in L(s)} \lambda_l \right) x_s \right] + \sum_l c_l \lambda_l = \sum_s L_s(x_s, q_s) + \sum_l c_l \lambda_l$$

where $q_s = \sum_{l \in L(s)} \lambda_l$. For each source s, $L_s(x_s, q_s) = U_s(x_s) - q_s x_s$ only depends on the local rate x_s and the path price q_s (i.e. the sum of λ_l on links used by source s).

The Lagrange dual function $g(\boldsymbol{\lambda})$ is defined as the maximized $L(\mathbf{x}, \boldsymbol{\lambda})$ over $\mathbf{x}$ for a given $\boldsymbol{\lambda}$. This 'net utility' maximization can obviously be conducted distributively by each source

$$x_S^*(q_s) = \text{argmax}[U_s(x_s) - q_s x_s], \ \forall s \tag{10.49}$$

The Lagrangian maximizer $\mathbf{x}^*(\boldsymbol{\lambda})$ will be referred to as the price-based rate allocation (for a given price $\boldsymbol{\lambda}$). The Lagrange dual problem of (10.1) is

$$\begin{aligned} &\text{Minimize } g(\boldsymbol{\lambda}) = L(x^*(\boldsymbol{\lambda}), \boldsymbol{\lambda}) \\ &\text{subject to } \boldsymbol{\lambda} \geq 0 \end{aligned} \tag{10.50}$$

In problem (10.50) the optimization variable is $\boldsymbol{\lambda}$. Since $g(\boldsymbol{\lambda})$ is the pointwise supremum of a family of affine functions in $\boldsymbol{\lambda}$, it is convex and (10.50) is a convex minimization problem. Since $g(\boldsymbol{\lambda})$ may be nondifferentiable, an iterative subgradient method can be used to update the dual variables $\boldsymbol{\lambda}$ to solve the dual problem (10.50):

$$\lambda_l(t+1) = \left\{ \lambda_l(t) - \beta(t) \left[c_l - \sum_{s \in S(l)} x_s(q_s(t)) \right] \right\}^+, \forall l \tag{10.51}$$

where $c_l - \sum_{s \in S(l)} x_s(q_s(t))$ is the lth component of a subgradient vector of $g(\boldsymbol{\lambda})$, t is the iteration index and $\beta(t) > 0$ is the step size. Certain choices of step sizes, such as $\beta(t) = \beta_0/t$, $\beta > 0$, guarantee that the sequence of dual variables $\boldsymbol{\lambda}(t)$ converges to the dual optimal $\boldsymbol{\lambda}^*$ as $t \to \infty$. It can be shown that the primal variable $\mathbf{x}^*$ ($\boldsymbol{\lambda}$(t)) also converges to the primal optimal variable $\mathbf{x}^*$. For a primal problem that is a convex optimization the convergence is toward a global optimum.

In summary, the sequence of source and link algorithms (10.49) and (10.51) forms a standard dual-decomposition-based distributed algorithm that globally solves NUM (10.1) and the dual problem (10.50), i.e. computes an optimal rate vector $\mathbf{x}^*$ and optimal link price vector $\boldsymbol{\lambda}^*$ without an explicit need for signaling. This is because the subgradient is precisely the difference between the fixed link capacity and the varying traffic load on each link, and the subgradient update equation has the interpretation of a weighted queuing delay update. This will be referred to as the *basic algorithm* (*BA*) or *price-based distributed algorithm.* The behaviour of this algorithm for nonconcave source utility functions will be discussed in Section 10.5.

A primal decomposition can be carried out when the problem has a coupling variable such that when fixed to some value the general problem decouples into several subproblems. For example, the following problem over $\mathbf{y}$, $\{\mathbf{x}_i\}$:

$$\begin{aligned} \text{Maximize } & \sum_i f_i(\mathbf{x}_i) \\ \text{subject to } & \mathbf{x}_i \in X_i, \ \forall i \\ & \mathbf{A}_i \mathbf{x}_i \leq \mathbf{y}, \ \forall i \\ & \mathbf{y} \in Y \end{aligned} \tag{10.52}$$

would decouple if variable $\mathbf{y}$ were fixed. This suggests separating the optimization in (10.52) into two levels of optimization. At the lower level, we have the subproblems, one for each i over $\mathbf{x}_i$, in which (10.52) decouples when $\mathbf{y}$ is fixed:

$$\begin{aligned} \text{Maximize } & f_i(\mathbf{x}_i) \\ \text{subject to } & \mathbf{x}_i \in X_i \\ & \mathbf{A}_i \mathbf{x}_i \leq \mathbf{y} \end{aligned} \tag{10.53}$$

At the higher level, we have the master problem in charge of updating the coupling variable $\mathbf{y}$ by solving

$$\begin{aligned} \text{Maximize } & \sum_i f_i^*(\mathbf{y}) \\ \text{subject to } & \mathbf{y} \in Y \end{aligned} \tag{10.54}$$

In (10.54), $f_i^*(\mathbf{y})$ is the optimal objective value of problem (10.53) for a given $\mathbf{y}$. A subgradient for each $f_i^*(\mathbf{y})$ is given by

$$\mathbf{s}_i(\mathbf{y}) = \boldsymbol{\lambda}_i^*(\mathbf{y}) \tag{10.55}$$

where $\boldsymbol{\lambda}_i^*(\mathbf{y})$ is the optimal Lagrange multiplier corresponding to the constraint $\mathbf{A}_i \mathbf{x}_i \leq \mathbf{y}$ in problem (10.53). The global subgradient in this case is $s(\mathbf{y}) = \sum_i \boldsymbol{\lambda}_i^*(\mathbf{y}) = \sum_i \boldsymbol{\lambda}_i^*(\mathbf{y})$. The subproblems in (10.53) can be locally and independently solved with knowledge of $\mathbf{y}$.

A dual decomposition is appropriate when the problem has a coupling constraint such that when relaxed the optimization problem decouples into several subproblems. Consider, for example, the following problem:

$$\begin{aligned} \text{Maximize } & \sum_i f_i(\mathbf{x}_i) \\ \text{subject to } & \mathbf{x}_i \in X_i, \forall i \\ & \sum_i \mathbf{h}_i(\mathbf{x}_i) \leq \mathbf{c} \end{aligned} \tag{10.56}$$

Without the constraint $\sum_i \mathbf{h}_i \mathbf{x}_i \leq \mathbf{c}$ the problem would decouple. This suggests relaxing the coupling constraint in (10.56) as

$$\begin{aligned} &\text{Maximize } \sum_i f_i(\mathbf{x}_i) - \lambda^T \left(\sum_i \mathbf{h}_i(\mathbf{x}_i) - \mathbf{c} \right) \\ &\text{subject to } \mathbf{x}_i \in X_i, \forall i \end{aligned} \tag{10.57}$$

such that the optimization operates at two levels of optimization. At the lower level, we have the subproblems, one for each i over $\mathbf{x}_i$, in which (10.57) decouples:

$$\begin{aligned} &\text{Maximize } f_i(\mathbf{x}_i) - \boldsymbol{\lambda}^T \mathbf{h}_i(\mathbf{x}_i) \\ &\text{subject to } \mathbf{x}_i \in X_i \end{aligned} \tag{10.58}$$

At the higher level, we have the master dual problem updating the dual variable $\boldsymbol{\lambda}$ by solving the dual problem

$$\begin{aligned} &\text{Minimize } g(\boldsymbol{\lambda}) = \sum_i g_i(\boldsymbol{\lambda}) + \lambda^{\mathrm{T}} \mathbf{c} \\ &\text{subject to } \boldsymbol{\lambda} \geq 0 \end{aligned} \tag{10.59}$$

In (10.59), $g_i(\boldsymbol{\lambda})$ is the dual fraction obtained as the maximum value of the Lagrangian solved in (10.58) for a given $\boldsymbol{\lambda}$. This approach is in fact solving the dual instead of the original primal problem. Hence, it will only give appropriate results if strong duality holds. A subgradient for each $g_i(\boldsymbol{\lambda})$ is given by

$$\mathbf{s}_i(\boldsymbol{\lambda}) = -\mathbf{h}_i(\mathbf{x}_i^*(\boldsymbol{\lambda})) \tag{10.60}$$

where $\mathbf{x}^*$ $(\boldsymbol{\lambda})$ is the optimal solution of problem (10.58) for a given $\boldsymbol{\lambda}$. The global subgradient is then

$$\mathbf{s}(\boldsymbol{\lambda}) = \sum_i \mathbf{s}_i(\boldsymbol{\lambda}) + \mathbf{c} = \mathbf{c} - \sum_i \mathbf{h}_i(\mathbf{x}_i^*(\boldsymbol{\lambda}))$$

The subproblems in (10.58) can be locally and independently solved with knowledge of $\boldsymbol{\lambda}$.

10.4.3 Coupling constraints

Not all coupling constraints can be readily decomposed through primal or dual decompositions. For example, the feasibility set of SIR in wireless cellular network power control problems is coupled in a way that has no obvious decomposability structure. A reparametrization of the constraint set is required prior to dual decomposition [46]. Sometimes, the coupling is time-invariant, as in more broadband access networks, and very efficient static pricing can be used to decouple such 'static coupling'.

10.4.4 Decoupling coupled objectives

Distributed and end-to-end algorithms can solve the basic NUM of (10.1) for the following reasons:

(1) *Separability in objective function: the network utility is a sum of individual source utilities.*

(2) *Additivity in constraint functions: the linear flow constraint sums over the individual flows.*

(3) *Interchangeability of iteration index:*

$$\sum_{l} \lambda_l \sum_{s \in S(l)} x_s = \sum_{s} x_s \sum_{l \in L(s)} \lambda_l$$

(4) *Zero duality gap.*

Property 3 is trivial. When property 2 is violated, decomposition is much harder and usually involves some reparametrization of the constraint set. For the case when property 4 does not hold, recent works have provided alternative solutions that will be discussed in Section 10.4.5.

The generalized NUM problem considered in this section is

$$\begin{aligned} &\text{Maximize } \sum_{k} U_k(\mathbf{x}_k, \{\mathbf{x}_l\}_{l \in L(k)}) \\ &\text{subject to } \mathbf{x}_k \in X_k, \forall k \\ &\qquad \sum_{k=1}^{K} \mathbf{h}_k(\mathbf{x}_k) \leq \mathbf{c} \end{aligned} \tag{10.61}$$

In (10.61), the (strictly concave) utilities U_k depend on a vector local variable $\mathbf{x}_k$ and on the variables of other utilities $\mathbf{x}_l$ for $l \in L(k)$, i.e. coupled utilities, $L(k)$ is the set of nodes coupled with the kth utility, the sets X_k are arbitrary convex sets and the coupling constraining function $\sum_k \mathbf{h}_k(\mathbf{x}_k)$ is not necessarily linear but still convex. Note that this model has two types of coupling: coupled constraint and coupled utilities.

One way to deal with the coupling problem in the utilities is to introduce auxiliary variable and additional equality constraints, thus moving the coupling in the objective function to coupling in the constraint. This can then be decoupled by dual decomposition and solved by introducing additional consistency pricing. If two nodes have their individual utilities dependent on each other's total variable then it is reasonable to assume that there must be some communication channels in which they can locally exchange pricing messages. It can be shown that the global link congestion price update of the standard dual-decomposition-based distributed algorithm is not affected by the total consistency price updates, which can be conducted via these local communication channels among the nodes.

The first step is to introduce in problem (10.61) the auxiliary variable $\mathbf{x}_{kl}$ for the coupled arguments in the utility functions and additional equality constraints to enforce consistency:

$$\begin{aligned} &\text{Maximize } \sum_{k} U_k(\mathbf{x}_k, \{\mathbf{x}_{kl}\}_{l \in L(k)}) \\ &\text{subject to } \mathbf{x}_k \in X_k, \forall k \\ &\qquad \sum_{k} \mathbf{h}_k(\mathbf{x}_k) \leq \mathbf{c} \\ &\qquad \mathbf{x}_{kl} = \mathbf{x}_l, \ \forall k, \ l \in L(k) \end{aligned} \tag{10.62}$$

To obtain a distributed algorithm, we take now a dual decomposition approach by relaxing all the coupling constraints in problem (10.62):

$$\begin{aligned} &\text{Maximize } \sum_{k} U_k(\mathbf{x}_k, \{\mathbf{x}_{kl}\}_{l \in L(k)}) + \lambda^{\mathrm{T}} \left(\mathbf{c} - \sum_{k} \mathbf{h}_k(\mathbf{x}_k) \right) + \sum_{k, l \in L(k)} \gamma_{kl}^{\mathrm{T}} (\mathbf{x}_l - \mathbf{x}_{kl}) \\ &\text{subject to } \mathbf{x}_k \in X_k, \forall k \\ &\qquad \mathbf{x}_{kl} \in X_l, \forall k, \ l \in L(k) \end{aligned} \tag{10.63}$$

In (10.63), $\boldsymbol{\lambda}$ are the congestion prices and $\boldsymbol{\gamma}_{kl}$ are the consistency prices. By exploiting the additivity structure the Lagrangian is separated into many subproblems where maximization is done using the total variables (the kth subproblem uses only the variable with the first subscript index k). The optimal value of problem (10.63) for a given set of $\boldsymbol{\gamma}_{kl}$ and $\boldsymbol{\lambda}$ defines the dual function $g(\{\boldsymbol{\gamma}_{kl}\}, \boldsymbol{\lambda})$. The dual problem is then

$$\begin{aligned} &\underset{\{\boldsymbol{\gamma}_{kl}\},\boldsymbol{\lambda}}{\text{Minimize}}\ g(\{\boldsymbol{\gamma}_{kl}\}, \boldsymbol{\lambda}) \\ &\text{subject to } \boldsymbol{\lambda} \geq \mathbf{0} \end{aligned} \tag{10.64}$$

One should notice that (10.64) is equivalent to

$$\begin{aligned} &\underset{\boldsymbol{\lambda}}{\text{Minimize}}(\underset{\{\boldsymbol{\gamma}_{kl}\}}{\text{Minimize}}\ g(\{\boldsymbol{\gamma}_{kl}\}, \boldsymbol{\lambda})) \\ &\text{subject to } \boldsymbol{\lambda} \geq \mathbf{0} \end{aligned} \tag{10.65}$$

Problem (10.64) can be solved by simultaneously updating the prices using a subgradient algorithm. In problem (10.65), the inner minimization is fully performed (by repeatedly updating $\{\boldsymbol{\gamma}_{kl}\}$) for each update of $\boldsymbol{\lambda}$. This latter approach implies two time scales: a fast time scale in which each cluster updates the corresponding consistency prices and a slow time scale in which the network updates the link prices, where the former approach has just one time scale.

In summary, the problem (10.61), where the utilities U_k are strictly concave, the sets X_k are arbitrary convex sets and the constraining functions h_k are convex, can be optimally solved by the distribute algorithm defined as:

(1) *Links update the congestion prices (each link autonomously only its own component):*

$$\boldsymbol{\lambda}(t+1) = \left\{ \boldsymbol{\lambda}(t) - \beta_1 \left[\mathbf{c} - \sum_k \mathbf{h}_k(\mathbf{x}_k) \right] \right\} \tag{10.66}$$

where β_1 is the step size.

(2) *The kth node, for all k, updates the consistency prices (at a faster or same time scale as the update of $\lambda(t)$, as*

$$\gamma_{kl}(t+1) = \gamma_{kl}(t) - \beta_2(x_l(t) - x_{kl}(t)), l \in L(k) \tag{10.67}$$

where β_2 is the stepsize, and then broadcast them to the coupled nodes within the cluster.

(3) *The kth node, for all k, locally solve the problem*

$$\begin{aligned} &\underset{x_k,\{x_{kl}\}r}{\text{Maximize}}\ U_k(\mathbf{x}_k, \{\mathbf{x}_{kl}\}_{l\in L(k)}) - \boldsymbol{\lambda}^{\mathrm{T}} \sum_k \mathbf{h}_k(\mathbf{x}_k) \\ &\qquad + \left(\sum_{l:k\in L(l)} \gamma_{lk} \right)^{\mathrm{T}} \mathbf{x}_k - \sum_{l\in L(k)} \gamma_{kl}^{\mathrm{T}} \mathbf{x}_{kl} \\ &\text{subject to } \mathbf{x}_k \in X_k \\ &\qquad \mathbf{x}_{kl} \in X_l, \forall l \in L(k) \end{aligned} \tag{10.68}$$

where $\{\mathbf{x}_{kl}\}_{l\in L(k)}$ are auxiliary local variables for the kth node.

In summary, all links must advertise their local variables $\mathbf{x}_k$ (not the auxiliary ones $\mathbf{x}_{kl}$); congestion prices $\boldsymbol{\lambda}$ are updated as before; each link can update the corresponding $\boldsymbol{\gamma}_{kl}$ with knowledge of the variables $\mathbf{x}_k$ of the coupled link and signal it to the coupled links; each link can update the local variable $\mathbf{x}_k$ as well as the auxiliary ones $\mathbf{x}_{kl}$. The only additional price due to the coupled utilities is limited signaling between the coupled links within each cluster.

10.4.5 Alternative decompositions

One of the techniques that lead to alternatives of distributed architectures is to apply primal and dual decompositions recursively, as illustrated in Figure 10.6.

The basic decompositions are repeatedly applied to a problem to obtain smaller and smaller subproblems. For example, consider the following problem over $\boldsymbol{y}$, $\{\mathbf{x}_i\}$, which includes both a coupling variable and a coupling constraint:

$$\begin{aligned} \text{Maximize } & \sum_i f_i(\mathbf{x}_i, \mathbf{y}) \\ \text{subject to } & \mathbf{x}_i \in X_i, \ \forall i \\ & \sum_i \mathbf{h}_i(\mathbf{x}_i) \leq \mathbf{c} \\ & \mathbf{A}_i \mathbf{x}_i \leq \mathbf{y}, \ \forall i \\ & \mathbf{y} \in Y \end{aligned} \tag{10.69}$$

This problem can be decomposed by taking first a primal decomposition with respect to the coupling variable $\boldsymbol{y}$ and then a dual decomposition with respect to the coupling constraint $\sum_i \mathbf{h}_i(\mathbf{x}_i) \leq \mathbf{c}$. An alternative approach would be to first take a dual decomposition and then a primal one.

Another example that shows flexibility in terms of different decompositions is the following problem with two sets of constraints:

$$\begin{aligned} \text{Maximize } & f_0(\mathbf{x}) \\ \text{subject to } & f_i(\mathbf{x}) \leq 0, \ \forall i \\ & h_i(\mathbf{x}) \leq 0, \ \forall i \end{aligned} \tag{10.70}$$

One way to deal with this problem is via the dual problem with a full relaxation of both sets of constraints to obtain the dual function $g(\boldsymbol{\lambda}, \boldsymbol{\mu})$. At this point instead of minimizing g directly with respect to $\boldsymbol{\lambda}$ and $\boldsymbol{\mu}$, it can be minimized over only one set of Lagrange multipliers first and then over the remaining one: $\min_{\lambda} \min_{\mu} g(\boldsymbol{\lambda}, \boldsymbol{\mu})$. This approach corresponds to first applying a full dual decomposition and then a primal one on the dual problem.

The following lemma characterizes the subgradient of the master problem at the top level.

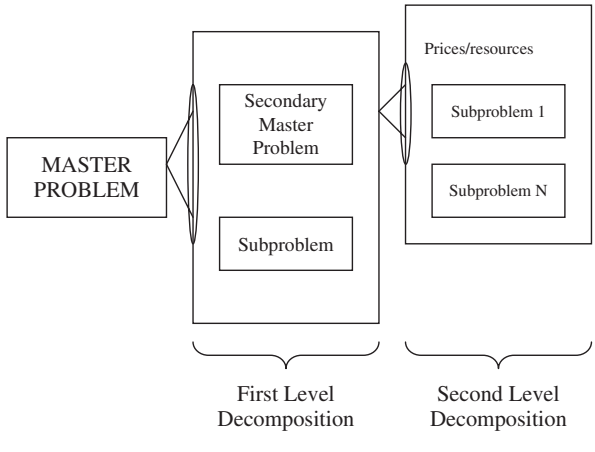

Figure 10.6 Multilevel decomposition.

Lemma [21].
Consider the following partial minimization of the dual function

$$g(\boldsymbol{\lambda}) = \inf_{\boldsymbol{\mu}} g(\boldsymbol{\lambda}, \boldsymbol{\mu}) \tag{10.71}$$

where $g(\boldsymbol{\lambda}, \boldsymbol{\mu})$ is the dual function defined as

$$g(\boldsymbol{\lambda}, \boldsymbol{\mu}) \triangleq \sup_{\mathbf{x} \in X} \left[f_0(\mathbf{x}) - \sum_i \lambda_i f_i(\mathbf{x}) - \sum_i \mu_i h_i(\mathbf{x}) \right] \tag{10.72}$$

Then $g(\boldsymbol{\lambda})$ is convex and a subgradient, denoted by $\mathbf{s}_{\boldsymbol{\lambda}}(\boldsymbol{\lambda})$, is given by

$$s_{\lambda_i}(\boldsymbol{\lambda}) = -f_i(\mathbf{x}^*(\boldsymbol{\lambda}, \boldsymbol{\mu}^*(\boldsymbol{\lambda}))) \tag{10.73}$$

where $\mathbf{x}^*(\boldsymbol{\lambda}, \boldsymbol{\mu})$ is the value of $\mathbf{x}$ that achieves the supremum in (10.72) for a given $\boldsymbol{\lambda}$ and $\boldsymbol{\mu}$, and $\boldsymbol{\mu}^*(\boldsymbol{\lambda})$ is the value of $\boldsymbol{\mu}$ that achieves the infimum in Equation (10.71).

Alternatively, problem (10.70) can be approached via the dual but with a partial relaxation of only one set of constraints, say $f_i(\mathbf{x}) \leq 0, \forall i$, obtaining the dual function $g(\boldsymbol{\lambda})$ to be minimized by the master problem. In order to compute $g(\boldsymbol{\lambda})$ for a given $\boldsymbol{\lambda}$, now the partial Lagrangian has to be maximized subject to the remaining constraints $g_i(\mathbf{x}) \leq 0, \forall i$, for which yet another relaxation can be used. This approach corresponds to first applying a partial dual decomposition and then, for the subproblem, another dual decomposition.

In addition to combinations of primal and dual decompositions, there can also be different orderings of updates, including the choice of parallel (Jacobi) or sequential (Gauss–Siedel) updates. When there is more that one level of decomposition, and all levels run some type of iterative algorithm, such as the subgradient methods, convergence and stability are guaranteed if the lower-level master problem is solved on a faster time scale than the high-level master problem, so that at each iteration of a master problem all the problems at a lower level have already converged. If the updates of the different subproblems operate on similar time scales, convergence of the overall system may still be possible but requires more proof techniques.

Partial and hierarchical decompositions can also be used for architectural alternatives of the protocol stack. As an example, consider the following special case of NUM in variables ($\mathbf{x}$, $\mathbf{y}$):

$$\begin{aligned} \text{Maximize} \quad & \sum_i U_i(x_i) \\ \text{subject to} \quad & f_i(x_i, y_i) \leq 0, \ \forall i \\ & y_i \in Y_i, \forall i \\ & \sum_i h_i(x_i, y_i) \leq 0 \end{aligned} \tag{10.74}$$

In problem (10.74), $\mathbf{x}$ models the performance metrics that user utilities depend on and $\mathbf{y}$ models the same resources that are globally coupled and have an impact on performance. This problem has applications in the distributed power control algorithm in wireless cellular networks, and can be decomposed in a number of different ways. In the three examples below, each decomposition results in a new possibility in achieving the most appropriate tradeoff between computation and communication.

(1) In a *primal decomposition approach* problem (10.74) decouples if y_i are fixed. We can decompose the original problem into the master problem over $\mathbf{y}$:

$$\begin{aligned} \text{Maximize} \quad & \sum_i \tilde{U}_i(y_i) \\ \text{subject to} \quad & y_i \in y_i \forall i \\ & \sum_i h_i(y_i) \leq 0 \end{aligned} \tag{10.75}$$

In (10.75), each $\tilde{U}_i(y_i)$ is the optimal objective value of the subproblem over x_i:

$$\begin{aligned} &\text{Maximize } U_i(x_i) \\ &\text{subject to } x_i \in X_i \\ &\qquad f_i(x_i, y_i) \leq 0 \end{aligned} \tag{10.76}$$

Each of the subproblems can be solved by using only its local information (U_i, f_i and the local set X_i) and the corresponding y_i given by the master problem. Once each subproblem is solved, the optimal value $U_i(y_i)$ and possibly a subgradient can be communicated to the master problem. In this case, the master problem needs to communicate to each of the subproblems the available amount of resources y_i allocated.

(2) In a *full dual decomposition approach* with respect to all coupling constraints $f_i(x_i, y_i) \leq 0$ and $\sum_i h_i(y_i) \leq 0$, the master dual problem is

$$\text{Minimize } g(\boldsymbol{\lambda}, \gamma) \tag{10.77}$$

over $\boldsymbol{\lambda}, \gamma \geq 0$. In (10.77) $g(\boldsymbol{\lambda}, \gamma)$ is given by the sum of the optimal objective values of the following subproblems over (x_i, y_i) for each i.

$$\begin{aligned} &\text{Maximize } U_i(x_i) - \lambda_i f_i(x_i, y_i) - \gamma h_i(y_i) \\ &\text{subject to } x_i \in X_i \end{aligned} \tag{10.78}$$

Each of the subproblems can be solved in parallel by using only its local information and the Lagrange multipliers λ_i and γ (given by the master problem). Once each subproblem is solved, the optimal value and possibly a subgradient (given by $-f_i(x_i, y_i)$ and $-h_i(y_i)$) can be communicated to the master problem. In this case, the master dual problem needs to communicate to each of the subproblems the private price λ_i and the common price γ.

(3) In a *partial dual decomposition approach* only with respect to the global coupling constraint $\sum_i h_i(y_i) \leq 0$, the master dual problem over $\gamma \geq 0$ is

$$\text{Minimize } g(\gamma) \tag{10.79}$$

In problem (10.79), $g(\gamma)$ is given by the sum of the optimal objective values of the following subproblems for all i:

$$\begin{aligned} &\text{Maximize } U_i(x_i) - \gamma h_i(y_i) \\ &\text{subject to } x_i \in X_i \\ &\qquad f_i(x_i, y_i) \leq 0 \end{aligned} \tag{10.80}$$

Each of the subproblems can be solved in parallel by using only its local information and the Lagrange multiplier γ (given by the master problem).

Once each subproblem is solved, the optimal value and (possibly) a subgradient, given by $-h_i(y_i)$, can be communicated to the master problem. In this case, the master dual problem needs to communicate to each of the subproblems simply the common price γ. For more details see References [46] to [57].

10.4.6 Application example of decomposition techniques to distributed crosslayer optimization

This section presents an application of the decomposition methods in the design of utility maximizing protocols for systems with orthogonal channels and a global resource constraint in the physical layer. The algorithms consist of two complementary problems based on decomposition

techniques, in which congestion control and resource allocations are performed on different time scales. The simulation parameters are the same as in Reference [58].

10.4.6.1 The system model

A network is assumed to consist of L directed links shared by N sources indexed by s. An increasing and strictly concave function $u_s(x_s)$ is associated to each source, which measures the ability of the utility source s to send at rate x_s.

It is assumed that data are routed along fixed paths, represented by a routing matrix $\mathbf{R} = [r_{ls}]$ with entries $r_{ls} = 1$ if source s uses link l and 0 otherwise. The aggregate communication rate on each link l is limited by its capacity $c_l(\varphi_l)$, where φ_l are the available resources on link l. We assume that the capacities are monotone increasing, concave functions, twice differentiable, and that there is a network-wide resource budget, i.e. that $\sum_L^{l=1} \varphi_i \leq \varphi_{\text{tot}}$ and $\varphi_l \geq 0$. We would like to find the combination of source rates and resource allocations that maximizes the total network utility. Introducing the vectors $\mathbf{x} = (x_1 \cdots x_s)$, $\varphi = (\varphi_1 \cdots \varphi_L)$ and $\mathbf{c}(\varphi) = (c_1(\varphi_1) \cdots c_L(\varphi_L))$, this amounts to solving the following convex optimization problem:

$$\begin{aligned} &\text{Maximize } \sum_{s=1}^{N} u_s(x_s) \\ &\text{subject to } \mathbf{R}\mathbf{x} \leq \mathbf{c}(\varphi), \mathbf{x}_{\min} \leq \mathbf{x} \\ &\qquad \sum_{l=1}^{L} \varphi_i \leq \varphi_{\text{tot}}, 0 \leq \varphi \end{aligned} \tag{10.81}$$

in the variables s and φ.

We assume that there should exist a resource allocation $\tilde{\varphi}$ such that $\mathbf{R}\mathbf{x}_{\min} \prec \mathbf{c}(\tilde{\varphi})$, and the routing matrix, $\mathbf{R}$, should be such that all sources have data to send and all links are at least used by one source. In wireless networks with Gaussian broadcast channels, the classical Shannon capacity formula gives

$$c_l = W_l \log\left(1 + \frac{P_l}{\sigma_l W_l}\right) \tag{10.82}$$

where the adjustable parameters are W_l, the assigned bandwidth, and P_l, the power used in the link.

(1) *Dual decomposition.* We introduce Lagrange multipliers λ_l for the capacities constraints in (10.81) and form the partial Lagrangian

$$L(\mathbf{x}, \varphi, \boldsymbol{\lambda}) = \left\{ \sum_s u_s(x_s) - \lambda^{\mathrm{T}}(\mathbf{R}\mathbf{x} - \mathbf{c}(\varphi)) \Big| \sum\nolimits_{\varphi_l} = \varphi_{\text{tot}}, \sum_l \varphi_l = \varphi_{tot}, \mathbf{x}_{\min} \leq \mathbf{x} \right\} \tag{10.83}$$

and the associated dual function

$$g(\boldsymbol{\lambda}) = \sup_{x,\varphi}\{L(\mathbf{x}, \varphi, \boldsymbol{\lambda})\} = \sup_{x_{\min} \leq x} \left\{ \sum_s u_s(x_s) - \boldsymbol{\lambda}^{\mathbf{T}}\mathbf{R}\mathbf{x} \right\} + \sup_{\substack{\sum_l \varphi_l = \varphi_{tot} \\ \varphi_{\min} \leq \varphi}} \boldsymbol{\lambda}^{\mathbf{T}}\mathbf{c}(\varphi)$$

The dual function decomposes into a network subproblem and a resource allocation subproblem. The corresponding Lagrange dual problem is

$$\begin{aligned} &\text{Minimize } g(\boldsymbol{\lambda}) \\ &\text{subject to } \boldsymbol{\lambda} \geq 0 \end{aligned}$$

If we assume that the link capacities are strictly concave, then the partial Lagrangian is strictly concave in $(\mathbf{x}, \varphi)$ and the dual function is differentiable [59] with

$$\nabla g(\boldsymbol{\lambda}) = \mathbf{c}(\varphi^*(\boldsymbol{\lambda})) - \mathbf{R}\mathbf{x}^*(\boldsymbol{\lambda})$$

The dual variables can be updated using a projected gradient method

$$\lambda_l(t+1) = \left[\lambda_l(t) - \gamma\left(c_l(\varphi_l^*(t)) - \sum_{s=1}^{N} r_{ls}x_s^*(t)\right)\right] \tag{10.84}$$

This update can be carried out locally by links based on their current excess capacities.

(2) *Primal decomposition.* To complement the dual approach, we will now develop a distributed solution in which optimization flow control is carried out on a fast time scale, while resource reallocations are performed on a slower time scale. We rewrite problem (10.81) as

$$\begin{aligned} &\text{Maximize } \nu(\varphi) = \sup_{x_{\min} \le x}\left\{\sum_s u_s(x_s) | \mathbf{R}\mathbf{x} \le \mathbf{c}(\varphi)\right\} \\ &\text{subject to } \sum_{l=1}^{L} \varphi_l = \varphi_{\text{tot}} \\ &\qquad \varphi_{\min} \le \varphi \end{aligned} \tag{10.85}$$

We use the optimal values to compute the subgradient

$$\mathbf{h}(\varphi) = (\lambda_1^* c_1'(\varphi_1) \cdots \lambda_L^* c_L'(\varphi_L))$$

where λ_l are optimal Lagrange multipliers for the capacity constraints in problem (10.81). We execute a distributed projection and use this to update φ with

$$\varphi_{t+1} = [\varphi_t + \alpha h(\varphi(t))]^+$$

We calculate the projection in a distributed fashion:

$$\begin{aligned} &\text{Minimize } ||\varphi - \varphi^0||_2^2 \\ &\text{subject to } \sum_{L}^{l=1} \varphi_l = \varphi_{\text{tot}}, \varphi_{\min} \le \varphi \end{aligned} \tag{10.86}$$

10.4.6.2 Performance example

We now demonstrate the algorithms on the sample network shown in Figure 10.7. The network has been generated by placing eight nodes randomly in a unit square and introducing direct links between all nodes that are within a distance d of each other. The value of d has been chosen to be as small as possible while guaranteeing that the network is strongly connected.

The link capacities are

$$c_l(\varphi_l) = \varphi_l \log\left(1 + \frac{\gamma_l}{\varphi_l}\right) \tag{10.87}$$

where $\gamma_l = 1/d_l^2$ and d_l is the distance between the communicating nodes. This is a special case of Equation (10.82). The resource limits $\varphi_{\min}$ and φ_{tot} are set to 0.1 and 10, respectively. The utility functions are $u_s(x_s) = \log(x_s)$, which corresponds to proportional fairness. The minimum source rate, $x_{\min}$, was set to 10^{-6}.

The norm of the differences between the current and optimal values of the decision variables versus the number of main loop iterations are shown in Figures 10.8 and 10.9.

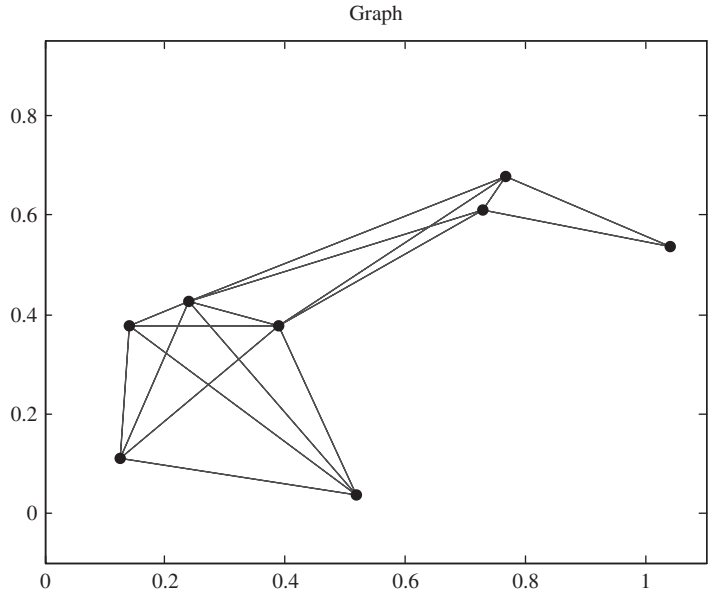

Figure 10.7 Example network topology.

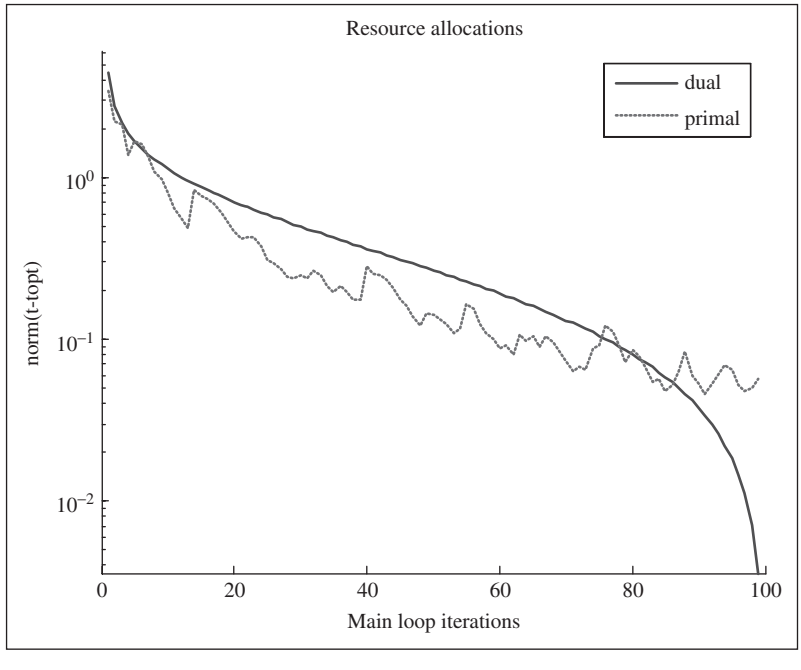

Figure 10.8 The norm of the resource allocation minus the optimal resource allocation versus main loop iterations.

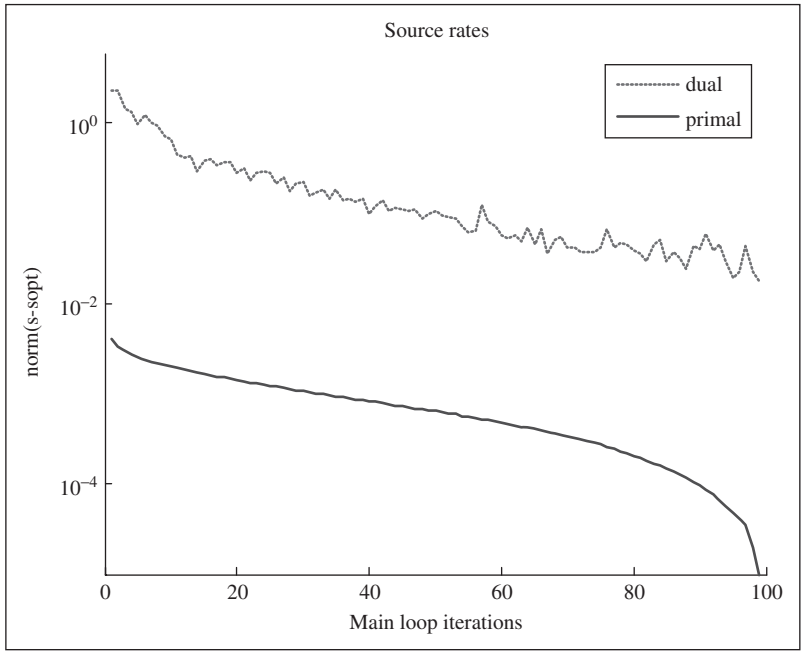

Figure 10.9 The norm of the source rates minus the optimal source rate versus main loop iterations.

10.5 OPTIMIZATION OF DISTRIBUTED RATE ALLOCATION FOR INELASTIC UTILITY FLOWS

In most of the recent research on network rate allocation it is common to assume that traffic flows are elastic, which means that they have concave and continuous utility functions. These critical assumptions lead to the tractability of the analytic models for rate allocation based on network utility maximization, discussed so far in this chapter, but also limit the applicability of the resulting rate allocation protocols.

There are two common ways to model the inelastic traffic utility function: a *nonconcave* utility function based on the user perception model (e.g. sigmoidal utility for voice traffic based on MOS scores) or a *discontinuous* utility function based on the model where real-time flows attain zero utility if the rate is below a threshold and a constant positive utility (or concave increasing utility) above the threshold.

If we remove the critical assumption that $\{U_s\}$ are concave functions and allow them to be any nonlinear functions, the resulting optimization problem becomes nonconvex and significantly harder to analyze and solve, even by centralized computational methods. In particular, a local optimum may not be a global optimum and the duality gap can be strictly positive. The standard distributive algorithms that solve the dual problem may produce infeasible or suboptimal rate allocation.

10.5.1 Nonconcave utility flows

Based on the basic formulation of the NUM problem (10.1) and its dual decomposition, we have developed the rate allocation algorithm for concave and continuous utility flows in Section 10.4.2,

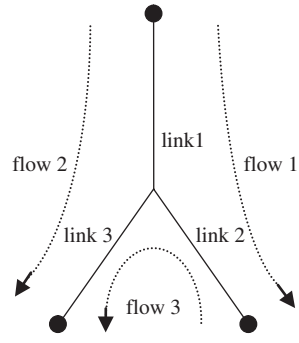

Figure 10.10 Example network topology.

where it was referred to as the *basic algorithm* (*BA*). With nonconcave utility functions, the BA may fail to converge to the primal optimal solution. One reason is that solving the dual problem (10.50) is no longer equivalent to solving the primal problem (10.1).

In this section, we discuss the general case where $\{U_s\}$ are nonconcave functions. The goal of this discussion is to investigate sufficient and necessary conditions under which the BA still converges to the globally optimal rate allocation, i.e. the primal optimizer $\mathbf{x}^*$.

In Figure 10.10 a *topology example* illustrates that the BA can converge even when the utility functions are nonconcave. In the example, there are only three flows over three links, so that the small number of flows and links allow an exhaustive search to compute the global optimum and check against the distributed algorithm's solution. All three utility functions are nonconcave: $U_s(x_s) = [1 - 2Q(\sqrt{2x_s})]^{\beta_s}$, where Q is the complementary cumulative distribution of the standard Gaussian variable and β_s are positive parameters. The link capacity vector is varied within the set $C = \{\mathbf{c}(\theta) = \theta[5, 10, 6] + (1 - \theta)[8, 6, 7], \theta \in [0, 1]\}$.

Each capacity vector gives one realization of a nonconcave NUM. The BA is executed for this problem in Reference [60] and the resulting rate allocation is indeed found to be globally optimal for all $\mathbf{c} \in C$. As shown in Figure 10.11 for some of the choices of $\mathbf{c}$, the maximized network utility using the BA matches precisely with that from exhaustive search. For the BA to work for inelastic flow rate allocation one necessary condition that immediately manifests itself is the zero duality gap condition.

If U^* is the globally optimal primal objective value and x^* its maximizer, and D^* is the globally optimal dual objective value and λ^* is its minimizer, then independentlyof the concavity of the utilities, $D^* \geq U^*$ (see Section 10.2). The duality gap for problem (10.1) is defined as $\eta = D^* - U^*$. The zero duality gap condition means that $\eta = 0$. It is easy to see that the zero duality gap is a necessary condition for the BA to converge to the primal optimal. Although concavity of all utility functions $\{U_s(x_s)\}$ is a sufficient condition to guarantee a zero duality gap in (10.1), it is not a necessary condition. The duality gap can be zero even for nonconvex optimization problems. However, proving the zero duality gap in these cases can be much more difficult and requires efforts beyond the standard arguments in convex optimization [1].

In the sequel we will discuss sufficient conditions for the convergence of the algorithm.

Theorem 1.
Continuity of price-based rate allocation $\mathbf{x}^*(\boldsymbol{\lambda})$ at all optimal prices $\boldsymbol{\lambda}^*$ implies that the price-based rate allocation $\mathbf{x}^*(\boldsymbol{\lambda})$ obtained through the BA converges to a globally optimal rate allocation $\mathbf{x}^*$.

Proof. In the sequel we summarize the proof along the lines presented in Reference [60]. We start by claiming that continuity of price-based rate allocation $\mathbf{x}^*(\boldsymbol{\lambda})$ at the optimal price $\boldsymbol{\lambda}^*$ implies

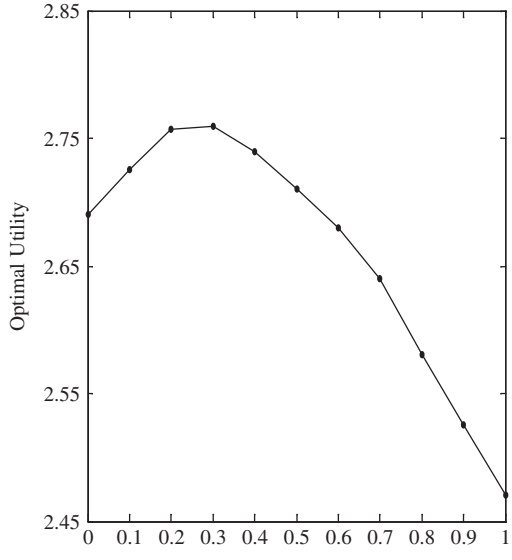

Figure 10.11 A cross-sectional sample is shown in the graph where the BA's converged results coincide with the globally optimal rate allocation computed through exhaustive search.

that $\mathbf{x}^*(\boldsymbol{\lambda}^{\text{opt}})$ and $\boldsymbol{\lambda}^{\text{opt}}$ satisfy complementary slackness and that $\mathbf{x}^*(\boldsymbol{\lambda}^{\text{opt}})$ is primal feasible. The complementary slackness condition between the optimal congestion price and price-based rate allocation is given by $\lambda_l^{\text{opt}}(\sum_{s:l\in L(s)} x_s^*(q_s^{\text{opt}}) - c_l) = 0, \forall l$. To check this, for any given l, consider first the case where $\lambda_l^{\text{opt}} > 0$. Let $\varepsilon > 0$ be sufficiently small such that we can define price vectors $\boldsymbol{\lambda}^{\min}$ where $\{\lambda_i^{\min} = \lambda_i^{\text{opt}}, i \neq l; \lambda_l^{\min} = \lambda_l^{\text{opt}} - \varepsilon > 0\}$ and $\boldsymbol{\lambda}^{\max}$ with $\{\lambda_i^{\max} = \lambda_i^{\text{opt}}, i \neq l; \lambda_l^{\max} = \lambda_l^{\text{opt}} + \varepsilon > 0\}$. Based on the definition of the subgradient, we have

$$\begin{aligned} g(\boldsymbol{\lambda}^{\text{opt}}) &\geq g(\boldsymbol{\lambda}^{\min}) + (\boldsymbol{\lambda}^{\text{opt}} - \boldsymbol{\lambda}^{\min})^{\text{T}} \delta g(\boldsymbol{\lambda}^{\min}) \\ &= g(\boldsymbol{\lambda}^{\min}) + \varepsilon \left(c_l - \sum_{s:l\in L(s)} x_s^*(\lambda^{\min}) \right) \end{aligned}$$

Since $g(\boldsymbol{\lambda}^{\text{opt}}) \leq g(\boldsymbol{\lambda}^{\min})$, the lth component of the subgradient evaluated at $\boldsymbol{\lambda}^{\min}$ is nonpositive, resulting in $\sum_{s:l\in L(s)} x_s^*(\boldsymbol{\lambda}^{\min}) \geq c_l$. Similarly, the ith component of the subgradient evaluated at $\lambda^{\max}$ is nonnegative, resulting in $\sum_{s:l\in L(s)} x_s^*(\lambda^{\max}) \leq c_l$. By continuity of $x^*(\boldsymbol{\lambda})$ at $\boldsymbol{\lambda}^{\text{opt}}$, $\sum_{s:l\in L(s)} x_s^*(q_s^{\text{opt}}) = c_l$, which implies both complementary slackness and primal feasibility.

Now, let us consider the case $\lambda_l^{\text{opt}} = 0$. While the complementary slackness condition is obvious, we need to show that the price-based rate allocation is primal feasible. Let $\varepsilon > 0$ and $\lambda_l^{\max}$ and $\boldsymbol{\lambda}^{\max}$ be as defined before. The lth component of the subgradient at $\boldsymbol{\lambda}^{\max}$ is nonnegative, resulting in $\sum_{s:l\in L(s)} x_s^*(\lambda^{\max}) \leq c_l$. Due to continuity of $\mathbf{x}^*(\boldsymbol{\lambda})$ at $\boldsymbol{\lambda}^{\text{opt}}$, in this case we have $\sum_{sl\in L(s)} x_s^*(q_s^{\text{opt}}) \leq c_l$, proving primal feasibility.

It can be shown that $D^* \leq U^*$ by the following set of equalities/nonequalities:

$$\begin{aligned} D^* &\overset{\text{(a)}}{=} g(\boldsymbol{\lambda}^{\text{opt}}) \overset{\text{(b)}}{=} \max_{\mathbf{x}} L(\mathbf{x}^*(\boldsymbol{\lambda}^{\text{opt}}),\ \boldsymbol{\lambda}^{\text{opt}}) \\ &\overset{\text{(c)}}{=} \sum_s U_s(x_s^*(q_s^{\text{opt}})) + \sum_l \lambda_l^{\text{opt}} \left[c_l - \sum_{s;l\in L(s)} x_s^*(q_s^{\text{opt}}) \right] \overset{\text{(d)}}{=} \sum U_s(x_s^*(q_s^{\text{opt}})) \overset{\text{(e)}}{\leq} U^* \end{aligned}$$

Equality (a) follows from the definition of the dual optimal value, (b) from the definition of the Lagrange dual function, (c) from the definition of the Lagrangian, (d) from complementary slackness and (e) from the definition of primal optimal value. Also, by weak duality we have $D^* \geq U^*$. Therefore, $D^* = U^*$; i.e. the inequality must be an equality. Thus, price-based rate allocation $\mathbf{x}^*(\boldsymbol{\lambda}^{opt})$ is a feasible rate vector that attains the globally optimal network utility, i.e. the BA converges to the globally optimal rate allocation.

10.5.2 Capacity provisioning for convergence of the basic algorithm

From the previous section, we can see that it is possible to achieve convergence of the BA to the optimal rate allocation, even with nonconcave utility functions, as long as certain path prices are avoided. Let $U_s(x_s)$ be a sigmoidal function as shown in Figure 10.12. An intuitive guess is that the BA would converge if link capacities can guarantee that the optimal rate for a sigmoidal utility source lies in the concave part of the sigmoidal curve. It is strictly increasing, has one inflection point x_s^i and $(\mathrm{d}^2U_s(x_s)/\mathrm{d}x_s^2) > 0$, for $x_s < x_s^i$, and $(\mathrm{d}^2U_s(x_s)/\mathrm{d}x_s^2) < 0$, for $x_s > x_s^i$. Let q_s^0 be the slope of the tangent from the origin to the sigmoidal curve $U_s(x_s)$. Let x_s^0 be the source rate at which the tangent intersects the sigmoidal curve $U_s(x_s)$. Theorem 1 from the previous section shows that continuity of $\mathbf{x}^*(\boldsymbol{\lambda})$ at the dual optimal $\boldsymbol{\lambda}^{\text{opt}}$ implies convergence of the BA and primal optimality of $\mathbf{x}^*(\boldsymbol{\lambda}^{\text{opt}})$. We note that for the sigmoidal function $U_s(x_s)$, $\mathbf{x}_s^*(\boldsymbol{\lambda})$ is discontinuous when $q_s = q_s^0$. For $q_s > q_s^0$, we have $x_s^*(\boldsymbol{\lambda}) = 0$ and the source gets a 0 rate. On the other hand, for $q_s < q_s^0$, we have $x_s^*(\boldsymbol{\lambda}) > x_s^0$ and the source gets a positive rate and utility. If the optimal price $\boldsymbol{\lambda}^{\text{opt}}$ is such that $q_s^{\text{opt}} < q_s^0$ for every sigmoidal utility source, then $x_s^*(\boldsymbol{\lambda}^{\text{opt}})$ is continuous at the optimal price and the sufficient condition is met. The BA can then be applied to this nonconvex optimization problem to obtain the global optimal.

The optimal price on a link depends on the link capacity and the load offered by all the sources using the link. In general, the link capacities can be increased to bring down the optimal prices to a desired value that ensures the convergence of the BA. Naturally we would like to use the minimal set of capacities that would ensure continuity of the price-based rate allocation. We elaborate this idea in the rest of this section.

Consider a network with L links and S sources as in the previous section. Let S_n of the sources have a nonconcave sigmoidal utility, and, without loss of generality, let these be the first S_n of the S

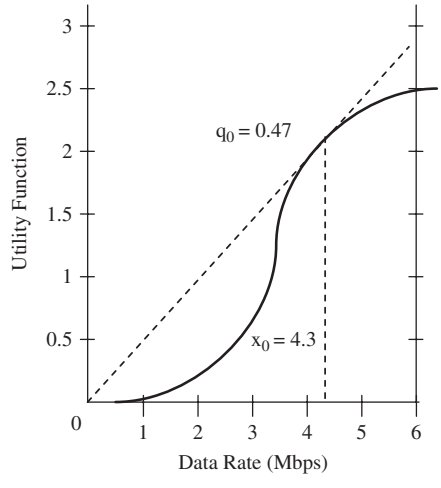

Figure 10.12 Sigmoidal utility function and illustration of x^0 and q^0.

sources. The other $S_c = S - S_n$ sources have concave utility functions. Without loss of generality, we assume that all of the L links considered serve some nonconcave sigmoidal source, because otherwise the links that do not serve any sigmoidal source can be ignored (increasing the capacity on those links does not contribute toward reducing the prices seen by the sigmoidal sources).

If the routing matrix corresponding to the S_n sigmoidal (nonconcave) sources is a $L \times S_n$ matrix $\mathbf{R}_n$ (where the (l, s) entry of the routing matrix is 1 if $l \in L(s)$ and 0 otherwise) and if the routing matrix of the other S_c sources is $\mathbf{R}_c$, then $\mathbf{R} = [\mathbf{R}_n \mathbf{R}_c]$ is the routing matrix of the entire network. For sigmoidal utility sources, let $\mathbf{x}_n^0$ and $\mathbf{q}_n^0$ be the vectors of source rates and slopes, respectively, at the point where the tangent from the origin intersects the sigmoidal curves.

One can show that the BA applied to the NUM problem with source utilities a mix of strictly concave and sigmoidal functions, as modeled above, converges to the primal optimal rate allocation, and sources with sigmoidal utilities obtain nonzero source rates if there is a dual price vector $\mathbf{p} \succeq 0$ satisfying the following inequality:

$$\mathbf{q}_n^0 \succ \mathbf{R}_n^T \mathbf{p} \tag{10.88}$$

and the link capacities $\mathbf{c} = \mathbf{c}(\mathbf{p})$, where

$$\mathbf{c}(\mathbf{p}) = \mathbf{R}_n \mathbf{x}_n^*(\mathbf{p}) + \mathbf{R}_c \mathbf{x}_c^*(\mathbf{p}) \tag{10.89}$$

Here, $\mathbf{x}_n^*(\mathbf{p})$ and $\mathbf{x}_c^*(\mathbf{p})$ are the price-based rate allocation at price p obtained by solving (10.49) for sources with nonconcave and concave utilities, respectively.

To prove this, we first recall that the subgradient of the Lagrangian dual function $g(\boldsymbol{\lambda})$ is given by $\delta g(\boldsymbol{\lambda}) = \mathbf{c} - \mathbf{R}\mathbf{x}^*(\boldsymbol{\lambda})$. If $\mathbf{c} = \mathbf{c}(\mathbf{p})$, then the subgradient at price $\mathbf{p}$ vanishes, i.e. $\delta g(\mathbf{p}) = 0$. The solution to the dual problem, $\boldsymbol{\lambda}^{\text{opt}}$, is unique under the modeling assumption in this section [61]. This implies that $\boldsymbol{\lambda}^{\text{opt}} = \mathbf{p}$. For the nonconcave sources, we have $q_s^{\text{opt}} = (\mathbf{R}_n^{\text{T}}\mathbf{p})_s$ and $\mathbf{q}_s^0 \geq (\mathbf{R}_n^{\text{T}}\mathbf{p})_s$, implying $q_s^{\text{opt}} < q_s^0$. This implies that the sigmoidal sources have an optimal pricing that is less than the critical pricing q_s^0; hence the price-based rate allocation $x_s^*(q_s^{\text{opt}})$ is continuous, implying that the BA converges to primal optimal. Furthermore, $x_s^*(q_s^{\text{opt}})$ is strictly positive; i.e. the rate allocation to each source is nonzero.

10.6 NONCONVEX OPTIMIZATION PROBLEM IN NETWORK WITH QoS PROVISIONING

In this section, we discuss an optimal joint congestion–contention control scheme that maximizes the network throughput while at the same time providing end-to-end QoS for multimedia traffic.

10.6.1 The system model

We consider a wireless mesh network (WMN) with topology consisting of a set of S sources communicating over $l \in L$ wireless links. We denote the flow rate of each source s as x_s. Some flows are transmitted over multiple hops, while others use a single hop. We want to determine, for such a communication scenario, the necessary means that a delay constrained multimedia flow can be supported successfully.

For these purposes, we define a parameter a_l that determines the medium access probability on link l. This parameter can be interpreted as the probability that link l captures the medium for transmission among the other contending links within a maximal clique n in the conflict graph, where $L'(n)$ denotes the set of links in clique n. We define a conflict matrix $\mathbf{F}$ with entries f_{nl} as

$$f_{nl} = \begin{cases} 1, & \text{if } l \in L'(n) \\ 0, & \text{otherwise} \end{cases} \tag{10.90}$$

and dimension $N \times L$, where N and L denote the total number of maximal cliques and links in the network, respectively.

For each maximal clique n, the sum of medium access probabilities of links that conflict should satisfy the inequality $\sum_{l \in L(n)} f_{nl} a_l \leq \varepsilon_n$, where $\varepsilon_n \in [0, 1]$ denotes the usable portion of a channel after excluding the effect of collisions; $\varepsilon_n = 1$ corresponds to the case of perfect scheduling where there is no collision. For IEEE 802.11, $\varepsilon_n \approx 0.85$ and it can keep the same value for a large number of stations when the ready-to-send/clear-to-send (*RTS/CTS*) mechanism is used [62, 63].

To model different sources of delay in the network we refer to the 802.11 example where the DCF (distributed coordination function) is used to share the channel fairly and resolve the collision problem by using RTS/CTS signaling and defining a backoff phase. The main goal of the backoff phase is to minimize the probability of collision, which happens after the channel is released by the capturing node and then nodes start to contend to capture it. In our delay model we use the standard binary exponential backoff (BEB) algorithm, which selects the *backoff time* from a geometric distribution with parameter p of a p-persistence algorithm [63].

A node m that tries to access link l continuously listens to (in a carrier sense) the channel except in the period when it captures the channel for transmission. During the listening phase, upon sensing the idle channel, it waits for a period of I (DIFS, or distributed interframe space). If no other node captures the channel during period I, node m starts transmission and holds the channel during a packet transmission time T. If another node captures the channel during the DIFS of node m, node m sends to the channel again and as soon as it detects the channel idle, it starts the *backoff phase*. The backoff time is divided into slots of duration Δ and measured by a backoff slot counter, which is initially set to *backoff time*$/\Delta$ and decremented at each idle slot. During the backoff period, another node may capture the channel and then the node m stops the countdown of the backoff counter until the channel is idle again. Transmission of node m starts only when the counter reaches zero and the average backoff slot count is given as $(1 - p)/p$, where the average backoff period $B(p)$ of the p-persistence algorithm is simply denoted as $B(p) = \Delta(1 - p)/p$.

In this model we allow 802.11 not necessarily to operate in the backoff mode. This means that a newly generated MAC packet can access the idle channel with some probability. Actually this is exactly the situation if transport layer flow is optimized together with the MAC layer. Given the above DCF algorithm and channel access probability a_l on link l, the average medium access delay $d_l^{(m)}(a_l)$ can be expressed as

$$d_l^{(m)}(a_l) = a_l(I + T) + \sum_{n=1}^{\infty} a_l(1 - a_l)^n[(n + 1)(1 + T) + B(a_l)] \tag{10.91}$$

The first term denotes the average delay for observing the medium idle for transmission over link l. Then, the summation represents the total delay that includes the n packets of transmission time $I + T$ with collisions with other conflicting links, the average backoff time for link l and the transmission time $I + T$ for link l after it captures the medium. After manipulating (10.91) and replacing $B(a_l)$, the average medium access delay is

$$\begin{aligned} d_l^{(m)}(a_l) &= a_l(I + T)\sum_{n=0}^{\infty}(1 - a_l)^n + a_l B(a_l)\sum_{n=1}^{\infty}(1 - a_l)^n + a_l(I + T)\sum_{n=1}^{\infty}(1 - a_l)^n \\ &= (I + T) + \frac{(1 - a_l)}{a_l}(I + T) + (1 - a_l)B(a_l) \\ &= \frac{I + T + \Delta(1 - a_l)^2}{a_l} \end{aligned} \tag{10.92}$$

The medium access delay $d_l^{(m)}(a_l)$ causes an extra queuing delay of $d_l^{(q)}(a_l)$ that occurs at the link layer. The amount of the average link layer queuing delay is determined by the amount of data

accumulated during $d_l^{(m)}(a_l)$ divided by the service rate of the link layer, given as

$$d_l^{(q)} = \left[d_l^{(m)}(a_l) \sum_s r_{ls} x_s \right] \Big/ c_l a_l \tag{10.93}$$

The total delay on link l is given as $d_l(x, a_l) = d_l^{(p)} + d_l^{(m)}(a_l) + d_l^{(q)}(x, a_l)$ and can be rewritten as follows by replacing $d_l^{(q)}$:

$$d_l(x, a_l) = d_l^{(p)} + \left(1 + \frac{\sum_s r_{ls} x_s}{c_l a_l} \right) d_l^{(m)}(a_l) \tag{10.94}$$

By simply using Equations (10.92) and (10.94) the average delay $d_l(x, a_l)$ on link l can be written as

$$d_l(x, a_l) = d_l^{(p)} + \left[1 + \frac{\sum_s r_{ls} x_s}{c_l a_l} \right] \left[\frac{1 + T + \triangle(1 - a_l)^2}{a_l} \right] \tag{10.95}$$

where r_{ls} indicates if the source s uses link l ($r_{ls} = 1$), T is the packet transmission time and Δ is the slot duration.

On this model we optimize, as before, for $U_s(x_s) = \log x_s$, which corresponds to proportional fairness. Given the WMN topology we formulate the NUM problem as

$$\begin{aligned} \underset{\mathbf{x},\mathbf{a}}{\text{Maximize}} \ & \sum_s U_s(x_s) \\ \text{subject to} \ & \mathbf{Rx} \leq \mathbf{C}a \\ & \mathbf{R^T d}(\mathbf{x}, a) \leq \mathbf{t} \\ & \mathbf{F}a \leq \boldsymbol{\varepsilon} \\ & x_s \geq 0 \text{ and } 0 \leq a_l \leq 1 \end{aligned} \tag{10.96}$$

In problem (10.96), the overall network utility is maximized in terms of the utilities $U_s(x_s)$ of each source $s \in S$ under the set of constraints. The first constraint denotes the restrictions on source rates $\mathbf{x} = [x_1, \ldots, x_S]^{\mathrm{T}}$ given that the routing matrix is $\mathbf{R}$ and the average MAC layer link capacities are $\mathbf{C}a$. The link access matrix is defined as $\mathbf{C} = \mathrm{diag}(c_1, \ldots, c_L)$ and entries of $\mathbf{R}$ are given by $r_{ls} = 1$ if source s uses link l and $r_{ls} = 0$ otherwise. The second constraint defines a bound $\mathbf{t} = [t_1, \ldots, t_S]^{\mathrm{T}}$ on the end-to-end delay of each source, where $\mathbf{d}(a) = [d_1(a_1), \ldots, d_L(a_L)]^{\mathrm{T}}$ represents the average delay of links in the network. For the sake of completeness, we refer the end-to-end delay vector of all sources as $\boldsymbol{\tau} = \mathbf{R}^T \mathbf{d}(a)$, where each entry τ_s gives the forward trip time of packets from source s to their destination. Finally, the third constraint is the restatement of the inequality on medium access parameters $a = [a_1, \ldots, a_L]^{\mathrm{T}}$ given below (10.90) as $\sum_{l \in L(n)} f_{nl} a_l \leq \varepsilon_n$ where $\boldsymbol{\varepsilon} = [\varepsilon_1, \ldots, \varepsilon_N]$.

This set of constraints essentially takes care of the packet losses due to both congestion and late arrivals. With the first constraint, sources are restricted to operate at a rate where their sum on each link is lower than the link's MAC layer capacity, and as a result packet losses due to congestion are minimized. With the second constraint, network parameters a and $\mathbf{x}$ are optimized such that the end-to-end delay of each source will conform to the application imposed delay requirement. The solution of the above constrained optimization problem will maximize the network throughput while minimizing the loss due to dropped packets and late arrivals.

10.6.2 Solving the nonconvex optimization problem for joint congestion–contention control

The above introduced NUM problem can be solved distributedly by means of dual decomposition, provided all the constraints are convex functions. For source s, the sum of the link delays (i.e.

end-to-end delay) $\tau_s = \sum_l r_{ls} d_l(\mathbf{x}, a_l)$ is, however, not a convex function. Fortunately, we can bypass the problem by making the following approximation [64]. Based on common values given in Reference [63], the slot duration in (10.95) is $\Delta = 50\,\mu s$, which becomes negligible compared to the sum of the packet transmission time, $T \approx 3500\,\mu s$, and the distributed interframe space (DIFS) time, $I = 2\Delta + SIFS = 128\,\mu s$ for the short interframe space $SIFS = 28\,\mu s$, while $(1 - a_l)$ is never greater than 1. Hence the second term of the product in Equation (10.95) can be approximated as $I + T/a_l$. On the other hand, due to the flow constraint, the aggregate flow on link l can never exceed the link's capacity, $\sum_s r_{ls} x_s \le c_l a_l$, and should be operated close to the capacity due to the utility maximization. Then the first term of the product in Equation (10.95) can be approximated (especially for congested nodes) as $1 + \sum_s r_{ls} x_s/(c_l a_l) \approx 2$ for the maximum utility case. In doing so, we can approximate the link delay function as

$$d_l(a_l) \approx d_l^{(p)} + 2(I + T)/a_l \tag{10.97}$$

while satisfying the convexity requirements over a.

We can now proceed with dual decomposition. First, we rewrite the primal NUM problem in (10.96) as an unconstrained dual problem in terms of the Lagrangian $L(\boldsymbol{\lambda}, \boldsymbol{\mu}, \boldsymbol{\nu}, \mathbf{x}, a)$ using $\boldsymbol{\lambda}$, $\boldsymbol{\mu}$ and $\boldsymbol{\nu}$. The resulting dual problem becomes

$$\begin{aligned} &\min_{\lambda,\mu,\iota} D(\boldsymbol{\lambda}, \boldsymbol{\mu}, \boldsymbol{\nu}), \\ &\text{subject to } \boldsymbol{\lambda}, \boldsymbol{\mu}, \boldsymbol{\nu} \ge 0 \end{aligned} \tag{10.98}$$

where the corresponding dual function is given as

$$\begin{aligned} D(\boldsymbol{\lambda}, \boldsymbol{\mu}, \boldsymbol{\nu}) &= \max_{x_s, a_l \ge 0} L(\boldsymbol{\lambda}, \boldsymbol{\mu}, \boldsymbol{\nu}, \mathbf{x}, a) \\ &= \max_{x_s, a_l \ge 0} \sum_s U_s(x_s) - \boldsymbol{\lambda}^{\mathrm{T}}(\mathbf{R}\mathbf{x} - \mathbf{C}a) - \boldsymbol{\mu}^{\mathrm{T}}(\mathbf{R}^{\mathrm{T}}\mathbf{d}(a) - \mathbf{t}) - \boldsymbol{\nu}^{\mathrm{T}}(\mathbf{F}a - \boldsymbol{\varepsilon}) \\ &= \max_{x_s, a_l \ge 0} \sum_s \left\{ U_s(x_s) - \sum_l \lambda_l r_{ls} x_s \right\} + \sum_l \left\{ \lambda_l a_l c_l - \sum_n \upsilon_n f_{nl} a_l \right\} \\ &\quad - \sum_s \sum_l \mu_s r_{ls} d_l(a_l) + \sum_s \mu_s t_s + \sum_n \upsilon_n \varepsilon_n \end{aligned} \tag{10.99}$$

When solving the dual problem, the dual parameters $\boldsymbol{\lambda}, \boldsymbol{\mu}, \boldsymbol{\nu}$ that minimize the dual function $D(\boldsymbol{\lambda}, \boldsymbol{\mu}, \boldsymbol{\nu})$ can be calculated by fixing the primal parameters $\mathbf{x}$ and a. The primal parameters are determined by fixing the dual parameters $\boldsymbol{\lambda}, \boldsymbol{\mu}, \boldsymbol{\nu}$. This iterative algorithm calculates the global optimal primal variables by means of exchanging price information (the dual variables) between the links and the sources. The resulting algorithm is a distributed joint congestion–contention protocol. The calculation of the various prices $\boldsymbol{\lambda}, \boldsymbol{\mu}, \boldsymbol{\nu}$ can be implemented by using the gradient algorithm described in Section 10.2.

10.7 OPTIMIZATION OF LAYERED MULTICAST BY USING INTEGER AND DYNAMIC PROGRAMMING

Layered transmission refers to the technique where information is encoded in layers, and a subset of these layers is sent to the receivers, depending on the receiver requirements, and the congestion of the path from the source to the receiver. Layered multicasting is a form of *multirate multicasting*, since different receivers in the same multicast group can receive traffic at different rates.

Multilayer transmission is preferred when receivers of the same multicast group have different characteristics. Typically, multilayer transmissions are achieved through hierarchical encoding of real-time signals. In this approach, a signal is encoded into a number of layers that can be incrementally combined to provide progressive re-finement. In layered multicasting, the receivers adapt to congestion by adding or dropping layers. With multilayer transmission, the network can be utilized more efficiently and receivers can receive data that are more commensurate with their capabilities.

In layered multicast, the receiver rates are constrained to take only a set of discrete values, which are determined by the layer bandwidths.

In this section, we take into account such constraints and pose the optimal rate control problem as a *discrete/integer* program. Unfortunately, even very simple special cases of the integer program can be shown to be NP-hard. Dealing with this integer programming directly and using a combination of *Lagrangian relaxation* and *dynamic programming* in this section, we show that it is possible to achieve rates that are very close to the optimal, without making the approximation that receiver rates take a continuous set of values.

10.7.1 The system model

In the sequel, we describe the network model and formulate the rate control problem as an optimization problem with discreteness constraints on the rates. In the subsequent sections, we discuss how we can achieve close-to-optimal rates for this problem.

We model a network with a set L of unidirectional links, where a link $l \in L$ has capacity c_l. The network is shared by a set of G multicast groups (sessions). Each multicast group is associated with a unique source, a set of receivers and a set of links that the multicast group uses (the set of links forms a tree). Any multicast group $g \in G$ is specified by $\{s^g, R^g, L^g\}$, where s^g is the source, L^g is the set of links in the multicast tree and R^g is the set of receivers in group g.

Using the example of a multicast tree shown in Figure 10.13, we introduce some additional terminology:

---

s, *source node*
$\{i_1, i_2, i_3, i_4\}$, *set of receiver nodes*
Junction nodes; in Figure 10.13, $\{i_5, i_6, i_7\}$ *is the set of junction nodes*
$R = \bigcup_{g \in G} R^g$, *set of all receiver nodes (over all groups)*
J^g, *junction nodes of any group* $g \in G$
$J = \bigcup_{g \in G} I^g$, *set of all junction nodes (over all groups)*
$I^g = R^g \cup J^g$
$I = \bigcup_{g \in G} I^g$
$I = R \cup J$, *set of all receiver and junction nodes (over all groups)*
$S = \{s^g, g \in G\}$, *set of all source nodes (over all groups)*
$I_l \subseteq I$, *set of receiver/junction nodes whose branches include link* $l \in L$
x_i, *a rate variable associated with each receiver/junction node* $i \in I$, *denoting the rate at which node* i *receives data from its parent* x_i, *rate variable for any node* $i \in S$
$\underline{x} = (x_i, i \in I \cup S)$ *denotes the vector of all rates*

$\underline{x}^g = (x_i, i \in I^g \cup \{s^g\})$, *the vector of rates associated with group* g *for each group* $g \in G$
C_i, *set of children of node* C, *each node* $i \in J \cup S$
K^g, *number of layers, for any group* $g \in G$
$b_1^g < b_2^g < \cdots < b_{K^g}^g$, *the cumulative layer bandwidths (the rates of the receivers belonging to group* g *are constrained to take only these discrete values) for any group* $g \in G$
b_k^g, *sum of the bandwidths of the layers* $1, 2, \ldots, k$ *for any* $k \in \{1, 2, \ldots, K^g\}$
$U_i : \Re_+ \to \Re$, *utility function (assumed increasing and concave) associated with* i, *for each receiver* $i \in R$

With the notation defined above, the utility maximization-based rate control problem is formulated as

$$P : \text{maximize} \sum_{i \in R} U_i(x_i) \tag{10.100}$$

$$\text{subject to} \sum_{i \in I_l} x_i \leq c_l \forall l \in L \tag{10.100a}$$

$$\underline{x}^g \in X^g \ \forall g \in G \tag{10.100b}$$

where $X^g = Y^g \cap Z^g$ and Y^g and Z^g are defined as

$$Y^g = \{\underline{x} : x_i \geq x_{i'} \forall i' \in C_i \forall i \in J^g \cup \{s^g\}\} \tag{10.101}$$

$$Z^g = \{\underline{x} : x_i \in \{b_1^g, b_2^g, \ldots, b_{K^g}^g\} \forall i \in I^g \cup \{s^g\}\} \tag{10.101a}$$

Relation (10.100a) represents the link capacity constraints. Relation (10.101) represents the fact that the rate at which a junction/receiver node receives data can be no greater than the rate at which its parent node receives data. Relation (10.101a) represents the discreteness constraints on the rates resulting in an integer optimization problem.

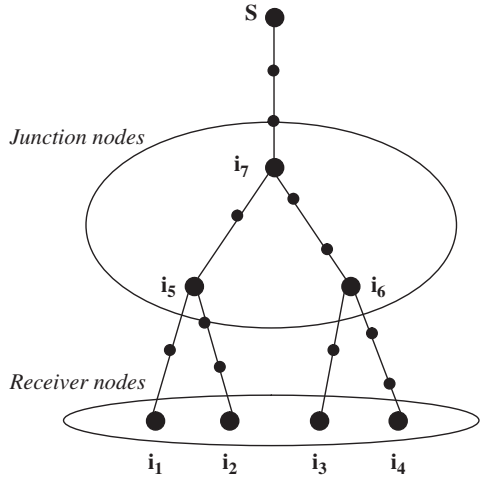

Figure 10.13 Example network topology for the multirate multicast tree.

10.7.2 Lagrangian relaxation for integer programs

In this section, we outline the opimization approach. The approach is based on *Lagrangian relaxation* for integer programs [65, 66].

In our case, this technique can help us develop an iterative algorithm that achieves rates that are close-to-optimal. In addition, along with dynamic programming, it leads to an algorithm that is completely distributed.

If λ_l is the dual variable associated with the link capacity constraint for link $l \in L$, $\underline{\lambda} = (\lambda_l, l \in L)$ the vector of the dual variables and $L_i \subseteq L$ the set of links in the branch of node i, then the Lagrangian dual $D(\underline{\lambda})$ can be written as

$$D(\underline{\lambda}) = \sum_{g \in G} \max_{\underline{x}^g \in X^g} \left\{ \sum_{i \in R^g} U_i(x_i) - \sum_{i \in I^g} \left(\sum_{l \in L_t} \lambda_l \right) x_i \right) + \sum_{l \in L} \lambda_l c_l \right\} \tag{10.102}$$

Since we are dealing with a discrete program, a duality gap exists, and dualization implicitly involves relaxation of the problem. Note that the dual is convex but nondifferentiable (the nondifferentiability is due to the presence of the discreteness constraints on the rates). Here we apply a subgradient method (with a constant step size α) to solve this problem. In this case, each iteration of the subgradient method reduces to two sets of updates: (1) dual variable updates and (2) rate updates. The dual variable update procedure for any link $l \in L$ at step n is

$$\lambda_l(n+1) = \lambda_l(n) + \alpha \left\{ \sum_{i \in I_l} x_i(n) - c_l \right\}$$

where $x_i(n)$ is the value of x_i at the nth iterative step. At the nth step, for any group $g \in G$, the rates of the receiver/junction nodes are updated as

$$\underline{x}^g(n+1) = \arg \max_{\underline{x}^g \in X^g} \left\{ \sum_{i \in R^g} U_i(x_i) - \sum_{i \in L_{lg}} \left[\sum_{i \in L_t} \lambda_l(n) \right] x_i \right\}$$

This relation states that given the link prices, each group chooses the junction/receiver rates so as to maximize its profit function.

Now we show how the group profit maximization problem can be solved in an efficient manner. Note that the group profit maximization problem needs to be solved for each group in every iteration of the rate control algorithm.

10.7.3 Group profit maximization by dynamic programming

Consider any particular multicast group $g \in G$. Now, consider any junction/receiver/source node $i \in I^g \cup \{s^g\}$. Let T_i denote the set of source/junction/receiver nodes that fall within the tree rooted at i (including i). Let $\underline{x}_i = (x_{i'}, i' \in T_i)$ denote the vector of the rate variables associated with the source/junction/receiver nodes in T_i. Let us define $P_i(\underline{x}_i)$, the tree profit function associated with node i, as

$$P_i(\underline{x}_i) = \sum_{i' \in T_i \cap R^g} U_i(x_i) - \sum_{i \in T_i \setminus \{i\}} \left(\sum_{i \in L'_r} \lambda_l \right) x_{i'} \tag{10.103}$$

In (10.103), P_i denotes the aggregate utility of all receivers in T_i minus the price charged to group g for using the links in tree T_i. Note that for any receiver i, $P_i(\underline{x}_i) = U_i(x_i)$. Also note that the group

profit function is P_{s^g}. For any node $i \in I^g \cup \{s^g\}$, we define $X_i = Y_i \cap Z_i$, where Y_i and Z_i are

$$Y_i = \{\underline{x}_i : x_{i'} \geq x_i, \forall i' \in C_{i'} \forall i' \in T_i \cap (J^g \cup \{s^g\})\}$$
$$Z_i = \{\underline{x}_i : x_{i'} \in \{b_1^g, b_2^g, \ldots, b_{K^g}^g\} \forall i' \in T_i\}$$

Next, for any $i \in I^g \cup \{s^g\}$ and $k \in \{1, 2, \ldots, K^g\}$, define $X_i(k)$ as $X_i(k) = \{\underline{x}_i : \underline{x}_i \in X_i, x_i = b_k^g\}$. Thus, $X_i(k)$ denotes the set of values in which the rates of source/junction/receiver nodes in tree T_i are constrained to lie if node i receives traffic up to layer k from its parent. Then, for any $i \in I^g \cup \{s^g\}$ and $k \in \{1, 2, \ldots, K^g\}$, define $p_i(k)$, the *conditional maximum profit* (CMP) of node i at level k, as

$$p_i(k) = \max_{\underline{x}_x \in X_t(k)} P_i(\underline{x}_i)$$

Parameter $p_i(k)$ represents the maximum profit derived from the tree T_i if the node i receives traffic up to layer k from its parent. Note that for any receiver node i, $p_i(k) = U_i(b_k^g)$. Also note that the maximum group profit that we are interested in obtaining is equal to $p_{s^g}(K^g)$. In the sequel, we demonstrate how the CMPs of node i can be derived from the CMPs of its children nodes. The results will help us in computing the maximum group profit recursively by breaking it up into smaller subproblems.

Considering the constraint $\underline{x}_i \in X_i(k)$, for any $i \in J^g \cup \{s^g\}$ and $k \in \{1, 2, \ldots, K^g\}$, we can show that this constraint is equivalent to a set of similar constraints involving the subtrees of T_i:

$$\{\underline{x}_i : \underline{x}_i \in X_i(k)\} = \{\underline{x}_i : \underline{x}_i \in X_i, x_i = b_k^g\} \tag{10.103a}$$
$$= \{\underline{x}_i : \underline{x}_{i'} \in X_{i'}, x_{i'} \leq b_k^g \forall i' \in C_i, x_i = b_k^g\} \tag{10.104}$$
$$= \{\underline{x}_i : \underline{x}_{i'} \in X_{i'}', x_{i'}, \in \{b_1, \ldots, b_k^g\} \forall i' \in C_i, x_i = b_k^g\} \tag{10.105}$$
$$= \{\underline{x}_i : \underline{x}_i, \in \bigcup_{k'=1}^{k} X_i'(k') \forall i' \in C_i, x_i = b_k^g\} \tag{10.106}$$

Relation (10.103a) follows from the definition of $X_i(k)$, while (10.104) follows from expanding the constraints in the set $\underline{x}_i \in X_i(k)$ and using the fact that $x_i = b_k^g$.

From (10.103), one can see that for any $i \in J^g \cup \{s^g\}$, we have

$$P_i(\underline{x}_i) = \sum_{i' \in C_i} \left\{ P_{i'}(\underline{x}_{i'}) - \left(\sum_{l \in L_{i'}} \lambda_l \right) x_{i'} \right\} \tag{10.107}$$

For any $i \in J^g \cup \{s^g\}$ and $k \in \{1, 2, \ldots, K^g\}$, we also have

$$p_i(k) = \max_{\underline{x}_i \in X_i(k)} P_i(\underline{x}_i) \tag{10.108}$$
$$= \max_{\underline{x}_i \in X_i(k)} \sum_{i' \in C_i} \left\{ P_{i'}(\underline{x}_{i'}) - \left(\sum_{l \in L_{i'}} \lambda_l \right) x_{i'} \right\} \tag{10.109}$$
$$= \max_{\substack{\underline{x}_{i'} \in \cup_{k'=1}^{k} X_{i'}(k') \forall i' \in C_i' \\ x_i = b_k^g}} \sum_{i' \in C_i} \left\{ P_{i'}(\underline{x}_{i'}) - \left(\sum_{i \in L_{i'}} \lambda_l \right) x_{i'} \right\} \tag{10.110}$$
$$= \max_{\underline{x}_{i'} \in \cup_{k'=1}^{k} X_{i'}(k') \forall i' \in C_i} \sum_{i' \in C_i} \left\{ P_{i'}(\underline{x}_{i'}) - \left(\sum_{i \in L_{i'}} \lambda_l \right) x_{i'} \right\} \tag{10.111}$$
$$= \sum_{i' \in C_i} \max_{\underline{x}_{i'} \in \bigcup_{k'=1}^{k} X_{i'}(k')} \left\{ P_{i'}(\underline{x}_{i'}) - \left(\sum_{i \in L_{i'}} \lambda_l \right) x_{i'} \right\} \tag{10.112}$$

$$= \sum_{i' \in C_i} \max_{k' \le k} \max_{x' \in x_{i'}(k')} \left\{ P_{i'}(\underline{x}_{i'}) - \left(\sum_{i \in L_{i'}} \lambda_l \right) x_{i'} \right\} \tag{10.113}$$

$$= \sum_{i' \in C_i} \max_{k} \left\{ \max_{x' \in x_i(k')} P_{i'}(\underline{x}_{i'}) - \left(\sum_{i \in L_{i'}} \lambda_l \right) \max_{\underline{x}_i \in x_{i'}(k')} x_{i'} \right\} \tag{10.114}$$

$$= \sum_{i' \in C_i} \max_{k' \le k} \left\{ P_{i'}(k') - \left(\sum_{i \in L_{i'}} \lambda_l \right) b_{k'}^g \right\} \tag{10.115}$$

Relation (10.108) follows from the definition of $p_i(k)$ and (10.109) follows from (10.107). Relation (10.110) follows from (10.106). Relation (10.111) follows from the fact that neither the term $\sum_{i' \in C_i} \{P_{i'}(\underline{x}_{i'}) - (\sum_{i \in L_{i'}} \lambda_l) x_{i'}\}$ nor the other constraints in (10.110) depends on the variable x_i. Relation (10.112) follows from the fact that the constraint set $\{\underline{x}_{i' \in \bigcup_{k'=1}^{k}} X_{i'}(k') \forall i' \in C_i\}$ and the objective function $\sum_{i' \in C_i} \{P_{i'}(\underline{x}_{i'}) - \sum_{l \in L_{i'}} \lambda_l) x_{i'}\}$ are both separable with respect to the variable vectors $\underline{x}_{i'} i' \in C_i$. In the above equations the constraint $k' \in \{1, \ldots, k\}$ is represented as $k' \le k$. Relation (10.115) follows from the definitions of $p_i(k')$ and $X_i(k')$. Relation (10.115) shows that the CMPs for a source/junction node i can be expressed in terms of the CMPs of its children nodes. This fact allows us to find $p_{s^g}(K^g)$ using a dynamic programming approach (index evolving utility). In other words, we can calculate the CMPs with a bottom-up approach: first, we compute the CMPs at the receiver nodes, then at junction nodes that are one level above that, and so on, until we reach the source node. Note that the dynamic programming computations at the nodes in any particular level of the tree can be executed simultaneously. This parallelism inherent in the structure of the dynamic program can be used to solve the group profit maximization problem in a single round-trip time.

10.8 QoS OPTIMIZATION IN TIME-VARYING CHANNELS

Problems and methodologies covered in Sections 10.6 and 10.7 are combined in this section to discuss the delay tradeoffs for utility optimal scheduling in a general network with time-varying channels, thus involving dynamic programming.

10.8.1 The system model

We start by considering first a one-hop data network with M links that operates in slotted time with timeslots $t \in \{0, 1, 2, \ldots\}$, where every timeslot data randomly enters the network. In the sequel we will use the following terminology and definitions:

$A_m(t)$, *the amount of new data over link* m *during slot* t
$\lambda_m = E\{A_m(t)\}$, *arrival rates (for* $m \in \{1, \ldots, M\}$*)*
$\boldsymbol{\lambda} = (\lambda_1, \ldots, \lambda_M)$, *vector of arrival rates*
$L_m(t)$, *amount of data currently stored in the type* m *transport layer storage reservoir*
$R_m(t)$, *the amount of type* m *data allowed to enter the network on slot* t *by flow control decisions,*
$R_m(S) \le A_m(t) + L_m(t)$
$\mu_m(t)$, *transmission rate over link* m *during slot* t
$U_m(t)$, *amount of type* m *data in network layer queue* m *at the beginning of slot* t*. The process* $U_m(t)$ *thus evolves as*

$$U_m(t+1) = \max[U_m(t) - \mu_m(t), 0] + R_m(t)$$

$\vec{S}(t) = (S_1(t), \ldots, S_M(t))$, *channel state vector at time* t
$\Omega_{\vec{S}}$, *set of all feasible transmission rate vectors* $\boldsymbol{\mu} = (\mu_1, \ldots, \mu_M)$ *available for resource allocation decisions when* $\vec{S}(t) = S$
Λ, *network capacity region, the closure of all arrival rate vectors* $\boldsymbol{\lambda}$ *that the network can stably support. An input rate vector* $\boldsymbol{\lambda}$ *is in the capacity region* Λ *if and only if there exists a stationary randomized resource allocation algorithm that chooses transmission rates* $\boldsymbol{\mu}(t)$ *in* $\Omega_{\vec{S}(t)}$ *based only on the current channel state* $\vec{S}(t)$ *and satisfies, for all slots* t, $E\{\mu_m(t)\} = \lambda_m$ *for all* $m \in \{1, \ldots, M\}$
r_m, *long-term rate that data from stream* $A_m(t)$ *is delivered to the network by its flow controller,* $\vec{r} = (r_1, \ldots, r_M); r_m \leq \lambda_m$ *for all* m
$\vec{r} \in \Lambda$, *to ensure stability*
$g_m(r)$, *utility function for stream* m
g^*, *optimal network utility, solution of the following problem:*

$$\begin{aligned} \text{Maximize} \quad & \sum_{m=1}^{M} g_m(r_m) \\ \text{subject to} \quad & \vec{r} \in \Lambda \\ & r_m \leq \lambda_m \text{ for all } m \in \{1, \ldots, M\} \end{aligned}$$

One should be aware of the fact that no control algorithm that stabilizes the network can achieve an overall utility larger than g^*. The objective is to develop a joint algorithm for flow control, routing and resource allocation that stabilizes the network and yields a total utility that can be pushed arbitrarily close to the optimal value g^*, with a corresponding optimal tradeoff in end-to-end network delay.

Because the capacity region Λ is compact and the utility functions are continuous, there exists an optimal rate vector $\vec{r}^*$ (referred to as an *optimally fair operating point*) such that $\sum_m g_m(r_m^*)$.

If $\overline{\lambda}$ is strictly interior to the capacity region, then $\vec{r}^* = \boldsymbol{\lambda}$, and hence the exact optimal utility can be achieved simply by stabilizing the network. This can be accomplished with finite average delay (for both one-hop and multihop networks). Hence, fundamental utility-delay tradeoff only makes sense in the case when the input rate vector is either on the boundary or strictly outside Λ.

In the next section, we focus on the case where the rate vector is strictly outside Λ. More precisely, we shall assume there exists a positive value $\varepsilon_{\max}$ and an optimally fair operating point $\vec{r}^*$ such that $\lambda_m \geq r_m^* + \varepsilon_{\max}$ for all sessions $m \in \{1, \ldots, M\}$. This would be a scenario, for example, where all sessions have infinite storage reservoirs that are infinitely backlogged so that there is always data to send.

10.8.2 Dynamic control algorithm

To discuss the control algorithm, we first represent the optimization problem in an equivalent form:

$$\begin{aligned} \text{Maximize} \quad & \sum_{m=1}^{M} g_m(\gamma_m) \\ \text{subject to} \quad & r_m \geq \gamma_m \text{ for all } m \\ & \vec{r} \in \Lambda \\ & r_m \leq \lambda_m \text{ for all } m \end{aligned} \tag{10.116}$$

The additional linear constraint $r_m \geq \gamma_m$ acts to decouple the throughput values $\vec{r}$ from the new optimization variables $\boldsymbol{\gamma}$.

If $\overline{\boldsymbol{\mu}}_m$ is the time-average transmission rate offered over link m and $\hat{\mu}_m$ the time-average rate that actual data are delivered over link m then $\hat{\mu}_m \leq \overline{\boldsymbol{\mu}}_m$, where strict inequality is possible due to 'edge effects' that arise when the queue backlog $U_m(t)$ is frequently zero or near-zero so that the offered transmission rate $\mu_m(t)$ is underutilized. The time-average departure rate of bits from link m must be less than or equal to the admitted input rate to this link, and hence $r_m \geq \hat{\mu}_m$. Only if we can by some means ensure that edge events occur very infrequently is $\hat{\mu}_m \approx \overline{\boldsymbol{\mu}}_m$, and hence for some small value $\delta > 0$, we have $r_m + \delta \geq \overline{\boldsymbol{\mu}}_m$.

Therefore, if we can design a stabilizing control algorithm that maximizes the utility function, keeps queues far away from the edge region and satisfies $\overline{\boldsymbol{\mu}}_m \geq \gamma_m$ for all m, then from $r_m + \delta \geq \overline{\boldsymbol{\mu}}_m$ we have that the constraint $r_m \geq \gamma_m$ will be within δ of being satisfied, and so the resulting network utility will be close to the optimal utility g^*. Proximity to the optimal solution thus depends entirely on the ability to avoid edge effects.

To design such a control policy, Reference [67] uses a combination of *stochastic optimal Lyapunov scheduling* [68–70], together with the concept of *buffer partitioning* from Reference [71]. For a threshold parameter $Q > 0$, the algorithm decreases the queue backlog $U_m(t)$ when this backlog is greater than or equal to Q, and *increases* the queue backlog when $U_m(t) < Q$. This ensures stability while also keeping the backlog sufficiently far from the edge region.

If $\vec{U}(t) = (U_1(t), \ldots, U_M(t))$ represents the vector of current queue backlogs, and assuming that these queues have maximum buffer size Q, the queueing dynamics are modified as

$$U_m(t+1) = \min[\max[U_m(t) - \mu_m(t), 0] + R_m(t), Q] \tag{10.117}$$

Thus, $U_m(t) \leq Q$ for all t. Any excess data admitted to the network layer according to the $R_m(t)$ process but that does not fit into the network layer queue $U_m(t)$ (due to the finite buffer constraint) is placed back into the transport layer storage, or dropped if there is no room for transport layer storage.

For given parameters $Q > 0, \omega > 0$, the nonnegative *Lyapunov function* is defined as

$$L(\vec{U}) \triangleq \sum_{m=1}^{M} (e^{\omega(Q-U_m)} - 1); U_m \leq Q \tag{10.118}$$

This function achieves its minimum value of $L(\vec{U}) = 0$ when $U_m = Q$ for all m, and increases exponentially when the backlog in any queue deviates from the Q threshold. Minimizing the drift of this Lyapunov function from one timeslot to the next thus tends to maintain all queue backlogs near the threshold Q.

Next, we must ensure that the constraints $\overline{\boldsymbol{\mu}}_m \geq \gamma_m$ are satisfied. For this, we use the concept of a *virtual queue* [69]. For each session $m \in \{1, \ldots, M\}$, a virtual queue $Z_m(t)$ is defined with a dynamic update equation as

$$Z_m(t+1) = \max[Z_m(t) - \mu_m(t), 0] + \gamma_m(t) \tag{10.119}$$

where $\mu_m(t)$ and $\gamma_m(t)$ are control decision variables used by the network controller. Equation (10.119) can be viewed as the dynamic equation of a discrete-time queue with input process $\gamma_m(t)$ and server process $\mu_m(t)$.

Assume that arrivals to any link are bounded by a value $A_{\max}$ every slot, so that $A_m(t) \leq A_{\max}$ for all t. Let $R_{\max}$ be any value greater than or equal to $A_{\max}$. Recall that $L_m(t)$ is the current data in transport layer queue m. Starting from Lyapunov function drift minimization the following control algorithm, defined in terms of positive constants ω, Q, V, is defined as in Reference [67].

Initialize all virtual queues so that $Z_m(0) = 0$ *for all* m.
In every timeslot:
Flow control: the flow controller for each link m *observes* $U_m(t)$ *and* $Z_m(t)$ *and makes these decisions*:

(1) *Choose* $R_m(t) = \min[A_m(t) + L_m(t), R_{\max}]$.

(2) *Choose* $\gamma_m(t) = \gamma_m$, *where* γ_m *solves*:

$$\text{Maximize } V g_m(\gamma_m) - 2Z_m(t)\gamma_m$$
$$\text{subject to } 0 \le \gamma_m \le R_{\max}$$

The virtual queues $Z_m(t)$ *are then updated according to* (10.119), *using the* $\gamma_m(t)$ *values computed above and the* $\mu_m(t)$ *values computed by the following resource allocation algorithm. The actual queues* $U_m(t)$ *are updated according to the finite buffer queueing law (10.117).*

Any admitted data that would cause the network layer queue to exceed its buffer constraint Q *is placed back in the transport layer reservoir, or dropped if there is no room for storage.*

Resource allocation: every timeslot t, *the network controllers observe the current channel state vector* $\vec{S}(t)$ *and allocate transmission rates* $\vec{\mu}(t) = (\mu_1(t), \ldots, \mu_m(t))$, *where* $\vec{\mu}(t)$ *solves the following optimization problem:*

$$\text{Maximize } \sum_{m=1}^{M} W_m(t)\mu_m$$
$$\text{subject to } \vec{\mu} \in \Omega_{\vec{S}(t)}$$

where $W_m(t) = -e^{\omega}(Q - U_m(t)) + (2/\omega)Z_m(t)$

Let $\varepsilon_{\max}$ be the largest value of ε that satisfies $\varepsilon \le \min[\lambda_m/2, \lambda_m - r_m^*]$ ($\vec{r}^*$ represent an optimally fair operating point), for all $m \in \{1, \ldots, M\}$, and assume that $\varepsilon_{\max} > 0$. We also define $\delta_{\max}$ as the largest possible change in the individual queue backlog at any link during a timeslot $\delta_{\max} \triangleq \max[R_{\max}, \mu_{\max}]$. For a given set of parameters $V > 0$, $0 < \varepsilon \le \varepsilon_{\max}$, any positive value ω that satisfies $\omega\delta_{\max}e^{\omega\delta_{\max}} \le 2\varepsilon/\delta_{\max}$ and $Q \triangleq 2\log(V)/\omega$, the above algorithm stabilizes all actual and virtual queues of the system, and yields [67] $U_m(t) \le Q = O(\log(V))$ for all t and $\liminf_{t\to\infty} \sum_m g_m(\bar{r}_m(t)) \ge g^* - O(1/V)$. Because V is an arbitrary control parameter, it can be made as large as desired, pushing total system utility arbitrarily close to the optimal utility g^* with a corresponding increase in average delay.

In the case of a *multihop network* with N nodes data arrive randomly at each node and must be delivered to a specific other node. All data destined for a particular node $c \in \{1, \ldots, N\}$ will be referred to as *commodity* c *data*, regardless of its source.

In the sequel we will use the following notation and terminology:

$A_n^{(c)}(t)$, *amount of new commodity* c *bits that exogenously enter node* n *during time slot* t.

$$\lambda_n^{(c)} = E\{A_n^{(c)}(t)\}$$

$\underline{\lambda} = (\lambda_n^{(c)})$, *arrival rate matrix*
$L_n^{(c)}(t)$, *commodity* c *data in the transport layer reservoir at node* n
$R_n^{(c)}(t)$, *the amount of commodity* c *data admitted to the network layer at node* n

$R_n^{(c)}(t) \le A_n^{(c)}(t) + L_n^{(c)}(t)$ *for all* t, *flow control decision constraints*
$\underline{S}(t) = (S_{ab}(t))$, *channel state matrix, specifying the state of all potential links* (a, b) *between each node pair* (a, b)
$\underline{\mu}(t) = (\mu_{ab}(t))$, *current transition rate matrix*
$\underline{\mu}(t) \in \Omega_{\underline{S}(t)}$
$\Omega_{\underline{S}(t)}$, *set of feasible transmission rate matrix options under channel state* $\underline{S}(t)$
$\mu_{ab}^{(c)}(t)$, *routing control variables, the transmission rate offered to commodity* c *data over link* (a, b) *during slot* t
These new control variables satisfy the following constraints: $\sum_c \mu_{ab}^{(c)}(t) \le \mu_{ab}(t)$ *for all* (a, b) *and* $\mu_{ab}^{(c)}(t) = 0$ *if* $(a, b) \notin L_c$
L_c, *the set of all links acceptable for commodity* c *data to traverse*
$U_n^{(c)}(t)$, *the amount of commodity* c *bits currently stored in network node* n *during slot* t

$$U_n^{(c)}(t+1) \le \max[U_n^{(c)}(t) - \sum_b \mu_{nb}^{(c)}(t), 0] + R_n^{(c)}(t) + \sum_a \mu_{an}^{(c)}(t)$$

Each network queue can receive both exogenous and endogenous data.
$\boldsymbol{\mu}_{ab}^{(c)}(t)$ *may be less than the actual commodity* c *data transmitted over link* (a, b) *during slot* t *if there is not enough of this commodity to transmit.*
$U_n^{(n)}(t) = 0$ *for all* t, *as data that reaches the destination are removed from the network.*
K, *set of all* (n, c) *pairs for which it is possible to have a nonzero* $U_n^{(c)}(t)$ *value* $|K|$, *number of such pairs*
$\lambda_n^{(c)} = 0$ *whenever* $(n, c) \notin K$
Λ, *the network capacity region consisting of all stabilizable rate matrices* $\underline{\lambda}$
$g_n^{(c)}(r)$, *utility functions for commodity* c *in node* n
Optimization process:

$$\text{Maximize} \sum_{(n,c)\in K} g_n^{(c)}(r_n^{(c)})$$

$$\text{subject to } (r_n^{(c)}) \in \Lambda \text{ and } r_n^{(c)} \le \lambda_n^{(c)} \text{ for all } (n, c) \in K$$

$(r_n^{*(c)})$, *an optimally fair throughput matrix that solves this problem* $g^* \triangleq \sum_{(n,c)\in K} g_n^{(c)}(r_n^{*(c)})$
$\gamma_n^{(c)}$, *auxiliary variables to modify the optimization problem to maximizing* $\sum_{(n,c)\in K} g_n^{(c)}(\gamma_n^{(c)})$, *with a new constraint* $r_n^{(c)} \ge \gamma_n^{(c)}$

$$r_n^{(c)} + \sum\nolimits_a \boldsymbol{\mu}_{an}^{(c)} \ge \sum_b \hat{\mu}_{nb}^{(c)}, \text{ constraint}$$

$\overline{\boldsymbol{\mu}}_{ab}^{(c)}, \hat{\mu}_{ab}^{(c)}$, *the time-average transmission rate offered to commodity* c *data over link* (a, b) *and the time-average rate of the actual commodity* c *data transferred over this link, respectively*
$\overline{\boldsymbol{\mu}}_{ab}^{(c)} \approx \hat{\mu}_{ab}^{(c)}$, *if edge events are rare and then the constraint* $r_n^{(c)} \ge \gamma_n^{(c)}$ *is close to being satisfied provided that we ensure for all* $(n, c) \in K$

$$\sum_b \overline{\boldsymbol{\mu}}_{nb}^{(c)} - \sum_a \mu_{an}^{(c)} \ge \gamma_n^{(c)}$$

$Z_n^{(c)}(t)$, *virtual queues for all* $(n, c) \in K$, *where* $Z_n^{(c)}(0) = 0$ *evolves as*

$$Z_n^{(c)}(t+1) = \max[Z_n^{(c)}(t) - \sum_b \boldsymbol{\mu}_{nb}^{(c)}(t), 0] + \gamma_n^{(c)}(t) + \sum_a \mu_{an}^{(c)}(t) \tag{10.120}$$

For given parameters $Q > 0, \omega > 0$, we define the following *bimodal Lyapunov function*:

$$L(\underline{U}) \triangleq \sum_{(n,c)\in K(c)} \left(e^{\omega(Q-U_n^{(c)})} + e^{\omega(U_n^{(c)}-Q)} - 2 \right) \tag{10.121}$$

The function has its minimum value of $L(\underline{U}) = 0$ when $U_n^{(c)} = Q$ for all $(n, c) \in K$ and increases exponentially when the backlog in any queue deviates from the Q threshold either to the right or to the left. For $\underline{X} \triangleq [\underline{U}, \underline{Z}]$, representing the combined system state, we define the Lyapunov function

$$\Psi(\underline{X}) \triangleq L(\underline{U}) + \sum_{(n,c)\in K} (Z_n^{(c)})^2$$

For the specification of the control algorithm we define the indicator functions $1_n^{(c)L}(t)$ and $1_n^{(c)R}(t)$ for all $(n, c) \in K$ as

$$1_n^{(c)L}(t) \triangleq \begin{cases} 1, & U_n^{(c)}(t) < Q \\ 0, & U_n^{(c)}(t) \geq Q \end{cases}$$

and $1_n^{(c)R}(t) = 1 - 1_n^{(c)L}(t)$. Designing a control policy to minimize the Lyapunov function drift every time slot leads to the following algorithm [67]:

Multihop Control Algorithm
Flow control: the flow controller at each node n observes $U_n^{(c)}(t)$ *and* $Z_n^{(c)}(t)$ *and makes the following decisions for each commodity c such that* $(n, c) \in K$:

(1) *If* $U_n^{(c)}(t) \geq Q$, *then choose* $R_n^{(c)}(t) = 0$. *Next, list all remaining (n, c) streams at node n in order of increasing* $U_n^{(c)}(t)$, *and sequentially assign* $R_n^{(c)}(t)$ *to be as large as possible for the commodities c with the smallest values of* $U_n^{(c)}(t)$, *having in mind that*

$$R_n^{(c)}(t) \leq A_n^{(c)}(t) + L_n^{(c)}(t), \text{ subject to the constraint } \sum_c R_n(t) \leq R_{\max}$$

(2) *Choose* $\gamma_n^{(c)}(t) = \gamma_n^{(c)}$, *where* $\gamma_n^{(c)}$ *solves*

$$\begin{aligned} &\text{Maximize } V g_n^{(c)}(\gamma_n^{(c)}) - 2Z_n^{(c)}(t)\gamma_n^{(c)} \\ &\text{subject to } 0 \leq \gamma_n^{(c)} \leq R_{\max} \end{aligned}$$

Update the virtual queues $Z_n^{(c)}(t)$ *according to (10.120), using the* $\gamma_n^{(c)}(t)$ *values computed above and the* $\boldsymbol{\mu}_{an}^{(c)}(t)$, $\boldsymbol{\mu}_{nb}^{(c)}(t)$ *values computed by the following routing and resource allocation algorithms.*
Routing: the controller at each node n observes the queue backlogs of its neighboring nodes, and for each neighbor node b and each commodity c such that $(n, b) \in L_c$, *it computes* $W_{nb}^{(c)}(t)$, *defined as*

$$\begin{aligned} W_{nb}^{(c)}(t) \triangleq &[1_n^{(c)R}(t) e^{\omega(U_n^{(c)}(t)-Q)} - 1_b^{(c)R}(t) e^{\omega(U_b^{(c)}(t)-Q)}] \\ &-[1_n^{(c)L}(t) e^{\omega(Q-U_n^{(c)}(t))} - 1_b^{(c)L}(t) e^{\omega(Q-U_b^{(c)}(t))}] + \frac{2}{\omega}[Z_n^{(c)}(t) - Z_b^{(c)}(t)] \end{aligned}$$

with $1_b^{(b)R}(t) = 1_b^{(b)L}(t) = 0$, $Z_b^{(b)}(t) = 0$ *for all t and* $b \in \{1, \ldots, N\}$.
The optimal commodity $c_{nb}^*(t)$ *is then chosen as the commodity* c^* *that maximizes* $W_{nb}^{(c)}(t)$ *over all* $c \in \{1, \ldots, N\}$ *such that* $(n, b) \in L_c$ *(ties are broken arbitrarily). For* $W_{nb}^*(t) \triangleq \max[W_{nb}^{(c^*)}(t), 0]$

routing variables are then chosen as

$$\mu_{nb}^{(c)}(t) = \begin{cases} 0, & \text{if } W_{nb}^{*}(t) = 0 \text{ or } c \neq c_{nb}^{*}(t) \\ \mu_{nb}^{(t)}, & \text{otherwise} \end{cases}$$

where the transmission rates $\boldsymbol{\mu}_{nb}(t)$ *are computed by the resource allocation algorithm below. Resource allocation: every timeslot t, the network controllers observe the current channel state matrix* $\underline{S}(t)$ *and allocate transmission rates* $\boldsymbol{\mu}_{ab}(t) = \boldsymbol{\mu}_{ab}$, *where* $\boldsymbol{\mu}_{ab}$ *solves the following optimization problem:*

$$\text{Maximize} \sum_{ab} W_{ab}^{*}(t)\boldsymbol{\mu}_{ab}$$

$$\text{subject to } (\mu_{ab}) \in \boldsymbol{\Omega}_{S(t)}$$

$W_{ab}^{*}(t)$ *weights are obtained from the routing algorithm.*

Assuming that exogenous arrivals to any node are bounded by a value $A_{\max}$ on every timeslot, so that $\sum_c A_n^{(c)}(t) \leq A_{\max}$ for all $n \in \{1, \ldots, N\}$, we define $R_{\max}$ to be any value greater than or equal to A_{ax}. In addition, we assume that there is an optimally fair operating point $(r_n^{*(c)})$ with $r_n^{*(c)} > 0$ for all $(n, c) \in K$, and that the input rate matrix $\underline{\lambda}$ strictly dominates this operating point. Define $\varepsilon_{\max}$ as the largest value of ε such that $\varepsilon \leq r_n^{*(c)} \leq \lambda_n^{(c)} - \varepsilon$ for all sessions $(n, c) \in K$ and $\delta_{\max}$ as the largest possible change in the total queue backlog at any node during a timeslot $\delta_{\max} = \max \triangle(R_{\max} + \mu_{\max}^{in}, \mu_{\max}^{out})$. The performance of the algorithm depends on the time averages $\overline{U}_n^{(c)}(t)$ and $\overline{r}_n^{(c)}(t)$ defined as $\overline{U}_n^{(c)}(t) \triangleq \frac{1}{t} \sum_{\tau=0}^{t-1} E\{U_n^{(c)}(\tau)\}$ and $\overline{r}_n^{(c)}(t) \triangleq \frac{1}{t} \sum_{\tau=0}^{t-1} E\{R_n^{(c)}(\tau)\}$

For parameters V, ε such that $V > 0$ and $0 < \varepsilon \leq \varepsilon_{\max}$, ω that satisfies $\omega\delta_{\max} e^{\omega\delta_{\max}} \leq \varepsilon/\delta_{\max}$ and $Q = -\log(V)\omega$, the algorithm stabilizes all actual and virtual queues of the system and provides [67]

$$\limsup_{t\to\infty} \frac{1}{|K|} \sum_{(n,c)\in K} \overline{U}_n^{(c)}(t) \leq O(\log(V))$$

$$\liminf_{t\to\infty} \sum_{(n,c)\in K} g_n^{(c)}(\overline{r}_n^{(c)}(t)) \geq g^* - O(1/V) \tag{10.122}$$

10.9 NETWORK OPTIMIZATION BY GEOMETRIC PROGRAMMING

Geometrical programming (GP) belongs to a class of nonlinear, nonconvex optimization problems that has been used to solve a number of problems in wireless communications due to its useful theoretical and computational properties. GP can be turned into a convex optimization problem; hence a local optimum is also a global optimum, Lagrange duality gap is zero under mild conditions and a global optimum can always be computed very efficiently.

There are two equivalent forms of GP: the standard form and the convex form. The first is a constrained optimization of a type of function called posynomial and the second form is obtained from the first through a logarithmic change of variable.

A monomial function is defined as $f : \mathbf{R}_{++}^n \to \mathbf{R}$:

$$f(\mathbf{x}) = d x_1^{a^{(1)}} x_2^{a^{(2)}} \cdots x_n^{a^{(n)}} \tag{10.123a}$$

where the multiplicative constant $d \geq 0$ and the exponential constants $a^{(j)} \in \mathbf{R}$, $j = 1, 2, \ldots, n$. A sum of monomials is called a posynomial:

$$f(\mathbf{x}) = \sum_{k=1}^{K} d_k x_1^{a_k^{(1)}} x_2^{a_k^{(2)}} \cdots x_n^{a_k^{(n)}} \tag{10.123b}$$

where $d_k \geq 0, k = 1, 2, \ldots, K$ and $a_k^{(j)} \in \mathbf{R}$, $j = 1, 2, \ldots, n, k = 1, 2, \ldots, K$.

GP in standard form. This consists of minimizing a posynomial subject to posynomial upper bound inequality constraints and monomial equality constraints, and can be formally expressed as

$$\begin{aligned} &\text{Minimize } f_0(\mathbf{x}) \\ &\text{subject to } f_i(\mathbf{x}) \leq 1, i = 1, 2, \ldots, m \\ &\qquad\qquad h_l(\mathbf{x}) = 1, l = 1, 2, \ldots, M \end{aligned} \tag{10.124}$$

In problem (10.123), $f_i, i = 0, 1, \ldots, m$, are posynomials, $f_i(\mathbf{x}) = \sum_{k=1}^{K_i} d_{ik} x_1^{a_{ik}^{(1)}} x_2^{a_{ik}^{(2)}} \ldots x_n^{a_{ik}^{(n)}}$ and $h_l, l = 1, 2, \ldots, M$ are monomials and $h_l(\mathbf{x}) = d_l x_1^{a_l^{(1)}} x_2^{a_l^{(2)}} \ldots x_n^{a_l^{(n)}}$.

GP in convex form. Since posynomials are not convex functions, GP in standard form is not a convex optimization problem. By introducing the following change of the variables, $y_i = \log x_i, b_{ik} = \log d_{ik}, b_l = \log d_l$, and a logarithmic change of the function values, we have an equivalent problem in $\boldsymbol{y}$:

$$\begin{aligned} &\text{Minimize } p_0(\mathbf{y}) = \log \sum_{k=1}^{K_0} \exp(\mathbf{a}_{0k}^{\mathrm{T}} \mathbf{y} + b_{0k}) \\ &\text{subject to } p_i(\mathbf{y}) = \log \sum_{k=1}^{K_l} \exp(\mathbf{a}_{ik}^{\mathrm{T}} \mathbf{y} + b_{ik} \leq 0, \forall i \\ &\qquad\qquad q_l(\mathbf{y}) = a_l^{\mathrm{T}} \mathbf{y} + b_l = 0, l = 1, 2, \ldots, M \end{aligned} \tag{10.125}$$

Since it can be verified that the log-sum-exponent function is convex, problem (10.125) is referred to as GP in *convex form*, which is a convex optimization problem. A detailed tutorial of GP and a comprehensive survey of its recent applications to communication systems can be found in Reference [72].

10.9.1 Power control by geometric programming: high SNR

In this section we consider a wireless (cellular or multihop) network with n logical transmitter/receiver pairs. Transmit powers are denoted as $P_1, \ldots, P_n$. In the cellular uplink case, all logical receivers reside in the base station. In the multihop case, since the transmission environment can be different on the links comprising an end-to-end path, power control schemes must consider each link along a flow's path.

In Rayleigh fading, the power received from transmitter j at receiver i is given by $G_{ij} F_{ij} P_j$, where $G_{ij} \geq 0$ represents the path gain. It may also include the antenna gain and coding gain. G_{ij} is often modeled to be proportional to $d_{ij}^{-\gamma}$, where d_{ij} denotes distance, γ is the power fall-off factor and the F_{ij} model Rayleigh fading and are independent and exponentially distributed with unit mean. The distribution of the received power from transmitter j at receiver i is then exponential with mean value $E[G_{ij} F_{ij} P_j] = G_{ij} P_j$. The SIR for the receiver on logical link i is

$$SIR_i = y_i = \frac{P_i G_{ii} F_{ii}}{\sum_{j \neq i}^{N} P_j G_{ij} F_{ij} + n_i} \tag{10.126}$$

where n_i is the noise power for receiver i.

The constellation size M used by a link can be closely approximated for M-ary quadrature amplitude modulation (MQAM) modulations as follows: $M = 1 + (-\phi_1 y)/[\ln(\phi_2 e)]$, where e is the bit error rate and ϕ_1, ϕ_2 are constants that depend on the modulation type [73]. Defining T as the symbol period and $K = (-\phi_1)/[\ln(\phi_2 e)]$ leads to an expression of the data rate R_{iota} on the ith link as a function of the SIR y as $R_i = \log_2(1 + Ky_i)/T$. When Ky is much larger than 1, it can be approximated as $R_i = \log_2(Ky_i)/T$. This approximation is reasonable either when the signal level is much higher than the interference level or, in CDMA systems, when the spreading gain is large. For notational simplicity in the rest of this section, we redefine G_{ii} as K times the original G_{ii}, thus absorbing constant K into the definition of SIR. The aggregate data rate for the system can then be written as

$$R_{\text{system}} = \sum_i R_i = (1/T) \log_2 \left(\prod_i y_i \right) \tag{10.127}$$

Outage probability is another parameter for QoS specification in wireless networks. A channel outage is considered when the received SIR falls below a given threshold value y_{th}, often computed from the BER requirement. In a high SIR environment the ith link outage probability is

$$P_{o,i} = \text{Prob}\{y_i \le y_{th}\} = \text{Prob}\{G_{ii} F_{ii} P_i \le y_{th} \sum_{j \ne i} g_{ii} F_{ij} P_j\}$$

The outage probability can be expressed as [74]

$$P_{o,i} = 1 - \prod_{j \ne i} 1/[1 + y_{th} G_{ij} P_j/(G_{ll} P_l)]$$

which means that the upper bound $P_{o,i} \le P_{o,i,\max}$ can be written as an upper bound on a posynomial in $\mathbf{P}$:

$$\prod_{j \ne i} [1 + y_{th} G_{ij} P_j/(G_{ii} P_l)] \le (1 - P_{o,i\,\max}) \tag{10.128}$$

The following constrained problem of maximizing the SIR of a particular user i^* is a GP:

$$\begin{aligned} &\text{Maximize } R_{\iota^*}(\mathbf{P}) \\ &\text{subject to } R_l(\mathbf{P}) \ge R_{\iota,\min}, \ \forall i \\ &\qquad P_{i1} G_{i1} = P_{i2} G_{i2} \\ &\qquad 0 \le P_i \le P_{i,\max}, \ \forall i \end{aligned} \tag{10.129}$$

The first constraint, equivalent to $y_i \ge y_{i,\min}$, sets a floor on the SIR of other users and protects these users from user i^* increasing its transmit power excessively. The second constraint reflects the classical power control criterion in solving the near–far problem in CDMA systems: the expected received power from one transmitter i_1 must equal that from another i_2. The third constraint is system limitations on transmit powers. All constraints can be verified to be inequality upper bounds on posynomials in the transmit power vector $\mathbf{P}$. On the system level, we have

$$\begin{aligned} &\text{Maximize } R_{\text{system}}(\mathbf{P}) \\ &\text{subject to } R_l(\mathbf{P}) \ge R_{i,\min}, \ \forall i \\ &\qquad P_{o,i}(\mathbf{P}) \le P_{o,i,\max}, \ \forall i \\ &\qquad 0 \le P_i \le P_{i,\max}, \ \forall i \end{aligned} \tag{10.130}$$

where the optimization variables are the transmit powers $\mathbf{P}$. The objective is equivalent to minimizing the posynomial $\prod_i ISR_i = \prod_i 1/y_i$. Each ISR is a posynomial in $\mathbf{P}$ and the product of posynomials is again a posynomial. The first constraint is from the data rate demand $R_{i,\min}$ by

each user. The second constraint represents the outage probability upper bounds $P_{o,i,\max}$. These inequality constraints put upper bounds on posynomials of $\mathbf{P}$. Thus problem (10.130) is indeed a GP and efficiently solvable for global optimality.

In wireless multihop networks, system throughput may be measured either by end-to-end transport layer utilities or by link layer aggregate throughput. GP application to the first approach has appeared in Reference [75], and Reference [76] presents the second approach, extending to the multihop case by indexing each logical link as i.

10.9.2 Power control by geometric programming: low SNR

If we maximize the total throughput R_{system} when SIR is low, the approximation of $\log(l + y)$ as $\log y$ does not hold. Unlike SIR, which is an inverted posynomial, $1 + SIR$ is not an inverted posynomial. Instead, $1/(1 + SIR)$ is a ratio between two posynomials:

$$\frac{f(\mathbf{P})}{g(\mathbf{P})} = \frac{\sum_{j \neq i} G_{ij} P_j + n_i}{\sum_j G_{ij} P_j + n_i} \tag{10.131}$$

Minimizing or upper bounding a ratio between two posynomials belongs to a truly nonconvex class of problems known as complementary GP [72], which is an intractable NP-hard problem.

An equivalent generalization of GP is signomial programming (SP) [72]. It consists of minimizing a signomial subject to upper bound inequality constraints on signomials, where a signomial $s(x)$ is a sum of monomials, possibly with *negative* multiplicative coefficients:

$$s(\mathbf{x}) = \sum_{i=1}^{N} c_i g_i(\mathbf{x})$$

where $\mathbf{c} \in \mathbf{R}^N$ and $g_i(\mathbf{x})$ are monomials.

The successive convex approximation method, in particular the logarithmic approximation, single condensation method and double condensation method for GP [72], are used to solve the above problem.

A limitation for GP-based power control in ad hoc networks without base stations is the need for centralized computation by interior point methods. The GP formulations of power control problems can also be solved in a distributed way. The basic idea is that each user solves its own local optimization problem and the coupling among users is taken care of by message passing among the users. The key step is to introduce auxiliary variables and to add extra equality constraints, thus transferring the coupling in the objective to coupling in the constraints, which can be solved by introducing 'consistency pricing', as discussed earlier in this chapter.

10.10 QoS SCHEDULING BY GEOMETRIC PROGRAMMING

In this section we present a throughput optimal scheduling policy called *queue proportional scheduling* (*QPS*) based on geometric programming GP. For fading broadcast channels (BCs), QPS finds a data rate vector such that the expected rate vector over all fading states is proportional to the current queue state vector and is on the boundary of the capacity region of a fading BC. The overall system is summarized in Figure 10.14.

In this section, a block fading channel is assumed where the fading state is constant over one scheduling period and takes a new independent state in the next slot. Both the transmitter and receivers are assumed to have perfect knowledge of CSI. In order to achieve the capacity region of a Gaussian BC, superposition coding is used at the transmitter in conjunction with successive interference cancellation at each receiver [77, 78]. With this optimal scheme, one user can remove

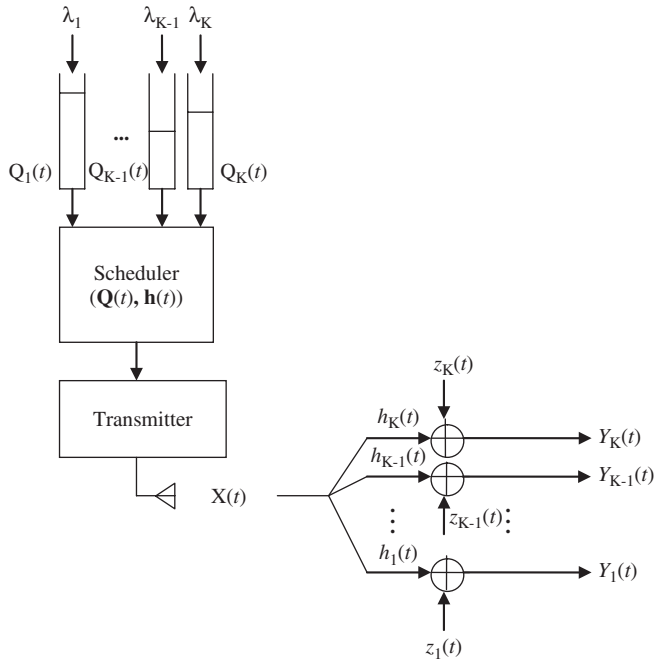

Figure 10.14 (a) Block diagram of the queuing system and scheduler. (b) Fading broadcast channel models.

the interference caused by other user messages encoded earlier. Consider a Gaussian broadcast channel with a single transmitter sending independent messages to K users over a two-sided bandwidth 2W. It is assumed that the transmitter has a peak power P. The received signal of user i is $Y_i(t) = h_i(t)X(t) + z_i(t), i = 1, \ldots, K$, where the transmitted signal $X(t)$ is composed of K independent messages, $h_i(t)$ is the complex channel gain of user and $z_i(t)$ are i.i.d. zero-mean Gaussian band-limited variables with power N_0W. If the channel gain is combined with the noise component by defining an effective noise $\tilde{z}_i(t) = z_i(t)/h_i(t)$, the equivalent received signal is given by $\tilde{Y}_i(t) = X(t) + \tilde{z}_i(t), \ i = 1, \ldots, K$, where the power of $\tilde{z}_i(t)$ conditioned on the channel gain is defined as $n_i(t) = N_0W/|h_i(t)|^2$. By assuming that $W = 1$ noise power, $\mathbf{n} = [n_1, n_2, \ldots, n_K]^{\mathrm{T}}$ will be used to denote a fading state. The ergodic capacity region of a fading BC is the set of all long-term average rate vectors achievable in a fading BC with an arbitrarily small probability of error. A power control policy $\wp$ over all possible fading states is defined as a function that maps from any fading state n to each user's transmit power $P_i(\mathbf{n})$. Let Ω denote the set of all power policies satisfying the sum power constraint P, which is given by $\Omega = \{\wp : \sum_{i=1}^{K} P_i(\mathbf{n}) \leq P$, for all $n\}$. For each fading state, the capacity region is achieved by encoding a message of the user with smaller effective noise power later [78]. With this optimal ordering, the capacity of user i for a fading state n is given by

$$R_i(\mathbf{P}(\mathbf{n})) = \log_2 \left[1 + P_i(\mathbf{n}) \Big/ \left(n_i + \sum_{k=1}^{K} P_k(\mathbf{n}) 1[n_i > n_k] \right) \right] \tag{10.132}$$

In Equation (10.132), $\mathbf{P}(\mathbf{n}) = [P_1(\mathbf{n}), P_2(\mathbf{n}), \ldots, P_K(\mathbf{n})]^{\mathrm{T}}$ and $1[\cdot]$ is the indicator function, which equals 1 if its argument is satisfied and 0 otherwise. The capacity region of a Gaussian BC

for the fading state $\mathbf{n}$ and transmit power P is $C(\mathbf{n}, P) = \{R_i : R_i \le R_i(\mathbf{P}(\mathbf{n})), i = 1, 2, \ldots, K,$ where $\sum_i P_i(\mathbf{n}) = P\}$.

If $C_{BC}(\wp) = \{R_i : R_i \le E_n[R_i(\mathbf{P}(\mathbf{n}))], i = 1, \ldots, K\}$ denotes the set of achievable rates averaged over all fading states for a power policy $\wp$ with the sum power constraint $P$and perfect CSI at the transmitter and receivers, the ergodic capacity region of a fading BC is given by [79] $C_{\text{erg}}(P) = \bigcup_{P\in\Omega} C_{BC}(P)$ where the region $C_{\text{erg}}(P)$ is convex.

We assume that K data sources generate packets according to independent Poisson arrival processes $\{A_i(t), i = 1, \ldots, K\}$, with $\lim_{t\to\infty} A_i(t)/t = a_i < \infty$ and $\text{var}[A_i(t + T) - A_i(t)] < \infty$ for $T < \infty$. Packet lengths in bits $\{B_i\}$ are i.i.d. exponentially distributed with $E[B_i] = \gamma_i < \infty$ and $E[B_i^2] < \infty$, and independent of packet arrival processes. Thus, user i's average arrival rate in bits is given by $\lambda_i = a_i\gamma_i$. The transmitter has K output queues assumed to have infinite capacity. Packets from source i enter queue i and wait until they are served to receiver i. The scheduling period is denoted by T_s and normalized to $T_s = 1$. The fading state is represented as $\mathbf{n}(t) = [n_1(t)n_2(t)\cdots n_K(t)]^{\text{T}}$, and the queue state vector is $\mathbf{Q}(t) = [Q_1(t)Q_2(t)\cdots Q_K(t)]^{\text{T}}$, where $Q_i(t)$ denotes the number of bits waiting to be sent to user i.

The allocated rate vector at time t is represented as $\mathbf{R}(t) = \mathbf{R}(\mathbf{n}(t), \mathbf{Q}(t)) = [R_1(\mathbf{n}(t), \mathbf{Q}(t))\cdots R_K(\mathbf{n}(t), \mathbf{Q}(t))]^{\text{T}}$, which is determined by the scheduler based on both fading and queue states. $\mathbf{R}(t)$ is achievable only when it is within the capacity region $C(\mathbf{n}(t), P)$.

If $Z_i(t)$ is the number of arrived bits at user i's queue in the time slot t, then, after a scheduling period, user i's queue state vector is equal to $Q_i(t + 1) = \max\{Q_i(t) - R_i(t), 0\} + Z_i(t)$. In this section, each scheduling policy has an explicit constraint of $\mathbf{R}(t) \preceq \mathbf{Q}(t)$; thus, the $\max\{\cdot, 0\}$ operation can be removed. With the overflow function defined by $g(M) = \limsup_{t\to\infty}(1/t)\int_t^0 1[Q_i(u) > M]\,\text{d}\tau$, queue i is said to be stable if $g(M) \to 0$ as $M \to \infty$. An arrival rate vector $\boldsymbol{\lambda}$ is feasible if there exists a feasible power and rate allocation policy that keeps all queues stable. A set of feasible arrival rate vectors forms the network capacity region and a scheduling method that achieves the entire network capacity region is called throughput optimal.

In this section, QPS is introduced and formulated via GP. At timeslot t, *maximum weight matching scheduling* (*MWMS*) assigns the following data rate vector $R_0(\mathbf{n}(t), \mathbf{Q}(t)) = \arg\max_{\mathbf{r}} Q'(t)^{\text{T}}\mathbf{r}$ such that $\mathbf{r} \in C(\mathbf{n}(t), P)$, where $\mathbf{r} = [r_1 r_2 \cdots r_K]^{\text{T}}$, $\mathbf{n}(t)$ is the fading state vector at time t and $\mathbf{Q}'(t) = [\beta_1 Q_1(t)\cdots\beta_K Q_K(t)]^{\text{T}}$. Parameter β_i is the user i's priority weight. Parameter $\beta_i = 1$ for all users if everyone has the same priority. This algorithm tends to allocate a higher data rate to the user with longer backlog or better channel conditions. By jointly considering queue and channel states, MWMS is shown to achieve the entire network capacity region [80].

The *QPS algorithm* allocates the data rate vector at timeslot t as

$$\mathbf{R}_{\text{QPS}}(\mathbf{n}(t), \mathbf{Q}(t)) \in C(\mathbf{n}(t), P)$$

such that

$$E_{\mathbf{n}(t)}[\mathbf{R}_{\text{QPS}}(\mathbf{n}(t), \mathbf{Q}(t))] = \mathbf{Q}'(t)\left(\max_{Q'(t)x\in C_{\text{erg}}(P)} x\right) \tag{10.133}$$

where x is a scalar. Assuming equal priority on each user, $\mathbf{Q}'(t) = \mathbf{Q}(t)$. Then the average rate vector under the QPS policy $E_{\mathbf{n}(t)}[\mathbf{R}_{QPS}(\mathbf{n}(t), \mathbf{Q}(t))]$ is proportional to the queue state vector and also lies on the boundary surface of the ergodic capacity region. As shown in Reference [81], each boundary point of $C_{\text{erg}}(P)$ in a fading BC is a solution to the optimization problem $\max_{\mathbf{r}} \boldsymbol{\mu}\cdot\mathbf{r}$, where $\mathbf{r} \in C_{\text{erg}}(P)$ for some $\boldsymbol{\mu} \in R_+^K$. When such $\boldsymbol{\mu}$ is given, $\mathbf{R}_{\text{QPS}}(\mathbf{n}(t), \mathbf{Q}(t))$ is a solution to the optimization problem $\max_{\mathbf{r}} \boldsymbol{\mu}\cdot\mathbf{r}$, where $\mathbf{r} \in C(\mathbf{n}(t), P)$ for any fading state $\mathbf{n}(t)$. Therefore, the data rate vector assigned by QPS at timeslot t can be expressed as $\mathbf{R}_{\text{QPS}}(\mathbf{n}(t), \mathbf{Q}(t)) = \arg\max_{\mathbf{r}} \boldsymbol{\mu}^{\text{T}}\mathbf{r}$ such that $\mathbf{r} \in C(\mathbf{n}(t), P)$. Under the QPS policy, $\boldsymbol{\mu}$ is determined based on the current queue state vector, as well as the ergodic capacity region of a fading BC. However, MWMS only considers the queue state vector in deriving the weight vector.

In Reference [82] the rate allocation of QPS is formulated via GP. The M most recent fading states $\{\mathbf{n}^{(1)}, \ldots, \mathbf{n}^{(M)}\}$ are sampled, with $\mathbf{n}^{(M)}$ denoting the current fading state $\mathbf{n}(t)$. For a family of M parallel Gaussian broadcast channels, such that in the mth component channel user i has effective noise variance $n_i^{(m)}$, rate $R_i^{(m)}$ and power $P_i^{(m)}$, QPS allocates the data rate vector $\mathbf{R}_{\text{QPS}}(\mathbf{n}^{(M)}, \mathbf{Q}(t))$, which is a solution of the following optimization problem:

$$\frac{1}{M}\sum_{m=1}^{M}\mathbf{R}_{\text{QPS}}(\mathbf{n}^{(m)}, \mathbf{Q}(t)) = \mathbf{Q}(t)\left(\max_{\mathbf{Q}(t)x\in C_{\text{erg}}(P)} x\right)$$
$$\mathbf{R}_{\text{QPS}}(\mathbf{n}^{(m)}, \mathbf{Q}(t)) \in C(\mathbf{n}^{(m)}, P) \text{ for all } m \tag{10.134}$$

The capacity region of the mth Gaussian BC is given by

$$C(\mathbf{n}^{(m)}, P) = \{R_{\pi_m(i)}^{(m)} \ : \ R_{\pi_m(i)}^{(m)} \le \log_2\left(1 + \frac{\alpha_{\pi_m}^{(m)}(i)P}{n_{\pi_m(i)}^{(m)} + \sum_{j<i}\alpha_{\pi_m(i)}^{(m)}P}\right), 1, 2, \ldots, K \tag{10.135}$$

where $\sum_i \alpha_{\pi_m(i)}^{(m)}$ and $\pi_m(\cdot)$ is the permutation such that $n_{\pi_m(1)}^{(m)} < n_{\pi_m(2)}^{(m)} < .. < n_{\pi(K)}^{(m)}, \cdots$ and $\alpha_{\pi_m(i)}^{(m)}$ is the fraction of the total transmit power used for the user $\pi_m(i)$ signal in the mth Gaussian BC. When $\mathbf{R}^{(m)}$ is on the boundary of the capacity region, solving the $\alpha_{\pi_m(i)}^{(m)}$ in terms of the rate vector $\mathbf{R}^{(m)}$ yields

$$\sum_{i=1}^{l}\alpha_{\pi_m(i)}^{(m)}P = \sum_{i=1}^{l}\left(n_{\pi_m(i)}^{(m)} - n_{\pi_m(i-1)}^{(m)}\right)$$
$$\times \exp\left(\log 2\sum_{j=i}^{l}R_{\pi_m(j)}^{(m)}\right) - n_{\pi_m(l)}^{(m)}, l = 1, \ldots, K \tag{10.136}$$

where $n_{\pi_m(0)}^{(m)} \equiv 0$. Equation (10.80) is equivalent to

$$C(\mathbf{n}^{(m)}, P) = \left\{R_{\pi_m(i)}^{(m)} \ : \ \sum_{i=1}^{K}\left(n_{\pi_m(i)}^{(m)} - n_{\pi_m(i-1)}^{(m)}\right) \times \exp\left(\log 2\sum_{j=i}^{K}R_{\pi_m(j)}^{(m)}\right) - n_{\pi_m(K)}^{(m)} \le P \text{ and}\right.$$
$$\left. R_{\pi_m(i)}^{(m)} \ge 0, i = 1, 2, \cdots, K\right\} \tag{10.137}$$

Using this relation, (10.134) can be converted into

$$\begin{aligned}
\text{Minimize} \quad & \log[\exp(-x)] \\
\text{subject to} \quad & \log\{\exp(-R_i^{(m)})\} \le 0, \forall i \text{ and } m \\
& \log\{\exp(-Q_i(t))\exp[R_i^{(M)}]\} \le 0, \ \forall i \\
& \log\sum_{i=1}^{K}\left(\frac{n_{\pi_m(i)}^{(m)} - n_{\pi_m(i-1)}^{(m)}}{P + n_{\pi_m(K)}^{(m)}}\right) \\
& \times \exp\left(\log 2\sum_{j=i}^{K}R_{\pi_m(j)}^{(m)}\right) \le 0, \forall m \\
& \mathbf{Q}(t)x - \frac{1}{M}\sum_{m=1}^{M}\mathbf{R}^{(m)} = 0
\end{aligned} \tag{10.138}$$

In problem (10.138), the second set of constraints is added to avoid allocating redundant power to some users with short queue lengths. If the optimization variable is defined as

$$\mathbf{y} = [x(\mathbf{R}^{(1)})^{\mathrm{T}} \cdots (\mathbf{R}^{(M)})^{\mathrm{T}}]^{\mathrm{T}} \in R_{+}^{(KM+1)}$$

problem (10.138) is a standard geometric program with the globally optimal solution

$$\mathbf{y}^* = [x^*(\mathbf{R}^{*(1)})^{\mathrm{T}} \cdots (\mathbf{R}^{*(M)})^{\mathrm{T}}]^{\mathrm{T}}$$

Then, the data rate vector supported under the QPS policy is $\mathbf{R}_{QPS}(\mathbf{n}^{(M)}, \mathbf{Q}(t)) = \mathbf{R}^{*(M)}$ and the corresponding power allocation can be obtained by solving Equation (10.136) for $m = M$.

10.10.1 Optimization of OFDM system by GP

The above GP formulation of QPS can be extended to OFDM systems in a fading BC. At tone l, M sampled fading state vectors $\{\mathbf{n}^{(l,1)}, \cdots, \mathbf{n}^{(l,M)}\}$ are collected with $\mathbf{n}^{(l,m)} = [n_1^{(l,m)} \ldots n_K^{(l,m)}]^{\mathrm{T}}$. For the mth sampled fading state, $n_i^{(l,m)}$, $R_i^{(l,m)}$ and $P_i^{(l,m)}$ denote the effective noise variance, rate and power on user i's tone l, respectively. As in the previous section, the Mth sample denotes the current fading state. If $\pi_{l,m}(\cdot)$ is the permutation such that $n_{\pi_{l,m}(1)}^{(l,m)} < n_{\pi_{l,m}(2)}^{(l,m)} < \cdots < n_{\pi_{l,m}(K)}^{(l,m)}$ by applying the above updates to Equations (10.137) and (10.138), QPS in OFDM systems can be converted into the following GP [82]:

$$\begin{aligned}
&\text{Minimize } \log[\exp(-x)] \\
&\text{subject to } \log[\exp\left(-R_i^{(l,m)}\right)] \le 0, \forall i, l \text{ and } m \\
&\qquad \log\left\{\exp[-Q_i(t)]\exp\left(\sum_{l=1}^{L} R_i^{(l,M)}\right)\right\} \le 0, \forall i \\
&\qquad \log\sum_{l=1}^{L}\sum_{i=1}^{K}\left(\frac{n_{\pi_{l,m}(i)}^{(l,m)} - n_{\pi_{l,m}(i-1)}^{(l,m)}}{P + \sum_{s=1}^{L} n_{\pi_{s,m}(K)}^{(s,m)}}\right) \times \exp\left(\log 2 \sum_{j=i}^{K} R_{\pi_{l,m}(j)}^{l,m}\right) \le 0, \forall m \\
&\qquad \mathbf{Q}(t)x \; - \frac{1}{M}\sum_{m=1}^{M}\sum_{l=1}^{L}\mathbf{R}^{(l,m)} = 0
\end{aligned} \tag{10.139}$$

where $n_{\pi_{l,m}(0)}^{(l,m)} \equiv 0$. If the optimization variable is defined as $\mathbf{y} = [x(\mathbf{R}^{(1,1)})^{\mathrm{T}} \cdots (\mathbf{R}^{(L,M)})^{\mathrm{T}}]^{\mathrm{T}} \in R_{+}^{(KLM+1)}$, problem (10.139) is a standard geometric program with the globally optimal solution $\mathbf{y}^* = [x^*(\mathbf{R}^{*(1,1)})^{\mathrm{T}} \cdots (\mathbf{R}^{*(L,M)})^{\mathrm{T}}]^{\mathrm{T}}$. Consequent rate allocation on tone l under the QPS policy is $\mathbf{R}_{QPS}^{(l)}(n^{(l,M)}, \mathbf{Q}(t)) = \mathbf{R}^{*(l,M)}$ for $l = 1, \ldots, L$, and the corresponding power allocation can be obtained by applying Equation (10.136) on each tone with $m = M$.

10.10.2 Maximum weight matching scheduling by GP

At timeslot t, the rate allocation under MWMS can be found by solving $R_0(\mathbf{n}(t), \mathbf{Q}(t)) = \arg\max_{\mathbf{r}} Q'(t)^{\mathrm{T}}\mathbf{r}$ such that $\mathbf{r} \in C(\mathbf{n}(t), P)$, which is the weighted sum-rate maximization problem over $C(\mathbf{n}(t), P)$ considering the queue state vector $\mathbf{Q}(t)$ as the weight vector. Utilizing Equation (10.137), MWMS can be formulated as the following GP [82]:

$$\begin{aligned}
&\text{Minimize } \log\{\exp[-\mathbf{Q}(t)^{\mathrm{T}}\mathbf{r}]\} \\
&\text{subject to } \log[\exp(-r_i)] \le 0, \forall i \\
&\qquad \log\{\exp[-Q_i(t)]\exp(r_i)\} \le 0, \;\; \forall i
\end{aligned}$$

$$\log \sum_{i=1}^{K} \left(\frac{n_{\pi_i}(t) - n_{\pi_{(i-l)}}(t)}{P + n_{\pi(K)}(t)} \right) \times \exp\left(\log 2 \sum_{j=i}^{K} r_{\pi(j)} \right) \leq 0 \tag{10.140}$$

where $\pi(\cdot)$ is the permutation such that $n_{\pi(1)}(t) < n_{\pi(2)}(t) < .. < n_{\pi(K)}(t)$. If $\mathbf{r}^*$ is the solution of problem (10.140), then $R_0(\mathbf{n}(t), \mathbf{Q}(t)) = \mathbf{r}^*$.

10.10.3 Opportunistic scheduling by GP

The general principles of opportunistic communications are discussed in Chapter 2. Within this section, under the *OS* (*opportunistic scheduling*) policy, a user with the better channel condition takes higher priority in resource allocation. Also, user i is served only if some transmit power remains after clearing queue backlogs of users with higher priorities than user i. This algorithm is equivalent to allocating a data rate vector that minimizes the l_1 -norm distance from the current queue state vector. The l_1-norm of a vector $x \in R^n$ is defined as $||x||_1 = |x_1| + \cdots + |x_n|$. At timeslot t, the OS policy supports the rate vector $\mathbf{R}_{os}(\mathbf{n}(t), \mathbf{Q}(t))$, which is a solution of the following optimization problem:

$$\begin{aligned} &\text{Minimize } ||\mathbf{Q}(t) - \mathbf{r}||_1 \\ &\text{subject to } \mathbf{r} \in C(\mathbf{n}(t), P) \end{aligned} \tag{10.141}$$

With the constraint of $\mathbf{r} \prec \mathbf{Q}(t)$, the solution of the above problem is unaffected by $\sum_{i=1}^{K} Q_i(t)$, which can be omitted from (10.141), resulting in the following GP:

$$\begin{aligned} &\text{Minimize } \log[\exp(-\mathbf{1}^{\mathrm{T}}\mathbf{r})] \\ &\text{subject to } \log[\exp(-r_i)] \leq 0, \forall i \\ &\qquad \log\{\exp[-Q_i(t)]\exp(r_i)\} \leq 0, \ \forall i \\ &\qquad \log \sum_{i=1}^{K} \left[\frac{n_{\pi_i}(t) - n_{\pi_{(i-l)}}(t)}{P + n_{\pi(K)}(t)} \right] \\ &\qquad \times \exp\left(\log 2 \sum_{j=i}^{K} r_{\pi(j)} \right) \leq 0 \end{aligned} \tag{10.142}$$

If r^* is the solution of problem (10.142), then $\mathbf{R}_{os}(\mathbf{n}(t), \mathbf{Q}(t)) = \mathbf{r}^*$. When $\mathbf{Q}(t) \succeq \mathbf{r}$ for any $\mathbf{r} \in C(\mathbf{n}(t), P)$, the OS policy only depends on channel conditions. At each scheduling time, it allocates total power to the single user with the best channel condition, which is a sum-rate maximizing scheme in a fading BC (see Chapter 2).

10.10.4 Rescue scheduling by GP

Rescue scheduling (RS) assigns a data rate vector such that the longest queue length is minimized, therefore minimizing the risk of buffer overflows. This is equivalent to selecting a rate vector minimizing the l_∞-norm distance from the current queue state vector. The l_∞ -norm of a vector $\mathbf{x} \in R^n$ is defined as $||x||_\infty = \max\{|x_1|, \ldots, |x_n|\}$. Hence, at timeslot t, the RS policy assigns the rate vector $\mathbf{R}_{rs}(\mathbf{n}(t), \mathbf{Q}(t))$, which is a solution of the following optimization problem:

$$\begin{aligned} &\text{Minimize } \ ||\mathbf{Q}(t) - \mathbf{r}||_\infty \\ &\text{subject to } \ \mathbf{r} \in C(\mathbf{n}(t), P) \end{aligned} \tag{10.143}$$

If x is the upper bound on $||\mathbf{Q}(t) - \mathbf{r}||_\infty$ such that $-x\mathbf{1} \prec \mathbf{Q}(t) - \mathbf{r} \prec x\mathbf{1}$, then problem (10.143) becomes

$$\begin{aligned}
&\text{Minimize } \log[\exp(x)] \\
&\text{subject to } \log[\exp(-r_i)] \le 0, \forall i \\
&\qquad \log\{\exp[-Q_i(t)]\exp(-x + r_i)\} \le 0, \ \forall i \\
&\qquad \log\{\exp[Q_i(t)]\exp(-x - r_i)\} \le 0, \ \forall i \\
&\qquad \log \sum_{i=1}^{K} \left[\frac{n_{\pi_i}(t) - n_{\pi_{(i-l)}}(t)}{P + n_{\pi(K)}(t)} \right] \\
&\qquad \times \exp\left(\log 2 \sum_{j=i}^{K} r_{\pi(j)} \right) \le 0
\end{aligned}$$

For the optimization variable $\mathbf{y} = [x\mathbf{r}^{\mathrm{T}}]^{\mathrm{T}}$, problem (10.144) is a standard geometric program with the globally optimal point $\mathbf{y}^* = [x^*\mathbf{r}^{*T}]^{\mathrm{T}}$. The data rate vector supported under RS is $\mathbf{R}_{rs}(\mathbf{n}(t), \mathbf{Q}(t)) = \mathbf{r}^*$. More details on the performance analysis of the above algorithms can be found in Reference [82].

REFERENCES

[1] S. P. Boyd and L. Vandenberghe, *Convex Optimization*. Cambridge University Press, 2004. Material available at www.stanford.edu/~boyd.

[2] N. Z. Shor, *Minimization Methods for Non-differentiable Functions*, Springer Series in Computational Mathematics. Springer, 1985.

[3] J.-B. Hiriart-Urruty and C. Lemaréchal, *Convex Analysis and Minimization Algorithms* (two volumes). Springer, 1993.

[4] J. E. Kelley. The cutting-plane method for solving convex programs, *J. Soc. Ind. Appl. Mathematics*, vol. 8, no. 4, 1960, pp. 703–712.

[5] J. Elzinga and T. G. Moore, A central cutting plane algorithm for the convex programming problem, *Math. Programming Studies*, vol. 8, 1975, pp. 134–145.

[6] J.-L. Goffin, Z.-Q. Luo and Y. Ye, Complexity analysis of an interior cutting plane method for convex feasibility problems, *SIAM J. Optimization*, vol. 6, 1996, pp. 638–652.

[7] N. Z. Shor, The development of numerical methods for nonsmooth optimization in the USSR, in *History of Mathematical Programming. A Collection of Personal Reminiscences*, J. K. Lenstra, A. H. G. Rinnooy Kan and A. Schrijver (eds), Centrum voor Wiskunde en Informatica and North-Holland: Amsterdam, 1991, pp. 135–139.

[8] R. G. Bland, D. Goldfarb and M. J. Todd, The ellipsoid method: a survey, *Ops Res.*, vol. 29, no. 6, 1981, pp. 1039–1091.

[9] D. Palomar and M. Chiang, A tutorial to decompositon methods for network utility maximization, *IEEE J. Selected Areas Commun.*, vol. 24, no. 8, August 2006, pp. 1439–1450.

[10] S. Floyd and V. Jacobson, Random early detection gateways for congestion avoidance, *IEEE/ACM Trans. Networking*, vol. 1, no. 4, August 1993, pp. 397–413.

[11] V. Jacobson, Congestion avoidance and control, in *Proc. ACM SIGCOMM*, August 1988.

[12] S. Kunniyur and R. Srikant, End-to-end congestion control: utility functions, random losses and ECN marks, *IEEE/ACM Trans. Networking*, vol. 11, no. 5, October 2003, pp. 689–702.

[13] S. H. Low, Duality model of TCP and queue management algorithms, *IEEE/ACM Trans. Networking*, vol. 11, no. 4, August 2003, pp. 525–536.

[14] S. H. Low, L. L. Perterson and L. Wang, Understanding Vegas: a duality model, *J. ACM*, vol. 49, no. 2, March 2002, pp. 207–235.
[15] J. Mo and J. Walrand, Fair end-to-end window-based congestion control, *IEEE/ACM Trans. Networking*, vol. 8, no. 5, October 2000, pp. 556–567.
[16] C. Jin, D. X. Wei and S. H. Low, FAST TCP: motivation, architecture, algorithms, and performance, in *Proc. IEEE INFOCOM*, March 2004.
[17] C. Jin, D. X. Wei, S. H. Low, G. Buhrmaster, J. Bunn, D. H. Choe, R. L. A. Cottrell, J. C. Doyle, W. Feng, O. Martin, H. Newman, F. Paganini, S. Ravot and S. Singh, FAST TCP: from theory to experiments, *IEEE Networks*, vol. 19, no. 1, January/February 2005, pp. 4–11.
[18] D. X. Wei, C. Jin, S. H. Low and S. Hegde, FAST TCP: motivation, architecture, algorithms, and performance, *IEEE/ACM Trans. Networks*, vol. 14, no. 6, December 2006, pp. 1246–1259.
[19] J. W. Lee, M. Chiang and R. A. Calderbank, Utility-optimal medium access control, *IEEE Trans. Wireless Commun.*, vol. 6, no. 7, July 2007, pp. 2741–2751.
[20] J. W. Lee, A. Tang, J. Huang, M. Chiang and A. R. Calderbank, Reverse engineering MAC: a game theoretic model, *IEEE J. Selected Areas Commun.*, vol. 25, no. 6, August 2007, pp. 1135–1147.
[21] Mung Chiang, S. H. Low, A. R. Calderbank and J. C. Doyle, Layering as optimization decomposition: a mathematical theory of network architectures, *Proc. IEEE*, vol. 95, no. 1, January 2007, pp. 255–312.
[22] T. Nandagopal, T. Kim, X. Gao and V. Bharghavan, Achieving MAC layer fairness in wireless packet networks, in *Proc. ACM MOBICOM*, August 2000.
[23] L. Chen, S. H. Low and J. C. Doyle, Joint TCP congestion control and medium access control, in *Proc. IEEE INFOCOM*, March 2005.
[24] Z. Fang and B. Bensaou, Fair bandwidth sharing algorithms based on game theory frameworks for wireless *ad-hoc* networks, in *Proc. IEEE INFOCOM*, vol. 2, 7–11 March 2004, pp. 1284–1295.
[25] T. Nandagopal, T. Kim, X. Gao and V. Bharghavan, Achieving MAC layer fairness in wireless packet networks, in *Proc. ACM MOBICOM*, August 2000.
[26] K. Kar, S. Sarkar and L. Tassiulas, Achieving proportional fairness using local information in Aloha networks, *IEEE Trans. Automatic Control*, vol. 49, no. 10, October 2004, pp. 1858–1862.
[27] K. Kar, S. Sarkar and L. Tassiulas, Optimization based rate control for multipath sessions, in *Proc. Int. Teletraffic Congr.*, December 2001.
[28] J. He, M. Bresler, M. Chiang and J. Rexford, Towards multi-layer traffic engineering: optimization of congestion control and routing, *IEEE J. Selected Areas Commun.*, vol. 25, no. 5, June 2007, pp. 868–880.
[29] K. Kar, S. Sarkar and L. Tassiulas, Optimization based rate control for multipath sessions, in *Proc. Int. Teletraffic Congr.*, December 2001.
[30] F. P. Kelly and T. Voice, Stability of end-to-end algorithms for joint routing and rate control, *Comput. Commun. Rev.*, vol. 35, no. 2, January 2005, pp. 5–12.
[31] P. Key, L. Massoulie and D. Towsley, Combining multipath routing and congestion control for robustness, in *Proc. CISS*, March 2006.
[32] F. Paganini, Congestion control with adaptive multipath routing based on optimization, in *Proc. CISS*, March 2006.
[33] L. Chen, S. H. Low and J. C. Doyle, Joint TCP congestion control and medium access control, in *Proc. IEEE INFOCOM*, March 2005.
[34] R. J. La and V. Anantharam, Utility-based rate control in the Internet for elastic traffic, *IEEE/ACM Trans. Networking*, vol. 10, no. 2, April 2002, pp. 272–286.

[35] X. Wang and K. Kar, Cross-layer rate optimization for proportional fairness in multihop wireless networks with random access, *IEEE J. Selected Areas Commun.*, vol. 24, no. 8, August 2006, pp. 1548–1559.
[36] C. Yuen and P. Marbach, Price-based rate control in random access networks, *IEEE/ACM Trans. Networking*, vol. 13, no. 5, December 2005, pp. 1027–1040.
[37] J. Zhang and D. Zheng, A stochastic primal-dual algorithm for joint flow control and MAC design in multihop wireless networks, in *Proc. CISS*, March 2006.
[38] J. Zhang, D. Zheng and M. Chiang, Impacts of stochastic noisy feedback in network utility maximization, *Proc. IEEE INFOCOM*, May 2007.
[39] L. Chen, S. H. Low, M. Chiang and J. C. Doyle, Joint optimal congestion control, routing, and scheduling in wireless *ad hoc* networks, in *Proc. IEEE INFOCOM*, April 2006.
[40] A. Eryilmaz and R. Srikant, Fair resource allocation in wireless networks using queue-length-based scheduling and congestion control, in *Proc. IEEE INFOCOM*, vol. 3, 13–17 March 2005, pp. 1794–1803.
[41] A. Eryilmaz and R. Srikant, Joint congestion control, routing and MAC for stability and fairness in wireless networks, *IEEE J. Selected Areas Commun.*, vol. 24, no. 8, August 2006, pp. 1514–1524.
[42] X. Lin and N. B. Shroff, Joint rate control and scheduling in multihop wireless networks, in *Proc. IEEE CDC*, vol. 2, 14–17 December 2004, pp. 1484–1489.
[43] X. Lin and N. B. Shroff, The impact of imperfect scheduling on cross-layer rate control in wireless networks, *IEEE/ACM Trans. Networking*, vol. 14, no. 2, April 2006, pp. 302–315.
[44] M. J. Neely, E. Modiano and C. P. Li, Fairness and optimal stochastic control for heterogeneous networks, in *Proc. IEEE INFOCOM*, vol. 3, 13–17 March 2005, pp. 1723–1734.
[45] A. L. Stolyar, Maximizing queueing network utility subject to stability: greedy primal-dual algorithm, *Queueing Systems*, vol. 50, no. 4, 2005, pp. 401–457.
[46] P. Hande, S. Rangan and M. Chiang, Distributed algorithms for optimal SIR assignment in cellular data networks, in *Proc. IEEE INFOCOM*, April 2006.
[47] R. Cendrillon, J. Huang, M. Chiang and M. Moonen, Autonomous spectrum balancing for digital subscriber lines, in *IEEE Trans. Signal Processing*, vol. 55, no. 8, August 2007, pp. 4241–4257.
[48] M. Chiang, C. W. Tan, D. Palomar, D. O'Neill and D. Julian, Power control by geometric programming, *IEEE Trans. Wireless Commun.*, vol. 6, no. 7, July 2007, pp. 2640–2651.
[49] C. W. Tan, D. Palomar and M. Chiang, Distributed optimization of coupled systems with applications to network utility maximization, in *Proc. IEEE ICASSP*, vol. 5, 14–19 May 2006, pp. V–981–V-984.
[50] A. Elwalid, C. Jin, S. H. Low and I. Widjaja, MATE:MPLS adaptive traffic engineering, in *Proc. IEEE INFOCOM*, vol. 3, 22–26 April 2001, pp. 1300–1309.
[51] H. Han, S. Shakkottai, C. V. Hollot, R. Srikant and D. Towsley, Overlay TCP for multi-path routing and congestion control, in *Proc. IMA Workshop on Measurement and Modeling of the Internet*, January 2004.
[52] J. He, M. Bresler, M. Chiang and J. Rexford, Towards multi-layer traffic engineering: optimization of congestion control and routing, *IEEE J. Selected Areas Commun.*, vol. 25, no. 5, June 2007, pp. 868–880.
[53] S. Kandula and D. Katabi, Walking the tightrope: responsive yet stable traffic engineering, in *Proc. ACM SIGCOMM*, August 2005.
[54] P. Key, L. Massoulie and D. Towsley, Combining multipath routing and congestion control for robustness, in *Proc. CISS*, March 2006.
[55] X. Lin and N. B. Shroff, Utility maximization for communication networks with multipath routing, *IEEE Trans. Automatic Control*, vol. 51, no. 5, May 2006, pp. 766–781.

[56] F. Paganini, Congestion control with adaptive multipath routing based on optimization, in *Proc. CISS*, March 2006.
[57] D. P. Bertsekas and J. N. Tsitsiklis, *Parallel and Distributed Computation*. Prentice-Hall, Englewood Cliffs, NJ, 1989.
[58] B. Johansson and M. Johansson, Primal and dual approaches to distributed cross-layer optimization, in *Proc. 16th IFAC World Congr.*, Prague, Czech Republic, July 2005, CD-ROM.
[59] D. Bertsekas, *Nonlinear Programming*, 2nd edn. Athena Scientific, 1999.
[60] P. Hande, S. Zhang and M. Chiang, Distributed rate allocation for inelastic flows, *IEEE/ACM Trans. Networking*, vol. 15, no. 6, December 2007, p. 1240.
[61] J. W. Lee, R. R. Mazumdar and N. Shroff, Non-convex optimization and rate control for multi-class services in the Internet, Presented at the *IEEE INFOCOM*, Hong Kong, China, March 2004.
[62] E. Gürses and A. N. Kim, Utility optimal real-time multimedia communication in wireless mesh networks, in *Packet Video 2007*, 12–13 November 2007, pp. 234–242.
[63] G. Bianchi, Performance analysis of the IEEE 802.11 distributed coordination function, *IEEE J. Selected Areas Commun.*, vol. 18, no. 3, March 2000, pp. 535–547.
[64] IEEE 802.11 WG, *International Standard for Information Technology Local and Metropolitan Area Networks – Specific Requirements. Part 11: Wireless LAN MAC and PHY Specifications*, 1999.
[65] K. Kar, L. Tassiulas, Layered multicast rate control based on Lagrangian relaxation and dynamic programming, *IEEE J. Selected Areas Commun.*, vol. 24, no. 8, August 2006, p. 1464.
[66] L. A. Wolsey, *Integer Programming*. John Wiley & Sons, Inc.: New York, 1998.
[67] M. J. Neely, Super-fast delay tradeoffs for utility optimal fair scheduling in wireless networks, *IEEE J. Selected Areas Commun.*, vol. 24, no. 8, August 2006, p. 1489.
[68] M. J. Neely, E. Modiano and C. Li, Fairness and optimal stochastic control for heterogeneous networks, in *Proc. IEEE INFOCOM*, March 2005, pp. 1723–1734.
[69] M. J. Neely, Energy optimal control for time varying wireless networks, in *Proc. IEEE INFOCOM*, March 2005, pp. 572–583.
[70] L. Georgiadis, M. J. Neely and L. Tassiulas, Resource allocation and cross-layer control in wireless networks, *Foundations and Trends in Networking*, vol. 1, no. 1, 2006, pp. 1–149.
[71] R. Berry and R. Gallager, Communication over fading channels with delay constraints, *IEEE Trans. Information Theory*, vol. 48, no. 5, May 2002, pp. 1135–1149.
[72] M. Chiang, Geomenic programming for communication systems, *Foundations and Trends of Commun. and Information Theory*, vol. 2, no. 1–2, August 2005, pp. 1–156.
[73] A. Goldsmith, *Wireless Communications*. Cambridge University Press, 2004.
[74] S. Kandukuri and S. Boyd, Optimal power control in interference limited fading wireless channels with outage probability specifications, *IEEE Trans. Wireless Commun.*, vol. 1, no. 1, January 2002, pp. 46–55.
[75] M. Chiang, Balancing transport and physical layers in wireless multihop networks: jointly optimal congestion control and power control, *IEEE J. Selected Area Commun.*, vol. 23, no. 1, January 2005, pp. 104–116.
[76] M. Chiang, C. W. Tan, D. Palomar, D. O'Neill and D. Julian, Power control by geometric programming, *IEEE Trans. Wireless Commun.*, vol. 6, no. 7, July 2007, p. 2640.
[77] T. Cover and J. Thomas, *Elements of Information Theory*. John Wiley & Sons, Inc.: New York, 1997.
[78] P. Whiting , and E. Yeh, Broadcasting over uncertain channels with decoding delay constraints, *IEEE Trans. Information Theory*, vol. 52, no. 3, March 2006, p. 904.
[79] L. Li and A. Goldsmith, Capacity and optimal resource allocation for fading broadcast channels. Part I: ergodic capacity, *IEEE Trans. Information Theory*, vol. 47, March 2001, pp. 1083–1102.

[80] L. Tassiulas and A. Ephremides, Stability properties of constrained queueing systems and scheduling policies for maximum throughput in multihop radio networks, *IEEE Trans. Automatic Control*, vol. 37, December 1992, pp. 1936–1948.

[81] D. Tse, Optimal power allocation over parallel Gaussian broadcast channels, in *Proc. Int. Symp. Information*, Ulm, Germany, June 1997, p. 27.

[82] K. Seong, R. Narasimhan and J. Cioffi, Queue proportional scheduling via geometric programming in fading broadcast channels, *IEEE J. Selected Areas Commun.*, vol. 24, no. 8, August 2006, p. 1593.

11

Mobility Management

11.1 INTRODUCTION

As already indicated in Chapter 1 (see Figure 1.1), 4G wireless networks will integrate services of different segments such as cellular networks, WLAN, WPAN and even LEO satellites. Several alternative backbone networks will be used, like the public land mobile networks (PLMN), mobile Internet protocol (mobile IP) networks, wireless asynchronous transfer mode (WATM) networks, and low Earth orbit (LEO) satellite networks. Regardless of the network, one of the most important and challenging problems for wireless communication and computing is mobility management [1–62]. Mobility management enables telecommunication networks to locate roaming terminals for call delivery and to maintain connections as the terminal is moving into a new service area, process known as *handoff*. The handoff may be executed between different segments (cells) of the same or different systems. *The handoff* event is caused by radio link degradation or initiated by the system that rearranges radio channels in order to avoid congestion. Our focus in this section is on the first kind of handoff, where the cause of handoff is poor radio quality due to a change in the environment or the movement of the wireless terminal. For example, the mobile user might cross cell boundaries and move to an adjacent cell while the call is in process. In this case, the call must be handed off to the neighboring cell in order to provide uninterrupted service to the mobile subscriber. If adjacent cells do not have enough channels to support the handoff, the call is forced to be blocked. In systems where the cell size is relatively small (microcellular systems), the handoff procedure has an important effect on the performance of the system. Here, an important issue is to limit the probability of forced call termination, because from the point of view of a mobile user, forced termination of an ongoing call is less desirable than blocking a new call. Therefore, the system must reduce the chances of unsuccessful handoffs by reserving some channels explicitly for handoff calls. For example, handoff prioritizing schemes are channel assignment strategies that allocate channels to handoff requests more readily than new calls.

Thus, mobility management supports mobile terminals, allowing users to roam while simultaneously offering them incoming calls and supporting calls in progress. Mobility management consists of location management and handoff management.

Location management is a process that enables the network to discover the current attachment point of the mobile user for call delivery. The main components of the process are shown in

Advanced Wireless Technologies: Cognitive, Cooperative & Opportunistic 4G Technology Second Edition Savo G. Glisic

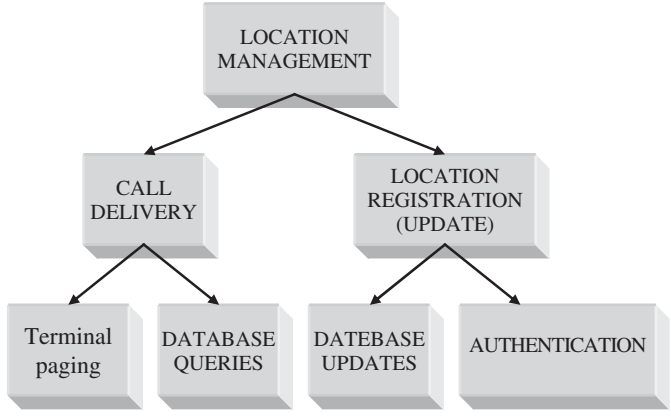

Figure 11.1 Components of location management process.

Figure 11.1. The first segment is location registration (or location update). In this stage, the mobile terminal periodically notifies the network of its new access point, allowing the network to authenticate the user and revise the user's location profile. The second segment is call delivery. Here the network is queried for the user location profile and the current position of the mobile host is found. The main issues in location management involve database architecture design, design of messaging procedures and the transmission of signaling messages between various components of a signaling network. Other issues include: security, dynamic database updates, querying delays, terminal paging methods and paging delays.

Handoff (or handover) management enables the network to maintain a user's connection as the mobile terminal continues to move and change its access point to the network. The three-stage process for handoff first involves *initiation*, where the user, a network agent or changing network conditions identify the need for handoff. The second stage is new *connection generation*, where the network must find new resources for the handoff connection and perform any additional routing operations. Under network-controlled handoff (NCHO) or mobile-assisted handoff (MAHO), the network generates a new connection, by finding new resources for the handoff and performing any additional routing operations. For mobile-controlled handoff (MCHO), the mobile terminal finds the new resources and the network approves. The final stage is *data-flow control*, where the delivery of the data from the old connection path to the new connection path is maintained according to agreed-upon QoS. The segments of handoff management are presented in Figure 11.2.

Handoff management includes two conditions: intracell handoff and intercell handoff. Intracell handoff occurs when the user moves within a service area (or cell) and experiences signal strength deterioration below a certain threshold that results in the transfer of the user's calls to new radio channels of appropriate strength at the same (BS). Intercell handoff occurs when the user moves into an adjacent cell and all of the terminal's connections must be transferred to a new BS. While performing handoff, the terminal may connect to multiple BSs simultaneously and use some form of signaling diversity to combine the multiple signals. This is called *soft handoff*. On the other hand, if the terminal stays connected to only one BS at a time, clearing the connection with the former BS immediately before or after establishing a connection with the target BS, then the process is referred to as *hard handoff*. Handoff management issues are: efficient and expedient packet processing, minimizing the signaling load on the network, optimizing the route for each connection, efficient bandwidth reassignment and refining quality of service for wireless connections. Below we will discuss the handoff management in some of the component networks of 4G integrated wireless network concept as suggested by Figure 1.1.

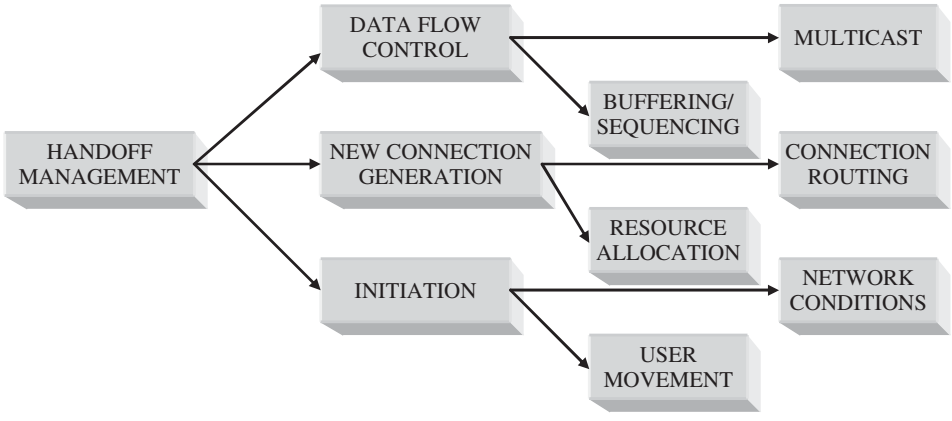

Figure 11.2 Components of handoff management.

11.1.1 Mobility management in cellular networks

Mobile terminals (MTs) are free to travel and thus the network access point of an MT changes as it moves around the network coverage area. As a result, the ID of an MT does not implicitly provide the location information of the MT and the call delivery process becomes more complex. The current systems for PLMN location management strategies require each MT to register its location with the network periodically. In order to perform the registration, update and call delivery operations described above, the network stores the location information of each MT in the location databases. Then the information can be retrieved for call delivery.

Current schemes for PLMN location management are based on a two-level data hierarchy such that two types of network location database, the home location register (HLR) and the visitor location register (VLR), are involved in tracking an MT. In general, there is an HLR for each network and a user is permanently associated with an HLR in his/her subscribed network. Information about each user, such as the types of services subscribed and location information, are stored in a user profile located at the HLR. The number of VLRs and their placements vary among networks. Each VLR stores the information of the MTs (downloaded from the HLR) visiting its associated area.

Network management functions, such as call processing and location registration, are achieved by the exchange of signaling messages through a signaling network. Signaling system 7 (SS7) [34, 38, 63], is the protocol used for signaling exchange, and the signaling network is referred to as the SS7 network.

The type of cell site switch (CSS) currently implemented for the PLMN is known as a mobile switching center (MSC). Figure 11.3 shows the SS7 signaling network which connects the HLR, the VLRs, and the MSCs in a PLMN-based network. The signal transfer points (STPs), as shown in Figure 11.3, are responsible for routing signaling messages.

As mentioned previously, location management includes two major tasks: location registration (or update) and call delivery. In order to correctly deliver calls, the PLMN must keep track of the location of each MT. As described previously, location information is stored in two types of databases, VLR and HLR. As the MTs move around the network coverage area, the data stored in these databases may no longer be accurate. To ensure that calls can be delivered successfully, the databases are periodically updated through the process called location registration.

Location registration is initiated by an MT when it reports its current location to the network. This reporting process is referred to as location update. Current systems adopt an approach such that the MT performs a location update whenever it enters a new location area (LA). Each LA

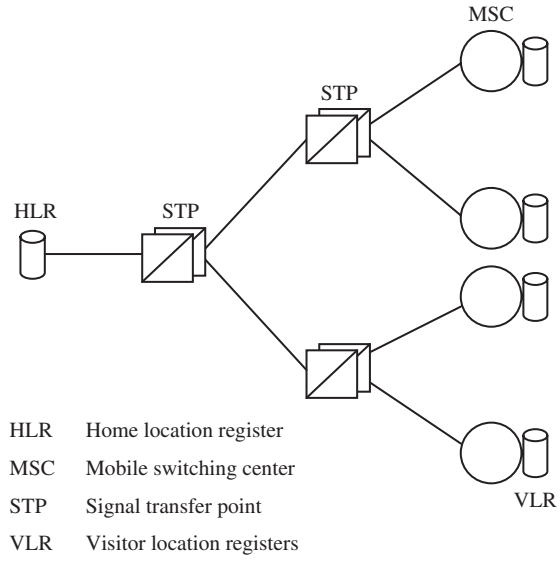

Figure 11.3 Location management SS7 signaling network.

consists of a number of cells and, in general, all base station transmission systems (BTSs) belonging to the same LA are connected to the same MSC.

When an MT enters an LA, if the new LA belongs to the same VLR as the old LA, the record at the VLR is updated to record the ID of the new LA. Otherwise, if the new LA belongs to a different VLR, a number of extra steps are required to: (1) register the MT at the new serving VLR; (2) update the HLR to record the ID of the new serving VLR; and (3) deregister the MT at the old serving VLR. Figure 11.4 shows the location registration procedure when an MT

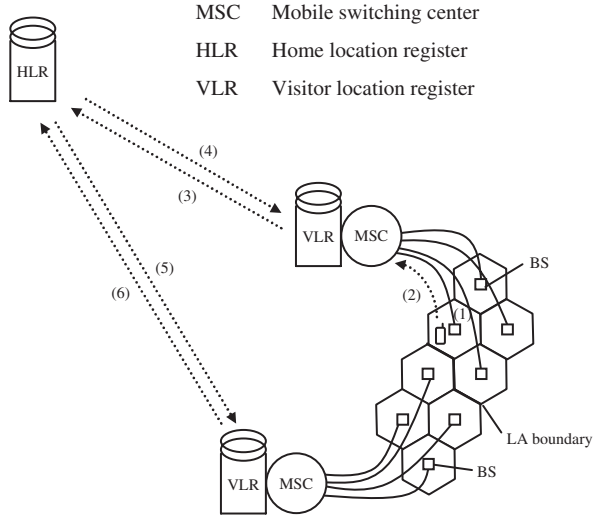

Figure 11.4 Location registration procedures.

moves to a new LA. The following is the ordered list of tasks that are performed during location registration.

(1) The MT enters a new LA and transmits a location update message to the new BS.

(2) The BS forwards the location update message to the MSC which launches a registration query to its associated VLR.

(3) The VLR updates its record on the location of the MT. If the new LA belongs to a different VLR, the new VLR determines the address of the HLR of the MT from its mobile identification number (MIN). This is achieved by a table lookup procedure called global title translation. The new VLR then sends a location registration message to the HLR. Otherwise, location registration is complete.

(4) The HLR performs the required procedures to authenticate the MT and records the ID of the newserving VLR of the MT. The HLR then sends a registration acknowledgment message to the new VLR.

(5) The HLR sends a registration cancellation message to the old VLR.

(6) The old VLR removes the record of the MT and returns a cancellation acknowledgment message to the HLR.

Call delivery consists of two major steps (1) determining the serving VLR of the called MT and (2) locating the visiting cell of the called MT. Locating the serving VLR of the MT involves the following procedure, shown in Figure 11.5:

(1) The calling MT sends a call initiation signal to the serving MSC of the MT through a nearby BS.

(2) The MSC determines the address of the HLR of the called MT by global title translation and sends a location request message to the HLR.

(3) The HLR determines the serving VLR of the called MT and sends a route request message to the VLR. This VLR then forwards the message to the MSC serving the MT.

(4) The MSC allocates a temporary identifier called temporary local directory number (TLDN) to the MT and sends a reply to the HLR together with the TLDN.

(5) The HLR forward this information to the MSC of the calling MT.

(6) The calling MSC requests a call setup to the called MSC through the SS7 network.

The procedure described above allows the network to set up a connection from the calling MT to the serving MSC of the called MT. Since each MSC is associated with an LA and there is more than one cell in each LA, a mechanism is therefore necessary to determine the cell location of the called MT. In current PLMN networks, this is achieved by a paging (or alerting) procedure, such that polling signals are broadcast to all cells within the residing LA of the called MT. On receiving the polling signal, the MT sends a reply which allows the MSC to determine its current residing cell. As the number of MTs increases, sending polling signals to all cells in an LA whenever a call arrives may consume excessive wireless bandwidth. We describe a number of proposed paging mechanisms for reducing the paging cost later.

11.1.2 Location registration and call delivery in 4G

Location registration involves the updating of location databases when current location information is available. On the other hand, call delivery involves the querying of location databases to

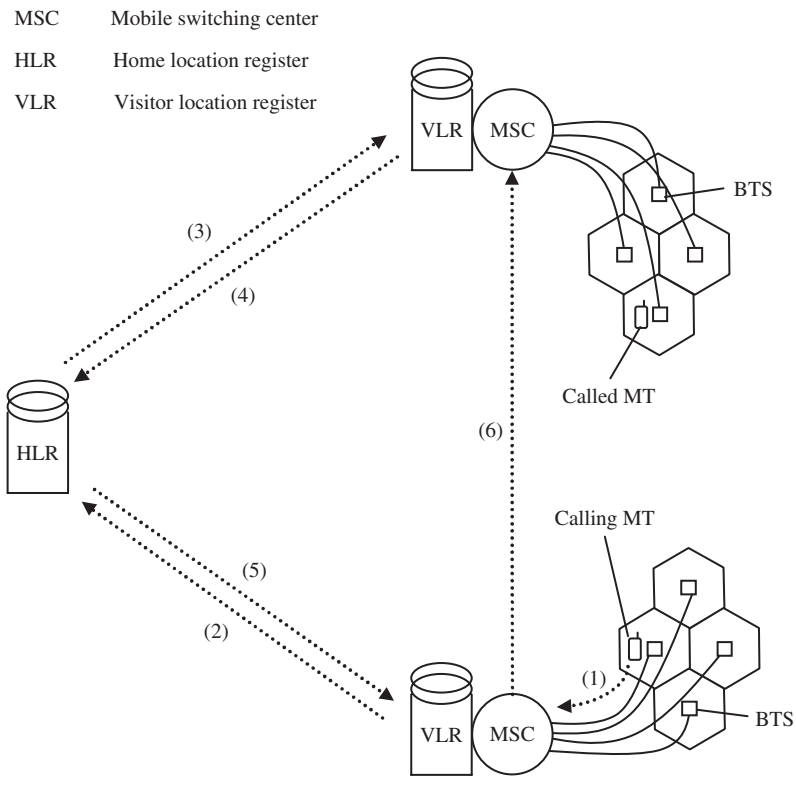

Figure 11.5 Call delivery procedures.

determine the current location of a called MT. These can be costly processes, especially when the MT is located far away from its assigned HLR. For example, if the MT is currently roaming USA and its HLR is in Finland, a location registration message is transmitted from USA to Finland whenever the MT moves to a new LA that belongs to a different VLR. Under the same scenario, when a call for the MT is originated from a nearby MT in USA, the MSC of the calling MT must first query the HLR in Finland before it finds out that the called MT is located in the same area as the caller. As the number of mobile subscribers keeps increasing, the volume of signaling traffic generated by location management is extremely high. Methods for reducing the signaling traffic in 4G networks are therefore needed.

Research in this area generally falls into two categories. In the first category, extensions to the existing location management strategy are developed which aim at improving the IS-41 (or GSM/UMTS) scheme while keeping the basic database network architecture unchanged. This type of solution has the advantage of easy adaptation to the current PLMN networks without major modification. These schemes are based on centralized database architectures inherited from the existing standards. Another category of research results lies in completely new database architectures that require a new set of schemes for location registration and call delivery. Most of these schemes are based on distributed database architectures. Some additional research efforts involve: the reverse virtual call setup – a new scheme for delivering mobile-terminated calls [23], an optimal routing scheme based on the ratio of source messaging to location update rates [61], and a single registration strategy for multitier PCS systems [33]. In what follows, we discuss centralized vs distributed database architectures.

11.1.2.1 Centralized database architectures

This solution consists of the two-tier database structure with additional optimizations that aim to reduce the location management cost. The extension to include inter-technology roaming is also expected.

Dynamic hierarchical database architecture
The first centralized database architecture is the dynamic hierarchical database architecture presented in Ho and Akyildtz [18]. The proposed architecture is based on that of the IS-41 standard with the addition of a new level of databases called directory registers (DRs). Each DR covers the service area of a number of MSCs. The primary function of the DRs is to compute periodically and store the location pointer configuration for the MTs in its service area. Each MT has its unique pointer configuration and three types of location pointers are available at the DR:

(1) A local pointer is stored at an MT serving DR, which indicates the current serving MSC of the MT.

(2) A direct remote pointer is stored at a remote DR, which indicates the current serving MSC of the MT.

(3) An indirect remote pointer is stored at a remote DR, which indicates the current serving DR of the MT.

In addition, the HLR of the MT may be configured to store a pointer to either the serving DR or the serving MSC of the MT. In some cases, it may be more cost-effective not to set up any pointers, and the original IS-41 scheme will be used.

As an example, *if the intertechnology roaming is supported*, suppose that the HLR of a given MT is located in Finland and it is currently roaming in Chicago. If a significant number of the incoming calls for the MT are originating from Los Angeles, a direct or indirect remote pointer can be set up for the MT in the DR at the Los Angeles area. When the next call is initiated for this MT from Los Angeles, the calling MSC first queries the DR and the call can be immediately forwarded to Chicago without requiring a query at the HLR, which is located in Finland. This reduces the signaling overhead for call delivery. On the other hand, the HLR can be set up to record the ID of the serving DR (instead of the serving MSC) of the MT. When the MT moves to another MSC within the same LA in Illinois area, only the local pointer at the serving DR of the MT has to be updated. Again, it is not necessary to access the HLR in Finland. This reduces the signaling overhead for location registration. The advantage of this scheme is that it can reduce the overhead for both location registration and call delivery.

11.1.2.2 Multiple-copy location information strategies

A number of different strategies have been considered to facilitate the search for the user location. The basic idea of the *per-user location caching* strategy [25] is that the volume of signaling and database access traffic for locating an MT can be reduced by maintaining a cache of location information at a nearby STP. Whenever the MT is accessed through the STP, an entry is added to the cache which contains a mapping from the ID of the MT to that of its serving VLR. When another call is initiated for an MT, the STP first checks if a cache entry exists for the MT. If no cache entry for the MT exists, the call delivery scheme as described earlier is used to locate the MT. If a cache entry exists, the STP will query the VLR as specified by the cache. If the MT is still residing under the same VLR, a hit occurs and the MT is found. If the MT has already moved to another location which is not associated with the same VLR, a miss occurs and the call delivery scheme is used to locate the MT.

In order to reduce the number of misses, it is suggested in Lin [35] that cache entries should be invalidated after a certain time interval. Based on the mobility and call arrival parameters, the author [35] introduces a threshold scheme which determines the time when a particular cached location information should be cleared such that the cost for call delivery can be reduced.

User profiles can be *replicated* at selected local databases. When a call is initiated for a remote MT, the network first determines if a replication of the called MTs user profile is available locally. If the user profile is found, no HLR query is necessary and the network can locate the called MT based on the location information available at the local database. Otherwise, the network locates the called MT following the standard procedures. When the MT moves to another location, the network updates all replications of the MT's user profile. This results in higher signaling overhead for location registration. Depending on the mobility rate of the MT and the call arrival rate from each location, this method may significantly reduce the signaling and database access overhead for local management.

11.1.2.3 Local extentions

Pointer forwarding and local anchoring are the strategies where only the far end segment of the rout is modified. The basic idea of the *pointer forwarding* strategy [24] is that, instead of reporting a location change to the HLR every time the MT moves to an area belonging to a different VLR, the reporting can be eliminated by simply setting up a forwarding pointer from the old VLR to the new VLR. When a call for the MT is initiated, the network locates the MT by first determining the VLR at the beginning of the pointer chain and then following the pointers to the current serving VLR of the MT. To minimize the delay in locating an MT, the length of the pointer chain is limited to a predefined maximum value K. Figure 11.6 demonstrates the operation of pointer forwarding. A slight modification of the above scheme is the local anchoring [19], where a VLR close to the MT is selected as its local anchor. Instead of transmitting registration messages to the HLR, location changes are reported to the local anchor. Since the local anchor is close to the

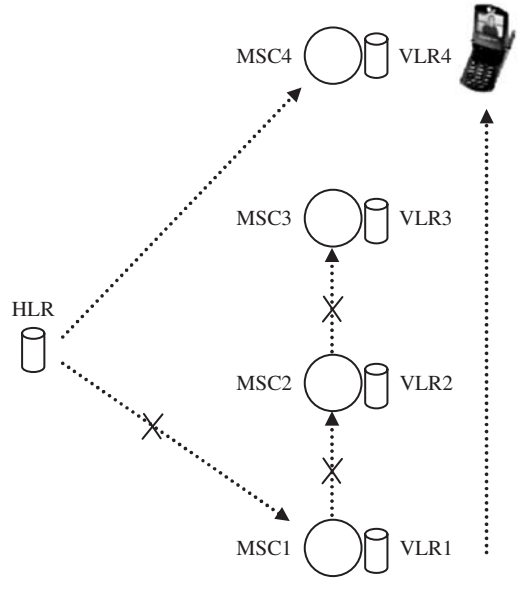

Figure 11.6 Pointer forwarding strategy.

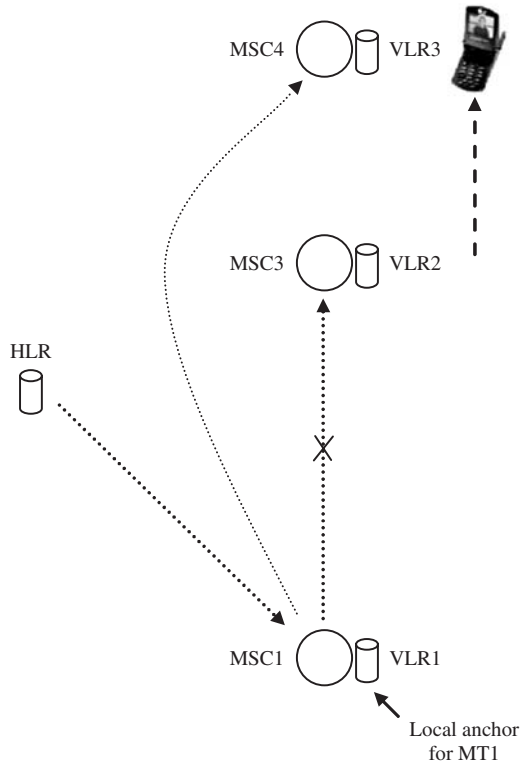

Figure 11.7 Local anchoring scheme.

MT, the signaling cost incurred in location registration is reduced. The HLR keeps a pointer to the local anchor. When an incoming call arrives, the HLR queries the local anchor of the called MT which, in turn, queries the serving VLR to obtain a routable address to the called MT. Figure 11.7 demonstrates the local anchoring scheme.

11.1.2.4 Distributed database architectures

This type of solution is a further extension of the *multiple copy concept* and consists of multiple databases distributed throughout the network coverage area. In a *fully distributed registration scheme* [18] the two-level HLR/VLR database architecture is replaced by a large number of location databases. These location databases are organized as a tree with the root at the top and the leaves at the bottom. The MTs are associated with the leaf (lowest level) location databases and each location database contains location information of the MTs that are residing in its subtree.

Database hierarchy, introduced in Anantharam *et al.* [10] is similar to the fully distributed registration scheme [58]. Here, MTs may be located at any node of the tree hierarchy (not limited to the leaf nodes). The root of the tree contains a database but it is not necessary for other nodes to have databases installed. These databases store pointers for MTs. If an MT is residing at the subtree of a database, a pointer is set up in this database pointing to the next database along the path to the MT. If there is no more database along this path, the pointer points to the residing node of the MT. When a call for an MT is initiated at a node on the tree, the called MT can be located by following the pointers of the MT.

Another form of distributed concept is *partitioning*. Since the mobility pattern of the MTs varies among locations, partitions can be generated by grouping location servers among which the MT moves frequently. Location registration is performed only when the MT enters a partition.

11.1.2.5 Location update and terminal paging options for 4G

Current PCS networks partition their coverage areas into a number of LAs. Each LA consists of a group of cells and each MT performs a location update when it enters an LA. When an incoming call arrives, the network locates the MT by simultaneously paging all cells within the LA. The main drawbacks of this location update and paging scheme are:

(1) Requiring the network to poll all cells within the LA each time a call arrives may result in excessive volume of wireless broadcast traffic.

(2) The mobility and call arrival patterns of MTs vary, and it is generally difficult to select an LA size that is optimal for all users. An ideal location update and paging mechanism should be able to adjust on a per-user basis.

(3) Finally, excessive location updates may be performed by MTs that are located around LA boundaries and are making frequent movements back and forth between two LAs.

In addition, the LA-based location update and paging scheme is a static scheme as it cannot be adjusted based on the parameters of an MT from time to time. Recent research efforts for 4G have attempted to reduce the effects of these inefficiencies. Excessive location updates are discussed in Rose [51] and Bar-Noy *et al.* [12]. A timer-based strategy that uses a universal timeout parameter is presented in Rose [51], while a tracking strategy for mobile users in PCS networks based on cell topology is explored and compared with the time-based strategy in Bar-Noy *et al.* [12]. For excessive polling, a one-way paging network architecture and the interfaces among paging network elements are examined in Lin [30]. Additional schemes attempt to reduce the cost of finding a user when the MT moves during the paging process [48, 62]. Many recent efforts have focused primarily on dynamic location update mechanisms which perform location update based on the mobility of the MTs and the frequency of incoming calls. In the following a number of dynamic location update and paging schemes is presented.

Location updating

The standard LA-based location update method does not allow adaptation to the mobility characteristics of the MTs. The 4G solutions should allow dynamic selection of location update parameters, resulting in lower cost. *Dynamic LA management* introduces a method for calculating the optimal LA size given the respective costs for location update and cell polling. A mesh cell configuration with square-shaped cells is considered. Each LA consists of $k \times k$ cells arranged in a square, and the value of k is selected on a per-user basis according to the mobility and call arrival patterns and the cost parameters. This mechanism performs better than the static scheme in which LA size is fixed. However, it is generally not easy to use different LA sizes for different MTs as the MTs must be able to identify the boundaries of LAs, which are continuously changing. The implementation of this scheme is complicated when cells are hexagonal shaped, or in the worst case, when irregular cells are used.

Dynamic update schemes are also examined in Reference [13]. In a *time based* scheme an MT performs location updates periodically at a constant time interval ΔT. Figure 11.8 shows the path of an MT. If a location update occurred at location A at time 0, subsequent location updates will occur at locations B, C and D if the MT moves to these locations at times ΔT, $2\Delta T$ and $3\Delta T$, respectively. In a *movement-based* scheme, an MT performs a location update whenever it completes a predefined number of movements across cell boundaries (this number is referred to

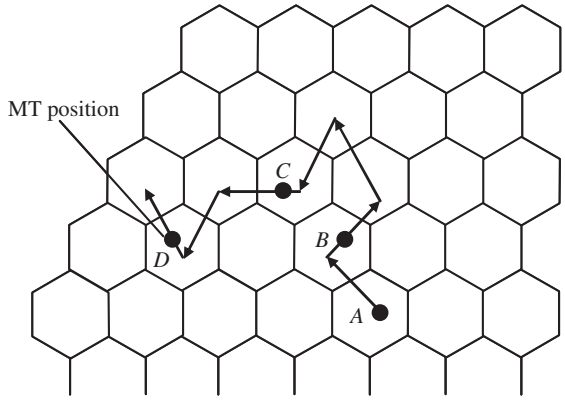

Figure 11.8 Time-based location update scheme.

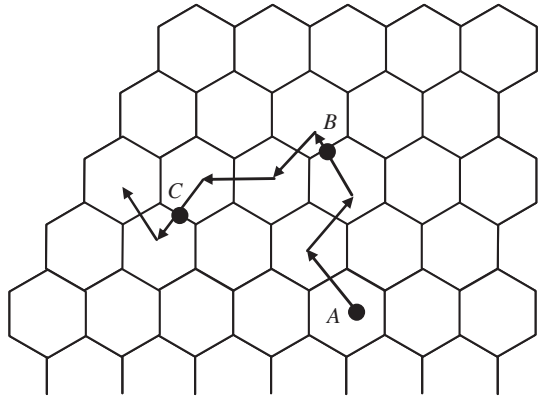

Figure 11.9 Movement-based location update scheme.

as the movement threshold). Assuming a movement threshold of three is used, the MT performs location updates at locations *B* and *C*, as shown in Figure 11.9. In a *distance-based* scheme an MT performs a location update when its distance from the cell where it performed the last location update exceeds a predefined value (this distance value is referred to as the distance threshold). Figure 11.10 shows the same path as Figure 11.8. A location update is performed at location *B* where the distance of the MT from location *A* exceeds the threshold distance (solid line).

An *iterative distance-based location* update scheme introduces an iterative algorithm that can generate the optimal threshold distance that results in the minimum cost. When an incoming call arrives, cells are paged in a shortest-distance-first order such that cells closest to the cell where the last location update occurred are polled first. The delay in locating an MT is, therefore, proportional to the distance traveled since the last location update. Results demonstrate that, depending on the mobility and call arrival parameters, the optimal movement threshold varies widely. This demonstrates that location update schemes should be per-user-based and should be dynamically adjusted according to the current mobility and call arrival pattern of the user. However, the number of iterations required for this algorithm to converge varies depending on the mobility and call arrival parameters considered. Determining the optimal threshold distance may require significant computation resources at the MT.

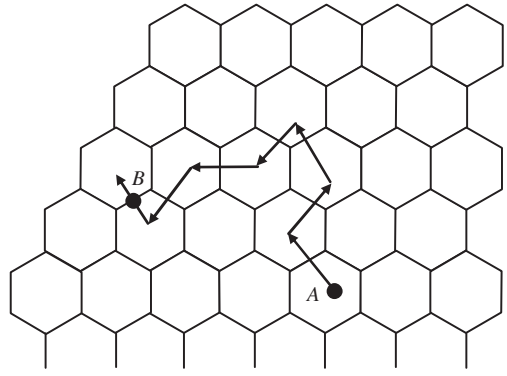

Figure 11.10 Distance-based location update scheme.

A dynamic time-based location update scheme is introduced in Akyildiz and Ho [8]. The location update time interval is determined after each movement based on the probability distribution of the call interarrival time. This scheme does not make any specific assumptions on the mobility pattern of the MT's, and the shortest-distance-first paging scheme as described above is used. It is demonstrated that the results obtained are close to the optimal results given in Ho and Akyildiz [20]. Computation required by this scheme is low and they are, therefore, feasible for application in MTs that have limited computing power. The time required to locate an MT is directly proportional to the distance traveled since the last location update.

Terminal paging optimization provides a trade-off between paging cost and paging delay. Paging subject to delay constraints is considered in Rose and Yates [52]. The authors assume that the network coverage area is divided into LAs, and the probability that an MT is residing in a LA is given. It is demonstrated that, when delay is unconstrained, the polling cost is minimized by sequentially searching the LAs in decreasing order of probability of containing the MT. For constrained delay, the authors obtain the optimal polling sequence that results in the minimum polling cost. However, the authors assume that the probability distribution of user location is provided. This probability distribution may be user-dependent. A location update and paging scheme that facilitates derivation of this probability distribution is needed in order to apply this paging scheme. The tradeoff between the costs of location update and paging is not considered in Rose and Yates [52].

Location update and paging subject to delay constraints is considered in Akyildiz and Ho [20]. Again, the authors consider the distance-based location update scheme. However, paging delay is constrained such that the time required to locate an MT is smaller than or equal to a predefined maximum value. When an incoming call arrives, the residing area of the MT is partitioned into a number of subareas. These subareas are then polled sequentially to locate the MT. By limiting the number of polling areas to a given value such as N, the time required to locate a mobile is smaller than or equal to the time required for N polling operations. Given the mobility and call arrival parameters, the threshold distance and the maximum delay, an analytical model is introduced that generates the expected cost of the proposed scheme. An iterative algorithm is then used to locate the optimal threshold distance that results in the lowest cost. It is demonstrated that the cost is the lowest when the maximum delay is unconstrained. However, by slightly increasing the maximum delay from its minimum value of 1, the cost is significantly lowered. Another scheme using the movement-based location update is reported in Akyildiz and Ho [7]. Similar to Ho and Akyildiz [20], paging delay is confined to a maximum value. Movement-based location update schemes have the advantage that implementation is simple. The MTs do not have to know the cell configuration of the network. The scheme introduced in Akyildiz and Ho [7] is feasible for use in current PLMN networks.

Thus as a summary, remaining open problems for the 4G PLMN-based backbone are: (1) research work should consider the development of dynamic schemes that limit or enhance the distribution of location information on a per-user basis; (2) ongoing research efforts should attempt to reach some middle ground between centralized database architectures and distributed database architectures; and (3) future research should focus on the design of dynamic location update and paging schemes that are simple to implement.

11.1.2.6 Mobility management for mobile IP

Existing standards for terminal mobility over the Internet are described in Perkins [43, 44]. The mobility-enabling protocol for the Internet, *mobile IP*, enables terminals to move from one subnetwork to another as packets are being sent, without interrupting this process. An MN is a host or router that changes its attachment point from one subnet to another without changing its IP address. The MN accesses the Internet via a home agent (HA) or a foreign agent (FA). The HA is an Internet router on the MNs home network, while the FA is a router on the visited network. The node at the other end of the connection is called the correspondent node (CN). A simple mobile IP architecture is illustrated in Figure 11.11. In this example, the CN sends packets to the MN via the MN's HA and the FA. [Note that the term mobile node (MN) is used instead of mobile terminal (MT) in order to follow mobile IP conventions.] As mentioned previously, network organization introduces some differences in the way mobility management is handled over the Internet. For example, mobile IP allows MNs to communicate their current reachability information to their home agent without the use of databases [42]. As a result, mobile IP defines new operations for location and handoff management:

(1) Discovery – how an MN finds a new Internet attachment point when it moves from one place to another.

(2) Registration – how an MN registers with its HA, an Internet router on the MNs home network.

(3) Routing and tunneling – how an MN receives datagrams when it is away from home [43].

Registration operations include mobile agent discovery, movement detection, forming care-of-addresses and binding updates, whereas handoff operations include routing and tunneling. Figure 11.12 illustrates the analogous relationships between the location management operations for mobile IP and those previously described in Figure 11.1 for PLMN.

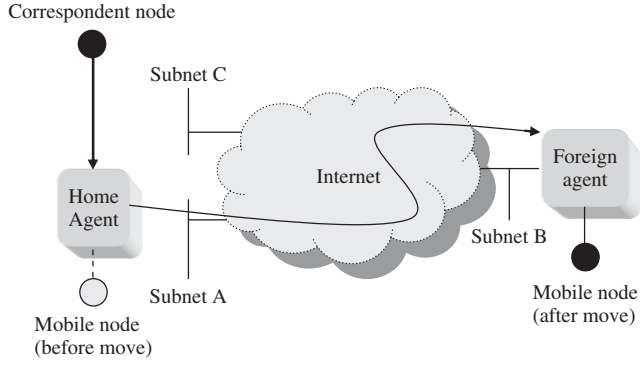

Figure 11.11 Mobile IP architecture.

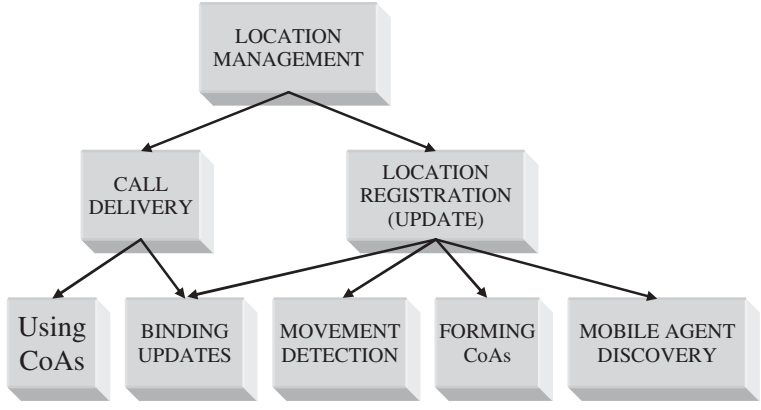

Figure 11.12 Mobile IP location management.

Location registration

When visiting any network away from home, each MN must have an HA. The MN registers with its home agent in order to track the MN's current IP address. There are two IP addresses associated with each MN, one for locating and the other one for identification. In the standard terminology, the new IP address associated with an MN while it visits a foreign link is called its *care of address* (CoA). The association between the current CoA and the MN's home address is maintained by a *mobility binding*, so that packets destined for the MN may be routed using the current CoA regardless of the MN's current point of attachment to the Internet. Each binding has an associated lifetime period, negotiated during the MN's registration, and after which time the registration is deleted. The MN must reregister within this period in order to continue service with this CoA.

Depending upon its method of attachment, the MN sends location registration messages directly to its HA, or through an FA that forwards the registration to the HA. In either case, the MN exchanges registration request and registration reply messages based on IPv4, as described below and shown in Figure 11.13.

(1) By using a registration request message (the request may be relayed to the HA by the current FA), the MN registers with its HA.

(2) The HA creates or modifies a mobility binding for that MN with a new lifetime.

(3) The appropriate mobile agent (HA or FA) returns a registration reply message. The reply message contains the necessary codes to inform the mobile node about the status of its request and to provide the lifetime granted by the HA [43].

Modifications in IPv6

In IPv6, the FAs in Figure 11.13 no longer exist. The entities formerly serving as FAs are now access points (APs).

Movement detection

For the other backbone networks, the movement of the user is determined by updates performed when the user moves into a new LA. Since mobile IP does not use LAs to periodically update the network, a new feature to determine whether the MN has moved to a new subnet after changing its network APs is used. Mobile agents make themselves known by sending agent advertisement messages. The primary movement detection method for mobile IPv6 uses the facilities of IPv6

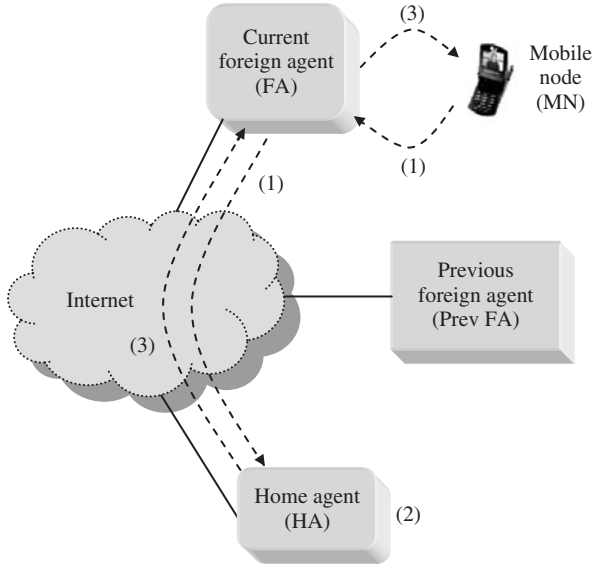

Figure 11.13 Mobile IP location registration.

neighbor discovery. Two mechanisms used by the MN to detect movement from one subnet to another are *the advertisement lifetime* and the *network prefix*.

Advertisement lifetime
The lifetime field within the main body of the Internet control message protocol (ICMP) router advertisement portion of the agent advertisement is used. A mobile node records the lifetime received in any agent advertisements, until that lifetime expires. If the MN has not maintained contact with its FA, the MN must attempt to solicit a new agent [42].

Network prefix
The second method uses the network prefix, a bit string that consists of some initial bits of an IP address, to detect movement. In some cases, an MN can determine whether or not a newly received agent advertisement was received on the same subnet as the MN's current CoA. If the prefixes differ, the MN can assume that it has moved. This method is not available if the MN is currently using an FA's CoA.

After discovering that MN is on a foreign network, it can obtain a new CoA for this new network from the prefix advertised by the new router and perform location update procedures. For the PLMN, registration is implemented using database storage and retrieval. In Mobile IP, the MN's registration message creates or modifies a mobility binding at the home agent, associating the MN's home address with its new CoA for the specified binding lifetime. The procedure is outlined below and shown in Figure 11.14.

(1) By sending a binding update, the MN registers a new CoA with its HA.

(2) The MN notifies its CN of the MN's current binding information.

(3) The CN and the HA send a binding request to the MN to get the MN's current binding information, if the binding update is allowed to expire.

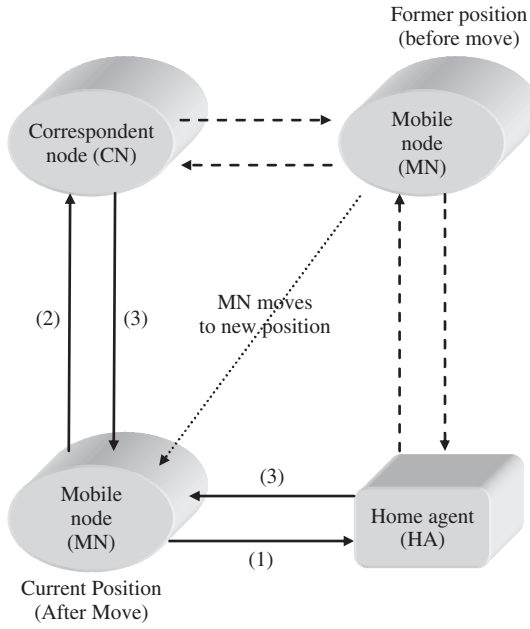

Figure 11.14 Mobile IP location management operations.

The MN responds to the binding request with its new binding update. After receiving the new CoA, the CN and HA send a binding acknowledgment to the MN. Once the registration process is complete, call delivery consists of reaching the MN via the new CoAs. A wireless network interface may allow an MN to be reachable on more than one link at a time (i.e. within the wireless transmitter range of routers on more than one separate link). This establishment of coexisting wireless networks can be very helpful for smooth handoff.

Handoff management

Current routing optimization schemes in IPv4 allow the previous foreign agent (or agents) to maintain a binding for their former mobile visitors, showing a current CoA for each. Then, as packets are sent to the old CoA, the corresponding previous foreign agents can forward the packets to the current CoA of the MN, as demonstrated in Figure 11.15. As a result, an MN is able to accept packets at its old CoA while it updates its home agent and correspondent nodes with a new CoA on a new link. If the previous FA does not have a fresh binding (the binding lifetime has expired), the previous FA forwards the packets to the home agent of the MN, which sends the packets to the CoA from the MN's last location registration update, as shown in Figure 11.16. This can potentially create unnecessary traffic if the HA's binding still refers to the previous FA. Alternatively, the previous FA can invoke the use of special tunnels which forward the packets, but also indicate the need for special handling at the HA.

When special tunnels are used, the packets that are sent to the HA are encapsulated with the FA's CoA address as the source IP address. Upon reception of the newly encapsulated packets, the HA compares the source IP address with the MN's most recent CoA. Thus, if the two addresses match, the packets will not be circled back to the FA. However, if the addresses do not match, the HA can decapsulate the packets and forward them to the MN's current CoA, as shown in Figure 11.16 [43]. In IPv6, the smooth handoff procedure is based on routers (IPv6 nodes) instead of FAs.

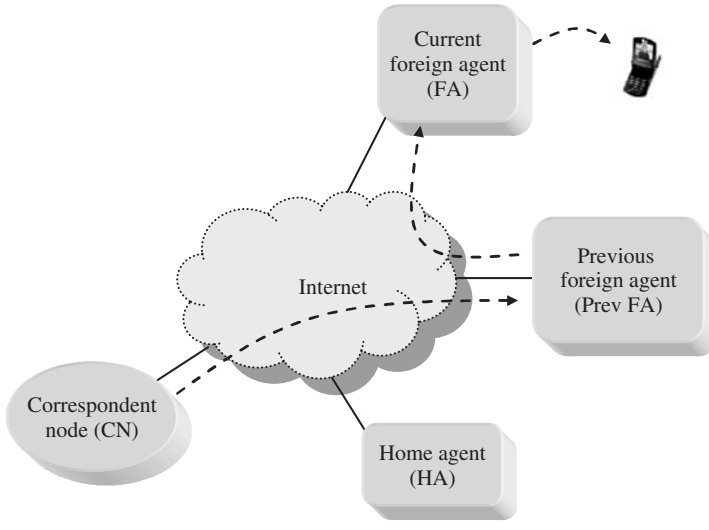

Figure 11.15 Mobile IP smooth handoff with fresh binding at previous FA.

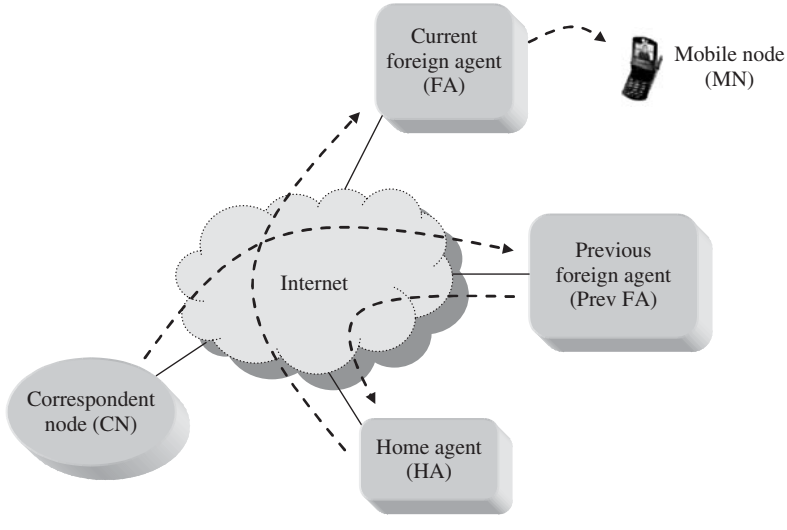

Figure 11.16 Mobile IP smooth handoff without fresh binding at previous FA.

The process of routing datagrams for an MN through its HA often results in the utilization of paths that are significantly longer than optimal. Route optimization techniques for mobile IP employ the use of tunnels, such as the special tunnels mentioned for smooth handoff, to minimize the inefficient path use. For example, when the HA tunnels a datagram to the CoA, the MN's home address is effectively shielded from intervening routers between its home network and its current location. Once the datagram reaches the agent, the original datagram is recovered and is delivered to the MN. Currently, there are two protocols for routing optimization and tunnel establishment: *route optimization in mobile IP* [64] and *the tunnel establishment protocol* [65].

The basic idea of route optimization is to define extensions to basic mobile IP protocols that allow for better routing, so that datagrams can travel from a correspondent node to a mobile node without going to the home agent first [64]. These extensions provide a means for nodes to cache the binding of an MN and then tunnel datagrams directly to the CoA indicated in that binding, bypassing the MN's home agent. In addition, extensions allow for direct forwarding to the MN's new CoA for cases such as datagrams that are in flight when an MN moves and datagrams that are sent based on an out-of-data cached binding.

In tunnel establishment protocol, Mobile IP is modified in order to perform between arbitrary nodes [65]. Upon establishing a tunnel, the encapsulating agent (HA) transmits PDUs to the tunnel endpoint (FA) according to a set of parameters. The process of creating or updating tunnel parameters is called tunnel establishment. Generally the establishment parameters will include a network address for the MN. In order to use tunnel establishment to transmit PDUs, the home agent must determine the appropriate tunnel endpoint (FA) for the MN. This is done by consulting a table that is indexed by the MN's IP address. Each table entry contains the address of the appropriate tunnel endpoint, as well as any other necessary tunnel parameters. After receiving the packets, the foreign agent may then make use of any of a variety of methods to transmit the decapsulated PDUs so that it can be received by the MN. If the MN resides at this particular FA, no further network operations are required.

4G mobile IP networks will have to additionally address several issues. *Security* is one of the most important. As mentioned for the PLMN, the authentication of the mobile becomes more complex as the MN's address loses its tie to a permanent access point. This allows for a greater opportunity for impersonating an MN in order to receive services. Thus security measures for the registration and update procedures, specifically protecting the CoAs and HAs, must be implemented in order to police terminal use [43]. Some authentication schemes for the MN, the HA, and the FA can be found in Troxel and Sanchez [66]. See also Chapter 15 of this book.

The next issue is *simultaneous binding*. Since an MN can maintain several CoAs at one time, the HA must be prepared to tunnel packets to several endpoints. Thus, the HA is instructed to send duplicate encapsulated datagrams to each CoA. After the MN receives the packets from the CoAs, it can invoke some process to remove the duplicates. If necessary, the duplicate packets may be preserved in order to aid signal reconstruction.

Options for *regionalized registration* should also be considered, the extreme case being the BIONET concept discussed in Chapter 16. Currently, three major concepts have been identified as potential methods for limiting location update and registration cost. First, there is a need for schemes that manage the local connectivity available to the MN and also to manage the buffering of datagrams to be delivered. Through this, the network can benefit from smooth handoffs without implementing route optimization procedures. Second, a multicast group of foreign agents is needed in order to allow the MN to use a multicast IP address as its CoA. Third, a hierarchy of foreign agents can be used in agent advertisement in order to localize the registrations to the lowest common FA of the CoA at the two points of attachments. To enable this method, the MN has to determine the tree-height required for its new registration message, and then arrange for the transmission of this message to reach each level of the hierarchy between itself and the lowest common ancestor of its new and previous CoA [44].

As already discussed in Chapter 1, 4G is all about integrating different wireless networks. So intertechnology roaming is the central issue in 4G wireless networks. The first steps in that direction have already been undertaken. Recently, there has been some discussion regarding Mobile IP with respect to the third-generation IMT 2000 system. A high-level IP mobility architecture is described in Becker *et al.* [69], in which the diverse nature of today's wireless and wireline packet data networks is explored. To support the seamless roaming among the heterogeneous networks, the mobility management based on mobile IP concepts is extended to the current third generation IMT2000 wireless architecture. Another concept, referred to as simple mobile IP (SMIP) [68], searches for a more simplistic approach to support the mobility of users, compared with the

asymmetric triangular approach proposed in IPv6. SMIP employs a more symmetric and distributed solution for location management based on MN connections to fixed network routers that have added mobility functions.

Mobility management in wireless ATM deals with transitioning from ATM cell transport based upon widely available resources over wireline to cell transport based upon the limited and relatively unreliable resources over the wireless channel. For details of networks architectures. Thus, the issues such as latency, message delivery, connection routing and QoS [67] will be in the focus of discussion. The ATM Forum (WATM Working Group), is developing basic mechanisms and protocol extensions for location and handoff management that address these issues. The Forum has specified that new procedures must be compatible with the current ATM standards in order to be implemented with relative ease and efficiency [45]. As a result, many of the procedures are also compatible with PCS, satellite and to a lesser degree mobile IP concepts. In this section, we discuss selected proposed solutions for location management, terminal paging, and handoff.

Options considered for 4G are summarized in Figure 11.17. Proposed protocols for WATM implement location management using three techniques: location servers, location advertisement and terminal paging.

Location servers refer to the use of databases to maintain records of the attachment point of MTs within the network. As discussed earlier, the storage and retrieval process can generate excessive signaling and querying operations. *Location advertisement* avoids the use of databases by passing location information throughout the network on broadcast messages. *Terminal paging* is employed to locate MTs within the service area of its attachment point, as discussed previously.

Location server techniques are based on location servers (the databases) used to store and retrieve a record of the current position of the mobile. They require querying operations, as well as signaling protocols for storage and retrieval. WATM server protocols employ the IS-41/GSM based techniques that were discussed for the PLMN backbone earlier in this section. The first method makes familiar use of the HLR/VLR database structure. The second algorithm, location registers (LRs), uses a hierarchy of databases.

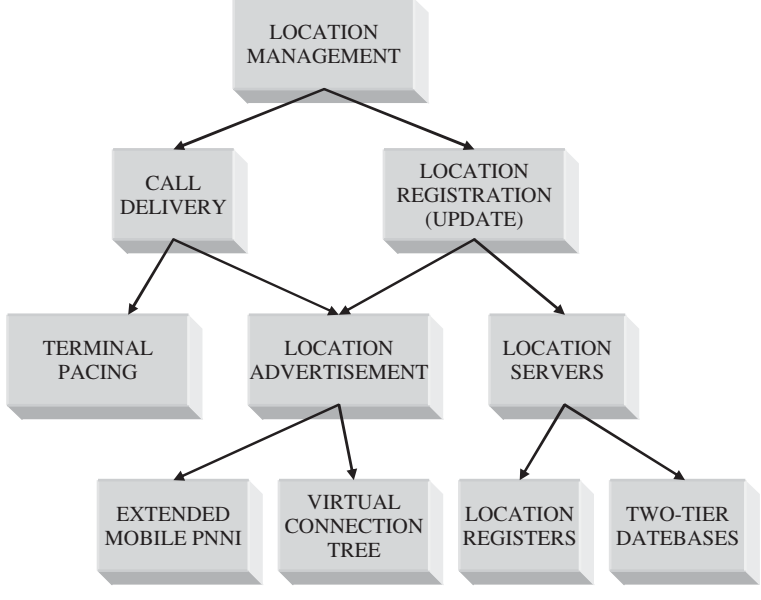

Figure 11.17 ATM location management techniques.

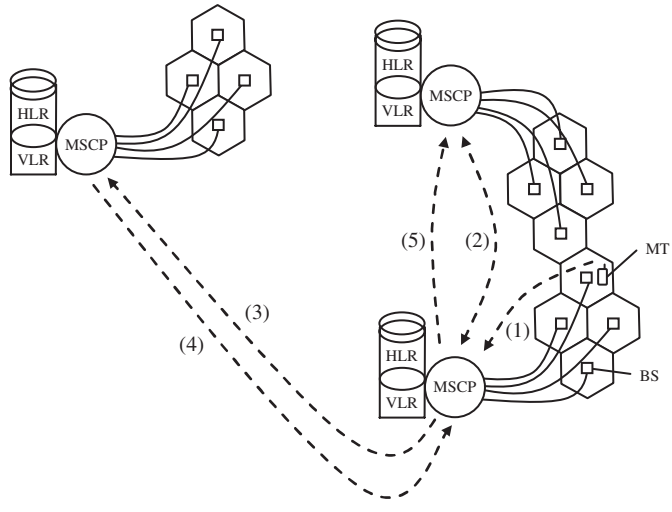

Figure 11.18 Two-tier database scheme.

The *two-tier database* uses bilevel databases that are distributed to zones throughout the network, as shown in Figure 11.18. The zones, analogous to the LAs, are maintained by a zone manager. The zone manager, analogous to the mobility service control point (MSCP) of the 4G wireless architecture, controls the zone's location update procedures. The home tier (HLR) of the zone's database stores location information regarding MTs that are permanently registered within that zone, while the second tier (VLR) of the zone's database stores location information on MTs that are visiting the zone. Each MT has a home zone, i.e. a zone in which it is permanently registered.

Upon entering a new zone, the MT detects the new zone identity broadcast from the BSs. The steps for registration, shown in Figure 11.19, are:

(1) The MT transmits a registration request message to the new MSCP that contains its user identification number, authentication data, and the identity of the previous zone.

(2) The current MSCP determines the home zone of the MT from the previous zone.

(3) The current and home MSCPs authenticate the user and update the home user profile with the new location information.

(4) The home zone sends a copy of the profile to the current zone, which stores the profile in the VLR tier of its database.

(5) The current MSCP sends a purge message to the previous zone so that the user's profile is deleted from the previous zone's VLR tier.

Call delivery is achieved by routing the call to the last known zone first. If the MT has moved and has been purged, the call is immediately forwarded to the home zone. The home zone's HLR is queried for the current location of the MT, which is forwarded back to the calling switch. The calling switch can then set up a connection to the current serving switch of the MT.

The advantage of the two-tier scheme is that it keeps the number of queries low, requiring at most two database lookups for each incoming call to find the MT. However, the use of a centralized HLR may cause increased signaling traffic and unnecessary connection set-up delays if the MT makes several localized moves for an extended period of time. A more localized approach may reduce the need for long-distance queries and thereby reduce connection set-up delays.

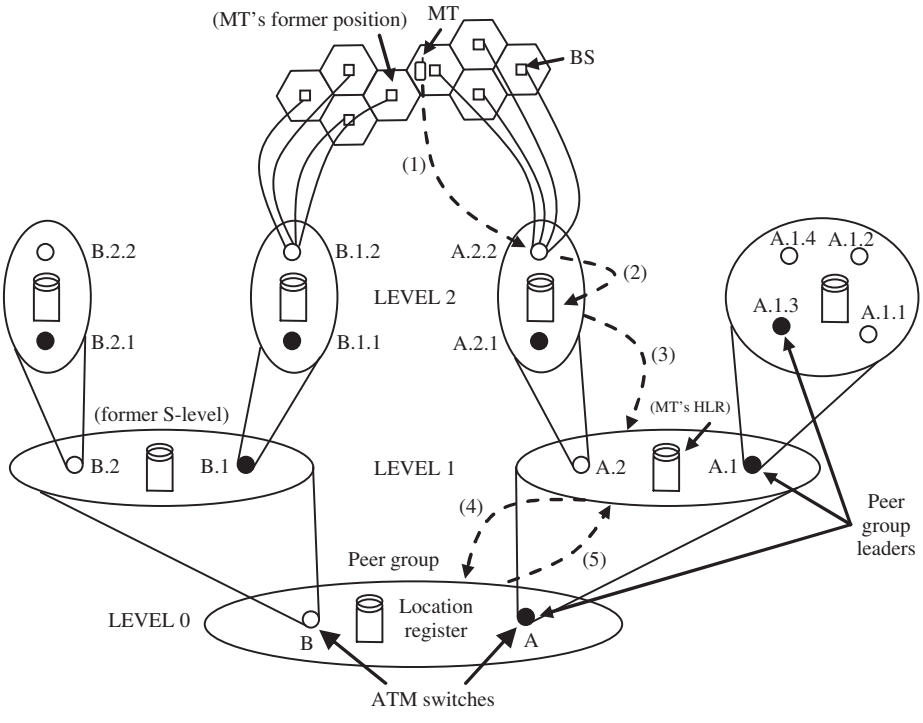

Figure 11.19 LR Hierarchy of WATM location registers scheme.

The *LR hierarchy*-based scheme, described in Veeraraghavan and Dommetry [56] and shown in Figure 11.19, distributes location servers throughout a hierarchical private network-to-network interface (PNNI) architecture. The PNNI procedure is based on a hierarchy of peer groups, each consisting of collections of ATM switches. Each switch can connect to other switches within its peer group. Special switches, *designated peer group leader*, can also connect to a higher ranking leader in the 'parent' peer group. Each peer group also has its own database, or LR, used to store location information on each of the MTs being serviced by the peer group.

The PNNI organization allows the network to route connections to the MT without requiring the parent nodes to have exact location information. Only the lowest referenced peer must record the exact location, and the number of LR updates then corresponds to the level of mobility of the MT. As an illustration, a connection being set up to a MT located at switch *A*.2.2 in Figure 11.19 is first routed according to the highest boundary peer group and switch *A*. Peer A can then route the connection to its 'child' peer group, level *A*.*x* to switch *A*.2. Finally, the connection is routed by *A*.2 to the lowest peer group level to switch *A*.2.2, which resolves the connection to the MT.

Thus, for movement within the *A*.2 peer group, the location update procedure can be localized to only the LR of that peer group. However, a movement from peer group *B*.1 to peer group *A*.2 requires location registration of a larger scope, and the maintenance of a home LR to store a pointer to the current parent peer position of the MT. To limit signaling for the larger scale moves to the minimum necessary level,Veeraraghavan and Dommetry [56] use two scope-limiting parameters, *S* and *L*. The *S* parameter indicates a higher level peer group boundary for LR queries, while the *L* parameter designates the lowest group. In Figure 11.19, the current *S* level is level one, while the *L* level is level two.

When the MT performs a location update by sending a registration notification message to the new BS, this message is relayed to the serving switch, which then stores the MT's location information in the peer group's LR. When the MT powers on or off, this message is relayed up the hierarchy until it reaches the preset boundary *S*. The *S*-level register records the entry and then relays the message to the MT's home LR. As an illustration, for movement from position *B*.1.2 to position *A*.2.2, the registration procedure, shown in Figure 11.19, is as follows:

(1) The MT sends a registration notification message to the new BS/switch.

(2) The new switch stores the MT in the peer group's LR.

(3) The peer group relays the new location info to the higher level LR's for routing, stopping at the first common ancestor of the former and current peer groups.

(4) In this case, the former S level is not a common ancestor, so a new S level is designated and the location info stops propagating at the new S level, level 0.

(5) The MT's home LR (located at group A.x) is notified of the new S-level location for the MT.

After the updates are complete, the new switch sends a purge message to the previous switch so that the former location can be removed from the LRs.

Call delivery
An incoming call request can be routed to the last known peer group or switch via the *S*-level LR. If the mobile has moved, the last known switch propagates a location request, querying the upstream LRs until the mobile endpoint's address is recognized by an LR that has a pointer to the mobile's current position. Then the request is sent to the *L*-level LR for that peer group, which resolves the query and sends the location information back to the calling switch.

Finally, if the call request reaches the *S* level before being recognized by an LR, the *S*-level LR forwards the location request directly to the home switch. Since the home LR keeps track of *S*-level changes for its mobile, the home switch can forward the request directly to the correct *S*-level switch, whose LR points to the current peer group position of the MT.

Location advertisement techniques
Although the *LR hierarchy* provides the advantages of simplicity, decreased computation costs and flexibility, the method can still require a substantial signaling and database querying load. This load can be reduced by using location advertisement. For WATM, advertisement refers to the notification of appropriate network nodes of the current location of the MT. The first method, *mobile PNNI*, uses the PNNI architecture described above by removing the LRs and by taking advantage of an internal broadcast mechanism [56]. The second method, *destination-rooted virtual connection trees*, advertises location information via provisioned virtual paths [57]. The third method, *integrated location resolution*, extends the signaling framework of ATM with location information elements that incorporate location resolution into the connection set-up process [4]. For more details see the references.

The *terminal paging problem* has not yet been explored enough for WATM applications, and additional work will be needed in this area.

11.1.2.7 WATM handoff management in 4G wireless networks

Handoff management controls the process of maintaining each connection at a certain level of QoS as the MT moves into different service areas [29]. As illustrated in Figure 11.20, potential

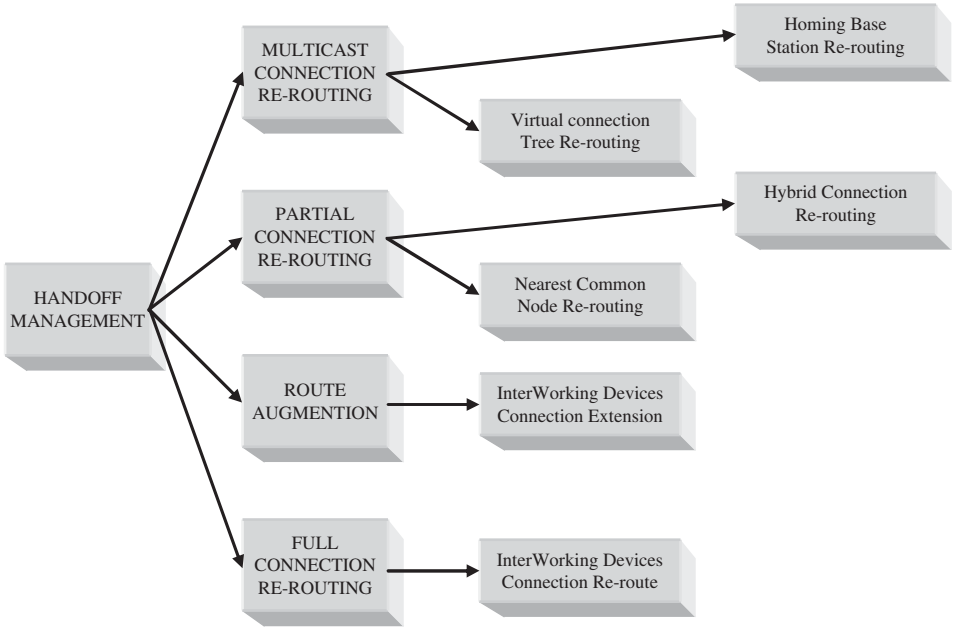

Figure 11.20 WATM handoff management techniques.

protocols to be used in 4G, can be grouped into four categories:

(1) full connection rerouting;

(2) route augmentation;

(3) partial connection rerouting; and

(4) multicast connection rerouting.

Full connection rerouting maintains the connection by establishing a completely new route for each handoff, as if it were a brand new call [46]. Route augmentation simply extends the original connection via a hop to the MT's next location [46]. Partial connection rerouting re-establishes certain segments of the original connection, while preserving the remainder [9]. Finally, multicast connection rerouting combines the former three techniques but includes the maintenance of potential handoff connection routes to support the original connection, reducing the time spent in finding a new route for handoff [9]. More details can be found in the above references.

11.1.2.8 Mobility management for satellite networks

In 4G integrated wireless networks the LEO satellites would cover regions where building terrestrial wireless systems are economically infeasible due to rough terrain or insufficient user population. A satellite system could also interact with terrestrial wireless network to absorb the instantaneous traffic overload of the terrestrial wireless network.

LEO satellites are usually those with altitudes between 500 and 1500 km above the Earth's surface [70–72]. This low altitude provides small end-to-end delays and low power requirements for both the satellites and the handheld ground terminals. In addition, intersatellite links (ISL) make it possible to route a connection through the satellite network without using any terrestrial resources.

These advantages come along with a challenge; in contrast to geostationary (GEO) satellites, LEO satellites change their position with reference to a fixed point on the Earth. Owing to this mobility, the coverage region of an LEO satellite is not stationary. A global coverage at any time is still possible if a certain number of orbits and satellites are used. The coverage area of a single satellite consists of small-sized cells, which are referred to as spotbeams. Different frequencies or codes are used in different spotbeams to achieve frequency reuse in the satellite coverage area.

Location management in the LEO satellite network environment represents more challenging problem because of the movement of satellite footprints. As a consequence, an LA cannot be associated with the coverage area of a satellite because of very fast movement of a LEO satellite. Thus, 4G will need the development of new LA definitions for satellite networks as well as the signaling issues mentioned for all of the location management protocols. In del Re [47], LAs are defined using (gateway, spotbeam) pairs. However, the very fast movement of the spotbeams results in excessive signaling for location updates. In Ananasso and Priscoli [73], LAs are defined using only gateways. However, the paging problem has not been addressed in the same reference.

Handoff management ensures that ongoing calls are not disrupted as a result of satellite movement, but rather transferred or handed off to new spotbeams or satellites when necessary. If a handoff is between two spotbeams served by the same satellite, handoff is *intrasatellite*. The small size of spotbeams causes frequent intrasatellite handoffs, which are also referred to as *spotbeam handoffs* [74]. If the handoff is between two satellites, it is referred to as *intersatellite* handoff. Another form of handoff occurs as a result of the change in the connectivity pattern of the network. Satellites near to polar regions turn off their links to other satellites in the neighboring orbits. Ongoing calls passing through these links need to be rerouted. This type of handoff is referred to as *link handoff* [59, 60]. Frequent link handoffs result in a high volume of signaling traffic. Moreover, some of the ongoing calls would be blocked during connection rerouting caused by link handoffs.

11.2 CELLULAR SYSTEMS WITH PRIORITIZED HANDOFF

The handoff attempt rate in a cellular system depends on cell radius and mobile speed as well as other system parameters. As a result of limited resources, some fraction of handoff attempts will be unsuccessful. Some calls will be forced to terminate before message completion. In this section we discuss analytical models to investigate these effects and to examine the relationships between performance characteristics and system parameters. For these purposes some assumptions about the traffic nature are needed. We assume that the new call origination rate is uniformly distributed over the mobile service area with the average number of new call originations per second per unit area Λ_a. A very large population of mobiles is assumed, thus the average call origination rate is for practical purposes independent of the number of calls in progress. A hexagonal cell shape is assumed. The cell radius R for a hexagonal cell is defined as the maximum distance from the center of a cell to the cell boundary. With the cell radius R, the average new call origination rate per cell Λ_R is $\Lambda_R = 3\sqrt{3}R^2\Lambda_a/2$. Average handoff attempt rate per cell is Λ_{Rh}. The ratio γ_0 of handoff attempt rate to new call origination rate (per cell) is $\gamma_0 \triangleq \Lambda_{Rh}/\Lambda_R$. If a fraction P_B of new call origination is blocked and cleared from the system, the average rate at which new calls are carried is $\Lambda_{Rc} = \Lambda_R(1 - P_B)$. Similarly, if a fraction P_{fh} of handoff attempts fails, the average rate at which handoff calls are carried is $\Lambda_{Rhc} = \Lambda_{Rh}(1 - P_{fh})$. The ratio γ_c of the average carried handoff attempt rate to the average carried new call origination rate is defined as $\gamma_c \triangleq \Lambda_{Rhc}/\Lambda_{Rc} = \gamma_0(1 - P_{fh})/(1 - P_B)$.

The channel holding time T_H in a cell is defined as the time duration between the instant that a channel is occupied by a call and the instant it is released by either completion of the call or a cell boundary crossing by the mobile. This is a function of system parameters such as cell size, speed and direction of mobiles, etc. To investigate the distribution of T_H we let the random variable T_M denote the message duration, that is, the time an assigned channel would be held if no handoff is

required. The random variable T_{M} is assumed to be exponentially distributed $f_{T_{\mathrm{M}}}(t) = \mu_{\mathrm{M}} \mathrm{e}^{-\mu_{\mathrm{M}} t}$ with the mean value $\bar{T}_{\mathrm{M}} (\triangleq 1/\mu_{\mathrm{M}})$. The speed in a cell is assumed to be uniformly distributed on the interval $[0, V_{\max}]$.

When a mobile crosses a cell boundary, the model assumes that vehicular speed and direction change. The direction of travel is also assumed to be uniformly distributed and independent of speed. More sophisticated models would assume that the higher the speed the fewer changes in direction are possible.

The random variable T_n is the time a mobile resides in the cell to which the call is originated. The time that a mobile resides in the cell in which the call is handed off is denoted T_{h}. The pdfs $f_{T_n}(t)$ and $f_{T\mathrm{h}}(t)$ will be discussed in Section 11.3.

When a call is originated in a cell and gets a channel, the call holds the channel until the call is completed in the cell or the mobile moves out of the cell. Therefore, the channel holding time $T_{\mathrm{H}n}$ is either the message duration T_{M} or the time T_n for which the mobile resides in the cell, whichever is less. For a call that has been handed off successfully, the channel is held until the call is completed in the cell or the mobile moves out of the cell again before call completion.

Because of the memoryless property of the exponential distributions, the remaining message duration of a call after handoff has the same distribution as the message duration. In this case the channel holding time T_{Hh} is either the remaining message duration T_{M} or mobile residing time T_{h} in the cell; whichever is less. The random variables $T_{\mathrm{H}n}$ and $T_{\mathrm{H}h}$ are therefore given by

$$T_{\mathrm{H}n} = \min(T_{\mathrm{M}}, T_n) \text{ and } T_{\mathrm{Hh}} = \min(T_{\mathrm{M}}, T_{\mathrm{h}}) \tag{11.1}$$

The cumulative distribution functions (CDF) of $T_{\mathrm{H}n}$ and T_{Hh} can be expressed as

$$\begin{aligned} F_{T_{\mathrm{H}n}}(t) &= F_{T_{\mathrm{M}}}(t) + F_{T_n}(t)[1 - F_{T_{\mathrm{M}}}(t)] \\ F_{T_{\mathrm{Hh}}}(t) &= F_{T_{\mathrm{M}}}(t) + F_{T_{\mathrm{h}}}(t)[1 - F_{T_{\mathrm{M}}}(t)] \end{aligned} \tag{11.2}$$

The distribution of channel holding time can be written as

$$\begin{aligned} F_{T_{\mathrm{n}}}(t) &= \frac{\Lambda_{R\mathrm{c}}}{\Lambda_{R\mathrm{c}} + \Lambda_{R\mathrm{hc}}} F_{T_{\mathrm{H}n}}(t) + \frac{\Lambda_{R\mathrm{hc}}}{\Lambda_{R\mathrm{c}} + \Lambda_{R\mathrm{hc}}} F_{T_{\mathrm{Hn}}}(t) \\ &= \frac{1}{1+\gamma_{\mathrm{c}}} F_{T_{\mathrm{H}n}}(t) + \frac{\gamma_{\mathrm{c}}}{1+\gamma_{\mathrm{c}}} F_{T_{\mathrm{Hh}}}(t) \\ &= F_{T_{\mathrm{M}}}(t) + \frac{1}{1+\gamma_{\mathrm{c}}} \left[1 - F_{T_{\mathrm{M}}}(t)\right] \left[F_{T_n}(t) + \gamma_{\mathrm{c}} F_{T_{\mathrm{n}}}(t)\right] \end{aligned} \tag{11.3}$$

From the initial definitions,

$$F_{T_{\mathrm{H}}}(t) = \begin{cases} 1 - \mathrm{e}^{-\mu_{\mathrm{M}} t} + \frac{\mathrm{e}^{-\mu_{\mathrm{M}} t}}{1+\gamma_{\mathrm{c}}} \left[F_{T_n}(t) + \gamma_{\mathrm{c}} F_{T_{\mathrm{h}}}(t)\right], & \text{for} \quad t \geq 0 \\ 0, & \text{elsewhere} \end{cases} \tag{11.4}$$

The complementary distribution function $F^{\mathrm{C}} T_{\mathrm{H}}(t)$ is

$$\begin{aligned} F^{\mathrm{C}} T_{\mathrm{H}}(t) &= 1 - F_{T_{\mathrm{H}}}(t) = F_{T_{\mathrm{H}}}(t) \\ &= \begin{cases} 1 - \mathrm{e}^{-\mu_{\mathrm{M}} t} - \dfrac{\mathrm{e}^{-\mu_{\mathrm{M}} t}}{1+\gamma_{\mathrm{c}}} \left[F_{T_n}(t) + \gamma_{\mathrm{c}} F_{T_{\mathrm{h}}}(t)\right], & \text{for} \quad t \geq 0 \\ 0, & \text{elsewhere} \end{cases} \end{aligned} \tag{11.5}$$

By differentiating Equation (11.4) we get the probability function (PDF) of T_{H} as

$$f_{T_{\mathrm{H}}}(t) = \mu_{\mathrm{M}} \mathrm{e}^{-\mu_{\mathrm{M}} t} + \frac{\mathrm{e}^{-\mu_{\mathrm{M}} t}}{1+\gamma_{\mathrm{c}}} \left[f_{T_n}(t) + \gamma_{\mathrm{c}} f_{T_{\mathrm{h}}}(t)\right] - \frac{\mu_{\mathrm{M}} \mathrm{e}^{-\mu_{\mathrm{M}} t}}{1+\gamma_{\mathrm{c}}} \left[F_{T_n}(t) + \gamma_{\mathrm{c}} F_{T_{\mathrm{h}}}(t)\right] \tag{11.6}$$

To simplify the analysis the distribution of T_{H} is approximated in References [75, 76] by a negative exponential distribution with mean $\bar{T}_{\mathrm{H}}$ ($\triangleq 1/\mu_{\mathrm{H}}$). From the family of negative exponential

distribution functions, a function which best fits the distribution of T_{H}, by comparing $F^{\mathrm{C}}_{T_{\mathrm{H}}}(t)$ and $\mathrm{e}^{-\mu_{\mathrm{H}}t}$ is chosen which is defined as

$$\mu_{\mathrm{H}} \Rightarrow \min_{\mu_{\mathrm{H}}} \int_0^\infty \left[F^{C}_{T_{\mathrm{H}}}(t) - \mathrm{e}^{-\mu_{\mathrm{H}}t}\right] \mathrm{d}t \tag{11.7}$$

Because a negative exponential distribution function is determined by its mean value, we choose $\bar{T}_{\mathrm{H}}(\triangleq 1/\mu_{\mathrm{H}})$, which satisfies the above condition. The 'goodness of fit' for this approximation is measured by

$$G = \frac{\displaystyle\int_0^\infty \left|F^{C}_{T_{\mathrm{H}}}(t) - \mathrm{e}^{-\mu_{\mathrm{H}}t}\right| \mathrm{d}t}{\displaystyle 2\int_0^\infty F^{\mathrm{C}}_{T_{\mathrm{H}}}(t)\,\mathrm{d}t} \tag{11.8}$$

In the sequel the following definitions will be used:

(1) The probability that a new call does not enter service because of unavailability of channels is called the blocking probability, P_{B}.

(2) The probability that a call is ultimately forced into termination (though not blocked) is P_{F}. This represents the average fraction of new calls which are not blocked but which are eventually uncompleted.

(3) P_{fh} is the probability that a given handoff attempt fails. It represents the average fraction of handoff attempts that are unsuccessful.

(4) The probability P_{N} that a new call that is not blocked will require at least one handoff before completion because of the mobile crossing the cell boundary is

$$\begin{aligned} P_{\mathrm{N}} = \Pr\{T_{\mathrm{M}} > T_n\} &= \int_0^\infty \left[1 - F_{T_{\mathrm{M}}}(t)\right] f_{T_n}(t)\,\mathrm{d}t \\ &= \int_0^\infty \mathrm{e}^{-\mu_{\mathrm{M}}t} f_{T_n}(t)\,\mathrm{d}t \end{aligned} \tag{11.9}$$

(5) The probability P_{H} that a call that has already been handed off successfully will require another handoff before completion is

$$P_{\mathrm{H}} = \Pr\{T_{\mathrm{M}} > T_{\mathrm{h}}\} = \int_0^\infty \left[1 - F_{T_{\mathrm{M}}}(t)\right] f_{T_{\mathrm{h}}}(t)\,\mathrm{d}t = \int_0^\infty \mathrm{e}^{-\mu_{\mathrm{M}}t} f_{T_{\mathrm{h}}}(t)\,\mathrm{d}t \tag{11.10}$$

Let the integer random variable K be the number of times that a nonblocked call is successfully handed off during its lifetime. The event that a mobile moves out of the mobile service area during the call will be ignored since the whole service area is much larger than the cell size. A nonblocked call will have exactly K successful handoffs if all of the following events occur:

(1) It is not completed in the cell in which it was first originated.

(2) It succeeds in the first handoff attempt.

(3) It requires and succeeds in $k-1$ additional handoffs.

(4) It is either completed before needing the next handoff or it is not completed but fails on the $(k+1)$st handoff attempt.

The probability function for K is therefore given by

$$\begin{aligned}\Pr\{K=0\} &= (1-P_{\mathrm{N}})+P_{\mathrm{N}}P_{\mathrm{fh}}\\ \Pr\{K=k\} &= P_{\mathrm{N}}(1-P_{\mathrm{fh}})(1-P_{\mathrm{H}}+P_{\mathrm{H}}P_{\mathrm{fh}})\{P_{\mathrm{H}}(1-P_{\mathrm{fh}})\}^{k-1}, \quad k=1,2,\ldots\end{aligned} \tag{11.11}$$

and the mean value of K is

$$\bar{K}=\sum_{k=0}^{\infty} k\Pr\{K=k\}=\frac{P_{\mathrm{N}}(1-P_{\mathrm{fh}})}{1-P_{\mathrm{H}}(1-P_{\mathrm{fh}})} \tag{11.12}$$

If the entire service area has M cells, the total average new call attempt rate which is not blocked is $M\Lambda_{Rc}$, and the total average handoff call attempt rate is $\bar{K}M\Lambda_{Rc}$. If these traffic components are equally distributed among cells, we have $\gamma_{\mathrm{c}}=(\bar{K}M\Lambda_{Rc})/(M\Lambda_{Rc})\equiv\bar{K}$.

11.2.1 Channel assignment priority schemes

The probability of forced termination can be decreased by giving priority (for channels) to handoff attempts (over new call attempts). In this section, two priority schemes are described, and the expressions for P_{B} and P_{fh} are derived. A subset of the channels allocated to a cell is to be exclusively used for handoff calls in both priority schemes. In the first priority scheme, a handoff call is terminated if no channel is immediately available in the target cell (*channel reservation – CR handoffs*). In the second priority scheme, the handoff call attempt is held in a queue until either a channel becomes available for it, or the received signal power level becomes lower than the receiver threshold level (*channel reservation with queueing – CRQ handoffs*).

11.2.2 Channel reservation – CR handoffs

Priority is given to handoff attempts by assigning C_{h} channels exclusively for handoff calls among the C channels in a cell. The remaining $C-C_{\mathrm{h}}$ channels are shared by both new calls and handoff calls. A new call is blocked if the number of available channels in the cell is less than or equal to C_{h} when the call is originated. A handoff attempt is unsuccessful if no channel is available in the target cell. We assume that both new and handoff call attempts are generated according to a Poisson point process with mean rates per cell of Λ_R and $\Lambda_{R\mathrm{h}}$, respectively. As discussed previously, the channel holding time T_{H} in a cell is approximated to have an exponential distribution with mean $\bar{T}_{\mathrm{H}}(\triangleq 1/\mu_{\mathrm{H}})$. We define the state E_j of a cell such that a total of j calls is in the progress for the base station of that cell. Let P_j represent the steady-state probability that the base station is in state E_j; the probabilities can be determined in the usual way for birth-death processes discussed in Chapter 6. The pertinent state-transition diagram is shown in Figure 11.21.

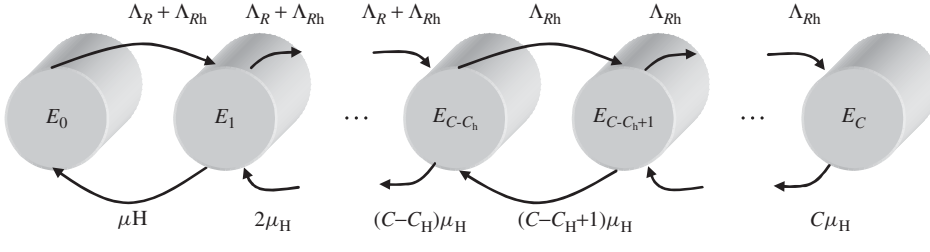

Figure 11.21 State-transition diagram for channel reservation – CR handoffs.

The state equations are

$$P_j = \begin{cases} \dfrac{\Lambda_R + \Lambda_{Rh}}{j\mu_H} P_{j-1}, & \text{for} \quad j = 1, 2, \ldots, C - C_h \\ \dfrac{\Lambda_{Rh}}{j\mu_H} P_{j-1}, & \text{for} \quad j = C - C_h + 1, \ldots, C \end{cases} \tag{11.13}$$

As in Chapter 6, by using Equation (11.13) recursively, along with the normalization condition $\sum_{j=0}^{\infty} P_j = 1$, the probability distribution $\{P_j\}$ is

$$P_0 = \left[\sum_{k=0}^{C-C_h} \frac{(\Lambda_R + \Lambda_{Rh})^k}{k!\mu_H^k} + \sum_{k=C-C_h+1}^{C} \frac{(\Lambda_R + \Lambda_{Rh})^{C-C_h} \Lambda_{Rh}^{k-(C-C_h)}}{k!{\mu_H}^k} \right]^{-1}$$

$$P_j = \begin{cases} \dfrac{(\Lambda_R + \Lambda_{Rh})^j}{j!\mu_H^j} P_0, & \text{for} \quad j = 1, 2, \ldots, C - C_h \\ \dfrac{(\Lambda_R + \Lambda_{Rh})^{C-C_h} \Lambda_{Rh}^{j-(C-C_h)}}{j!\mu_H^j} P_0, & \text{for} \quad j = C - C_h + 1, \ldots, C \end{cases} \tag{11.14}$$

The probability of blocking a new call is $P_B = \sum_{j=C-C_h}^{C} P_j$ and the probability of handoff attempt failure P_{fh} is the probability that the state number of the base station is equal to C. Thus $P_{fh} = P_c$.

11.2.3 Channel reservation with queueing – CRQ handoffs

When a mobile moves away from the base station, the received power generally decreases. When the received power gets lower than a handoff threshold level, the handoff procedure is initiated. The *handoff area* is defined as the area in which the average received power level from the base station of a mobile receiver is between the handoff threshold level (*upper bound*) and the receiver threshold level (*lower bound*). If the handoff attempt finds all channels in the target cell occupied, we consider that it can be queued. If any channel is released while the mobile is in the handoff area, the next queued handoff attempt is accomplished successfully. If the received power level from the source cell's base station falls below the receiver threshold level prior to the mobile being assigned a channel in the target cell, the call is forced into termination. When a channel is released in the cell, it is assigned to the next handoff call attempt waiting in the queue (if any). If more than one handoff call attempt is in the queue, the first-come-first-served queuing discipline is used. The prioritized queueing is also possible where the fast moving (fast signal level losing) users may have higher priority. We assume that the queue size at the base station is unlimited. Figure 11.22 shows a schematic representation of the flow of call attempts through a base station.

The time for which a mobile is in the handoff area depends on system parameters such as the speed and direction of mobile travel and the cell size. We call it the dwell time of a mobile in the handoff area T_Q. For simplicity of analysis, we assume that this dwell time is exponentially distributed with mean $\bar{T}_Q (\triangleq 1/\mu_H)$. We define E_j as the state of the base station when *j is the sum of the number of channels being used in the cell and the number of handoff call attempts in the queue*. For those states whose state number j is less than equal to C, the state transition relation is the same as for the CR scheme. Let X be the elapsed time from the instant a handoff attempt joins the queue to the first instant that a channel is released in the fully occupied target cell. For state numbers less than C, X is equal to zero. Otherwise, *X is the minimum remaining holding time* of those calls in progress in the fully occupied target cell. When a handoff attempt joins the queue for a given target cell, other handoff attempts may already be in the queue (each is associated with

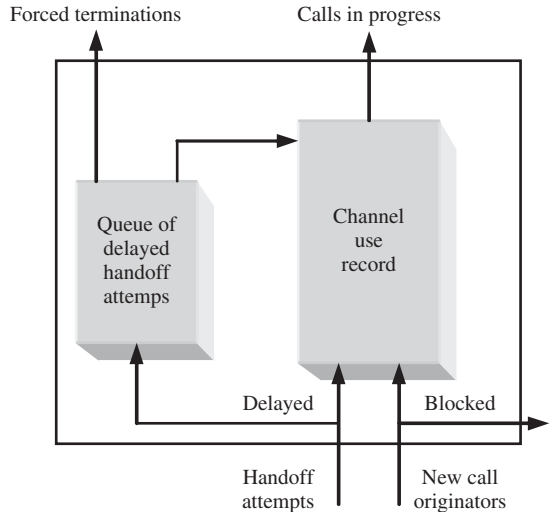

Figure 11.22 Call flow diagram for channel reservation with queueing-CRQ handoffs.

a particular mobile). When any of these first joined the queue, the *time* that it could remain on the queue *without succeeding* is denoted by T_Q (according to our previous definition). Let T_i be the remaining dwell time for that attempt which is in the ith queue position when another handoff attempt joins the queue. Under the memoryless assumptions here, the distributions of all T_i and T_Q are identical. Let $N(t)$ be the state number of the system at time t. From the description of this scheme and the properties of the exponential distribution it follows that

$$\begin{aligned} P_r\{N(t+h) &= C+k-1 | N(t) = C+k\} \\ &= P_r\{X \le h \quad \text{or} \quad T_1 \le h \quad \text{or} \ldots T_k \le h\} \\ &= 1 - P_r\{X > h \quad \text{and} \quad T_1 > h \quad \text{or} \ldots T_k > h\} \\ &= 1 - P_r\{X > h\} P_r\{T_1 > h\} \ldots P_r\{T_k > h\} \\ &= 1 - \mathrm{e}^{-(C\mu_{\mathrm{H}} + k\mu_Q)h} \end{aligned} \tag{11.15}$$

since the random variables $X, T_1, T_2, \ldots, T_k$ are independent. From Equation (11.15) we see that it follows the birth-and-death process and the resulting state transition diagram is as shown in Figure 11.23.

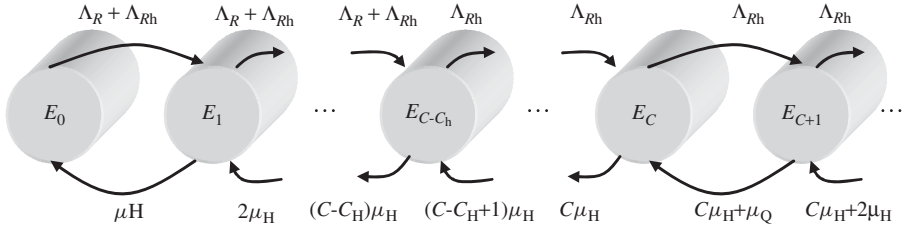

Figure 11.23 State-transition diagram for CRQ priority scheme.

As before, the probability distribution $\{P_j\}$ is easily found to be

$$P_0 = \left[\sum_{k=0}^{C-C_h} \frac{(\Lambda_R + \Lambda_{Rh})^k}{k!\mu_H{}^k} + \sum_{k=C-C_h+1}^{C} \frac{(\Lambda_R + \Lambda_{Rh})^{C-C_h}\, \Lambda_{Rh}^{k-(C-C_h)}}{k!\mu_H^k} + \sum_{k=C+1}^{\infty} \frac{(\Lambda_R + \Lambda_{Rh})^{C-C_h}\, \Lambda_{Rh}^{k-(C-C_h)}}{C!\mu_H^C \prod_{i=1}^{k-C} \left(C\mu_H + i\mu_Q\right)} \right]^{-1}$$

$$P_j = \begin{cases} \dfrac{(\Lambda_R + \Lambda_{Rh})^j}{j!\mu_H^j} P_0, & \text{for} \quad 1 \le j \le C - C_h \\ \dfrac{(\Lambda_R + \Lambda_{Rh})^{C-C_h}\, \Lambda_{Rh}^{j-(C-C_h)}}{j!\mu_H^j} P_0, & \text{for} \quad C - C_h + 1 \le j \le C \\ \dfrac{(\Lambda_R + \Lambda_{Rh})^{(C-C_h)}\, \Lambda_{Rh}^{j-(C-C_h)}}{C!\mu_H^C \prod_{i=1}^{j-C} \left(C\mu_H + i\mu_Q\right)} P_0, & \text{for} \quad j \ge C + 1 \end{cases} \tag{11.16}$$

The probability of blocking is $P_B = \sum_{j=C-C_h}^{\infty} P_j$. A given handoff attempt that joins the queue will be successful if both of the following events occur before the mobile moves out of the handoff area:

(1) All of the attempts that joined the queue earlier than the given attempt have been disposed.

(2) A channel becomes available when the given attempt is at the front of the queue.

Thus the probability of a handoff attempt failure can be calculated as the average fraction of handoff attempts whose mobiles leave the handoff area prior to their coming into the queue front position and getting a channel. Noting that arrivals that find k attempts in queue enter position $k + 1$, this can be expressed as

$$P_{fh} \triangleq \sum_{k=0}^{\infty} P_{C+k} P_{fh|k} \tag{11.17}$$

where $P_{fh|k} = P_r\{\text{attempt fails given it enters the queue in position } k - 1\}$.

Since handoff success for those attempts which enter the queue in position $k + 1$ requires coming to the head of the queue and getting a channel, under the memoryless conditions assumed in this development, we have

$$\left(1 - P_{fh|k}\right) = \left[\prod_{i=1}^{k} P\left(i \mid i + 1\right) \right] P_r\{\text{get channel in first position}\} \tag{11.18}$$

where $P(i \mid i + 1)$ is the probability that an attempt in position $i + 1$ moves to position i before its mobile leaves the handoff area.

There are two possible outcomes for an attempt in position $i + 1$. It will either be cleared from the system or will advance in queue to the next (lower) position. It will advance if the remaining dwell time of its mobile exceeds either:

(1) at least one of the remaining dwell times T_j, $j = 1, 2, \ldots, i$, for any attempt ahead of it in the queue; or

(2) the minimum remaining holding time X of those calls in progress in the target cell.

Thus

$$1 - P(i \mid i+1) = P_r\{T_{i+1} \le X, T_{i+1} \le T_j, \quad j = 1, 2, \ldots, i\} \quad i = 1, 2, \ldots. \tag{11.19}$$

$$\begin{aligned} 1 - P(i \mid i+1) &= P_r\{T_{i+1} \le X, T_{i+1} \le T_1, \ldots, T_{i+1} \le T_i\} \\ &= P_r\{T_{i+1} \le \min(X, T_1, T_2, \ldots, T_i)\} \\ &= P_r\{T_{i+1} \le Y_i\} \quad i = 1, 2, \ldots \end{aligned} \tag{11.19a}$$

where $Y_i \equiv \min(X, T_1, T_2, \ldots, T_i)$. Since the mobiles move independently of each other and of the channel holding times, the random variables, X, T_j, $(j = 1, 2, \ldots, i)$ are statistically independent. Therefore, the cumulative distribution of Y_i in Equation (11.19) can be written as

$$F_{Y_i}(\tau) = 1 - \{1 - F_X(\tau)\}\{1 - F_{T_1}(\tau)\} \ldots \{1 - F_{T_i}(\tau)\}$$

Because of the exponentially distributed variables, this gives

$$F_{Y_i}(\tau) = 1 - \mathrm{e}^{-C\mu_{\mathrm{H}}\tau}\mathrm{e}^{-\mu_Q\tau} \ldots \mathrm{e}^{-\mu_Q\tau} = 1 - \mathrm{e}^{-(C\mu_{\mathrm{H}} + i\mu_Q)\tau}$$

and Equation (11.19) becomes

$$\begin{aligned} 1 - P(i \mid i+1) = P_r\{T_{i+1} \le Y_i\} &= \int_0^\infty \{1 - F_{Y_i}(\tau)\} f_{T_{i+1}}(\tau)\, \mathrm{d}\tau \\ &= \int_0^\infty \mathrm{e}^{-(C\mu_{\mathrm{H}} + i\mu_Q)\tau} \mu_Q \mathrm{e}^{-\mu_Q\tau} \mathrm{d}\tau \\ &= \frac{\mu_Q}{C\mu_{\mathrm{H}} + (i+1)\mu_Q}, \quad i = 1, 2, \ldots \end{aligned} \tag{11.20}$$

The handoff attempt at the head of the queue will get a channel (succeed) if its remaining dwell time T_1 exceeds X. Thus

$$\begin{aligned} P_r\{\text{get channel in front position}\} &= P_r\{T_1 > X\} \text{ and} \\ P_r\{\text{does not get channel in front position}\} &= P_r\{T_1 \le X\} \\ &= \int_0^\infty \mathrm{e}^{-C_{\mu\mathrm{H}}\tau} \mu_Q \mathrm{e}^{-\mu_Q\tau}\, \mathrm{d}\tau = \frac{\mu_Q}{C\mu_{\mathrm{H}} + \mu_Q} \end{aligned} \tag{11.21}$$

The probability Equation (11.21) corresponds to letting $i = 0$ in Equation (11.20) Then from Equation (11.18) we have

$$\begin{aligned} 1 - P_{\mathrm{fh}|k} &= \left[\prod_{i=1}^{k} P(i \mid i+1)\right] P_r\{\text{get channel in first position}\} \\ &= \frac{C\mu_{\mathrm{H}} + \mu_Q}{C\mu_{\mathrm{H}} + 2\mu_Q} \frac{C\mu_{\mathrm{H}} + 2\mu_Q}{C\mu_{\mathrm{H}} + 3\mu_Q} \cdots \frac{C\mu_{\mathrm{H}} + k\mu_Q}{C\mu_{\mathrm{H}} + (k+1)\,\mu_Q} \frac{C\mu_{\mathrm{H}}}{C\mu_{\mathrm{H}} + \mu_Q} \\ &= \frac{C\mu_{\mathrm{H}}}{C\mu_{\mathrm{H}} + (k+1)\,\mu_Q} \end{aligned} \tag{11.22}$$

and

$$P_{\mathrm{fh}|k} = \frac{(k+1)\,\mu_Q}{C\mu_{\mathrm{H}} + (k+1)\,\mu_Q} \tag{11.23}$$

The above equations form a set of simultaneous nonlinear equations which can be solved for system variables when parameters are given. Beginning with an initial guess for the unknowns, the equations are solved numerically using the method of successive substitutions.

A call which is not blocked will be eventually forced into termination if it succeeds in each of the first $(l-1)$ handoff attempts which it requires but fails on the lth. Therefore,

$$P_{\mathrm{F}} = \sum_{l=1}^{\infty} P_{\mathrm{fh}} \left[P_n \left(1 - P_{\mathrm{fh}}\right)^{l-1} P_{\mathrm{H}}^{l-1} \right] = \frac{P_{\mathrm{fh}} P_{\mathrm{N}}}{1 - P_{\mathrm{H}} \left(1 - P_{\mathrm{fh}}\right)} \tag{11.24}$$

where P_{N} and P_{H} are the probabilities of handoff demand of new and handoff calls, as defined previously. Let P_{nc} denote the *fraction of new call attempts* that will *not* be *completed* because of either blocking or unsuccessful handoff. This is also an important system performance measure. This probability P_{nc} can be expressed as

$$P_{\mathrm{nc}} = P_{\mathrm{B}} + P_{\mathrm{F}} \left(1 - P_{\mathrm{B}}\right) = P_{\mathrm{B}} + \frac{P_{\mathrm{fh}} P_{\mathrm{N}} \left(1 - P_{\mathrm{B}}\right)}{1 - P_{\mathrm{H}} \left(1 - P_{\mathrm{fh}}\right)} \tag{11.25}$$

where the first and second terms represent the effects of blocking and handoff attempt failure, respectively. In Equation (11.25) we can guess roughly that, when cell size is large, the probabilities of cell crossing P_{N} and P_{H} will be small and the second term of Equation (11.25) (i.e. the effect of cell crossing) will be much smaller than the first term (i.e. effect of blocking). However, when the cell size is decreased, P_{N} and P_{H} will increase. The noncompleted call probability P_{nc} can be considered as a unified measure of both blocking and forced termination effects.

Another interesting measure of system performance is the weighted sum of P_{B} and P_{F}

$$CF = (1 - \alpha) P_{\mathrm{B}} + \alpha P_{\mathrm{F}} \tag{11.26}$$

where α is in the interval $[(0, 1)]$ and indicates the relative importance of the blocking and forced termination effects. For some applications P_{F} may be more important than P_{B} from the user's point of view, and the relative cost α can be assigned using the system designer's judgment.

11.2.4 Performance examples

For the calculations, the average message duration was taken as $\bar{T}_{\mathrm{M}} = 120\,\mathrm{s}$ and the maximum speed of a mobile of $V_{\max} = 60\,\mathrm{miles/h}$ was used. The probabilities P_{B} and P_{F} as functions of (new) call origination rate per unit area Λ_{a} can be seen in Figure 11.24, with cell radius R being a parameter. A total of 20 channels per cell ($C = 20$) and one channel per cell for handoff priority

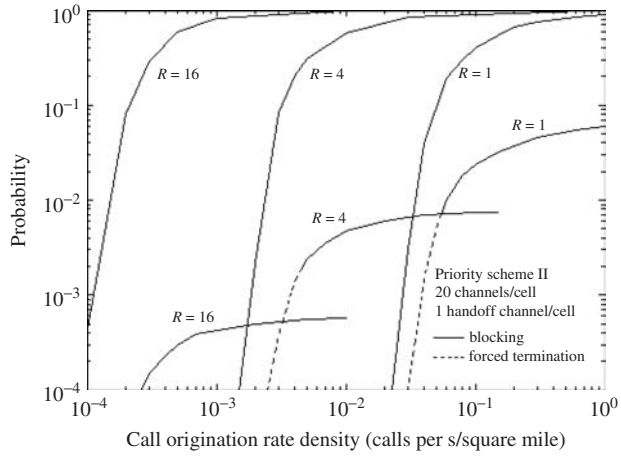

Figure 11.24 Blocking and forced termination probabilities for CRQ priority scheme.

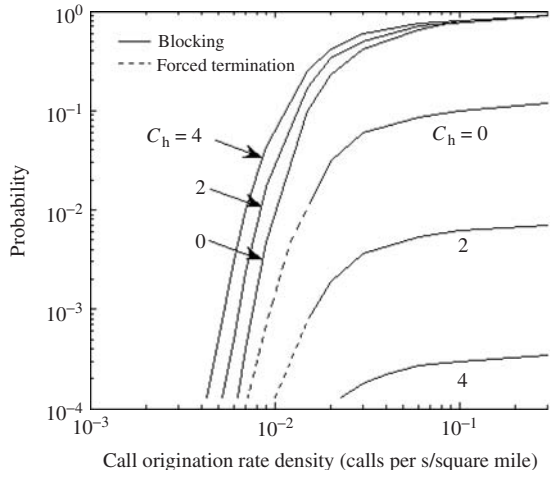

Figure 11.25 Blocking and forced termination probabilities for CRQ systems with 20 channels/cell, $R = 2$ miles.

($C_h = 1$) was assumed. The CRQ scheme was used for this figure, and the mean dwell time for a handoff attempt $\bar{T}_Q$ was assumed to be $\bar{T}_H/10$. As can be seen, P_F is much smaller than P_B and the difference between them decreases as cell size decreases. As expected, for larger R the effect of handoff attempts and forced terminations on system performance is smaller.

Figure 11.25 shows P_B and P_F as functions of Λ_a. As the effects of increasing priority given to handoff calls over new calls by increasing C_h, P_F decreases by orders of magnitude with only small to moderate increase in P_B this exchange is important because (as was mentioned previously) forced terminations are usually considered much less desirable than blocked calls.

Blocking and forced termination probabilities for the two priority schemes are shown in Figure 11.26 as functions of call origination rate density Λ_a. The forced termination probability P_F is smaller for th CRQ scheme, but almost no difference exists in blocking probability P_B. We get this superiority of the CRQ priority scheme by queuing the delayed handoff attempts for the dwell time of the mobile in the handoff area.

11.3 CELL RESIDING TIME DISTRIBUTION

In this section we discuss the probability distributions of the residing times T_n and T_h. The random variable T_n is defined as the time (duration) that a mobile resides in the cell *in which its call originated*. Also T_h is defined as the time a mobile resides in a cell to *which its call is handed off*. To simplify analysis we approximate the hexagonal cell shape as a circle. For a hexagonal cell having radius R, the approximating circle with the same area has a radius, R_{eq}, which is given by $R_{eq} = \sqrt{(3\sqrt{3}/2\pi)}\, R \approx 0.91R$ and illustrated in Figure 11.27. The base station is assumed to be at the center of a cell and is indicated by a letter B in the figure. The location of a mobile in a cell, which is indicated by a letter A in the figure, is represented by its distance r and direction ϕ from the base station as shown. To find the distributions of T_n and T_h, we assume that the mobiles are spread evenly over the area of the cell. Then r and ϕ are random variables with PDFs

$$f_r(r) = \begin{cases} \dfrac{2r}{R_{eq}^2}, & 0 \le r \le R_{eq} \\ 0, & \text{elsewhere} \end{cases}, \quad f_\phi(\phi) = \begin{cases} \dfrac{1}{2\pi}, & 0 \le \phi \le 2\pi \\ 0, & \text{elsewhere} \end{cases} \tag{11.27}$$

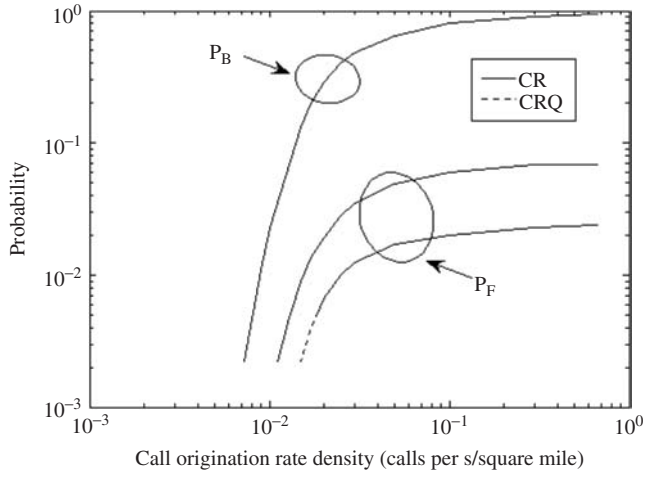

Figure 11.26 Blocking and forced terminations for priority CR and CRQ schemes (20 channels/cell, one handoff channel/cell, $R = 2$ miles).

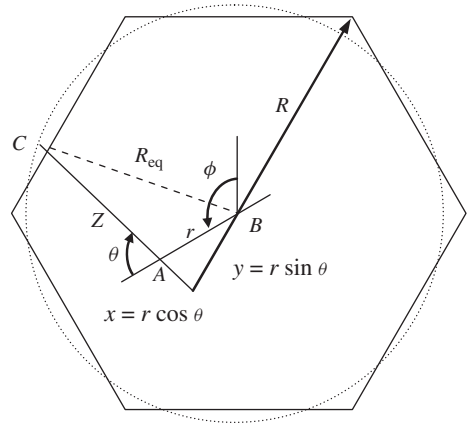

Figure 11.27 Illustration of distance from point A in cell (where call is originated), to point C on cell boundary (where mobile exits from cell).

Next it is assumed that a mobile travels in any direction with equal probability and its direction remains constant during its travel in the cell. If we define the direction of mobile travel by the angle θ (with respect to a vector from the base station to the mobile), as shown in the figure, the distance Z from the mobile to the boundary of approximating circle is $Z = \sqrt{[R_{eq}^2 - (r \sin\theta)^2]} - r\cos\theta$. Because ϕ is evenly distributed in a circle, Z is independent of ϕ and from the symmetry we can consider the random variable θ is in interval $[0, \pi]$ with PDF

$$f_\theta(\theta) = \begin{cases} \dfrac{1}{\pi}, & 0 \le \theta \le \pi \\ 0, & \text{elsewhere} \end{cases} \tag{11.28}$$

If we define new random variables x, y as $x = r\cos\theta,\ y = r\sin\theta$, then $Z = (R_{eq}^2 - y^2) - x$ and $W = x$. Since the mobile is assumed to be equally likely to be located anywhere in the approximating circle

$$f_{XY}(x, y) = \begin{cases} \dfrac{2}{\pi R_{eq}^2}, & -R_{eq} \le x \le R_{eq}, \quad 0 \le x^2 + y^2 \le R_{eq}^2, \quad 0 \le y \le R_{eq} \\ 0, \quad \text{elsewhere} \end{cases}$$

From Equations (11.27)–(11.28), the joint density function of Z and W can be found by standard methods

$$\begin{aligned} f_{ZW}(z, w) &= \frac{|z + w|}{\sqrt{{R_{eq}}^2 - (z + w)^2}} f_{XY}(x, y) \\ &= \frac{2}{\pi R_{eq}^2} \frac{|z + w|}{\sqrt{R_{eq}^2 - (z + w)^2}}, \quad 0 \le z \le 2R_{eq}, -\frac{1}{2}z \le w \le -z + R_{eq} \end{aligned}$$

The PDF of the distance Z then becomes

$$\begin{aligned} f_Z(z) &= \int_{-z/2}^{R_{eq}-z} \frac{2}{\pi R_{eq}^2} \frac{(z + w)}{\sqrt{R_{eq}^2 - (z + w)^2}} \mathrm{d}w, \quad 0 \le z \le 2R_{eq} \\ &= \begin{cases} \dfrac{2}{\pi R_{eq}^2} \sqrt{R_{eq}^2 - \left(\dfrac{z}{2}\right)^2}, & 0 \le z \le 2R_{eq} \\ 0, \text{ elsewhere} \end{cases} \end{aligned} \tag{11.29}$$

If the speed V of a mobile is constant during its travel in the cell and random variable which is uniformly distributed on the interval $[0, V_{max}]$ with PDF

$$f_V(v) = \begin{cases} \dfrac{1}{V_{max}}, & 0 \le v \le V_{max} \\ 0, \text{ elsewhere} \end{cases}$$

then the time T_n is expressed by $T_n = Z/V$ with PDF

$$\begin{aligned} f_{T_n}(t) &= \int_{-\infty}^{\infty} |w|\, f_Z(tw) f_V(w) \mathrm{d}w \\ &= \begin{cases} \dfrac{2}{V_{max}\pi R_{eq}^2} \displaystyle\int_0^{V_{max}} w \sqrt{R_{eq}^2 - \left(\frac{tw}{2}\right)^2}\, \mathrm{d}w, & 0 \le t \le \dfrac{2R_{eq}}{V_{max}} \\ \dfrac{2}{V_{max}\pi R_{eq}^2} \displaystyle\int_0^{2R_{eq}/t} w \sqrt{R_{eq}^2 - \left(\frac{tw}{2}\right)^2}\, \mathrm{d}w, & t \ge \dfrac{2R_{eq}}{V_{max}} \end{cases} \\ &= \begin{cases} \dfrac{8R_{eq}}{3V_{max}\pi t^2} \left[1 - \sqrt{\left\{ 1 - \left(\dfrac{tV_{max}}{2R_{eq}}\right)^2 \right\}^3} \right], & 0 \le t \le \dfrac{2R_{eq}}{V_{max}} \\ \dfrac{8R_{eq}}{3V_{max}\pi t^2}, & t \ge \dfrac{2R_{eq}}{V_{max}} \end{cases} \end{aligned} \tag{11.30}$$

and the cdf of T_n is

$$F_{T_N}(t) = \int_{-\infty}^{t} f_{T_n}(x)\mathrm{d}x\, F_{T_n} = \begin{cases} \dfrac{2}{\pi}\arcsin\left(\dfrac{V_{\max}t}{2R_{\text{eq}}}\right) - \dfrac{4}{3\pi}\tan\left[\dfrac{1}{2}\arcsin\left(\dfrac{V_{\max}t}{2R_{\text{eq}}}\right)\right] \\ +\dfrac{1}{3\pi}\sin\left[2\arcsin\left(\dfrac{V_{\max}t}{2R_{\text{eq}}}\right)\right],\ 0 \le t \le \dfrac{2R_{\text{eq}}}{V_{\max}} \\ 1 - \dfrac{8R_{\text{eq}}}{3\pi V_{\max}}\dfrac{1}{t},\ t \ge \dfrac{2R_{\text{eq}}}{V_{\max}} \end{cases} \tag{11.31}$$

To find the distribution of T_{h}, in the next step we note that, when a handoff call is attempted, it is always generated at the cell boundary, which is taken as the boundary of the approximating circle. Therefore, to find T_{h} one must recognize that the mobile will move from one point on the boundary to another. The direction of a mobile when it crosses the boundary is indicated by the angle θ between the direction of the mobile and the direction from the mobile to the center of a cell as shown in Figure 11.28 [75, 76].

If the mobile moves in any direction with equal probability, the random variable θ has PDF given by

$$f_\theta(\theta) = \begin{cases} \dfrac{1}{\pi}, & -\dfrac{\pi}{2} \le \theta \le \dfrac{\pi}{2} \\ 0, & \text{elsewhere} \end{cases}$$

The distance Z as shown in Figure 11.28 is $Z = 2R_{\text{eq}}\cos\theta$, which has a CDF given by

$$F_Z(z) = P_r\{Z \le z\} = \begin{cases} 0,\ z < 0 \\ 1 - \dfrac{2}{\pi}\arccos\left(\dfrac{z}{2R_{\text{eq}}}\right),\ 0 \le z \le 2R_{\text{eq}} \\ 1,\ z > 2R_{\text{eq}} \end{cases} \tag{11.32}$$

The PDF of Z is

$$f_Z(z) = \frac{\mathrm{d}}{\mathrm{d}z}F_Z(z) = \begin{cases} \dfrac{1}{\pi}\dfrac{1}{\sqrt{R_{\text{eq}}^2 - \left(\frac{z}{2}\right)^2}},\ 0 \le z \le 2R_{\text{eq}} \\ 0,\ \text{elsewhere} \end{cases} \tag{11.33}$$

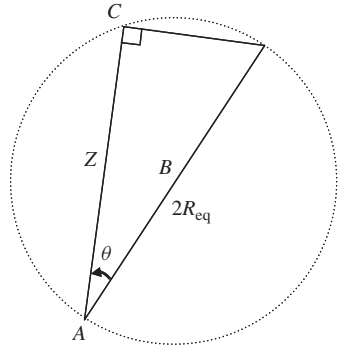

Figure 11.28 Illustration of distance from cell entering point (A on cell boundary), to cell exiting point (C on cell boundary).

The time in the cell T_h is the time that a mobile travels the distance Z with speed V, then $T_h = Z/V$. With the same assumption about V, the PDF of T_h is

$$f_{T_h}(t) = \int_0^\infty |w|\, f_Z(tw) f_V(w) \mathrm{d}w = \begin{cases} \dfrac{1}{\pi V_{\max}} \displaystyle\int_0^{V_{\max}} \dfrac{w}{\sqrt{R_{eq}^2 - \left(\dfrac{tw}{2}\right)^2}} \mathrm{d}w, & 0 \le t \le \dfrac{2R_{eq}}{V_{\max}} \\ \dfrac{1}{\pi V_{\max}} \displaystyle\int_0^{2R_{eq}/t} \dfrac{w}{\sqrt{R_{eq}^2 - \left(\dfrac{tw}{2}\right)^2}} \mathrm{d}w, & t \ge \dfrac{2R_{eq}}{V_{\max}} \end{cases}$$

$$= \begin{cases} \dfrac{4R_{eq}}{\pi V_{\max}} \dfrac{1}{t^2} \left[1 - \sqrt{1 - \left(\dfrac{V_{\max} t}{2R_{eq}}\right)^2} \right], & 0 \le t \le \dfrac{2R_{eq}}{V_{\max}} \\ \dfrac{4R_{eq}}{\pi V_{\max}} \dfrac{1}{t^2}, & t \ge \dfrac{2R_{eq}}{V_{\max}} \end{cases} \tag{11.34}$$

and the CDF of T_h is

$$F_{T_h}(t) = \int_{-\infty}^{t} f_{T_h}(x)\, \mathrm{d}x$$

$$= \begin{cases} 0, & t < 0 \\ \dfrac{2}{\pi} \arcsin\left(\dfrac{V_{\max} t}{2R_{eq}}\right) - \dfrac{2}{\pi} \tan\left[\dfrac{1}{2} \arcsin\left(\dfrac{V_{\max} t}{2R_{eq}}\right)\right], & 0 \le t \le \dfrac{2R_{eq}}{V_{\max}} \\ 1 - \dfrac{4R_{eq}}{\pi V_{\max}} \dfrac{1}{t}, & t > \dfrac{2R_{eq}}{V_{\max}} \end{cases} \tag{11.35}$$

Figure 11.29 shows the mean channel holding time in a cell $\overline{T_H}$. Notice that $\overline{T_H}$ becomes smaller with smaller cell size, but sensitivity to change in cell size is smaller for larger cells. Finally, earlier

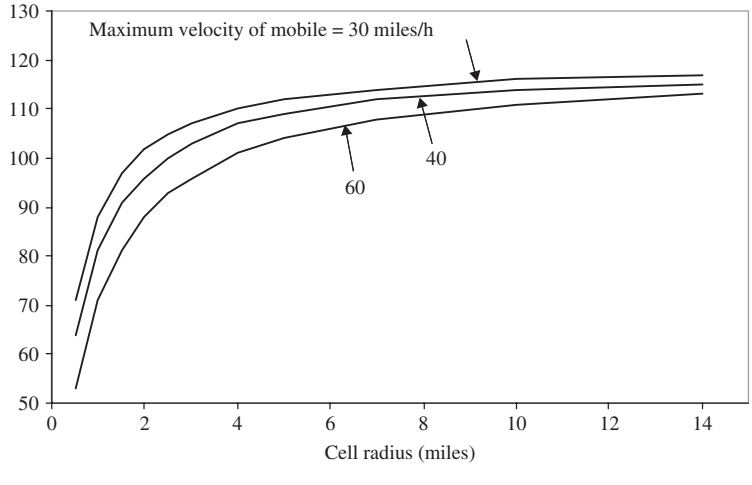

Figure 11.29 Mean channel holding time (s) in cell vs R (average call duration = 120 s).

Table 11.1 The goodness-of-fit G of the approximation

Cell radius, R	G
1.0	0.020220
2.0	0.000120
4.0	0.000003
6.0	0.000094
8.0	0.000121
10.0	0.000107
12.0	0.000086
14.0	0.000066
16.0	0.000053

in Section 11.2 we approximated the cumulative distribution function of the channel holding time in a cell as suggested in References [75, 76]. The goodness-of-fit G of this approximation, defined in Equation (11.8), is shown in Table 11.1 for various cell sizes. We see that G is very small for a wide ranges of cell radius R. These values support the use of the approximation in the calculations.

11.4 MOBILITY PREDICTION IN PICO- AND MICROCELLULAR NETWORKS

It should be expected that 4G networks will further reduce the size of the cells. In a micro-and picocellular network, resources availability varies frequently as users move from one access point to another. In order to deterministically guarantee QoS support for a mobile unit, the network must have prior exact knowledge of the mobile's path, along with arrival and departure times to every cell along the path. With this knowledge, the network can verify the feasibility of supporting the call during its lifetime, as the mobile moves across the network. It is impractical, however, to require the users to inform the network of their exact movement, since they may not know this information *a priori*. Even if the path is known, the exact arrival and departure times to the cells along the path are still hard to determine in advance. Therefore, it becomes crucial to have an accurate mechanism to predict the trajectory of the mobile user.

As an example, the virtual connection tree is designed to support QoS guarantees for mobile units [77]. In this scheme, a number of adjacent cells are grouped into a cell cluster in a static fashion. Upon the admission of a call, the scheme pre-establishes a connection between a root switch and each base station in the cell cluster. The scheme does not take user mobility into consideration to predict the set of base stations which may potentially be visited by the mobile unit. This may result in an unnecessary resource overloading that may underutilize the network resources and cause severe congestion.

The *shadow cluster* (SC) scheme [78] provides a distributed call-admission control (CAC) based on the estimated bandwidth requirements in the SC. An SC is a collection of base stations to which a mobile unit is likely to attach in the future. The admission decision is made in a distributed fashion by all the base stations within the SC. The scheme partitions the time into predefined intervals and verifies the feasibility of supporting calls over those intervals. This requires the communication of large number of messages between base stations during every time interval. Moreover, since bandwidth estimates are calculated at the beginning of each time interval and the admission decisions are made at the end of each time interval, admission of new calls is delayed for at least a time equal to the length of these predefined time intervals.

Both of the above two schemes lack the mechanism to predict the mobile's trajectory and determine the future cells to which the mobile may hand off. Several techniques have been proposed in the literature to address this issue. In Bharghavan and Mysore [79], a profile-based algorithm is proposed to predict the next cell that the mobile unit will hand off, using a user profile and a cell profile, which are simply the aggregate values of the handoff's history. In Liu and Maguire [80], a mobile motion prediction (MMP) algorithm is proposed to predict the future locations of the mobile unit. This algorithm is based on a pattern matching technique that exploits the regularity of the users' movement patterns. The MMP algorithm was further expanded to a two-tier hierarchical location prediction (HLP) algorithm [81]. In the latter case, the two-tiered prediction scheme involves both an intercell and an intracell tracking and prediction component. The first tier uses an approximate pattern matching technique to predict the global intercell direction and the second tier uses an extended self-learning Kalman filter to predict the trajectory within the cell using the measurements received by the mobile unit.

In order to support QoS guarantees of multiple classes of services, the scheme must integrate call and admission control with the mobility profile of the mobile user. The integration of these two components makes it possible to use mobility prediction to verify the feasibility of admitting a new call and make sure that the required QoS can be supported during the lifetime of the call. In other words we should be able to predict location (space) and time when a certain resources well be needed in the network. This concept will be referred to as *space time predictive QoS* or STP QoS. The mobility prediction algorithm must be easy to implement and maintain, since it will be invoked on a per-user basis. Furthermore, the admission control procedure must be invoked only when needed with minimum overhead and in a distributed fashion, where each network cell, potentially involved in supporting the QoS requirements of the call, participates in the decision process [82, 83].

In this section, we present such a framework, which efficiently integrates mobility prediction and CAC, to provide support for PST-QoS guarantees, where each call is guaranteed its QoS requirements for the time interval that the mobile unit is expected to spend within each cell it is likely to visit during the lifetime of the call.

In this framework, efficient support of PST-QoS guarantees is achieved based on an accurate estimate of mobile's trajectory as well as the arrival and departure times for each cell along the path. Using these estimates, the network can determine if enough resources are available in each cell along the mobile's path to support the QoS requirements of the call. The framework is designed to easily accommodate dynamic variations in network resources. The basic components of this framework are:

(1) a predictive service model to support timed-QoS guarantees;

(2) a mobility model to determine the mobile's most likely cluster (MLC); the MLC represents a set of cells that are most likely to be visited by a mobile unit during its itinerary; and

(3) a CAC model to verify the feasibility of supporting a call within the MLC.

The service model accommodates different types of applications by supporting *integral* and *fractional* predictive QoS guarantees over a predefined time-guarantee period. The MLC model is used to actively predict the set of cells that are most likely to be visited by the mobile unit. For each MLC cell, the mobile's earliest arrival time latest arrival time and latest departure time are estimated. These estimates are then used by the CAC to determine the feasibility of admitting a call by verifying that enough resources are available in each of the MLC cells during the time interval between the mobile's earliest arrival time and its latest departure time. If available, resources are then reserved for the time interval between the mobile's earliest arrival time and latest departure time and leased for the time interval between the mobile's earliest and latest arrival times. If the mobile unit does not arrive before the lease expires, the reservation is canceled and the resources

are returned to the pool of available resources. The unique feature of the this frame-work is the ability to combine the mobility model with the CAC model to determine the level of PST-QoS guarantees that the network can provide to a call and dynamically adjust these guarantees as the mobile unit moves across the network.

11.4.1 PST-QoS guarantees framework

The first approach, to achieve a high level of QoS support guarantees in mobile environments, is to allocate resources for the duration of the call in all future cells that the mobile unit will visit. This means that the resources within each cell that is to be visited will be held, possibly for the duration of the call, even if the mobile never moves into the cell. This approach is similar to the one proposed in Talukdar *et al.* [85] and will be referred to as a *predictive space* or PS QoS model. Clearly, such an approach will result in underutilization of the network resources as resources are being held, but not used by any call.

The second approach is to only reserve resources in all future cells that the mobile unit may visit for the time interval during which the mobile will reside in each cell. If t_i and t_{i+1} represent the expected arrival and departure times of the mobile unit to cell i along the path, respectively, resources in cell i will only be reserved for the time interval $[t_i, t_{i+1}]$ [84]. Unlike the first approach, this approach is likely to increase resource utilization, since resources in every cell remain available to other calls outside the reservation intervals. This approach, however, is only feasible if exact knowledge of the mobile path and arrival and departure times to every cell along the path is available. Obtaining exact knowledge of mobile mobility is not possible in most cases, due to the uncertainty of the mobile environments and the difficulty in specifying the mobility profiles of mobile units. An acceptable level of service guarantees, however, can be achieved if the path of the mobile can be predicted accurately. This approach is discussed in this section and will be referred to as *predictive space and time* or the PST QoS model. The model attempts to achieve a balance between an acceptable level of service guarantees and a high level of network resource utilization. Based on this model, the required QoS support level is guaranteed by reserving resources in advance in each cell that is *most likely* to be visited by the mobile unit. These reservations only extend for a time duration equal to the time interval the mobile unit is expected to spend within a cell, starting from the time of its arrival time to the cell until its departure time from the cell. In order to characterize the set of 'most likely' cells and capture the level of QoS guarantees requested by the application, the service model uses the following parameters:

(1) the time guarantee period T_G;

(2) a cluster-reservation threshold τ, and a

(3) bandwidth-reservation threshold, γ.

All of these parameters are application-dependent. The parameter T_G specifies the time duration for which the required QoS level is guaranteed; τ defines the minimum percentage of the most likely cells to be visited by the mobile unit that must support the required QoS level for the guarantee period T_G. The parameter γ represents the minimum percentage of the required bandwidth that must be reserved in every cell that is most likely to be visited.

To accommodate different types of applications, the service model provides two types of predictive service guarantees, namely, *integral guaranteed* service and *fractional guaranteed* service. The integral guaranteed service ensures that all cells, which are most likely to be visited by the mobile unit, can support the requested bandwidth requirements for the lifetime of the call. In this case, T_G must be equal to the call duration and τ and γ are both equal to 100 %. The fractional guaranteed service, on the other hand, guarantees that at least τ % of these cells can support at

least the γ % of the requested bandwidth requirements for the next T_G interval. A special case arises when either the value of τ or γ is zero. In this case, the service is referred to as *best effort*.

11.4.2 Most likely cluster model

The MLC model considers that the 'most likely to be visited' property of a cell is directly related to the position of the cell with respect to the estimated direction of the mobile unit. This likelihood is referred to as directional probability. Based on this metric, cells that are situated along the mobile unit's direction have higher directional probabilities and are more likely to be visited than those that are situated outside of this direction.

Based on the above, the MLC at any point in time during the lifetime of a call is defined as a collection of contiguous cells, each of which is characterized by a directional probability that exceeds a certain threshold. For each MLC cell, the expected arrival and departure times of the mobile are estimated. Using these estimates, the feasibility of supporting the requested level of timed-QoS guarantees during the mobile's residence time within each cell along path is verified. In the following, we present the method used to predict the direction of a mobile unit and the scheme used to construct its MLC. We then describe the algorithm used to estimate the expected times of arrival and departure of the mobile unit to a given cell within the MLC [84].

The *direction-prediction method* used by MLC to predict the mobile user's direction is based on the history of its movement. It is clear, however, that the prediction method used should not be greatly affected by small deviations in the mobile direction. Furthermore, the method should converge rapidly to the new direction of the mobile unit. To take the above properties into consideration, a first-order autoregressive filter, with a smoothing factor α, is used. More specifically, let D_0 be the current direction of the mobile unit when the call is made. Notice that, when the mobile is stationary within a cell, it is assumed that the current cell is the only member of the MLC, so reservations are done only within the current cell. If D_t represents the observed direction of the mobile unit at time t and $\tilde{D}_t$ represents the estimated direction at time t, the predicted direction $\tilde{D}_{t+1}$ at $t+1$ is obtained as $\tilde{D}_{t+1} = (1-\alpha)\,\tilde{D}_t + \alpha D_t$. In order to track the actual direction of the mobile unit more accurately, the smoothing factor α is computed as $\alpha = cE_s^2/\sigma_{s+1}$ where $0 < c < 1$, $E_s = D_s - \tilde{D}_s$ is the prediction error, and σ_s is the average of the past square prediction errors at time s. σ_s can be expressed as $\sigma_{s+1} = cE_s^2 + (1-c)\,\sigma_s$.

The *directional probability*, at any point in time t, of any cell being visited next by a mobile unit, can be derived based on the current cell, where the mobile resides, and the estimated direction $\tilde{D}_t$ of the mobile unit at time t. The basic property of this probability distribution is that for a given direction, the cell that lies on the estimated direction from the current cell has the highest probability of being visited in the future [83]. Consider a mobile unit currently residing at cell i coming from cell m and let $j = 1, 2, \ldots$, represent a set of adjacent cells to cell i. Each cell j is situated at an angle ω_{ij} from the x-axis passing by the center of cell i, as presented in Figure 11.30. If we define the *directional path* from i to j as the direct path from the center of cell i to the center of cell j, the *directionality* D_{ij} for a given cell j can be expressed as

$$D_{ij} = \begin{cases} \dfrac{\theta_{ij}}{\phi_{ij}}, & \phi_{ij} > 0 \\ \theta_{ij}, & \phi_{ij} = 0 \end{cases} \tag{11.36}$$

where ϕ_{ij} is an integer representing the deviation angle between the straight path to destination and the directional path from i to j, while θ_{ij} represents the angle between the directional path from m to i and the directional path from i to j.

Based on its directionality D_{ij}, the directional probability $P_{i\to j}$ of cell j being visited next by a mobile unit currently at cell i can be expressed as $P_{i\to j} = D_{ij}/\sum_k D_{ik}$ where k is a cell at the

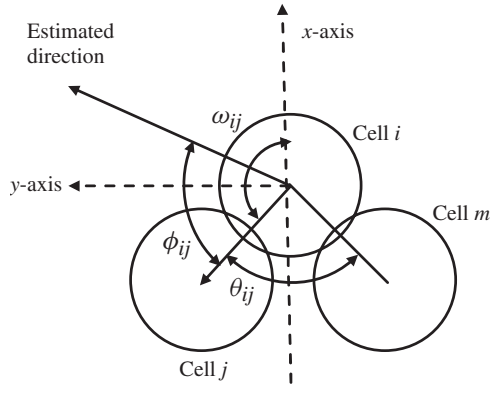

Figure 11.30 Parameters used to calculate the directional probability.

same ring as j with respect to i. A cell k is said to be at ring L with respect to cell i if it is located at a ring L cells away from i. For a given cell i, the directional probabilities $P_{i\rightarrow j}$ provide the basis upon which MLCs are formed as the mobile units moves across the network.

11.4.2.1 Forming the most likely cluster

Starting from the cell where the call originated, a mobile unit is expected to progress toward its destination. The mobile unit, however, can temporarily deviate from its long-term direction to the destination, but is expected to converge back at some point in time toward its destination. This mobility behavior can be used to determine the cells that are likely to be visited by a mobile unit.

Let us define the forward span as the set of cells situated within an angle with respect to the estimated direction $\tilde{D}_t$ of the mobile unit as illustrated in Figure 11.31. Based on the directional probabilities and the definition of a forward span, the MLC of a given mobile unit u currently located at cell i, denoted as $C_i^{\text{MLC}}(u)$, can be expressed as $C_i^{\text{MLC}}(u) = \{\text{cells } j \mid \phi_{ij} \leq \delta_i,\ j = 1, 2, \ldots\}$ where ϕ_{ij} is the deviation angle between the straight path to destination and the directional path

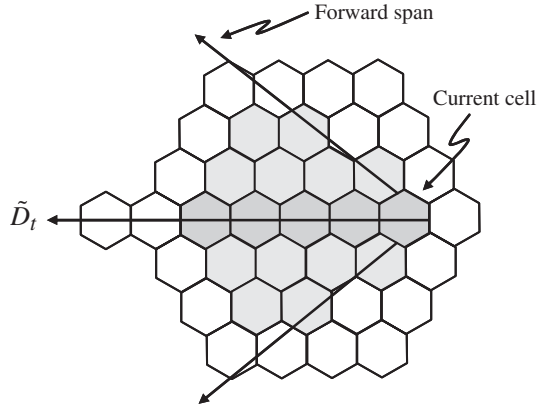

Figure 11.31 Definition of the MLC.

from i to j. The angle δ_i is defined such that $P_{i\to j} \geq \mu$, where μ represents a system defined threshold on the likelihood that cell is to be visited. More specifically, δ_i can be expressed as $\delta_i = \max |\phi_{ij}|$ such that $P_{i\to j} \geq \mu$.

The next step in the process of forming the MLC is to decide on the size of the MLC window, W_{MLC}, which represents the number of adjacent rings of cells to be included in the MLC. Define $\text{Ring}_{i,j}$ to be the ring at which cell j is located with respect to cell i. Therefore, a cell k is included in $C_i^{\text{MLC}}(u)$, if $\text{Ring}_{i,k} \leq W_{\text{LMC}}$ which gives $C_i^{\text{MLC}}(u) = \{\text{cells } j \mid \Phi_{ij} \leq \delta_i, \text{ and } \text{Ring}_{i,j} \leq W_{\text{MLC}} \quad j = 1, 2, \ldots\}$. The size of the MLC window has a strong impact on the performance of the scheme. Increasing the MLC window size, by including more rings, increases the likelihood of supporting the required QoS if the mobile moves along the predicted direction $\tilde{D}(t)$. On the other hand, if the mobile deviates from the predicted direction, increasing the MLC window size may not ensure the continued support of the call, as the mobile unit may move out from the MLC. A possible approach is to reward users who move within the predicted direction by increasing their MLC window size up to a maximum $R_{\max}$. The value of $R_{\max}$ depends on the value of the guarantee period T_G. Higher values of T_G result in larger values of $R_{\max}$.

When the user deviates from the estimated direction, the MLC window size is decreased by an amount proportional to the degree of deviation. As a result, support of the predictable users' QoS requirements can be achieved with high probability, whereas users with unpredictable behavior do not unnecessarily overcommit the network resources. The algorithm dynamically updates the size of the MLC window based on the observed movement patterns of the mobile users. If Δ_t is the measure of the mobile's deviation with respect to the estimated direction at time t, defined as $\Delta_{t+1} = \beta\Delta_t + (1-\beta)|\tilde{D}_t - D_t|$ with $0 < \beta < 1$ and Δ_0 equal to zero, the MLC window size W_{MLC} at time t can be defined as follows:

$$W_{\text{LMC}} = \min\left(R_{\max}, \left\lfloor \left(1 - \frac{\Delta_t}{\pi}\right)^2 \right\rfloor R_{\max}\right) \tag{11.37}$$

The MLC window size is recalculated at every handoff; therefore, the window size shrinks and grows depending on the mobile's behavior.

The method can be easily extended to cellular network with cells of different sizes. When a cellular network has cells of different sizes, the definition of rings is different. The rings are imaginary circles centered at the current cell. The radius of the first ring R_1 is equal to the distance from the center of the current cell to the center of the neighboring cell whose center is farthest away. Consequently, the radius of a ring i, where $i = 1, 2, \ldots$, is equal $i \times R_1$. Any cell that has its center within the boundaries of a ring is considered in that ring.

The *time of arrival* and *residence time* of the mobile can be estimated for each MLC cell. Based on these estimates, the feasibility of supporting the requested level of timed-QoS guarantees within the residence time can then be verified. The cell residence time within cell j for a mobile unit currently in cell i is characterized by three parameters, namely, expected earliest arrival time $[T_{\text{EA}}(i, j)]$, expected latest arrival time $[T_{\text{LA}}(i, j)]$, and expected latest departure time $[T_{\text{LD}}(i, j)]$. Consequently, $[T_{\text{EA}}(i, j), T_{\text{LD}}(i, j)]$ is the expected residence time of the mobile unit within cell j. This interval is referred to as the resource reservation interval (RRI), while the interval $[T_{\text{EA}}(i, j), T_{\text{LA}}(i, j)]$ is referred to as the resource leasing interval (RLI). Resources are reserved for the entire duration of RRI. However, if the mobile does not arrive to cell before RLI expires, all resources are released and the reservation is canceled. This is necessary to prevent mobile units from holding resources unnecessarily.

In order to derive these time intervals, one can adopt the method used in the SC and consider all possible paths from the current cell to each cell in the cluster [78]. This method can be complex, since there are many possible paths that a mobile unit may follow to reach a cell. The approach taken in the MLC model is based on the concept of most likely paths [84].

Consider a mobile unit u, currently located at cell m, and let $C_m^{\text{MLC}}(u)$ denote its MLC. Define $G = (V, E)$ to be a directed graph, where V is a set of vertices and E a set of edges. A vertex $v_i \in V$ represents MLC cell i. For each cell i and j in $C_m^{\text{MLC}}(u)$, an edge (v_i, v_j) is in E if and only if j is a *reachable direct neighbor* of i. Each directed edge is (v_i, v_j) in G is assigned a cost $1/P_{i\to j}$.

A path Π between MLC cells i and k is defined as a sequence of edges $(v_i, v_{i+1}), (v_{i+1}, v_{i+2}), \ldots, (v_{k-1}, v_k)$. The cost of a path between MLC cells i and k is derived from the cost of its edges so that the least costly path represents the most likely path to be followed by the mobile. A *k-shortest paths* algorithm [86] is then used to obtain the set K of *k-most likely paths* to be followed by the mobile unit.

For each path $\Pi \in K$ between MLC cell i and j, we define the *path residence time* as the sum of the residence time of each cell in the path. Let Π_s and Π_1 in K, represent the paths with the shortest and longest path residence time, respectively. Π_s is used to derive the expected earliest arrival time , while Π_1 is used to derive expected latest arrival $T_{\text{LA}}(i, j)$. So, $T_{\text{EA}}(i, j)$ and $T_{\text{LA}}(i, j)$ can be expressed, respectively, as

$$T_{\text{EA}}(i, j) = \sum_{k\in\Pi_1} \frac{d(m, k, n)}{\bar{S}_{\max}(k)}, \quad T_{LA}(i, j) = \sum_{k\in\Pi_1} \frac{d(m, k, n)}{\bar{S}_{\min}(k)} \tag{11.38}$$

where $\bar{S}_{\max}(k)$ and $\bar{S}_{\min}(k)$ represent the average maximum and minimum speed for cell k, respectively. $\bar{S}_{\max}(k)$ and $\bar{S}_{\min}(k)$ are provided by the network support based on the observed mobile units' speeds. $d(m, k, n)$ is the main distance within cell k given that cells m, k, and n are three consecutive cells in the path. The value of $d(m, k, n)$ depends on whether cell k is the cell where the call originated, an intermediate cell or the last cell in the path, i.e. cell j

$$d(m, k, n) = \begin{cases} d_{\text{O}}(k, n), & \text{if } k \text{ is the originating cell} \\ d_{\text{I}}(m, k, n), & \text{if } k \text{ is the intermediate cell} \\ d_{\text{LI}'}(k, n), & \text{if } m = n \\ d_{\text{L}}(m, k), & \text{if } k \text{ is the last cell, k = j} \end{cases} \tag{11.39}$$

When k is the originating cell, the pdf $f_Y(y)$ of the distance Y, within cell k as shown in Figure 11.32, is derived, assuming that the mobile units are evenly spread over a cell area of radius R

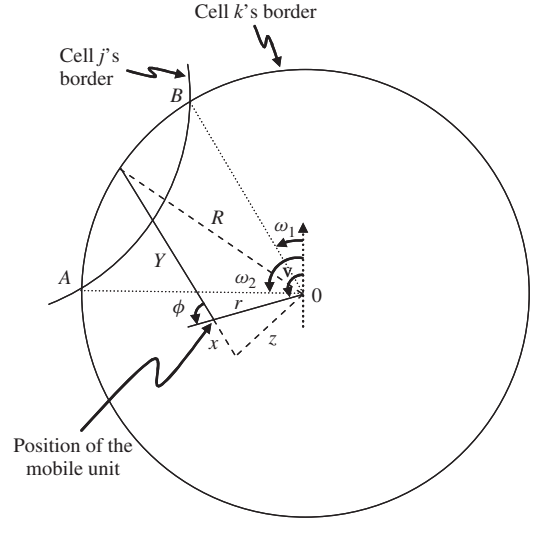

Figure 11.32 Distance Y in originating cell k.

travel along a constant direction within the cell and can exit from the cell from any point along the border with cell n. Therefore, the position of the mobile unit is determined by the angle v and the distance r from the center of the cell. v is uniformly distributed between 0 and 2π; r is uniformly distributed between 0 and R. Since v is uniformly distributed, ϕ is also uniformly distributed between 0 and π. Therefore, $d(k, n)$ is equal to the mean distance $E[Y]$ of the PDF $f_Y(y)$. Based on these assumptions the PDF $f_Y(y)$in a cell where the call originates can be obtained using the standard methods as described in [75]:

$$f_Y(y) = \begin{cases} \dfrac{2}{\pi R^2}\sqrt{\left\{R^2 - \left(\dfrac{y}{2}\right)^2\right\}}, & \text{for} \quad 0 \le y \le 2R \\ 0, & \text{otherwise} \end{cases}$$

which gives

$$d_o(k, n) = E[Y] = \int_0^{2R} y \cdot f_Y(y)\,\mathrm{d}y = \frac{8R}{3\pi} \tag{11.40}$$

When k is an intermediate cell, the PDF $f_Y(y)$ of the distance Y, within cell k, as shown in Figure 11.33, is derived assuming that the mobile units enter cell k from cell m at any point along the arc AB of cell k. This arc is defined by the angles β_1 and β_2: The mobile travels along a constant direction within the cell and can exit from cell k to n from any point along the arc CD of cell k, which is defined by the angles ω_1 and ω_2. The direction of the mobile is indicated by the angle ϕ, which is uniformly distributed; $d(m, k, n)$ is equal to the mean distance $E[Y]$ of the PDF $f_Y(y)$, which is derived in Aljadhai and Znati [84] (see also the Appendix for details) as

$$d_I(m, k, n) = E[Y] = \begin{cases} \dfrac{8R}{(\omega_2 - \omega_1)(\beta_2 - \beta_1)}\left[\sin\left(\dfrac{\beta_2 - \omega_2}{2}\right) - \sin\left(\dfrac{\beta_1 - \omega_2}{2}\right)\right. \\ \qquad \left. - \sin\left(\dfrac{\beta_2 - \omega_1}{2}\right) + \sin\left(\dfrac{\beta_1 - \omega_1}{2}\right)\right] \quad \text{for} \quad \beta_1 \ge \omega_2 \\ \dfrac{8R}{(\omega_2 - \omega_1)\,(\beta_2 - \beta_1)}\left[\sin\left(\dfrac{\omega_1 - \beta_2}{2}\right) - \sin\left(\dfrac{\omega_1 - \beta_1}{2}\right)\right. \\ \qquad \left. - \sin\left(\dfrac{\omega_2 - \beta_1}{2}\right) + \sin\left(\dfrac{\omega_2 - \beta_1}{2}\right)\right] \quad \text{for} \quad \beta_2 \le \omega_1 \end{cases} \tag{11.41}$$

The mean distance in the last cell in the path is derived as follows:

$$d_L(m, k) = \max d(m, k, q) \quad \forall q \text{ adjacent to } k, q \ne m \tag{11.42}$$

The mean distance in the cell k when the path makes a loop within cell k is derived as follows:

$$d_{LP}(m, k, n) = 2d_o(k, n) \tag{11.43}$$

Similarly, the expected latest departure time $T_{LD}(i, j)$ from cell j can be computed as:

$$T_{LD}(i, j) = T_{LA}(i, j) + d(m, k)/\bar{S}_{\min}(k) \tag{11.44}$$

The estimates of $T_{EA}(i, j)$, $T_{LD}(i, j)$ and $T_{LD}(i, j)$ for a mobile u currently located at cell i are used to compute RLI and RRI for each cell $j \in C_i^{MLC}(u)$. The CAC uses these values to verify the feasibility of supporting u's call in each cell $j \in C_i^{MLC}(u)$.

A good agreement between the results of the analytical model of the distance, based on Equations (11.40) and (11.41), and the simulation results of mobile units traveling along the same path, is demonstrated in Aljadhai and Znati: [84].

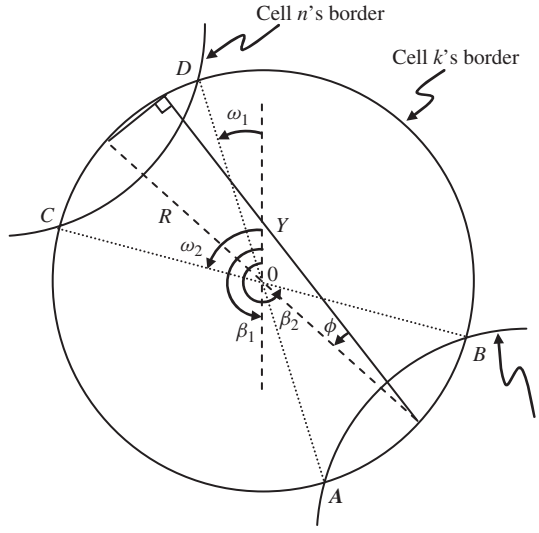

Figure 11.33 Distance Y in an intermediate cell k.

11.4.2.2 Performance example

The MLC CAC scheme is compared with the SC scheme based on the following assumptions [78, 84].

(1) Each cell covers 1 km along a highway. The highway is covered by 10 cells. Mobile units can appear anywhere along a cell with equal probability.

(2) Call holding time is exponentially distributed with mean $T_H = 130$ and 180 s.

(3) Total bandwidth of each cell is 40 bandwidth units (BUs). Three types of calls are used: voice, audio, and video, requiring $B_{voice} = 1$ BU, $B_{audio} = 5$ BUs and $B_{video} = 10$ BUs, respectively. The probabilities of each type are, $P_{voice} = 0.7$, $P_{audio} = 0.2$, and $P_{video} = 0.1$.

(4) Mobile units may have one of three different speeds: 70, 90 or 105 km/h. The probability of each speed is 1/3.

(5) In the SC scheme, the time is quantized in time interval of length 10 s.

(6) A reference scheme, referred to as clairvoyant scheme (CS), is introduced. In this scheme, the exact behavior of every mobile unit is assumed to be known at the admission time. CS reserves bandwidth in exactly the cells that the mobile unit will visit and for the exact residence time interval in every cell. Therefore, CS produces the maximum utilization and minimum blocking ratio for a specific dropping ratio, which is zero in this case.

Since mobile units can appear anywhere along a cell, the residence time within the initial cell (the cell in which the call originates) is selected to be uniformly distributed between zero, and a duration equal to cell length/speed. The initial direction probability is assumed to be 0.5 for both possible directions, i.e. left and right directions. After the first handoff, the direction and position of the call become known and, therefore, it is possible to determine the arrival and departure time in other cells.

Figure 11.34 shows the blocking ratio and Figure 11.35 utilization of the three schemes as functions of the call arrival rate. As expected, CS produces the maximum utilization and minimum

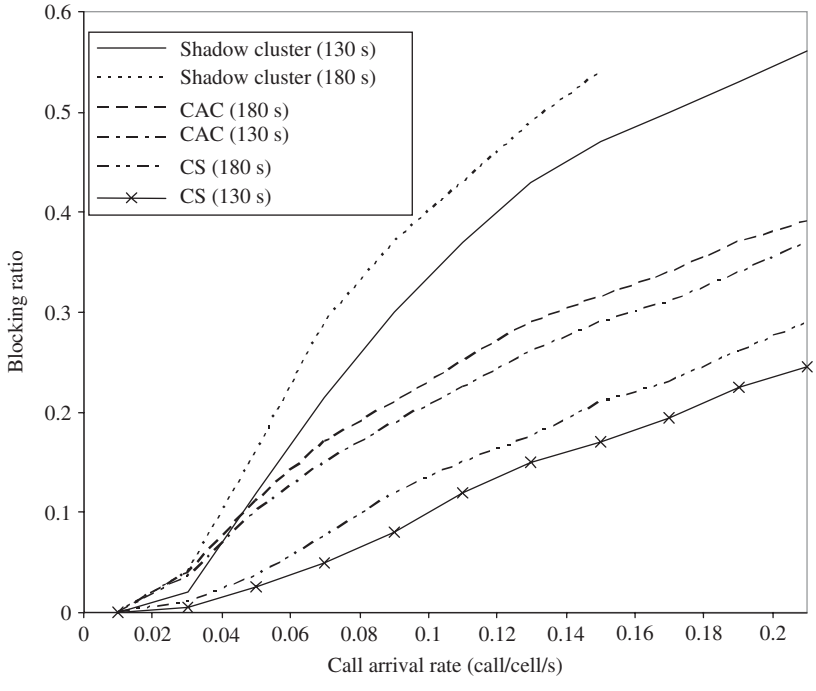

Figure 11.34 Blocking ratio in three systems.

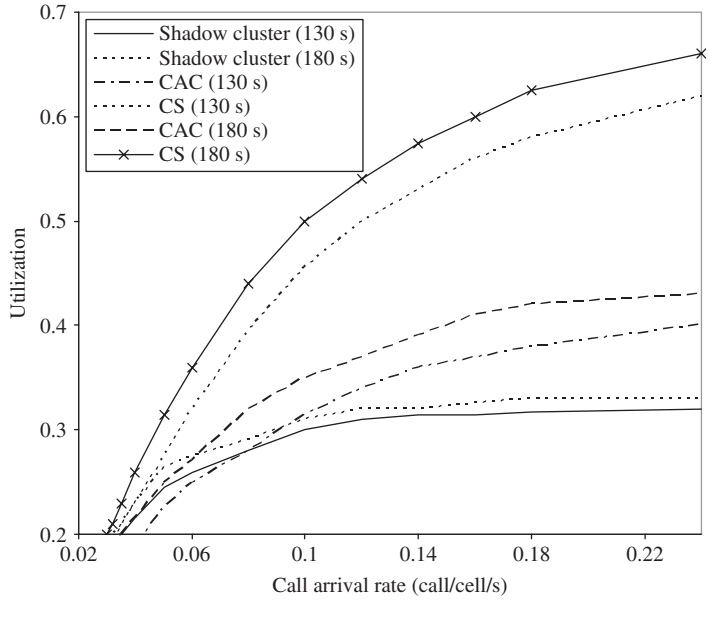

Figure 11.35 Utilization in three systems.

blocking ratio assuming a zero dropping ratio condition. The utilization in the MLC CAC is better than SC as the call arrival rate exceeds 0.06 for all mean call holding times. Moreover, the call blocking in MLC CAC is much less than that of the SC scheme. This behavior shows that, by simply reserving bandwidth between the earliest arrival time and latest departure time at a cell, the MLC scheme accepts more calls and increases utilization. Moreover, the increase in the utilization in the SC scheme is very slow when the call arrival rate is greater than 0.06. The reason for this behavior is that the SC bases its estimates on the exponential holding time PDF, which decreases as time increases. Therefore, the bandwidth estimates decreases as the distance to a future cell increases. As a result, the chance of dropping the call in subsequent cells is increased unless the minimum survivability estimate is increased. In Figures 11.34 and 11.35, the MLC CAC always outperforms the SC regardless of the mean holding time.

APPENDIX: DISTANCE CALCULATION IN AN INTERMEDIATE CELL

Given an intermediate cell on the path of the mobile unit, the PDF of the distance can be derived based on the angles β and ω, as shown in Figure 11.33. The entry point to the cell is assumed to be the point E, as shown in Figure 11.33. The mobile unit move in a direction evenly distributed leading to the next cell (Figure 11.33), where 2ψ is the range of the direction angle ϕ. The angle β is uniformly distributed between β_1 and β_2. Therefore, $f_\beta(\beta)$ is

$$f_\beta(\beta) = \begin{cases} \dfrac{1}{\beta_2 - \beta_1}, & \beta_1 \le \beta \le \beta_2 \\ 0, & \text{elsewhere} \end{cases} \tag{11.45}$$

Since ϕ is evenly distributed, we have

$$f_\phi(\phi \mid \beta) = \begin{cases} \dfrac{2}{\psi_2 - \psi_1}, & \dfrac{\psi_1}{2} \le \phi \le \dfrac{\psi_2}{2} \\ 0, & \text{elsewhere} \end{cases} \tag{11.46}$$

The CDF of the above function can be represented as

$$F_\phi(\phi \mid \beta) = \begin{cases} 0, & \phi < \dfrac{\psi_1}{2} \\ \dfrac{2\phi - \psi_1}{\psi_2 - \psi_1}, & \dfrac{\psi_1}{2} \le \phi \le \dfrac{\psi_2}{2} \\ 1, & \phi > \dfrac{\psi_2}{2} \end{cases} \tag{11.47}$$

where ψ is defined as

$$\psi_i = \begin{cases} \pi - (\beta - \omega_i), & \beta \ge \omega_2 \\ \pi - (\omega_j - \beta), & \beta < \omega_1 \quad \text{and} \quad i \ne j. \end{cases} \tag{11.48}$$

If Y is the distance traveled from E to X, as in Figure 11.33 then, Y becomes $Y = 2R\cos\phi$ and gives in Equation (11.47) the following four cases.
Case 1: $\psi_2/2 > \psi_1/2 \ge 0$

$$F_Y(y \mid \beta) = \begin{cases} 0, & y < 2R\cos\left(\dfrac{\psi_2}{2}\right) \\ 1 - \dfrac{2\text{arco}\cos\left(\dfrac{y}{2R}\right) - \psi_1}{\psi_2 - \psi_1}, & 2R\cos\left(\dfrac{\psi_2}{2}\right) \le y \le 2R\cos\left(\dfrac{\psi_1}{2}\right) \\ 1, & y > 2R\cos\left(\dfrac{\psi_1}{2}\right). \end{cases} \tag{11.49}$$

The PDF of y is

$$f_Y(y \mid \beta) = \begin{cases} \dfrac{1}{(\psi_2 - \psi_1)\sqrt{R^2 - \left(\dfrac{y}{2}\right)^2}}, & 2R\cos\left(\dfrac{\psi_2}{2}\right) \le y \le 2R\cos\left(\dfrac{\psi_1}{2}\right) \\ 0, & \text{elsewhere} \end{cases} \tag{11.50}$$

The mean distance $E[Y \mid \beta]$ is

$$E[Y \mid \beta] = \begin{cases} \displaystyle\int_{2R\cos(\psi_2/2)}^{2R\cos(\psi_1/2)} y \cdot \frac{1}{(\psi_2 - \psi_1)\sqrt{R^2 - \left(\dfrac{y}{2}\right)^2}}\,\mathrm{d}y \end{cases} \tag{11.51}$$

$$= \left\{ \frac{4R}{\psi_2 - \psi_1}\left[\sin\left(\frac{\psi_2}{2}\right) - \sin\left(\frac{\psi_1}{2}\right)\right] \right. \tag{11.52}$$

The mean distance $E[Y]$ for cell $id(m, i, j)$ for a mobile path entering cell i from cell m and exiting cell i to cell j is

$$d(m, i, j) = E[Y] = \int_{\beta_1}^{\beta_2} E[Y \mid \beta] f_\beta(\beta)\,\mathrm{d}\beta \tag{11.53}$$

$$= \left\{ \int_{\beta_1}^{\beta_2} \frac{1}{\beta_2 - \beta_1} \cdot \frac{4R}{\psi_2 - \psi_1}\left[\sin\left(\frac{\psi_2}{2}\right) - \sin\left(\frac{\psi_1}{2}\right)\right] \right.$$

$$= \begin{cases} \dfrac{8R}{(\omega_2 - \omega_1)(\beta_2 - \beta_1)}\left[\sin\left(\dfrac{\beta_2 - \omega_2}{2}\right) - \sin\left(\dfrac{\beta_1 - \omega_1}{2}\right)\right. \\ \qquad \left. - \sin\left(\dfrac{\beta_2 - \omega_1}{2}\right) + \sin\left(\dfrac{\beta_1 - \omega_2}{2}\right)\right] \quad \beta_1 \ge \omega_2 \\ \dfrac{8R}{(\omega_2 - \omega_1)(\beta_2 - \beta_1)}\left[\sin\left(\dfrac{\omega_1 - \beta_2}{2}\right) - \sin\left(\dfrac{\omega_1 - \beta_1}{2}\right)\right. \\ \qquad \left. - \sin\left(\dfrac{\omega_2 - \beta_1}{2}\right) + \sin\left(\dfrac{\omega_2 - \beta_1}{2}\right)\right] \quad \beta_2 \le \omega_1 \end{cases} \tag{11.54}$$

Case 2: $\psi_1/2 < \psi_2/2 \le 0$

$$F_Y(y \mid \beta) = \begin{cases} 0, & y < 2R\cos\left(\dfrac{\psi_2}{2}\right) \\ 1 - \dfrac{2\arccos\left(\dfrac{y}{2R}\right) - \psi_1}{\psi_2 - \psi_1}, & 2R\cos\left(\dfrac{\psi_1}{2}\right) \le y \le 2R\cos\left(\dfrac{\psi_1}{2}\right) \\ 1, & y > 2R\cos\left(\dfrac{\psi_2}{2}\right). \end{cases} \tag{11.55}$$

The PDF of y is

$$f_Y(y \mid \beta) = \begin{cases} \dfrac{-1}{(\psi_2 - \psi_1)\sqrt{R^2 - \left(\dfrac{y}{2}\right)^2}}, & 2R\cos\left(\dfrac{\psi_2}{2}\right) \le y \le 2R\cos\left(\dfrac{\psi_1}{2}\right) \\ 0, & \text{elsewhere} \end{cases} \tag{11.56}$$

The mean distance $E[Y \mid \beta]$ is

$$E[Y \mid \beta] = \begin{cases} \int_{2R\cos(\psi_1/2)}^{2R\cos(\psi_2/2)} y \cdot \dfrac{1}{(\psi_1 - \psi_2)\sqrt{R^2 - \left(\dfrac{y}{2}\right)^2}} \mathrm{d}y \end{cases} \tag{11.57}$$

$$= \left\{ \frac{4R}{\psi_2 - \psi_1} \left[\sin\left(\frac{\psi_2}{2}\right) - \sin\left(\frac{\psi_1}{2}\right) \right] \right. \tag{11.58}$$

The mean distance $E[Y]$ for cell $id(m, i, j)$ for a mobile path entering cell i from cell m and exiting cell i to cell j is

$$d(m, i, j) = E[Y] = \int_{\beta_1}^{\beta_2} E[Y \mid \beta] f_\beta(\beta) \mathrm{d}\beta \tag{11.59}$$

$$= \left\{ \int_{\beta_1}^{\beta_2} \frac{1}{\beta_2 - \beta_1} \cdot \frac{4R}{\psi_2 - \psi_1} \left[\sin\left(\frac{\psi_2}{2}\right) - \sin\left(\frac{\psi_1}{2}\right) \right] \right.$$

$$= \begin{cases} \dfrac{8R}{(\omega_2 - \omega_1)(\beta_2 - \beta_1)} \left[\sin\left(\dfrac{\beta_2 - \omega_2}{2}\right) - \sin\left(\dfrac{\beta_1 - \omega_1}{2}\right) \right. \\ \qquad \left. - \sin\left(\dfrac{\beta_2 - \omega_1}{2}\right) + \sin\left(\dfrac{\beta_1 - \omega_2}{2}\right) \right] \quad \beta_1 \geq \omega_2 \\ \dfrac{8R}{(\omega_2 - \omega_1)(\beta_2 - \beta_1)} \left[\sin\left(\dfrac{\omega_1 - \beta_2}{2}\right) - \sin\left(\dfrac{\omega_1 - \beta_1}{2}\right) \right. \\ \qquad \left. - \sin\left(\dfrac{\omega_2 - \beta_1}{2}\right) + \sin\left(\dfrac{\omega_2 - \beta_1}{2}\right) \right] \quad \beta_2 \leq \omega_1 \end{cases} \tag{11.60}$$

Case 3: $|\psi_1/2| < \psi_2/2$

$$f_Y(y \mid \beta) = f'_Y(y \mid \beta) + f''_Y(y \mid \beta) \tag{11.61}$$

$$F'_Y(y \mid \beta) = \begin{cases} 0, & y < 2R\cos\left(\dfrac{\psi_2}{2}\right) \\ 1 - \dfrac{2\mathrm{arc}\cos\left(\dfrac{y}{2R}\right) - \psi_1}{\psi_2 - \psi_1}, & 2R\cos\left(\dfrac{\psi_2}{2}\right) \leq y \leq 2R \\ 1, & y > 2R \end{cases} \tag{11.62}$$

$$F''_Y(y \mid \beta) = \begin{cases} 0, & y < 2R\cos\left(\dfrac{\psi_2}{2}\right) \\ 1 - \dfrac{2\mathrm{arc}\cos\left(\dfrac{y}{2R}\right) - \psi_1}{\psi_2 - \psi_1}, & 2R\cos\left(\dfrac{\psi_2}{2}\right) \leq y \leq 2R \\ 1, & y > 2R \end{cases} \tag{11.63}$$

The PDF of y is

$$f_Y(y \mid \beta) = f'_Y(y \mid \beta) + f''_Y(y \mid \beta) \tag{11.64}$$

$$f'_Y(y \mid \beta) = \begin{cases} \dfrac{1}{(\psi_2 - \psi_1)\sqrt{R^2 - \left(\dfrac{y}{2}\right)^2}}, & 2R\cos\left(\dfrac{\psi_2}{2}\right) \le y \le 2R \\ 0, & \text{elsewhere} \end{cases} \tag{11.65}$$

$$f''_Y(y \mid \beta) = \begin{cases} \dfrac{-1}{(\psi_2 - \psi_1)\sqrt{R^2 - \left(\dfrac{y}{2}\right)^2}}, & 2R\cos\left(\dfrac{\psi_1}{2}\right) \le y \le 2R \\ 0, & \text{elsewhere} \end{cases} \tag{11.66}$$

The mean distance $E[Y \mid \beta]$ is

$$E[Y \mid \beta] = \begin{cases} \displaystyle\int_{2R\cos(\psi_2/2)}^{2R} y \cdot \frac{1}{(\psi_2 - \psi_1)\sqrt{R^2 - \left(\dfrac{y}{2}\right)^2}} \mathrm{d}y \\ + \displaystyle\int_{2R\cos(\psi_1/2)}^{2R} y \cdot \frac{-1}{(\psi_2 - \psi_1)\sqrt{R^2 - \left(\dfrac{y}{2}\right)^2}} \mathrm{d}y \end{cases} \tag{11.67}$$

$$= \left\{ \frac{4R}{\psi_2 - \psi_1}\left[\sin\left(\frac{\psi_2}{2}\right) - \sin\left(\frac{\psi_1}{2}\right)\right] \right. \tag{11.68}$$

The mean distance $E[Y]$ for cell $id(m, i, j)$ for a mobile path entering cell i from cell m and exiting cell i to cell j is

$$d(m, i, j) = E[Y] = \int_{\beta_1}^{\beta_2} E[Y \mid \beta] f_\beta(\beta)\, \mathrm{d}\beta \tag{11.69}$$

$$= \left\{ \int_{\beta_1}^{\beta_2} \frac{1}{\beta_2 - \beta_1} \cdot \frac{4R}{\psi_2 - \psi_1}\left[\sin\left(\frac{\psi_2}{2}\right) - \sin\left(\frac{\psi_1}{2}\right)\right] \right.$$

$$= \begin{cases} \dfrac{8R}{(\omega_2 - \omega_1)(\beta_2 - \beta_1)}\left[\sin\left(\dfrac{\beta_2 - \omega_2}{2}\right) - \sin\left(\dfrac{\beta_1 - \omega_1}{2}\right)\right. \\ \qquad \left. - \sin\left(\dfrac{\beta_2 - \omega_1}{2}\right) + \sin\left(\dfrac{\beta_1 - \omega_2}{2}\right)\right] \quad \beta_1 \ge \omega_2 \\ \dfrac{8R}{(\omega_2 - \omega_1)(\beta_2 - \beta_1)}\left[\sin\left(\dfrac{\omega_1 - \beta_2}{2}\right) - \sin\left(\dfrac{\omega_1 - \beta_1}{2}\right)\right. \\ \qquad \left. - \sin\left(\dfrac{\omega_2 - \beta_1}{2}\right) + \sin\left(\dfrac{\omega_2 - \beta_1}{2}\right)\right] \quad \beta_2 \le \omega_1 \end{cases} \tag{11.70}$$

Case 4: $|\psi_1/2| < \psi_2/2$

$$F_Y(y \mid \beta) = F'_Y(y \mid \beta) + F''_Y(y \mid \beta) \tag{11.71}$$

$$F'_Y(y \mid \beta) = \begin{cases} 0, & y < 2R\cos\left(\dfrac{\psi_1}{2}\right) \\ 1 - \dfrac{2\arccos\left(\dfrac{y}{2R}\right) - \psi_1}{\psi_2 - \psi_1}, & 2R\cos\left(\dfrac{\psi_2}{2}\right) \le y \le 2R \\ 1, & y > 2R \end{cases} \tag{11.72}$$

$$F_Y''(y \mid \beta) = \begin{cases} 0, & y < 2R\cos\left(\dfrac{\psi_1}{2}\right) \\ 1 - \dfrac{2\text{arco}\cos\left(\dfrac{y}{2R}\right) - \psi_1}{\psi_2 - \psi_1}, & 2R\cos\left(\dfrac{\psi_2}{2}\right) \le y \le 2R \\ 1, & y > 2R \end{cases} \tag{11.73}$$

The PDF of y is

$$f_Y(y \mid \beta) = f_Y'(y \mid \beta) + f_Y''(y \mid \beta) \tag{11.74}$$

$$f_Y'(y \mid \beta) = \begin{cases} \dfrac{-1}{(\psi_2 - \psi_1)\sqrt{R^2 - \left(\dfrac{y}{2}\right)^2}}, & 2R\cos\left(\dfrac{\psi_1}{2}\right) \le y \le 2R \\ 0, & \text{elsewhere} \end{cases} \tag{11.75}$$

$$f_Y'(y \mid \beta) = \begin{cases} \dfrac{1}{(\psi_2 - \psi_1)\sqrt{R^2 - \left(\dfrac{y}{2}\right)^2}}, & 2R\cos\left(\dfrac{\psi_2}{2}\right) \le y \le 2R \\ 0, & \text{elsewhere} \end{cases} \tag{11.76}$$

The mean distance $E[Y|\beta]$ is

$$E[Y \mid \beta] = \begin{cases} \displaystyle\int_{2R\cos(\psi_1/2)}^{2R} y \cdot \frac{-1}{(\psi_2 - \psi_1)\sqrt{R^2 - \left(\dfrac{y}{2}\right)^2}}\,\mathrm{d}y \\ \displaystyle + \int_{2R\cos(\psi_2/2)}^{2R} y \cdot \frac{1}{(\psi_2 - \psi_1)\sqrt{R^2 - \left(\dfrac{y}{2}\right)^2}}\,\mathrm{d}y \end{cases} \tag{11.77}$$

$$= \left\{ \frac{4R}{\psi_2 - \psi_1}\left[\sin\left(\frac{\psi_2}{2}\right) - \sin\left(\frac{\psi_1}{2}\right)\right] \right. \tag{11.78}$$

The mean distance $E[Y]$ for cell $id(m, i, j)$ for a mobile path entering cell i from cell m and exiting cell i to cell j is

$$\begin{aligned} d(m, i, j) = E[Y] &= \int_{\beta_1}^{\beta_2} E[Y \mid \beta] f_\beta(\beta)\,\mathrm{d}\beta \\ &= \left\{ \int_{\beta_1}^{\beta_2} \frac{1}{\beta_2 - \beta_1} \cdot \frac{4R}{\psi_2 - \psi_1}\left[\sin\left(\frac{\psi_2}{2}\right) - \sin\left(\frac{\psi_1}{2}\right)\right] \right. \end{aligned} \tag{11.79}$$

$$= \begin{cases} \dfrac{8R}{(\omega_2 - \omega_1)(\beta_2 - \beta_1)}\left[\sin\left(\dfrac{\beta_2 - \omega_2}{2}\right) - \sin\left(\dfrac{\beta_1 - \omega_1}{2}\right) \right. \\ \quad \left. - \sin\left(\dfrac{\beta_2 - \omega_1}{2}\right) + \sin\left(\dfrac{\beta_1 - \omega_2}{2}\right)\right] \quad \beta_1 \ge \omega_2 \\ \dfrac{8R}{(\omega_2 - \omega_1)(\beta_2 - \beta_1)}\left[\sin\left(\dfrac{\omega_1 - \beta_2}{2}\right) - \sin\left(\dfrac{\omega_1 - \beta_1}{2}\right) \right. \\ \quad \left. - \sin\left(\dfrac{\omega_2 - \beta_1}{2}\right) + \sin\left(\dfrac{\omega_2 - \beta_1}{2}\right)\right] \quad \beta_2 \le \omega_1 \end{cases} \tag{11.80}$$

REFERENCES

[1] A. Acampora, Wireless ATM: A perspective on issues and prospects, *IEEE Person. Commun.*, vol. 3, 1996, pp. 8–17.

[2] A. Acampora, An architecture and methodology for mobile-executed handoff in cellular ATM networks, *IEEE J. Select. Areas Commun.*, vol. 12, 1994, pp. 1365–1375.

[3] A. Acharya, J. Li, F. Ansari and D. Raychaudhuri, Mobility support for IP over wireless ATM, *IEEE Commun. Mag.*, vol. 36, 1998, pp. 84–88.

[4] A. Acharya, J. Li, B. Rajagopalan and D. Raychaudhuri, Mo-bility management in wireless ATM networks, *IEEE Commun. Mag.*, vol. 35, 1997, pp. 100–109.

[5] I.F. Akyildiz, J. McNair, J.S.M. Ho, H. Uzunalioglu and W. Wang, Mobility management in current and future communication networks, *IEEE Network Mag.*, vol. 12, 1998, pp. 39–49.

[6] I.F. Akyildiz and J.S.M. Ho, On location management for personal communications networks, *IEEE Commun. Mag.*, vol. 34, 1996, pp. 138–145.

[7] I.F. Akyildiz, J.S.M. Ho and Y.B. Lin, Movement-based location update and selective paging for PCS networks, *IEEE/ACM Trans. Networking*, vol. 4, 1996, pp. 629–636.

[8] I.F. Akyildiz and J.S.M. Ho, Dynamic mobile user location update for wireless PCS networks, *ACM-Baltzer J. Wireless Networks*, vol. 1, no. 2, 1995, pp. 187–196.

[9] B. Akyol and D. Cox, Re-routing for handoff in a wireless ATM network, *IEEE Personal Commun.*, vol. 3, 1996, pp. 26–33.

[10] V. Anantharam, M.L. Honig, U. Madhow and V.K. Wei, Optimization of a database hierarchy for mobility tracking in a personal communications network, *Performance Eval.*, vol. 20, no. 1–3, 1994, pp. 287–300.

[11] E. Ayanoglu, K. Eng and M. Karol, Wireless ATM: Limits, challenges, and proposals, *IEEE Personal Commun.*, vol. 3, 1996, pp. 19–34.

[12] A. Bar-Noy, I. Kessler and M. Sidi, Topology-based tracking strategies for personal communication networks, *ACM-Baltzer J. Mobile Networks and Applications (MONET)*, vol. 1, no. 1, 1996, pp. 49–56.

[13] A. Bar-Noy, I. Kessler, and M. Sidi, Mobile users: to update or not to update? *ACM-Baltzer J. Wireless Networks*, vol. 1, no. 2, 1995, pp. 175–186.

[14] S. Dolev, D.K. Pradhan and J.L. Welch, Modified tree structure for location management in mobile environments, *Comput. Commun.*, vol. 19, no. 4, 1996, pp. 335–345.

[15] F. Dosiere, T. Zein, G. Maral and J.P. Boutes, A model for the handover traffic in low earth-orbiting (LEO) satellite networks for personal communications, *Int. J. Satellite Commun.*, vol. 11, 1993, pp. 145–149.

[16] N. Efthymiou, Y.F. Hu and R. Sheriff, Performance of inter-segment handover protocols in an integrated space/terrestrial-UMTS environment, *IEEE Trans. Veh. Technol.*, vol. 47, 1998, pp. 1179–1199.

[17] E. Guarene, P. Fasano and V. Vercellone, IP and ATM integration perspectives, *IEEE Commun. Mag.*, vol. 36, 1998, pp. 74–80.

[18] J.S.M. Ho and I.F. Akyildiz, Dynamic hierarchical data-base architecture for location management in PCS networks, *IEEE/ACM Trans. Networking*, vol. 5, no. 5, 1997, pp. 646–661.

[19] J.S.M. Ho and I.F. Akyildiz Local anchor scheme for reducing signaling cost in personal communication networks, *IEEE/ACM Trans. Networking*, vol. 4, no. 5, 1996, pp. 709–726.

[20] J.S.M. Ho and I.F. Akyildiz, A mobile user location update and paging mechanism under delay constraints, *ACM-Baltzer J. Wireless Networks*, vol. 1, no. 4, 1995, pp. 413–425.

[21] D. Hong and S. Rappaport, Traffic model and performance analysis for cellular mobile radio telephone systems with prioritized and nonprioritized handoff procedures, *IEEE Trans. Veh. Technol.*, vol. 35, 1986, pp. 77–92.

[22] L.-R. Hu and S. Rappaport, Adaptive location management scheme for global personal communications, in *Proc. IEEE Communications*, vol. 144, no. 1, 1997, pp. 54–60.

[23] C.-L. I, G.P. Pollini and R.D. Gitlin, PCS mobility manage-ment using the reverse virtual call setup algorithm, *IEEE/ACM Trans. Networking*, vol. 5, 1997, pp. 13–24.
[24] R. Jain and Y.B. Lin, An auxiliary user location strategy employing forwarding pointers to reduce network impact of PCS, *ACM-Baltzer J. Wireless Networks*, vol. 1, no. 2, 1995, pp. 197–210.
[25] R. Jain, Y.B. Lin and S. Mohan, A caching strategy to reduce network impacts of PCS, *IEEE J. Select. Areas Commun.*, vol. 12, 1994, pp. 1434–1444.
[26] D. Johnson and D. Maltz, Protocols for adaptive wireless and mobile networking, *IEEE Personal Commun.*, vol. 3, 1996, pp. 34–42.
[27] S.J. Kim and C.Y. Lee, Modeling and analysis of the dynamic location registration and paging in microcellular systems, *IEEE Trans. Veh. Technol.*, vol. 45, 1996, pp. 82–89.
[28] P. Krishna, N. Vaidya, and D.K. Pradhan, Static and adaptive location management in mobile wireless networks, *Comput. Commun.*, vol. 19, no. 4, 1996, pp. 321–334.
[29] B. Li, S. Jiang and D. Tsang, Subscriber-assisted handoff support in multimedia PCS, *Mobile Comput. Commun. Rev.*, vol. 1, no. 3, 1997, pp. 29–36.
[30] Y.B. Lin Paging systems: network architectures and inter-faces, *IEEE Network*, vol. 11, 1997, pp. 56–61.
[31] Y.B. Lin, Reducing location update cost in a PCS network, *IEEE/ACM Trans. Networking*, vol. 5, 1997, pp. 25–33.
[32] Y.-B. Lin and I. Chlamtac, Heterogeneous personal communication services: Integration of PCS systems, *IEEE Commun. Mag.*, vol. 34, 1996, pp. 106–113.
[33] Y.B. Lin, F.C. Li, A. Noerpel and I.P. Kun, Performance modeling of multitier PCS system, *Int. J. Wireless Information Networks*, vol. 3, no. 2, 1996, pp. 67–78.
[34] Y.B. Lin and S.K. DeVries, PCS network signaling using SS7, *IEEE Commun. Mag.*, vol. 33, 1995, pp. 44–55.
[35] Y.B. Lin, Determining the user locations for personal communications services networks, *IEEE Trans. Veh. Technol.*, vol. 43, 1994, pp. 466–473.
[36] J. Markoulidakis, G. Lyberopoulos, D. Tsirkas and E. Sykas, Mobility modeling in third-generation mobile telecommunications systems, *IEEE Personal Commun.*, vol. 4, 1997, pp. 41–56.
[37] M. Marsan, C.-F. Chiasserini, R. Lo Cigno, M. Munafo and A. Fumagalli, Local and global handovers for mobility management in wireless ATM networks, *IEEE Personal Commun.*, vol. 4, 1997, pp. 16–24.
[38] A.R. Modarressi and R.A. Skoog, Signaling system 7: a tutorial, *IEEE Commun. Mag.*, vol. 28, 1990, pp. 19–35.
[39] S. Mohan and R. Jain, Two user location strategies for personal communications services, *IEEE Personal Commun.*, vol. 1, 1994, pp. 42–50.
[40] R. Pandya, D. Grillo, E. Lycksell, P. Mieybegue, H. Okinaka and M. Yabusaki, IMT-2000 standards: Network aspects, *IEEE Personal Commun.*, 1997, pp. 20–29.
[41] C.E. Perkins, *Mobile IP: Design Principles and Practices*, Addison-Wesley Wireless Communications Series. Reading, MA: Addison Wesley, 1998.
[42] C.E. Perkins, IP mobility support version 2, Internet Engineering Task Force, Internet draft, draft-ietf-mobileip-v2-00.text, November 1997.
[43] C. Perkins, Mobile IP, *IEEE Commun. Mag.*, vol. 35, 1997, pp. 84–99.
[44] C. Perkins, Mobile-IP local registration with hierarchical foreign agents, Internet Engineering Task Force, Internet draft; draft-perkins-mobileip-hierfa-00.txt, February 1996.
[45] B. Rajagopalan, An overview of ATM forum's wireless ATM standards activities, *ACM Mobile Comput. Commun. Rev.*, vol. 1, no. 3, 1997.
[46] B. Rajagopalan, Mobility management in integrated wireless-ATM networks, *ACM-Baltzer J. Mobile Networks Applicat. (MONET)*, vol. 1, no. 3, 1996, pp. 273–285.

[47] E. del Re, A coordinated European effort for the definition of a satellite integrated environment for future mobile communications, *IEEE Commun. Mag.*, vol. 34, 1996, pp. 98–104.
[48] C. Rose, State-based paging/registration: A greedy technique, *IEEE Trans. Veh. Technol.*, vol. 48, 1999, pp. 166–173.
[49] C. Rose and R. Yates, Ensemble polling strategies for in-creased paging capacity in mobile communication networks, *ACM/Baltzer Wireless Networks J.*, vol. 3, no. 2, 1997, pp. 159–167.
[50] C. Rose and R. Yates, Location uncertainty in mobile networks: a theoretical framework, *IEEE Commun. Mag.*, vol. 35, 1997, pp. 94–101.
[51] C. Rose, Minimizing the averagecost of paging and reg-istration: a timer-based method, *ACM-Baltzer J. Wireless Networks*, vol. 2, no. 2, 1996, pp. 109–116.
[52] C. Rose and R. Yates, Minimizing the average cost of paging under delay constraints, *ACM-Baltzer J. Wireless Networks*, vol. 1, no. 2, 1995, pp. 211–219.
[53] S. Tabbane, Location management methods for 3rd generation mobile systems, *IEEE Commun. Mag.*, vol. 35, 1997, pp. 72–78.
[54] C.-K. Toh, A unifying methodology for handovers of het-erogeneous connections in wireless ATM networks, *ACM SIGCOMM Comput. Commun. Rev.*, vol. 27, no. 1, 1997, pp. 12–30.
[55] C.-K. Toh, A hybrid handover protocol for local area wireless ATM networks, *ACM-Baltzer J. Mobile Networks Applicat. (MONET)*, vol. 1, no. 3, 1996, pp. 313–334.
[56] M. Veeraraghavan and G. Dommetry, Mobile location man-agement in ATM networks, *IEEE J. Select. Areas Commun.*, vol. 15, 1997, pp. 1437–1454.
[57] M. Veeraraghavan, M. Karol, and K. Eng, Mobility and connection management in a wireless ATM LAN, *IEEE J. Select. Areas Commun.*, vol. 15, 1997, pp. 50–68.
[58] J.Z. Wang, A fully distributed location registration strategy for universal personal communication systems, *IEEE J. Select. Areas Commun.*, vol. 11, 1993, pp. 850–860.
[59] M. Werner, C. Delucchi, H.-J. Vogel, G. Maral, and J.-J. De Ridder, ATM-based routing in LEO/MEO satellite networks with intersatellite links, *IEEE J. Select. Areas Commun.*, vol. 15, 1997, pp. 69–82.
[60] M. Werner, A. Jahn, E. Lutz, and A. Bottcher, Analysis of system parameters for LEO/ICO-satellite communication net-works, *IEEE J. Select. Areas Commun.*, vol. 13, 1995, pp. 371–381.
[61] R. Yates, C. Rose, B. Rajagopalan and B. Badrinath, Analysis of a mobile-assisted adaptive location management strategy, *ACM-Baltzer J. Mobile Networks Applicat. (MONET)*, vol. 1, no. 2, 1996, pp. 105–112.
[62] A. Yenerand C. Rose, Highly mobile users and paging: Optimal polling strategies, *IEEE Trans. Veh. Technol.*, vol. 47, 1998, pp. 1251–1257.
[63] D.R. Wilson, Signaling system no. 7, IS-41 and cellular telephony networking, *Proc. IEEE*, vol. 80, 1992, pp. 664–652.
[64] C. Perkins and D. Johnson, Route optimization in mobile IP, Internet Engineering Task Force, Internet draft; draft-ietf-mobileip-optom-07.txt, 20 November 1997.
[65] P. Calhoun and C. Perkins, Tunnel establishment protocol, Internet Engineering Task Force, Internet draft; draft-ietfmobileip- calhoun-tep-00.txt, 21 November 1997.
[66] G. Troxel and L. Sanchez, Rapid authentication for mobile IP, Internet Engineering Task Force, Internet draft; draft-ietf-mobileip-ra-00.txt, December 1997.
[67] R. Yuan, S.K. Biswas, L.J. French, J. Li, and D. Raychaudhuri, A signaling and control architecture for mobility support, *ACM-Baltzer J, Mobile Networks Applicat. (MONET)*, vol. 1, no. 3, 1996, pp. 287–298.
[68] M. Johnsson, Simple mobile IP, Internet Engineering Task Force, Internet-draft, Ericsson; draft-ietf-mobileip-simple-00.txt, March 1999.
[69] C.B. Becker, B. Patil and E. Qaddoura, IP mobility architecture framework, Internet Engineering Task Force, Internet draft; draft-ietf-mobileip-ipm-arch-00.txt, March 1999.

[70] J.M. Benedetto, Economy-class ion-defying IC's in orbit, *IEEE Spectrum*, vol. 35, 1998, pp. 36–41.
[71] E. Lutz, Issues in satellite personal communication systems, *ACM J. Wireless Networks*, vol. 4, no. 2, 1998, pp. 109–124.
[72] B. Miller, Satellite free mobile phone, *IEEE Spectrum*, vol. 35, 1998, pp. 26–35.
[73] F. Ananasso and F.D. Priscoli, Issues on the evolution toward satellite personal communication networks, in *Proc. GLOBECOM'95*, London, pp. 541–545.
[74] E. del Re, R. Fantacci and G. Giambene, Call blocking performance for dynamic channel allocation technique in future mobile satellite systems, *Proc. Inst. Elect. Eng., Commun.*, vol. 143, no. 5, 1996, pp. 289–296.
[75] D. Hong and S.S. Rappaport, Traffic model and performance analysis for cellular mobile radio telephone systems with prioritized and non-prioritized handoff procedures, *IEEE Trans. Vehic. Technol.,* vol. VT- 35, no. 3, 1986, pp. 77–92.
[76] CEAS Technical Report no. 773, 1 June 1999, College of Engineering and Applied Sciences, State University of New York, Stony Brook, NY, USA.
[77] A. Acampora and M. Naghshineh, Control and quality-of-service provisioning in high speed microcellular networks, *IEEE Person. Commun.*, vol. 1, 1994, pp. 36–42.
[78] D. Levine, I. Akyildiz and M. Naghshineh, Resource estimation and call admission algorithm for wireless multimedia using the shadow cluster concept, *IEEE/ACM Trans. Networking*, vol. 5, no. 1, 1997, pp. 1–12.
[79] V. Bharghavan and J. Mysore, Profile based next-cell prediction in in-door wireless LANs, in *Proc. IEEE Singapore Int. Conf. Networking*, April 1997, pp. 147–152.
[80] G. Liu and G.Q. Maguire Jr, Transmit activity and intermodal route planner, Technical Report, Royal Institute of Technology, Stockholm, February 1995.
[81] P. Bahl, T. Liu and I. Chlamtac, Mobility modeling, location tracking, and trajectory prediction in wireless ATM networks, *IEEE J. Select. Areas Commun.*, vol. 16, 1998, pp. 922–937.
[82] A. Aljadhai and T. Znati, A framework for call admission control and QoS support in wirelessnetworks, in *Proc. INFOCOM99*, vol. 3, New York, March 1999, pp. 1014–1026.
[83] A. Aljadhai and T. Znati, A predictive bandwidth allocation scheme for multimedia wireless networks, in *Proc. Conf. Communication Networks and Distributed Systems Modeling and Simulation,* Phoenix, AZ, January 1997, pp. 95–100.
[84] A.R. Aljadhai and T.F. Znati. Predictive mobility support for QoS provisioning in mobile wireless environments *IEEE J. Selected Areas Commun.*, vol. 19, no. 10, 2001, pp. 1915–1931.
[85] A. Talukdar, B.R. Badrinath, and A. Acharya, On accommodating mo-bile hosts in an integrated services packet network, in *Proc. IEEE IN-FOCOM*, vol. 3, Kobe, Japan, April 1997, pp. 1046–1053.
[86] S.E. Dreyfus, An appraisal of some shortest-path algorithms, *Opns. Res.*, vol. 17, 1969, pp. 395–412.

12

Cognitive Radio Resource Management

Network optimization, including radio resource management, discussed in Chapter 10, provides algorithms that optimize system performance defined by a given utility function. In this chapter we present suboptimum solutions for resource management that include a high level of cognition and cooperation to mitigate intercell interference. An important segment of this topic dealing with the flexible spectra sharing is covered in another book on advanced wireless communications, which focuses more on the physical layer [1].

12.1 CHANNEL ASSIGNMENT SCHEMES

A given radio spectrum (or bandwidth) can be divided into a set of disjoint or noninterfering radio channels. All such channels can be used simultaneously while maintaining an acceptable received radio signal. In order to divide a given radio spectrum into such channels many techniques such as frequency division (FDMA/OFDMA), time division (TDMA/TH-UWB), or code division (CDMA/MC-CDMA) can be used, as discussed in Chapter 2. In FDMA, the spectrum is divided into disjoint frequency hands, whereas in TDMA the channel separation is achieved by dividing the usage of the channel into disjoint time periods called timeslots. In CDMA, the channel separation is achieved by using different spreading codes. The major criteria in determining the number of channels with a certain quality that can be used for a given wireless spectrum is the level of received signal quality that can be achieved in each channel.

If $S_i(k)$ is the set (i) of wireless terminals that communicate with each other using the same channel k then, due to physical characteristics of the radio environment, the same channel k can be reused simultaneously by another set j if the members of sets i and j are spaced sufficiently apart. All such sets that use the same channel are referred to as cochannel sets or simply cochannels. The minimum distance at which cochannels can be reused with acceptable interference is called the 'cochannel reuse distance' D. For an illustration see Figure 12.1.

Advanced Wireless Technologies: Cognitive, Cooperative & Opportunistic 4G Technology Second Edition Savo G. Glisic

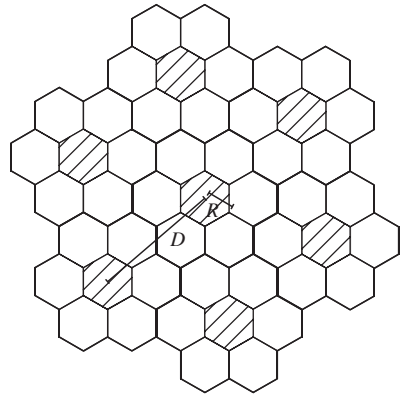

a) Uniform hexagonal cellular layout with reuse 7.

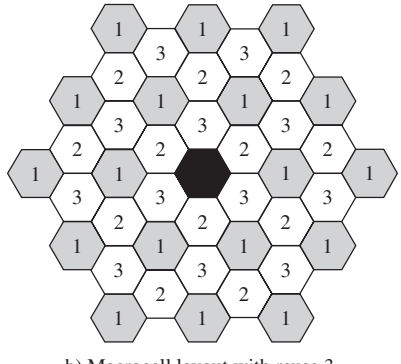

b) Macrocell layout with reuse 3.

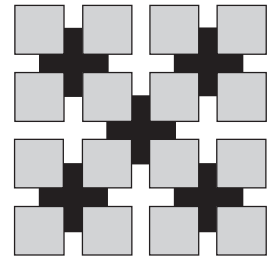

c) Street microcell layout with reuse 2.

Figure 12.1 Examples of the frequency reuse factor.

This is possible because due to propagation path loss in the radio environment, the average power received from a transmitter at distance d is proportional to $P_T d^{-\alpha}$, where α is a number in the range of 3–5 depending on the physical environment and P_T is the average transmitter power. Thus, by adjusting the transmitter power level and/or the distance d between cochannels, a channel can be reused by a number of cochannels if the CIR (carrier-to-interference ratio) in each cochannel is above the required value $CIR_{\min}$.

In general, for a wireless station R at distance d from a transmitter T using the same reference radio channel as the set of other transmitters T_i at distances d_i from R, we have

$$CIR = \frac{S}{I + N_0} = \frac{Pd^{-\alpha}}{\sum_i P_i d_i^{-\alpha} + N_0} \tag{12.1}$$

where N_0 represents the background noise. To achieve a certain level of CIR at the reference station R, different methods can be used. In general, we can represent the residual interference signal power as

$$I \rightarrow I_r(d, \theta, f, t) = (1 - C_f)(1 - C_p)(1 - C_\theta)(1 - C_t) I(d, \theta, f, t) \tag{12.1a}$$

where C_f, C_p, C_θ and C_t are frequency, propagation (distance + shadowing + fading), angle (space) and time isolation coefficients, respectively. $I(d, \theta, f, t)$ is the interference signal power without any suppression techniques [2]. For perfect isolation at least one of these coefficients

is equal to one and the interference has no influence on the received signal. In practice, it is rather difficult and economically impractical to reach the point where $C_i = 1$. Instead, the product $(1 - C_r)(1 - C_\theta)(1 - C_t)$ depending on these coefficients should be kept as low as possible, with an affordable effort measured by cost, power consumption and physical size of the hardware required for the solution.

Coefficient C_f is related to the frequency assignment in the cellular network while coefficient C_p is related to the propagation conditions. $C_f = 1$ if the interfering signal frequency is different from the frequency of the useful signal. $C_p = 1$ if, due to propagation losses, the interfering signal cannot reach the site of the useful reference signal. In general, the same frequency can be used in two cells only if the propagation losses between the two cells are high enough so that the interfering signals are attenuated to the acceptable level. Coefficient C_θ is related to antenna beamforming and possibilities of reducing the interference level by spatial filtering. Finally, interference cancellation and equalization in the time domain can also be used to reduce the level of interference.

In this chapter we will focus on two methods for reducing the interference level. First, the distance between interfering stations using the cochannel and the reference station R can be increased to reduce the cochannel interference level. Many channel allocation schemes are based on this idea of physical separation. Another solution to reduce the CIR at R is to reduce the interfering powers transmitted from interfering stations and/or to increase the desired signal's power level P. This is the idea behind power control schemes. These two methods present the underlying concept for channel assignment algorithms in cellular systems. Each of these algorithms uses a different method to achieve a $CIR_{\min}$ at each mobile terminal by separating cochannels and/or by adjusting the transmitter power.

12.1.1 Different channel allocation schemes

Channel allocation schemes can be divided into a number of different categories depending on the comparison basis. For example, when channel assignment algorithms are compared based on the way in which cochannels are separated, they can be divided into fixed channel allocation (FCA), dynamic channel allocation (DCA) and hybrid channel allocation (HCA).

In *FCA schemes*, the area is partitioned into a number of cells, and a number of channels are assigned to each cell according to some reuse pattern, depending on the desired signal quality. In *DCA*, all channels are placed in a pool and are assigned to new calls as needed such that the criterion is satisfied. At the cost of higher complexity, DCA schemes provide flexibility and traffic adaptability. However, DCA strategies are less efficient than FCA under high-load conditions. To overcome this drawback, HCA techniques were designed by combining FCA and DCA schemes.

Channel assignment schemes can be implemented in many different ways. For example, a channel can be assigned to a radio cell based on the coverage area of the radio cell and its adjacent cells such that the $CIR_{\min}$ is maintained with high probability in all radio cells. Channels could also be assigned by taking the local CIR measurements of the mobile and base station receivers into account; i.e. instead of allocating a channel blindly to a cell based on worst-case conditions (such as letting cochannels be located at the closest boundary), a channel can be allocated to a mobile based on its local CIR measurements [3, 4].

Channel assignment schemes can be implemented in a centralized or distributed fashion. In centralized schemes the channel is assigned by a central controller, whereas in distributed schemes a channel is selected either by the local base station of the cell from which the call is initiated or selected autonomously by the mobile. In a system with cell-based control, each base station keeps information about the current available channels in its vicinity. Here the channel availability information is updated by exchange of status information between base stations. In autonomously organized distributed schemes, the mobile chooses a channel based on its local CIR measurements without the involvement of a central call assignment entity. This scheme is simpler but less efficient. The channel assignment based on local assignment can be done for both FCA and DCA schemes.

12.1.2 Fixed channel allocation

In the FCA strategy a set of nominal channels is permanently allocated to each cell for its exclusive use. Here a definite relationship is assumed between each channel and each cell, in accordance with cochannel reuse constraints [5–9].

The total number of available channels in the system C is divided into sets and the minimum number of channel sets N (reuse factor) required to serve the entire coverage area is related to the reuse distance s as follows [6]: $N = \sigma^2/3$ for hexagonal cells. Here σ is defined as D/R, where R is the radius of the cell and D is the physical distance between the two cell centres [4]. N can assume only the integer values 3, 4, 7, 9, ... as generally presented by the series $(i + j)2 - ij$, with i and j being integers [5]. Figure 12.1(a) and (b) gives the allocation of channel sets to cells for $N = 3$ and $N = 7$, respectively.

In the simple FCA strategy, the same number of nominal channels is allocated to each cell. This uniform channel distribution is efficient if the traffic distribution of the system is also uniform. In that case, the overall average blocking probability of the mobile system is the same as the call blocking probability in a cell. Because traffic in cellular systems can be nonuniform with temporal and spatial fluctuations, a uniform allocation of channels to cells may result in high blocking in some cells, while others might have a sizable number of spare channels. This could result in poor channel utilization. Therefore, the number of channels in a cell can match the load in it by nonuniform channel allocation [10, 11] or static borrowing [12, 13].

In nonuniform channel allocation the number of nominal channels allocated to each cell depends on the expected traffic profile in that cell. Thus, heavily loaded cells are assigned more channels than lightly loaded ones. In Reference [10] an algorithm, called *nonuniform compact pattern allocation*, is proposed for allocating channels to cells according to their traffic distributions. The technique attempts to allocate channels to cells in such a way that the average blocking probability in the entire system is minimized. A similar technique for nonuniform channel allocation is also employed in the algorithms proposed in Reference [11].

Simulation results in Reference [10] show that the blocking probability using nonuniform compact pattern allocation is always lower than the blocking probability of uniform channel allocation. Also, for the same blocking probability, the system can carry, on the average 10 % (maximum 22 %) more traffic with the use of the nonuniform pattern allocation [10].

In the static borrowing schemes proposed in References [12] and [13], unused channels from lightly loaded cells are reassigned to heavily loaded ones at distances $>$ the minimum reuse distance σ. Although in static borrowing schemes channels are permanently assigned to cells, the number of nominal channels assigned in each cell may be reassigned periodically according to spatial inequities in the load. This can be done in a scheduled or predictive manner, with changes in traffic known in advance or based on measurements, respectively.

12.1.3 Channel borrowing schemes

In a channel borrowing scheme, an acceptor cell that has used all its nominal channels can borrow free channels from its neighboring cells (donors) to accommodate new calls. A channel can be borrowed by a cell if the borrowed channel does not interfere with existing calls. When a channel is borrowed, several other cells are prohibited from using it. This is called channel locking. In contrast to static borrowing, channel borrowing strategies deal with short-term allocation of borrowed channels to cells: once a call is completed, the borrowed channel is returned to its nominal cell. The proposed channel borrowing schemes differ in the way a free channel is selected from a donor cell to be borrowed by an acceptor cell.

The channel borrowing schemes can be divided into simple and hybrid. In simple channel borrowing schemes, any nominal channel in a cell can be borrowed by a neighboring cell for temporary use. In hybrid channel borrowing strategies, the set of channels assigned to each cell is

divided into two subsets, A (standard or local channels) and B (nonstandard or channels that can be borrowed). Subset A is for use only in the nominally assigned cell, while subset B is allowed to be lent to neighboring cells.

The channel borrowing schemes can be categorized as:

Simple channel borrowing
- *Simple borrowing* (*SB*)
- *Borrow from the richest* (*SBR*)
- *Basic algorithm* (*BA*)
- *Basic algorithm with reassignment* (*BAR*)
- *Borrow first available* (*BFA*)

Hybrid channel borrowing
- *Simple hybrid borrowing scheme* (*SHCB*)
- *Borrowing with channel ordering* (*BCO*)
- *Borrowing with directional channel locking* (*BDCL*)
- *Sharing with bias* (*SHB*)
- *Channel assignment with borrowing and reassignment* (*CABR*)
- *Ordered dynamic channel assignment with rearrangement* (*ODCA*)

In the next two subsections we discuss the simple and hybrid borrowing schemes in detail.

12.1.4 Simple channel borrowing schemes

In the simple borrowing (SB) strategy [12–15], a nominal channel set is assigned to a cell, as in the FCA case. After all nominal channels are used, an available channel from a neighboring cell is borrowed. To be available for borrowing, the channel most not interfere with existing calls. Although channel borrowing can reduce call blocking, it can cause interference in the donor cells from which the channel is borrowed and prevent future calls in these cells from being completed [16].

As shown in Reference [15] the SB strategy gives lower blocking probability than static FCA under light and moderate traffic, but static FCA performs better in heavy traffic conditions. This is due to the fact that in light and moderate traffic conditions, borrowing of channels provides a means to serve the fluctuations of offered traffic, and as long as the traffic intensity is low the number of donor cells is small. In heavy traffic, the channel borrowing may proliferate to such an extent, due to channel locking, that the channel usage efficiency drops drastically, canting an increase in blocking probability and a decrease in channel utilization [17].

Because the set of channels that can be borrowed in a cell may contain more than one candidate channel, the way a channel is selected from the set plays an important role in the performance of a channel borrowing scheme. The objective of all the schemes is to reduce the number of locked channels caused by channel borrowing. The difference between them is the specific algorithm used for selecting one of the candidate channels for borrowing. Along these lines, several variations of the SB strategy have been proposed where channels are borrowed from nonadjacent cells [10, 12–15]. In the following, we discuss briefly each of the proposed schemes.

12.1.4.1 Borrow from the richest (SBR)

In this scheme, channels that are candidates for borrowing are available channels nominally assigned to one of the adjacent cells of the acceptor cell [12]. If more than one adjacent cell has channels available for borrowing, a channel is borrowed from the cell with the greatest number of channels available for borrowing. As discussed earlier, channel borrowing can cause channel locking. The SBR scheme does not take channel locking into account when choosing a candidate channel for borrowing.

12.1.4.2 Basic algorithm (BA)

This scheme is an improved version of the SBR strategy which takes channel locking into account when selecting a candidate channel for borrowing [12, 13]. This scheme tries to minimize the future call blocking probability in the cell that is most affected by the channel borrowing. As in the SBR ease, channels that are candidates for borrowing are available channels nominally assigned to one of the adjacent cells of the acceptor cell. The algorithm chooses the candidate channel that maximizes the number of available nominal channels in the worst-case nominal cell in distance σ to the acceptor cell.

12.1.4.3 Basic algorithm with reassignment (BAR)

This scheme [13] provides for the transfer of a call from a borrowed channel to a nominal channel whenever a nominal channel becomes available. The choice of the particular borrowed channel to be freed is again made in a manner that minimizes the maximum probability of future call blocking in the cell most affected by the borrowing, as in the BA scheme.

12.1.4.4 Borrow first available (BFA)

Instead of trying to optimize when borrowing, this algorithm selects the first candidate channel it finds [12]. Here the philosophy of the nominal channel assignment is also different. Instead of assigning channels directly to cells, the channels are divided into sets, and then each set is assigned to cells at reuse distance σ. These sets are numbered in sequence. When setting up a call, channel sets are searched in a prescribed sequence to find a candidate channel.

A general conclusion reached by most studies on the performance comparison of the previous schemes is that adopting a simple test for borrowing (e.g. borrowing the first available channel that satisfies the σ constraint) yields performance results quite comparable to systems that perform an exhaustive and complex search method to find a candidate channel [10, 12–14]. SBR, BA and BFA were evaluated by simulation in Reference [12] using a two-dimensional hexagonal cell layout with 360 service channels. The offered load was adjusted for an average blocking of 0.02. The results show that all three schemes exhibit nearly the same average blocking probability versus load. The BFA has an advantage over the other two in that its computing effort and complexity are significantly less. Here the complexity of each algorithm is determined based on the average number of channel tests per call while searching for a candidate channel to borrow. In Reference [12], simulation results showed a large variation in the complexity of these algorithms depending on the network load. For example, for a 20 % increase in the traffic, SBR requires 50 % and the BA 100 % more channel tests compared to BFA.

12.1.5 Hybrid channel borrowing schemes

12.1.5.1 Simple hybrid channel borrowing strategy (SHCB)

In the SHCB strategy [5, 10, 14] the set of channels assigned to each cell is divided into two subsets, A (standard) and B (borrowable) channels. Subset A is nominally assigned in each cell, while subset B is allowed to be lent to neighboring cells. The ratio A/B is determined a priori, depending on an estimation of the traffic conditions, and can be adapted dynamically in a scheduled or predictive manner [14].

12.1.5.2 Borrowing with channel ordering (BCO)

The BCO [10, 14, 15] outperforms SHCB by dynamically varying A/B channel ratio according to changing traffic conditions [14, 15]. In the BCO strategy, all nominal channels are ordered such

that the first channel has the highest priority for being assigned to the next local call and the last channel is given the highest priority for being borrowed by the neighboring cells. A variation of the BCO strategy, called BCO with reassignment, allows intercellular handoff, i.e. immediate reallocation of a released high-rank channel to a call existing in a lower-rank channel in order to minimize the channel locking effect.

12.1.5.3 Borrowing with directional channel locking (BDCL)

In this strategy, a channel is suitable for borrowing only if it is simultaneously free in three nearby cochannel cells. This requirement is too stringent and decreases the number of channels available for borrowing. In the BDCL strategy, the channel locking in the cochannel cells is restricted to those directions affected by the borrowing. Thus, the number of channels available for borrowing is greater than that in the BCO strategy. To determine in which case a 'locked' channel can he borrowed, 'lock directions' are specified for each locked channel. The scheme also incorporates reallocation of calls from borrowed to nominal channels and between borrowed channels in order to minimize the channel borrowing of future calls, especially the multiple-channel borrowing observed during heavy traffic.

It was shown in Reference [10] by simulation that BDCL gives the lowest blocking probability, followed by HCO and FCA, for both uniform and nonuniform traffic. The reduction of the blocking probability for BDCL and BCO over FCA for the system in Reference [10] is almost uniformly 0.04 and 0.03, respectively, for the range of traffic load tested.

The nonuniform pattern allocation FCA scheme, discussed in the previous section, can also be applied in the case of the hybrid channel borrowing strategies. With the use of nonuniform pattern allocation the relative performance of the BDCL, BCO and uniform FCA schemes remain the same as before, but the traffic-carrying capacity of a system can be increased by about 10 %. This advantage is in addition to those gained from the channel borrowing strategies [10].

12.1.5.4 Sharing with bias (SHB)

In Reference [18] a scheme of channel borrowing with coordinated sectoring is described. The SHB strategy is similar to the join biased queue rule, which is a simple but effective way to balance the load of servers in the presence of unbalanced traffic. Each cell in the system is divided into three sectors, X, Y, Z, as shown in Figure 12.2. Only calls initiated in one of these sectors can borrow channels from the two adjacent cells neighboring it (donor cells). In addition, the nominal channels in donor cells are divided into two subsets, A and B, as in the SHCB case. Channels

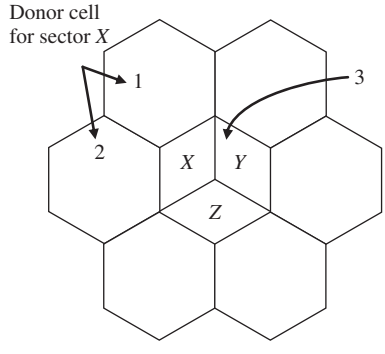

Figure 12.2 Sharing with bias.

from set A can only be used inside the donor cell, while channels in set B can be loaned to an acceptor cell.

For the example shown in Figure 12.2 a call initiated in sector X of cell number 3 can only borrow a channel from set A of the cells numbered 1 and 2.

12.1.5.5 Channel assignment with borrowing and reassignment (CARB)

The scheme was proposed in Reference [13] and is statistically optimum in a certain min–max sense. Here channels are borrowed on the basis of causing the least harm to neighboring cells in terms of a future call blocking probability. Likewise, reassignment of borrowed channels is done in a way to cause maximum relief to neighboring cells.

12.1.5.6 Ordered channel assignment scheme with rearrangement (ODCA)

This scheme, proposed in Reference [19], combines the merits of CARB and BCO with improvements to yield a higher performance. In ODCA, when a call requests service, the base station of the cell checks to see if there are any nominal channels available. If there are channels available, the user will be assigned one on an ordered basis, as in BCO. Here all channels are numbered in a predetermined order according to the same criterion as in the CARB scheme, and the lowest-numbered available idle channel is always selected. If all nominal channels are busy, the cell may borrow a nonstandard channel from a neighboring cell. Once a nonstandard channel is assigned, the availability lists of all affected cells where the assigned channel can cause interference are updated. Whenever a channel is no longer required, the availability lists of the affected cells are updated accordingly. Whenever a standard channel is available, the channel reassignment procedure is initiated to ensure efficient utilization. If there is a nonstandard channel in use in the cell, the call served by that channel is switched to the newly freed standard channel; the necessary availability lists are also updated. If no nonstandard channels are used in the cell, a call served by a standard channel with lower priority than the newly freed one is switched to the newly freed channel [19].

The performance of ODCA was studied in Reference [19] for a highway microcellular environment with a nonuniform teletraffic load. A performance comparison with the FCA and CARB shows significant improvement. The ODCA scheme exhibits better channel utilization compared to the CARE and FCA; the OUCA scheme also performs better than CARE and FCA at blocking probabilities below 0.1. For example, at a blocking probability of 0.05, ODCA is capable of supporting 4 % more traffic than CARE and 35 % more traffic than FCA [19]. However, the ODCA scheme incurs a higher computational overhead in assigning and reassigning channels, and more frequent switching of channels due to the reassignment propagation effect.

12.1.6 Dynamic channel allocation

Due to short-term temporal and spatial variations of traffic in cellular systems, FCA schemes are not able to attain high channel efficiency. To overcome this, DCA schemes have been studied during the past 20 years. In contrast to FCA, there is no fixed relationship between channels and cells in DCA. All channels are kept in a central pool and are assigned dynamically to radio cells as new calls arrive in the system [20]. After a call is completed, its channel is returned to the central pool.

In DCA, a channel is eligible for use in any cell provided that signal interference constraints are satisfied. Because, in general, more than one channel might be available in the central pool to be assigned to a cell that requires a channel, some strategy must be applied to select the assigned channel [9]. The main idea of all DCA schemes is to evaluate the cost of using each candidate

channel and select the one with the minimum cost provided that certain interference constraints are satisfied. The selection of the cost function is what differentiates DCA schemes [9]. The selected cost function might depend on the future blocking probability in the vicinity of the cell, the usage frequency of the candidate channel, the reuse distance, channel occupancy distribution under current traffic conditions, radio channel measurements of individual mobile users or the average blocking probability of the system [17].

Based on information used for channel assignment, DCA strategies could be classified either as call-by-call DCA or adaptive DCA schemes [21]. In the call-by-call DCA, the channel assignment is based only on current channel usage conditions in the service area, while in adaptive DCA the channel assignment is adaptively carried out using information on the previous as well as present channel usage conditions [21]. DCA schemes can also be divided into centralized and distributed schemes with respect to the type of control they employ. In general, the schemes can be classified into the following groups:

(1) *Centralized DCA*
   First available (FA)
   Locally optimized dynamic assignment (LODA)
   Selection with maximum usage on the reuse ring (RING)
   Mean square (MSQ)
   Nearest neighbor (NN)
   Nearest neighbor + 1 (NN + 1)
   1, clique
(2) *Distributed DCA*
   Locally packing distributed DCA (LP-DDCA)
   LP-DDCA with ACI constraint
   Moving direction (MD)
(3) *CIR measurement DCA schemes*
   Sequential channel search (SCS)
   MSIR
   Dynamic channel selection (DCS)
   Channel segregation
(4) *One dimension systems*
   MINMAX
   Minimum interference (MI)
   Random minimum interference (RMI)
   Random minimum interference with reassignment (RMIR)
   Sequential minimum interference (SMI)

12.1.7 Centralized DCA schemes

In centralized DCA schemes, a channel from the central pool is assigned to a call for temporary use by a centralized controller. The difference between these schemes is the specific cost function used for selecting one of the candidate channels for assignment.

12.1.7.1 First available (FA)

FA is the simplest of the DCA schemes strategy. In FA the first available channel within the reuse distance found during a channel search is assigned to the call. The FA strategy minimizes the system computational time and, as shown by the simulation in Reference [9] for a linear cellular mobile system, it provides an increase of 20 % in the total handled traffic compared to FCA for low and moderate traffic loads.

12.1.7.2 Locally optimized dynamic assignment (LODA)

LODA uses a cost function based on the future blocking probability in the vicinity of the cell in which a call is initiated [10, 14].

12.1.7.3 Channel reuse optimization schemes

The objective of any mobile system is to maximize the efficiency of the system. Maximum efficiency is equivalent to maximum utilization of every channel in the system. It is obvious that the shorter the channel reuse distance, the greater the channel reuse over the whole service area. The cost functions selected in the following schemes attempt to maximize the efficiency of the system by optimizing the reuse of a channel in the system area.

12.1.7.4 Selection with maximum usage on the reuse ring (RING)

RING selects a candidate channel that is in use in the most cells in the cochannel set. If more than one channel has this maximum usage, an arbitrary selection among such channels is made to serve the call. If none is available, the selection is made based on the FA scheme.

12.1.7.5 Mean square (MSQ), nearest neighbor (NN), nearest neighbour plus one (NN + 1)

The MSQ scheme selects the available channel that minimizes the mean square of the distance among the cells using the same channel. The NN strategy selects the available channel occupied in the nearest cell in distance $\geq \sigma$, while the NN + 1 scheme selects an eligible channel occupied in the nearest cell within distance $\geq \sigma + 1$ or distance σ if an available channel is not found in distance $\sigma + 1$ [9].

Computer simulations of FCA, MSQ, NN and NN + 1 strategies show that under light traffic conditions, NN exhibits the lowest blocking rate, followed by MSQ, FA and NN + 1 [21]. When applied to a microcellular system, the NN + 1 strategy leads to lower forced call termination and channel changing because the mobile unit is more likely to keep the same channel when it moves to an adjacent cell [22]. In addition, simulation results of FA, RING and NN [9, 23] show that for both one- and two-dimensional mobile systems, all of the above schemes operate at very low blocking rates until the offered traffic reaches some threshold. A small increase in the offered traffic above this threshold produces a considerable increase in the blocking probability of new calls and results in very little increase in the traffic carried by the system. The load at which blocking begins to occur in one-dimensional systems [23] is somewhat greater than that in two-dimensional systems [9]. Finally, the simulation results in Reference [23] show that strategies like RING and NN, which use a channel reuse optimization approach, are able to carry 5 % more traffic at a given blocking rate of 3 % compared to a channel assignment strategy like FA, which does not employ any channel reuse optimization.

12.1.7.6 The 1-clique scheme

All four previous schemes employ local channel reuse optimization schemes. A global channel reuse optimization approach is used in the 1-clique strategy. The 1-clique scheme uses a set of graphs, one for each channel, expressing the non-cochannel interference structure over the whole service area for that channel. In each graph a vertex represents a cell, and cells without cochannel interference are connected with edges. Therefore, each graph reflects the results of a possible channel assignment. A channel is assigned from several possibilities such that as many vertices

as possible still remain available after the assignment. This scheme shows a low probability of blocking, but when there are a lot of cells the required computational time makes quick channel selection difficult [20].

12.1.7.7 Schemes with channel rearrangement

Compared to FCA schemes, DCA schemes do not carry as much traffic at high blocking rates because they are not able to maximize channel reuse as they serve the randomly offered call attempts. In order to improve the performance of DCA schemes at high traffic density, channel reassignment techniques have been suggested [6, 9]. The basic goal of channel reassignment is to switch calls already in process, whenever possible, from the channels these calls are using to other channels, with the objective of keeping the distance between cells using the same channel simultaneously to a minimum. Thus, channel reuse is more concentrated and more traffic can be carried per channel at a given blocking rate.

12.1.7.8 Distributed DCA schemes

Microcellular systems have shown great potential for capacity improvement in high-density personal communication networks. However, propagation characteristics will be less predictable and network control requirements more complex than in the other systems. Centralized DCA schemes can produce near-optimum channel allocation, but at the expense of a high centralization overhead. Distributed schemes are therefore more attractive for implementation in microcellular systems, due to the simplicity of the assignment algorithm in each base station.

The proposed distributed DCA schemes use either local information about the current available channels in the cell's vicinity (cell-based) [24] or signal strength measurements [25].

In cell-based schemes a channel is allocated to a call by the base station at which the call is initiated. The difference with the centralized approach is that each base station keeps information about the current available channels in its vicinity. The channel pattern information is updated by exchanging status information between base stations. The cell-based scheme provides near-optimum channel allocation at the expense of excessive exchange of status information between base stations, especially under heavy traffic loads.

Particularly appealing are the DCA interference adaptation schemes, which rely on signal strength measurements where a base station uses only local information, without the need to communicate with any other base station in the network. Thus, the system is self-organizing and channels can be placed or added everywhere, as needed, to increase capacity or to improve radio coverage in a distributed fashion. These schemes allow fast real-time processing and maximal channel packing at the expense of increased cochannel interference probability with respect to ongoing calls in adjacent cells, which may lead to undesirable effects such as interruption, deadlock and instability.

12.1.8 Cell-based distributed DCA schemes

12.1.8.1 Local packing dynamic distributed channel assignment (LP-DDCA)

LP-DDCA is a scheme where each base station assigns channels to calls using the augmented channel occupancy (ACO) matrix, which contains necessary and sufficient local information for the base station to make a channel assignment decision. With M available channels in the system and k neighboring cells to cell i within the cochannel interference distance, the ACO matrix is shown in Table 12.1. It has $M + 1$ columns and $k_i + 1$ rows. The first M columns correspond to the M channels. The first row indicates the channel occupancy in cell i and the remaining k_i rows

Table 12.1 ACO matrix at base station i. (Reproduced by permission of IEEE [77])

Base station number	Channel number								Number of assignable channels
	1	2	3	4	5	6	$\cdots$	M	
i		×					$\cdots$		0
i_1	×			×			$\cdots$		0
i_2		×					$\cdots$		2
$\vdots$	$\vdots$	$\vdots$	$\vdots$	$\vdots$	$\vdots$	$\vdots$	$\vdots$	$\vdots$	$\vdots$
i_{k_i}			×		×				4

indicate the channel occupancy pattern in the neighborhood of i, as obtained from neighboring base stations. The last column of the matrix corresponds to the number of current available channels for each of the $k_i + 1$ cochannel cells. Therefore, an empty column indicates an idle channel, which can be assigned to cell i. When a call requests service from cell i, its base station will use the ACO matrix to assign the first channel with an empty column. The content of the ACO table is updated by collecting channel occupancy information from interfering cells. Whenever a change of channel occupancy happens in one cell, the base station of the cell informs the base stations of all the interfering cells about the change in order to update the data in the local ACO matrices.

In addition to constraining cochannel interference, the design of a wireless cellular systems must also include measures to limit adjacent channel interference (ACI). In Reference [9] a modified version of the LP-DDCA scheme was proposed that incorporates the ACI constraint.

12.1.8.2 Moving direction (MD)

The MD strategy was proposed in Reference [24] for one-dimensional microcellular systems. In these systems, forced call termination and channel changing occur frequently because of their small cell size [24]. The MD strategy uses information on moving directions of the mobile units to decrease both the forced call termination blocking probability and the channel changing. An available channel is selected among those assigned to mobile units that are elsewhere in the service area and moving in the same direction as the mobile in question. The search for such a channel starts from the nearest noninterfering cell to the one where the new call was initiated and stops at the cell that is α reuse distances away, where α is a parameter.

A channel assignment example is given in Figure 12.3, where b, c, d and e are the available channels and DR is the minimum reuse distance. For this example the parameter α is set to one. The new call attempt is assigned channel b because the mobile requesting the channel is moving in the same direction as the mobile in cell number 5.

The sets of mobiles moving in the same direction and assigned the same channel are thus formed. When a mobile of a set crosses a cell boundary it is likely that a same set of mobiles has already crossed out of its cell to the next cell. In this manner a mobile can use the same channel after handoff with higher probability. This lowers the probability of both changing channels and forced call termination. The strategy is efficient in systems where mobiles move at nearly the same speed through the cells laid along a road or a highway and for one-dimensional microcellular systems.

The simulation results in Reference [24] for a one-dimensional system show that the MD strategy provides a lower probability of forced call termination compared to the NN, NN + 1 and FCA strategies. Although the MD scheme has attractive features, it is not obvious how it could be expanded to a two-dimensional system.

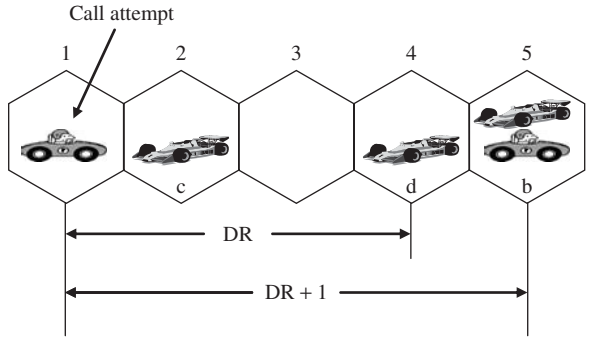

Figure 12.3 Moving direction strategy illustration.

12.1.9 Signal strength measurement-based distributed DCA schemes

A large body of research has been published on the performance analysis of traditional channel allocation schemes, both FCA and DCA [3, 5, 26], in which knowledge of the mobile locations is not taken into account. In all of these schemes, channels are allocated to cells based on the assumption that the mobile may be located anywhere within the boundary of the cell. Thus, the packing of channels is not maximal. These schemes suffer from the fact that the selected fixed reusability distance might be too pessimistic.

In the interference adaptation schemes, mobiles measure the amount of cochannel interference to determine the reusability of the channel. If a mechanism is assumed to exist by which mobiles and base stations can measure the amount of interference, then maximal channel packing could be achieved. An example of a system based on this principle is the digital European cordless telecommunications (DECT) standard.

However, local decisions can lead to suboptimal allocation. In interference adaptation DCA schemes, mobiles and base stations estimate CIR and allocate a channel to a call when predicted CIRs are above a threshold. It is possible that this allocation will cause the CIR of established calls to deteriorate, in which case a service interrupt occurs. If the interrupted call cannot find an acceptable new channel immediately, the result is a premature service termination, referred to as deadlock. Even if the interrupted call finds an acceptable channel, setting up a link using the new channel can cause interruption of another established link. These successive interruptions are referred to as instability. If no channel is available for the initial call request, the call is blocked.

12.1.9.1 Sequential channel search (SCS)

The simplest scheme among the interference adaptation DCA schemes is the SCS strategy, where all mobile–base station pairs examine channels in the same order and choose the first available with an acceptable CIR. It is expected that SCS will support a volume of traffic by suboptimal channel packing at the expense of causing many interruptions.

12.1.9.2 Dynamic channel selection (DCS)

DCS is a fully distributed algorithm for flexible mobile cellular radio resource sharing based on the assumption that mobiles are able to measure the amount of interference they experience in each channel. In DCS, each mobile station estimates the interference probability and selects the base station that minimizes its value. The interference probability is a function of a number of

parameters, such as the received signal power from base stations, the availability of channels and cochannel interference. In order to evaluate the interference probability, specific models for each of the above parameters should be developed. In Reference [27], models are developed to calculate probabilities of channel availability, desired carrier power and the CIR for constant traffic load.

12.1.9.3 Channel segregation

The channel segregation strategy was proposed in Reference [25] as a self-organized dynamic channel assignment scheme. By scanning all channels, each cell selects a vacant channel with an acceptable cochannel interference level. The scanning order is formed independently for each cell in accordance with the probability of channel selectability, $P(i)$, which is renewed by learning. For every channel i in the system, each cell keeps the current value of $P(i)$. When a call request arrives at the base station, the base station channel with the highest value of $P(i)$ under observation is selected. Subsequently, the received power level of the selected channel is measured in order to determine whether the channel is used or not. If the measured power level is below (or above) a threshold value, the channel is considered to be idle (or busy). If the channel is idle, the base station starts communication using the channel, and its priority is increased. If the channel is busy, the priority of the channel is decreased and the next-highest-priority channel tried. If all channels are busy, the call is blocked. The value of $P(i)$ and the update mechanism determine the performance of the algorithm. In Reference [28], $P(i)$ is updated to show the successful transmission probability on channel i as follows:

$P(i) = [P(i)N(i) + 1]/[N(i) + 1]$ and
$N(i) = N(i) + 1$ if the channel is idle
$P(i) = [P(i)N(i)]/[N(i) + 1]$ and
$N(i) = N(i) + 1$ if the channel is busy

Here $N(i)$ is the number of times channel i is accessed. In Reference [25] the update mechanism for $P(i)$ is defined as $F(i) = N_s(i)/N(i)$ where $N_s(i)$ is the number of successful uses of channel i.

Simulation results show that interference due to carrier sense error is reduced by 1/10–1/100 with channel segregation [28]. Also, the blocking probability is greatly reduced compared to FCA and DCA schemes.

12.1.10 One-dimensional cellular systems

All the DDCA schemes described in this section are applicable for one-dimensional cellular mobile systems. One-dimensional structures can be identified in cases such as streets with tall buildings shielding interference on either side (see Figure 12.1(c)).

12.1.10.1 Minimum Interference (MI) scheme

The MI scheme is well known and among the simplest for one-dimensional cellular systems. It is incorporated in the enhanced cordless telephone (CT-2) and DECT systems. In an MI scheme, a mobile signals its need for a channel to its nearest base station. The base station then measures the interfering signal power on all channels not already assigned to other mobiles. The mobile is assigned the channel with the minimum interference. The order in which mobiles are assigned

channels affects the efficiency of channel reuse. Taking into consideration the order of service we discuss three variations of the MI scheme:

- *Random minimum interference* (*RMI*) is the scheme where mobiles are served according to the MI scheme in a random order or, equivalently, in the order in which calls arrive in the system.
- *Random minimum interference with reassignment* (*RMIR*) is a modification where mobiles are first served according to the RMI scheme. Each mobile is then reassigned a channel by its base station according to the MI scheme. Those mobiles denied service by the initial RMI scheme also try to obtain a channel again. The order in which mobiles are reassigned is random. The number of times this procedure is carried out is the number of reassignments, R.
- *Sequential minimum interference* (*SAI*) is a modification where mobiles are assigned channels according to the MI scheme in a sequential order. The sequence followed is such that any mobile is served only after all the mobiles that are ahead of it have had a chance to be served. This procedure would require some coordination between base stations because of the sequential order of service.

In general, there is a tradeoff between the quality of service, the implementation complexity of the channel allocation algorithms and spectrum utilization efficiency. Simulation [5, 8, 9] results show that under low traffic intensity DCA strategies performs better. However, FCA schemes become superior at high offered traffic, especially in the case of uniform traffic. In the ease of nonuniform traffic and light to moderate loads, it is believed that the DCA scheme will perform better due to the fact that under low traffic intensity DCA uses channels more efficiently than FCA.

In DCA, the assignment control is made independently in each cell by selecting a vacant channel among those allocated to that cell in advance. In DCA the knowledge of occupied channels in other cells as well as in the cell in question is necessary. The amount of control is different in each DCA strategy. If the DCA requires a lot of processing and complete knowledge of the state of the entire system, the call setup delay would be significantly long without high-speed computing and signaling. The implementation complexity of the DCA is discussed in Reference [29].

12.1.10.2 Hybrid channel assignment schemes

HCA schemes are a mixture of the FCA and DCA techniques. In HCA, the total number of channels available for service is divided into fixed and dynamic sets. The fixed set contains a number of nominal channels that are assigned to cells as in the FCA schemes and, in all cases, are to be preferred for use in their respective cells. The second set of channels is shared by all users in the system to increase flexibility. When a call requires service from a cell and all of its nominal channels are busy, a channel from the dynamic set is assigned to the call. The channel assignment procedure from the dynamic set follows any of the DCA strategies described in the previous section. For example, in the studies presented in References [5] and [30], the FA and RING strategies are used, respectively, for DCA. Variations of the main RCA schemes include HCA with channel reordering [30] and HCA schemes where calls that cannot find an available channel are queued instead of blocked [6]. The call blocking probability for an HCA scheme is defined as the probability that a call arriving to a cell finds both the fixed and dynamic channels busy.

Performance evaluation results of different HCA schemes have been presented in References [5] to [7] and [31]. In Reference [5], a study is presented for an HCA scheme with Erlang-b service discipline for uniform size and shape cells where traffic is uniformly distributed over the whole system. The measure of interest is the probability of blocking as the load increases for different ratios of fixed to dynamic cells. As shown in Reference [5], for a system with a fixed-to-dynamic channel ratio of 3:1, the HCA gives a better grade of service than FCA for load increases up

to 50 %. Beyond this load HCA performs better in all cases studied in Reference [5]. A similar pattern of behaviour is obtained for the HCA scheme with the FA-DCA scheme and Ertang-c service discipline (calls that cannot find an available channel are queued instead of blocked). In addition, the HCA scheme with Erlang-c service discipline [6] has a lower probability of blocking than the HCA scheme with Erlang-b service discipline [5]. This phenomenon is expected because in the former case calls are allowed to be queued until they can be served.

In Reference [31], two different approximating models were presented. In the first model the traffic offered in the dynamic channels is modeled as an interrupted poison process, while the second used GI/M/m(m). The blocking probability versus the arrival rate for both models present the same pattern of behaviour as the simulation results of References [5] and [6].

12.1.10.3 Flexible channel allocation (FlCA)

FlCA schemes divide the set of available channels into fixed and flexible sets. Each cell is assigned a set of fixed channels that typically suffices under a light traffic load. The flexible channels are assigned to those cells whose channels have become inadequate under increasing traffic loads. The assignment of these emergency channels among the cells is done in either a scheduled or predictive manner [32]. In the literature proposed F1CA techniques differ according to the time at which and the basis on which additional channels are assigned.

In the predictive strategy, the traffic intensity or, equivalently, the blocking probability is constantly measured at every cell site so that the reallocation of the flexible channels can be carried at any point in time [17]. Fixed and flexible channels are determined and assigned (or released) to (or from) each cell according to the change in traffic intensity or blocking probability measured in each cell. The number of dynamic channels required in a cell is determined according to the increase in measured traffic intensity. The acquired flexible channels can be used in a manner identical to the fixed channels in a cell as long as the cell possesses the channels. As long as a cell has several free fixed channels, no flexible channels are assigned to it if the traffic intensity is below a certain threshold [32].

If the flexible channels are assigned on a scheduled basis, it is assumed that the variation of traffic, such as the movement of traffic peaks in time and space, are estimated a priori. The change in assignment of flexible channels is then made at the predetermined peaks of traffic change [17]. Flexible assignment strategies use centralized control and require the central controller to have up-to-date information about the traffic pattern in its area in order to manage the assignment of the flexible channels [17].

12.1.11 Reuse partitioning (RUP)

RUP is an effective concept to get high spectrum efficiency in cellular systems. In RUP, as shown in Figure 12.4, each cell in the system is divided into two or more concentric subcells (zones). Because the inner zones are closer to the base station located at the center of the cell, the power level required to achieve a desired CIR in the inner zones can be much lower compared to the outer zones. Thus, the channel reuse distance (i.e. the distance between cells using the same channel) can be smaller for the inner zones than for the outer ones, resulting in higher spectrum efficiency.

Reuse partitioning schemes could be divided into fixed and adaptive:

(1) *Fixed reuse partitioning*
    Simple reuse partitioning
    Simple sorting channel assignment algorithm
(2) *Adaptive reuse partitioning*
    Autonomous reuse partitioning (ARP)
    Flexible reuse (FRU)

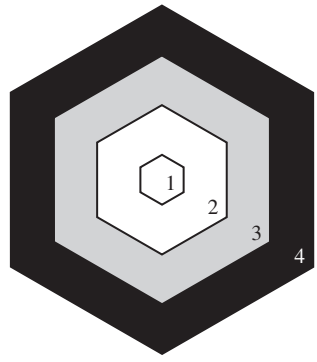

Figure 12.4 Concentric subcells.

DDCA
All-channel concentric allocation (ACCA)
Self-organized reuse partitioning (SPRP)

12.1.11.1 Fixed reuse partitioning

Simple reuse partitioning was introduced in Reference [33]. In this scheme, available channels are split among several overlaid cell plans with different reuse distances. The underlying principle behind RUP is to reduce the signal-to-interference ratio (SIR) for those units that already have more than adequate transmission quality while offering greater protection to those units that require it. The goal is to produce an overall SIR distribution that satisfies system quality objectives while bringing about a general increase in system capacity. For the same SIR objective, those partitioning have the potential to obtain a significant increase in system capacity when compared to a system that uses only a single reuse factor [33].

Simple RUP can be implemented by dividing the spectrum allocation into two [33] or more [34] groups of mutually exclusive channels. Channel assignment within the ith group is then determined by the reuse factor N for that group. Mobile units with the best received signal quality will be assigned to the group of channels with the smallest reuse factor value, while those with the poorest received signal quality will be assigned to the group of channels with the largest reuse factor value. As the received signal quality for a mobile unit changes, it can be handed off to:

(a) a channel that belongs to a different reuse group on the same zone at the same cell,

(b) a channel that belongs to the same or to a different group on another zone at the same cell,

(c) a channel belonging to the same or a different group at another cell.

Typically, the mobile units closer to a cell site will be served by channels from a group having a small value of N [33].

There are two main design issues related to the simple RUP concept. The first issue is the capacity allocation problem, which is to decide how many channels should be assigned to each zone. The second issue is the actual assignment of channels to calls. In Reference [34] the performance limits of the RUP concept were explored and methods for allocating capacity to the different cell zones as well as optimum real-time channel assignment schemes have been presented.

The *simple sorting channel assignment algorithm* also divides each cell into a number of cocentric zones and assigns a number of channels, as in simple RUP. For each mobile in the

cell, the base station measures the level of SIR and places the measurements in a descending order. Then it assigns channels to the set of at most M mobiles with the largest values of SIR, where M is the number of available channels in the entire cell. The mobile in the set with the smallest value of SIR is assigned a channel from the outer cell zone. The assignment of mobile channels according to ascending values of SIR continues until all channels from the outer zone are used. The base station continues to assign channels in the next zone, and so on, until all mobiles in the set have been assigned channels.

The simple sorting channel algorithm achieves almost optimum performance. It also allows 1.4–3 times more traffic than the FCA scheme. An important remaining issue is that the sorting scheme only determines which cell plan each mobile should use. It does not assign actual channels, which must be done with some care. In addition, if all cells using a certain channel group started the channel assignment by using the first channel in the group, we would get an exceptionally high interference level on that particular channel. A random selection procedure would be one way to solve this problem.

12.1.11.2 Adaptive Channel Allocation Reuse Partitioning (ACA-RUP)

In this case any channel in the system can be used by any base station, as long as the required CIR is maintained.

Autonomous reuse partitioning (*ARP*) is based on the RUP concept and real-time CIR measurements. In this technique, all the channels are viewed in the same order by all base stations, and the first channel that satisfies the threshold condition is allocated to the mobile attempting the call. Therefore, each channel is reused at a minimum distance with respect to the strength of the received desired signal. In ARP, base stations conduct their allocations independent of one another and no cooperative control is necessary.

As compared to simple FCA, ARP doubles the traffic handling capacity of the system and decreases the cochannel interference by 1/4 [35]. ARP improves traffic handling at the cost of the SIR margin in each channel. This creates problems to fast-moving mobile stations such as car-mounted units, which suffer from rapid fluctuations in signal level.

The *flexible reuse* (*FRU*) scheme is based on the principle that whenever a call requests service, the channel with the smallest CIR margin among those available is selected. If there is no available channel, the call is blocked. Simulations in Reference [36] showed that FRU can effectively improve system capacity, especially for users with portable units. More specifically, a capacity gain of 2.3–2.7 of FRU over FCA was observed. However, the FRU strategy requires a large number of CIR measurements, which makes it virtually impractical for high-density microcellular systems.

The *self-organized reuse partitioning* (*SORP*) scheme uses the method where each base station has a table in which average power measurements for each channel in its cell and the surrounding cells are stored. When a call arrives, the base station measures the received power of the calling mobile station (in order to define at which subcell the mobile station is located) and selects a channel that shows the average power closest to the measured power. The channel is used if available; otherwise the second closest candidate is tried. The content of the table for the chosen channel is updated with the average value of the measured power and the power of the mobile stations using the same channel. The power level of the other mobile stations is broadcast by their base station. As a consequence of this procedure, in each base station channels that correspond to the same power are grouped autonomously for self-organized partitioning.

In Reference [37], a performance comparison is made between SORP, conventional ARP and random DCA schemes. The simulation analysis showed that SORP and ARP show almost the same performance, which is far superior to random DCA. SORP can reduce the occurrence of intracell handoff and can reach a desired channel quickly, while achieving high traffic capacity. The essential difference between ARP and SORP is that ARP always senses the channels in the

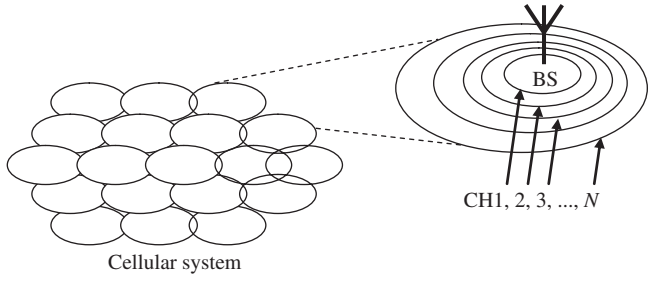

Figure 12.5 Principle of the oil-channel concentric allocation.

same order until one is available, while SORP learns which channel is correct for the calling mobile so it can find a desired channel more quickly.

All-channel concentric allocation (*ACCA*) is an extension of the RUP concept. All radio channels of a system are now allocated nominally in the same manner for each cell, as in Figure 12.5. Each cell is divided into N concentric regions. Each region has its own channel allocation. Here each channel is assigned a mobile belonging to the concentric region in which that channel is allocated and has a specific desired signal level corresponding to the channel location. Therefore, each channel has its own reuse distance determined from the desired signal level. Thus, ACCA accomplishes effective channel allocation in a global sense, though it is a self-organizing distributed control algorithm. Computer simulations showed that the system capacity at a blocking rate of 3 % is improved by a factor of 2.5 compared to the FCA [38]. If, in addition, a transmitter power control is implemented on top of ACCA, the system accomplishes a capacity 3.4 times greater than FCA.

The *distributed control channel allocation* (*DCCA*) is a dynamic channel allocation scheme based on the ARP concept. In this scheme all cells are identical and channels are ordered in the same manner, starting with channel number one, by all the base stations in the network. The decision to allocate a channel is made locally based on CIR measurements. The architecture of a cell in DCCA is shown in Figure 12.6. It consists of an omnidirectional central station connected to six symmetrically oriented substations [39, 40]. The substations are simple transceivers and can be switched on and off under the control of the main station. When the traffic density of the cell is

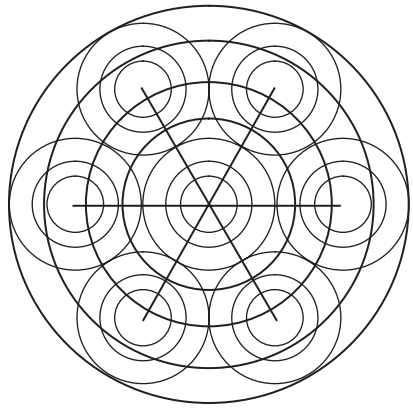

Figure 12.6 DCCA cell structure.

low all the substations are off and the only operating station is the main station, at the centre of the cell covering the entire cell area. Gradually, as call traffic increases, forced call blocking will occur due to an unacceptable level of cochannel interference or the unavailability of resources. In this case, the main base station switches on the nearest substation to the mobile unit demanding access. This in effect relocates the main base station closer to the mobile requesting service; therefore, CIR measurements will now be higher, thus improving the probability of finding an acceptable channel. If the traffic is reduced, the main station switches off a number of substations. The system therefore automatically adapts itself to time-variant cell traffic density. As a result, an improvement in both system efficiency and traffic capacity can be achieved. As discussed in Reference [40], the DCCA system results in a lower probability of forced termination of calls. Computer simulation showed a drastic reduction in the number of handoffs and almost 50 % less forced termination of calls compared to the ARP scheme.

For additional information on the subject see also References [41] to [58].

12.2 DYNAMIC CHANNEL ALLOCATION WITH SDMA

12.2.1 Single-cell environment

We start by considering the down-link of a single cell with K users and N channels. Later we will extend the basic concept to more realistic scenarios with multiple interfering cells in wireless networks. Depending on the multiple access scheme (TDMA, CDMA or OFDMA), *channels are timeslots, codes or subcarrier frequencies*. The base station (BS) has a uniform linear array of M antennas, while each receiver has an omnidirectional antenna. Introduction of some directivity at the mobile receiver will be considered later. Each user k has a minimum rate requirement of r_k bits/s over some time interval $(0, t)$, which consists of several slots. This requirement denotes QoS that the MAC layer requests from the physical layer. A fixed number of symbols S are transmitted in one slot and the symbol (signaling) interval is T. Single-rate transmission is assumed and r_k is mapped to a minimum number of required channels x_k. Occasionally, for simplicity, we will assume that there is one channel per user.

The block diagram of a generic space division multiple access (SDMA) transmitter is depicted in Figure 12.7. User bits enter the channel allocation module, which determines cochannel sets of

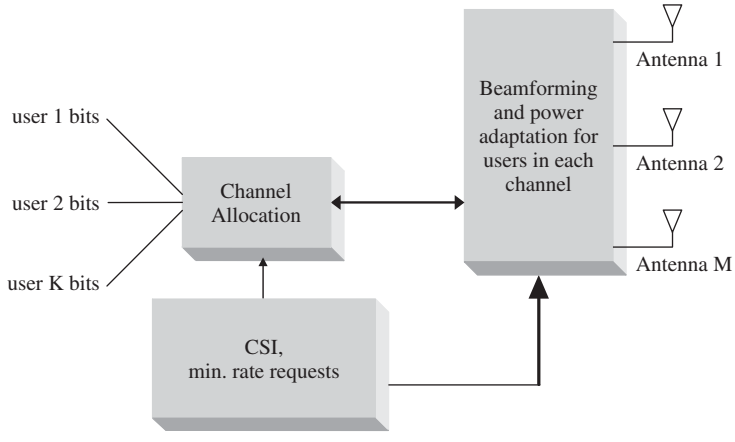

Figure 12.7 SDMA transmitter with a generic multiple access scheme.

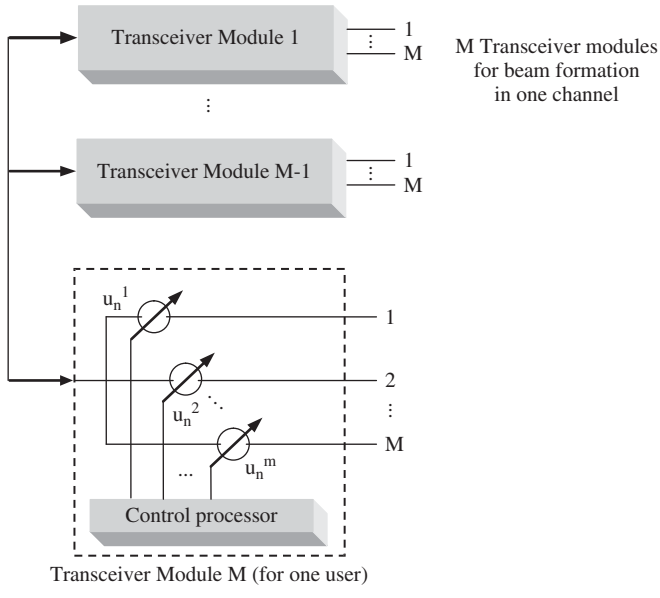

Figure 12.8 The structure of M transceiver modules for channel n.

users in different channels. Beamforming and power adaptation are subsequently performed for each user that is allocated to a channel. Under SDMA, the transmitter can form at most M beams for each channel and transmit to M cochannel users at the same time. A beam $\mathbf{u}_{n,k} = (u_{n,k}^1, \ldots, u_{n,k}^M)^{\mathrm{T}}$ is formed by a dedicated transceiver and a power $p_{n,k}$ is assigned to user k in channel n. Beams are normalized to unit power, i.e. $\|\mathbf{u}_{n,k}\| = 1$. We assume that M transceivers (beamformers) are available for each channel, so that a separate beam can be formed for each one of the M users that can be separated in a channel. A set of M transceivers for a channel is shown in Figure 12.8. Channel allocation and beamforming are interdependent operations and they also depend on user minimum rate requirements and channel state information (CSI), which are assumed to be available at the transmitter.

An *OFDM/SDMA transmitter* is shown in Figure 12.9. After subcarrier allocation, beamforming and power adaptation, user bits are forwarded into M parallel modules of N modulators. Each modulator modulates the corresponding subcarrier with bits of users that are allocated to the subcarrier. For single-rate transmission, b bits of each assigned user modulate a subcarrier and constitute a subsymbol. Subsymbols of each user are then fed into an inverse discrete Fourier transform (IDFT) module and are transformed into N time-domain samples, which form an OFDM user symbol. A cyclic prefix of some time samples is appended to eliminate ISI. After D/A conversion, continuous signals are transmitted from the M antennas.

Assuming that OFDM symbols do not interfere with each other, the transmitted base-band signal to user k from the mth antenna is

$$x_k^m(t) = \sum_{n=0}^{N-1} \sqrt{p_{n,k}} u_{n,k}^m d_{n,k} g(t) \mathrm{e}^{\mathrm{j}2\pi m t/T}, \quad \text{for } 0 \le t \le T$$

where the complex coefficient $d_{n,k}$ represents the subsymbol of user k at the output of the nth modulator. If user k uses n_k subcarriers, it achieves rate $(bS/T_s)n_k$ bits/s in a timeslot. In this case the previous expression is modified so that the channel $n \to n_k$ represents the subset of subcarriers

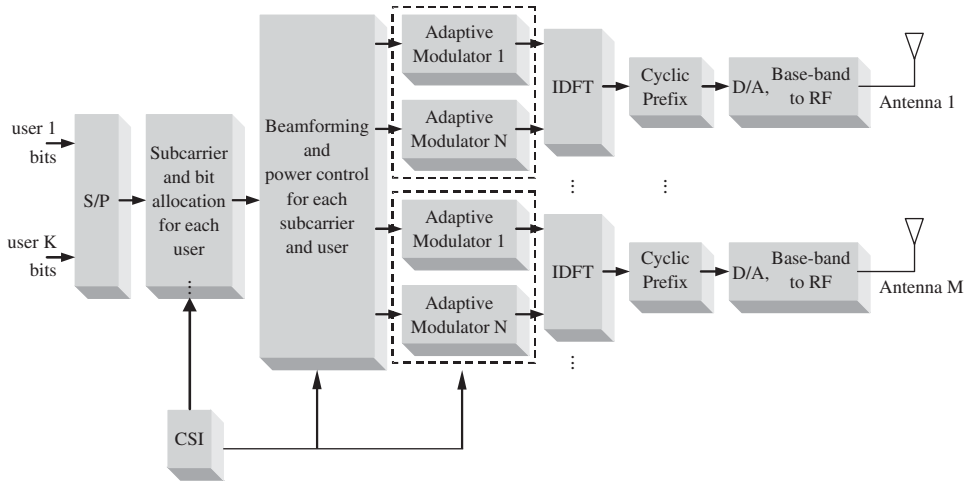

Figure 12.9 Block diagram of a multiuser OFDM/SDMA transmitter.

allocated to one user at a given location. The multipath channel between antenna m and user k is

$$h_k^m(t) = \sum_{l=1}^{L} \beta_{k,l}\delta(t - \tau_{k,l} + \tau_{k,l}^m)$$

where $\tau_{k,l}^m = (\delta/c)(m-1)\cos\theta_{k,l}$ captures the delay difference between the mth antenna element and the reference element, where δ is the distance between two elements, $\theta_{k,l}$ is the angle of the lth path of user k with respect to the array and c is the electromagnetic wave propagation speed. The received signal for user k, from its own BS, after down-conversion is

$$r_{ko}(t) = \sum_{j=1}^{K}\sum_{m=1}^{M}\sum_{l=1}^{L} \beta_{k,l}x_l^m(t - \tau_{k,l} + \tau_{k,l}^m) + z(t)$$

After the DFT the subsymbol at subcarrier n is

$$y_{n,k} = \sum_{m=1}^{M} u_{n,k}^m \sum_{l=1}^{L} d_{n,k}\sqrt{p_{n,k}}\xi_{k,l}(n)\exp[\mathrm{j}2\pi(f_c + n/T)\tau_{k,l}^m] + y_{n,k}^u + z_{n,k}$$

where $y_{n,k}^u$ is the undesired interference from users other than k in subcarrier n, $z_{n,k}$ is the noise at subcarrier n, f_c is the carrier frequency and

$$\xi_{k,l}(n) = \beta_{k,l}\exp[-\mathrm{j}2\pi(f_c + n/T)\tau_{k,l}^m]$$

The vector

$$\mathbf{a}_{n,k} = \sum_{l=1}^{L} \xi_{k,l}^*(n)\mathbf{v}_n(\theta_{k,l})$$

is called the spatial signature of user k at subcarrier n. The received signal for user k at subcarrier n is

$$y_{n,k} = \sqrt{p_{n,k}}(\mathbf{a}_{n,k}^H\mathbf{u}_{n,k})d_{n,k} + \sum_{\substack{j\in U^{(n)}\\ j\neq k}} \sqrt{p_{n,k}}(\mathbf{a}_{n,k}^H\mathbf{u}_{n,k})d_{n,j} + z_{n,k} \tag{12.2}$$

where $U^{(n)}$ is the set of users in subcarrier n. If paths are resolvable, their angles, complex gains and delays are known to the transmitter and the SINR of user k at subcarrier n is

$$SINR_{n,k} = W_{n,k} = \frac{p_{n,k}(\mathbf{u}_{n,k}^H H_{n,k}\,\mathbf{u}_{n,k})}{\sum\limits_{\substack{j \in U^{(n)} \\ j \neq k}} p_{n,j}(\mathbf{u}_{n,k}^H H_{n,k}\,\mathbf{u}_{n,j}) + \sigma^2} \tag{12.3}$$

where σ^2 is the noise variance and matrix $H_{n,k}$ is defined as

$$H_{n,k} = \sum_{l_1=1}^{L}\sum_{l_2=1}^{L}[\xi_{k,l_1}(n)\xi_{k,l_2}^*(n)\mathbf{v}_n(\theta_{k,l_1})\mathbf{v}_n^H(\theta_{k,l_2})]$$

If CSI is provided in terms of a statistical characterization of the parameters above, gains $\beta_{k,l}$ can be modeled as complex Gaussian random variables with zero mean and variance $A_{k,l}$ and delays $\tau_{k,l}$ are uniformly distributed in $[0, T]$. The expected useful received signal power is

$$E\left\{\left|\sqrt{p_{n,k}}(\mathbf{a}_{n,k}^H\mathbf{u}_{n,k})d_{n,k}\right|^2\right\} = p_{n,k}(\mathbf{u}_{n,k}^H H_{n,k}\mathbf{u}_{n,k})$$

with

$$H_{n,k} = \sum_{l_1=1}^{L}\sum_{l_2=1}^{L}\mathbf{v}_n(\theta_{k,l_1})\mathbf{v}_n^H(\theta_{k,l_2})E\{\xi_{k,l_1}(n)\xi_{k,l_2}^*(n)\}$$

where user symbols are normalized to unit power. If paths are uncorrelated,

$$E\{\xi_{k,l_1}(n)\xi_{k,l_2}^*(n)\} = \begin{cases} 0, & \text{if } l_1 \neq l_2 \\ A_{k,l}, & \text{if } l_1 = l_2 = l \end{cases} \tag{12.4}$$

and

$$H_{n,k} = \sum_{l=1}^{L} A_{k,l}\mathbf{v}_n(\theta_{k,l})\mathbf{v}_n^H(\theta_{k,l})$$

is called the spatial covariance matrix of user k at subcarrier n.

In *single-carrier TDMA*, the N available channels are timeslots. The transmitted base-band signal for user k that is assigned to slot n is $s_{n,k}(t) = \Sigma_i d_{n,k}(i)g(t - iT)$, where $\{d_{n,k}(i)\}$ is the symbol sequence, T is the symbol duration and $g(t)$ is the pulse shaping filter. If there is no pulse overlap, we have $s_{n,k}(t) = d_{n,k}g(t)$. At most M users can be assigned to a timeslot. User signals are then multiplied by beamforming weights and powers and are transmitted from the M antennas. A modulation level of b bits/symbol is used and a rate of bS/T_s bits/s is achieved for a user in a timeslot. The received symbol for user k is

$$r_{n,k}(t) = \sum_{j \in U^{(n)}} \sqrt{p_{n,j}} \sum_{m=1}^{M} u_{n,j}^m \sum_{l=1}^{L} \xi_{k,l}(\omega_c)\mathrm{e}^{\mathrm{j}2\pi f_c \tau_{k,l}^m} s_{n,j}(t)$$

where $\xi_{k,l}(\omega_c)$ is the complex gain of the lth path of user k at carrier frequency $\omega_c = 2\pi f_c$. For the received symbol of user k we obtain an expression similar to that in Equation (12.2) and the SINR at the output of the matched filter of k at timeslot n is given by Equation (12.3).

In *CDMA,* the N channels are deterministic real codes with fixed spreading gain G. Let $\mathrm{c}_n = (c_{n1}, \ldots, c_{nG})$ denote the normalized vector corresponding to code n. Each code pair (n, m) is characterized by cross-correlation $\rho_{nm} = \mathrm{c}_n^{\mathrm{T}}\mathrm{c}_m$, where $\rho_{nn} = 1$. In the time domain, code n is represented as $c_n(t) = \sum_{r=1}^{G} c_{nr}\,p(t - (r-1)T_c)$, where $p(t)$ is the chip pulse and T_c is the chip duration. The transmitted signal to user k with code n is $s_{n,k}(t) = \Sigma_i d_{n,k}(i)c_n(t - iT)$. By setting $i = 0$, a single symbol is denoted as $s_{n,k}(t) = d_{n,k}\,c_n(t)$. User signals are multiplied by beamforming

weights and powers and are transmitted from the M antennas. Each code is associated with rate $1/(GT_c)$ and user k with n_k codes achieves rate $n_k/(GT_c)$ bits/s.

The receiver of user k consists of a bank of matched filters, each of which is matched to a code used by the user. The signal at the output of the matched filter to code n is $y_{n,k} = \mathbf{c}_n^{\mathrm{T}} \mathbf{y}_k$, where $\mathbf{y}_k$ is the signal at the input of the kth receiver. Note that $y_{n,k} = y_{n,k}^d + y_{n,k}^u$, where $y_{n,k} = \sqrt{p_{n,k}}(\mathbf{a}_k^H \mathbf{u}_{n,k}) d_{n,k}$ is the desired signal of user k that is transmitted with code n and $y_{n,k}^u$ is the undesired interference signal. The latter is

$$y_{n,k}^u = \sum_{\substack{j \in U^{(n)} \\ j \neq k}} \sqrt{p_{n,j}}(\mathbf{a}_k^H \mathbf{u}_{n,j}) d_{n,j} + \sum_{\substack{m=1 \\ m \neq n}}^{N} \sum_{j \in U^{(m)}} \rho_{nm} \sqrt{p_{m,j}}(\mathbf{a}_k^H \mathbf{u}_{m,j}) d_{m,j}$$

and the SIR at the output of the matched filter to code n of k is

$$W_{n,k} = \frac{p_{n,k}(\mathbf{u}_{n,k}^H H_k \mathbf{u}_{n,k})}{\sum\limits_{\substack{j \in U^{(n)} \\ j \neq k}} p_{n,j}(\mathbf{u}_{n,k}^H H_k \mathbf{u}_{n,k}) + \sum\limits_{\substack{m=1 \\ m \neq n}}^{N} \sum\limits_{j \in U^{(m)}} \rho_{nm}^2 p_{m,j}(\mathbf{u}_{m,j}^H H_k \mathbf{u}_{m,j})} \tag{12.5}$$

The first term in the denominator of Equation (12.5) captures cochannel interference from other users that use code n and the second term denotes interchannel interference from other utilized codes due to code cross-correlation. Note that spatial signatures a_k and spatial covariance matrices H_k are independent of channel n.

Consider beamforming and power control in the up-link. The relationship between the up-link and the down-link will be used in the sequel. Beamforming is performed at the BS and power is adapted for the up-link transmission of each user. The SIR for user k in channel n is

$$\tilde{W}_{n,k} = p_{n,k}(\mathbf{u}_{n,k}^H H_k \mathbf{u}_{n,k}) / \mathbf{u}_{n,k}^H \left(\sum_{\substack{j \in U^{(n)} \\ j \neq k}} p_{n,j} H_k \right) \mathbf{u}_{n,k} \tag{12.6}$$

12.2.2 Resource allocation

The algorithms are general and include TDMA, OFDMA and CDMA.

Algorithm 1

(1) *Beamforming vector adaptation.* For the moment let us fix attention on channel n and let k be the user to be inserted next in n. Let $\mathbf{u}_{m,j}$ and $p_{m,j}$ denote the beamforming vector and power of user j in channel m. Insertion of user k in n creates a new interference instance for cochannel users in channel n and for users in other correlated channels m. Thus beamforming vectors that result in acceptable SIRs are needed. For each user $j \in U^{(m)}$ define the ratio of desired power generated by beam $\mathbf{u}_{m,j}$ over interference power, which is caused by $\mathbf{u}_{m,j}$ to other users, including the new user k in channel n. In fact, we are interested in the maximum value of this ratio, $\Psi_{m,j}^{(n,k)}$, over all directions $\mathbf{u}_{m,j}$:

$$\Psi_{m,j}^{(n,k)} = \max_{\mathbf{u}_{m,j}} \frac{\mathbf{u}_{m,j}^H H_{m,j} \mathbf{u}_{m,j}}{\mathbf{u}_{m,j}^H \left(\sum\limits_{\substack{\mu=1 \\ \mu \neq m}}^{N} \sum\limits_{i \in U^{(m)}} \rho_{\mu m}^2 H_{\mu,i} + \sum\limits_{\substack{i \in U^{(m)} \\ \imath \neq j}} H_{m,i} + \rho_{mn}^2 H_{n,k} \right) \mathbf{u}_{m,j}} \tag{12.7}$$

such that $\|u_{m,j}\| = 1$. Vector $\mathbf{u}^*_{m,j}$ that maximizes this ratio is the dominant generalized eigenvector of the pair of matrices that appear in the numerator and denominator. We also compute the corresponding ratio for user k that is tentatively inserted in channel n:

$$\Psi_{n,k} = \max_{\mathbf{u}_{m,j}} \frac{\mathbf{u}_{n,k}^H H_{n,k} \mathbf{u}_{n,k}}{\mathbf{u}_{n,k}^H \left(\sum_{j \in U^{(n)}} H_{n,j} + \sum_{\substack{m=1 \\ m \neq n}}^{N} \sum_{i \in U^{(m)}} \rho_{mn}^2 H_{m,i} \right) \mathbf{u}_{n,k}} \tag{12.8}$$

such that $\|\mathbf{u}_{n,k}\| = 1$, where the denominator captures cochannel and interchannel interference caused by the beam of k to other users. With the computed beamforming vectors, we evaluate the SIRs for user k in channel n and for users in other channels.

(2) *Power adaptation.* If SIRs of some users do not exceed the minimum SIR γ, we fix the computed beamforming vectors and activate power control. Given a set of assigned users to some channels, the question is whether there exist powers such that all SIRs exceed γ. For each channel i, let κ_i, l_i be indices of users in that channel. Define $\mathbf{U}$ as the ensemble of computed beamforming vectors for users and channels, i.e. $\mathbf{U} = \{\mathbf{u}_{n,k} : k \in U^{(n)}, n = 1, \ldots, N\}$. Then we define the $\left(\sum_{n=1}^{N} |U^{(n)}|\right) \times \left(\sum_{n=1}^{N} |U^{(n)}|\right)$ block matrix $\mathbf{A}(\mathbf{U})$ as $\mathbf{A}(\mathbf{U}) = \|\mathbf{A}_{ij}(\mathbf{U})\|$ for $i, j = 1, \ldots, N$. The $[\kappa_i, l_i]$th element of the $(|U^{(i)}| \times |U^{(i)}|)$ matrix $\mathbf{A}_{ii}(\mathbf{U})$ in the diagonal of $\mathbf{A}(\mathbf{U})$ specifies interference that is caused by the beam of the l_ith user to the receiver of the κ_ith user in channel i, namely

$$\mathbf{A}_{ii}(\mathbf{U})[k_i, l_i] = \begin{cases} \mathbf{u}_{i,l_i}^{*H} H_{i,k_i} \mathbf{u}_{i,l_i}^*, & \text{if } k_i \neq l_i \\ 1, & \text{if } k_i = l_i \end{cases} \tag{12.9}$$

The $[\kappa_i, l_j]$th element of the $(|U^{(i)}| \times |U^{(j)}|)$ matrix $\mathbf{A}_{ij}(\mathbf{U})$, $i \neq j$, denotes the interchannel interference caused by the beam of the l_jth user in channel j to the receiver of the κ_ith user in channel i:

$$\mathbf{A}_{ij}(\mathbf{U})[k_i, l_i] = \rho_{ij}^2 (\mathbf{u}_{i,l_i}^{*H} H_{i,k_i} \mathbf{u}_{i,l_i}^*)$$

Define also

$$\mathbf{\Delta} = \text{diag}\left(1/\mathbf{u}_{i,l_i}^{*H} H_{i,k_i} \mathbf{u}_{i,l_i}^*,\ i = 1, \ldots, n,\ k_i = 1, \ldots, \left|U^{(i)}\right|\right)$$

and the $\left(\sum_{n=1}^{N} |U^{(n)}|\right) \times 1$ vector $\mathbf{p}$ of transmission powers to users in all channels. Then, the requirement $W_{n,k} \geq \gamma$ can be written in matrix form as

$$[(1 + \gamma)/\gamma]\mathbf{p} \geq \mathbf{\Delta A}(\mathbf{U})\mathbf{p}. \tag{12.10}$$

Matrix $\mathbf{\Delta A}(\mathbf{U})$ is nonnegative definite and irreducible. From the Perron–Frobenius theorem, it has a positive, real eigenvalue $\lambda_{\max}(\mathbf{\Delta A}(\mathbf{U})) = \max_i\{|\lambda_i|\}$, where λ_i, $i = 1, \ldots$, and $\left(\sum_n \left|U^{(n)}\right|\right)$ are the eigenvalues of $\mathbf{\Delta A}(\mathbf{U})$. The eigenvalue $\lambda_{\max}(\mathbf{\Delta A}(\mathbf{U}))$ has an associated eigenvector with strictly positive entries. Furthermore, the minimum real λ for which the inequality $\lambda\mathbf{p} \geq \mathbf{\Delta A}(\mathbf{U})\mathbf{p}$ has solutions $\mathbf{p} > 0$ is $\lambda = \lambda_{\max}(\mathbf{\Delta A}(\mathbf{U}))$. In our case, we start by finding the maximum real positive eigenvalue of $\mathbf{\Delta A}(\mathbf{U})$ to request the existence of a power vector with positive entries. If $\lambda_{\max}(\mathbf{\Delta A}(\mathbf{U})) \leq (1 + \gamma)/\gamma$, then the inequality (12.10) holds and the SIR level γ is achievable. The power vector that leads to an achievable γ is the eigenvector that corresponds to $\lambda_{\max}(\mathbf{\Delta A}(\mathbf{U}))$.

Next, we define an *assignment preference factor* $\Phi_{n,k}$ for channel n and user k. First, the beam and power must yield a strong desired signal for user k. Furthermore, all beams and powers should be such that interference $I_{n,k}$ caused by user k to other users, as well as induced interference $I'_{n,k}$ on k by other users, is low. These requirements are captured by the ratio

$\Phi_{n,k} = p_{n,k}(\mathbf{u}_{n,k}^{*H} H_{n,k} \mathbf{u}_{n,k}^{*}) / \max\{I_{n,k}, I'_{n,k}\}$, where

$$I_{n,k} = p_{n,k} \mathbf{u}_{n,k}^{*H} \left(\sum_{j \in U^{(n)}} H_{n,j} + \sum_{\substack{m=1 \\ m \neq n}}^{N} \sum_{i \in U^{(m)}} \rho_{mn}^2 H_{m,i} \right) \mathbf{u}_{n,k}^{*}$$

$$I'_{n,k} = \sum_{j \in U^{(n)}} p_{n,j} (\mathbf{u}_{n,j}^{*H} H_{n,k} \mathbf{u}_{n,j}^{*}) + \sum_{\substack{m=1 \\ m \neq n}}^{N} \sum_{i \in U^{(m)}} \rho_{mn}^2 p_{m,i} (\mathbf{u}_{m,i}^{*H} H_{n,k} \mathbf{u}_{m,i}^{*})$$

If power control is not activated (when all SIRs exceed γ after initial beam computations with Equations (12.7) and (12.8)), the ratios above do not include powers.

At each step of the algorithm, $\Phi_{n,k}$ are computed for all channels n, for which a user insertion leads to acceptable SIRs and for all users k that have not satisfied minimum rate requirements x_k. Among assignments that yield acceptable SIRs for users, we select the one with the maximum $\Phi_{n,k}$. After each assignment, the rate of user k is updated. When a user reaches x_k, it is not considered for assignment until all users reach their minimum rate requirements. Then, all users are again considered for assignment. If the cardinality of a cochannel user set reaches M, the corresponding channel is not included for user assignment. The algorithm terminates when no further assignments are possible to any channel.

Algorithm 2

The second class of algorithms is based on the criterion of maximizing the minimum SIR of users defined as

$$\Phi_{n,k} = \min \left\{ W_{n,k}, \min_{\substack{j \in U^{(m)} \\ m = 1, \ldots, N}} W_{m,j} \right\}$$

With this assignment, we intend to facilitate future assignments and ultimately increase the number of users with SIRs above γ.

Algorithm 3

This algorithm attempts to provide the maximum common SIR for users in the system. It performs joint adaptation of beamforming vectors and powers in order to obtain the highest common SIR. Consider channel n in isolation with the set of users $U^{(n)}$. Let $\mathbf{p}_n$ and $\mathbf{U}_n$ be the power vector and the ensemble of computed beamforming vectors for users in n. Define the $(|U^{(n)}| \times |U^{(n)}|)$ matrix $\mathbf{B}(\mathbf{U}_n)$ with elements

$$\mathbf{B}(\mathbf{U}_n)[i, j] = \begin{cases} \mathbf{u}_{n,j}^{H} H_{n,i} \mathbf{u}_{n,j}, & \text{if } i \neq j \\ 0, & \text{if } i = j \end{cases} \tag{12.11}$$

$\mathbf{B}(\mathbf{U}_n)$ is the interference matrix for users in channel n. Define also the diagonal matrix

$$\mathbf{D} = \text{diag}(1/\mathbf{u}_{n,i}^{H} H_{n,i} \mathbf{u}_{n,i} : i \in U^{(n)})$$

An instance in which all users achieve a common SIR γ_c in the *down-link* by using the ensemble of beamforming vectors $\mathbf{U}_n$ and power vector $\mathbf{p}_n$ is described by the set of equations $\mathbf{DB}(\mathbf{U}_n)\mathbf{p}_n = \mathbf{p}_n/\gamma_c$. Thus, γ_c is a reciprocal eigenvalue of matrix $\mathbf{DB}(\mathbf{U}_n)$. Matrix $\mathbf{DB}(\mathbf{U}_n)$ has the same properties as $\mathbf{\Delta A}(\mathbf{U})$ with respect to the existence of an eigenvector $\mathbf{p}_n$ with positive entries. Therefore, we have $1/\gamma_c = \lambda_{\max}(\mathbf{DB}(\mathbf{U}_n))$ and the maximum possible common SIR γ_c^* is

$$\gamma_c^* = 1/\min_{\mathbf{U}_n} \lambda_{\max}(\mathbf{DB}(\mathbf{U}_n)) \tag{12.12}$$

We now consider the corresponding problem of beamforming and power control for the same users in the *up-link*. It can be verified that the instance in which all users achieve a common SIR $\tilde{\gamma}_c$ in the up-link by using an ensemble of beamforming vectors $\tilde{\mathbf{U}}_n$ and transmit power vector $\tilde{\mathbf{p}}_n$ is described by $\mathbf{D}\mathbf{B}^{\mathrm{T}}(\tilde{\mathbf{U}}_n)\tilde{\mathbf{p}}_n = \tilde{\mathbf{p}}_n/\tilde{\gamma}_c$ and the maximum possible common SIR $\tilde{\gamma}_c^*$ for the up-link is

$$\tilde{\gamma}_c^* = \frac{1}{\min\limits_{\tilde{\mathbf{U}}_n} \lambda_{\max}(\mathbf{D}\mathbf{B}^{\mathrm{T}}(\tilde{\mathbf{U}}_n))} \tag{12.13}$$

For the relationship between the down-link problem (12.12) and the up-link problem (12.13), the following properties (P) have been proved in References [59] and [60]:

P1. *For a given set of beamforming vectors* $\mathbf{U}_n$, *we have* $\lambda_{\max}(\mathbf{D}\mathbf{B}(\mathbf{U}_n)) = \lambda_{\max}(\mathbf{D}\mathbf{B}^{\mathrm{T}}(\mathbf{U}_n))$.

P2. *The up-link and down-link problems have the same solution in terms of maximum achievable common SIR, i.e. we have* $\gamma_c^* = \tilde{\gamma}_c^*$.

P3. *The beamforming vectors that solve the downlink problem (12.12) and the up-link problem (12.13) are the same, namely* $\mathbf{U}_n^* = \tilde{\mathbf{U}}_n^*$.

P4. *In the following iterative algorithm (i-algorithm), the sequence of eigenvalues* $\lambda_{\max}^{(t)}$ *is monotonically decreasing with the iteration number t and the algorithm converges to a minimum, which is related to the maximum common SIR through problems (12.12) and (12.13).*

i-algorithm

1. *Set* $t = 0$. *Start with arbitrary beamforming vectors* $\mathbf{U}_n^{(0)}$.
2. $t \leftarrow t + 1$. *For given* $\mathbf{U}_n$, *solve the following eigenproblem for the uplink:*
$$\mathbf{D}\mathbf{B}^{\mathrm{T}}(\mathbf{U}_n^{(t)})\mathbf{p}_n^{(t)} = \lambda_{\max}^{(t)}\mathbf{p}_n^{(t)}$$
3. *For the computed* $\mathbf{p}_n^{(t)}$, *solve a set of decoupled generalized eigenproblems*
$$\mathbf{u}_{n,k} = \arg\max_{\mathbf{u}_{n,k}} \frac{\mathbf{u}_{n,k}^H H_{n,k}\mathbf{u}_{n,k}}{\mathbf{u}_{n,k}^H R_{n,k}(\mathbf{p}_n^{(t)})\mathbf{u}_{n,k}^H}$$
subject to $\|\mathbf{u}_{n,k}\| = 1$, for all $k \in U^{(n)}$, where
$$R_{n,k}(\mathbf{p}_n^{(t)}) = \sum_{\substack{j \in U^{(n)} \\ \neq k}} \mathbf{p}_{n,j}^{(t)} H_{n,j}$$
4. *With the computed* $\mathbf{U}_n^{(t)}$, *go to step 2. Continue until convergence.*

In step 3, the quantity to be maximized is the up-link SIR of user k. The beamforming vectors $\mathbf{U}_n^*$ at the end of the algorithm are the required down-link beams. If $\lambda_{\max}^* = \lambda_{\max}(\mathbf{D}\mathbf{B}^{\mathrm{T}}(\mathbf{U}_n^*))$ is the eigenvalue at the end of the algorithm, the down-link power vector is given by the eigenvector of $\mathbf{B}(\mathbf{U}_n^*)$ that corresponds to $\lambda_{\max}^*$.

The rationale of Algorithm 3 is based on a simple observation that eliminates the need for channel assignment in a multiuser multichannel system, where channel allocation, beamforming and power adaptation need to be performed jointly. A K-user system with N nonorthogonal channels can be viewed as a single-channel system. For a given user assignment to channels, users interfere with each other based on their spatial covariance matrices and channel cross-correlations.

For this system we define the block interference matrix $\mathbf{F}(\mathbf{U})$ with matrix elements as

$$\mathbf{F}_{ij}(\mathbf{U}) = \begin{cases} \mathbf{A}_{ij}(\mathbf{U}), & \text{if } i \neq j \\ \mathbf{A}_{ii}(\mathbf{U}) - \mathbf{I}, & \text{if } i = j \end{cases} \tag{12.14}$$

where $\mathbf{I}$ is the identity matrix and the matrix elements of block matrix $\mathbf{A}(\mathbf{U})$ are defined in Equation (12.9). A system in which all users achieve a common SIR γ_c in the down-link is described by the set of linear equations $\mathbf{\Delta F}(\mathbf{U})\mathbf{p} = (1/\gamma_c)\mathbf{p}$. In step 3 of the *i-algorithm*, a set of decoupled generalized eigenproblems are solved, for which

$$R_{n,k}(\mathbf{p}^{(t)}) = \sum_{\substack{j \in U^{(n)} \\ j \neq k}} p_{n,j}^{(t)} H_{n,j} + \sum_{\substack{m=1 \\ m \neq n}}^{N} \sum_{j \in U^{(m)}} \rho_{nm}^2 p_{m,j}^{(t)} H_{m,j} \tag{12.15}$$

For a given assignment of users to channels, let γ_c^* denote the maximum common SIR, which is computed by applying the i-algorithm. For each user $k \in \mathbf{U}^{(n)}$, let $\gamma_{c,n}(k)$ denote the common SIR of remaining users when k is removed from subcarrier n. Again, $\gamma_{c,n}(k)$ is found by the *i-algorithm* after deleting the appropriate row and column from $\mathbf{F}^{\mathrm{T}}(\mathbf{U})$. The main steps of Algorithm 3 are as follows:

- *Start by assigning all K users in each channel n.*
- *Run the i-algorithm and find the maximum common SIR γ_c^* of users.*
- *If $\gamma_c^* \geq \gamma$, desirable SIRs are achieved for all users and the algorithm is terminated. Otherwise, go to step 3 of the i-algorithm.*
- *For each $k \in U^{(n)}$, compute $\gamma_{c,n}(k)$.*
- *Select pair (n^*, k^*) with maximum $\gamma_{c,n}(k)$ and remove user k^* from channel n^*.*
- *Update user rates. If a user reaches minimum rate requirements, do not consider it for further removal. Go to the second step of this algorithm.*

By removing the user that yields the highest common SIR each time, we intend to remove fewer users until a desired common SIR is obtained, in order to achieve high system rate.

The three algorithms were presented for the general case that encompasses TDMA, OFDMA and CDMA. Algorithms 1 and 2 are applicable to these multiple access schemes with minor modifications that reflect their special features. In single-carrier TDMA with orthogonal timeslots, we have $\rho_{nm} = 0$ for different slots n, m. In a time interval of N slots where channel quality does not change for user k, the spatial covariance matrix of k is the same across all channels, i.e . $H_{n,k} = H_k$, for $n = 1, \ldots, N$. The spatial covariance matrix varies according to temporal channel variations from slot to slot. The interference factors given by Equations (12.7) and (12.8) are now defined as $\Psi_j^{(n,k)}$ only for cochannel users $j \in U^{(n)}$ and the denominator denotes cochannel interference only. Since $\mathbf{A}_{ij} = 0$ for $i \neq j$, the problem of finding feasible power vectors that satisfy Algorithms 1, 2 and 3 decomposes into N separate problems of the form $[(1+\gamma)/\gamma]\mathbf{p}_n = \Delta_n \mathbf{A}_{nn}(\mathbf{U}_n) \cdot \mathbf{p}_n$ for each channel n, where Δ_n is the diagonal matrix that contains the reciprocal of useful signal powers of users in channel n, $\mathbf{U}_n$ is the ensemble of beamforming vectors of users in n and $\mathbf{p}_n$ is a $(|U^{(n)}| \times 1)$ power vector. In OFDMA with orthogonal subcarriers, each user k has a different spatial covariance matrix $H_{n,k}$ for each subcarrier n. Finally, in CDMA, codes are nonorthogonal due to cross-correlations and user spatial covariance matrices do not depend on codes; namely it is $H_{n,k} = H_k$, for $n = 1, \ldots, N$. For these multiple access schemes, Algorithms 1 and 2 are executed whenever channel quality varies with time.

A special note should be made for Algorithm 3. In CDMA, the algorithm is executed as described previously and the objective is to provide the highest acceptable common SIR to users. In TDMA and OFDMA with orthogonal channels and $\mathbf{F}_{ij} = 0$ for $i \neq j$, a separate problem of the form (12.12) is solved for each channel n. Algorithm 3 is modified as follows. We start by assigning all K users in each channel n and we execute the *i-algorithm* for each channel. The outcome is a vector of common SIRs $\gamma_c = (\gamma_{c,1}, \ldots, \gamma_{c,N})$, where $\gamma_{c,n}$ is the resulting common SIR of users in channel n. If $\gamma_{c,n} \geq \gamma$ for all n, desirable SIRs are achieved for cochannel users in all channels and the algorithm terminates. Otherwise some users need to be removed from channels in which the common SIR does not exceed γ. For each user k in such a channel n, let $\gamma_{c,n}(k)$ denote the common SIR of users in channel n after k is removed from n. At each step, we remove the user k from a channel n so that the resulting $\gamma_{c,n}(k)$ is maximum over possible user removals from channels. User rates are updated after each step of the algorithm and if a user k reaches x_k, it is not considered in further removals. If $\gamma_{c,n} \geq \gamma$ for a channel n at some stage of the algorithm, no further users are removed from this channel. The algorithm terminates when $\gamma_{c,n} \geq \gamma$ for all n.

As an illustration in the special case of $K = 2$ users in a channel for $M \geq 2$, let H_i, $\mathbf{u}_i$ and p_i be the spatial covariance matrix, beamforming vector and power for user i, $i = 1, 2$. Start with initial beamforming vectors $\mathbf{u}_i^{(0)}$. In the first iteration of the *i-algorithm*, we find $\lambda_{\max}^{(1)}$ as a function of H_i and $\mathbf{u}_i^{(0)}$ and power ratio $\mu^{(1)} = p_2/p_1$ in step 2. In step 3, we find beamforming vectors $\mathbf{u}_1 = \mathbf{u}_{\max}(H_1, H_2)$ and $\mathbf{u}_2 = \mathbf{u}_{\max}(H_2, H_1)$. In the second iteration, we have $\lambda_{\max}^{(2)} = \sqrt{\lambda_{\max}(H_1, H_2)\lambda_{\min}(H_1, H_2)}$ and power ratio $\mu^{(2)} >= \sqrt{\lambda_{\max}(H_1, H_2)/\lambda_{\min}(H_1, H_2)}$, where $\lambda_{\max}(H_1, H_2)$ and $\lambda_{\min}(H_1, H_2)$ are the maximum and minimum generalized eigenvalues of (H_1, H_2). These do not change in subsequent iterations. Thus the maximum common SIR is $\gamma_c^* = 1/\sqrt{\lambda_{\max}(H_1, H_2)\lambda_{\min}(H_1, H_2)}$ with beamforming vectors $\mathbf{u}_1$, $\mathbf{u}_2$ and power ratio given above.

12.2.3 Performance examples

A single-cell system is considered with $K = 10$ users that are uniformly distributed in the cell area. The BS uses TDMA, CDMA or OFDMA and is equipped with an antenna array with $M = 4$ elements and $\delta = \lambda/2$ and $N = 10$ available channels. Each user k needs at least $x_k = 3$ channels. The received power decays with distance d from the BS as d^{-4}. For each link corresponding to an antenna and a user receiver, multipath fading is simulated with a two-ray model. The angle of the first path, θ_1, is uniformly distributed in $[0, 2\pi]$, while the angle of the second path, θ_2, deviates from θ_1 by a random amount, uniformly distributed in $[0, 0.1\pi]$. The complex gain of each path is an independent lognormal random variable with standard deviation $\sigma = 6$ dB, which accounts for shadow fading. System performances are illustrated in Figures 12.10 to 12.14. For more details see References [59] to [71].

12.3 PACKET-SWITCHED SDMA/TDMA NETWORKS

Researchers have recently also considered the use of smart antennas in packet-switched systems. In Reference [72], smart antennas were used to improve the uplink performance of a slotted ALOHA packet radio network. During packet reception, the base station uses the smart antenna to enhance gain in the direction of a desired packet and attempts to minimize interference from other transmissions. As a result, the capacity of the system can be increased compared with conventional ALOHA due to a reduction in the effect of collisions.

The functionality described above can be improved upon in systems where the base station uses time-division duplexing (TDD). In TDD, the base station can first measure the characteristics of the channel between itself and a station and then use this information as a basis for future communications using the smart antenna. In Reference [73], a protocol was proposed that uses this technique to improve system performance in a harsh fading environment.

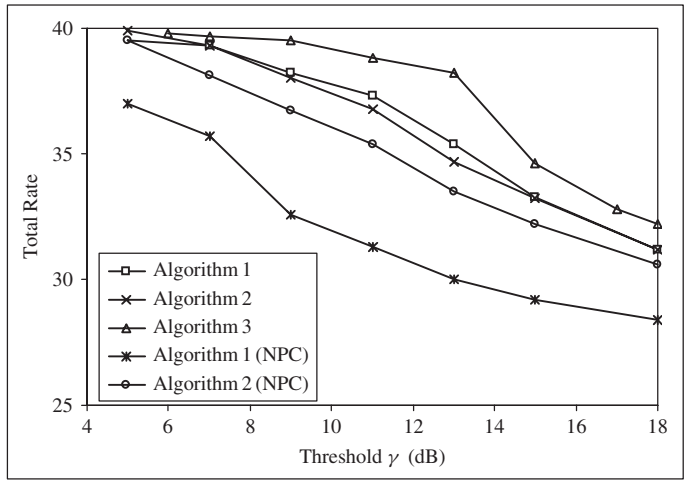

Figure 12.10 Total achievable system rate versus the SIR threshold for OFDMA.

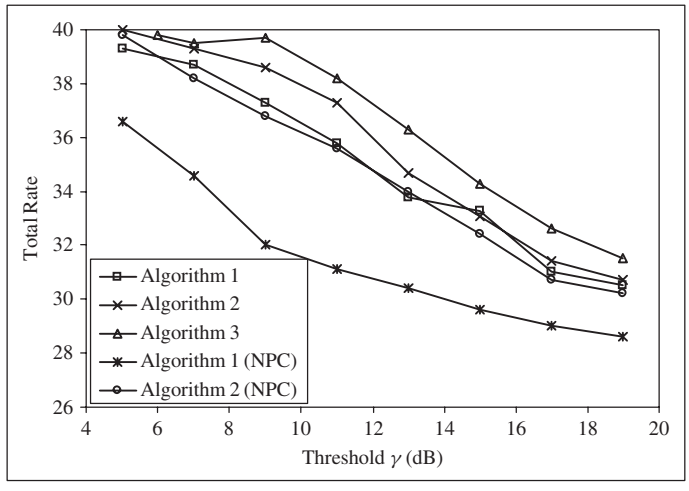

Figure 12.11 Total achievable system rate versus the SIR threshold for TDMA.

In Reference [74], a media access control protocol was proposed based on a slot reservation mechanism combined with SDMA. The work reported in Reference [75] studies the capacity performance of reservation ALOHA protocols that support SDMA. The tradeoffs involved in operating the reservation channel in multibeam versus single-beam modes were assessed. The system described in Reference [76] uses smart antennas in a packet radio network with slotted nonpersistent CSMA as the media access control protocol. Multibeam protocols are also described in Reference [77], which use carrier sensing as a mechanism for synchronizing smart antenna adaptation. In addition, signaling mechanisms are proposed for reducing the detrimental effects of hidden stations. It should be noted that an important practical concern in random access SDMA protocols is the complexity and latency of the dynamic packet acquisition process. Finally, in Reference [78], smart antennas were proposed for use in indoor local area networks based on protocols derived from the IEEE 802.11 wireless LAN standard.

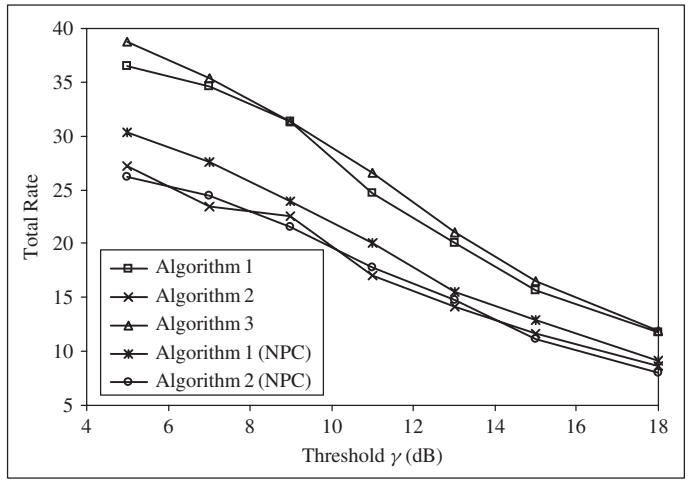

Figure 12.12 Total achievable system rate versus the SIR threshold for CDMA ($\rho_{\max} = 0.02$).

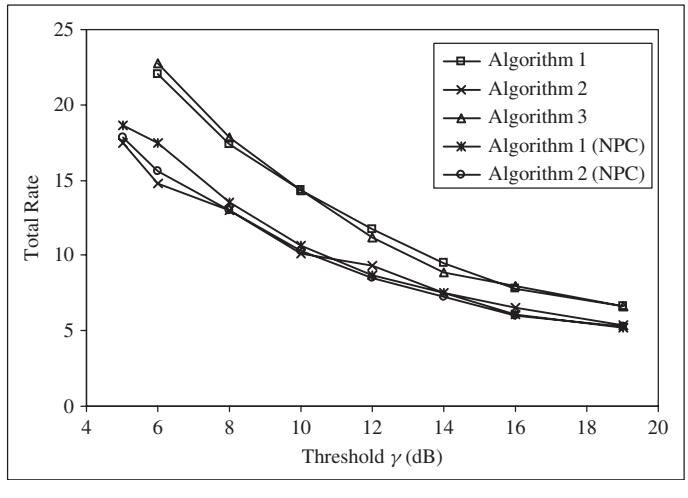

Figure 12.13 Total achievable system rate versus the SIR threshold for CDMA ($\rho_{\max} = 0.1$).

In this section we discuss dynamic slot allocation (DSA) for packet-switched SDMA. As in Reference [73], we assume that the system is TDD and narrow-band and that the base station can measure the spatial channel characteristics for a station when it is transmitting in the up-link direction. In dynamic slot allocation, the base station then uses these spatial channel measurements to construct subsequent SDMA/TDMA frames intelligently.

12.3.1 The system model

The base station utilizes a smart antenna array with N elements and communicates with a set of portable stations. The stations use single omnidirectional antennas. We will assume that the system considered uses time-division duplexing (TDD). As discussed above, the base station may be able

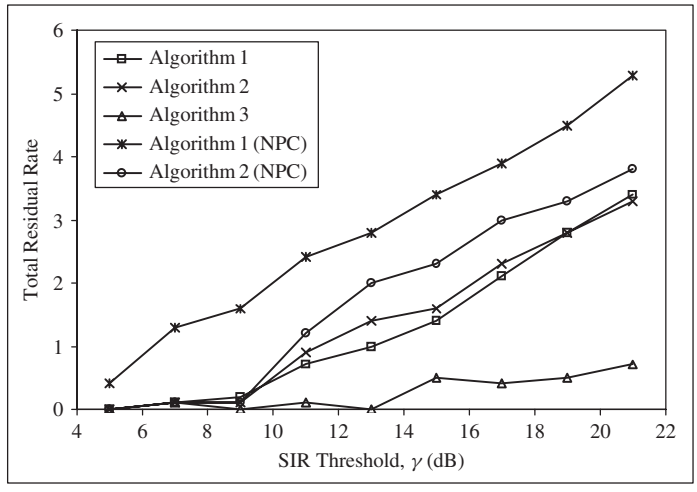

Figure 12.14 Total residual rate versus the SIR threshold for OFDMA.

to determine the correct beamforming for both transmission and reception after first measuring the vector channel response between a set of active stations and the array.

Under multiple beamforming SDMA operation, the base station can attempt to transmit or receive up to M packets simultaneously by forming M antenna beam patterns. In the following discussion, we focus on the activities of a single beamforming module, in the reverse-link (up-link) direction. A similar analysis can be done for the forward-link direction [79]. The system considered is given in Figure 2.15. In the figure we show the details of a single beamforming module and the set of complex beamforming weights, $\mathbf{w} = [w_1, w_2, \ldots, w_N]$, one for each antenna element.

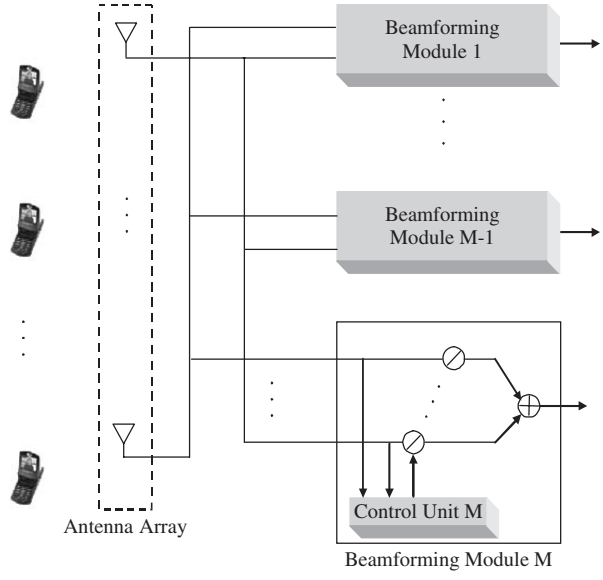

Figure 12.15 Multibeam smart antenna in receive mode.

In the following development we assume that the delay spread is small compared to symbol durations (e.g. indoors OFDM signaling). We also assume a time-invariant situation where the channel conditions are essentially constant from the time the channel is sampled until transmissions occur. Under these conditions we can define the beamforming required to maximize the post-beamforming SINR for each desired signal [80, 81].

The received base station signal vector at time sample k is defined by $\mathbf{x}(k) = [r_1(k)r_2(k)\cdots r_N(k)]^{\mathrm{T}}$, where $r_i(k)$ is a complex received signal on antenna element i at time k. S stations transmitting simultaneously. The received signal $\mathbf{x}(k)$ is the superposition of the desired signal vector, $\mathbf{x}_d(k)$, $S-1$ interfering signal vectors, $\mathbf{x}_i(k)$ and an additive white Gaussian noise vector, $\mathbf{x}_\eta$. In Figure 12.15 the first desired signal is shown as $d = 1$, corresponding to beamforming module 1. This can be written as

$$\mathbf{x}(k) = \mathbf{x}_d(k) + \sum_{\substack{i=1 \\ i \neq d}}^{S} \mathbf{x}_i(k) + \mathbf{x}_\eta(k)$$

The interfering and noise signals collectively form the undesired signal $\mathbf{x}_u(k)$, so $\mathbf{x}(k)$ can also be written as $\mathbf{x}(k) = \mathbf{x}_d(k) + \mathbf{x}_u(k)$. If the signal transmitted by station j is $s_j(k)$ and the channel is not varying with time, then the received signal can be written as

$$\mathbf{x}(k) = \mathbf{v}_d s_d(k) + \sum_{\substack{i=1 \\ i \neq d}}^{S} \mathbf{v}_i s_i(k) + \mathbf{x}_\eta(k)$$

where $\mathbf{v}_d$ and $\mathbf{v}_i$ are referred to as the $N \times 1$ station signature (or station code) vectors of the desired station d and the ith interfering signal, respectively. Note that, in general, the station signatures result from a superposition of multipath components, as discussed in Section 12.2.

We will assume that each transmitted signal has unit power and is uncorrelated with the other transmitted signals. The $N \times N$ undesired signal covariance matrix is

$$\mathbf{\Phi}_u = E[\mathbf{x}_u^*(k)\mathbf{x}_u^{\mathrm{T}}(k)] = \sigma_\eta^2 \mathbf{I} + \sum_{\substack{i=1 \\ i \neq d}}^{S} \mathbf{v}_i^* \mathbf{v}_i^{\mathrm{T}}$$

where $\mathbf{I}$ is the identity matrix and σ_η^2 is the mean noise power per element. The mean SINR, after beamforming, is given by

$$SINR = E\left[\left|\mathbf{w}^{\mathrm{T}}\mathbf{x}_d(k)\right|^2\right] / E\left[\left|\mathbf{w}^{\mathrm{T}}\mathbf{x}_u(k)\right|^2\right] \tag{12.16}$$

The value of $\mathbf{w}$ that minimizes the MMSE between the output of the beam former and the desired signal is

$$\mathbf{w}_{\mathrm{opt}} = \mathbf{\Phi}_u^{-1}\mathbf{v}_d^* \tag{12.17}$$

12.3.2 Multibeam SDMA/TDMA capacity and slot allocation

In smart antenna base stations using TDD, the station signatures can be obtained by polling the active stations before actual user data are transmitted [73, 74]. Once a set of station signatures is known, the base station then generates an SDMA/TDMA frame so that transmission can proceed. As in Reference [74], we will assume that all of these activities occur well within the coherence time of the channel.

Given a set of T stations, a slot allocation algorithm generates an SDMA/TDMA frame consisting of L timeslots. We assume that each station is allocated a single slot in the generated frame,

into which a fixed-length packet can be transmitted. The timeslots and stations are indexed by the sets of integers $1, 2, \ldots, L$ and $1, 2, \ldots, T$, respectively. Here, L is a random variable that is dependent upon the particular stations chosen and the slot allocation algorithm used. In this process, CS(i) is defined to be the set of stations that have been allocated to slot i. If CS(2) = {1, 2, 4}, for example, then stations 1, 2 and 4 have been assigned to timeslot 2. The output of the slot allocation process consists of the integer L and CS(i) for $i = 1, 2, \ldots, L$.

The objective of the slot allocation process is to perform this allocation such that the length of the frame, L, is minimized. This assignment is done under the constraint that the post-beamforming SINR from Equation (12.16) (using the optimal beamforming weights from Equation (12.17)) exceeds the $SINR_{\min}$ threshold for each assigned packet; i.e. if the SINR for packet i is given by Equation (12.16), we must have $SINR_i \geq SINR_{\min}$. The expected frame length $E[L]$ for a given T is obtained by repeating the allocation many times under the same slot allocation algorithm. It can easily be seen that minimizing the expected frame length is the same as maximizing the frame capacity C_f, defined by $C_f = T/E[L]$. The maximum number of stations per slot is bounded by the number of available beamforming modules, M. M is set to N in this section, which would normally be the maximum number of simultaneous transmissions possible. In this section we are only interested in the frame capacity, so we will refer to C_f simply as capacity from here on.

We now consider the output SINR when optimal SINR beamforming is used for a given desired signal. Consider a set of stations that are assigned to the same SDMA/TDMA timeslot. Without any loss in generality, we will consider a particular antenna beam and identify the desired station signature vector as $\mathbf{x}_d$. The optimal SINR, after beamforming, can be written as

$$SINR = \max_{\mathbf{w}} \langle \mathbf{x}_d, \mathbf{w} \rangle^2 / \sum_{i=1}^{I} \langle \mathbf{x}_i, \mathbf{w} \rangle^2 + \sigma^2 \|\mathbf{w}\|^2$$

where we have assumed that there are I interfering stations assigned to the slot in addition to the desired station. We have also assumed that the interfering stations are numbered from 1 to I. In this expression, σ^2 is the Gaussian noise power at the input to the beamforming module.

In general, the I interferers will consist of I_0 orthogonal interferers and I_{no} nonorthogonal interferers, as discussed above, where $I = I_0 + I_{\text{no}}$. We will denote the set of nonorthogonal interfering station indices as $\mathbf{I}_{\text{no}}$. It can be seen from the form of the SINR that we can choose the appropriate terms in $\mathbf{w}$ such that $\langle \mathbf{x}_i, \mathbf{w} \rangle = 0$ for all I_0 orthogonal interferers. This can be done without affecting the other terms in the SINR. As a result, we have

$$\begin{aligned} SINR &\leq \max_{\mathbf{w}} \langle \mathbf{x}_d, \mathbf{w} \rangle^2 / \sum_{i \in \mathbf{I}_{\text{no}}}^{I} \langle \mathbf{x}_i, \mathbf{w} \rangle^2 + \sigma^2 \|\mathbf{w}\|^2 \\ &\leq \max_{\mathbf{w}} \langle \mathbf{x}_d, \mathbf{w} \rangle^2 / \langle \mathbf{x}_S, \mathbf{w} \rangle^2 + \sigma^2 \|\mathbf{w}\|^2 \end{aligned}$$

The second inequality follows from setting $I = 1$. When there is only a single nonorthogonal interferer, we denote its signature vector by $\mathbf{x}_s$ as shown. It is clear that the SINR is a nonincreasing function of I_{no}. Therefore, the optimal SINR obtained with one or more nonorthogonal interferers in a slot (i.e. $\overline{SINR}_1$) is strictly less than the optimum SINR, which can be obtained with zero nonorthogonal interferers (i.e. $\overline{SINR}_0$). Accordingly, if we choose the required SINR for each station to satisfy $\overline{SINR}_1 < SINR_{\min} < \overline{SINR}_0$, then only those stations that have orthogonal spatial signatures will be permitted to be assigned to the same slot. Thus, by making this selection, an optimal slot allocation algorithm can only allocate stations with orthogonal spatial signatures to the same timeslot. Stations that have nonorthogonal signatures must be assigned to separate timeslots.

12.3.3 SDMA/TDMA slot allocation algorithms

The following definitions and variables will be used to define the algorithms:

- Station index $\{1, 2, \ldots, T\}$.
- CS(i) the set of stations currently allocated to slot i. At the start of each algorithm this set is initialized to be empty for all i.
- UA is the current set of unallocated stations. This set is initialized to contain all stations at the start of each algorithm.
- CsID is the current slot ID and Stn is a variable to hold the current station under consideration.

Reference [82] gives pseudo code descriptions for the three algorithms summarized below.

Random SDMA/TDMA

1. *CsID =1*
2. *for each Stn in UA*
3. ***begin***
4. *CS(CsID) = CS(CsID) + {Stn}*
5. *if (SINR$_i$ < SINR$_{min}$ for any station, i, in CS(CsID))*
6. ***begin***
7. *CS(CsID) = CS(CsID) − {Stn}*
8. *CsID = CsID + 1*
9. *CS(CsID) = CS(CsID) + {Stn}*
10. ***end***
11. *UA = UA − {Stn}*
12. ***end***

The slot ID (CsID) is first initialized to 1. The algorithm then executes block 3–12 once for each station. The algorithm either adds the station under consideration to the current slot or to the next slot by itself. First, the station is added to the current slot (line 4). The stations in the current slot are then tested to check that the SINR for each is above the desired threshold (line 5), i.e. 8. If not (block 6–10), the added station is removed from the current slot, the slot index is incremented (line 8) and the station in question is added to the next slot (line 9). If the SINR is sufficient for all stations in slot CsID (line 5), then the station in question is left in the current slot and the algorithm continues with the next station in UA. In either case the station is allocated and thus removed from UA (line 11).

The problem with this method is that if two consecutive stations are incompatible, the algorithm will advance to the next slot even if an unallocated compatible station exists. However, the complexity of this algorithm is very low.

Equal Norm SDMA/TDMA

1. *for each* $i, j \in \{1, 2, \ldots, T\}$ *let* $C_{i,j} = \min(\|\mathbf{v}_i\|_2^2/\|\mathbf{v}_j\|_2^2, \|\mathbf{v}_j\|_2^2/\|\mathbf{v}_i\|_2^2)$
2. *CsID = 1*
3. *Stn = 1*
4. *CS(CsID) = CS(CsID) + {Stn}*
5. *while (UA* $\neq \{\ \}$*)*

```
6.  begin
7.  for each station i in UA
8.    begin
9.    Find station, k, such that C(i, k) ≤
          C(i,j) for all k, j in CS(CsID)
10.     COMP(i) = C(i, k)
11.     end
12.   Find the station, n, such that
          COMP(n) ≥ COMP(i) for all n, i in UA
13.   UA = UA − {n}
14.   CS(CsID) = CS(CsID) + {n}
15.   if (SINR_i < SINR_min for any station,
          i, in CS(CsID))
16.     begin
17.     CS(CsID) = CS(CsID) − {n}
18.     UA = UA + {n}
19.     CsID = CsID + 1
20.     Pick a station, k, randomly from UA
21.     CS(CsID) = CS(CsID) + {k}
22.     UA = UA − {k}
23.     end
24.   end
```

Compared with the Random algorithm, in Equal Norm more sophisticated tests are used to assign a station to a slot. We first form the compatibility matrix, **C**, using the station spatial codes, as shown in line 1. The algorithm then initializes the slot ID (CsID) to 1 and begins with station 1. This station is added to slot 1 (line 4). Block 6–24 then executes until all stations have been assigned. Stations are added to the current slot as follows. For each station in UA the algorithm finds the station in CS(CsID) to which it has minimum compatibility. This is done in line 9. The compatibility value is recorded in line 10. COMP(i) is a variable used to record the compatibility value for station i. Line 12 then selects the station in UA with the largest of these compatibility values. This is the candidate station in the current slot. In line 14 this station is added to the slot. All of the station SINRs are then tested in line 15. If all SINRs are above the desired threshold, then this station is left assigned to the current slot. Otherwise the station is removed from that slot (line 17) and returned to UA (line 18). The slot index is then incremented (line 19) and a station is randomly selected from UA and assigned to the new slot (lines 20 to 22). It can be seen that the ijth entry in **C** is proportional to the ratio of the received powers of signals i and j. The physical interpretation of this algorithm is that it attempts to place stations with similar power levels in the same timeslot. This is done to provide less opportunity for stronger interferers to corrupt weaker transmissions.

First Fit SDMA/TDMA

```
1.  CsID = 1
2.  while (UA ≠ { })
3.    begin
4.    for each Stn in UA
5.      begin
6.      CS(CsID) = CS(CsID) + {Stn}
7.      if (SINR_i < SINR_min for any Station,i, in CS(CsID))
```

```
8.              begin
9.                CS(CsID) = CS(CsID) − {Stn}
10.               end
11.           else
12.             begin
13.               UA = UA − {Stn}
14.             end
15.       end
16. CsID = CsID + 1
17. end
```

The First Fit algorithm is similar to the Random algorithm. In First Fit, however, instead of advancing to the next slot whenever a station assignment is infeasible, all stations in UA are tried first. Block 3–17 is executed until all stations have been allocated. For a given timeslot (i.e. CsID), block 5–15 checks every remaining station in UA to see if it can be added to the slot in question. In line 6 the station is temporarily added to the slot and tested for feasibility in line 7. If the assignment is feasible the station remains assigned to slot CsID and is removed from UA by line 13. Otherwise line 9 removes the station from this slot. In either case the loop continues by testing the next station in UA. Once all stations have been tested, CsID is incremented and the procedure repeats for the next timeslot.

Best Fit SDMA/TDMA

```
1. CsID = 1
2. Find Station k such that ‖v_k‖_2 ≤ ‖v_j‖_2 for all k, j in UA
3. CS(CsID) = CS(CsID) + {k}
4. UA = UA − {k}
5. while (UA ≠ { })
6.   begin
7.   SINRmaxmin = −∞
8.   for each Stn ∈ UA
9.     begin
10.      CS(CsID) = CS(CsID) + {Stn}
11.      if (SINR_i > SINR_m in for all stations in CS(CsID))
12.        begin
13.        SINRx = Minimum SINR of stations
               in CS(CsID)
14.        if (SINRx > SINRmaxmin)
15.          begin
16.          SINRmaxmin = SINRx
17.          MaxminStn = Stn
18.          end
19.        end
20.        CS(CsID) = CS(CsID) − {Stn}
21.    end
22.  if (SINRmaxmin > −∞)
23.    begin
24.    CS(CsID) = CS(CsID) + {MaxminStn}
25.    UA = UA − {MaxminStn}
26.    end
```

27. *else*
28. ***begin***
29. $CsID = CsID + 1$
30. *Find Station k such that* $\|v_k\|_2 \leq \|v_j\|_2$ *for all k, j in UA*
31. $CS(CsID) = CS(CsID) + \{k\}$
32. $UA = UA - \{k\}$
33. ***end***
34. ***end***

The Best Fit algorithm is the most sophisticated of the algorithms. We start by slot 1 (line 1). The algorithm selects stations for consideration in ascending order of received power at the base station. This is shown in line 2, where we start with the station in UA with the lowest receive power. In lines 1 to 4 this station is assigned to slot 1. The block 6–34 then executes until all stations have been allocated. In each iteration of the block, the station in UA is found whose addition to the current slot would result in the largest minimum SINR for those stations in the slot in question. This station is found in the block 9–21 as follows. In line 10, a test station is temporarily added to the current slot, CsID. If all stations in CS(CsID) satisfy the minimum SINR constraint (line 11), then the SINRx variable records the minimum SINR of all stations allocated to slot CsID. In line 14 the algorithm then tests to see if this minimum SINR is the largest found so far. If so, then the SINR is recorded in the variable SINRmaxmin (line 16) and the new station is recorded in the variable MaxminStn (line 17). The test in line 22 is used to determine if a feasible station has been found to add to the current slot, CsID. If so, the recorded station is added (lines 24 and 25). Otherwise there is no station that can be added to the current slot. In this case the slot ID is incremented (line 29) and the station with the lowest receive power is drawn from UA and added to the new slot. The above procedure is then repeated.

Note that sorting the station signatures in order of ascending power is beneficial since it helps prevent those with higher power from overpowering the others. Also, since lower power signals are competing with a relatively large amount of noise, it is best to allocate them at the start of the frame when there are more unallocated stations to test. Both Random and First Fit algorithms using power pre-sorting are also defined. In the following descriptions the differences between their unsorted versions are noted.

Random Sorted SDMA/TDMA

At the start of the algorithm, the stations in UA are sorted in order of ascending received power. The remaining algorithm is identical to Random SDMA/TDMA discussed above. In line 2 of that description, stations are drawn from UA in sorted order.

First Fit Sorted SDMA/TDMA

As in the Random Sorted case, the stations in UA are first sorted in order of ascending received power. The remaining algorithm is identical to First Fit SDMA/TDMA discussed above. In line 4 of that description, stations are drawn from UA in sorted order.

If $T \gg N$, the approximate worst-case orders of complexity of the dynamic slot allocation algorithms are given in Table 12.2 [82]. It can be seen that the algorithms fall into two groups. The most complex group consists of First Fit Sorted and Best Fit. For $N = 4$, over the range of stations considered, the computation required is at least an order of magnitude greater for these algorithms compared with the other group. In the $N = 8$ element case, this difference increases about half an order of magnitude when the number of stations is large.

Table 12.2 Approximate worst-case algorithm orders. (Reproduced by permission of IEEE © 2001 from Shad *et al*. [82])

Alorithm	$O(N, T)$
FCFS	$\frac{T}{N-1}\left(4N^5 + \frac{145}{12}N^4\right)$
FCFS Sorted	$T(8N-2) + O(\text{FCFS})$
First Fit	$\frac{T^2}{2(N-1)}\left(4N^5 + \frac{145}{12}N^4\right)$
First Fit Sorted and Best Fit	$T(8N-2) + O(\text{First Fit})$
Equal Norm	$T(11T - 13 + 8N) + O(\text{FCFS})$

12.3.4 SDMA/TDMA performance examples

Performance examples for the system with $N = 8$ antenna array are shown in Figures 12.16 and 12.17.

In Figure 12.16, we first show the case where the SNR is very high, i.e. 20 dB. In this low-noise case, the smart antenna can almost always accommodate eight packets per slot. Note that this is the theoretical maximum since the antenna has only eight elements. The sawtooth drop of the curves is caused when a station is added that must be placed into a new slot by itself, and therefore there are not enough stations to fill the slot in question. Under these conditions, the antenna is doing such a good job there is very little value in performing dynamic slot allocation, and thus there is virtually no distinction between the algorithms. Note that in the limit as the SNR becomes infinite, the SDMA/TDMA capacity is given by $T/\lceil T/N \rceil$, where $\lceil \cdot \rceil$ is the ceiling operation that rounds

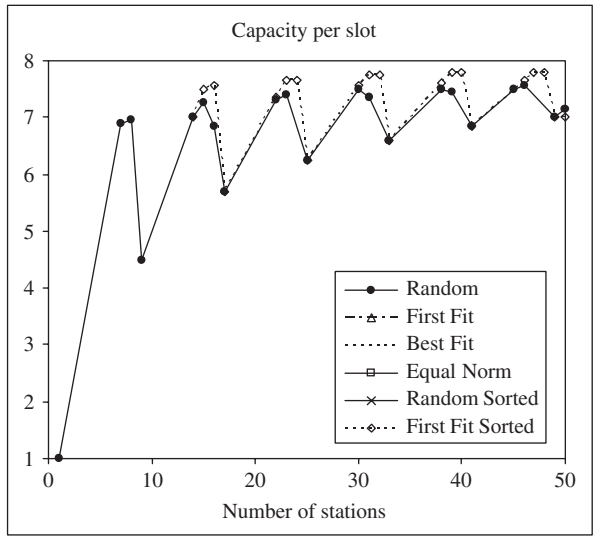

Figure 12.16 SDMA/TDMA capacity with simulated Rayleigh station signatures, 20 dB SNR. (Reproduced by permission of IEEE © 2001 from Shad *et al*. [82].)

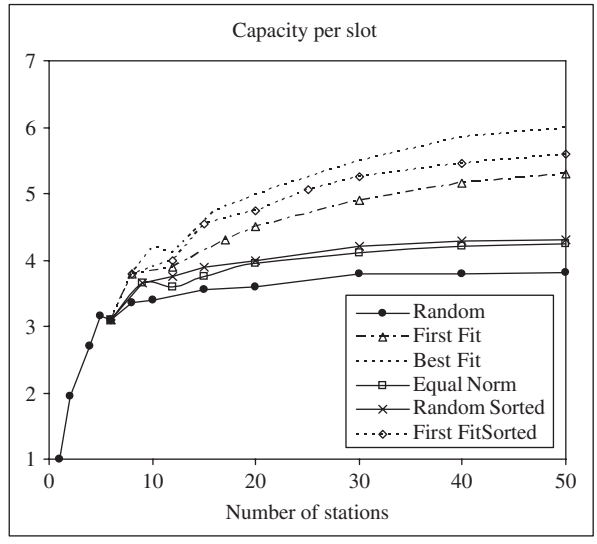

Figure 12.17 SDMA/TDMA capacity with simulated Rayleigh station signatures, 6 dB SNR. (Reproduced by permission of IEEE © 2001 from Shad *et al.* [82].)

its argument up to the next integer. This happens because each beamforming module can always null-out seven interferers and yet achieve the required $SINR_{\min}$ for the desired station, since it does not have to combat random noise.

In Figure 12.17, a similar graph is shown for a much higher noise (6 dB SNR). It can now be seen that variations between the different algorithms become very significant, especially when a higher number of stations is considered. This is because the more sophisticated algorithms have more stations to consider, so they are better able to generate good slot assignments. In the example shown, the Best Fit algorithm has a capacity roughly 58 % higher than the Random algorithm, when 50 stations are considered. As the propagation conditions deteriorate, one expects increasing value in performing intelligent slot allocation, since the system performs less well under a random allocation of stations.

12.4 SDMA/OFDM NETWORKS WITH ADAPTIVE DATA RATE

12.4.1 The system model

In this section we further elaborate details of resource allocation in SDMA/OFDM because this particular format is of special interest for 4 G wireless networks. Special focus is on adaptation of the bit rate depending on available SNR after resource allocation.

We consider basically the same model again as in Section 12.2 with a base station that provides coverage to a cell and serves K users, but this time we introduce additional details. The base station has an M-element adaptive linear antenna array, capable of separating at most $M' \leq M$ cochannel users. We will assume that all degrees of freedom of the array are exploited, so that $M' = M$. Each one of the K receivers has a single omnidirectional antenna. The base station employs OFDM transmission with N subcarriers.

An underlying slotted transmission scheme is assumed. Packetized data arrive from higher layers for transmission over the radio channel and each packet occupies one timeslot of duration T_s. A packet consists of S OFDM information symbols and one training symbol, which is used

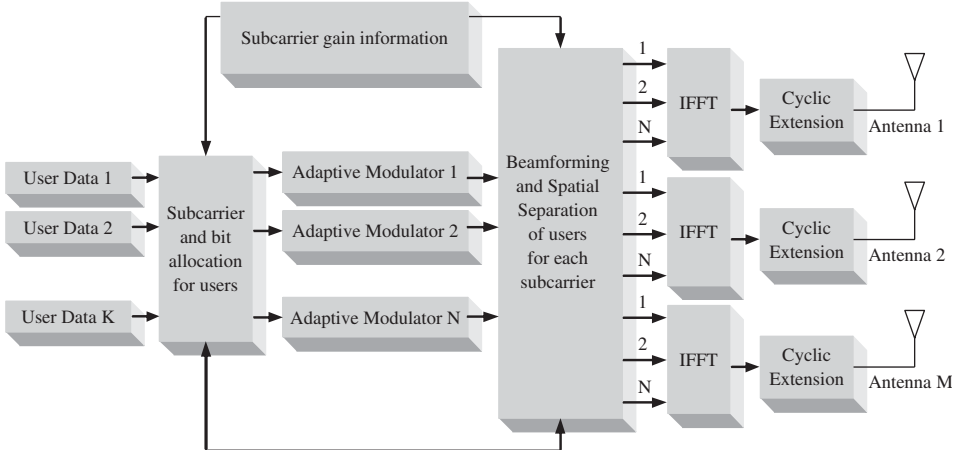

Figure 12.18 Block diagram of OFDM/SDMA transmitter with adaptive subcarrier and bit allocation and spatial user separation.

for channel estimation. Each OFDM symbol of a user consists of bits that must be assigned to different subcarriers. If $b_{n,k}$ bits of user k are assigned to subcarrier n, the total number of bits per OFDM symbol for k is $\sum_{n=1}^{N} b_{n,k}$. These $b_{n,k}$ bits constitute the nth subsymbol of user k that modulates subcarrier n. User subsymbols can have different numbers of bits in subcarriers, by using different modulation levels from a set of available QAM constellations. Assuming that the channel is invariant for a slot duration, subsymbols of all symbols of a user within a packet modulate the same subcarriers. The instantaneous transmission rate R_k (in bits/s) for user k in a slot is $R_k = S(\sum_{n=1}^{N} b_{n,k})/T_s$. Under SDMA, the base station can transmit up to M subsymbols of M different users in each subcarrier by forming M different beam patterns. The configuration of a K-user OFDM/SDMA transmitter is redrawn in Figure 12.18 obtained by slight modification of Figure 12.9. The serial bit streams of users are inserted into the subcarrier and bit allocation module. This module determines the number of allocated user bits to different subcarriers and the users that share the same subcarriers.

After that, user bits are forwarded into N adaptive modulators. Each modulator modulates the corresponding subcarrier with an appropriate signal that depends on the bits of all users that share the subcarrier. Since linear modulation methods (such as QAM) are assumed, the superposition principle holds and the signal that modulates a subcarrier is given by superimposing the constellation points of users that share the subcarrier. Then the outputs of modulators enter the beamforming and spatial separation module. The beamforming and spatial separation submodule for subcarrier n is redrawn in Figure 12.18 with slightly different notation. Bits of each of the ($M' \leq M$) users assigned to subcarrier n are forwarded to one of the parallel beamforming modules. A beamforming vector $\mathbf{w}_{n,k} = [w_{n,k}^1, \ldots, w_{n,k}^M]^{\mathrm{T}}$ is computed for each user k. The output of the beamforming and spatial separation module is a set of beamforming vectors $\{\mathbf{w}_{n,k}\}$ for each subcarrier n and each user k assigned to a subcarrier. With this notation $SINR_{n,k}$ can be represented by rewriting Equation (12.3) as

$$SINR_{n,k} = \frac{\mathbf{w}_{n,k}^H H_{n,k} \mathbf{w}_{n,k}}{\sum_{j \neq k} \mathbf{w}_{n,j}^H \mathbf{H}_{n,k} \mathbf{w}_{n,j} + \sigma^2} \tag{12.3a}$$

The link quality for all users, subcarriers and antennas is assumed to be known at the transmitter, which means that matrices $H_{n,k}$ are available for all n, k. With a bidirectional link and time-division duplexing (TDD), each subcarrier can be considered as a reciprocal link.

Then spatial signatures of users at each subcarrier remain unchanged for one up-link and down-link transmission. Link quality estimation can be performed at the base station with training symbols that are included in up-link user packets. A user k sends training symbol e_k, consisting of known complex subcarrier coefficients $\{E_{n,k}\}$, $n = 1, \ldots, N$. Antenna m receives N time samples $\{z^m_{n,k}\}$, $n = 1, \ldots, N$ and uses FFT to transform them to frequency-domain coefficients $\{Z^m_{n,k}\}$, $n = 1, \ldots, N$. The received coefficient at antenna m and subcarrier n from user k is $Z^m_{n,k} = E_{n,k}H^m_{n,k} + N^m_{n,k}$, where $N^m_{n,k}$ is the noise component. Then the MMSE estimate of complex gain is $\hat{H}^m_{n,k} = Z^m_{n,k}/E_{n,k}$. Under the assumption of reciprocity and reasonable time variance of the link, the transmitter can use these estimates in down-link computations.

The BER of a user that uses M-QAM modulation in a subcarrier is approximated as [25] $\text{BER} \approx 0.2\exp[-1.5 \cdot SINR/(M-1)]$. The minimum SINR to maintain $\text{BER} \leq q$ for M-QAM modulation is the following SINR threshold: $\gamma_M = -\ln(5q)(M-1)/(1.5)$. A higher SINR (lower interference level) in a subcarrier enables the utilization of high M-QAM modulation levels and yields a higher transmission rate.

12.4.2 Resource allocation algorithm

The basic idea of the algorithm is to assign each user to an appropriate subcarrier by evaluating the incurred rate benefit of the allocation, defined as the increase in total number of bits of user subsymbols in the subcarrier. Cochannel users in a subcarrier must be spatially separable, while SIRs at receivers must be as high as possible, so as to exceed the largest possible SIR threshold, which corresponds to a large number of bits per subsymbol. Since joint computation of beamforming vectors of users to increase all receiver SIRs is not straightforward, we focus on the impact of the allocation to each user separately. If inserted users cause the least interference to other users that are already assigned in the channel and receive the least interference from them, then spatial separability with larger numbers of bits per user subsymbol are possible, since SIRs at receivers are higher.

For each subcarrier n and user k, we construct the ratio of desired power for user k over undesired power caused to other users by user k. The desired power is the useful signal power that reaches receiver k, while the undesired power is a measure of interference induced by user k to receivers of other users that use the same subcarrier n. In fact, we are interested in computing the maximum value of this ratio, $D_{n,k}$, by appropriately adjusting the direction of beamforming vector $\mathbf{w}_{n,k}$. Thus, we define

$$D_{n,k} = \max_{\mathbf{w}_{n,k}} \frac{\mathbf{w}^H_{n,k} H_{n,k} \mathbf{w}_{n,k}}{\mathbf{w}^H_{n,k} \left(\sum_{i \in U^n} \mathbf{H}_{n,i}\right) \mathbf{w}_{n,k}}, \text{ s.t. } |\mathbf{w}_{n,k}| = c \tag{12.18}$$

where c is a constant and U^n is the set of users that are already assigned to subcarrier n. The vector $\mathbf{w}^*_{n,k}$ that maximizes the ratio above is known to be the generalized eigenvector of the matrix pair $(H_{n,k}, \sum_{i \in U^n} H_{n,i})$. A user k should be inserted in subcarrier n if the ratio $D_{n,k}$ is maximum. In addition, we take into consideration the impact of insertion of user k on other users that share the subcarrier. For each such user i already assigned in subcarrier n, we compute the following ratios:

$$D^-_{n,i} = \max_{\mathbf{w}_{n,k}} \mathbf{w}^H_{n,i} H_{n,i} \mathbf{w}_{n,i} / \mathbf{w}^H_{n,i} \left(\sum\nolimits_{j \in U^n : j \neq i} H_{n,j}\right) \mathbf{w}_{n,i}$$

and

$$D^+_{n,i} = \max_{\mathbf{w}_{n,k}} \mathbf{w}^H_{n,i} H_{n,i} \mathbf{w}_{n,i} / \mathbf{w}^H_{n,i} \left(\sum\nolimits_{j \in U^n : j \neq i} H_{n,j} + H_{n,k}\right) \mathbf{w}_{n,i}$$

where in both equations we assume $|\mathbf{w}_{n,i}| = c$. The quantity $\Delta D^k_{n,i} = D^-_{n,i} - D^+_{n,i}(k)$ denotes the impact of insertion of new user k on user i that is already assigned in the subcarrier. Insertion of user k causes interference to user i and this is shown in the denominator of $D^+_{n,i}(k)$. A new user k is preferable for the subcarrier if it causes the least total interference to users in the subcarrier, so that quantities $\Delta D^k_{n,i}$ are minimum for as many users i as possible, among all subcarriers n. The interference preference factor (IPF), $I_{n,k}$, is defined as $I_{n,k} = D_{n,k} / \sum_{i \in U^n} \Delta D^k_{n,i}$.

The allocation process should select a user k and assign it to subcarrier n, so that IPF is maximum. The new cochannel set of users is then more likely to be spatially separable.

Let us assume now that user k is tentatively assigned to subcarrier n, according to the criterion above. The beamforming vectors for users in U^n are then computed as the solutions to appropriate generalized eigenproblems. These beamforming vectors are used to calculate SIR at each receiver. However, it may happen that insertion of new user k decreases SIR at a receiver of a cochannel user in such a way that the number of bits per subsymbol for that user (and thus the corresponding SIR threshold) needs to be reduced in order to maintain acceptable subcarrier BER and spatial separability of all users. The assignment of a user in a subcarrier is beneficial if the total number of user bits for spatially separable users in $U^n \cup \{k\}$ exceeds that of U^n before insertion of user k. If the inserted user does not possess desirable spatial or multipath properties, e.g. it is not sufficiently separated in angle from other users, the resulting total number of user bits in the subcarrier may be reduced. Clearly, the most appropriate allocation pair (n^*, k^*) of user and subcarrier is the one for which the total increase in number of user bits in that subcarrier is maximized. In order to formalize these arguments, let $b_{n,k}$ denote the number of bits of tentatively inserted user k in subcarrier n. For each user i, already assigned in subcarrier n, let $b^-_{n,i}$ and $b^+_{n,i}(k)$ denote the number of bits for user i before and after insertion of user k. An increase in the number of bits of a user means an increase in the rate of that user in the subcarrier. Thus, we define the rate increment factor (RIF) for user subcarrier n and user k as $T_{n,k} = b_{n,k} + \sum_{i \in U^n} (b^+_{n,i}(k) - b^-_{n,i})$.

An efficient allocation of users to subcarriers that leads to spatially separable users and a large total number of user bits is one where user insertion in a subcarrier results in least induced or received interference to and from already assigned cochannel users, respectively, as well as in a maximum increase in the total number of user bits. To capture this objective, we define the assignment preference factor (APF) $A_{n,k}$ as $A_{n,k} = I_{n,k} T_{n,k}$.

Among assignments with the same amount of induced or received interference, we prefer the one that results in a larger rate increase. In addition, among assignments with the same rate benefit, we consider the one with the least induced or received interference, in order to improve the situation for future allocations. The preference factors for the first assigned user in an empty subcarrier n in the absence of cochannel users are computed as follows:

(1) The IPF is given by the maximum achievable SIR at the receiver, subject to a power constraint for the user subsymbol,

$$I_{n,k} = \max_{\mathbf{w}_{n,k}} (\mathbf{w}^H_{n,k} H_{n,k} \mathbf{w}_{n,k}), \text{ s.t. } |\mathbf{w}_{n,k}| = c \tag{12.19}$$

where c is a constant. The solution $\mathbf{w}^*_{n,k}$ is the eigenvector that corresponds to the maximum positive eigenvalue of matrix $H_{n,k}$.

(2) The RIF is the maximum number of bits per subsymbol, which is determined by the maximum available modulation level.

The algorithm selects the allocation that yields the maximum APF and assigns that user to the corresponding subcarrier. The procedure is repeated until no further user assignments in subcarriers can increase the total number of user bits in a subcarrier, i.e. until $T_{n,k} < 0$ for all subcarriers n

and users k, or until the cardinality of cochannel sets of users assigned to all subcarriers is M. The main steps of the algorithm are outlined as follows [70]:

Algorithm 4

(1) *Compute spatial covariance matrices $H_{n,k}$ for all K users and N subcarriers. Initially all subcarriers are included in list C of candidate subcarriers for allocation.*

(2) *Select pair (n^*, k^*) of subcarrier and user that yields* the *maximum APF and performs the assignment.*

(3) *Update APF factors of cochannel users for n^*.*

(4) *If $|U^{\overline{n}}| = M$ or if $T_{\overline{n},k} < 0$ for a subcarrier $\tilde{n}$ and all users k, remove subcarrier $\tilde{n}$ from list C.*

(5) *If list C is not empty, go to step 2. Otherwise, terminate the algorithm and go to step 6.*

(6) *Repeat the same allocation of users to subcarriers for all packet symbols and all user packets until the next adaptation.*

The computationally intense part of the algorithm is the computation of dominant generalized eigenvectors for the APF factors. For one user, this involves Cholesky decomposition of an $M \times M$ matrix and calculation of the maximum eigenvalue of an appropriate matrix. Both of these procedures are known to be of complexity $O(M^3)$. For N subcarriers, K users and M antenna elements, the complexity of the algorithm is $O(NKM^4)$, which is not prohibitive, given that the number of antennas that is used in practice is relatively small (less than eight).

12.4.3 Impact of OFDM/SDMA system specifications on resource allocations

In the previous section, we considered the problem of resource allocation with beamforming for spatially separable users and presented an algorithm for spatial separability with a large total number of user bits per subcarrier. However, in a realistic scenario additional system specifications, which will be referred to as constraints, may come into use. For instance, the algorithm generates an allocation of spatially separable users to subcarriers, without any guarantees on total achievable rates for individual users. It may happen that users with certain spatial and multipath properties, (e.g. spatial covariance matrices) achieve high rates, whereas other users do not. In addition, beamforming power constraints were only utilized to facilitate the assignment. Thus, the only limiting factor in user assignment in a subcarrier was the number of antennas and no statement was made on the impact of beamforming power constraints on the assignment.

Each user k should satisfy a minimum rate requirement ρ_k (in bits/s), which is usually issued by the MAC layer in order to ensure satisfaction of QoS requirements for users and, to some extent, fairness in resource allocation. In addition, in a multicarrier transmission scheme such as OFDM, symbol transmission across subcarriers is subject to transmission power constraints per subcarrier. These constraints account for transmission limitations, such as the requirement for a low peak-to-average power ratio (PAPR) to avoid symbol distortion [1, 83]. Although the incorporation of constraints in the problem formulation approximates realistic scenarios, the complexity may become prohibitive. For instance, in the assignment procedure of the previous section, user reassignments among subcarriers and additional beamforming calculations should be performed if the aforementioned constraints are present.

In order to bring the problem closer to practical implementation, in this section we consider the impact of these constraints in the context of a simplified problem, where subcarrier reuse is not applicable. In this system, beamforming per subcarrier is used as another dimension to improve subcarrier quality. The OFDM/SDMA transmission system is the one in Figure 12.18,

with the difference that there exists only one beamforming module per subcarrier. Spatial covariance matrices $H_{n,k}$ are known to the transmitter for each subcarrier n and user k. Due to the absence of cochannel interference, the system is assumed to be noise-limited. Noise variance is incorporated in matrix $H_{n,k}$, so that the SNR at subcarrier n of receiver k is $\mathbf{w}_{n,k}^H H_{n,k} \mathbf{w}_{n,k}$. Each user k is assigned to some subcarriers in order to satisfy the minimum rate requirement ρ_k. A fixed BER at each subcarrier must also be satisfied. The number of user bits in a subcarrier depends on the user spatial covariance matrix and the beamforming vector. These determine SNR at the receiver and thus the maximum SNR threshold γ that is satisfied. The beamforming vector for user k in the subcarrier is assumed to have fixed power $P_{n,k}$, i.e. $\mathbf{w}_{n,k}^H \mathbf{w}_{n,k} = P_{n,k}$. A beamforming vector is feasible if it satisfies the power constraint. Clearly, the assignment of different users to a subcarrier leads to different feasible beamforming vectors that give a certain SNR at the receiver. A subcarrier and bit assignment to users is *admissible* if there exists a family of feasible beamforming vectors, one for each subcarrier, such that minimum SNR constraints at receivers corresponding to the given number of user bits per subcarrier are satisfied and minimum rate requirements for all users are fulfilled. The identification of the admissible subcarrier and bit assignment to users that yields maximum total user throughput is not straightforward. It involves selection of the user to be assigned to a subcarrier, computation of the number of user bits in the subcarrier, as well as determination of feasible beamforming vectors. Ideally, each subcarrier should be assigned to the user that can support the largest number of bits in that subcarrier. The problem is that this policy may not lead to an admissible allocation, since some users may not satisfy minimum rate requirements. In the sequel, we discuss a heuristic method that identifies an admissible allocation that yields high total user throughput.

12.4.3.1 Maximization of the total throughput

Let us focus on a subcarrier n and a user k. The problem of maximizing receiver SNR subject to a beamforming vector power constraint is

$$\max_{\mathbf{w}_{n,k}} \left(\mathbf{w}_{n,k}^H H_{n,k} \mathbf{w}_{n,k} \right), \text{ s.t. } \mathbf{w}_{n,k}^H \mathbf{w}_{n,k} = P_{n,k} \tag{12.20}$$

Since matrix $H_{n,k}$ is symmetric and invertible, it can be decomposed to $H_{n,k} = U_{n,k} \Lambda_{n,k} U_{n,k}^H$, where $U_{n,k}$ is a unitary matrix, whose columns are the eigenvectors of $H_{n,k}$, and $\Lambda_{n,k}$ is a diagonal matrix of the corresponding eigenvalues. Thus $SNR_{n,k} = \tilde{\mathbf{w}}_{n,k} \Lambda_{n,k} \tilde{\mathbf{w}}_{n,k}$ or

$$SNR_{n,k} = \sum_{m=1}^{M} \lambda_{n,k}^m \left(\tilde{\mathbf{w}}_{n,k}^m \right)^2$$

where $\tilde{\mathbf{w}}_{n,k} = U_{n,k}^{\mathrm{T}} \tilde{\mathbf{w}}_{n,k}$ and $\{\lambda_{n,k}^m\}_{m=1}^M$ are the eigenvalues of $H_{n,k}$. Note that $\tilde{\mathbf{w}}_{n,k}^H \tilde{\mathbf{w}}_{n,k} = P_{n,k}$, since $U_{n,k}$ is unitary. The maximization of problem (12.20) subject to the power constraint is achieved by vector [84]

$$\tilde{\mathbf{w}}_{n,k}^* = \sqrt{P_{n,k}} [0, \ldots, 0, \underbrace{1}_{\mu_{n,k}-\text{elem}}, 0, \ldots, 0]$$

where $\mu_{n,k} = \arg\max_m \lambda_{n,k}^m$. Thus, the optimal beamforming vector is $\mathbf{w}_{n,k}^* = U_{n,k} \tilde{\mathbf{w}}_{n,k}^* = \sqrt{P_{n,k}} \mathbf{u}_{n,k}^{\mu_{n,k}}$, where $\mathbf{u}_{n,k}^{\mu_{n,k}}$ is the eigenvector corresponding to the largest eigenvalue of $H_{n,k}$ and the maximum SNR value is $P_{n,k} \lambda_{n,k}^m$.

Consider now the multiuser case. For each user k and subcarrier n, we compute $SNR_{n,k} = P_{n,k} \lambda_{n,k}^m$. At each subcarrier n, we assign the user k^* that achieves maximum SNR, namely $k^*(n) = \arg\max_{k=1,\ldots,K} (P_{n,k} \lambda_{n,k}^{\mu_{n,k}})$. The total number of bits (total rate) for each user over all subcarriers is then evaluated by using $R_k = S(\sum_{n=1}^N b_{n,k})/T_s$. If all users satisfy the minimum rate requirements,

then this is the optimal solution, whereas if no user satisfies the minimum rate requirements, then an admissible user and bit allocation does not exist. Assume now that after this initial assignment only a subset of users satisfies the minimum rate requirements. Let S and U denote the sets of 'satisfied' and 'unsatisfied' users respectively. Then, the rate of unsatisfied users must be increased, so as to approach and exceed the minimum rate requirements. This can be achieved by subcarrier exchange (reassignment) between satisfied and unsatisfied users.

Consider a pair of users $k \in S$ and $l \in U$ that are initially assigned to subcarriers m and n respectively. Let $r_{n,k}$ denote the number of transmitted bits (rate) for a user k when it is assigned to subcarrier n and let τ_k, τ_l denote the total user rates after the initial assignment. A subcarrier exchange between users k and l is *acceptable* if the satisfied user does not become unsatisfied and if the rate of the unsatisfied user is increased, or in other words if $r_{m,k} - r_{n,k} \leq \tau_k - \rho_k$ and $r_{m,l} \geq r_{n,l}$. Subcarrier exchange should cause the *least decrease* in total achievable throughput. For the exchange of subcarriers m and n that are initially occupied by users k and l, we define the reassignment rate cost as $C_{m,n} = (r_{m,k} + r_{n,l}) - (r_{m,l} + r_{n,k})$, where terms in parentheses denote rates before and after reassignment and $C_{m,n} \geq 0$. Another significant parameter is the associated rate benefit for *unsatisfied* users. Rate benefit is captured by the metric $U_{m,n} = (\rho_l - \tau_l) - [\rho_l - (\tau_l - r_{n,l} + r_{m,l})]^+$, where the two terms denote the marginal rate that is required in order for l to reach the minimum rate ρ_l before and after reassignment and $(x)^+ = x$, if $x > 0$; otherwise it is 0.

If the unsatisfied user reaches ρ_l with the subcarrier exchange, then the second term is 0. A preferable reassignment is one with a small reassignment rate cost $C_{m,n}$ and a high rate benefit $U_{m,n}$ for unsatisfied users. We define $E_{m,n} = C_{m,n}/U_{m,n}$ as the exchange preference factor (EPF). After the initial assignment, admissible subcarrier reassignments with *minimum EPF* are performed, by selecting appropriate subcarriers occupied by a satisfied and an unsatisfied user. EPFs and user rates are updated after each reassignment. This procedure is iterated until either all users satisfy their minimum rate requirements or no further acceptable subcarrier reassignments exist. Observe that by requiring maximum rate benefit $U_{m,n}$ for unsatisfied users, we reduce the number of algorithm iterations until user minimum rate requirements are satisfied.

12.4.3.2 Illustration

In a simple example of two users, analyzed in Reference [70], let b_i, $\mathbf{w}_i$ and H_i, respectively, be the number of bits, beamforming vector and spatial covariance matrix for user i, $i = 1, 2$. In order to have a fixed BER at each receiver for b_i user bits, the minimum required SIR is γ_i, $i = 1, 2$, where the mapping $b \mapsto \gamma$ is performed by using $\gamma_M = -\ln(5q)(M-1)/1.5$, with $b = \log_2 M$.

Vector $\mathbf{w}_i$ is written as $\mathbf{w}_i = |\mathbf{w}_i|\mathbf{u}_i$, where $\mathbf{u}_i$ is a unit vector that specifies the beamforming orientation. Two users with a vector of bits (b_1, b_2) are spatially separable if *both* SIRs at corresponding receivers SIR exceed the required thresholds, $SIR_1 = \mathbf{w}_1^H H_1 \mathbf{w}_1 / \mathbf{w}_2^H H_1 \mathbf{w}_2 \geq \gamma_1$ and $SIR_2 = \mathbf{w}_2^H H_2 \mathbf{w}_2 / \mathbf{w}_1^H H_2 \mathbf{w}_1 \geq \gamma_2$. Then the vector of bits is called achievable. The arising spatial separability issue is whether beamforming vectors $\mathbf{w}_1$ and $\mathbf{w}_2$ exist so that the same condition is satisfied. The determination of beamforming vectors is not straightforward, since SIR of each user depends on both beamforming vectors. Observe that the product of SIRs can be written as

$$SIR_1 \cdot SIR_2 = \frac{\mathbf{w}_1^H H_1 \mathbf{w}_1}{\mathbf{w}_1^H H_2 \mathbf{w}_1} \cdot \frac{\mathbf{w}_2^H H_2 \mathbf{w}_2}{\mathbf{w}_2^H H_1 \mathbf{w}_2} = z_1(\mathbf{w}_1) \cdot z_2(\mathbf{w}_2)$$

Then

$$\max_{\mathbf{w}_1, \mathbf{w}_2} (SIR_1 \cdot SIR_2) = \max_{\mathbf{w}_1} z_1 \cdot \max_{\mathbf{w}_2} z_2 \tag{12.21}$$

Let z_1^*, z_2^* denote the maximum values of z_1, z_2, which can be determined by finding the dominant generalized eigenvectors, $\mathbf{u}_1 = \mathbf{u}(H_1, H_2)$ and $\mathbf{u}_2 = \mathbf{u}(H_2, H_1)$. These eigenvectors are unit vectors, since vector magnitudes are cancelled. Then, if $z_1^* z_2^* < \gamma_1 \gamma_2$, the vector of bit numbers (b_1, b_2) is not

achievable and users are not separable. However, if $z_1^* z_2^* \geq \gamma_1 \gamma_2$, we cannot claim that individual bit numbers are achievable. In this case, if we know the beamforming orientation vectors $\mathbf{u}_1$ and $\mathbf{u}_2$, we can write the SIR constraints in the form of a linear inequality system, $F\mathbf{x} \geq \mathbf{0}$, as

$$\begin{pmatrix} (\mathbf{u}_1^H H_1 \mathbf{u}_1)/\gamma_1 & -\mathbf{u}_2^H H_1 \mathbf{u}_2 \\ -\mathbf{u}_1^H H_2 \mathbf{u}_1 & (\mathbf{u}_2^H H_2 \mathbf{u}_2)/\gamma_2 \end{pmatrix} \begin{pmatrix} |\mathbf{w}_1| \\ |\mathbf{w}_2| \end{pmatrix} \geq \begin{pmatrix} 0 \\ 0 \end{pmatrix} \tag{12.22}$$

If the system has a solution $(x_1, x_2) = (|\mathbf{w}_1|, |\mathbf{w}_2|)$ with $x_i \geq 0, i = 1, 2$, then users are spatially separable for the beamforming orientation $(\mathbf{u}_1, \mathbf{u}_2)$ and the beamforming vectors are given by $\mathbf{w}_i = x_i \mathbf{u}_i$, for $i = 1, 2$. Note that this method cannot be applied for more than two users, since (12.21) does not hold.

12.4.4 Performance examples

Results presented in this section are obtained by simulation of a single-cell system with 20 users that are uniformly distributed in the cell area [70]. The system uses OFDM transmission with an array of eight antennas at 5 GHz, in a frequency band that is divided into 50 subcarriers. The received power decreases with distance d from the base station as d^{-4}. Links corresponding to different receivers are uncorrelated. For each such link, multipath fading is modeled with a two-ray model. The angle of each path is uniformly distributed in $[0, \pi]$. The delay between paths is uniformly distributed in $[0, T]$, where T is the symbol period. The complex gain of each path is an independent lognormal random variable with standard deviation $\sigma = 6$ dB, which accounts for shadow fading.

The multipath channel between the mth antenna and the kth receiver is modeled as

$$h_{m,k}(t) = \sum_{l=1}^{L} \beta_k^l \alpha_m(\theta_{l,k}) \delta(t - \tau_k^l)$$

where L is the total number of paths, β_k^l and τ_k^l are, respectively, the complex gain and time delay for path l, and $\alpha_m(\theta_{l,k})$ is the mth element of the $M \times 1$ antenna steering vector at direction $\theta_{l,k}$, $\alpha(\theta_{l,k})$. The vector $\mathbf{a}_k = \sum_{l=1}^{L} \beta_k^l \alpha(\theta_{l,k})$ is called the spatial signature of user k and captures spatial properties and the multipath channel of that user.

The array steering vector for angle θ is given by vector $\boldsymbol{\alpha}(\theta) = (1, e^{(j2\pi d \sin\theta/\lambda_w)}, \ldots, e^{(j2\pi(M-1)d \sin\theta/\lambda_w)})$, where d is the distance between antenna elements and λ_w is the subcarrier wavelength. The steering vector is thus dependent on subcarrier frequency. Using this model, the spatial covariance matrices $H_{n,k}$ are determined for each user and subcarrier. A slotted transmission scheme based on TDD is assumed, so that reciprocity between the up-link and down-link is ensured. A subcarrier quality estimation is performed by means of training symbols that are transmitted in up-link packets and no estimation errors occur. A target BER of 10^{-3} is assumed for all users and subcarriers and the SINR threshold corresponding to a given number of user bits per subsymbol is computed by $\gamma_M = -\ln(5q)(M-1)/1.5$.

Three algorithms are compared:

(1) Subcarrier allocation and spatial separation of users. This is Algorithm 4. defined in Section 12.4.2. It employs combined subcarrier allocation and beamforming, under the criteria of minimal induced and received interference and large numbers of transmitted user bits. It will be referred to here as Algorithm A.

(2) Random subcarrier allocation (RSA) and spatial separation of users. This algorithm does not apply the criteria above to assign users to subcarriers. Thus, a user is always assigned to an arbitrary subcarrier. Once user assignment takes place, beamforming vectors are computed as usual and the number of user bits per subcarrier are determined. This algorithm is referred to as Algorithm A-RSA.

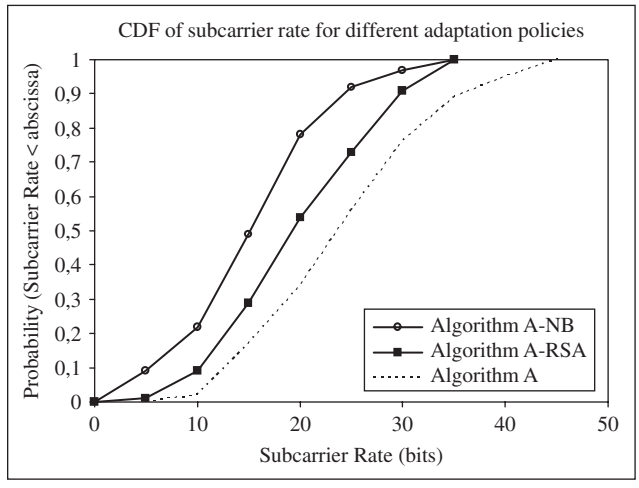

Figure 12.19 CDF of subcarrier rate for different adaptive transmissions. (Reproduced by permission of IEEE © 2002 from Koutsopoulos and Tassiulas [70].)

(3) Subcarrier allocation with no beamforming (NB). This algorithm does not apply beamforming in the criteria for user insertion in a subcarrier. In the absence of beamforming, preference factors, such as $D_{n,k}$ in Equation (12.18), are given as $D_{n,k} = \|H_{n,k}\| / \sum_{i \in U^n} \|H_{n,k}\|$. Other preference factors are computed accordingly. This method is referred to as Algorithm A-NB.

The performance criterion is the aggregate subcarrier transmission rate, which is proportional to the total number of bits of users in the subcarrier. Different numbers of bits per subsymbol are achieved by employing six different M-QAM modulation levels, which yield up to 6 bits per user of the OFDM subsymbol in a subcarrier. The user rates were computed over all subcarriers of symbols during transmission of 10 000 data packets, where the channel conditions varied randomly between consecutive packets. Results were averaged over 100 such random experiments with different user locations. The results are presented in Figures 12.19 to 12.22.

12.5 INTERCELL INTERFERENCE CANCELLATION–SP SEPARABILITY

In this section we discuss how a more advanced receiver structure can significantly increase the capacity of MIMO systems with adjacent-cell interference. Any BLAST-like receiver [1, 84, 85] is by its nature a multiuser detector that separates the data streams from the transmit antennas of the desired base station. It thus seems logical to extend this principle to the data streams from the interfering base stations as well. In this section, turbo space–time multiuser detection (ST-MUD) is employed for intracell communications; then, on top of this, various multiuser detection methods are applied to combat intercell interference, hopefully to increase the capacity in this interference-limited scenario. We concentrate here on the down-link, as this is usually the bottleneck for wireless data transmission. Furthermore, we assume first that there is no cooperation between base stations during the normal operation status and that the base stations have no knowledge of the down-link propagation channel. These assumptions are well fulfilled in typical wireless local area network (LAN) situations. In the next step, however, we will address whether it is worth devoting more system resources to these tasks for performance improvement.

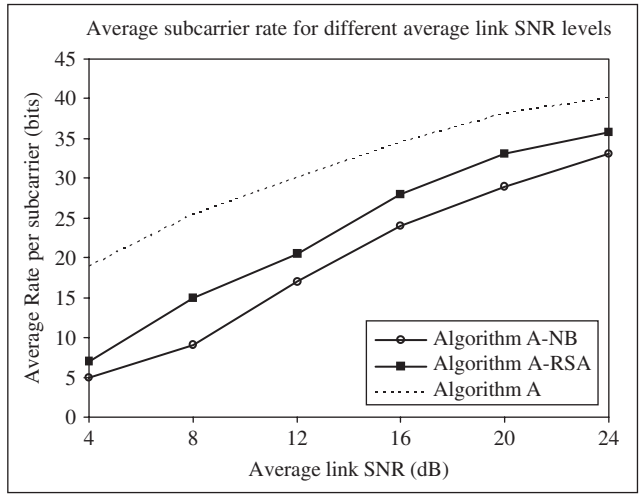

Figure 12.20 Subcarrier rate for different channel conditions (SNR values). (Reproduced by permission of IEEE © 2002 from Koutsopoulos and Tassiulas [70].)

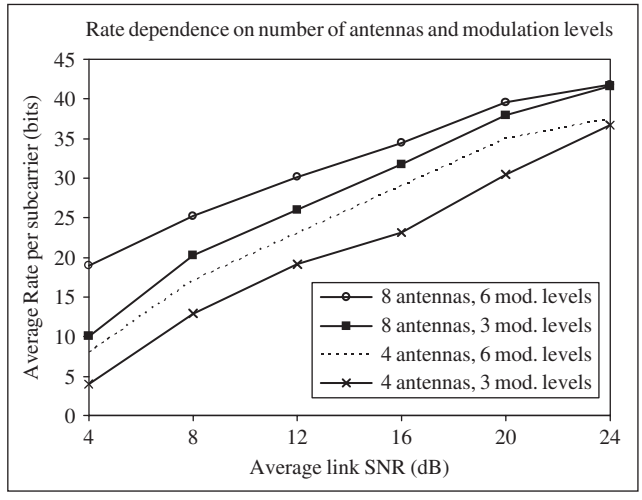

Figure 12.21 Subcarrier rate versus different numbers of antennas and modulation levels. (Reproduced by permission of IEEE © 2002 from Koutsopoulos and Tassiulas [70].)

12.5.1 Channel and cellular system model

For a MIMO system we use a well-known mathematical model, which is given by [1, 84, 85] $\mathbf{y} = \mathbf{H}\mathbf{x} + \mathbf{n}$, where $\mathbf{y}$ is the received vector, $\mathbf{x}$ is the transmitted signal, $\mathbf{H}$ is a channel matrix, which captures the channel characteristics between transmit and receive antenna arrays, and $\mathbf{n}$ is the background noise. Without loss of generality, we assume an $N \times N$ MIMO system with the transmitted signal vector constrained to have overall power $E\{\mathrm{x}^H\mathrm{x}\} \leq P$ and circularly symmetric Gaussian background noise with covariance matrix $\Phi_N = \sigma^2\mathbf{I}$. The entries of the complex

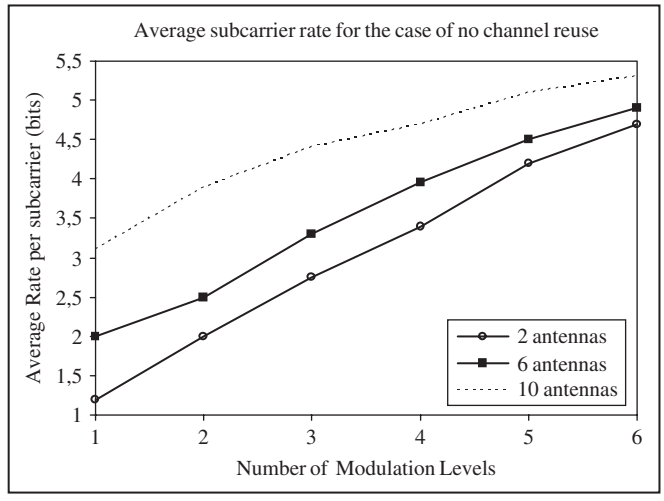

Figure 12.22 Subcarrier rate versus different modulation levels for no subcarrier reuse. (Reproduced by permission of IEEE © 2002 from Koutsopoulos and Tassiulas [70].)

matrix $\mathbf{H}$ are independent with uniformly distributed phase and normalized Rayleigh distributed magnitude, modeling a Rayleigh fading channel with sufficient physical separation between transmit and receive antennas. The signal-to-noise ratio (SNR) is given by $\rho = P/\sigma^2$. If the channel matrix $\mathbf{H}$ is unknown at the transmitter, then the capacity for the interference-free (single-cell) case is given by [1] $C = \log_2 \det [\mathbf{I} + P\mathbf{H}^H \Phi_N^{-1} \mathbf{H}/N]$, where the channel state information (CSI) is assumed to be known at the receiver. When $\Phi_N = \sigma^2 \mathbf{I}$, this can be lower-bounded as $C_L = \sum_i \log_2(1 + \rho\chi_{2i}^2/N)$, where χ_{2i}^2 is a chi-square distributed random variable with $2i$ degrees of freedom and mean value I; i.e. χ_{2i}^2 is the sum of the squares of $2i$ real Gaussian variables, each with zero mean and variance 1/2.

We consider a TDMA/FDMA multicell system where each base station (BS) and mobile station (MS) has the same number of antennas. The extension to CDMA and OFDMA will be discussed later. We take into account interference from the first tier of the center-excited cell configuration with a reuse factor of one, which is depicted in Figure 12.23. Note that no sectorization of the cell is intended. We assume a frequency-flat quasistatic fading environment, and the complex baseband channel gain between the jth transmit and the ith receive antenna is modeled by

$$h_{ij} = \sqrt{c\frac{1}{d_{ij}^{\gamma}}}\sqrt{s_{ij}}\left[\sqrt{\frac{K}{K+1}}e^{j\Phi_{ij}} + \sqrt{\frac{1}{K+1}}z_{ij}\right] \tag{12.23}$$

where d_{ij} is the length of the link, γ is the path loss exponent, c is a propagation constant (e.g. the free distance path loss at the break point) and $s_{ij} = 10^{S_{ij}/10}$ is a lognormal shadow fading variable, where S_{ij} is a zero mean Gaussian random variable with standard deviation v.

K is the so-called Ricean K factor, which denotes the ratio of the direct received power (LOS component) to average scattered power (NLOS component), $\Phi_{ij} = 2\pi d_{ij}/\lambda$ is the phase shift of the LOS path (λ is the wavelength) and z_{ij} is modeled as a set of normalized complex Gaussian random variables, assumed to be independent for each transmit–receive link.

With these assumptions, the multicell system model is given by [86]

$$\mathbf{y} = \mathbf{H} \cdot \mathbf{x} + \sum_i \mathbf{H}_{\text{if}i} \cdot \mathbf{x}_{\text{if}i} + \mathbf{n}$$

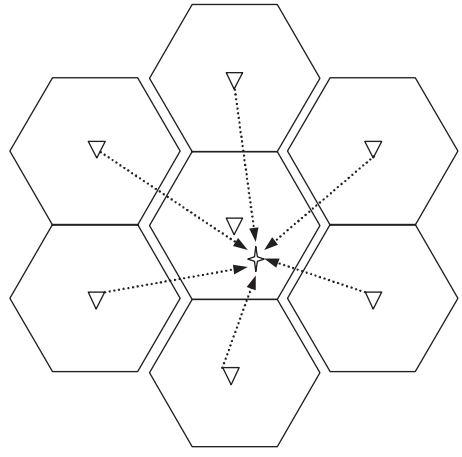

Figure 12.23 Cellular system with one tier of interferers in the down-link case.

where the subscript 'if' denotes interference. This model is further simplified to

$$\mathbf{y} = \mathbf{H} \cdot \mathbf{x} + \sum_{i=1}^{2} \mathbf{H}_{\text{if}i} \cdot \mathbf{x}_{\text{if}i} + \sum_{i=3}^{4} \mathbf{H}_{\text{if}i} \cdot \mathbf{x}_{\text{if}i} + \mathbf{n}$$

with $P_{if1} = \alpha P_{if2}$, $P_{if3} = \beta P_{if4}$ and $(P_{if1} + P_{if2})/(P_{if3} + P_{if4}) = \gamma \gg 1$, where $P_{\text{if}i} = E\{\mathrm{x}_{\text{if}i}^H \mathrm{x}_{\text{if}i}\}$. Different choices of the parameters α, β and γ define the structure of the interfering signals, as will be addressed later. We use the same assumptions for the channel matrices and noise as in the single-cell case, while assuming that the channel matrices for different cells are independent. The signal-to-noise ratio is given by $\rho = P/\sigma^2$ and the signal-to-interference ratio (SIR) is given by $\eta = P/\sum_i P_{\text{if}i}$.

12.5.2 Turbo space–time multiuser detection for intracell communications

Turbo multiuser detection can be applied to the coded BLAST system, resulting in two *turbo space–time multiuser detection* structures, shown in Figures 12.24 and 12.25, respectively.

The turbo decoding procedure of coded V-BLAST is analogous to that of the Turbo-BLAST to be discussed and, therefore, is omitted here. The Turbo-BLAST detection algorithm involves two components: demodulation and decoding. An MAP algorithm is employed in the decoding stage to take in soft metrics from the demodulation stage and produce soft estimates of information and coded data bits. The demodulation stage with ML detection is straightforward. Suppose an $N \times N$ MIMO system is employed by one cell and each substream adopts M-ary quadrature amplitude modulation (M-QAM). Then, for each symbol interval $B = N \log_2 M$ bits are jointly detected. The extrinsic information [1] for the ith bit $1 \leq i \leq B$ is given by

$$L_e(i) = \log \left\{ \sum_{\mathbf{x} \in X_i^+} p(\mathbf{y}|\mathbf{x}) p(\mathbf{x}) / \sum_{\mathbf{x} \in X_i^-} p(\mathbf{y}|\mathbf{x}) p(\mathbf{x}) \right\} - L_a(i)$$

where

$$X_i^+ = \left\{ (x_1, x_2, \ldots, x_N)^{\mathrm{T}} : b_i = 1 \right\}, \; X_i^- = \left\{ (x_1, x_2, \ldots, x_N)^{\mathrm{T}} : b_i = -1 \right\}$$

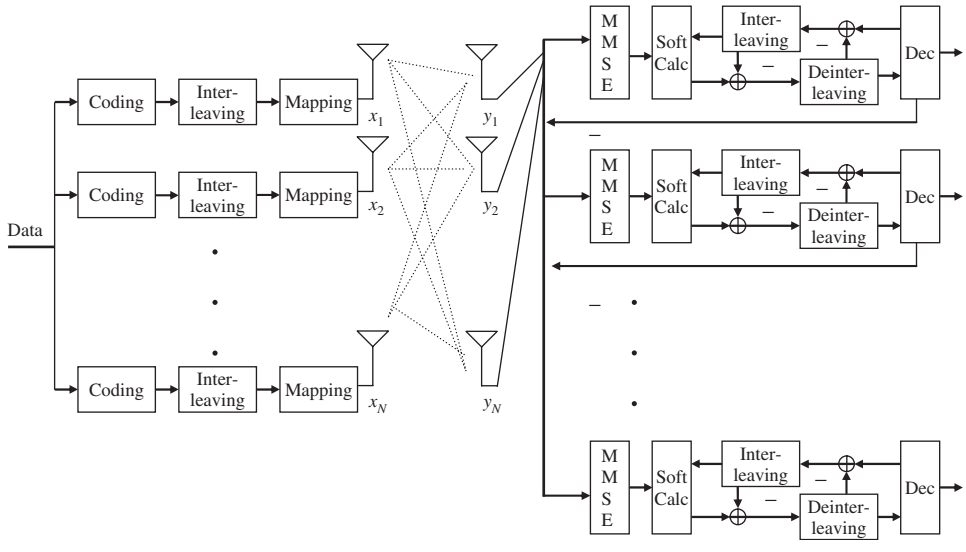

Figure 12.24 Structure of the coded V-BLAST.

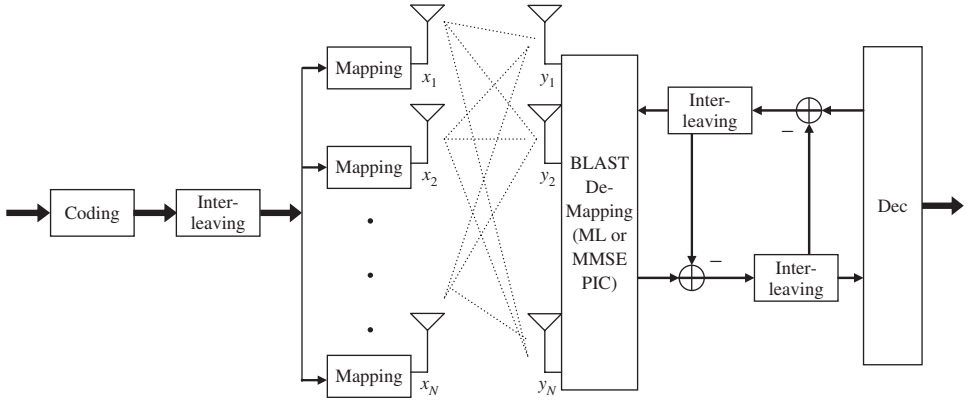

Figure 12.25 Structure of Turbo-BLAST.

$p(\mathbf{y}|\mathbf{x})$ is a multivariate Gaussian distribution, $p(\mathbf{x}) = \prod_{i=1}^{B} p(b_i)$ and $L_a(i) = \log[P(b_i = 1)/P(b_i = -1)]$ comprises a priori information from the decoding stage.

The demodulation stage with PIC is more subtle. First, the interference signals are estimated from the soft metric from the decoding stage and subtracted from the received signal, with which we have for some substream $1 \leq k \leq N$, $\tilde{\mathbf{y}}_k = \mathrm{H}(\mathbf{x} - \tilde{\mathbf{x}}_{\mathbf{k}}) + \mathbf{n}$, where $\tilde{\mathbf{x}}_k = (\tilde{x}_1, \tilde{x}_2, \ldots, \tilde{x}_{k-1}, \tilde{x}_k = 0, \tilde{x}_{k+1}, \ldots \tilde{x}_N)^{\mathrm{T}}$ is the estimated interference vector. Then, an MMSE filter is applied to $\tilde{\mathbf{y}}_k$ to suppress the residual interference plus noise further, given by [1]

$$\mathbf{w}_k = E\{\tilde{\mathbf{y}}_{\mathrm{k}}\tilde{\mathbf{y}}_{\mathrm{k}}^H\}^{-1}E\{\tilde{\mathbf{y}}_{\mathrm{k}}\mathbf{x}_{\mathrm{k}}^*\} = \left(\mathbf{h}_{\mathrm{k}}\mathbf{h}_k^H + \mathbf{H}_{\mathrm{k}}\mathbf{Q}\mathbf{H}_k^H + \frac{N}{\rho}\mathbf{I}\right)^{-1}\mathbf{h}_k$$

where $\mathbf{h}_k$ is the kth column of matrix $\mathbf{H}$, $\mathbf{H}_k$ is the complement of $\mathbf{h}_k$ in $\mathbf{H}$ and

$$\mathbf{Q} = \text{diag}\left[1 - \frac{N}{P}|\tilde{x}_1|^2, \ldots, 1 - \frac{N}{P}|\tilde{x}_{k-1}|^2, 1 - \frac{N}{P}|\tilde{x}_{k+1}|^2, \ldots, 1 - \frac{N}{P}|\tilde{x}_N|^2\right]$$

which approaches zero when estimates from the decoding stage are accurate enough for constant-modulus signals. As shown in Reference [87], the output of the MMSE filter $z_k = \mathbf{w}_k^H \tilde{\mathbf{y}}_k$ can be written as $z_k = \mu_k x_k + \eta_k$, where $\mu_k = N/PE[z_k x_k^*] = \mathbf{w}_k^H \mathbf{h}_k$ and η_k is well-approximated by a Gaussian variable with zero mean and variance

$$v_k^2 = E\left[|z_k - \mu_k x_k|^2\right] = E\left[|z_k|^2\right] - \frac{P}{N}|\mu_k|^2 = \frac{P}{N}\left(\mu_k - |\mu_k|^2\right)$$

The extrinsic information is given in the same form as before, but with $\mathbf{y}$ replaced by z_k and $\mathbf{x}$ with x_k, and therefore with much lower complexity.

12.5.3 Multiuser detection in the presence of intercell interference

Maximum likelihood multiuser detection is infeasible for most current applications due to its complexity. For linear MMSE MUD, we assume knowledge of channel information for the interfering users, which (although difficult to implement) can be obtained either through an initial joint training phase with the coordination of base stations or through adaptive tracking algorithms from the received signals directly. MMSE MUD, which is generally the most favorable linear MUD, has a detection matrix given by [1]

$$\mathbf{W} = \left(\mathbf{H}\mathbf{H}^H + \sum_i \frac{P_{\text{if}i}}{P}\mathbf{H}_{\text{if}i}\mathbf{H}_{\text{if}i}^H + \frac{N}{\rho}\mathbf{I}\right)^{-1}\mathbf{H} \tag{12.24}$$

Thus, the detection process would be first to apply the weight matrix of Equation (12.24) to the received signal to combat cochannel interference and then to process the modified signal. As mentioned, linear MMSE MUD cannot effectively suppress the intercell interference as the receive antenna array does not have enough degrees of freedom. However, the distribution of the residual interference plus noise at the output of a linear MMSE multiuser detector is well approximated by a Gaussian distribution [87]. This property will guarantee good performance of the Gaussian-metric-based receivers (e.g. Turbo ST MUD), which would otherwise deteriorate greatly in a multiuser environment.

The multicell capacity of the desired MIMO system with the linear MMSE preprocessing is asymptotically (in the sense of large dimensional systems) given by

$$C_{M-\text{mmse}} = \log\,\det\left[\mathbf{I} + P\mathbf{H}\mathbf{H}^H\sum^{-1}/N\right] \text{ and } \sum = \sum_i P_{\text{if}i}\mathbf{H}_{\text{if}i}\mathbf{H}_{\text{if}i}^H/P + \sigma^2\mathbf{I}$$

To prove this we represent the system model after linear MMSE filtering with (12.23), as $\mathbf{y}' = \mathbf{W}^H\mathbf{H}\cdot\mathbf{x} + \boldsymbol{\eta}$, where $\boldsymbol{\eta}$ is approximately Gaussian distributed with a covariance matrix of $\mathbf{W}^\mathbf{H}\sum\mathbf{W}$[86]. This is verified in Reference [88] as $N \to \infty$. This gives

$$C_{M-\text{mmse}} = \log\,\det\left[\mathbf{I} + \frac{P}{N}\mathbf{H}^H\mathbf{W}(\mathbf{W}^H\sum\mathbf{W})^{-1}\mathbf{W}^H\mathbf{H}\right]$$

With Equation (12.24), it is easy to verify that (note that $\mathbf{W}^H\mathbf{H} = \mathbf{H}^H\mathbf{W}$)

$$\mathbf{W}^H\sum\mathbf{W} = \frac{P}{N}(\mathbf{I} - \mathbf{W}^H)\mathbf{H}^H\mathbf{W}$$

By defining $\mathbf{Q} = (P/N)\mathbf{H}^H \sum^{-1} \mathbf{H}$, it can be shown that the probability that $\mathbf{Q}$ is nonsingular goes to one as $N \to \infty$ [37]. Then

$$\mathbf{W}^H\mathbf{H} = \mathbf{H}^H \left(\mathbf{H}\mathbf{H}^H + \frac{N}{P}\sum\right)^{-1} \mathbf{H} = \mathbf{H}^H \left(\frac{P}{N}\sum^{-1} - \left(\frac{P}{N}\sum^{-1}\right)\mathbf{H}\Delta^{-1}\mathbf{H}^H\left(\frac{P}{N}\sum^{-1}\right)\right)\mathbf{H}$$

with

$$\Delta = \mathrm{I} + \mathbf{H}^H\left(\frac{P}{N}\sum^{-1}\right)\mathbf{H} = \mathrm{I} + \mathbf{Q}$$

by the matrix inversion formula. It then follows that

$$\mathbf{W}^H\mathbf{H} = \mathbf{Q} - \mathbf{Q}(\mathbf{I} + \mathbf{Q})^{-1}\mathbf{Q} = (\mathbf{I} + \mathbf{Q})^{-1}\mathbf{Q}$$

and

$$\mathbf{I} - \mathbf{W}^H\mathbf{H} = \mathbf{I} - (\mathbf{I} + \mathbf{Q})^{-1}\mathbf{Q} = (\mathbf{I} + \mathbf{Q})^{-1}$$

both of which are invertible asymptotically. Therefore,

$$\begin{aligned} C_{M-\mathrm{mmse}} &= \log\,\det\left[\mathbf{I} + (\mathbf{I} - \mathbf{W}^H\mathbf{H})^{-1}\mathbf{W}^H\mathbf{H}\right] = \log\,\det\left[(\mathbf{I} - \mathbf{W}^H\mathbf{H})^{-1}\right] \\ &= \log\,\det\left[\mathbf{I} + \mathbf{Q}\right] = \log\,\det\left[\mathbf{I} + \frac{P}{N}\mathbf{H}\mathbf{H}^H\sum^{-1}\right] \end{aligned}$$

Another linear MUD technique of interest to combat the intercell interference is the so-called channel-shortening multiuser detector [89]. For detecting data originating in the desired cell, the idea is to apply some form of array processing to maximize the signal-to-interference-plus-noise ratio (SINR), where the signal power refers to the power contributions of all the substreams in the cell to be detected, while interference refers to the power contributions of data streams in other cells. Note that this criterion is different from linear MMSE MUD (which also maximizes the SINR), in which the signal refers to the very substream to be detected while all other data streams, both in the cell and out of the cell, are treated as interferers. In short, the optimal detection matrix for channel-shortening linear MUD is the collection of the first N principal general eigenvectors of the matrix pencil $\left(\mathbf{H}\mathbf{H}^H, \sum_i P_{\mathrm{ifi}}/P\mathbf{H}_{\mathrm{ifi}}\mathbf{H}_{\mathrm{ifi}}^i + N/\rho\mathrm{I}\right)$. This scheme also serves as a linear preprocessing stage, often followed by much more complex processing, such as ML processing, within the desired cell.

Since ML-MUD is highly complex, while linear MUD is limited in its interference cancellation capability, nonlinear MUD often provides a tradeoff between performance and complexity. In the context of multicell MIMO systems, group detection techniques naturally call for attention, in which information bits for one group (one-cell MIMO) are detected at a time. Following a natural extension from BLAST, we can detect one MIMO system at a time and feed decisions to other group detectors for interference cancellation. Successive interference cancellation, even though far from the optimal detection scheme, is nonetheless asymptotically optimal under the assumption of perfect interference cancellation [1, 90]. Note that, generally, the success of interference cancellation relies on the correct detection of interference. In an adverse environment where we cannot get good estimates of interference, IC schemes will worsen the performance instead of improving it. The potential benefit of group IC-MUD depends greatly on the interference structure.

12.5.4 Performance examples

The results presented are based on a simulation scenario for a down-link cellular system with one tier of interferers as shown in Figure 12.23 and the same set of parameters as in Reference [86]. A center-excited pico-cell structure with radius $d = 200$ m is assumed. The transmit antenna array sends out signals simultaneously from all elements with a total power of 1 W in the 2.45 GHz band, which undergo free-space path loss up to a distance of 10 m and then suffers path loss according

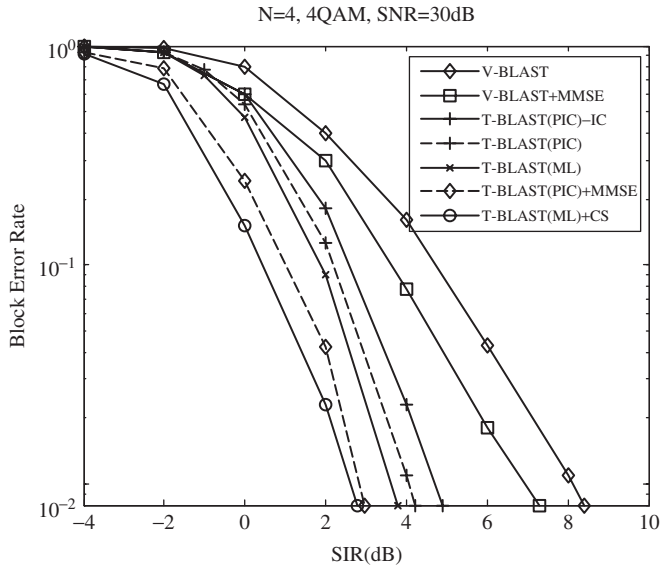

Figure 12.26 Performance comparison of various MIMO receivers when two equal-power interferers dominate.

to a power law with exponent $\eta = 3.7$. The lognormal shadow fading standard deviation $v = 8$ dB and Ricean K-factor $= 0$. The multipath fading is assumed to be a zero-mean complex Gaussian with variance 1/2 per dimension. A mobile is randomly located, according to a uniform distribution over the cell. The simulations confirm that the percentage environment is interference-limited. In most cases the power of the two strongest users dominates. The result also indicates that the one-dominant-interferer scenario (the power of the strongest interferer is at least 3 dB higher than the sum of the rest) accounts for one-third of all the cases. For the remaining two-thirds of cases, which belongs to the two-dominant-interferer scenario, the ratio between the two largest interferer powers varies mostly from 0 to 5 dB. These observations verify in part the effectiveness of the approximate expression for the received signal $\mathbf{y}$ (given after Figure 12.23 in Section 12.5.1), as interference from the two farthest adjacent cells can typically be ignored.

We assume that each cell employs a 4×4 MIMO system, operating at SNR $= 30$ dB. The modulation scheme employed is 4QAM. The coding scheme used is a rate-1/3 64-state convolutional code with generators $(G_1, G_2, G_3) = (115, 117, 123)_8$ (this code has been proposed for EDGE).

The receiver structure is either coded V-BLAST or Turbo-BLAST, combined with various MUD schemes to combat the intercell interference as indicated in the figures. Two scenarios are simulated: (a) $P_{if1} = P_{if2} = 4P_{if3} = 4P_{if4}$ and (b) $P_{if1} = 6P_{if2} = 6P_{if3} = 6P_{if4}$. Scenario (a) corresponds to a two-equal-power-dominant interferer, while situation (b) reflects a one-dominant-interferer case. The results are shown in Figures 12.26 to 12.36. For more details on the topic see References [86] and [91] to [98].

12.6 INTERCELL INTERFERENCE AVOIDANCE IN SDMA SYSTEMS

In this section we consider a fixed, broadband, packet-switched time division multiple access (TDMA) wireless network, which supports multimedia services that may require a high data rate.

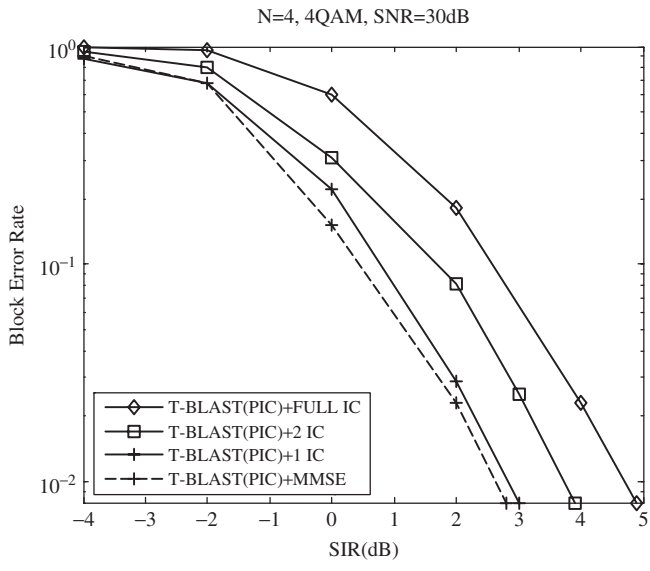

Figure 12.27 Performance comparison of various versions of group IC-MUD when two equal-power interferers dominate.

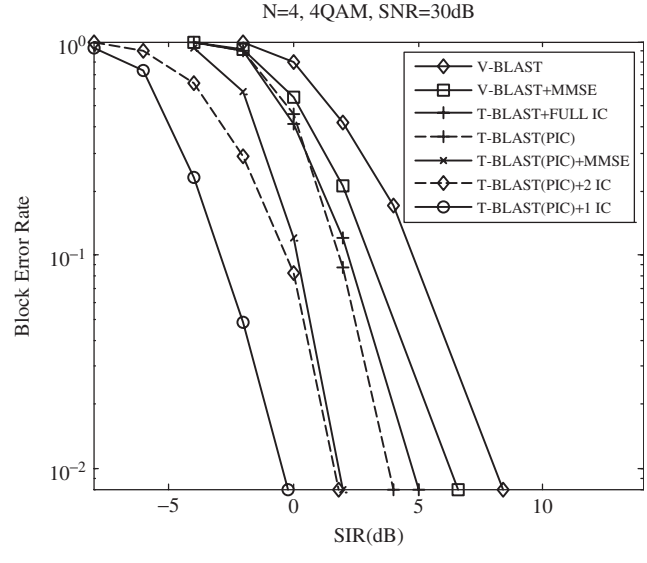

Figure 12.28 Performance comparison of various MIMO receivers when one interferer dominates.

The system consists of multiple cells and each cell has multiple sectors or can form fixed or adaptive beams, using phased arrays or adaptive arrays. User terminals have directional antennas that point to the serving base. To support a high bit rate, each cell has the ability to use the allocated spectrum fully. In this system, time is divided into fixed length time frames, which in turn are divided into a fixed number of subframes. A subframe consists of one or more timeslots, such that

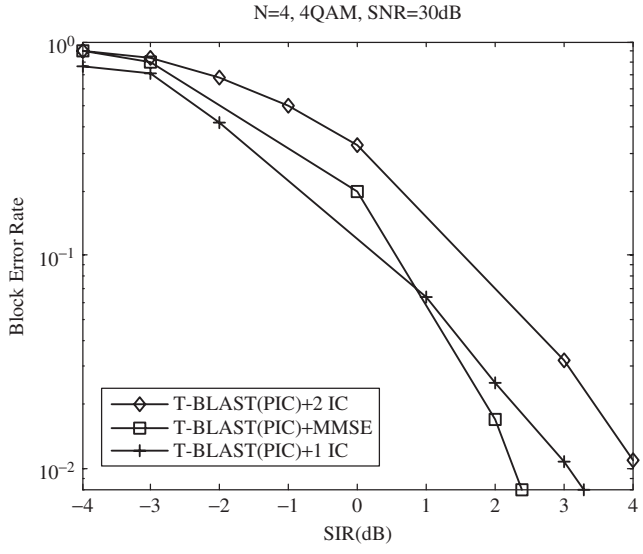

Figure 12.29 Performance comparison of linear MMSE and group IC-MUD when two interferers dominate with a power ratio of 1 dB.

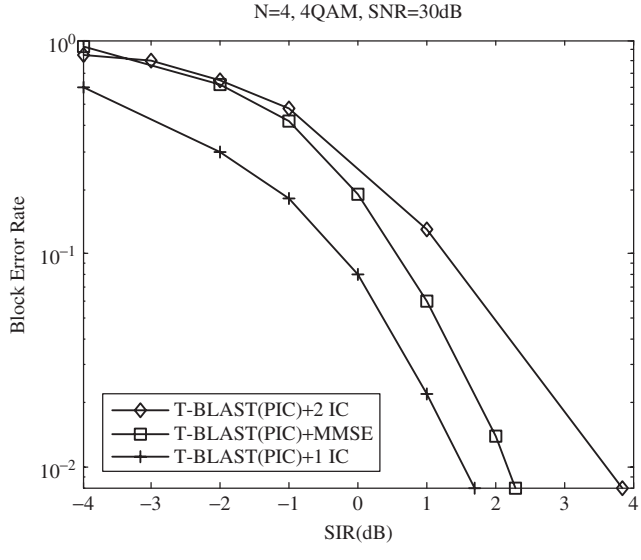

Figure 12.30 Performance comparison of linear MMSE and group IC-MUD when two interferers dominate with a power ratio of 3 dB.

a packet may be transmitted in one timeslot. The problem is how to schedule the transmissions in timeslots so as to maximize the system capacity. The focus in this section is on the problem of down-link scheduling to include intercell interference management.

Several techniques, with different levels of coordination among bases, have been proposed for the intercell interference management in packet-switched, broadband wireless systems. Capture

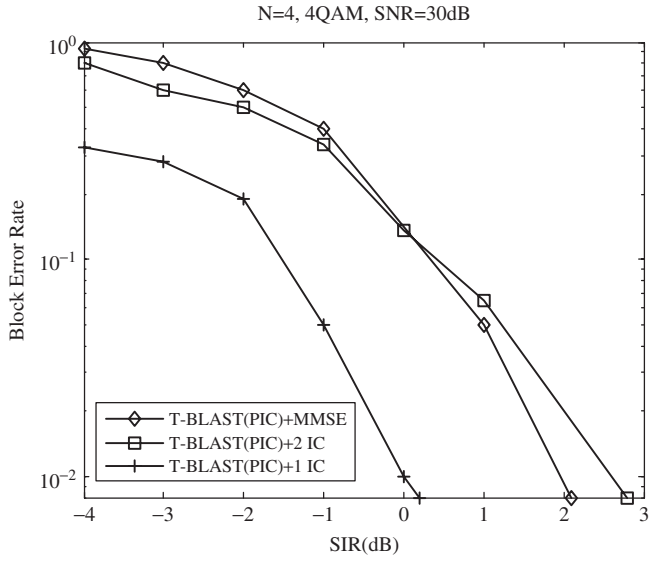

Figure 12.31 Performance comparison of linear MMSE and group IC-MUD when two interferers dominate with a power ratio of 5 dB.

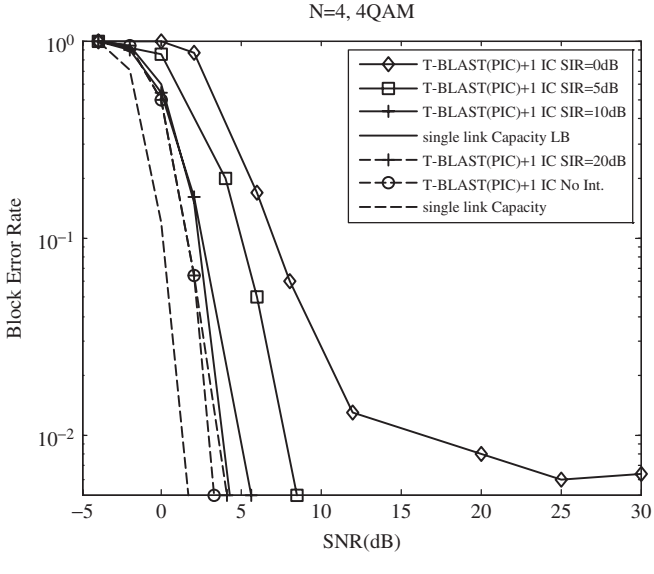

Figure 12.32 Down-link capacity of interference-limited MIMO when one interferer dominates.

division packet access (CDPA), which is targeted for mobile applications, uses the system resource in a completely uncoordinated fashion [99]. A base transmits whenever it has a packet to transmit, and this packet is received successfully as long as the interference from nearby bases is acceptable.

Transmission failures are taken care of by higher layer protocols such as an automatic repeat request (ARQ). A similar scheme, for mobile systems with multibeam adaptive antenna arrays, has

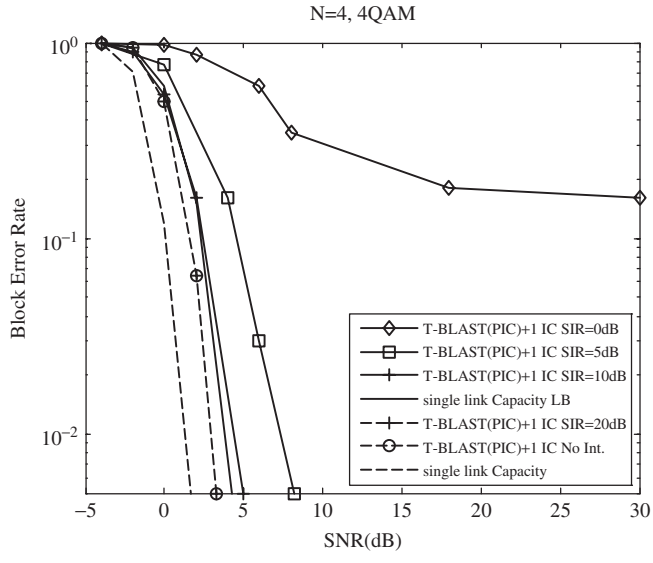

Figure 12.33 Down-link capacity of interference-limited MIMO when two interferers dominate.

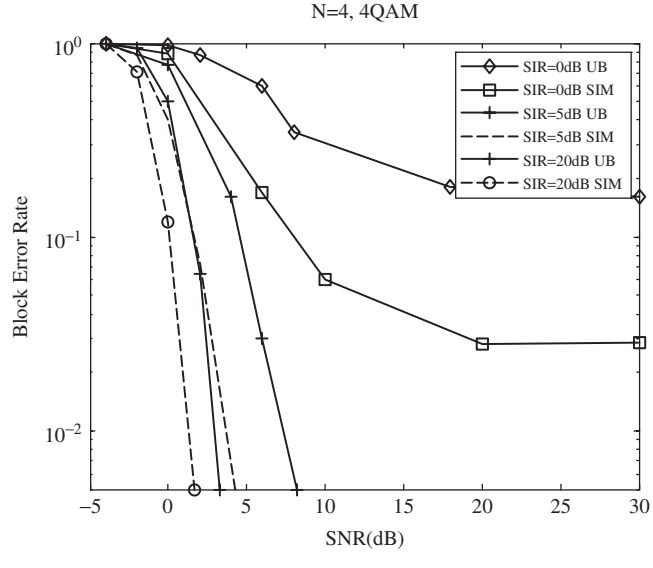

Figure 12.34 Comparison of theoretical and simulated results of the capacity of interference-limited MIMO systems with a linear MMSE front end.

been proposed and analyzed in Reference [100]. Because these schemes are designed for mobile applications, they do not use a crucial asset of the fixed environment – the ability to predict interference levels at a terminal based upon long-term measurements.

Other techniques, targeted for a fixed environment, have been proposed in References [101] to [105]. All of these techniques involve some system planning or engineering to ensure that the

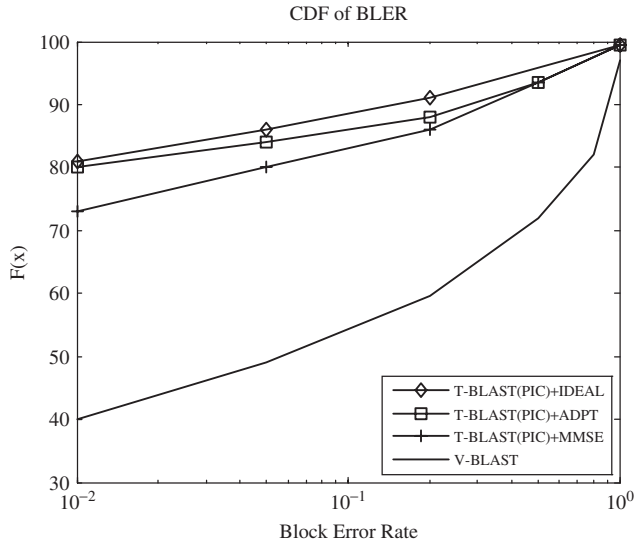

Figure 12.35 CDF of the block error rate for different receivers experienced by a mobile in Rayleigh fading.

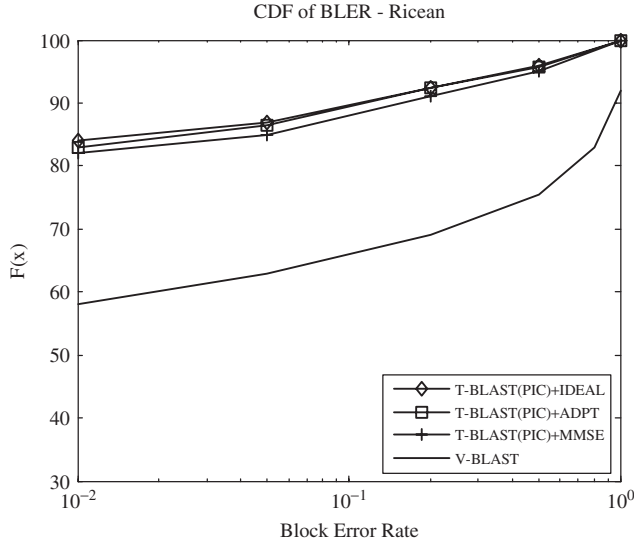

Figure 12.36 CDF of the block error rate for different receivers experienced by a mobile in Ricean fading.

transmissions of different bases are coordinated. The key concept of the staggered resource allocation algorithm (SRA) proposed in Reference [102] is to identify the major sources of interference for each sector and to schedule transmissions accordingly to avoid these sources. A limitation of this approach is that the interference sources are identified assuming ideal base locations and a uniform propagation environment. In practice, the interference may arise from very different sources

and reduce the effectiveness of the preplanning. A key observation in Reference [101] is that, in a fixed wireless system, the performance varies widely across different terminals. Therefore, a timeslot reuse partitioning (TSRP) scheme is proposed for handling the intercell interference. The reuse partitioning provides a terminal with differing levels of performance assurance, which can then be used both to equalize performance among terminals and to offer different levels of performance at a given terminal.

In this section we discuss the intercell interference management technique, which belongs to a broader family of the so-called beam-off window (BOW) technique, although the presentation here is following what is in Reference [106] called quasi-static resource allocation with interference avoidance (QRA-IA). The basic idea of BOW is for every base to periodically turn off each of its beams (sectors) for a certain amount of time (window). This permits each terminal to identify preferred time periods for transmission. For example, a terminal that receives high interference from a particular beam of another base would see significantly better performance in the time period when this beam is turned off.

This requires each base to have a beam-off sequence that specifies the subframe during which the corresponding beam is always turned off. Note that because of the intracell scheduling, a beam may also be turned off in timeslots of other subframes. In contrast to the subframe specified by the beam-off sequence, however, these timeslots may change from frame to frame. Each terminal continuously senses the interference during each frame and identifies timeslots during which it consistently receives lower interference. The information about these preferred timeslots is then used by the base for transmission scheduling and also for generating a suitable beam-off schedule.

12.6.1 The BOW scheme

BOW uses the following procedure:

(1) *Each base periodically turns off each of its beams according to its beam-off sequence.*

(2) *Terminals measure the received interference over time, identify their preferred transmission timeslots and report this information to the serving bases.*

(3) *The bases schedule data transmissions to the terminals accordingly.*

Consider a system consisting of M cells, each with N beams or sectors. It is always possible to find beam-off sequences (BOSs) with no conflicts if we permit sufficiently long BOSs, i.e. if we permit a large number of subframes per frame. For example, if there are $(M \times N)$ subframes per frame, each beam in the system can be assigned a unique subframe to be switched off. In this case, there is no conflict between the preferred transmission period of a terminal and the subframe when the terminal's serving beam is off. For many reasons, however, it is undesirable to have a large number of subframes per frame.

Using a result from graph theory, it can be shown that there exist shorter conflict-free beam-off sequences. Let K denote the number of subframes per frame. Assume that each beam in the system interferes with terminals served by at most C_1 other beams and, conversely, terminals in any beam experience interference from at most C_2 other beams. We model this system as a simple graph and relate the length of the frame to the chromatic number of the graph. A graph G has a chromatic number equal to K if it is K-colorable but not $(K-1)$-colorable.

Each beam in the system is represented by a vertex. Two vertices are connected by an edge if they should not be switched off at the same time. Therefore, the vertices representing beams in the same cell are fully connected. In addition, if beam i interferes with terminals of beam j (i and j necessarily have to belong to different cells), the two corresponding vertices are connected by an edge. This is because the time period at which beam i is switched off is most likely the preferred timeslots of terminals in beam j. If these two beams are switched off at the same time, terminals

in beam j have no opportunity to use their preferred timeslots. Each subframe is represented by one color. A vertex with color s implies that the beam is turned off in the corresponding subframe s. To ensure no scheduling conflict, vertices connected by an edge should have different colors. Therefore, the problem of finding conflict-free beam-off sequences is equivalent to the graph coloring problem. It can be shown [106] that the chromatic number of this graph is between N and $(N + C_1 + C_2)$.

12.6.2 Generating beam-off sequences

A simple beam-switching algorithm is proposed in Reference [106] for generating BOS. This algorithm uses a cost matrix for each base, $\mathrm{C}^{(l)} = \{c_{ij}^{(l)}\}_{N\times K}, l = 1, \ldots, M$, defined as follows. For convenience, we omit the base index (l) in the following discussion; c_{ij} denotes the number of terminals in beam i that prefer subframe j, N denotes the number of beams and K denotes the number of subframes per frame. A terminal is said to prefer subframe j if this is the only subframe that contains preferred timeslots of the terminal. Therefore, terminals with preferred timeslots in more than one subframe do not count toward c_{ij}. If beam i is scheduled to be switched off during subframe j, the cost caused by switching off this beam is c_{ij}. In general, if $\{s(i)\}(i = 1 \text{ to } N)$ is the beam-off sequence of a base, where $s(i) \in [1, K]$ denotes the subframe when the beam is scheduled to be switched off, the cost of the current beam-off sequence at this base is given by $\sum_i c_{is(i)}$. The system cost is the cumulative sum of the cost at each base.

The following algorithm is used for obtaining suitable beam-off sequences:

(1) *Assign an initial beam-off sequence to each base. This sequence can be a random sequence or a sequence designed according to some engineering rules. The following steps are then repeated independently at each base.*

(2) *Each terminal continuously measures the interference in each time slot and reports these measurements to its serving base.*

(3) *Based upon this gathered information, each base evaluates the cost associated with its current beam-off sequence. Note that this cost calculation can be done at predefined or random times.*

(4) *If the cost is above a threshold, the base rearranges its beam-off sequence as follows. In order not to perturb the system drastically, this rearrangement is an alteration of the current schedule and not a complete rescheduling.*
   (a) *Identify the beam that generates most of the cost.*
   (b) *Reschedule the beam to be off in a subframe that leads to the most cost reduction.*

Figure 12.37 illustrates one step of this algorithm. The figure shows the cost matrices and beam-off sequences at a given base before and after one rearrangement. The costs of the beam-off sequences are circled in the corresponding cost matrices. In this example, the cost of the original beam-off sequence is five. Switching off beam 3 during subframe 1 generates most of this cost. To minimize the cost, it is better to switch this beam-off in subframe 4 rather than 1. The beam-off sequence is rearranged accordingly and the final cost of the new sequence is one. We show later via a simulation that this simple procedure helps the system converge to an acceptable state.

12.6.3 Constrained QRA-IA

To obtain the full benefit of BOW, it is necessary to assign every terminal to its preferred timeslot. This may not always be possible if many terminals prefer the same timeslot. Terminals that cannot

1. Original cost matrix

beam \ subframe	1	2	3	4
1	2	(0)	1	1
2	1	1	(0)	1
3	(3)	1	2	0
4	1	2	2	(2)

Original beam-off sequence

Beam No.	1	2	3	4
Sub-frame	2	3	1	4

Total cost = 5

2. Identify beam 3 as the major cost contributor

3. Cost matrix after adjust

beam \ subframe	1	2	3	4
1	2	(0)	1	1
2	1	1	(0)	1
3	3	1	2	(0)
4	(1)	2	2	2

New beam-off sequence

Beam No.	1	2	3	4
Sub-frame	2	3	1	4

Total cost = 1

Figure 12.37 Illustration of the proposed procedure for finding appropriate beam-off sequences. (Reproduced by permission of IEEE © 1999 from Chawla and Qiu [106].)

be assigned to their preferred timeslots in the current frame have to either be assigned to some other timeslots in the current frame or wait until the next frame. The first case degrades the PER performance of the terminal and the second one introduces delay. Both of them cause performance degradation. This resulting loss in performance depends on the specific scheduling scheme used at the base.

In this section, we estimate this performance loss by assuming a first-in-first-out (FIFO) scheduler at each base, which schedules packet transmissions on a frame-by-frame basis. Let $F = (K \times L \times S)$ denote the maximum number of packets that may be transmitted in each frame, where K is the number of subframes per frame, L is the number of timeslots per subframe and S is the timeslot capacity, i.e. the number of packets that may be transmitted simultaneously in a timeslot. The scheduler takes the first F packets waiting for transmission from its packet queue and schedules them in the next frame. Some of these packets may not be assigned to preferred timeslots of the corresponding terminals. Therefore, the resulting PER performance may be worse than that of an ideal assignment, where every packet is assigned to a preferred timeslot of the corresponding terminal.

Assume that the base has the knowledge of the measured or estimated performance of each terminal during each timeslot. Also, assume that a base can transmit at most one packet to each terminal in a frame. As a result, among the F packets to be transmitted in a frame, there is a one-to-one correspondence between a packet and a terminal. Let $\mathbf{P} = \{p_{ij}\}_{F \times KL}$ denote the PER matrix corresponding to the F chosen terminals that need to be scheduled in the next frame, where p_{ij} is the PER of terminal i in timeslot j. The problem then is to assign terminals to timeslots such that the overall PER is minimized. Let $\mathbf{X} = \{x_{ij} = 0 \text{ or } 1\}_{F \times KL}$ denote a binary solution matrix, where $x_{ij} = 1$ implies that terminal i is assigned to timeslot j. Let $y(i)$ denote the beam serving terminal i. An acceptable assignment satisfies the following constraints: (1) each terminal is assigned to a timeslot, (2) no more than S terminals can be assigned to a time slot and (3) a beam

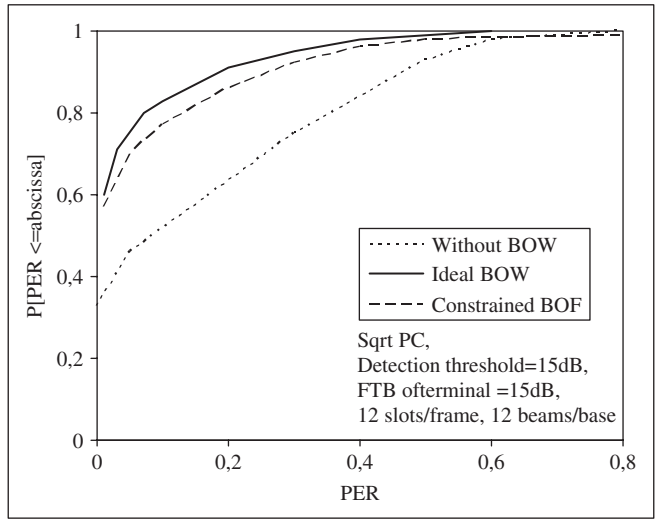

Figure 12.38 CDF of the PER with and without BOW: $\gamma = 4$ (the path loss exponent), $\sigma = 6\,\text{dB}$ (the shadow fading).

can serve at most one terminal in a timeslot. The problem is formulated as follows:

$$\begin{aligned} &\text{Minimize} && \sum_{i,j} p_{ij} x_{ij} \\ &\text{subject to} && x_{ij} \geq 0, \ \forall i, j \\ & && \sum_{j} x_{ij} = 1, \ \forall i \\ & && \sum_{i} x_{ij} \leq S, \ \forall j \\ & && y(i) \neq y(k) \quad \text{if } x_{ij} = x_{kj} = 1, \ \forall j \end{aligned} \tag{12.25}$$

This is a constrained optimization problem [107] (see also Chapter 10) and well-elaborated techniques can be used to solve it. The performance of the resulting timeslot assignment may be compared to that of the corresponding ideal assignment. This comparison provides an estimate of the performance loss. The results show that this loss is reasonably small.

Figure 12.38 shows cumulative distribution function (CDF) of PER. The figure also shows the PER of the constrained BOW with $S = 5$. The dashed–dotted line, the dashed line and the solid line represent the PER with ideal BOW, with constrained BOW and without BOW, respectively. We see that the fraction of terminals with PER better than 0.1 is 83 % with ideal BOW, 77 % with constrained BOW and 51 % without BOW.

12.7 MULTILAYER RRM

In a fixed wireless network, cell sectorization and directional antennas at fixed terminal locations are key components in reducing interference from neighboring sectors and cells.

In 4G wireless systems the sophisticated resource management schemes may want to split the terminals in the wireless network into different classes based on the mobility and still apply on the low-mobility terminals rules of engagement designed for fixed networks. This will be referred to as multilayer RRM or RRM overlay. Fong *et al*. [108] proposes the *staggered resource allocation*

(SRA) method as a distributed dynamic resource allocation (DRA) algorithm for the fixed network, where the same radio spectrum is used (shared) by each sector in every cell on a dynamic time-division basis. With the use of directional antennas to suppress interference, the SRA method is particularly effective in avoiding both intercell and intracell interference.

Qiu and Chawla [109] observe that, depending on terrain and fading, certain terminals (e.g. houses), due to their fixed locations, may be consistently unable to receive signals with satisfactory SIR while transmission for other terminals may always be successful. Thus, terminals at 'good' and 'poor' locations should be served according to different timeslot reuse patterns, which is called *timeslot reuse partitioning* (TSRP) in Reference [109]. The main idea is that many BSs can transmit simultaneously if the intended receiving terminals are located at good positions. On the contrary, when the receiving locations are poor, few BSs are scheduled to transmit at the same time so that a target SIR threshold can be met for successful reception at the receiving ends.

The specific implementation of TSRP in Reference [109] divides the time frame (i.e. bandwidth) into a dedicated portion and a shared portion. At most, one packet is transmitted among four neighboring cells during each timeslot in the dedicated portion and up to three packets can be transmitted simultaneously in every cell in the shared portion. The purpose is to allow terminals at 'good' and 'poor' locations to use timeslots in the dedicated and shared portion, respectively. Because of the bandwidth partitioning into the dedicated and shared portion, many terminal locations with moderate reception quality either may be overprotected when transmitting in the dedicated portion or may not receive the packets successfully when sent during the shared portion. It results in a potential waste of bandwidth.

The SRA method in Reference [108] can be enhanced by considering the reception quality of terminals [110]. The method, to be referred to as the *enhanced staggered resource allocation* (ESRA) method, has the capability of avoiding major interference as the SRA method does, and makes use of the knowledge of the reception quality at terminals to improve throughput and maintain the success probability of one (or as close to one as practically possible) for down-link transmission.

12.7.1 The SRA protocol

For illustration purposes, consider the hexagonal cell layout in Figure 12.39. Each cell is divided into six sectors, each of which is served by a BS antenna with a 60° beamwidth, and terminal antennas can have a beamwidth smaller than 60°. In the SRA method, timeslots are grouped into six subframes and sectors are labeled by 1 to 6 anticlockwise, as shown in Figure 12.39. The sector labeling patterns for adjacent cells differ by a 120° rotation, thus creating a cluster of three cells whose patterns can be repeated across the entire system. Note that the time frame shown in the figure is applicable to both the down-link and up-link, which are provided by the TDD or FDD technique.

Each sector assigns timeslots for transmitting packets to or from its terminals according to a special order shown in Figure 12.40 (in case a terminal needs to send packets to its BS, it is assumed that the BS is made aware of the need, perhaps via a separate dedicated channel or a contention channel). The traffic to be transmitted in a sector is divided into blocks a, b, c, d, e and f of different sizes to be discussed later. For example, a sector with label 1 first schedules packets for transmission in timeslots of subframe 1 (block a) in the figure. If it has more traffic to send, it then uses subframe 4 (b), subframe 5 (c), etc., until subframe 6 (f). The reason for such an order is that if interference due to concurrent packet transmission in the same cell can be tolerated, then after using all slots in the first subframe a, a sector should use the first subframe of the opposite sector in the same cell, in order to make the best use of the BS directional antennas. Following that, timeslots in the first subframes for the sectors next to the opposite sector are used. To avoid interference due to overlapping antenna patterns of neighboring sectors, their first subframes are used as the

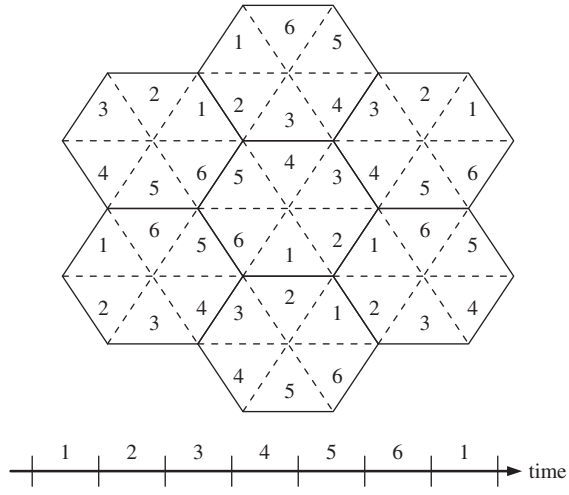

Figure 12.39 Cell layout and frame structure. (Reproduced by permission of IEEE © 1998 from Fong *et al*. [108].)

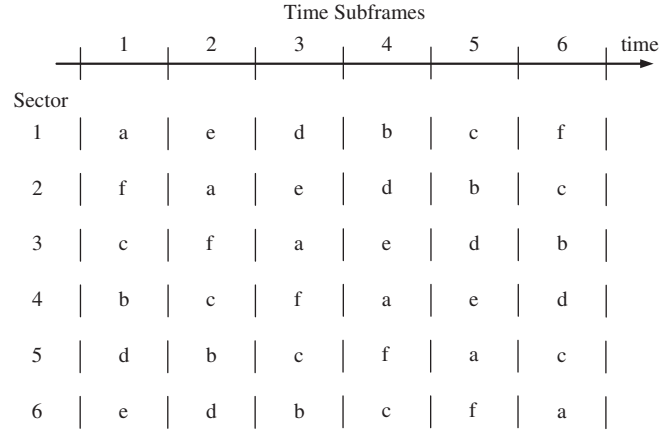

Figure 12.40 Order of slot assignment for the SRA method. (Reproduced by permission of IEEE © 1998 from Fong *et al*. [108].)

last resort. For simplicity (while causing very minor throughput degradation), Figure 12.40 does not show the assignment from the left- and right-hand sides of the subframes, as suggested in Reference [108]. As depicted in the figure, the assignment order for the next sector is 'staggered' by a right rotation by one subframe based on the order for the previous sector. In the sequel, the assignment order, regardless of the associated sector, is generally referred to as the *staggered order*.

If all sectors have traffic loads of less than one-sixth of the total channel capacity, all packets are transmitted in different time subframes (only block a), thus causing no interference within the same cell. Of course, as the traffic load increases, packets are transmitted simultaneously, thus increasing the level of interference. Nevertheless, the staggered order exploits the characteristics of

directional antennas to allow multiple concurrent packet transmissions while reducing the intracell interference.

Besides managing intracell interference, the SRA method also helps avoid interference from major sources in the neighboring cells. This is particularly so when traffic load is low to moderate. To see this, let us consider the down-link for sector 1 in the middle cell of Figure 12.39. Sector 2 in the bottom cell and sector 3 in the upper cell are the major sources of interference. By examining the staggered order for sectors 1, 2 and 3, we find that they will not transmit simultaneously, so they will not interfere with each other provided that all of them have a traffic load of less than one-third of the total channel capacity (i.e. using only subframes a and b for transmission). The same comment also applies to the up-link, where sectors 2 and 5 of the bottom cell in the figure now become the major sources of interference. Due to the symmetry of the staggered order and cell layout, this same comment applies to each sector in every cell.

12.7.2 The ESRA protocol

The basic idea of the terminal classification in the ESRA method is to categorize terminals based on their ability to tolerate various degrees of concurrent packet transmissions according to the staggered order. Certainly such tolerance depends on the reception quality of the terminal locations, which in turn depends on the distance between the BSs and terminals, transmission power, antenna characteristics, terrain and fading. For the layout with six sectors per cell in Figure 12.39, there are six levels of concurrent transmission, and terminals are categorized into six classes, indexed by 1 to 6.

As shown in Figure 12.40, each time frame has six subframes, indexed by 1 to 6. If J_m^i is the index of the mth subframe for use by sector i in the staggered order, then $J_1^3 = 3$, $J_2^3 = 6$, $J_3^3 = 1$, $J_4^3 = 5$, $J_5^3 = 4$ and $J_6^3 = 2$ for sector 3 as it first uses slots in subframes 3, 6, 1 and so on, as shown in Figure 12.40. Further, for $c = 1, 2, \ldots, 6$, let $I_c(j) \subseteq \{1, 2, \ldots, 6\}$ denote the set of sectors allowed to transmit in subframe j when each sector can use only the first c subframes in the staggered order for transmission (which results in c concurrent packet transmissions in each cell). For instance, $I_2(1) = \{1, 4\}$, $I_3(1) = \{1, 4, 3\}$, $I_4(3) = \{3, 6, 5, 1\}$ and $I_5(3) = \{3, 6, 5, 1, 2\}$.

For terminal classification, the system can activate one or a set of BS antennas to send a special signal such as a pilot tone for measurement purposes. The pilot tone is first activated by the BS antenna of the home sector where a terminal belongs. The received power of the pilot tone represents the signal strength at the terminal. Then, according to the possible concurrent transmissions allowed by the staggered order in different time subframes, a combination of BS antennas (including that of the home sector) in each cell is activated in a systematic way to send the pilot tone simultaneously. The total received power at the terminal is now the signal plus interference power. Thus, we can compute the SIR at the terminal for these different combinations. The terminal is categorized based on the highest degree of concurrent transmissions with its SIR exceeding a given threshold.

Each time frame in the ESRA method consists of six subframes, indexed by 1 to 6 in Figure 12.40. Each subframe is further divided into six *miniframes,* which are also labeled from 1 to 6. Each miniframe with the same label consists of a multiple but fixed number of timeslots in each subframe. The sizes of miniframes are chosen to match the expected traffic demand of the terminal classes, as will be discussed in the sequel.

Each sector uses the subframes according to the staggered order, given by a, b, c, d, e and f in the figure (where a and f indicate the first and last subframe to be used, respectively). However, it is important to note that timeslots of only those miniframes marked with dashed lines are available to the corresponding sector indicated on the left-most side of the figure. Clearly, varying from subframe to subframe, each sector is allowed to schedule packet transmission in one or more miniframes in some subframes, but not in others.

For instance, sector 2 can use all miniframes in subframe 2, but it can schedule transmission only in miniframe 5 and 6 in subframe 3; other miniframes in subframe 3 are *unavailable* to sector 2. It is also noteworthy that there are different degrees of concurrent packet transmission in various miniframes. For $c = 1, 2, \ldots, 6$, as many as c packets are transmitted simultaneously in each cell during miniframe c in each subframe. On one extreme, only one packet is transmitted in each cell during miniframe 1, while on the other extreme, up to six packets are sent during miniframe 6. The main idea here is that various miniframes allow different degrees of concurrent packet transmissions. Thus, the miniframe structure is compatible with the terminal classification so that packets for class-c terminals transmitted in miniframe c will be successfully received, as verified in the classification procedure. In fact, as discussed further later, packet transmission for a class-k terminal in miniframe c with $c < k$ (referred to as *upgraded sharing*) will also be successfully received. The upgraded sharing helps avoid loss of 'trunking efficiency' by partitioning subframes into miniframes.

Based on the compatibility between the miniframe structure and terminal classes, each sector schedules packet transmissions in the ascending order of terminal class indices; i.e. traffic for class 1 and 6 terminals are arranged for transmission first and last, respectively. Timeslots in miniframes with small indexes, starting from those miniframes in the first subframe of the staggered order, are used first, thus enabling upgraded sharing as much as possible in case miniframes are not fully utilized by traffic of their associated terminal classes.

The miniframe structure can be viewed as a means to divide the bandwidth into multiple 'channels' that allow different degrees of concurrent packet transmissions tolerable in terms of SIR by various terminals. Therefore, in order to maximize the system throughput, the sizes of miniframes should be chosen to match the traffic load from the respective terminal classes.

Without loss of generality, consider that terminals of all classes have identical traffic loads. Let α_i be the fraction of class-i terminals (relative to the total number of terminals served by the ESRA method) in the whole network for $i = 1$ to 6. Further, let N_t be the 'target' number of timeslots in each subframe, which is determined by considering packet delay requirements, scheduling overheads and so on. In addition, let miniframe i in each subframe have n_i timeslots. Observe that each sector can use miniframe i in i different subframes (see Figure 12.41). Therefore, to handle

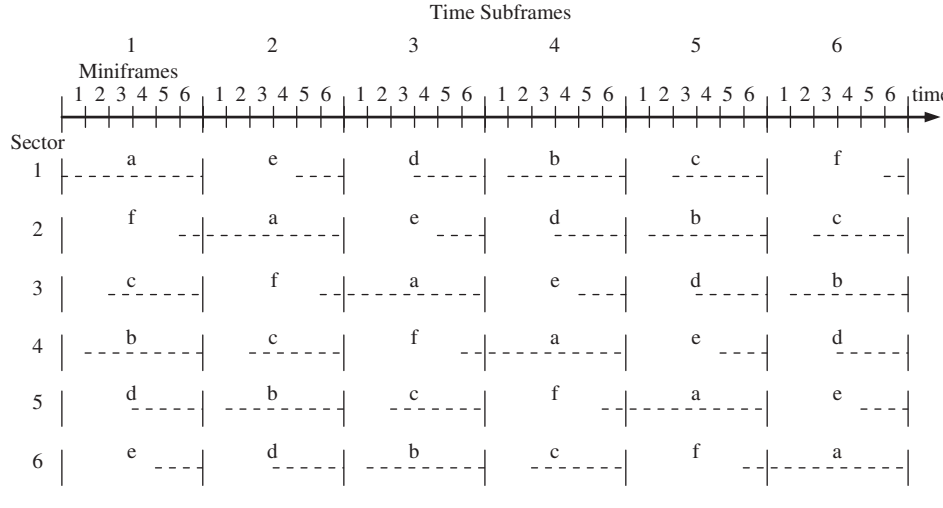

Figure 12.41 Use order of subframes and miniframes in the ESRA method. (Reproduced by permission of IEEE © 2004 from Tralli *et al*. [111].)

the uniform traffic load among terminals $n_i = \beta\alpha_i / i$, where β is a proportionality constant and the rounding of the integer is ignored at the present moment. Since $\sum_i n_i = N_t$, $\beta = (N_t)/(\sum_j \alpha_j / j)$. Substituting this into $n_i = \beta\alpha_i / i$ yields $n_i = [(N_t\alpha_i / i)/(\sum_j \alpha_j / j)]$, where $[x]$ denotes the integer closest to x. With these miniframe sizes, each subframe has $N = \sum_i n_i$ timeslots and the frame size is KN, where K is the number of sectors in each cell (six for the setting under consideration).

To analyze the packet throughput for the ESRA method, we continue to assume that terminals of all classes have identical traffic loads. Further, assume that there are always packets pending for transmission. Based on the size of each miniframe i, the maximum throughput for class-i terminals is in_i/KN packets per timeslot in each sector. This is so because (1) each sector can transmit during miniframe i in i different subframes of each frame and (2) each packet transmission for class-i terminals in miniframe i will be successful by the definition of terminal classification. Thus, the maximum throughput in each sector for all terminal classes is

$$\gamma_m = \sum_i \frac{in_i}{KN} = \sum_i \frac{i}{KN}\left[\frac{N_t\alpha_i / i}{\sum_j \alpha_j / j}\right] \tag{12.26}$$

Ignoring the rounding of the integer and applying the facts that $\sum_i \alpha_i = 1$ and $N_t \approx N$, we obtain the maximum downlink throughput per sector

$$\gamma_m \approx \frac{1}{K\sum_j \alpha_j / j} \tag{12.27}$$

12.8 RESOURCE ALLOCATION WITH POWER PREASSIGNMENT (RAPpA)

Within this section we discuss a technique named power-shaped advanced resource assignment (PSARA) [111], which exploits an appropriate set of power profiles that limit (preassignment) the power transmitted in each slot of the frame with the aim of helping the allocation algorithm to distribute the intercell and intersector interference efficiently within the frame and make it partially predictable.

We consider again the down-link of a full reuse cellular system in which packet traffic is to be transmitted from the base station to fixed users. The base stations, placed on a regular grid depending on the (hexagonal or squared) geometry and sectorized into four or six beams, are assumed to be frame synchronous. There are S sectors per cell: square cells have four sectors and hexagonal cells have six. Each sector is illuminated by an antenna whose 3 dB beamwidth is 90° or 60° as a default case. Each sector is assigned a label (A or B for the square geometry, A, B or C for the hexagonal geometry), which is suitably reused according to a given reuse plan, as in Figure 12.42. The labels and its use will be discussed later in more detail.

The model includes M cells and U user terminals randomly placed in the service area with uniform spatial distribution. Each terminal is equipped with a directional antenna and served by the sector/cell with the smallest channel loss. The propagation model includes path loss and lognormal shadowing. The latter is assumed to be constant in time due to the fixed positions of the users. Once all user antennas are oriented, the relationship between the power $P_t(s, b)$ transmitted by the sector antenna $s(s \in [0, 1, \ldots, S-1])$ of the base station $b(b \in [0, 1, \ldots, M-1])$ and the corresponding power $P_r(u)$ received at the terminal u is given by $P_r(u) = g(s, b, u)P_t(s, b)$ with $g(s, b, u) = kd^{-\beta}\log[1, \sigma]f_t(\varphi_t)f_r(\varphi_r)$, where k is a constant that accounts for the effects of carrier frequency and antenna gains, d is the link length between the base station and the user u, β is the propagation coefficient and $\log[1, \sigma]$ is a lognormal random variable with unit average value and variance σ. The functions $f_t(\varphi_t)$ and $f_r(\varphi_r)$ represent the radiation pattern of transmitter and receiver antennas, where $\varphi_t(\varphi_r)$ is the angle between the direction of maximum gain and the

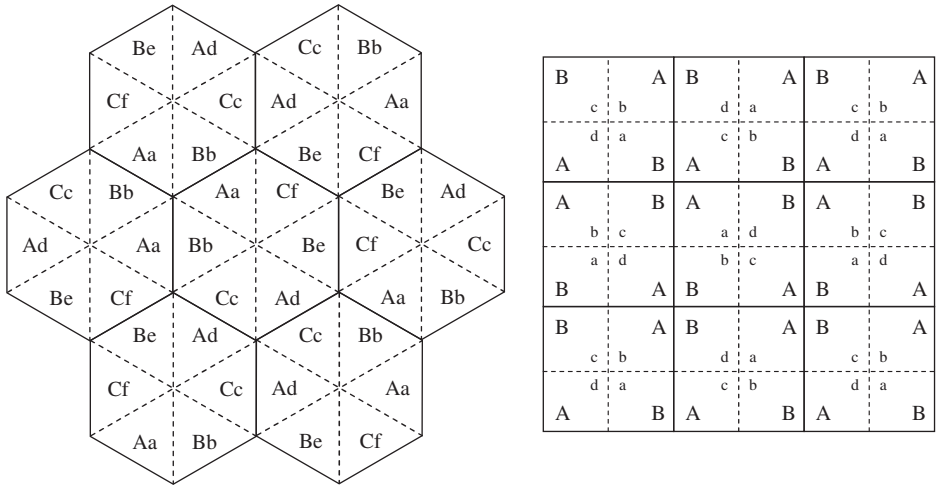

Figure 12.42 Label pattern for square and hexagonal cells (lowercase labels refer to ESRA).

direction of an ideal line joining the transmitter and the receiver. We also assume $\varphi_r = 0$ between a user and its serving sector. Antenna heights are not taken into account.

The delivery of the packets to users is performed on a TDM frame composed of N slots. As a first step in determining the throughput efficiency, we do not consider any arrival process but rather assume that each user always has packets to transmit and that the base station tries to schedule one packet per user per frame. The SIR is computed as $\text{SIR} = g(s_o, b_o, u)P_t(s_o, b_o)/\sum_{(s,b)\neq(s_o,b_o)} g(s, b, u)P_t(s, b)$, where u is the user and s_o is the serving sector belonging to the serving base (b_o). Only packets whose SIR is above a reference threshold SIR_{thr} are collected for throughput statistics, and we assume that the packet is lost when $SIR < SIR_{\text{thr}}$.

12.8.1 Resource assignment protocol

We consider a simplified case where each sector of each cell independently performs allocation of timeslots and power to users. Once packets have been allocated slots they can be transmitted at the maximum allowed power or the transmit power can be lowered by an SIR-based power control procedure. Hence, the power assigned to users becomes

$$P_t(s_0, b_0, u) = \min[P_t^{(\max)}(s_0, b_0),\ SIR_{\text{thr}} I_{\text{worst}}(u)/\text{g}(s_0, b_0, u)] \tag{12.28}$$

where the estimated worst-case interference is

$$I_{\text{worst}}(u) = \sum_{(a,b)\neq(s,b_o)} g(s, b, u)P_t^{(\max)}(s, b) + \sum_{s\neq s_o, s \text{ active}} g(s, b_0, u)P_t^{(\max)}(s, b_0) \tag{12.29}$$

In the ideal case where intersector interference is zero (i.e. when nonoverlapping sector antenna patterns are used) the power assignment is trivial.

For the sake of comparison, and in order to highlight the benefits of the PSRA scheme, we consider here the following resource allocation strategies:

(1) *Random resource assignment with power control (RRA + PC)* takes place where the assignment of packets to slots is done randomly, i.e. no channel information is taken into account during allocation. Channel information is exploited only in order to decide how much power to use based

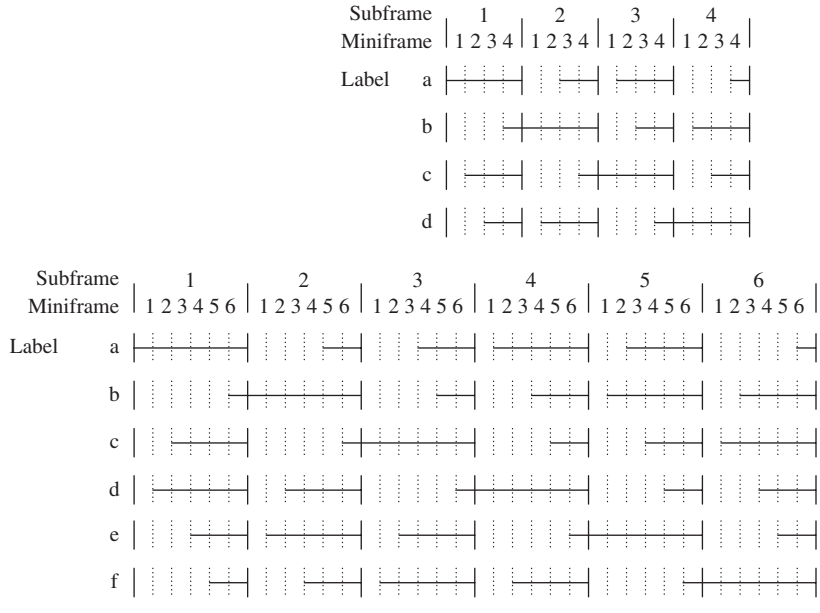

Figure 12.43 ESRA: frame structure for the hexagonal and square scenarios. (Reproduced by permission of IEEE © 2004 from Tralli *et al*. [111].)

on channel attenuation measurements. This scheme is very simple and will be considered here as the baseline case.

(2) *ESRA* exploits staggered resource assignment to manage concurrent transmissions in the slots of the frame, as described in the previous section. For sector labeling as in Figure 12.42, each sector is allowed to transmit only in those slots marked with solid lines (Figure 12.43) according to the pattern corresponding to its label.

(3) *PSRA* aims partially to organize the use of power across the cellular system in order to determine different predictable levels of interference in each slot of the frame. Within this framework, the allocation algorithm can assign slots according to the different levels of protection against interference required by the user. The allocation algorithm also tries to assign the power level needed to ensure the predefined SIR_{thr}. To achieve the outlined tasks, each sector of each base is assigned a power curve, called a power profile, that is a function of the label of the sector. It determines the maximum transmission power that a sector antenna which uses such a profile is allowed to radiate in timeslot i.

With a two-label pattern two different power profiles are considered, $P(i, A)$ and $P(i, B)$, with $P(i, A) = P(N - 1 - i, B)$, $i = 0, 1, \ldots, N - 1$ (symmetric profiles). Two simple choices for the power profiles proposed in Reference [111] are the straight line (linear shaping) $P(i, A) = P_{\min} + i(P_{\max} - P_{\min})/(N - 1)$ and the symmetric step (step shaping)

$$P(i, A) = \begin{cases} P_{\min}, & \text{if } i \leq \frac{N}{2} - 1 \\ P_{\max}, & \text{otherwise.} \end{cases} \tag{12.30}$$

By expressing the power profiles as vectors of power levels, $P_l = [P(0, l), P(1, l), \ldots, P(N - 1, l)]^{\text{T}}$ (l is the label), suitable three-label symmetric power profiles can be simply designed

Table 12.3 Three-label star patterns. (Reproduced by permission of IEEE © 2002 from Tralli *et al*. [112])

Slots	A-Profile	B-Profile	C-Profile
A-edge			
0	p_5	p_0	p_0
1	p_4	p_1	p_1
2	p_3	p_2	p_2
5 8	p_2 p_2	p_3 p_2	p_2 p_3
4 7	p_1 p_1	p_4 p_1	p_1 p_4
3 6	p_0 p_0	p_5 p_0	p_0 p_5
B-edge C-edge			

slot	0	1	2	3	4	5	6	7	8
P_A	p_5	p_4	p_3	p_0	p_1	p_2	p_0	p_1	p_2
P_B	p_0	p_1	p_2	p_5	p_4	p_3	p_0	p_1	p_2
P_C	p_0	p_1	p_2	p_0	p_1	p_2	p_5	p_4	p_3

through a geometric approach, by exploiting two-dimensional patterns that are invariant to rotations of 120°, such as, for example, the simple star (Table 12.3) proposed in Reference [112], where even some other geometries were shown and tested. These patterns have positions numbered from 0 to $N-1$ and can be used by placing on the N pattern positions the N power levels of a power profile. In this way, three symmetric profiles can be obtained by means of a simple rotation of the pattern, i.e. $P_B = \Pi P_A$, $P_C = \Pi P_B$, $P_A = \Pi P_C$, where Π is a suitable permutation matrix. Now, if we define R as a positive integer corresponding to the number of slots in each branch of the star, the allowed values of the frame length is $N = 3R$ constraint on the number of the slots, i.e. if we want $N \neq 3R$, other geometries can be used (e.g. a triangle [112]).

The implementation of the optimal allocation algorithm is a hard task and in Reference [111] an algorithm is proposed that does not try to search exhaustively for the best fitting users in the frame. Instead, it considers a single slot allocation based on the set of powers required in each slot to achieve a predefined SIR.

The user allocation for each sector s_0 of each base station b_0 acts as follows:

(1) For each user u in sector s_0 of base b_0:
   (a) Compute the sum of the maximum values of intercell and intracell interference in each slot i,

$$I_{\max}(i,u) = I_{\max(\text{in})}(i,u) + I_{\max(\text{out})}(i,u)$$

where

$$I_{\max(\text{in})}(i,u) = \sum_{b \neq b_0} \sum_{s=0}^{S-1} g(b,s,u) P(i, l_{(b,s)})$$

$$I_{\max(\text{out})}(i,u) = \sum_{s \neq s_0} g(b_0,s,u) P(i, l_{(b_0,s)})$$

are the intercell and intracell contributions, respectively, and $l_{(b,s)}$ is the label of sector s of base station b.

(b) Compute the power that the sector antenna should radiate to counteract $I_{\max}$, in slot i, with $i = 0, \ldots, N-1$, i.e. $P_c(i,u) = SIR_{\text{thr}} I_{\max}(i,u)/g(b_0, s_0, u)$. Based on $P_c(i,u)$, we have slots (*insecure slots*) where $P_c(i,u)$ exceeds the power profile and other slots (*secure slots*) where $P_c(i,u)$ is lower than the power profile. In a *secure slot* a packet will be received by user u with $SIR \geq SIR_{\text{thr}}$. On the other hand, since the interference evaluation is performed by considering a worst-case scenario, transmission in an insecure slot does not necessarily imply that the packet will be received with $SIR < SIR_{\text{thr}}$. Some users have no *secure slots*; such users are called *bad users*. Users that have at least one secure slot are called *good users*.

(2) Sort *good users* by increasing number of their *secure slots*. Therefore, the priority is given to users that have fewer secure slots.

(3) Allocate *good users* in the order found at the previous point and for each user among the secure slots choose the slot i that corresponds to the minimum value of $P_c(i,u)$. If no secure slot is available for the user, suspend its allocation and go to the next user. This is done because it may subtract secure slots from other users to which they should be allocated.

(4) Allocate previously suspended good users, i.e. the ones with no secure slots left. All these good users will obviously have to be allocated in *insecure* slots.

(5) Allocate *bad users* with the same criterion adopted at the previous points (i.e. minimum $P_c(i,u)$).

Once the allocation algorithm is terminated, the power control procedure previously described is launched for each slot i of each base station b.

12.8.2 Analytical modeling of RAPpA

Let us consider the simplest downlink scenario where the users in a sector are interfered by only one sector antenna of a neighboring cell, having a different label. This is usually a good approximation of the actual scenario, where, due to the use of directional antennas, users typically have one dominant interferer in the first tier of cells and few other weak interferers in the second and third tiers. Let us also approximate the region that includes all the users in a sector that see the same interfering station with a slice of circle with unit radius and angular width 2θ, as in Figure 12.44 [111]. We assume that the dominant interferer has a normalized distance d from the base station serving the user. It can be easily verified in Figures 12.42 and 12.44 that $d = 2$ for both the four-sectored and the six-sectored cellular scenarios. We consider here a two-label pattern and we will show in the next section that it is very simple to extend this framework to the case of three or more labels. If we denote the power of the serving base station (label A) in slot i with $P(i,A)$ and the power of the interfering base station with $P(i,B)$, the SIR in slot i for the user placed in the point (ρ, ϑ) (polar coordinates, with $0 \leq \rho \leq 1$, $\vartheta = \angle\overrightarrow{ab}, \overrightarrow{ac}$ and $-\theta \leq \vartheta \leq \theta$ on the distance $D = \sqrt{(d + \rho\cos\vartheta)^2 + (\rho\cos\vartheta)^2}$ from base station B, can be expressed as

$$SIR_{(\rho,\vartheta,i)} = \frac{P(i,A)}{P(i,B)} \times \left(\frac{\rho}{\sqrt{\rho^2 + 2d\rho\cos\vartheta + d^2}} \right)^{-\beta} \log\left[1, \sqrt{2}\sigma\right] \tag{12.31}$$

For simplicity, we will consider here after the minimum of the median value of the SIR on the interval $[-\theta, \theta]$ obtained for $\vartheta = 0$:

$$SIR_0(\rho, i) = \frac{P(i,A)}{P(i,B)} \left(\frac{d+\rho}{\rho} \right)^{\beta} \tag{12.32}$$

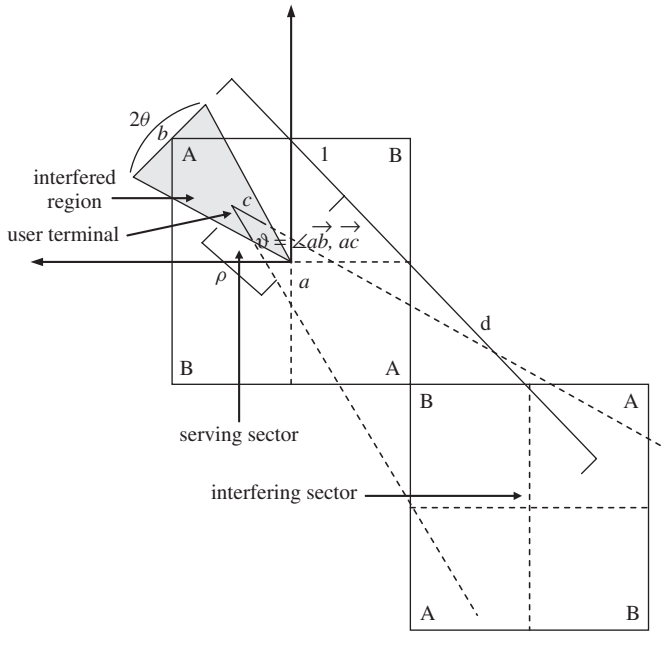

Figure 12.44 Interference model for the FBWA system.

Because of this approximation we use a different reference threshold, which we denote with $SIR_{0\text{thr}}$, such that

$$SIR_{0\text{thr}}[\text{dB}] = SIR_{\text{thr}}[\text{dB}] + M_{\text{SIR}}[\text{dB}],$$

where M_{SIR} is a suitable fading margin. Since $SIR_0(\rho, i)$ is a monotonic function of ρ, we can define $\overline{\rho}_i$ as the solution of $SIR_0(\rho, i) = SIR_{0\text{thr}}$, leading to

$$\overline{\rho}_i = \frac{d}{\left(SIR_{0\text{thr}} \frac{P(i,B)}{P(i,A)}\right)^{1/\beta} - 1} \tag{12.33}$$

The fraction of the area of the slice where users have $SIR_0(\rho, i) \geq SIR_{0\text{thr}}$ in slot i is $A_c(i) = \min[\overline{\rho}_i^2, 1]$. For the users uniformly distributed in the area, $A_c(i)$ also corresponds to the average fraction of users that can be served in slot i with $SIR_0(\rho, i) \geq SIR_{0\text{thr}}$.

In the case where $A_c(i)$ is a nondecreasing function of i and there are N users per sector, an ideal allocation algorithm, having the task of allocating (uniformly distributed) users fulfilling the quality requirement, will try to serve with each slot at least $1/N$th of the area. It achieves its goal only when $A_c(i) \geq (i+1)/N$ for all i. If there is a value of i such that $A_c(i) < (i+1)/N$, the allocation algorithm is unable to fill some slots in the set of slots with an index between 0 and i. Moreover, if $A_c(i)(N-1) < 1$, there are no slots able to serve the users with ρ close to one. This concept can be expressed by the function $F(i)$ recursively defined as

$$F(i) = \min[F(i-1) + 1/N, A_c(i)]$$

starting from $F(-1) = 0$, which indicates the fraction of the user served from slot 0 to slot i. This is intuitive and consistent with previous assertions, since all terminals have identical traffic

load and are uniformly distributed (that means each slot can ideally serve a fraction of users up to $1/N$). Moreover, $F(N-1)$ also indicates the total fraction of served users per frame. For this reason, it can be used to compare and analyze the effectiveness of power profiles.

It can easily be verified that $F(N-1)=1$ if $A_c(i) \geq (i+1)/N$ for all i and $F(N-1)<1$ for some values of i. In fact, it is possible to show that $1-F(N-1)=\max_i[(i+1)/N - A_c(i)]$. When it is not possible to have $A_c(i) \geq (i+1)/N$ for every i, the function $A_c(i)$ has to be designed to stay as close as possible to the linear function $(i+1)/N$. This is possible, in this framework, by suitably designing the functions $P(i, A)$ and $P(i, B)$.

The previous discussion holds if $A_c(i)$ is a nondecreasing function of i. To obtain this, we should have a nondecreasing ratio $r(i)=P(i, A)/P(i, B)$, which can be carried out by properly designing $P(i, A)$ and $P(i, B)$ or simply by doing a slot permutation $i \rightarrow i^*$ in order to get a nondecreasing $r(i^*)$.

In a system without power shaping, $P(i, A)=P(i, B)$ for all timeslots i; hence, all users are covered in all slots when $A_c(i)=1$, i.e. only when $SIR_{0\text{thr}} \leq (d+1)^{\beta}$. Without power shaping, from Equation (12.33) we obtain

$$F(N-1)=\overline{A_c}=\min\left\{d^2\left[(SIR_{0\text{thr}})^{1/\beta}-1\right]^{-2}, 1\right\}$$

When $\overline{A_c}<1$, i.e. if $SIR_{0\text{thr}} > (d+1)^{\beta}$, power shaping can improve the performance. For this reason, we consider hereafter $SIR_{0\text{thr}} > (d+1)^{\beta}$.

For two-label power profiles, we can take a nondecreasing $P(i, A)$ with $P(N-1, A)=P_{\max}$. To maintain equal behavior among the cells, a symmetric profile is chosen for $P(i, B)$, i.e. $P(i, B)=P(N-1-i, A)$, which is not increasing with i and has $P(0, B)=P_{\max}$. This also implies that $r(i)$ is nondecreasing with $r(i)=1/r(N-1-i)$. The simplest case of power profile (step shaping) by modifying (12.30) is given as

$$P(i, A)=\begin{cases} P_{\min}, & i=0, \ldots, M_p-1 \\ P_{\max}, & i=M_p, \ldots, N-1 \end{cases} \tag{12.34}$$

where $M_p \leq N/2$. It produces $r(i)=P_{\min}/P_{\max}, i=0, \ldots, M_p-1, r(i)=1, i=M_p, \ldots, N-M_p-1$, and $r(i)=P_{\max}/P_{\min}, i=N-M_p, \ldots, N-1$, where $A_c(i)$ can be easily evaluated through (12.33). In this case, we can choose M_p and $P_{\max}/P_{\min}$ to optimize $A_c(i)$. As an example, with $M_p=N/2$, the optimal choice would be to have, for the first half of the frame ($i=0, \ldots, N/2-1$), $A_c(i) \geq 1/2$ and, for the second half of the frame ($i=N/2, \ldots, N-1$), $A_c(i)=1$. Due to the symmetry of profiles, we can constrain half of the values of the function $A_c(i)$ by considering $A_c(i)=1$ for $i=N/2, \ldots, N-1$, which means $SIR(1, i)=SIR_{0\text{thr}}$ and (12.32) gives $P_{\max}/P_{\min}=SIR_{0\text{thr}}(1+d)^{-\beta}$.

By using (12.33) we have $F(N-1)=1/2+\min\{A_c(N/2-1), 1/2\}$, where $A_c(N/2-1)=[d/(SIR_{0thr}^2/(1+d)^{\beta})^{1/\beta}-1]^2$. If $A_c(N/2-1)<0.5$ some users cannot be served, but in every case at least $N/2$ users are allocated. It is worth emphasizing that the step profile is also the simplest extension of TSRP [113, 114] that is obtained with $P_{\min}=0$. It is worth noting that instead of keeping several slots unused (zero serving power), as TSRP or ESRA do, it is useful to allow in those slots transmission at minimum power in order to serve interference-resistant users while maintaining good protection for interference-exposed terminals. When an additional noise or interference is added to the dominant interference, it is easy to note that the ratio $P_{\max}/P_{\min}$ should be increased, as in an equivalent situation where a larger $SIR_{0\text{thr}}$ is adopted. Therefore, we will design hereafter the power profiles by considering a larger SIR threshold, $SIR_{0\text{thr}}$, which is the same as taking a higher value for M_{SIR}. The simple step shaping can be further improved by considering the more general case of different values of $r(i)$ for different indexes i. As before, the design can be done by constraining only half of the values of the function $A_c(i)$.

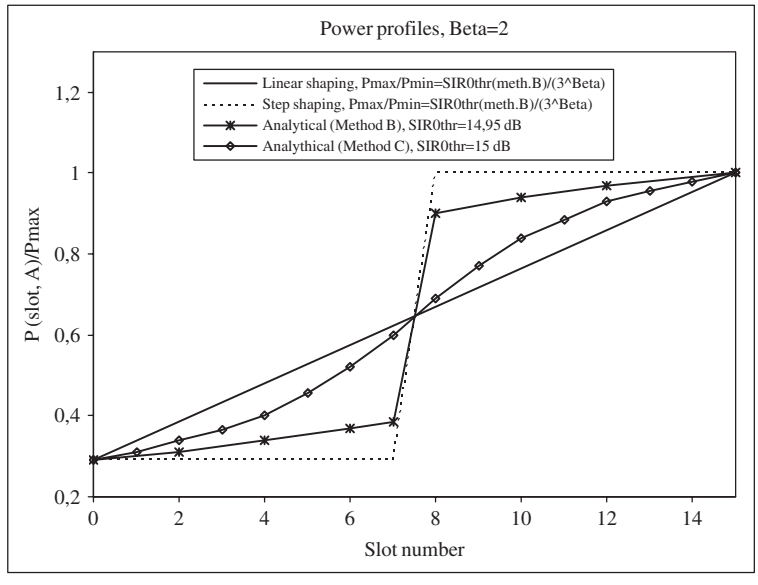

Figure 12.45 Power profiles. (Reproduced by permission of IEEE © 2004 from Tralli *et al.* [111].)

We obtain two design methods. In the first one, named 'method A', we can pose $A_c(i) = [(i+1)/N]$, $i = 0, \ldots, N/2-1$, which leads, by using (12.33), to

$$P(i, A) = P_{\max} \begin{cases} \frac{SIR_{0\text{thr}}}{\alpha(i)}, & i = 0, \ldots, \frac{N}{2} - 1 \\ 1, & i = \frac{N}{2}, \ldots, N-1 \end{cases} \tag{12.35}$$

where $\alpha(i) = \{1 + d[(i+1)/N]^{-1/2}\}^{\beta}$. In 'method B', $A_c(i) = [(i+1)/N]$, $i = N/2, \ldots, N-1$, leading to

$$P(i, A) = P_{\max} \begin{cases} \frac{\alpha(N-1-i)}{SIR_{0\text{thr}}}, & i = 0, \ldots, \frac{N}{2} - 1 \\ 1, & i = \frac{N}{2}, \ldots, N-1 \end{cases} \tag{12.36}$$

Previous methods provide a feasible solution when $\alpha(N/2-1) \geq SIR_{0\text{thr}}$ for method A or $\alpha(N/2) \leq SIR_{0\text{thr}}$ for method B.

It can be shown that the conditions imposed for methods A and B guarantee a nondecreasing $P(i, A)$ and $A_c(i)$. We should emphasize that in both cases we obtain a solution for $r(i)$, which is the ratio of two powers. One of them has been arbitrarily fixed to $P_{\max}$ although other choices are possible, e.g. pairs of symmetric values around $(P_{\max} + P_{\min})/2$, as in the case of Figure 12.45.

Another method (method C) to improve power shaping can be designed with the task of making $A_c(i)$ as close as possible to the linear function $(i+1)/N$. Since $r(i) = 1/r(N-1-i)$, the task can be achieved by solving with respect to $r(i)$:

$$A_c(i) - (i+1)/N = A_c(N-1-i) - (N-i)/N$$

for $i = 0, \ldots, N/2-1$ or $i = N/2, \ldots, N-1$. As before, one of the terms of $r(i)$ can be arbitrarily fixed to $P_{\max}$. This method will be more efficient for resource allocation. It leads to a monotonic profile and consequently to a nondecreasing $A_c(i)$.

Figure 12.46 shows a comparison (for $N = 16$) between profiles in terms of $F(i)$ and $A_c(i)$. As expected, $A_c(i)$ obtained for method C leads to a higher value of $F(N-1)$ since it is closer to

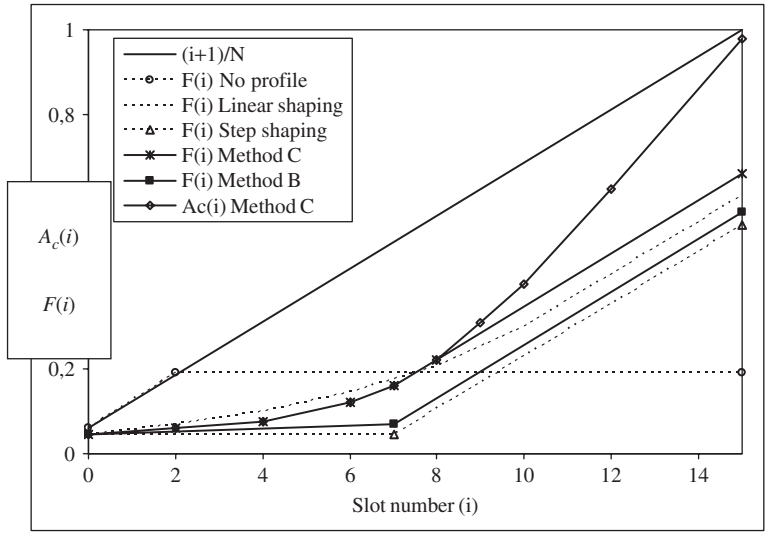

Figure 12.46 Comparison between profiles in terms of $F(i)$ and $A_c(i)$: $\beta = 2$, $SIR_{0\text{thr}} = 15\,\text{dB}$. (Reproduced by permission of IEEE © 2004 from Tralli *et al.* [111].)

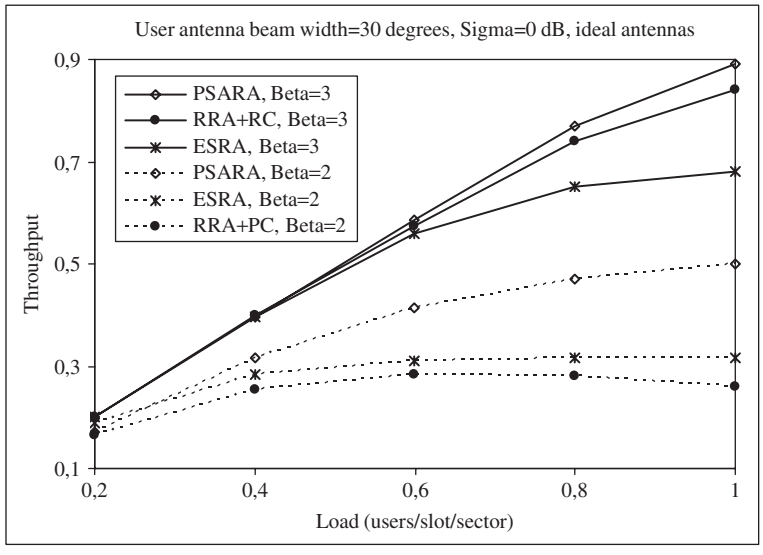

Figure 12.47 Throughput versus load for different resource allocation strategies: the effect of the propagation exponent. PSARA uses a linear power profile with $P_{\max}/P_{\min} = 20\,\text{dB}$: square cells. (Reproduced by permission of IEEE © 2004 from Tralli *et al.* [111].)

$[(i + 1)/N]$, but even the basic step profile leads to a considerable gain over the use of no profile (i.e. a flat profile). The throughput curves are shown in Figure 12.47.

In the case of design of three-label power profiles, the easiest way to choose the K levels of power P_j, $j = 0, \ldots, K - 1$, which define the power profiles according to Table 12.3, is to apply

the step or the straight line. However, analytical curves obtained for the two-label case are also valid. In fact, Figure 12.42 shows that in the hexagonal scenario the assumption of having only one main interferer per user is accurate (provided that the user antenna beamwidth is sufficiently narrow).

To design analytical profiles, due to the symmetries among profile patterns and to the fact that we consider only one main interferer, we can choose $P(i, A)$ and $P(i, B)$ as serving and interfering powers, respectively, without any loss of generality. Once $P(i, A)$ is found, $P(i, B)$ and $P(i, C)$ are computed by means of the permutation matrix. As shown before, the goal of the design is to find $r(i) = P(i, A)/P(i, B)$. By means of a suitable slot permutation $i \rightarrow i^*$ (that does not lead to a loss of generality), a nondecreasing $r(i^*)$ can be derived, such as, for example, the star, which has

$$r(i^*) = r(N - 1 - i^*)^{-1} \text{ for } i^* = 0, \cdots, R - 1 \text{ and } r(i^*) = 1$$
$$\text{for } i^* = R, \ldots, N - 1 - R$$

where $R = N/3$.

The geometric approach to design the three-label pattern presented above can be easily extended to a general L-label pattern.

12.9 COGNITIVE AND COOPERATIVE DYNAMIC RADIO RESOURCE ALLOCATION

In this section we discuss a solution that unifies radio resource management (RRM) for TDMA, CDMA and OFDM signal formats and achieves a near-optimum channel reuse factor close to one [115]. In the sequel we will use interchangeably the terms radio resources, spectra or channel, representing the frequency beam in OFDM, the timeslot in TDMA or the code for CDMA signal formats, respectively. Occasionally, term resources may also include power, which will be explicitly pointed out to avoid ambiguity. As will be explained in the sequel, the solution requires a certain level of cognition and cooperation designed to reduce the intercell interference on the down-link.

As discussed in the previous sections in this chapter, in space division multiple access (SDMA), within each channel, multiple beams are formed by a smart antenna array at the base station. The radiation pattern of each beam is adjusted so that the main lobe is steered to the direction of the desired user and nulls are placed in the direction of interfering users, which is referred to as angle or θ *separability*.

It should be intuitively clear that if two users, due to their position in the network, are not θ*-separable*, then we have to use additional steps to reduce the intercell interference. For example,

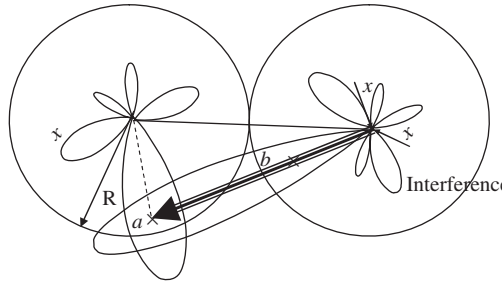

Figure 12.48 Transmission for user b cannot be spatially filtered at the location of user a by θ separation, because the transmission and interfering direction coincide; d-separation has to be used.

in Figure 12.48, transmission to user b will also be received by user a. On the other hand, transmission to user a, in Figure 12.49, will not be received by user b because that direction can be spatially notched out while still transmitting successfully to user a. For these purposes, in the sequel we present channel allocation schemes based on *d-separability.* The scheme can be further enhanced by using intercell interference cancellation, referred to as signal processing or *sp-separability*, which will be required only by a limited number of users and that number can be controlled.

In this model we assume that the beamforming has generated M spatial channels, which are reused across each cell. Within each spatial channel, N additional channels are generated by using either timeslot (TDMA), frequency beam (subcarrier in OFDM) or code (CDMA).

In order to minimize the intercell cochannel interference, special, intercell coordinated, channel allocation patterns are used. For a simple model with two cells, the channel allocation scheme will assign the channel index $(1, 2, \ldots, n, \ldots, N)$, depending on the user distance from the BS, differently in a reference cell and its neighboring cell. We will use notation

$$a[(\text{start, direction})n, (\text{start, direction})r] \tag{12.37}$$

to denote the channel allocation pattern. As an example,

$$a[(1, \text{up})n, (0, \text{up})r] \tag{12.38}$$

means that channels (n) are allocated in increasing order (up) of indices starting from index 1 to the users on increasing (up) distances (r) from the BS, starting with distance 0. In other words, the channel with the lowest index is allocated to the user on the shortest distance from the BS. In order to avoid the situation where two users from different cells positioned close to each other at the borders of their cells receive at the same channel, the assignment in the neighboring cell should use the complementary pattern

$$a[(1, \text{up})n, (R, \text{down})r] \tag{12.39}$$

This means that the channels (n) are allocated in increasing order (up) of indices starting from index 1 to the users on decreasing (down) distances (r), starting with the maximum distance R. This suggests an alternative notation for IIC RRM as SDMA (θ, r, c), where c stands for channel.

For example, if two users, in Figure 12.50, from different cells are using the same channel, their distance for $\theta = 0$ will be approximately R (cell radius) and for the same receiving power the minimum signal-to-interference ratio, in the absence of fading, will depend on R. This basic concept will be further elaborated in more detail. In general, if user k uses n_k channels) (subcarriers, slots or codes) Equations (12.37) to (12.39) should be modified so that the channel $n \to n_k$ represents the subset of channels allocated to one user at a given location.

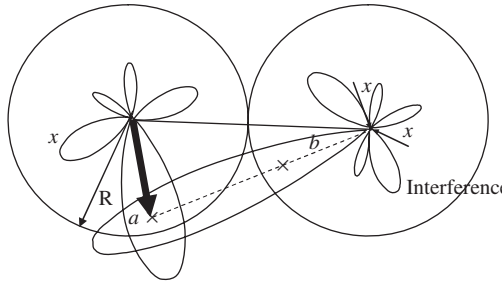

Figure 12.49 Transmission for user a can be avoided at the location of user b by θ separation.

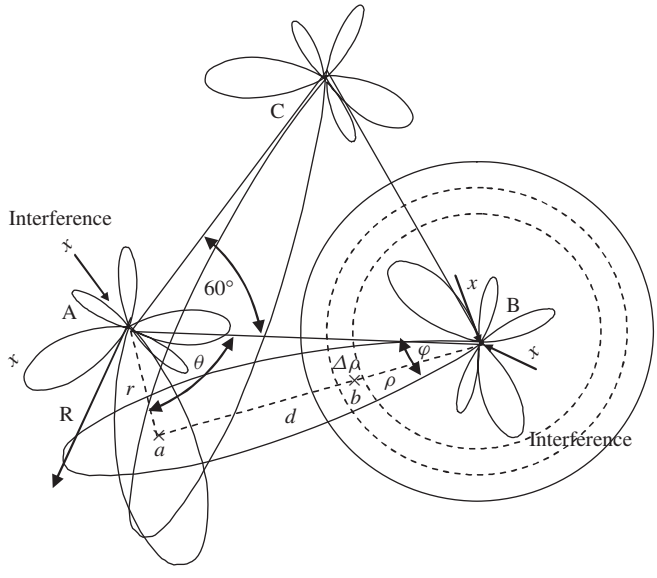

Figure 12.50 Size 3 cell cluster scenario.

An alternative presentation for assignment $a[(\text{start, direction})n, (\text{start, direction})r]$ can be obtained if the following notation is used:

$\Uparrow$ *direction up,*

$\Downarrow$ *direction down,*

$\Updownarrow$ *alternating directions (up/down and down/up) at the end of the sweep* (12.40)

As already mentioned, in TDMA the channel is a timeslot while in OFDM the channel is a frequency beam (subcarrier). In CDMA, for a given set of available codes $C = \{c_k\}$, we form the set of the cross-correlations $\rho = \{\rho_{km}(\tau)\}$ between codes c_k and c_m $\forall k, m$. If $\max_\tau \rho_{km}(\tau)$ are sorted in increasing order indexed by index $l \Rightarrow (k, m)$, then the code assignment in two adjacent cells will be defined with a pair:

$$A(a_1, a_2) = \begin{cases} a_1[(1, \Uparrow)l(k), (R, \Downarrow)r] \\ a_2[(1, \Uparrow)l(m), (R, \Downarrow)r] \end{cases} \tag{12.41}$$

This means that for two of the closest users belonging to two different cells (largest $r = R$), two codes with indices (k, m) corresponding to the lowest cross-correlation $l = 1$ will be allocated. For the users with smaller r, the distance between the two interfering mobile will be larger and the larger indices of l, corresponding to larger cross-correlations $\rho = \{\rho_{km}(\tau)\}$, can be used.

12.9.1 Signal-to-interference ratio

For the analysis of the signal-to-interference ratio we will initially suppose that the mobile stations a and b are located in two adjacent cells, as shown in Figure 12.50. In a conventional system these two mutually interfering stations may be at an arbitrary distance. Formally we will refer to this as the arbitrary distance (AD) protocol.

12.9.1.1 Arbitrary distance (AD) protocol

AD protocol with no power control

With the transmit power P, power of the signal transmitted by base station A and received at the location of mobile a is $p_a = \xi_a \beta_a P / r_a^{\alpha}$, where α is the propagations constant, r_a is the distance of mobile a from the base A, ξ_a represents Rayleigh fading and β_a lognormal shadowing. Similarly, power of the signal transmitted by base B and received at the location of mobile b is $p_b = \xi_b \beta_b P / r_b^{\alpha}$ and the interference power at the location of mobile a is $p_{b\to a} = \xi_{b+d} \beta_{b+d} P (r_b + d)^{-\alpha}$, where d is the distance between mobiles a and b. The signal-to-interference ratio is

$$SIR = y_1 = \frac{p_a}{p_{b\to a}} = \frac{\xi_a \beta_a P (r_b + d)^{\alpha}}{r_a^{\alpha} P \xi_{b+d} \beta_{b+d}} = \frac{\xi_a \beta_a}{\xi_{b+d} \beta_{b+d}} \left(\frac{r_b + d}{r_a} \right)^{\alpha} \tag{12.42}$$

Having in mind Figure 12.50, and by using the cosine theorem, we get

$$(d + r_b)^2 = (2R)^2 + r_a^2 - 4 R r_a \cos\theta \tag{12.43}$$

$$\left(\frac{d + r_b}{r_a} \right)^2 = \left(\frac{2R}{r_a} \right)^2 + 1 - 4 \frac{R}{r_a} \cos\theta \tag{12.44}$$

$$\frac{d + r_b}{r_a} = \sqrt{4/g^2 + 1 - 4/g \cos\theta} \tag{12.45}$$

where $g = r_a / R$. Now we have

$$y_1 = \frac{\xi_a \beta_a}{\xi_{b+d} \beta_{b+d}} (4/g^2 + 1 - 4/g \cos\theta)^{\alpha/2} \tag{12.46}$$

The interference-to-signal ratio is $i_1 = 1/y_1$.

AD protocol with power control

In the case of power control, the received signal power at the location of mobiles a and b, transmitted by their base stations, is the same and is defined by $p = \xi_a \beta_a \Pr_a^{-\alpha} = \xi_b \beta_b P_b r_b^{-\alpha}$, where P_a and P_b are the transmit powers of base stations A and B, respectively. The interference power at the location of mobile a is $p_{b\to a} = \xi_{b+d} \beta_{b+d} P_b (r_b + d)^{-\alpha}$ and the interference-to-signal ratio is

$$SIR = y_2 = \frac{p}{p_{b\to a}} = \frac{\xi_b \beta_b}{\xi_{b+d} \beta_{b+d}} \left(1 + \frac{d}{r_b} \right)^{\alpha} \tag{12.47}$$

By dividing Equation (12.45) by r_b we get

$$1 + \frac{d}{r_b} = \frac{r_a}{r_b} \frac{1}{g} \sqrt{4 + g^2 - 4g \cos\theta} = \frac{1}{h} \sqrt{4 + g^2 - 4g \cos\theta} \tag{12.48}$$

and the signal-to-interference ratio is now

$$y_2 = \frac{\xi_b \beta_b}{\xi_{b+d} \beta_{b+d}} \left(\frac{1}{h} \sqrt{4 + g^2 - 4g \cos\theta} \right)^{\alpha}, \quad i_2 = 1/y_2 \tag{12.49}$$

where $h = r_b / R$. The same equations stand for the case of no fading if we set $\xi_a = \beta_a = \xi_b = \beta_b = \xi_{b+d} = \beta_{b+d} = 1$.

12.9.1.2 Constant distance CD protocol

As already mentioned, in order to avoid the situation where two users from different cells positioned close to each other at the borders of their cells receive at the same channel, therefore to keep a low

interference level, the assignment of channels in the two neighboring cells should use the pattern

$$a[(1, \Uparrow)n,\ (0, \Uparrow)r] \tag{12.50}$$

$$b[(1, \Uparrow)n,\ (R, \Downarrow)r] \tag{12.51}$$

In this case the following condition is always satisfied: $r_b = R - r_a$. The set of equations derived in the previous section for the case with and without power control can be applied in this case if we set $h = 1 - g$. Therefore, we have

$$y_3 = y_1 = \frac{\xi_a \beta_a}{\xi_{b+d}\beta_{b+d}}(4/g^2 + 1 - 4/g\cos\theta)^{\alpha/2},\ i_3 = 1/y_3 \tag{12.52}$$

$$y_4 = y_2|_{h=1-g} = \frac{\xi_b \beta_b}{\xi_{b+d}\beta_{b+d}}\left(\frac{1}{1-g}\sqrt{4 + g^2 - 4g\cos\theta}\right)^{\alpha},\ i_4 = 1/y_4 \tag{12.53}$$

12.9.1.3 Linearly varying distance LVD protocol

The protocol is defined as

$$a[(1, \Uparrow)n,\ (0, \Uparrow)r] \tag{12.54}$$

$$b[(1, \Uparrow)n,\ (0, \Uparrow)r] \tag{12.55}$$

Therefore, $r_a = r_b, h = g$. Equations from the previous sections can also be applied in this case and we have

$$y_5 = y_1 = \frac{\xi_a \beta_a}{\xi_{b+d}\beta_{b+d}}(4/g^2 + 1 - 4/g\cos\theta)^{\alpha/2},\ i_5 = 1/y_5 \tag{12.56}$$

$$y_6 = y_2|_{h=g} = \frac{\xi_b \beta_b}{\xi_{b+d}\beta_{b+d}}\left(\frac{1}{g}\sqrt{4 + g^2 - 4g\cos\theta}\right)^{\alpha},\ i_6 = 1/y_6 \tag{12.57}$$

12.9.2 System performance

12.9.2.1 The outage probability

The outage probability is defined as

$$P_{\text{out}}(x, \theta) = P(i > \varepsilon) = 1 - P(i < \varepsilon) = 1 - P\left(\frac{\xi_{b+d}\beta_{b+d}}{\xi_b \beta_b} i_0(x, \theta) < \varepsilon\right) \tag{12.58}$$

where ε is a given threshold which depends on the receiver implementation. In general, there will be a correlation between the spatial samples of ξ_{b+d} and ξ_b as well as between β_{b+d} and β_b. The amount of correlation will depend on both the beam width and the mutual distance d between interfering users. Both larger distance and larger beamwidth will result in less correlation. Although the modeling of the channel resemblance (correlation) for the two interfering users is beyond the scope of this book, we can make some suggestions that can be used in the further evaluation of the protocols. For a very narrow beam we can use the approximation $\xi_{b+d} = \xi_b \xi_d$ and, for $d \to 0$, $\xi_{b+d} \to \xi_b$. For larger beamwidths we can use the approximation $\xi_{b+d} = (1 - \rho)\xi_{-b} + \rho\xi_b$, where ξ_{-b} represents the portion of the signal received at point $b + d$ not seen by point b, and the resemblance factor ρ can be represented as $\rho(\varphi, d) = (1 - d/d_0)(1 - \varphi/\varphi_0)$. For a precise analysis of P_{out} we need a joint probability distribution function of ξ_{b+d} and ξ_b. However, for a relatively wide beam and d large enough (e.g. $d = R$ is of particular interest), we can assume that the fading at the two mutually interfering terminal locations is independent. In this case, if β is lognormal variable with zero mean and variance σ then in this calculus we can use the fact that $\beta = \beta_{b+d}/\beta_b = 10^{n_{b+d} - n_b} = 10^n$ is also lognormal variable with zero mean and variance $\sqrt{2}\sigma$.

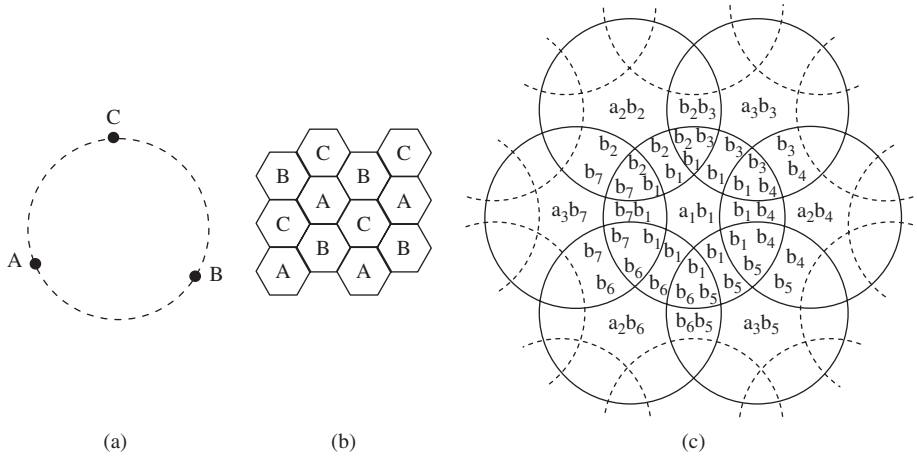

Figure 12.51 Multiple-cell scenarios.

Therefore, we have

$$P_{\text{out}}(x,\theta) = P(i > \varepsilon) = 1 - P(i < \varepsilon) = 1 - P\left(\beta \frac{\xi_{b+d}}{\xi_b} i_0(x,\theta) < \varepsilon\right)$$

$$= 1 - \int_0^\infty P(\beta)\mathrm{d}\beta \int_0^\infty P(\xi_{b+d})\mathrm{d}\xi_{b+d} \int_{i_0\beta\xi_{b+d}/\varepsilon}^\infty P(\xi_b)\mathrm{d}\xi_b \tag{12.59}$$

12.9.2.2 Intercell collision recovery protocol and channel reuse factor

After channel allocation in the system with connection-oriented services, SIR outage may occur, which will be referred to as an intercell collision. If this happens the mobile will notify the base station and the collision recovery protocol, described in the sequel, will be activated.

In a network with packet access, data link and network connections are established with an entity called a mobile switching point (MSP), which is physically connected to all the BSs that constitute a radio service area, as shown in Figure 12.51(a). A number of simplified protocols for packet-switched transmission dealing with intercell interference can be used.

In this concept we define an *intercell collision* when the packets belonging to different BSs send NACK at the same channel. When such a collision occurs the BSs may simultaneously reschedule packet retransmission (R) and reallocate (R) the packet from different cells to different channels – hence the name *R^2-ALOHA protocol.*

In order to design an effective intercell collision recovery protocol in the sequel, we first identify different possible reasons for collision and based on this elaborate protocol for collision resolution.

(1) *Noncooperative cellular system*

In this system there is neither a mutual exchange of information nor coordinated action between the cells in the network. As a consequence we have the following events:

(a) If the base station does not have information about the user's location it cannot make any assumption as to whether the NACK was due to noise and fading or due to collision with the packet from other cells, and can relay on a standard technique of packet retransmission (R) with a random backoff period. A longer backoff time reduces the probability of a new collision with the retransmitted packet in the adjacent cell, but at the same time this increases the delay.

(b) If the given cell has information about the user location and based on that information makes an assumption about whether or not the NACK was due to intercell or intracell interference, we have the following possibilities. If the assumption was that the NACK was due to intracell interference (the user was not close to the cell border), only retransmission (action R) would take place. If the assumption was that the NACK was due to intercell interference (the user was close to the cell border) retransmission plus rescheduling (action R^2) would take place. If there is no cooperation between the base stations, in the case where two interfering users belonging to two different cells collide, both base stations will take R^2 action. This would result in a double effort in the sense that both base stations would do the recomputation of the schedules and even without coordination both base stations may again choose the same new channels for the two users, resulting in a new collision.

(2) *Cooperative cellular system*
In the case where two bases cooperate, they would agree that only one base would take action R^2 and another could use only R. This would reduce complexity of such action and at the same time eliminate the possibility that after R^2 action of both bases the interfering users would collide again. The reduced scope of the R^2 action will be referred to as mutation, which is part of a broader family of genetic algorithms.

(3) *Collision exclusion protocol*
For a given number k of jointly registered collisions in both bases, the collided channels will not be used in the next K frames, where KT is the fading constant. The *intercell throughput* in such a system is defined as $S(k) = (N - k)/N = 1 - k/N$. The average intercell throughput is derived in Appendix 12B as

$$S = \sum_k S(k) p_{\text{out}}(k) = 1 - P_{\text{out}} \tag{12.60}$$

where the probability of having k channels with $i > \varepsilon$ can be presented as

$$p_{\text{out}}(k) = \sum_s \prod_{i \in s \in S(k\Uparrow)} P_{\text{out}}^{(i)} \prod_{j \in s \in S(k\Downarrow)} (1 - P_{\text{out}}^{(j)}) \tag{12.61}$$

and $p_{\text{out}}^{(i)}$ is the channel outage probability given by Equations (12.58) and (12.59). In Equation (12.61) $S(k^{\Uparrow})$ stands for the set of all possible combinations of k channels, where $i > \varepsilon$ and $S(k^{\Downarrow})$ for the set of all possible complementary combinations of $N - k$ channels where $i < \varepsilon$. For each element with index s in $S(k^{\Uparrow})$ there is one corresponding element in $S(k^{\Downarrow})$. The size of the set is

$$|S(k^{\Uparrow})| = \binom{N}{k} = |S(k_{\Downarrow})| \tag{12.62}$$

(4) *Collision sharing protocol*
In this protocol, after k collisions, in each next packet interval k collided channels are alternatively allocated only to one BS. The throughput is now $S(k) = (2N - k)/2N = 1 - k/2N$ and the average throughput defined by Equation (12.60) is $S = 1 - P_{\text{out}}/2$.

In a network with connection-oriented services, the collision recovery protocol is the same but we still use slightly different terminology. Instead of an intercell packet collision we have an intercell channel assignment collision. Also, instead of intercell throughput S we use the term intercell channel assignment efficiency E. If there is no cooperation, collided assignments will not be used (collision exclusion) in any of the two collided cells and E will be given by $S(k) = 1 - k/N$. In collision sharing the cells may agree to use each $k/2$ collided channels, resulting in E given by $S(k) = (2N - k)/2N = 1 - k/2N$. For both of these two services we define the channel reuse factor as $CRF = 1/S$ for packet services and $CRF = 1/E$ for connection-oriented services.

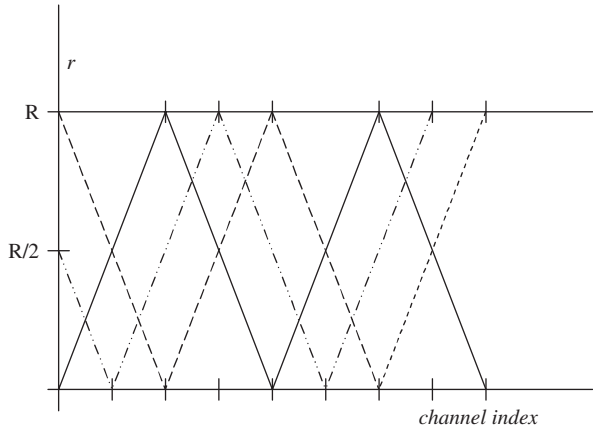

Figure 12.52 Channel assignment in the case of a size 3 cluster.

12.9.3 Multicell operation

A multiple-cell scenario with cluster size $c = 3$ is shown in Figure 12.51.

12.9.3.1 CD protocol

For the time being let us focus only on assignment $A(a_1, a_2, a_3)$, where the cell assignment a_k covers the whole cell k, as shown in Figure 12.51(b). Channel assignments a_k are defined as

$$a_k[(1, \Uparrow)n, ((k-1)R/2, \Updownarrow))r] \tag{12.63}$$

which is illustrated in Figure 12.52. The constant interference distance is now $> R/2$. The general extension to cluster size c is defined as

$$a_k[(1, \Uparrow)n, ((k-1)R/(c-1), \Updownarrow))r] \tag{12.64}$$

with constant interference distance $d > R/(c-1)$.

If in Figure 12.51(c) we use the notation A_1, A_2, A_3 for the nonoverlapping area, the area where two cells' transmissions overlap and the area where three cells' transmissions overlap, respectively, then with uniform distribution of users in the area, the average reuse factor can be represented as $c = A_1 + 2A_2 + 3A_3$, where $A_1 + A_2 + A_3 = 1$. Here we assume that in the overlapping areas the overlapping cells share available resources (channels) evenly. Equivalently, from C available channels we can use effectively $C_{\text{eff}} = A_1C + A_2C/2 + A_3C/3$ channels per cell.

For the allocation (12.63) starting at $r = 0$ and $r = R/2$ (see Figure 12.52), in the adjacent cell we have, similarly as previously, $p_{b\to a} = \xi_{b+d}\beta_{b+d}P_b(r_b + d)^{-\alpha}$, where $r_b = |R/2 - r_a|$. The interference-to-signal ratio is

$$SIR = y = \frac{p}{p_{b\to a}} = \frac{\xi_a\beta_a}{\xi_{b+d}\beta_{b+d}}\left(1 + \frac{d}{|R/2 - r_a|}\right)^{\alpha} \tag{12.65}$$

Finally, we have

$$1 + \frac{d}{|R/2 - r_a|} = \frac{r_a}{|R/2 - r_a|}\frac{1}{g}\sqrt{4 + g^2 - 4g\cos\theta} = \frac{1}{|1/2 - g|}\sqrt{4 + g^2 - 4g\cos\theta} \tag{12.66}$$

$$y = \frac{\xi_a\beta_a}{\xi_{b+d}\beta_{b+d}}\left(\frac{1}{|1/2 - g|}\sqrt{4 + g^2 - 4g\cos\theta}\right)^{\alpha},\ i = 1/y \tag{12.67}$$

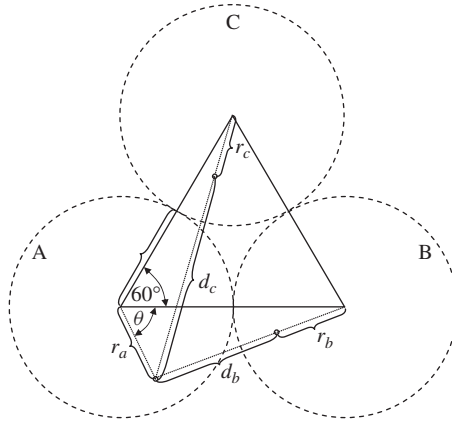

Figure 12.53 Size 3 cell cluster scenario.

In the case of the size 3 cluster scenario (cells A, B and C), as shown in Figure 12.50, the angle between directions $\overline{AB}$ and $\overline{AC}$ is $\varphi = 60^\circ$. Therefore, if the previous equations are used for cells A and B then for cells A and C we use the same equations with $\theta_1 = \theta + \varphi = \theta + 60^\circ$. For more details see Figure 12.53 and Appendix 12A.

12.9.3.2 LVD protocol

In this case in all cells an LVD protocol defined as

$$a_k[(1, \Uparrow)n, (0, \Uparrow)r] \tag{12.68}$$

is used. The concept is based on ICC and partial intercell interference cancellation. The maximum possible spatial separation is used for a subset of users and then this distance is linearly reduced for other subsets of users depending on their location. For the subset of users with the distance below a certain threshold, interference cancellation is used.

12.9.4 Performance examples

In this section we present some performance illustrations of the protocols. In the figures the signal-to-interference ratio for the IIC-CD protocol is designated as SIR_{CD} whereas the same parameter for the system without the intercell interference coordination (NIIC-AD) protocol is designated as SIR_{AD}. These parameters for isolated clusters of two and three cells are presented in Figures 12.54 and 12.55. In Figure 12.54, one can see that in most of the terminal positions $SIR_{CD} > SIR_{AD}$. The results are shown for $h = 0.8$. In Figure 12.55, when the user is at the cell border ($h = 1$) the minimum value for $SIR_{AD} = 0\,\text{dB}$, so that $SIR_{CD} - SIR_{AD}$ is of the order of 20–30 dB for $g > 0.5$. Of course, if the user is close to the base station (say $h = 0.2$ as in Figure 12.55) SIR_{AD} is significantly larger than SIR_{CD}. The advantage of the IIC protocol is that independent of user location, including the cell border area, SIR remains acceptable (larger than 15 dB), which ensures complete cell coverage. On the other hand, without IIC the SIR becomes unacceptably low in the cell border area and unnecessarily high in the area close to the base station. In this way the coverage is not ensured across the entire network.

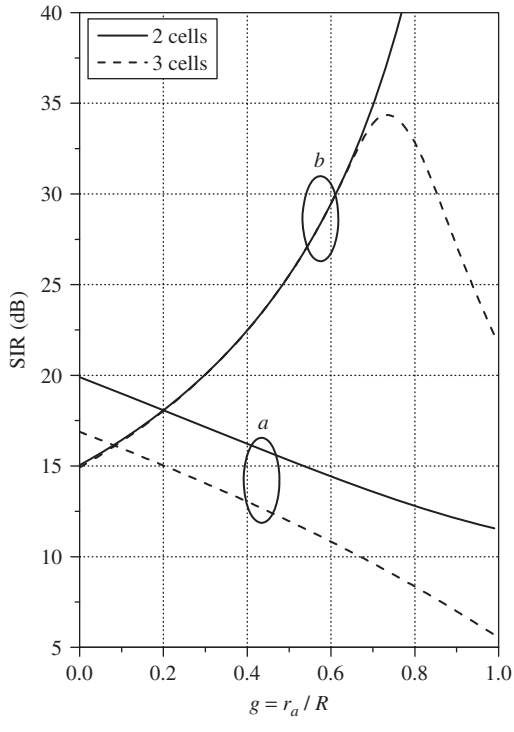

Figure 12.54 Signal-to-interference ratio as a function of normalized distance g: (a) power control, no fading, AD protocol; (b) power control, no fading, CD protocol. Averaged over θ in the range $[-60^\circ, 0^\circ]$: $\alpha = 5$; $h_b = r_b/R = h_c = r_c/R = h = 0.8$.

Figure 12.56 additionally presents the signal-to-interference ratio for the LVD protocol (SIR_{LVD}) where a cluster of three cells unfolds into the network scenario from Figure 12.51(c). For $g < 0.5$, SIR_{LVD} is larger than SIR_{CD} and then falls down to the value 0 dB. Depending on the receiver processing capability, when SIR_{LVD} falls below a certain threshold, the receiver will have to use *sp*-separability techniques in order to provide proper data detection. In Figure 12.56 the values of SIR are in general lower due to the impact of all seven surrounding cells.

Parameter P_{out} is shown in Figure 12.57 for a given set of channel parameters. One can see that for $\alpha = 5$, which is a typical value for an urban network, and $\sigma = 8$ dB, P_{out} takes values between 0 and 20 % across the network. For smaller values of $\sigma = 6$ dB and 3 dB, P_{out} is much lower.

Figure 12.58 shows the average intercell throughput for a set of channel parameters. For the collision exclusion protocol, we have $0.73 < S < 0.98$ for $\sigma = 8$ dB and $0.89 < S < 0.9998$ for $\sigma = 3$ dB, and for the collision sharing protocol, it can be seen that $0.87 < S < 0.99$ for $\sigma = 8$ dB and $0.95 < S < 0.9999$ for $\sigma = 3$ dB.

Fixed wireless networks can use antenna directivity in both base stations (access point) and user terminals. For these reasons the resource reuse factor would be better for such schemes than for the schemes developed here, where we assume omnidirectional antennas, which is a more appropriate model for a mobile terminal.

In 4G wireless systems, sophisticated resource management schemes may want to split the terminals in the wireless network into different classes based on mobility, while still applying

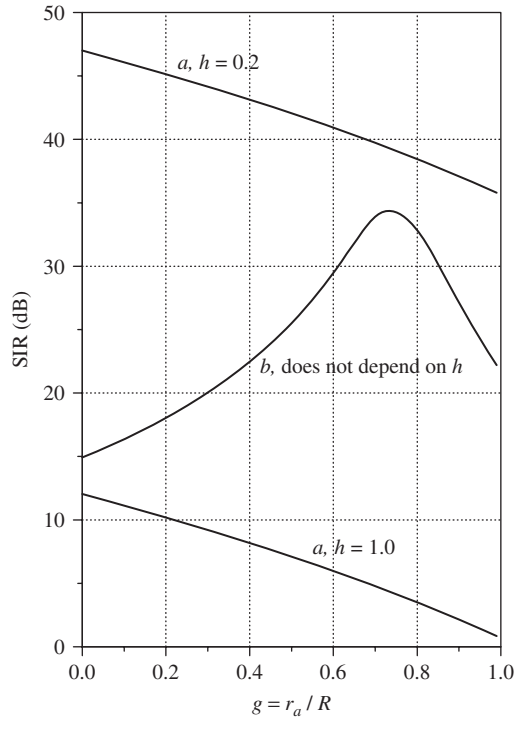

Figure 12.55 Signal-to-interference ratio as a function of normalized distance g for a three-cell scenario: (a) power control, no fading, AD protocol; (b) power control, no fading, CD protocol. Averaged over θ in the range $[-60^\circ, 0^\circ]$: $\alpha = 5$; $h_b = r_b/R = h_c = r_c/R = h$.

low-mobility terminal rules of engagement designed for fixed networks. This will be referred to as multilayer RRM or RRM overlay. This raises three fundamental questions:

1. How to dynamically split the users between the two groups.
2. How to control the handover between the two groups.
3. How to partition the overall resources for the two groups and provide flexible spectra sharing so as to maximize the spectra utilization.

Different options may also include pricing. Switching from the mobile to the fixed user status may enable more efficient RRM and effectively less usage of the overall resources of the network, resulting in a lower price.

12.10 APPENDIX 12A: POWER CONTROL, CD PROTOCOL, IN THE PRESENCE OF FADING

If ξ represents Rayleigh fading, β lognormal shadowing and α is the propagation constant, it was shown (see Equation (12.53)) for users a and b, for the geometry from Figure 12.48, that the

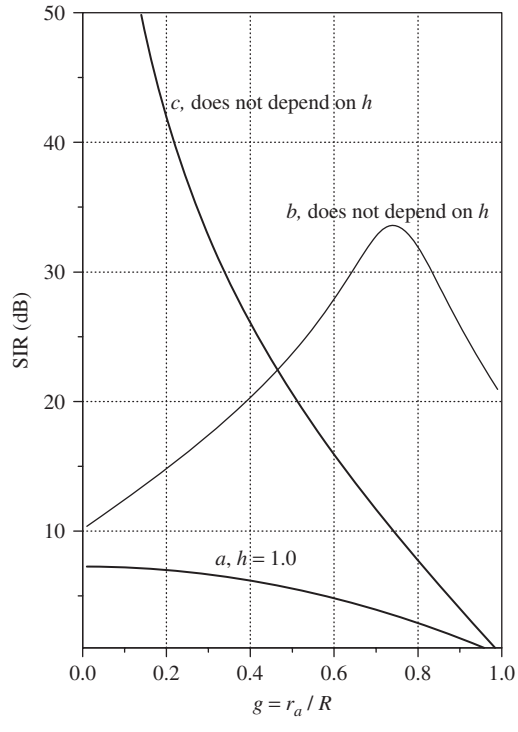

Figure 12.56 Signal-to-interference ratio as a function of normalized distance g for a seven-cell scenario with cluster size 3: (a) power control, no fading, AD protocol; (b) power control, no fading, CD protocol; (c) power control, no fading, LVD protocol. Averaged over $\theta \in [0, 2\pi]$: $\alpha = 5$; $h_b = r_b/R = h_c = r_c/R = h_d = \cdots = h_g = h$.

signal-to-interference ratio has the following form:

$$SIR = y_b = \frac{\xi_b \beta_b}{\xi_{b+d} \beta_{b+d}} \left(\frac{1}{1-g} \sqrt{4 + g^2 - 4g\cos\theta} \right)^{\alpha} \tag{12.69}$$

The interference-to-signal ratio is

$$i_b = 1/y_b = \frac{\xi_{b+d_b} \beta_{b+d_b}}{\xi_b \beta_b} \left(\frac{1-g}{\sqrt{4 - 4g\cos\theta + g^2}} \right)^{\alpha} = \frac{\xi_{b+d_b} \beta_{b+d_b}}{\xi_b \beta_b} f_b(\theta) \tag{12.70}$$

where

$$f_b(\theta) = \left(\frac{1-g}{\sqrt{4 - 4g\cos\theta + g^2}} \right)^{\alpha} \tag{12.71}$$

If β_{b+d_b} and β_b are independent lognormal random variables with the following probability density functions (PDFs):

$$p_{\beta_{b+d}}(x) = p_{\beta_b}(x) = \frac{1}{x\sigma_\beta \sqrt{2\pi}} \exp\left(-\frac{(\ln x)^2}{2\sigma_\beta^2} \right) \tag{12.72}$$

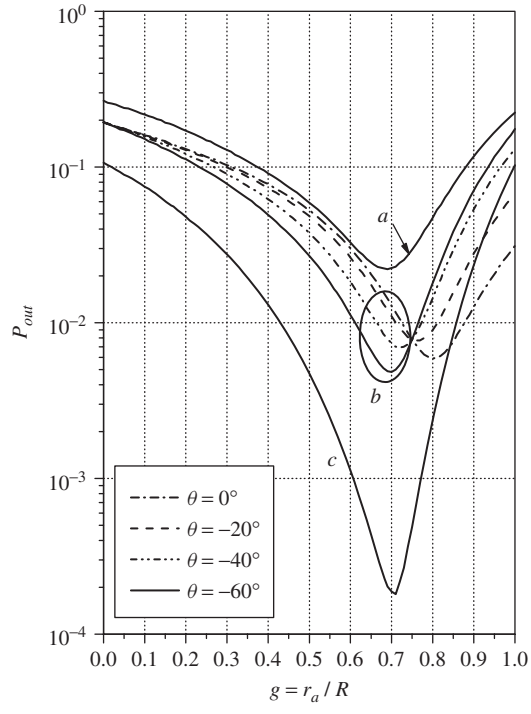

Figure 12.57 Outage probability as a function of normalized distance g for a three-cell scenario and CD protocol $\alpha = 5$: (a) $\sigma_{\beta b} = \sigma_{\beta c} = 3$ dB; (b) $\sigma_{\beta b} = \sigma_{\beta c} = 6$ dB; (c) $\sigma_{\beta b} = \sigma_{\beta c} = 8$ dB; $\sigma_{b+d} = \sigma_{c+d} = \sigma_c = \sigma_d = 1$; $\varepsilon = 0.5$.

then $\beta_{b1} = \beta_{b+d_b}/\beta_b$ is also a lognormal random variable with parameter $\sqrt{2}\sigma_\beta$. Also, if ξ_{b+d_b} and ξ_b are independent Rayleigh random variables:

$$\begin{aligned} p_{\xi_{b+d}}(x) &= \frac{x}{\sigma_{b+d}^2} \exp\left(-\frac{x^2}{2\sigma_{b+d}^2}\right) \\ p_{\xi_b}(x) &= \frac{x}{\sigma_b^2} \exp\left(-\frac{x^2}{2\sigma_b^2}\right) \end{aligned} \tag{12.73}$$

then $\xi_{b1} = \xi_{b+d_b}/\xi_b$ is the random variable with the following PDF:

$$p_{\xi_{b1}}(x) = \frac{2\sigma_{b+d}^2 \sigma_b^2 x}{(\sigma_{b+d}^2 + \sigma_b^2 x^2)^2} \tag{12.74}$$

The probability density function of $(\xi_{b+d_b}/\xi_b) f_b(\theta)$ is

$$p_{\xi f_b}(x) = \frac{1}{f_b(\theta)} p_{\xi_{b1}}(x/f_b(\theta)) \tag{12.75}$$

Finally, the PDF of i_b is

$$p_b(x) = \int_0^{+\infty} p_{\beta 1}(x/z) p_{\xi f}(z)/z \cdot \mathrm{d}z \tag{12.76}$$

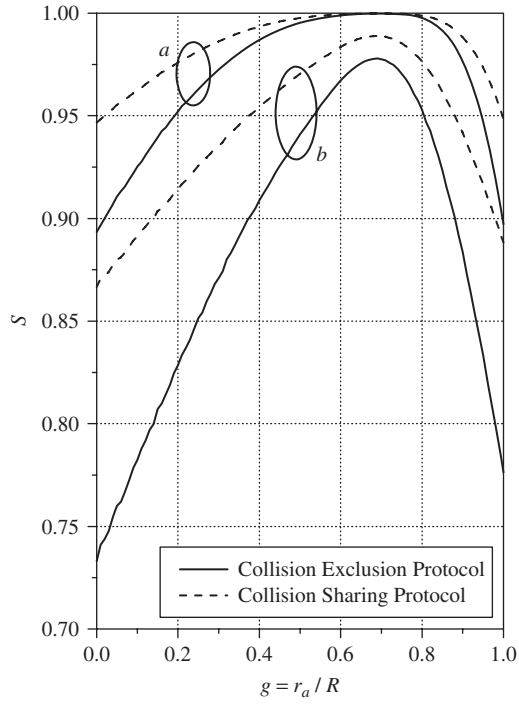

Figure 12.58 Average intercell throughput as a function of normalized distance g for a three-cell scenario and CD protocol: (a) $\sigma_{\beta b} = \sigma_{\beta c} = 3\,\text{dB}$; (b) $\sigma_{\beta b} = \sigma_{\beta c} = 8\,\text{dB}$; $\sigma_{b+d} = \sigma_{c+d} = \sigma_c = \sigma_d = 1$ $\theta = -60°$: $\alpha = 5$; $\varepsilon = 0.5$.

Similarly, it can be shown that for users a and c, Equation (12.70) may be written as

$$i_c = \frac{\xi_{c+d_c}\beta_{c+d_c}}{\xi_c\beta_c}\left(\frac{|0.5-g|}{\sqrt{4-4g\cos(\theta+\pi/3)+g^2}}\right)^{\alpha} = \frac{\xi_{c+d_c}\beta_{c+d_c}}{\xi_c\beta_c} f_c(\theta)$$

$$f_c(\theta) = \left(\frac{|0.5-g|}{\sqrt{4-4g\cos(\theta+\pi/3)+g^2}}\right)^{\alpha} \tag{12.77}$$

since $r_c = |R/2 - r_a|$. The probability density function for the variable i_c is

$$p_c(x) = \int_0^{+\infty} p_{\beta 2}(x/z)\, p_{\xi f_c}(z)/z \cdot \mathrm{d}z \tag{12.78}$$

where

$$p_{\xi f_c}(x) = \frac{1}{f_c(\theta)} p_{\xi_{c1}}(x/f_c(\theta)) \tag{12.79}$$

$$p_{\xi_{c1}}(x) = \frac{2\sigma_{c+d}^2\sigma_c^2 x}{(\sigma_{c+d}^2 + \sigma_c^2 x^2)^2} \tag{12.80}$$

Now the probability density function of $i_b + i_c$ is

$$p(x) = \int_0^x p_b(x-u)\,p_c(u)\,\mathrm{d}u \tag{12.81}$$

The outage probability is, after averaging over θ,

$$P_{\text{out}} = P(i_b + i_c > \varepsilon) = \frac{1}{2\pi}\int_0^{2\pi}\int_{\varepsilon}^{+\infty} p(x)\,\mathrm{d}x\,\mathrm{d}\theta \tag{12.82}$$

12.11 APPENDIX 12B: AVERAGE INTERCELL THROUGHPUT

$$\begin{aligned} S &= \sum_{k=0}^{N}\left(1-\frac{k}{N}\right)\underbrace{\binom{N}{k}P_{\text{out}}^{k}(1-P_{\text{out}})^{N-k}}_{p_{\text{out}}(k)} \\ &= \sum_{k=0}^{N}\binom{N}{k}P_{\text{out}}^{k}(1-P_{\text{out}})^{N-k} - \frac{1}{N}\sum_{k=0}^{N}k\binom{N}{k}P_{\text{out}}^{k}(1-P_{\text{out}})^{N-k} \\ &= 1-\frac{1}{N}\sum_{k=0}^{N}k\binom{N}{k}P_{\text{out}}^{k}(1-P_{\text{out}})^{N-k} \end{aligned} \tag{12.83}$$

The second term may be written as follows:

$$E = \frac{1}{N}\sum_{k=0}^{N}k\binom{N}{k}P_{\text{out}}^{k}(1-P_{\text{out}})^{N-k} \tag{12.84}$$

The first term of the series (with index $k = 0$) has the value 0 since the first factor, k, is zero. It may thus be discarded, i.e. we can change the lower limit to $k = 1$:

$$\begin{aligned} E &= \frac{1}{N}\sum_{k=1}^{N}k\frac{N!}{k!(N-k)!}P_{\text{out}}^{k}(1-P_{\text{out}})^{N-k} \\ &= \frac{1}{N}\sum_{k=1}^{N}k\frac{N(N-1)!}{k(k-1)!(N-k)!}P_{\text{out}}P_{\text{out}}^{k-1}(1-P_{\text{out}})^{N-k} \end{aligned} \tag{12.85}$$

We have pulled factors of N and k out of the factorials, and one power of P_{out} has been split off. We are preparing to redefine the indices:

$$E = \frac{1}{N}N\;P_{\text{out}}\sum_{k=1}^{N}\frac{(N-1)!}{(k-1)!(N-k)!}P_{\text{out}}^{k-1}(1-P_{\text{out}})^{N-k} \tag{12.86}$$

We rename $M = N - 1$ and $s = k - 1$. The value of the sum is not changed by this, but it now becomes readily recognizable. The ensuing sum is a sum over a complete binomial distribution:

$$\begin{aligned} E &= P_{\text{out}}\sum_{s=0}^{M}\frac{M!}{s!(M-s)!}P_{\text{out}}^{s}(1-P_{\text{out}})^{M-s} \\ &= P_{\text{out}}\sum_{s=0}^{M}\binom{M}{s}P_{\text{out}}^{s}(1-P_{\text{out}})^{M-s} = P_{\text{out}}\times 1 = P_{\text{out}} \end{aligned} \tag{12.87}$$

Finally, we have

$$S = 1 - P_{\text{out}} \tag{12.88}$$

REFERENCES

[1] S. Glisic, *Advanced Wireless Communications, 4G Cognitive Broadband Technology*, 2nd edn. John Wiley & Sons, Ltd: London, 2007.

[2] S. G. Glisic and P. Pirinen, Co-channel interference in digital cellular TDMA networks, in *John Wiley Encyclopedia of Telecommunications*, J. Proakis (ed.), John Wiley & Sons, Ltd, 2003.

[3] J. Zander, Asymptotic bounds on the performance of a class of dynamic channel assignment algorithms, *IEEE J. Selected Areas Commun.*, vol. 11, 1993, pp. 926–933.

[4] J. C.-I. Chuang, Performance issues and algorithms for dynamic channel assignment, *IEEE J. Selected Areas Commun.*, vol. 11, 1993, p. 6.

[5] T. J. Kahwa and N. Georganas, A hybrid channel assignment scheme in large scale cellular-structured mobile communication systems, *IEEE Trans. Commun.*, vol. COM-26, 1978, pp. 432–438.

[6] J. Sin and N. Georganas, A simulation study of a hybrid channel assignment scheme for cellular land mobile radio systems with Erlang C service, *IEEE Trans. Commun.*, vol. COM-9, 1981, pp. 143–147.

[7] D. Cox and D. O. Reudink, Increasing channel occupancy in large scale mobile radio systems: dynamic channel reassignment, *IEEE Trans. Vehicular Technol.*, vol. VT-22, 1973, pp. 218–222.

[8] D. Cox and D. O. Reudink, A comparison of some non-uniform spatial demand profiles on mobile radio system performance, *IEEE Trans. Commun.*, vol. COM-20, 1972, pp. 190–195.

[9] D. C. Cox and D. O. Reudink, Dynamic channel assignment in two-dimensional large-scale mobile radio systems, *Bell Systems Technol. J.*, vol. 51, 1972, pp. 1611–1628.

[10] M. Zhang and T.-S. Yum, The non-uniform compact pattern allocation algorithm for cellular mobile systems, *IEEE Trans. Vehicular Technol.*, vol. VT-40, 1991, pp. 387–391.

[11] S.-H. Oh *et al*., Prioritized channel assignment in a cellular radio network, *IEEE Trans. Commun.*, vol. 40, 1992, pp. 1259–1269.

[12] T. Anderson, A simulation study of some dynamic channel assignment algorthms in high capacity mobile telecommunications system, *IEEE Trans. Vehicular Technol.*, vol. VT-22, 1973, p. 210.

[13] J. S. Engel and M. Peritsky, Statistically optimum dynamic server assignment in systems with interfering servers, *IEEE Trans. Vehicular Technol.*, vol. VT-22, 1973, pp. 203–209.

[14] M. Zhang, Comparisons of channel assignment strategies in cellular mobile telephone systems, *IEEE Trans. Vehicular Technol.*, vol. VT-38, 1989, pp. 211–215.

[15] R. Singh, S. M. Elnoubi and C. Gupta, A new frequency channel assignment algorithm in high capacity mobile communications systems, *IEEE Trans. Vehicular Technol.*, vol. VT-31, 1982.

[16] P. John, An insight into dynamic channel assignment in cellular mobile communication systems, *Eur. J. Opl Res.*, vol. 74, 1994, pp. 70–77.

[17] S. Tekinay and B. Jabbari, Handover and channel assignment in mobile cellular networks, *IEEE Commun. Mag.*, vol. 29, 1991.

[18] T.-S. P. Yum and W.-S. Wong, Hot spot traffic relief in cellular systems, *IEEE J. Selected Areas Commun.*, vol. 11, 1993, pp. 934–940.

[19] S. Kuek, Ordered dynamic channel assignment scheme with reassignment in highway microcell, *IEEE Trans. Vehicular Technol.*, vol. 41, 1992, pp. 271–277.
[20] K. Okada and F. Kubota, On dynamic channel assignment in cellular mobile radio systems, in *Proc. IEEE Int. Symp. Circuits and Systems*, vol. 2, 1991, pp. 938–941.
[21] K. Okada and F. Kubota, On dynamic channel assignment strategies in cellular mobile radio systems, *IEICE Trans. Fundamentals*, vol. 75, 1992, pp. 1634–1641.
[22] D. Cox and D. Reudink, A comparison of some channel assignment strategies in large mobile communication systems, *IEEE Trans. Commun.*, vol. 20, 1972, pp. 190–195.
[23] D. Cox and D. Reudink, Dynamic channel assignment in high capacity mobile communications systems, *Bell Systems Technol. J.*, vol. 50, 1971, pp. 1833–1857.
[24] K. Okada and F. Kubota, A proposal of a dynamic channel assignment strategy with information of moving directions, *IEICE Trans. Fundamentals*, vol. E75-a, 1992, pp. 1667–1673.
[25] V. Akaiwa and H. Andoh, Channel segregation – a self organized dynamic allocation method: application to TDMA/FDMA microcellular system, *J. Selected Areas Commun.*, vol. 11, 1993, pp. 949–954.
[26] V. Prabhl and S. S. Rappaport, Approximate analysis of dynamic channel assignment in large systems with cellular structure, *IEEE Trans. Commun.*, vol. 22, 1974, pp. 1715–1720.
[27] D. Hong and S. Rappaport, Traffic modelling and performance analysis for cellular mobile radio telephone systems with prioritized and nonprioritized handoff procedures, *IEEE Trans. Vehicular Technol.*, vol. VT-35, 1986, pp 77–92.
[28] Y. Furuya and V. Akaiwa, Channel segregation – a distributed channel allocation scheme for mobile communication systems, *IEICE Trans.*, vol. 74, 1991, pp. 1531–1537.
[29] J. Vucetic, A hardware implementation of channel allocation algorithm based on a space–bandwidth model of a cellular network, *IEEE Trans. Vehicular Technol.*, vol. 42, 1993, pp. 444–455.
[30] D. Cox and D. Reudink, Increasing channel occupancy in large scale mobile radio systems: dynamic channel reassignment, *IEEE Trans. Commun.*, vol. 21, 1973, pp. 1302–1306.
[31] W. Yue, Analytical methods to calculate the performance of a cellular mobile radio communication system with hybrid channel assignment, *IEEE Trans. Vehicular Technol.*, vol. VT-40, 1991, pp. 453–459, 1991.
[32] J. Tajime and K. Imamura, A strategy for flexible channel assignment in mobile communication systems, *IEEE Trans. Vehicular Technol.*, vol. VT-37, 1988, pp. 92–103.
[33] S. W. Halpern, Reuse partitioning in cellular systems, *IEEE Trans. Vehicular Technol.*, 1983, pp. 322–327.
[34] J. Zande and J. Frodigh, Capacity allocation and channel assignment in cellular radio systems using reuse partitioning, *Electronic Lett.*, vol. 28, 1991.
[35] T. Kanai, Autonomous reuse partitioning in cellular systems, in *Proc. IEEE Vehicular Technol. Conf.*, 1992, pp. 782–785.
[36] S. Onoe and S. Yasuda, Flexible re-use for dynamic channel assignment in mobile radio systems, in *Proc. IEEE ICC*, 1989, pp. 472–476.
[37] S. Verdu and S. Shamai(Shitz), Spectral efficiency of CDMA with random spreading, *IEEE Trans. Information Theory*, vol. 45, March 1999, pp. 622–640.
[38] T. Takenaka, T. Nakamura and V. Tajima, All-channel concentric allocation in cellular systems, in *Proc. IEEE ICC'93*, 1993, pp. 920–924.
[39] K. Madani and A. H. Aghvami, Performance of distributed control channel allocation (DCCA) under uniform and non-uniform traffic conditions in microcellular radio communications, in *Proc. IEEE ICC*, 1994.
[40] K. Madani and A. H. Aghvami, Investigation of handover in distributed control channel allocation (DCCA) for microcellular radio systems, *PIMRC*, 1994, p. 82.1.
[41] A. Gamst, Some lower bounds for a class of frequency assignment problems, *IEEE Trans. Vehicular Technol.*, vol. 35, 1986.

[42] J. B. Punt and D. Sparreboom, Mathematical models for the analysis of dynamic channel selection or indoor mobile wireless communications systems, *PIMRC*, vol. E6.5, 1994, pp. 1081–1085.
[43] J. Ward and R. T. Compton, High throughput slotted ALOHA packet radio networks with adaptive 171 arrays, *IEEE Trans. Commun.*, vol. 41, March 1993, pp. 460–470.
[44] A. J. Goldsmith and S.-G. Chua, Variable-rate variable-power MQAM for fading channels, *IEEE Trans. Commun.*, vol. 45, no. 10, October 1997, pp. 1218–1230.
[45] T. Keller and L. Hanzo, Adaptive modulation techniques for duplex OFDM transmission, *IEEE Trans. Vehicular Technol.*, vol. 49, no. 5, September 2000, pp. 1893–1905.
[46] W. Rhee and J. M. Cioffi, Increase in capacity of multiuser OFDM system using dynamic subcarrier allocation, in *Proc. IEEE Vehicular Technol. Conf.*, vol. 2, Fall 2000, pp. 1085–1089.
[47] C. Yih and E. Geraniotis, Adaptive modulation, power allocation and control for OFDM wireless networks, in *Proc. IEEE Int. Symp. Personal, Indoor, Mobile Radio Commun.*, vol. 2, 2000, pp. 819–813.
[48] C. Y. Wong, R. S. Cheng, K. B. Letaief and R. D. Murch, Multiuser OFDM with adaptive subcarrrier, bit and power allocation, *IEEE J. Selected Areas Commun.*, vol. 17, no. 10, October 1999, pp. 1747–1758.
[49] I. Koutsopoulos and L. Tassiulas, Channel-state adaptive techniques for throughput enhancement in wireless broadband networks, in *Proc. IEEE INFOCOM 2001*, vol. 2, 2001, pp. 757–766.
[50] F. Rashid-Farrokhi, K. J. R. Liu and L. Tassiulas, Transmit beamforming and power control for cellular wireless systems, *IEEE J. Selected Areas Commun.*, vol. 16, no. 8, October 1998, pp. 1437–1450.
[51] E. Visotsky and U. Madhow, Optimum beamforming using transmit antenna arrays, in *Proc. IEEE Vehicular Technol. Conf.*, vol. 1, 1999, pp. 851–856.
[52] M. Olfat, K. J. R. Liu and F. Rashid-Farrokhi, Low complexity adaptive beamforming and power allocation for OFDM over wireless networks, in *Proc. IEEE Int. Conf. Commun.*, vol. 1, 1999, pp. 523–527.
[53] C. Farsakh and J. A. Nossek, Spatial covariance based downlink beamforming in an SDMA mobile radio system, *IEEE Trans. Commun.*, vol. 46, no. 11, November 1998, pp. 1497–1506.
[54] G. J. Foschini and M. J. Gans, On limits of wireless communications in a fading environment when using multiple antennas, *Wireless Personal Commun.*, vol. 6, no. 3, March 1998, pp. 311–335.
[55] E. Telatar, Capacity of multi-antenna Gaussian channels, *Eur. Trans. Telecommun.*, vol. 10, no. 6, November/December 1999, pp. 585–595.
[56] A. Wyner, Shannon theoretic approach to a Gaussian cellular multiple-access channel, *IEEE Trans. Information Theory*, vol. 40, November 1994, pp. 1713–1727.
[57] C. Berrou *et al*., Near Shannon limit error-correction coding and decoding: Turbo codes, in *Proc. IEEE Int. Conf. Commun.*, Geneva, Switzerland, May 1993, pp. 1064–1070.
[58] J. A. Bondy and U. S. R. Murty, *Graph Theory with Applications*. North-Holland: New York, 1985.
[59] M. Schubert and H. Boche, A unifying theory for uplink and downlink multiuser beamforming, in *Proc. Int. Zurich Sem. Broadband Commun., Access, Transmission, Networking*, 2002, pp. 27.1–27.6.
[60] H. Boche and M. Schubert, SIR balancing for multiuser downlink beamforming – a convergence analysis, *IEEE Int. Conf. Commun.*, vol. 2, 2002, pp. 841–845.
[61] I. Katzela and M. Naghshineh, Channel assignment schemes for cellular mobile telecommunication systems: a comprehensive survey, *IEEE Personal Commun.*, vol. 3, no. 3, June 1996, pp. 10–31.

[62] C. Y. Wong, R. S. Cheng, K. B. Letaief and R. D. Murch, Multiuser OFDM with adaptive subcarrrier, bit and power allocation, *IEEE J. Selected Areas Commun.*, vol. 17, no. 10, October 1999, pp. 1747–1758.

[63] I. Koutsopoulos and L. Tassiulas, Channel-state adaptive techniques for throughput enhancement in wireless broadband networks, in *Proc. IEEE INFOCOM*, vol. 2, 2001, pp. 757–766.

[64] G. Okamoto, *Smart Antenna Systems and Wireless LANs*. Kluwer Academic Publishers: Boston, 1999.

[65] C. Farsakh and J. A. Nossek, Spatial covariance based downlink beam-forming in an SDMA mobile radio system, *IEEE Trans. Commun.*, vol. 46, no. 11, November 1998, pp. 1497–1506.

[66] F. Rashid-Farrokhi, L. Tassiulas and K. J. R. Liu, Joint optimal power control and beamforming in wireless networks using antenna arrays, *IEEE Trans. Commun.*, vol. 46, no. 10, October 1998, pp. 1313–1324.

[67] F. Rashid-Farrokhi, K. J. R. Liu and L. Tassiulas, Transmit beamforming and power control for cellular wireless systems, *IEEE J. Selected Areas Commun.*, vol. 16, no. 8, October 1998, pp. 1437–1450.

[68] F. Shad, T. D. Todd, V. Kezys and J. Litva, Dynamic slot allocation (DSA) in indoor SDMA/TDMA using a smart antenna basestation, *IEEE/ACM Trans. Networking*, vol. 9, no. 1, February 2001.

[69] H. Yin and H. Liu, An SDMA protocol for wireless multimedia networks, *Proc. IEEE ICASSP*, vol. 5, 2000, pp. 2613–2616.

[70] I. Koutsopoulos and L. Tassiulas, Adaptive resource allocation in wireless broadband networks with OFDM signaling, in *Proc. IEEE INFOCOM*, 2002.

[71] T. Fong, P. Henry, K. Leung, X. Qiu and N. Shankaranarayanan, Radio resource allocation in fixed broadband wireless networks, *IEEE Trans. Commun.*, vol. 46, no. 6, June 1998, pp. 806–817.

[72] J. Ward and R. T. Compton, Improving the performance of slotted ALOHA packet radio network with an adaptive array, *IEEE Trans. Commun.*, vol. 40, February 1992, pp. 292–300.

[73] A. Acampora, Wireless ATM: a perspective on issues and prospects, *IEEE Personal Commun.*, August 1996, pp. 8–17.

[74] G. Xu and S. Q. Li, Throughput multiplication of wireless LANs for multimedia services: SDMA protocol design, in *Proc. GLOBECOM*, August 1994, pp. 1326–1332.

[75] F. Shad and T. D. Todd, Capacity of s-aloha protocols using a smart antenna at the basestation, in *9th Int. Symp. Personal, Indoor, and Mobile Radio Commun. (PIMRC'98)*, September 1998, pp. 1101–1105.

[76] A. Sugihara, K. Enomoto and I. Sasase, Throughput performance of a slotted nonpersistent CSMA with an adaptive array, in *Proc. IEEE: Personal, Indoor, and Mobile Radio Commun.*, vol. 2, September 1995, pp. 75–80.

[77] C. Sakr and T. D. Todd, Carrier-sense protocols for packet-switched smart antenna basestations, in *IEEE Int. Conf. Network Protocols*, October 1997, pp. 45–52.

[78] G. Okamoto and G. Xu, Throughput multiplication of wireless LANs for multimedia services: spread spectrum with SDMA, in *IEEE Vehicular Technol. Conf.*, April 1996, pp. 1371–1375.

[79] J. Litva and T. K. Lo, *Digital Beamforming in Wireless Communications*. Artech, Norwood, MA, 1996.

[80] R. T. Compton, *Adaptive Antennas, Concepts and Performance*. Prentice-Hall: Englewood Cliffs, NJ, 1988.

[81] G. T. Okamoto, *Smart Antenna Systems and Wireless LANs*. Kluwer: Norwell, MA, 1998.

[82] F. Shad, T. D. Todd, V. Kezys and J. Litva, Dynamic slot allocation (DSA) in indoor SDMA/TDMA using a smart antenna basestation, *IEEE/ACM Trans. Networking*, vol. 9, no. 1, February 2001.

[83] M. Friese, On the achievable information rate with peak-power-limited orthogonal frequency-division multiplexing, *IEEE Trans. Information Theory*, vol. 46, no. 7, November 2000, pp. 2579–2587.
[84] D. C. Lay, *Linear Algebra and Its Applications*. Addison-Wesley, 1997.
[85] G. J. Foschini, Layered space–time architecture for wireless communication in a fading environment when using multi-element antennas, *Bell Labs Technol. J.*, vol. 2, no. 2, 1996, pp. 41–59.
[86] H. Dai, A. Molisch and H. V. Poor, Downlink capacity of interference-limited MIMO systems with joint detection, *IEEE Trans. Wireless Commun.*, vol. 3, no. 2, March 2004, p. 442.
[87] H. V. Poor and S. Verdu, Probability of error in MMSE multiuser detection, *IEEE Trans. Information Theory*, vol. 43, May 1997, pp. 858–871.
[88] J. Zhang, E. K. P. Chong and D. Tse, Output MAI distributions of linear MMSE multiuser receivers in CDMA systems, *IEEE Trans. Information Theory*, vol. 47, May 2001, pp. 1128–1144.
[89] I. Medvedev and V. Tarokh, A channel-shortening multiuser detector for DS-CDMA systems, in *Proc. IEEE Vehicular Technol. Conf.*, vol. 3, Rhodes, Greece, May 2001, pp. 1834–1838.
[90] M. Varanasi, Decision feedback multiuser detection: a systematic approach, *IEEE Trans. Information Theory*, vol. 45, January 1999, pp. 219–240.
[91] S. L. Ariyavisitakul, Turbo space–time processing to improve wireless channel capacity, *IEEE Trans. Commun.*, vol. 48, August 2000, pp. 1347–1359.
[92] S. Catreux, P. F. Driessen and L. J. Greenstein, Simulation results for an interference-limited multiple-input multiple-output cellular system, *IEEE Commun. Lett.*, vol. 4, November 2000, pp. 334–336.
[93] J. Hagenauer *et al*., Iterative decoding of binary block and convolutional codes, *IEEE Trans. Information Theory*, vol. 42, March 1996, pp. 429–445.
[94] H. V. Poor, Turbo multiuser detection: a primer, *J. Commun. Networks*, vol. 3, no. 3, September 2001, pp. 196–201.
[95] S. Shamai and A. Wyner, Information theoretic considerations for symmetric, cellular multiple-access fading channels. Parts I and II, *IEEE Trans. Information Theory*, vol. 43, November 1997, pp. 1877–1911.
[96] A. Van Zelst, R. Van Nee and G. A. Awater, Turbo-BLAST and its performance, in *Proc. IEEE Vehicular Technol. Conf.*, vol. 2, Rhodes, Greece, May 2001, pp. 1282–1286.
[97] X. Wang and H. V. Poor, Iterative (turbo) soft interference cancellation and decoding for coded CDMA, *IEEE Trans. Commun.*, vol. 47, July 1999, pp. 1046–1061.
[98] X. Wang and H. V. Poor, Space–time multiuser detection in multipath CDMA channels, *IEEE Trans. Signal Processing*, vol. 47, September 1999, pp. 2356–2374.
[99] F. Borgonovo, M. Zorzi, L. Fratta, V. Trecordi and G. Bianchi, Capture-division packet access for wireless personal communications, *IEEE J. Selected Areas Commun.*, vol. 14, no. 4, May 1996, pp. 609–622.
[100] S. C. Swales, M. A. Beach, D. J. Edwards and J. P. McGeehan, The performance enhancement of multibeam adaptive base-station antennas for cellular land mobile radio systems, *IEEE Trans. Vehicular Technol.*, vol. 39, no. 1, February 1990, pp. 56–67.
[101] X. Qiu and K. Chawla, Resource assignment in a fixed broadband wireless system, *IEEE Commun. Lett.*, vol. 1, no. 4, July 1997, pp. 108–110.
[102] T. Fong, P. Henry, K. Leung, X. Qiu and N. K. Shankaranarayanan, Radio resource allocation in fixed broadband wireless networks, *IEEE Trans. Commun.*, vol. 46, no. 6, June 1998, pp. 806–818.
[103] K. Leung and A. Srivastava, Dynamic resource allocation for broadband services in fixed wireless networks, in *Proc. MMT'97*, 1998, pp. 301–314.

[104] A. Srivastava, K. Leung and N. K. Shankaranarayanan, Sector based resource allocation for fixed broadband services networks, in *Proc. Vehicular Technol. Conf.*, May 1998, pp. 1680–1684.

[105] S. Glisic, *Advanced Wireless Networks, 4G Technology*. John Wiley & Sons, Ltd: London, 2006.

[106] K. Chawla, and X. Qiu, Quasi-static resource allocation with interference avoidance for fixed wireless systems, *IEEE J. Selected Areas Commun.*, vol. 17, no. 3, March 1999, pp. 493–504.

[107] D. G. Luenberger, *Optimization by Vector Space Methods*. John Wiley & Sons, Inc.: New York, 1969.

[108] T. K. Fong, P. S. Henry, K. K. Leung, X. Qiu and N. K. Shankaranarayanan, Radio resource allocation in fixed broadband wireless networks, *IEEE Trans. Commun.*, vol. 46, June 1998, pp. 806–818.

[109] X. Qiu and K. Chawla, Resource assignment in a fixed wireless system, *IEEE Commun. Lett.*, vol. 1, July 1997, pp. 108–110.

[110] K. K. Leung, and A. Srivastava, Dynamic allocation of downlink and uplink resource for broadband services in fixed wireless networks, *IEEE J. Selected Areas Commun.*, vol. 17, no. 5, May 1999, pp. 990–1006.

[111] V. Tralli, R. Veronesi and M. Zorzi, Power-shaped advanced resource assignment (PSARA) for fixed broadband wireless access systems, *IEEE Trans. Wireless Commun.*, vol. 3, no. 6, November 2004, pp. 2207–2220.

[112] V. Tralli, R. Veronesi and M. Zorzi, Resource allocation with power-shaping in TDMA-based mobile radio systems, in *Proc. IEEE PIMRC*, vol. 1, September 2002, pp. 354–358.

[113] X. Qiu and K. Chawla, Resource assignment in a fixed broadband wireless system, *IEEE Commun. Lett.*, vol. 1, July 1997, pp. 108–110.

[114] X. Qiu and K. Chawla, Intra-cell interference management for fixed broadband wireless systems, in *Proc. 48th IEEE Vehicular Technol. Conf.*, vol. 2, 1998, pp. 914–919.

[115] N. Milosevic, B. Lorenzo, S. Glisic and Z. Nikolic, Intercell Cooperative Dynamic Radio Resource Allocation, submitted to PIMRC'09.

13

Ad Hoc *Networks*

13.1 ROUTING PROTOCOLS

Self-organizing wireless networks composed of mobile nodes and requiring no fixed infrastructure will be referred to as mobile *ad hoc* networks (MANET). These networks are characterized by dynamic topology. In other words, nodes can join or leave the network as well as being able to change the range of their transmissions. Each node acts as an independent router. Because of the wireless mode of communication, links will be bandwidth-constrained and of variable capacity. In addition, there will be limited transmitter range, energy-limitations and limited physical security. MAC and network protocols are of a distributed nature. Also, complex routing protocols with large transmission overheads and large processing loads on each node will be used.

Dynamic topology is illustrated in Figure 13.1. Node mobility creates a dynamic topology, i.e. changes in the connectivity between the nodes as a direct function of the distance between each other, the characteristics of the area where they are deployed and, of course, the power of their transmitters. Node mobility and architecture reconfigurability in *ad hoc* networks have had a major effect on the design of routing protocols. MANETs are used for military applications and rescue and recovery scenarios, in local areas like offices, building WLANs, home networks, robot networks, sensor networks and personal Area networking, also for interconnection of wireless devices like games, and habitat, wildlife and micro climate monitoring.

Based on the above characteristics of MANET the routing protocols should be distributed, based on both uni- and bi-directional links, energy efficient and secure. Performance metrics include:

(1) data throughput, i.e. how well the network delivers packets from the source to destination;

(2) delay, e.g. end-to-end delay of packet delivery;

(3) overhead costs, i.e. average of control packets produced per node;

(4) power consumption, i.e. average power used by each node.

Two classes of routing protocols are considered for these applications, proactive and reactive routing. Proactive routing, illustrated in Figure 13.2, maintains routes to every other node in the network. This is a table-driven protocol where regular routing updates impose large overhead.

Advanced Wireless Technologies: Cognitive, Cooperative & Opportunistic 4G Technology Second Edition Savo G. Glisic

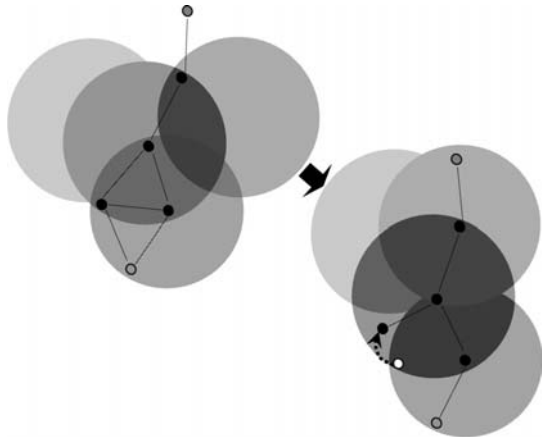

Figure 13.1 Illustration of dynamic topology.

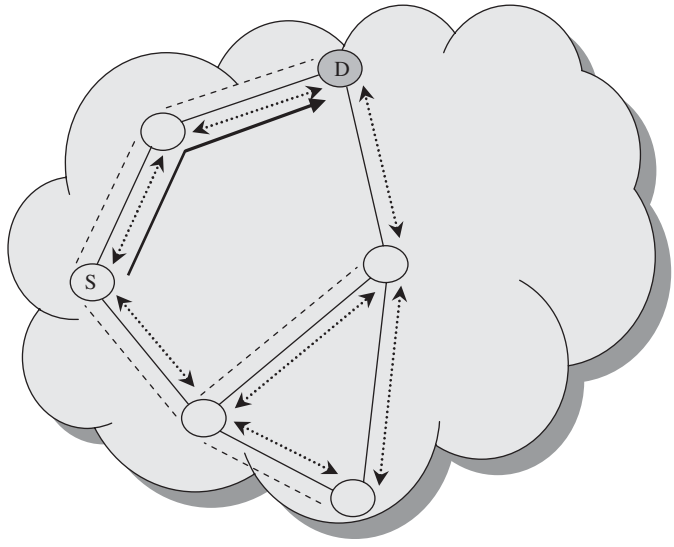

Figure 13.2 Proactive/timer: route updates (◂·····▸), routes (------) and data (——▸).

On the other hand, there is no latency in route discovery, i.e. data can be sent immediately. The drawback is that most routing information might never be used. These protocols are suitable for high traffic networks and most often are based on Bellman–Ford type algorithms. Reactive routing, illustrated in Figure 13.3 maintains routes to only those nodes which are needed. The cost of finding routes is expensive since flooding is involved. Owing to the nature of the protocol, there might be a delay before transmitting data. The protocol may not be appropriate for real-time applications but is good for low/medium traffic networks.

When the network topology is changed, the two protocols will behave differently, as can be seen in Figure 13.4(a, b). Proactive/timer-based protocol must wait for the updates to be transmitted and processed and for new routing tables to be built. For reactive/on demand protocol a new route request is sent and a new route is found independently.

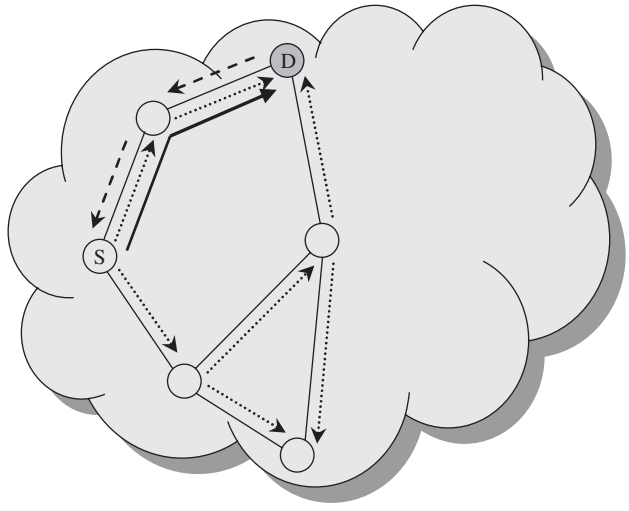

Figure 13.3 Reactive/on demand: route REQ (⟷), route REP (------) and data flow (⟶).

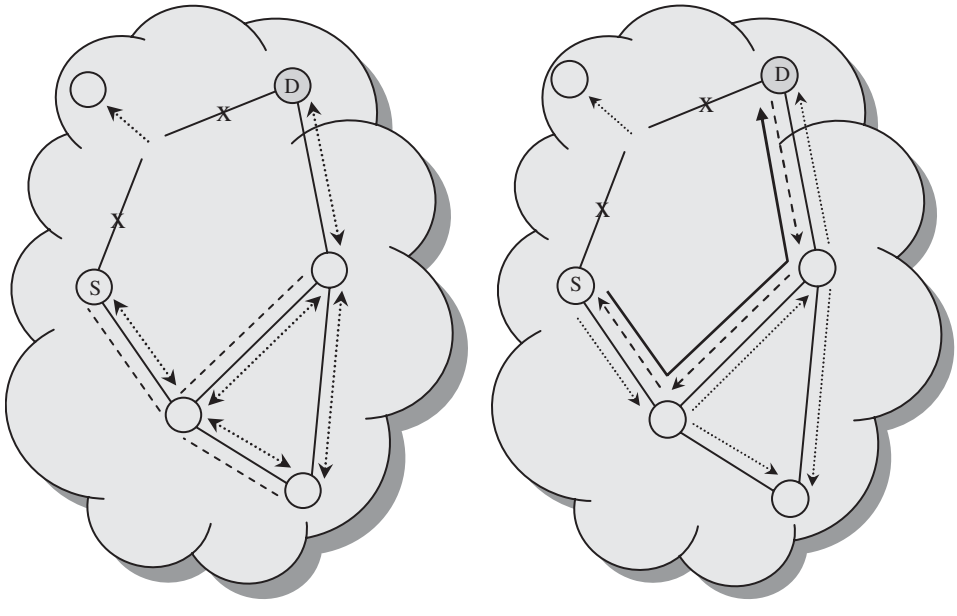

(a) (b)

Figure 13.4 (a) Proactive/timer protocol operation when the topology is changed. (b) Reactive/on demand protocol operation when the topology is changed.

13.1.1 Routing protocols

Classification of *ad hoc* routing protocols, discussed in References [1–24] is given in Figure 13.5. Table-driven routing protocols attempt to maintain consistent, up-to-date routing information from

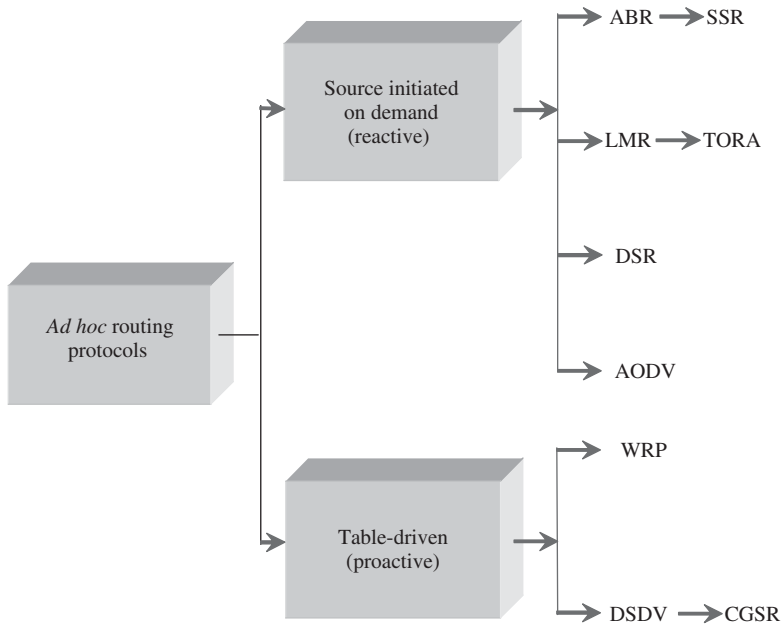

Figure 13.5 Classification of *ad hoc* routing protocols [destination sequenced distance vector (DSDV), clusterhead gateway switch routing (CGSR), wireless routing protocol (WRP), *ad hoc* on-demand distance vector (AODV), dynamic source routing (DSR), temporally ordered routing algorithm (TORA), lightweight mobile routing (LMR), signal stability routing (SSR) and associativity based routing (ABR)].

each node to every other node in the network. These protocols require each node to maintain one or more tables to store routing information, and they respond to changes in network topology by propagating updates throughout the network in order to maintain a consistent network view. The areas in which they differ are the number of necessary routing-related tables and the methods by which changes in network structure are broadcast. We start this section by discussing some of the existing table-driven *ad hoc* routing protocols.

13.1.1.1 Destination sequenced distance vector, DSDV

Traditional distance vector algorithms are based on the classical Bellman–Ford (DBF) algorithm discussed in Chapter 7. This algorithm has the drawback that routing loops can occur. To eliminate or minimize the formation of loops the nodes are required to often coordinate and communicate among themselves. The problem is caused by frequent topological changes. The RIP is based on this type of algorithm. The application of RIP to *ad hoc* networks is limited since it was not designed for such an environment. The objective of DSDV protocols is to preserve the simplicity of RIP and avoid the looping problem in a mobile wireless environment. The main features of DSDV are:

- routing tables have entries with number of hops to each network destination;
- each route table entry is tagged with a sequence number originated by the destination;

- nodes periodically communicate their routing table to their neighbors and when there is a significant new information available;
- routing information is normally transmitted using a broadcasting or multicasting mode.

Route tables entry consists of:

(1) destination address;

(2) number of hops required to reach the destination;

(3) sequence number of the information received regarding that destination, as originally stamped by the destination.

Within the headers of the packet, the transmitter route tables usually carry the node hardware address, the network address and the route transmission sequence number. Receiving a transmission from a neighbor does not indicate immediately the existence of a bi-directional link with that neighbor. A node does not allow routing through a neighbor until that neighbor shows that it also has the node as a neighbor. This means that DSDV algorithms use only bi-directional links.

An important parameter value is the time between broadcasting routing information packets. However when any new and substantial route information is received by a mobile node, the updated route information is transmitted as soon as possible.

Broken links are a normal occurrence in *ad hoc* networks. They are detected by the MAC layer or inferred if no transmissions are received from a neighbor for some time. A broken link is given a metric of ∞ and an updated sequence number. A broken link translates into a substantial route change and thus this new routing information is immediately broadcasted to all neighbors. To propagate new routing information, particularly the one generated by broken links, and to avoid large transmission overheads, two types of routing packets are used: (1) full dump – carries all the available information; and (2) incremental – carries only information changed after the last dump. When a node receives a new routing packet the information is compared with the one already available at the node. Routes with a more recent sequence number are always used. Newly computed routes are scheduled for immediate advertisement. The route updating process is illustrated in Figure 13.6.

When A moves and it is detected as a routing neighbor by G and H, it causes these nodes to advertise their updated routing information (incremental update). Upon reception of this update, F updates its own routing tables and broadcasts the new information. D receives this update and carries out an update of its routing table. The steps are illustrated in Figure 13.7.

13.1.1.2 Clusterhead gateway switch routing

The clusterhead gateway switch routing (CGSR) protocol differs from the previous protocol in the type of addressing and network organization scheme employed. Instead of a 'flat' network, CGSR is a clustered multihop mobile wireless network with several heuristic routing schemes [4]. In the next section we will see that, by having a cluster head controlling a group of *ad hoc* nodes, a framework for code separation (among clusters), channel access, routing and bandwidth allocation can be achieved. A cluster head selection algorithm is utilized to elect a node as the cluster head using a distributed algorithm within the cluster. The disadvantage of having a cluster head scheme is that frequent cluster head changes can adversely affect routing protocol performance since nodes are busy in cluster head selection rather than packet relaying. Hence, instead of invoking cluster head reselection every time the cluster membership changes, a least cluster change (LCC) clustering algorithm is introduced. Using LCC, cluster heads only change when two cluster heads come into contact, or when a node moves out of contact of all other cluster heads.

Destination	Next hop	Metric	Sequence no.	Install time
A	B	2	S123_A	T002_D
B	B	1	S137_B	T001_D
C	B	2	S201_C	T003_D
D	D	0	S312_D	T001_D
E	F	2	S400_E	T005_D
F	F	1	S150_F	T001_D
G	F	2	S111_G	T007_D
H	F	3	S233_H	T007_D
I	I	1	S150_I	T001_D
J	J	1	S130_J	T001_D

D's advertised routing table		
Destination	Metric	Sequence no.
A	2	S123_A
B	1	S137_B
C	2	S201_C
E	2	S312_E
F	1	S150_F
G	2	S111_G
H	3	S233_H
I	1	S150_I
J	1	S130_J

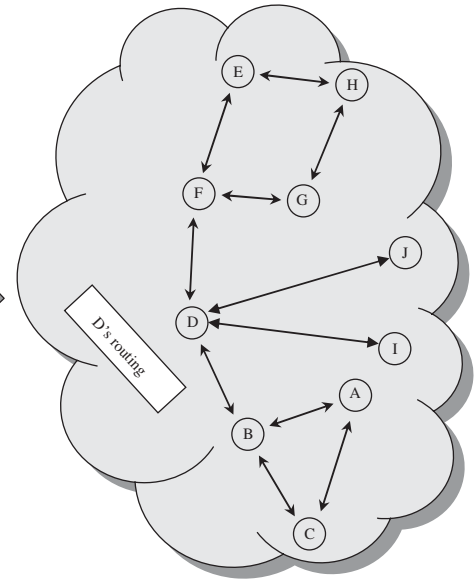

Figure 13.6 Illustration of route updating process. Metric = number of hops to reach destination; sequence number = the freshness of received route, used to avoid routing loops; install time = when a received route was installed, used for damping route fluctuations.

CGSR uses DSDV as the underlying routing scheme, and hence has much of the same overhead as DSDV. However, it modifies DSDV by using a hierarchical cluster-head-to-gate way routing approach to route traffic from source to destination. Gateway nodes are nodes that are within a communication range of two or more cluster heads. A packet sent by a node is first routed to its cluster head, and then the packet is routed from the cluster head to a gateway to another cluster head, and so on until the cluster head of the destination node is reached. The packet is then transmitted to the destination. Using this method, each node must keep a "cluster member table" where it stores the destination cluster head for each mobile node in the network. These cluster member tables are broadcast by each node periodically using the DSDV algorithm. Nodes update their cluster member tables on reception of such a table from a neighbor.

In addition to the cluster member table, each node must also maintain a routing table which is used to determine the next hop in order to reach the destination. On receiving a packet, a node will consult its cluster member table and routing table to determine the nearest cluster head along the route to the destination. Next, the node will check its routing table to determine the next hop used to reach the selected cluster head. It then transmits the packet to this node.

13.1.1.3 The wireless routing protocol

The wireless routing protocol (WRP) described in Murthy and Garcia-Luna-Aceves [5] is a table-based protocol with the goal of maintaining routing information among all nodes in the network. Each node in the network is responsible for maintaining four tables: (1) distance table; (2) routing table; (3) link-cost table; and (4) message retransmission list (MRL) table.

D's updated routing table				
Destination	Next hop	Metric	Sequence no.	Install time
A	**F**	**4**	**S412_A**	**T509_D**
B	B	1	S137_B	T001_D
C	B	2	S201_C	T003_D
D	D	0	S312_D	T001_D
E	F	2	S400_E	T005_D
F	F	1	S150_F	T001_D
G	F	2	S111_G	T007_D
H	F	3	S233_H	T007_D
I	I	1	S150_I	T001_D
J	J	1	S130_J	T001_D

D's updated advertised routing table		
Destination	Metric	Sequence no.
A	**3**	**S412_A**
B	1	S137_B
C	2	S201_C
E	2	S400_E
F	1	S150_F
G	2	S111_G
H	3	S233_H
I	1	S150_I
J	1	S130_J

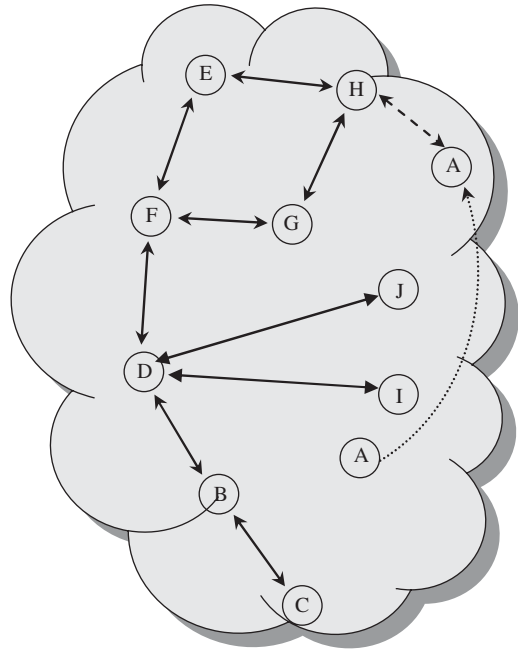

Figure 13.7 Illustration of route updating process after A moves.

Each entry of the MRL contains the sequence number of the update message, a retransmission counter, an acknowledgment-required flag vector with one entry per neighbor, and a list of updates sent in the update message. The MRL records which updates in an update message need to be retransmitted and which neighbors should acknowledge the retransmission [5].

Mobiles inform each other of link changes through the use of update messages. An update message is sent only between neighboring nodes and contains a list of updates (the destination, the distance to the destination and the predecessor of the destination), as well as a list of responses indicating which mobiles should acknowledge (ACK) the update. Mobiles send update messages after processing updates from neighbors or detecting a change in a link to a neighbor. In the event of the loss of a link between two nodes, the nodes send update messages to their neighbors. The neighbors then modify their distance table entries and check for new possible paths through other

nodes. Any new paths are relayed back to the original nodes so that they can update their tables accordingly. Nodes learn of the existence of their neighbors from the receipt of acknowledgments and other messages. If a node is not sending messages, it must send a hello message within a specified time period to ensure connectivity. Otherwise, the lack of messages from the node indicates the failure of that link. This may cause a false alarm. When a mobile receives a hello message from a new node, that new node is added to the mobile's routing table, and the mobile sends the new node a copy of its routing table information. Part of the novelty of WRP stems from the way in which it achieves loop freedom. In WRP, routing nodes communicate the distance and second-to-last hop information for each destination in the wireless networks. WRP belongs to the class of path-finding algorithms with an important exception. It avoids the 'count-to-infinity' problem [6], also discussed in Chapter 7, by forcing each node to perform consistency checks of predecessor information reported by all its neighbors. This ultimately (although not instantaneously) eliminates looping situations and provides faster route convergence when a link failure event occurs.

13.1.2 Reactive protocols

13.1.2.1 Dynamic source routing (DSR)

In this case every packet carries the routing sequence. Intermediate nodes may learn routes from 'heard' traffic (RREQ, RREP, DATA). No periodic sending of routing packets occurs. The system may piggyback route requests on route replies and must use link layer feedback to find broken links. To send a packet the sender constructs a *source route* in the packet's header.

The source route has the address of every host through which the packet should be forwarded to reach its destination. Each host in the *ad hoc* network maintains a *route cache* in which it stores source routes it has learned. Each entry in the route cache has an expiration period, after which it will be deleted. If the sender does not have a route to a destination it then attempts to find out by using a *routing discovery* process. This process is illustrated in Figures 13.8–13.10. While waiting for the routing discovery to complete, the sender continues sending and receiving packets with other hosts. Each host uses a *route maintenance* procedure to monitor the correct operation of a route.

Usually the data link layer has a mechanism to detect a link failure. When a link failure is detected the host sends a *route error packet* to the original sender of the packet. The route error packet has the address of the host who detected the failure and the host to which it was attempting to transmit the packet. When a route error packet is received by a host, the hop in error is removed from the host's route cache, and all routes which contain this hop are truncated at that point.

To return the route error packet the host uses a route in its route cache to the sender of the original packet. If the host does not have a route it can reverse the route information carried in the packet that could not be forwarded because of the link error. The later assumes that only bidirectional links are being used for routing. Another option to return route error packets is to perform a route discovery process to find a route to the original sender and use that route. Several optimizations are possible to reduce the amount of overhead traffic.

13.1.2.2 Route cache

During the process of route discovery and maintenance a host receives, directly or indirectly, information about routes to other hosts, thus minimizing the need to search for that information in the future. For example in the *ad hoc* network shown in Figure 13.11 let us assume that node A1 performs a route discovery to A5.

Since hosts A2, A3 and A4 are on the route to A5, host A1 also learns the routes to A2, A3 and A4. Likewise, these 'intermediate hosts' learn about routes to each other by looking into the content of the route reply packet.

13.1.2.3 Piggybacking on route discoveries

To minimize the delay in delivering a data packet when there is no route to the destination and a route discovery process is needed, one can piggyback the data on the route request packets.

13.1.2.4 Learning by 'listening'

If the host operate in promiscuous receiving mode, i.e. they receive and process every transmission in their range, then they can obtain substantial information about routing, e.g. in the network in Figure 13.12. Nodes A2, A3 and A5 listen to the route error packet from A4 to A1. Since the

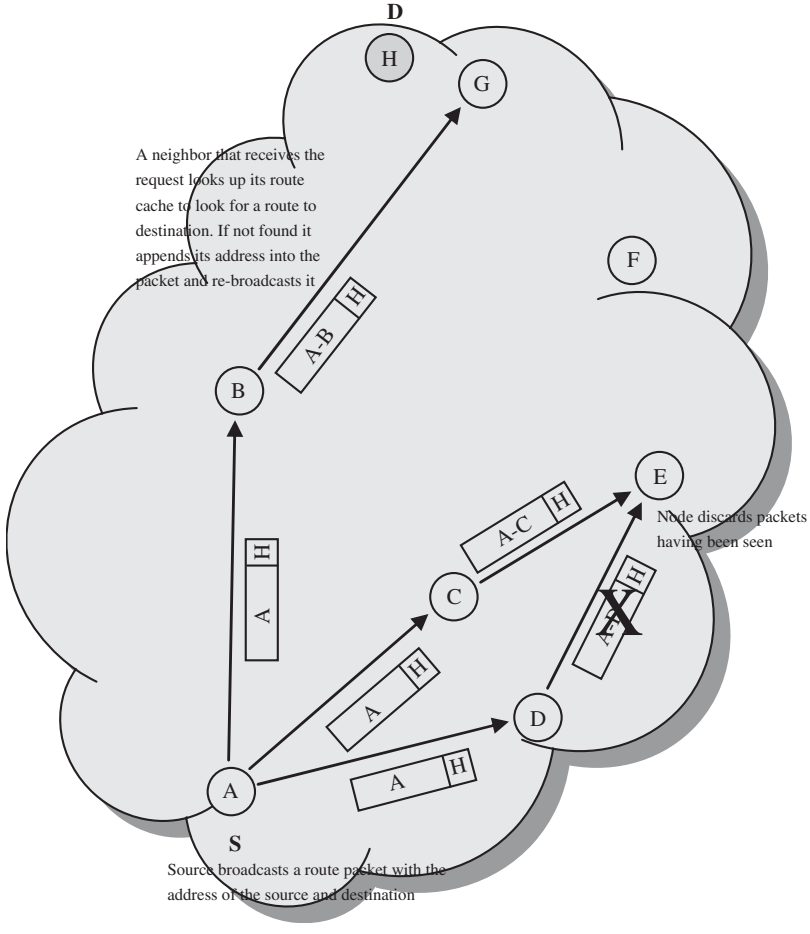

Figure 13.8 DSR – route discovery.

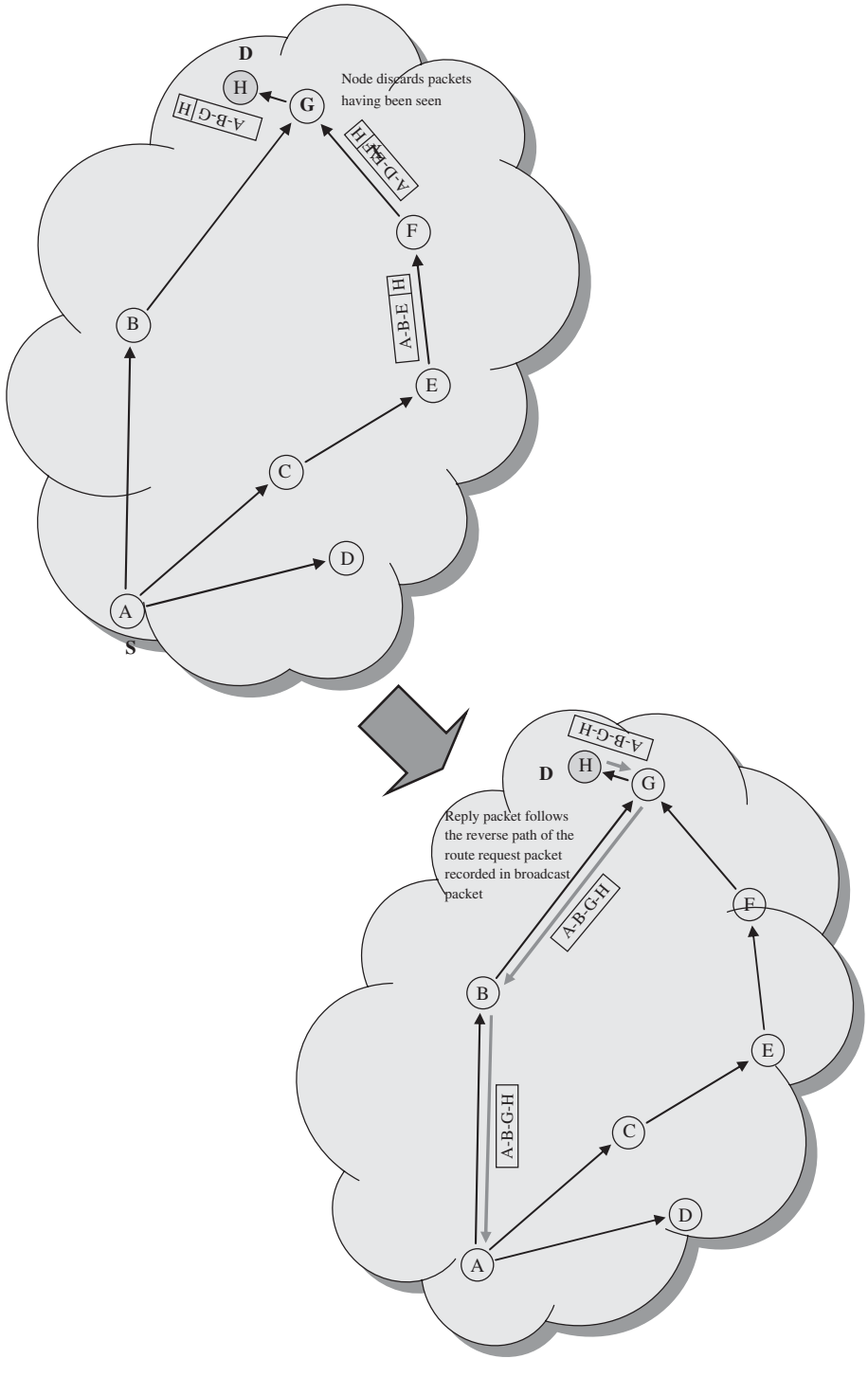

Figure 13.8 *(continued.)*

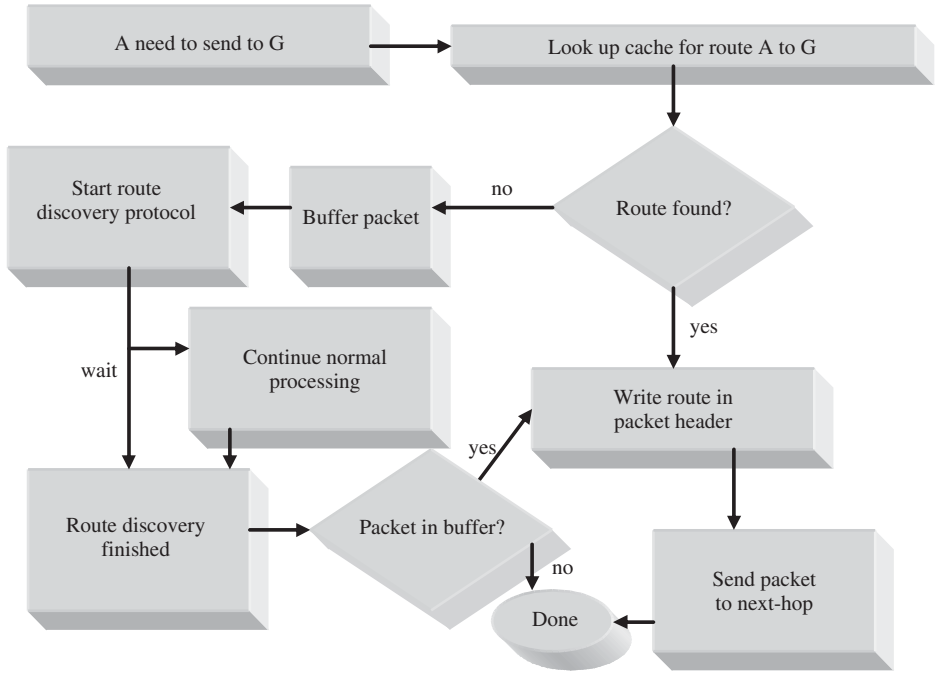

Figure 13.9 DSR – route discovery decision process at source A.

route error packet identifies precisely the hop where the failure was detected, hosts B, C and D can update their route cache with this information.

In summary, SDR is an on-demand protocol, with potentially zero control message overhead if the topology does not change frequently. Packet delays/jitters are associated with on-demand routing. It can work with unidirectional links as well as bidirectional links. Route caching is used to minimize the route discovery overhead. Promiscuous mode operations can translate in excessive use of power. This is not easily scalable to large networks since the protocol design assumes a small network diameter. The need to place the entire route in the route replies and data packets translates in large on-the-air packet overheads. Protocol allows for the possibility to keep multiple routes to a destination in the route cache. CPU and memory use demands on each host are high, since the routes have to be continuously maintained and updated.

13.1.2.5 Ad-hoc *on demand distance vector (AODV)*

The protocol uses 'traditional' routing tables. Hello messages are sent periodically to identify neighbors. Sequence numbers guarantee freshness. Route requests are sent in the reverse direction, i.e. they only use bi-directional links. The system may use link layer feedback to find broken links. The protocol is based on the destination-sequenced distance-vector (DSDV) algorithm. It provides on-demand route acquisition. Nodes maintain the route cache and use a destination sequence number for each route entry. The protocol does nothing when connection between end points is still valid. The route discovery mechanism, illustrated in Figure 13.13, is initiated by broadcasting a route request packet (RREQ), when a route to new destination is needed.

The neighbors forward the request to their neighbors until either the destination or an intermediate node with a 'fresh enough' route to the destination is located. Route reply packets are

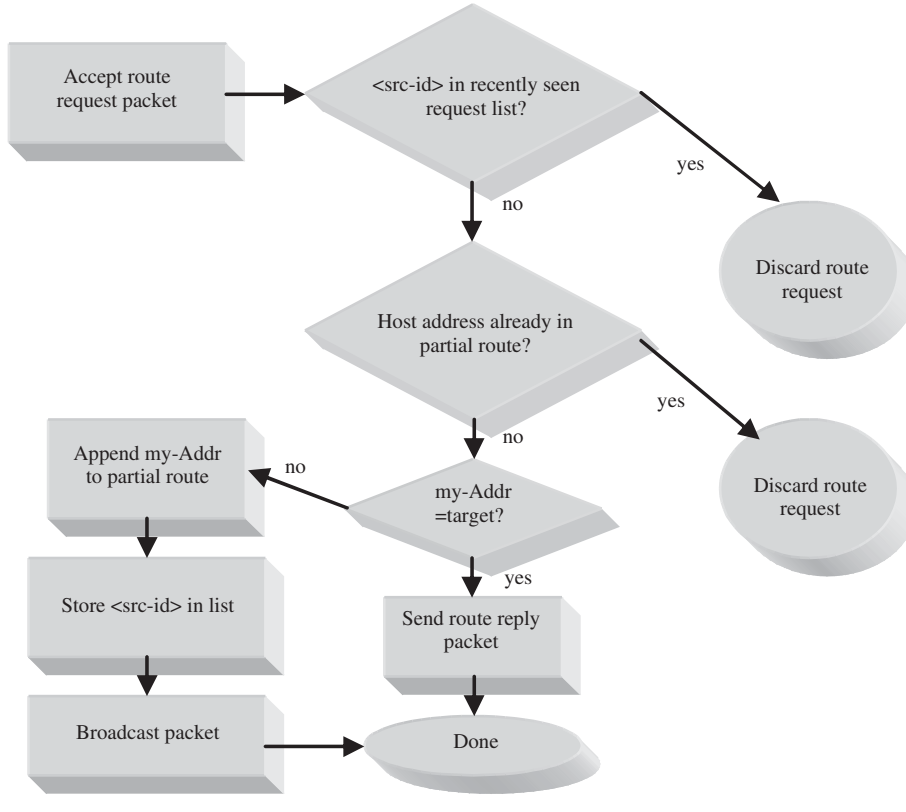

Figure 13.10 DSR – route discovery decision process at an intermediate node.

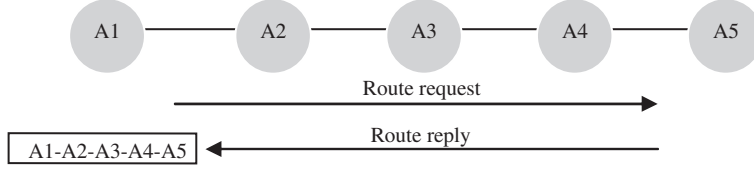

Figure 13.11 DSR – optimizations.

transmitted upstream of the path taken by the route request packet to inform the original sender (an intermediate nodes) of the route finding. Route error packets (RERR) are used to erase broken links.

13.1.2.6 AODV–path maintenance

Periodic hello messages can be used to ensure symmetric links and to detect link failures. Hello messages include a list of nodes that the host has heard of. Once the next hop becomes unavailable the host upstream of the link failure propagates an unsolicited RREP with a hop count of ∞ to all active upstream neighbors. Upon receiving notification of a broken link, a source node can restart the discovery process if they still need a route to destination.

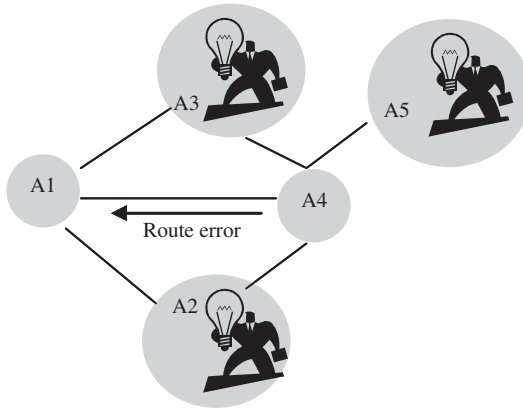

Figure 13.12 Learning about the routes by 'listening'.

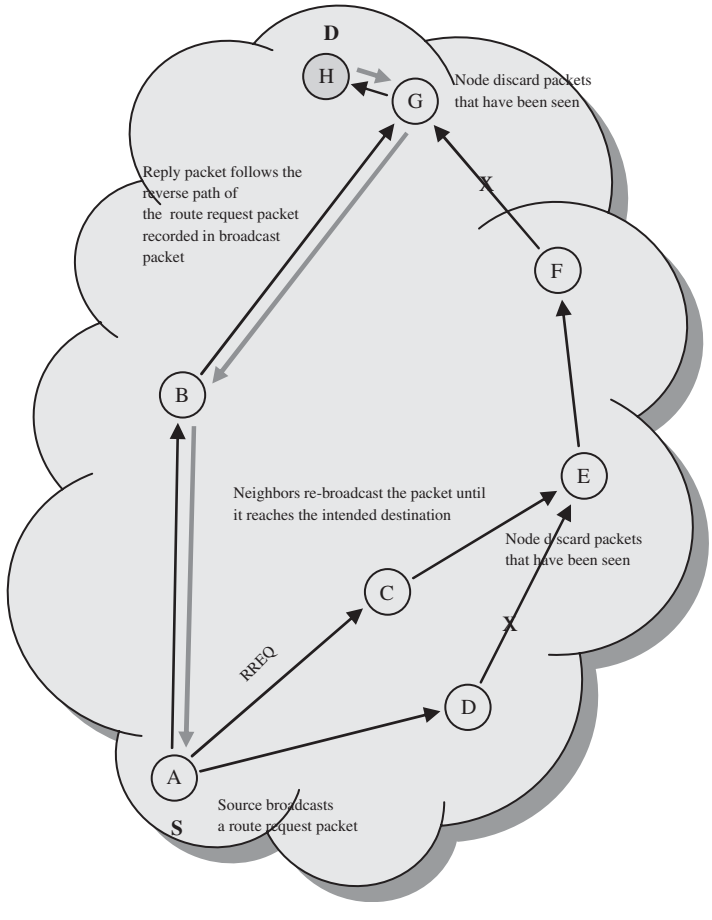

Figure 13.13 AODV – path finding.

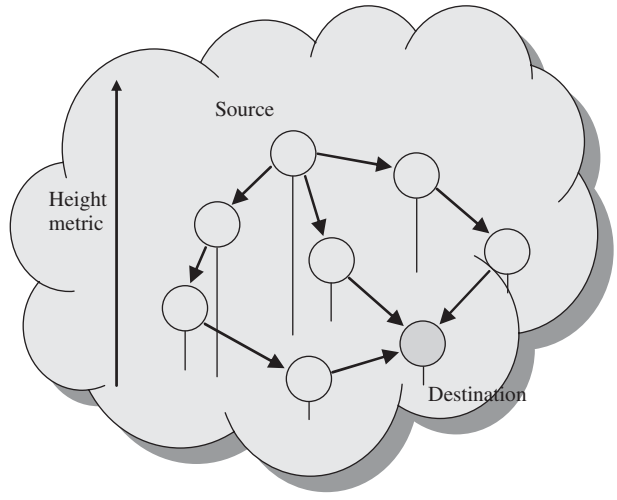

Figure 13.14 TORA.

13.1.2.7 Temporal order routing algorithm (TORA)

TORA is also a distributed protocol. It provides loop-free routes and multiple routes. It is source-initiated and creates routes to destination only when desired.

The protocol minimizes reaction to topological changes, by localizing reaction to a very small group of nodes near the change and provides fast recovery upon route failures. Also, it detects a network partition when there is one and erases all invalid routes within a finite time.

The protocol has three basic functions: route creation, route maintenance and route erasure. During the route creation, nodes use a 'height' metric to build a directed acyclic graph (DAG) rooted at the destination. Links are assigned that have a direction (upstream or downstream) based on the relative height metric of neighboring nodes, as illustrated in Figure 13.14.

From Chapter 7, *G(V, E)* represents the network, where V is the set of nodes and E is the set of links. Each node $i \in V$ is assumed to have a unique identifier (ID), and each link $(i, j) \in E$, is assumed to be bidirectional, i.e. it allows two-way communications. The height metric associated with each node is of the form $Hi = (\tau i, oidi, ri, \delta i, i)$ where:

- τi is the logical time of a link failure, and defines a new reference level;
- $oidi$ is the unique ID of the node that defined the reference level;
- ri denotes two unique sub-levels of a reference level;
- δi is used to order the nodes with respect to a common reference level; and
- i is the unique ID of the node itself.

Each node i (other than the destination) maintains its height Hi. Initially the height is set to NULL, $Hi = [-, -, -, -, i]$. The height of the destination is always ZERO, $H_{\text{dID}} = [0, 0, 0, 0, dID]$. At each node there is a height array with an entry $NH_{i,j}$ for each neighbor $i, \epsilon V$. Initially the height of each neighbor is set to NULL; if a neighbor is a destination its corresponding entry in the height array is set to ZERO.

The operation of TORA protocols is illustrated in Figures 13.15–13.18. The protocols are well suited for networks with large dense populations of nodes. They posses the ability to detect network partitions and erase all invalid routes within a finite time.

Protocol quickly creates and maintains routes for a destination for which routing is desired. It minimizes the number of nodes reacting to topological changes. It needs a synchronization mechanism to achieve a temporal order of events.

13.1.2.8 Associativity-based routing

The associativity based routing (ABR) protocol [12] is free from loops, deadlock and packet duplicates, and defines a different routing metric for *ad hoc* mobile networks. This metric is

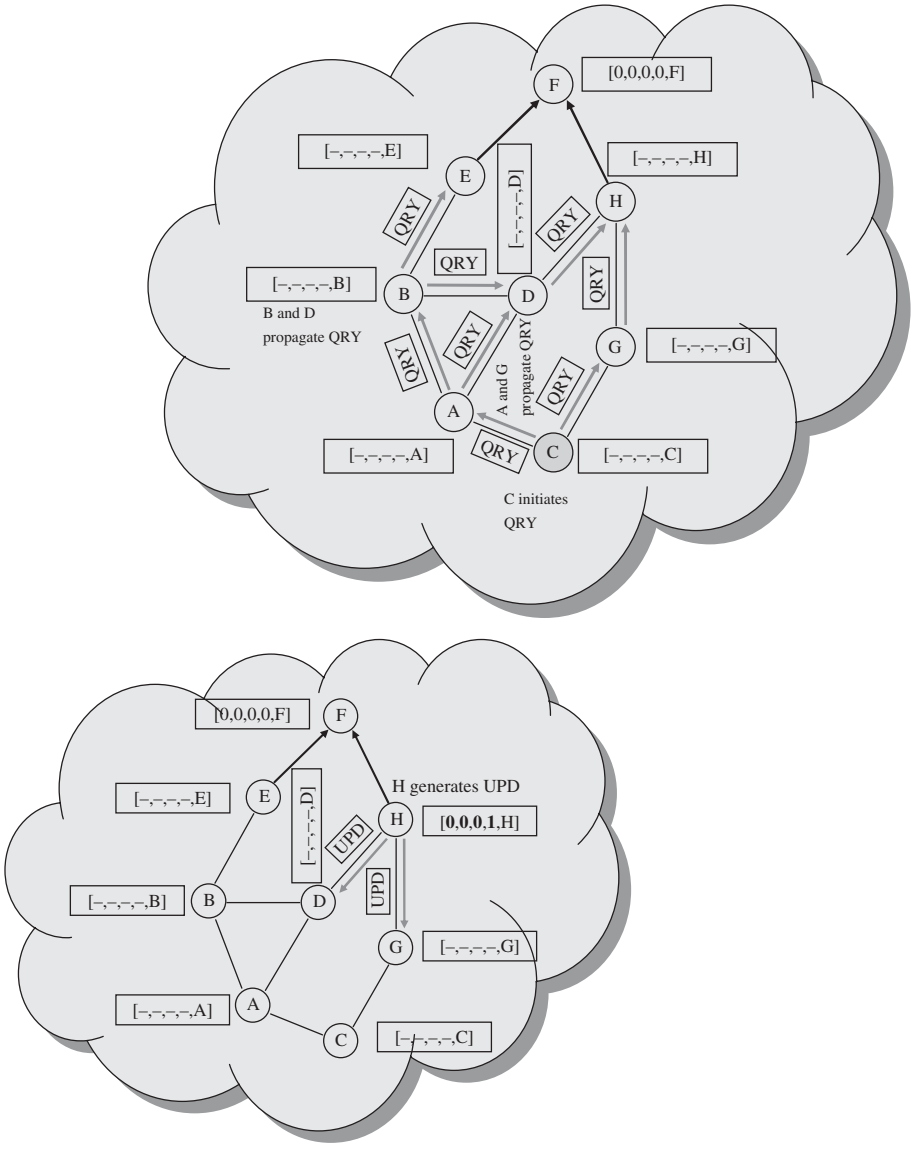

Figure 13.15 TORA – route creation.

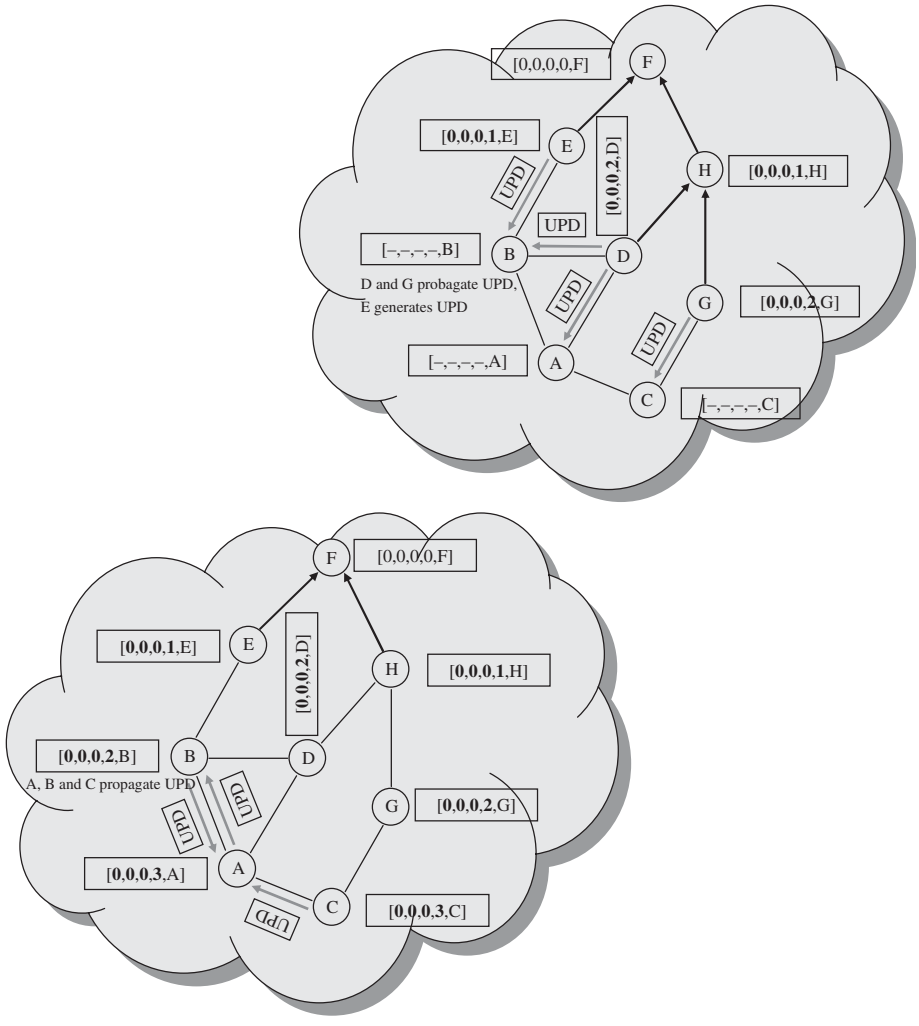

Figure 13.15 *(continued.)*

known as the degree of association stability. In ABR, a route is selected based on the degree of association stability of mobile nodes. Each node periodically generates a beacon to signify its existence. When received by neighboring nodes, this beacon causes their associativity tables to be updated. For each beacon received, the associativity tick of the current node with respect to the beaconing node is incremented. Association stability is defined by connection stability of one node with respect to another node over time and space. A high degree of association stability may indicate a low state of node mobility, while a low degree may indicate a high state of node mobility. Associativity ticks are reset when the neighbors of a node or the node itself move out of proximity. A fundamental objective of ABR is to derive longer-lived routes for *ad hoc* mobile networks.

The three phases of ABR are: (1) route discovery; (2) route reconstruction (RRC); and (3) route deletion. The route discovery phase is accomplished by a broadcast query and await-reply (BQ-REPLY) cycle. A node desiring a route broadcasts a BQ message in search of mobiles

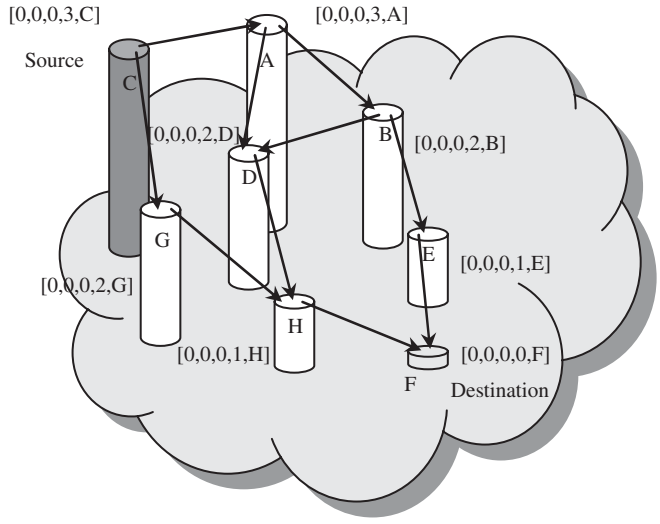

Figure 13.16 TORA – route creation (visualization).

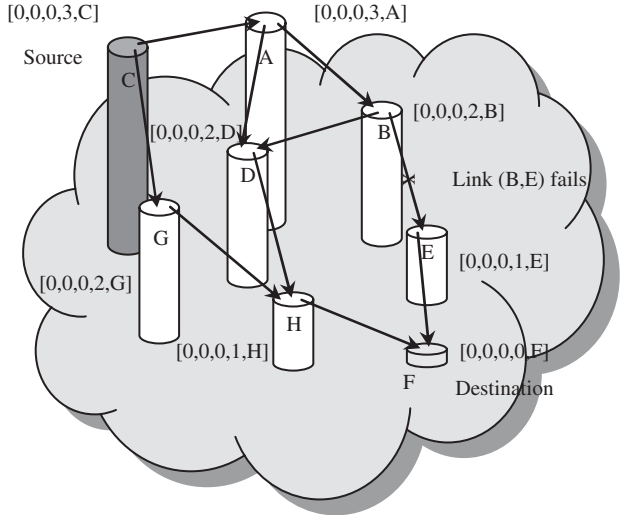

Figure 13.17 TORA – maintaining routes link failure with no reaction.

that have a route to the destination. All nodes receiving the query (that are not the destination) append their addresses and their associativity ticks with their neighbors along with QoS information to the query packet. A successor node erases its upstream node neighbors' associativity tick entries and retains only the entry concerned with itself and its upstream node. In this way, each resultant packet arriving at the destination will contain the associativity ticks of the nodes along the route to the destination. The destination is then able to select the best route by examining the associativity ticks along each of the paths. When multiple paths have the same overall degree of association stability, the route with the minimum number of hops is selected. The destination then sends a REPLY packet back to the source along this path. Nodes propagating the REPLY

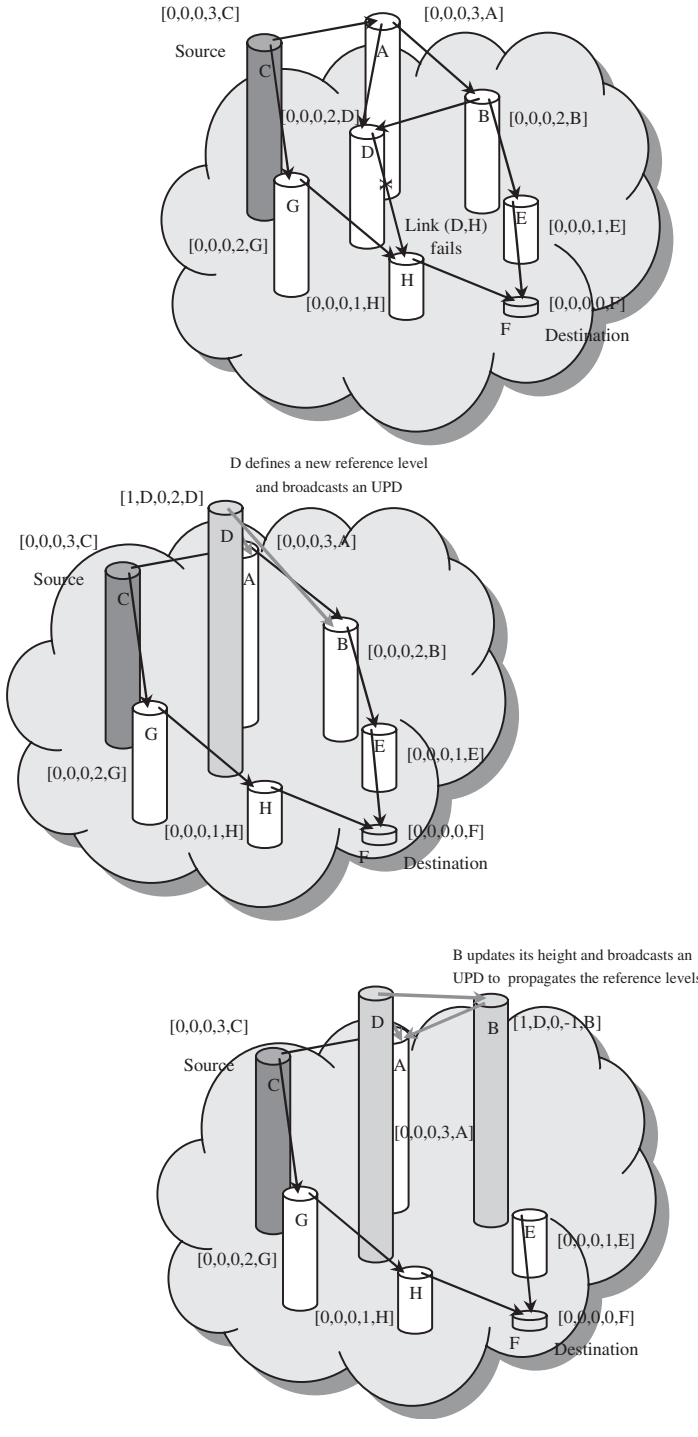

Figure 13.18 TORA – re-establishing routes after link failure of last downstream link.

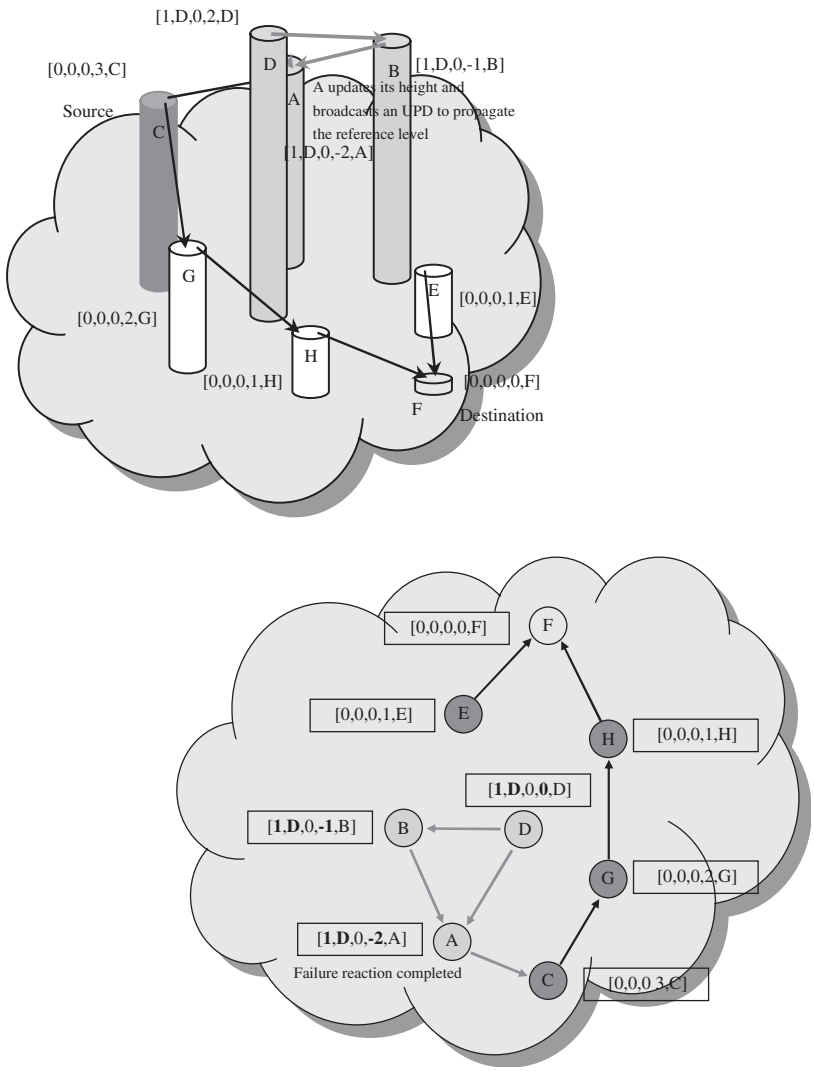

Figure 13.18 *(continued.)*

mark their routes as valid. All other routes remain inactive, and the possibility of duplicate packets arriving at the destination is avoided. RRC may consist of partial route discovery, invalid route erasure, valid route updates and new route discovery, depending on which node(s) along the route move. Movement by the source results in a new BQ-REPLY process. The RN message is a route notification used to erase the route entries associated with downstream nodes. When the destination moves, the immediate upstream node erases its route and determines if the node is still reachable by a localized query (LQ[H]) process, where H refers to the hop count from the upstream node to the destination. If the destination receives the LO packet, it REPLYs with the best partial route; otherwise, the initiating node times out and the process backtracks to the next upstream node. Here an RN message is sent to the next upstream node to erase the invalid route and inform this node that it should invoke the LQ process. If this process results in backtracking more than halfway to

the source, the LO process is discontinued and a new BQ process is initiated at the source. When a discovered route is no longer desired, the source node initiates a route delete (RD) broadcast so that all nodes along the route update their routing tables. The RD message is propagated by a full broadcast, as opposed to a directed broadcast, because the source node may not be aware of any route node changes that occurred during RRCs.

13.1.2.9 Signal stability routing

Another on-demand protocol is the signal stability-based adaptive routing protocol (SSR) presented in Dube *et al.* [13]. Unlike the algorithms described so far, SSR selects routes based on the signal strength between nodes and a node's location stability. This route selection criteria has the effect of choosing routes that have 'stronger' connectivity. SSR can be divided into two cooperative protocols: the dynamic routing protocol (DRP) and the static routing protocol (SRP). The DRP is responsible for the maintenance of the signal stability table (SST) and routing table (RT). The SST records the signal strength of neighboring nodes, which is obtained by periodic beacons from the link layer of each neighboring node. Signal strength may be recorded as either a strong or weak channel. All transmissions are received by, and processed in, the DRP. After updating all appropriate table entries, the DRP passes a received packet to the SRP.

The SRP processes packets by passing the packet up the stack if it is the intended receiver or looking up the destination in the RT and then forwarding the packet if it is not. If no entry is found in the RT for the destination, a route-search process is initiated to find a route. Route requests are propagated throughout the network, but are only forwarded to the next hop if they are received over strong channels and have not been previously processed (to prevent looping). The destination chooses the first arriving route-search packet to send back because it is most probable that the packet arrived over the shortest and/or least congested path. The DRP then reverses the selected route and sends a route-reply message back to the initiator. The DRP of the nodes along the path update their RTs accordingly.

Route-search packets arriving at the destination have necessarily chosen the path of strongest signal stability, since the packets are dropped at a node if they have arrived over a weak channel. If there is no route-reply message received at the source within a specific timeout period, the source changes the PREF field in the header to indicate that weak channels are acceptable, since these may be the only links over which the packet can be propagated. When a failed link is detected within the network, the intermediate nodes send an error message to the source indicating which channel has failed. The source then initiates another route-search process to find a new path to the destination. The source also sends an erase message to notify all nodes of the broken link.

13.2 HYBRID ROUTING PROTOCOL

The zone routing protocol (ZRP) is a hybrid routing protocol that proactively maintains routes within a local region of the network (referred to as the routing zone). Knowledge of this routing zone topology is leveraged by the ZRP to improve the efficiency of a reactive route query/reply mechanism. The ZRP can be configured for a particular network through adjustment of a single parameter, the routing zone radius. A routing zone of radius r is defined for each node and includes the nodes whose minimum distance in hops from a given node is at most r hops. An example of a routing zone (for node S) of radius two hops is shown in Figure 13.19. Nodes within the circle, are said to be within the routing zone of the central node S. Nodes outside the circle are said to be outside S's routing zone. Peripheral nodes are nodes whose minimum distance to S is exactly equal to the zone radius. The remaining nodes are categorized as interior nodes.

For a routing zone of radius r, the number of routing zone nodes can be regulated through adjustments in each node's transmitter power. Subject to the local propagation conditions and

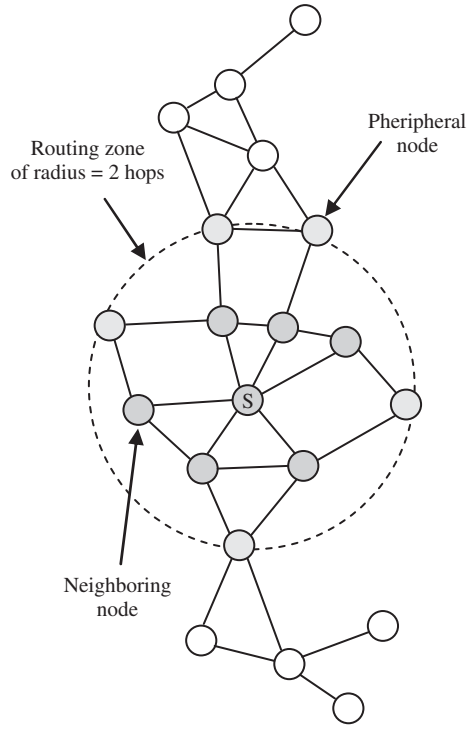

Figure 13.19 A routing zone of radius $r = 2$ hops.

receiver sensitivity, the transmission power determines the set of neighbor nodes, i.e. those nodes that are in direct communication with a node. To provide adequate network reachability, it is important that a node be connected to a sufficient number of neighbors. However, more is not necessarily better. As the transmitters' coverage areas grow larger, so does the membership of the routing zones. This can result in an excessive amount of route update traffic.

Each node is assumed to continuously (proactively) maintain routing information only to those nodes that are within its routing zone. Because the updates are only propagated locally, the amount of update traffic required to maintain a routing zone does not depend on the total number of network nodes (which can be quite large). This is referred to as the *intrazone routing protocol* (IARP). The *interzone routing protocol (IERP)* is responsible for reactively discovering routes to destinations located beyond a node's routing zone. The IERP operates as follows: the source node first checks whether the destination is within its zone. If so, the path to the destination is known, and no further route discovery processing is required. If the destination is not within the source's routing zone, the source broadcasts a route request (referred to as request) to all its peripheral nodes. Now, in turn, all the peripheral nodes execute the same algorithm: they check whether the destination is within their zone. If so, a route reply (referred to as reply) is sent back to the source indicating the route to the destination. If not, the peripheral node forwards the query to its peripheral nodes, which in turn execute the same procedure.

An example of this route discovery procedure is demonstrated in Figure 13.20. The source node S needs to send a packet to the destination D. To find a route within the network, S first checks whether D is within its routing zone. If so, S knows the route to D. Otherwise, S broadcasts a query to its peripheral nodes; that is, S sends a query to nodes H, G and C. Now, in turn, after verifying that D is not in its routing zone, each one of these nodes forwards the query by broadcasting the

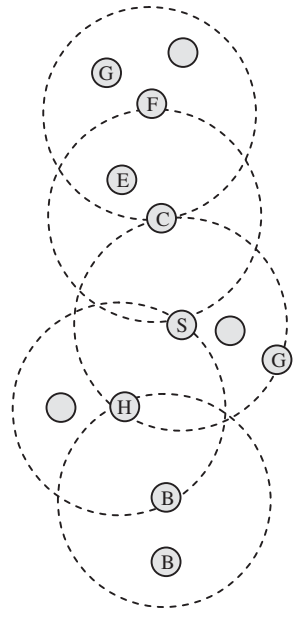

Figure 13.20 Illustration of IERP operation.

query to its peripheral nodes. In particular, H sends the query to B, which recognizes D as being in its routing zone and responds to the query, indicating the forwarding path: S–H–B–D. As indicated by this example, a route can be specified by a sequence of nodes that have received the successful IERP query thread. The manner in which this information is collected and distributed is specified by a route accumulation procedure. In the basic route accumulation, a node appends its ID to a received query packet. When a node finds the destination in its zone, the accumulated sequence of IDs specifies a route between querying source and destination. By reversing the accumulated route, a path is provided back to the query source. This information can be used to return the route reply through source routing.

The intuition behind the ZRP is that querying can be performed more efficiently by broadcasting queries to the periphery of a routing zone rather than flooding the queries over the same area. However, problems can arise once the query leaves the initial routing zone. Because the routing zones heavily overlap, a node can be a member of many routing zones. It is very possible that the query will be forwarded to all the network nodes, effectively flooding the network.

Yet a more disappointing result is that the IERP can result in much more traffic than the flooding itself, due to the fact that broadcasting involves sending the query along a path equal to the zone radius. Excess route query traffic can be regarded as a result of overlapping query threads (i.e. overlapping queried routing zones). Thus, the design objective of query control mechanisms should be to reduce the amount of route query traffic by steering threads outward from the source's routing zone and away from each other, as indicated in Figure 13.21. This problem is addressed primarily through appropriate mechanisms of query detection and query termination.

13.2.1 Loop-back termination

The query is terminated when the accumulated route (excluding the previous node) contains the host which lies in routing zone, e.g. for route $= \{S \rightarrow A \rightarrow B \rightarrow C\}$ in Figure 13.22, C terminates the query, because S is in C's routing zone.

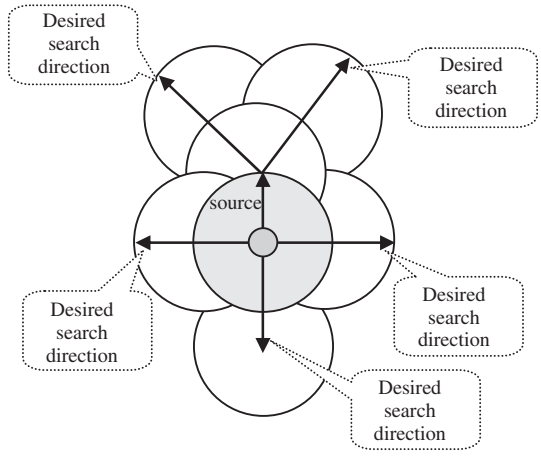

Figure 13.21 Guiding the search in desirable directions.

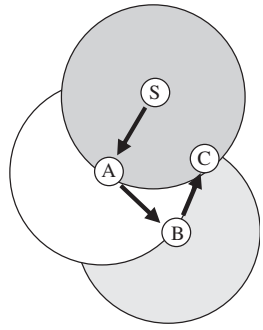

Figure 13.22 Loop-back termination.

13.2.2 Early termination

When the ability to terminate route query threads is limited to peripheral nodes, threads are allowed to penetrate into previously covered areas, which generates unnecessary control traffic. This excess traffic can be eliminated by extending the thread termination capability to the intermediate nodes that relay the thread. This approach is referred to as early termination (ET). Figure 13.23 illustrates the operation of the ET mechanism. Node S broadcasts a route query with node C as one of the intended recipients. Intermediate node A passes along the query to B. Instead of delivering the query to node C, node B terminates the thread because a different thread of this query was previously detected. Intermediate nodes may terminate existing queries but are restricted from issuing new queries. Otherwise, the ZRP would degenerate into a flooding protocol. The ability to terminate an overlapping query thread depends on the ability of nodes to detect that a routing zone they belong to has been previously queried. Clearly, the central node in the routing zone (which processed the query) is aware that its zone has been queried. In order to notify the remaining routing zone nodes without introducing additional control traffic, some form of 'eavesdropping' needs to be implemented. The first level of query detection (QD1) allows the intermediate nodes, which transport queries to the edge of the routing zone, to detect these queries. In single channel networks, it may be possible for queries to be detected by any node within the range of a query-transmitting node. This extended query detection capability (QD2) can be implemented by using IP

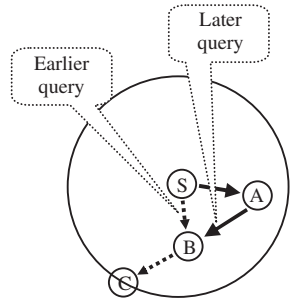

Figure 13.23 Early termination.

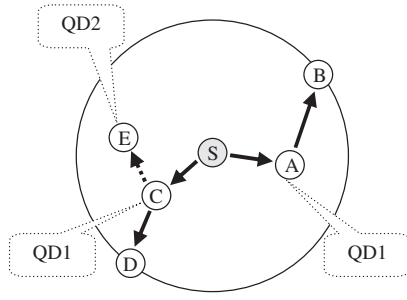

Figure 13.24 Query detection (QD1/QD2).

broadcasts to send route queries. Figure 13.24 illustrates both levels of advanced query detection. In this example, node S broadcasts to two peripheral nodes, B and D. The intermediate nodes A and C are able to detect passing threads using QD1. If QD2 is implemented, node E will be able to 'eavesdrop' on A's transmissions and record the query as well.

The techniques just discussed improve the efficiency of the IERP by significantly reducing the cost of propagating a single query. Further improvements in IERP performance can be achieved by reducing the frequency of route queries, initiating a global route discovery procedure only when there is a substantial change in the network topology. More specifically, active routes are cached by nodes: the communicating end nodes and intermediate nodes. Upon a change in the network topology, such that a link within an active path is broken, a local path repair procedure is initiated. The path repair procedure substitutes a broken link by a minipath between the ends of the broken link. A path update is then generated and sent to the end points of the path. Path repair procedures tend to reduce the path optimality (e.g. increase the length for shortest path routing). Thus, after some number of repairs, the path endpoints may initiate a new route discovery procedure to replace the path with a new optimal one.

13.2.3 Selective broadcasting (SBC)

Rather than broadcast queries to all peripheral nodes, the same coverage can be provided by broadcasting to a chosen subset of peripheral nodes. This requires IARP to provide network topology information for an extended zone that is twice the radius of the routing zone.

A node will first determine the subset of other peripheral nodes covered by its assigned inner peripheral nodes. The node will then broadcast to this subset of assigned inner peripheral nodes which forms the minimal partitioning set of the outer peripheral nodes.

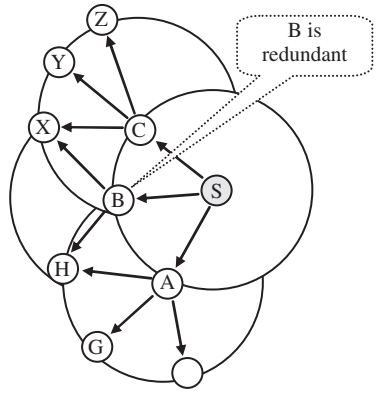

Figure 13.25 Selective broadcasting.

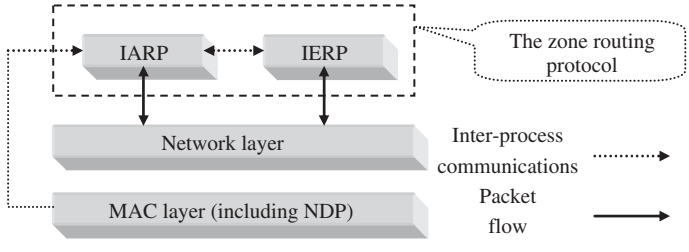

Figure 13.26 The position of the routing functions in the protocol stack.

Table 13.1 Simulation parameters

Parameter	Symbol	Values	Default
Zone radius [hops]	ρ	1–8	—
Node density [neighbors/node]	δ	3–9	6
Relative node speed [neighbors/s]	V	0.1–2.0	1.0
Number of nodes [nodes]	N	200–1000	500

This is illustrated in Figure 13.25. S's inner peripheral nodes are A, B and C. Its outer peripheral nodes are F, G, H, X, Y and Z. Two inner peripheral nodes of B (H and X) are also inner peripheral nodes of A and C. S can then choose to eliminate B from its list of broadcast recipients since A can provide coverage to H and C can cover X.

The position of the routing functions in the protocol stack are illustrated in Figure 13.26. Route updates are triggered by the MAC-level neighbor discovery protocol (NDP). IARP is notified when a link to a neighbor is established or broken. IERP reactively acquires routes to nodes beyond the routing zone. IERP forwards queries to its peripheral nodes (BRP) keeping track of the peripheral nodes through the routing topology information provided by IARP.

Pearlman and Haas [38] present the performance evaluation of the hybrid protocol, described above for the simulation set of parameters given in Table 13.1. From Figure 13.27 one can see that the IARP control traffic per node is increased as the radius of the zone is increased.

At the same time IERP traffic generated per zone would be reduced. So, the total ZRP traffic has a minimum value for some zone diameter r, which is demonstrated in Figure 13.28.

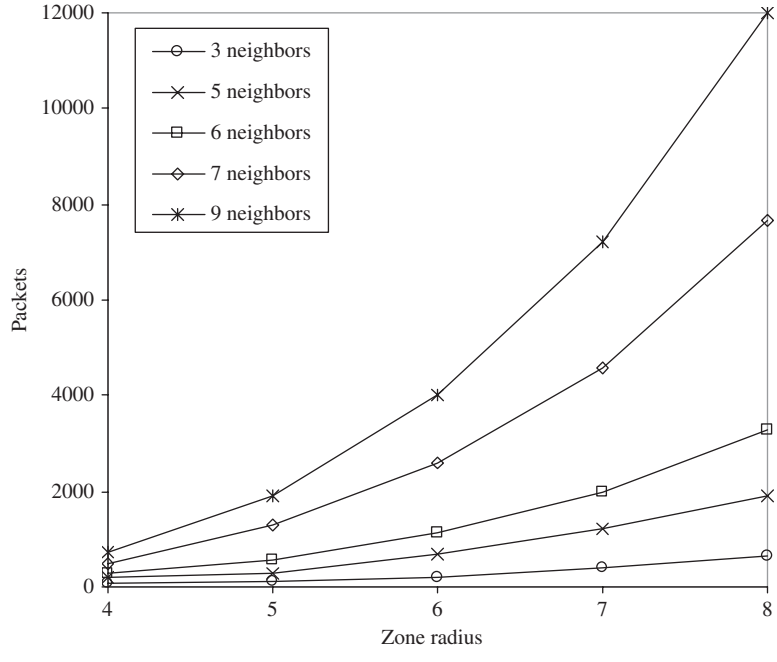

Figure 13.27 IARP traffic generated per neighbor.

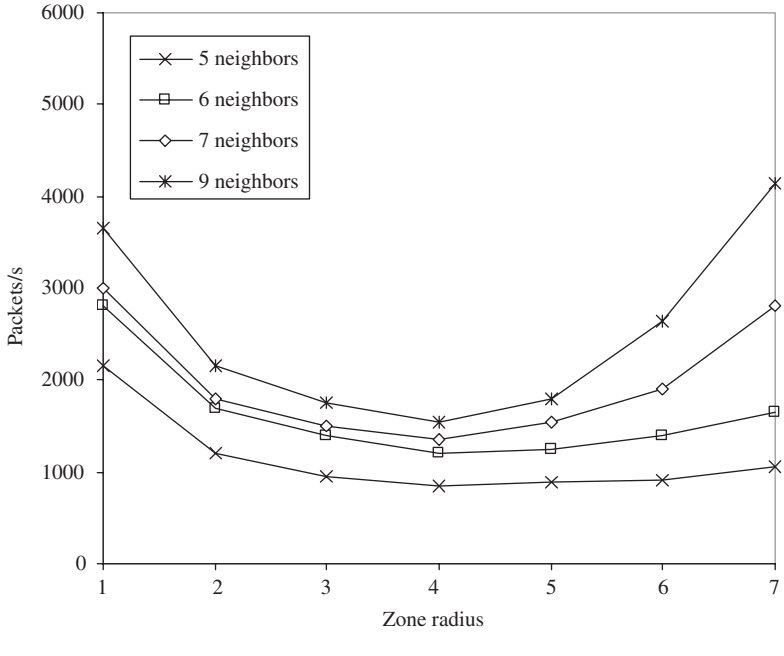

Figure 13.28 ZRP traffic per node ($N = 1000$ nodes, $v = 0{:}5$ neighbors/s).

13.3 SCALABLE ROUTING STRATEGIES

13.3.1 Hierarchical routing protocols

A hierarchical approach to routing, often referred to as *hierarchical state routing* (HSR), has been a traditional option when the network has a large number of nodes. The approach has a lot in common with routing with aggregation presented in Chapter 7. Commontable-driven protocols and on-demand protocols are for flat topologies and thus have a *scalability* problem when the network is large. For table-driven protocols there is high volume of overhead transmissions. On the other hand, for on-demand protocols there is large discovery latency.

The experience gained in wired networks suggests the use of a hierarchical structure to address the scalability problem. The use of hierarchical routing protocol in *ad-hoc* networks reduces overhead traffic and discovery latency but it has drawbacks, such as: suboptimal routes and complex management of the network hierarchical structure due to its dynamic nature. The basic idea is to divide the network into clusters or domains, as illustrated in Figures 13.29 and 13.30.

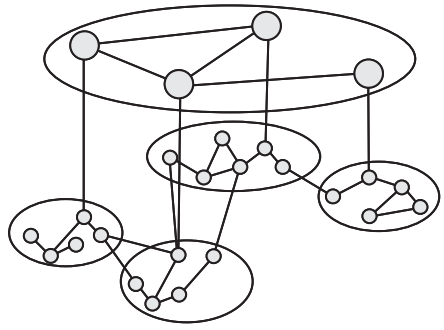

Figure 13.29 The network hierarchical structure.

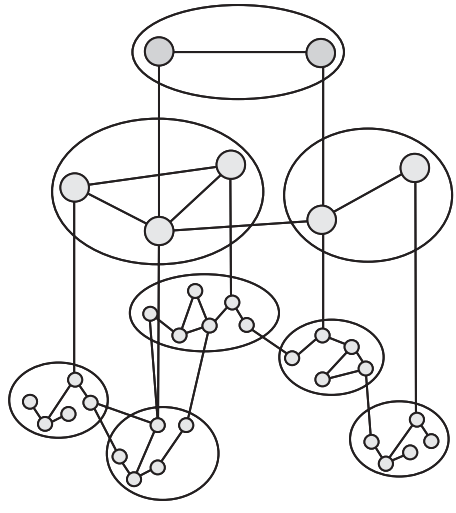

Figure 13.30 Three layers network hierarchical structure.

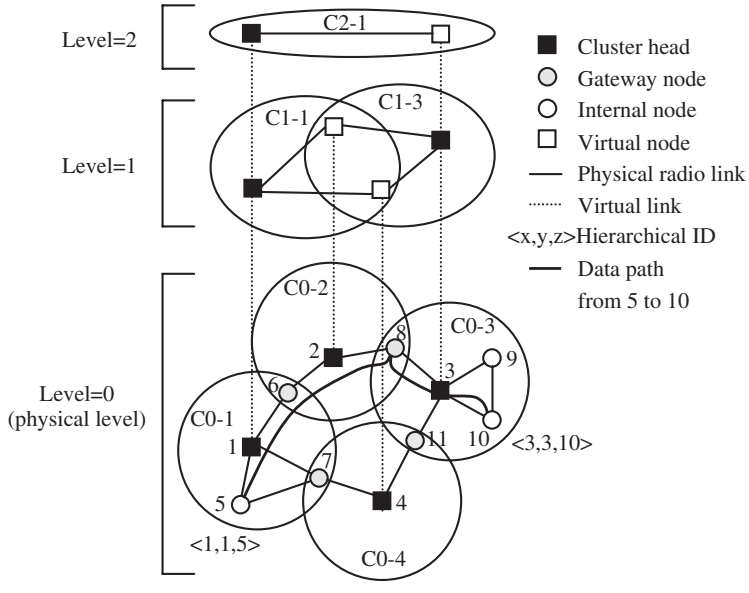

Figure 13.31 Physical multilevel clustering.

The mobile nodes are grouped into regions, regions are grouped into super-regions, and so on, as shown in Figure 13.30. A specific mobile host is chosen as the clusterhead for each region. In hierarchical routing, mobile nodes know how to route packets to their destination within its own region, but do not know the route outside of its own region. Clusterheads know how to reach other regions.

Figure 13.31 shows an example of physical clustering in more detail. At level $l = 0$, we have four physical level clusters, C0–1, C0–2, C0–3 and C0–4. Level 1 and level 2 clusters are generated by recursively selecting cluster heads. Different clustering algorithms can be used for the dynamic creation of clusters and the election of cluster heads [39, 40]. At level 0 clustering, spread-spectrum radios and CDMA can be introduced for spatial reuse across clusters. Within a level 0 cluster, the MAC layer can be implemented by using a variety of different schemes (polling, MACA, CSMA, TDMA, etc.).

Generally, as in ZRP, there are three kinds of nodes in a cluster, namely, the cluster head node (e.g. nodes 1–4), gateway node (e.g. nodes 6–8, and 11) and internal nodes (e.g. nodes 5, 9 and 10). The cluster head node acts as a local coordinator of transmissions within the cluster. The node IDs shown in Figure 13.31 (at level $l = 0$) are physical (e.g. MAC layer) addresses. They are hardwired and are unique to each node.

Within a physical cluster, each node monitors the state of the link to each neighbor (i.e. up/down state and possibly QoS parameters such as bandwidth) and broadcasts it within the cluster. The cluster head summarizes LS information within its cluster and propagates it to the neighbor cluster heads (via the gateways). The knowledge of connectivity between neighbor cluster heads leads to the formation of level 1 clusters. For example, as shown in Figure 13.31, neighbor cluster heads 1 and 2 become members of the level 1 cluster C1–1. To carry out LS routing at level 1, an LS parameter of the 'virtual' link in C1–1 between nodes 1 and 2 (which are neighbor cluster heads) is calculated from the LS parameters of the physical path from cluster head 1 to next cluster head 2 through gateway 6. More precisely, gateway 6 passes the LS update for link (6–2) to cluster head 1. Cluster head 1 estimates the parameters for the path (1–6–2) using its local estimate for (1–6) and

the estimate for (6–2) it just received from gateway 6. The result becomes the LS parameter of the 'virtual link' between nodes 1 and 2 in C1–1. This is equivalent to the aggregation process discussed in Chapter 7. The virtual link can be viewed as a 'tunnel' implemented through lower level nodes.

Applying the aforementioned clustering procedure (aggregation) recursively, new cluster heads are elected at each level and become members of the higher level cluster (e.g. node 1 is elected as a cluster head at level 1 and becomes a member of level 2 cluster C2–1).

Nodes within a cluster exchange virtual LS information as well as summarized lower-level cluster information. After obtaining the LS information at this level, each virtual node floods it down to nodes within the lower level cluster. As a result, each physical node has a 'hierarchical' topology information, as opposed to a full topology view as in flat LS schemes. The hierarchy so developed requires a new address for each node, the hierarchical address. There are many possible solutions for the choice of the hierarchical address scheme. In hierarchical state routing (HSR), we define the hierarchical ID (HID) of a node as the sequence of the MAC addresses of the nodes on path from the top hierarchy to the node itself. For example, in Figure 13.31 the hierarchical address of node 6 [called HID(6)], is 3, 2, 6. In this example, node 3 is a member of the top hierarchical cluster (level 2). It is also the cluster head of C1–3. Node 2 is member of C1–3 and is the cluster head of C0–2. Node 6 is a member of C0–2 and can be reached directly from node 2. The advantage of this hierarchical address scheme is that each node can dynamically and locally update its own HID upon receiving the routing updates from the nodes higher up in the hierarchy. The hierarchical address is sufficient to deliver a packet to its destination from anywhere in the network using HSR tables.

Referring to Figure 13.31, consider for example the delivery of a packet from node 5 to node 10. Note that HID(5) = <1, 1, 5> and HID(10) = <3, 3, 10>. The packet is forwarded upwards (to node 1) to the top hierarchy by node 5. Node 1 delivers the packet to node 3, which is the top hierarchy node for destination 10. Node 1 has a 'virtual link', i.e. a tunnel, to node 3, namely, the path (1, 6, 2, 8, 3). It thus delivers the packet to node 3 along this path. Finally, node 3 delivers the packet to node 10 along the downwards hierarchical path, which in this case reduces to a single hop.

Gateways nodes can communicate with multiple cluster heads and thus can be reached from the top hierarchy via multiple paths. Consequently, a gateway has multiple hierarchical addresses, similar to a router in the wired Internet, equipped with multiple subnet addresses.

13.3.2 Performance examples

Performance analysis of the system described above can be found in Iwata *et al.* [41]. In most experiments, the network consistes of 100 mobile hosts roaming randomly in all directions at a predefined average speed in a 1000×1000 m area(i.e. no group mobility models are used). A reflecting boundary is assumed. The radio transmission range is 120 m. A free space propagation channel model is assumed. The data rate is 2 Mb/s. The packet length is 10 kb for data, 2 kb for a cluster head neighbor list broadcast, and 500 b for MAC control packets. Transmission time is 5 ms for a data packet, 1 ms for a neighboring list, and 0.25 ms for a control packet. The buffer size at each node is 15 packets. Figures 13.32 and 13.33 illustrate the tradeoffs between throughput and control overhead (O/H) in HSR when the route refresh rate is varied.

In Figure 13.32 (at 90 km/h), we note that the O/H increases linearly with refresh rate until the network becomes saturated with control packets and starts dropping them. The data throughput first increases rapidly with the refresh rate, owing to more accurate routes and lower packet drops due to the lack of a route. Eventually, throughput peaks and then starts decreasing as the network becomes saturated, and data packets are dropped because of buffer overflow. Figure 13.33 reports the 'optimal' HSR refresh rate as a function of speed.

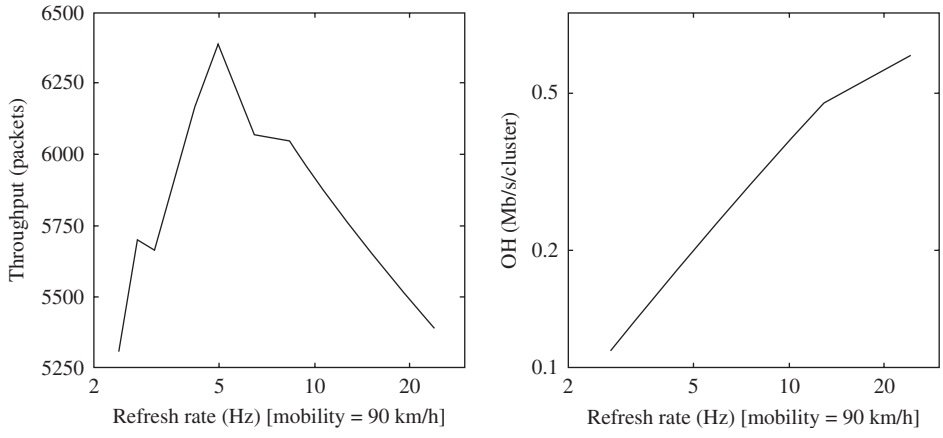

Figure 13.32 System performance vs the routing information refresh rate with $v = 90$ km/h.

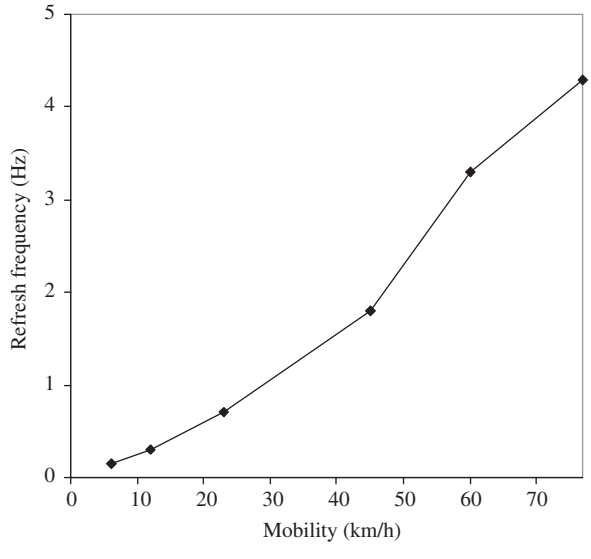

Figure 13.33 Optimum routing information refresh rate vs mobility.

13.3.3 FSR (fisheye routing) protocol

This protocol represents a different way to reduce (aggregate) the amount of information used for routing purposes. In Kleinrock and Stevens [42], a 'fisheye' technique was proposed to reduce the size of information required to represent graphical data. The eye of a fish captures with high detail the pixels near the focal point. The detail decreases as the distance from the focal point increases. In routing, the fisheye approach translates to maintaining accurate distance and path quality information about the immediate neighborhood of a node, with progressively less detail as the distance increases.

The FSR scheme presented in Iwata *et al.* [41] is built on top of another routing scheme called 'global state routing' (GSR) [43]. GSR is functionally similar to LS routing in that it maintains a

topology map at each node. The key is the way in which routing information is disseminated. In LS, LS packets are generated and flooded into the network whenever a node detects a topology change. In GSR, LS packets are not flooded. Instead, nodes maintain an LS table based on the up-to-date information received from neighboring nodes and periodically exchange it with their local neighbors only (no flooding).

Through this exchange process, the table entries with larger sequence numbers replace the ones with smaller sequence numbers. The GSR periodic table exchange resembles the DSDV, discussed earlier in this chapter, where the distances are updated according to the time stamp or sequence number assigned by the node originating the update. In GSR (like in LS), LSs are propagated, a full topology map is kept at each node, and shortest paths are computed using this map.

In a wireless environment, a radio link between mobile nodes may experience frequent disconnects and reconnects. The LS protocol releases an LS update for each such change, which floods the network and causes excessive overhead. GSR avoids this problem by using periodic exchange of the entire topology map, greatly reducing the control message overhead [43]. The drawbacks of GSR are the large size update message that consumes a considerable amount of bandwidth and the latency of the LS change propagation, which depends on the update period. This is where the fisheye technique comes to help, by reducing the size of update messages without seriously affecting routing accuracy.

Figure 13.34 illustrates the application of fisheye in a mobile wireless network. The circles with different shades of gray define the fisheye scopes with respect to the centre node (node 11). The

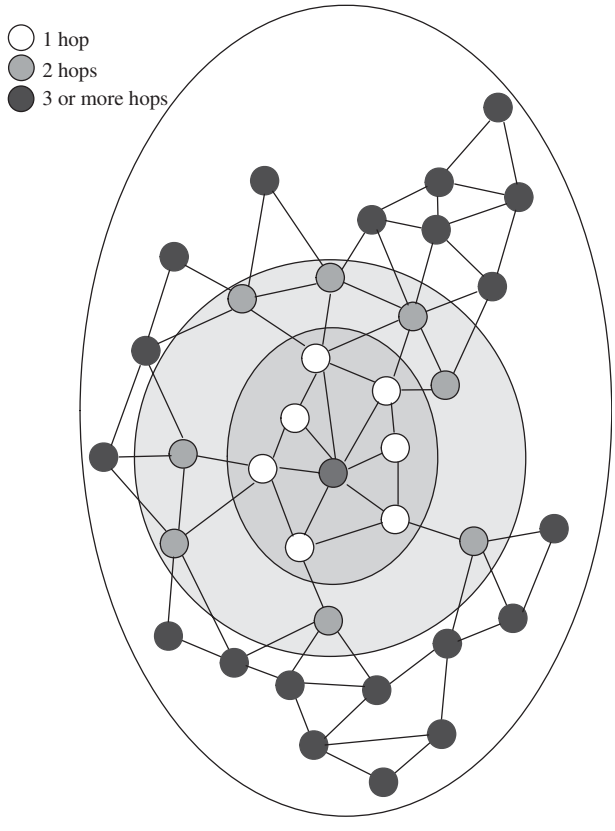

Figure 13.34 Illustration of a fisheye.

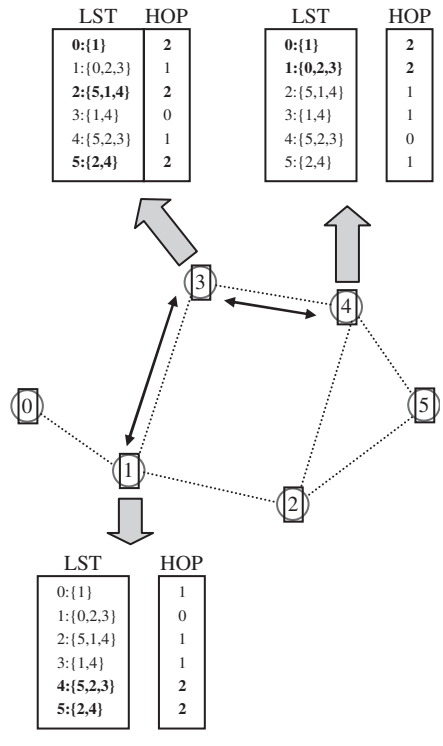

Figure 13.35 Message reduction using fisheye.

scope is defined as the set of nodes that can be reached within a given number of hops. In our case, three scopes are shown for one, two and three hops, respectively. Nodes are color-coded as black, gray and white, accordingly. The reduction of update message size is obtained by using different exchange periods for different entries in the table. More precisely, entries corresponding to nodes within the smaller scope are propagated to the neighbors with the highest frequency. Referring to Figure 13.35, entries in bold are exchanged most frequently. The rest of the entries are sent out at a lower frequency. As a result, a considerable fraction of LS entries are suppressed, thus reducing the message size. This strategy produces timely updates from near stations, but creates large latencies from stations that are far away. However, the imprecise knowledge of the best path to a distant destination is compensated for by the fact that the route becomes progressively more accurate as the packet gets closer to its destination.

In summary, FSR scales well to large networks, by keeping LS exchange overhead (O/H) low without compromising route computation accuracy when the destination is near. By retaining a routing entry for each destination, FSR avoids the extra work of 'finding' the destination (as in on-demand routing) and thus maintains low-single packet transmission latency. As mobility increases, routes to remote destinations become less accurate. However, when a packet approaches its destination, it finds increasingly accurate routing instructions as it enters sectors with a higher refresh rate.

Figure 13.36 shows the increase in the control O/H as a function of number of nodes. Geographical node density is kept the same for all runs, as shown in Table 13.2 [41]. One can see that as network size grows larger, the fisheye technique aggressively reduces the O/H.

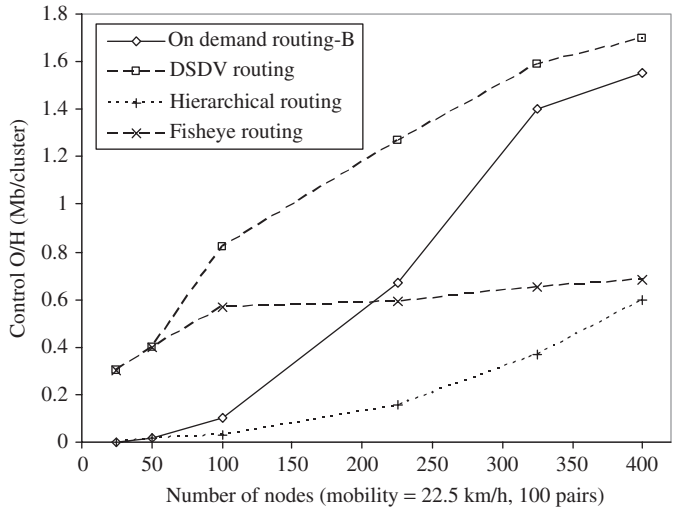

Figure 13.36 Control O/H vs number of nodes.

Table 13.2 Node density (nodes vs area)

Number of nodes	Simulation area
25	500 × 500
49	700 × 700
100	1000 × 1000
225	1500 × 1500
324	1800 × 1800
400	2000 × 2000

13.4 MULTIPATH ROUTING

A routing scheme that uses multiple paths simultaneously by splitting the information between a multitude of paths, so as to increase the probability that the essential portion of the information is received at the destination without incurring excessive delay is referred to as *multipath routing*. Such a scheme is needed to mitigate the instability of the topology (e.g. failure of links) in an *ad hoc* network due to nodal mobility and changes in wireless propagation conditions. The scheme works by adding an overhead to each packet, which is calculated as a linear function of the original packet bits. The process has its analogy in coding theory. The resulting packet (information and overhead) is fragmented into smaller blocks and distributed over the available paths. The probability of reconstructing the original information at the destination is increased as the number of used paths is increased.

A lot of research has been done in the area of multipath routing in wired networks. One of the initial approaches to this problem was the dispersity routing [44]. In order to achieve self-healing and fault tolerance in digital communication networks, diversity coding is suggested in Ayanoglu *et al.* [45]. In Krishnan and Silvester [46], a per-packet allocation granularity for multipath source routing schemes was shown to perform better than a per-connection allocation.

An exhaustive simulation of the various tradeoffs associated with dispersity routing is presented in Banerjea [47]. The inherent capability of this routing method to provide a large variety of services was pointed out. Owing to this fact, numerous schemes employing multipath routing have been proposed for wired networks in order to perform QoS routing [48–55]. All these protocols are based on proactive routing, since they maintain tables that reflect the state of the entire network. For this reason, owing to the unreliability of the wireless infrastructure and the nodal mobility, which can trigger an excessive amount of updates in the state tables, they cannot be successfully applied to mobile networks.

The application of multipath techniques in mobile *ad hoc* networks seems natural, as multipath routing allows reduction of the effect of unreliable wireless links and the constantly changing topology. The on-demand multipath routing scheme is presented in Nasipuri and Das [56] as a multipath extension of dynamic source routing (DSR) [57], described in Section 13.1. The alternate routes are maintained, so that they can be utilized when the primary one fails. TORA [58], routing on demand acyclic multipath (ROAM) [59] and *ad hoc* on-demand distance vector-backup routing (AODV-BR) [60], which is based on the *ad hoc* on-demand distance vector (AODV) protocol [61], are also examples of schemes that maintain multiple routes and utilize them only when the primary root fails. However, these protocols do not distribute the traffic into the multiple available paths.

Another extension of DSR, multiple source routing (MSR) [62], proposes a weighted round-robin heuristic-based scheduling strategy among multiple paths in order to distribute load, but provides no analytical modeling of its performance. The split multipath routing (SMR), proposed in Lee and Gerla [63], focuses on building and maintaining maximally disjoint paths; however, the load is distributed only in two routes per session. In Papadimitratos *et al.* [64], the authors propose a novel and nearly linear heuristic for constructing a highly reliable path set. In Pearlman *et al.* [65], the effect of alternate path routing (APR) on load balancing and end-to-end delay in mobile *ad hoc* networks has been explored. It was argued, however, that the network topology and channel characteristics (e.g. route coupling) can severely limit the gain offered by APR strategies. In an interesting application [66], multipath path transport (MPT) is combined with multiple description coding (MDC) in order to send video and image information in a multihop mobile radio network. In this section, we discuss a multipath scheme for mobile *ad hoc* networks based on diversity coding [45]. Data load is distributed over multiple paths in order to minimize the packet drop rate and achieve load balancing in a constantly changing environment.

Suppose that $n_{\max}$ paths are available for the transmission of data packets from a source to a destination. Any of the multipath schemes mentioned in the introduction can be employed in order to acquire these paths. No paths have nodes in common (mutually disjoint).

Each path, indexed as $i, i = 1, \ldots n_{\max}$, is either down at the time that the source attempts to transmit with probability of failure p_i or the information is received correctly with probability $1 - p_i$. Since there are no common nodes among the paths, they are considered independent in the sense that success or failure of one path cannot imply success or failure of another. It should be noted here that, in wireless *ad hoc* networks, nodes are sharing a single channel for transmission, so node disjointness does not guarantee the independence of the paths. Taking this into account, the paths are ideally considered independent as an approximation of a realistic *ad hoc* wireless network. For a more realistic modeling of the paths in a wireless network, one may refer to Tsirigos and Haas [67], where path correlation is included in the analysis. The failure probabilities of the available paths are organized in the probability vector $\mathbf{p} = \{p_i\}$, in such a way that $p_i \leq p_{i+1}$. The vector of success probabilities is defined as $\mathbf{q}\{q_i\} = 1 - \mathbf{p} = \{1 - p_i\}$.

Let us now suppose that we have to send a packet of D data bits utilizing the set of available independent paths in such a way as to maximize the probability that these bits are successfully communicated to the destination. This probability is denoted as P. In order to achieve this goal, we employ a coding scheme in which C extra bits are added as overhead. The resulting $B = D + C$ bits are treated as one network-layer packet. The extra bits are calculated as a function of the information bits in such a way that, when splitting the B-bit packet into multiple equal-size

nonoverlapping blocks, the initial D-bit packet can be reconstructed, given any subset of these blocks with a total size of D or more bits. First, we define the overhead factor $r = B/D = b/d$ where b and d take integer values and the fraction b/d cannot be further simplified. One should note that $1/r$ would be equivalent to coding gain in channel coding theory.

Next we define the vector $\mathbf{v} = \{v_i\}$, where v_i is the number of equal-size blocks that is allocated to path i. Some of the paths may demonstrate such a poor performance that there is no point in using them at all. This means that we might require using only some of the available paths. If n is the number of the paths we have to use in order to maximize P, it would be preferable to define the block allocation vector $\mathbf{v} = \{v_i\}$ as a vector of a variable size n, instead of fixing its size to the number of available paths $n_{\max}$.

Given the fact that the probability failure vector is ordered from the best path to the worst one, a decision to use n paths implies that these paths will be the first n ones. Based on these observations, the allocation vector $\mathbf{v} = \{v_i\}$ has the following form: $\mathbf{v} = \{v_1, v_2, \ldots, v_n\},\ n \le n_{\max}$.

If the block size is w, then $w \sum_{i=1}^{n} v_i = B = rD$. Therefore, the total number of blocks that the B-bit packet is fragmented into is $a = \sum_{i=1}^{n} v_i = rD/w$. From $p_i \le p_{i+1}$ it follows that $v_i \ge v_{i+1}$, because a path with higher failure probability cannot be assigned fewer blocks than a path with a lower failure probability. The original D-bit packet is fragmented into N w-size blocks, $d_1, d_2, d_3, \ldots, d_N$, and the C-bit overhead packet into M w-size blocks, $c_1, c_2, c_3, \ldots, c_M$. Based on this we have $N = D/w = a/r$ and $M = C/w = (r-1)N = (r-1)a/r$. Path 1 will be assigned the first v_1 blocks of the B-bitsequence, path two will receive the next v_2 blocks, and so on. Thus, path i will be assigned v_i blocks, each block of size w. Like parity check bits in error correcting $(N + M, M)$ block coding, the overhead symbols are generated as linear combination of the original packets as

$$c_j = \sum_{i=1}^{N} \beta_{ij} d_i; \quad 1 \le j \le M \tag{13.1}$$

where multiplication and summation are performed in Galois Fields $GF(2^m)$. The relations between probability of successful packet transmission P, parameters N and M and link failure probabilities are available from coding theory and will not be repeated here. One of the important results from that theory is that the block size has to satisfy the following inequality, so that the original information can be recovered [45]:

$$w \ge \left\lceil \log_2(N + M + 1) \right\rceil \ge \log_2(a + 1) \tag{13.2}$$

By incorporating the previous definitions in Equation (13.2), we obtain an inequality for the number of blocks, into which we can split the B-bit packet

$$B \ge a \log_2(a + 1) \equiv B_{\min} \tag{13.3}$$

13.5 CLUSTERING PROTOCOLS

13.5.1 Introduction

In dynamic cluster-based routing, described so far in this chapter, the network is dynamically organized into partitions called clusters, with the objective of maintaining a relatively stable effective topology [70]. The membership in each cluster changes over time in response to node mobility and is determined by the criteria specified in the clustering algorithm. In order to limit far-reaching reactions to topology dynamics, complete routing information is maintained only for intracluster routing. Intercluster routing is achieved by hiding the topology details within a cluster from external nodes and using hierarchical aggregation, reactive routing or a combination of both techniques. The argument made against dynamic clustering is that the rearrangement of the clusters and the

assignment of nodes to clusters may require excessive processing and communications overhead, which outweigh its potential benefits. If the clustering algorithm is complex or cannot quantify a measure of cluster stability, these obstacles may be difficult to overcome. A desirable design objective for an architectural framework capable of supporting routing in large *ad hoc* networks subject to high rates of node mobility incorporates the advantages of cluster-based routing and balances the tradeoff between reactive and proactive routing while minimizing the shortcomings of each. Furthermore, the consequences of node mobility suggest the need to include a quantitative measure of mobility directly in the network organization or path selection process.

Specifically, a strategy capable of evaluating the probability of path availability over time and of basing clustering or routing decisions on this metric can help minimize the reaction to topological changes. Such a strategy can limit the propagation of far-reaching control information while supporting higher quality routing in highly mobile environments.

In this section we present the (c,t) cluster framework, which defines a strategy for dynamically organizing the topology of an *ad hoc* network in order to adaptively balance the tradeoff between proactive and on demand-based routing by clustering nodes according to node mobility. This is achieved by specifying a distributed asynchronous clustering algorithm that maintains clusters which satisfy the (c,t) criteria that there is a probabilistic bound c on the mutual availability of paths between all nodes in the cluster over a specified interval of time t. In order to evaluate the (c,t) criteria, a mobility model is used that characterizes the movement of nodes in large *ad hoc* networks. It is shown how this model is used to determine the probability of path availability when links are subject to failure due to node mobility.

Based on the (c,t) cluster framework, intracluster routing requires a proactive strategy, whereas intercluster routing is demand-based. Consequently, the framework specifies an adaptive-hybrid scheme whose balance is dynamically determined by node mobility. In networks with low rates of mobility, (c,t) clustering provides an infrastructure that is more proactive. This enables more optimal routing by increasing the distribution of topology information when the rate of change is low. When mobility rates become very high, cluster size will be diminished and reactive routing will dominate. The (c,t) cluster framework decouples the routing algorithm specification from the clustering algorithm, and thus, it is flexible enough to support evolving *ad hoc* network routing strategies described so far in both the intra- and intercluster domains.

Several dynamic clustering strategies have been proposed in the literature [70–73]. These strategies differ in the criteria used to organize the clusters and the implementation of the distributed clustering algorithms. McDonald and Znati [74] use prediction of node mobility as a criteria for cluster organization. Clustering decisions in [70–73] are based on static views of the network at the time of each topology change. Consequently, they do not provide for a quantitative measure of cluster stability. In contrast, the (c, t) cluster strategy [74] forms the cluster topology using criteria based directly on node mobility. According to Ramanathan and Steenstrup [73], the ability to predict the future state of an *ad hoc* network comprising highly mobile nodes is essential if the network control algorithms are expected to maintain any substantive QoS guarantees to real-time connections. The multimedia support for wireless network (MMWN) system proposed by Ramanathan and Steenstrup [73] is based upon a hybrid architecture that includes the characteristics of *ad hoc* and cellular networks. Their framework uses hierarchical routing over dynamic clusters that are organized according to a set of system parameters that control the size of each cluster and the number of hierarchical levels. Aggregation of routing information is used to achieve scalability and limit the propagation of topological change information. A multilevel strategy is used to repair virtual circuit (VC) connections that have been disturbed due to node mobility. MMWN does not predict node movement. Consequently, it is unable to provide a quantitative bound on the stability of its cluster organization.

Vaidya *et al.* [72] proposed a scheme that dynamically organizes the topology into k clusters, where nodes in a cluster are mutually reachable via k-hop paths. The algorithm considers $k = 1$ and reduces to finding cliques in the physical topology. Using a first-fit heuristic, the algorithm attempts

to find the largest cliques possible. Although the algorithm does not form optimal clusters, it still requires a three-pass operation each time a topology change occurs: one for finding a set of feasible clusters, a second for choosing the largest of the feasible clusters that are essential to maintain cluster connectivity, and a third to eliminate any existing clusters that are made superfluous by the new clusters.

The objective of the scheme proposed by Lin and Gerla [70] differs significantly from the previous examples. Rather than using clustering to minimize the network's reaction to topological changes, their scheme is intended to provide controlled access to the bandwidth and scheduling of the nodes in each cluster in order to provide QoS support. Hierarchical routing and path maintenance were a secondary concern. The proposed algorithm is very simple and uses node ID numbers to deterministically build clusters of nodes that are reachable by two-hop paths.

The zone routing protocol (ZRP), described in Section 13.2 is a hybrid strategy that attempts to balance the tradeoff between proactive and reactive routing. The objective of ZRP is to maintain proactive routing within a zone and to use a query–response mechanism to achieve interzone routing. In ZRP, each node maintains its own hop-count constrained routing zone; consequently, zones do not reflect a quantitative measure of stability, and the zone topology overlaps arbitrarily. These characteristics differ from (c,t) clusters, which are determined by node mobility and do not overlap. Both strategies assume a proactive routing protocol for intrazone/cluster routing, and each organizes its topology based upon information maintained by that protocol. ZRP also defines the query control scheme to achieve interzone routing. Although ZRP is not a clustering algorithm and the (c,t) cluster framework is not a routing protocol, the comparison demonstrates a close relationship that could be leveraged by incorporating the (c,t) cluster into ZRP. The use of (c,t) clusters in ZRP could achieve more efficient and adaptive hybrid routing without significantly increasing its complexity.

13.5.2 Clustering algorithm

The objective of the clustering algorithm is to partition the network into several clusters. Optimal cluster size is dictated by the tradeoff between spatial reuse of the channel (which drives toward small sizes) and delay minimization (which drives toward large sizes). Other constraints also apply, such as power consumption and geographical layout. Cluster size is controlled through the radio transmission power. For the cluster algorithm, we assume that transmission power is fixed and is uniform across the network. Within each cluster, nodes can communicate with each other in at most two hops. The clusters can be constructed based on node ID.

The following algorithm partitions the multihop network into some nonoverlapping clusters. The following operational assumptions underlying the construction of the algorithm in a radio network are made. These assumptions are common to most radio data link protocols [75–78]:

(A1) Every node has a unique ID and knows the IDs of its one-hop neighbors. This can be provided by a physical layer for mutual location and identification of radio nodes.

(A2) A message sent by a node is received correctly within a finite time by all of its one-hop neighbors.

(A3) Network topology does not change during the algorithm execution.

The distributed clustering algorithm is shown in Figure 13.37

As an example, the topology from Figure 13.38 after clustering is given in Figure 13.39. From Figures 13.37–13.39 one can see that the cluster ID of each node is equal to either its node ID or the lowest cluster ID of its neighbors. Every node must have its cluster ID once it becomes the lowest ID node in its locality. This cluster ID will be broadcast at this time, and will not be changed before the algorithm stops. Hence, every node can determine its cluster and only one cluster.

```
Γ: the set of ID's of my one-hop neighbors and myself
{
        if (my_id == min(Γ))
        {
                my_cid = my_id;
                broadcast cluster(my_id,my_cid);
                Γ = Γ -{my_id};
        }

        for (:;)
        {
                on receiving cluster(id, cid)
                {
                        set the cluster ID of node id to cid;
                        if (id==cid and (my_cid==UNKNOWN or my_cid>cid))
                                my_cid = cid;
                        Γ =Γ -{id};
                        if (my_id == min(Γ))
                        {
                                if (my_cid==UNKNOWN) my_cid = my_id;
                                broadcast cluster(my_id,my_cid);
                                Γ = Γ - {my_id};
                        }
                }
                if (Γ==Ø) stop;
        }
}
```

Figure 13.37 Distributed clustering algorithm (cluster ID – cid). (Reproduced by permission of IEEE [70].)

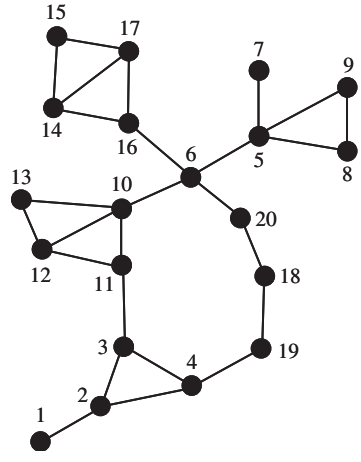

Figure 13.38 System topology.

13.5.3 Clustering with prediction

13.5.3.1 (c,t) Cluster framework

The objective of the (*c,t*) cluster framework is to maintain an effective topology that adapts to node mobility so that routing can be more responsive and optimal when mobility rates are low and more

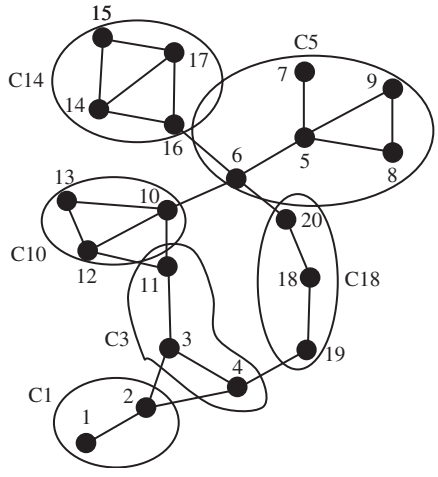

Figure 13.39 Clustering.

efficient when they are high. This is accomplished by a simple distributed clustering algorithm using a probability model for path availability as the basis for clustering decisions. The algorithm dynamically organizes the nodes of an *ad hoc* network into clusters where probabilistic bounds can be maintained on the availability of paths to cluster destinations over a specified interval of time.

The (c,t) cluster framework can also be used as the basis for the development of adaptive schemes for probabilistic QoS guarantees in *ad hoc* networks. Specifically, support for QoS in time-varying networks requires addressing: (1) connection-level issues related to path establishment and management to ensure the existence of a connection between the source and the destination; and (2) packet-level performance issues in terms of delay bounds, throughput and acceptable error rates.

Ideally, it is desirable to guarantee that the QoS requirements of ongoing connections are preserved for their entire duration. Unfortunately, this is not possible in a time-varying network environment as connections may fail randomly due to user mobility.

A more realistic and practical approach is to provide some form of probabilistic QoS guarantees by keeping connection failures below a prespecified threshold value and by ensuring with high probability that a minimum level of bandwidth is always available to ongoing connections.

The basic idea of the (c,t) cluster strategy is to partition the network into clusters of nodes that are mutually reachable along cluster internal paths that are expected to be available for a period of time t with a probability of at least c. The union of the clusters in a network must cover all the nodes in the network. Assume, without loss of generality, that t is identical at every node in a cluster. If the cluster's topology remains stable over the interval of length t, then routing will be deterministic during this interval, and standard assumptions permit the *ad hoc* network to be modeled as a network of Jackson queues. Assuming that path availability is an ergodic process, c represents the average proportion of time a (c,t) path is available to carry data. Consequently, c places a lower bound on the effective capacity of the path over an interval of length t.

Let the link capacity be C b/s and the mean packet length $1/\mu$ b. The effective packet service rate μ_{eff} over the interval t can be determined based upon the path availability according to Equation (13.4). Based on the Jackson model, each node can be treated as an independent M/M/1 queue. Using knowledge of the current aggregate arrival rate λ and the effective service rate μ_{eff}, the M/M/1 results can be applied to find the mean total packet delay T. Since this delay must

be less than t, this approach establishes a lower bound on the path availability, as shown in Equation (13.7)

$$\mu_{\text{eff}} = cC\mu \tag{13.4}$$

$$T = \frac{1}{\mu_{\text{eff}} - \lambda} \tag{13.5}$$

$$t \geq \frac{1}{cC\mu - \lambda} \tag{13.6}$$

$$c \geq \frac{1 + \lambda t}{\mu t C} \tag{13.7}$$

An effective adaptive strategy for determining the value of c controls the minimum level of cluster stability required to support the traffic load and QoS requirements of established connections. The choice of the parameter t is a system design decision that determines the maximum cluster size achievable for different rates of mobility when no traffic exists in the network.

13.5.3.2 (c,t) Cluster algorithm

There are five events which drive the (c,t) cluster algorithm, namely, node activation, link activation, link failure, expiration of the timer and node deactivation.

Node activation
The primary objective of an activating node is to discover an adjacent node and join its cluster. In order to accomplish this, it must be able to obtain topology information for the cluster from its neighbor and execute its routing algorithm to determine the (c,t) availability of all the destination nodes in that cluster. The source node can join a cluster if and only if all the destinations are reachable via (c,t) paths. The first step upon node activation is the initialization of the source node's CID (cluster ID) to a predefined value that indicates its unclustered status. The network-interface layer protocol is required to advertise the node's CID as part of the neighbor greeting protocol [79] and in the header of the encapsulation protocol. This enables nodes to easily identify the cluster status and membership of neighboring nodes and of the source of the routing updates – a necessary function to control the dissemination of routing information. When its network-interface layer protocol identifies one or more neighboring nodes, the source node performs the following actions. First, the source node identifies the CIDs associated with each neighbor. Next, it evaluates the link availability associated with each neighbor according to either a system default mobility profile or mobility information obtained through the network-interface layer protocol or physical-layer sensing. The precise methodology and the information required for the evaluation of link availability is described later in this section.

Finally, the neighbors, having discovered the unclustered status of the source node, automatically generate and transmit complete cluster topology information, which they have stored locally as a result of participating in the cluster's intracluster routing protocol. This topology synchronization function is a standard feature of typical proactive routing protocols when a router discovers the activation of a link to a new router. The source node does not immediately send its topology information to any of the neighbors.

Link activation
A link activation detected by a clustered node that is not an orphan is treated as an intracluster routing event. Hence, the topology update will be disseminated throughout the cluster. Unlike reactive routing that responds after path failure, the dissemination of link activation updates is a

key factor to an (*c,t*) cluster node's ability to find new *(c,t)* paths in anticipation of future link failures or the expiration of the timer.

Link failure
The objective of a node detecting a link failure is to determine if the link failure has caused the loss of any (*c,t*) paths to destinations in the cluster. A node's response to a link failure event is twofold. First, each node must update its view of the cluster topology and re-evaluate the path availability to each of the cluster destinations remaining in the node's routing table. Second, each node forwards information regarding the link failure to the remaining cluster destinations.

Expiration of c timer
The *c* timer controls cluster maintenance through periodic execution of the intracluster routing algorithm at each node in a cluster. Using the topology information available at each node, the current link availability information is estimated and maximum availability paths are calculated to each destination node in the cluster. If any of the paths are not (*c,t*) paths, then the node leaves the cluster.

Node deactivation
The event of node deactivation encompasses four related events, namely, graceful deactivation, sudden failure, cluster disconnection and voluntary departure from the cluster. In general, each of these events triggers a response by the routing protocol. As a result, nodes determine that the node that has deactivated is no longer reachable.

13.5.3.3 Ad hoc *mobility model*

The *random ad hoc mobility model* used in this section is a continuous-time stochastic process, which characterizes the movement of nodes in a two-dimensional space. Based on the random *ad hoc* mobility model, each node's movement consists of a sequence of random length intervals called mobility epochs during which a node moves in a constant direction at a constant speed. The speed and direction of each node varies randomly from epoch to epoch. Consequently, during epoch i of duration T_n^i, node n moves a distance of $V_n^i T_n^i$ in a straight line at an angle of θ_n^i. The number of epochs during an interval of length t is the discrete random process $N_n(t)$. Figure 13.40(a) illustrates the movement of the node over six mobility epochs, each of which is characterized by its direction, θ_n^i, and distance $V_n^i T_n^i$. The mobility profile of node n moving according to the random *ad hoc* mobility model requires three parameters: λ_n, μ_n and σ_n^2. The following list defines these parameters and states the assumptions made in developing this model:

(1) The epoch lengths are identically, independently distributed (i.i.d.) exponentially with mean $1/\lambda_n$.

(2) The direction of the mobile node during each epoch is i.i.d. uniformly distributed over $(0, 2\pi)$ and remains constant only for the duration of the epoch.

(3) The speed during each epoch is an i.i.d. distributed random variable (e.g. i.i.d. normal, i.i.d. uniform) with mean μ_n and variance σ_n^2 and remains constant only for the duration of the epoch.

(4) Speed, direction and epoch length are uncorrelated.

(5) Mobility is uncorrelated among the nodes of a network, and links fail independently.

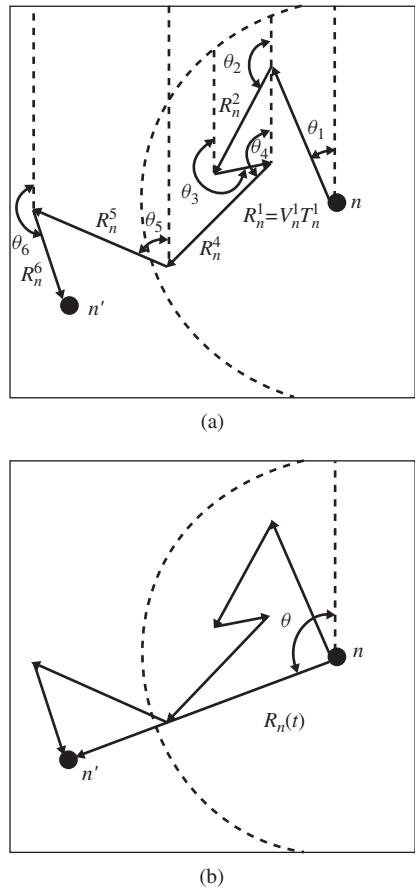

Figure 13.40 *Ad hoc* mobility model node movement: (a) epoch random mobility vectors; (b) *ad hoc* mobility model node movement.

Nodes with limited transmission range are assumed to experience frequent random changes in speed and direction with respect to the length of time a link remains active between two nodes. Furthermore, it is assumed that the distributions of each node's mobility characteristics change slowly relative to the rate of link failure. Consequently, the distribution of the number of mobility epochs is stationary and relatively large while a link is active. Since the epoch lengths are i.i.d. exponentially distributed, $N_n(t)$ is a Poisson process with rate λ_n. Hence, the expected number of epochs experienced by node n during the interval $(0,t)$ while a link is active is $\lambda_n t \triangleq 1$.

These assumptions reflect a network environment in which there are a large number of heterogeneous nodes operating autonomously in an *ad hoc* fashion, which conceptually reflects the environment considered in the design of the (c,t) cluster framework. In order to characterize the availability of a link between two nodes over a period of time $(t_0, t_0 + 1)$, the distribution of the mobility of one node with respect to the other must be determined. To characterize this distribution, it is first necessary to derive the mobility distribution of a single node in isolation. The single node distribution is extended to derive the joint mobility distribution that accounts for the mobility of one node with respect to the other. Using this joint mobility distribution, the link availability distribution is derived.

The random mobility vector can be expressed as a random sum of the epoch random mobility vectors

$$\mathbf{R}_n(t) = \sum_{i=1}^{N_n(t)} \mathbf{R}_n^i$$

as shown in Figure 13.40(b). Let be $\mathbf{R}_n(t)$ the resulting random mobility vector of a mobile node which is located at position $[X(t_0), Y(t_0)]$ at time t_0 and moves according to a random *ad hoc* mobility profile, $\langle \lambda_n, \mu_n, \sigma_n^2 \rangle$. The phase of the resultant vector $\mathbf{R}_n(t)$ is uniformly distributed over $(0, 2\pi)$ and its magnitude represents the aggregate distance moved by the node and is approximately Raleigh distributed with parameter

$$\alpha_n = (2t/\lambda_n)(\sigma_n^2 + \mu_n^2)$$

$$\Pr(\theta_n \le \phi) = \phi/2\pi, \quad 0 \le \phi \le 2\pi \tag{13.8}$$

$$\Pr[R_n(t) \le r] \approx 1 - \exp(-r^2/\alpha_n), \quad 0 \le r \le \infty \tag{13.9}$$

The derivation of these distributions is an application of the classic theory of uniform random phasor sums [80] that applies central limit theorem to a large number of i.i.d. variables.

Joint node mobility

Based on the assumption of random link failures, we can consider the mobility of two nodes at a time by fixing the frame of reference of one node with respect to the other. This transformation is accomplished by treating one of the nodes as if it were the base station of a cell, keeping it at a fixed position. For each movement of this node, the other node is translated an equal distance in the opposite direction. So, the vector $\mathbf{R}_{m,n}(t) = \mathbf{R}_m(t) - \mathbf{R}_n(t)$, representing the equivalent random mobility vector of node m with respect to node n, is obtained by fixing m's frame of reference to n's position and moving m relative to that point. Its phase is uniformly distributed over $(0, 2\pi)$ and its magnitude has Raleigh distribution with parameter $\alpha_{m,n} = \alpha_m + \alpha_n$.

Random ad hoc *link availability*

If $L_{m,n}(t) = 1$ denotes an active and $L_{m,n}(t) = 0$ an inactive link, then for nodes n and m, link availability is defined as

$$A_{m,n}(t) \equiv \Pr[L_{m,n}(t_0 + t) = 1 \mid L_{m,n}(t_0) = 1] \tag{13.10}$$

Note that a link is still considered available at time t even if it experienced failures during one or more intervals (t_i, t_j); $t_0 < t_i < t_j < t_0 + t$. By definition, if m lies within the circular region of radius R centered at n, the link between the two nodes is considered to be active.

Depending on the initial status and location of nodes m and n, two distinct cases of link availability can be identified.

(1) Node activation – node m becomes active at time t_0, and it is assumed to be at a random location within range of node n. In this case we have

$$A_{m,n}(t) \approx 1 - \Phi\left\{\frac{1}{2}, 2, -R^2/\alpha_{m,n}\right\}$$

$$\Phi\left\{\frac{1}{2}, 2, z\right\} = e^{z/2}\left[I_0(z/2) - I_1(z/2)\right] \tag{13.11}$$

$$\alpha_{m,n} = 2t\left\{\frac{\sigma_m^2 + \mu_m^2}{\lambda_m} + \frac{\sigma_n^2 + \mu_n^2}{\lambda_n}\right\}$$

(2) Link activation: node m moves within range of node n at time t_0 by reaching the boundary defined by R, and it is assumed to be located at a random point around the boundary. In this case we have

$$A_{m,n}(t) = \frac{1}{2}\left\{1 - I_0(-2R^2/\alpha_{m,n})\exp(-2R^2/\alpha_{m,n})\right\} \tag{13.12}$$

Random ad hoc *path availability*
Let $P^k_{m,n}(t)$ indicate the status of path k from node n to node m at time t. $P^k_{m,n}(t) = 1$ if all the links in the path are active at time t, and $P^k_{m,n}(t) = 0$ if one or more links in the path are inactive at time t. The path availability $\pi^k_{m,n}(t)$ between two nodes n and m at time $t \geq t_0$ is given by the following probability

$$\pi^k_{m,n}(t) \equiv \Pr\left\{P^k_{m,n}(t_0 + t) = 1 \;\middle|\; P^k_{m,n}(t_0 = 1)\right\} = \prod_{(i,j)\in k} A_{i,j}(t_0 + t) \tag{13.13}$$

If $\pi^k_{m,n}(t)$ is the path availability of path k from node n to node m at time t, then path k is defined as an (c,t) path if and only if

$$\pi^k_{m,n}(t) \geq c \tag{13.14}$$

Node n and node m are (c,t) available if they are mutually reachable over (c,t) paths. An (c,t) cluster is a set of (c,t) available nodes. This definition states that every node in an (c,t) cluster has a path to every other node in the cluster that will be available at time $t_0 + t$ with a probability $\geq c$.

Path availability cost calculation
The above discussion demonstrates how the link availability can be calculated, thereby providing a link metric that represents a probabilistic measure of path availability. This metric can be used by the routing algorithm in order to construct paths that support a lower bound c on availability of a path over an interval of length t. The availabilities of each of the links along a path are used by the (c,t) cluster protocol to determine if the path is an (c,t) path, and consequently, if a cluster satisfies the (c,t) criteria. In order to support this functionality in an *ad hoc* network, the routing protocol must maintain and disseminate the following status information for each link:

(1) the initial link activation time, t_0;

(2) the mobility profiles for each of the adjacent nodes $\langle \lambda_i, \mu_i, \sigma_i^2 \rangle$, $i = m, n$;

(3) the transmission range of each of the adjacent nodes, R;

(4) the event which activated the link: (a) node activation at time t_0 or (b) nodes moving into range of each other at time t_0.

Based on this information, any node in an (c,t) cluster can estimate, at any time τ, the availability of a link at time $t + \tau$. This can be achieved because each node knows the initial link activation time t_0; hence, link availability is evaluated over the interval $(t_0, t + \tau)$. Nodes can use conditional probability to evaluate the availability of their own links because they have direct knowledge of such a link's status at time τ, whereas remote nodes do not. Specifically, for an incident link that activated at time t_0, a node will evaluate the availability at time t, given that it is available at time $\tau \geq t_0$.

13.5.3.4 Performance example

A range of node mobility with mean speeds between 5.0 and 25.0 km/h was simulated in McDonald and Znati [74]. The speeds during each mobility epoch were normally distributed, and the direction

was uniformly distributed over $(0, 2\pi)$. A node activation rate of 250 nodes/h was used. The mean time to node deactivation was 1 h. Nodes were initially randomly activated within a bounded region of 5×5 km. Nodes that moved beyond this boundary were no longer considered to be part of the *ad hoc* network and were effectively deactivated. (c,t) path availability was evaluated using Dijkstra's algorithm.

For each simulation run, data was collected by sampling the network status once per second over an observation interval of 1 h. The first 2 h of each run were discarded to eliminate transient effects, and each simulation was rerun 10 times with new random seeds. Simulation results for cluster size and cluster survival times are given in Figures 13.40 and 13.41. Finally logical relationships among MANET network-layer entities is given in Figure 13.42.

13.6 CASHING SCHEMES FOR ROUTING

A large class of routing protocols for MANETs, namely reactive protocols, employ some form of caching to reduce the number of route discoveries. The simplest form of caching is based on timeouts associated with cache entries. When an entry is cached, a timer starts. When the timeout elapses, the entry is removed from the cache. Each time the entry is used, the timer restarts. Therefore, the effectiveness of such a scheme depends on the timeout value associated with a cached route. If the timeout is well-tuned, the protocol performance increases; otherwise, a severe degradation arises as entries are removed either prematurely or too late from the cache.

13.6.1 Cache management

A cache scheme is characterized by the following set of design choices that specify cache management in terms of space (cache structure) and time (i.e. when to read/add/ delete a cache entry): store policy, read policy, writing policy and deletion policy.

The *store policy* determines the structure of the route cache. Recently, two different cache structures were studied [81], namely link cache and path cache, and applied to DSR. In a link cache structure, each individual link in the routes returned in RREP packets is added to a unified graph data structure, managed at each node, that reflects the node's current view of the network topology. In so doing, new paths can be calculated by merging route information gained from different packets. In the path cache, however, each node stores a set of complete paths starting from itself. The implementation of the latter structure is easier compared with the former, but it does not permit inference of new routes and exploitation of all topology information available at a node.

The *reading policy* determines rules of using a cache entry. Besides the straightforward use from the source node when sending a new message, several other strategies are possible. For example, DSR defines the following policies:

- *cache reply* – an intermediate node can reply to a route request with information stored in its own cache;
- *salvaging* – an intermediate node can use a path from its own cache when a data packet meets a broken link on its source route;
- *gratuitous reply* – a node runs the interface in the promiscuous mode and it listens for packets not directed to itself. If the node has a better route to the destination node of a packet, it sends a gratuitous reply to the source node with this new better route.

The *writing policy* determines when and which information has to be cached. Owing to the broadcast nature of radio transmissions, it is quite easy for a node to learn about new paths by running its radio interface in the promiscuous mode. The main problem for the writing policy is indeed to

cache valid paths. Negative caches are a technique proposed in Johnson and Maltz [82] and adapted in Marina and Das [83] to filter the writing of cache entries in DSR out. A node stores negative caches for broken links seen either via the route error control packets or link layer for a period of time of δt s. Within this time interval, the writing of a new route cache that contains a cached broken link is disabled.

The *deletion policy* determines which information has to be removed from the cache and when. Deletion policy is actually the most critical part of a cache scheme. Two kinds of 'errors' can occur, owing to an imprecise erasure: (1) *early deletion*, a cached route is removed when it is still valid; and (2) *late deletion*, a cached route is not removed even if it is no longer valid.

The visible effect of these kinds of errors is a reduction in the packet delivery fraction and an increase in the routing overhead (the total number of overhead packets) [84]. Late deletions create the potential risk of an avalanche effect, especially at high load. If a node replies with a stale route, the incorrect information may be cached by other nodes and, in turn, used as a reply to a discovery. Thus, cache 'pollution' can propagate fairly quickly [83].

Caching schemes in DSR

All such schemes rely on a local timer-based deletion policy [81, 84]. The only exception has been proposed in Marina and Das [83]. They introduce a reactive caching deletion policy, namely, the wider error notification, that propagates route errors to all the nodes, forcing each node to delete stale entries from its cache.

Simulation results reported in References [81, 83] show that performance of a timer-based caching deletion policy is highly affected by the choice of the timeout associated with each entry. In the path cache, for a value of timeout lower than the optimal one (i.e. early deletion), the packet delivery fraction and routing overhead are worse than caching schemes that do not use any timeout. In the link cache, late deletion errors increase the routing overhead while the packet delivery fraction falls sharply.

The cache timeout can obviously be tuned dynamically. However, adaptive timer-based deletion policies have their own drawbacks. This policy suffers from late or early deletion errors during the transition time from one optimal timeout value to the successive one. So, the more the network and the data load are variable, the worse the performance will be.

To reduce the effect of such imprecise deletions, the adaptive timer-based cache scheme has been combined with the wide error notification deletion technique and studied for DSR in Perkins and Royer [17]. According to such a combined scheme, routes that become stale before their timeout expiration are removed reactively from all the sources using that route. In this combined technique, however, two more points remain unresolved: (1) Owing to the reactive nature of the deletions, if a cache entry is not used, it remains in the cache, even if no longer valid, thus it can be used as a reply to a path discovery and (2) the effect of early deletions cannot be avoided.

Caching schemes in ZRP

The caching zone with radius k^* for a cache leader n is defined as the set of nodes at a distance of at most k^* hops from n. An active path is created as a result of the discover phase and it is composed of a set of nodes, referred to as active nodes, forming a path from a source node S to a destination node D. Cache leader nodes are a subset of the active nodes.

The key consideration is to avoid the possibility that nodes can cache route information autonomously. Therefore, a cache leader n is the only node that is authorized to advertise route information inside its caching zone which is written into caches. On receiving the advertising message, a node proactively maintains a path to n so that it can be used as the next-hop node to any of the advertised routes. A cache leader is responsible for the validity of the advertised routes. Thus, it monitors such routes and forces each node in its caching zone to remove a route as soon as it becomes stale, so the deletion policy is proactive. Let us note that, if we consider $k^* = k$ and

each node of a ZRP interzone path as a cache leader, we get the same underlying zone structure of ZRP (this implies that each active node is a cache leader). However, more generally, a cache leader can decide to advertise paths only to those nodes located at a distance $k^* < k$, and not all active nodes need to be cache leaders.

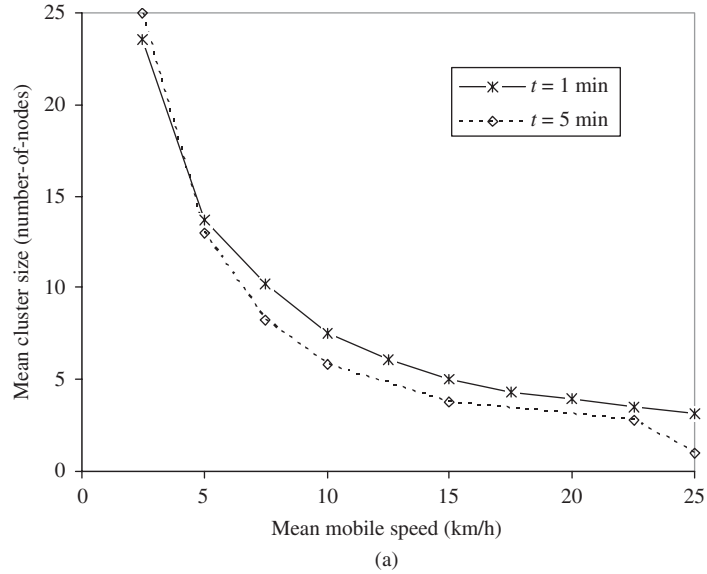

(a)

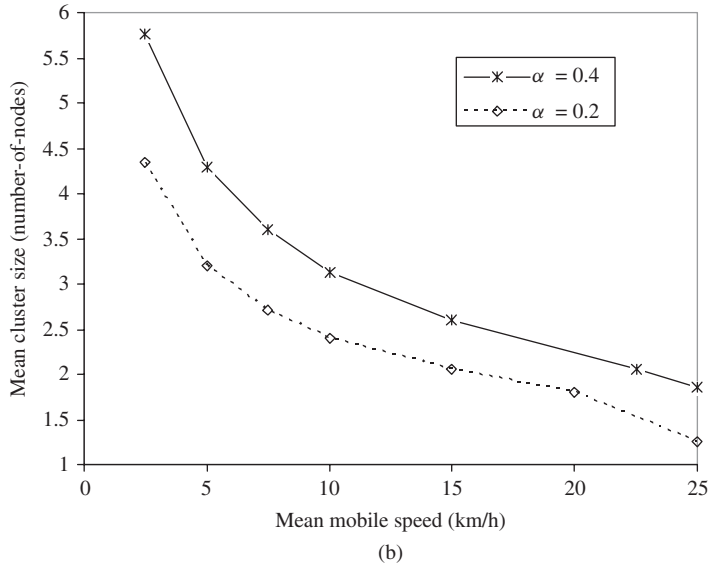

(b)

Figure 13.41 Simulation results: (a) cluster size ($R = 1000$ m); (b) cluster size ($R = 500$ m); (c) cluster survival ($R = 1000$ m); and (d) cluster survival ($R = 500$ m). (Reproduced by permission of IEEE [74].)

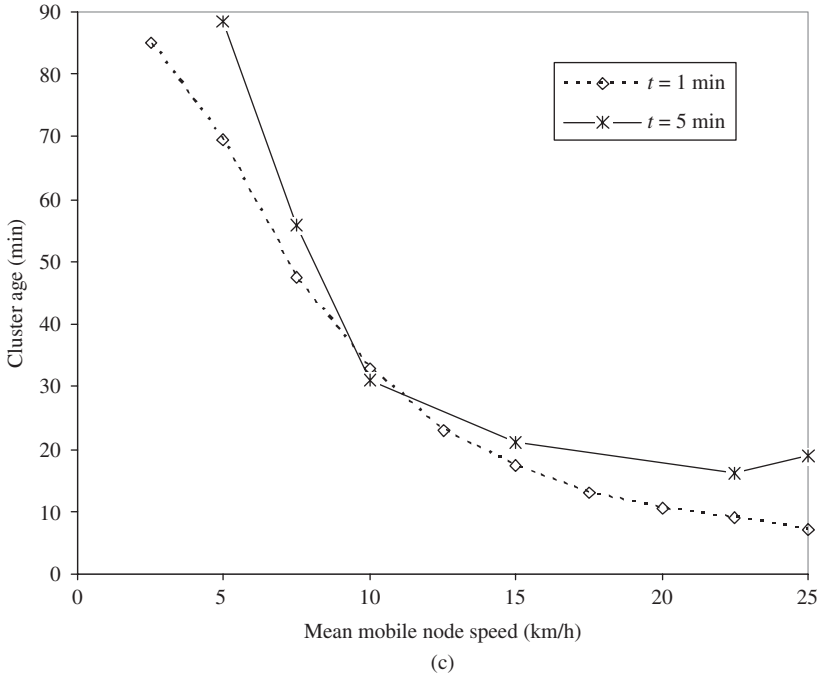

(c)

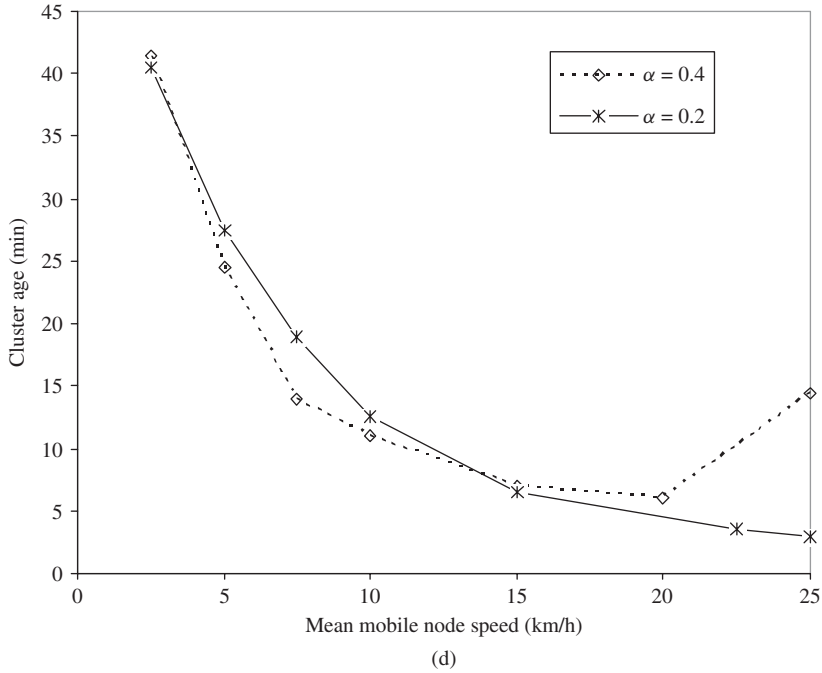

(d)

Figure 13.41 *(continued.)*

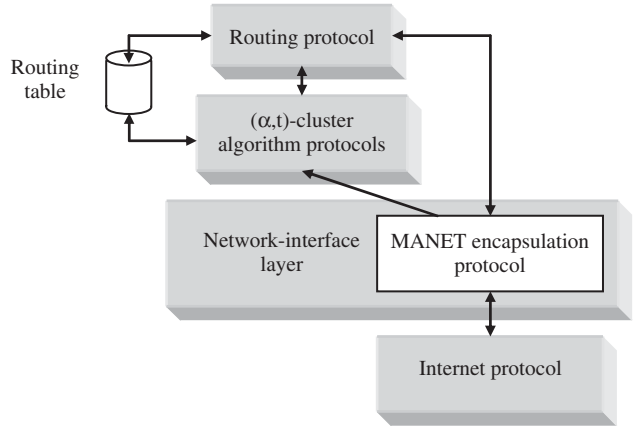

Figure 13.42 Logical relationships among MANET network-layer entities.

Implementation of C-ZRP
For simplicity, the implementation assumes:

(1) $k = k^*$.

(2) All active nodes act as cache leader nodes and vice versa.

(3) Only paths to active nodes are advertised as external routes.

(4) Caches are managed using explicit injection/deletion messages.

(5) To stop redundant query threads, LT (loop back termination), QD2 (query detection) and ET (early termination) redundant filtering rules are used which have been described earlier in this chapter.

When a node S, in Figure 13.43, executes a route request for a node D, an interzone path from S to D is identified. A node B_i belonging to an interzone path is an active node for the caching scheme. In Figure 13.43 an interzone path between S and D is formed by nodes b, e, p and t. Thus, an interzone path is also an active path. An interzone path is stored according to a distributed next-hop fashion, where the next-hop node is an active node. B_i stores B_{i+1} as the next-hop active node for all the downstream nodes from B_{i+2} to B_{M+1} and B_{i-1} as the next-hop active node for all the upstream nodes from B_0 to B_{i-2}. These two active nodes will be referred to as companion nodes (as an example, the companion nodes of node b, with respect to the interzone path from S to D are S and e).

All routing information concerning nodes belonging to an interzone path is advertised inside the caching zone of each member of the path, which thus acts as cache leader for that information. Such routes are then maintained proactively by the IARP. If a new node joins B_i's zone, it acquires, by means of the IARP, all previously advertised routing information by B_i. Since a node may belong to more than one overlapping zone, it can acquire more than a single path to the same destination.

When a node, say B_{i+1}, leaves B_i's routing zone, not all the routing information gathered during the route request/reply is lost. Roughly speaking, two active paths from S to B_{i-1} and from B_{i+1} to D are still up. Hence, all the routing information concerning these subpaths is still valid. However, nodes $B_0, \ldots, B_{i-1}$ ($B_{i-1}, \ldots, B_{M+1}$) notify the nodes inside their own zones, using a delete control message, that the destinations $B_{i-1}, \ldots, B_{M+1}$ ($B_0, \ldots, B_i$) are no longer reachable.

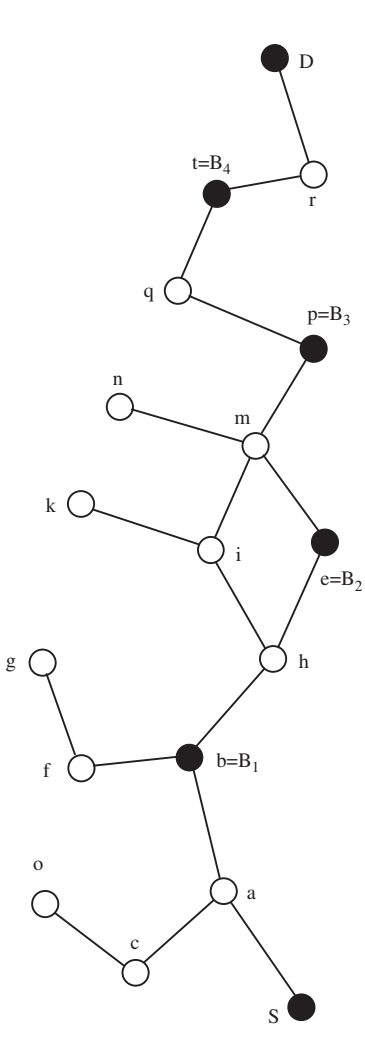

IZT

r	r	1
t	r	2

EZT

p	t	2
e	t	3
b	t	4
S	t	5

Node D

IZT

q	q	1
r	r	1
p	q	2
D	r	2

EZT

S	p	4
b	p	3
e	p	2

IZP=(ID,B3,D)
Node B4

IZT

m	m	1
q	q	1
e	m	2
t	q	2

EZT

S	e	3
b	e	2
D	t	2

IZP=(ID,B2,B4)
Node B3

IZT

h	h	1
m	m	1
l	h	2
p	m	2
n	m	2
b	h	2

EZT

S	b	2
t	p	2
D	p	3

IZP=(ID,B1,B3)
Node B2

IZT

a	a	1
f	f	1
h	h	1
S	a	2
c	a	2
g	f	2
l	h	2
e	h	2

EZT

p	e	2
t	e	3
D	e	4

IZP=(ID,S,B2)
Node B1

IZT

a	a	1
c	a	2
b	a	2

EZT

e	b	2
p	b	3
t	b	4
D	b	5

Node S

Figure 13.43 An example of values of data structures used in C-ZRP, $k = 2$.

Data structures
Each node X uses the following local data structures:

- *Internal zone routing table (IZT)* – an entry of IZT is a triple (d, n, #*h*), where d is the destination node, n is the next-hop node (located in X's transmission range), and *#h* is the path cost in number of hops.
- *External zone routing table (EZT)* – a row of EZT is a triple (d, n, #*z*), where d is the destination node, n is the next-hop active node (n belongs to X's routing zone and is not restricted to be

in its transmission range), and #z is the cost of the path from X to d, given as the number of active nodes that have to be traversed. For example, in Figure 13.43, node b sets node e as the next-hop active node for p with cost two (nodes e and p).

- *Interzone path table (IZP)* – an interzone path corresponds to an entry in X's IZP table provided that X is an active node and (X $\neq$ S,D). In this case, let the path id be ID and X = B_i. The entry is the triple (ID, B_{i-1}, B_{i+1}).
- *Reachable nodes (RN) list* – this is a sequence of pairs (d, #z), where d is an active node belonging to an interzone path and #z is the cost of the path from X expressed as number of active nodes that must be traversed to reach d. A node X advertises RN to nodes belonging to Z_k(X). RN includes the projection of EZT along the first and third components. For example, node *b* of Figure 13.43 will include the pairs (p, 2), (t, 3), and (D, 4) in RN.
- *Unreachable nodes (UN) set* – this set of nodes is used to advertise destinations that become unreachable.

Interzone path creation

A single interzone path from S to D is created during a route request/reply cycle by allowing only the destination D to send a single reply for a given request. The path is tagged with a unique identifier ID, for example, obtained by using increasing sequence numbers generated by the requesting node. When S triggers a new route discovery for a node D, it bordercasts a query message to all its border nodes. The message contains the identifier ID and a route accumulation vector AV[ ], initialized with AV[0] = S. Let M be the number of active nodes (not including S and D).

(1) When a border node X $\neq$ D receives a query message, if the message is received for the first time and the redundant query filter rules are satisfied:
   (a) It adds its own identification into the accumulation vector. As an example, if the node X corresponds to node B_j in the interzone path, then AV[j] = X.
   (b) If D belongs to X's routing zone, then the latter unicasts the query message to D. Otherwise, it executes a bordercast.

(2) When the destination node D receives a query message with identifier ID for the first time:
   (a) It stores the tuples (AV[i], AV[M], $M + 1 - i$, for $0 \leq i \leq M - 1$ in EZT.
   (b) It prepares the list RN = (AV[i], $M + 1 - i$)], for $0 \leq i \leq M$.
   (c) It sets AV[$M + 1$] = D.
   (d) It sends a reply message to AV[M]. The message contains the AV vector accumulated in the query message.

   An example of path creation is given in Figure 13.44(a).

(3) When a border node B_j receives a reply message:
   (a) If $B_j \neq$ S, then it stores the triple (ID, AV[$j - 1$], AV[$j + 1$]) in the IZP table, thus becoming an active node.
   (b) It stores the following tuples in EZT: (AV[i], AV[$j - 1$], $j - i$), for $0 \leq i \leq j - 2$; (AV[i], AV[$j + 1$], $j - i$), for $j + 2 \leq i \leq M + 1$.
   (c) It prepares RN = [(AV[$j + i$], $|i|$)] for $-j \leq i \leq M + 1$.
   (d) If $B_j \neq$ S, then it forwards the reply message to the node AV[$j - 1$].

Figure 13.43(b) shows the state at node B2 after the reception of the reply message with AV [S,B1,B2,B3,B4,D] that caused the execution of the following actions:

(1) B_2 becomes a member of an interzone path [it stores the triple (ID,B_1,B_3) in IZP].

(2) B_2 adds the entries (S, B_1, 2), (B_4, B_3, 2), (D, B_3, 3) in EZT.

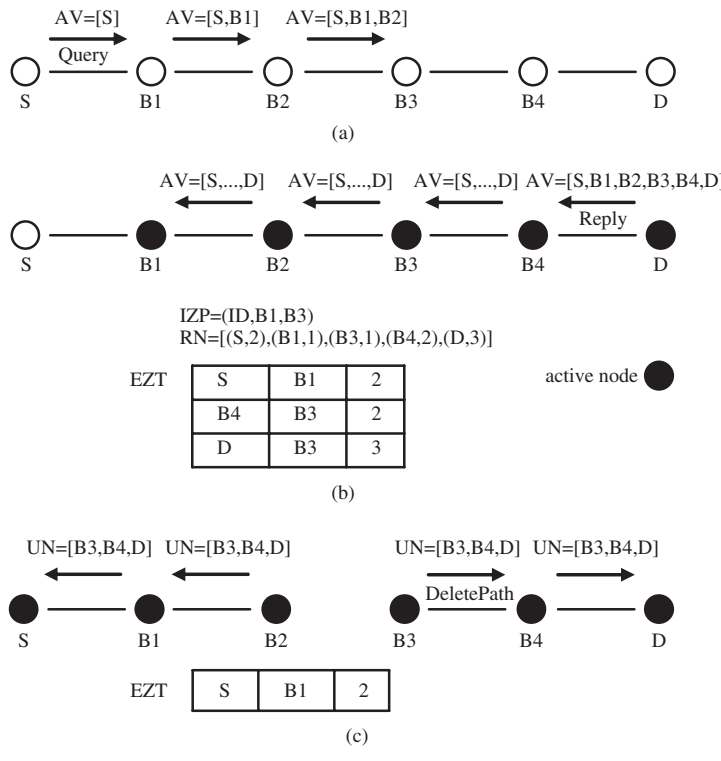

Figure 13.44 An example of interzone path creation and deletion.

(3) B_2 prepares the list of reachable nodes, RN = [(S,2), (B1,1), (B3,1), (B4, 2), (D,3)].

(4) B_2 forwards the reply to B1.

Interzone path deletion

An interzone path is broken at node B_j when B_{j-1} (or B_{j+1}) is no longer in B_j's routing zone. In this case, the path is divided in two subpaths and the source node is notified with an error message. An active node B_j executes the following actions (in the following notation '–' means any):

(1) Deletes the entry (–, B_{j-1}, –) or (–, B_{j+1}, –) from EZT.

(2) Checks for the companion node B_{j+1} or B_{j-1} in the IZP table.

(3) If the companion node is found, then it prepares the following list of unreachable nodes: $N = [B_0, B_1, \ldots, B_{j-1}]$ (UN = $[B_{j+1}, B_{j+2}, \ldots, B_{M+1}]$); and sends a Delete_Path message, containing UN and the path identifier ID, to the companion node.

(4) Deletes the entry (ID, B_{j-1}, B_{j+1}) from IZP after the successful transmission of the message.

When an active path is broken, the source node either receives the Delete_Path message from B_1 [if the link is broken between (B_j, B_{j+1}), with $j > 0$], or is able to detect the break autonomously via IARP. The source node thus triggers a new route discovery if required to send other packets, while the two subpaths ($B_0, B_1, \ldots, B_{j-1}$ and $B_{j+1}, B_{j+2}, \ldots, B_{M+1}$) remain active. Figure 13.44(c) shows the case when the 'link' between B_2 and B_3 is broken (i.e. their distance becomes higher

than k). Two interzone subpaths, (S, B_1, B_2) and (B_3, B_4, D), are generated. In the figure, B_2's EZT data structure is also shown.

When an active node receives a Delete_Path message from one of its companion nodes X, it deletes the entries stored in the UN list from EZT and forwards the message to the other companion node. If the receiving node has some another route to a node stored in UN, then it does not include such a node when forwarding UN.

Cache management

In order to allow all the nodes of B_j's routing zone to use the acquired information, B_j broadcasts RN inside its zone. Such a message is referred to as *the inject message*. On receiving an inject message carrying the reachable node list RN from a node $X = B_j$, a node Y creates a set of entries (RN[i].d, X, RN[i].#z) into its own EZT, $0 \leq i \leq |RN|$, where RN[i].d is the first component (destination node) of the ith pair of RN, RN[i], #z, the second component (i.e. the length), and |RN| is the number of elements of RN. Figure 13.44(a) shows node B_2 injecting the external routes to nodes S, B_1, B_3, B_4, D into its zone. Note that Y now has two routes to node B_1 since such a node is in Y' routing zone.

Deleting external routes

When a node B_j either detects a path breakage or receives a Delete_Path message, it broadcasts a Delete message into its zone containing the list of unreachable nodes UN. When an internal node receives a Delete message it deletes all the matching entries from EZT. Figure 13.45(b) shows the delete mechanism on node Y.

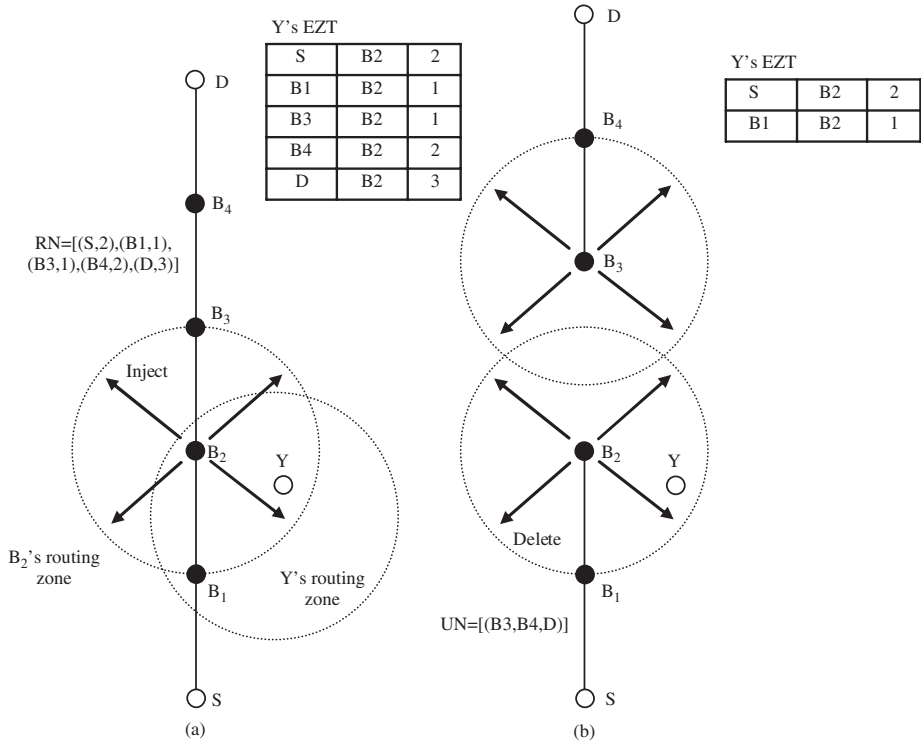

Figure 13.45 An example of (a) injection and (b) deletion of external nodes.

13.7 DISTRIBUTED QoS ROUTING

In this section a distributed QoS routing scheme for *ad hoc* networks is discussed. Two routing problems are presented, *delay constrained least cost routing* (DCLC) and *bandwidth constrained least cost routing* (BCLC). As before, the path that satisfies the delay (or bandwidth) constraint is called a feasible path. The algorithms can tolerate the imprecision of the available state information. Good routing performance in terms of success ratio, message overhead and average path cost is achieved even when the degree of information imprecision is high. Note that the problem of information imprecision exists only for QoS routing; all best-effort routing algorithms, such as DSR and ABR, do not consider this problem because they do not need the QoS state in the first place. Multipath parallel routing is used to increase the probability of finding a feasible path. In contrast to the flooding-based path discovery algorithms, these algorithms search only a small number of paths, which limits the routing overhead. In order to maximize the chance of finding a feasible path, the state information at the intermediate nodes is collectively utilized to make intelligent hop-by-hop path selection. The logic behind this is very much equivalent to using the Viterbi instead of ML (maximum likelihood) algorithm in trellis-based demodulation processes.

The algorithms consider not only the QoS requirements, but also the optimality of the routing path. Low-cost paths are given preference in order to improve the overall network performance. In order to reduce the level of QoS disruption, fault-tolerance techniques are brought in for the maintenance of the established paths. Different levels of redundancy provide tradeoff between the reliability and the overhead. The dynamic path repairing algorithm repairs the path at the breaking point shifts the traffic to a neighbor node, and reconfigures the path around the breaking point without rerouting the connection along a completely new path. Rerouting is needed in two cases. One case is when the primary path and all secondary paths are broken. The other case is when the cost of the path grows large and hence it becomes beneficial to route the traffic to another path with a lower cost.

13.7.1 Wireless links reliability

One element of the cost function will be reliability of the wireless links. The links between the stationary or slowly moving nodes are likely to exist continuously. Such links are called *stationary links*. The links between the fast moving nodes are likely to exist only for a short period of time. Such links are called *transient links.* A routing path should use stationary links whenever possible in order to reduce the probability of a path breaking when the network topology changes. A *stationary neighbor* is connected to a node with a stationary link. As in Chapter 7, delay of path P between two nodes equals the sum of the link delays on the path between the two nodes and will be denoted as *delay(P).* Similarly *bandwidth(P)* equals the minimum link bandwidth on the path P, and *cost(P)* equals the sum of the link costs.

13.7.2 Routing

Given a source node s, a destination node t, and a delay requirement D, the problem of delay-constrained routing is to find a feasible path P from s to t such that $delay(P) \leq D$. When there are multiple feasible paths, we want to select the one with the least cost. Another problem is bandwidth-constrained routing, i.e. finding a path P such that $bandwidth(P) \geq B$, where B is the bandwidth requirement. When there are multiple such paths, the one with the least cost is selected. Finding a feasible path is actually the first part of the problem. The second part is to maintain the path when the network topology changes.

13.7.3 Routing information

The following end-to-end state information is required to be maintained at every node i for every possible destination t. The information is updated periodically by a distance-vector protocol discussed in Section 13.1:

(1) Delay variation – $\Delta D_i(t)$ keeps the estimated maximum change of $D_i(t)$ before the next update. That is, based on the recent state history, the actual minimum end-to-end delay from i to t is expected to be between $D_i(t) - \Delta D_i(t)$ and $D_i(t) + \Delta D_i(t)$ in the next update period.

(2) Bandwidth variation – $\Delta B_i(t)$ keeps the estimated maximum change of $B_i(t)$ before the next update. The actual maximum bandwidth from i to t is expected to be between $B_i(t) - \Delta B_i(t)$ and $B_i(t) + \Delta B_i(t)$ in the next period.

(3) The cost metric $C_i(t)$ is used for optimization, in contrast to the delay and bandwidth metrics used in QoS constraints.

Consider an arbitrary update of $\Delta D_i(t)$ and $D_i(t)$. Let $\Delta D_i(t)$ and $\Delta D_i'(t)$ be the values of $\Delta D_i(t)$ before and after the update, respectively. Similarly, let $D_i(t)$ and $D_i'(t)$ be the values of $D_i(t)$ before and after the update, respectively. $D_i'(t)$ is provided by a distance-vector protocol. $\Delta D_i'(t)$ is calculated as follows:

$$\Delta D_i'(t) = \alpha \Delta D_i(t) + (1 - \alpha) \left| D_i'(t) - D_i(t) \right| \tag{13.15}$$

The factor $\alpha(<1)$ determines how fast the history information $\Delta D_i(t)$ is forgotten, and $1 - \alpha$ determines how fast $\Delta D_i'(t)$ converges to $|D_i'(t) - D_i(t)|$. By the previous formula, it is still possible for the actual delay to be out of the range $[D_i(t) - \Delta D_i(t), D_i(t) + \Delta D_i(t)]$.

One way to make such probability sufficiently small is to enlarge $\Delta D_i(t)$. Hence, we shall modify the formula and introduce another factor $\beta(>1)$:

$$\Delta D_i'(t) = \alpha \Delta D_i(t) + (1 - \alpha)\beta \left| D_i'(t) - D_i(t) \right| \tag{13.16}$$

$\Delta D_i'(t)$ converges to $\beta \left| D_i'(t) - D_i(t) \right|$ at a speed determined by $1 - \alpha$.

13.7.4 Token-based routing

There are numerous paths from s to t. We shall not randomly pick several paths to search. Instead, we want to make an intelligent hop-by-hop path selection to guide the search along the best candidate paths. This is what, for example, the Viterbi algorithm would be doing in trying to avoid search through all possible trajectories of a trellis (ML approach) in a signal demodulation/decoding process.

The basic idea of token-based probing is outlined below. A token is the permission to search one path. The source node issues a number of tokens based on the available state information. One guideline is that more tokens are issued for the connections with tighter requirements. Probes (routing messages) are sent from the source toward the destination to search for a low-cost path that satisfies the QoS requirement. Each probe is required to carry at least one token. At an intermediate node, a probe with more than one token is allowed to be split into multiple ones, each searching a different downstream subpath. The maximum number of probes at any time is bounded by the total number of tokens. Since each probe searches a path, the maximum number of paths searched is also bounded by the number of tokens. See Figure 13.46 for an example. Upon receipt of a probe, an intermediate node decides, based on its state: (1) whether the received probe should be split; and

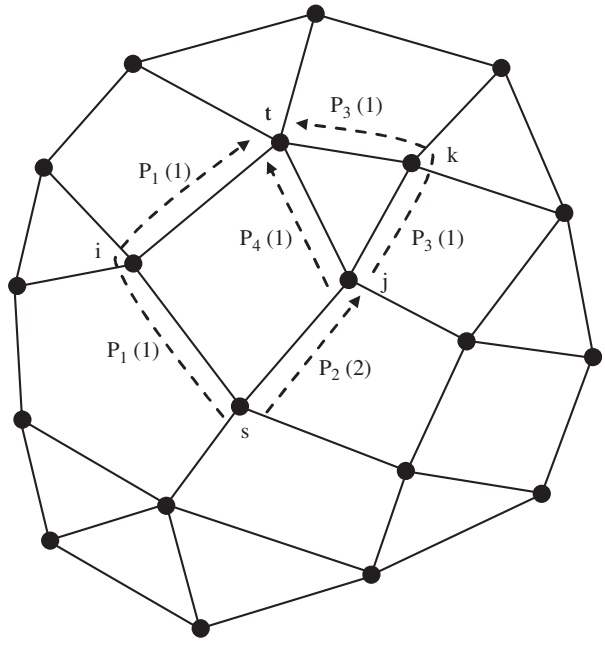

Figure 13.46 Generation of probes p (number of tokens).

(2) to which neighbor nodes the probe(s) should be forwarded. The goal is to collectively utilize the state information at the intermediate nodes to guide the limited tickets (the probes carrying them) along the best paths to the destination, so that the probability of finding a low-cost feasible path is maximized.

13.7.5 Delay-constrained routing

When a connection request arrives at the source node, a certain number N_0 of tokens are generated, and probes are sent toward the destination t. Each probe carries one or more tokens. Since no new tokens are allowed to be created by the intermediate nodes, the total number of tokens is always N_0, and the number of probes is at most N_0 at any time. When a node receives a probe p with $N(p)$ tokens, it makes at most $N(p)$ copies of p, distributes the received tickets among the new probes, and then forwards them along to selected outgoing links toward t. Each probe accumulates the delay of the path it has traversed so far. A probe can proceed only when the accumulated delay does not violate the delay requirement. Hence, any probe arriving at the destination detects a feasible path, which is the one it has traversed.

There are two basic guidelines for how to determine N_0 and how to distribute the tokens in a received probe among the new probes:

(1) Different numbers of tokens are assigned to different connections based on their 'needs'. For a connection whose delay requirement is large and can be easily satisfied, one token is issued to search a single path; for a connection whose delay requirement is smaller, more tokens are issued to increase the chance of finding a feasible path; for a connection whose delay requirement is too small to be satisfied, no tokens are issued, and the connection is immediately rejected.

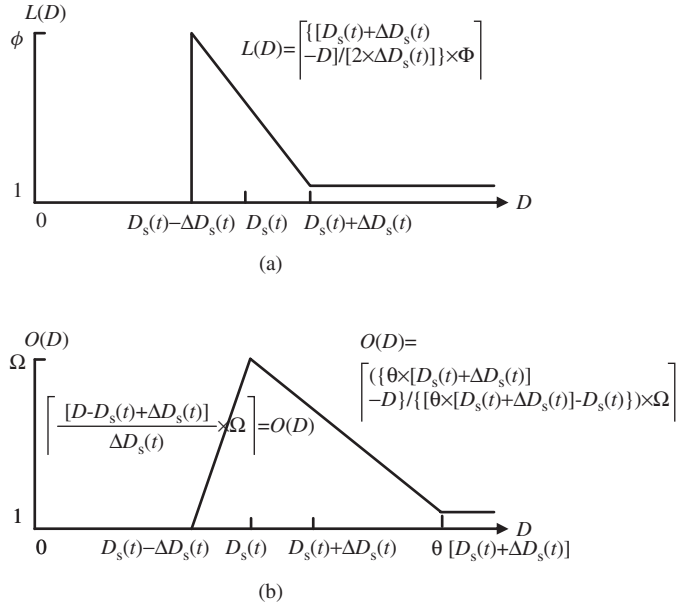

Figure 13.47 Token curves.

(2) When a node i forwards the received tokens to its neighbors, the tokens are distributed unevenly among the neighbors, depending on their chances of leading to reliable low-cost feasible paths. A neighbor having a smaller end-to-end delay to the destination should receive more tickets than a neighbor having a larger delay; a neighbor having a smaller end-to-end cost to the destination should receive more tokens than a neighbor having a larger cost; a neighbor having a stationary link should be given preference over a neighbor having a transient link to i. Note that some neighbors may not receive any tokens because i may have only a few or just one token to forward.

13.7.6 Tokens

The two types of tokens, constraint (limitation) tokens (CT) and optimization tokens (OT) have different purposes. CT tokens prefer paths with smaller delays, so that the chance of satisfying a given delay (constraints) requirement is higher. OT tokens prefer the paths with smaller costs. The overall strategy is to use the more aggressive OT tokens to find a low-cost feasible path with relatively low success probability and to use the CT tokens as a backup to guarantee a high success probability of finding a feasible path. The number of CT tokens L, and OT tokens O is determined based on the delay requirement D. If D is very large and can definitely be satisfied, a single CT token will be sufficient to find a feasible path. If D is too small to be possibly satisfied, no CT token is necessary, and the connection is rejected. Otherwise, more than one CT token is issued to search multiple paths for a feasible one. Based on the previous guideline, a linear token curve shown in Figure 13.47(a) was chosen in Chen and Nahrstedt [85] for simplicity and efficient computation.

Parameter Φ is a system parameter specifying the maximum allowable number of CT. It shows that more CT are assigned for smaller D. Number of optimization tokens O is also determined based on the delay requirement D as shown in Figure 13.47(b).

13.7.7 Forwarding the received tokens

13.7.7.1 Candidate neighbors

If $L + O = 0$, the connection request is rejected. Otherwise, probes carrying the tokens are sent from s to t. A probe proceeds only when the path has a delay of no more than D. Hence, once a probe reaches t, it detects a delay-constrained path. Each probe accumulates the delay of the path it has traversed so far. A data field, denoted as *delay(p)*, is defined in a probe p. Initially, *delay(p)*$\Rightarrow 0$; whenever p proceeds for another *link (i,j)*, *delay(p)* $\Rightarrow$ *delay(p)* + *delay(i,j)*. Suppose a node i receives a probe p with $L(p)$ constraint tokens and $O(p)$ optimization tokens. Suppose k is the sender of the probe p. The set $R_i^p(t)$ of candidate neighbors, to which i will forward the received tokens, is determined as follows. We first consider only the stationary neighbors (V_i^s) of i. Let

$$R_i^p(t) = \left\{ j \,\middle|\, delay(p) + delay(i, j) + D_j(t) - \Delta D_j(t) \le D,\ j \in V_i^s - \{k\} \right\}$$

$R_i^p(t)$is the set of neighbors to which the tickets should be forwarded. If $R_i^p(t) = \{0\}$, we take the transient neighbors into consideration and redefine $R_i^p(t)$ to be

$$R_i^p(t) = \left\{ j \,\middle|\, delay(p) + delay(i, j) + D_j(t) - \Delta D_j(t) \le D,\ j \in V_i - \{k\} \right\}$$

If we still have $R_i^p(t) = \{0\}$, all received tokens are invalidated and discarded. If $R_i^p(t) \neq \{0\}$, then for every $j \in R_i^p(t)$, i makes a copy of p, denoted as p_j. Let p_j have $L(p_j)$ constraint tokens and $O(p_j)$ optimization tokens. These parameters are calculated as

$$L(p_j) = \frac{\left[delay(i, j) + D_j(t)\right]^{-1}}{\sum_{j' \in R_i^p(t)} \left[delay(i, j') + D_{j'}(t)\right]^{-1}} \times L(p)$$

$$O(p_j) = \frac{\left[\cos t(i, j) + C_j(t)\right]^{-1}}{\sum_{j' \in R_i^p(t)} \left[\cos t(i, j') + C_{j'}(t)\right]^{-1}} \times O(p) \tag{13.17}$$

These numbers will be rounded to the closest integer.

The *data structure* carried by a probe p is shown in Table 13.3. The last six fields, *k, path, L(p), O(p), delay(p)* and *cost(p)*, are modified as the probe traverses. Tokens are logical entities, and only the number of tokens is important: there can be at most $L(p) + O(p)$ new probes descending from p, among which probes with constraint tokens choose paths based on delay, probes with optimization tokens choose paths based on cost, and probes with both types of tokens choose paths based on both delay and cost.

13.7.8 Bandwidth-constrained routing

The algorithm shares the same computational structure with the delay-constrained routing algorithm. The differences are the metric-dependent token curves and token distribution formulas. The token curves are given in Figure 13.48.

13.7.9 Forwarding the received tickets

Suppose a node i receives a probe p with $L(p)$ constraint tokens and $O(p)$ optimization tokens. Suppose k is the sender of the probe p. The set $R_i^p(t)$ of candidate neighbours, to which i will

Table 13.3

id	System-wide unique identification for the connection request
s	Source node
t	Destination node
D	Delay requirement
$L + O$	Total number of tokens
k	Sender of *p*
path	Path *p* has traversed so far
L(*p*)	Number of constrained tokens carried by *p*
O(*p*)	Number of optimization tokens carried by *p*
delay(p)	Accumulated delay of the path traversed so far
cost(p)	Accumulated cost of the path traversed so far

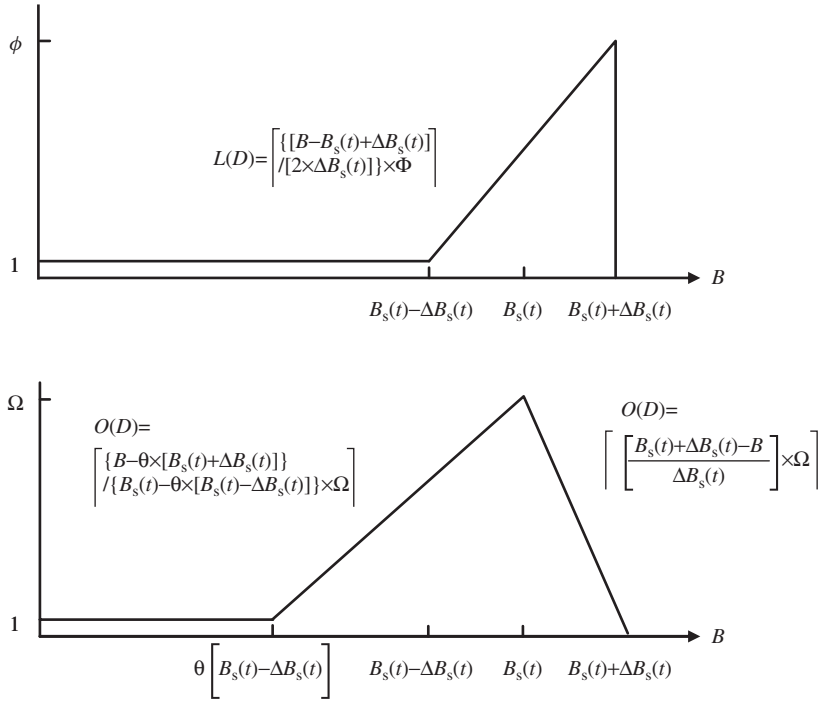

Figure 13.48 Token curves as functions of B.

forward the received tokens, is determined as follows. Define

$$R_i^p(t) = \left\{ j \,\middle|\, bandwidth(i, j) \geq B \wedge B_j(t) + \Delta B_j(t) \geq B,\ j \in V_i^s - \{k\} \right\}$$

If $R_i^p(t) = \{0\}$, we take the transient neighbours into consideration and redefine $R_i^p(t)$ to be

$$R_i^p(t) = \left\{ j \,\middle|\, bandwidth(i, j) \geq B \wedge B_j(t) + \Delta B_j(t) \geq B,\ j \in V_i - \{k\} \right\}$$

If we still have $R_i^p(t) = \{0\}$ all received tokens are invalidated and discarded. If $R_i^p(t) \neq \{0\}$, then for every $j \in R_i^p(t)$, i makes a copy of p, denoted as p_j. Let p_j have $L(p_j)$ constraint tokens and $O(p_j)$ optimization tokens. $L(p_j)$ is determined based on the observation that a probe sent toward the direction with a larger residual bandwidth should have more L tokens. These parameters are now calculated as

$$L(p_j) = \frac{\min\left[bandwidth(i, j), B_j(t)\right]}{\sum_{j' \in R_i^p(t)} \min\left[bandwidth(i, j'), B_{j'}(t)\right]} \times L(p)$$

$$O(p_j) = \frac{\left[\cos t(i, j) + C_j(t)\right]^{-1}}{\sum_{j' \in R_i^p(t)} \left[\cos t(i, j') + C_{j'}(t)\right]^{-1}} \times O(p) \tag{13.18}$$

13.7.10 Performance example

Three performance metrics: (1) success ratio = number of connections accepted/total number of connection requests; (2) avg msg overhead = total number of messages sent/total number of connection requests; and (3) avg path cost = total cost of all established paths/number of established paths, are analysed by simulation in Cher and Nahrstedt [85].

Sending a probe over a link is counted as one message. Hence, for a probe that has traversed a path of l hops, l messages are counted. The network topology used in simulation is randomly generated. Forty nodes are placed randomly within a 15×15 m area. The transmission range of a node is bounded by a circle with a radius of 3 m. A link is added between two nodes that are in the transmission range of each other. The average degree of a node is 3.4.

The source node, the destination node, and parameter D of each connection request are randomly generated. D is uniformly distributed in the range of [30, 160 ms]. The cost of each link is uniformly distributed in [0, 200]. Each link (j, k) is associated with two delay values: delay-old denoted as *delay(j,k)* and delay-new denoted as *delay'(j,k); delay(j,k)* is the last delay value advertised by the link to the network. Parameter *delay'(j,k)* is the actual delay of the link at the time of routing. Parameter *delay (j,k)* is uniformly distributed in [0, 50 ms], while *delay'(j,k)* is uniformly distributed in $\left[(1-\xi)delay(j,k), (1+\xi)delay(j,k)\right]$, where ξ is a simulation parameter, called the imprecision rate, defined as

$$\xi = \sup\left\{\left[delay'(j,k) - delay(j,k)\right]/delay(j,k)\right\}$$

Three algorithms are simulated: the flooding algorithm, the token-based probing algorithm (TBP) and the shortest-path algorithm (SP). The flooding algorithm is equivalent to TBP with infinite number of constraint tokens and zero optimization tokens. It floods routing messages from the source to the destination. Each routing message accumulates the delay of the path it has traversed, and the message proceeds only if the accumulated delay does not exceed the delay bound. The system parameters of the TBP algorithm are $\Phi = 4$, $\theta = 1.5$, $\Omega = 3$. The values are obtained by extensive simulation runs. The SP algorithm maintains a state vector at each node I by a distance-vector protocol.

Comparison of the performance results shown in Figures 13.49–13.52 demonstrates advantages of the TBP. The protocol presented in this section is a brief interpretation of Ticket Based Protocol represented in Chen and Nahrstedt [85] with slightly modified terminology adjusted to that of the rest of the book. The problem of QoS routing in wireline and wireless networks has been attracting much attention in both academia and industry. For more information see References [86–88]. A comprehensive overview of the literature is given in Chen and Nahrstedt [88]. The problem will be revisited again in Chapter 21 in more detail.

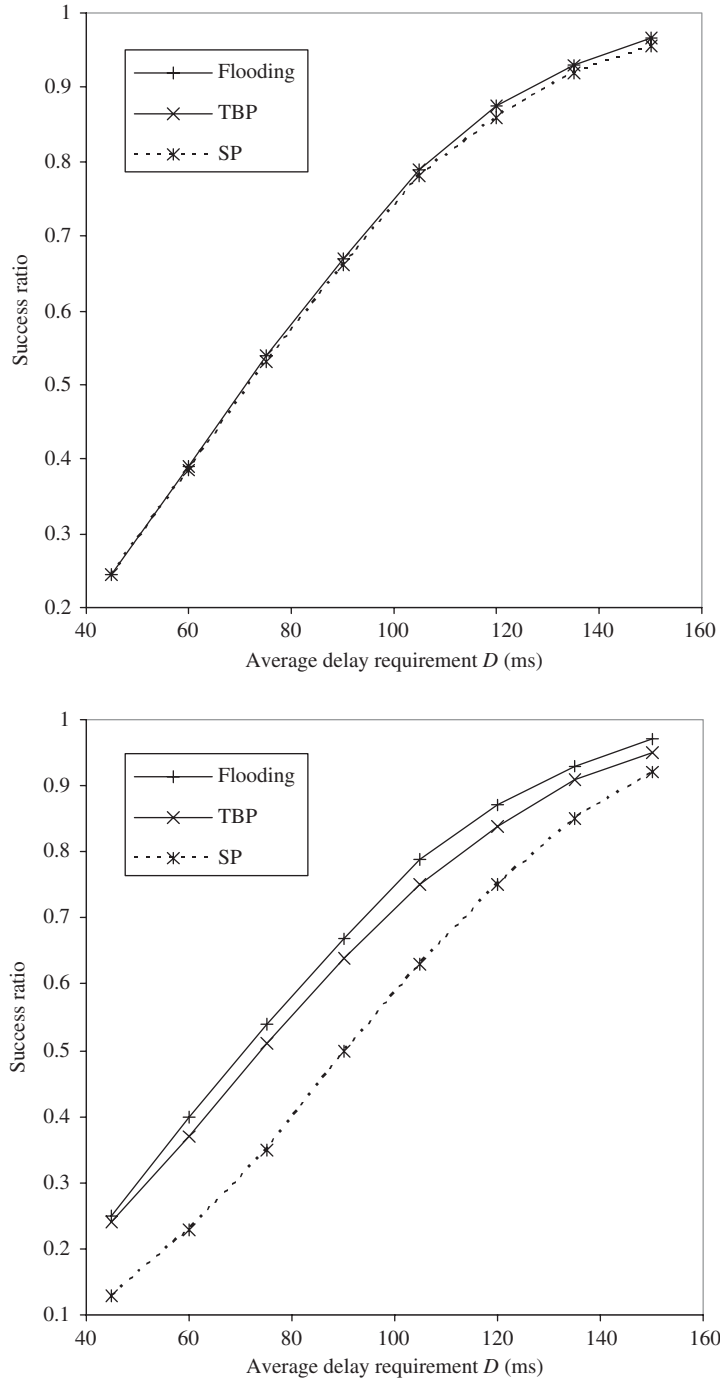

Figure 13.49 Success ratio [imprecision rate: (a) 5 % and (b) 50 %]. (Reproduced by permission of IEEE [85].)

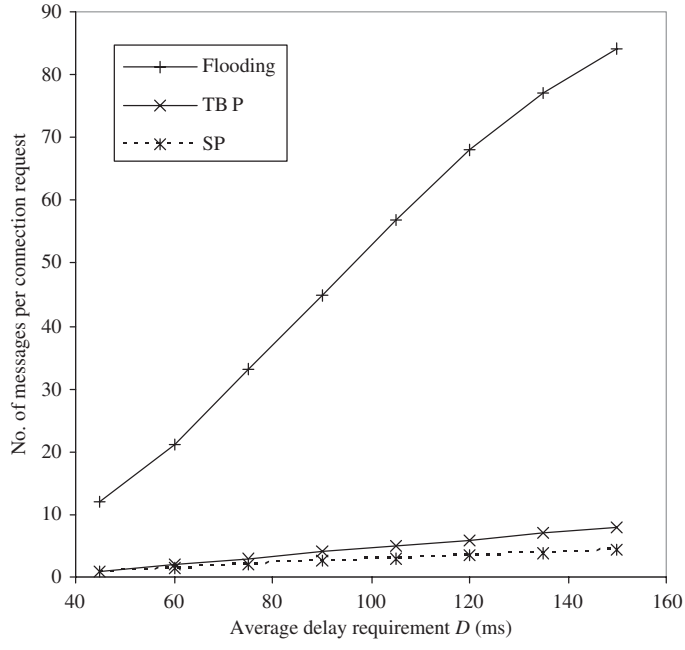

Figure 13.50 Messages overhead (imprecision rate: 10 %). (Reproduced by permission of IEEE [85].)

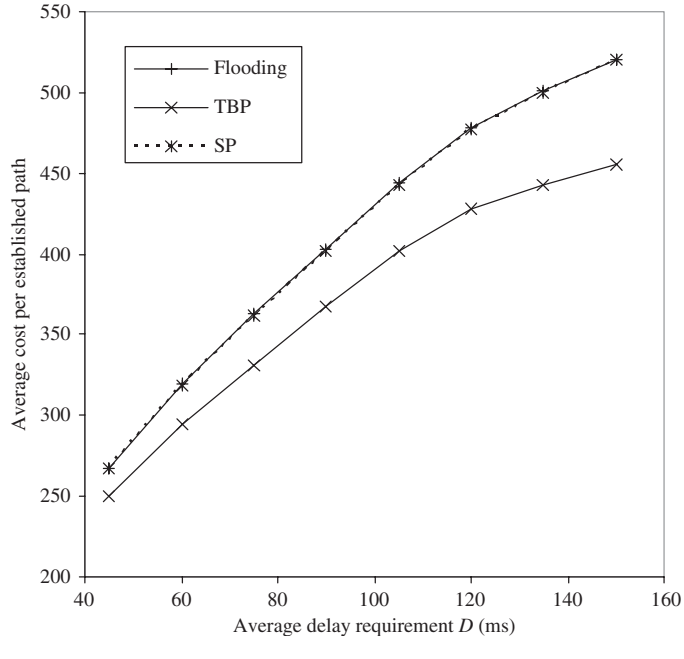

Figure 13.51 Cost per established path (imprecision rate: 5 %). (Reproduced by permission of IEEE [85].)

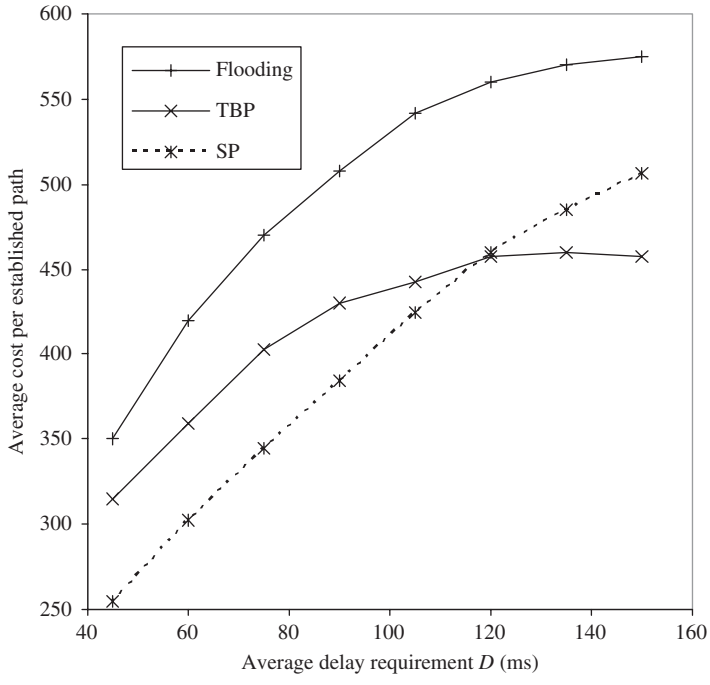

Figure 13.52 Cost per established path (imprecision rate: 50 %). (Reproduced by permission of IEEE [85].)

REFERENCES

[1] C.E. Perkins and P. Bhagwat, Highly dynamic destination-sequenced distance-vector routing (DSDV) for mobile computers, *Comput. Commun. Rev.*, October 1994, pp. 234–244.

[2] J. Jubin and J. Tornow, The DARPA packet radio network protocols, *Proc. IEEE*, vol. 75, no. 1, 1987, pp. 21–32.

[3] E. Royer and C.K. Toh, A review of current routing protocols for *ad hoc* mobile wireless networks, *IEEE Person. Commun.*, April 1999, pp. 46–54.

[4] C.-C. Chiang, Routing in clustered multihop, mobile wireless networks with fading channel, in *Proc. IEEE SICON* '97, April 1997, pp. 197–211.

[5] S. Murthy and I.I. Garcia-Luna-Aceves, An efficient routing protocol for wireless networks, *ACM Mobile Networks App. J.*, (Special Issue on Routing in Mobile Communication Networks), October 1996, pp. 183–197.

[6] A.S. Tanenbaum, *Computer Networks*, 3rd edn, Ch. 5, Prentice Hall: Englewood Cliffs, NJ, 1996, pp. 357–358.

[7] C.E. Perkins and E.M. Royet, *Ad-hoc* on-demand distance vector routing, in *Proc 2nd IEEE Workshop. Mobile Comput*. Technol. and Applications, Feb. 1999, pp. 90–100.

[8] D.B. Johnson and O.A. Maltz, Dynamic source routing in *ad-hoc* wireless networks, in *Mobile Computing*, L. Irnielinski and H. Korth (Eds). Kluwer: Norwell, MA, 1996, pp. 153–181.

[9] J. Broch, O.B. Johnson, and D.A. Maltz, The dynamic source routing protocol for mobile *ad hoc* networks, IETF Internet draft, draft-ietf manet-dsr-01.txt, December 1998 (work in progress).

[10] V.D. Park and M.S. Corson, A highly adaptive distributed routing algorithm for mobile wireless networks, in *Proc. INFOCOM* '97, April 1997.
[11] M.S. Corson and A. Ephremides, A distributed routing algorithm for mobile wireless networks, *ACM/Baltzer Wireless Networks J.*, vol. 1, no. 1, 1995, pp. 61–81.
[12] C.-K. Toh, A novel distributed routing protocol to support *ad-hoc* mobile computing, in *Proc. 1996 IEEE 15th Annual Int. Phoenix Conf. Computing and Communications*, March 1996, pp. 480–486.
[13] R. Dube *et al*., Signal stability based adaptive routing (SSA) for *ad-hoc* mobile networks, *IEEE Person. Commun.*, February 1997, pp. 36–45.
[14] C.-K. Toh, Associativity-based routing for *ad-hoc* mobile networks, *Wireless Person. Commun.*, vol. 4, no. 2, March 1997, pp. 1–36.
[15] S. Murthy and I.I. Garcia-Luna-Aceves, Loop-free internet routing using hierarchical routing trees, in *Proc. INFOCOM '97*, 7–11, April 1997.
[16] C-C. Chiang, M. Gerla and S. Zhang, Adaptive shared tree multicast in mobile wirelesa networks, in *Proc. GLOBECOM '98*, November 1998, pp. 1817–1822.
[17] C.E. Perkins and E.M. Royer, *Ad hoc* on demand distance vector (AODV) routing, IETF Internet draft, draft-ietf-manet-aodv-02.txt, November 1998 (work in progress),
[18] L. Ji and M.S. Corson, A lightweight adaptive multicast algorithm, in *Proc. GLOBECOM '98*, November 1998, pp. 1036–1042.
[19] C.-K. Toh and G. Sin, Implementing associativity-based routing for *ad hoc* mobile wireless networks, Unpublished article, March 1998.
[20] D. Baker *et al*., Flat vs. hierarchical network control architecture, in *ARO/DARPA Workshop mobile ad-hoc Networking*; www.isr.umd. edu, Mar, 1997.
[21] M. Gerla, C-C. Chiang and L. Zhang, Tree multicast strategies in mobile, multihop wireless networks, *ACM/Baltzer Mobile Networks Applic. J.*, 1998.
[22] S. Singh, T. Woo and C.S. Raghavendra, Power-aware routing in mobile *ad hoc* networks, in *proc. ACM/IEEE MO6'ICOM '98*, October 1998.
[23] Y. Ko and N.H. Vaidya, Location-aided routing (LAR) in mobile *ad hoc* networks, in *Proc. ACM/IEEE MCIBCOM '98*, October 1998.
[24] C.R. Sin and M. Gerla, MACNPR: an asynchronous multimedia multi- hop wireless network, in *Proc. IEEE INFOCOM '97*, March 1997.
[25] Z.J. Haas and M.R. Pearlman, The performance of a new routing protocol for the reconfigurable wireless networks, in *Proc. ICC'98*, pp. 156–160.
[26] Z.J. Haas and M.R. Pearlman, Evaluation of the *ad-hoc* connectivity with the reconfigurable wireless networks, in *Virginia Tech's Eighth Symp. Wireless Personal Communications*, 1998, pp. 156–160.
[27] Z.J. Haas and M.R. Pearlman, The performance of query control schemes for the zone routing protocol, in *Proc. SIGCOMM'98*, pp. 167–177.
[28] P. Jacquet, P. Muhlethaler and A. Qayyum, Optimized link state routing protocol, *IETF MANET,* Internet Draft, November 1998. http://www.ietf.cnri.reston.va.us
[29] D.B. Johnson and D.A. Maltz, Dynamic source routing in ad hoc wireless networking, in *Mobile Computing*, T. Imielinski and H. Korth (Eds). Kluwer: Norwell, MA, 1996.
[30] J. Moy, OSPF version 2, RFC 2178, March 1997.
[31] S. Murthy and J.J. Garcia-Luna-Aceves, A routing protocol for packet radio networks, in *Proc. ACM Mobile Computing and Networking Conf. (MOBICOM'95)*, pp. 86–94.
[32] An efficient routing protocol for wireless networks, *MONET*, vol. 1, 1986, pp. 183–197.
[33] V.D. Park and M.S. Corson, A highly adaptive distributed routing algorithm for mobile wireless networks, in *Proc. IEEE INFOCOM '97*, Kobe, pp. 1405–1413.
[34] C.E. Perkins and P. Bhagwat, Highly dynamic destination-sequenced distance-vector routing (DSDV) for mobile computers, in *Proc. ACM SIGCOMM,* vol. 24, no. 4, October 1994, pp. 234–244.

[35] C.E. Perkins and E.M. Royer, *Ad hoc* on-demand distance vector routing, in *Proc. IEEE WMCSA'99,* vol. 3, New Orleans, LA, 1999, pp. 90–100.
[36] J. Sharony, A mobile radio network architecture with dynamically changing topology using virtual subnets, *MONET*, vol. 1, 1997, pp. 75–86.
[37] P.F. Tsuchiya, The landmark hierarchy: a new hierarchy for routing in very large networks, *ACM Comput. Commun. Rev.*, vol. 18, 1988, pp. 35–42.
[38] M.R. Pearlman and Z.J. Haas, Determining the optimal configuration for the zone routing protocol, *IEEE J. Selected Areas Commun.*, vol. 17, no. 8, 1999, pp. 1395–1414.
[39] C.-C. Chiang, H.-K. Wu, W. Liu and M. Gerla, Routing in clustered multihop, mobile wireless networks, in *Proc. IEEE Singapore Int. Conf. Networks*, 1997, pp. 197–211.
[40] M. Gerla and J. Tsai, Multicluster, mobile, multimedia radio network, *ACM-Baltzer J. Wireless Networks*, vol. 1, no. 3, 1995, pp. 255–265.
[41] A. Iwata, C.-C. Chiang, G. Pei, M. Gerla and T.-W. Chen, Scalable routing strategies for *ad hoc* wireless networks, *IEEE J. Selected Areas Commun.* vol. 17, no. 8, 1999, pp. 1369–1379.
[42] L. Kleinrock and K. Stevens, Fisheye: a lenslike computer display transformation, Computer Science Department, University of California, Los Angeles, CA, Technical Report, 1971.
[43] T.-W. Chen and M. Gerla, Global state routing: a new routing schemes for *ad-hoc* wireless networks, in *Proc. IEEE ICC'98*, 7–11 June 1998, pp. 171–175.
[44] N.F. Maxemchuk, Dispersity routing, in *Proc. IEEE ICC '75*, June 1975, pp. 41.10–41.13.
[45] E. Ayanoglu, C.-L. I, R.D. Gitlin and J.E. Mazo, Diversity coding for transparent self-healing and fault-tolerant communication networks, *IEEE Trans. Commun.*, vol. 41, 1993, pp. 1677–1686.
[46] R. Krishnan and J.A. Silvester, Choice of allocation granularity in multipath source routing schemes, in *Proc. IEEE INFOCOM '93*, vol. 1, 1993, pp. 322–329.
[47] A. Banerjea, Simulation study of the capacity effects of dispersity routing for fault-tolerant realtime channels, in *Proc. ACM SIGCOMM'96*, vol. 26, 1996, pp. 194–205.
[48] D. Sidhu, R. Nair and S. Abdallah, Finding disjoint paths in networks, in *Proc. ACM SIGCOMM '91*, 1991, pp. 43–51.
[49] R. Ogier, V. Rutemburg and N. Shacham, Distributed algorithms for computing shortest pairs of disjoint paths, *IEEE Trans. Inform. Theory*, vol. 39, 1993, pp. 443–455.
[50] S. Murthy and J.J. Garcia-Luna-Aceves, Congestion-oriented shortest multipath routing, in *Proc. IEEE INFOCOM '96*, March 1996, pp. 1028–1036.
[51] W.T. Zaumen and J.J. Garcia-Luna-Aceves, Loop-free multipath routing using generalized diffusing computations, in *Proc. IEEE INFOCOM '98*, March 1998, pp. 1408–1417.
[52] J. Chen, P. Druschel and D. Subramanian, An efficient multipath forwarding method, in *Proc. IEEE INFOCOM '98*, 1998, pp. 1418–1425.
[53] N. Taft-Plotkin, B. Bellur and R. Ogier, Quality-of-service routing using maximally disjoint paths, in *Proc. 7th Int. Workshop Quality of Service (IWQoS'99)*, June 1999, pp. 119–128.
[54] S. Vutukury and J.J. Garcia-Luna-Aceves, An algorithm for multipath computation using distance vectors with predecessor information, in *Proc. IEEE ICCCN '99*, October 1999, pp. 534–539.
[55] I. Cidon, R. Rom, and Y. Shavitt, Analysis of multi-path routing, *IEEE/ACM Trans. Networking*, vol. 7, 1999, pp. 885–896.
[56] A. Nasipuri and S.R. Das, On-demand multipath routing for mobile *ad hoc* networks, in *Proc. IEEE ICCCN*, October 1999, pp. 64–70.
[57] D. Johnson and D. Maltz, Dynamic source routing in *ad hoc* wireless networks, in *Mobile Computing*, T. Imielinski and H. Korth (Eds). Kluwer: Norwell, MA, 1996.
[58] V.D. Park and M.S. Corson, A highly adaptive distributed routing algorithm for mobile wireless networks, in *Proc. IEEE INFOCOM '99*, 1999, pp. 1405–1413.
[59] J. Raju and J.J. Garcia-Luna-Aceves, A new approach to on-demand loop-free multipath routing, in *Proc. IEEE ICCCN*, October 1999, pp. 522–527.

[60] S.J. Lee and M. Gerla, AODV-BR: backup routing in *ad hoc* networks, in *Proc. IEEE WCNC*, 2000, pp. 1311–1316.
[61] C.E. Perkins and E.M. Royer, *Ad-hoc* on-demand distance vector routing, in *Proc. IEEE WMCSA*, New Orleans, LA, February 1999, pp. 90–100.
[62] L. Wang, L. Zhang, Y. Shu and M. Dong, Multipath source routing in wireless *ad hoc* networks, in *Proc. Canadian Conf. Electrical and Computer Engineering*, vol. 1, 2000, pp. 479–483.
[63] S.J. Lee and M. Gerla, Split multipath routing with maximally disjoint paths in *ad hoc* networks, in *Proc. ICC 2001*, vol. 10, June 2001, pp. 3201–3205.
[64] P. Papadimitratos, Z.J. Haas and E.G. Sirer, Path set selection in mobile *ad hoc* networks, in *Proc. ACM MobiHOC 2002*, Lausanne, 9–11, June 2002, pp. 160–170.
[65] M.R. Pearlman, Z.J. Haas, P. Sholander and S.S. Tabrizi, On the impact of alternate path routing for load balancing in mobile *ad hoc* networks, in *Proc. MobiHOC*, 2000, pp. 150–310.
[66] N. Gogate, D. Chung, S. Panwar and Y. Wang, Supporting video/image applications in a mobile multihop radio environment using route diversity, in *Proc. IEEE ICC '99*, vol. 3, June 1999, pp. 1701–1706.
[67] A. Tsirigos and Z.J. Haas, Analysis of Multipath Routing: part 2 – mitigation of the effects of frequently changing network topologies, *IEEE Trans. Wireless Commun.*, vol. 3, No. 2, March 2004, pp. 500–511.
[68] A.B. McDonald and T. Znati, A path availability model for wireless ad hoc networks, in *Proc. IEEE WCNC*, vol. 1, 1999, pp. 35–40.
[69] A. Tsirigos and Z.J. Haas, Analysis of multipath routing: part 1 – the effect on packet delivery ratio, *IEEE Trans. Wireless Commun.*, vol. 3, no. 1, 2004, pp. 138–146.
[70] C.R. Lin and M. Gerla, Adaptive clustering for mobile wireless networks," *IEEE J. Selected Areas Commun.*, vol. 15, no. 7, 1997, pp. 1265–1275.
[71] M. Gerla and J.T. Tsai, Multicluster, mobile, multimedia radio network, *Wireless Networks,* vol. 1, 1995, pp. 255–265.
[72] N.H. Vaidya, P. Krishna, M. Chatterjee and D.K. Pradhan, A cluster-based approach for routing in dynamic networks, *ACM Comput. Commun. Rev.*, vol. 27, no. 2, 1997.
[73] R. Ramanathan and M. Steenstrup, Hierarchically-organized, multihop mobile wireless networks for quality-of-service support, *Mobile Networks Applic.*, vol. 3, no. 1, 1998, pp. 101–119.
[74] A.B. McDonald and T.F. Znati, A Mobility-based framework for adaptive clustering in wireless *ad hoc* Networks, *IEEE J. Selected Areas Commun.*, vol. 17, No. 8, 1999, pp. 1466–1488.
[75] D.J. Baker and A. Ephremides, The architectural organization of a mobile radio network via a distributed algorithm, *IEEE Trans. Commun.*, 1981, pp. 1694–1701.
[76] D.J. Baker, J. Wieselthier and A. Ephremides, A distributed algorithm for scheduling the activation of links in a self-organizing, mobile, radio network, in *Proc. IEEE ICC'82*, pp. 2F.6.1–2F.6.5.
[77] I. Chlamtac and S.S. Pinter, Distributed nodes organization algorithm for channel access in a multihop dynamic radio network, *IEEE Trans. Comput.*, 1987, pp. 728–737.
[78] M. Gerla and J. T.-C. Tsai, Multicluster, mobile, multimedia radio network, *ACM-Baltzer J. Wireless Networks*, vol. 1, no. 3, 1995, pp. 255–265.
[79] A.B. McDonald and T. Znati, Performance evaluation of neighbour greeting protocols: ARP versus ES-IS, *Comput. J.,* vol. 39, no. 10, 1996, pp. 854–867.
[80] P. Beckmann, *Probability in Communication Engineering*. Harcourt Brace World: New York, 1967.
[81] Y. Hu and D.B. Johnson, Caching strategies in on-demand routing protocols for wireless *ad hoc* networks, in *Proc. MobiCom 2000*, August 2000, pp. 231–242.

[82] D.B. Johnson and D.A. Maltz, Dynamic source routing in *ad hoc* wireless networks, www.ietf.org/internet-drafts/draft-ietf-manet-dsr-03.txt, IETF Internet Draft (work in progress), October 1999.

[83] M.K. Marina and S.R. Das, Performance of route cache strategies in dynamic source routing: *Proc. Second Wireless Networking and Mobile Computing (WNMC)*, April 2001.

[84] D. Maltz, J. Broch, J. Jetcheva and D.B. Johnson, The effects of on-demand behavior in routing protocols for multi-hop wireless *ad hoc* networks, *IEEE J. Selected Areas in Commun.*, Special Issue on Mobile and Wireless Networks, August 1999.

[85] S. Chen and K. Nahrstedt, Distributed quality-of-service routing in *ad hoc* Networks, *IEEE J. Selected Areas Commun.*, vol. 17, no. 8, August 1999, pp. 1488–1505.

[86] H.F. Soloma, S. Reeves and Y. Viniotis, Evaluation of multicast routing algorithms for real-time communication on high-speed networks, *IEEE J. Selected Area Commun.* vol. 15, no. 3, 1997, pp. 332–345.

[87] I. Cidon, R. Ram and V. Shavitt, Multi-path routing combined with resource reservation,: *IEEE INFOCOM '97*, Japan, April 1997, pp. 92–100.

[88] S. Chen and K. Nahrstedt, An overview of quality-of-service routing for the next generation high-speed networks: problems and solutions, *IEEE Networks*, Special Issue on Transmission and Distribution of Digital Video, November/December 1998, pp. 64–79.

14

Sensor Networks

14.1 INTRODUCTION

A sensor network is composed of a large number of sensor nodes, which are densely deployed either inside the phenomenon they are observing, or very close to it. Most of the time the nodes are randomly deployed in inaccessible terrains or disaster relief operations. This also means that sensor network protocols and algorithms must possess self-organizing capabilities. Another unique feature of sensor networks is the cooperative effort of sensor nodes. Sensor nodes are fitted with an on-board processor. Instead of sending the raw data to the nodes responsible for the fusion, sensor nodes use their processing abilities to locally carry out simple computations and transmit only the required and partially processed data.

The above described features ensure a wide range of applications for sensor networks. Some of the application areas are health, military and security. For example, the physiological data about a patient can be monitored remotely by a doctor. While this is more convenient for the patient, it also allows the doctor to better understand the patient's current condition. Sensor networks can also be used to detect foreign chemical agents in the air and the water. They can help to identify the type, concentration and location of pollutants. In essence, sensor networks will provide the end user with intelligence and a better understanding of the environment. It is expected that, in future, wireless sensor networks will be an integral part of our lives, even more than the present-day personal computers.

Realization of these and other sensor network applications require wireless *ad hoc* networking techniques. Although many protocols and algorithms have been proposed for traditional wireless *ad hoc* networks, as described in Chapter 13, they are not well suited for the unique features and application requirements of sensor networks. To illustrate this point, the differences between sensor networks and *ad hoc* networks (see Chapter 13, and references therein) are outlined below [1–5]:

- sensor nodes are densely deployed;
- sensor nodes are prone to failure;
- the number of sensor nodes in a sensor network can be several orders of magnitude higher than the nodes in an *ad hoc* network;

Advanced Wireless Technologies: Cognitive, Cooperative & Opportunistic 4G Technology Second Edition Savo G. Glisic

- the topology of a sensor network changes very frequently;
- sensor nodes mainly use broadcast communication paradigms whereas most *ad hoc* networks are based on point-to-point communications;
- sensor nodes are limited in power, computational capacities and memory;
- sensor nodes may not have global identification (ID) because of the large amount of overhead and large number of sensors.

One of the most important constraints on sensor nodes is the low power consumption requirement. Sensor nodes carry limited, quite often irreplaceable, power sources. Therefore, while traditional networks aim to achieve high QoS provisions, sensor network protocols must focus primarily on power conservation. They must have inbuilt trade-off mechanisms that give the end user the option of prolonging network lifetime at the cost of lower throughput or higher transmission delay. This problem will be the focus of this chapter.

Sensor networks may consist of many different types of sensors such as seismic, low sampling rate magnetic, thermal, visual, infrared, acoustic and radar. These sensors are able to monitor a wide variety of ambient conditions that include the current characteristics such as speed, direction and size of an object, temperature, humidity, vehicular movement, lightning condition, pressure, soil makeup, noise levels, the presence or absence of certain kinds of objects, mechanical stress levels on attached objects etc.

Sensor nodes can be used for continuous sensing, event detection, event ID, location sensing, and local control of actuators. The concept of micro-sensing and wireless connection of these nodes promises many new application areas. Usually these applications are categorized into military, environment, health, home and other commercial areas. It is possible to expand this classification with more categories such as space exploration, chemical processing and disaster relief.

Wireless sensor networks can be an integral part of military command, control, communications, computing, intelligence, surveillance, reconnaissance and targeting (C4ISRT) systems. They

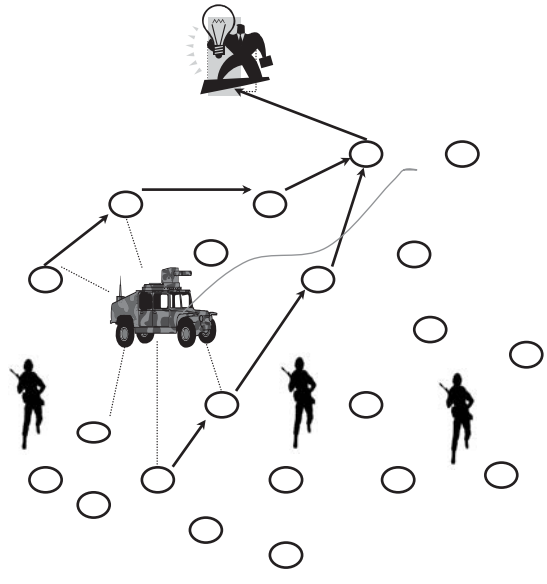

Figure 14.1 Battlefield surveillance.

are used for monitoring friendly forces, equipment and ammunition and battlefield surveillance (Figure 14.1). Sensor networks can be deployed in critical terrains, and some valuable, detailed and timely intelligence about the opposing forces and terrain can be gathered within minutes before the opposing forces can intercept them. Sensor networks can also be incorporated into the guidance systems of intelligent ammunition.

Sensor networks deployed in the friendly region and used as a chemical or biological warning system can provide friendly forces with critical reaction time, which decreases casualty numbers drastically. Environmental applications of sensor networks include tracking the movements of birds, small animals and insects; monitoring environmental conditions that affect crops and livestock; irrigation; macroinstruments for large-scale Earth monitoring and planetary exploration; chemical/biological detection; precision agriculture; biological, Earth and environmental monitoring in marine, soil and atmospheric contexts; forest fire detection; meteorological or geophysical research; flood detection; bio-complexity mapping of the environment; and pollution study.

The health applications for sensor networks are providing interfaces for the disabled, integrated patient monitoring, diagnostics, drug administration in hospitals, monitoring the movements and internal processes of insects or other small animals, telemonitoring of human physiological data, and tracking and monitoring doctors and patients inside a hospital. More details on sensor networks applications can be found in References [6–64].

14.2 SENSOR NETWORKS PARAMETERS

A sensor network design is influenced by many parameters, which include fault tolerance, scalability, production costs, operating environment, sensor network topology, hardware constraints, transmission media and power consumption. The failure of sensor nodes should not affect the overall task of the sensor network. This is the reliability or fault tolerance issue. Fault tolerance is the ability to sustain sensor network functionalities without any interruption due to sensor node failures [25, 49].

The protocols and algorithms may be designed to address the level of fault tolerance required by the sensor networks. If the environment where the sensor nodes are deployed has little interference, then the protocols can be more relaxed. For example, if sensor nodes are being deployed in a house to keep track of humidity and temperature levels, the fault tolerance requirement may be low since this kind of sensor networks is not easily damaged or interfered with by environmental noise. On the other hand, if sensor nodes are being deployed in a battlefield for surveillance and detection, then the fault tolerance has to be high because the sensed data are critical and sensor nodes can be destroyed by hostile actions. As a result, the fault tolerance level depends on the application of the sensor networks, and the schemes must be developed with this in mind. The number of sensor nodes deployed in studying a phenomenon may be in the order of hundreds or thousands. The networks must be able to work with this number of nodes. The density can range from few sensor nodes to few hundred sensor nodes in a region, which can be less than 10 m in diameter [12]. The node density depends on the application in which the sensor nodes are deployed. For machine diagnosis application, the node density is around 300 sensor nodes in a $5 \times 5\,m^2$ region, and the density for the vehicle tracking application is around 10 sensor nodes per region [51]. In some cases, the density can be as high as 20 sensor nodes/m^3 [51]. A home may contain around two dozen home appliances containing sensor nodes [42], but this number will grow if sensor nodes are embedded into furniture and other miscellaneous items. For habitat monitoring application, the number of sensor nodes ranges from 25 to 100 per region. The density will be extremely high when a person normally containing hundreds of sensor nodes, which are embedded in eye glasses, clothing, shoes, watch, jewelry and the human body, is sitting inside a stadium watching a basketball, football or baseball game.

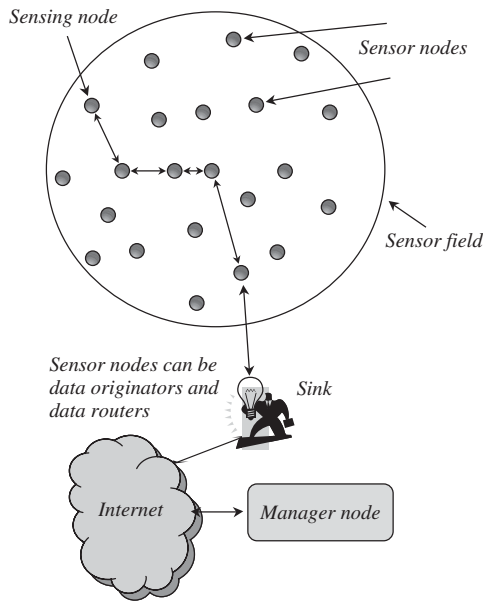

Figure 14.2 Sensor network topology.

As a consequence, the cost of each sensor node has to be kept low. The state-of-the-art technology allows a Bluetooth radio system to be less than US$10 [46]. Also, the price of a PicoNode is targeted to be less than US$1 [45]. The cost of a sensor node should be much less than US$1 in order for the sensor network to be feasible [45]. The cost of a Bluetooth radio, which is known to be a low-cost device, is 10 times more expensive than the targeted price for a sensor node. Note that a sensor node also has some additional units such as sensing and processing units. In addition, it may be equipped with a location-finding system, mobilizer or power generator depending on the applications of the sensor networks. As a result, the cost of a sensor node is a very challenging issue given the amount of functionality with a price of much less than a dollar.

An illustration of sensor network topology is shown in Figure 14.2. Deploying a high number of nodes densely requires careful handling of topology maintenance. Issues related to topology maintenance and change can be classified in three phases [66–77].

14.2.1 Pre-deployment and deployment phase

Sensor nodes can be either thrown in mass or placed one by one in the sensor field. They can be deployed by dropping from a plane, delivering in an artillery shell, rocket or missile, throwing by a catapult (from a ship, etc.), placing in factory or placing one by one either by a human or a robot. Although the sheer number of sensors and their unattended deployment usually preclude placing them according to a carefully engineered deployment plan, the schemes for initial deployment must reduce the installation cost, eliminate the need for any preorganization and preplanning, increase the flexibility of arrangement and promote self-organization and fault tolerance.

14.2.2 Post-deployment phase

After deployment, topology changes are due to change in sensor nodes' [27, 34] position, reachability (due to jamming, noise, moving obstacles, etc.), available energy, malfunctioning and task

details. Sensor nodes may be statically deployed. However, device failure is a regular or common event due to energy depletion or destruction. It is also possible to have sensor networks with highly mobile nodes. In addition, sensor nodes and the network experience varying task dynamics, and they may be a target for deliberate jamming. Therefore, all these factors cause frequent changes in sensor network topologies after deployment.

14.2.3 Re-deployment of additional nodes phase

Additional sensor nodes can be re-deployed at any time to replace the malfunctioning nodes or due to changes in task dynamics. Addition of new nodes poses a need to re-organize the network. Coping with frequent topology changes in an *ad hoc* network that has myriad nodes and very stringent power consumption constraints requires special routing protocols.

In a multihop sensor network, communicating nodes are linked by a wireless medium. One option for radio links is the use of industrial, scientific and medical (ISM) bands, listed in Table 14.1, which offer license-free communication in most countries.

Some of these frequency bands are already being used for communication in cordless phone systems and wireless local area networks (WLANs). For sensor networks, a small-sized, low-cost, ultralow power transceiver is required. According to Porret *et al.* [43], certain hardware constraints and the trade-off between antenna efficiency and power consumption limit the choice of a carrier frequency for such transceivers to the ultrahigh frequency range. They also propose the use of the 433 MHz ISM band in Europe and the 915 MHz ISM band in North America. The transceiver design issues in these two bands are addressed in References [16, 35].

14.3 SENSOR NETWORKS ARCHITECTURE

The sensor nodes are usually scattered in a *sensor field* as shown in Figure 14.2. Each of these scattered sensor nodes has the capabilities to collect data and route data back to the *sink* and the end users. Data are routed back to the end user by a multihop infrastructureless architecture through the sink, as shown in Figure 14.2. The sink may communicate with the *task manager node* via Internet or satellite.

The protocol stack used by the sink and all sensor nodes is given in Figure 14.3. This protocol stack combines power and routing awareness, integrates data with networking protocols,

Table 14.1 Frequency bands available for ISM applications

Frequency band	Center frequency
6765–6795 kHz	6780 kHz
13 553–13 567 kHz	13,560 kHz
26 957–27 283 kHz	27,120 kHz
40.66–40.70 MHz	40.68 MHz
433.05–434.79 MHz	433.92 MHz
902–928 MHz	915 MHz
2400–2500 MHz	2450 MHz
5725–5875 MHz	5800 MHz
24–24.25 GHz	24.125 GHz
61–61.5 GHz	61.25 GHz
122–123 GHz	122.5 GHz
244–246 GHz	245 GHz

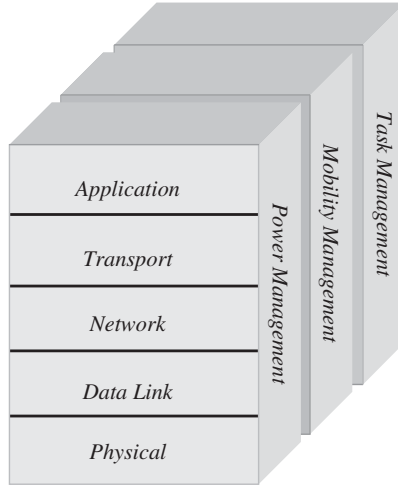

Figure 14.3 The sensor networks protocol stack.

communicates power efficiently through the wireless medium and promotes cooperative efforts of sensor nodes. The protocol stack consists of the *application layer*, *transport layer*, *network layer*, *data link layer*, *physical layer*, *power management plane*, *mobility management plane* and *task management plane* [81–94]. Depending on the sensing tasks, different types of application software can be built and used on the application layer. The transport layer helps to maintain the flow of data if the sensor networks application requires it. The network layer takes care of routing the data supplied by the transport layer. Since the environment is noisy and sensor nodes can be mobile, the MAC protocol must be power aware and able to minimize collision with neighbors' broadcast. The physical layer addresses the needs of a simple but robust modulation, transmission and receiving techniques. In addition, the power, mobility and task management planes monitor the power, movement and task distribution among the sensor nodes. These planes help the sensor nodes coordinate the sensing task and lower the overall power consumption.

14.3.1 Physical layer

The physical layer is responsible for frequency selection, carrier frequency generation, signal detection, modulation and data encryption. The choice of a good modulation scheme is critical for reliable communication in a sensor network. Binary and *M*-ary modulation schemes are compared in Shih *et al.* [51]. While an *M*-ary scheme can reduce the transmit on-time by sending multiple bits per symbol, it results in complex circuitry and increased radio power consumption. These tradeoff parameters are formulated in Shih *et al.* [51] and it is concluded that under start-up power dominant conditions, the binary modulation scheme is more energy-efficient. Hence, *M*-ary modulation gains are significant only for low start-up power systems.

14.3.2 Data link layer

The data link layer is responsible for the multiplexing of data streams, data frame detection, medium access and error control.

14.3.2.1 Medium access control

The MAC protocol in a wireless multihop self-organizing sensor network must achieve two goals [61, 62, 138]. The first is the creation of the network infrastructure. Since thousands of sensor nodes are densely scattered in a sensor field, the MAC scheme must establish communication links for data transfer. This forms the basic infrastructure needed for wireless communication hop by hop and gives the sensor network self-organizing ability. The second objective is to fairly and efficiently share communication resources between sensor nodes. Traditional MAC schemes, described in Chapter 5, are summarized in Figure 14.4 and Table 14.2.

A lot of modifications are needed in MAC protocols when applied in sensor networks. In a cellular system, the base stations form a wired backbone. A mobile node is only a single hop away from the nearest base station. The primary goal of the MAC protocol in such systems is the provision of high QoS and bandwidth efficiency. Power conservation assumes only secondary importance as base stations have unlimited power supply and the mobile user can replenish exhausted batteries in the handset. Hence, medium access is focused on dedicated resource assignment strategy. Such an access scheme is impractical for sensor networks as there is no central controlling agent like the base station.

The mobile *ad hoc* networks (MANET), discussed in Chapter 13, are probably the closest peers to the sensor networks. The MAC protocol in a MANET has the task of forming the network infrastructure and maintaining it in the face of mobility. Hence, the primary goal is the provision of high QoS under mobile conditions. Although the nodes are portable battery-powered devices, they can be replaced by the user and hence power consumption is only of secondary importance.

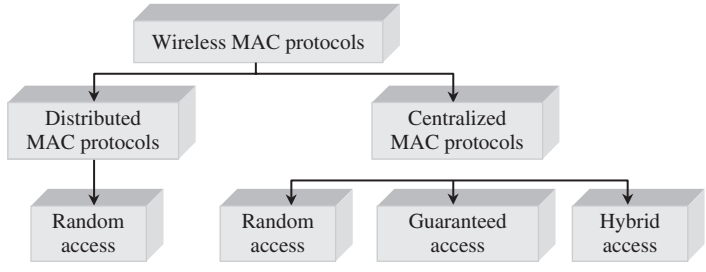

Figure 14.4 Classification of MAC schemes.

Table 14.2 Categorization of MAC protocols

Category	Resource sharing mode	Application domain	Disadvantages
Dedicated assignment or fixed allocation	Pre-determined fixed allocation	Continuous traffic/provides bounded delay	Inefficient for bursty traffic
Demand based	On demand or user request	Variable rate and multimedia traffic	Overhead and delay due to reservation process
Random access or contention-based	Contention when transmission packets are available	Bursty traffic	Inefficient for delay-sensitive traffic

Therefore, the MAC protocol for sensor networks must have built-in power conservation, mobility management and failure recovery strategies. Although many schemes for medium access have been proposed for MANETs (see Chapter 13), the design of an efficient MAC scheme for the new regime of sensor networks is still an open research issue. The *fixed allocation* and *random access* versions of medium access have been discussed in References [54, 60]. *Demand-based* MAC schemes may be unsuitable for sensor networks due their large messaging overhead and link set-up delay. Power conservation is achieved by the use of power saving operation modes and by preferring time-outs to acknowledgements, wherever possible.

Since radios must be turned off during idling for precious power savings, the MAC scheme should include a variant of TDMA [39]. Such a medium access mechanism is presented in Sohrabi *et al.* [54]. Further, contention-based channel access is deemed unsuitable due to its requirement to monitor the channel at all times. It must be noted, however, that random medium access can also support power conservation, as in the IEEE 802.11 standard for WLANs, by turning off radios depending on the status of the net allocation vector. Constant listening times and adaptive rate control schemes can also help achieve energy efficiency in random access schemes for sensor networks [60].

14.3.2.2 Self-organizing MAC for sensor networks (SMACS)

The SMACS protocol [54] achieves network start-up and link-layer organization, and the *eavesdrop-and-register* (*EAR*) algorithm enables seamless connection of mobile nodes in a sensor network. SMACS is a distributed infrastructure-building protocol which enables nodes to discover their neighbors and establish transmission/reception schedules for communication without the need for any local or global master nodes. In this protocol, the neighbor discovery and channel assignment phases are combined so that, by the time nodes hear all their neighbors, they will have formed a connected network. A communication link consists of a pair of time slots operating at a randomly chosen, but fixed frequency (or frequency hopping sequence). This is a feasible option in sensor networks, since the available bandwidth can be expected to be much higher than the maximum data rate for sensor nodes. Such a scheme avoids the necessity for network-wide synchronization, although communicating neighbors in a subnet need to be time-synchronized. *Power conservation* is achieved using a random wake-up schedule during the connection phase and by turning the radio off during idle time slots. The process is based on using an ultralow power radio to wake-up the neighbors. This second radio uses much less power via either a low duty cycle or hardware design. Usually this second radio can only transmit a busy tone. This broadcast tone should not disrupt any on-going data transmission, e.g. use a different channel.

The amount of time and power needed to wake-up (start-up) a radio is not negligible and thus just turning off the radio whenever it is not being used is not necessarily efficient. The energy characteristics of the start-up time should also be taken into account when designing the size of the data link packets.

The EAR protocol [49] attempts to offer continuous service to the mobile nodes under both mobile and stationary conditions. Here, the mobile nodes assume full control of the connection process and also decide when to drop connections, thereby minimizing messaging overhead. The EAR is transparent to the SMACS, so that the SMACS is functional until the introduction of mobile nodes into the network. In this model, the network is assumed to be mainly static, i.e. any mobile node has a number of stationary nodes in its vicinity. A drawback of such a time-slot assignment scheme is the possibility that members already belonging to different subnets might never get connected. For more details see Sohrabi *et al.* [54]. *Carrier sense media access* (CSMA)-based MAC scheme for sensor networks is presented in Woo and Culler [60]. Traditional-CSMA based schemes are deemed inappropriate as they all make the fundamental assumption of stochastically distributed traffic and tend to support independent point-to-point flows. On the contrary, the MAC protocol for sensor networks must be able to support variable, but highly correlated and dominantly

periodic traffic. Any CSMA-based medium access scheme has two important components, the *listening mechanism (sensing)* and the *backoff scheme*. Based on simulations in References [60–64], the constant listen periods are energy-efficient and the introduction of random delay (*p-persistance*) provides robustness against repeated collisions. Fixed window and binary exponential decrease backoff schemes are recommended to maintain proportional fairness in the network. A phase change at the application level is also advocated to get over any capturing effects. It is proposed in this work that the energy consumed/throughput can serve as a good indicator of *energy efficiency*.

14.3.3 Network layer

The *ad hoc* routing techniques, already discussed in Chapter 13, do not usually fit the requirements of the sensor networks. The networking layer of sensor networks is usually designed according to the following principles. First of all, power efficiency is always an important design parameter, see Figure 14.5. Sensor networks are mostly data centric. Data aggregation is useful only when it does not hinder the collaborative effort of the sensor nodes. An ideal sensor network has attribute-based addressing and location awareness. One of the following approaches can be used to select an energy efficient route.

(1) *Maximum available power* (*PA*) *route* – the route that has maximum total available power is preferred.

(2) *Minimum energy* (*ME*) *route* – the route that consumes ME to transmit the data packets between the sink and the sensor node is the ME route.

(3) *Minimum hop* (*MH*) *route* – the route that makes the MH to reach the sink is preferred. Note that the ME scheme selects the same route as the MH when the same amount of energy is

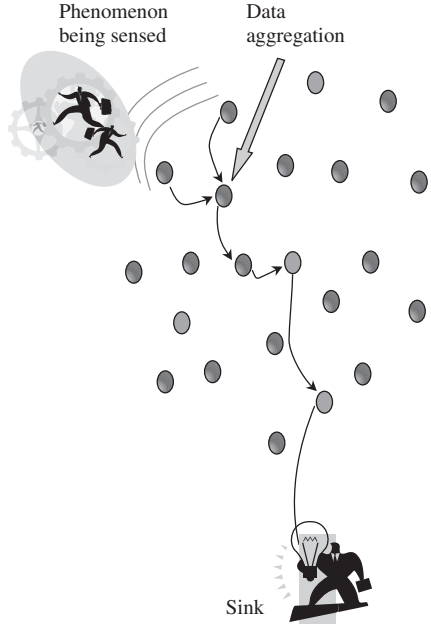

Figure 14.5 Multihop routing due to limited transmission range.

used on every link. Therefore, when nodes broadcast with same power level without any power control, MH is then equivalent to ME.

(4) *Maximum minimum PA node route* – the route along which the minimum PA is larger than the minimum PAs of the other routes is preferred. This scheme precludes the risk of using up a sensor node with low PA much earlier than the others because they are on a route with nodes which have very high PAs.

14.3.3.1 Data centric routing

In data-centric routing, the interest dissemination is performed to assign the sensing tasks to the sensor nodes. There are two approaches used for interest dissemination: sinks broadcast the interest [27], and sensor nodes broadcast an advertisement for the available data [23] and wait for a request from the interested sinks. For an illustration see Figure 14.6.

The data-centric routing requires attribute-based naming [49, 65]. For attribute-based naming, the users are more interested in querying an attribute of the phenomenon, rather than querying an individual node. For instance 'the areas where the moisture is over 70 %' is a more common query than 'the moisture read by a certain node'. The attribute-based naming is used to carry out queries using the attributes of the phenomenon. The attribute-based naming also makes broadcasting, attribute-based multicasting, geo-casting and any-casting important for sensor networks.

Data aggregation is a technique used to solve the implosion and overlap problems in data-centric routing [23]. In this technique, a sensor network is usually perceived as a reverse multicast tree, as shown in Figure 14.7, where the sink asks the sensor nodes to report the ambient condition of the phenomena. Data coming from multiple sensor nodes are aggregated as if they are about the same attribute of the phenomenon when they reach the same routing node on the way back to the sink. Data aggregation can be perceived as a set of automated methods of combining the data that comes from many sensor nodes into a set of meaningful information [22]. With this respect, data aggregation is known as data fusion [23]. Also, care must be taken when aggregating data, because the specifics of the data, e.g. the locations of reporting sensor nodes, should not be left out. Such specifics may be needed by certain applications.

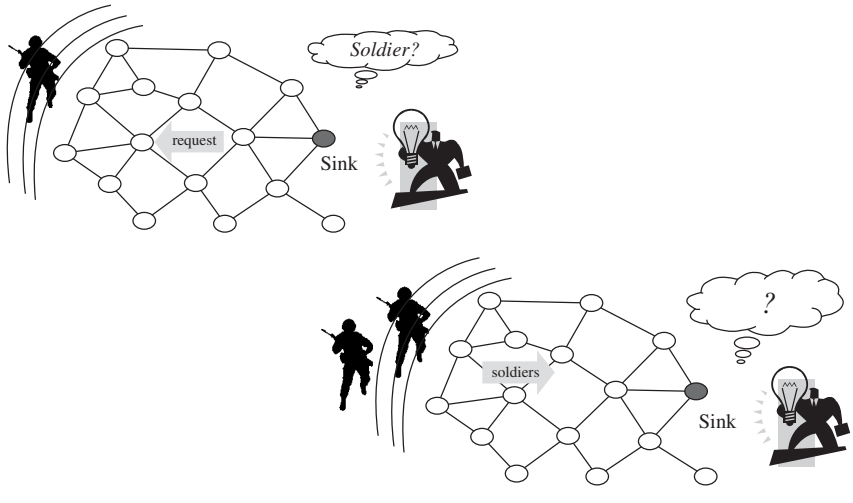

Figure 14.6 Broadcasting the interest (are there any soldiers in the area?) and advertising (there are soldiers in the area).

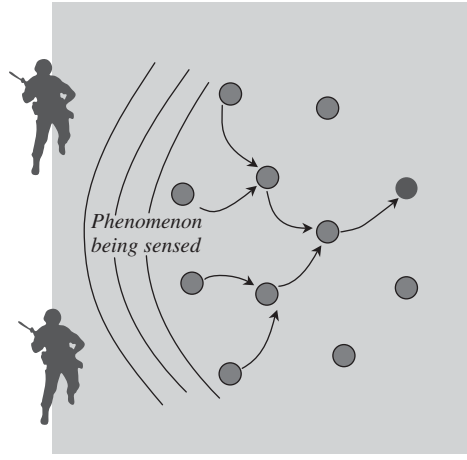

Figure 14.7 The data aggregation.

14.3.3.2 Internetworking

One other important function of the network layer is to provide internetworking with external networks such as other sensor networks, command and control systems and the Internet. In one scenario, the sink nodes can be used as a gateway to other networks. Another option is creating a backbone by connecting sink nodes together and making this backbone access other networks via a gateway.

14.3.3.3 Flooding and gossiping

Flooding has already been described in Chapters 7 and 13 as a technique used to disseminate information across a network. The drawbacks are [23]: (1) *implosion*, when duplicated messages are sent to the same node; (2) *overlap* – when two or more nodes share the same observing region, they may sense the same stimuli at the same time, and as a result, neighbor nodes receive duplicated messages; and (3) *resource blindness*, not taking into account the available energy resources. Control of the energy consumption is of paramount importance in WSNs; a promiscuous routing technique such as flooding wastes energy unnecessarily.

Gossiping is a variation of flooding attempting to correct some of its drawbacks [21]. Nodes do not indiscriminately broadcast but instead send a packet to a randomly selected neighbor who, once it receives the packet, repeats the process. It is not as simple to implement as the flooding mechanism and it takes longer for the propagation of messages across the network.

Data funneling by data aggregation concentrates, e.g. funnels, the packet flow into a single stream from the group of sensors to the sink. It reduces (compresses) the data by taking advantage of the fact that the destination is not that interested in a particular order of how the data packets arrive.

In the setup phase, the controller divides the sensing area into regions and performs a directional flood towards each region. When the packet reaches the region the first receiving node becomes a border node and modifies the packet (add fields) for route cost estimations within the region. Border nodes flood the region with modified packets. Sensor nodes in the region use cost information to schedule which border nodes to use.

In the data communication phase, when a sensor has data it uses the schedule to choose the border node that is to be used. It then waits for a time inversely proportional to the number of

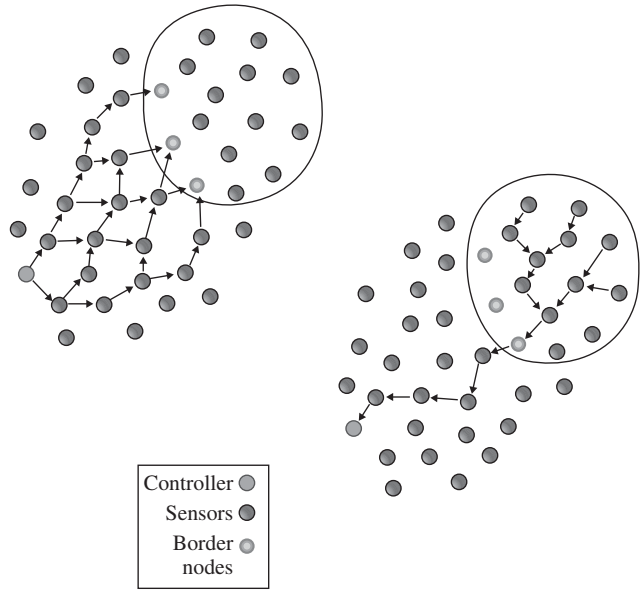

Figure 14.8 Data funneling: (a) setup phase; (b) data communication phase.

hops from the border. Along the way to the border node, the data packets joined together until they reach the border node. The border node collects all packets and then sends one packet with all the data back to the controller These steps are illustrated in Figure 14.8.

14.3.3.4 Sensor protocols for information via negotiation (SPIN)

A family of adaptive protocols called SPIN [23] is designed to address the deficiencies of classic flooding by negotiation and resource adaptation. The SPIN family of protocols is designed based on two basic ideas: sensor nodes operate more efficiently and conserve energy by sending data that describe the sensor data instead of sending the whole data, e.g. image, and sensor nodes must monitor the changes in their energy resources.

The *sequential assignment routing* (*SAR*) [54] algorithm creates multiple trees where the root of each tree is a one-hop neighbor from the sink. Each tree grows outward from the sink while avoiding nodes with very low QoS (i.e. low-throughput/high delay) and energy reserves. At the end of this procedure, most nodes belong to multiple trees. This allows a sensor node to choose a tree to relay its information back to the sink.

The *low-energy adaptive clustering hierarchy* (*LEACH*) [22] is a clustering-based protocol that minimizes energy dissipation in sensor networks. The purpose of LEACH is to randomly select sensor nodes as cluster-heads, so the high-energy dissipation in communicating with the base station is spread to all sensor nodes in the sensor network. During the set-up phase, a sensor node chooses a random number between 0 and 1. If this random number is less than the threshold $T(n)$, the node is a cluster-head. $T(n)$ is calculated as

$$T(n) = \begin{cases} \dfrac{P}{1 - P[rmod(1/P)]} & \text{if } n \in G \\ 0 & \text{otherwise,} \end{cases}$$

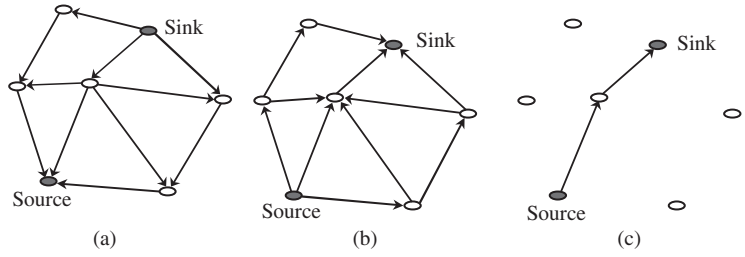

Figure 14.9 An example of directed diffusion [27]: (a) propagate interest, (b) set up gradient and (c) send data.

where P is the desired percentage to become a cluster-head; r, the current round; and G, the set of nodes that have not being selected as a cluster-head in the last $1/P$ rounds. After the cluster-heads are selected, the cluster-heads advertise to all sensor nodes in the network that they are the new cluster-heads. During the steady phase, the sensor nodes can begin sensing and transmitting data to the cluster-heads. After a certain period of time spent on the steady phase, the network goes into the set-up phase again and entering into another round of selecting the cluster-heads.

14.3.3.5 Directed diffusion

The directed diffusion data dissemination is discussed in Intanagonwiwat *et al.* [27]. The sink sends out interest, which is a task description, to all sensors, as shown in Figure 14.9(a). The task descriptors are named by assigning attribute-value pairs that describe the task. Each sensor node then stores the interest entry in its cache. The interest entry contains a timestamp field and several gradient fields. As the interest is propagated throughout the sensor network, the gradients from the source back to the sink are set up as shown in Figure 14.9(b). When the source has data for the interest, the source sends the data along the interest's gradient path as shown in Figure 14.9(c). The interest and data propagation and aggregation are determined locally. Also, the sink must refresh and reinforce the interest when it starts to receive data from the source. The directed diffusion is based on data-centric routing where the sink broadcasts the interest.

14.3.4 Transport layer

The need for transport layer is discussed in References [44, 46]. This layer is especially needed when access to the system is planned through Internet or other external networks. TCP with its current transmission window mechanisms, as discussed in Chapter 9, does match to the extreme characteristics of the sensor network environment. In Bakre and Badrinath [62] an approach called TCP splitting is considered to make sensor networks interact with other networks such as the Internet. In this approach, TCP connections are ended at sink nodes, and a special transport layer protocol can handle the communications between the sink node and sensor nodes. As a result, the communication between the user and the sink node is by UDP or TCP via the Internet or Satellite. Owing to sensor node limited memory, the communication between the sink and sensor nodes may be purely by UDP type protocols.

Unlike protocols such as TCP, the end-to-end communication schemes in sensor networks are not based on global addressing. These schemes must consider that attribute-based naming is used to indicate the destinations of the data packets.

As a conclusion, TCP variants developed in Chapter 9 for the traditional wireless networks are not suitable for WSNs where the notion of *end-to-end reliability* has to be redefined due to the

specific nature of the sensor network which comes with features such as: (1) multiple senders, the sensors and one destination, the sink, which creates a reverse multicast type of data flow; (2) for the same event there is a high level of redundancy or correlation in the data collected by the sensors and thus there is no need for end-to-end reliability between individual sensors and the sink, but instead between the event and the sink; (3) on the other hand there is need of end-to-end reliability between the sink and individual nodes for situations such as re-tasking or reprogramming; (4) the protocols developed should be energy aware and simple enough to be implemented in the low-end type of hardware and software of many WSN applications.

Pump slowly, fetch quickly (PFSQ) is designed to distribute data from a source node by pacing the injection of packets into the network at relatively low speed (*pump slowly*) which allows nodes that experience data loss to aggressively recover missing data from their neighbors (*fetch quickly*). The goals of this protocols are: (1) to ensure that all data segments are delivered to the intended destinations with minimum especial requirements on the nature of the lower layers; (2) to minimize the number of transmissions to recover lost information; (3) to operate correctly even in situations where the quality of the wireless links is very poor; and (4) to (5) provide loose delay bounds for data delivery to all intended receivers. PFSQ has been designed to guarantee sensor-to-sensor delivery and to provide end-to-end reliability for control management distribution from the control node (sink) to the sensors. It does not address congestion control.

Event-to-sink reliable transport (ESRT), illustrated in Figure 14.10, is designed to achieve reliable event detection (at the sink node) with a protocol that is energy aware and has congestion control mechanisms.

The protocol provides self-configuration, even in the case of a dynamic topology. For energy awareness sensor nodes are notified to decrease their frequency of reporting if the reliability level at the sink node is above the minimum. Congestion control takes advantage of the high level of correlation between the data flows corresponding to the same event. Sink is only interested in the collective information from a group of sensors, not in their individual report. Most of the complexity of the protocol falls on the sink node, minimizing the requirements on the sensor nodes.

14.3.5 Application layer

In this section, we discuss three application layer protocols, i.e. sensor management protocol (SMP), task assignment and data advertisement protocol (TADAP), and sensor query and data dissemination protocol (SQDDP). Additional work is expected in this segment of sensor networks.

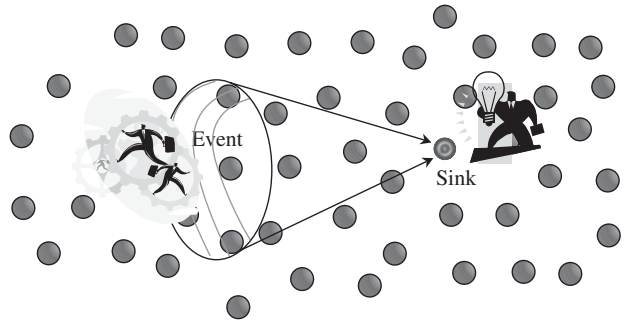

Figure 14.10 Event-to-sink reliable transport (ESRT).

14.3.5.1 Sensor management protocol

Sensor networks have many different application areas, and accessing them through networks such as the Internet is an option [44]. Designing an application layer management protocol has several advantages. It makes the hardware and software of the lower layers transparent to the sensor network management applications. System administrators interact with sensor networks using the sensor management protocol (SMP). Unlike many other networks, sensor networks consist of nodes that do not have global IDs, and they are usually infrastructureless. Therefore, SMP needs to access the nodes by using attribute-based naming and location-based addressing, which are explained in detail earlier in this section. SMP is a management protocol that provides the software operations needed to perform the following administrative tasks: introducing the rules related to data aggregation, attribute-based naming and clustering to the sensor nodes, exchanging data related to the location-finding algorithms, time synchronization of the sensor nodes, moving sensor nodes, turning sensor nodes on and off, querying the sensor network configuration and the status of nodes, re-configuring the sensor network, and authentication, key distribution and security in data communications. Discussion of these issues is given in References [15, 41, 48, 49, 65, 95–97].

The *task assignment and data advertisement protocol* controls interest dissemination in sensor networks. As discussed earlier in this section (Figure 14.6), users send their interest to a sensor node, a subset of the nodes or whole network. This interest may be about a certain attribute of the phenomenon or a triggering event. Another approach is the advertisement of available data in which the sensor nodes advertise the available data to the users, and the users query the data they are interested in. An application layer protocol that provides the user software with efficient interfaces for interest dissemination is useful for lower layer operations, such as routing, as explained in Figure 14.6.

The *sensor query and data dissemination protocol* (SQDDP) provides user applications with interfaces to issue queries, respond to queries and collect incoming replies. Note that these queries are generally not issued to particular nodes. Instead, attribute-based or location-based naming is preferred. For instance, ‘the locations of the nodes in the supermarket where the selling items stock is bellow a threshold and should be re-supplied’ is an attribute-based query. Similarly, ‘the selling item stock size at the node A’ is an example for location-based naming.

Sensor query and tasking language (SQTL) [49] is proposed as an application that provides even a larger set of services. SQTL supports three types of events, which are defined by the keywords *receive*, *every* and *expire*. Receive keyword defines events generated by a sensor node when the sensor node receives a message; every keyword defines events occurring periodically due to a timer time-out; and the expire keyword defines the events occurring when a timer is expired. If a sensor node receives a message that is intended for it and contains a script, the sensor node then executes the script. Although SQTL is proposed, different types of SQDDP can be developed for various applications. The use of SQDDPs may be unique to each application.

14.4 MOBILE SENSOR NETWORKS DEPLOYMENT

A mobile sensor network is composed of a distributed collection of *nodes*, each of which in addition to sensing, computation and communication also has locomotion capabilities. Locomotion facilitates a number of useful network capabilities, including the ability to self-deploy and self-repair. The use of mobile sensor networks includes applications ranging from urban combat scenarios to search-and-rescue operations and emergency environment monitoring. An example is a scenario involving a hazardous materials leak in an urban environment. In general, we would like to be able to throw a number of sensor nodes into a building through a window or doorway.

The nodes are equipped with chemical sensors that allow them to detect the relevant hazardous material, and deploy themselves throughout the building in such a way that they maximize the area 'covered' by these sensors. Data from the nodes are transmitted to a base station located safely outside the building, where they are assembled to form a live map showing the concentration of hazardous compounds within the building.

For the sensor network to be useful in this scenario, the location of each node must be determined. In urban environments, accurate localization using GPS is generally not possible (due to occlusions or multipath effects), while landmark-based approaches require prior models of the environment that may be either unavailable (destroyed), incomplete or inaccurate. This is particularly true in disaster scenarios, were the environment may have undergone recent (and unplanned) structural modifications. Therefore it is of interest to determine the location of network nodes using the nodes *themselves* as landmarks. This particular technique, however, requires that nodes maintain line-of-sight relationships with one another. This condition also enables establishment of line-of-sight communications links which operate with minimum energy consumption. An additional demand is that nodes should deploy in such a way that they maximize the area 'covered' by the network, while simultaneously ensuring that each node can be seen by at least one other node.

The concept of *coverage* as a paradigm for evaluating *multi-robot* [98–114] systems was introduced in Gage [93]. Three basic types of coverage were defined: *blanket coverage*, where the objective is to achieve a static arrangement of nodes that maximizes the total detection area; *barrier coverage*, where the objective is to minimize the probability of undetected penetration through the barrier; and *sweep coverage*, which is more or less equivalent to a moving barrier. The problem of exploration and map-building by a single robot in an unknown environment has been considered by a number of authors [113–115]. The frontier-based approach described in References [113, 114] proceeds by incrementally building a global occupancy map of the environment, which is then analyzed to find the 'frontiers' between free and unknown space. The robot is directed to the nearest such frontier. The network deployment algorithm described in Howard *et al.* [98] shares a number of similarities with [113]. It also builds a global occupancy grid of the environment and direct nodes to the frontier between free and unknown space. However, in this deployment algorithm the map is built entirely from live, rather than stored, sensory data. It also satisfies an additional constraint: that each node must be visible to at least one other node.

Multi-robot exploration and map-building has been explored by a number of authors [100, 106, 109, 111] who use a variety of techniques ranging from topological matching [100] to fuzzy inference [106] and particle filters [111]. Once again, there are two key differences between these earlier works and the work described in Howard *et al.* [98], where maps are built entirely from live, not stored, sensory data, and the deployment algorithm must satisfy an additional constraint (i.e. line-of-sight visibility).

A distributed algorithm for the deployment of mobile robot teams has been described in [108], where the concept of 'virtual pheromones' is introduced. These are localized messages that are emitted by one robot and detected by nearby robots. Virtual pheromones can be used to generate either 'gas expansion' or 'guided growth' deployment models. The key advantage of this approach is that the deployment algorithm is entirely distributed, and has the potential to respond dynamically to changes in the environment. This algorithm does, however, lead to relatively slow deployment; it is also unclear, from the published results, how effective this algorithm is at producing good area coverage. A somewhat similar algorithm based on artificial potential fields is described in Howard *et al.* [104].

The algorithm elaborated in this section is an *incremental* deployment algorithm [98], where nodes are deployed one at a time, with each node making use of information gathered by the previously deployed nodes to determine its ideal deployment location. The algorithm aims to maximize the total network *coverage*, i.e. the total area that can be 'seen' by the network. At the

same time, the algorithm must ensure that the *visibility constraint* is satisfied, i.e. each node must be visible to at least one other node. The algorithm relies on a number of key assumptions:

(1) *Homogeneous nodes* – all nodes are assumed to be identical. We also assume that each node is equipped with a range sensor, a broadcast communications device, and is mounted on some form of mobile platform.

(2) *Static environment* – the environment is assumed to be static, at least to the extent that gross topology remains unchanged while the network is deploying.

(3) *Model-free* – this algorithm is intended for applications in which environment models are unavailable; indeed, a key task for the network may be to *generate* such models.

(4) *Full communication* – all nodes in the network can communicate with some remote base station on which the deployment algorithm is executed. Note that this does not automatically imply that *all* nodes must be within radio range of the base station; the nodes may, for example, form an *ad hoc* multihop network.

(5) *Localization* – the position of each node is known in some arbitrary global coordinate system. This technique does not require external landmarks or prior models of the environment, but does require that each node is visible to at least one other node. It is this requirement that gives rise to the *visibility constraint*, i.e. each node must be visible to at least one other node at its deployed location.

Two performance metrics are of interest: *coverage*, i.e. the total area visible to the network's sensors; and *time*, i.e. the total deployment time, including both the time taken to perform the necessary computations and the time taken to physically move the nodes. The objective is to maximize the coverage while minimizing the deployment time.

The algorithm has four phases: *initialization, selection, assignment* and *execution*.

- *Initialization* – nodes are assigned one of three states: *waiting, active* or *deployed*. As the names suggest, a *waiting* node is waiting to be deployed, an *active* node is in the process of deploying, and a *deployed* node has already been deployed. Initially, the state of all nodes is set to *waiting*, with the exception of a single node that is set to *deployed*. This node provides a starting point, or 'anchor', for the network, and is not subject to the visibility constraint.

- *Selection* – sensor data from the deployed nodes is combined to form a common map of the environment (*occupancy grid*). This map is analyzed to select the deployment location, or goal, for the next node. Each cell in this grid is assigned one of three states: *free*, *occupied* or *unknown*. A cell is *free* if it is known to contain no obstacles, *occupied* if it is known to contain one or more obstacles, and *unknown* otherwise. In the combined occupancy grid, any cell that can be seen by one or more nodes will be marked as either free or occupied; only those cells that cannot be seen by *any* node will marked as unknown. We can therefore ensure that the visibility constraint is satisfied by always selecting goals that lie somewhere in free space.

- *Assignment* – in the simplest case, the selected goal is assigned to a waiting node, and the node's state is changed from *waiting* to *active*. More commonly, assignment is complicated by the fact that deployed nodes tend to obstruct waiting nodes, necessitating a more complex assignment algorithm. That is, the algorithm may have to re-assign the goals of a number of previously deployed nodes, changing their state from *deployed* to *active*.

- *Execution* – active nodes are deployed sequentially to their goal locations. The state of each node is changed from *active* to *deployed* upon arrival at the goal. The algorithm iterates through the selection, assignment and execution phases, terminating only when all nodes have been deployed. Performance examples of the algorithm can be found in Howard *et al.* [98].

14.5 DIRECTED DIFFUSION

As already indicated in Section 14.3.3, directed diffusion consists of several elements. Data is *named* using attribute-value pairs. A sensing task (or a subtask thereof) is disseminated throughout the sensor network as an *interest* for named data. This dissemination sets up *gradients* within the network designed to 'draw' events (i.e. data matching the interest). Events start flowing towards the originators of interests along multiple paths. The sensor network *reinforces* one, or a small number of these paths as illustrated in Figure 14.9. In this section we elaborate these elements in more detail.

In directed diffusion, task descriptions are *named* by, for example, a list of attribute-value pairs that describe a task. For example a surveillance system (military or civil application) which is expected to report an intrusion in a given area might be described as

type = human // *detect location*
interval = 20 ms // *send back events every 20 ms*
duration = 10 s // .. *for the next 10 s*
rect = [−100, 100, 200, 400] // *from sensors within rectangle*

For simplicity, we choose the subregion representation to be a rectangle defined on some coordinate system; in practice, this might be based on GPS coordinates. The task description specifies an interest for data matching the attributes. For this reason, such a task description is called an *interest*. The data sent in response to interests are also named using a similar naming scheme. Thus, for example, a sensor that detects an intrusion might generate the following data:

type = human // *type of intruder seen*
instance = military // *instance of this type*
location = [125, 220] // *node location*
intensity = 0.6 // *signal amplitude measure*
confidence = 0.85 // *confidence in the match*
timestamp = 01:20:40 // *event generation time*

Given our choice of naming scheme, we now describe how interests are *diffused* through the sensor network. Suppose that a task, with a specified *type* and *rect*, a *duration* of 10 min and an *interval* of 10 ms, is instantiated at a particular node in the network. The interval parameter specifies an event data rate; thus, in our example, the specified data rate is 100 events per second. This sink node records the task; the task state is purged from the node after the time indicated by the duration attribute.

For each active task, the sink periodically *broadcasts* an interest message to each of its neighbors. This initial interest contains the specified *rect* and *duration* attributes, but contains a much larger *interval* attribute. Intuitively, this initial interest may be thought of as exploratory; it tries to determine if there indeed are any sensor nodes that detect the human intrusion. To do this, the initial interest specifies a low data rate (in our example, one event per second). Then, the initial interest takes the following form:

type = human
interval = 1 s
rect = [−100, 200, 200, 400]
timestamp = 01:20:40
expiresAt = 01:30:40

The interest is periodically *refreshed* by the sink. To do this, the sink simply re-sends the same interest with a monotonically increasing timestamp attribute. Every node maintains an interest cache. Each item in the cache corresponds to a *distinct* interest. Two interests are distinct if their

type, *interval* or *rect* attributes are different. Interest entries in the cache *do not contain information about the sink*. Thus, interest state scales with the number of distinct active interests. The definition of distinct interests also allows interest *aggregation*. Two interests I_1 and I_2, with identical types, completely overlapping *rect* attributes, can, in some situations, be represented by a single interest entry.

An entry in the interest cache has several fields. A *timestamp* field indicates the timestamp of the last received matching interest. The interest entry also contains several *gradient fields*, up to one per neighbor. Each gradient contains a *data rate* field requested by the specified neighbor, derived from the *interval* attribute of the interest. It also contains a *duration* field, derived from the *timestamp* and *expiresAt* attributes of the interest, and indicating the approximate lifetime of the interest.

When a node receives an interest, it checks to see if the interest exists in the cache. If no matching entry exists (where a match is determined by the definition of distinct interests specified above), the node creates an interest entry. The parameters of the interest entry are instantiated from the received interest. This entry has a single gradient towards the neighbor from which the interest was received, with the specified event data rate. In the above example, a neighbor of the sink will set up an interest entry with a gradient of one event per second towards the sink. For this, it must be possible to distinguish individual neighbors. Any locally unique neighbor identifier may be used for this purpose.

If there exists an interest entry, but no gradient for the sender of the interest, the node adds a gradient with the specified value. It also updates the entry's timestamp and duration fields appropriately. Finally, if there exist both an entry *and* a gradient, the node simply updates the timestamp and duration fields.

After receiving an interest, a node may decide to re-send the interest to some subset of its neighbors. To its neighbors, this interest *appears to originate from the sending node*, although it might have come from a distant sink. This is an example of a *local interaction*. In this manner, interests *diffuse* throughout the network. Not all received interests are re-sent. A node may suppress a received interest if it recently re-sent a matching interest.

Generally speaking, there are several possible choices for neighbors, as presented in Figure 14.11. The simplest alternative is to *re-broadcast* the interest to all neighbors. It may also be possible to perform geographic routing, using some of the techniques described in Chapters 7 and 13. This can limit the topological scope for interest diffusion, thereby resulting in energy savings. Finally, in an immobile sensor network, a node might use cached data to direct interests. For example, if in response to an earlier interest, a node heard from some neighbor A data sent by some sensor within the region specified by the *rect* attribute, it can direct this interest to A, rather than broadcasting to all neighbors.

Figure 14.11(a) shows the gradients established in the case where interests are flooded through a sensor field. Unlike the simplified description in Figure 14.9(b), notice that every pair of neighboring nodes establishes a gradient towards each other. This is a consequence of local interactions.

For a sensor network, a gradient specifies both a data rate and a direction in which to send events. More generally, a gradient specifies a *value* and a direction. Figure 14.9(c) implicitly depicts binary valued gradients. In the sensor networks presented in this section, gradients have two values that determine the event reporting rate. In other sensor networks, gradient values might be used to, for example, probabilistically forward data along different paths, achieving some measure of load balancing.

14.5.1 Data propagation

A sensor node that is within the specified *rect* processes interests as described in the previous section. In addition, the node tasks its local sensors to begin collecting samples. A sensor node

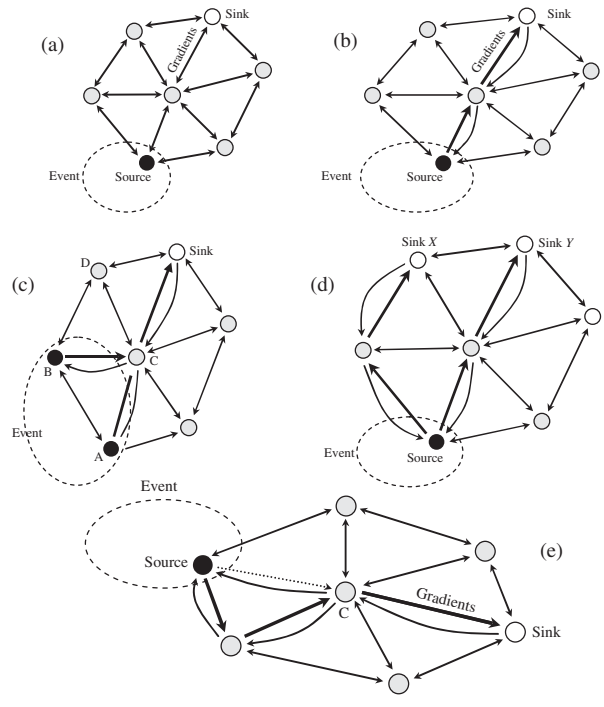

Figure 14.11 Diffusion: (a) gradient establishment; (b) reinforcement; (c) multiple sources; (d) multiple sinks; and (e) repair.

that detects a target searches its interest cache for a matching interest entry. In this case, a matching entry is one whose *rect* encompasses the sensor location, and the type of the entry matches the detected target type. When it finds one, it computes the highest requested event rate among all its outgoing gradients. The node tasks its sensor subsystem to generate event samples at this highest data rate. In the previous example, this data rate is initially one event per second (until reinforcement is applied). The source then sends to each neighbor for whom it has a gradient, an event description every second of the form:

type = human	*// type of intruder seen*
instance = military	*// instance of this type*
location = [125, 220]	*// node location*
intensity = 0.6	*// signal amplitude measure*
confidence = 0.85	*// confidence in the match*
timestamp = 01:20:40	*// local time when event was generated*

This *data* message is unicast individually to the relevant neighbors. A node that receives a data message from its neighbors attempts to find a matching interest entry in its cache. The matching rule is as described in the previous paragraph. If no match exists, the data message is silently dropped. If a match exists, the node checks the *data cache* associated with the matching interest entry for loop prevention. If a received data message has a matching data cache entry, the data message is silently dropped. Otherwise, the received message is added to the data cache and the data message is re-sent to the node's neighbors.

By examining its data cache, a node can determine the data rate of received events. To re-send a received data message, a node needs to examine the matching interest entry's gradient list. If all

gradients have a data rate that is greater than or equal to the rate of incoming events, the node may simply send the received data message to the appropriate neighbors. However, if some gradients have a lower data rate than others (caused by selectively reinforcing paths) then the node may *downconvert* to the appropriate gradient.

14.5.2 Reinforcement

The sink initially diffuses an interest for a low event-rate notification (one event per second). Once sources detect a matching target, they send low-rate events, possibly along multiple paths, towards the sink. After the sink starts receiving these low data rate events, it *reinforces* one particular neighbor in order to 'draw down' higher quality (higher data rate) events. In general, this feature of directed diffusion is achieved by *data driven* local rules. One example of such a rule is to reinforce any neighbor from which a node receives a previously unseen event. To reinforce this neighbor, the sink re-sends the original interest message but with a smaller interval (higher data rate). The reinforcement propagates back, and one way to chose reinforced path is to pick up one with low delay, as shown in Figure 14.11(b). Similar mechanisms are used to handle multiple source and multiple sinks scenarios, as shown in Figure 14.11(c) and (d).

In directed diffusion, *intermediate* nodes on a previously reinforced path can also apply the reinforcement rules. This is useful to enable *local repair* of failed or degraded paths as indicated in Figure 14.11(e).

14.6 AGGREGATION IN WIRELESS SENSOR NETWORKS

Data fusion or aggregation is an important concept in sensor networks. The key idea is to combine data from different sensors to eliminate redundant transmissions, and still provide a rich, multidimensional view of the environment being monitored. This concepts shifts the focus from address-centric approaches (finding routes between pairs of end nodes) to a more data-centric approach (finding routes from multiple sources to a destination that allows in-network consolidation of data).

Consider a network of n sensor nodes $1, 2, \ldots, n$ and a sink node t labeled $n + 1$ distributed over a region. The locations of the sensors and the sink are fixed and known apriori. Each sensor produces some information as it monitors its vicinity. We assume that each sensor generates one data packet per time unit to be transmitted to the base station. For simplicity, we refer to each time unit as a transmission cycle or simply *cycle*. We assume that all data packets have size k bits. The information from all the sensors needs to be gathered at each cycle and sent to the sink for processing. We assume that each sensor has the ability to transmit its packet to any other sensor in the network or directly to the sink. Further, each sensor i has a battery with finite, non-replenishable energy E_i. Whenever a sensor transmits or receives a data packet, it consumes some energy from its battery. The sink has an unlimited amount of energy available to it. Typical assumptions used in the modeling of energy consumption are that sensor consumes $\epsilon_{\text{elec}} = 50\,\text{nJ/b}$ to run the transmitter or receiver circuitry and $\epsilon_{\text{amp}} = 100\,\text{pJ/bit/m}^2$ for the transmitter amplifier. Thus, the energy consumed by a sensor i in receiving a k-bit data packet is given by, $Rx_i = \epsilon_{\text{elec}} \times k$, while the energy consumed in transmitting a data packet to sensor j is given by, $Tx_{i,j} = \epsilon_{\text{elec}} \times k + \epsilon_{\text{amp}} \times d_{i,j}^2 \times k$, where $d_{i,j}$ is the distance between nodes i and j.

We define the *lifetime* T of the system to be the number of cycles until the first sensor is drained of its energy. A *data gathering schedule* specifies, for each cycle, how the data packets from all the sensors are collected and transmitted to the base station. A schedule can be thought of as a collection of T directed trees, each rooted at the base station and spanning all the sensors, i.e. a schedule has one tree for each round. The lifetime of a schedule equals the lifetime of the system under that schedule. The objective is to find a schedule that maximizes the system lifetime T.

Data aggregation performs in-network fusion of data packets, coming from different sensors enroute to the sink, in an attempt to minimize the number and size of data transmissions and thus save sensor energies. Such aggregation can be performed when the data from different sensors are highly correlated. As usual, we make the simplistic assumption that an intermediate sensor can aggregate multiple incoming packets into a single outgoing packet.

The problem is to find a data gathering schedule with maximum lifetime for a given collection of sensors and a sink, with known locations and the energy of each sensor, where sensors are permitted to aggregate incoming data packets.

Consider a schedule S with lifetime T cycles. Let $f_{i,j}$ be the total number of packets that node i (a sensor) transmits to node j (a sensor or sink) in S. The energy constraints at each sensor, impose

$$\sum_{j=1}^{n+1} f_{i,j} \cdot Tx_{i,j} + \sum_{j=1}^{n} f_{j,i} \cdot Rx_i \leq E_i, i = 1, 2, \ldots, n.$$

The schedule S induces a flow network $G = (V, E)$. The flow network G is a directed graph having as nodes all the sensors and the sink, and edges (i, j) with capacity $f_{i,j}$ whenever $f_{i,j} > 0$.

If S is a schedule with lifetime T, and G is the flow network induced by S, then, for each sensor s, the maximum flow from s *to the sink t in G is $\geq T$*. This is due to the fact that each data packet transmitted from a sensor must reach the base station. The packets from s could possibly be aggregated with one or more packets from other sensors in the network. Intuitively, we need to guarantee that each of the T values from s *influences* the final value(s) received at the sink. In terms of network flows, this implies that sensor s must have a maximum $s - t$ flow of size $\geq T$ to the sink in the flow network G. Thus, a necessary condition for a schedule to have lifetime T is that each node in the induced flow network can push flow T to the sink.

Now, we consider the problem of finding a flow network G with maximum T, that allows each sensor to push flow T to the base station, while respecting the energy constraints at all the sensors. What needs to be found are the capacities of the edges of G. Such a flow network G will be referred to as an *admissible* flow network with lifetime T. An admissible flow network with maximum lifetime is called an *optimal admissible* flow network.

An optimal admissible flow network can be found using the integer program with linear constraints. If for each sensor $k = 1, 2, \ldots, n$, $\pi_{i,j}^{(k)}$ is a flow variable indicating the flow that k sends to the sink t over the edge (i, j), the integer program is given by:

Maximize T with

$$\sum_{j=1}^{n+1} f_{i,j} \cdot Tx_{i,j} + \sum_{j=1}^{n} f_{j,i} \cdot Rx_i \leq E_i, i = 1, 2, \ldots, n$$

$$\sum_{j=1}^{n} \pi_{j,i}^{(k)} = \sum_{j=1}^{n+1} \pi_{i,j}^{(k)}, \text{ for all } i = 1, 2, \ldots, n \text{ and } i \neq k,$$

$$T + \sum_{j=1}^{n} \pi_{j,k}^{(k)} = \sum_{j=1}^{n+1} \pi_{k,j}^{(k)},$$

$$0 \leq \pi_{i,j}^{(k)} \leq f_{i,j}, \text{ for all } i = 1, 2, \ldots, n \text{ and } j = 1, 2, \ldots, n+1$$

$$\sum_{i=1}^{n} \pi_{i,n+1}^{(k)} = T, \; k = 1, 2, \ldots, n,$$

The first line imposes the energy constraint per node; the next two lines enforce the flow conservation principle at a sensor; the next line ensures that the capacity constraints on the edges of the flow network are respected and the last line ensures that T flow from sensor k reaches the sink.

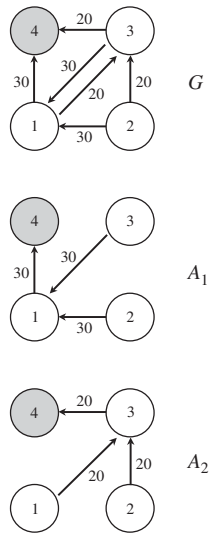

Figure 14.12 An admissible flow network G with lifetime 50 rounds and two aggregation trees A_1 and A_2 with lifetimes 30 and 20 rounds, respectively. The depth of the schedule with aggregation trees A_1 and A_2 is 2.

Now we can get a schedule from an admissible flow network. A schedule is a collection of directed trees rooted at the sink that span all the sensors, with one such tree for each cycle. Each such tree specifies how data packets are gathered and transmitted to the sink. These trees are referred to as *aggregation trees*. An aggregation tree may be used for one or more cycles. The number of cycles f for which an aggregation tree is used is indicated by associating the value f with each one of its edges. In the following f is referred to as the lifetime of the aggregation tree. The *depth* of a sensor v is the average of its depths in each of the aggregation trees, and the depth of the schedule is be $\max\{depth(v) : v \in V\}$.

Figure 14.12 shows an admissible flow network G with lifetime $T = 50$ and two aggregation trees A_1 and A_2, with lifetimes 30 and 20, respectively. By looking at one of these trees, say A_1, we see that, for each one of 30 cycles, sensor 2 transmits one packet to sensor 1, which in turn aggregates it with its own data packet and then sends one data packet to the base station. Given an admissible flow network G with lifetime T and a directed tree A rooted at the sink t with lifetime f, we define the (A, f)-*reduction* G' *of* G to be the flow network that results from G after reducing the capacities of all of its edges, that are also in A, by f. We call G' the (A, f)-*reduced* G. An (A, f)-reduction G' of G is *feasible* if the maximum flow from v to the sink t in G' is $\geq T - f$ for each vertex v in G'. Note that A does not have to span all the vertices of G, and thus it is not necessarily an aggregation tree. Moreover, if A is an aggregation tree, with lifetime f, for an admissible flow network G with lifetime T, and the (A, f)-reduction of G is feasible, then the (A, f)-reduced flow network G' of G is an admissible flow network with lifetime $T - f$. Therefore, we can devise a simple iterative algorithm, to construct a schedule for an admissible flow network G with lifetime T, provided we can find such an aggregation tree A.

```
Aggretree (G, T, t)
 1  initialize f ← 1
 2  let A = (V_o, E_o) where V_o = {t} and E_o = Ø
```

```
while A does not span all the nodes of G do
    for each edge e = (i, j) ∈ G such that i ∉ V_o and j ∈ V_o do
        let A' be A together with the edge e
        / / check if the (A', 1)-reduction of G is feasible
        let G_r be the (A', 1)-reduction of G
        if MAXFLOW(v, t, G_r) ≥ T − 1 for all nodes v of G
            / / replace A with A'
            V_o ← V_o ∪ {i}, E_o ← E_o ∪ {e}
            break
let c_min be the minimum capacity of the edges in A
let G_r be the (A, c_min)-reduction of G
if MAXFLOW(v, t, G_r) ≥ T − c_min for all nodes v of G
    f ← c_min
replace G with the (A, f)-reduction of G
return f, G, A
```

The aggretree (G, T, t) algorithm can be used to obtain an aggregation tree A with lifetime f from an admissible flow network G with lifetime $T \geq f$. Tree A is formed as follows. Initially A contains just the sink t. While A does not span all the sensors, we find and add to A an edge $e = (i, j)$, where $i \notin A$ and $j \in A$, provided that the (A', f)-reduction of G is feasible – here A' is the tree A together with the edge e and f is the minimum of the capacities of the edges in A'. Given a flow network G and sink t such that each sensor has a minimum $s - t$ cut of size $\geq T$ (i.e. the maximum flow from s to t in G is $\geq T$), we can prove that it is always possible to find a sequence of aggregation trees, via the algorithm, that can be used to aggregate T data packets from each of the sensors. The proof of correctness is based on a minimax theorems in graph theory [116, 117].

Experimental results show [118] that, for a network with 60 nodes, the above algorithm can improve the network lifetime by a factor of more than 20.

14.7 BOUNDARY ESTIMATION

An important problem in sensor networking applications is *boundary estimation* [79, 80, 127, 129]. Consider a network sensing a field composed of two or more regions of distinct behavior (e.g. differing mean values for the sensor measurements). An example of such a field is depicted in Figure 14.13(a). In practice this may represent the bound of the area under the fire or contaminated area. Boundary estimation is the process of determining the delineation between homogeneous regions. By transmitting to the sink only the information about the boundary instead of the transmission from each sensor, a significant aggregation effect can be achieved. There are two fundamental limitations in the boundary estimation problem. First, the accuracy of a boundary estimate is limited by the spatial density of sensors in the network and by the amount of noise associated with

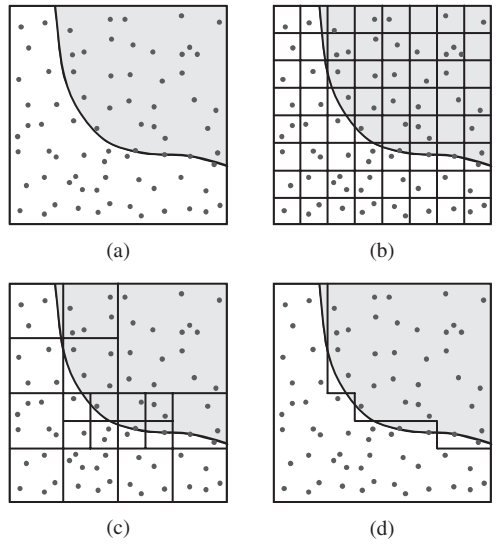

Figure 14.13 Sensing an inhomogeneous field. (a) Points are sensor locations. The environment has two conditions indicated by the gray and white regions of the square. (b) The sensor network domain is partitioned into square cells. (c) Sensors within the network operate collaboratively to determine a pruned partition that matches the boundary. (d) Final approximation to the boundary between the two regions which is transmitted to a remote point.

the measurement process. Second, energy constraints may limit the complexity of the boundary estimate that is ultimately transmitted to a desired destination.

The objective is to consider measurements from a collection of sensors and determine the boundary between two fields of relatively homogeneous measurements.

We presume a hierarchical structure of 'clusterheads' which manage measurements from nodes below them in the hierarchy. Thus, the nodes in each square of the partition communicate their measurements to a clusterhead in the square. Index the squares at the finest scale by row and column (i, j). The clusterhead in square (i, j) computes the average of these measurements to obtain a value $x_{i,j}$: $N(\mu_{i,j}, \sigma^2/m_{i,j})$, where $\mu_{i,j}$ is the mean value, σ^2 is the noise variance for each sensor measurement, and $m_{i,j}$ is the number of nodes in square (i, j). Thus we assume sensor measurements that have a Gaussian distribution. For simplicity, we assume $m_{i,j} = 1$. The random distribution is to account for noise in the system as well as for the small probability of node failure.

A possible approach to the boundary estimation problem is to devise a hierarchical processing strategy that enables the nodes to collaboratively determine a nonuniform rectangular partition of the sensor domain that is adapted to the boundaries [119–125]. The partition will have high, fine resolution along the boundary, and low, coarse resolution in homogeneous regions of the field, as depicted in Figure 14.13. The partition effectively provides a 'staircase'-like approximation to the boundary.

The estimation process partitions the sensor domain of a normalized unit square $[0, 1]$ into n sub-squares of sidelength $1/\sqrt{n}$, as shown in Figure 14.13(b). The sidelength $1/\sqrt{n}$ is the finest resolution in the analysis. In principle, this initial partition can be generated by a *recursive dyadic partition* (RDP). First divide the domain into four sub-squares of equal size. Repeat this process again on each sub-square. Repeat this $(1/2)\log_2 n = J$ times. This gives rise to a *complete* RDP of resolution $1/\sqrt{n}$ (the rectangular partition of the sensing domain shown in Figure 14.13(b)).

The RDP process can be represented with a quadtree structure. The quadtree can be pruned back to produce an RDP with nonuniform resolution as shown in Figure 14.13(c). The key issues are: (1) how to implement the pruning process in the sensor network; and (2) how to determine the best pruned tree.

Let P_n denote the set of all RDPs, including the initial complete RDP and all possible prunings. For a certain RDP $P \in P_n$, on each square of the partition, the estimator of the field averages the measurements from the sensors in that square and sets the estimate of the field to that average value. This results in a piecewise constant estimate, denoted by θ, of the field. This estimator will be compared with the data $x = \{x_{i,j}\}$. The empirical measure of performance is the sum-of-squared errors between $\theta = \theta(P)$ and the data $x = \{x_{i,j}\}$.

$$\Delta(\theta, x) = \sum_{i,j=1}^{\sqrt{n}} [\theta(i, j) - x_{i,j}]^2 \tag{14.1}$$

The complexity penalized estimator is defined by References [119–125]:

$$\hat{\theta}_n = \arg \min_{\theta(P) P \in P_n} \Delta[\theta(P), x] + 2\sigma^2 p(n) N_{\theta(P)} \tag{14.2}$$

where σ^2 is the noise variance, $N_{\theta(P)}$ denotes the total number of squares in the partition P, and $p(n)$ is a certain monotonically increasing function of n that discourages unnecessarily high-resolution partitions [appropriate choices of $p(n)$ will be discussed below]. The optimization in Equation (14.2) can be solved using a bottom-up tree pruning algorithm in $O(n)$ operations [122, 126, 128]. At each level of the hierarchy, the clusterhead receives the best sub-partition/subtree estimates from the four clusterheads below it, and compares the total cost of these estimates with the cost of the estimate equal to the average of all sensors in that cluster to make the decision on pruning.

14.7.1 Number of RDPs in *P*

Set P of RDPs consists of all RDPs resulting from pruning P_J, the uniform partition of the unit square into n squares of sidelength $1/\sqrt{n}$. We need to determine how many RDPs there are in P or, more specifically, we need to know how many partitions there are with exactly ℓ squares/leafs. Since the RDP is based on recursive splits into four, the number of leafs in every partition in P is of the form $\ell = 3m + 1$, for some integer $0 \le m \le (n - 1)/3$. The integer m corresponds to the number of recursive splits. For each RDP having $3m + 1$ leafs there is a corresponding partially ordered sequence of m split points (at dyadic positions in the plane). In general, there are

$$\binom{n}{m} \equiv \frac{n!}{(n-m)!m!}$$

possible selections of m points from n (n corresponding to the vertices of the finest resolution partition, P_J). This number is an upper bound on the number of partitions in P with $\ell = 3m + 1$ leafs (since RDPs can only have dyadic split points).

14.7.2 Kraft inequality

Let Θ_n denote the set of all possible models of the field. This set contains piecewise constant models (constant on the dyadic squares corresponding to one of the partitions in P_n). The constant values are in a prescribed range $[-R, R]$, and are quantized to k bits. The range corresponds to the upper and lower limits of the amplitude range of the sensors. The set Θ_n consists of a finite number of models derived in the previous section. Here we show that with the number of bits k

employed per transmission and $p(n)$ properly calibrated, we have

$$\sum_{\theta\in\Theta_n} \mathrm{e}^{-p(n)|\theta|} \le 1 \tag{14.3}$$

where for simplicity notation $N_{\theta(P)} = |\theta|$ is used. If $\Theta_n^{(m)}$ denotes the subset of Θ_n consisting of models based on $\ell = 3m + 1$ leaf partitions, then we have

$$\begin{aligned}\sum_{\theta\in\Theta_n} \mathrm{e}^{-p(n)|\theta|} &= \sum_{m=0}^{(n-1)/3} \sum_{\theta\in\Theta_n^{(m)}} \mathrm{e}^{-(3m+1)p(n)} \le \sum_{m=0}^{(n-1)/3} \binom{n}{m} (2^k)^{3m+1} \mathrm{e}^{-(3m+1)p(n)} \\ &\le \sum_{m=0}^{(n-1)/3} \frac{n^m}{m!} (2^k)^{3m+1} \mathrm{e}^{-(3m+1)p(n)} \\ &= \sum_{m=0}^{(n-1)/3} \frac{1}{m!} \mathrm{e}^{-[m\log n + (3m+1)\log(2^k) - (3m+1)p(n)]}\end{aligned}$$

If $A \equiv m\log n + (3m+1)\log(2^k) - (3m+1)p(n) < -1$ (then $\mathrm{e}^A < \mathrm{e}^{-1}$), then we have

$$\sum_{\theta\in\Theta_n} \mathrm{e}^{-p(n)|\theta|} \le 1/\mathrm{e} \sum_{m=0}^{(n-1)/3} \frac{1}{m!} \le 1 \tag{14.4}$$

To guarantee $A < -1$, we must have $p(n)$ growing at least like $\log n$. Therefore, set $p(n) = \gamma \log n$, for some $\gamma > 0$. Also, as we will see later in the next section, to guarantee that the quantization of our models is sufficiently fine to contribute a negligible amount to the overall error we must select 2^k: $n^{1/4}$. With these calibrations we have $A = [(7/4 - 3\gamma)m + (1/4 - \gamma)]\log n$. In order to guarantee that the MSE converges to zero, we will see in the next section that m must be a monotonically increasing function of n. Therefore, for n sufficiently large, the term involving $(\frac{1}{4} - \gamma)$ is negligible, and the condition $A < -1$ is satisfied by $\gamma > 7/12$. In References [119–125] $\gamma = 2/3$ is used.

14.7.3 Upper bounds on achievable accuracy

Assume that $p(n)$ satisfies the condition defined by Equation (14.4) where again $|\theta|$ denotes the number of squares (alternatively we shall call this the number of leafs in the pruned tree description of the boundary) in the partition θ. It is shown in the above section that $p(n) \le \gamma \log n$ satisfies Equation (14.4). Let $\hat{\theta}_n$ denote the solution to

$$\hat{\theta}_n = \arg\min_{\theta\in\Theta_n} \Delta(\theta, x) + 2\sigma^2 p(n)|\theta| \tag{14.5}$$

where, as before, x denotes the array of measurements at the finest scale $\{x_{i,j}\}$, and $|\theta|$ denotes the number of squares in the partition associated with θ. This is essentially the same estimator as defined in Equation (14.2) except that the values of the estimate are quantized in this case.

If θ_n^* denote the true value of the field at resolution $1/\sqrt{n}$ [i.e. $\theta_n^*(i,j) = E[x_{i,j}]$] then, applying Theorem 7 in References [119, 124], the MSE of the estimator $\hat{\theta}_n$ is bounded above as

$$\frac{1}{n}\sum_{i,j=1}^{\sqrt{n}} E\{[\hat{\theta}_n(i,j) - \theta_n^*(i,j)]^2\} \le \min_{\theta\in\Theta_n} \frac{1}{n}\left\{2\sum_{i,j=1}^{\sqrt{n}} [\theta(i,j) - \theta_n^*(i,j)]^2 + 8\sigma^2 p(n)|\theta|\right\} \tag{14.6}$$

The upper bound involves two terms. The first term, $2\sum_{i,j=1}^{\sqrt{n}}[\theta(i,j)-\theta_n^*(i,j)]^2$, is a bound on the bias or approximation error. The second term, $8\sigma^2 p(n)|\theta|$, is a bound on the variance or estimation error. The bias term, which measures the squared error between the best possible model in the class and the true field, is generally unknown. However, if we make certain assumptions on the smoothness of the boundary, then the rate at which this term decays as function of the partition size $|\theta|$ can be determined.

If the field being sensed is composed of homogeneous regions separated by a one-dimensional boundary and if the boundary is a Lipschitz function [122, 128], then by carefully calibrating quantization and penalization [taking $k: 1/4\log n$ and setting $p(n) = 2/3\log n$] we have [119, 125]

$$\frac{1}{n}\sum_{i,j=1}^{\sqrt{n}} E\{[\hat{\theta}_n(i,j)-\theta_n^*(i,j)]^2\} \le O\left[\sqrt{(\log n)/n}\right] \tag{14.7}$$

This result shows that the MSE decays to zero at a rate of $\sqrt{[(\log n)/n]}$.

14.7.4 System optimization

The system optimization includes energy-accuracy trade-off. Energy consumption is defined by two communication costs: the cost of communication due to the construction of the tree (*processing cost*) and the cost of communicating the final boundary estimate (*communication cost*). We will show that the expected number of leafs produced by the algorithm is $O(\sqrt{n})$, and that the *processing* and *communication* energy consumption is proportional to this number. Having in mind MSE : $\sqrt{[(\log n)/n]}$ and ignoring the logarithmic factor, the accuracy-energy trade-off required to achieve this optimal MSE is roughly MSE : 1/energy. If each of the n sensors transmits its data, directly or by multiple hops, to an external point, the processing and communication energy costs are $O(n)$, which leads to the trade-off MSE : $1/\sqrt{\text{energy}}$, since we know that no estimator exists that can result in an MSE decaying faster than $O(1/\sqrt{n})$. Thus, the hierarchical boundary estimation method offers substantial savings over the naive approach while optimizing the tradeoff between accuracy and complexity of the estimate.

Communication cost is proportional to the final description of the boundary, thus it is of interest to compute the expected size of the tree, or $E[|\hat{\theta}|]$. We construct an upperbound for $E[|\hat{\theta}|]$ under the assumption of a homogeneous field with no boundary. Let P denote the tree-structured partition associated with $\hat{\theta}$. Note that, because P is an RDP, it can have $d+1$ leafs (pieces in the partition), where $d = 3m, m = 0, \ldots, (n-1)/3$. Therefore, the expected number of leafs is given by

$$E[|\hat{\theta}|] = \sum_{m=0}^{(n-1)/3} (3m+1)\Pr(|\hat{\theta}| = 3m+1)$$

The probability $\Pr(|\hat{\theta}| = 3m+1)$ can be bounded from above by the probability that one of the possible partitions with $3m+1$ leafs, $m > 0$, is chosen in favor of the trivial partition with just a single leaf. That is, the event that one of the partitions with $3m+1$ leafs is selected implies that partitions of all other sizes were not selected, including the trivial partition, from which the upper bound follows. This upper bound allows us to bound the expected number of leafs as follows:

$$E[|\hat{\theta}|] \le \sum_{m=0}^{(n-1)/3} (3m+1) N_m P_m$$

where N_m denotes the number of different $(3m+1)$-leaf partitions, and p_m denotes the probability that a particular $(3m+1)$-leaf partition is chosen in favor of the trivial partition (under the homogeneous assumption). The number N_m can be bounded above by $\binom{n}{m}$, just as in the verification of

the Kraft inequality. The probability p_m can be bounded as follows. Note this is the probability of a particular outcome of a comparison of two models. The comparison is made between their respective sum-of-squared errors plus complexity penalty, as given by Equation (14.2). The single leaf model has a single degree of freedom (mean value of the entire region), and the alternate model, based on the $(3m+1)$-leaf has $3m+1$ degrees of freedom. Thus, under the assumption that the data are i.i.d. zero-mean Gaussian distributed with variance σ^2, it is easy to verify that the difference between the sum-of-squared errors of the models [single-leaf model sum-of-squares minus $(3m+1)$-leaf model sum-of-squares] is distributed as $\sigma^2 W_{3m}$, where W_{3m} is a chi-square distributed random variable with $3m$ degrees of freedom (precisely the difference between the degrees of freedom in the two models). This follows from the fact that the difference of the sum-of-squared errors is equal to the sum-of-squares of an orthogonal projection of the data onto a $3m$-dimensional subspace.

The single-leaf model is rejected if $\sigma^2 W_{3m}$ is greater than the difference between the complexity penalties associated with the two models; that is, if $\sigma^2 W_{3m} > (3m+1)2\sigma^2 p(n) - 2\sigma^2 p(n) = 6m\sigma^2 p(n)$, where $2\sigma^2 p(n)$ is the penalty associated with each additional leaf in P. According to the MSE analysis in the previous section, we require $p(n) = \gamma \log n$, with $\gamma > 7/12$. In References [119–125] $\gamma = 2/3$, in which case the rejection of the single-leaf model is equivalent to $W_{3m} > 4m \log n$. The probability of this condition, $p_m = \Pr(W_{3m} > 4m \log n)$, is bounded from above using Lemma 1 of Laurent and Massart [130]: 'If W_d is chi-square distributed with d degrees of freedom, then for $s > 0$ $\Pr(W_d \geq d + s\sqrt{2d} + s^2) \leq \mathrm{e}^{-s^2/2}$'. Making the identification $d + g\sqrt{2d} + s^2 = 4m \log n$ produces the bound

$$p_m = \Pr(W_{3m} > 4m \log n) \leq \mathrm{e}^{-2m \log n + m\sqrt{[3/2(4 \log n - 3/2)]}}$$

Combining the upper bounds above, we have

$$\begin{aligned} E[|\hat{\theta}|] &\leq \sum_{m=0}^{(n-1)/3} (3m+1) \binom{n}{m} \mathrm{e}^{-2m \log n + m\sqrt{3/2(4 \log n - 3/2)}} \\ &= \sum_{m=0}^{(n-1)/3} (3m+1) \binom{n}{m} n^{-m} \mathrm{e}^{-m \log n + m\sqrt{3/2(4 \log n - 3/2)}} \end{aligned} \tag{14.8}$$

For $n \geq 270$ the exponent $-\log n + \sqrt{3/2(4 \log n - 3/2)} < 0$ and therefore

$$E[|\hat{\theta}|] \leq \sum_{m=0}^{(n-1)/3} (3m+1) \binom{n}{m} n^{-m} \leq \sum_{m=0}^{(n-1)/3} (3m+1) \frac{n^m}{m!} n^{-m} \leq \sum_{m=0}^{(n-1)/3} (3m+1)/m! < 11$$

Furthermore, note that, as $n \to \infty$, the exponent $-\log n + \sqrt{[3/2(4 \log n - 3/2)]} \to \infty$. This fact implies that the factor $\mathrm{e}^{-m \log n + m\sqrt{[3/2(4 \log n - 3/2)]}}$ tends to zero when $m > 0$. Therefore, the expected number of leafs $E[|\hat{\theta}|] \to 1$ as $n \to \infty$.

Thus, for large sensor networks, the expected number of leafs (partition pieces) in the case where there is no boundary (simply a homogeneous field) is one. To consider the inhomogeneous case where a boundary does exist, if the boundary is a Lipschitz function or has a box counting dimension of 1, there exists a pruned RDP with at most $C'\sqrt{n}$ squares (leafs) that includes the $O(\sqrt{n})$ squares of sidelength $1/\sqrt{n}$ that the boundary passes through. Thus an upper bound on the number of leafs required to describe the boundary in the noiseless case is given by $C'\sqrt{n}$.

In the presence of noise, we can use the results above for the homogeneous case to bound the number of spurious leafs due to noise (zero as n grows); as a result, for large sensor networks, we can expect at most $C'\sqrt{n}$ leafs in total. Thus, the expected energy required to transmit the final boundary description is energy $= O(\sqrt{n})$.

The *processing cost* is intimately tied to the expected size of the final tree, as this value determines how much pruning will occur. We have seen above that the communication cost is

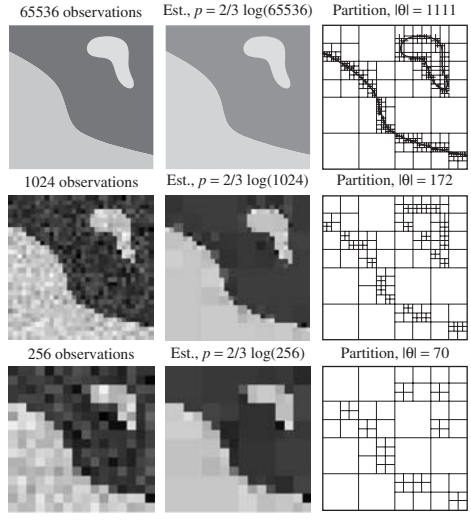

Figure 14.14 Effect of sensor network density (resolution) on boundary estimation. Column 1, noisy set of measurements; column 2, estimated boundary; and column 3, associated partition. (Reproduced by permission of IEEE [121].)

proportional to $\sqrt{n}$ and herein we shall show that the processing cost is also $O(\sqrt{n})$. At each scale $2^j/\sqrt{n}$, $j = 0, \ldots, 1/2 \log_2 n - 1$, the hierarchical algorithm passes a certain number of data or averages, n_j, corresponding to the number of squares in the best partition (up to that scale), up the tree to the next scale. We assume that a constant number of bits k is transmitted per measurement. These $k\, n_j$ bits must be transmitted approximately $2^j/\sqrt{n}$ meters (assuming the sensor domain is normalized to 1 square meter). Thus, the total in-network communication energy in bit-meters is:

$$\varepsilon = k \sum_{j=0}^{1/2 \log_2 n - 1} n_j 2^j / \sqrt{n}$$

In the naive approach, $n_j = n$ for all j, and therefore $\varepsilon \approx kn$. In the hierarchical approach, first consider the case when there is no boundary. We have already seen that in such cases the tree will be pruned at each stage with high probability. Therefore, $n_j = n/4^j$ and $\varepsilon \approx 2k\sqrt{n}$. Now if a boundary of length $C\sqrt{n}$ is present, then $n_j \leq n/4^j + C\sqrt{n}$. This produces $\varepsilon \leq k(C+2)\sqrt{n}$. Thus, we see that the hierarchical algorithm results in $\varepsilon = O(\sqrt{n})$.

Finally, a performance example is shown in Figure 14.14 [121].

14.8 OPTIMAL TRANSMISSION RADIUS IN SENSOR NETWORKS

In this section we discuss the problem of finding an optimal transmission radius for flooding in sensor networks. On one hand, a large transmission radius implies that fewer retransmissions will be needed to reach the outlying nodes in the network; therefore, the message will be heard by all nodes in less time. On the other hand, a larger transmission radius involves a higher number of neighbors competing to access the medium, and therefore each node has a longer contention delay for packet transmissions. In this section we discuss this tradeoff in CSMA/CA wireless MAC protocols.

Even though flooding has some unique advantages – it maximizes the probability that all reachable nodes inside a network will receive the packet – it has several disadvantages as well.

Several works have proposed mechanisms to improve flooding efficiency. The broadcast storm paper by Ni *et al*. [131] suggests a way to improve flooding by trading robustness. The authors propose to limit the number of nodes that transmit the flooded packet. The main idea is to have some nodes refrain from forwarding their packet if its transmission will not contribute to a larger coverage. Nevertheless, the basic flooding technique is in wide use for a number of querying techniques for sensor networks (in large part because of its guarantee of maximal robustness), and in this section we focus on analyzing its MAC-layer effects and improving its performance by minimizing the settling time of flooding.

Other studies have looked at the impact of the transmission radius in wireless networks. In Gupta and Kumar [132] the authors analyzed the critical transmission range to maintain connectivity in wireless networks and present a statistical analysis of the probability of connectivity. On the same line of work, Kleinrock and Silvester [133] analyze the minimum number of neighbors that a node should have to keep the network connected.

In Takagi and Kleinrock [134], the authors describe a similar tradeoff for increasing the transmission radius: a shorter range implies fewer collisions and a longer range implies moving a packet further ahead in one hop. However, in that work the authors want to maximize a parameter called *the expected one-hop progress in the desired direction*, which essentially measures how fast a packet can reach its destination in point-to-point transmissions.

All these studies were not analyzing a protocol like flooding, but instead trying to obtain an optimal transmission radius for other metrics such as connectivity, throughput or energy. In Ganesan *et al.* [135] an experimental testbed of 150 Berkeley motes [136] run flooding as the routing protocol. The study showed empirical relations between the reception and settling times – parameters used in this section – for different transmission ranges.

In this section we discuss an optimal transmission radius. However, in this case the important metric is the amount of time that a flooded packet captures the transmission medium. To accomplish the goal of minimizing the settling time, the tradeoff between reception and contention times is studied including the interaction between the MAC-layer and network-level behavior of an information dissemination scheme in wireless networks.

The network model is based on the following assumptions:

(1) The MAC protocol is based on a CSMA/CA scheme.

(2) All the nodes have the same transmission radius R.

(3) The area of the network can be approximated as a square.

(4) No mobility is considered.

(5) The nodes are deployed in either a grid or uniform topology. In a uniform topology, the physical terrain is divided into a number of cells based on the number of nodes in the network, and each node is placed randomly within each cell.

The analytical model is described by the following terms:

(1) Reception time (T_R) – average time when all the nodes in the network have received the flooded packet.

(2) Contention time (T_C) – average time between reception and transmission of a packet by all the nodes in the network.

(3) Settling time (T_S) – average time when all the nodes in the network have transmitted the flooded packet and signals the end of the flooding event.

From these definitions we observe that $T_S = T_R + T_C$. If the transmission radius of the nodes is not carefully chosen, the flooded packet may take too long to be transmitted by all the nodes

in the network, impacting overall network throughput. *The more time the channel is captured by a flooding event, the fewer queries can be disseminated, and the less time the channel is available for other packet transmissions*. We can state the relation between settling time and throughput *Th* in sensor networks as $Th \propto 1/T_S$. So, the goal is to minimize the settling time T_S. Since the settling time is the sum of the reception and contention times, the remainder of this section will analyze the relationships between T_R and T_C with respect to the range of the transmission radius.

The reception time T_R represents the average time at which nodes received the packet. If the transmission radius of each node is increased, the reception time in the network will decrease, because there are fewer hops needed to reach outlying nodes. Therefore, the reception time T_R is directly proportional to the maximum distance between any two nodes in the network, and inversely proportional to the transmission radius. Owing to the kind of topologies considered here (grid or uniform), the maximum distance between the nodes is the diagonal of the network area. If R is transmission radius (m) and S the length of the side of the square area (m) then $T_R = cS/R$, where c is a constant.

If a node increases its transmission radius, it will increase its number of neighbors, which will cause an increase in the contention time. If we consider the area covered by the network as S^2 then the expected number of neighbors of a given node is described by $m = \pi R^2 n/S^2$, where n is the total number of nodes in the network. However, the contention time is not directly proportional to above equation. There are two phenomena that influence T_c, the *edge phenomenon* and the *back-off phenomenon*.

The *edge phenomenon* can be described as follows: nodes close to the edges of the network area will not increase their number of neighbors proportionally to the square of the radius. The reason is that only a fraction of the area covered by its transmission radius intersects the area of the network. This phenomenon is illustrated in Figure 14.15, which shows a square topology with a given node (black point). In this figure, we can observe three regions as the transmission radius is increased:

- Region 1 – when R ranges from 0 to the edge of the network (R_e).
- Region 2 – when R ranges from R_e until it covers the entire network (R_w).
- Region 3 – when R is greater than R_w.

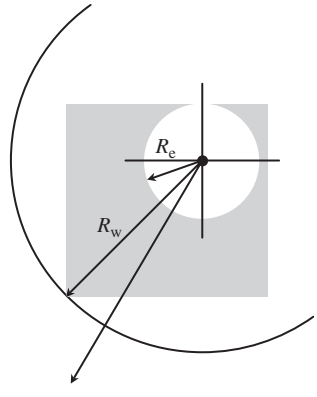

Figure 14.15 Different regions to calculate the number of neighbors versus the transmission radius of the node.

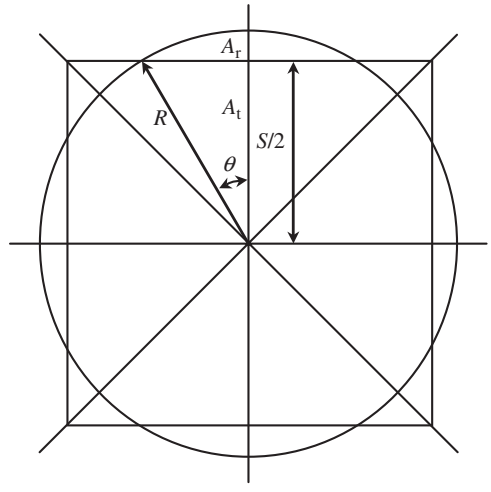

Figure 14.16 The overlapping area between the transmission radius coverage and the effective area of the network.

Each of these regions will have a different expression for the number of neighbors. For the first region, the number of nodes inside the transmission radius is directly proportional to the square of the radius. In the second region, the number of neighbors increases proportionally to the overlapping area between the transmission range and the network area. The overlapping area (A_O) is shown in Figure 14.16.

Defining A_r as the residual area beyond $S/2$, because of symmetry, the total overlapping area is given by

$$A_O = 8\left(\frac{\pi R^2}{8} - A_r\right)$$

where $A_\theta = A_r + A_t$. Since $\theta = \arccos(S/2R)$, we have $A_\theta = \theta(R^2/2)$ and $A_t = R^2 \sin(\theta)\cos(\theta)$.

As a consequence $A_r = \theta(R^2/2) - R^2 \sin(\theta)\cos(\theta)$ and we get for the center (+) and corner position ($\angle$)

$$A_{O+} = 8\left[\frac{\pi R^2}{8} - \theta\frac{R^2}{2} - R^2 \sin(\theta)\cos(\theta)\right]$$

$$A_{O+} = R^2[\pi - 4\theta - 4\sin(\theta)\cos(\theta)]$$

In the case of the lower bound, we have one quarter of a circle and ϕ is given by $\phi = \arccos(S/R)$ and

$$A_{O\angle} = 2\left[\frac{\pi R^2}{8} - \theta\frac{R^2}{2} - R^2 \sin(\theta)\cos(\theta)\right], A_{O\angle} = R^2\left[\frac{\pi}{4} - \theta - \sin(\theta)\cos(\theta)\right]$$

In the third region, the number of neighbors remains constant and is equal to the total number of nodes in the network. Since the values of R for the three different regions depend on the position of the node in the network, only the bounds of the edge phenomenon will be analyzed.

The node closest to the center of the network is the one increasing its number of neighbors most aggressively, hence it represents the upper bound. For this node, the second region begins when R is greater than $S/2$ and the third region begins when R is greater than $(S/2)\sqrt{2}$. The

following equation shows the upper bound $\lceil m \rceil$for the number of neighbors of this node:

$$\lceil m \rceil = \begin{cases} \pi \dfrac{R^2}{S^2} n & 0 < R < \dfrac{S}{2} \\ R^2[\pi - 4\theta + 4\cos(\theta)\sin(\theta)] & \dfrac{S}{2} < R \dfrac{S}{2}\sqrt{2} \\ n & \dfrac{S}{2}\sqrt{2} < R \end{cases}$$

where $\theta = \arccos(S/2R)$. The lower bound is given by nodes located on the corners of the network. In this case, there is no region 1 as such but rather the number of nodes increases as $\pi(R^2/4)$ and finishes when R equals S. The second region finishes when R equals $S\sqrt{2}$. The next equation represents the lower bound for the number of neighbors $\lfloor m \rfloor$:

$$\lfloor m \rfloor = \begin{cases} \pi \dfrac{R^2}{4S^2} n & 0 < R < S \\ R^2 \left[\dfrac{\pi}{4}\pi - \theta + \cos(\theta)\sin(\theta) \right] & S < R < S\sqrt{2} \quad \text{where } \theta = \arccos\left(\dfrac{S}{R}\right) \\ n & S\sqrt{2} < R \end{cases}$$

14.8.1 Back-off phenomenon

In CSMA/CA protocols, a node checks if the medium is clear before sending a packet; when the medium is clear for a small period of time, the node transmits the packet. If the channel becomes busy during this waiting period, it chooses a random time in the future to transmit the packet. This mechanism leads to a non linear relationship between the contention time and the number of neighbors. This nonlinear relationship is referred to as the back-off phenomenon.

By simulating a one-hop network with a varying number of nodes the nonlinear relationship between the number of neighbors and the contention time can be numerically approximated by [137] $f(m) = J \log^3(m)$, where m is the number of neighbors and J is a constant. If we incorporate the edge and back-off phenomena explained above, we obtain that the upper bound for the contention time T_C is given by:

$$\lceil T_C \rceil = \begin{cases} Kf\left(\pi \dfrac{R^2}{S^2} n\right) & 0 < R < \dfrac{S}{2} \\ Lf\{R^2[\pi - 4\theta + 4\cos(\theta)\sin(\theta)]\} & \dfrac{S}{2} < R < \dfrac{S}{2}\sqrt{2} \\ Mf(n) & \dfrac{S}{2}\sqrt{2} < R \end{cases}$$

and the lower bound is:

$$\lfloor T_C \rfloor = \begin{cases} Kf\left(\pi \dfrac{R^2}{4S^2} n\right) & 0 < R < S \\ Lf\left\{R^2 \left[\dfrac{\pi}{4} - \theta - \cos(\theta)\sin(\theta)\right]\right\} & S < R < S\sqrt{2} \\ Mf(n) & S\sqrt{2} < R \end{cases}$$

where K, L and M are constants and $f(.)$ is the function described above. The settling time is the sum of the reception and contention times. Figure 14.17 shows the analytical settling time, for a network with four hundred nodes. For illustration purposes, the analytical reception and contention times are also plotted. The settling time curve shows a minimum, as expected.

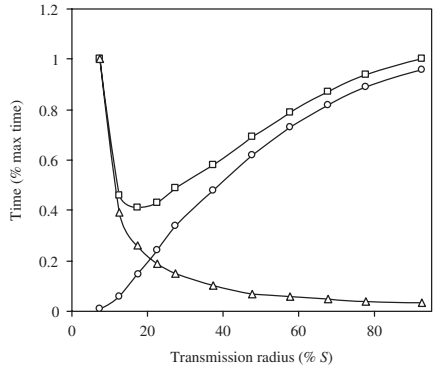

Figure 14.17 Analytical curve for the settling time, which is the sum of the reception and contention times.

14.9 DATA FUNNELING

In this section, a combination of two methods is discussed which improve the lifetime of energy constrained networks by reducing the amount of communication needed to send readings from a set of sensors to a controller. The first scheme is a packet aggregation technique, which has been already discussed, while the second scheme performs data compression. While either of the two schemes can be used separately, using them together provides maximum gain.

The main idea behind the algorithm, called data funneling [139], is the following. The controller breaks up the space into different regions (e.g. cuboids) and sends interest packets to each region, as shown in Figure 14.8(a). Upon receiving the interest packet, each node in the region will start periodically sending its readings back to the controller at an interval specified in the interest packet, usually every few minutes. Since many or all of the nodes within the region will be sending their readings back to the controller at the same time, it would be much more efficient to combine these readings into a single packet, so that only one packet with only one header travels from the region to the controller. The question is, how can all these reading be collected at a single point and combined into a single packet?

As already discussed in Section 14.3.3, the data funneling algorithm works as follows. The interest packets are sent toward the region using directional flooding. Each node that receives the interest packet checks if it is in the target region. If it is not, it computes its cost for communicating back to the controller, updates the cost field within the interest packet, and sends it on toward the specified region. This is the *directional flooding phase*.

When a node that is in the target region receives the interest packet from a neighbor node that lies outside the target region, the directional flooding phase concludes. The node realizes that it is on the border of the region and designates itself to be a border node, as shown in Figure 14.8(b). Each border node computes its cost for communicating with the controller in the same manner as was done by the nodes outside the region during the directional flooding phase. It then floods the entire region with a modified version of the interest packet. The 'cost to reach the controller' field is reset to zero and becomes the 'cost to reach the border node field.' Within the region, each node only keeps track of its cost for communicating with the border node, not its cost for communicating with the controller. Intuitively, it is as if the border node becomes the controller of the specified region. It is at one of the border nodes that all the readings from within the region will be collated into a single packet.

In addition, two new fields are added to the modified interest packet. One field keeps track of the number of hops that have been traversed between the border node and the node currently

processing the packet. The other field specifies the border node's cost for communicating with the controller, and this field, once defined by the border node, does not change as the packet travels from one node to another.

Once the nodes within the region receive the modified interest packet from the border nodes, they will then route their readings to the controller via each of the border nodes in turn. Since there are several border nodes within the region, maximizing aggregation of sensor readings requires all the nodes within the region to agree to route their data via the same border node during every given round of reporting back to the controller. This is accomplished by having every node compute an identical schedule of which border node to use during each round of reporting. This is achieved by each node in the region applying the same deterministic function to the vector of costs to reach the controller seen by each border node. Since all the nodes apply the same function to the same inputs, they will all compute the same schedule, allowing them to collect all of their data at one border node during each round of reporting. The function used to compute the schedule can be similar to the function used to compute the probabilities for selecting different paths in probabilistic routing. This allows border nodes with a low cost for communicating to the controller to be used more frequently than the ones with a high cost.

As data flows within the region from the sensors to the border nodes it can be aggregated along the way, as shown in Figure 14.8(b). When the time comes to send a new round of observations back to the controller, the sensor nodes do not immediately start sending their packets. Instead, they wait an amount of time inversely proportional to their distance (in number of hops) to the border node that will be used in that round of reporting before sending their readings toward that border node. This allows the nodes that are far away from the border node to send their data earlier than the nodes that are closer to the border node. This way, nodes close to the border will first receive the readings from upstream nodes and bundle those readings with their own. In the end, all of the data to be sent out by all the nodes within the region will be collated at one border node and sent back to the controller in a single packet, as shown in Figure 14.8(b).

If α is the ratio of bits in a packet header to the total number of bits in a packet containing the header and a single sensor reading for a particular application, and m is the average number of sensor readings per transmitted packet when data funneling is employed, then the total energy expended by the network on communication is reduced by $\alpha \times (m - 1/m) \times 100$ % due to data funneling if no compression of the sensor readings is done at the aggregation points. Performing compression on the sensor readings at the aggregation points within a region, as discussed in the sequel, would result in even greater energy savings. For this purpose *coding by ordering* is used.

The main idea behind 'coding by ordering' is that, when transmitting many unique pieces of data, and the order in which the data is sent is not important to the application (i.e. the transmitter may choose the order in which to send those pieces of data), then the choice of the order in which those pieces of data are sent can be used to convey additional information to the receiver. In fact it is possible to avoid explicitly transmitting some of those pieces of data, and use the ordering of the other information to convey the information contained in the pieces of data that were not sent.

Consider the case of the data funneling algorithm. In each round of reporting, the border node receives the packets containing sensor readings from n sensors in its region. It then places each node's packet (containing the node ID, which may be just the node's position, and payload) into a large superpacket containing the data of all the nodes and sends the superpacket to the controller. The border node has to include the ID of each node, which is unique, along with the node's sensor reading so as to make it clear which payload corresponds to which node. Since all of the sensor readings from the region will reach the controller at the same time and the ordering of the packets within the superpacket does not affect the application, the border node has the freedom to choose the ordering of the packets within the superpacket. This allows the border node to choose to 'suppress' some of the packets (i.e. choose not to include them in the superpacket), and order the other packets within the super-packet in such a way as to indicate the values contained within the suppressed packets.

For example, consider the case when there are four nodes with IDs 1, 2, 3 and 4 in the region. Each of the four sensors generates an independent reading, which is a value from the set $\{0, \ldots, 5\}$. The border node can choose to suppress the packet from node 4 and, instead, choose the appropriate ordering among the $3! = 6$ possible orderings of the packets from nodes 1, 2 and 3 to indicate the value generated by node 4. Note that in this case the border node need not encode the ID of the suppressed node because that information can be recovered from the fact that there are only four nodes and the packets of three of them were explicitly given in the superpacket. The question is, how many packets can be suppressed? Let n be the number of packets present at the encoder, k be the range of possible values generated by each sensor (e.g. if each sensor generates a 4-b value, then $k = 2^4$), and d be the range of node IDs of the sensor nodes. Given n, k and d, what is the largest number of packets, l, that can be suppressed?

One strategy is to have the encoder (located at the border node) throw away any l packets and appropriately order the remaining $n - l$ packets to indicate what values were contained in the suppressed packets. A total of $(n - l)!$ values can be indexed by ordering $n - l$ distinct objects. Each of the suppressed packets contains a payload that can take on any of the k possible values and an ID, which can be any value from the set of d valid IDs except for the ones that belong to the packets included in the super packet. The values contained within the suppressed packets can be regarded as symbols from a $(d - n + l) \times k$ ary alphabet, giving $(d - n + l)^l \times k^l$ possible values for the suppressed packets. In order for it to be possible to suppress l out of n packets in this manner, the following relationship must be satisfied $(n - l)! \geq (d - n + l)^l k^l$; or by using approximation, $n! = \sqrt{2\pi n}(n/e)^n$ we have

$$(n - l)[\ln(n - i) - 1] + 0.5 \ln[2\pi(n - l)] - l \ln k - l \ln(d - n + l) \geq 0$$

If this inequality is satisfied, then it is possible to suppress l packets. The suppressed packets can contain identical values. While their payloads may be identical, each packet has to have a unique ID. Since each packet has to be identified with a unique ID from among the d possible IDs, and $n - l$ of the possible IDs are taken up by the transmitted packets, there are $\binom{d-n+l}{l}$ possible combinations of IDs that the l suppressed packets can take on; therefore, when enumerating the possible values contained within the suppressed packets, the $(d - n + l)^l$ term should be replaced by $\binom{d-n+l}{l}$ giving $(n - l)! \geq \binom{d-n+l}{l} k^l$ as the relationship that must be satisfied in order for it to be possible to suppress l out of n packets. Again, approximation can be used to convert the inequality to the following equivalent relationship with more manageable terms:

$$\begin{aligned} \ln(2\pi) + l + (l + 0.5) \ln l + (n - l + 0.5) \ln(n - l) + (d - n + 0.5) \ln(d - n) - l \ln k \\ - (d - n + l + 0.5) \ln(d - n + l) - n \geq 0 \end{aligned}$$

The two schemes presented above assume that the encoder will suppress l packets without giving much consideration to which l packets are suppressed; however, since the encoder has the freedom to choose which l packets to suppress, the number of values that may be indexed by dropping l out of n packets and ordering the remaining $n - l$ packets increases by a factor of $\binom{n}{l}$. Combining this with the previous condition gives the following relationship, which must be satisfied if it is to be possible to suppress l out of n packets:

$$\frac{n!}{l!} \geq \binom{d - n + l}{l} k^l$$

As before, applying approximation and some manipulation can reduce the inequality to an equivalent one:

$$\begin{aligned} (n + 0.5) \ln n + (d - n + 0.5) \ln(d - n) + 0.5 \ln(2\pi) - d - 0.5 \ln(d - n + l) \\ + (d - n + l)[\ln(d - n + l) - 1] + l \ln k \geq 0 \end{aligned}$$

For example when $n = 30$, using the low-complexity scheme allows the encoder to suppress $l = 6$ packets, a 20 % saving in energy spent on transmitting sensor data. The bound on the number of packets that can be suppressed at $n = 30$ is 10. As n grows, the savings also increase. When $n = 100$, the low-complexity scheme provides 32 % savings, the higher-complexity scheme guarantees 44 % savings, while the bound is 53 %.

14.10 EQUIVALENT TRANSPORT CONTROL PROTOCOL IN SENSOR NETWORKS

The need for a transport layer for data delivery in WSN can be questioned under the premise that data flows from source to sink are generally loss tolerant. While the need for end-to-end reliability may not exist due to the sheer amount of correlated data flows, an event in the sensor field still needs to be tracked with a certain accuracy at the sink. So, instead of a traditional TCP layer, the sensor network paradigm necessitates an *event-to-sink* reliability notion at the transport layer that will be referred to as equivalent TCP (ETCP) [143–148]. Such a notion of collective identification of data flows from the event to the sink was illustrated earlier in Figure 14.10. An example of ETCP is event-to-sink reliable transport (ESRT) protocol for WSN, discussed in Sankarasubramaniam *et al.* [123]. Some of its features are

(1) *Self-configuration* – ESRT is self-configuring and achieves flexibility under dynamic topologies by self-adjusting the operating point.

(2) *Energy awareness* – if reliability levels at the sink are found to be in excess of that required, the source nodes can conserve energy by reducing their reporting rate.

(3) *Congestion control* – required event detection accuracy may be attained even in the presence of packet loss due to network congestion. In such cases, however, a suitable congestion control mechanism can help conserve energy while maintaining desired accuracy levels at the sink. This is done by conservatively reducing the reporting rate.

(4) *Collective identification* – ESRT does not require individual node IDs for operation. This is also in tune with ESRT model rather than the traditional end-to-end model. More importantly, this can ease implementation costs and reduce overhead.

(5) *Biased Implementation* – the algorithms of ESRT mainly run on the sink with minimum functionalities required at sensor nodes.

In another example [141, 142], the PSFQ mechanism is used for reliable retasking/reprogramming in WSN. PSFQ is based on slowly injecting packets into the network, but performing aggressive hop-by-hop recovery in case of packet loss. The pump operation in PSFQ simply performs controlled flooding and requires each intermediate node to create and maintain a data cache to be used for local loss recovery and in-sequence data delivery. Although this is an important transport layer solution for WSN, it is applicable only for strict sensor-to-sensor reliability and for purposes of control and management in the reverse direction from the sink to sensor nodes. Event detection/tracking in the forward direction does not require guaranteed end-to-end data delivery as in PSFQ. Individual data flows are correlated and loss-tolerant to the extent that desired event features are collectively and reliably informed to the sink. Hence, the use of PSFQ for the forward direction can lead to a waste of valuable resources. In addition to this, PSFQ does not address packet loss due to congestion. For this reason in the sequel we elaborate more ESRT algorithm.

The operation of the algorithm is based on the notion of *observed event reliability*, r_i (the number of received data packets in decision interval i at the sink), and *desired event reliability*, R (the number of data packets required for reliable event detection). R depends on the application.

If the observed event reliability, r_i, is greater than the desired reliability, R, then the event is deemed to be reliably detected. Else, appropriate action needs to be taken to achieve the desired reliability, R. With the above definition, r_i can be computed by stamping source data packets with an event ID and incrementing the received packet count at the sink each time the ID is detected in decision interval i. Note that this does not require individual identification of sensor nodes. Further, we model any increase in source information about the event features as a corresponding increase in the reporting rate, f, of sensor nodes. The reporting rate of a sensor node is defined as the number of packets sent out per unit time by that node. The transport problem in WSN is to *configure the reporting rate, f, of source nodes so as to achieve the required event detection reliability, R, at the sink with minimum resource utilization.*

In order to study the relationship between the observed reliability at the sink, r, and the reporting frequency, f, of sensor nodes, Sankarasubramaniam *et al.* [140] developed an evaluation environment using *ns*-2 . The parameters used in the study are:

Area of sensor field: $100 \times 100\,m^2$
Number of sensor nodes: 200
Radio range of a sensor node: 40 m
Packet length: 30 bytes
IFQ length: 65 packets
Transmit power: 0.660 W
Receive power: 0.395 W
Decision interval (τ): 10 s

Event centers (X_{ev}, Y_{ev}) were randomly chosen and all sensor nodes within the event radius behave as sources for that event. Let the desired reliability as laid down by the application be R. Hence, a normalized measure of reliability is $\eta = r/R$. Parameter, η_i denotes the normalized reliability at the end of decision interval i. The results of the above experiment are shown in Figure 14.18.

The aim is to operate as close to $\eta = 1$ as possible, while utilizing minimum network resources (f close to f^* in Figure 14.18). We call this the *optimal operating point*, marked as P_1 in Figure 14.18. For practical purposes, we define a tolerance zone of width 2ε around P_1. Here, ε is a

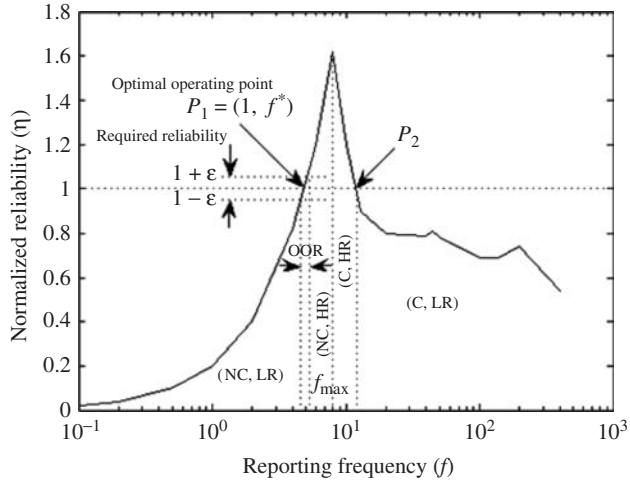

Figure 14.18 The five characteristic regions in the normalized reliability, η, vs reporting frequency, f, behavior. Number of source nodes-81. (Reproduced by permission of IEEE [140].)

protocol parameter to be optimized. Although the event is reliably detected at P_2 too, the network is congested and some source data packets are lost. Event reliability is achieved only because the high reporting frequency of source nodes compensates for this congestion loss. However, this is a waste of limited energy reserves and hence is not the operating point of interest. Similar reasoning holds for $\eta > 1 + \varepsilon$.

From Figure 14.25, we identify five characteristic regions (bounded by dotted lines) using the following decision boundaries:

(NC,LR): $f < f_{\max}$ and $\eta < 1 - \varepsilon$ (no congestion, low reliability)
(NC,HR): $f \leq f_{\max}$ and $\eta > 1 + \varepsilon$ (no congestion, high reliability)
(C,HR): $f > f_{\max}$ and $\eta > 1$ (congestion, high reliability)
(C,LR): $f > f_{\max}$ and $\eta \leq 1$ (congestion, low reliability)
OOR: $f < f_{\max}$ and $1 - \varepsilon \leq \eta \leq 1 + \varepsilon$ (optimal operating region)

As seen earlier, the sink derives a reliability indicator η_i at the end of decision interval i. Coupled with a congestion detection mechanism (to determine $f \lessgtr f_{\max}$), this can help the sink determine in which of the above regions the network currently resides. Hence, these characteristic regions identify the state of the network. Let S_i denote the network state variable at the end of

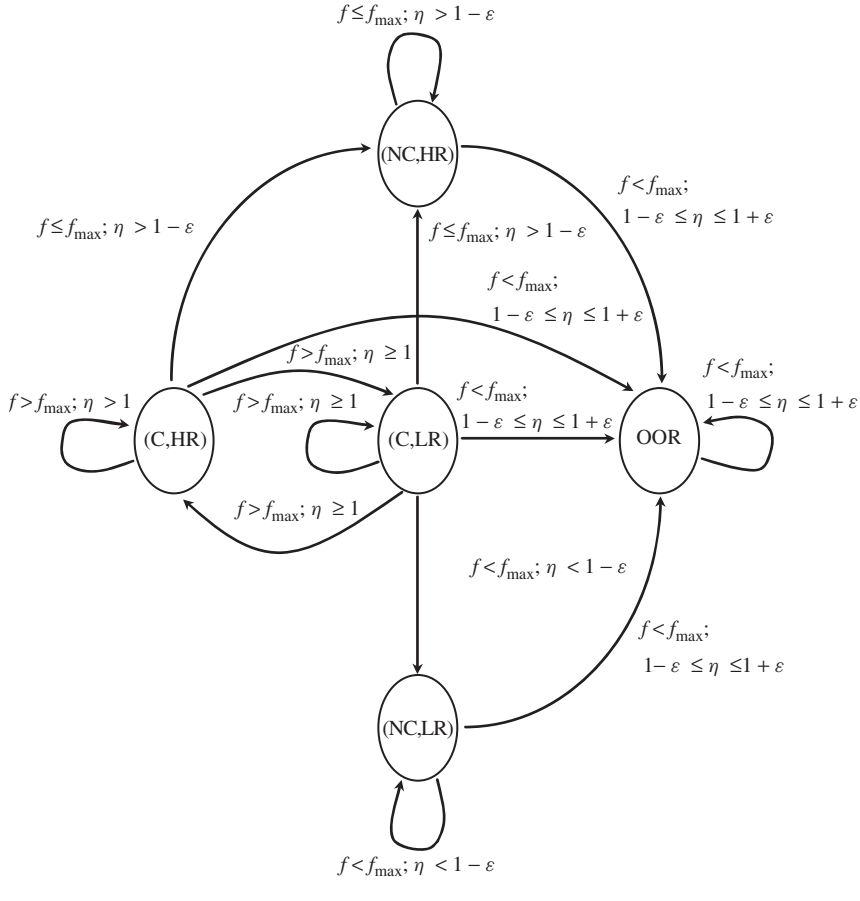

Figure 14.19 ESRT protocol state model and transitions. (Reproduced by permission of IEEE [27].)

decision interval i. Then,

$$S_i \in \{(NC, LR), (NC, HR), (C, HR), (C, LR), OOR\}$$

The operation of ESRT is closely tied to the current network state S_i. The ESRT protocol state model and transitions are shown in Figure 14.19. ESRT identifies the current state S_i from: (1) reliability indicator η_i computed by the sink for decision interval i; (2) a congestion detection mechanism, using the decision boundaries as defined above. Depending on the current state S_i, and the values of f_i and η_i, ESRT then calculates the updated reporting frequency f_{i+1} to be broadcast to the source nodes. At the end of the next decision interval, the sink derives a new reliability indicator η_{i+1} corresponding to the updated reporting frequency f_{i+1} of source nodes. In conjunction with any congestion reports, ESRT then determines the new network state S_{i+1}. This process is repeated until the optimal operating region (state OOR) is reached. The state model of the ESRT protocol and state transitions are shown in Figure 14.19. The following reporting rate updating rules are used [140]:

(NC,LR) $$f_{i+1} = \frac{f_i}{\eta_i}$$

(NC,HR) $$f_{i+1} = \frac{f_i}{2}\left(1 + \frac{1}{\eta_i}\right)$$

(C,HR) $$f_{i+1} = \frac{f_i}{\eta_i}$$

(C,LR) $$f_{i+1} = f_i^{(\eta_i/k)}$$

where k denotes the number of successive decision intervals for which the network has remained in state (C,LR) including the current decision interval

OOR $$f_{i+1} = f_i$$

In order to determine the current network state S_i in ESRT, the sink must be able to detect congestion in the network. ESRT uses a congestion detection mechanism based on local buffer level monitoring in sensor nodes. Any sensor node whose routing buffer overflows due to excessive incoming packets is said to be congested and it informs the sink of the same. For more on system performance see Sankarasubramaniam *et al.* [140].

REFERENCES

[1] I.F. Akyildiz, W. Su, Y. Sankarasubramaniam and E. Cayirci, A survey on sensor networks, *Comput. Networks*, 2002, pp. 393–422.

[2] G.J. Pottie and W.J. Kaiser, Wireless integrated network sensors, *Commun. ACM*, vol. 43, no. 5, 2000, pp. 51–58.

[3] J. Rabaey, M.J. Ammer, J.L. da Silva Jr, D. Patel and S. Roundy, Picoradio supports *ad hoc* ultra-low power wireless networking, *Comput. Mag.*, July 2000, pp. 42–48.

[4] S. Tilak, N. Abu-Ghazaleh and W. Heinzelman, A taxonomy of wireless micro-sensor network models, *ACM Mobile Comput. Commun. Rev. (MC2R)*, vol. 6, no. 2, April 2002, pp. 28–36.

[5] A. Mainwaring, J. Polastre, R. Szewczyk, D. Culler and J. Anderson, Wireless sensor networks for habitat monitoring, in *1st Workshop on Sensor Networks and Applications*, Atlanta, GA, October 2002, pp. 88–97.

[6] G.D. Abowd and J.P.G. Sterbenz, Final report on the interagency workshop on research issues for smart environments, *IEEE Person. Commun.*, October 2000, pp. 36–40.

[7] J. Agre and L. Clare, An integrated architecture for cooperative sensing networks, *IEEE Comput. Mag.*, May 2000, pp. 106–108.
[8] A. Bakre and B.R. Badrinath, I-TCP: indirect TCP for mobile hosts, in *Proc. 15th Int. Conf. Distributed Computing Systems*, Vancouver, BC, May 1995, pp. 136–143.
[9] P. Bonnet, J. Gehrke and P. Seshadri, Querying the physical world, *IEEE Person. Commun.*, October 2000, pp. 10–15.
[10] B.G. Celler, T. Hesketh, W. Earnshaw and E. Ilsar, An instrumentation system for the remote monitoring of changes in functional health status of the elderly, in *Int. Conf. IEEE-EMBS*, NewYork, 1994, pp. 908–909.
[11] A. Chandrakasan, R. Amirtharajah, S. Cho, J. Goodman, G. Konduri, J. Kulik, W. Rabiner and A. Wang, Design considerations for distributed micro-sensor systems, in *Proc. IEEE 1999 Custom Integrated Circuits Conf.*, San Diego, CA, May 1999, pp. 279–286.
[12] S. Cho and A. Chandrakasan, Energy-efficient protocols for low duty cycle wireless microsensor, in *Proc. 33rd Annual Hawaii Int. Conf. System Sciences*, Maui, HI, vol. 2, 2000, p. 10.
[13] G. Coyle *et al*., Home telecare for the elderly, *J. Telemed. Telecare*, vol. 1, 1995, pp. 183–184.
[14] I.A. Essa, Ubiquitous sensing for smart and aware environments, *IEEE Person. Commun.*, October 2000, pp. 47–49.
[15] D. Estrin, R. Govindan, J. Heidemann and S. Kumar, Next century challenges: scalable coordination in sensor networks, in *ACM MobiCom'99*, Washingtion, DC, 1999, pp. 263–270.
[16] P. Favre, N. Joehl, A. Vouilloz, P. Deval, C. Dehollain and M. J. Declerz, A 2 V, 600 A, 1 GHz BiCMOS super regenerative receiver for ISM applications, *IEEE J. Solid St. Circuits*, vol. 33, 1998, pp. 2186–2196.
[17] K. Govil, E. Chan and H. Wasserman, Comparing algorithms for dynamic speed-setting of a low-power CPU, in *Proc. ACM MobiCom'95*, Berkeley, CA, November 1995, pp. 13–25.
[18] M.P. Hamilton and M. Flaxman, Scientific data visualization and biological diversity: new tools for spatializing multimedia observations of species and ecosystems, *Landscape Urban Plann.*, vol. 21, 1992, pp. 285–297.
[19] M.P. Hamilton and Hummercams, robots, and the virtual reserve, Directors Notebook, 6 February 2000; available from www.jamesreserve.edu/news.html
[20] B. Halweil, Study finds modern farming is costly, *World Watch*, vol. 14, no. 1, 2001, pp. 9–10.
[21] S. Hedetniemi and A. Liestman, A survey of gossiping and broadcasting in communication networks, *Networks*, vol. 18, no. 4, 1988, pp. 319–349.
[22] W.R. Heinzelman, A. Chandrakasan and H. Balakrishnan, Energy-efficient communication protocol for wireless microsensor networks, in *IEEE Proc. Hawaii Int. Conf. System Sciences*, January 2000, pp. 1–10.
[23] W.R. Heinzelman, J. Kulik and H. Balakrishnan, Adaptive protocols for information dissemination in wireless sensor networks, *Proc. ACM MobiCom'99*, Seattle, WA, 1999, pp. 174–185.
[24] C. Herring and S. Kaplan, Component-based software systems for smart environments, *IEEE Person. Commun.*, October 2000, pp. 60–61.
[25] G. Hoblos, M. Staroswiecki and A. Aitouche, Optimal design of fault tolerant sensor networks, *IEEE Int. Conf. Control Applications*, Anchorage, AK, September 2000, pp. 467–472.
[26] T. Imielinski and S. Goel, DataSpace: querying and monitoring deeply networked collections in physical space, in *ACM Int. Workshop on Data Engineering for Wireless and Mobile Access MobiDE 1999*, Seattle, WA, 1999, pp. 44–51.
[27] C. Intanagonwiwat, R. Govindan and D. Estrin, Directed diffusion: a scalable and robust communication paradigm for sensor networks, in *Proc. ACM Mobi- Com'00, Boston,* MA, 2000, pp. 56–67.

[28] P. Johnson *et al*., Remote continuous physiological monitoring in the home, *J. Telemed. Telecare*, vol. 2, no. 2, 1996, pp. 107–113.
[29] J.M. Kahn, R.H. Katz and K.S.J. Pister, Next century challenges: mobile networking for smart dust, in *Proc. ACM MobiCom'99*, Washington, DC, 1999, pp. 271–278.
[30] T.H. Keitt, D.L. Urban and B.T. Milne, Detecting critical scales in fragmented landscapes, *Conserv. Ecol.*, vol. 1, no. 1, 1997, p. 4. Available from www.consecolo.org/vol1/iss1/art4
[31] R. Kravets, K. Schwan and K. Calvert, Power-aware communication for mobile computers, in *Proc. Mo-MUC'99*, San Diego, CA, November 1999, pp. 64–73.
[32] H. Lee, B. Han, Y. Shin and S. Im, Multipath characteristics of impulse radio channels, in *Proc. IEEE Vehicular Technology Conf.*, Tokyo, vol. 3, 2000, pp. 2487–2491.
[33] P. Letteri and M.B. Srivastava, Adaptive frame length control for improving wireless link throughput, range and energy efficiency, in *Proc. IEEE INFOCOM'98*, San Francisco, CA, March 1998, pp. 564–571.
[34] S. Meguerdichian, F. Koushanfar, G. Qu and M. Potkonjak, Exposure in wireless *ad-hoc* sensor networks, in *Proc. ACM MobiCom'01*, Rome, 2001, pp. 139–150.
[35] T. Melly, A. Porret, C.C. Enz and E.A. Vittoz, A 1.2 V, 430 MHz, 4 dBm power amplifier and a 250 W frontend, using a standard digital CMOS process, in *IEEE Int. Symp. Low Power Electronics and Design Conf.*, San Diego, CA, August 1999, pp. 233–237.
[36] F.R. Mireles and R.A. Scholtz, Performance of equicorrelated ultra-wideband pulse-position-modulated signals in the indoor wireless impulse radio channel, in *IEEE Conf. Communications, Computers and Signal Processing*, vol. 2, 1997, pp. 640–644.
[37] Y.H. Nam, Z. Halm, Y.J. Chee and K.S. Park, Development of remote diagnosis system integrating digital telemetry for medicine, in *Int. Conf. IEEE-EMBS*, Hong Kong, 1998, pp. 1170–1173.
[38] N. Noury, T. Herve, V. Rialle, G. Virone, E. Mercier, G. Morey, A. Moro and T. Porcheron, Monitoring behavior in home using a smart fall sensor, in *IEEE-EMBS Special Topic Conf. Microtechnologies in Medicine and Biology*, October 2000, pp. 607–610.
[39] M. Ogawa, T. Tamura and T. Togawa, Fully automated biosignal acquisition in daily routine through 1 month, in *Int. Conf. IEEE-EMBS*, Hong Kong, 1998, pp. 1947–1950.
[40] N. Priyantha, A. Chakraborty and H. Balakrishnan, The cricket location-support system, in *Proc. ACM MobiCom'00*, August 2000, pp. 32–43.
[41] A. Perrig, R. Szewczyk, V. Wen, D. Culler and J.D. Tygar, SPINS: security protocols for sensor networks, in *Proc. ACM MobiCom'01*, Rome, 2001, pp. 189–199.
[42] E.M. Petriu, N.D. Georganas, D.C. Petriu, D. Makrakis and V.Z. Groza, Sensor-based information appliances, in *IEEE Instrum. Msmt. Mag.*, December 2000, pp. 31–35.
[43] A. Porret, T. Melly, C.C. Enz and E.A. Vittoz, A low-power low-voltage transceiver architecture suitable for wireless distributed sensors network, in *IEEE Int. Symp. Circuits and Systems'00*, Geneva, vol. 1, 2000, pp. 56–59.
[44] G.J. Pottie and W.J. Kaiser, Wireless integrated network sensors, *Commun. ACM*, vol. 43, no. 5, 2000, pp. 551–558.
[45] J. Rabaey, J. Ammer, J.L. da Silva Jr and D. Patel, Pico-radio: *ad-hoc* wireless networking of ubiquitous low-energy sensor/monitor nodes, in *Proc. IEEE Computer Society Annual Workshop on VLSI (WVLSI'00)*, Orlanda, FL, April 2000, pp. 9–12.
[46] J.M. Rabaey, M.J. Ammer, J.L. da Silva Jr, D. Patel and S. Roundy, Picoradio supports *ad hoc* ultra-low power wireless networking, *IEEE Comput. Mag.*, 2000, pp. 42–48.
[47] V. Rodoplu and T.H. Meng, Minimum energy mobile wireless networks, *IEEE J. Selected Areas Commun.*, vol. 17, no. 8, 1999, pp. 1333–1344.
[48] A. Savvides, C. Han and M. Srivastava, Dynamic fine-grained localization in ad-hoc networks of sensors, in *Proc. ACM MobiCom'01*, Rome, July 2001, pp. 166–179.
[49] C. Shen, C. Srisathapornphat and C. Jaikaeo, Sensor information networking architecture and applications, *IEEE Person. Commun.*, August 2001, pp. 52–59.

[50] E. Shih, B.H. Calhoun, S. Cho and A. Chandrakasan, Energy-efficient link layer for wireless microsensor networks, in *Proc. IEEE Computer Society Workshop on VLSI 2001*, Orlando, FL, April 2001, pp. 16–21.

[51] E. Shih, S. Cho, N. Ickes, R. Min, A. Sinha, A. Wang and A. Chandrakasan, Physical layer driven protocol and algorithm design for energy-efficient wireless sensor networks, in *Proc. ACM MobiCom'01*, Rome, July 2001, pp. 272–286.

[52] B. Sibbald, Use computerized systems to cut adverse drug events: report, *CMAJ. Can. Med. Assoc. J.*, vol. 164, no. 13, 2001, p. 1878.

[53] S. Singh, M. Woo and C.S. Raghavendra, Power-aware routing in mobile *ad hoc* networks, in *Proc. ACM MobiCom'98*, Dallas, TX, 1998, pp. 181–190.

[54] K. Sohrabi, J. Gao, V. Ailawadhi and G.J. Pottie, Protocols for self-organization of a wireless sensor network, *IEEE Person. Commun.*, October 2000, pp. 16–27.

[55] Y. Tseng, S. Wu, C. Lin and J. Sheu, A multi-channel MAC protocol with power control for multi-hop mobile *ad hoc* networks, in *IEEE Int. Conf. Distributed Computing Systems*, Mesa, AZ, April 2001, pp. 419–424.

[56] B. Walker and W. Steffen, An overview of the implications of global change of natural and managed terrestrial ecosystems, *Conserv. Ecol.*, vol. 1, no. 2, 1997. Available from www.consecol.org/vol1/iss2/art2

[57] B. Warneke, B. Liebowitz and K.S.J. Pister, Smart dust: communicating with a cubic-millimeter computer, *IEEE Comput.*, January 2001, pp. 2–9.

[58] www.fao.org/sd/EIdirect/EIre0074.htm

[59] www.alertsystems.org

[60] A. Woo and D. Culler, A transmission control scheme for media access in sensor networks, in *Proc. ACM MobiCom'01*, Rome, July 2001, pp. 221–235.

[61] S. Wu, C. Lin, Y. Tseng and J. Sheu, A new multi channel MAC protocol with on-demand channel assignment for multihop mobile *ad hoc* networks, *Int. Symp. Parallel Architectures, Algorithms, and Networks, I-SPAN 2000*, Dallas, TX, 2000, pp. 232–237.

[62] S. Wu, Y. Tseng and J. Sheu, Intelligent medium access for mobile *ad hoc* networks with busy tones and power control, *IEEE J. Selected Areas Commun.*, September 2000, pp. 1647–1657.

[63] Y. Xu, J. Heidemann and D. Estrin, Geography-informed energy conservation for *ad hoc* routing, in *Proc. ACM MobiCom'2001*, Rome, July 2001.

[64] M. Zorzi and R. Rao, Error control and energy consumption in communications for nomadic computing, *IEEE Trans. Computers*, vol. 46, no. 3, 1997, pp. 279–289.

[65] J. Elson and D. Estrin, Random, ephemeral transaction identifiers in dynamic sensor networks, in *Proc. 21st Int. Conf. Distributed Computing Systems*, Mesa, AZ, April 2001, pp. 459–468.

[66] A. Howard, M. J. Mataric and G. S. Sukhatme, An incremental self-deployment algorithm for mobile sensor networks, *Autonomous Robots*, Special Issue on Intelligent Embedded Systems, vol. 13, 2002, pp. 113–126.

[67] T. Clouqueur, V. Phipatanasuphorn, P. Ramanathan and K. Saluja, Sensor deployment strategy for target detection, in *1st Workshop on Sensor Networks and Applications*, Atlanta, GA, October 2002, pp. 42–48.

[68] W. Rabiner Heinzelman, A. Chandrakasan and H. Balakrishnan, Energy-efficient communication protocol for wireless microsensor networks, in *Proc. 33rd Int. Conf. System Sciences (HICSS '00)*, January 2000, pp. 1–10.

[69] S. Lindsey and C. S. Raghavendra, PEGASIS: power efficient gathering in sensor information systems, in *2002 IEEE Aerospace Conf.*, March 2002, pp. 1–6.

[70] B. Krishnamachari, S. Wicker, R. Bejar and Marc Pearlman, Critical density thresholds in distributed wireless networks, in *Communications, Information and Network Security*, H. Bhargava, H.V. Poor, V. Tarokh and S. Yoon (eds). Kluwer: Norwell, MA, 2002, pp. 1–15.

[71] C. Intanagonwiwat, R. Govindan and D. Estrin, Directed diffusion: a scalable and robust communication paradigm for sensor networks, *Proc. ACM Mobicom*, Boston MA, August 2000, pp. 1–12.

[72] D. Braginsky and D. Estrin, Rumor routing algorithm for sensor networks, in *First Workshop on Sensor Networks and Applications (WSNA)*, Atlanta, GA, October 2002, pp. 1–12.

[73] D. Petrovic, R.C. Shah, K. Ramchandran and J. Rabaey, Data funneling: routing with aggregation and compression for wireless sensor networks, in *Proc. 1st IEEE Int. Workshop Sensor Network Protocols and Applications*, Anchorage, AK, May 2003, pp. 1–7.

[74] S. Verdu, Recent advances on the capacity of wideband channels in the low-power regime, *IEEE Wireless Commun.*, August 2002, pp. 40–45.

[75] E. J. Duarte-Melo and M. Liu, Data-gathering wireless sensor networks: organization and capacity, *Comput. Networks*, November 2003, pp. 519–537.

[76] K. Kalpakis, K. Dasgupta and P. Namjoshi, Maximum Lifetime Data Gathering and Aggregation in Wireless Sensor Networks, in *Proc. 2002 IEEE Int. Conf. Networking (ICN'02)*, Atlanta, GA, 26–29 August 2002. pp. 685–696.

[77] M. Bhardwaj, T. Garnett and A.P. Chandrakasan, Upper bounds on the lifetime of sensor networks, *Proc. ICC 2001*, Helsinki, June 2001, pp. 1–6.

[78] K. Kant Chintalapudi and R. Govindan, Localized edge detection in a sensor field, *SNPA*, 2003, pp. 1–11.

[79] R. Nowak and U. Mitra, Boundary estimation in sensor networks: theory and methods, in *2nd Int. Workshop on Information Processing in Sensor Networks*, Palo Alto, CA, 22–23 April 2003, pp. 1–16.

[80] D. Li, K. Wong, Y.H. Hu and A. Sayeed, Detection, classification and tracking of targets in distributed sensor networks, *IEEE Signal Proc. Mag.*, vol. 19, no. 2, March, 2002 pp. 1–23.

[81] C.-Y. Wan, A.T. Campbell and L. Krishnamurthy, PSFQ: a reliable transport protocol for wireless sensor networks, in *First ACM International Workshop on Wireless Sensor Networks and Applications (WSNA 2002)*, Atlanta, GA, 28 September 2002, pp. 1–11.

[82] W. Ye, J. Heidemann and D. Estrin, An energy-efficient MAC protocol for wireless sensor networks, in *Proc. 21st Int. Annual Joint Conf. IEEE Computer and Communications Societies (INFOCOM 2002)*, New York, June, 2002 pp. 1–10.

[83] Y. Sankarasubramaniam, O.B. Akan and I.F. Akyildiz, ESRT: event-to-sink reliable transport in wireless sensor networks, in *Proc. ACM MobiHoc'03*, Annapolis, MD, June 2003, pp. 177–188.

[84] F. Stann and J. Heidemann, RMST: reliable data transport in sensor networks, in *Proc. 1st IEEE Int. Workshop Sensor Networks Protocols and Applications*, Anchorage, AK, May 2003, pp. 1–11.

[85] M. Zuniga and B. Krishnamachari, Optimal transmission radius for flooding in large scale sensor networks, in *Workshop on Mobile and Wireless Networks, MWN 2003*, held in conjunction with the *23rd IEEE Int. Conf. Distributed Computing Systems (ICDCS)*, May 2003, pp. 1–29.

[86] G. Lu, B. Krishnamachari and C.S. Raghavendra, An adaptive energy efficient and low-latency MAC for data gathering in sensor networks, in *4th Int. Workshop on Algorithms for Wireless, Mobile, Ad Hoc and Sensor Networks (WMAN 04)*, held in conjunction with the *IEEE IPDPS Conf. 18th Int. Parallel and Distributed Processing Symp.*, April 2004, pp. 1–12.

[87] A. Depedri, A. Zanella and R. Verdone, An energy efficient protocol for wireless sensor networks, in *Autonomous Intelligent Networks and Systems (AINS 2003)*, Menlo Park, CA, 30 June to 1 July 2003, pp. 1–6.

[88] A. P. Chandrakasan, R. Min, M. Bhardwaj, S. Cho and A. Wang, Power aware wireless microsensor systems, Keynote Paper ESSCIRC, Florence, September 2002, pp. 1–8.

[89] P. Chen, B. O'Dea and E. Callaway, Energy efficient system design with optimum transmission range for wireless *ad hoc* networks, in *IEEE Int. Conf. Communication (ICC 2002)*, vol. 2, 28 April to 2 May 2002, pp. 945–952.

[90] S. Banerjee and A. Misra, Energy efficient reliable communication for multi-hop wireless networks, *J. Wireless Networks*, pp. 1–23.

[91] N. Lay, C. Cheetham, H. Mojaradi and J. Neal, Developing low-power transceiver technologies for *in situ* communication applications, IPN Progress Report 42–147, 15 November 2001, pp. 1–22.

[92] Y. Prakash and S.K.S Gupta, Energy efficient source coding and modulation for wireless applications, *IEEE Wireless Commun. Networking Conf.*, 2003, vol. 1, 16–20 March 2003, pp. 212–217.

[93] M. Khan, G. Pandurangan and B. Bhargava, Energy-efficient routing schemes for wireless sensor networks, Technical Report CSD TR 03-013, Department of Computer Science, Purdue University, 2003, pp. 1–12.

[94] E. Shih, S-H Cho, N. Ickes, R. Min, A. Sinha, A. Wang and A. Chandrakasan, Physical layer driven protocol and algorithm design for energy-efficient wireless sensor networks, in *Proc. 7th Annual Int. Conf. Mobile Computing and Networking*, Rome, 2001, pp. 272–287.

[95] D. Ganesan, R. Govindan, S. Shenker and D. Estrin, Highly resilient, energy efficient multipath routing in wireless sensor networks, *Mobile Comput. Commun. Rev. (MC2R)*, vol. 1, no. 2, 2002, pp. 10–24.

[96] B. Krishnamachari and S. Iyengar, Distributed bayesian algorithms for fault-tolerant event region detection in wireless sensor networks, *IEEE Trans. Comput.*, vol. 53, 2004, pp. 241–250.

[97] C. Karlof and D. Wagner, Secure routing in sensor networks: attacks and countermeasures, in *Proc. 1st IEEE Int. Workshop Sensor Networks Protocol and Applications*, Anchorage, AK, May 2003, pp. 1–15.

[98] A. Howard, M. Matari and G. Sukhatme, An incremental self-deployment algorithm for mobile sensor networks, in *Autonomous Robots, Special Issue on Intelligent Embedded Systems*, vol. 13(2). Kluwer Academic: Norwell, MA, 2002, pp. 113–126.

[99] T. Balch and M. Hybinette: Behavior-based coordination of large-scale robot formations, in *Proc. Fourth Int. Conf. Multiagent Systems (ICMAS')*, Boston, MA, 2000, pp. 363–364.

[100] G. Dedeoglu and G.S. Sukhatme, Landmark-based matching algorithms for cooperative mapping by autonomous robots, in *Distributed Autonomous Robotics Systems*, L.E. Parker, G.W. Bekey and J. Barhen (eds), vol. 4. Springer: Berlin, 2000, pp. 251–260.

[101] A. Elfes, Sonar-based real-world mapping and navigation, in *IEEE J. Robot. Autom.*, vol. RA-3, 1987, pp. 249–265.

[102] D.W. Gage, Command control for many-robot systems, in *AUVS-, the Nineteenth Annual AUVS Technical Symp.*, Hunstville AB, 1992, pp. 22–24. Reprinted in *Unmanned Syst. Mag.*, vol. 10, no. 4, Fall 1992, pp. 28–34.

[103] B.P. Gerkey, R.T. Vaughan, K. Stoy, A. Howard, G.S. Sukhatme and M. J. Matarić, Most valuable player: a robot device server for distributed control, in *Proc. of the IEEE/RSJ Int. Conf. on Intelligent Robots and Systems (IROSOl)*, Wailea, HJ, 2001, pp. 1226–1231.

[104] A. Howard, M.J. Matarić and G.S. Sukhatme, Mobile sensor network deployment using potential fields: a distributed, scalable solution to the area coverage problem, in *Distributed Autonomous Robotic Systems 5: Proc. 6th Int. Conf. Distributed Autonomous Robotic Systems (DARS02)*, Fukuoka, 2002, pp. 299–308.

[105] C. Intanagonwiwat, R. Govindan and D. Estrin, Directed diffusion: a scalable and robust communication paradigm for sensor networks, in *Proc. Sixth Annual International Conf. on Mobile Computing and Networks (MobiCOM 2000)*, Boston, MA, 2000, pp. 56–67.

[106] M. López-Sánchez, F. Esteva, R.L. de Mántaras, C. Sierra and J. Amat, Map generation by cooperative low-cost robots in structured unknown environments, *Autonomous Robots*, vol. 5, 1998, pp. 53–61.
[107] T. Lozano-Perez and M. Mason, Automatic synthesis of fine-motion strategies for robots, *Int. J. Robot. Res.*, vol. 3, 1984, pp. 3–24.
[108] D. Payton, M. Daily, R. Estkowski, M. Howard and C. Lee, Pheromone robotics, *Autonomous Robots*, vol. 11, 2001, pp. 319–324.
[109] I.M. Rekleitis, G. Dudek and E.E. Milios, Graph-based exploration using multiple robots, in L.E. Parker, G.W. Bekey and J. Barhen (eds.), *Distributed Autonomous Robotics Systems*, vol. 4, Springer: Berlin, 2000, pp. 241–250.
[110] F.E. Scheider, D. Wildermuth and H.-L. Wolf, Motion coordination in formations of multiple mobile robots using a potential field approach, in L.E. Parker, G.W. Bekey and J. Barhen (eds). *Distributed Autonomous Robotics Systems*, vol. 4, Springer: Berlin, 2000, pp. 305–314.
[111] S. Thrun, D. Fox, W. Burgard and F. Dellaert, Robust Monte Carlo localization for mobile robots, *Artif. Intell. J.* vol. 128, 2001, pp. 99–141.
[112] A.F. Winfield, Distributed sensing and data collection via broken *ad hoc* wireless connected networks of mobile robots, in L.E. Parker, G.W. Bekey and J. Barhen (eds). *Distributed Autonomous Robotics Systems*, vol. 4. Springer: Berlin, 2000, pp. 273–282.
[113] B. Yamauchi, Frontier-based approach for autonomous exploration, in *Proc. IEEE Int. Symp. Computational Intelligence, Robotics and Automation*, 1997, pp. 146–151.
[114] B. Yamauchi, A. Shultz and W. Adams, Mobile robot exploration and map-building with continuous localization, in *Proc. 1998 IEEE/RSJ Int. Conf. Robotics and Automation*, vol. 4, San Francisco, CA, 1998, pp. 3175–3720.
[115] A. Zelinksy, A mobile robot exploration algorithm, *IEEE Trans. Robot. Autom.*, vol. 8, 1992, pp. 707–717.
[116] J. Edmonds, Edge-disjoint branchings, in *Combinatorial Algorithms*. Academic Press: London, 1973.
[117] L. Lovász, On two minimax theorems in graph theory, *J. Combin. Theory Ser. B*, 1976.
[118] K. Dasgupta, K. Kalpakis and P. Namjoshi, An efficient clustering-based heuristic for data gathering and aggregation in sensor networks, in *IEEE Wireless Communications and Networking, WCNC 2003*, vol. 3, 16–20 March 2003, pp. 1948–1953.
[119] R.D. Nowak, E.D. Kolaczyk, Multiscale maximum penalized likelihood estimators, *IEEE Int. Symp. Information Theory*, Lozana, 2002, p. 156.
[120] R.D. Nowak and E.D. Kolaczyk, A statistical multiscale framework for Poisson inverse problems, *IEEE Trans. Inform. Theory*, vol. 46, no. 5, August 2000, pp. 1811–1825.
[121] R. Nowak, U. Mitra and R. Willett, Estimating inhomogeneous fields using wireless sensor networks, *IEEE J. Select. Areas Commun.*, vol. 22, no. 6, August 2004, pp. 999–1006.
[122] R.M. Willett and R.D. Nowak, Platelets: a multiscale approach for recovering edges and surfaces in photon-limited medical imaging, *IEEE Trans. Medical Imag.*, vol. 22, no. 3, March 2003, pp. 332–350.
[123] R.M. Willett, A.M. Martin and R.D. Nowak, Adaptive sampling for wireless sensor networks, in *Int. Symp. Information Theory, ISIT*, 27 June to 2 July 2004, p. 519.
[124] www.ece.rice.edu/∼nowak/pubs.html (www.ece.rice.edu/∼nowak/msla.pdf).
[125] R. Nowak and U. Mitra, *Boundary Estimation in Sensor Networks: Theory and Methods, 2nd International Workshop on Information Processing in Sensor Networks*, Palo Alto, CA, 22–23 April 2003, pp. 1–15.
[126] L. Breiman, J. Friedman, R. Olshen and C. J. Stone. *Classification and Regression Trees*. Wadsworth: Belmont, CA, 1983.

[127] K. Chintalapudi and R. Govindan. Localized edge detection in sensor fields. University of Southern California, Computer Science Department, Technical Report, 2002; available at www.cs.usc.edu/tech-reports/techniathrmca1-reports.html

[128] D. Donoho and Wedgelets: nearly minimax estimation of edges, *Ann. Statist.*, vol. 27, 1999, pp. 859–897.

[129] A.P. Korostelev and A. B. Tsybakov. *Minimax Theory of Image Reconstruction*. Springer: New York, 1993.

[130] B. Laurent and P. Massart. Adaptive estimation of a quadratic functional by model selection. *Ann. Stat.*, vol. 5, October 2000, pp. 37–52.

[131] S. Ni, Y. Tseng, Y. Chen and J. Chen, The broadcast storm problem in a mobile *ad hoc* network, in *Annual ACM/IEEE Int. Conf. Mobile Computing and Networking (MOBICOM)*, August 1999, pp. 151–162.

[132] P. Gupta and P.R. Kumar, Critical power for asymptotic connectivity in wireless networks, in *Stochastic Analysis, Control, Optimization and Applications*, W.M. McEneany *et al*. (eds). Birkhauser: Boston, MA, 1998, pp. 547–566.

[133] L. Kleinrock and J.A. Silvester. Optimum transmission radii for packet radio networks or why six is a magic number, in *Record National Telecommun. Conf.*, December 1978, pp. 4.3.1–4.3.5.

[134] H. Takagi and L. Kleinrock, Optimal transmission ranges for randomly distributed packet radio Terminals, *IEEE Trans. Commun.*, vol. COM-32, no. 3, March 1984, pp. 246–257.

[135] D. Ganesan, B. Krishnamachari, A. Woo, D. Culler, D. Estrin and S. Wicker, Complex behavior at scale: an experimental study of low-power wireless sensor networks, UCLA Computer Science Technical Report UCLA/CSD-TR 02-0013.

[136] TinyOS Homepage; http://webs.cs.berkeley.edu/tos/

[137] Z.M. Zuniga and B. Krishnamachari, Optimal transmission radius for flooding in large scale wireless sensor networks, in *Int. Workshop on Mobile and Wireless Networks*, Providence, RI, May 2003.

[138] K. Sohrabi, J. Gao, V. Ailawadhi and G.J. Pottie. Protocols for self-organization of a wireless sensor network, *IEEE Person. Commun.*, vol. 7, no. 5, October 2000, pp. 16–27.

[139] D. Petrovic, R.C. Shah, K. Ramchandran and J. Rabaey, Data funneling: routing with aggregation and compression for wireless sensor networks, *IEEE Int. Workshop on Sensor Network Protocols and Applications*, 11 May 2003, pp. 156–162.

[140] Y. Sankarasubramaniam, Ö. B. Akan and I.F. Akyildiz, ESRT: event-to-sink reliable transport in wireless sensor networks, in *MobiHoc'03,* Annapolis, MD, 1–3 June 2003, pp. 177–188.

[141] C.-Y. Wan, A.T. Campbell and L. Krishnamurthy, Pump-slowly, fetch-quickly (PSFQ): a reliable transport protocol for sensor networks, *IEEE J. Select. Areas Commun.*, volume 23, no. 4, 2005, pp. 862–872.

[142] C.-Y. Wan, A.T. Campbell and L. Krishnamurthy, PSFQ: a reliable transport protocol for wireless sensor networks, in *Proc. 1st ACM Int. Workshop Wireless Sensor Network Applications (WSNA)*, Atlanta, GA, 28 September 2002, pp. 1–11.

[143] S. Floyd, V. Jacobson, C. Liu, S. Macanne and L. Zhang, A reliable multicast framework for lightweight session and application layer framing, *IEEE/ACM Trans. Networks*, vol. 5, no. 2, 1997, pp. 784–803.

[144] R. Stann and J. Heidemann, RMST: reliable data transport in sensor networks, in *Proc. 1st IEEE Int. Workshop Sensor Network Protocols Applications*, Anchorage, AK, May 2003, pp. 102–112.

[145] C.-Y. Wan, S.B. Eisenman and A.T. Campbell, CODA: congestion detection and avoidance in sensor networks, in *Proc. 1st ACM Conf. Embedded Networked Sensor Syst. (SenSys)*, Los Angeles, CA, 5–7 November 2003, pp. 266–279.

[146] C.-Y. Wan, A resilient transport system for wireless sensor networks, Ph.D. dissertation, Department of Electronic Engineering, Columbia University, New York, 2005. Available at: http://comet.columbia.edu/armstrong/wan-2005.pdf

[147] H. Balakrishnan, V.N. Padmanabhan, S. Seshan and R.H. Katz, A comparison of mechanisms for improving TCP performance over wireless links, *IEEE/ACM Trans. Networking*, vol. 5, no. 6, 1997, pp. 756–769.

[148] B. Langen, G. Lober and W. Herzig, Reflection and transmission behavior of building materials at 60 GHz, in *Proc. IEEE PIMRC'94*, The Hague, September 1994, pp. 505–509.

15

Security

A necessary component of network security is the ability to reliably authenticate communication partners and other network entities.For this reason we will start this chapter by discussing authentication protocols [1–19]. The focus will be on a systematic approach to the design of the protocols rather then describing a specific protocol used in practice. The following session will discuss the security architectures. Principles of key distribution will be covered in the third section followed up by some specific solutions in *ad hoc* networks, sensor networks, GSM and UMTS systems.

15.1 AUTHENTICATION

Many designs dealing with authentication in networks or distributed systems combine the issues of authentication with those of key distribution. These designs typically assume that all network parties share a key with a common trusted entity, a key distribution center (KDC), from which they can get pair-wise shared keys to carry out mutual authentication protocols. These protocols are called three-party authentication protocols, and have been studied extensively [5, 6, 10–12, 15, 16]. Most of the corresponding implementations [10] require the exchange of long messages, which is possible for application layer protocols, but makes them unsuitable for use in lower-layer networking protocols where limited packet sizes are an important consideration. Some require synchronized clocks or counters [10] that pose system management and initialization issues, as will be discussed below.

Two-party authentication protocols are used in many networks. Some of these use public key cryptography [1–3, 18]. With a public key cryptographic system, each party only has to know and verify the public key of the other party, and there is no need to share secret keys. The authentication method most widely used in network environments today consists of asking users to prove their identity by demonstrating knowledge of a secret they know, *a password*. This widespread but old technique has several weaknesses.

In most password systems, the password typed by a user is sent in cleartext over the network to the computer that requested it. This means that an intruder can spy on passing traffic to collect passwords. Since users need to memorize their passwords, they typically select passwords that they

Advanced Wireless Technologies: Cognitive, Cooperative & Opportunistic 4G Technology Second Edition Savo G. Glisic

can easily remember. So, such passwords are selected from within a relatively small vocabulary, and are thus easily guessed by potential intruders [4].

Of all authentication techniques that circumvent the drawbacks of passwords, the most promising ones are those using cryptographic means. With such techniques, users are typically provided with smart cards or chip cards equipped with a processor capable of cryptographic operations. Authentication is based upon using the card to compute or verify cryptographic messages exchanged with the computer.

Cryptographic authentication consists of challenging the user or communicating party being authenticated to prove its identity by demonstrating its ability to encipher or decipher some item with a secret or private key known to be stored inside the smart card. Of course, since the secret or private key stored on the card or secure device changes infrequently, the item to be enciphered or deciphered with it must change for every execution of the authentication protocol, otherwise, even though the secret never flows in cleartext over the network, an intruder could still tap a line, record the cryptic message that flows over it, and play that recording back at a later time without even knowing what it means.

To guarantee that the item that gets enciphered (or deciphered), called the *challenge*, is different for every execution of the authentication protocol, three techniques are used. The challenge may be derived either from a real-time clock reading, in which case it is called a *timestamp*, from a *counter* that is incremented for every protocol execution, or from a random number generator, in which case it is called a *nonce*. In any case, a new challenge (timestamp, counter value or nonce) is generated for each protocol run.

With timestamps, the user being authenticated, A, enciphers the current reading of its clock and sends the result to the party requesting the authentication B. B then deciphers the received message, and verifies that the timestamp corresponds to the current realtime. The drawback of timestamps is thus immediately apparent. A and B must have synchronized real-time clocks for the verification to be possible. However, since clocks can never be perfectly synchronized and messages take time to travel across networks anyway, B cannot expect that the deciphered timestamp received from A will ever be equal to its own real-time clock reading. A's time-stamp at best can (and normally should) be within some limited time window of B's real-time clock. However, as soon as a time window of tolerance is defined, a potential intruder could exploit it to impersonate A by replaying one of A's recent authentication messages within that time window. Preventing this requires putting a limit to the number of authentication protocol runs allowable during the time window, and having B save all the authentication messages within the window. Thus, both efficiency and security require pretty good clock synchronization. Achieving such synchronization is often difficult, and making it secure would itself require using some other authentication method not depending on time.

With counting challenges, A and B maintain synchronized counters of the number of times they have authenticated one another. Every time A wants to communicate with B, it enciphers its counter and sends the result to B, who deciphers it and verifies that it matches its own counter value, whereupon both parties increment their respective counters for the next time. The drawback of such counting challenges is that both parties must maintain synchronized counters, which poses stable storage and counter management problems in the long run. The counters must be long enough to prevent an attacker from waiting for a (deterministic) counter wraparound; using counters complicates resolution of conflicts when both parties want to initiate protocol executions at the same time; after detecting loss of synchronization between two counters, some other method of authentication must be used to securely resynchronize them; and an undetected error in the counter values may have catastrophic effects.

Therefore, both timestamps and counter techniques, while useful, are not a complete solution, especially for protocols in the lower layers of a network architecture. The best technique for this purpose, and also the simplest one to implement, consists of using nonces. The price for this

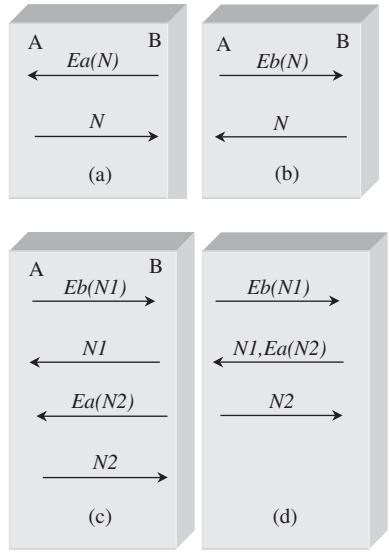

Figure 15.1 Authentication protocols: (a) one-way authentication of A; (b) one-way authentication of B; (c) two-way authentication; and (d) two-way authentication with three messages.

simplicity is an extra network message. While *A* can authenticate itself to *B* with a single message if timestamps or counters are used, two messages are necessary with nonces. Indeed, it is *B* and not *A* who needs to be sure that the nonce has never been used before. Thus, it is *B* and not *A* who must generate it. *B* must encipher it and send it to *A*, then *A* must decipher it and send it back in cleartext for *B* to authenticate it, which costs a total of two messages. The cost of one more message is usually tolerable, especially since the extra message can often be piggy-backed onto regular traffic or its cost can be amortized over many subsequent messages authenticated with sequence counters. Given these advantages of nonces over timestamps and counters, the rest of this section focuses on nonce-based authentication protocols.

Figure 15.1 is a simple representation of the nonce-based one-way authentication protocol, where *N* is a nonce generated by *B* and *Ea*(*N*) is its value enciphered under some key *Ka* that *B* knows is associated with *A*. It may be a secret key shared between *A* and *B* or the public key of *A*. The protocol allows *B* to authenticate *A*. A number of modifications are shown in the same figure.

The simple and elegant two-way authentication protocol, which was derived most naturally by combining two instances of the simplest possible one-way protocol, presents a number of undesirable characteristics. In particular, we will show that an intruder may break this protocol by interleaving messages from different executions of it, if the same shared key is used by both parties *or* if the same key is always used by the party who starts the protocol. One could still argue that the protocol is safe if used with four different keys; however, this creates additional overhead and key management issues, as well as migration problems for existing designs.

15.1.1 Attacks on simple cryptographic authentication

The simple two-way authentication protocol illustrated in Figure 15.1(d) suffers from a number of defects.

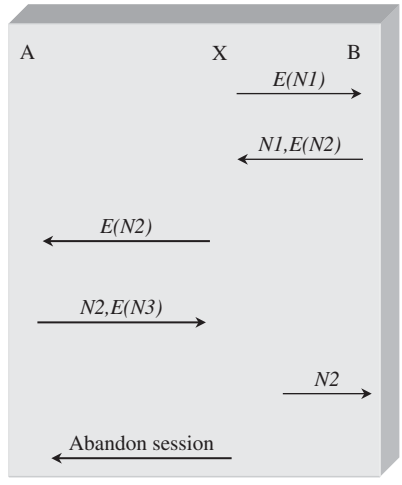

Figure 15.2 An oracle session attack.

15.1.1.1 Known plaintext attacks

A first weakness of the protocol is its openness to known plaintext attacks. Every enciphered message flowing between A and B is the ciphertext of a bit string (the nonce) that flows in plaintext in a subsequent message between A and B. This enables a passive wiretapping intruder to collect two cleartext–ciphertext pairs every time the protocol is run, which at the very least helps it accumulate encryption tables in the long run, and may even help it break the scheme and discover the encryption key, depending on the quality of the encryption algorithm used. It is in general desirable that the plaintext of exchanged enciphered messages not be known or derivable by intruders.

15.1.1.2 Chosen ciphertext attacks

A potential intruder may even turn known plaintext attacks into selected text attacks by playing an active instead of passive role. Pretending that it is A or B, an intruder may send the other party (B or A) a ciphertext message that it selected itself and wait for that other party to reply with the deciphered value of that text. Of course, the intruder, not knowing the right key, may not be able to complete the third protocol flow. However, it can accumulate knowledge about cleartext–ciphertext pairs *of which it selected the ciphertext itself* (or the cleartext, if the challenge was enciphered instead of deciphered). So it may try specific ciphertext strings such as all zeros, all ones, or whatever else might help it break the key faster, depending on the cryptographic method used. It is in general desirable that an intruder not be able to trick legitimate parties into generating deciphered versions of selected ciphertext messages (or enciphered versions of selected cleartext).

15.1.1.3 Oracle session attacks

If A and B use the same key in the simple protocol suggested earlier, the intruder actually *can* break the authentication without even breaking the key. This is illustrated in Figure 15.2, where the intruder, noted X and posing as A, starts a session with B by sending B some enciphered nonce $E(N1)$. B replies with the deciphered value $N1$ and its own enciphered challenge $E(N2)$. X cannot decipher $N2$, but it can take advantage of a selected ciphertext attack on A, using A

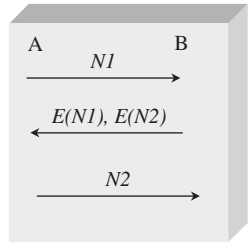

Figure 15.3 Improved two-way protocol.

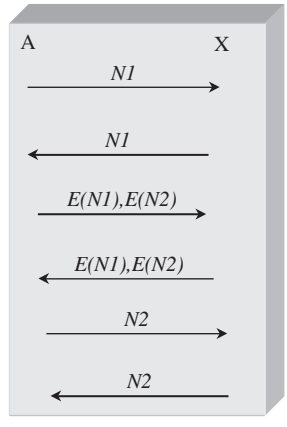

Figure 15.4 A parallel session attack.

as an oracle who will provide the necessary deciphered value $N2$.X accomplishes this by posing now as B to start a separate 'oracle' session with A, sending $E(N2)$ as the initial message on that session. A will reply with the needed value $N2$ and some own enciphered nonce $E(N3)$. X then drops the oracle session with A since it cannot and does not care about deciphering $N3$, but it then turns around and successfully assumes its faked identity A with respect to B by sending $N2$ to B. This may be prevented by modifying protocol as shown in Figure 15.3. This is an ISO SC27 protocol [19].

15.1.1.4 Parallel session attacks

Another defect commonly found in simple protocols, such as those seen above, is depicted in Figure 15.4, where the intruder assumes a passive role instead of an active one. It intercepts a call from A to B with challenge $N1$ and since it cannot answer the challenge $N1$ by replying $E(N1)$, it simply pretends that it is B trying to start a *parallel session* with A. Of course, it selects to use just the same $N1$ as the first challenge on the original session, thus causing A to provide it with precisely the answer $E(N1)$ needed to complete the first authentication. The remaining communication shown in the figure will complete the second authentication as well.

Parallel session attacks illustrate another fundamental flaw of many simple authentication protocols: the cryptographic expression used in the second message must be asymmetric (i.e. direction-dependent) so that its value in a protocol run initiated by A cannot be used in a protocol run initiated by B. Based on the above observations, i.e. that the cryptographic message in the second

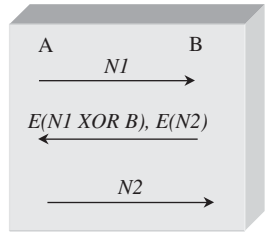

Figure 15.5 An asymmetric two-way authentication.

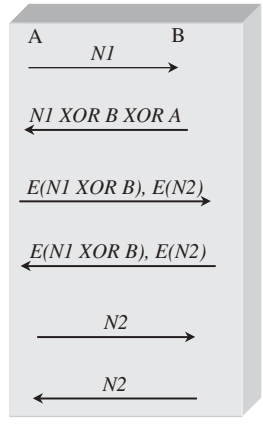

Figure 15.6 An offset attack (through a parallel session).

flow must be asymmetric (direction-dependent) and different from the one in the third flow, one may think that a protocol such as the one in Figure 15.5 should be secure. Unfortunately, in addition to that the fact that known- and selected-text attacks are still possible, the problem now is that the simple function XOR has not fixed anything since an intruder can still resort to a parallel session attack. It merely needs to use proper offsetting in addition, as illustrated in Figure 15.6.

The simple and apparently sound protocol of Figure 15.1(d) is thus broken in many ways. In the following, oracle-session attacks, parallel-session attacks, offset attacks and/or other types or combinations of attacks that involve replaying messages and functions of challenges observed in other runs of the protocol will be collectively referred to as *interleaving* attacks. Based on the above observations we can specify the following design requirements for authentication protocols:

(1) nonce-based (avoid synchronization and stable counter storage);

(2) resistant to common attacks;

(3) usable at any layer of any network architecture (small messages);

(4) usable on any processing base (few computations);

(5) using any cryptographic algorithm, either symmetric ones, such as DES [20] or asymmetric ones such as RSA [7];

(6) exportable – the chance to receive proper licensing for a technology is larger if it provides only message authentication code (MAC) functions and does not require full-fledged encryption and decryption of large messages;

(7) extendable – it should support the sharing of secret keys between multiple users and should allow additional fields to be carried in the messages, which would thus be authenticated as part of the protocol.

15.1.2 Canonical authentication protocol

A number of protocols meeting the above requirements have been developed [13, 14]. Some of these protocols are summarized in Figure 15.7. Given that the focus is on authentication protocols using nonces, the most general canonical form for all such protocols is depicted in Figure 15.7 (P1). Here, A sends some nonce $N1$ to B.B authenticates itself by sending back a function $u(\ )$ of several parameters, including at least its secret $K1$ and the challenge $N1$ it received from A. It also sends a challenge $N2$ to A. A finally completes the protocol by authenticating itself with a function $v(\ )$ of several parameters including at least its secret $K2$ and the challenge $N2$ from B. As indicated in the earlier section on attacks, in order for this protocol to resist oracle attacks, the functions $u(\ )$ and $v(\ )$ must be different from one another, meaning that a cryptographic message from flow (2) can never be used to derive the necessary message for flow (3).

The protocols must work with either symmetric or asymmetric cryptographic systems. With the latter, the secrets $K1$ and $K2$ would be the private keys of B and A, respectively. However, with symmetric systems, $K1$ and $K2$ would be shared secret keys. In fact, in many typical scenarios, they would be the same shared secret key. In the sequel we will continue under that assumption because it opens the door to attacks that would not be possible otherwise, yet it has advantages of efficiency and ease of migration of existing systems over solutions which use different keys for A and B. Any protocol that resists interleaving attacks using equal symmetric keys is also safe with asymmetric ones while the opposite is not true.

Under the assumption of symmetric cryptography with a single shared secret key K protocol P1 becomes as depicted in Figure 15.7 (P2), where the functions $u(K1,$ decryption) are represented by operations $E(\ )$ under the same key K of two different functions $p(\ )$ and $q(\ )$ of the remaining parameters. As indicated earlier in the section on attacks, the prevention of parallel session attacks suggests that function $p(\ )$ must be asymmetric, i.e. direction-dependent. In other words, the

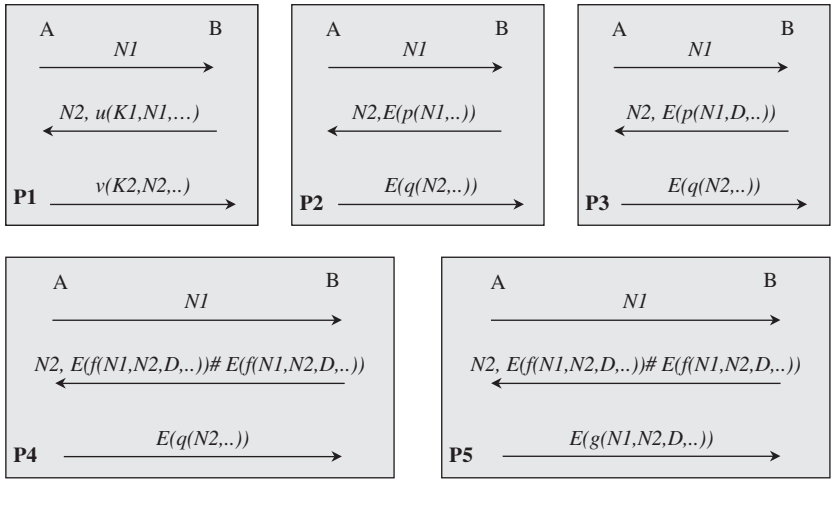

Figure 15.7 P1, resistance to replay attacks through use of nonces; P2, use of symmetric cryptography; P3, resistance to parallel session attacks; P4, resistance to selected-text and offset attacks; P5, minimal number of encryptions.

arguments to $p(\ )$ must be different depending on whether A or B starts the communication session. This is depicted in Figure 15.7 (P3) by the addition of a parameter D in $p(\ )$, which stands for anything indicating or tied to the direction of the flow (e.g. the name or address of one of the parties).

As shown in Figure 15.7 (P3), the complete protocol P3 requires three messages. In any networking environment, these messages need not travel in packets of their own. In practice, they can and typically would be piggy-backed onto other network packets, such as, for instance, connection requests and confirmations at whatever layer entities are being authenticated (e.g. link, network, transport, application, etc.). Within packets at any such layer, the authentication fields should take as little space as possible. As it stands presently, the canonical protocol requires a nonce to be carried on the first flow, a nonce and a cryptographic expression on the second one, and a cryptographic expression on the third one. The cleartext of the directional parameter, e.g. party name or address, is implicitly known or already present in the enclosing packet headers. The required size of nonces is given by the amount of security desired: the larger they are, the lower the probability will be that a given nonce gets reused. The size of the cryptographic expressions depends on the encryption algorithm used and on the amount of information being encrypted.

As an example, if the DES is used, the smallest cryptographic expression will be 64 b (key 56 b) long. Since the security of the whole authentication protocol rests on the unforgeability of the cryptographic expressions, if expressions of 64 b are used, the statistical security, ss, of the expressions is $ss = 1/p(\text{expression}) = 2^{64}$, the inverse of the probability that an intruder can successfully guess a cryptographic expression. For many environments, such a degree of security is already quite satisfactory, although longer cryptographic expressions are already being used. Triple DEA (ANSI X9.17, DEA 1999) uses three keys and three executions of DEA with effective key length 112 and 168 b. Advanced encryption standard (AES, 1997) uses blocks of length 128 b and key lengths 128, 192 and 256 b. If 64 b nonces are used, $p(\ )$ and $q(\ )$ may be restricted to 64 b functions of their parameters without compromising the degree of security. We further make this simplifying assumption.

Restricting $p(\ )$ and $q(\ )$ to 64 b functions to limit message size has its own implications. Many simple and attractive 64 b functions of only $N1$ and D (e.g. XOR, rotations, conditional permutations, etc.) could be subjected to selected-plaintext and offset attacks by an intruder. By including inside function $p(\ )$ an additional internal encrypted function of the same parameters $N1$ and D, one can separate these parameters cryptographically and thus bar the way to offset attacks. By including $N2$ inside function $p(\ )$, one bars the way to a potential intruder using B as an oracle to get some selected plaintext enciphered in the second flow because the cleartext of that flow then depends on nonce $N2$ which is not under the control of the intruder initiating a protocol run. These further conditions on $p(\ )$ are represented in Figure 15.7 (P4), where $p(\ )$ would thus be a 64 b function (noted #) of two operands, which themselves include functions $f(\ )$ and $g(\ )$ of $N1$, N2 and D.

The different fields in the message should be cryptographically separated, so that the attacker should not be able to control one field through another field. This separation should be ensured by an appropriate selection of the functions $f(\ )$ and $g(\ )$. We will later give exact conditions on $f(\ )$ and $g(\ )$ to prevent interleaving attacks, and give specific examples for these functions.

Any peer authentication protocol requires at least two cryptographic expressions. In Figure 15.7 (P5) a third cryptographic operation is used to protect against offset attacks. To keep the protocol simple, by putting additional conditions on $q(\ )$, we can return to a protocol requiring only two cryptographic block operations. This can be achieved by imposing that the functions $g(\ )$ and $q(\ )$ actually be the same, as represented in Figure 15.7 (P5). Indeed, in this case, the innermost cryptographic expression required to produce or verify the second flow is the same as the cryptographic expression of the third flow, and can thus be computed only once and saved to minimize computation.

Finally, it may be instructive at this point to describe the operation of public key encryption system used for authentication. In this case user generates pair of keys and places one key in the

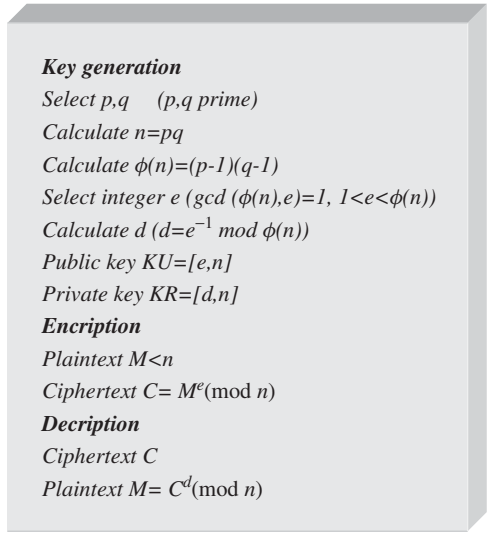

(a)

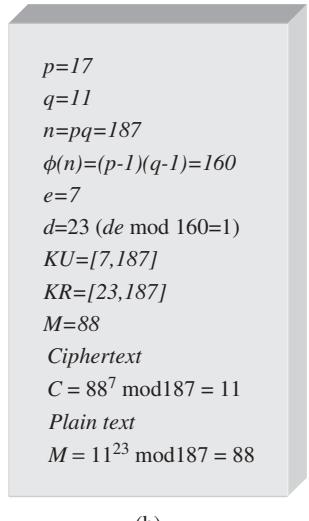

(b)

Figure 15.8 (a) Operation of a public key encryption system; (b) numerical example of operation of a public key encryption system.

public domain. To send a message the user encrypts using the public key and decrypts using a private key as illustrated in Figure 15.8(a); a numerical example is given in Figure 15.8(b).

15.2 SECURITY ARCHITECTURE

Cryptography provides only two fundamental services, namely, *confidentiality* and *authentication.* All communications security services are concerned with the identity of the senders or recipients

of information. Cryptography allows users to be identified by allocating secret keys to them. There are only two ways that cryptography can work, and these define the fundamental services [22, 23]:

- *Confidentiality* – only the user (or set of users) in possession of the secret key can read the message;
- *Authentication* – only the user (or set of users) in possession of the secret key can write the message.

A *secure channel* can be thought of as a relationship between two system users which provides some security services.

In this section, two basic types of secure channel are considered, namely, confidentiality channels and authentication channels. In addition, we define symmetric channels, each of which may coincide with a confidentiality channel, an authentication channel or both.

In a conventional symmetric cipher, a pair of users share the same key. This symmetric channel typically provides both a confidentiality and an authentication channel between a specific pair of users. Symmetric ciphers can also be used to provide authentication alone, as when a message authentication code is used [25].

A public key cryptosystem, as described above, usually has one public key and a corresponding secret key. For certain algorithms, such as RSA [31], the public key may be used for confidentiality and the secret key may be used for authentication. However, for other algorithms, it may be that only one channel is provided. For example, signature schemes provide authentication but not confidentiality,while schemes such as the McEliece algorithm [25] are suitable for authentication but not confidentiality.

There are three components that make up a *security architecture* in the model of this paper: (1) *users*; (2) *trusted users*, including information on who trusts whom; and (3) *secure channels*, which may provide confidentiality authentication or both.

The *formal model* is a relatively simple specification and defines a state-based sequential system as described in Spivey [32]. The first line of the specification defines the abstract types which will be used. These are users and keys [*User, Key*] and they are fundamental values in the model. Other components, such as secure channels and trusted users, will be defined in terms of these sets.

Next, some global, or axiomatic, definitions are made. These are things that are not expected to change within the model and so can be excluded from the rest of the system state. Five sets of keys are defined concerning two separate properties. A key must be in exactly one of the sets *public*, *secret*, *shared*; in other words, these sets partition ($\mathbb{P}$) the keys. In addition, a key must be a confidentiality key (in the set *Conf*) or an authentication key (in the set *Auth*) or both. The

Table 15.1 Special Z symbols

Symbol	Meaning
$f: X \to Y$	Function between X and Y
$f: X \leftrightarrow Y$	Relation between X and Y
id X	The identity function on X
dom f	The domain of f
ran f	The range of f
$f(\|X\|)$	Image of the set X under the function f
$f \oplus g$	Function which takes values of the function f except on the domain of g, where it takes the values of g
$f \circ g$	Functional composition where the domain of g must equal the range of f
$X \setminus Y$	Set difference of X and Y
$\mathbb{P} X$	the set of sets with elements of X as values

dual, or inverse, is defined for each key. Taking the dual of a key is a self-inverse operation. The dual of a confidentiality key is still a confidentiality key and similarly for authentication keys. Secret and public keys are interchanged under the dual map, while the dual of a shared key is still shared. The trusted users are defined by a map which defines those users trusted by each user. For a formal representation of the system components, notation from Table 15.1 known as *Z* notation [32] is used, resulting in [21]:

$$
\begin{array}{l}
Shared, Public, Secret, Auth, Conf : \rightarrowtail Key \\
dual : Key \rightarrow Key \\
Trusted : User \rightarrow \rightarrowtail User \\
\hline
(Shared, Public, Secret)\ partition\ Key \\
Auth \cup Conf = Key \\
dual \circ dual = id\ Key \\
dual(|Conf|) = Conf \\
dual(|Auth|) = Auth \\
dual(|Shared|) = Shared \\
dual(|Public|) = Secret \\
dual(|Secret|) = Public
\end{array}
$$

The first ordinary schema defines the variable that records what keys are known by each user, and with whom they are associated.

Keys

$$keys : User \rightarrow \rightarrowtail (User \times Key)$$

A set of (*user, key*) pairs is associated to each user, where 'x maps to (y, k)' means that x knows key k and uses it in communications with user y. The following three schemas define the state space of the model by giving formal definitions of secure channels in terms of possession of keys.

Confidentiality channels

$$
\begin{array}{l}
Keys \\
ConfChannels : User \rightarrow User \\
\hline
\forall\, x, y : User \bullet (x, y) \in ConfChannels \Leftrightarrow \\
\{\exists k : Conf \setminus Secret;\ z : \\
\qquad User \bullet (y, k) \in keys(x) \wedge [z, dual(k)] \in keys\ (y)\}
\end{array}
$$

Confidentiality channels define relations between pairs of users. These are ordered pairs as the channel may be in only one direction. It will be noticed that the definition is not symmetrical with respect to x and y. The predicate states that, for a confidentiality channel to exist from x to y, there must be a key whose use includes confidentiality and is either shared or public; x must associate this key with y; y must know the dual of the key. In the model, this means that y must associate it with some user(s), but it is not of any concern to y exactly which users know the key. To see why this is reasonable, consider a public key system providing confidentiality to y. Any user z who knows the public key of y has a confidentiality channel to y, and it is important to z that it is only y who has the secret dual key; y must of course know the secret key, but it does

not matter to y who knows the public key. This corresponds to the viewpoint that confidentiality is a service provided to the sender of information.

Authentication channels

$$Keys$$

$$AuthChannels : User \rightarrow User$$

$$\forall x, y : User \bullet (x, y) \in AuthChannels \Leftrightarrow$$

$$\{\exists k : Auth \setminus Public; z : User \bullet$$

$$(z, k) \in keys(x) \land [x, dual(k)] \in keys(y)\}$$

Authentication channels also define relations between pairs of users. The definition of authentication channels is dual to the definition of confidentiality channels and corresponds to the viewpoint that authentication is a service provided to the receiver of information.

Symmetric channels

$$Keys$$

$$SymmChannels : \mathbb{P}\{\mathbb{P}(User)\}$$

$$SymmChannels \subseteq \{x, y : User | x \neq y \bullet \{x, y\}\}$$

$$\forall x, y : User \bullet (x, y) \in SymmChannels \Leftrightarrow$$

$$\{(\exists k : Shared \bullet (y, k) \in keys(x) \land [x, dual(k)] \in keys(y)\}$$

Symmetric channels are in both directions and so are defined as sets of two different users. They correspond to the situation where neither key is public, and in practice the key and its dual are usually equal.

State

$$ConfidentialityChannels$$

$$AuthenticationChannels$$

$$SymmetricChannels$$

The system state is defined exactly by what keys are known by each user, thereby defining what secure channels exist.

Transfer

$$\Delta State$$

$$orig?, dest?, recip?, sender? : User$$

$$k? : Key$$

$$(orig?, k?) \in keys\ (sender?)$$

$$keys' = keys \oplus \{recip? \rightarrow keys(recip?) \cup (orig?, k?)\}$$

This schema says that if a key $k?$ is sent from one user to another, then the keys known to the recipient are updated to associate the key sent with the originator. In this model, the only state changes are those which happen as a result of passing keys from one user to another. Such a key exchange may or may not result in new channels being formed. The key passes from the sender to the recipient. It may be that the users between whom communication is intended (originator and destination) are different from the sender and recipient involved in a particular exchange. This is the situation if the sender is a key server. The recipient will therefore associate the received key with the originator, who may or may not be the sender.

SecureTransfer

Transfer

$k? \in Secret \Rightarrow (sender?, recip?) \in ConfChannels$

$k? \in Public \Rightarrow (sender?, recip?) \in AuthChannels$

$k? \in Shared \Rightarrow (sender?, recip?) \in ConfChannels \cap AuthChannels$

$orig? \neq sender? \wedge k? \in Public \cup Shared \Rightarrow$
$\quad sender? \in Trusted(recip?)$

$recip? \neq dest? \wedge k? \in Secret \cup Shared \Rightarrow$
$\quad recip? \in Trusted(sender?)$

This schema specifies the conditions which must exist if a key exchange should be performed securely: (1) secret keys may only be transferred over a confidentiality channel; (2) public keys must be transferred over authentication channels; (3) if the key is to be shared, the channel should provide both confidentiality and authentication since both users need to associate the key only with each other; (4) if the key is public or shared then the recipient must trust the sender, unless the sender is the originator; this is because the key must be correctly assigned to the originator; and (5) if the key is secret or shared, then the sender must trust the recipient not to reveal it, unless the recipient is the destination. More details on formal protocol presentation can be found in References [21–32].

15.3 KEY MANAGEMENT

Information protection mechanisms, discussed so far in this chapter, assume cryptographic keys to be distributed to the communicating parties prior to secure communications. The secure management of these keys is one of the most critical elements when integrating cryptographic functions into a system, since even the most elaborate security concept will be ineffective if the key management is weak.

An automatic distribution of keys typically employs different types of messages. A transaction usually is initiated by requesting a key from some central facility (e.g. a key distribution center, KDC), or from the entity a key is to be exchanged with. Cryptographic service messages (CSMs) are exchanged between communicating parties for the transmission of keying material, or for authentication purposes. CSMs may contain keys, or other keying material, such as the distinguished names of entities, key-IDs, counters or random values. CSMs have to be protected depending on their contents and on the security requirements. Generic requirements include the following:

(1) *Data confidentiality* should be provided while secret keys and possibly other data are being transmitted or stored.

(2) *Modification detection* prevents the active threat of unauthorized modification of data items. In most environments, all cryptographic service messages have to be protected against modification.

(3) *Replay detection* is to counter unauthorized duplication of data items.

(4) *Timeliness* requires that the response to a challenge message is prompt and does not allow for playback of some authentic response message by an impersonator.

(5) *Entity authentication* is to corroborate that an entity is the one claimed.

(6) *Data origin authentication* (*proof/nonrepudiation of origin*) is to make certain that the source of a message is the one claimed.

(7) *Proof/nonrepudiation of reception* shows the sender of a message that the message has been received by its legitimate receiver correctly.

(8) *Notarization* is the registration of messages to attest at a later stage its content, origin, destination or time of issue.

The correctness of key management protocols requires more than the existence of secure communication channels between entities and key management servers. For example, it critically depends on the capability of those servers to reliably follow the protocols. Therefore, each entity has to base its deductions not only on the protocol elements sent and received, but also on its trust in the server which, for that reason, often is called the *trusted party.*

Key management is facilitated by the key management services, which include entity registration, key generation, certification, authentication, key distribution and key maintenance.

Entity registration is a procedure by which an individual or a device is authenticated to the system. An absolute identification is provided if a link between an ID (e.g. a distinguished name or a device-ID) and some physical representation of the identified subject (e.g. a person or a device) can be established. An identification can be carried out manually or automatically. Absolute identification always requires at least one initial manual identification (e.g. by showing a passport or a device-ID).

Mutual authentication is usually based on the exchange of certificates. In any system, an entity is represented by some public data, called its (public) credentials (e.g. ID and address). Besides that, an entity may own secret credentials (e.g. testimonials) that may or may not be known by some trusted party. Whenever an entity is registered, a certificate based upon its credentials is issued as a proof of registration. This may involve various procedures, from a protected entry in a specific file to a signature by the certification authority on the credentials.

Key generation refers to procedures by which keys or pairs of keys of good cryptographic quality are securely and unpredictably generated. This implies the use of a random or pseudorandom process involving random seeds, which cannot be manipulated. The requirements are that certain elements of the key space are not more probable than others, and that it is not possible for the unauthorized to gain knowledge about keys.

Certificates are issued for authentication purposes. A credential containing identifying data together with other information (e.g. public keys) is rendered unforgeable by some certifying information (e.g. a digital signature provided by the key certification center). Certification may be an on-line service where some certification authority provides interactive support and is actively involved in key distribution processes, or it may be an off-line service so that certificates are issued to each entity only at some initial stage.

Authentication/Verification may be either (1) entity authentication or identification, (2) message content authentication and (3) message origin authentication. The term verification refers to the process of checking the appropriate claims, i.e. the correct identity of an entity, the unaltered message content or the correct source of a message. The validity of a certificate can be verified

using some public information (e.g. a public key of the key certification center), and can be carried out without the assistance of the certification authority, so that the trusted party is only needed for issuing the certificates.

Key distribution refers to procedures by which keys are securely provided to parties legitimately asking for them. The fundamental problem of key exchange or distribution is to establish keying material to be used in symmetric mechanisms whose origin, integrity and confidentiality can be guaranteed. As a result of varied design decisions appropriate to different circumstances, a large variety of key distribution protocols exist [37, 39]. The basic elements of a key distribution protocol are as follows.

15.3.1 Encipherment

The confidentiality of a data item D can be ensured by enciphering D with an appropriate key K which is denoted $eK(D)$. Depending on whether a secret key algorithm or a public key algorithm is used for the enciphering process, D will be enciphered with a secret key K shared between the sender and the legitimate recipient of the message, or with the legitimate recipient B's public key K_{Bp}. Encipherment with the sender A's private key K_{As}, may be used to authenticate the origin of data item D, or to identify A. Encipherment with a secret key provides modification detection if B has some means to check the validity of D (e.g. if B knows D beforehand, or if D contains suitable redundancy).

15.3.2 Modification detection codes

To detect the modification of a data item D, one can add some redundancy that has to be calculated using a collision-free function, i.e. it must be infeasible to find two different values of D that render the same result. Moreover, this process has to involve a secret parameter K in order to prevent forgery. Appropriate combination of K and D also allows for data origin authentication. Examples of suitable building blocks are message authentication codes, or hash functions combined with encipherment. The generic form of this building block is $D||mdcK(D)$. Modification detection codes (*mdc*) enable the legitimate recipient to detect unauthorized modification of the transmitted data immediately after receipt. The correctness of distributed keying material can also be checked if the sender confirms his knowledge of the key in a second step (see below).

15.3.3 Replay detection codes

To detect the replay of a message and to check its timeliness, some explicit or implicit challenge-and-response mechanism has to be used, since the recipient has to be able to decide on the acceptance. In most applications, the inclusion of a replay detection code denoted by $D||rdc$ (e.g. a timestamp TD, a counter CT, or a random number R) will only make sense if it is protected by modification detection. With symmetric cryptographic mechanisms, key modification, i.e. some combination (e.g. XOR) of the secret key with an *rdc*, can be used to detect the replay of a message. A special case is the process of key offsetting used to protect keying material enciphered for distribution where the key used for encipherment is XORed with a count value.

15.3.4 Proof of knowledge of a key

Authentication can be implemented by showing knowledge of a secret (e.g. a secret key). Nevertheless, a building block that proves the knowledge of a key K can also be useful, when K is public. There are several ways for A to prove to B the knowledge of a key that are all based on the principle of challenge and response in order to prevent a replay attack. Depending on the challenge

which may be a data item in cleartext or in ciphertext, A has to process the key K and the *rdc* in an appropriate way (e.g. by encipherment, or by calculating a message authentication code), or A has to perform a deciphering operation. The challenge may explicitly be provided by B (e.g. a random number R) or implicitly be given by a synchronized parameter (e.g. a timestamp TD or a counter CT). For some building blocks, the latter case requires only one pass to prove knowledge of K; its tradeoff is the necessary synchronization. If B provides a challenge enciphered with a key K^*, the enciphered data item has to be unpredictable (e.g. a random number R, or a key K^{**}). The generic form of this building block is *authK*(*A to B*).

15.3.5 Point-to-point key distribution

This is the basic mechanism of every key distribution scheme. If based on symmetric cryptographic techniques, point-to-point key distribution requires that the two parties involved already share a key that can be used to protect the keying material to be distributed. If based on asymmetric techniques, point-to-point key distribution requires that each of the two parties has a public key with its associated secret key, and the certificate of the public key produced by a certification authority known to the other party. General assumptions are: (1) the initiator A is able to generate or otherwise acquire a secret key K^*; (2) security requirements are confidentiality of K^*, modification and replay detection, mutual authentication of A and B, and a proof of delivery for K^*. For point-to-point key distribution protocols based on symmetric cryptographic techniques we additionally assume: (3) a key K_{AB} is already shared by A and B. In generic form, a point-to-point key distribution protocol meeting those requirements can be described as shown in Table 15.2 [33].

Table 15.3 is an example of a specific point-to-point key distribution protocol [33] (N denotes a nonrepeating number, R a random number).

For a point-to-point key distribution protocol based on public key techniques, we make the following supplementary assumptions: (4) there is no shared key known to A and B before the key exchange process starts; (5) there is a trusted third party C, where A can receive a certificate that contains the distinguished names of A and C, A',s public key K_{Ap}, and the certificate's expiration date TE. The integrity of the certificate is protected by C's signature. As an example, A's certificate can look like $ID_C || ID_A || K_{Ap} || TE || eK_{Cs}[h(ID_C || ID_A || K_{Ap} || TE)]$.

The exchange of certificates can be performed off-line and is not shown in the following protocol. In this protocol, A sends a message (often referred to as *token*) to B that consists of a secret key K^* enciphered with B's public key and an appended *rdc*. The integrity of the token is protected by A's signature. This guarantees modification and replay detection, as well as data origin

Table 15.2 Generic point-to-point key distribution

A		B
(1) $\rightarrow$	$eK_{AB}(K^*\|\|rdc)$	
(2) $\rightarrow$	$authK^*(A\ to\ B)$	
	$authK^*(B\ to\ A)$	$\leftarrow$ (3)

Table 15.3 Point-to-point key distribution

A	(ISO/IEC CD 9798-2)	B
(1) $\rightarrow$	$eK_{AB}(K^*\|\|N)$	
	$eK^*(N\|\|R)$	$\leftarrow$ (2)
(3) $\rightarrow$	R	

Table 15.4 Point-to-point key distribution

A	(ISO/IEC CD 9798-2)	B
(1) $\rightarrow$	$eK_{Bp}(K^*)\|\| rdc\|\| eK_{As}(h(eK_{Bp}(K^*)\|\| rdc))$	
	$eK^*(rdc)$	$\leftarrow$ (2)

authentication. B responds with the enciphered *rdc*, thereby acknowledging that it has received the key K^*, as shown in Table 15.4.

Key maintenance includes procedures for key activation, key storage, key replacement, key translation, key recovery, black listing of compromised keys, key deactivation and key deletion. Some of the issues of key maintenance are addressed below.

Storage of keying material refers to a key storage facility which provides secure storage of keys for future use, e.g. confidentiality and integrity for secret keying material, or integrity for public keys. Secret keying material must be protected by physical security (e.g. by storing it within a cryptographic device) or enciphered by keys that have physical security. For all keying material, unauthorized modification must be detectable by suitable authentication mechanisms.

Key archival refers to procedures by which keys for notarization or nonrepudiation services can be securely archived. Archived keys may need to be retrieved at a much later date to prove or disprove certain claims.

Key replacement enables parties to securely update their keying material. A key shall be replaced when its compromise is known or suspected. A key shall also be replaced within the time deemed feasible to determine it by an exhaustive attack. A replaced key shall not be reused. The replacement key shall not be a variant or any nonsecret transformation of the original key.

Key recovery refers to cryptographic keys which may become lost due to human error, software bugs or hardware malfunction. In communication security, a simple handshake at session initiation can ensure that both entities are using the same key. Also, message authentication techniques can be used for testing that plaintext has been recovered using the proper key. Key authentication techniques permit keys to be validated prior to their use. In the case where a key was lost, it still may be possible to recover that key by searching part of the key space. This approach may be successful, if the number of likely candidates is small enough.

Key deletion refers to procedures by which parties are assured of the secure destruction of keys that are no longer needed. Destroying a key means eliminating all records of this key, such that no information remaining after the deletion provides any feasibly usable information about the destroyed key.

More information on key management can be found in References [33–39].

15.4 SECURITY MANAGEMENT IN GSM NETWORKS

The *authentication* generic process is shown in Figure 15.9 [41,42]. The authentication algorithm (called A3 in the GSM specifications) computes from a random number RAND, both at the MS (mobile station) and at the AuC, a signed response (SRES), using an individual secret key K_i attached to the mobile subscriber. The number RAND, whose value is drawn randomly between 0 and $2^{128} - 1$, is used to generate the response by the mobile as well as by the fixed part of the network. The authentication process is carried out both at the mobile and at the MSC simultaneously. The BSS remains transparent to this process. The mobile only receives the random number over the radio path and in turn returns the signed response to the network. Thus, an air interface mobile designation is not disclosed. At subscription time, the subscriber authentication key K_i is allocated to the subscriber together with its IMSI (international mobile station identity). The

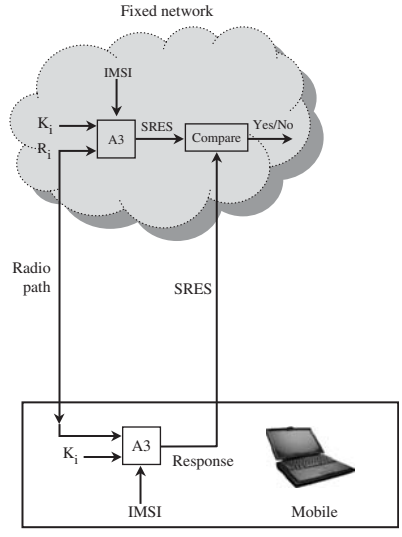

Figure 15.9 Generic authentication process.

key K_i is stored in the AuC and used to generate a triplet (K_c, signed response, RAND) within the GSM system. As stated above, the same K_i is also stored at the mobile in the subscriber ID (SIM). In the AuC, the following steps are carried out in order to produce one triplet. A nonpredictable RAND is produced. RAND and K_i are used to calculate the signed response and the ciphering key (K_c) using two different algorithms (A3, A8). This triplet (RAND, signed response, and K_c) is generated for each and every user and is then delivered to the HLR. This procedure is shown in Figure 15.10 [41–43].

The AuC begins the authentication and cipher key generation procedures after receiving an identification of the subscriber from the MSC/VLR. The AuC first queries the HLR for the subscriber's authentication key K_i. It then generates a 128 b RAND for use as a challenge (nonce), to be sent to the MS for verification of the MS's authenticity. RAND is also used by the AuC, with K_i in the algorithm A3 for authentication, to calculate the expected correct signed response from the MS. RAND and K_i are also used in the AuC to calculate the cipher key K_c with algorithm A8. The signed response is a 32 b number, and K_c is a 64 b number.

The values of RAND, signed response and K_c are transmitted to the MSC/VLR for interaction with the MS. Algorithms A3 and A8 are not fully standardized by GSM and may be specified at the direction of PLMN operators. Different PLMNs may use different and proprietary versions of these algorithms. Also, to protect the secrecy of the user, the authentication key K_i is not sent to the MSC/VLR. Based on the discretion of the PLMN operator, K_i can be of any format and length. The MSC/VLR forwards the value of the RAND to the MS, which also has the correct K_i and algorithm A3, which is stored in its SIM. The SIM then uses RAND and K_c in these algorithms to calculate the authentication SRESc and the cipher key, K_c. The MS sends the calculated response, SRESc, back to the MSC/VLR, which compares it with the value signed response received from the HLR/AuC. If the SRESc and the signed response agree, the subscriber access to the system is granted, and the cipher key K_c is transferred to the BTS for use in encrypting and decrypting messages to and from the MS. If the SRESc (computed signed response at the mobile) and the signed response disagree, the subscriber access to the system is denied. In summary, the VLR initiates authentication toward the MS and checks the authentication result. The complete process is shown in Figure 15.11.

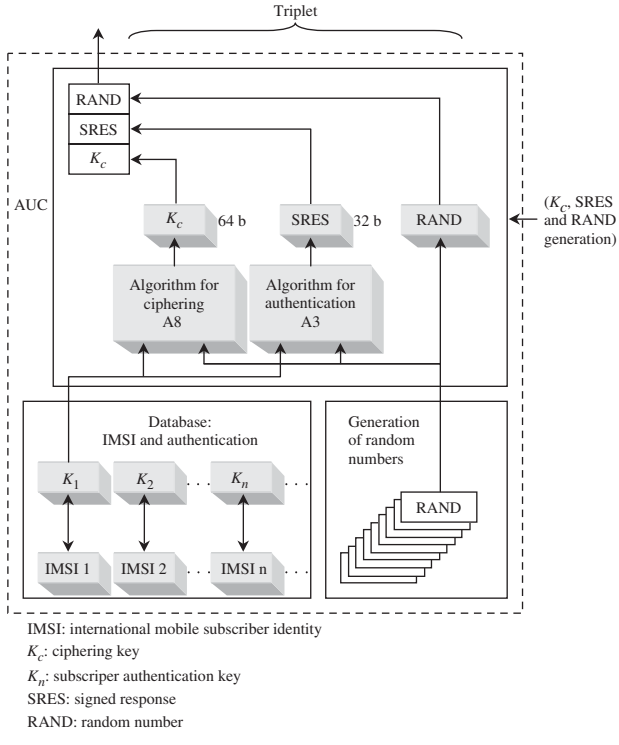

Figure 15.10 Generation of K_c, signed response, and RAND at the AuC.

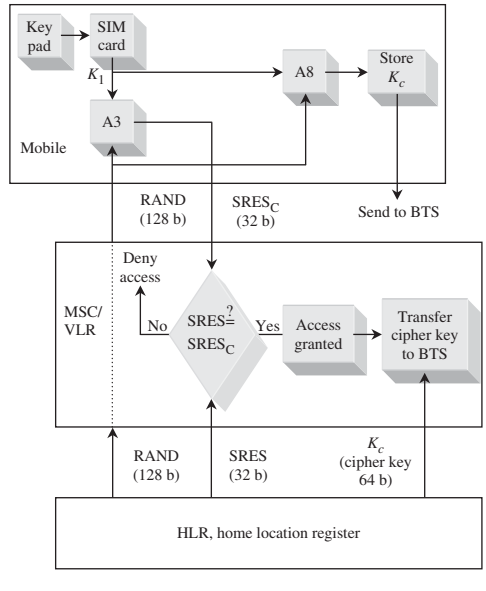

Figure 15.11 Authentication process in GSM system.

The *ciphering/deciphering* algorithm (called A5) uses a cipher key K_c, which is allocated to each mobile subscriber during the authentication procedures. The key K_c is computed from the RAND by an algorithm (called A8) driven by the mobile subscriber authentication key K_i. Algorithm A8 is common to all GSMs. Figure 15.10 has shown the process of generating K_c. For the authentication procedure, when a signed response is being calculated at the mobile, the ciphering key (K_c) is also calculated using another algorithm (A8), as shown in Figure 15.11. This key is set in the fixed system and in the MS. At the ciphering start command (from VLR to BSS), K_c is used by the MS and the BTS in order to cipher and decipher the bitstream that is sent over the radio path. In addition to the authentication procedures, a key setting may be initiated by the network as often as the network operator wishes. The command to use the encryption key is sent over the logical channel and dedicated control channel, as soon as the identity of the mobile subscriber is known by the network.

The key K_c must be agreed upon by the mobile station and the network prior to the start of encryption. The choice in GSM is to compute the key K_c independently from the effective start of encryption during the authentication process. K_c is then stored in a nonvolatile memory inside the SIM so as to be remembered even after a switched-off phase. This key is also stored in the visited MSC/VLR on the network side and is ready to be used for the start of encryption. The actual encryption/decryption of user data takes place within the mobile station and the BSS. For this purpose, the encryption key is downloaded from the MSC to the BTS via the BSC. After authentication, the transmission is ciphered, and K_c is used for ciphering/deciphering. This process is shown in Figure 15.12. Data flow on the radio path is obtained by a bit-per-bit binary addition of the user data flow and ciphering bitstream generated by the GSM algorithm A5 using a ciphering key (K_c). This exact process of encryption/decryption at the mobile and at BTS is shown in Figure 15.13. Code words S_1 and S_2 for downlinks and uplinks are changed at every frame. When modulo 2 is added with plain text, S_1 outputs cipher text. On the other side, the cipher text, when modulo 2 is added with S_1, outputs the plain text. The ciphering/deciphering function is placed on the transmission chain between the interleaver and the modulator. Since A3 and A8 are always running together, these two are implemented as a single algorithm in most cases. The algorithm A3 is standardized in the whole of GSM.

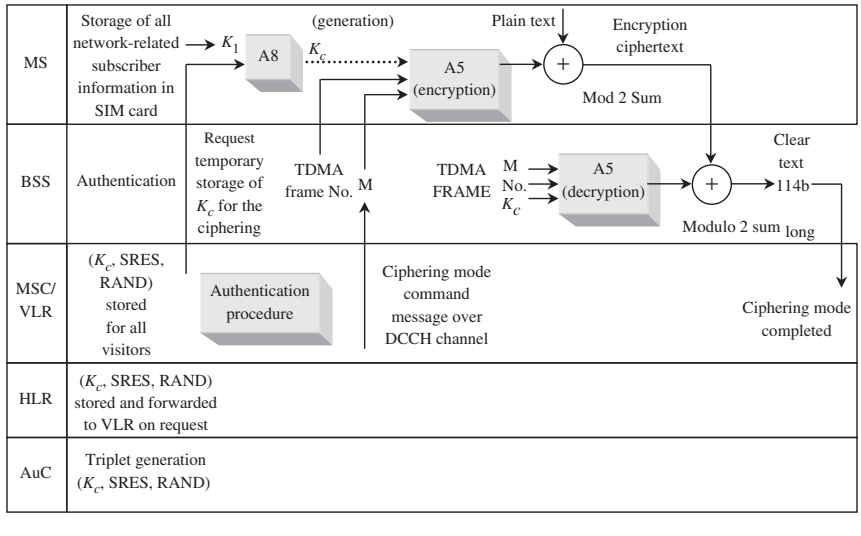

Figure 15.12 Sequential steps for encryption and decryption process.

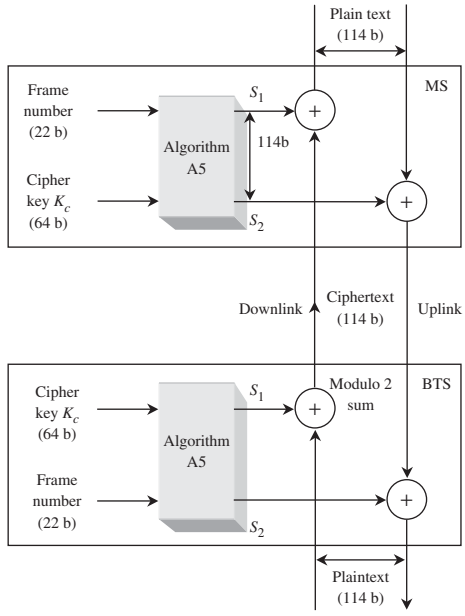

Figure 15.13 Encryption/decryption process.

15.5 SECURITY MANAGEMENT IN UMTS

Cryptographic functions used in UMTS are specified below:

Algorithm: Purpose/usage *O,S (operator specific, fully standardized)/location in the network*
f0 : *random challenge generating function*
O /AuC
f1 : *network authentication function*
O – (MILENAGE) /USIM and AuC
*f1** : *resynchronization message authentication function*
O – (MILENAGE) /USIM and AuC
f2 : *user challenge-response authentication function*
O – (MILENAGE) /USIM and AuC
f3 : *cipher key derivation function*
O – (MILENAGE) /USIM and AuC
f4 : *integrity key derivation function*

O – (MILENAGE) /USIM and AuC

f5 : *anonymity key derivation function for normal operation*

O – (MILENAGE) /USIM and AuC

*f5** : *anonymity key derivation function for resynchronization*

O – (MILENAGE) /USIM and AuC

f6 : *MAP encryption algorithm*

S/MAP nodes

f7 : *MAP integrity algorithm*

S/MAP nodes

f8 : *UMTS encryption algorithm*

S – (KASUMI)/ MS and RNC

f9 : *UMTS integrity algorithm*

S – (KASUMI) / MS and RNC

More details on these functions can be found in References [46–60] especially [52, 53, 56, 57]. A simplified UMTS security architecture is shown in Figure 15.14.

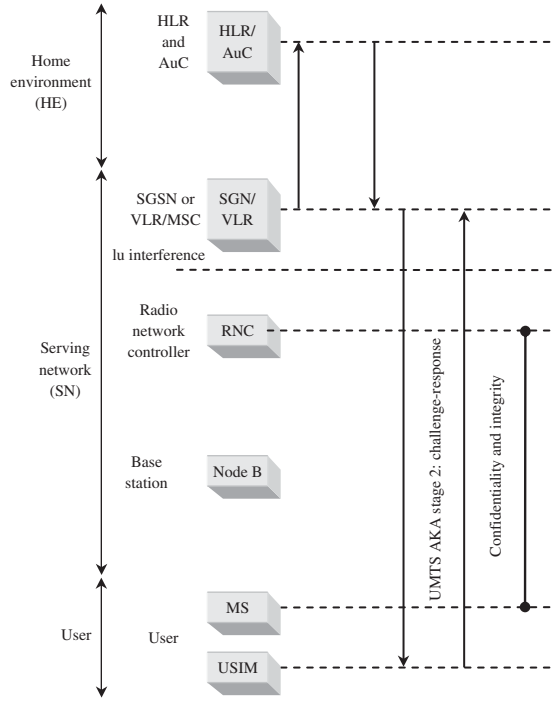

Figure 15.14 Simplified UMTS security architecture.

The security architecture is designed around a mutual authentication procedure that is executed between the user (USIM) and the SGSN/VLR3 at the network end. The procedure is called the UMTS Authentication and Key Agreement (AKA) since, in addition to providing authentication services, it also includes generation of session keys for confidentiality and integrity protection at the user end. The cryptographic algorithms/functions are defined in a requirements specification [49]. The AKA procedure is executed in two stages, as shown in Figure 15.14. The first stage involves transfer of security credentials (authentication vector, AV) from the home environment (HE) to the serving network (SN). The HE mainly consists of the home location register (HLR) and authentication center (AuC); the SN consists of the parts of the core network that are directly involved in setting up connections. With respect to access security, the SN network elements of interest are the SGSN, which handles packet-switched traffic, and the circuit-switched GSM nodes VLR/MSC (mobile switching center). An operator with a physical access infrastructure will normally have both HE and SN nodes.

The authentication vectors contain sensitive data like *challenge-response* authentication data and cryptographic keys. It is therefore clear that the transfer of authentication vectors between the HLR/AuC and the SGSN/VLR needs to be secured against eavesdropping and modification (i.e. both the transfer's confidentiality and integrity must be protected). The actual transfer mechanism for the AVs is the SS7-based mobile application part (MAP) protocol. The MAP protocol itself contains no security functionality, but a security extension to MAP called MAPsec [50] has been developed by the 3G Partnership Project (3GPP). The MAPsec protocol belongs to the Network Domain Security (NDS) work area in 3GPP. NDS covers both the MAPsec specification and specifications for how to protect IP connections on the control plane of the UMTS core network [51].

The second AKA stage is where the SGSN/ VLR executes the one-pass challenge-response procedure to achieve mutual entity authentication between the USIM and the network (SN, HE). A point to be made is that, in a two-staged AKA approach, the HE delegates responsibility for executing the security procedures to the SN. There must therefore be a trust relationship between the HE and the SN in this matter. In the GSM environment, this trust relationship is regulated through roaming agreements; the same model should be applicable to UMTS. The cryptographic functions ($f0 - f5^*$) used in the AKA procedure are implemented exclusively in the USIM and AuC. UMTS operators are free to choose any algorithm they want provided it complies with the function input/output specification given in Reference [49]. However, 3GPP has developed the MILENAGE [51, 52] algorithm set to provide the AKA functions. The formal status of MILENAGE is that it is provided as an example algorithm set, but in practice it is the recommended algorithm set for the AKA functions.

MILENAGE itself is built around the symmetric block cipher Rijndael. A consequence of having mutual authentication is that the USIM is now an active entity. In GSM, the user could not authenticate the network; hence, the UE could not reject the network. In UMTS, the USIM will attempt to authenticate the network and it is now possible that the USIM will reject the network. Details on the implementation of different security services in UMTS can be found in References [46–60].

15.6 SECURITY ARCHITECTURE FOR UMTS/WLAN INTERWORKING

As specified in Chapter 1, 4G will integrate different wireless systems and provide intertechnology roaming. Security architectures will depend on the type (tight or loose) of interworking. A tight UMTS/WLAN interworking solution would mandate the full 3GPP security architecture and require the 3GPP protocol stacks and interfaces to be present in the WLAN system [64]. The loose interworking options merely require the 3GPP authentication method to be implemented. To avoid link layer modifications, the authentication protocol is allowed to run at the link layer using Internet protocols – extensible authentication protocol (EAP) [63] and authentication, authorization and

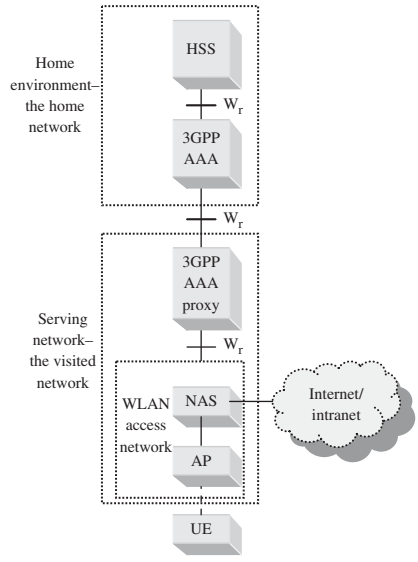

Figure 15.15 3GPP-WLAN architecture.

accounting (AAA) – as transport mechanisms. When used in WLAN the protocol EAP will be referred to as EAPOL. The main 3GPP-WLAN interworking architecture is defined in 3GPP TS 23.234 [61]; the security architecture is found in 3GPP TS 33.234 [62].

A benefit of the loose interworking approach is that the 3GPP-WLAN architecture is a fairly simple architecture. The architecture contains the WLAN access network and a UMTS core network in addition to glue technology to connect the two systems. Figure 15.15 gives an overview of the proposed architecture [64]. The two key glue components of the interworking solution are the AAA and EAP technologies. These are used to execute the UMTS AKA protocol from the 3G system's home domain toward the WLAN user equipment. The AAA architecture and the RADIUS and/or Diameter protocol are to be used as the bridge between the 3GPP system and the WLAN access network. Both Diameter and RADIUS are generic protocols and are intended to provide support for a diverse set of AAA applications, including network access, IP mobility and interoperator roaming. The EAP-AKA [67] protocol allows the UMTS AKA security protocol, which was originally designed for execution over UTRAN, to be executed over the WLAN access toward the user equipment. EAP [63] is a key element in the 3GPP-WLAN security architecture. EAP provides, in essence, a generic peer-to-peer based *request–response* transaction environment for authentication dialogs, and supports multiple authentication mechanisms. EAP typically runs directly over the link layer without requiring IP. EAP has its own flow control mechanisms, and is capable of removing duplicate messages and retransmitting lost messages. EAP can be used over different link layer protocols including the IEEE WLAN link layer. The necessary EAP encapsulation is described in the EAP-over-LAN specification [68].

The EAP protocol does not natively provide much in terms of authentication mechanisms. Instead, its power lies in its generic mechanism to support existing authentication methods through specialized EAP methods. EAP contains a negotiation sequence where the authenticator requests information about which authentication method to use. The EAP architecture does not require the authenticator to support all authentication methods. Instead, the authenticator can request assistance from a backend authentication server to complete the authentication processing. The specific authentication methods supported are defined in separate specifications detailing how the EAP

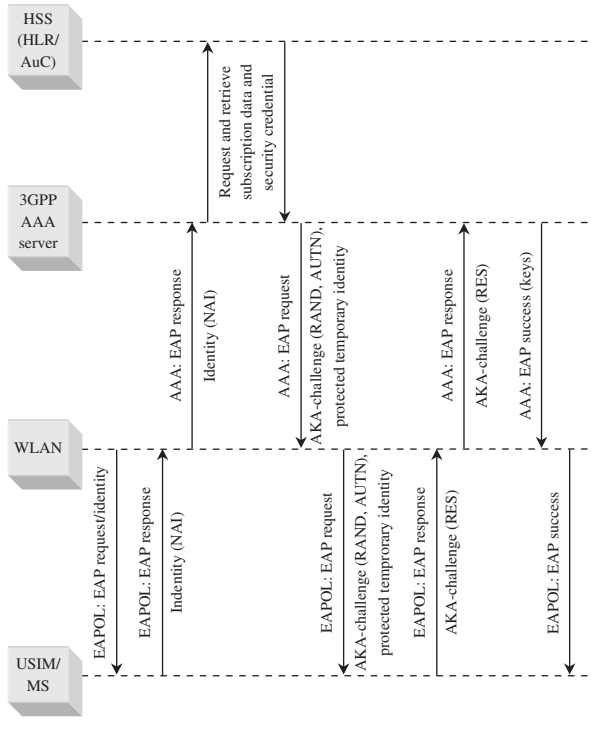

Figure 15.16 UMTS AKA procedure between a 3GPP network and an 802.11 WLAN MS.

framework is to be used to run the target authentication methods. For 3GPPWLAN interworking, primary interest is in the EAP-AKA [64, 67] methods. An execution of the EAP-AKA procedure specific to the IEEE 802.11 WLAN is illustrated in Figure 15.16.

15.7 SECURITY IN *AD HOC* NETWORKS

Traditional security mechanisms, such as authentication protocols, digital signature and encryption, still play important roles in achieving confidentiality, integrity, authentication and nonrepudiation of communication in *ad hoc* networks. However, these mechanisms are not sufficient by themselves.

In Zhou and Haas [69], two additional principles are discussed. First, the *redundancies* in the network topology (i.e. multiple routes between nodes) are exploited to achieve availability. The second principle is *distribution of trust.* Although no single node is trustworthy in an *ad hoc* network because of low physical security and availability, the trust can be distributed to an aggregation of nodes. Assuming that any $t + 1$ nodes will be unlikely to all be compromised, consensus of at least $t + 1$ nodes is trustworthy.

Although certain physical layer countermeasures, such as spread spectrum and coding, are possible [70, 79, 83, 84], we will only focus on how to defend against denial of service attacks towards routing protocols.

In most routing protocols, discussed in Chapter 13, routers exchange information on the topology of the network and this information could become a target for malicious adversaries who intend to bring the network down.

There are two sources of threats to routing protocols. The first comes from external attackers. By injecting erroneous routing information replaying old routing information or distorting routing information, an attacker could successfully partition a network or introduce excessive traffic load into the network by causing retransmission and inefficient routing. The second and also the more severe kind of threats comes from compromised nodes, which might advertise incorrect routing information to other nodes. Detection of such incorrect information is difficult. Merely requiring routing information to be signed by each node would not work, because compromised nodes are able to generate valid signatures using their private keys.

In the first case, nodes can protect routing information in the same way they protect data traffic, i.e. through the use of cryptographic schemes such as digital signature. However, this defense is ineffective against attacks from compromised servers. Worse yet, we cannot neglect the possibility of nodes being compromised in an *ad hoc* network. Detection of compromised nodes through routing information is also difficult in an *ad hoc* network because of its dynamically changing topology. When a piece of routing information is found to be invalid, the information could be generated by a compromised node, or, it could have become invalid as a result of topology changes. It is difficult to distinguish between the two cases.

On the other hand, certain properties of *ad hoc* networks can be exploited to achieve secure routing. For example, the routing protocols for *ad hoc* networks must handle outdated routing information to accommodate the dynamically changing topology. False routing information generated by compromised nodes could, to some extent, be considered outdated information. As long as there are sufficiently many correct nodes, the routing protocol should be able to find routes that go around these compromised nodes. Such capability of the routing protocols usually relies on the inherent redundancies due to multiple, possibly disjoint, routes between nodes in *ad hoc* networks. If routing protocols can discover multiple routes (e.g. protocols in ZRP, DSR, TORA and AODV, discussed in Chapter 13; all can achieve this), nodes can switch to an alternative route when the primary route appears to have failed.

Diversity coding, discussed in Chapter 7, takes advantage of multiple paths in an efficient way without message retransmission. The basic idea, discussed in Chapter 7, is to transmit redundant information through additional routes for error detection and correction. For example, if there are n disjoint routes between two nodes, then we can use $n - r$ channels to transmit data and use the other r channels to transmit redundant information. Even if certain routes are compromised, the receiver may still be able to validate messages and to recover messages from errors using the redundant information from the additional r channels.

Key management service using a single CA (*certification authority*) in *ad hoc* networks is problematic. The CA, responsible for the security of the entire network, is a vulnerable point of the network. If the CA is unavailable, nodes cannot obtain the current public keys of other nodes or to establish secure communication with others. If the CA is compromised and leaks its private key to an adversary, the adversary can then sign any erroneous certificate using this private key to impersonate any node or to revoke any certificate.

A standard approach to improve availability of a service is replication. However, a simple replication of the CA makes the service more vulnerable. Compromise of any single replica, which possesses the service private key, could lead to collapse of the entire system. To solve this problem, the trust can be distributed to a set of nodes with a collective key management responsibility [69].

In such a system, the service as a whole has a public/private key pair. All nodes in the system know the public key of the service and trust any certificates signed using the corresponding private key. Nodes, as clients, can submit *query* requests to get other clients' public keys or submit *update* requests to change their own public keys.

The key management service, with an $(n, t + 1)$ configuration ($n \geq 3t + 1$), consists of n special nodes, called *servers*, located within an *ad hoc* network. Each server also has its own key pair and stores the public keys of all the nodes in the network. In particular, each server knows the public

keys of other servers. Thus, servers can establish secure links among them. It is assumed that the adversary can compromise up to t servers in any period of time with a certain duration.

If a server is compromised, then the adversary has access to all the secret information stored on the server. A compromised server might be unavailable or exhibit Byzantine behavior (i.e. it can deviate arbitrarily from its protocols). It is also assumed that the adversary lacks the computational power to break the cryptographic schemes employed. The service is correct if *robustness* and *confidentiality* are preserved. Robustness assumes that the service is always able to process *query* and *update* requests from clients. Every *query* always returns the last updated public key associated with the requested client, assuming no concurrent *updates* on this entry. Confidentiality assumes that the private key of the service is never disclosed to an adversary so that an adversary is never able to issue certificates, signed by the service private key, for erroneous bindings.

Threshold cryptography is used to accomplish distribution of trust in the key management service [71, 72]. An $(n, t + 1)$ threshold cryptography scheme allows n parties to share the ability to perform a cryptographic operation (e.g. creating a digital signature), so that any $t + 1$ parties can perform this operation jointly, whereas it is infeasible for at most t parties to do so, even by collusion.

In this case, the n servers of the key management service share the ability to sign certificates. For the service to tolerate t compromised servers, an $(n, t + 1)$ threshold cryptography scheme is employed and the private key k of the service is divided into n shares $(s_1, s_2, \ldots, s_n)$, by assigning one share to each server. In this context $(s_1, s_2, \ldots, s_n)$ is referred to as an $(n, t + 1)$ *sharing* of k. The service is configured as illustrated in Figure 15.17.

For the service to sign a certificate, each server generates a partial signature for the certificate using its private key share and submits the partial signature to a combiner. With $t + 1$ correct partial signatures, the combiner is able to compute the signature for the certificate as illustrated in Figure 15.18, where servers generate a signature using a (3, 2) threshold signature scheme. The compromised servers (there are at most t of them) cannot generate correctly signed certificates by themselves, because they can generate at most t partial signatures.

If K/k is the public/private key pair of the service then by using a (3, 2) threshold cryptography scheme in Figure 15.18, each server i gets a share s_i of the private key k. For a message m, server i can generate a partial signature $PS(m, s_i)$ using its share s_i. Correct servers 1 and 3 both generate partial signatures and forward the signatures to a combiner c. Even though server 2 fails to submit a partial signature, c is able to generate the signature $(m)_k$ of m signed by service private key k [71, 72].

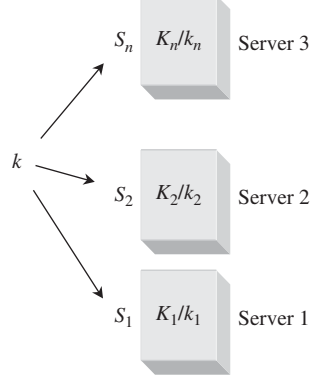

Figure 15.17 The configuration of a key management service.

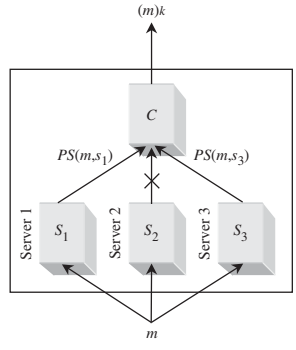

Figure 15.18 Threshold signature with three servers.

A compromised server could generate an incorrect partial signature, and use of this partial signature would yield an invalid signature. Fortunately, a combiner can verify the validity of a computed signature using the service public key. In case verification fails, the combiner tries another set of $t + 1$ partial signatures. This process continues until the combiner constructs the correct signature from $t + 1$ correct partial signatures. More efficient robust combining schemes are proposed [73, 74]. These schemes exploit the inherent redundancies in the partial signatures (note that any $t + 1$ correct partial signatures contain all the information of the final signature) and use error correction codes to mask incorrect partial signatures. In Gennaro *et al.* [73], a robust threshold DSS (digital signature standard) scheme is proposed. The process of computing a signature from partial signatures is essentially an interpolation. The authors uses the Berlekamp and Welch decoder, so that the interpolation still yields a correct signature despite a small portion (fewer than one-quarter) of partial signatures being missing or incorrect.

Even if the compromised servers are detected and excluded from the service, the adversary could still gather more than t shares of the private key from compromised servers over time. This would allow the adversary to generate any valid certificates signed by the private key.

Proactive schemes [75, 76] are proposed as a countermeasure to mobile adversaries. A proactive threshold cryptography scheme uses share refreshing, which enables servers to compute new shares from old ones in collaboration without disclosing the service private key to any server. The new shares constitute a new $(n, t + 1)$ sharing of the service private key. After refreshing, servers remove the old shares and use the new ones to generate partial signatures. Because the new shares are independent of the old ones, the adversary cannot combine old shares with new shares to recover the private key of the service. Thus, the adversary is challenged to compromise $t + 1$ servers between periodic refreshing.

Share refreshing must tolerate missing newly generated shares (called subshares) and erroneous subshares from compromised servers. A compromised server may not send any subshares. However, as long as correct servers agree on the set of subshares to use, they can generate new shares using only subshares generated from $t + 1$ servers. For servers to detect incorrect subshares, verifiable secret sharing schemes are used, for example, those in Pedersen [77]. A verifiable secret sharing scheme generates extra public information for each (sub)share using a one-way function. The public information can testify the correctness of the corresponding (sub)shares without disclosing the (sub)shares.

A variation of share refreshing also allows the key management service to change its configuration from $(n, t + 1)$ to $(n', t' + 1)$. This way, the key management service can adapt itself, on the fly, to changes in the network. If a compromised server is detected, the service should exclude the compromised server and refresh the exposed share. If a server is no longer available or if

a new server is added, the service should change its configuration accordingly. For example, a key management service may start with the (7, 3) configuration. If, after some time, one server is detected to be compromised and another server is no longer available, then the service could change its setting to the (5, 2) configuration. If two new servers are added later, the service could change its configuration back to (7, 3) with the new set of servers.

15.7.1 Self-organized key management

In this section we discuss a *self-organizing public-key management system* that allows users to create, store, distribute and revoke their public keys without the help of any trusted authority or fixed server [85]. In the system model, the public keys and the certificates of the system are represented as a directed graph $G(V, E)$, where V and E stand for the set of vertices and the set of edges, respectively. This graph will be referred to as the certificate graph. The vertices of the certificate graph represent public keys and the edges represent certificates. More precisely, there is a directed edge from vertex *Ku* to vertex *Kw* if there is a certficate signed with the private key of *u* that binds *Kw* to an identity. A certificate chain from a public key *Ku* to another public key *Kv* is represented by a directed path from vertex *Ku* to vertex *Kv* in *G*. Thus, the existence of a certificate chain from *Ku* to *Kv* means that vertex *Kv* is reachable from vertex *Ku* in *G* (denoted below $K_{u \to G} K_v$). In the following, the certificate graph *G* designates the graph comprising only the valid (not expired) certificates of the whole network. In the model, the updated and the nonupdated certificate repositories of user *u* are represented by the certificate graphs *Gu* and *Gnu*, respectively. Therefore, for any *u*, *Gu* is a subgraph of *G*, but *Gnu* is not necessarily a subgraph of *G*, as it may also contain some implicitly revoked certificates.

As shown in Figure 15.19, the initial phase of the scheme is executed in four steps: the creation of public/private key pairs, the issuing of certificates, the certificate exchange, and the creation of nodes' updated certificate repositories.

In step 0, *the user creates her own public/private key pair.*

In step 1, *she issues public-key certificates based on her knowledge about other users' public keys. The issuing of public-key certificates also continues when the system is fully operational (i.e. when the updated and nonupdated repositories are already constructed) as users get more information about other users' public keys. During this process, the certificate graph G is created. The speed of the creation of a usable (i.e. sufficiently connected) certificate graph heavily depends on the motivation of the users to issue certificates.*

In step 2, *the node performs the certificate exchange. During this step, the node collects certificates and thus creates its nonupdated certificate repository. Along with the creation of new certificates, the certificate exchange also continues even when the system is fully operational. This means that nodes' nonupdated repositories will be continuously upgraded with new certificates. The nodes' mobility determines the speed at which certificates are accumulated by the nodes themselves.*

In step 3, *the node constructs its updated certificate repository. The node can perform this operation in two ways, either by communicating with its certificate graph neighbors (**Step 3a**), or by applying the repository construction algorithm on the nonupdated certificate repository (**Step 3b**). When the node constructed its updated certificate repository, it is ready to perform authentication.*

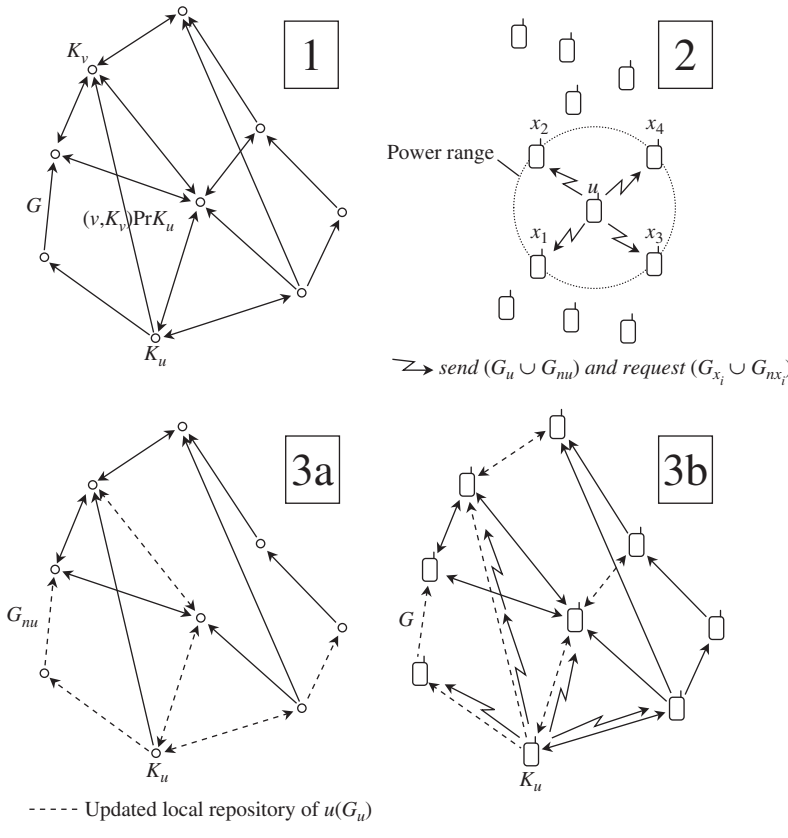

Figure 15.19 The creation of nodes' updated and nonupdated repositories (where $G_u^N = G_{nu}$).

The *authentication* is performed in such a way that, when a user u wants to verify the authenticity of the public key Kv of another user v, u tries to find a directed path from Ku to Kv in $Gu \cup Gv$. The certificates on this path are then used by u to authenticate Kv. An example of a certificate graph with updated local repositories of the users is shown in Figure 15.20. If there is no path from Ku to Kv in $Gu \cup G$v, u tries to find a path from Ku to Kv in $Gu \cup Gn$v. If such a path is found, u updates the expired certificates, checks their correctness and performs authentication. If there is no path from Ku to Kv in $Gu \cup Gn$v, u fails to authenticate Kv. A detailed description of each operation can be found in Capkun *et al.* [85].

15.8 SECURITY IN SENSOR NETWORKS

Owing to its inherent simplicity, sensor network routing protocols are sometimes even more susceptible to attacks against general *ad-hoc* routing protocols. Most network layer attacks against sensor networks fall into one of the following categories: *spoofed, altered or replayed routing information, selective forwarding, sinkhole attacks, sybil attacks, wormholes, HELLO flood attacks or acknowledgement spoofing. Spoofing, altering or replaying* routing information may be used by adversaries to create routing loops, attract or repel network traffic, extend or shorten source routes, generate false error messages, partition the network, increase end-to-end latency, etc.

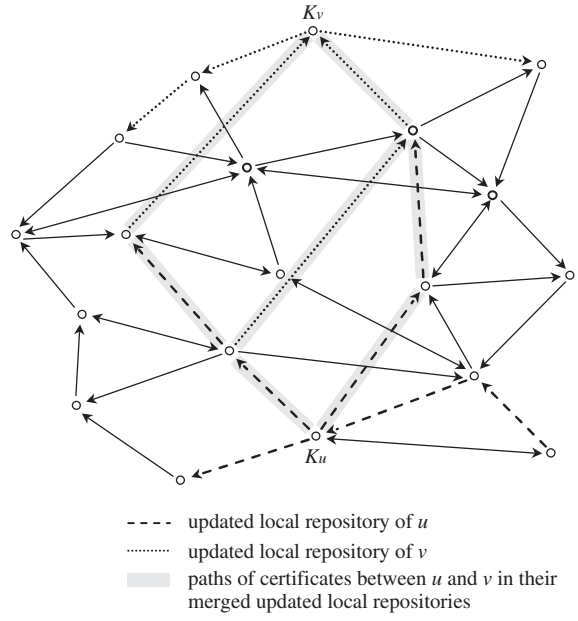

Figure 15.20 A certificate graph and paths of certificates between users u and v in their merged updated local repositories.

Selective forwarding attack refers to the case where malicious nodes refuse to forward certain messages and simply drop them, ensuring that they are not propagated any further. Selective forwarding attacks are typically most effective when the attacker is explicitly included on the path of a data flow. In the next two sections, we discuss sinkhole attacks and the Sybil attack, two mechanisms by which an adversary can efficiently include herself on the path of the targeted data flow.

Sinkhole attacks typically work by making a compromised node look especially attractive to surrounding nodes with respect to the routing algorithm. For instance, an adversary could spoof or replay an advertisement for an extremely high quality route to a base station.

One motivation for mounting a sinkhole attack is that it makes selective forwarding trivial. By ensuring that all traffic in the targeted area flows through a compromised node, an adversary can selectively suppress or modify packets originating from any node in the area.

Sybil attack refers to the case where a single node presents multiple identities to other nodes in the network. Sybil attacks pose a significant threat to geographic routing protocols. Location-aware routing often requires nodes to exchange coordinate information with their neighbors to efficiently route geographically addressed packets. It is only reasonable to expect a node to accept but a single set of coordinates from each of its neighbors, but by using the Sybil attack an adversary can 'be in more than one place at once'.

The *wormhole attack* refers to the case where an adversary tunnels messages received in one part of the network over a low latency link and replays them in a different part. Wormhole attacks most commonly involve two distant malicious nodes colluding to understate their distance from each other by relaying packets along an out-of-bounds channel available only to the attacker. An adversary situated close to a base station may be able to completely disrupt routing by creating a well-placed wormhole. An adversary could convince nodes who would normally be multiple hops from a base station that they are only one or two hops away via the wormhole. This can create a sinkhole: since the adversary on the other side of the wormhole can artificially provide a

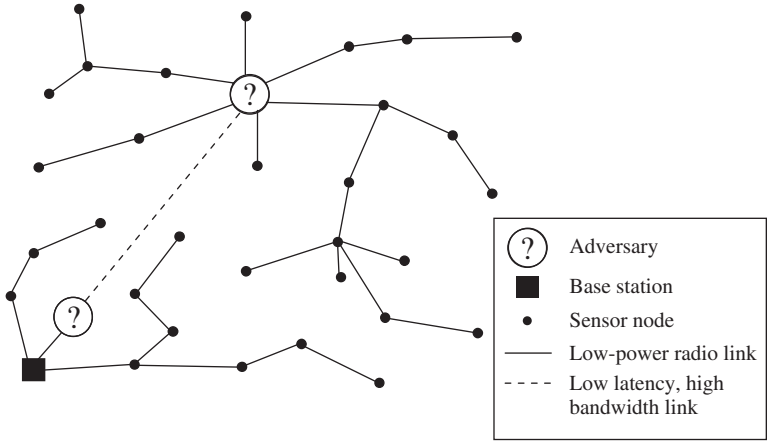

Figure 15.21 A laptop-class adversary using a wormhole to create a sinkhole in TinyOS beaconing.

high-quality route to the base station, potentially all traffic in the surrounding area will be drawn through it if alternate routes are significantly less attractive. This will most likely always be the case when the endpoint of the wormhole is relatively far from a base station. Figure 15.21 shows an example of a wormhole being used to create a sinkhole. Wormholes can also be used simply to convince two distant nodes that they are neighbors by relaying packets between the two of them. Wormhole attacks would probably be used in combination with selective forwarding or eavesdropping. Detection is potentially difficult when used in conjunction with the Sybil attack.

HELLO floods can be thought of as one-way, broadcast wormholes. Many protocols require nodes to broadcast HELLO packets to announce themselves to their neighbors, and a node receiving such a packet may assume that it is within (normal) radio range of the sender. This assumption may be false: a laptop-class attacker broadcasting routing or other information with large enough transmission power could convince every node in the network that the adversary is its neighbor.

An adversary does not necessarily need to be able to construct legitimate traffic in order to use the HELLO flood attack. It can simply re-broadcast overheard packets with enough power to be received by every node in the network.

Acknowledgement spoofing refers to the case where an adversary can spoof link layer acknowledgments for 'overheard' packets addressed to neighboring nodes. Goals include convincing the sender that a weak link is strong or that a dead or disabled node is alive. For example, a routing protocol may select the next hop in a path using link reliability. Artificially reinforcing a weak or dead link is a subtle way of manipulating such a scheme. Since packets sent along weak or dead links are lost, an adversary can effectively mount a selective forwarding attack using acknowledgement spoofing by encouraging the target node to transmit packets on those links.

Attacks on specific sensor networks routing protocol and possible countermeasures are discussed in References [86, 87].

REFERENCES

[1] *OSI Directory – Part 8: Authentication Framework.* ISO 9594-8. ISO: Geneva, 1988.

[2] J.J. Jueneman, S.M. Matyas and C.H. Meyer, Message authentication, *IEEE Commun. Mag.*, 1985, pp. 29–40.

[3] C.H. Meyer and S.M. Matyas, *Cryptography: a New Dimension in Computer Data Security*. Wiley: New York, 1982.
[4] R. Morris and K. Thompson, Password security: a case history, *CACM*, vol. 22, no. 11, 1979, pp. 594–597.
[5] R.M. Needham and M.D. Schroeder, Using encryption for authentication in large networks of computers, *CACM*, vol. 21, no. 12, 1978, pp. 993–998.
[6] D. Otway and O. Rees, Efficient and timely mutual authentication, *ACM OSR*, vol. 21, no. 1, 1987, pp. 8–10.
[7] R.L. Rivest, A. Shamir and L. Adlcman, A method for obtaining digital signatures and public-key crypto-systems, *CACM,* vol. 21, no. 2, 1978, pp. 120–126; *CACM*, vol. 26, no. 1, 1983, pp. 96–99.
[8] R. Rivest, The MD4 message digest algorithm, *Internet RFC,* vol. 1320, April 1992.
[9] R. Rivest, The MD5 message digest algorithm, *Internet RFS,* vol. 1321, April 1992.
[10] *Banking – key Management (Wholesale)*. ISO 8732. ISO: Geneva, 1988.
[11] R.K. Bauer, T.A. Berson and R.J. Freiertag, A key distribution protocol using event markers, *ACM TOCS,* vol. 1, no. 3, 1983, pp. 249–255.
[12] S.M. Bellovin and M. Merritt, Limitations of the Kerberos authentication system, *ACM CCR,* vol. 20, no. 5, 1990, pp. 119–132.
[13] R. Bird, I. Gopal, A. Herzberg, P.A. Janson, S. Kutten, R. Mowa and M. Yung, Systematic design of a family of attack-resistant authentication protocols, *IEEE J. Select. Area Commun.*, vol. 11. no. 5, 1993, pp. 679–692.
[14] R. Bird, I. Gopal, A. Herzberg, P.A. Janson, S. Kutten, R. Mowa and M. Yung, Systematic design of two-party authentication protocols, in *Proc. Crypto* 91, Santa Barbara, CA, Aug. 1991, pp. 44–61, available as *Advances in Cryptology, Lecture Notes in Computer Science* 576, J. Feigenbaum (ed.). Springer: New York, 1991.
[15] M. Burrows, M. Abadi and R.M. Needham, A logic of authentication, in *Proc. 12th ACM SOSP, ACM OSR,* vol. 23, no. 5, 1989, pp. 1–13.
[16] D.E. Denning and G.M. Sacco, Timestamps in key distribution systems, *CACM,* vol. 24, no. 8, 1981, pp. 533–536.
[17] L. Gong, Using one-way functions for authentication, *ACM CCR,* vol. 19, no. 5, 1989, pp. 8–11.
[18] C. I'Anson and C. Mitchell, Security defects in CCITT Recommendation X.509 – The Directory Authentication Framework, *ACM CR,* vol. 20, no. 2, 1990, pp. 30–34.
[19] *Entity Authentication Using Symmetric Techniques*. ISO-IEC JTC1.27.02.2 (20.03.1.2). ISO: Geneva, June 1990.
[20] *Data Encryption Standard*, FIPS 46, NBS, January 1977.
[21] C. Boyd, Security architectures using formal methods, *IEEE J. Select. Areas Commun.*, vol. 11, no. 5, June 1993, pp. 694–701.
[22] C.A. Boyd, Hidden assumptions in cryptographic protocols, *Proc. IEE, Part E*, vol. 137, 1990, pp. 433–436.
[23] M. Burrows, M. Abadi and R. Needham, A logic of authentication, *ACM Trans. Comput. Syst.,* vol. 8, no. 1, 1990, pp. 18–36.
[24] *CCITT, The Directory, Part 8: Authentication Framework, Recommendation X.509*. ISO: Geneva, 1989.
[25] D.W. Davies and W.L. Price, *Security in Computer Networks*. Wiley: New York, 1989.
[26] L. Gong, R. Needham and R. Yahalom, Reasoning about belief in cryptographic protocols, in *Proc. 1990 IEEE Computer Soc. Symp. Security Privacy*. IEEE Computer Society Press, 1990, pp. 234–248.
[27] *Information Processing Systems – Open Systems Interconnection Reference Model, Security Architecture*, ISO 7498-2. ISO: Geneva, 1988.

[28] R. Kailar and V.D. Gligor, On belief evolution in authentication protocols, in *Proc. Computer Security Foundations Workshop IV*. IEEE Press: New York, 1991, pp. 103–116.
[29] C. Meadows, A system for the specification and analysis of key management protocols, in *Proc. 1991 IEEE Computer Soc. Symp. Security Privacy*. IEEE Computer Society Press: New York, 1991, pp. 182–195.
[30] R.M. Needham and M.D. Schroeder, Using encryption for authentication in large networks of computers, *Commun. ACM,* vol. 21, no. 12, 1978, pp. 993–999.
[31] R. Rivest, A Shamir and L. Adelman, A method for obtaining digital signatures and public key cryptosystems, *Commun. ACM,* vol. 21, no. 2, 1978, pp. 120–126.
[32] J.M. Spivey, *The Z Notation*. Prentice-Hall: Englewood Cliffs, NJ, 1989.
[33] W. Fumy and P. Landrock, Principles of key management, *IEEE J. Select. Areas Commun.*, vol. 11, no. 5, 1993, pp. 785–793.
[34] D.M. Balenson, Automated distribution of cryptographic keys using the financial institution key management standard. *IEEE Commun. Mag.,* July 1985, pp. 41–46.
[35] W. Diffie and M.E. Hellman, New directions in cryptography, *IEEE Trans. Inform. Theory,* vol. 22, 1976, pp. 644–654.
[36] S.M. Matyas, Key handling with control vectors, *IBM Syst. J.,* vol. 30, no. 2, 1991, pp. 151–174.
[37] R.M. Needham and M.D. Schroeder, Using encryption for authentication in large networks of computers, *Commun. ACM,* vol. 21, 1978, pp. 993–999.
[38] E. Okamoto, Proposal for identity-based key distribution systems, *Electron. Lett.,* vol. 22, 1986, pp. 1283–1284.
[39] D. Otway and O. Rees, Efficient and timely mutual authentication. *Opns. Syst. Rev.*, vol. 21, 1987, pp. 8–10.
[40] A. Mehrotra and L.S. Golding, Mobility and security management in the GSM system and some proposed future improvements, *Proc. IEEE*, vol. 86, no. 7, 1998, pp. 1480–1486.
[41] A. Mehrotra, *GSM System Engineering*. Artech House: Norwood, MA, 1997.
[42] A. Mehrotra, *Cellular Radio Analog and Digital Systems*. Artech House: Norwood, MA, 1994, section 7.5.2.4, pp. 305–309.
[43] S.M. Redl, M.K. Weber and M.W. Oliphant, Security parameter, in *An Introduction to GSM*. Artech House: Norwood, MA, 1995, section 3.8, pp. 44–48.
[44] European Telecommunication Standard Institute/Global System for Mobility, ETSI/GSM specification vol. 2.17, section 3, Jan. 1993.
[45] G. Koien, An Introduction to Access Security in UMTS, *IEEE Wireless Commun.*, February 2004, pp. 8–18.
[46] 3G TS 33.120, *3G Security; Security Principles and Objectives*.
[47] 3G TS 21.133, *3G Security; Security Threats and Requirements*.
[48] 3G TS 33.102, *3G Security; Security Architecture*.
[49] 3G TS 33.105, *3G Security; Cryptographic Algorithm Requirements*.
[50] 3G TS 33.200, *3G Security; Network Domain Security; MAP Application Layer Security*.
[51] 3G TS 33.210, *3G Security; Network Domain Security; IP Network Layer Security*.
[52] 3G TS 35.205, *3G Security; Specification of the MILENAGE Algorithm Set: An Example Algorithm Set for the 3GPP Authentication and Key Generation Functions f1, f1*, f2, f3, f4, f5, and f5*; Document 1: General*.
[53] 3G TS 35.206, *3G Security; Specification of the MILENAGE Algorithm Set: An Example Algorithm Set for the 3GPP Authentication and Key Generation Functions f1, f1*, f2, f3, f4, f5, and f5*; Document 2: Algorithm Specification*.
[54] *Information Technology – Security Techniques – Entity Authentication - Part 4: Mechanisms Using a Cryptographic Check Function*. ISO/IEC 9798-4. ISO: Geneva.
[55] National Institute of Standards and Technology. *FIPS-197, Advanced Encryption Standard (AES)* (FIPS PUB 197). NIST: Gaithersburg, MD, 26 November 2001.

[56] 3G TS 35.201, *3G Security; Specification of the 3GPP Confidentiality and Integrity Algorithms; Document 1: f8 and f9 Specification*.

[57] 3G TS 35.202, *3G Security; Specification of the 3GPP Confidentiality and Integrity Algorithms; Document 2: KASUMI specification*.

[58] 3GPP, *Document TSGS#14(01)0622, Work Item Description: Support for Subscriber Certificates, SA#14*, Tokyo, Japan, Dec. 2001.

[59] S. Murphy and M. J. B. Robshaw, Essential algebraic structure within the AES: in *Proc. Crypto2002, LNCS*, vol. 2442. Springer: Berlin, 2002, pp. 1–16.

[60] 3G TS 33.904, *3GPP, SAGE; Report on the Evaluation of 3GPP Standard Confidentiality and Integrity Algorithms (SAGE v. 2.0)*.

[61] 3G TS 23.234, *3GPP System to Wireless Local Area Network (WLAN) Interworking System Description, Release 6*, work in progress.

[62] 3G TS 33.234 v050, *3G Security; Wireless Local Area Network (WLAN) Interworking Security, Release 6*, work in progress.

[63] L. Blunk *et al*., Extensible Authentication Protocol (EAP), Internet draft, draft-ietf-eap-rfc2284bis-04.txt, June 2003, work in progress.

[64] G. Koien and T. Haslestad, Security Aspects of'3G-WLAN Interworking, *IEEE Commun. Mag*., November 2003, pp. 82–88.

[65] ETSI TR 101 957, *Broadband Radio Access Networks (BRAN); HIPERLAN Type 2; Requirements and Architectures for Interworking between HIPERLAN/2nd and 3rd Generation Cellular Systems*.

[66] IEEE Std 802.11i/D4.0, *Draft Amendment to Standard for Telecommunications and Information Exchange Between Systems – LAN/MAN Specific Requirements – Part 11: Wireless Medium Access Control (MAC) and Physical Layer (PHY) specifications: Medium Access Control (MAC) Security Enhancements*, May 2003, work in progress.

[67] J. Arkko and H. Haverinen, EAP AKA Authentication, Internet Draft: draft-arkko-pppext-eap-aka-10.txt, June 2003, work in progress.

[68] IEEE Std 802.1X-2001, *IEEE Standard for Local and Metropolitan Area Networks – Port-Based Network Access Control*, July 2001.

[69] L. Zhou and Z. Haas, Securing *ad hoc* Networks, *IEEE Networks*, November/December 1999, pp. 24–30.

[70] E. Ayanoglu, C.-L. I, R. D. Gitlin and J. E. Mazo, Diversity coding for transparent self-healing and fault-tolerant communication networks. *IEEE Trans. Commun.*, vol. 41, 1993, pp. 1677–1686.

[71] Y. Desmedt and Y. Frankel, Threshold cryptosystems. In G. Brassard (ed.), *Advances in Cryptology – Crypto'89, Proc. 9th Annual International Cryptology Conference*, Santa Barbara, CA A, 20–24 August 1989, vol. 435 of Lecture Notes in Computer Science. Springer: Berlin, 1990, pp. 307–315.

[72] Y. Desmedt, Threshold cryptography. *Eur. Trans. Telecommun.*, vol. 5, 1994, pp. 449–457.

[73] R. Gennaro, S. Jarecki, H. Krawczyk and T. Rabin, Robust threshold DSS signatures. In U. M. Maurer (ed.), *Advances in Cryptology – Proc. Eurocrypt'96, International Conference on the Theory and Application of Cryptographic Techniques*, Saragossa, 12–16 May 1996, vol. 1233 of Lecture Notes in Computer Science. Springer: Berlin, 1996, pp. 354–371.

[74] R. Gennaro, S. Jarecki, H. Krawczyk and T. Rabin, Robust and efficient sharing of RSA functions. In N. Koblitz (ed.), *Advances in Cryptology – Proc. Crypto'96, the 16th Annual International Cryptology Conference*, Santa Barbara, CA, 18–22 August 1996, vol. 1109 of Lecture Notes in Computer Science. Springer: Berlin, 1996, pp. 157–172.

[75] A. Herzberg, S. Jarecki, H. Krawczyk and M. Yung, Proactive secret sharing or: How to cope with perpetual leakage. In D. Coppersmith (ed.), *Advances in Cryptology – Proc. Crypto'95, the 15th Annual International Cryptology Conference*, Santa Barbara, CA USA, 27–31 August 1995, vol. 963 of Lecture Notes in Computer Science. Springer: Berlin, 1995, pp. 457–469.

[76] Y. Frankel, P. Gemmell, P. MacKenzie and M. Yung, Proactive RSA. In B. S. Kaliski Jr. (ed.), *Advances in Cryptology – Proc. Crypto'97, the 17th Annual International Cryptology Conference*, Santa Barbara, CA, 17–21 August 1997, vol. 1294 of Lecture Notes in Computer Science. Springer: Berlin, 1997, pp. 440–454.

[77] T. Pedersen, Non-interactive and information-theoretic secure verifiable secret sharing. In J. Feigen-baum (ed.), *Advances in Cryptology – Proc. Crypto'91, the 11th Annual International Cryptology Conference*, Santa Barbara, CA, 11–15 August 1991, vol. 576 of Lecture Notes in Computer Science. Springer: Berlin, 1992, pp. 129–140.

[78] B. Kumar, Integration of security in network routing protocols. *SIGSAC Rev.*, vol. 11, 1993, pp. 18–25.

[79] K.E. Sirois and S.T. Kent, Securing the Nimrod routing architecture, in *Proc. Symp. Network and Distributed System Security*, Los Alamitos, CA, February 1997. The Internet Society, IEEE Computer Society Press, 1997, pp. 74–84.

[80] B.R. Smith, S. Murphy and J.J. Garcia-Luna-aceves, Securing distance-vector routing protocols. In *Proc. Symp. Network and Distributed System Security,* Los Alamitos, CA, February 1997. The Internet Society, IEEE Computer Society Press, 1997, pp. 85–92.

[81] R. Hauser, T. Przygienda and G. Tsudik, Lowering security overhead in link state routing. *Comput. Networks,* vol. 31, 1999, pp. 885–894.

[82] M.K. Reiter, Distributing trust with the Rampart toolkit, *Commun. ACM,* vol. 39, 1996, pp. 71–74.

[83] M.K. Reiter, M.K. Franklin, J.B. Lacy and R.N. Wright. The Ω key management service, *J. Comput. Security,* vol. 4, 1996, pp. 267–297.

[84] L. Gong, Increasing availability and security of an authentication service. *IEEE J. Select. Areas Commun.*, vol. 11, 1993, pp. 657–662.

[85] S. Capkun, L. Buttyán and J.-P. Hubaux, Self-organized public-key management for mobile *ad hoc* networks, *IEEE Trans. Mobile Comput.*, vol. 2, no. 1, 2003, pp. 52–64.

[86] C. Karlof and D. Wagner, Secure routing in wireless sensor networks: attacks and countermeasures, *Proc. First IEEE Int. Workshop on Sensor Network Protocols and Applications*, 11 May 2003, pp. 113–127.

[87] J. Kulik, W. Heinzelman and H. Balabishnan, Negotiation-based protocols for disseminating information in wireless sensor networks, *Wireless Networks*, vol. 8, nos 2–3, 2002, pp. 169–185.

16

Active Networks

16.1 INTRODUCTION

The basic goals of active networking (AN) are to create networking technologies that, in contrast to current networks, are easy to evolve and which allow application specific customization. To achieve these goals, AN uses a simple idea, that the network would be easier to change and customize if it were programmable [1–6]. While AN has the high-level goals of improving evolvability and customizabilty, there are a number of low-level concerns that must be balanced to achieve these goals. The first of these concerns is flexibility. AN systems aim to significantly improve the flexibility with which we can build networks. The second concern is safety and security. It is crucial that, while adding flexibility, we do not compromise the safety or security of the resulting system. The third concern is performance. If adding flexibility results in a system that cannot achieve its performance goals, it will be pointless. The final concern is usability. It is important that the resulting system not be so complex as to be unusable.

One of the basic techniques of AN is that code (program) is moved to the node at which it should execute. One place this idea first arose was in distributed systems supporting process migration. Another significant early influence was in generalization of remote procedure call (RPC) to support remote evaluation (RE). Both of these techniques will be discussed in detail in applications for network management in Chapter 18. The next important step in this direction was a DARPA proposal on the topic of 'Protocol boosters for distributed computing systems'. The idea was to *dynamically construct* protocols using protocol element insertion and deletion on an as-needed basis, to respond to network dynamics. Protocols were constructed *optimistically*; that is, ideal operating conditions (no errors, low delays, adequate throughput, etc.) were assumed, and protocol elements (such as error detection and correction mechanisms) were inserted into protocols on-demand, as conditions were encountered that deviated from the best case where the protocol element would not be needed.

On the network level the previous concepts resulted in middleboxes [7]. Domain-specific 'middleboxes' [7] are appearing such as firewalls, network address translators (NATs) and intrusion detection systems (IDSs). Examples of such middleboxes include NATs [8–10], NAT with protocol translator (NAT-PT) [11], SOCKS gateway [12], Packet classifiers, markers and schedulers [13], TCP performance enhancing proxies [14], IP firewalls [15, 16], gatekeepers/session control boxes [17, 18], transcoders, proxies [17, 19]. These various application-driven *ad hoc*

Advanced Wireless Technologies: Cognitive, Cooperative & Opportunistic 4G Technology Second Edition Savo G. Glisic

examples of STF (store, translate and forward) functionality can be unified in a common framework, and embedded in a common programming model reinforced with the safety and security.

The IETF's forwarding and control element separation (ForCES) working group [20] models router architectures in a way that allows the introduction of programmable and active technologies into the Internet control plane, in the style of base building block (BBN)s FIRE [21].

The principal observation here is that forwarding and routing are distinct activities. Routing is part of the 'control plane' of the IP Internet, while forwarding is the 'transport plane'. These activities were consolidated in traditional IP routers, but are now recognized as logically separate (viz. MPLS). The separation permits more general network elements to replace IP routers in performing control plane activities, allowing distributed routing with improved performance, slightly more global optimization, and perhaps surprisingly, an increase in security. In addition, the separation of routing and forwarding functions permits decoupling of their performance, allowing better tracking of technology improvements in both forwarder mechanics and routing algorithms.

Active router control uses fast forwarders as a virtual link layer, managed by specialized active router controllers (ARCs), as shown in Figure 16.1. Using a set of routers as a 'router in a room' is not uncommon; one could simply reduce their autonomy and specialize them to IP forwarding, making way for source routing over all optical networks or routing/router control internal to the network. The use of general purpose network elements permits this separation of concerns, while offering the *potential* for improvement of the Internet on a number of axes.

In this configuration, choices of routes are made by the ARC. A significant advantage is that specialized forwarding tables can be loaded into each forwarder; these tables can be small since entries must exist only for adjacent nodes.

A key advantage of the ARC model is that, for computationally centered tasks (routing, or more general computations if the programmability of ARCs is exploited), a computer which tracks computer technology trend exponentials (faster CPU, larger RAM) is used, while the forwarders independently track networking technology trend exponentials such as bandwidth improvements.

The basic distributed control architecture of Figure 16.1 can be replicated throughout an Internetwork, with the active elements using the managed Internet routes as link layers. This is shown in Figure 16.2, where a set of active nodes has been grafted into a larger collection of forwarders to create an active Internet.

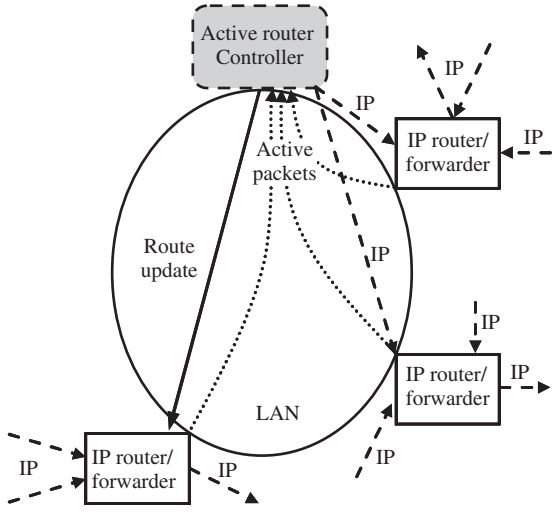

Figure 16.1 Active router controller managing a set of forwarder/routers.

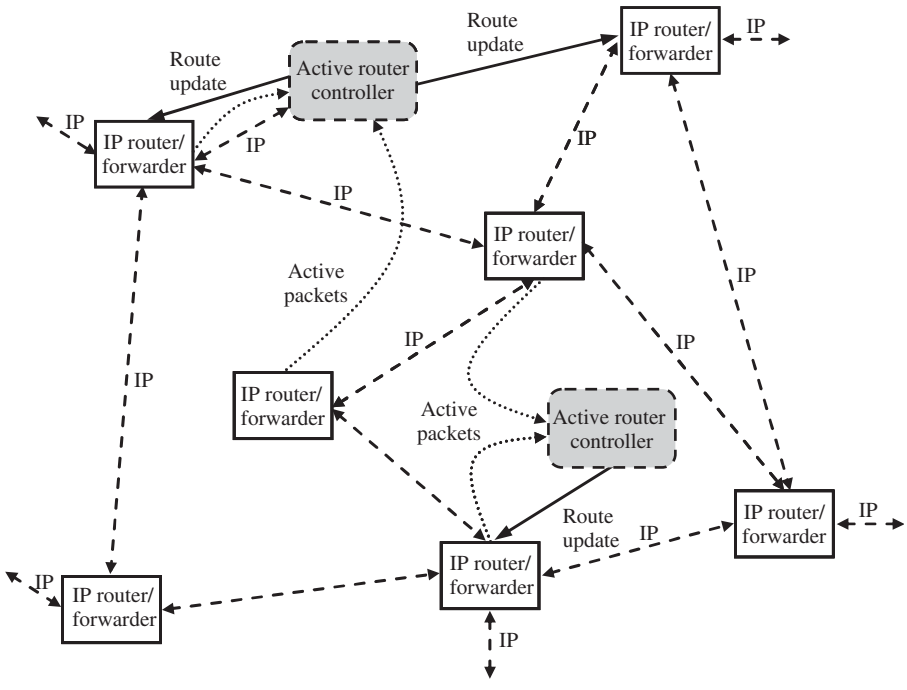

Figure 16.2 ARCs distributed throughout an Internet.

16.2 PROGRAMABLE NETWORKS REFERENCE MODELS

IEEE P1520 is formalized by the IEEE Project 1520 standards initiative for programmable network interfaces and its corresponding reference model [22]. The IEEE P1520 RM, depicted in Figure 16.3, defines the following four interfaces.

(1) CCM interface – the connection control and management interface is a collection of protocols that enable the exchange of state and control information at a very low level between the NE and an external agent.

(2) L-interface – this defines an application program interface (API) that consists of methods for manipulating local network resources abstracted as objects. This abstraction isolates upper layers from hardware dependencies or other proprietary interfaces.

(3) U-interface – this mainly provides an API that deals with connection setup issues. The U-interface isolates the diversity of connection set-up requests from the actual algorithms that implement them.

(4) V-interface – it provides a rich set of APIs to write highly customized software, often in the form of value-added services.

CCM and L-interfaces fall under the category of NE (network element) interfaces, whereas U- and V-interfaces constitute network-wide interfaces. Initial efforts through the ATM sub-working group (P1520.2) focused on telecommunication networks based on ATM and introduced programmability in the control plane [23]. Later, the IP Sub-working Group extended these principles to IP networks and routers.

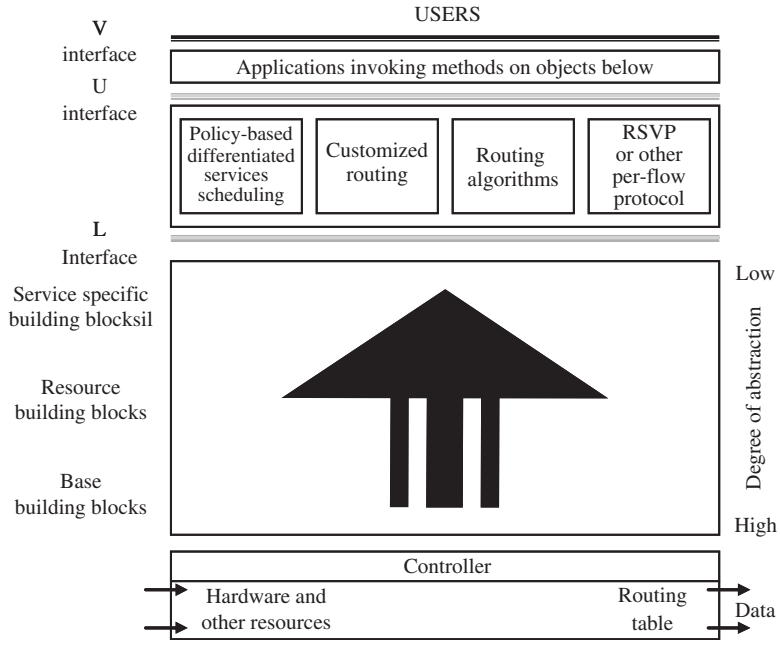

Figure 16.3 P1520 reference model and the L-interface abstraction model.

16.2.1 IETF ForCES

Recently, a working group of IETF, called forwarding and control element separation (ForCES) was formed with a similar objective to that of P1520 [24, 25]. Document [25] classifies the NE as a collection of components of two types: control elements (CE) and forwarding elements (FE) operating in the control and forwarding (transport) planes, respectively. CE's host controls functionality, like routing and signaling protocols, whereas FEs perform operations on packets, like header processing, metering, scheduling, etc., when passing through them. CEs and FEs may be interconnected with each other in every possible combination (CE-CE, CE-FE, FE-FE), thus forming arbitrary types of logical topologies (see Figure 16.4). Every distinct combination defines a reference point, namely, F_r, F_p and F_i. Each one of these reference points may define a protocol or a collection thereof, but ForCES protocol is only defined for the F_p reference point.

16.2.2 Active networks reference architecture

Active networks transform the store-and-forward network into store-compute-and-forward network. The difference here is that packets are no longer passive but rather active in the sense that they carry executable code together with their data payload. This code is dispatched and executed at designated (active) nodes performing operations on the packet data as well as changing the current state of the node to be found by the packets that follow. Two approaches are possible based on whether programs and data are carried discretely, within program and data packets (out-of-band) or in an integrated manner, i.e. in-band.

In the discrete case, injecting code into the node and processing packets are two separated jobs. The user or network operator first injects his customized code into the routers along a path. Then the data packet arrives, its header is examined and the appropriate preinstalled code is loaded to

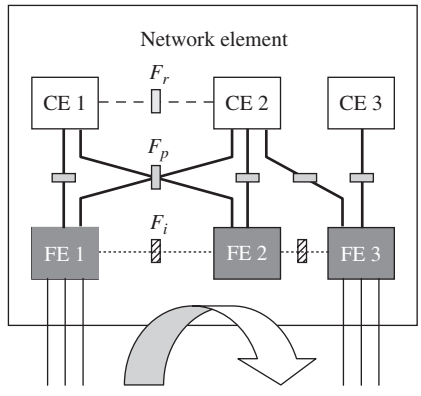

Figure 16.4 ForCES architectural representation of NE.

operate on its contents [26, 27]. Separate mechanisms for loading and executing may be required for the control thereof. This separation enables network operators to dynamically download code to extend a node's capabilities, which in turn become available to customers through execution.

At the other extreme lies the integrated approach where code and data are carried by the same packet [28]. In this context, when a packet arrives at a node, code and data are separated, and the code is loaded to operate on the packet or change the state of the node. A hybrid approach has also been proposed [29].

The *active networks reference architecture* model [30, 31] is shown in Figure 16.5. An active network is a mixture of active and legacy (nonactive) nodes. The active nodes run the node operating system (NodeOS) – not necessarily the same, while a number of execution environments (EE) coexist at the same node. Finally a number of active applications (AA) make use of services offered by the EEs.

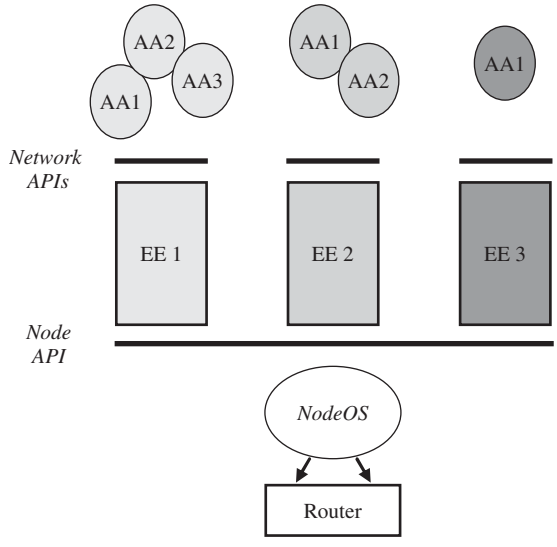

Figure 16.5 Active node architecture.

The NodeOS simultaneously supports multiple EEs. Its major functionality is to provide isolation among EEs through resource allocation and control mechanisms, and to provide security mechanisms to protect EEs from each other. It may also provide other basic facilities like caching or code distribution that EEs may use to build higher abstractions to be presented to their AAs. All these capabilities are encapsulated by the node interface through which EEs interact with the NodeOS. This is the minimal fixed point at which interoperability is achieved [31]. In contrast EEs implement a very broad definition of a network API ranging from programming languages to virtual machines, to static APIs in the form of a simple list of fixed-size parameters, etc. [32]. EE takes the form of a middleware toolkit for creating, composing and deploying services.

The AN reference architecture [30] is designed for simultaneously supporting a multiplicity of EEs at a node. Only EEs of the same type are allowed to communicate with each other, whereas EEs of different type are kept isolated from each other. A thorough analysis and comparison of programmable networks may be found in References [33, 34].

The *FAIN (future active IP network) NE* reference architecture is depicted in Figure 16.6. It describes how the ingredients identified previously may synergistically be combined in building next-generation NEs capable of seamlessly incorporating new functionality or dynamically configured to change their behavior according to new service requirements. One of the key concepts defined by the FAIN architecture is the EE. In FAIN, drawing from an analogy based on the concepts of class and object in object-oriented systems, we distinguish EEs between the *EE type* and the *EE instances* thereof.

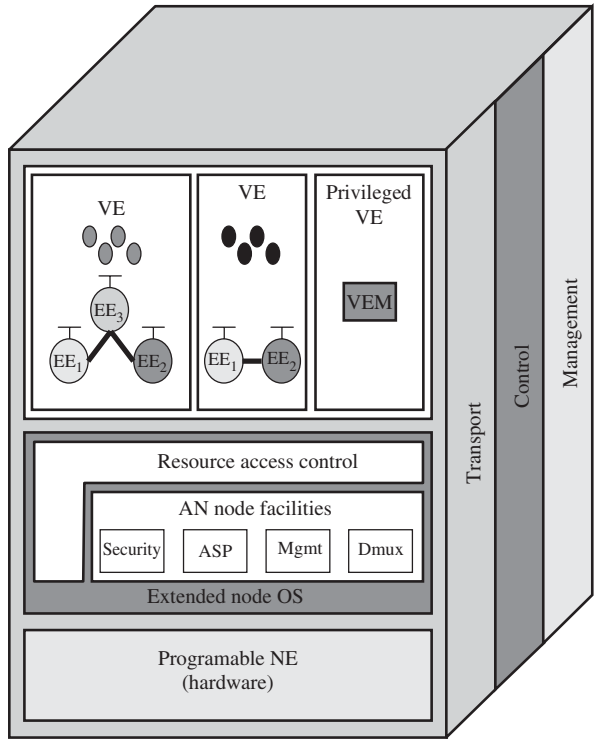

Figure 16.6 FAIN NE reference architecture.

An EE type is characterized by the programming methodology and the programming environment that is created as a result of the methodology used. The EE type is free of any implementation details. In contrast, an EE instance represents the realization of the EE type in the form of a runtime environment by using specific implementation technology, e.g. programming language and binding mechanisms to maintain operation of the runtime environment. For details see References [21, 35].

16.3 EVOLUTION TO 4G WIRELESS NETWORKS

Given the volume of investments in existing networks infrastructure, a possible way to 4G might be evolution rather than any revolution. By 'network evolution' we mean any incremental change to a network that modifies or enhances existing functionality or adds new functionality. In the context of active networking, evolution should be able to occur at remote nodes while the network is operational with only minimal disruption to existing services. AN achieves evolution by changing the programs that operate the network. Thus the ways in which we can evolve the network are dictated by the programmability mechanisms that are available to make such changes.

Active packets (AP) are perhaps the most radical AN technology for evolution and they are the only mechanism that, at a high-level, are specific to AN. Such packets carry (or literally are) programs that execute as they pass through the nodes of network. A packet can perform management actions on the nodes, effect its own routing, or form the basis of larger protocols between distributed nodes, e.g. routing protocols. Such packets (ANTS [38], Smart Packets [39] and PLAN [40]) are like conventional packets, but with qualitatively more power and flexibility.

Active packet evolution does not require changes to the nodes of the network. Instead, it functions solely by the execution of APs utilizing standard services. The disadvantage of this approach is that taking advantage of new functionality requires the use of new packet programs. This means that at some level the applications using the functionality must be aware that the new functionality exists. This is the kind of evolution facilitated by pure AP systems, such as ANTS [38] and in essence it embodies the AN goal of application-level customization.

The programmability mechanism that is broadly familiar outside the AN community is the *plug-in extension*. Plug-in extensions can be downloaded and dynamically linked into a node to add new node-level functionality. For this new functionality to be used, it must be callable from some prebuilt and known interface. For example, a packet program will have a standard way of calling node resident services. If it is possible to add a plug-in extension to the set of callable services (typically by extending the service name space) then such an extension 'plugs in' to the service call interface.

The programmability mechanism known as the *update extensions* may also be downloaded, but they go beyond plug-in extensions in that they can update or modify existing code and can do so even while the node remains operational. Thus, such extension can add to or modify a system's functionality even when there does not exist an interface for it to hook into.

An example of AP evolution program written in a special-purpose language, PLAN (packet language for AN) [40], for mobility management protocol can be found in Song *et al.* [36]. Before a mobile node leaves its home network, it must identify the router that serves as its home agent. For simplicity, it is assumed that its default router serves this purpose. Once the node has attached itself to a new network and has a unique address, it sends an AP containing a control program to register itself to its home agent. When executed, this program simply adds the information to the home agent's soft-state keyed by the mobile node's home network address. Both the application aware and transparent versions share the same soft-state entries, allowing them to use the same control program and to co-exist.

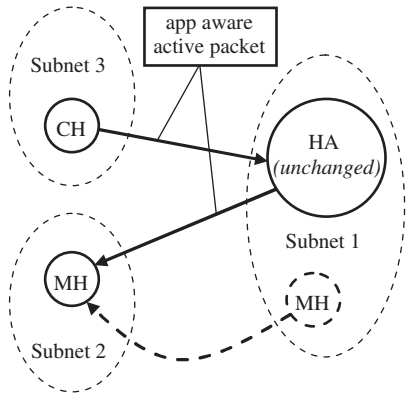

Figure 16.7 Active packets for mobile-IP (MH, mobile host; HA, home agent; CH, corresponding host.)

Figure 16.7 illustrates how we detect that a packet is at the home agent of a mobile host and how the packet is then tunneled to the unique address. The PLAN code for the packet that must be sent by the application is [36]:

```
fun getToAgent(dest, payload, port) =
  try
    let val fagent = lookupTuple(dest) in
      OnRemote(|FoundFA|(dest, payload, port), fagent, getRB( ), defRoute)
    end
  handle NotFound =>
    if (thisHostIs(dest)) then deliver(payload, port)
    else
      let val next = defaultRoute(dest) in
        OnNeighbor(|getToAgent|(dest, payload, port), #1 next, getRB( ),#2 next))
      end
fun FoundFA(dest, payload, port) =
  let val hop = defaultRoute(dest) in
    OnNeighbor(|deliver|(payload, port), #1 hop, getRB(), #2 hop))
  end
```

GetToAgent is the main function and, when it executes, it first looks up *dest* in the soft-store using *lookupTuple*. If that succeeds, it has found the home agent and it uses *OnRemote* to send a new packet, the tunnel, that will execute *FoundFA* at the foreign agent with the same arguments as *getToAgent*.

OnRemote provides multihop transmission of the packet without execution until it reaches the foreign agent. If the lookup fails the handle will execute. If we have actually reached the host then we deliver the packet. Otherwise, it looks up the next hop toward *dest*. It then uses *OnNeighbor*, which only transmits a packet one hop, to send the packet. Thus the packet travels hop-by-hop looking for the home agent. *FoundFA* function executes on the foreign agent, which in this case is the mobile host, but might be some other node on the same sub-net. It sends a packet to the *dest* that does the delivery. This is where the original packet is removed from the tunnel. Notice that all of that functionality is encoded in the tunnel packet program itself; the foreign agent does not need to have any knowledge of its role as a tunnel endpoint – it just has to support PLAN.

If a node defines an extensible interface, new extensions can be loaded and plugged into this interface to provide extended or enhanced functionality. This is the essence of plug-in extension evolution. As an illustration consider the pseudocode shown below for a simple AP that implements route discovery [36]:

```
Route Discover(Simple DSR)
procedure Route Request(Target,RouteRec)
  if Duplicate Request Packet Or My Address Already In Route Rec
    then Discard
    else { if This Host is Target
             then Route Reply(RouteRec)
           else { Append My Address To Route
                  Flood To All Neighbours
```

The packet itself embodies many key aspects of the protocol directly. In particular, it does duplicate elimination, tests for routing loops, detects termination and sends a reply, and performs flooding. In general, since many protocols have relatively simple control flow, simple APs can implement key aspects of the protocol directly. This algorithm benefits from noderesident services that are specific to the protocol, particularly to detect if this is a duplicate request or if the current node is already in the route record.

16.4 PROGRAMMABLE 4G MOBILE NETWORK ARCHITECTURE

In this section, we introduce a possible high-level architecture for future mobile systems with the focus on programmability [37, 41]. To address the creation and provisioning of unanticipated services, the whole system has to be designed to be as flexible as possible. Openness and configurability, not only at the service level but also with respect to the whole system architecture, will attract third-party vendors to evolve the system as it unfolds and is therefore the key to viable solutions. As pointed out in Chapter 1, 4G systems are expected to provide an integration platform to seamlessly combine heterogeneous environments. Core abstraction layers cover hardware platform, network platform, middleware platform and applications. The abstraction layers can interact with each other using well-defined interfaces. Besides their regular cooperation in an operational setting, each layer can be configured separately and independently via configuration interfaces.

The generic architecture for the network elements of a mobile network is shown in Figure 16.8 (excluding applications). In this architecture, the following abstraction layers are considered, each programmable with configurable components:

- Middleware platform, typically with a virtual execution environment for platform-independent distributed processing.
- The computing platform serves as a general purpose platform for processing stateful protocols, e.g. routing, QoS signaling or connection management.
- The forwarding engine is in the data path of a network node and it connects the interface modules, e.g. by a switch matrix. This engine can be implemented as dedicated hardware or as a kernel module of common operating systems. The forwarding engine is programmable for performance-critical tasks which are performed on a per-packet basis.
- The interface modules are medium specific for different wireless or wired standards. They can be configured or programmed to adapt to new physical layer protocols or for triggering events in higher layers.

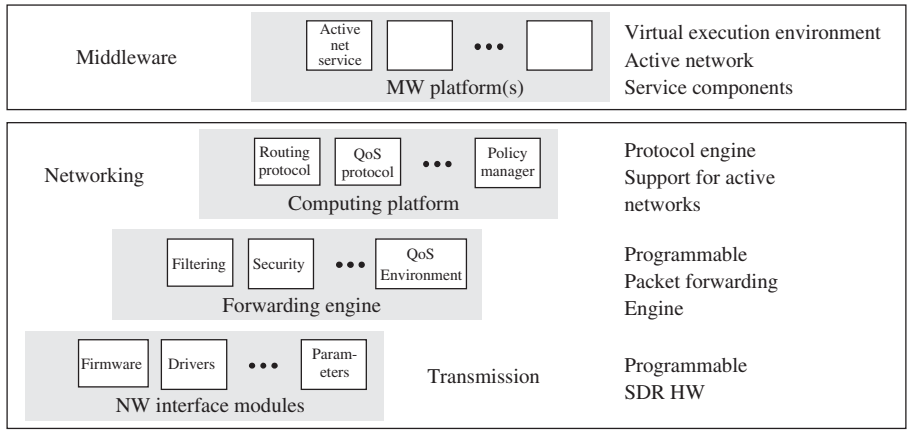

Figure 16.8 Programmable network element model.

There are different approaches to active networking in this architecture. Some approaches offer a virtual execution environment, e.g. a Java virtual machine, on the middleware layer. Some options also include native code in the computing platform, e.g. for flexible signaling. Others employ programmable hardware for forwarding.

A key ingredient in these approaches is interfaces to the lower layers and programmable filters for identifying the packets to be processed in the active networking environment. The terminal architecture is shown in Figure 16.9. It consists of:

- Middleware platform, typically with a limited virtual execution environment.
- Smart Card, e.g. USIM for UMTS, which includes subscriber identities and also a small, but highly secure execution environment. This can be used ideally for personal services like electronic wallet.
- Programmable hardware, which is designed for one or more radio standards.
- Native operating system which provides real-time support, needed for stacks and certain critical applications, e.g. multimedia codecs.

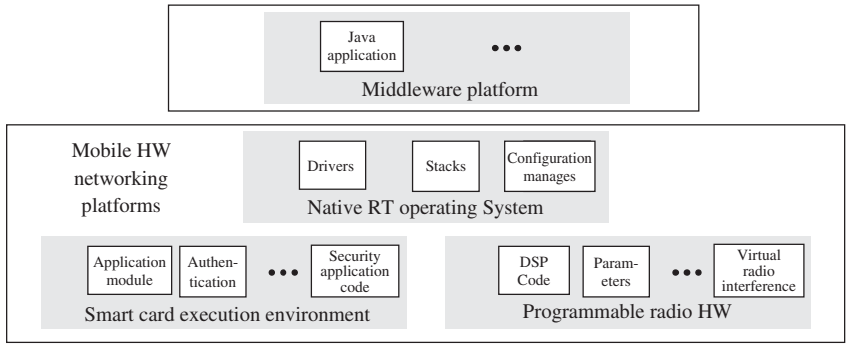

Figure 16.9 Mobile terminal architecture.

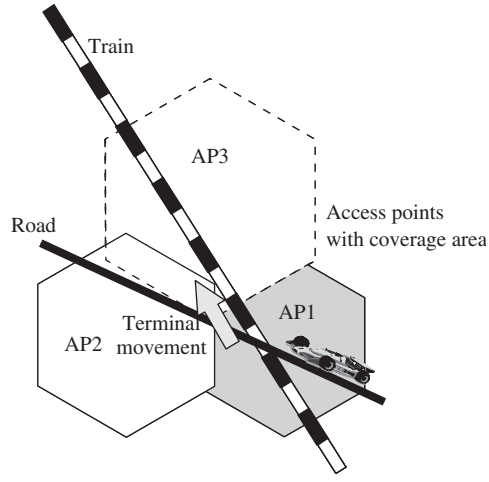

Figure 16.10 Context-aware hand-over prediction.

Compared with network elements, the SmartCard is a new, programmable component. Owing to resource limitations, the forwarding engine and computation platform just collapse to one operating system platform. Also, the middleware layers are typically quite restricted. Service deployment and control of reconfigurations are complex since there is a split of responsibility between operator and manufacturer. For instance, the manufacturer has to provide or digitally sign appropriate low-level code for reconfigurations. On the other hand, the operator is interested in controlling the configuration to fit the user and network needs.

There are a number of examples to show the importance of flexible networking protocols and the need of dynamic cross layer interfaces in future mobile networks. As an example we show that hand-over can be optimized by information about the user context [37, 42, 43] as shown in Figure 16.10. In this scenario, the terminal moves into an area covered by both AP2 and AP3. The problem is to decide which access point (AP) to choose. State of the art are many algorithms based on signal strength analysis or on available radio resources. Even if one AP is slightly better regarding these local measurements, the decision may not be the best. For instance, if the terminal in Figure 16.10 is on the train, it is obviously better to hand over to AP3, even if AP2 is more reachable for a short period of time. In many cases, the hand-over can be optimized by knowledge of terminal movement and user preferences. For instance, if the terminal is in a car or train, its route may be constrained to certain areas. Also, the terminal profile may contain the information that the terminal is built in a car. Alternatively, the movement pattern of a terminal may suggest that the user is in a train. A main problem is that hand-over decisions have to be executed fast. However, the terminal profile and location information is often available on a central server in the core network. Retrieving this information may be too slow for hand-over decisions.

Furthermore, the radio conditions during hand-over may be poor and hence limit such information exchange. The idea of the solution is to proactively deploy a context-aware decision algorithm onto the terminal which can be used to assist hand-over decisions. A typical example is the information about the current movement pattern, e.g. by knowledge of train or road routes. For implementation, different algorithms can be deployed by the network on the terminal, depending on the context information. This implementation needs a cross layer interface, which collects the context information from different layers and makes an optimized decision about deploying a decision algorithm.

16.5 COGNITIVE PACKET NETWORKS

We now discuss packet switching networks in which intelligence is incorporated into the packets, rather than at the nodes or in the protocols. Networks which contain such packets are referred to as cognitive packet networks (CPN). Cognitive packets in CPN route themselves, and learn to avoid congestion and being lost or destroyed. Cognitive packets learn from their own observations about the network and from the experience of other packets. They rely minimally on routers. Each cognitive packet progressively refines its own model of the network as it travels through the network, and uses the model to make routing decisions. Cognitive packets (CPs) store information in their private cognitive map (CM) and update the CM and make their routing decisions using the code which is in each packet. This code may include neural networks or other adaptive algorithms. Figure 16.11 presents the format of a cognitive packet. The manner in which cognitive memory at a node is updated by the node's processor is shown in Figure 16.12. In a CPN, the packets use nodes as 'rented space', where they make decisions about their routes. They also use nodes as places where they can read their mailboxes. *Mailboxes may be filled by the node, or by other packets which pass through the node.* Packets also use nodes as processors which execute their code to update their CM and then execute their routing decisions. As a result of code execution, certain information may be moved from the CP to certain mailboxes. The nodes may execute the code of CPs in some order of priority between classes of CPs, for instance as a function of QoS requirements which are contained in the identification field).

As a routing decision, a CP will be placed in some output queue, in some order of priority, determined by the CP code execution. A CPN and a CPN node are schematically represented in Figures 16.13 and 16.14. CPs use units of information 'signals' to communicate with each other via mailboxes (MBs) in the nodes. These signals can also emanate from the environment (nodes,

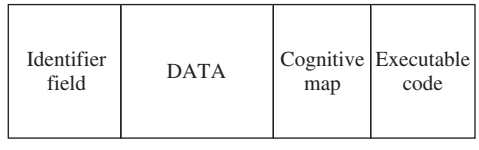

Figure 16.11 Format of cognitive packet.

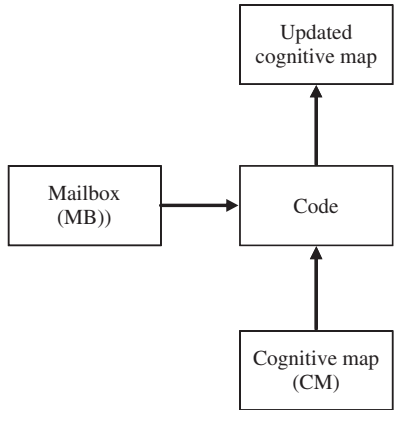

Figure 16.12 CP update by a CPN node.

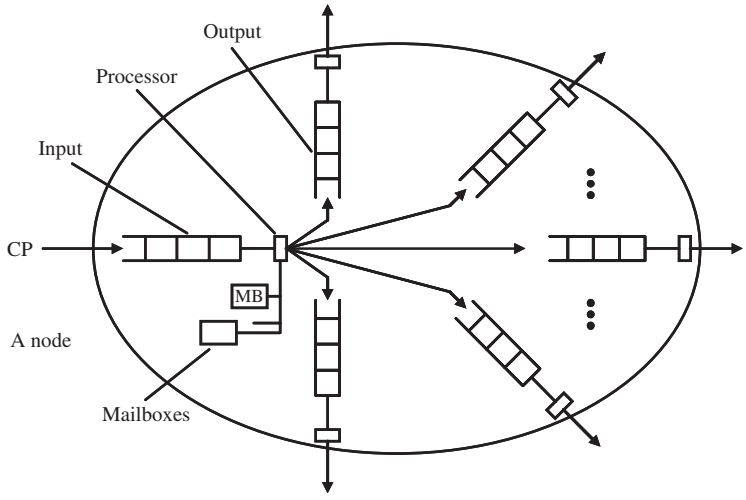

Figure 16.13 CPN node model.

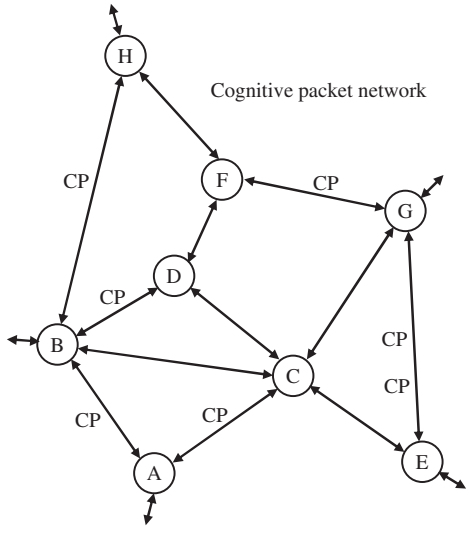

Figure 16.14 CPN example.

existing end-to-end protocols) toward the CPs. CP, shown in Figure 16.11, contain the following fields [44]:

(1) The *identifier field* (IF), which provides a unique identifier for the CP, as well as information about the class of packets it may belong to, such as its quality of service (QoS) requirements.

(2) The *data field* containing the ordinary data it is transporting.

(3) A *cognitive map* (CM), which contains the usual source and destination (S-D) information, as well as a map showing where the packet currently 'thinks' it is, the packet's view of the

state of the network, and information about where it wants to go next; the S-D information may also be stored in the IF.

(4) *Executable code* that the CP uses to update its CM. This code will contain learning algorithms for updating the CM, and decision algorithms which use the CM.

A node in the CPN provides a storage area for CPs and for mailboxes which are used to exchange data between CPs, and between CPs and the node. It has an input buffer for CPs arriving from the input links, a set of mailboxes, and a set of output buffers which are associated with output links. Nodes in a CPN carry out the following functions [44]:

(1) A node receives packets via a finite set of ports and stores them in an input buffer.

(2) It transmits packets to other nodes via a set of output buffers. Once a CP is placed in an output buffer, it is transmitted to another destination node with some priority indicated in the output buffer.

(3) A node receives information from CPs which it stores in MBs. MBs may be reserved for certain classes of CPs, or may be specialized by classes of CPs. For instance, there may be different MBs for packets identified by different source-destination (S-D) pairs.

(4) A node executes the code for each CP in the input buffer. During the execution of the CPs code, the CP may ask the node to decline its identity, and to provide information about its local connectivity (i.e. this is node A, and I am connected to nodes B, C, D via output buffers) while executing its code. In some cases, the CP may already have this information in its CM as a result of the initial information it received at its source, and as a result of its own memory of the sequence of moves it has made.

As a result of this execution:

(1) The CMs of the packets in the input buffer are updated.

(2) Certain information is moved from CPs to certain MBs.

(3) A CP which has made the decision to be moved to an output buffer is transfered there, with the priority it may have requested.

We have been already discussing some networks which offer users the capability of adding network executable code to their packets. Additional material can be found in References [44–68].

16.5.1 Adaptation by cognitive packets

Each cognitive packet starts with an initial representation of the network from which it then progressively constructs its own cognitive map of the network state and uses it to make routing decisions. Learning paradigms are used by CPs to update their CM and reach decisions using the packet's prior experience and the input provided via mailboxes. In the adaptive approach for CPs, each packet entering the network is assigned a goal before it enters the network, and the CP uses the goal to determine its course of action each time it has to make a decision [44]. For instance if the CP contains part of a telephone conversation, a typical goal assigned to the packet should reflect the concern about the delay. A more sophisticated goal in this case could be delay and sequenced (in order) delivery. On the other hand, if these were data packets, the goal may simply be packet loss rate. These goals are translated into numerical quantities (e.g. delay values, loss probabilities and weighted combinations of such numerical quantities), which are then used directly in the adaptation. An example is where all the packets were assigned a common goal, which was

to minimize a weighted combination of delay (W) and loss (L) as

$$G = \alpha W + \beta L \tag{16.1}$$

A simple approach to adaptation is to respond in the sense of the most recently available data. Here the CP's cognitive memory contains data which is updated from the contents of the node's mailbox. After this update is made, the CP makes the decision which is most advantageous (lowest cost or highest reward) simply based on this information. This approach is referred to as the Bang-Bang algorithm. Instead some other learning paradigms for CPs can be also used like *learning feedforward random neural networks* (LFRNN) [57, 68] or *random neural networks with reinforcement learning* (RNNRL) [57]. Adaptive stochastic finite-state machines (ASFSM) [55, 56, 58] are another class of adaptive models which could be used for these purposes.

16.5.2 The random neural networks-based algorithms

For the reinforcement learning approach to CP adaptation, as well the feed-forward neural network predictor, the RNN [57] was used in Gelenbe *et al.* [44]. IT is an analytically tractable model whose mathematical structure is akin to that of queueing networks. It has product form just like many useful queueing network models, although it is based on nonlinear mathematics. The state qi of the ith neuron in the network is the probability that it is excited. *Each neuron i is associated with a distinct outgoing link at a node.* These quantities satisfy the following system of nonlinear equations:

$$q_i = \lambda^+(i)/\left[r(i) + \lambda^-(i)\right] \tag{16.2}$$

with

$$\lambda^+(i) = \sum_j q_j w^+_{ji} + \Lambda_i, \;\; \lambda^-(i) = \sum_j q_j w^-_{ji} + \lambda_i \tag{16.3}$$

Here w^+_{ij} is the rate at which neuron i sends 'excitation spikes' to neuron j when i is excited, and w^-_{ij} is the rate at which neuron i sends "inhibition spikes" to neuron j when i is excited and $r(i)$ is the total firing rate from the neuron i. For an n neuron network, the network parameters are these n by n 'weight matrices' $\mathbf{W}^+ = \|w^+_{ij}\|$ and $\mathbf{W}^- = \|w^-_{ij}\|$ which need to be 'learned' from input data. Various techniques for learning may be applied to the RNN. These include reinforcement learning and gradient-based learning, which are used in the following.

Given some goal G that the CP has to achieve as a function to be minimized [i.e. transit delay or probability of loss, or a weighted combination of the two as in Equation (16.1)], a reward R is formulated which is simply $R = 1/G$. Successive measured values of the R are denoted by Rl, $l = 1, 2, \ldots$ These are first used to compute a decision threshold:

$$T_l = aT_{l-1} + (1 - a)R_l \tag{16.4}$$

where a is some constant $0 < a < 1$, typically close to 1. Now an RNN with (at least) as many nodes as the decision outcomes is constructed. Let the neurons be numbered $1, \ldots, n$. Thus for any decision i, there is some neuron i. Decisions in this RL algorithm with the RNN are taken by selecting the decision j for which the corresponding neuron is the most excited, i.e. the one with has the largest value of q_j. Note that the lth decision may not have contributed directly to the lth observed reward because of time delays between cause and effect. Suppose that we have now taken the lth decision which corresponds to neuron j, and that we have measured the lth reward Rl. Let us denote by r_i the firing rates of the neurons before the update takes place. We first determine whether the most recent value of the reward is larger than the previous 'smoothed' value of the reward, which is referred to as the threshold T_{l-1}. If that is the case, then we increase

very significantly the excitatory weights going into the neuron that was the previous winner (in order to reward it for its new success), and make a small increase of the inhibitory weights leading to other neurons. If the new reward is not better than the previously observed smoothed reward (the threshold), then we simply increase moderately all excitatory weights leading to all neurons, except for the previous winner, and increase significantly the inhibitory weights leading to the previous winning neuron (in order to punish it for not being very successful this time). This is detailed in the algorithm given below. We compute T_{l-1} and then update the network weights as follows for all neurons $i \neq j$:

$$
\begin{aligned}
&\text{If} \quad T_{l-1} \leq R_l \\
&\quad - w^+(i,j) \leftarrow w^+(i,j) + R_l \\
&\quad - w^-(i,k) \leftarrow w^-(i,k) + R_l/(n-2), \qquad \text{if} \quad k \neq j \\
&\text{Else} \\
&\quad - w^+(i,j) \leftarrow w^+(i,j) + R_l/(n-2), \qquad \text{if} \quad k \neq j \\
&\quad - w^-(i,k) \leftarrow w^-(i,k) + R_l
\end{aligned}
$$

Then we re-normalize all the weights by carrying out the following operations, to avoid obtaining weights which indefinitely increase in size. First for each i we compute:

$$
\bar{r}_i = \sum_{m=1}^{n} [w^+(i,m) + w^-(i,m)] \tag{16.5}
$$

and then renormalize the weights with

$$
\begin{aligned}
w^+(i,j) &\leftarrow w^+(i,j) r_i / \bar{r}_i \\
w^-(i,j) &\leftarrow w^-(i,j) r_i / \bar{r}_i
\end{aligned}
$$

The probabilities qi are computed using the nonlinear iterations in Equations (16.2) and (16.3), leading to a new decision based on the neuron with the highest probability of being excited.

16.5.2.1 Performance examples

Simulation results are generated in a scenario as in Gelenbe *et al.* [44]. The CPN included $10 \times 10 = 100$ nodes, interconnected within rectangular grid topology. All link speeds were normalized to 1, and packets were allowed to enter and leave the network either from the top 10 nodes or the bottom 10 nodes in the grid. All the packets were assigned a common goal, which was to minimize a weighted combination of delay (W) and loss (L) as defined by Equation (16.1). All the algorithms are allowed to use four items of information which are deposited in the nodes' mailboxes:

(1) the length of the local queues in the node;

(2) recent values of the downstream delays experienced by packets which have previously gone through the output links and reached their destinations;

(3) the loss rate of packets which have passed through the same node and gone through the output links;

(4) estimates made by the most recent CPs which have used the output links headed for some destination d of its estimated delay D_d and loss L_d from this node to its destination.

The value D_d is updated by each successive CP passing through the node and whose destination is d. Samples of the simulation results are given in Figures 16.15–16.18.

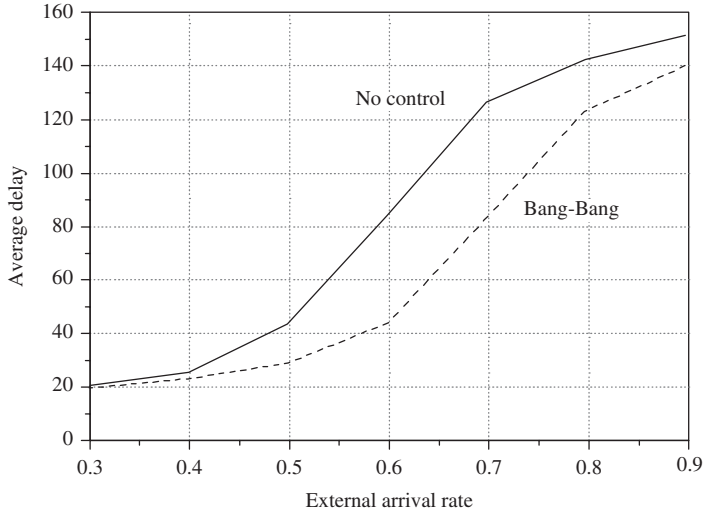

Figure 16.15 Comparison of average delay through the CPN with Bang-Bang control based on estimated delay.

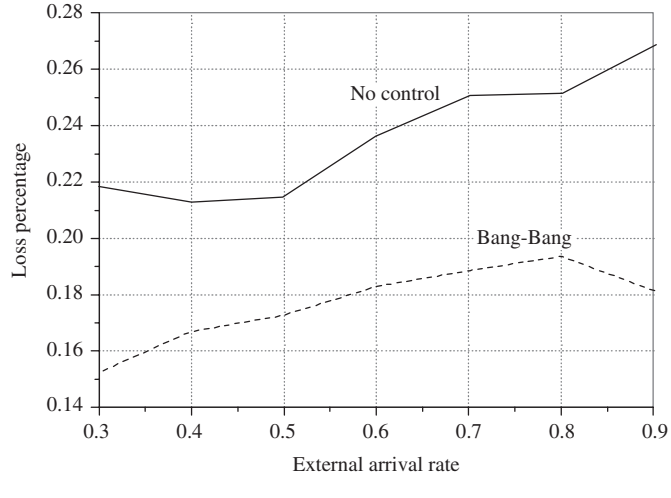

Figure 16.16 Comparison of average loss through the CPN with Bang-Bang control based on delay and loss.

16.6 GAME THEORY MODELS IN COGNITIVE RADIO NETWORKS

Game theory is a set of mathematical tools used to analyze interactive decision makers. We will show how these tools can be used in the analysis of cognitive networks [71–77]. The fundamental component of game theory is the concept of a game, formally expressed in *normal form* as [69, 70]:

$$G = \langle N, A, \{u_i\} \rangle$$

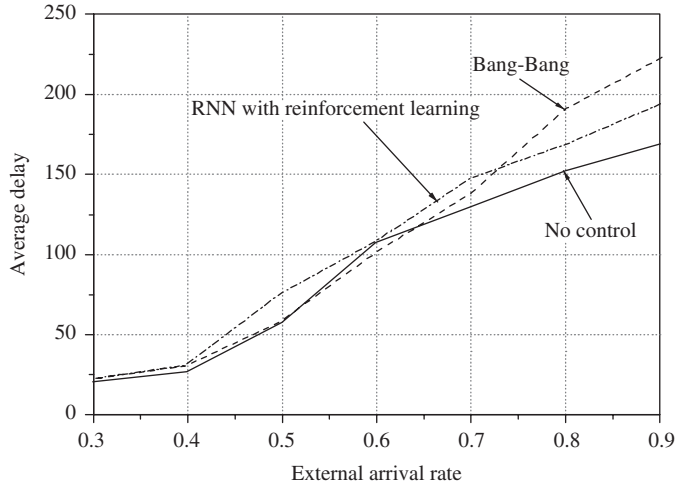

Figure 16.17 Comparison of average delay through the CPN with reinforcement learning-based control using delay and loss as the goal.

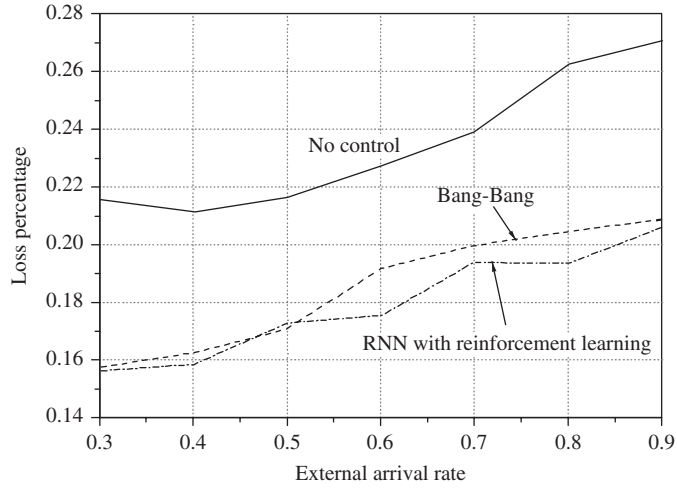

Figure 16.18 Comparison of average loss through the CPN with reinforcement learning-based control using delay and loss as the goal.

Where

(1) G is a particular game;

(2) $N = \{1, 2, \ldots, n\}$ is a finite set of players (decision makers);

(3) A_i is the set of actions available to player i;

(4) $A = A_1 \times A_2 \times \cdots \times A_n$ is the action space; and

(5) $\{u_i\} = \{u_1, u_2, \cdots, u_n\}$ is the set of utility (objective) functions that the players wish to maximize.

Each player's objective function, u_i, is a function of the particular action chosen by player i, a_i and the particular actions chosen by all of the other players in the game, a_{-i}, and yields a real number. Other games may include additional components, such as the information available to each player and communication mechanisms. In a *repeated game*, players are allowed to observe the actions of the other players, remember past actions, and attempt to predict future actions of players. An action vector a is said to be a *Nash equilibrium* (NE) if

$$u_i(a) \geq u_i(b_i, a_{-i}) \forall i \in N, b_i \in A_i \tag{16.6}$$

Restated, an NE is an action vector from which no player can profitably unilaterally deviate. NE correspond to the steady-states of the game and are then predicted as the most probable outcomes of the game.

A *repeated game* is a sequence of stages where each stage is the same normal form game. When the game has an infinite number of stages, the game is said to be an infinite horizon game. Players choose strategies (actions at each stage), based on their knowledge of the game-past actions, future expectations and current observations. These strategies can be fixed, contingent on the actions of other players or adaptive. These strategies can be also designed to punish players who deviate from agreed upon behavior. When punishment occurs, players choose their actions to minimize the payoff of the offending player. However, i is still able to achieve some payoff v_i. Thus there is a limit to the how much a player can be punished.

As estimations of future values of u_i are uncertain, many repeated games modify the original objective functions by discounting the expected payoffs in future stages by δ, where $0 < \delta < 1$ such that the anticipated value in stage k to player i is given by

$$u_{i,k}(a) = \delta^k u_i(a) \tag{16.7}$$

It can be shown that, in a repeated game with an infinite horizon and discounting, for every feasible payoff vector $v > v_i$ for all $i \in N$, there exists a $\delta < 1$ such that for all $\delta \in (\delta, 1)$ there is an NE with payoffs v (*Folk theorem* [69]). To generalize the Folk theorem, given a discounted infinite horizon repeated game, nearly any behavior can be designed to be the steady-state through the proper choice of punishment strategies and δ. Thus convergent behavior of a repeated game can be achieved nearly independent of the objective function.

A *myopic game* is defined as a repeated game in which there is no communication between the players, memory of past events or speculation of future events. Any adaptation by a player can still be based on knowledge of the current state of the game. As players have no consideration of future payoffs, the Folk theorem does not hold for myopic games and the convergence to steady-state behavior must occur through other means. Two convergence dynamics possible in a myopic game are the *best response dynamic* and the *better response dynamic*. Both dynamics require additional structure in the stage game to ensure convergence. Best response dynamic [70] refers to the case where, at each stage, one player $i \in N$ is permitted to deviate from a_i to some randomly selected action $b_i \in A_i$ if

$$u_i(b_i, a_{-i}) \geq u_i(c_i, a_{-i}) \forall c_i \neq b_i \in A_i \text{ and } u_i(b_i, a_{-i}) > u_i(a)$$

Better response dynamic [70] refers to the case where, at each stage, one player $i \in N$ is permitted to deviate from a_i to some randomly selected action $b_i \in A_i$ if $u_i(b_i, a_{-i}) > u_i(a_i, a_{-i})$.

An *S-modular game* restricts $\{u_j\}$ such that, for all $i \in N$, either Equation (16.8) or (16.9) is satisfied.

$$\frac{\partial^2 u_i(a)}{\partial a_i \partial a_j} \geq 0 \forall j \neq i \in N \tag{16.8}$$

$$\frac{\partial^2 u_i(a)}{\partial a_i \partial a_j} \leq 0 \forall j \neq i \in N \tag{16.9}$$

In the former case, the game is said to be *supermodular*; in the latter the game is said to be *submodular*. Myopic games whose stages are *S*-modular games with a unique NE and follow a best response dynamic converge to the NE when the NE is unique [71].

A *potential game* is a special type of game where $\{u_j\}$ are such that the change in value seen by a unilaterally deviating player is reflected in a function $P\colon A \to \Re$. All myopic games where the stages are the same potential game converge to a NE when decisions are updated according to a better response dynamic [70].

An *exact potential game* (EPG) is the game where there exists some function (EPF) $P\colon A \to \Re$ such that $\forall i \in N, \forall a \in A$

$$u_i(a_i, a_{-i}) - u_i(b_i, a_{-i}) = P(a_i, a_{-i}) - P(b_i, a_{-i}) \tag{16.10}$$

A necessary and sufficient condition for a game to be an exact potential game is [72]

$$\frac{\partial^2 u_i(a)}{\partial a_i \partial a_j} = \frac{\partial^2 u_j(a)}{\partial a_j \partial a_i} \forall i, j \in N, a \in A \tag{16.11}$$

Coordination-dummy game [72] is a composite of a coordination game with identical interest function V and a dummy game with dummy function D_i whose value is solely dependent on the actions of the other players and can be expressed as

$$u_i(a) = V(a) + D_i(a_{-i}) \tag{16.12}$$

An EPF for this game can be written as

$$P(a) = V(a) \tag{16.13}$$

Self-motivated games' utility functions are a function solely of that player's actions.

$$u_i(a) = h_i(a) \tag{16.14}$$

A self-motivated game can be shown to be an EPG by introducing the EPF as

$$P(a) = \sum\nolimits_{i \in N} h_i(a_i) \tag{16.15}$$

Bilateral symmetric interaction (BSI) game [73] refers to the case where every player's objective function can be characterized by

$$u_i(a) = \sum\nolimits_{j \in N \setminus \{i\}} w_{ij}(a_i, a_j) - h_i(a_i) \tag{16.16}$$

where $w_{ij}\colon A_i \times A_j \to \Re$ and $h_i\colon A_i \to \Re$ such that for every $(a_i, a_j) \in A_i \times A_j$, $w_{ij}(a_i, a_j) = w_{ji}(a_j, a_i)$. An EPF for a BSI game is given by

$$P(a) = \sum_{i \in N} \sum_{j=1}^{i-1} w_{ij}(a_i, a_j) - \sum_{i \in N} h_i(a_i) \tag{16.17}$$

Ordinal potential games (OPG) refer to the case where there exists some function (OPF) $P\colon A \to \Re$ such that, in addition to Equation (16.10), we also have

$$u_i(a_i, a_{-i}) > u_i(b_i, a_{-i}) \Leftrightarrow P(a_i, a_{-i}) > P(b_i, a_{-i}), \forall i \in N, \forall a \in A \tag{16.18}$$

All EPG are also OPG.

16.6.1 Cognitive radio networks as a game

The cognitive radios in the network form the game's set of decision makers. The set of physical layer parameters which a radio is permitted to alter forms the player's action set. From these

action sets, the action space is formed. Preference relations over the action space are formed by an exhaustive evaluation of the adaptation algorithms. Objective functions are then formed by mapping the preference relations to the real number line so that preferable action vectors are larger than less preferable action vectors.

16.6.1.1 Distributed power control

As an example we examine distributed power control algorithms within the context of CRNs [71, 74, 77]. Below, the following notation is used:

- N, the set of decision-making (cognitive) radios in the network;
- i,j, two different cognitive radios, $i, j \in N$;
- P_j, the set of power levels available to radio j; this is presumed to be a segment of the real number line $\Re$;
- p_j, a power level chosen by j from P_j;
- $\mathbf{P}$, the power space ($\Re^n$) formed from the Cartesian product of all P_j; $\mathbf{P} = P_1 \times P_2 \times \cdots P_n$;
- $\mathbf{p}$, a power profile (vector) from $\mathbf{P}$ formed as $\mathbf{p} = \{p_1, p_2, \cdots p_n\}$;
- $u_j(p)$, the utility that j receives from $\mathbf{p}$; this is the specific objective function that j is looking to maximize.

Based on these conventions, a power control game G can be formulated as $G = \langle N, P, \{u_j\}\rangle$.

16.6.1.2 Repeated power games

MacKenzie and Wicker [74] consider a discounted repeated power control game implemented on a packet-based network wherein the original objective function for each radio j is the modified function of throughput given as

$$u_j(\mathbf{p}) = R\left[1 - 2BER(\mathbf{p})\right]^L / p_j \tag{16.19}$$

where R is the transmission rate, L is the packet length and BER is the bit error rate which is a function of the SINR seen by j. As the modeled game has an infinite horizon, a CRN implemented in this manner will exhibit convergent behavior if:

(1) some mechanism exists for broadcasting the desired operating vector, the discount factor, and the punishment strategy;

(2) there is full knowledge of the environment so the radios can differentiate deviant behavior from fades and jammers external to the CRN;

(3) there is knowledge of the action chosen by each radio at each stage.

16.6.1.3 S-modular games

Altman and Altman [71] examines the application of super-modular games to distributed power control. Thus the objective functions for this game are characterized by Equations (16.8) and (16.9). Herein each game follows a general updating algorithm (GUA), which is actually a best response dynamic. Thus if these network games have a unique NE, behavior converges to the NE from any initial p. For a CRN which satisfies this characterization, the conditions for convergence are:

(1) The adaptation algorithms must incorporate perfect knowledge of the objective function.

(2) The network must have a unique steady state.

(3) Some method must exist for measuring current performance and for sensing relevant environmental parameters. Depending on the particular adaptation algorithm, it might be necessary to know the number and type of other radios in the network.

Altman and Altman [71] assert that the classes of power control algorithms considered in by Yates [75] are *S*-modular games. Yates examines power control in the context of the uplink of a cellular system under five scenarios:

(1) fixed assignment where each mobile is assigned to a particular base station;

(2) minimum power assignment where each mobile is assigned to the base station where its SINR is maximized;

(3) macro diversity where all base stations combine the signals of the mobiles;

(4) limited diversity where a subset of the base stations combine the signals of the mobiles; and

(5) multiple connection reception where the target SINR must be maintained at a number of base stations.

In each scenario, each mobile, j, tries to achieve a target SINR γ_j as measured by a function, $I(\mathbf{p})$. $I(\mathbf{p})$ is the standard effective interference function which has the following properties: (1) *positivity*, e.g. $I(\mathbf{p}) > 0$; (2) *monotonicity*, e.g. if $\mathbf{p} \geq \mathbf{p}^*$, then $I(\mathbf{p}) \geq I(p^*)$; (3) *scalability*, e.g. for all $\alpha > 1$, $\alpha I(\mathbf{p}) > I(\alpha \mathbf{p})$, where the convention that $\mathbf{p} > \mathbf{p}^*$ means that $\mathbf{p}_i > \mathbf{p}_i{}^* \forall i \in N$.

Single-cell target SINR games are also ordinal potential games. To prove it, consider a modified game where the action sets are the received power levels at the base station. A received power level for mobile j, r_j, is the product of its path loss to base station k, $h_{j,k}$, and its transmitted power level. Then the objective functions of a target SINR game can be expressed as

$$u_j(p) = 1 - \left\{ -\gamma_j + \left[r_j - \left(\sum_{i \in N \setminus j} r_i \right) - \sigma_k \right] \right\}^2 \tag{16.20}$$

where σ_k is the noise power at k. Expanding the above expression gives

$$u_j(\mathbf{p}) = 1 - \gamma_j^2 - \sigma_k^2 - 2\gamma_j\sigma_k - \left(\sum_{i \in N \setminus j} r_i \right)^2 - 2\gamma_j \left(\sum_{i \in N \setminus j} r_i \right) - 2\sigma_k \left(\sum_{i \in N \setminus j} r_i \right)$$

$$-r_j^2 + 2\gamma_j r_j + 2\sigma_k r_j + 2r_j \left(\sum_{i \in N \setminus j} r_i \right) \tag{16.21}$$

The first line of Equation (16.21) is a dummy game; the following three terms in Equation (16.21) are a self-motivated game, EPG. The final term is also an EPG as it is a BSI game. Since a composite game formed from a linear combination of two EPGs is itself an EPG, it is seen that the target SINR game is an EPG. As other forms of target SINR games are ordinal transformations (OT) of Equation (16.21), all target SINR games are OPG, since OT of an OPG is an OPG. It can be also shown that all target throughput power control games are OPG (all throughput maximization power control games are OPG).

16.6.1.4 Nonlinear group pricing

Goodman and Mandayam [76] consider a scenario wherein mobile devices are trying to maximize a function of their throughput. Note that the only NE of games whose utility functions are pure throughput function is the power vector where all mobiles transmit at maximum power. To avoid this problem, Goodman and Mandayam [76] introduce the modified throughput function as

$$u_j(\mathbf{p}) = \frac{BT(\mathbf{p})}{p_j} - cRp_j \tag{16.22}$$

where R is the transmission rate, c is a constant, B is the battery life, and T is the throughput function. This can neither be shown to be an OPG nor an OPG. The left-most term is generally only an OPG, whereas the pricing function is an EPG as it is a self-motivated game.

Goodman and Mandayam [76] use a best response dynamic in their experiments, which converge to a NE. Although not stated in Goodman and Mandayam [76], Saraydar *et al.* [78] show that Equation (16.22) is indeed a supermodular game. Also note that, without the cost function, Equation (16.19) is a particular instance of Equation (16.22). So a CRN implementing the repeated games of References [74], [76] or [78] is a supermodular game and will exhibit convergent behavior if the properties specified above for S-modular games are satisfied. However, it should be noted that, when left as a repeated game, there is greater flexibility in dynamically selecting the steady-state.

16.6.1.5 Nonlinear group pricing

Sung and Wong [77] consider another single cell distributed power control game with pricing characterized by

$$u_j(\mathbf{p}) = R_j T(\mathbf{p}) - \frac{\lambda h_j p_j}{\sum_{i\in N} h_i p_i} \tag{16.23}$$

where λ is a constant and the base station subscript has been dropped in this case as all mobiles are communicating with the same base station. The pricing function is to reflect that the damage caused by p_j to the other devices in the network is a function of the relative difference in powers rather than absolute power level. Note that Equation (16.23) is just a composite game of throughput maximization and a cost function. As we have indicated that throughput maximization is an OPG, Equation (16.23) can only be guaranteed to be an OPG only if, though not necessarily if, the pricing function has an EPF which can only be true if Equation (16.11) is satisfied. Differentiating the price function twice yields:

$$\frac{\partial^2 C_i}{\partial p_i \partial p_j} = \frac{\left(\sum_{k\in N} h_k p_k\right)^2 \lambda h_i h_j - 2h_j \left(\sum_{k\in N} h_k p_k\right) g_i(\mathbf{p})}{\left(\sum_{k\in N} h_k p_k\right)^4}$$

$$\frac{\partial^2 C_j}{\partial p_j \partial p_i} = \frac{\left(\sum_{k\in N} h_k p_k\right)^2 \lambda h_i h_j - 2h_i \left(\sum_{k\in N} h_k p_k\right) g_j(\mathbf{p})}{\left(\sum_{k\in N} h_k p_k\right)^4}$$

where $g_i(\mathbf{p}) = \lambda h_i \sum_{k\in N} h_k p_k - \lambda h_i^2 p_i$. Further evaluation leads to the result that this price function has an EPF if $h_j p_j = h_i p_i$. Note that this is only satisfied when the received powers are identical, which will generally not be true. Thus the cost function does not have an EPF and the nonlinear group priced game is not an OPG. Also note that Equation (16.23) cannot be guaranteed to be a supermodular game either as properly chosen power vectors p and p^* will yield different signs for the second partial derivative of the cost functions.

Therefore neither the better response dynamic nor the best response dynamic will assuredly converge, and a more complex convergence dynamic is required. As the repeated game dynamic is guaranteed for convergence, it can still be used. Thus this modification of the pricing function significantly complicated the network.

Additional examples of game theory applications in resource allocation modeling can be found in References [116–127] and routing in [79–115].

16.7 BIOLOGICALLY INSPIRED NETWORKS

Current Internet protocols were never planned for the emerging pervasive environments where the amount of information will be enormous. The communications requirements placed by these protocols on the low cost sensor and tag nodes are in direct contradiction to the fundamental goals of these nodes, being small, inexpensive and maintenance-free. Biological systems provide insights into principles which can be adopted to completely redefine the basic concepts of control, structure, interaction and function of the emerging pervasive environments. The study of the rules of genetics and evolution combined with mobility leads to the definition of service-oriented communication systems which are autonomous and autonomously self-adaptive. Based on References [128–131] in this section we discuss how this paradigm shift, which views a network only as a randomly self-organizing by-product of a collection of self-optimizing services, may become the enabler of the new world of omnipresent low cost pervasive environments of the future.

16.7.1 Bio-analogies

In Carreras *et al.* [131] the depicted scenario services are associated with living organisms. Service is defined by chromosomes. In this way service evolves and adapts to the environment constantly and autonomously. By analogy with living organisms, chromosomes are collections of *genes* that are the smallest service (related) data unit and inborn intelligence/instincts and thus represent all the information needed for the organism to function and service to be executed. Like in nature, this concept defines a complete life-cycle of the organisms and therefore of services. The life cycle starts from the birth of an organism, goes through the reproduction and ends with the death. *Reproduction and evolution* occur, applying evolution rules inherited from nature. Fitness is measuring the correspondence of the organism's genetic information with the environment and determines the exchange of information (genetic information). Therefore no-end-to-end communication concept exists in these systems. Information is only exchanged as needed, locally, between mating organisms.

Environment is determining the *natural selection* based on the *fitness* of the organisms, with the environment leading to the best services possible as a function of the environment. In this concept *the service is the organism.* A scenario is envisioned where users will be more and more interested in a service able to provide reliable localized information. The role of the service will be, for instance, to provide answers to questions like *How is the weather around the train station?* or *Where will I find a free parking space around there?* Services will be hosted on users' devices and will go around through the physical movement of the users. Each service is constituted by a program and its related data that is organized into *chromosomes.* Each chromosome consists of:

(1) data that is the genetic information of the organism, organized in *genes*;

(2) a *plugin* that stores a syntax notation describing the actions dictated by the chromosome and the fitness (degree of attraction) operator yielding *natural selection* through preferred *mating*;

Genes are a tuple of information and consist of: (a) *value*; (b) *timing information*; (c) *information source ID/location information*; and (d) *other data depending on the service*.

Organisms are diploid, which means that there is always two homologous chromosomes associated with each service. The two homologous chromosomes have the same genes but in different forms. Alleles are different forms of the same gene and correspond to different values in the tuple of gene information. They may differ in timing information or in the source value information. Each allele may be dominant or recessive depending on the service behavior. Having two chromosomes allows us to estimate the reliability of the data. We would probably always choose the youngest data value to be the actual one if it is a parking lot, but we might also average the sensor data if it represents temperature.

The choice of the preferred value among the two reflects the concept of dominant and recessive genes. As in nature, recessive information enables the service to survive in different environments, providing the service with higher resilience against data corruption and fraud, and may even allow for additional features. Analogy with the *life cycle* is also possible. In this concept service is born when the user downloads the chromosome onto his device. From that moment on, the user is able to interact with the other organisms (i.e. users carrying chromosomes) and with the environment where the users are physically moving. When gathering information from the environment the service *grows*. While growing, the service improves its functionalities, meaning that it becomes able to increase performance. When a user meets another user while moving, services may reproduce and produce offspring. It is in this phase that evolution and natural selection occur. In order to be able to reproduce the service must satisfy some fitness requirements, since it is not willing to spread useless information. We assume a service to be dead when it cannot reproduce anymore.

Analogies with *birth*, *growth*, *reproduction* and *death* are even further elaborated in this concept. As we have already said, the service is born when the user obtains (downloads) an empty chromosome of a certain service that consists only of the plugin. From that instant on the user can read data from sensors and use the syntax definition from the plugin. At this stage the user is haploid, i.e. it has only one chromosome per service. When reading sensor data, the user fills the chromosomes both at the same time. This information is in any case more reliable than the previous information on the chromosomes.

The concept of mating is performed the following way: in *meiosis*, the diploid cell splits into two haploid reproductive cells (the eggs or sperm). In real life, four haploid cells would appear because of one step of copying the chromosomes, including cross-over. Each two copies would be identical. This means that the chromosome pair is being split and copied. Two packets are sent out one after another containing one chromosome each. In the best case when all the sent packets reach the receiver, it has four different combinations of the chromosome pairs. This is the best case; the user may for energy reasons decide to send out only one chromosome, or receive only one because of packet loss. A selection has to take place to decide which of these combinations survives. This selection could be influenced by the quality of the plugin (by the version number). Having such a selection can help to spread new versions of plugins. It also may help to repair broken chromosomes (that were damaged during the wireless transmission). In a sense, we allow for truly spontaneous mutations and we may even find that mutations spread. It remains to be seen if this is any good. The selection occurs as a consequence of localization and age. The fitness of a chromosome is defined as the average of the timing information of the genes weighted with the localization information. In this sense the environment participates in the selection, since the survival of a service also depends on where the user is (but not only) when he mates with another user.

If the sensor data in the chromosome is too old, it is very likely useless. Thus we forbid sending out the chromosome after a certain threshold (coded in the plugin). This way the chromosome can die, but it may be reborn through reading new sensor data or receiving a fresh chromosome. The service is considered *alive* as long as it is able to answer to questions. Death is therefore a consequence of outdated chromosomal information (sensor-gathered information is aging). It is in the interest of the user to exchange information and to gather sensor information and this same interest drives the service *instinct to survive*. This defines a complete life cycle of the service.

As an example of the environmental monitoring applications, Carreras *et al.* [132] describe a parking lot finding application as a possible application scenario of the above concept for the nomadic sensor network:

> *Each parking spot in a city is equipped with a sensor that is capable of notifying whether the parking lot is free or not together with its geographical position (or ID). Each user subscribing to the service is equipped with a hand-held device that communicates both with the sensor nodes and with other users who subscribed to the service. The users, while moving around the city, collect information on the status (free/not free) of the parking lots they encounter on their way. This information is stored in their devices, together with a time stamp of when the information has been collected. Whenever two users come into communication range, they exchange their knowledge of the parking lot status (and update their own if the information is 'fresh' enough). The basic service of the system to the user would be the assistance in finding the nearest parking lot. The user queries his device (which might be some PDA), asking for the nearest free parking lot in a specific area of the city. The device will provide this information based on the data that has stored so far. Of course, the information cannot be considered real-time.*

16.7.2 Bionet architecture

The bio-networking architecture [130–134] applies key concepts and mechanisms described above to design network applications. One of the key concepts in biological systems is emergence. In biological systems, beneficial system properties (e.g. adaptability) often emerge through the simple and autonomous interactions among diverse biological entities (see the above example). The bio-networking architecture applies the concept of emergence by implementing network applications as a group of distributed, autonomous and diverse objects called cyber-entities (CEs). In Itao *et al.* [134], analogy to a bee colony (a network application) consisting of multiple bees (CEs) is used. Each CE implements a functional service related to the application and follows simple behaviors similar to biological entities, such as *reproduction*, *death*, *migration and environment sensing*, as discussed in the previous section.

In the bio-networking architecture, CEs are designed based on the three principles described below in order to interact and collectively provide network applications that are autonomous, scalable, adaptive, and simple.

(1) *CEs are decentralized* – there are no central entities to control and coordinate CEs (i.e. no directory servers and no resource managers). Decentralization allows network applications to be scalable and simple by avoiding a single point of performance bottleneck and failure and by avoiding any central coordination in developing and deploying CEs.

(2) *CEs are autonomous* – CEs monitor their local network environments, and based on the monitored environmental conditions, they autonomously interact without any intervention from human users or from other controlling entities.

(3) *CEs are adaptive* to dynamically changing environnemental conditions (e.g. user demandes, user locations and resource availability) over the short- and long-term.

The bionet platform described in Suzuki *et al.* [130], and presented in Figure 16.19, provides an execution environment for CEs. It consists of two types of software components. The first type of components, *supporting components*, abstracts low-level operating and networking details (e.g.

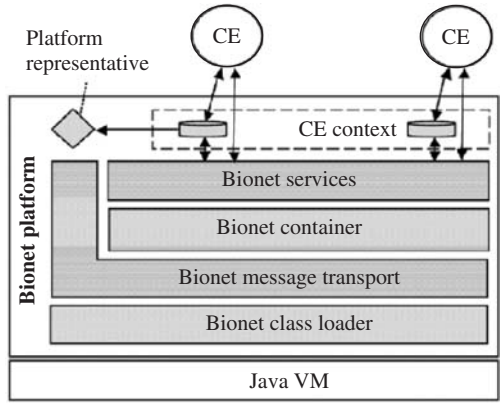

CE, cyber-entity.

Figure 16.19 Bionet platform architecture. (Reproduced by permission of IEEE [130].)

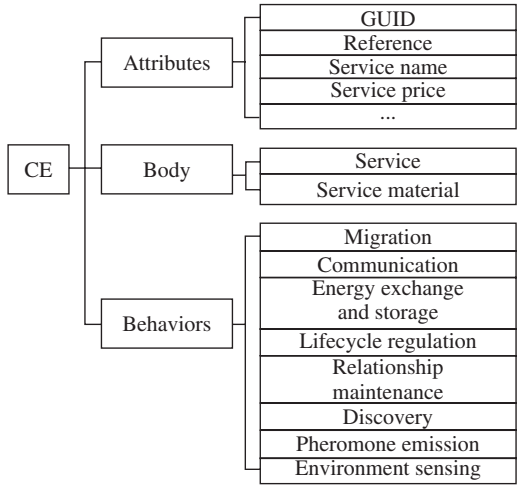

Figure 16.20 Design of a CE.

network I/O and concurrency control for executing CEs). The second type of components, *runtime components*, provides runtime services that CEs use to perform their services and behaviours. The bionet platform is implemented in Java, and each bionet platform runs on a Java virtual machine (JVM). Each CE is implemented as a Java object and runs on a bionet platform.

As shown in Figure 16.20, a CE consists of three main segment: *attributes, body* and *behaviours*. *Attributes* carry descriptive information regarding the CE (e.g. CE ID and description of a service it provides). The *body* implements a service that the CE provides and contains materials relevant to the service (e.g. data, application code or user profiles). CE *behaviors* implement nonservice-related actions that are inherent to all CEs. Examples of behavior include migration, reproduction and energy exchange. More information on different segments of the architecture can be found in Suzuki *et al.* [130].

REFERENCES

[1] D.S. Alexander, M. Shaw, S. Nettles and J. Smith, Active bridging, in *Proc. ACM SIGCOMM Conf.*, 1997, pp. 101–111.

[2] B. Schwartz, A.W. Jackson, W.T. Strayer, W. Zhou, D. Rockwell and C. Partridge, Smart packets for active networks, *ACM Trans. Comput. Syst.*, vol. 18, no. 1, 2000, pp. 67–88.

[3] D. Tennenhouse and D. Wetherall, Toward an active network architecture, *Comput. Commun. Rev.*, vol. 26, no. 2, 1996.

[4] D.L. Tennenhouse, J.M. Smith, W.D. Sincoskie, D.J. Wetherall and G.J. Minden, A survey of active network research, *IEEE Commun.*, vol. 35, 1997, pp. 80–86.

[5] D.S. Alexander, W.A. Arbaugh, M.W. Hicks, P. Kakkar, A.D. Keromytis, J.T. Moore, C.A. Gunter, S.M. Nettles and J.M. Smith, The SwitchWare active network architecture, *IEEE Network*, 1998, pp. 29–36.

[6] *FAIN – Future Active IP Networks*. Available at: www.ist-fain.org/publications/publications.html

[7] B. Carpenter and S. Brim, *Middleboxes: Taxonomy and Issues*. Internet Engineering Task Force, RFC 3234. Available at: www.iets.org, February 2002.

[8] T. Hain, *Architectural Implications of NAT*. Internet RFC 2993, Available at: www.iets.org, November 2000.

[9] P. Srisuresh and K. Egevang, *Traditional IP Network Address Translator* (*Traditional NAT*). Internet RFC 3022. Available at: www.iets.org, January 2001.

[10] M. Holdrege and P. Srisuresh, *Protocol Complications With the IP Network Address Translator*. Internet RFC 3027. Available at: www.iets.org, January 2001.

[11] G. Tsirtsis and P. Srisuresh, *Network Address Translation – Protocol Translation* (*NAT-PT*). Internet RFC 2766. Available at: www.iets.org, February 2000.

[12] M. Leech, M. Ganis, Y. Lee, R. Kuris, D. Koblas and L. Jones, *SOCKS Protocol Version 5*. Internet RFC 1928. Available at: www.iets.org, March 1996.

[13] S. Blake, D. Black, M. Carlson, E. Davies, Z. Wang and W. Weiss, *An Architecture for Differentiated Service*. Internet RFC 2475. Available at: www.iets.org, December 1998.

[14] J. Border, M. Kojo, J. Griner, G. Montenegro and Z. Shelby, *Performance Enhancing Proxies Intended to Mitigate Link-Related Degradations*. Internet RFC 3135. Available at: www.iets.org, June 2001.

[15] N. Freed, *Behavior of and Requirements for Internet Fire-Walls*. Internet RFC 2979. Available at: www.iets.org, October 2000.

[16] B. Cheswick and S. Bellovin, *Firewalls and Internet Security: Repelling the Wily Hacker*. Addison-Wesley: Reading, MA, 1994.

[17] M. Handley, H. Schulzrinne, E. Schooler and J. Rosenberg, *SIP: Session Initiation Protocol*. Internet RFC 2543. Available at: www.iets.org, March 1999.

[18] F. Cuervo, N. Greene, A. Rayhan, C. Huitema, B. Rosen and J. Segers, *Megaco Protocol 1.0*. Internet RFC 3015. Available at: www.iets.org, November 2000.

[19] R. Fielding, J. Gettys, J. Mogul, H. Frystyk, L. Masinter, P. Leach and T. Berners-Lee. *Hypertext Transfer Protocol* – HTTP/1.1. Internet RFC 2616. Available at: www.iets.org, June 1999.

[20] IETF Forwarding Control Element Separation Working Group Home Page; www.ietf.org/html.charters/forces-charter.html

[21] C. Partridge, A.C. Snoeren, W.T. Strayer, B. Schwartz, M. Condell and I. Castineyra, FIRE: flexible intra-AS routing environment, *IEEE J. Select. Areas Commun.*, vol. 19, no. 3, 2001, pp. 410–425.

[22] J. Biswas, A.A. Lazer, J.-F. Huard, K. Lim, H. Mahjoub, L.-F. Pau, M. Suzuki, S. Torstensson, W. Wang and S. Weinstein, The IEEE P1520 standards initiative for programmable network interfaces, *IEEE Commun. Mag.*, vol. 36, no. 10, 1998, pp. 64–70.

[23] IEEE P1520.2, *Draft 2.2, Standard for Application Programming Interfaces for ATM Networks*. Available at: www.ieee-pin.org/pin-atm/intro.html
[24] IETF ForCES; www.ietf.org/html.charters/forces-charter.html
[25] IETF For CES, *Draft-IETF-Forces-Framework-04.txt*. Available at: www.ietf.org/internet-drafts/draft-ietf-forces-framework-04.txt, 2002.
[26] D.J. Wetherall, J.V. Guttag and D.L. Tennenhouse, *ANTS: a Toolkit For Building and Dynamically Deploying Network Protocols IEEE Openarch*. Available at: ftp://ftp.tns.lcs.mit.edu/pub/papers/openarch98.ps.gz, 1998.
[27] D. Decasper, G. Parulkar, S. Choi, J. DeHart, T. Wolf and B. Plattner, *A Scalable, High Performance Active Network Node IEEE Network*. Available at: www.tik.ee.ethz.ch/∼dan/papers/ieee_ann_1.pdf
[28] B. Schwartz, A.W. Jackson, W.T. Strayer, W. Zhou, D. Rockwell and C. Partridge, *Smart Packets for Active Networks OPENARCH'99*. Available at: ftp://ftp.bbn.com/pub/AIR/smart.ps, 1999.
[29] D. Scott Alexander, W.A. Arbaugh, M.W. Hicks, P. Kakkar, A.D. Keromytis, J.T. Moore, C.A. Gunter, S.M. Nettles and J.M. Smith, The switchware active network architecture, *IEEE Network*, vol. 12, 1998, pp. 29–36.
[30] K.L. Calvert (ed.), *Architectural Framework for Active Networks Draft Version 1.0*. Available at: protocols.netlab.uky.edu/∼calvert/arch-latest.ps, 1999.
[31] L. Peterson (ed.), *Node OS interface specification AN node OS working group*. Available at: www.cs.princeton.edu/nsg/papers/nodeos-02. ps, 2001.
[32] K. Calvert, S. Bhattacharjee, E. Zegura and J. Sterbenz, Directions in active networks, *IEEE Commun.*, vol. 36, 1998, pp. 72–78.
[33] A.T. Campbell, H. De Meer, M.E. Kounavis, K. Miki, J. Vicente and D. Villela, A survey of programmable networks. *ACM Comput. Commun. Rev.* April, 1999.
[34] *Initial Active Network and Active Node Architecture FAIN Project Deliverable* 2. Available at: www.ist-fain.org/deliverables/del2/d2.pdf
[35] *Revised Active Network and Active Node Architecture FAIN Project Deliverable* 4. Available at: www.ist-fain.org/deliverables/del4/d4.pdf
[36] S.-K. Song *et al*., *Evolution in Action: Using Active Networking to Evolve Network Support for Mobility*, J. Sterbenz *et al*. (eds). IWAN 2002. LNCS 2546, Springer: Berlin, 2002, pp. 146–161.
[37] C. Prehofer and Q. Wei, *Active Networks for 4G Mobile Communication:Motivation, Architecture, and Application Scenarios*, J. Sterbenz *et al*. (eds). IWAN 2002, LNCS 2546. Springer: Berlin, 2002, pp. 132–145.
[38] D.J. Wetherall, J. Guttag and D.L. Tennenhouse. ANTS: a toolkit for building and dynamically deploying network protocols, in *IEEE OPENARCH*, April 1998, pp. 117–129.
[39] B. Schwartz, A.W. Jackson, W.T. Strayer, W. Zhou, R.D. Rockwell and C. Partridge. Smart packets: Applying active networks to network management, *ACM Trans. Comput. Systems*, vol. 18, no. 1, February 2000.
[40] M. Hicks, P. Kakkar, J.T. Moore, C.A. Gunter and S. Nettles. PLAN: a packet language for active networks, in *Proc. Third ACM SIGPLAN Int. Conf. Functional Programming*. ACM, 1998, pp. 86–93.
[41] WWRF, Wireless World Research Forum (WWRF); www.wireless-worldresearch. org/
[42] M. Kounavis and A. Campbell, *Design, Implementation and Evaluation of Programmable Handoff in Mobile Networks, Mobile Networks and Applications*, vol. 6. Kluwer Academic: Norwell, MA, 2001, pp. 443–461.
[43] H.J. Wang, R.H. Katz and J. Giese, Policy-enabled handoffs across heterogeneous wireless networks, in *WMCSA* 99, New Orleans, LA, 25–26 February 1999, pp. 51–60.
[44] E. Gelenbe, Z. Xu and E. Seref, Cognitive packet networks, *11th IEEE Int. Conf. Tools with Artificial Intelligence*, 9–11 November 1999, pp. 47–54.

[45] E. Gelenbe, R. Lent and A. Nunez, Self-aware networks and QoS, *Proc. IEEE*, vol. 92, no. 9, 2004, pp. 1478–1489.
[46] R.E. Ramos and K. Madani, A novel generic distributed intelligent re-configurable mobile network architecture, in *IEEE VTS 53rd Vehicular Technology Conf.* vol. 3, 6–9 May 2001, pp. 1927–1931.
[47] T. Kocak and J. Seeber, Smart packet processor design for the cognitive packet network router, in *The 2002 45th Midwest Symp. Circuits and Systems, MWSCAS-2002*, vol. 2, 4–7 August 2002, pp. II–513–II-516.
[48] X. Hu, A.N. Zincir-Heywood and M.I. Heywood, Testing a cognitive packet concept on a LAN, in *IEEE CCECE 2002. Canadian Conf. Electrical and Computer Engineering*, vol. 3, 12–15 May 2002, pp. 1577–1582.
[49] Y. Miao, Z.-Q. Liu, C.K. Siew and C.Y. Miao, Dynamical cognitive network – an extension of fuzzy cognitive map, *IEEE Trans. Fuzzy Syst.*, vol. 9, no. 5, 2001, pp. 760–770.
[50] J. Neel, R.M. Buehrer, B.H. Reed and R.P. Gilles, Game theoretic analysis of a network of cognitive radios, in *The 2002 45th Midwest Symp. Circuits and Systems. MWSCAS-2002*, vol. 3, 4–7 August 2002, pp. III–409–III-412.
[51] E. Gelenbe, M. Gellman, R. Lent, P. Liu and P. Su, Autonomous smart routing for network QoS, in *Int. Conf. Autonomic Computing*, 17–18 May 2004, pp. 232–239.
[52] W.-R. Zhang, S.-S. Chen, W. Wang and R.S. King, A cognitive-map-based approach to the coordination of distributed cooperative agents, *IEEE Trans. Syst. Man Cybernet.*, vol. 22, no. 1, 1992, pp. 103–114.
[53] J.O. Neel, J.H. Reed and R.P. Gilles, Convergence of cognitive radio networks, in *2004 IEEE Wireless Communications and Networking Conf., WCNC*, vol. 4, 21–25 March 2004, pp. 2250–2255.
[54] P. Mahonen, Cognitive trends in making: future of networks, in *15th IEEE Int. Symp. Personal, Indoor and Mobile Radio Communications, PIMRC 2004*, vol. 2, 5–8 September 2004, pp. 1449–1454.
[55] R. Viswanathan and K.S. Narendra, Comparison of expedient and optimal reinforcement schemes for learning systems, *J. Cybernet.* vol. 2, 1972, pp. 21–37.
[56] K.S. Narendra and P. Mars, The use of learning algorithms in telephone traffic routing – a methodology, *Automatica*, vol. 19, 1983, pp. 495–502.
[57] E. Gelenbe, Learning in the recurrent random neural network, *Neural Comput.*, vol. 5, no. 1, 1993, pp. 154–164.
[58] P. Mars, J.R. Chen and R. Nambiar, *Learning Algorithms: Theory and Applications in Signal Processing, Control and Communications*. CRC Press: Boca Raton, FL, 1996.
[59] D.L. Tennenhouse, J.M. Smith, D.W. Sincoskie, D.J. Wetherall and G.J. Minden, A survey of active network research, *IEEE Commun. Mag.*, vol. 35, no. 1, 1997, pp. 80–86.
[60] M. Bregust and T. Magedanz, Mobile agents-enabling technology for active intelligent network implementation, *IEEE Network Mag.*, vol. 12, no. 3, 1998, pp. 53–60.
[61] T. Faber, ACC: using active networking to enhance feedback congestion control mechanisms, *IEEE Network Mag.*, vol. 12, no. 3, 1998, pp. 61–65.
[62] S. Rooney, J.E. van der Merwe, S.A. Crosby and I.M. Leslie, The tempest: a framework for safe, resource-assured, programmable networks, *IEEE Commun. Mag.* vol. 36, no. 10, 1998, pp. 42–53.
[63] J.-F. Huard and A.A. Lazar, A programmable transport architecture with QoS guarantee, *IEEE Commun.*, vol. 36, no. 10, 1998, pp. 54–63.
[64] J. Biswas, A.A. Lazar, S. Mahjoub, L.-F. Pau, M. Suzuki, S. Torstensson, W. Wang and S. Weinstein, The IEEE P1520 standards initiative for programmable network interface, *IEEE Commun.*, vol. 36, no. 10, 1998, pp. 64–72.
[65] K.L. Calvert, S. Bhattacharjee, E. Zegura and J. Sterbenz, Directions in active networks, *IEEE Commun.*, vol. 36, no. 10, 1998, pp. 64–72.

[66] W. Marcus, I. Hadzic, A.J. McAuley and J.M. Smith Protocol boosters: applying programmability to network infrastructures, *IEEE Commun.*, vol. 36, no. 10, 1998, pp. 79–83.
[67] D.S. Alexander, W.A. Arbaugh, A.D. Keromytis and J.M. Smith, Safety and security of programmable networks infrastructures, *IEEE Commun.*, vol. 36, no. 10, 1998, pp. 84–92.
[68] E. Gelenbe, Zhi-Hong Mao and Y. Da-Li, Function approximation with spiked random networks, *IEEE Trans. Neural Networks*, vol. 10, no. 1, 1999, pp. 3–9.
[69] D. Fudenberg and J. Tirole, *Game Theory*. MIT Press: Cambridge, MA, 1991.
[70] J. Friedman and C. Mezzetti, Learning in games by random sampling, *J. Econ. Theory*, vol. 98, 2001, pp. 55–84.
[71] E. Altman and Z. Altman. *S*-modular games and power control in wireless networks, *IEEE Trans. Autom. Control*, vol. 48, 2003, pp. 839–842.
[72] D. Monderer and L. Shapley, Potential games, *Games Econ. Behav.*, vol. 14, 1996, pp. 124–143.
[73] T. Ui, A shapley value representation of potential games, *Games Econ. Behav.*, vol. 14, 2000, pp. 121–135.
[74] A. MacKenzie and S. Wicker, Game theory in communications: motivation, explanation, and application to power control, in *Globecom 2001*, pp. 821–825.
[75] R. Yates, A framework for uplink power control in cellular radio systems, *IEEE J. Select. Areas Commun.*, vol. 13, no. 7, 1995, pp. 1341–1347.
[76] D. Goodman and N. Mandayam. Power control for wireless data, *IEEE Person. Commun.*, April 2000, pp. 48–54.
[77] C. Sung and W. Wong, A noncooperative power control game for multirate CDMA data networks, *IEEE Trans. Wireless Commun.*, vol. 2, no. 1, 2003, pp. 186–219.
[78] C. Saraydar, N. Mandayam and D. Goodman, Pareto efficiency of pricing-based power control in wireless data networks, *Wireless Commun. Networking Conf.*, 21–24 September 1999, pp. 231–235.
[79] J.P. Hespanha and S. Bohacek, Preliminary results in routing games, in *Proc. 2001 American Control Conf.*, vol. 3, 25–27 June 2001, pp. 1904–1909.
[80] R. Kannan and S.S. Iyengar, Game-theoretic models for reliable path-length and energy-constrained routing with data aggregation in wireless sensor networks, *IEEE J. Select. Areas Commun.*, vol. 22, no. 6, 2004, pp. 1141–1150.
[81] V. Anantharam, On the Nash dynamics of congestion games with player-specific utility, in *43rd IEEE Conf. Decision and Control*, *CDC*, vol. 5, 14–17 December 2004, pp. 4673–4678.
[82] A.A. Economides and J.A. Silvester, A game theory approach to cooperative and non-cooperative routing problems, in *SBT/IEEE Int. Telecommunications Symp. ITS '90 Symposium Record*, 3–6 September 1990, pp. 597–601.
[83] A.A. Economides and J.A. Silvester, Multi-objective routing in integrated services networks: a game theory approach, in *INFOCOM '91. Tenth Annual Joint Conf. IEEE Computer and Communications Societies. Networking in the 90s*, 7–11 April 1991, vol. 3. IEEE: New York, 1991, pp. 1220–1227.
[84] J. Cai and U. Pooch, Play alone or together – truthful and efficient routing in wireless *ad hoc* networks with selfish nodes, in *2004 IEEE Int. Conf. Mobile Ad-hoc and Sensor Systems*, 25–27 October 2004, pp. 457–465.
[85] I. Sahin and M.A. Simaan, A game theoretic flow and routing control policy for two-node parallel link communication networks with multiple users, in *15th IEEE Int. Symp. Personal, Indoor and Mobile Radio Communications*, *PIMRC 2004*, vol. 4, 5–8 September 2004, pp. 2478–2482.
[86] E. Altman, T. Basar and R. Srikant, Nash equilibria for combined flow control and routing in networks: asymptotic behavior for a large number of users, *IEEE Trans. Autom. Control*, vol. 47, no. 6, 2002, pp. 917–930.

[87] T. Boulogne, E. Altman, H. Kameda and O. Pourtallier, Mixed equilibrium (ME) for multiclass routing games, *IEEE Trans. Autom. Control*, vol. 47, no. 6, 2002, pp. 903–916.

[88] A. Orda, R. Rom and N. Shimkin, Competitive routing in multi-user communication networks, in *INFOCOM '93. IEEE Twelfth Annual Joint Conf. IEEE Computer and Communications Societies. Networking: Foundation for the Future*, 28 March to 1 April 1993, vol. 3, pp. 964–971.

[89] C.-H. Yeh and E.A. Varvarigos, A mathematical game and its applications to the design of interconnection networks, in *Int. Conf. Parallel Processing*, 3–7 September 2001, pp. 21–30.

[90] E. Altman and H. Kameda, Equilibria for multiclass routing in multi-agent networks, in *IEEE Conf. Decision and Control*, vol. 1, 4–7 December 2001, pp. 604–609.

[91] V. Marbukh, QoS routing under adversarial binary uncertainty, in *IEEE Int. Conf. Communications*, *ICC 2002*, vol. 4, 28 April to 2 May 2002, pp. 2268–2272.

[92] R.J. La and V. Anantharam, Optimal routing control: repeated game approach, *IEEE Trans. Autom. Control*, vol. 47, no. 3, 2002, pp. 437–450.

[93] R.J. La and V. Anantharam, Optimal routing control: game theoretic approach, in *IEEE Conf. Decision and Control*, vol. 3, 10–12 December 1997, pp. 2910–2915.

[94] Y.A. Korilis, A.A. Lazar and A. Orda, Capacity allocation under noncooperative routing, *IEEE Trans. Autom. Control*, vol. 42, no. 3, 1997, pp. 309–325.

[95] W. Wang, X.-Y. Li and O. Frieder, *k*-Anycast game in selfish networks, in *Int. Conf. Computer Communications and Networks*, 11–13 October 2004, pp. 289–294.

[96] V. Marbukh, Minimum cost routing: robustness through randomization, in *IEEE Int. Symp. Information Theory*, 2002, p. 127.

[97] R.E. Azouzi, E. Altman and O. Pourtallier, Properties of equilibria in competitive routing with several user types, in *IEEE Conf. Decision and Control*, vol. 4, 10–13 December 2002, pp. 3646–3651.

[98] O. Kabranov, A. Yassine and D. Makrakis, Game theoretic pricing and optimal routing in optical networks, in *Int. Conf. Communication Technology Proc.*, vol. 1, 9–11 April 2003, pp. 604–607.

[99] M. Kodialam and T.V. Lakshman, Detecting network intrusions via sampling: a game theoretic approach, in *IEEE Joint Conf. IEEE Computer and Communications Societies, INFOCOM 2003*. vol. 3, 30 March to 3 April 2003, pp. 1880–1889.

[100] J. Zander, Jamming in slotted ALOHA multihop packet radio networks, *IEEE Trans. Commun.*, vol. 39, no. 10, 1991, pp. 1525–1531.

[101] O. Ercetin and L. Tassiulas, Market-based resource allocation for content delivery in the Internet, *IEEE Trans. Comput.*, vol. 52, no. 12, 2003, pp. 1573–1585.

[102] Y.A. Korilis, A.A. Lazar and A. Orda, Achieving network optima using Stackelberg routing strategies, *IEEE/ACM Trans. Networking*, vol. 5, no. 1, 1997, pp. 161–173.

[103] J. Zander, Jamming games in slotted Aloha packet radio networks, *IEEE Military Communications Conf.*, *MILCOM '90, 'A New Era'*, vol. 2, 30 September to 3 October 1990, pp. 830–834.

[104] K. Yamamoto and S. Yoshida, Analysis of distributed route selection scheme in wireless *ad hoc* networks, in *IEEE Int. Symp. Personal, Indoor and Mobile Radio Communications*, vol. 1, 5–8 September 2004, pp. 584–588.

[105] Y.A. Korilis and A. Orda, Incentive compatible pricing strategies for QoS routing, in *INFOCOM '99*, vol. 2, 21–25 March 1999, pp. 891–899.

[106] K. Yamamoto and S. Yoshida, Stability of selfish route selections in wireless *ad hoc* networks, in *Int. Symp. Multi-Dimensional Mobile Communications, 2004 and Joint Conf. 10th Asia-Pacific Conf. Communications*, vol. 2, 29 August to 1 September 2004, pp. 853–857.

[107] R. Kannan and S.S. Iyengar, Game-theoretic models for reliable path-length and energy-constrained routing with data aggregation in wireless sensor networks, *IEEE J. Select. Areas Commun.*, vol. 22, no. 6, August 2004, pp. 1141–1150.

[108] J. Cai and U. Pooch, Allocate fair payoff for cooperation in wireless *ad hoc* networks using Shapley value, in *Int. Parallel and Distributed Processing Symp.*, 26–30 April 2004, p. 219.

[109] M. Alanyali, Learning automata in games with memory with application to circuit-switched routing, in *IEEE Conf. Decision and Control*, vol. 5, 14–17 December 2004, pp. 4850–4855.

[110] R. Atar and P. Dupuis, Characterization of the value function for a differential game formulation of a queueing network optimization problem, in *IEEE Conf. Decision and Control*, vol. 1, 7–10 December 1999, pp. 131–136.

[111] E. Altman, T. Basar and R. Srikant, Nash equilibria for combined flow control and routing in networks: asymptotic behaviour for a large number of users, in *IEEE Conference on Decision and Control*, vol. 4, 7–10 December 1999, pp. 4002–4007.

[112] A. Orda, R. Rom and N. Shimkin, Competitive routing in multiuser communication networks, *IEEE/ACM Trans. Networking*, vol. 1, no. 5, 1993, pp. 510–521.

[113] S. Irani and Y. Rabani, On the value of information in coordination games, in *Annual Symp. Foundations of Computer Science*, 1993, 3–5 November 1993, pp. 12–21.

[114] K. Loja, J. Szigeti and T. Cinkler, Inter-domain routing in multiprovider optical networks: game theory and simulations, in *Next Generation Internet Networks*, 18–20 April 2005, pp. 157–164.

[115] J.A. Almendral, L.L. Fernandez, V. Cholvi and M.A.F. Sanjuan, Oblivious router policies and Nash equilibrium, in *Int. Symp. Computers and Communications*, vol. 2, 28 June to 1 July 2004, pp. 736–741.

[116] J. Virapanicharoen and W. Benjapolakul, Fair-efficient guard bandwidth coefficients selection in call admission control for mobile multimedia communications using game theoretic framework, in *Int. Conf. Communications*, vol. 1, 20–24 June 2004, pp. 80–84.

[117] L. Berlemann, B. Walke and S. Mangold, Behavior based strategies in radio resource sharing games, in *IEEE Int. Symp. Personal, Indoor and Mobile Radio Communications*, vol. 2, 5–8 September 2004, pp. 840–846.

[118] N. Feng, S.-C. Mau and N.B. Mandayam, Pricing and power control for joint network-centric and user-centric radio resource management, *IEEE Trans. Commun.*, vol. 52, no. 9, September 2004, pp. 1547–1557.

[119] R. Kannan, S. Sarangi, S.S. Iyengar and L. Ray, Sensor-centric quality of routing in sensor networks, in *IEEE Joint Conf. IEEE Computer and Communications Societies*, vol. 1, 30 March to 3 April 2003, pp. 692–701.

[120] C.U. Saraydar, N.B. Mandayam and D.J. Goodman, Efficient power control via pricing in wireless data networks, *IEEE Trans. Commun.*, vol. 50, no. 2, 2002, pp. 291–303.

[121] V. Anantharam, On the Nash dynamics of congestion games with player-specific utility, in *Conf. on Decision and Control, CDC*, vol. 5, 14–17 December 2004, pp. 4673–4678.

[122] Y. Zheng and Z. Feng, Evolutionary game and resources competition in the Internet, in *The IEEE-Siberian Workshop of Students and Young Researchers Modern Communication Technologies*, 28–29 November 2001, pp. 51–54.

[123] A. Aresti, B.M. Ninan and M. Devetsikiotis, Resource allocation games in connection-oriented networks under imperfect information, in *IEEE Int. Conf. Communications*, vol. 2, 20–24 June 2004, pp. 1060–1064.

[124] L. Libman and A. Orda, Atomic resource sharing in noncooperative networks, in *INFOCOM '97*, vol. 3, 7–11 April 1997, pp. 1006–1013.

[125] T. Heikkinen, On distributed resource allocation of a multimedia network, in *IEEE Vehicular Technology Conf.*, vol. 4, 19–22 September 1999, pp. 2116–2118.

[126] P. Fuzesi and A. Vidacs, Game theoretic analysis of network dimensioning strategies in differentiated services networks, in *IEEE Int. Conf. Communications*, vol. 2, 28 April to 2 May 2002, pp. 1069–1073.

[127] T. Alpcan and T. Basar, A game-theoretic framework for congestion control in general topology networks, in *IEEE Conf. Decision and Control*, vol. 2, 10–13 December 2002, pp. 1218–1224.

[128] M. Chatterjee, Haitao Lin, S.K. Das and K. Basu, A game theoretic approach for utility maximization in CDMA systems, *IEEE Int. Conf. Commun., ICC '03*, vol. 1, 11–15 May 2003, pp. 412–416.

[129] I. Chlamtac, I. Carreras and H. Woesner, *From Internets to BIONETS: Biological Kinetic Service Oriented Networks*. Springer Science: Berlin, 2005, pp. 75–95.

[130] T. Nakano and T. Suda, Adaptive and evolvable network services, in K. Deb *et al*. (eds). *Genetic and Evolutionary Computation GECCO 2004*, vol. 3102. Springer: Heidelberg, 2004, pp. 151–162.

[131] J. Suzuki and T. Suda, A middleware platform for a biologically inspired network architecture supporting autonomous and adaptive applications, *IEEE J. Select. Areas Commun.*, vol. 23, no. 2, February 2005, pp. 249–260.

[132] I. Carreras, I. Chlamtac, H. Woesner and C. Kiraly, BIONETS: bio-inspired next generation networks, private communication, January 2005.

[133] I. Carreras, I. Chlamtac, H. Woesner and H. Zhang, Nomadic sensor networks, private communication, January 2005.

[134] T. Suda, T. Itao and M. Matsuo, The bio-networking architecture: the biologically inspired approach to the design of scalable, adaptive, and survivable/available network applications, in *The Internet as a Large-Scale Complex System*, K. Park (ed.). Princeton University Press: Princeton, NJ, 2005.

[135] T. Itao, S. Tanaka, T. Suda and T. Aoyama, A framework for adaptive UbiComp applications based on the jack-in-the-net architecture, *Kluwer/ACM Wireless Network J.*, vol. 10, no. 3, 2004, pp. 287–299.

17

Network Deployment

17.1 CELLULAR SYSTEMS WITH OVERLAPPING COVERAGE

The concept of cellular communication systems is based on the assumption that a mobile user is served by the base station that provides the best link quality [1, 2]. Spectrum allocation strategies, discussed in Chapter 12, are based on this assumption. In many cases, however, a mobile user can establish a communication link of acceptable quality with more than one base. Therefore, at many locations there is overlapping coverage, usually by nearby base stations [3].

The *coverage overlap* can be used to improve the system performance. Several schemes that consider this have been suggested [4–8]. Generalized fixed channel assignment (GFCA), a scheme that allows a call to be served by any of several nearby base stations, was considered in Choudhury and Rappaport [4]. Directed retry, discussed in References [5, 6], allows a new call that cannot be served at one base to attempt access via a nearby alternative base. Load sharing is an enhancement of directed retry that allows calls in congested cells to be served by neighboring base stations. In Chu and Rappaport [7] overlapping coverage for highway microcells was considered. The use of overlapping coverage with channel rearrangement was discussed in Chu and Rappaport [8].

Reuse partitioning [9–11] can also improve traffic performance of fixed channel assignment (FCA). The method divides the channels into several disjoint partitions. These partitions are associated with different cluster sizes (or reuse factors). Channels are allocated to base stations according to these cluster sizes. To meet the same signal quality requirement, channels corresponding to smaller cluster sizes are used within a smaller area than that for channels associated with larger cluster sizes [9]. Since channels are reused more often for a smaller cluster size, there may be more channels available at a base in reuse partitioning than in FCA. Therefore, improved traffic performance can be obtained. Because there is a fixed relationship between channels and base stations, reuse partitioning is a fixed channel assignment scheme. In this section the acronym FCA is used only to refer fixed channel assignment without utilizing overlapping coverage or reuse partitioning. That is, in FCA all channels are allocated using a single cluster size and overlapping coverage is not exploited.

When overlapping coverage exists in a system and is being used to provide enhanced access, users in overlapping areas may benefit. However, this may be at the expense of users in nonoverlapping areas who may encounter increased blocking or handoff failure because of the higher

Advanced Wireless Technologies: Cognitive, Cooperative & Opportunistic 4G Technology Second Edition Savo G. Glisic

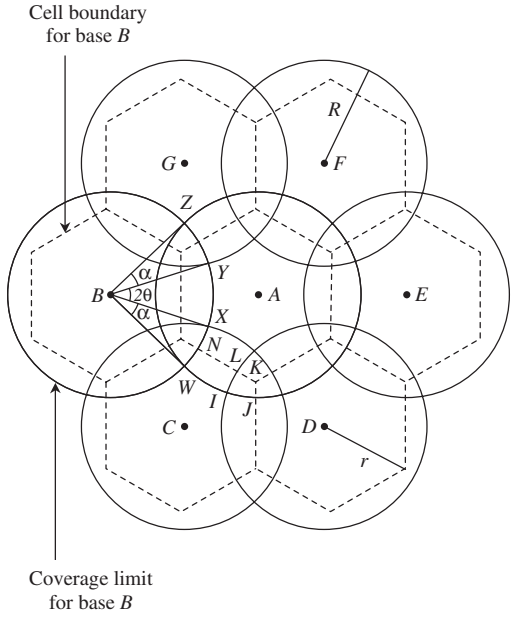

Figure 17.1 System layout for overlapping coverage.

channel occupancy of the system. Generally, overlapping areas tend to occur at the periphery of cells (i.e. distant from bases). In reuse partitioning, on the other hand, calls that are close to base stations can access channels from both the smaller cluster and larger cluster partitions. Those calls distant from bases cannot use channels from partitions of smaller cluster sizes. Such calls may in fact do more poorly than in FCA. When *both* overlapping coverage and reuse partitioning are used, they can complement one another. Such a combination will be discussed in this section.

The *system layout* is shown in Figure 17.1. The *cell radius*, r, is defined as the distance from a base to a vertex of its own cell. The *coverage* of a base is the area in which users can establish a link with acceptable signal quality with that base. This area can be modeled by a circle with the center at the corresponding base station. The *coverage radius*, R, is defined as the distance from a base to its coverage boundary.

The coverage of a base is overlapped with coverages of neighboring bases. Therefore, calls can potentially access one, two, three or even more base stations depending on the platform location and the ratio of the coverage radius to the cell radius (R/r). For the interesting range of R/r, there are three kinds of regions in which calls have potential access to one, two or three base stations. These regions in Figure 17.2 are denoted A_1, A_2 and A_3, respectively. A_1 is the nonoverlapping region while both A_2 and A_3 are overlapping regions. We consider (without loss of generality) the cell radius, r, to be normalized to unity. The coverage radius, R, is determined by the requirement of the link quality. Once R is found, the percentage of a cell that belongs to region A_1, A_2 or A_3 can be calculated. They are denoted by p_1, p_2 and p_3, respectively. These relationships are discussed letter in the section.

Reuse partitioning that has two partitions of channels, denoted a and b, is used. Systems with more partitions can be considered similarly. Channels of these two partitions are referred to as a- and b-type channels, respectively. These two partitions are used with different cluster sizes, N_a and N_b, to allocate channels to base stations. Channels of type a are equally divided into N_a groups each with C_a channels. Similarly, b-type channels are equally divided into N_b groups each with C_b channels. Every base station is assigned one group of channels from each partition in such

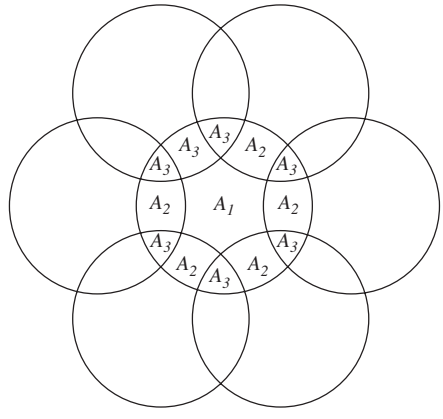

Figure 17.2 Three kinds of regions in the coverage of a base.

a way that co-channel interference is minimized. As a result, there are totally $C_a + C_b$ channels available at a base. Let C_T denote the total number of available channels and f denote the fraction of channels that are assigned to partition a. So,

$$f = N_a \cdot C_a / C_T \quad \text{and} \quad 1 - f = N_b \cdot C_b / C_T$$

Since N_a and N_b are different, N_a is assumed to be the smaller one. Consequently a-type channels must be used in a smaller area. Channels of type a are intended for use by users who can access only one base, which corresponds to users in region A_1. Channels of type b can be used by all users. Figure 17.3 shows the channel assignment and the available channel groups in a specific region for such a system with $N_a = 3$ and $N_b = 7$. The three groups of a-type channels are labeled a_1, a_2 and a_3, and the seven groups of b-type channels are labeled $b_1, b_2, \ldots, b_7$. Because of overlapping coverage, users in region A_2 can access two groups of channels from partition b. Similarly, users in A_3 can access three groups of b-type channels.

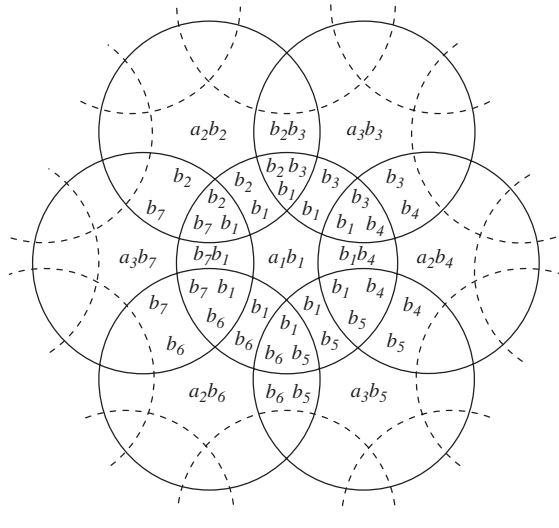

Figure 17.3 The relationship between channel groups and various regions for $N_a = 3$ and $N_b = 7$.

Priority to handoff calls is given at each base, by allocating C_{ha} of the C_a a-type channels to handoffs. Similarly, C_{hb} of the C_b b-type channels are reserved at a base. Specific channels are not reserved, only the numbers, C_{ha} and C_{hb}. As a result, new calls that arise in region A_1 can access $C_a - C_{ha}$ a-type channels and $C_b - C_{hb}$ b-type channels at the corresponding base. New calls that arise in region A_2 or A_3 can access $C_b - C_{hb}$ channels of b-type at each potential base. New calls that arise in region A_1 are served by b-type channels only when no a-type channel is available. When more than one base has a channel available to serve a new call that arises in region A_2 or A_3, the one with the best link quality is chosen. Most likely, it is the nearest one under uniform propagation and flat terrain conditions.

The possible types of handoffs are shown in Figure 17.3. The received signal power is inversely proportional to the distance raised to an exponent, γ, which is called path loss exponent. The coverage radius, R, is determined such that the worst case SIR of a-type calls is equal to the worst case SIR of b-type calls. Therefore, the desired R is the one that satisfies $\text{SIR}_a(R, N_a, \gamma) = \text{SIR}_b(R, N_b, \gamma)$. Mobile users are assumed to be uniformly distributed throughout the service area. Call arrivals follow a Poisson point process with a rate Λ_n per cell, and this rate is independent of the number of calls in progress. Session duration, T, is a random variable with a negative exponential probability density function with mean $\bar{T}(= \mu^{-1})$. An a (or b)-type call resides within the pertaining region during the dwell time T_a (or T_d).

These are random variables with a negative exponential distribution of mean $\bar{T}_a(= \mu_a^{-1})$ (or $\bar{T}_d(= \mu_d^{-1})$. $\bar{T}_a$ and $\bar{T}_d$ are assumed to be proportional to the radii of the corresponding areas. Although region A_1 is not circular, an equivalent radius (which is the radius of a circle that has the same area as A_1) can be used. *System modeling* is based on using two variables to specify the state of a base. One is the number of a-type channels in use; the other is the number of b-type channels in use. A complete state representation for the whole system will be a string of base station states with two variables for each base. This state representation can keep track of all events that occur in the system. Unfortunately, the huge number of system states precludes using this approach for most cases of interest. A simplified approach is to decouple a base from others using average teletraffic demands related to neighboring bases. This is similar to the approach used in References [13, 14]. As a result, the state, s, is characterized from a given base by $a(s)$, $b(s)$, where $a(s)$ is the number of a-type channels in use in state s, and $b(s)$ is the number of b-type channels in use in state s with constraint $0 \leq a(s) \leq C_a$ and $0 \leq b(s) \leq C_b$. The state probabilities, $P(s)$, in statistical equilibrium are needed for determining the performance measures of interest. To calculate state probabilities, the state transitions and the corresponding transition rates must be identified and calculated. Owing to overlapping coverage and reuse partitioning, state transitions result from six driving processes:

(1) new call arrivals;

(2) call completions;

(3) handoff departures of a type; calls that use a-type channels are a-type calls and those that use b-type channels are b-type calls. An a-type call initiates a handoff (a-type handoff) when it leaves region A_1. An a-type handoff may be an inter-base or an intra-base handoff depending on which base continues its service (see Figure 17.3);

(4) hand-off arrivals of a type;

(5) handoff departures of b type; a b-type call initiates a handoff (b-type handoff) only when it leaves the coverage of the serving base. A b-type handoff that enters region A_1 of a neighboring base (out of the coverage of the serving base) can access channels from both a-type and b-type (a-type channels first) at that target base. A b-type handoff that enters region A_2 can access all channels of b-type at each potential target base; and

(6) hand-off arrivals of b type.

The transition rates from a current state s to next state s_n due to these driving processes are denoted by $r_n(s, s_n)$, $r_c(s, s_n)$, $r_{da}(s, s_n)$, $r_{ha}(s, s_n)$, $r_{db}(s, s_n)$, and $r_{hb}(s, s_n)$, respectively. The details for state transition rate derivation and solving the system of state probabilities equations is based on the general principles discussed in Chapter 6. Some specific details can be found also in References [7, 8, 13, 14–16] and especially [17].

Some examples of performance results with $C_T = 180$, $N_a = 3$, $N_b = 9$, $\bar{T} = 100$ s, $\bar{T}_d = 60$ s, $C_{ha} = 0$, $C_{hb} = 0$ and $\gamma = 4$, are shown in Figures 17.4–17.6.

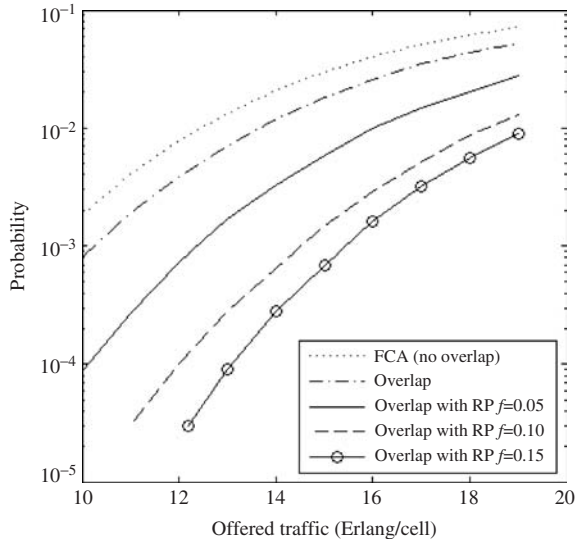

Figure 17.4 Overall blocking probability for FCA, coverage overlap and coverage overlap with reuse partitioning.

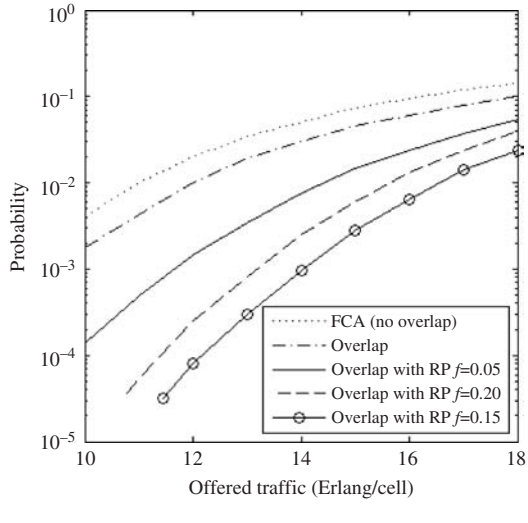

Figure 17.5 Forced termination probability for FCA, coverage overlap, and coverage overlap with reuse partitioning.

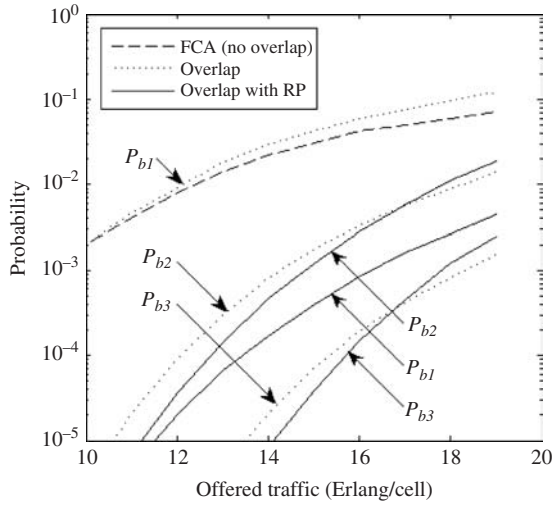

Figure 17.6 Blocking probability in areas A_1, A_2 and A_3 for FCA, coverage overlap and coverage overlap with reuse partitioning.

17.2 IMBEDDED MICROCELL IN CDMA MACROCELL NETWORK

Combining a macrocell and microcell with a two-tier overlaying and underlaying structure for a CDMA system is to become an increasingly popular trend in 4G wireless networks. However, the cochannel interference from a microcell to macrocell and vice versa in this two-tier structure is different from that in the homogeneous structure (i.e. consisting of only macrocells or only microcells).

A possibility of embedding a CDMA micro cell into a TDMA macrocell is discussed in References [18, 19] and a CDMA micro cell into a CDMA macrocell in Wu *et al.* [20]. Figure 17.7 presents the geometry of overlayed and underlayed CDMA macrocell (radius R)/CDMA microcell (radius r) structures where a microcell is located at distance d_1 from the BS of the central macrocell. Propagation loss before breakpoint (bp) is assumed to be proportional to d^2, otherwise, it is proportional to d^4, where d is the distance away from the transmitter. The received power is represented as

$$P_l = \begin{cases} \dfrac{(\lambda/4\pi)^2 P_t}{d^2}, & d \le bp = \dfrac{4\pi h_{\mathrm{m}} h_{\mathrm{b}}}{\lambda} \\ \dfrac{(h_{\mathrm{m}} h_{\mathrm{b}})^2 P_{\mathrm{t}}}{d^4}, & \text{otherwise} \end{cases} \tag{17.1}$$

where P_{t} is the power of the transmitter, h_{m} and h_{b} are the height of the mobile and BS antennas respectively, and bp is the breakpoint [17–20]. The MS will access a cell BS with the strongest pilot signal. After an MS determines to access a certain cell BS, the cell BS will verify whether or not the ratio for uplink signal to interference (C/I) from a mobile is less than a threshold of $(C/I)_{\mathrm{tu}}$. If the C/I is less than the threshold of $(C/I)_{\mathrm{tu}}$, the MS is inhibited and blocked. In other words, for a call to be accepted we should have

$$\left(\frac{C}{I}\right)_{\mathrm{u}} = \frac{P_{\mathrm{r}j}}{\sum_{i=1, i\neq j}^{M} P_{\mathrm{r}i} + \sum_{k=1}^{N} P'_{\mathrm{t}k} \times (\beta)'_k} \ge \left(\frac{C}{I}\right)_{\mathrm{tu}} \tag{17.2}$$

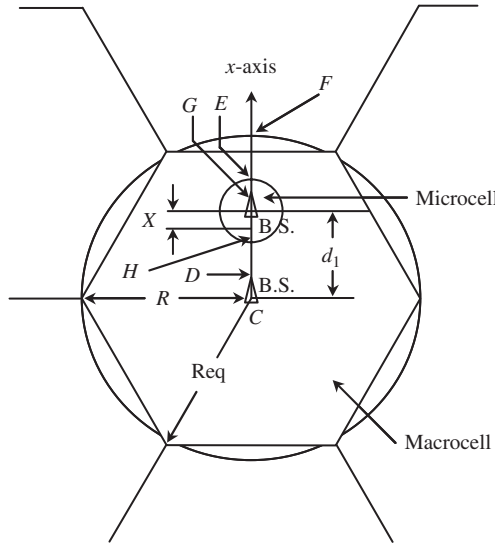

Figure 17.7 Macrocell/microcell overlayed/underlayed structure.

where P_{rj} is the power received from the desired jth MS by a dedicated BS, P'_{tk} is the power transmitted from the kth MS belonging to other BSs, and $(\beta)'_k$ is the path loss from the kth MS to the dedicated BS. The first and second terms in the denominator represent the interference from other MSs in the same BS and from MSs belonging to other BSs, respectively. Thermal noise is rather small relative to the cells' interference, so it is neglected. If P_r is increased, the interference from other cells is relatively smaller so that the C/I requirement for newly active users can be satisfied.

17.2.1 Macrocell and microcell link budget

For the handoff analysis we want to find the point where the strength of pilot signal emitted from a microcell BS is equal to that from a macrocell at the microcell boundary. The microcell boundary is assumed here to be distant from the macrocell bp. The distance from the microcell BS to the center of microcell is x. Therefore, the pilot power (emitted from microcell BS) received at boundary point D shown in Figure 17.7 is represented as

$$P_{\mathrm{rsD}} = \frac{(h_{\mathrm{m}} h_{\mathrm{bs}})^2 \alpha_{\mathrm{s}} P_{\mathrm{ts}}}{(r - x)^4} \tag{17.3}$$

where α_{s} is the power fraction of the pilot signal for microcells. Similarly, the pilot power received from the macrocell BS at boundary D is represented by

$$P_{\mathrm{rlD}} = \frac{(h_{\mathrm{m}} h_{\mathrm{bl}})^2 \alpha_{\mathrm{l}} P_{\mathrm{tl}}}{(d_1 - x)^4} \tag{17.4}$$

where α_l is the ratio of pilot power to the BS's downlink power and d_1 is the distance between the centers of macrocells and microcells. The above equation is similar to (17.1). The subscripts xs (or xl) of $P_{x\mathrm{s}}$ (or $P_{x\mathrm{l}}$) denote symbols for the microcell (*small cell*) or for the macrocell (*large cell*). Since the strengths of the pilot signals emitted from both the microcell BS and macrocell BS at D point are equal (i.e. $P_{\mathrm{rsD}} = P_{\mathrm{rlD}}$), the transmission power emitted from both BSs must satisfy

the following formula:

$$P_{ts} = \frac{h_{bl}^2 (r-x)^4 \alpha_l}{h_{bs}^2 (d_1 - x)^4 \alpha_s} P_{tl} \tag{17.5}$$

Similarly, it holds for point E which is on distance $r + x$ from the BS as shown in Figure 17.7. Thus, we obtain

$$P_{rsE} = \frac{(h_m h_{bs})^2 \alpha_s P_{ts}}{(r+x)^4} \quad \text{and} \quad P_{rlE} = \frac{(h_m h_{bl})^2 \alpha_l P_{tl}}{(d_1 + r)^4} \tag{17.6}$$

Equating P_{rsE} and P_{rlE} yields

$$P_{ts} = P_{tl} \left(\frac{h_{bl}}{h_{bs}}\right)^2 \left(\frac{r+x}{d_1 + r}\right)^4 \left(\frac{\alpha_l}{\alpha_s}\right) \tag{17.7}$$

Dividing Equation (17.5) by Equation (17.7) gives $x = r^2/d_1$, which means that the microcell BS must shift from its center by x distance. When d_1 is getting smaller, the value x is getting larger. This fact will cause an asymmetric environment and make the site engineering more difficult. Substituting $x = r^2/d_1$ into Equation (17.5) gives the power ratio of

$$\frac{P_{tl}}{P_{ts}} = \frac{h_{bs}^2 d_1^4 \alpha_s}{h_{bl}^2 r^4 \alpha_l} \tag{17.8}$$

The *downlink C/I*s for the central macrocell and for the microcell can be expressed as [1]:

$$\left(\frac{C}{I}\right)_l = \frac{\frac{P_{tl}(1-\alpha_l)}{N} \times \beta}{\left[1 - \frac{(1-\alpha_l)}{N}\right] P_{tl}\beta + P_{ts}\beta' + \sum_{i=1}^{6} P_{tl} \times \beta_i} \tag{17.9}$$

$$\left(\frac{C}{I}\right)_s = \frac{\frac{P_{ts}(1-\alpha_s)}{M}\beta'}{\left[1 - \frac{(1-\alpha_s)}{M}\right] P_{ts}\beta' + P_{ts}\beta + \sum_{i=1}^{6} P_{tl}\beta_i} \tag{17.10}$$

where N and M denote the number of active users in the central macrocell BS and microcell BS, β, β' and β_i are path loss for macrocell, microcell and adjacent macrocell, respectively, and the third term in the denominator represents the interference from the six adjacent macrocells. The above formulas are the decision rules for the downlink to accept a newly active MS. For a given threshold *C/I* they determined maximum N and M (*capacity*).

The *uplink C/I*s measured by both the macrocell and microcell BSs are derived as

$$\left(\frac{C}{I}\right)_l = \frac{P_r}{(N-1)P_r + \sum_{i=1}^{M} P_r' \left(\frac{r_i}{d_i}\right)^4 \left(\frac{h_{bl}}{h_{bs}}\right)^2 + I_{ll}} \tag{17.11}$$

and

$$\left(\frac{C}{I}\right)_s = \frac{P_r'}{(M-1)P_r' + \sum_{i=1}^{N} P_r \left(\frac{d_i}{r_i}\right)^4 \left(\frac{h_{bs}}{h_{bl}}\right)^2 + I_{ls}} \tag{17.12}$$

respectively, where P_r and P_r' are mobile powers received by the macrocell's BS and microcell's BS, respectively, M and N denote the number of active mobiles in each microcell and macrocell, respectively. The first term and the second term in the denominator represent the interference from

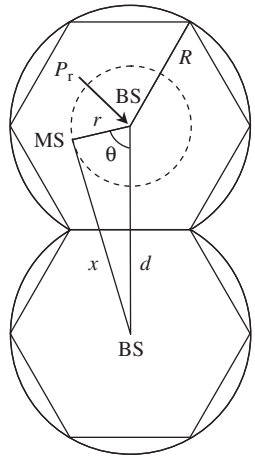

Figure 17.8 Cell geometry for calculation of interference.

other MSs in the same BS and from all MSs in the other kind of BS, and r_i and d_i are the distance from the ith mobile to its own BS and to the other kind of BS, respectively. Finally, the third term I_{ll} (or I_{ls}) represents the interference from adjacent macrocells to the central macrocell BS (or microcell BS). The above formulas are the decision rules for the uplink to accept a newly active MS. To find expression for I_{ll} (or I_{ls}), N mobile units are assumed to be uniformly distributed in an equivalent disc of radius R shown in Figure 17.8. The density of mobile unit is $\rho = N/\pi R^2$ [1, 20].

The power received in the BS from each mobile is assumed here to be P_r with a path loss proportional to the fourth power of distance. The interference caused by mobiles in an adjacent macrocell is

$$P(d) = \frac{2NP_r}{\pi R^2} \int_0^R r^5 \, dr \int_0^\pi \frac{d\theta}{(d^2 + r^2 - 2\,dr\cos\theta)^2} \tag{17.13}$$

where r is the distance between the mobile and the adjacent macrocell BS, $x = \sqrt{(d^2 + r^2 - 2dr\cos\theta)}$ is the distance between the mobile in the adjacent macrocell and the interfered BS, and d is the distance between two BSs. Therefore, the interference to the central macrocell BS caused by the six adjacent macrocells can be calculated as

$$I_{ll} = \sum_{i=1}^{6} P(d_i = 2R) = 0.378NP_r \tag{17.14}$$

Similarly, the interference to the microcell BS caused by the six adjacent macrocells is expressed as

$$I_{ls} = \sum_{i=1}^{6} P(d_i)(h_{bs}/h_{bl})^2 = i_s NP_r \tag{17.15}$$

where

$$i_s = \sum_{i=1}^{6} 2(h_{bs}/h_{bl})^2 \left[2(d_i^2/R^2) \ln \frac{d_i^2}{d_i^2 - R^2} - \left(\frac{4d_i^4 - 6d_i^2R^2 + R^4}{2(d_i^2 - R^2)^2} \right) \right] \tag{17.16}$$

depending on the location of microcell.

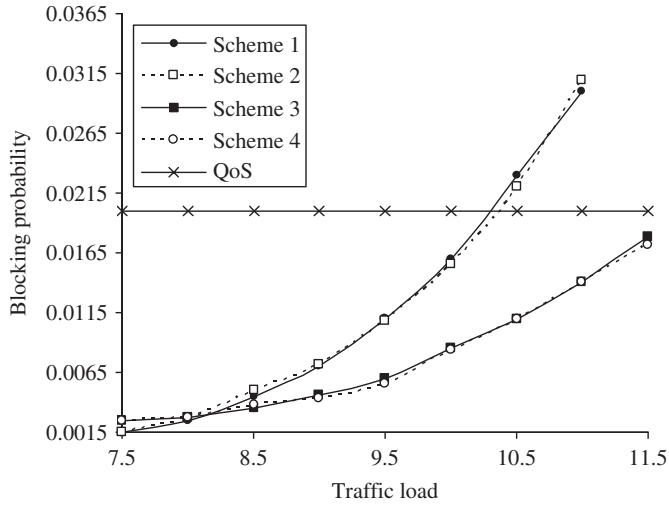

Figure 17.9 Blocking probability of macrocell. (Reproduced by permission of IEEE [20].)

17.2.2 Performance example

A detailed analysis of the above system by simulation is given in Wu *et al.* [20]. Four different power control schemes are analyzed:

(1) both the macrocell and microcell use the signal-strength-based power control for the uplink and there is no power control for the downlink;

(2) (a) [or scheme 2(b)], both the macrocells and microcells use the signal-strength-based power control for the uplink, and downlink power control is also applied for the microcell (or applied for macrocells and microcells);

(3) both the macrocells and microcells use the C/I power control for the uplink and there is no power control for the downlink;

(4) both the macrocells and microcells apply the C/I power control for uplink, however, but only the microcell uses power control for the downlink.

In addition, antenna heights of macrocells and microcells are 45 and 6 m, respectively. The radius of the microcell is $r = 1000$ m, the radius of the macrocell is R, and $R = 10r$. The bps are 342 m for the microcell and 2569 m for the macrocell.

The arrival process for users in a cell is Poisson distributed with a mean arrival rate of λ, and the holding time for a call is exponentially distributed with the mean of $1/\mu$. The required E_b/N_0 for uplink and downlink in a CDMA system is around 7 and 5 dB, respectively, if the bit error rate is less than 10^{-3}. The major performance we are concerned with is the capacity. Under this maximum loading condition, the background noise is very little relative to interference, so that C/I is the only index to survey. The processing gain for a CDMA system is defined as the ratio of bandwidth over data rate, that is, 21.0 dB (i.e. 1.2288 MHz/9.6 kbs), so that the threshold of $(C/I)_{tu}$ is 14 dB for uplink and the threshold $(C/I)_{td}$ is 16 dB for the downlink. For this set of parameters the blocking probabilities for the two cells are given in Figures 17.9 and 17.10.

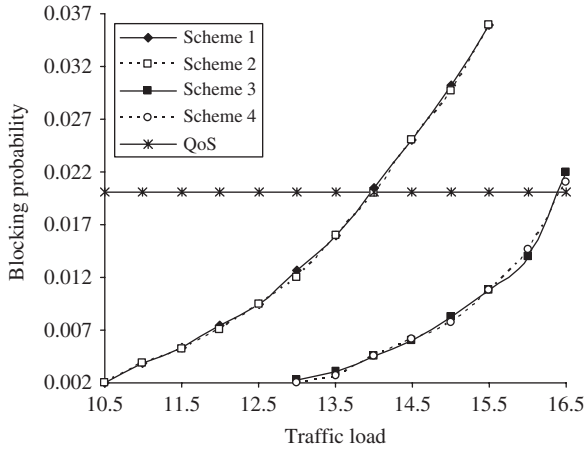

Figure 17.10 Blocking probability in microcell. (Reproduced by permission of IEEE [20].)

17.3 MULTITIER WIRELESS CELLULAR NETWORKS

In this section we further extend the previous problem to a general cell-design methodology in multitier wireless cellular network. Multitier networks may be a solution when there are a multitude of traffic types with drastically different parameters and/or different requirements, such as different mobility parameters or quality-of-service requirements. In such situations, it may be cost-effective to build a multitude of cellular infrastructures, each serving a particular traffic type. The network resources (channels) are then partitioned among the multitude of tiers. In general terms, we are interested in quantifying the cost reduction due to the *multitier* network design, as opposed to a single-tier network. 4G networks are expected to serve different mobility platforms and support multimedia applications through a newly deployed infrastructure based on the multitier approach.

The cellular systems for the 4G of wireless multimedia networks will rely on cells that are smaller than those used today. In particular, in the proposed microcellular systems, the cell radius can shrink to as small as 50 m (compared with 0.5–10 mile radius range for today's macrocellular systems). Smaller cell radii are also possible for systems with smaller coverage, such as pico- and nanocells in a local-area environment. The size of the cells is closely related to the expected speed of the mobiles that the system is to support. In other words the faster the mobiles move, the larger the cells should be. This will keep the complexity of handoffs at a manageable level. The cell size is also dependent on the expected system load (Erlangs per area unit). The larger the system load, the smaller the cell should be. This is the direct outcome of the limited wireless resources assigned to handle cell traffic. Smaller cells result in channels being reused a greater number of times and thus greater total system capacity. Finally, the cell size also depends on the required QoS level. This includes the probability of call blocking, call dropping or call completion. In general, the more stringent the QoS, the smaller the cells need to be, since smaller cells increase the total system capacity. Unfortunately, smaller cells require more base stations, and hence higher costs.

In this section, we discuss the multitier concept to show how to optimize the design of a system with differing traffic requirements and mobile characteristics. We examine how to lay out a multitier cellular system, given a total number of channels, the area to be covered, the average speed of mobiles in a tier, call arrival and duration statistics for each tier, and a constraint on the

QoS (i.e. blocking and dropping probabilities). We discuss how to design a multitier cellular system in terms of the number of tier-i cells (e.g. of macrocells and microcells in a two-tier system) and the number of channels allocated to each tier so that the total system cost is minimized.

17.3.1 The network model

For each tier, the total area of the system (*coverage* area) is partitioned into cells. All cells of the same tier are of equal size. The network resources are also partitioned among the network tiers. Channels allocated to a particular tier are then reused based on the reuse factor determined for the mobiles of that tier (i.e. within each tier, channels are divided into channel sets). One such set is then allocated to each cell of that tier. For simplicity, FCA for the allocation of channels both among the tiers and within a tier is used.

In this section, connection-oriented traffic is considered. Each tier is identified by several parameters: *call arrival rate*, *call duration time*, *call data rate*, *average speed of mobiles*, *performance factors* and *QoS factors.* Additional assumptions are that:

- handoffs and new calls are served from the same pool of available channels which means that, for a given tier, the probability of blocking equals the probability of dropping;
- the speed of each class of mobiles is constant for each tier;
- new call arrivals and call terminations are independent of the handoff traffic;
- the traffic generation is spatially uniformly distributed;
- call arrivals follow a Poisson process;
- the spatial and time distribution of call arrivals are the same over all cells in a given tier, but can be different from tier to tier;
- call duration for a given tier is exponentially distributed, and may vary from tier to tier.

In the presentation the following notation is used [21]:

- λ_i^0, rate of tier i calls initiated per unit area, calls/(s m^2);
- λ_i, call initiation rate in a tier i cell (calls/s);
- $1\mu_i$, average call duration of a tier i cell (s call);
- h_i, mean number of handoffs for a tier i call (handoffs/p call);
- γ_i, the relative cost of a tier i base station to the cost of a tier S base-station ($\gamma_S \equiv 1$);
- A, total area to be covered (m^2);
- S, number of tiers;
- C, total number of available network channels;
- C_i, number of channels allocated to tier i;
- N_i, number of channels allocated to a tier i cell;
- f_i, number of tier i cells in the frequency reuse cluster;
- m_i, number of tier i cells contained in a tier $(i-1)$ cell; tier 0 defines the total coverage area; $m_1 \stackrel{def}{=}$ total number of tier 1 cells;
- R_i, radius of a tier i cell (m);

- V_i, average speed of tier i mobile users (ms);
- $P_{\mathrm{B}}(i)$, actual blocking probability for a tier i cell;
- $P_{\mathrm{D}}(i)$, actual dropping probability for a tier i cell;
- $P_{\mathrm{B}}^{\max}(i)$, the maximum acceptable blocking probability for tier i calls;
- $P_{\mathrm{D}}^{\max}(i)$, the maximum acceptable dropping probability for tier i calls;
- $P_{\mathrm{L}}(i)$, loss probability of tier i;
- PLT, overall system loss probability, weighted by the amount of traffic of each tier;
- $\mathrm{PLT}_{\max}$, the maximum acceptable weighted system loss probability;
- TSC, total system cost;
- $\mathrm{TSC}_{\max}$, maximum allowable total system cost; input design parameter tabbing.

Cost optimization is supposed to minimize the cost of the multitier infrastructure. In our model, we assume that the major part of the total system cost is the cost of base station deployment, which in our model is proportional to the total number of base stations. Thus, the total system cost, TSC, is:

$$\mathrm{TSC} = m_1\{\gamma_1 + m_2[\gamma_2 + m_3(\cdots)]\} = \sum_{i=1}^{S} \gamma_i \cdot \prod_{j=1}^{i} m_j, \quad S \geq 1 \tag{17.17}$$

In the above equation, we assume that cells are arbitrary split so that the location of tier i base stations is independent of the location of the base stations of the other tiers. In a more structured splitting cells of tier i form rings within a cell of tier $(i-1)$ as shown for the two-tier case in Figure 17.11. Thus, if a base station already exists in a cell for tier i, the cost of placing an additional base station for a higher tier is negligible. Therefore, for example, in the case of a two-tier network the total cost can be reduced by the cost of the tier 2 base stations. In such a case, the total cost is

$$\mathrm{TSC} = \sum_{i=1}^{S} \gamma_i \left(\prod_{j=1}^{i} m_j - \prod_{j=1}^{i-1} m_j \right) = \gamma_1 m_1 + \sum_{i=2}^{S} \gamma_i (m_i - 1) \prod_{j=1}^{i-1} m_j, \quad S \geq 1 \tag{17.18}$$

It will be further assumed that the set of all the available channels to tier i, C_i, is equally divided among the f_i cells in the frequency reuse cluster, which means no channel sharing between the cells. There is no channel sharing among the tiers either. It is also assumed that no channels are put aside for handling handoffs. Therefore, the blocking and dropping probabilities are equal, and

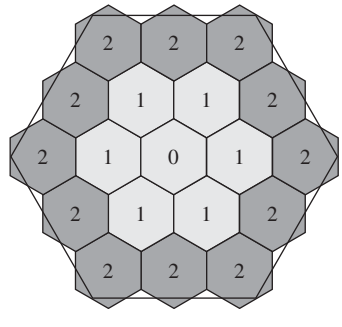

Figure 17.11 Cell splitting in multitier network.

will be referred to as the probability of loss, $P_{\mathrm{L}}(i)$; that is,

$$\forall i,\ P_{\mathrm{L}}(i) = P_{\mathrm{B}}(i) = P_{\mathrm{D}}(i) \text{ and } P_{\mathrm{L}}^{\max}(i) = \min\left\{P_{\mathrm{B}}^{\max}(i),\, P_{\mathrm{D}}^{\max}(i)\right\}$$

The overall system loss probability, PLT, is given by:

$$\mathrm{PLT} = \frac{\sum_{i=1}^{S} P_{\mathrm{L}}(i)\lambda_i^0}{\sum_{i=1}^{S} \lambda_i^0} \tag{17.19}$$

The layout design problem is to minimize TSC, when the total number of available channels is at most C, and subject to the following QoS constraints: $\mathrm{PLT} \le \mathrm{PLT}_{\max}$ and $\bar{P}_{\mathrm{L}} \le \bar{P}_{\mathrm{L}}^{\max}$. In other words: Find $\{m_i\}$ minimizing TSC with $\sum_{j=1}^{S} C_j \le C$ and $\mathrm{PLT} \le \mathrm{PLT}_{\max}$ and $\bar{P}_L \le \bar{P}_L^{\max}$ [21].

The average number of handoffs, h_i, that a call of tier i will undergo during its lifetime is

$$h_i = (3 + 2\sqrt{3})V_i/9\mu_i R_i, \quad i = 1, 2, \ldots, S \text{ [22]}$$

Now assume that there are a total of M_i cells in tier-i ($M_i = \prod_{j=1}^{i} m_j$). Then the total average number of handoffs per second in all the cells is $h_i\lambda_i M_i$. The total arrival rate of handoff and initial calls in all tier i cells is $\lambda_i M_i\ (h_i + 1)$, and the average total (handoffs and initial calls) rate per cell is $\lambda_i^{\mathrm{total}} = \lambda_i(h_i + 1)$. It was assumed that the total arrival process to a cell is still Markovian, with the average rate of $\lambda_i^{\mathrm{total}}$. Since the area of a hexagon with radius R is $3\sqrt{3}/2R^2$, we obtain $\lambda_i = 3\sqrt{2}\lambda_i^0 R_i^2/2$. This leads to

$$\lambda_i^{\mathrm{total}} = \lambda_i^0 R_i \frac{\left[(2 + \sqrt{3})V_i + 3\sqrt{3}\mu_i R_i\right]}{2\mu_i} \tag{17.20}$$

The average call termination rate is [22] $\mu_i^{\mathrm{total}} = \mu_i(1 + 9h_i)$. We can use the Erlang-B formula (see Chapter 6) extended to *M/G/c/c* systems. The probability of loss of a tier i call is therefore

$$P_{\mathrm{L}}(i) = \frac{\left(\lambda_i^{\mathrm{total}}/\mu_i^{\mathrm{total}}\right)^{N_i}/N_i!}{\sum_{j=0}^{C_i}\left(\lambda_i^{\mathrm{total}}/\mu_i^{\mathrm{total}}\right)^{j}/j!} \tag{17.21}$$

$$= \frac{\{[\lambda_i(1 + h_i)]/[\mu_i(1 + 9h_i)]\}^{N_i}/N_i!}{\sum_{j=0}^{C_i}\{[(\lambda_i(1 + h_i)]/[\mu_i(1 + 9h_i)]\}^{j}/j!}, \quad i = 1, 2, \ldots, S$$

where $\lambda_i^{\mathrm{total}}$, μ_i^{total}, λ_i and h_i are given above, and $N_i = \lfloor C_i/f \rfloor, i = 1, 2, \ldots, S$.

For a two-tier system ($S = 2$), the cost function simplifies to $\mathrm{TSC} = \lambda_1 \cdot m_1 + \lambda_2 \cdot m_1 \cdot (m_2 - 1)$. Parameters m_1, m_2 and R_2 as a function of the area, A and the tier 1 cell radius, R_1, can be expressed as

$$m_1 = \lceil A/A_1 \rceil = \left\lceil 2\sqrt{3}A/9R_1^2 \right\rceil \tag{17.22}$$

where $A1$ is area of tier 1 cell. We assume that both tier 1 and tier 2 cells are hexagonally shaped and that tier 2 cells are obtained by suitably splitting the tier 1 cells. Each tier 1 cell will contain k layers of tier 2 cells. Figure 17.11 shows an example of a tier 1 cell which contains three layers (0, 1 and 2). From the geometry of a hexagon, the number of tier 2 cells in a tier 1 cell is given by $m_2 = 1 + 6 + \cdots + 6k = 1 + 3k(k + 1), \quad k = 0, 1, \ldots,$ where $(k + 1)$ denotes the number of 'circular layers' in the cell splitting. Also, the radius of a tier-2 cell is given by $R_2 = R_1/\sqrt{m_2}$.

The *constrained optimization problem* outlined above consists of finding optimal values of R_1, R_2, C_1, C_2, m_1 and m_2, which are the system design parameters. The optimal values will be

referred to as R_1^*, R_2^*, C_1^*, C_2^*, m_1^* and m_2^*. The parameters m_1, m_2, C_1 and C_2 are integers, while R_1 and R_2 are continuous variables. However, we only need to consider a discrete subset of the possible values of R_1. From Equation (17.22), it is sufficient to consider just those values of R_1 for which $R_1 = \sqrt{(2\sqrt{3}A/9\ell)}$ where $\ell = m_{\min 1}, \ldots, m_{\max 1}$; $m_{\min 1}$ and $m_{\max 1}$ are the lower and upper bounds, respectively, of the number of tier 1 cells in the system. Thus, R_1 can only assume one of $m_{\max 1} - m_{\min 1} + 1$ values.

The lower bound, $m_{\min 1}$, is usually assumed to be equal to 1, while the upper bound, $m_{\max 1}$, can be estimated from $\mathrm{TSC}_{\max}$, which is given to the designer, as $m_{\max 1} = \lceil \mathrm{TSC}_{\max}/\gamma_1 \rceil$. The following search procedure is used in Ganz *et al.* [21] to find the design parameters.

$$\mathrm{TSC}^* = \mathrm{TSC}_{\max}$$
$$m_{\max 1} = \lceil \mathrm{TSC}_{\max}/\gamma_1 \rceil$$
$$a_1 = 3\sqrt{2}\lambda_1^0/2$$
$$a_2 = 3\sqrt{2}\lambda_2^0/2$$
$$b_1 = (3 + 2\sqrt{3})V_1/9\mu_1$$
$$b_2 = (3 + 2\sqrt{3})V_2/9\mu_2$$
$$c = \sqrt{2\sqrt{3}A/9}$$

`while` $(m_{\min 1} \leq m_1 \leq m_{\max 1})$ `do`

$$R_1 = c/\sqrt{m_1}$$
$$\lambda_1 = a_1 R_1^2$$
$$h_1 = b_1/R_1$$

`while` $(1 \leq C_1 < C)$ `do`

$$N_1 = \lfloor C_1/f_1 \rfloor$$
$$N_2 = \lfloor (C - C_1)/f_2 \rfloor$$
$$P_L(1) = \frac{\{[\lambda_1(1+h_1)]/[\mu_1(1+9h_1)]\}^{N_1}/N_1!}{\sum_{j=0}^{N_i}\{[\lambda_1(1+h_1)]/[\mu_1(1+9h_1)]\}^j/j!}$$

`for` $(k = 1;;$ k++$)$ `do`

$$m_2 = 1 + 3k(k+1)$$
$$\mathrm{TSC} = \gamma_1 m_1 + \gamma_2 m_1(m_2 - 1)$$

`if` $(\mathrm{TSC} > \mathrm{TSC}^*)$ `then break`

$$R_2 = R_1/\sqrt{m_2}$$
$$\lambda_2 = a_2 R_2^2$$
$$h_2 = b_2/R_2$$
$$P_L(2) = \frac{\{[\lambda_2(1+h_2)]/[\mu_2(1+9h_2)]\}^{N_2}/N_2!}{\sum_{j=0}^{N_2}\{[\lambda_2(1+h_2)]/[\mu_2(1+9h_2)]\}^j/j!}$$
$$\mathrm{PLT} = \frac{\lambda_1^0 P_L(1) + \lambda_2^0 P_L(2)}{\lambda_1^0 + \lambda_2^0}$$

```
    if (PLT < PLT_max) and [P_L(1) < P_L^max(1)] and [P_L(2) < P_L^max(1)] then break
    end for
    if (TSC < TSC*) then
```

$$\hat{k} = k$$

$$m_1^* = m_1$$

$$m_2^* = m_2$$

$$R_1^* = R_1$$

$$R_2^* = R_1/\sqrt{m_2}$$

$$C_1^* = C_1$$

$$C_2^* = C - C_1$$

```
    end if
  end while
end while
```

The outputs are: TSC*, m_1^*, m_2^*, R_1^*, R_2^*, C_1^* and C_2^*.

17.3.2 Performance example

To generate numerical results, a system with the parameters shown in Table 17.1 is used [21]. The performance of the two-tier system is compared with that of a one-tier system. To obtain results for a one-tier system the optimization algorithm with $R_1 = R_2$ was run. This results in both tiers sharing the same cells and $m_2 = 1$. The total cost is then computed as TSC $= m_1\gamma_1$.

Figure 17.12 depicts the total system cost as a function of tier 2 mobile speed, while tier 1 mobile speed is fixed for one-tier and a two-tier systems. The tier 1 mobile speeds considered are 30, 90, 180, 270, 360 and 540 km/h.

Table 17.1 Example system parameters

Parameter	Value/range	Units
A	100	km^2
C	90	Channels
S	2	
λ_1^0	0.23.0	Calls/(min km^2)
λ_2^0	5.040.0	Calls/(min km^2)
μ_1, μ_2	0.33	Calls/min
γ_1	10.0	\$ (in 1000 s)/base
γ_2	1.0	\$ (in 1000 s)/base
V_1	30540	km/h
V_2	1.512.0	km/h
f_1, f_2	3	
TSC$_{max}$	10 000–20 000	\$ (in 1000 s)
PLT$_{max}$	0.01	
P_B^{max}(*)	0.01	
P_D^{max}(*)	0.01	

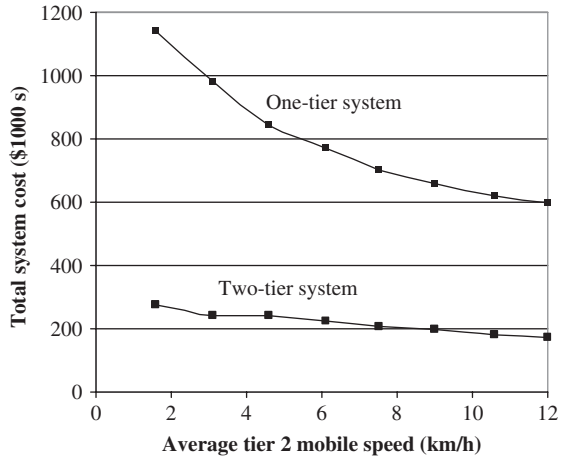

Figure 17.12 Comparison of the total system costs between the one-tier and two-tier systems, $\lambda_1^0 = 1$[calls/(min km^2)] and $\lambda_2^0 = 20$[calls/(min km^2).]

The main conclusion from Figure 17.12 and many other similar runs [21] is that, for the parameter ranges used in this study, the two-tier system outperforms the single-tier system for all the values of the slower and faster mobile speeds.

17.4 LOCAL MULTIPOINT DISTRIBUTION SERVICE

Wireless systems can establish area-wide coverage with the deployment of a single base station. The local multipoint distribution service (LMDS) offers a wireless method of access to broadband interactive services. The system architecture is considered point-to-multipoint since a centralized hub, or base station, simultaneously communicates with many fixed subscribers in the vicinity of the hub. Multiple hubs are required to provide coverage over areas larger than a single cell. Because of the fragile propagation environment at 28 GHz, LMDS systems have small cells with a coverage radius on the order of a few kilometers. Digital LMDS systems can flexibly allocate bandwidth across a wide range of bi-directional broadband services including telephony and high-speed data access.

Multiple LMDS hubs are arranged in a cellular fashion to reuse the frequency spectrum many times in the service area. Complete frequency reuse in each cell of the system is attempted with alternating polarization in either adjacent cells or adjacent hub antenna sectors within the same cell. Subscriber antennas are highly directional with roughly a 9 inch diameter (30–35 dBi) to provide additional isolation from transmissions in adjacent cells and to reduce the received amount of multipath propagation that may cause signal degradation. Since cells are small and the entire spectrum is reused many times, the overall system capacity is quite high, and backhaul requirements can be large. Backhaul networks will probably be a combination of fiber-optics and point-to-point radio links.

The system capacity comes mainly from the huge radio frequency (RF) bandwidth available: block A, 1150 MHz (27.50–28.35, 29.100–29.250 and 31.075–31.225 GHz); and block B, 150 MHz (31.000–31.075 and 31.225–31.300 GHz). For the purpose of frequency planning for two-way usage it is essential to solve the problem of LMDS spectrum partitioning for the upstream and downstream. The standard duplexing options, frequency-division duplex (FDD) and time-division duplex (TDD), are applicable in LMDS too and will not be discussed here in any more detail.

Instead, as a wireless point-to-multipoint system, the deployment of LMDS will be assessed by the basic parameters of cell size and capacity. Obviously, an operator would want to cover as large an area as possible with a minimum number of cell sites, hence maximizing cell size. The modulation and coding, and the ensuing E_b/N_0, are factors in determining cell size. However, because of high rain attenuation at LMDS frequencies, there is a major trade-off between cell size and system availability determined by the rain expectancy for a given geographical area. In most of the United States, for the forthright aim of providing 'wireless fiber' availability of 0.9999–0.99999, the cells would only be between 0.3 and 2 miles [23]. Consequently, the deployment of LMDS will extensively involve multicell scenarios. In the following we review the methods of optimizing system capacity in these scenarios through frequency reuse. The main problem related to frequency reuse is the interference between different segments of the system. Therefore, patterns that create bound and predictable values of S/I are essential to device deployment. Frequency reuse and capacity in interference-limited systems have been discussed in previous sections for mobile cellular and personal communications services (PCS) systems. As the basic methods and principles also apply to fixed systems, there are several major differences in the treatment of fixed broadband wireless systems such as LMDS.

Unlike mobile cellular, in LMDS the subscriber antennae are highly directional and point toward one specific base station. This, together with the nonmoving nature of the subscriber, results in much lower link dynamics. The channel can mostly be described as Rician (with a strong main ray) and not Rayleigh-like in mobile cellular. Since the subscriber employs directive antennae, it is compelled to communicate with only one base station, which excludes the use of macro diversity (or cell diversity) – a very beneficial method with mobile cellular, but one that complicates the interference and frequency reuse analysis.

Also, mobile cellular service was originally intended for voice; therefore, it is designed for symmetric loading, while broadband wireless services generally have more downstream traffic than upstream. This reflects in the main issue of concern for interference study, which in PCS and mobile cellular is upstream interference because the base station receiver has the hard task of receiving from a multitude of mobiles transmitting through nondirectional antennae and suffering different fast fading.

In LMDS the upstream is usually lower-capacity and employs lower-order modulation, which offers better immunity. Also, the slower fading environment allows a closed-loop transmission power control system to operate relatively accurately. Consequently, upstream most subscribers transmit at a power lower than nominal, unlike the downstream transmission. Also, the narrow beam of their antennae is an interference-limiting factor. Therefore, downstream interference is the most problematic, as opposed to the mobile cellular case.

Another parallel with mobile cellular refers to cellular patterns. Owing to the mobile nature of its subscribers, a mobile cellular system has to provide service from the start to a whole area (town, region), with a large number of adjacent cells. The number of sectors is relatively low (2–4); otherwise, the mobile would go through frequent handoffs.

In LMDS, in the long run, owing to the small cell size, the ever increasing hunger for bandwidth and the availability of radio and networking technologies, deployment is also expected to be blanket coverage. However, the economics of LMDS do not require this from the beginning. Operators will probably first offer the service in clusters of business clients with high data bandwidth demands and with the financial readiness for the new service, and later will gradually expand the service to larger areas. Second, the sectorization will be in denser patterns determined by the increasing demand for bandwidth and not limited by the requirement for handoff. The narrower sectors employing higher antenna gain in the base station also provide for larger cell size.

Frequency reuse in one cell is illustrated in Figure 17.13 with three examples of frequency reuse by sectorization. The first step in frequency planning is to assume the division of the available spectrum into subbands, so adjacent sectors will operate on different subbands. Also, the sector structure has to be designed as a function of the capacity required and the S/I specification of

the modem used. The need to divide into subbands is a function of base station antenna quality, specifically the steepness of the rolloff from the main lobe to sidelobes in the horizontal antenna pattern. If the antenna sidelobes roll off very steeply after the main lobe, it is possible to reuse the frequency every two sectors, resulting in patterns of the type A, B, A, B, ..., as in Figure 17.13(b). In this context the reuse factor, F_R, is the number of times the whole band is used in the cell, which for the simplified regular patterns is the number of sectors divided by the number of subbands; in this case $F_R = 3$. In a more conservative deployment the frequency is reused only in back-to-back sectors as in Figure 17.13(a), which has six sectors with reuse pattern A, B, C, A, B, C. Figure 17.13(c) shows a higher-capacity cell where the pattern A, B, C, ..., is repeated in 12 sectors, resulting in $F_R = 4$. Obviously, to keep the equipment cost low, we want a low number of sectors; schemes where we divide the spectrum in as few subbands as possible (two is best).

With present antenna technology at 28 GHz it is possible to achieve sidelobes under −33 dB, but the radiation pattern of the deployed antenna is different. The sidelobes are significantly higher because of scattering effects such as diffraction, reflection or dispersion caused by foliage. The very narrow beamwidth of the subscriber antenna (which at 28 GHz can be reasonably made 3° or lower) helps limit the scattering effect. Obviously, the sum of such effects depends on the millimeter-wave effects in the specific buildings and terrain in the area, and have to be estimated through simulation and measurements for each particular case. Another uncertain factor in the estimation of S/I is the fading encountered by the direct signal. As a starting assessment, we shall consider the above-mentioned effects accountable for increasing the equivalent antenna sidelobe radiation to −25 dB.

Based on this, the following estimations of S/I are only orientative. For each particular deployment the worst case has to be estimated considering the particular conditions.

17.4.1 Interference estimations

To allow A, B, C, ..., type sectorization, in Figure 17.13(a) and (c) the base station antenna sidelobe is $\alpha = -25$ dB at an angle more than 2.5 $B_{3\,dB}$ from boresight, where $B_{3\,dB}$ is the −3 dB beamwidth (the main lobe is between $\pm 0.5\ B_{3\,dB}$). In Figure 17.13(a) and (b), $B_{3\,dB} = 60°$, while in Figure 17.13(c) $B_{3\,dB} = 30°$. In Figure 17.13(b), better-quality antennas are considered, which would achieve the same sidelobe rejection at 1.5 $B_{3\,dB}$, driving frequency reuse higher for the same number of sectors.

17.4.2 Alternating polarization

Figure 17.14(a) shows how a high reuse factor of 6 can be achieved in 12 sectors by alternating the polarity in sectors. The lines' orientations show the polarization, horizontal (H) or vertical (V). The amount of discrimination that can be achieved depends on the environment. Although the antenna technology may provide for polarization discrimination of 30–40 dB, we shall consider that the combination of depolarization effects raises the cross-polarization level to $p = -7$ dB.

The interference is reduced, so the same frequency at the same polarization comes only in the fourth sector. The problem is that a deployment has to allow for gradual sectorization – start by deploying minimum equipment, then split into more sectors as demand grows. However, if alternating polarization is employed in sectors, the operator would have to visit the subscriber sites in order to reorient the antennas. A more conservative approach would be to set two large areas of different polarity, as in Figure 17.14(b). This does not reduce the close-in sidelobes but reduces overall interference and also helps in the multiplecell design. Following is an approximation for the S/I:

$$\frac{S}{I} = \frac{S}{\sum_i I_i + N_R} = \frac{S}{\sum_i \alpha_i S_i + \sum_j p_j \alpha_j S_j + N_R} \tag{17.23}$$

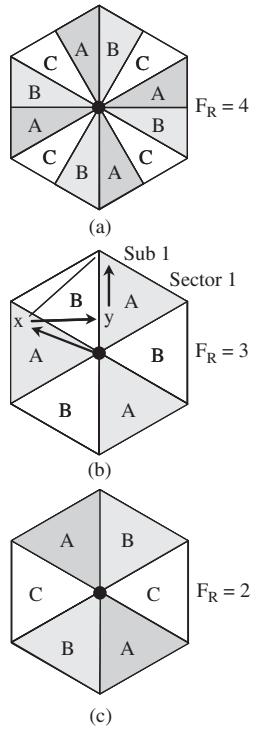

Figure 17.13 Cells with reuse factors of 2, 3 and 4.

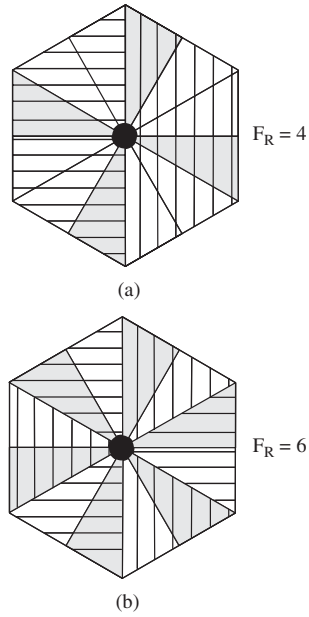

Figure 17.14 Twelve-sector cells with cross-polarization.

Table 17.2 The S/I level at the subscriber receiver

	Figure 17.13(a)	Figure 17.13(b)	Figure 17.13(c)	Figure 17.14(a)	Figure 17.14(b)
S/I in dB	25	22	20	22	25

where S_i are the transmission powers in other sectors using the same subband, I_i the interferers, and N_R the receiver input noise. Later the case will be considered where all transmission powers in sectors are equal to $S_i = S$, and, N_R is neglected. N_1 and N_2 are the number of sectors with the same polarization and the cross-polarized ones, respectively. As well, the worst case values α and p will be taken for the sidelobe gains and cross-polarization:

$$\frac{S}{I} = \frac{1}{\alpha(N_1 + N_2 p)}. \tag{17.24}$$

Thus, in a first approximation [24], by applying Equation (17.24), the S/I level (or co-channel interference, CCI) at the subscriber receiver is given in Table 17.2. The type of modulation and the subsequent modem S/I specification have to be specified with sufficient margin. A modem receiver operates in a complex environment of challenges of which the S/I or CCI is only one. Other impairments such as equalizer errors, adjacent channel interference, phase noise and inter-modulation induced by the RF chain limit the S/I with which the modem can work in the real operation environment. The above technique can be extended to multiple cell scenario. Details can be found in Roman [24].

17.5 SELF-ORGANIZATION IN 4G NETWORKS

17.5.1 Motivation

Self-organization is an emerging principle that will be used to organise 4G cellular networks [25–40]. It is a functionality that allows the network to detect changes, make intelligent decisions based upon these inputs, and then implement the appropriate action, either minimizing or maximizing the effect of the changes. Figure 17.15 illustrates a multitier scenario where numerous self-organizing technologies potentially could be applied.

Frequency planning discussed so far in this chapter was performed by choosing a suitable reuse pattern. Individual frequencies are then assigned to different base stations according to propagation predictions based on terrain and clutter databases.

The need to move away from this type of frequency planning has been expressed in the literature [28] as well as being emphasized by ETSI in the selection criteria for the UMTS air–interface technique. The main reason for this departure is the need for very small cell sizes in urban areas with highly varying morphology, making traditional frequency planning difficult. Another reason lies in the difficulty associated with the addition of new base stations to the network, which currently requires extensive reconfiguration. In view of these two arguments, a desirable solution would require the use of unconfigured base transceiver stations (BTSs) at all sites; these BTSs are installed without a predefined set of parameters and select their operating characteristics on the basis of information achieved from runtime data. For instance, they may operate at all the available carriers and select their operating frequencies to minimize mutual interference with other BTSs [28].

The increasing demand for data services means that the next generation of communication networks must be able to support a wide variety of services. The systems must be location- and situation-aware, and must take advantage of this information to dynamically configure themselves in a distributed fashion [29].

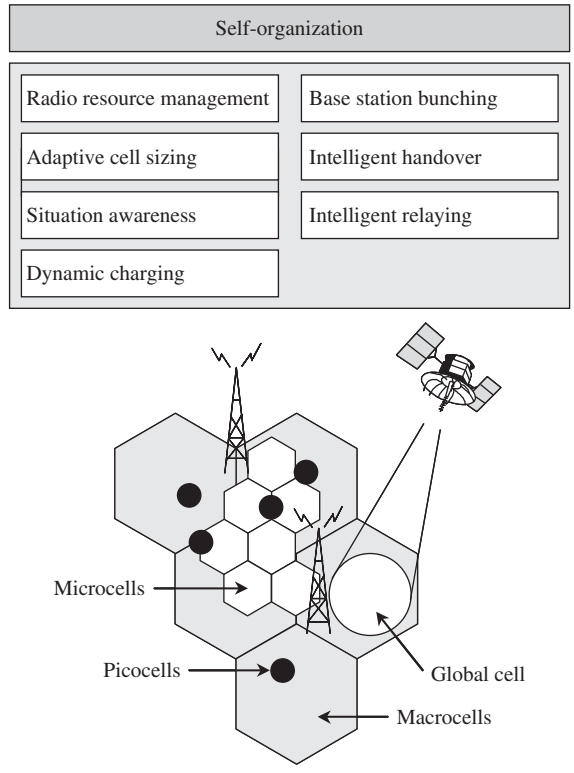

Figure 17.15 Multitier scenario with self-organising technologies.

There will be no central control strategy in 4G, and all devices will be able to adapt to changes imposed by the environment. The devices are intelligent and clearly employ some form of self-organization [30, 31]. So far in our previous discussion, coverage and capacity have been the two most important factors in cellular planning. To have good coverage in both rural and urban environments is important so as to enable customers to use their terminals wherever they go. Coverage gaps mean loss of revenue and can also lead to customers moving to a different operator (which they believe is covering this area better). On the other hand, some areas may not be economically viable to cover from the operator's point of view due to a low population density. Other locations, for instance a sports stadium, may only require coverage at certain times of the day or even week.

Capacity is equally important. Without adequate capacity, users will not be able to enter the network even though there might be suitable coverage in the area. Providing the correct capacity in the correct location is essential to minimize the amount of infrastructure, while ensuring a high utilization of the hardware that has actually been installed. Based on the traffic distribution over the duration of a day reported in Lam *et al*. [32], an average transceiver utilization of only 35 % has been estimated. Improving this utilization is therefore of great interest.

A flexible architecture is essential to enable the wide variety of services and terminals expected in 4G to co-exist seamlessly in the same bandwidth. In addition, future upgrades and reconfigurations should require minimum effort and cost. The initial investment, the running costs and the cost of future upgrades are expected to be the three most important components in determining the total cost of the system.

17.5.2 Networks self-organizing technologies

Capacity, both in terms of bandwidth and hardware, will always be limited in a practical communication system. When a cell becomes congested, different actions are possible. The cell could borrow resources, bandwidth or hardware, from a neighboring cell. It could also make a service handover request to a neighbor in order to minimize the congestion. Thirdly, a service handover request could be made to a cell in a layer above or below in the hierarchical cell structure. Finally, the cell could try to reduce the path loss to the mobile terminal to minimise the impact of other cell interference. If neighboring cells are unable to 'assist' the congested cell, the options left for the cell are to degrade the users' service quality (if it is interference limited) or to try and influence the users' behavior. This can be achieved through service pricing strategies. The pricing scheme can be regarded as a protection mechanism for the network. Since it cannot create capacity, only utilise what it already has, it needs to force the users to adapt their behavioral pattern until the network is upgraded or there is more capacity available. Self-organizing technologies fall into one of these categories.

17.5.2.1 Bunching of base stations

In a micro- and picocellular environment there will be severe fluctuations in traffic demand, user mobility and traffic types. This highly complex environment will require advanced radio resource management (RRM) algorithms and it will be beneficial to have a central intelligent unit that can maximize the resource utilization. The bunch concept has been proposed as a means to deal with this issue. It involves a central unit (CU) that controls a set of remote antennas or base stations (which have very little intelligence). The central units will deal with all decisions on channel allocation, service request and handover. Algorithms for layers 1 and 2 (such as power control) may be controlled by the remote unit itself. The bunch concept can be viewed simply as a very advanced base station with a number of small antennas for remote sensing. The central unit will therefore have complete control over all the traffic in its coverage area and will be able to maximize the resource utilization for the current traffic. This provides opportunities for uplink diversity and avoids intercell handovers in its coverage area. The bunch approach will typically be deployed in city centres, large buildings or even a single building floor.

17.5.2.2 Dynamic charging

The operators need to encourage users to utilize the network more efficiently, something that can be achieved through a well thought-out pricing strategy. Pricing becomes particularly important for data services such as e-mail and file transfer as these may require considerable resources but may not be time-critical. A large portion of e-mails (which are not time-critical) could, for example, be sent during off-peak hours, hence improving the resource utilization. In this area two main approaches are used, *user utility method* and *maximum revenue method*.

User utility algorithms assume that the user associates a value to each service level that can be obtained. The service level is often referred to as the user's *utility function* and it can be interpreted as the amount the user is willing to pay for a given quality of service. It is assumed that the user acts 'selfishly', always trying to maximize their own utility (or service). The whole point with a pricing strategy is to enable the operator to predict how users will react to it, something which is not trivial. Current proposals do not try to determine the exact user's utility function, but rather to postulate a utility function which is based on the characteristics of the application or service. Two prime examples are voice and data services, which exhibit very different characteristics. Although speech applications are very sensitive to time delays, they are relatively insensitive to data errors. Similarly, although data services are relatively insensitive to time delays, they are very sensitive to data errors.

The *maximum revenue method* suggested in Bharghavan *et al*. [36] is based on letting the network optimize its revenue by allocating resources to users in a manner which is beneficial for the network. The two main principles are to maximize the resources allocated to static flows and to minimize the variance in resources allocated to mobile flows. These rules are based on the assumption that, whereas a static user's preference is for maximum data rate, mobile users are more concerned with the variance in service quality as they move from cell to cell. The actual revenue model is based on a 4-tuple, $<A, T, C_a, F>$, namely admission fee, termination credit, adaptation credit and revenue function. The network uses these parameters to optimize its revenue. Maximum revenue is calculated according to the following rules: (1) the flow pays an admission fee once it is granted its minimum requested resource allocation; (2) if a flow is prematurely terminated by the network, the latter pays the flow a termination credit; (3) the network pays the flow an adaptation credit if the resource allocation is changed during the transmission, regardless of whether the allocation is increased or reduced; (4) the flow pays a positive but decreasing marginal revenue for each extra unit granted by the network. The flow does not pay for resources allocated above its maximum requested resource allocation.

Intelligent relaying is a technique that can minimize the amount of planning and the number of base stations required in a cellular network. A network employing intelligent relaying includes mobiles that are capable of passing data directly to other mobiles, rather then directly to a base station, as for a conventional cellular network. In order to plan a network incorporating intelligent relaying, it is convenient to consider each mobile as a 'virtual cell', acting as a base station at its center. The coverage area of this virtual cell, as seen in Figure 17.16, can be varied according to the circumstances, as the mobile changes its transmit power and according to the mobility of the user. The mobile will set the radius of its virtual cell according to the number of other mobiles in the vicinity available to relay data; the size of the virtual cell will be minimized to improve frequency reuse.

Context awareness in 4G will, for example, be a scenario in which devices such as personal digital assistants (PDAs) should be able to communicate at short range with a number of other devices. These devices might be a fax machine, a computer, a mobile phone, a printer or a photocopier. Assuming all these devices have a low-power radio, then the PDA would be able to engage any of the devices. The task could be printing documents, downloading documents, faxing a message or uploading data for storage. To the user, the interdevice communication will be transparent. The user will only be concerned with the task they are performing, not the devices they

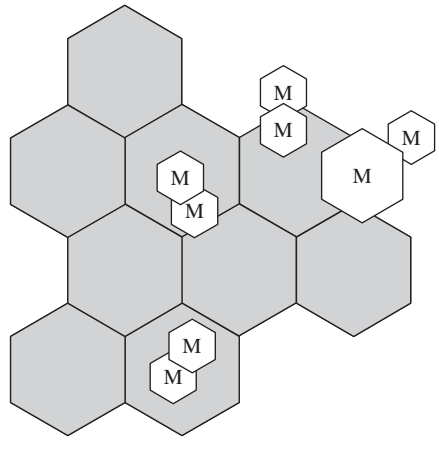

Figure 17.16 An intelligent-relaying overlay.

are connected with. This sort of communication between electronic devices can be achieved through transmission of beacon signals, which provide relevant information such as device capability and identification. As manufacturers throughout the world are incorporating the Bluetooth technology into their products, this concept is about to materialize [41].

The context or situation awareness concept can also be exploited in cellular networks. In current cellular systems, base stations transmit information on their broadcast control channel, which can be used to implement this idea. Assuming this information includes $I = [id, x\_lat, y\_long, Tx]$ (base station identity, position in latitude and longitude, broadcast control channel transmit power), then this would enable the network to reconfigure its base station coverage areas when a base station is removed or added to the network.

Dynamic cell sizing is another emerging technique that has received considerable interest in the literature [40]. By dynamically adjusting the coverage areas of the cells, optimum network performance can be achieved under any traffic conditions. When a single cell is heavily occupied, which the surrounding cells are lightly loaded, it is possible with this scheme to reduce the cell size of the loaded cell and to increase the size of the surrounding cells. In this manner, more users can be accommodated in the centre cell. This can be implemented in such a way that the base station controls its attachment area by increasing or decreasing its beacon transmit power, hence increasing or decreasing the area in which mobiles will connect to the base station. Under congestion the cell will contract such as to limit its service area and reduce the inter-base-station interference. This will enable it to serve more users closer to the base station. In the limit, the cell is so small that the interference contribution of neighboring base stations can be ignored and maximum capacity is achieved. In light traffic conditions it will expand and hence improve the network coverage with cells overlapping the same area. The cell to which the user connects will therefore be a function not only of the path loss between the base station and the user but also of the beacon transmit power.

Intelligent handover (IH) techniques can be made more intelligent, also considering parameters such as resource utilization. A fast-moving mobile user who is currently served by a cell may run into problems in the next cell because it is fully congested. An intelligent handover algorithm would be able to recognize this problem and try to solve it by handing the user to the microcellular layer. The user will stay in this layer until the blocked cell has been passed, upon which it will be handed back to the macro layer. Similarly, if there is no coverage on the user's home network in the area in which they are moving, then the IH algorithm should seek to maintain the connection by handing over to a competitor's network or a private network offering capacity to external users. Performance evaluation of the above techniques can be found in Spilling *et al*. [42].

REFERENCES

[1] S.G. Glisic, *Adaptive WCDMA, Theory and Practice*. Wiley: Chichester, 2003.

[2] S.G. Glisic and P. Pirinen, Co-channel interference in digital cellular TDMA networks, in *Encyclopedia of Telecommunications*, ed. J. Proakis. Wiley: Chichester, 2003.

[3] N. Srivastava and S.S. Rappaport, Models for overlapping coverage areas in cellular and micro-cellular communication systems, in *IEEE GLOBECOM '91*, Phoenix, AZ, 2–5 December 1991, pp. 26.3.1–26.3.5.

[4] G.L. Choudhury and S.S. Rappaport, Cellular communication schemes using generalized fixed channel assignment and collision type request channels, *IEEE Trans. Vehicular Technol.*, vol. VT-31, 1982, pp. 53–65.

[5] B. Eklundh, Channel utilization and blocking probability in a cellular mobile telephone system with directed retry, *IEEE Trans. Commun.*, vol. COM-34, 1986, pp. 329–337.

[6] J. Karlsson and B. Eklundh, A cellular mobile telephone system with load sharing – an enhancement of directed retry, *IEEE Trans. Commun.*, vol. COM-37, 1989, pp. 530–535.

[7] T.-P. Chu and S.S. Rappaport, Generalized fixed channel assignment in microcellular communication systems, *IEEE Trans. Vehicular Technol.*, vol. 43, 1994, pp. 713–721.
[8] T.-P. Chu and S.S. Rappaport, Overlapping coverage and channel rearrangement in microcellular communication systems, *IEEE Proc. Comm.*, vol. 142, no. 5, 1995, pp. 323–332.
[9] S.W. Halpern, Reuse partitioning in cellular systems, in *IEEE Vehicular Technology Conf.*, *VTC '83*, Toronto, 25–27 May 1983, pp. 322–327.
[10] K. Sallberg, B. Stavenow and B. Eklundh, Hybrid channel assignment and reuse partitioning in a cellular mobile telephone system, in *IEEE Vehicular Technology Conf. VTC '87*, Tampa, FL 1–3 June 1987, pp. 405–411.
[11] J. Zander and M. Frodigh, Capacity allocation and channel assignment in cellular radio systems using reuse partitioning, *Electron. Lett.*, vol. 28, no. 5, 1992, pp. 438–440.
[12] D. Hong and S.S. Rappaport, Traffic model and performance analysis for cellular mobile radio telephone systems with prioritized and non-prioritized handoff procedures, *IEEE Trans. Vehicular Technol.*, vol. VT-35, 1986, pp. 77–92.
[13] S.S. Rappaport, The multiple-call handoff problem in high-capacity cellular communications systems, *IEEE Trans. Vehicular Technol.*, vol. 40, 1991, pp. 546–557.
[14] S.S. Rappaport, Blocking, handoff and traffic performance for cellular communication systems with mixed platforms, *IEEE Proc. I*, vol. 140, no. 5, 1993, pp. 389–401.
[15] L.P.A. Robichaud, M. Boisvert and J. Robert, *Signal Flow Graphs and Applications*. Prentice-Hall: Englewood Cliffs, NJ, 1962.
[16] H. Jiang and S.S. Rappaport, Handoff analysis for CBWL schemes in cellular communications, College of Engineering and Applied Science, State University of New York, Stony Brook, CEAS Technical Report no. 683, 10 August 1993.
[17] T.-P. Chu and S. Rappaport, Overlapping coverage with reuse partitioning in cellular communication systems, *IEEE Trans. Vehicular Technol.*, vol. 46, no. 1, 1997, pp. 41–54.
[18] D. Grieco, The capacity achievable with a broadband CDMA microcell underlying to an existing cellular macrosystem, *IEEE J. Select. Areas Commun.*, vol. 12, no. 4, 1994, pp. 744–750.
[19] S. Glisic and B. Vucetic, *Spread Spectrum CDMA Systems for Wireless Communications*. Artech House: Norwood, MA, 1997.
[20] J.-S. Wu, J.-K. Chung and Y.-C. Yang, Performance study for a microcell hot spot embedded in CDMA macrocell systems, *IEEE Trans. Vehicular Technol.*, vol. 48, no. 1, 1999 pp. 47–59.
[21] A. Ganz, C.M. Krishna, D. Tang and Z.J. Haas, On optimal design of multitier wireless cellular systems, *IEEE Commun. Mag.*, vol. 35, 1997, pp. 88–94.
[22] R. Guérin, Channel occupancy time distribution in a cellular radio system, *IEEE Trans. Vehicular Technol.*, vol. VT-35, no. 3, 1987, pp. 627–635.
[23] P.B. Papazian, G.A. Hufford, R.J. Achate and R. Hoffman, Study of the local multipoint distribution service radio channel, *IEEE Trans. Broadcasting*, vol. 43, no. 2, 1997, pp. 175–184.
[24] V.I. Roman, Frequency reuse and system deployment in local multipoint distribution service, *IEEE Person. Commun.*, December 1999, pp. 20–28.
[25] M. Schwartz, Network management and control issues in multimedia wireless networks, *IEEE Person. Commun.*, June 1995, pp. 8–16.
[26] A.O. Mahajan, A.J. Dadej and K.V. Lever, Modelling and evaluation network formation functions in self-organising radio networks, in *Proc. IEEE Global Telecommunications Conf., GLOBECOM*, London, 1995, pp. 1507–1511.
[27] R.W Nettleton and G.R. Schloemar, Selforganizing channel assignment for wireless systems, *IEEE Commun. Mag.*, August 1997, pp. 46–51.
[28] M. Frullone, G. Rira, P. Grazioso and G. Fabciasecca, Advanced planning criteria for cellular systems, *IEEE Person. Commun.*, December 1996, pp. 10–15.

[29] R. Katz, Adaptation and mobility in wireless information systems, *IEEE Person. Commun.*, vol. 1, 1994, pp. 6–17.
[30] M. Flament, F. Gessler, F. Lagergen, O. Queseth, R. Stridh, M. Unbedaun, J. Wu and J. Zander, An approach to 4th Generation wireless infrastructures – scenarios and key research issues, *IEEE 49th Vehicular Technology Conf.*, Houston, TX, 16–20 May 1999, vol. 2, pp. 1742–1746.
[31] M. Flament, F. Gessler, F. Lagergen, O. Queseth, R. Stridh, M. Unbedaun, J. Wu and J. Zander, Telecom scenarios 2010 – a wireless infrastructure perspeclive. A PCC report is available at: www.s3,kth.se/radio/4GW/publk7Papers/ScenarioRcport.pdf
[32] D. Lam, D.C. Cox and J. Widom, Teletraffic modelling for personal communications services, *IEEE Commun. Mag.*, vol. 35, no. 2, 1997, pp. 79–87.
[33] E.K. Tameh and A.R. Nix, The use of measurement data to analyse the performance of rooftop diffraction and foliage loss algorithms in 3-D integrated urban/rural propagation model, in *Proc. IEEE 48th Vehicular Technology Conf.*, Ottawa, vol. 1, May 1998, pp. 303–307.
[34] First European initiative on re-configurable radio systems and networks, European Commission Green Paper version 1.0.
[35] A.G. Spilling, A.R. Nix, M.P. Fitton and C. Van Eijl, Adaptive networks for UMTS, in *Proc. 49th IEEE Vehicular Technology Conf.*, Houston, TX, vol. 1, 16–18 May 1999, pp. 556–560.
[36] V. Bharghavan, K.-W. Lee, S. Lu, S. Ha, J.-R. Li and D. Dwyer, The TIMELY adaptive resource management architecture, *IEEE Person. Commun.*, August 1998, pp. 20–31.
[37] T.J. Harrold and A.R. Nix, Intelligent relaying for future personal communication systems, in *IRK Colloquium on Capacity and Range Enhancement Techniques for Third Generation Mobile Communications and Beyond*, February 2000, IEEE Colloquium Digest no. 00/003, pp. 9/l–5.
[38] N. Bambos, Toward power-sensitive network architectures in wireless communications: concepts, issues and design aspects, *IEEE Person. Commun.*, June 1998, pp. 50–59.
[39] A.G. Spilling and A.R. Nix, aspects of self-organisation in cellular networks, in *9th IEEE Symp. Personal Indoor and Mobile Radio Communications*, Boston, MA, 1998, pp. 682–686.
[40] T. Togo, I. Yoshii and R. Kohro, Dynamic cell-size control according to geographical mobile distribution in a DS/CDMA cellular system, in *9th IEEE Symp. Personal Indoor and Mobile Radio Communications*, Boston, MA, 1998, pp. 677–681.
[41] J.C. Tiaartson, The Bluetooth radio system, *IEEE Person. Commun.*, vol. 7, no. 1, February 2000, pp. 28–36.
[42] A.G. Spilling, A.R. Nix, M.A. Beach and T.J. Harrold, Self-organisation in future mobile communications, *Electron. Commun. Engng. J.*, June 2000, pp. 133–147.

18

Network Management

18.1 THE SIMPLE NETWORK MANAGEMENT PROTOCOL

Back in 1988, the simple network management protocol (SNMP), was designed to provide an easily implemented, low-overhead foundation for multivendor network management of different network resources. The SNMP specification: (1) defines a protocol for exchanging information between one or more management systems and a number of agents; (2) provides a framework for formatting and storing management information; and (3) defines a number of general-purpose management information variables, or objects. The model of network management that is used for SNMP includes the following key elements: management station, management agent, management information base and network management protocol.

The *management station* will have, at least: (1) a set of management applications for data analysis, fault recovery, and so on; (2) an interface by which the network manager may monitor and control the network by communicating with the managed elements of the network; (3) a protocol by which the management station and managed entities exchange control and management information; (4) The management station maintains at least a summary of the management information maintained at each of the managed elements in the network in its own database of information. Only the last two elements are the subject of SNMP standardization.

The *management agent* is a piece of SNMP software in key platforms, such as hosts, bridges, routers and hubs, by which they may be managed from a management station. The management agent responds to requests for information from a management station, responds to requests for actions from the management station, and may asynchronously provide the management station with important but unsolicited information. In order to manage the resources in a network, these resources are represented as objects. Each object is essentially a data variable that represents one aspect of the managed system. The collection of objects is referred to as a management information base (MIB). The MIB functions as a collection of access points at the agent for the management station; the agent software maintains the MIB. These objects are standardized across systems of a particular class (e.g. bridges all support the same management objects). A management station performs the monitoring function by retrieving the value of MIB objects. A management station can cause an action to take place at an agent or can change the configuration settings of an agent

Advanced Wireless Technologies: Cognitive, Cooperative & Opportunistic 4G Technology Second Edition Savo G. Glisic

by modifying the value of specific variables. The management station and agents are linked by a network management protocol, which includes the following key capabilities:

(1) Get – used by the management station to retrieve the values of objects at the agent.

(2) Set – used by the management station to set the values of objects at the agent.

(3) Trap – used by an agent to notify the management station of significant events.

SNMP was designed to be an application-level protocol that is part of the TCP/IP protocol suite and typically operates over the user datagram protocol (UDP), although it may also operate over TCP. A manager process controls access to the central MIB at the management station and provides an interface to the network manager. The manager process achieves network management by using SNMP, which is implemented on top of UDP and IP.

Each agent must also implement SNMP, UDP and IP. In addition, there is an agent process that interprets the SNMP messages and controls remote access to the agent's MIB. For an agent device that supports other applications, such as FTP, TCP as well as UDP is required. From a management station, three types of SNMP messages are issued on behalf of a management application: *GetRequest*, *GetNextRequest* and *SetRequest.* The first two are variations of the *get* function. All three messages are acknowledged by the agent in the form of a *GetResponse* message, which is passed up to the management application. In addition, an agent may issue a *trap* message in response to an event that affects the MIB and the underlying managed resources. SNMP relies on UDP, which is a connectionless protocol, and SNMP is itself connectionless. No ongoing connections are maintained between a management station and its agents. Instead, each exchange is a separate transaction between a management station and an agent.

Trap-directed polling technique is used if a management station is responsible for a large number of agents, and if each agent maintains a large number of objects. In this case it becomes impractical for the management station to regularly poll all agents for all of their readable object data. Instead, at initialization time, and perhaps at infrequent intervals, such as once a day, a management station can poll all the agents it knows of for some key information, such as interface characteristics, and perhaps some baseline performance statistics, such as average number of packets sent and received over each interface over a given period of time. Once this baseline is established, the management station refrains from polling. Instead, each agent is responsible for notifying the management station of any unusual event. Examples are if the agent crashes and is rebooted, the failure of a link or an overload condition as defined by the packet load crossing some threshold. These events are communicated in SNMP messages known as traps.

Once a management station is alerted to an exception condition, it may choose to take some action. At this point, the management station may direct polls to the agent reporting the event and perhaps to some nearby agents in order to diagnose any problem and to gain more specific information about the exception condition. Having in mind that traps are communicated via UDP and are therefore delivered unreliably, a management station may wish to infrequently poll agents. All these options should be used in such a way as to provide a reliable network management with minimum overhead traffic generated in the network.

The use of SNMP requires that all agents, as well as management stations, must support UDP and IP. This limits direct management to such devices and excludes other devices, such as some bridges and modems, that do not support any part of the TCP/IP protocol suite. Furthermore, there may be numerous small systems (personal computers, workstations, programmable controllers), that do implement TCP/IP to support their applications, but for which it is not desirable to add the additional burden of SNMP, agent logic and MIB maintenance.

To accommodate devices that do not implement SNMP, the concept of proxy was developed. In this scheme an SNMP agent acts as a proxy for one or more other devices; that is, the SNMP agent acts on behalf of the proxied devices. Figure 18.1 indicates the type of protocol architecture that is often involved. The management station sends queries concerning a device to its proxy agent.

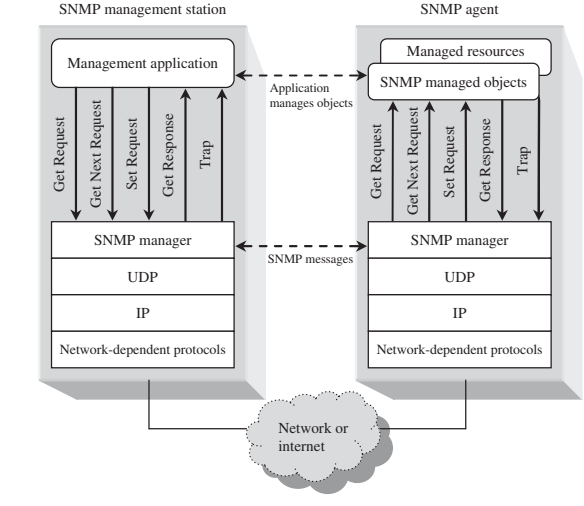

(a)

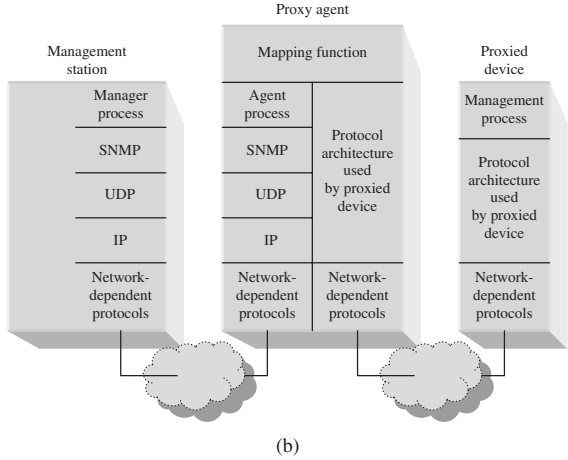

(b)

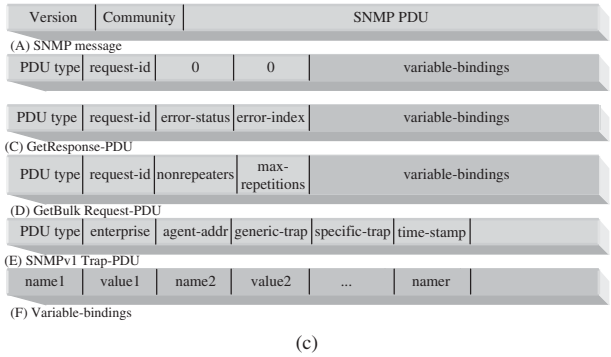

(c)

Figure 18.1 (a) Position of SNMP in the protocol stack; (b) proxy protocol architecture; (c) SNMP formats (reproduced by permission of IEEE [47]); (d) SNMP message and PDU fields (reproduced by permission of IEEE [47]).

Field	Description
Version	SNMP version; RFC 1157 is version 1
Community	A pairing of an SNMP agent with some arbitrary set of SNMP application entities. The name of the community functions as a password to authenticate the SNMP message
Request-id	Used to distinquish among outstanding request by providing each request with unique ID
Error-status	Used to indicate that an expection occured while processing a request. Values are: noError (0), tooBig (1), noSuchname (2), badValue (3), readOnly (4), genErr (5)
Error-index	When error-status is nonzero, error-index may provide additional information by indicating which variable in a list caused the exception. A variable is an instance of a managed object
Variable-bindings	A list of variable names and corresponding values. In some cases (e.g. GetRequest-PDU), the values are null
Enterprise	Type of object generating trap; based on sysObjectID
Agent-addr	Address of object generating trap
Generic-trap	Generic trap type. Values are: coldStart (0), warmStart (1), linkDown (2), linkUp (3), authenticationFailure (4), egpNeighborLoss (5), enterpriseSpecific (6)
Specific-trap	Specific trap code
Time-stamp	Time elapsed between the last (re)initialization of the network entity and the generation of the trap; contains the value of sysUpTime
Non-repeaters	Indicates how many listed variables are to return just one value each
Max-repetitions	Indicates number of values to be returned for each of the remaining variables

(d)

Figure 18.1 *(continued.)*

The proxy agent converts each query into the management protocol that is used by the device. When a reply to a query is received by the agent, it passes that reply back to the management station. Similarly, if an event notification of some sort from the device is transmitted to the proxy, the proxy sends that on to the management station in the form of a trap message. The format of the SNMPv1 message is given in Figure 18.1. More data for versions $v2 - v3$ and any additional detail on SNMP protocols can be found in References [1–6].

In a traditional centralized network management scheme, one host in the configuration has the role of a network management station; there may possibly be one or two other management stations in a backup role. The remainder of the devices on the network contain agent software and an MIB, to allow monitoring and control from the management station. As networks grow in size and traffic load, such a centralized system is unworkable. Too much burden is placed on the management station, and there is too much traffic, with reports from every single agent having to wend their way across the entire network to headquarters. In such circumstances, a decentralized, distributed approach works better. In a decentralized network management scheme, there may be multiple top-level management stations, which might be referred to as management servers. Each such server might directly manage a portion of the total pool of agents. However, for many of the agents, the management server delegates responsibility to an intermediate manager. The intermediate manager plays the role of manager to monitor and control the agents under its responsibility. It also plays an agent role to provide information and accept control from a higher-level management server. This type of architecture spreads the processing burden and reduces total network traffic and will be discussed in more detail in the next section.

The *common management information protocol* (CMIP) [8, 9] was proposed as a standard to supercede SNMP. The standards are exhaustive in their specifications and include almost every possible detail for network management functions. CMIP was specified to work over the OSI protocol stack. The drawbacks of CMIP are: (1) it is complex to use and implement; (2) it requires many resources to execute; (3) it has high overhead; and (4) few networks use the OSI protocol suites.

The *LAN man management protocol* (LMMP) [8] was developed as a network management solution for LANs. LMMP was built over the IEEE 802 logical link layer (LLC). Therefore, it is independent of the network layer protocol. Functionally, it is equivalent to common management information service over IEEE 802 LLC (CMOL). The advantages of LMMP are that it is easier to implement and protocol-independent. The disadvantages are that LMMP messages cannot go beyond a LAN boundary because LMMP does not use any network layer facilities. LMMP agents are also not dynamically extensible.

The *telecommunications management network* (TMN) [11] was built over the OSI reference model, but it includes support for signaling system number 7, TCP/IP, ISDN, X.25 and 802.3 LAN-based networks. TMN has some advantages over the existing standards. For instance, TMN supports a larger number of protocols suites, incorporates features from existing management protocols, has wider domain of acceptance, and is 'future proof'. The disadvantages are that large amounts of processing are required, and agents are not extensible at run time.

18.2 DISTRIBUTED NETWORK MANAGEMENT

As already indicated in Section 18.1, centralized network management systems (NMSs) are clients to management agents (servers) residing permanently in each managed network element (NE). Although adequate for most practical management applications, the limitations of SNMP, such as the potential processing and traffic bottleneck at the NMS, have been recognized for many years.

The inefficiency can be reduced by distributing network management functions to a hierarchy of mid-level managers, each responsible for managing a portion of the entire network, as in SNMPv2. Subnetworks can be managed in parallel, reducing the traffic and processing burden on the highest level NMS. Typically, the distribution of network management functions and the organization of managers are fairly static. It has been observed that decentralizing network management functions may achieve several benefits [12–22].

(1) network traffic and processing load in the NMS can be both reduced by performing data processing closer to the NEs;

(2) scalability to large networks is improved;

(3) searches can be performed closer to the data, improving speed and efficiency; and

(4) distributed network management is inherently more robust without depending on continuous communications between the NMS and NEs.

In general in this context, the network management approaches will be classified as shown in Figure 18.2. In Figure 18.2(a), the *client–server* (CS) model represents the traditional SNMP paradigm where a centralized NMS polls a network of network elements. The communications between the NMS (*client*) and agents (*server*) is characterized by pairs of query–response messages for every interaction. Figure 18.2(b) represents a *hierarchical static* (HS) approach modeled as mid-level managers, each managing a separate subnetwork of network elements.

A two-level hierarchy is considered here, although multiple hierarchical layers may be possible. Each subnetwork is managed in a client–server manner and mid-level managers may communicate with a centralized high-level NMS as needed.

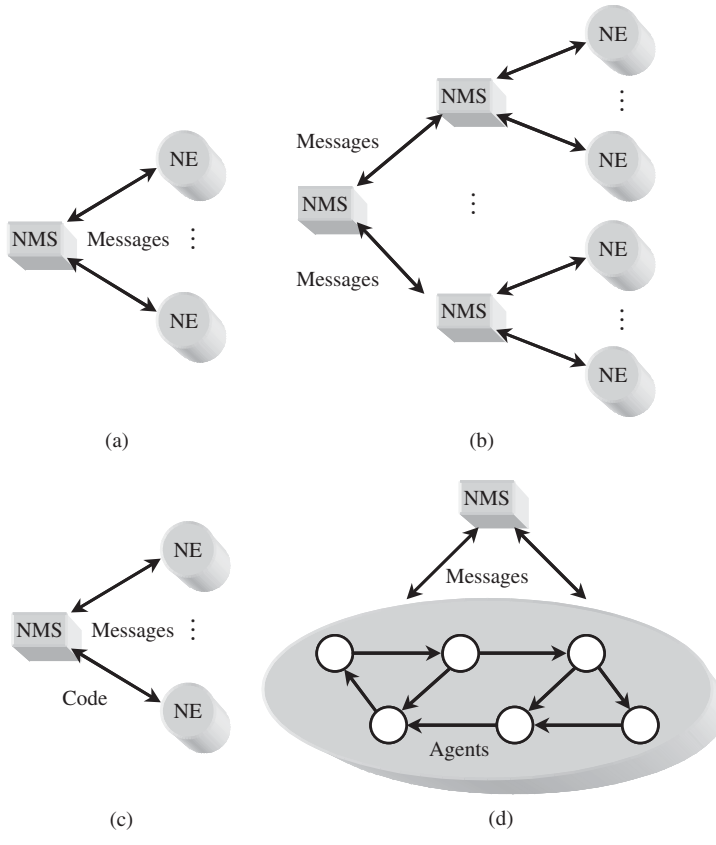

Figure 18.2 Centralized and distributed network management approaches. (a) Client–server; (b) hierarchical static; (c) weak mobility; and (d) strong mobility.

In the *weak mobility* (WM) approach, the NMS distributes code to specific NEs where the code is executed, as shown in Figure 18.2(c). After performing its specific task, the code will typically report results back to the NMS and expire at the NE. During execution, the code does not have a capability for autonomous migration to other NEs. In the *strong mobility* (SM) approach, the NMS dispatches one or more agents to carry out a specific task, as shown in Figure 18.2(d). Agents have the capability to autonomously travel (execution state and code) among different NEs to complete their tasks. The route may be predetermined or chosen dynamically, depending on the results at each NE.

18.3 MOBILE AGENT-BASED NETWORK MANAGEMENT

As already discussed in Chapters 1 and 16, 4G itself will become a competitive marketplace with a diversity of vendors, operators and customers. In this environment, users will be able to choose from a wide range of network services, which provide different bandwidth requirements and various QoS, and which will operate under different pricing schemes. Technical and market forces are driving the evolution of 4G toward the traded resource service architecture (TRSA) model, whereby network resources such as bandwidth, buffer space and computational power will be traded in the same manner as existing commodities.

In such complicated environments, users, whether buyers or sellers, need tools that facilitate expertise brokering activities such as buying or selling the right products, at the right price and at the right time. The brokering process will be guided by user preferences, which need to be processed according to some customized logic. The mobile agent technology seems to be a feasible option for dealing with these issues [23–34]. In other words, an *ad hoc* software sent across the network may allow network resources to be used more effectively, as they can be directly controlled at the application level.

In order to provide each customer with the opportunity of implementing his/her own policy, trading costs with service quality according to his/her own preferences and capacities, network service must be open, flexible and configurable upon demand. A first step toward the realization of a programmable network is that of using an agent-based approach, in order to obtain a faster time scale of service deployment. A major incentive for an agent-based approach is that policies can be implemented dynamically, allowing for a resource-state-based admission and reservation strategy. Agents are used to discover about resources available inside the network and claim resources on behalf of customers according to some 'figures of merit' [25], which represent tradeoffs between bandwidth claimed and loss risk incurred due to high utilization. Different customers may pay for resources in a different way, negotiating the costs for obtaining a certain 'figure of merit'. Agents are able to trigger adaptation of applications inside the network on behalf of customers. This allows for an immediate response to resource shortages, decreases the amount of useless data transported and reduces the signaling overhead. Mobile agents [26] provide the highest possible degree of flexibility and can carry application-specific knowledge into the network to locations where it is needed, following an approach similar to the one shown in some other programmable network projects discussed in Chapter 16 [23, 27].

As already indicated in Section 18.2, by adopting mobile code technology in network management it is possible to overcome some limitations of the centralized management approach. In general, such technology is based on the idea of reversing the logic according to which the data produced by network devices are periodically transferred to the central management station. Management applications can then be *moved* to the network devices, thus, performing (locally) some micromanagement operations, and reducing the workload for the management station and the traffic overhead in the network.

The *code on demand* paradigm, used in this concept, relies on a client which can dynamically download and execute code modules from a remote code server. The client has no need for unnecessary code installed, except for the runtime system allowing these mechanisms. Java applets are a very common example of such type of technology. The use of an approach based on code on demand increases the flexibility of the system, and maintains agents simple and *small* at the same time.

The *remote evaluation* paradigm, is based on the idea that a client sends a procedure to be executed on a remote host, where it is run up to the end; the results are, therefore, returned to the client host which sent the code. This paradigm allows the issue of the bandwidth waste that occurs in a centralized system when micromanagement operations are needed to be dealt with. In a traditional system, no matter which processing has to be performed on the data of the device, they have to be moved from the SNMP-agent to the NMS, where they are processed. Conversely, thanks to the mechanism of remote evaluation, the actions to be performed can be developed and sent to the remote device, where they will be executed without generating traffic in the network (except the initial one for sending the code to be executed). A typical example is the computation of the so-called *health functions* [24]. In general, by health function we mean an expression consisting of several elementary management variables. Each variable provides a particular measure concerning the device to be controlled. By using a technology based on remote evaluation, we can compute these functions directly on the devices, and only when necessary. The code that performs such computations will be sent by the NMS and dynamically executed. This approach allows obtaining what is called '*semantic compression of data*'. In general the manager

of a network is not interested in the single value of an MIB variable, but in aggregate values containing higher-level '*information*'. We can, therefore, develop a system in which the manager writes its management functions (or they might be already available), and then invokes their remote execution on specific devices, when necessary.

The *mobile agent* adds more benefits to the ones that can be obtained with remote evaluation. In fact, in this case the action on a device is always expressly started by the NMS. Conversely, in the case of mobile agents, the ability to store the state during the movements allows applications to be developed in which the agent moves from one device to another, performing the management functions required. In addition, the agent can be delegated the task of deciding where and when to migrate according to its current state, thus reducing the interaction with the NMS, and making processing more distributed.

18.3.1 Mobile agent platform

Different platforms have been designed for the development and the management of mobile agents that give all the primitives needed for their creation, execution, communication, migration, etc. [24, 32, 35, 36]. The following agents are used:

The *browser agent* (BA) collects some MIB variables from a set of nodes specified by the user. Both the variables of the MIB-tree to be collected and the servers to be visited are selected through an appropriate dialog box of the application '*SNMP-monitoring*'. After being started, the agent reaches the first node to be visited, opens an SNMP local communication session, builds a PDU-request containing the MIB variables to be searched, waits for the reply from the SNMP daemon, and saves the data obtained in an internal structure. Then, if other nodes need to be visited, it reaches them, and repeats the procedure mentioned above. Otherwise, it returns to the platform from which it has been launched, where the results of the research are presented.

The *daemon agent* (DA) monitors a 'health function' defined by the user. For starting the agent, the function to be computed and the node of the network (where the computation has to be done) must be provided. Then this agent moves to the node in question, where it records the value of the function: if the value is higher than a fixed threshold (defined by the user), a notification message is sent to the server from which the agent has departed. The two agents described before directly interact with the SNMP daemon present in the different nodes.

The *messenger agent* (MA), during its migration through the nodes of the network, interacts with other agents for collecting specific information produced by them. During the configuration, the agents to be contacted and the servers where they have to be searched need to be selected and (if necessary) also the number of times the agent has to contact such agents. Thus, the MA performs operations at a higher abstraction level than the mere retrieval of MIB variables. In fact, since DAs can perform the computation of any function on the different nodes of the network, the messenger allows collection of such information, thus obtaining a general description about the state of the network.

The *verifier agent* does not perform an actual network management action. Its task is that of collecting important information, which might be useful for further operations of network management, from remote network devices to the starting host. It visits the nodes selected during the configuration, and computes a function whose purpose is the evaluation of the presence of a specific property of the system visited (for example, a software version, or the available space on disk, or the verification of some log files, etc.). The verifier agent then reports to the server, from which it departed, the list of the nodes that satisfy this property.

18.3.2 Mobile agents in multioperator networks

In 4G networks, many types of providers will be usually involved in order to complete the end-to-end service offering. Specifically, the SP (service provider) is responsible for the definition

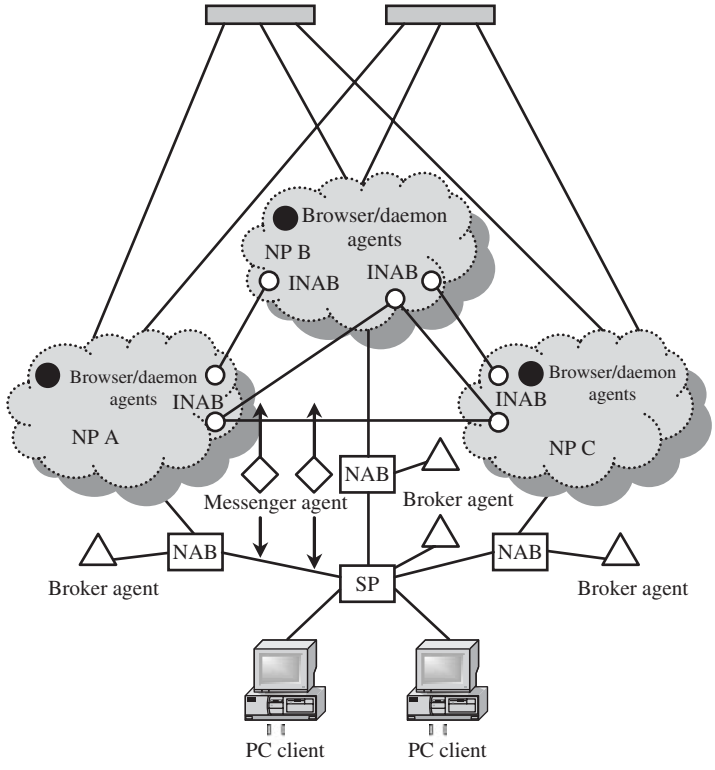

Figure 18.3 Network model for agent brokering environment.

end delivery of the service characteristics, while the NP (network provider) provides the network infrastructure (i.e. high-speed network). In such an arrangement, the SP is essentially a customer of the NP, while the SP provides the service to its own customers or end-users (usually multiple customers with small to medium size). As a means of competition, many different NPs offer access to a remote CP (content provider) which provides multimedia services such as voice, data and video. Similarly, the SP is capable of accessing many different NPs to request service. The various network operators (providers) will then be competing to sell their network links to clients through a representative agent host, the *network access broker* (NAB)/the *internetwork access broker* (INAB).

A scenario that involves three competing NPs and two SPs is illustrated in Figure 18.3. The three networks are owned by three different operators, and each one of them is responsible for resource allocation and pricing strategies within its own environment.

Moreover, the three networks have some interconnection points with each other, therefore allowing traffic to flow among the different networks, as expected in an open marketplace. The SP is informed periodically about the cost changes associated with each of those interconnection points. As a means of competition, all three networks offer the same access to the remote CP. The SP serving a particular client is responsible for identifying the best/optimal connection path (routing) per request of the customer.

In Chapter 7, QoS routing with multiconstraint has been shown to be an NP-hard problem [34]. For this reason, in this section we additionally consider a genetic algorithm (GA), which presents a good method to handle multiconstraint optimization problems and does not depend on

the properties of the problem itself [37, 38]. The remaining issue is how the underlying agent architecture may interact with the genetic algorithm itself. It is assumed that an SP may host a particular kind of agent [named *broker agent* (BrkA)] which is in charge of identifying the optimal path to manage a specific connection request. The interaction between a BrkA and the algorithm may occur according to the following strategies:

(1) The BrkA is able to execute the algorithm in run-time upon the request from the PC client.

(2) The BrkA sends a request to a network node where the genetic algorithm can be executed. The optimal path is then sent back to the BrkA, which activates the setup procedure.

(3) A set of optimal paths for different pairs of PC client and CPs is stored in a database (eventually distributed), which is accessed from the BrkA to retrieve the more convenient path to satisfy the specific request. Once the connection is established, the genetic algorithm can be re-executed in order to identify a more convenient path, if the case.

If network performance and reliability change for some reason, monitoring agents distributed in the system will promptly react to pass the genetic algorithm the new data to recompute the new optimal paths.

18.3.3 Integration of routing algorithm and mobile agents

When network conditions change, SP always wants to find a good route for its customers in real time. That is, with certain QoS constraints, SP wants to find a cost-reasonable route for its costumers. The routing algorithm in SP needs to know:

(1) traffic from SP to CP;

(2) QoS requirements/constraints (i.e. time delay constraint from SP to CP);

(3) connectivity of nodes of NPs,

(4) bandwidth available for each link between nodes;

(5) cost for the traffic to pass through each link; and

(6) time delay for the traffic to pass through each link.

The use of mobile agents provides the complementary underlying structure in order to obtain this information in a distributed and efficient manner. In Section 18.3.1, we provided a brief description of how the agents can be used to deal with the collection of information [31, 33] about the state of the network and the monitoring of health functions that can be defined by the SP. The definition and creation of BAs and DAs serve the purpose of collecting specific variables from a set of nodes (e.g. NABs and INABs) specified by the SP. Then, MAs, during their migration through specific nodes of the network, interact with the other agents for collecting specific information produced by them and, therefore, obtain a general description about the state of the network. Moreover due to the mechanisms of remote evaluation and mobile agents described in the previous sections, the actions to be performed can be developed by the BrkA of a specific SP and sent to other remote devices where they will be executed on behalf of the BrkA, therefore limiting the generated traffic in the network and distributing the computational load and effort. Once the data are collected the routing algorithms can be executed.

A number of these algorithms were discussed in Chapter 6. For this reason in this section we additionally discuss only the GA. In general, GA is a stochastic algorithm searching process in the solution space by emulating biological selection and reproduction. It has been used to solve various optimization problems [38]. In this section, we discuss a genetic-based algorithm in order to

address the problem described in the previous sections. In the following, we describe the different features and phases of the algorithm [35].

Encoding is used to map the search space of the specific problem into the space where GA can operate. In the literature, related work in using GA as an optimization tool to solve the famous Traveling Salesman Problem [37] has been reported. There are several encoding approaches mentioned in the literature, such as adjacency representation, ordinal representation and path representation. Some encoding approaches are not suitable for GA operation (crossover and mutation), and some other encoding approaches are inefficient in searching the solution space. In this section, *path representation approach* is used to naturally encode a route due to its easy implementation. That is, all the nodes that the route passes through are listed in sequence. In order to encode the route in a fixed data structure, 'zeroes' are filled into the empty space of the code.

For instance, in a scenario with 10 nodes in addition to the CP and SP, an array with 10 elements can be used to represent the route. Once the number of nodes that the route passes is less than 10, the corresponding element will be zero. For example [1 2 3 4 0 0 0 0 0 0] is used to represent the SP–1–2–3–4–CP route.

Population initialization is used to start GA computation. In the population initialization process, the number of nodes the route will pass through, which node will be in the route and the sequence of the nodes of the route can be randomly determined. However, there will be some solutions that may violate constraints of delay or interconnectivity. The 'penalty method' is used to deal with these constraints, as follows:

(1) for those links that do not exist, a very large delay value is assigned; and

(2) for those routes that violate the delay constraint, a penalty to their cost is added.

In the algorithm, the following expression is used to evaluate the weighted cost of those illegal routes:

$$C'(r) = C(r)[\alpha + D(r)/D_{\max}]$$

where $C'(r)$ is the weighted cost of route r, $C(r)$ is the function that evaluates the total cost of the links that the route may pass through, $D(r)$ is the function that evaluates the time delay of the route, $D_{\max}$ is the upper bound of the time delay constraint, and α is the penalty constant (in the algorithm it is set to 2).

The *fitness* $F(r)$ of the solutions is proportional to their survivability during the algorithm computation. The selection operation, defined below, will use these values to keep 'good' solutions and discard the 'bad' solutions. For simplicity, we can use the cost of each route as the fitness of each solution. In order to prevent those solutions with very low fitness from being discarded by selection operation of GA at the first several computation loops of GA, the value of fitness of those 'bad' solutions is increased. In this way, some 'bad' solutions still have chances to survive at the beginning of the evolution of GA and the 'good' parts in them will have chances to transfer to new generations. For convenience, we normalize the fitness of solutions to [0,1] by the following expression:

$$F(r) = \frac{[C_{\max} - C(r)]C_{\min}}{(C_{\max} - C_{\min})C(r)}$$

where $C_{\max}$ and $C_{\min}$ and are maximum and minimum cost of routes in each generation of population, respectively.

Selection operation keeps 'good' solutions while discard 'bad' solutions at the same time. This operation tries to simulate 'natural selection' in real life. Those readers with background in communications theory will easily recognize the similarities between GA and the Viterbi algorithm (VA) used to approximate maximum likelihood (ML) demodulators.

Two selection operators are used in the algorithm. The first one is based on the 'fitness proportional model'. It is also called 'Monte Carlo selection'. The algorithm is as follows:

(1) add the fitness of all solutions;

(2) randomly generate a number between zero and the sum of fitness; this number is called the pointer of the Monte Carlo wheel; and

(3) add the fitness of each solution one by one until the value is greater than the pointer. Then the last solution is being selected.

Using this algorithm, the higher the fitness value, the bigger the chance of that solution being chosen. The second selection operator used in the algorithm is the 'best solution reservation'. The best solution in the population will always survive and several duplicated copies will be generated for mutation operation. In this way, the GA will always converge to a certain 'good' solution. Moreover, there will be a good chance to find a better solution on the base of the best solution of each generation.

Crossover operation enables any pair of solutions in the population to have a chance to exchange part of their solution information with others. Therefore, those 'good' parts from different solutions may be combined together to create a new, better solution. The two original solutions are the 'parents' of the new solutions generated. There are many crossover operators designed to solve different problems. In this section, we use traditional one-point crossover method. That is, we find a certain point of the array and swap the part before and after the cross point to generate two new solutions. However, because the number of nodes the route may pass through is not fixed, it is difficult to determine a fixed crossover point. In Papavassiliou *et al.* [35] the crossover point is determined by $\lfloor (A + B)/4 \rfloor$, where A and B are the numbers of nodes that the two routes will pass through, respectively, and the operator '$\lfloor\ \rfloor$' is a rounding function, e.g. if it is before the crossover operation, there are two routes: [1 2 3 4 5 0 0 0 0 0] and [6 7 8 0 0 0 0 0 0 0]. According to this procedure ($\lfloor (A + B)/4 \rfloor = 2$), after the crossover we get: [1 2 8 0 0 0 0 0 0 0] and [6 7 3 4 5 0 0 0 0 0]. Note that only part of the population will experience crossover operation; this rate is called the crossover rate.

The *mutation operation* randomly chooses a solution in the population and then slightly change it to generate a new solution. In this way, there is a chance to find better solution that cannot be found by only crossover operation. In the algorithm, four mutation operators are used:

(1) randomly delete a node from a route;

(2) randomly add a node into a route;

(3) randomly delete two nodes from a route; and

(4) randomly add two nodes into a route.

Only part of population will experience the mutation operation (this is characterized by mutation rate). In order to enhance the local searching ability, those copies of the best solution of each generation are all treated by mutation operator. In this way, the GA may find a better solution that is 'close' to the best solution of each generation.

In the *repair operation*, during crossover and mutation operation, illegal representation of route may be generated because duplicated elements (nodes) may appear in the same route. In the algorithm, those duplicated nodes that would bring high cost to the route are deleted. For example, there may be a route like [1 2 3 4 5 3 7 0 0 0], where node '3' is duplicated. We can evaluate the cost of strings (2 3 4), (5 3 7) and the delay of strings (2 3 4), (5 3 7). If the weighted cost of string (2 3 4) is less than (5 3 7), node 3 in (5 3 7) will be discarded.

The *computation efficiency* can be improved if after a minimum number of trails (MinTrails), when the algorithm has found a feasible solution and has made no more improvement for a

specific period of time, the computation process is stopped. In the algorithm, the 'improvement' is presented by the average cost change rate of the best solution of certain generation. This change rate is evaluated by the following expression:

$$\frac{\Delta C}{\Delta t} = \Delta R(k) = \frac{C(i) - C(i+1)}{k - i}$$

where we assume the cost of the best solution of that generation changes at ith step and ChangeRate $(k) = \Delta R(k)$ is the average change rate of cost at kth step $(k > i)$. Once this value is less than a certain lower-bound MinChangeRate, GA computation may be stopped.

The *updating process* may be improved by assuming that the price of each link and the congestion of the network will change gradually. So when new traffic comes, the SP will recompute routes for its customers. During the dynamic operation of the system, in order to improve the efficiency of the algorithm, the results of the last computation can be partly reused. One possibility is to mix certain 'training genes' into the initial population of the new route computation. However, this may lead to premature discards and prevent GA from finding better solutions. Instead of mixing the past solution into the initial solution of GA, they may be mixed into population after, for example, 70 % of MinTrails of GA loops. In this way, we can still take advantage of the results of the last computation and prevent premature discards at the same time. If the network conditions change smoothly, we can take advantage of the past best solution of last computation. If the network conditions change dramatically at a certain time and the optimal route may totally differ from the past solution, GA will not take advantage of the past best solution by mixing the past solution into the population during the GA computation. The flow chart in Figure 18.4 summarizes the operation of the algorithm. The integration of the mobile agents into the routing algorithm is presented in Figure 18.5.

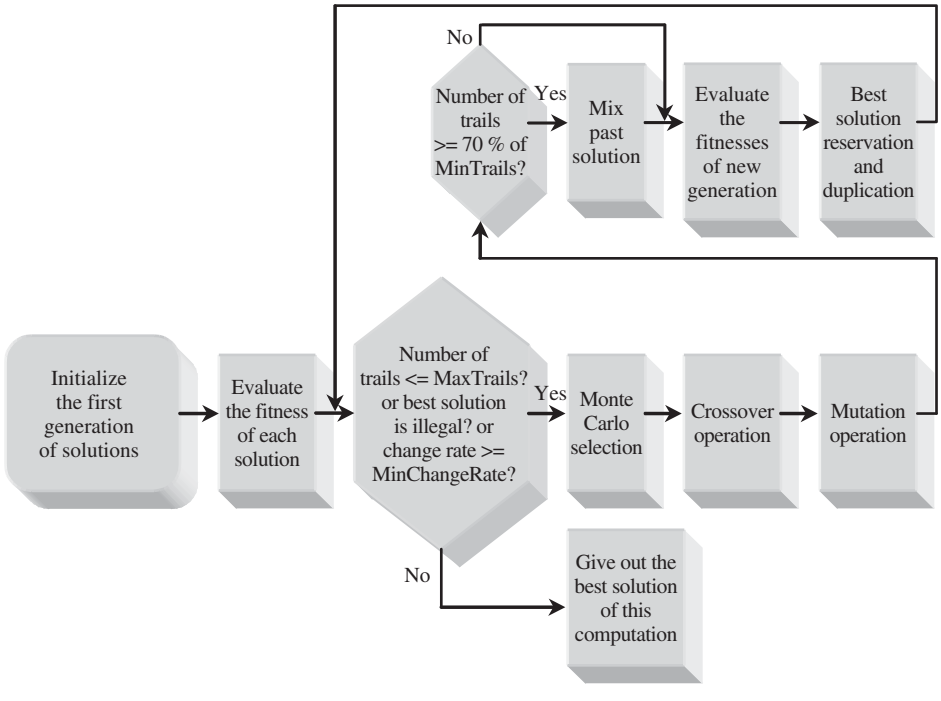

Figure 18.4 Flow chart of GA.

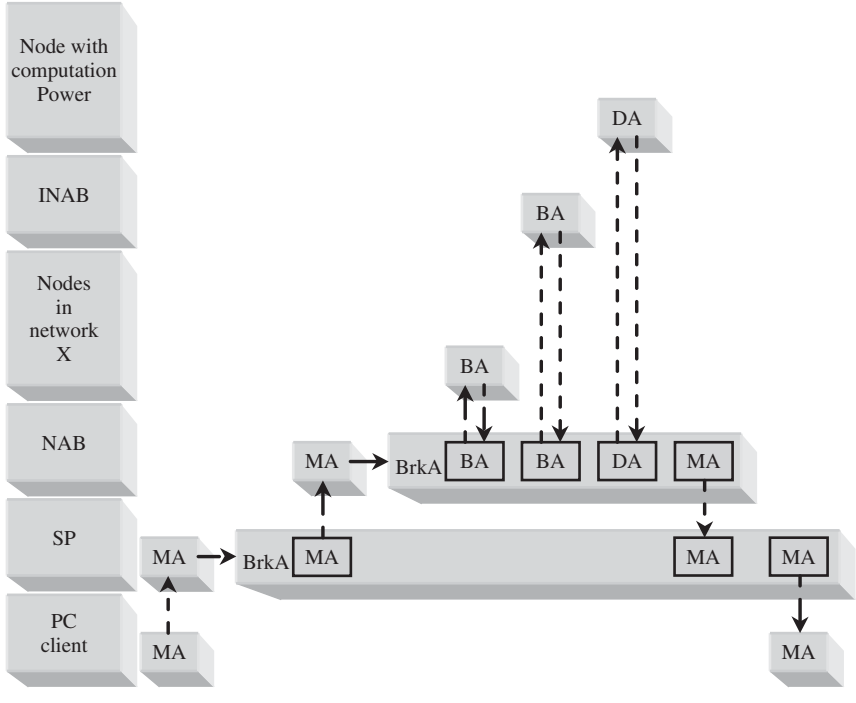

Figure 18.5 Agents used to implement routing algorithms based on GA.

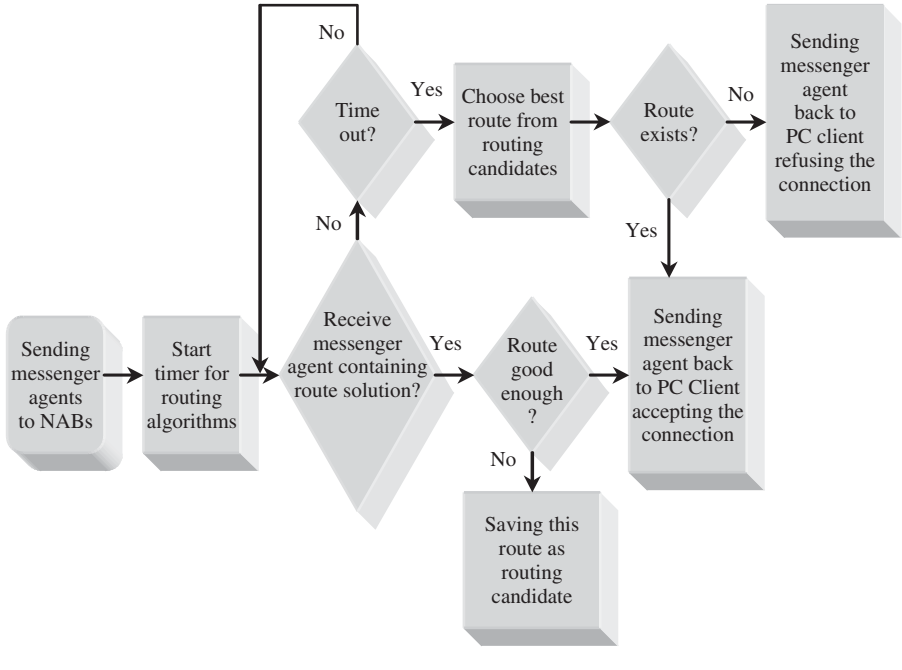

Figure 18.6 Algorithm for BrkAs in SP to choose a route for its client.

As shown in the figure, BrkAs, MAs, BAs and DAs are used to migrate among different network elements to implement the proposed routing algorithm. Once the PC client needs a connection to the CP, an MA will be sent from PC client to SP containing information about the upper bound of setup time delay of the connection and the corresponding QoS requirements. After receiving the MAs from PC client, the SP creates a BrkA to deal with this connection requirement.

This BrkA creates MAs containing source and destination information, as well as QoS requirements, and multicasts the agents to each NAB that it is connected with. Then the BrkA in SP waits for the agents from NABs to obtain the routing solution according to the scheme depicted in Figure 18.6.

As seen by the flow chart, in order to control the connection setup time, a timer is used to determine the deadline of the route searching procedure. If the BrkA receives an MA from NAB with satisfactory routing solution before the expiration of the timer, the route searching process stops and this solution is selected. Otherwise, when the timer expires the agent chooses the best route among the route candidates found until that time. Each NAB also creates a BrkAs to deal with the connection when it receives the MAs with the corresponding connection request from the SP. Then, three kinds of agents are used to implement the routing algorithm as follows.

A *browser* agent will be created and sent to nodes inside the individual private network that the NAB belongs to. These agents will collect resource information such as available bandwidth, delay of the link, price of the link, etc. In a similar way, the BrkA in each NAB will also send out BAs to INABs to see if it can take advantage of network resources from other NPs.

A *daemon* agent containing the GA code and resource-related information will be created after collecting the necessary resource information, to implement the routing algorithm described in detail in the previous section. Instead of executing the algorithm in each NAB, the BrkA sends DAs to the most suitable nodes inside its private network (e.g. nodes with enough computation resources such as CPU, memory, etc). In this way, we can balance the computation load among nodes in the private networks, if needed.

A *messenger agent* will be used to bring results back to the BrkA from DAs after the genetic-based route computation. This agent will be forwarded to the BrkA in the SP. Performance results for the algorithm can be found in Papavassiliou *et al.* [35].

18.4 *AD HOC* NETWORK MANAGEMENT

We start by identifying some of the properties of *ad hoc* networks that make them difficult to manage.

18.4.1 Heterogeneous environments

First of all, nodes of an *ad hoc* network can range in complexity from simple sensors located in the field to fully functional computers such as laptops. An implication of this diversity is that not all nodes will be able to contribute equally to the management task. For instance, it is likely that sensors and small personal digital assistant (PDA)-type devices will contribute minimally to the task of management, while more powerful machines will need to take on responsibilities such as collecting data before forwarding it to the management station, tracking other mobiles in the neighborhood as they move, etc. Thus, the management protocol needs to function in very heterogeneous environments.

18.4.2 Time varying topology

One mission of a network management protocol is to present the topology of the network to the network manager. In wireline networks, this is a very simple task because changes to the topology

are very infrequent (e.g. a new node gets added, failure of a node, or addition/deletion of a subnetwork, etc.). In mobile networks, on the other hand, the topology changes very frequently because the nodes move about constantly. Thus, the management station needs to collect connectivity information from nodes periodically. An implication of this is an increased message overhead in collecting topology information.

18.4.3 Energy constraints

Most nodes in *ad hoc* networks run on batteries. Thus, we need to ensure that the network management overhead is kept to a minimum so that energy is conserved. Different energy is consumed by a radio when a packet is transmitted or received. In addition, the CPU expends energy in processing these packets. Thus, we need to reduce the number of packets transmitted/received/processed at each node. This requirement is contradictory to the need for topology update messages previously discussed.

18.4.4 Network partitioning

Energy constraints and mobility can result in the network becoming partitioned frequently. For instance, nodes may power themselves off to conserve energy resulting in partitions, or a node may move out of transmission range of other nodes. Similarly, a node may die when its battery runs out of power. In all these cases, the partitioned subnetworks need to continue running independently, and the management protocol must be robust enough to adapt. For instance, when the network gets partitioned, the management protocol entities must quickly learn that the partition has occurred and reconfigure the subnetwork(s) to function autonomously. Furthermore, when partitions merge, the management protocol must be capable of updating the network view without too much of an overhead.

18.4.5 Variation of signal quality

Signal quality can vary quite dramatically in wireless environments. Thus, fading and jamming may result in a link going down periodically. An effect of this is that the network topology from a graph theoretic point of view changes. However, the physical layout of the network may not change at all. The management protocol must be able to distinguish this case from the case when node moves cause topology changes, because in the case of changing link quality/connectivity, it may not be necessary to exchange topology update messages at all. In order to be able to do this, the management protocol entity (which resides at the application layer) must be able to query the physical layer. This obviously violates the layering concept of OSI, but it results in enormous savings.

18.4.6 Eavesdropping

Ad hoc networks are frequently set up in hostile environments (e.g. battlesite networks) and are therefore subject to eavesdropping, destruction and possibly penetration (i.e. a node is captured and used to snoop). Thus, the management protocol needs to incorporate encryption as well as sophisticated authentication procedures.

18.4.7 *Ad hoc* network management protocol functions

In this section we will discuss some main functions of *ad hoc* network management protocol (ANMP). *Data collection* is a necessary function in ANMP where the management entities collect

node and network information from the network. SNMP specifies a large list of information items that can be collected from each node. However, this list does not include some crucial data items that are specific to the *ad hoc* environment like the status of the battery power (expected remaining lifetime), link quality, location (longitude and latitude), speed and direction, etc. All this information needs to be collected as (and when) it changes 'significantly'. For example, the location of a mobile node changes continuously, but there is little point in updating it constantly because the overhead in message complexity is high. The best solution is to update this information when some other aspect of the node changes. For instance, if the node's connectivity changes as a result of the motion, then we may need to update its location.

One problem that arises in *ad hoc* networks in relation to data collection is the message overhead. *Ad hoc* networks have limited bandwidth (whose quality is variable), and we must ensure that the process of management does not consume significant amounts of this resource. Since network management runs at the application layer, the simplest way to implement data collection (at the manager station) is to poll each node individually. This method, unfortunately, results in a very high message overhead. A more efficient method of data collection is to use a spanning tree rooted in the manager station.

Configuration/fault management is needed because nodes in *ad hoc* networks die, move or power themselves off to save energy. In all of these cases, the network topology changes, and the manager station needs to know the fate of these nodes. In cases when a node is unavailable for the reasons just stated, the manager records that fact in its database. However, even in the case when a manager knows that a node is dead, the entry for that node is not removed from the database because the node may be resurrected (e.g. we put in a new battery) or, keeping in mind that *ad hoc* networks are temporary, we may need a complete history of the network's behavior to effect a redesign of protocols, evaluate security breaches, etc.

New nodes may join a network periodically, and these nodes must be incorporated seamlessly into the network. A network may also be partitioned periodically. In this case, we need to ensure that each partition selects its own manager. However, when these partitions merge, one common manager needs to be chosen. Manager selection must be done based on the hardware and software capabilities of nodes and the available battery power. We may also have geographically coexisting but independent networks. An example is a battlefield, where a naval unit may be physically collocated with an infantry unit, each of which is using its own *ad hoc* network. In this case, the two networks may decide to be managed together or continue being managed independently but exchange information (such as link quality, presence of jamming, etc.) with each other as an aid to better deploy the network resources. It is also possible that a node may belong to two different networks and be managed by two (or more) managers. An example is a disaster relief model, where a police officer may remain on a police (secure) *ad hoc* network but simultaneously be connected (and managed) to an *ad hoc* network of medical relief teams. In 4G management, protocols for *ad hoc* networks must be able to operate in all these scenarios.

Security management deals with security threats [42–53, 55]. *Ad hoc* networks are very vulnerable to security threats because the nodes (e.g. the unmanned nodes) can easily be tampered with, and signals can be intercepted, jammed or faked. Current protocols, such as SNMPv3 [41, 56, 62, 63], do provide us with some mechanisms to guard against eavesdropping and replay attacks using secure unicast, which is not efficient for all incoming network architectures.

ANMP designing should address the issues raised above. It should be also compatible with SNMP. This is necessary because: (1) SNMP is a widely used management protocol today; and (2) *ad hoc* networks can be viewed as extensions of today's networks that are used to cover areas lacking a fixed infrastructure. In operation, it is quite likely that an *ad hoc* network would be connected to a local area wireline network (using a gateway). In such cases, ANMP manager should be designed to be viewed either as a peer of the SNMP manager (which is managing the wireline network) or as an agent of the SNMP manager. This flexibility is a major strength of ANMP. Obviously ANMP can operate in isolated *ad hoc* networks as well. In the

next section, we provide an overview of the possible design choices in ANMP with the following constraints [39]:

(1) the PDU structure used is identical to SNMP's PDU structure;

(2) UDP is the transport protocol used for transmitting ANMP messages;

(3) lost data is not retransmitted by ANMP because information is periodically updated anyway. Furthermore, if the application sitting on top of ANMP wishes to obtain the lost information, it can request the ANMP manager to solicit that information again.

18.4.8 ANMP architecture

In order to have a protocol that is message-efficient, a hierarchical model for data collection is appropriate, since intermediate levels of the hierarchy can collect data (possibly producing a digest) before forwarding it to upper layers of the hierarchy. A problem, however, with utilizing a hierarchical approach in *ad hoc* networks is the cost of maintaining a hierarchy in the face of node mobility. A good tradeoff is to use a three-level hierarchical architecture for ANMP. Figure 18.7 illustrates this architecture. The lowest level of this architecture consists of individual managed nodes called agents. Several agents (that are close to one another) are grouped into clusters and are managed by a cluster head (the nodes with squares around them in the figure). The cluster heads in turn are managed by the network manager. It is important to emphasize that: (a) clustering for management (in ANMP) is very different from clustering for routing, as we discuss in Chapter 13; and (b) a manager is frequently more than one hop away from the cluster heads (Figure 18.7 is a logical view and not a physical view).

The structure of the clusters is dynamic. Thus, as nodes move about, the number and composition of the clusters change. Similarly, the nodes serving as cluster heads also change over time. Different algorithms for forming and maintaining clusters will be discussed below. The clusters should have the following properties:

(1) The clusters are neither too large nor too small. The message overhead of collecting data within large clusters will be high. Likewise, if we have very small clusters, then there will be many cluster heads, all of which will be controlled by the manager. Thus, the message overhead in transactions between the cluster heads and the manager is high.

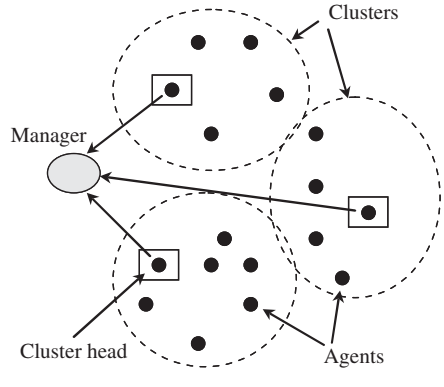

Figure 18.7 ANMP's hierarchical architecture.

(2) The clusters are formed such that node mobility does not result in frequent recomputation of the clusters. This property is necessary if we want to reduce the message overhead of maintaining clusters.

(3) Sometimes nodes move out of one cluster and into another but are not incorporated into the new cluster immediately. This is because cluster maintenance algorithms only run periodically and not continuously. The effect of this is that some percentage of nodes may be unmanaged by cluster heads for short periods of time. This is not really a problem (except for the message overhead in data collection) because these nodes are still in communication with the overall manager, and they can be directly managed by the manager.

It is important to make a distinction between the use of clusters for management vs clusters for routing. Clustering in ANMP is used to logically divide the network into a three-level hierarchy in order to reduce the message overhead of network management. Since ANMP is an application-layer protocol, ANMP presupposes the existence of an underlying routing protocol. Thus, the manager node can always reach any of the nodes in the *ad hoc* network (so long as they both lie in the same partition) and can manage them directly. Clustering simply introduces intermediate nodes called cluster heads for the purpose of reducing the message overhead. Thus, clustering algorithms used for management serve a weaker and different objective when compared with clustering algorithms used for routing.

In cluster-based routing [40], neighboring nodes form clusters and select a cluster head. Cluster heads have the responsibility of routing packets sent to nodes outside the cluster. It is easy to see that clustering here serves a fundamental goal of maintaining routes. Finally, we note that if the underlying routing protocol is cluster-based, ANMP could simply use these clusters for management as well. However, if the routing protocol is not cluster-based [41], the two clustering algorithms describe here form clusters and rely on routing support to exchange control messages.

Graph-based clustering is described first as a basic concept. After that the maintenance algorithm that deals with node mobility after clusters have been formed will be discussed. A node in the graph represents a mobile host in the network. There is an undirected link between two nodes if they are within transmission range of each other. For the purpose of clustering we assume the following.

(1) each node in the network has a unique ID;

(2) each node in the network maintains a list of its one-hop neighbors (recall that ANMP runs at the application layer, and therefore it can obtain this information from the network or MAC layer);

(3) Messages sent by a node are received correctly by all its neighbors within a finite amount of time.

In the algorithm, the node with minimum ID among its neighbors (which have not joined any other cluster) forms a cluster and becomes the cluster head. Upon hearing from a cluster head, each node that has not yet joined any cluster declares that it has joined a cluster. If any node has been included in more than one cluster, then all but one cluster head prunes the node entry from their list when they do not hear any information from that node.

Figure 18.8 illustrates cluster formation in a simple *ad hoc* network. The node with the minimum ID forms the cluster and becomes the cluster head. Here node 1 is the minimum ID node among its neighbors; therefore, it forms a cluster C1. Node 4 does not initiate cluster formation because it is not the minimum ID node among its neighbors. When node 2 broadcasts a message that it has joined cluster C1, node 4 realizes that it is now the minimum ID node. Since the cluster formation runs in a distributed way, it is possible that, by the time node 4 receives the broadcast message

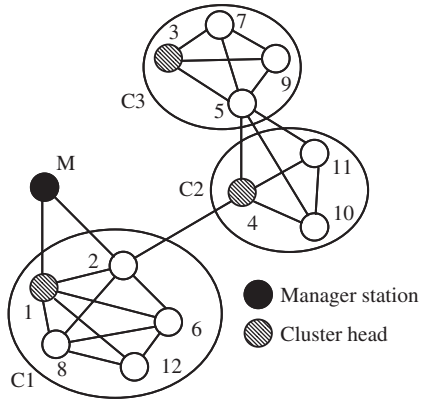

Figure 18.8 Clusters formed using graphical clustering.

from node 2, node 3 has already initiated cluster formation, and node 5 also sends a message that it has joined some cluster C3. Thus, when node 4 starts cluster formation, it only includes the remaining nodes among its neighbors and from C2.

Because the node with minimum ID considers only its one-hop neighbors while forming the cluster, the nodes in a cluster are one hop away from the cluster head and at most two hops away from any other cluster mate when the cluster is formed. The information maintained by each node after clusters are formed is:

- a neighbor list – a list of nodes that are one hop away;
- a cluster list – a list of all nodes that are its cluster mates;
- a ping counter – a counter that indicates the time steps elapsed since it last heard from its cluster head.

Cluster maintenance for graph-based clustering deals with the changes in the network topology. As a result, the clusters and cluster membership have to be updated. Changes in cluster membership are triggered when a node moves out of a cluster (and into another) or when the cluster head itself moves out of a cluster (or, relatively speaking, cluster members move away from the cluster head). Figure 18.9 presents some illustrative cases. Figure 18.9(a) shows a situation where nodes move about but are still connected to at least one of their cluster mates (see Figure 18.8). Here, there is no need to recompute clusters. Figure 18.9(b) shows two scenarios: (1) when a node moves across the cluster boundary; and (2) when the cluster head gets disconnected. It can be seen that node 4 gets disconnected from all the members of its previous cluster. Since node 4 is two hops away from the cluster head of cluster C1, it sends a join request to node 2. On receiving such event from node 4, node 2 adds node 4 to its cluster list and broadcasts it to all the members. Meanwhile, nodes 10 and 11 discover that their cluster head has moved away, and they initiate cluster formation and form a new cluster C4. The previous example indicates an important property of the maintenance algorithm.

When new clusters are formed, all nodes in the cluster are one hop away from the cluster head. However, as nodes move about, we allow nodes to join clusters even if they are two hops away from the cluster head of an existing cluster. This flexibility drastically reduces the message overhead of the algorithm.

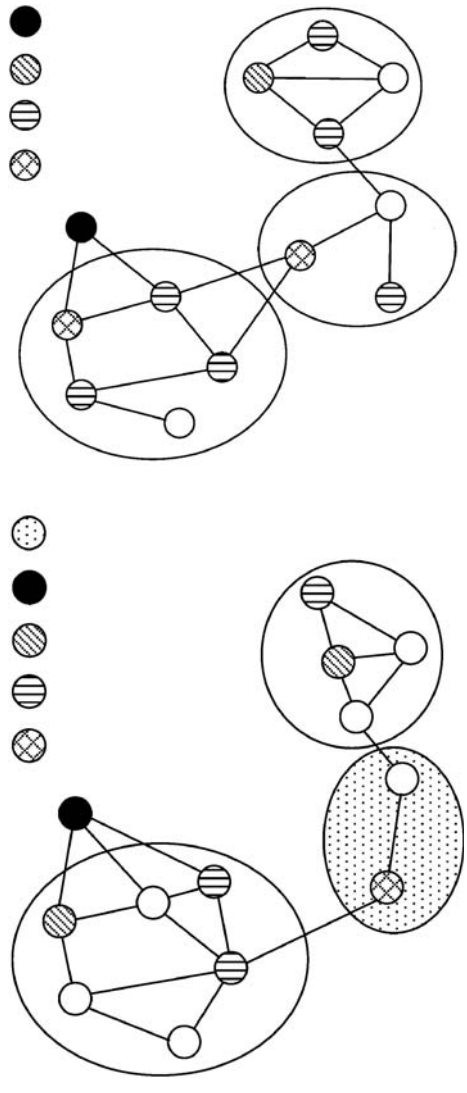

Figure 18.9 Effect of node mobility on clusters.

18.4.8.1 Performance of cluster maintenance algorithm

If a node is connected to at least one node in its cluster list, it is still considered to be part of that cluster. If a node detects that it has no links to any of its previous cluster mates, it either forms a new cluster by itself or joins another cluster. The algorithm should be able to differentiate between node movements within the cluster and movements across the cluster boundary. Four types of events that a node can detect as a result of mobility are identified. A node can detect: (1) a new neighbor, who is also a cluster mate; (2) that a previous neighbor and cluster mate has moved; (3) that it was previously directly connected to the cluster head but is no longer directly connected,

or it was previously not directly connected but is now directly connected; (4) a new neighbor, who wants to join the cluster.

At every fixed interval, called a time step, each node locally creates a list of events that it has observed and sends it to its cluster head. The cluster heads collects these events and recomputes the cluster list. If there is any change in the cluster membership, the cluster head broadcasts the new list. Thus, whenever a node moves out of a cluster or joins a cluster, the message exchange is restricted to within that cluster. In order to minimize the number of cluster changes, a node is allowed to join a cluster if the cluster head is two hops away. The restriction of two hops (as opposed to, say, three hops) has been enforced to avoid the creation of big clusters.

In such a division of the network, the cluster head plays an important role. That is why a major event that can occur is the movement of the cluster head. To determine if the cluster head has moved away, a ping counter is used at each node. This counter gets incremented at every time step. If the counter at the cluster head crosses some threshold value, then the cluster head sends a ping message to all its cluster mates, indicating that it is still alive. If the cluster mates do not hear a ping after their ping counters cross a threshold, they assume that the cluster head is either dead or has moved out. Once a node detects such an event, it cannot be certain about its cluster list. New cluster(s) are formed with one-hop neighbors in the same way as the clusters were initially formed. It is easy to see that the frequency at which these pings are sent plays an important role in maintaining the clusters. If the ping frequency is small, then between consecutive pings, some nodes may be unmanaged by a cluster head (i.e. they do not belong to any cluster). Unfortunately, even though a high frequency of pings minimizes the number of nodes unmanaged by cluster heads, it results in a higher message overhead.

One method of reducing the number of ping messages while simultaneously keeping the fraction of nodes unmanaged by clusterheads small is to exploit information available at the MAC layer. The MAC layer in wireless networks periodically transmits a beacon to announce itself to its neighbors. Thus, the MAC layer keeps an updated list of its one-hop neighbors. If nodes transmit this list to their neighbors, changes in the cluster membership can be detected quickly. If the cluster head moves away, its departure will be noticed by the MAC layer of its one-hop neighbors. These nodes can act on this information to quickly reform clusters.

Another characteristic of *ad hoc* networks are partitions. If a subnetwork gets partitioned from the main network, it is treated as any other cluster because the protocol does not require any information exchange between clusters. If a single node gets partitioned, it forms a cluster by itself. However, when it gets reconnected, it tries to join another cluster because the clusters of too small or too large a size are both inefficient from the point of view of network management.

To study the performance of this clustering algorithm, an ad hoc network was simulated in Chen *et al.* [39] in which the 30 nodes move randomly within a 1500×1500 unit box (for 60 nodes, the area of the playground was twice that, and so on). Each node selects a direction randomly uniformly in the range [0, 360] degrees. It moves along that direction for a length of time that is exponentially distributed. At the end of this time, it recomputes the direction and traveling time. When a node hits the edge of the box, it wraps around and emerges from the opposite edge. In the simulation, the same transmission power was used for all the nodes in the network and the *ad hoc* network was represented as an undirected graph with links between two nodes if they are within transmission range of each other. The average speed of nodes is 1–50 unit/s in different runs. The transmission range of a node is fixed at 450 units. Each reading is an average of 10 readings, and the simulation time is 1000 s. Finally, a packet loss probability of 10^{-3} in all simulations was assumed.

Figure 18.10 (upper part) shows the message overhead of the protocol for the case when only pings to detect topology changes (graph on the left) and when pings along with MAC-layer information (the graph on the right) are used. The x-axis indicates the speed in units per second, and the y-axis shows the number of messages exchanged per second for cluster maintenance.

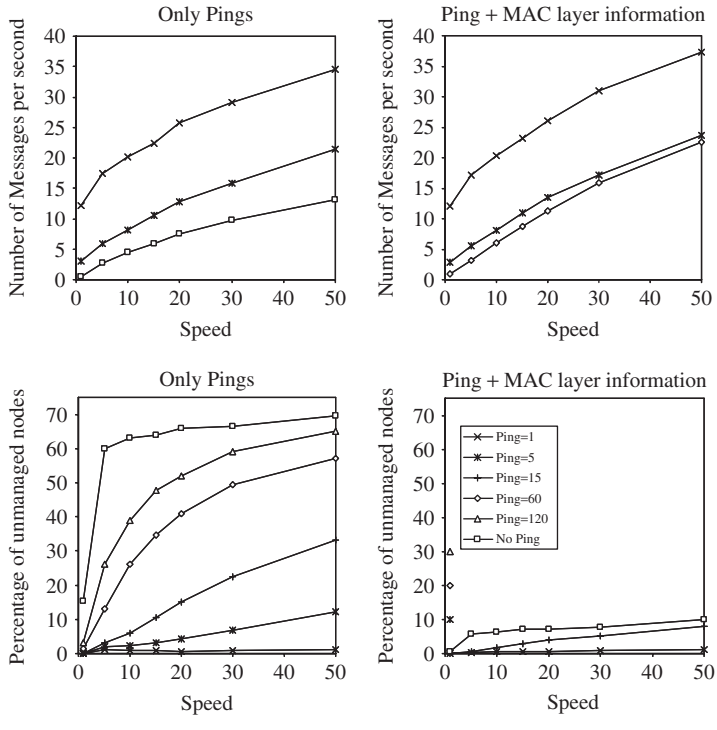

Figure 18.10 Message overhead and percentage of nodes unmanaged by cluster heads.

Each curve in the graph depicts the message overhead incurred for different ping intervals, which vary from no ping (equivalent to infinite time steps) down to one ping message every time step. It may be noted that message overhead increases almost linearly with increase in speed. The message overhead when we use MAC-layer information shows similar behavior, but there are more messages exchanged. This is obvious because of the fact that nodes do not wait for the ping message from the cluster head. The clustering algorithm is triggered as soon as the nodes detect cluster head movement.

The same figure (lower part) shows the percentage of nodes unmanaged by cluster heads. The plot on the left is for the case when only pings are used to detect topology changes, while the graph on the right is for the case when pings as well as MAC-layer information to detect topology changes are used. It can be seen from the graph that at higher speeds the percentage of nodes unmanaged by cluster heads goes up. This is mainly because of frequent disconnections and partitions generated in the network. Interestingly, the percentage of nodes unmanaged by cluster heads is as high as 50–70 % when we only use pings, but stays below 10 % when we use MAC-layer connectivity information as well.

REFERENCES

[1] www.snmp.com/

[2] W. Stallings, *SNMP, SNMPv2, and RMON: Practical Network Management*, 2nd edn., Addison-Wesley: Reading, MA, 1996.

[3] M. Rose, *The Simple Book: an Introduction to Network Management*, 3rd edn. Prentice Hall: Upper Saddle River, NJ, 1996.
[4] http://netman.cit.buffalo.edu/index.html
[5] J. Case, M. Fedor, M. Schoffstall and J. Davin, a simple network management protocol (SNMP), IETF, RFC 1157, 1990.
[6] *Information Technology – Open Systems Interconnection-Common Management Information Protocol Definition*, ITU-T, Geneva, ITU Recommendation X.711, 1992.
[7] W. Stallings, SNMP and SNMPv2: the infrastructure for network management, *IEEE Commun. Mag.*, vol. 36, 1998, pp. 37–43.
[8] A. Leinwand and K. Fang, *Network Management: A Practical Perspective*. Addison-Wesley: Reading, MA, 1993.
[9] W. Stallings, *SNMP, SNMPv2, and CMIP: the Practical Guide to Network Management Standards*, 1st edn. Addison-Wesley: Reading, MA, 1993.
[10] L. Raman, OSI systems and network management, *IEEE Commun. Mag.*, vol. 36, 1998, pp. 46–53.
[11] M. Kahani and H.W.P. Beadle, Decentralised approach for network management, *ACM SIGCOM Comput. Commun. Rev.*, 1997, pp. 36–47.
[12] G. Goldszmidt and Y. Yemini, Delegated agents for network management, *IEEE Commun. Mag.*, vol. 36, 1998, pp. 66–70.
[13] M. Kahani and H. Beadle, Decentralized approaches for network management, *Computer Commun. Rev.*, vol. 27, 1997, pp. 36–47.
[14] S. Vinoski, CORBA: integrating diverse applications within distributed heterogeneous environments, *IEEE Commun. Mag.*, vol. 35, 1997, pp. 46–55.
[15] M. Greenberg, J. Byington and D. Harper, Mobile agents and security, *IEEE Commun. Mag.*, vol. 36, 1998, pp. 76–85.
[16] V. Pham and A. Karmouch, Mobile software agents: an overview, *IEEE Commun. Mag.*, vol. 36, 1998, pp. 26–37.
[17] D. Milojicic, F. Douglis and R. Wheeler, *Mobility Processes, Computers and Agents*, D. Milojicic, F. Douglis and R. Wheeler (eds). ACM Press, 1999.
[18] A. Fuggetta, G. Picco and G. Vigna, Understanding code mobility, *IEEE Trans. Software Engng*, vol. 24, 1998, pp. 342–361.
[19] M. Baldi and G. Picco, Evaluating the tradeoffs of mobile code design paradigms in network management applications, in *Proc. ICSE'98*, Kyoto, 19–25 April 1998, pp. 146–155.
[20] M. Siegl and G. Trausmuth, Hierarchical network management: A concept and its prototype in SNMPv2, *Comput. Networks ISDN Syst.*, vol. 28, 1996, pp. 441–452.
[21] J. Stamos and D. Gifford, Remote evaluation, *ACMTrans. Prog. Lang. and Syst.*, vol. 12, 1990, pp. 537–565.
[22] A. Bieszczad, B. Pagurek and T. White, Mobile agents for network management, *IEEE Commun. Surv.*, vol. 1, no. 4Q, 1998, pp. 2–9.
[23] A.T. Campbell, H.G. de Meer, M.E. Kounavis, K. Miki, J. Vicente and D. Villela, A survey of programmable networks, *ACM Comput. Commun. Rev.*, vol. 29, 1999, pp. 7–23.
[24] A. Puliafito, O. Tomarchio and L. Vita, MAP: design and implementation of a mobile agent platform, *J. Syst. Architect.*, vol. 46, 2000, pp. 256–267.
[25] H. De Meer, A. La Corte, A. Puliafito and O. Tomarchio, Programmable agents for flexible QoS management in IP networks, *IEEE J. Select. Areas Commun.*, vol. 18, 2000, pp. 145–162.
[26] M.R. Genesereth and S.P. Ketchpel, Software agents, *Commun. ACM*, vol. 37, 1994, pp. 48–53.
[27] D.S. Alexander, W.A. Arbaugh, A.D. Keromytis and J.M. Smith, The switchware active network architecture, *IEEE Network*, vol. 12, 1998, pp. 29–36.
[28] D. Tennenhouse, S.M. Smith W.D. Sincoskie, D.J. Weatheall and G.J. Minden, A survey of active networks research, *IEEE Commun. Mag.*, vol. 35, 1997, pp. 80–85.

[29] *IEEE Networks*, Special Issue on Programmable Networks, vol. 12, May/June 1998.
[30] *AdventNet Management APIs*. Available at: www.adventnet.com
[31] A. Bivens, L. Gao, M.F. Hulber and B. Szymanski, Agent-based network monitoring, in *Proc. Autonomous Agents99 Conf., Workshop 1*, *Agent Based High Performance Computing: Problem Solving Applications and Practical Deployment*, Seattle, WA, May 1999, pp. 41–53.
[32] M.S. Greenberg, J.C. Byington and T. Holding, Mobile agents and security, *IEEE Commun. Mag.*, vol. 7, 1998 pp. 76–85.
[33] A. Puliafito and O. Tomarchio, Using mobile agents to implement flexible network management strategies, *Comput. Commun. J.*, vol. 23, 2000, pp. 708–719.
[34] Z. Wang and J. Crowcroft, Quality-of-service routing for supporting multimedia applications, *IEEE J. Select. Areas Commun.*, vol. 14, 1996, pp. 1228–1234.
[35] S. Papavassiliou, A. Puliafito, O. Tomarchio and J. Ye, Mobile agent-based approach for efficient network management and resource allocation: framework and applications, *IEEE J. Select. Areas Commun.*, vol. 20, no. 4, 2002, pp. 858–872.
[36] R. Zahavi and T.J. Mowbray, *The Essential CORBA: Systems Integration Using Distributed Objects*. Wiley: New York, 1995.
[37] D.E. Goldberg, *Genetic Algorithms in Search, Optimization and Machine Learning*. Addison-Wesley: Reading, MA, 1989.
[38] Z. Michalewicz, *Genetic Algorithms + Data Structure = Evolution Programs*. Springer: New York, 1992.
[39] W. Chen, N. Jain and S. Singh, ANMP: *ad hoc* network management protocol, *IEEE J. Select. Areas Commun.*, vol. 17 no. 8, 1999, pp. 1506–1531.
[40] M. Gerla and T.J. Tzu-Chich, Multicluster, mobile, multimedia radio network, *ACM-Baltzer J. Wireless Networks*, vol. 1, 1995, pp. 255–266.
[41] D.B. Johnson and D.A. Maltz, Dynamic source routing in ad hoc wireless networks, in *Mobile Computing*, T. Imielinski and H. F. Korth (eds). Kluwer: Norwell, MA, 1996, pp. 153–181.
[42] K. Terplan, *Communication Network Management.* Prentice-Hall: Englewood Cliffs, NJ, 1989.
[43] Mobile MIB Taskforce, *System Components*, Available at: www.epilogue.com/mmtf/
[44] J. Pavon and J. Tomas, CORBA for network and service management in the TINA framework, *IEEE Trans. Commun.*, vol. 36, 1998, pp. 72–79.
[45] G. Goldszmidt and Y. Yemini, Delegated agents for network management, *IEEE Trans. Commun.*, vol. 36, 1998, pp. 66–70.
[46] V.S. Acosta, OSF/DME *(Distributed Management Environment).* Available at: www.frontiernet.net/vsa184/papers/osf_dme.htm, 1998.
[47] OMG. *CORBA Overview.* Available at: www.infosys.tuwien.ac.at/Research/Corba/OMG/arch2.htm#446864, 1998.
[48] U. Blumenthal and B. Wijnen, User-based security model (USM) for version 3 of the simple network management protocol (SNMPv3), RFC 2274, January 1998.
[49] B. Wijnen, R. Presuhn and K. McCloghrie, View-based access control for the simple network management protocol (SNMP), RFC 2275, January 1998.
[50] C.P. Pfleeger, *Security in Computing*, 2nd edn. Prentice-Hall: Englewood Cliffs, NJ, 1997.
[51] G.-H. Chiou and W.-T. Chen, Secure broadcasting using secure lock, *IEEE Trans. Software Engng*, vol. 15, 1989, pp. 929–933.
[52] L. Gong and N. Shacham, Multicast security and its extension to a mobile environment, *Wireless Networks*, vol. 1, August 1995, pp. 281–295.
[53] J. McLean, The specification an modeling of computer security, *IEEE Comput.* vol. 3, 1990, pp. 9–17.
[54] *Network Management Server.* Available at: http://netman.cit.buffalo.edu/index.html, 1998.
[55] U. Blumenthal and B. Wijnen, User-based security model (USM) for version 3 of the simple network management protocol (SNMPv3), RFC 2274, January 1998.

[56] B. Wijnen, R. Presuhn and K. McCloghrie, View-based access control for the simple network management protocol (SNMP), RFC 2275, January 1998.
[57] R. Lin Chunhung and M. Gerla, Adaptive clustering for mobile wireless networks, *IEEE J. Select. Areas Commun.*, vol. 15, 1997, pp. 1265–1274.
[58] SNMP Research Group, *The EMANATE run-time extensible agent system*, *SNMP Version 3 Charter*. Available at: www.snmp.com/emanateintro.html, 1998.
[59] *SNMP Version3 Charter*. Available at: www.ieft.org/html.charters/snmpv3-charter.html, 1998.
[60] D.J. Sidor, TMN Standards: Satisfying today's needs while preparing for tomorrow, *IEEE Commun. Mag.*, vol. 36, 1998, pp. 54–64.
[61] Mobile Management Task Force, *Mobile MIB Draft 2.0*, Available at: www.epilogue.com/mmtf/, 1998.
[62] C.E. Perkins and P. Bhagwat, Routing over multi-hop wireless network of mobile computers, in *Mobile Computing*, T. Imielinski and H. F. Korth (eds). Kluwer: Norwell, MA, 1996, pp. 183–205.
[63] C.-K. Toh, The Cambridge ad hoc mobile routing protocol, in *Wireless ATM and Ad Hoc Networks*, Chap. 9. Kluwer: Reading, MA, 1997.

19

Network Information Theory

Information theory has made a significant contribution to the development of communication theory and practice. This is especially true in the domain of physical layer including channel capacity issues, coding and modulation. Unfortunately, information theory has not yet made a comparable mark in the field of communication networks, which is today the center of activity and attention in most information technology areas. The principal reason for this is twofold. First, by focusing on the classical point-to-point, source–channel–destination model of communication, information theory has ignored the bursty nature of real sources. In advanced networks, source burstiness is the central phenomenon that underlies the process of resource sharing for communication. Secondly, by focusing on the asymptotic limits of the tradeoff between accuracy and rate of communication, information theory ignored the role of delay as a parameter that may affect this tradeoff. In networking, delay is a fundamental quantity, not only as a performance measure, but also as a parameter that may control and affect the fundamental limits of the rate–accuracy tradeoff.

A comprehensive survey of information theory contributions to the study of different network layers is given in Ephremides and Hajek [1]. The effective capacity of communications links including time-varying channel capacity, adaptive coding and modulation and queueing has already been discussed in Chapters 4 and 8. In this chapter we additionally discus the effective capacity of advanced cellular network, transport capacity of wireless networks and network coding.

19.1 EFFECTIVE CAPACITY OF ADVANCED CELLULAR NETWORKS

In this section we discuss effective capacity and capacity losses in an advanced CDMA network due to imperfections in the operation of the system components. In addition to the standard WCDMA technology both base stations and mobile units use antenna beam forming and self-steering to track the incoming (and transmitted) signal direction. By using high directivity antennas and antenna pointer tracking, the level of multiple access interference (MAI) and the required transmitted power are reduced. In order to exploit the available propagation diversity signals arriving from different directions (azimuth ψ, elevation φ) and delay τ are combined in a three-dimensional (ψ, φ, τ) RAKE receiver. This is expected to significantly improve the system performance. In this section we present a systematic mathematical framework for capacity evaluation of such a

Advanced Wireless Technologies: Cognitive, Cooperative & Opportunistic 4G Technology Second Edition Savo G. Glisic

CDMA network in the presence of implementation imperfections and a fading channel. The theory is general and some examples of a practical set of channel and system parameters are used as illustrations. As an example, it was shown that, in the case of voice applications and a two-dimensional (4antennas $\times$ 4multipaths) RAKE receiver, up to 90 % of the system capacity can be lost due to the system imperfections. Further elaboration of these results, including extensive numerical analysis based on the offered analytical framework, would provide enough background for understanding of possible evolution of advanced W-CDMA and MC CDMA towards the fourth generation of mobile cellular communication networks.

The physical layer of the third generation of mobile communication system (3G) is based on wideband CDMA. The CDMA capacity analysis is covered in a number of papers and recently has become a subject in standard textbooks [2–8].

The effect of more sophisticated receiver structures (like multiuser detectors MUD or joint detectors) on CDMA or hybrid systems capacity has been examined in [9–13]. The results in Hämäläinen *et al.* [9] show roughly twofold increase in capacity with MUD efficiency 65 % compared with conventional receivers. The effect of the fractional cell load on the coverage of the system is presented in [10]. The coverage of MUD-CDMA uplink was less affected by the variation in cell loading than in conventional systems. References [11] and [12] describe a CDMA system where joint data estimation is used with coherent receiver antenna diversity. This system can be used as hybrid multiple access scheme with TDMA and FDMA component. In Manji and Mandayam [13] significant capacity gains are reported when zero forcing multiuser detectors are used instead of conventional single-user receivers.

In most of the references it has been assumed that the service of interest is low rate speech. In next generation systems (4G), however, mixed services including high rate data have to be taken into account. This has been done in Huang and Bhargava [14], where the performance of integrated voice/data system is presented. It is also anticipated that 4G will be using adaptive antennas to further reduce the MAI. The effects of adaptive base station antenna arrays on CDMA capacity have been studied [6, 7]. The results show that significant capacity gains can be achieved with quite simple techniques.

One conventional way to improve cellular system capacity, used in 3G systems, is cell splitting, i.e. sub-dividing the coverage area of one base station to be covered by several base stations (smaller cells) [15]. Another simple and widely applied technique to reduce interference spatially in 3G is to divide cells into sectors, e.g. three 120° sectors. These sectors are covered by one or several directional antenna elements. The effects of sectorization to spectrum efficiency are studied in Chan [16]. The conclusion in Chan [16] is that sectorization reduces co-channel interference and improves the signal-to-noise ratio of the desired link at the given cluster size. However, at the same time the trunking efficiency is decreased [17]. Owing to the improved link quality, a tighter frequency reuse satisfies the performance criterion in comparison to the omnicellular case. Therefore, the net effect of sectorization is positive at least for large cells and high traffic densities.

By using M-element antenna arrays at the base station the spatial filtering effect can be further improved. The multiple beam adaptive array would not reduce the network trunking efficiency, unlike sectorization and cell splitting [18]. These adaptive or smart antenna techniques can be divided into switched-beam, phased array and pure adaptive antenna systems. Advanced adaptive systems are also called spatial division multiple access (SDMA) systems. Advanced SDMA systems maximize the gain towards the desired mobile user and minimize the gain towards interfering signals in real time.

According to Winters [19], by applying a four-element adaptive array at the TDMA, uplink frequencies can be reused in every cell (three-sector system) and sevenfold capacity increase is achieved. Correspondingly, a four-beam antenna leads to reuse of three or four and doubled capacity at small angular spread.

Some practical examples of the impact of the use of advanced antenna techniques on the existing cellular standards are described in References [20, 21]. In Petrus *et al.* [20] the reference system is AMPS and in Mogensen *et al.* [21] it is GSM. The analysis in Kudoh and Matsumoto [22] uses ideal and flat-top beamformers. The main lobe of the ideal beamformer is flat and there are no sidelobes, whereas the flat-top beamformer has a fixed sidelobe level. The ideal beamformer can be seen as a realization of the underloaded system, i.e. there are less interferers than elements in the array. The overloaded case is better modeled by the flat-top beamformer because all interferers cannot be nulled as the sidelobe level is increased. Performance results show that reuse factor of one is not feasible in AMPS, but reuses four and three can be achieved with uniform linear arrays (ULA) with five and eight elements, respectively. Paper [21] concentrates on the design and performance of the frequency hopping GSM network using conventional beamforming. Most of the results are based on the simulated and measured data of eight-element ULA. The simulated C/I improvement follows closely the theoretical gain at low azimuth spreads. In urban macrocells the C/I gain is reduced from the theoretical value 9 dB down to approximately 5.5–7.5 dB. The designed direction of arrival (DoA) algorithm is shown to be very robust to co-channel interference. The potential capacity enhancement is reported to be threefold in a $1/3$ reuse FH-GSM network for an array size of $M = 4$–6. A number of papers [23–30] present the analysis of capacity improvements using spatial filtering.

Solutions in 4G will go even beyond the above options and assume that both base station and the mobile unit are using beam forming and self-steering to continuously track transmitter–receiver direction (two side beam pointer tracking 2SBPT). Owing to user mobility and tracking imperfections there will be always tracking error that will result in lower received signal level, causing performance degradation. In this chapter we provide a general framework for performance analysis of a network using this technology. It is anticipated that this technology will be used in 4G systems.

19.1.1 4G cellular network system model

Although the general theory of MIMO system modeling is applicable for the system description, performance analysis will require more details and a slightly different approach will be used. This model will explicitly present signal parameters sensitive to implementation imperfections.

19.1.1.1 Transmitted signal

The complex envelope of the signal transmitted by user $k \in \{1, 2, \ldots, K\}$ in the nth symbol interval $t \in [nT, (n+1)T]$ is

$$s_k = A_k T_k(\psi, \varphi) \mathrm{e}^{j\phi_{k0}} S_k^{(n)}(t - \tau_k) \tag{19.1}$$

where A_k is the transmitted signal amplitude of user k, $T_k(\psi, \varphi)$ is the transmitting antenna gain pattern as a function of azimuth ψ and elevation angle φ, τ_k is the signal delay, ϕ_{k0} is the transmitted signal carrier phase, and $S_k^{(n)}(t)$ can be represented as

$$S_k^{(n)}(t) = S_k^{(n)} = S_k = S_{ik} + jS_{qk} = d_{ik}c_{ik} + jd_{qk}c_{qk} \tag{19.2}$$

In this equation d_{ik} and d_{qk} are two information bits in the I- and Q-channels, respectively, and $c_{ikm}^{(n)}$ and $c_{qkm}^{(n)}$ are the mth chips of the kth user PN codes in the I- and Q-channel respectively. Equations (19.58) and (19.63) are general and different combinations of the signal parameters over most of the signal formats of practical interest. In practical systems the codes will be a combination of a number of component codes [2].

19.1.1.2 Channel model

The channel impulse responses consist of discrete multipath components represented as

$$h_k^{(n)}(\psi,\varphi,t)=\sum_{l=1}^{L}h_{kl}^{(n)}(\psi,\varphi)\delta\left(t-\tau_{kl}^{(n)}\right)=\sum_{l=1}^{L}H_{kl}^{(n)}(\psi,\varphi)\mathrm{e}^{j\phi_{kl}}\delta(t-\tau_{kl}^{(n)})$$

If antenna lobes are narrow we can use a discrete approximation of this functions in spatial domain too and implement 3D RAKE receive as follows:

$$\begin{aligned}h_k^{(n)}(\psi,\varphi,t)&=\sum_{l=1}^{L}h_{kl}^{(n)}\delta\left(\psi-\psi_{kl},\varphi-\varphi_{kl},t-\tau_{kl}^{(n)}\right) &\text{(19.3a)}\\&=\sum_{l=1}^{L}H_{kl}^{(n)}\mathrm{e}^{j\phi_{kl}}\delta\left(\psi-\psi_{kl},\varphi-\varphi_{kl},t-\tau_{kl}^{(n)}\right)\\h_{kl}^{(n)}&=H_{kl}^{(n)}\mathrm{e}^{j\phi_{kl}} &\text{(19.3b)}\end{aligned}$$

where L is the overall number of spatial-delay multipath components of the channel. Each path is characterized by a specific angle of arrival (ψ,φ) and delay τ. Parameter $h_{kl}^{(n)}$ is the complex coefficient (gain) of the lth path of user k at symbol interval with index n, $\tau_{kl}^{(n)}\in[0,T_m)$ is the delay of the lth path component of user k in symbol interval n and $\delta(t)$ is the Dirac delta function. We assume that T_m is the delay spread of the channel. In what follows, indices n will be dropped whenever this does not produce any ambiguity. It is also assumed that $T_m<T$.

19.1.2 The received signal

The base station receiver block diagram is shown in Figure 19.1 [31]. The overall received signal at the base station site during N_b symbol intervals can be represented as

$$\begin{aligned}r(t)&=\mathrm{Re}\left\{\mathrm{e}^{j\omega_0 t}\sum_{n=0}^{N_b-1}\sum_{k=1}^{K}s_k^{(n)}(t)*h_k^{(n)}(t)\right\}+\mathrm{Re}\left\{z(t)\mathrm{e}^{j\omega_0 t}\right\}\\&=\mathrm{Re}\left\{\mathrm{e}^{j\omega_0 t}\sum_{n=0}^{N_b-1}\sum_{k}\sum_{l}a_{kl}S_k^{(n)}(t-nT-\tau_k-\tau_{kl})\right\}+\mathrm{Re}\left\{z(t)\mathrm{e}^{j\omega_0 t}\right\} &\text{(19.4)}\end{aligned}$$

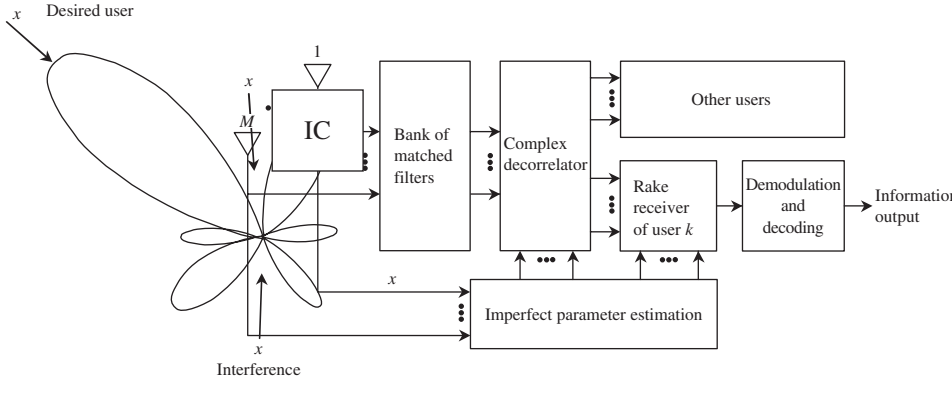

Figure 19.1 Receiver block diagram.

where $a_{kl} = A_k T_k(\psi, \varphi) H_{kl}^{(n)} e^{j\Phi_{kl}} = A'_{kl} e^{j\Phi_{kl}}$, $A_k T_k(\psi, \varphi) H_{kl}^{(n)} = A'_{kl}$, $\Phi_{kl} = \phi_0 + \phi_{k0} - \phi_{kl}$, ϕ_0 is the frequency down-conversion phase error and $z(t)$ is a complex zero mean additive white Gaussian noise process with two-sided power spectral density σ^2 and ω_0 is the carrier frequency. In general, in the sequel we will refer to A'_{kl} as received signal amplitude. This amplitude will be further modified by the receiver antenna gain pattern. The complex matched filter of user k with receiver antenna pattern $R_k(\psi, \varphi)$ will create two correlation functions for each path:

$$\begin{aligned} y_{ikl}^{(n)} &= \int_{nT+\tau_k+\tau_{kl}}^{(n+1)T+\tau_k+\tau_{kl}} r(t) R_k(\psi, \varphi) c_{ik}(t - nT - \tau_k + \tau_{kl}) \cos(\omega_0 t + \tilde{\Phi}_{kl})\, \mathrm{d}t \\ &= \sum_{k'} \sum_{l'} A_{k'l'} [d_{ik'} \rho_{ik'l',ikl} \cos \varepsilon_{k'l',kl} + d_{qk'} \rho_{qk'l',ikl} \sin \varepsilon_{k'l',kl}] \\ &= \sum_{k'} \sum_{l'} y_{ikl}(k'l') \end{aligned} \tag{19.5}$$

where $A_{k'l'} = A'_{k'l'} R_k(\psi, \varphi)$, parameter $\tilde{\Phi}_{kl}$ is the estimate of Φ_{kl} and

$$\begin{aligned} y_{ikl}(k'l') &= y_{iikl}(k'l') + y_{iqkl}(k'l') \\ &= A_{k'l'} [d_{ik'} \rho_{ik'l',ikl} \cos \varepsilon_{k'l',kl} + d_{qk'} \rho_{qk'l',ikl} \sin \varepsilon_{k'l',kl}] \end{aligned} \tag{19.6}$$

$$\begin{aligned} y_{qkl}^{(n)} &= \int_{nT+\tau_k+\tau_{kl}}^{(n+1)T+\tau_k+\tau_{kl}} r(t) R_k(\psi, \varphi) c_{qk}(t - nT - \tau_k + \tau_{kl}) \sin(\omega_0 t + \tilde{\Phi}_{kl})\, \mathrm{d}t \\ &= \sum_{k'} \sum_{l'} A_{k'l'} [d_{qk'} \rho_{qk'l',qkl} \cos \varepsilon_{k'l',kl} - d_{ik'} \rho_{ik'l',qkl} \sin \varepsilon_{k'l',kl}] \\ &= \sum_{k'} \sum_{l'} y_{qkl}(k'l') \end{aligned} \tag{19.7a}$$

$$\begin{aligned} y_{qkl}(k'l') &= y_{qqkl}(k'l') + y_{qikl}(k'l') \\ &= A_{k'l'} [d_{qk'} \rho_{qk'l',qkl} \cos \varepsilon_{k'l',kl} - d_{ik'} \rho_{ik'l',qkl} \sin \varepsilon_{k'l',kl}] \end{aligned} \tag{19.7b}$$

where $\rho_{x,y}$ are cross-correlation functions between the corresponding code components x and y. Each of these components is defined with three indices. Parameter $\varepsilon_{a,b} = \Phi_a - \tilde{\Phi}_b$ where a and b are defined with two indices each. In order to receive the incoming signal without any losses, the receiving antenna should be directing (pointing) the maximum of its radiation diagram towards the angle of arrival of the incoming signal. In this segment we will use the following terminology. The direction of the signal arrival is characterized by the pointer $\boldsymbol{p}_{\mathrm{a}} = (\psi_{\mathrm{a}}, \varphi_{\mathrm{a}})$. In order to receive the maximum signal available, the receiver antenna pointer should be $\boldsymbol{p}_{\mathrm{r}} = (\psi_{\mathrm{r}}, \varphi_{\mathrm{r}}) = (\psi_{\mathrm{a}} + \pi, \varphi_{\mathrm{a}} + \pi)$. Owing to mobility, the receiver will be tracking the incoming signal pointer and the pointer tracking error will be defined as $\Delta \boldsymbol{p} = \boldsymbol{p}_{\mathrm{r}} - \boldsymbol{p}_{\mathrm{a}} = (\psi_{\mathrm{r}} - \psi_{\mathrm{a}}, \varphi_{\mathrm{r}} - \varphi_{\mathrm{a}}) = (\Delta\psi, \Delta\varphi)$. Owing to this error the amplitude of the received signal will be reduced by ε_p with respect to the maximum value. These issues will be elaborated later. When necessary, we should make a distinction between the amplitude seen by the receiver *(asr)* for a given pointer tracking error $\Delta \boldsymbol{p}$ and the maximum available amplitude *(maa)* obtained when $\Delta \boldsymbol{p} = 0$. Let the vectors $\Im(\,)$ of MF output samples for the nth symbol interval be defined as

$$\boldsymbol{y}_{ik}^{(n)} = \Im^L \left(y_{ikl}^{(n)} \right) = \left(y_{ik1}^{(n)}, y_{ik2}^{(n)}, \ldots., y_{ikL}^{(n)} \right), \quad \in C^L \tag{19.8a}$$

$$\boldsymbol{y}_{qk}^{(n)} = \Im^L \left(y_{qkl}^{(n)} \right) = \left(y_{qk1}^{(n)}, y_{qk2}^{(n)}, \ldots., y_{qkL}^{(n)} \right), \quad \in C^L \tag{19.8b}$$

$$\mathrm{y}_k^{(n)} = \mathrm{y}_{ik}^{(n)} + j \mathrm{y}_{qk}^{(n)}; \quad \boldsymbol{y}^{(n)} = \Im^K \left(\boldsymbol{y}_k^{(n)} \right), \quad \in \mathrm{C}^{KL}; \quad \boldsymbol{y} = \Im^{N_b}(\boldsymbol{y}^{(n)}), \quad \in C^{N_b KL} \tag{19.8c}$$

19.1.2.1 CDMA system capacity

The starting point in the evaluation of CDMA system capacity is the parameter $Y_m = E_{bm}/N_0$, the received signal energy per symbol per overall noise density in a given reference receiver with index m. For the purpose of this analysis we can represent this parameter in general case as

$$Y_m = \frac{E_{bm}}{N_0} = \frac{ST}{I_{\text{oc}} + I_{\text{oic}} + I_{\text{oin}} + \eta_{\text{th}}} \tag{19.9}$$

where I_{oc}, I_{oic} and I_{oin} are power densities of intracell-, intercell- and overlay-type internetwork interference, respectively, and η_{th} is thermal noise power density. S is the overall received power of the useful signal and $T = 1/R_{\text{b}}$ is the information bit interval. Contributions of I_{oic} and I_{oin} to N_0 have been discussed in a number of papers [2]. In order to minimize repetition in our analysis, we will parameterize this contribution by introducing $\eta_0 = I_{\text{oic}} + I_{\text{oin}} + \eta_{\text{th}}$ and concentrate on the analysis of the intracell interference in the CDMA network based on advanced receivers using imperfect rake and MAI cancellation. A general block diagram of the receiver is shown in Figure 19.1. An extension of the analysis, to both intercell and internetwork interference, is straightforward.

19.1.3 Multipath channel: near--far effect and power control

We start with the rejection combiner, which will choose the first multipath signal component and reject (suppress) the others. In this case, Equation (19.9) for the I-channel becomes

$$\begin{aligned} Y_{ibm} &= \frac{\alpha_{iim1}(m1)S/R_{\text{b}}}{\{\alpha_{iqm1}(m1) + I(k'l')\}S/R_{\text{b}} + \eta_0} \\ &= \frac{\alpha_{iim1}(m1)}{\alpha_{iqm1}(m1) + I(k'l') + \eta_0 R_{\text{b}}/S} \end{aligned} \tag{19.10}$$

where $\alpha_x(z)$, (for $x = iim1, iqm1, im1$ and $z = m1, k'l'$) is the power coefficient defined as $\alpha_x(z) = E_\varepsilon\{|y_x(z)|^2\}/S$, S is normalized power level of the received signal and parameters $y_x(z)$ are in general defined by Equation (19.6).

$$I(k'l') = \sum_{k'=1}^{K} \sum_{\substack{l'=1(k'\neq m) \\ l'=2(k'=m)}}^{L} \alpha_{im1}(k'l')$$

is the equivalent MAI. $E_\varepsilon\{\ \}$ stands for averaging with respect to corresponding phases $\varepsilon_{a,b}$ defined by Equation (19.7). Based on this, we have

$$\begin{aligned} \alpha_{im1}(k'l') &= E_\varepsilon\left\{y^2_{im1}(k'l')\right\} \\ &= A^2_{k'l'}\rho^2_{im1}(k'l')/2 \Rightarrow A^2_{k'l'}/2 \Rightarrow \{A_{k'}H_{k'l'}T_{k'}(\psi,\varphi)R_m(\psi,\varphi)\}^2 \end{aligned} \tag{19.11}$$

where

$$\rho^2_{im1}(k'l') = \rho^2_{ik'l',im1} + \rho^2_{qk'l',im1},\ \ \rho^2 = E_\rho\left\{\rho^2_{ik'l',im1} + \rho^2_{qk'l',im1}\right\}$$

and normalization $A^2_{k'l'}\rho^2/2 \Rightarrow A^2_{k'l'}/2$.

A similar equation can be obtained for the Q-channel too. It has been assumed that all 'interference per path' components are independent. In what follows we will simplify the notation by dropping all indices $im1$ so that $\alpha_{im1}(k'l') \Rightarrow \alpha_{kl}$. With no power control (*npc*) α_{kl} will depend only on the channel characteristics. In partial power control (*ppc*) only the first multipath component of the signal is measured and used in a power control (open or closed) loop. Full power control (*fpc*) will normalize all components of the received signal and rake power control (*rpc*) will normalize

only those components combined in the rake receiver. The (*rpc*) control seems to be more feasible because these components are already available. These concepts for ideal operation are defined by the following equations

$$\begin{aligned} &npc \Rightarrow \alpha_{kl} = \alpha_{kl}, \quad \forall k, l; \quad ppc \Rightarrow \alpha_{k1} = 1, \quad \forall k \\ &fpc \Rightarrow \sum_{l=1}^{L} \alpha_{kl} = 1, \quad \forall k; \quad rpc \Rightarrow \sum_{l=1}^{L_0} \alpha_{kl} = 1, \quad \forall k \end{aligned} \tag{19.12}$$

where L_0 is the number of fingers in the rake receiver. The contemporary theory in this field does not recognize these options which causes a lot of misunderstanding and misconceptions in the interpretation of the power control problem in the CDMA network. Although *fpc* is not practically feasible, the analysis including *fpc* should provide the reference results for the comparison with other, less efficient options. Another problem in the interpretation of the results in the analysis of the power control imperfections is caused by the assumption that all users in the network have the same problem with power control. Hence, the imperfect power control is characterized with the same variance of the power control error. This is more than pessimistic assumption and yet it has been used very often in analyses published so far. The above discussion is based on the signal amplitude seen by the receiver (asr). System losses due to difference between the *asr* and *maa* will be discussed in the next section. If we now introduce matrix $\boldsymbol{\alpha}_m$ with coefficients $\|\alpha_{kl}\|, \forall k, l$ except for $\alpha_{m1} = 0$ and use notation $\mathbf{1}$ for vector of all ones, Equation (19.10) becomes

$$Y_{bm} = \frac{\alpha_{m1}}{\mathbf{1} \cdot \boldsymbol{\alpha}_m \cdot \mathbf{1}^T + \eta_0 R_b / S} \tag{19.13}$$

Compared with Equation (19.10), the index i is dropped in order to indicate that the same form of equation is valid for both, the I- and Q-channel defined by Equation (19.8).

19.1.4 Multipath channel: pointer tracking error, rake receiver and interference canceling

If L_0-fingers rake receiver ($L_0 \leq$ L) with combiner coefficients $w_{mr} (r = 1, 2, \ldots, L_0)$ and interference canceller are used, the signal-to-noise ratio will become

$$Y_{bm} = \frac{r_m^{(L_0)}}{f(m, \boldsymbol{\alpha}, \mathbf{c}, \mathbf{r}) K + \varsigma_0 \eta R_\mathrm{b} / S} \tag{19.14}$$

where

$$\varsigma_0 = \sum_{r=1}^{L_0} w_{mr}^2 = \mathbf{w}_m \mathbf{w}_m^\mathrm{T}; \quad \mathbf{w}_m = (w_{m1}, w_{m2}, \ldots, w_{mn}) \tag{19.15}$$

is due to Gaussian noise processing in the rake receiver, and noise density η_0 becomes η due to additional signal processing. Also we have

$$\begin{aligned} f(m, \boldsymbol{\alpha}, \mathbf{c}, \mathbf{r}) &= \frac{1}{K} \sum_{\substack{k=1 \\ k \neq m}}^{K} \sum_{r=1}^{L_0} \sum_{l=1}^{L} w_{mr}^2 \bar{\alpha}_{kl} (1 - C_{kl}) + \frac{1}{K} \sum_{r=1}^{L_0} \sum_{\substack{l=1 \\ l \neq r}}^{L} w_{mr}^2 \bar{\alpha}_{ml} (1 - C_{ml}) \\ &= \frac{1}{K} \left\{ \mathbf{w}_m \left(\mathbf{1} \cdot \boldsymbol{\alpha}_{cmr} \cdot \mathbf{1}^\mathrm{T} \right) \mathbf{w}_m^\mathrm{T} \right\} \end{aligned} \tag{19.16}$$

with $\boldsymbol{\alpha}_{cmr}$ being a matrix of size $K \times L$ with coefficients $\|\bar{\alpha}_{kl}(1 - C_{kl})\|$ except for $\bar{\alpha}_{mr}(1 - C_{mr}) = 0$ and C_{ml} is efficiency of the canceller. The parameter $\bar{\alpha}_{kl} = E_{p(\phi,\psi)} \{\alpha_{kl}\}$ is the average value of the interfering signal power α_{kl} coming from direction (azimuth, elevation) $(\psi_{kl}, \varphi_{kl}) = (\psi_m + \Delta\psi_{kl}, \varphi_m + \Delta\varphi_{kl})$ with respect to the reference pointer $p(\psi_m, \varphi_m)$ of the useful signal. Formally

this can be represented as

$$\bar{\alpha}_{kl} = \int\int_{\phi,\psi} \int\int_{\Delta\psi,\Delta\varphi} \alpha_{kl}(\psi,\varphi)\mathrm{PDF}(\Delta\psi_{kl},\Delta\varphi_{kl})\ \mathrm{d}\psi\ \mathrm{d}\varphi\ \mathrm{d}(\Delta\psi_{kl})\ \mathrm{d}(\Delta\varphi_{kl}) \tag{19.16a}$$

were $\mathrm{PDF}(\Delta\psi_{kl},\Delta\varphi_{kl})$ is probability density function of the arguments. For the first insight into the system performance a uniform distribution of $\Delta\psi_{kl}$ and $\Delta\varphi_{kl}$ can be assumed along with a rectangular shape of $T(\psi,\varphi)$ and $R(\psi,\varphi)$ in the range $\psi \in \psi_0 + \Psi$, $\varphi \in \varphi_0 + \Phi$, so that evaluation of Equation (19.16a) becomes trivial. For the amplitudes A_{kl} seen by the receiver *asr*, the parameter $r_m^{(L_0)}$ in Equation (19.14), called rake receiver efficiency, is given as

$$r_m^{(L_0)} = \left(\sum_{r=1}^{L_0} w_{mr}\cos\varepsilon_{\theta mmr}\sqrt{\alpha_{mr}}\right)^2 = \left(\mathrm{W}_m \cdot \boldsymbol{\alpha}_{mm\surd}\right)^2 \tag{19.17}$$

with

$$\boldsymbol{\alpha}_{mm\surd} = \left(\cos\varepsilon_{\theta mm1}\sqrt{\alpha_{m1}}, \cos\varepsilon_{\theta mm2}\sqrt{\alpha_{m2}}, \ldots\right)^{\mathrm{T}}$$

Parameter $\varepsilon_{\theta mmr} = \theta_{mmr} - \hat{\theta}_{mmr}$ is the carrier phase synchronization error in receiver m for signal of user m in path r. We will drop index *mkl* whenever it does not result into any ambiguity. In the sequel we will use the following notation: $\alpha_{kl} = A_{kl}^2/2$, $\hat{A}_{mkl}$ is the estimation of A_{kl} by the receiver m, $\varepsilon_a = \Delta A_{mkl}/A_{kl} = (A_{kl} - \hat{A}_{mkl})/A_{kl}$ is the relative amplitude estimation error, $\varepsilon_m = BER =$ bit error rate that can be represented as $\overline{m\hat{m}} = 1 - 2BER$, and $\varepsilon_\theta =$ carrier phase estimation error.

For the equal gain combiner (EGC) the combiner coefficients are given as $w_{mr} = 1$. Having in mind the notation used so far in the sequel, we will drop index m for simplicity. For the maximal ratio combiner (MRC) the combiner coefficients are based on estimates as

$$\hat{w}_r = \frac{\cos\varepsilon_{\theta r}}{\cos\varepsilon_{\theta 1}} \cdot \frac{\hat{A}_r}{\hat{A}_l} \cong \frac{\left(1-\varepsilon_{\theta r}^2/2\right)}{\left(1-\varepsilon_{\theta l}^2/2\right)} \cdot \frac{A_r(1-\varepsilon_{ar})}{A_l(1-\varepsilon_{al})} \tag{19.18}$$

$$E\{\hat{w}_r\} = w_r\left(1-\sigma_{\theta r}^2\right)\left(1+\sigma_{\theta 1}^2\right)(1-\varepsilon_{ar})(1+\varepsilon_{a1}) \tag{19.19}$$

$$E\left\{\hat{w}_r^2\right\} = w_r^2\left(1-2\sigma_{\theta r}^2+3\sigma_{\theta r}^4\right)\left(1+2\sigma_{\theta l}^2-3\sigma_{\theta l}^4\right)(1-\varepsilon_{ar})^2(1+\varepsilon_{a1})^2$$

Averaging Equation (19.17) gives for EGC

$$\begin{aligned} E\left\{r^{(L_0)}\right\} &= E\left\{\left(\sum_{r=1}^{L_0}\cos\varepsilon_{\theta r}\sqrt{\alpha_r}\right)^2\right\} = E\left\{\left(\sum_{r=1}^{L_0}\left(1-\varepsilon_{\theta r}^2/2\right)\sqrt{\alpha_r}\right)^2\right\} \\ &= \sum_r\sum_{\substack{l\\ l\neq r}}\left(1-\sigma_{\theta r}^2\right)\left(1-\sigma_{\theta l}^2\right)\sqrt{\alpha_r\alpha_l} + \sum_r \alpha_r\left(1-2\sigma_{\theta r}^2+3\sigma_{\theta r}^4\right) \end{aligned} \tag{19.20}$$

For MRC the same relation becomes

$$\begin{aligned} E\left\{r^{(L_0)}\right\} &= E\left\{\left(\sum_{r=1}^{L_0}\frac{\alpha_r}{\sqrt{\alpha_1}}\frac{\left(1-\varepsilon_{\theta r}^2/2\right)^2}{\left(1-\varepsilon_{\theta l}^2/2\right)}\frac{(1-\varepsilon_{ar})}{(1-\varepsilon_{al})}\right)^2\right\} \\ &= E\left\{\sum_{r=1}^{L_0}\frac{\alpha_r^2}{\alpha_l}\frac{\left(1-\varepsilon_{\theta r}^2/2\right)^4}{\left(1-\varepsilon_{\theta l}^2/2\right)^2}\frac{(1-\varepsilon_{ar})^2}{(1-\varepsilon_{a1})^2}\right\} \\ &+ \sum_r\sum_{\substack{l\\ l\neq r}}\frac{\alpha_r\alpha_l}{\alpha_l}\left(1-2\sigma_{\theta r}^2+3\sigma_{\theta r}^4\right)\left(1-2\sigma_{\theta l}^2+3\sigma_{\theta l}^4\right) \\ &\quad\times\left(1+2\sigma_{\theta 1}^2-3\sigma_{\theta 1}^4\right)(1-\varepsilon_{ar})(1-\varepsilon_{al})(1+\varepsilon_{al})^2 \end{aligned} \tag{19.21}$$

In order to evaluate the first term we use limits. For the upper limit we have $\varepsilon_{\theta r}^2 \Rightarrow \varepsilon_{\theta l}^2$. By using this we have

$$(1-\varepsilon_{\theta r}^2/2)^4/(1-\varepsilon_{\theta l}^2/2)^2 \Rightarrow (1-\varepsilon_{\theta l}^2/2)^2$$

and the first term becomes

$$\sum_{r=l}^{L_0} \frac{\alpha_r^2}{\alpha_l}\left(1-2\sigma_{\theta 1}^2+3\sigma_{\theta 1}^4\right)(1-\varepsilon_{ar})^2/(1-\varepsilon_{a1})^2$$

For the lower limit we use $\varepsilon_{\theta l}^2 \Rightarrow \varepsilon_{\theta r}^2$ and the first term becomes

$$\sum_{r=l}^{L_0} \frac{\alpha_r^2}{\alpha_l}\left(1-2\sigma_{\theta \mathrm{r}}^2+3\sigma_{\theta \mathrm{r}}^4\right)(1-\varepsilon_{ar})^2/(1-\varepsilon_{al})^2$$

For a signal with the I- and Q-component the parameter $\cos\varepsilon_{\theta r}$ should be replaced by $\cos\varepsilon_{\theta r} \Rightarrow \cos\varepsilon_{\theta r} + m\rho\sin\varepsilon_{\theta r}$, where m is the information in the interfering channel (I or Q), and ρ is the cross-correlation between the codes used in the I- and Q-channel. For small tracking errors this term can be replaced as $\cos\varepsilon_{\theta r} + m\rho\sin\varepsilon_{\theta r} \approx 1 + m\rho\varepsilon - \varepsilon^2/2$, where the notation is further simplified by dropping the subscript $(\,)_{\theta r}$. Similar expressions can be derived for the complex signal format. In the above discussion the signal amplitude seen by the receiver *(asr)* is used for A_r. In the presence of pointer estimation error this is related to the (*maa*) as $A_r \Rightarrow A_r - \varepsilon_p$. So, to account for the losses due to ε_p, parameter α_r in the above equation should be replaced by $\alpha_r \Rightarrow E(A_r-\varepsilon_p)^2 = \alpha_r - 2\bar{\varepsilon}_p\sqrt{\alpha_r+\sigma_p^2}$ where $\bar{\varepsilon}_p$ and $\sigma_p^2 = E(\varepsilon_p^2)$ are the mean and variance of the pointer tracking error. The power control will compensate for the pointer tracking losses by increasing the signal power by the amount equal to the losses. This means that the level of interference will be increased which can be taken into account in our model by modifying the parameters α_{kl} as follows: $\alpha_{kl} \Rightarrow \alpha_{kl} + 2\bar{\varepsilon}_p\sqrt{\alpha_{kl}-\sigma_{pkl}^2}$

19.1.5 Interference canceler modeling: nonlinear multiuser detectors

For the system performance evaluation a model for the canceller efficiency is needed. Linear multiuser structure might not be of much interest in the next generation of the mobile communication systems where the use of long codes will be attractive. An alternative approach is nonlinear (multistage) multiuser detection, that would include channel estimation parameters too. This would be based on interference estimation and cancellation schemes (OKI standard-IS-665/ITU recommendation M.1073 or UMTS defined by ETSI)

In general if the estimates of Equation (19.8) are denoted $\hat{\mathbf{y}}_i$ and $\hat{\mathbf{y}}_q$, then the residual interference after cancellation can be expressed as

$$\Delta\mathbf{y}_i = \mathbf{y}_i - \hat{\mathbf{y}}_i, \quad \Delta\mathbf{y}_q = \mathbf{y}_q - \hat{\mathbf{y}}_q, \quad \Delta\mathbf{y} = \Delta\mathbf{y}_i + j\Delta\mathbf{y}_q = \mathrm{Vec}\left\{\Delta y_\varsigma\right\} \tag{19.22}$$

where index $\varsigma \Rightarrow k, l$ spans all combinations of k and l. By using Equation (19.22), each component $\alpha_{kl}(1-C_{kl})$ in Equation (19.16) can be obtained as a corresponding entry of $\mathrm{Vec}\{|\Delta y_\varsigma|^2\}$.

To further elaborate these components we will use a simplified notation and analysis. After frequency downconversion and despreading, the signal from user k, received through path l at the receiver m, would have the form

$$\hat{S}_{mkl} = \hat{A}_{mkl}\hat{m}_k\cos\hat{\theta}_{mkl} = (A_{mkl}+\Delta A_{mkl})\hat{m}_k\cos(\theta_{mkl}+\varepsilon_{\theta mkl}) \tag{19.23}$$

for a single signal component and

$$\begin{aligned}\hat{S}_{mkl}^i &= \hat{A}_{mkl}\hat{m}_{ki}\cos\theta_{mkl} + \hat{A}_{mkl}\hat{m}_{kq}\sin\theta_{mkl};\\ \hat{S}_{mkl}^q &= -\hat{A}_{mkl}\hat{m}_{ki}\sin\theta_{mkl} + \hat{A}_{mkl}\hat{m}_{kq}\cos\theta_{mkl}\end{aligned} \tag{19.24}$$

for a complex (I&Q) signal structure. In a given receiver m, components $\hat{S}^i_{mkl}$ and $\hat{S}^q_{mkl}$ correspond to Δy_{ikl} and Δy_{qkl}. Parameter A_{mkl} includes both amplitude and correlation function. In Equation (19.23) ΔA_{mkl} and $\varepsilon_{\theta mkl}$ are amplitude and phase estimation errors. The canceller would create $S_{mkl} - \hat{S}_{mkl} = \Delta S_{mkl}$ and the power of this residual error (with index m dropped for simplicity) would be

$$E_\theta\left[(\Delta S_{kl})^2\right] = E_\theta\left[A_{kl} m_k \cos\theta_{kl} - (A_{kl} + \Delta A_{kl})\,\hat{m}_k \cos(\theta_{kl} + \varepsilon_{\theta k})\right]^2 \tag{19.25}$$

where $E_\theta[\,]$ stands for averaging with respect to θ_{kl} and m_k. Parameter $(\Delta S_{kl})^2$ corresponds to $|\Delta y_n|^2$. This can be represented as

$$E_\theta\left[(\Delta S_{kl})^2\right] = \alpha_{kl}\left[1 + (1+\varepsilon_a)^2 - 2(1+\varepsilon_a)\cdot(1-2\varepsilon_m)\cos\varepsilon_\theta\right] \tag{19.26}$$

From this equation we have $1 - C_{kl} = E_\theta\lfloor(\Delta S_{kl})^2\rfloor/\alpha_{kl}$ and $C_{kl} = 2(1+\varepsilon_a)(1-2\varepsilon_m)\cos\varepsilon_\theta - (1+\varepsilon_a)^2$. Expanding $\cos\varepsilon_\theta$ as $1 - \varepsilon_\theta^2/2$ and averaging gives

$$C_{kl} = 2(1+\varepsilon_a)(1-2\varepsilon_m)\left(1-\sigma_\theta^2\right) - (1+\varepsilon_a)^2 \tag{19.27}$$

For zero mean ε_θ, $\sigma_\theta^2 = E\lfloor\varepsilon_\theta^2/2\rfloor$ is the carrier phase tracking error variance. For the complex (I&Q) signal structure cancellation efficiencies in I- and Q-channels can be represented as

$$\begin{aligned} C^i_{kl} &= 4(1+\varepsilon_a)(1-2\varepsilon_m)\left(1+\sigma_\theta^2\right) - 2(1+\varepsilon_a)^2 - 1 \\ C^q_{kl} &= 4(1+\varepsilon_a)(1-2\varepsilon_m)\left(1+\sigma_\theta^2\right) - 2(1+\varepsilon_a)^2 - 1 \end{aligned} \tag{19.28}$$

So, in this case the canceller efficiency is expressed in terms of amplitude, phase and data estimation errors. These results should be now used for analysis of the impact of large-scale channel estimators on overall CDMA network sensitivity. The performance measure of any estimator is parameter estimation error variance that should be directly used in Equations (19.28) for cancellation efficiency and Equations (19.19)–(19.22) for the rake receiver. If joint parameter estimation is used, based on ML criterion, then the Cramer–Rao bound could be used for these purposes. For the Kalman type estimator, the error covariance matrix is available for each iteration of estimation. If each parameter is estimated independently, then for carrier phase and code delay estimation error a simple relation $\sigma^2_{\theta,\tau} = 1/SNR_{\mathrm{L}}$ can be used where SNR_{L} is the signal-to-noise ratio in the tracking loop. For the evaluation of this SNR_{L} the noise power is in general given as $N = B_{\mathrm{L}} N_0$. For this case, the noise density N_0 is approximated as a ratio of the overall interference plus noise power divided by the signal bandwidth. The loop bandwidth will be proportional to f_{D} where f_{D} is the fading rate (Doppler). The higher the f_{D}, the higher the loop noise bandwith, the higher the equivalent noise power ($N_0 f_{\mathrm{D}}$). If interference cancellation is performed prior to parameter estimation, N_0 is obtained from $f(\,)$ defined by Equation (9.16). If parameter estimation is used without interference cancellation the same $f(\,)$ is used with $C_{kl} = 0$. In addition to this

$$\varepsilon_a \Rightarrow \frac{A - \hat{A}(1-\varepsilon_\tau)}{A} = \frac{\Delta A + \hat{A}\varepsilon_\tau}{A} \quad ; \quad \varepsilon_a \Rightarrow \varepsilon_A + \varepsilon_\tau(1-\varepsilon_A) \tag{19.29}$$

where ε_τ is the code delay estimation error and $\varepsilon_A = (A - \hat{A})/A = 1 - \hat{A}/A$. For noncoherent estimation we have

$$\frac{\hat{A}}{A} = \left(\frac{\pi}{4y}\right)^{1/2} \exp\left(-\frac{y}{2}\right)\left\{1 + yI_0\left(\frac{y}{2}\right) + yI_1\left(\frac{y}{2}\right)\right\} \tag{19.30}$$

where $I_0(\,)$ and $I_1(\,)$ are the zeroth- and first- order Bessel functions, respectively, and y is the signal-to-noise ratio.

19.1.6 Approximations

If we assume that the channel estimation is perfect ($\varepsilon_a = \varepsilon_\theta = 0$) the parameter C_{mkl} becomes $C_{kl} = 2(1 - 2\varepsilon_m) - 1 = 1 - 4\varepsilon_m$. For DPSK modulation $\varepsilon_m = (1/2)\exp(-y/2)$ where y is signal-to-noise ratio and for CPSK $\varepsilon_m = (1/2)\text{erfc}(\sqrt{y})$. So $C_{kl} = 1 - 2e^{-y}$ for DPSK, and $C_{kl} = 1 - 2\,\text{erfc}(\sqrt{y})$ for CPSK. For large y, $C_{kl} \Rightarrow 1$ and for small y in DPSK system we have $e^{-y} \cong 1 - y$ and $C_{kl} \cong 2y - 1$. This can be presented as $C_{kl} = 2Y_b - 1$, where Y_b is given by Equation (19.14). Bearing in mind that Y_b depends on C_{kl} the whole equation can be solved through an iterative procedure starting up with an initial value of $C_{kl} = 0, \forall m, k, l$. Similar approximations can be obtained for σ_θ^2 and ε_a. From practical point of view an attractive solution could be a scheme that would estimate and cancel only the strongest interference (e.g. successive interference cancellation schemes [2]).

19.1.7 Outage probability

The previous section already completely defines the simulation scenario for the system performance analysis. For the numerical analysis further assumptions and specifications are necessary. First of all we need the channel model. The exponential multipath intensity profile (MIP) is widely used analytical model realized as a tapped delay line [2]. It is very flexible in modeling different propagation scenarios. The decay of the profile and the number of taps in the model can vary. Averaged power coefficients in the multipath intensity profile are

$$\overline{\alpha_l} = \overline{\alpha_0} e^{-\lambda l} \quad l, \lambda \geq 0 \tag{19.31}$$

where λ is the decay parameter of the profile. Power coefficients should be normalized as $\sum_{l=0}^{L-1} \overline{\alpha_0} e^{-\lambda l} = 1$. For $\lambda = 0$ the profile will be flat. The number of resolvable paths depends on the channel chip rate and this must be taken into account. We will start from Equation (19.14) and look for the average system performance for $\rho^2 = 1/G$ where $G = W/R_b$ is the system processing gain and W is the system bandwidth (chip rate). The average signal to noise ratio will be expressed as

$$\overline{Y_b} = \frac{r^{(L_0)} G}{f(\boldsymbol{\alpha}) K + \varsigma_0 \eta' W / S} \tag{19.32}$$

Now, if we accept some quality of transmission, BER $= 10^{-e}$, that can be achieved with the given SNR $= Y_0$, then with the equivalent average interference density $\eta_0 = I_{\text{oic}} + I_{\text{oin}} + \eta_{\text{th}}$ SNR will be

$$Y_0 = \frac{r^{(L_0)} G}{\eta_0} \tag{19.33}$$

To evaluate the outage probability P_{out} we need to evaluate [2]

$$\begin{aligned} P_{\text{out}} &= \Pr\left(\text{BER} > 10^{-e}\right) = \Pr\left(\text{MAI} + \frac{\eta W}{S} > \eta_0\right) \\ &= \Pr\left(\text{MAI} > \eta_0 - \frac{\eta W}{S}\right) = \Pr\left(\text{MAI} > \delta\right) \end{aligned} \tag{19.34}$$

where δ is given as

$$\delta = \frac{r^{(L_0)} G}{Y_0} - \frac{\eta W}{S}$$

It can be shown that this outage probability can be represented by Gaussian integral

$$P_{\text{out}} = Q\left(\frac{\delta - m_g}{\sigma_g}\right) \tag{19.35}$$

where m_g and σ_g are the mean value and the standard variance respectively of the overall interference. From Equation (19.32) we have for the system capacity K with ideal system components

$$K_{\max} = \frac{r_0^{(L_0)} G}{Y_0 f_0(\alpha)} - \varsigma_0 \eta W / S f_0(\boldsymbol{\alpha}) \tag{19.36}$$

Owing to imperfections in the operation of the rake receiver and interference canceller, this capacity will be reduced to

$$K' = \frac{r^{(L_0)} G}{Y_0 f(\boldsymbol{\alpha})} - \varsigma_0 \eta' W / S f(\boldsymbol{\alpha}) \tag{19.37}$$

where $r_0^{(L_0)}$ and $f_0(\alpha)$ are now replaced by real parameters $r^{(L_0)}$ and $f(\boldsymbol{\alpha})$ that take into account those imperfections. The system sensitivity function is defined as

$$\Re = \frac{K_{\max} - K'}{K_{\max}} = \frac{1}{K_{\max}} \left\{ \frac{\Delta r^{(L_0)} G}{Y_0 f(\alpha) f_0(\alpha)} - \frac{\varsigma_0 \eta' W \Delta f(\boldsymbol{\alpha})}{S f(\boldsymbol{\alpha}) f_0(\boldsymbol{\alpha})} \right\} \tag{19.38}$$

where $\Delta r^{(L_0)} = r_0^{(L_0)} f(\boldsymbol{\alpha}) - r^{(L_0)} f_0(\boldsymbol{\alpha})$ and $\Delta f(\boldsymbol{\alpha}) = f(\boldsymbol{\alpha}) - f_0(\boldsymbol{\alpha})$.

19.1.7.1 Performance example

In this section we present some numerical results for illustration purposes. The results are obtained for a channel with double exponential (space and delay) profile with decay factors λ_s and λ_t. Graphical results are presented with: solid line, 4×4 rake; dashed line, 4×1 rake. In the case of a *3 dB approximation of the real antenna*, the beam forming is approximated by the rectangular shape of the antenna pattern in the range $\varphi_{3\,\mathrm{dB}} = 30^\circ$ (for $\rho_c = 1$), and uniform distribution of $\Delta\psi_{kl}$ and $\Delta\varphi_{kl}$ ([0, π], [0, 2 π], respectively) , $\lambda_s = \lambda_t = 0$ if not specified otherwise, $Y_0 = 2$, $L = 4$, interference margin SNR $= (20 * \alpha_0 / alfa\_mean)^{-1}$.

The users are uniformly distributed in the sphere (φ, ψ) with $\varphi, \psi \in (0, 360^\circ)$. The results can be easily scaled down for a more realistic scenario where $\varphi \in (0, 360^\circ)$ and $\psi \in (\psi_{\min}, \psi_{\max})$. The canceling efficiency for maximum capacity is calculated by assuming no estimation errors in Equation (19.27). When estimation errors are included, canceling efficiencies are given by Equation (19.27). Carrier phase tracking error variance is assumed to be $\sigma_\theta^2 = 1/\mathrm{SNR_L}$. For MRC the amplitude estimation error is approximated from Equation (19.30) to follow $\varepsilon_a = 1/4\ \mathrm{SNR_L}$. For *real antennas* the amplitude patterns are specified in Figure 19.2. The base station amplitude antenna pattern is given as

$$A(\varphi,\ \psi) = \frac{1}{N} \sum_{n=1}^{N} \exp\left\{ -\pi \left[\rho_c \sin\psi \cos\left(\varphi - 2\pi \frac{n}{N} \right) \right]^2 \right\}$$

and four examples cover a relatively wide range of shapes, from a wide lobe for $\rho_c = 1$ to a rather narrow lobe for $\rho_c = 12$. At mobile stations an omnidirectional antenna pattern $A(\varphi,\ \psi) = 1$ is assumed. Capacity curves, defined as the number of users with data rate $R =$ chip rate/$G = 4.096/G$, for different antenna patterns, are shown in Figure 19.3. The highest capacity is obtained for $\rho_c = 12$ because with the narrowest lobe the spatial division multiple access effect is the most effective. With increased receiver velocity the capacity will be reduced due to the increased effect of imperfections. A comparison of the systems using ideal and real antennas is shown in Figure 19.4. Figure 19.4 presents the system capacity vs G. In general higher G means more users in the network and more MAI resulting in more impact of imperfections. A 4×4 rake performs better for lower G but for higher G (more users) it deteriorates faster. The degradation is more severe for higher receiver velocities.

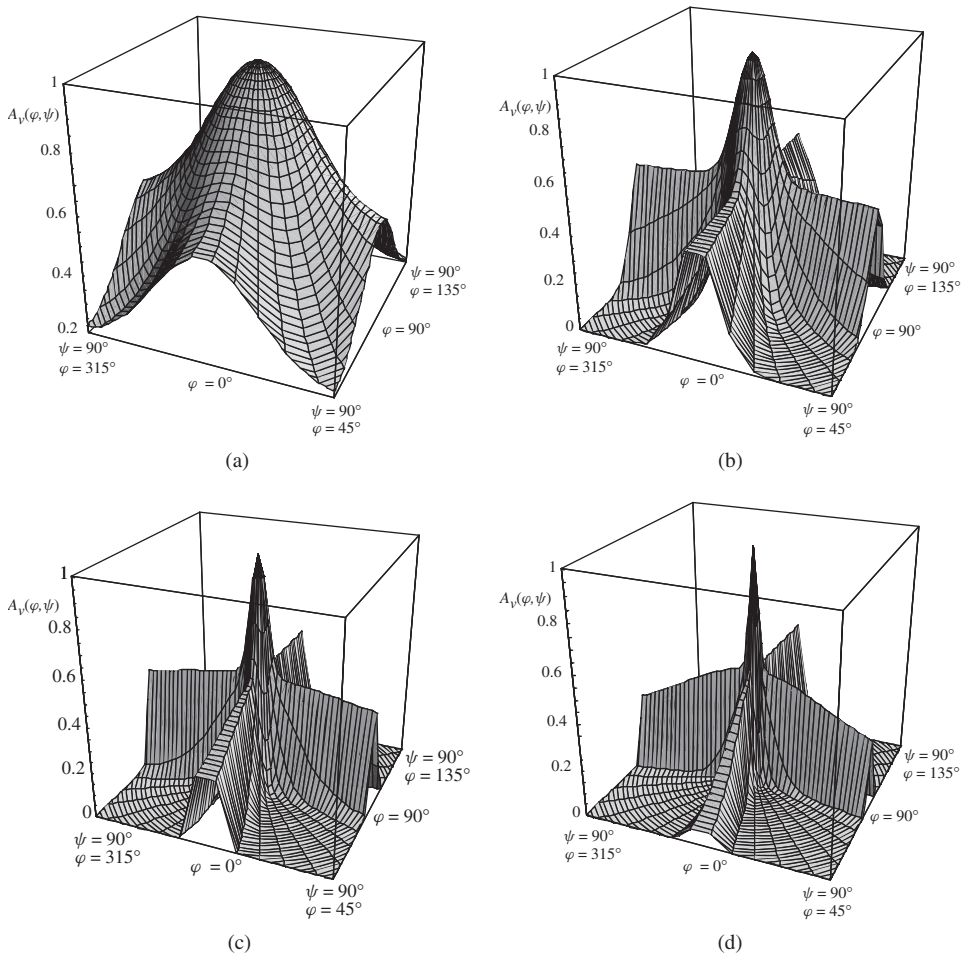

Figure 19.2 Peak-amplitude pattern $A(\varphi, \psi)$ for nonsinusoidal Gaussian pulses received by the circular array with $N = 4$ elements and (a) $\rho_c = 1$; (b) $\rho_c = 3$; (c) $\rho_c = 6$; (d) $\rho_c = 12$.

Figure 19.5 represents the same results as a function of the receiver velocity. The system sensitivity function defined by Equation (19.38) is shown in Figure 19.6. Sensitivity equal to 1 means that all capacity has been lost due to imperfections. Figure 19.6 demonstrates that very high values for the system sensitivity, even in the range close to 0.9, can be expected if a large number of users (low data rate corresponding to high G) are in the network.

In this section we have presented a systematic analytical framework for the capacity evaluation of an advanced CDMA network. This approach provides a relatively simple way to specify the required quality of a number of system components. This includes multiple access interference canceller and rake receiver, taking into account all their imperfections. The system performance measure is the network sensitivity function representing the relative losses in capacity due to all imperfections in the system implementation. Some numerical examples are presented for illustration purposes. These results are obtained for a channel with double exponential (space and delay)

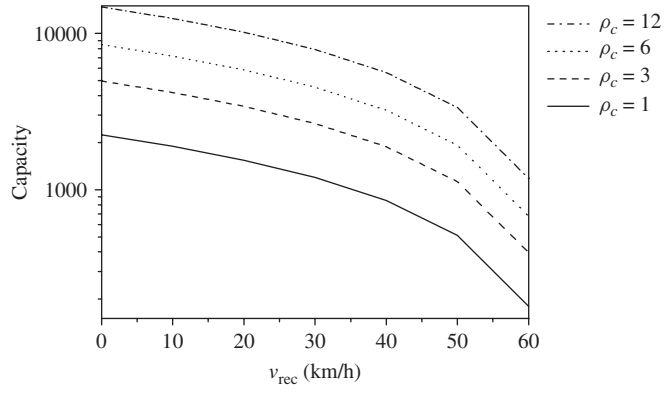

Figure 19.3 Capacity vs receiver velocity for EGC for different antenna patterns $A(\varphi, \psi)$. $N = 4$, 4×4 rake, $G = 256$, $\lambda_t = \lambda_s = 0$, $Y_0 = 2$, $L = 4$, SNR $= (20^*\alpha_0/\text{alpha\_mean})^{-1}$.

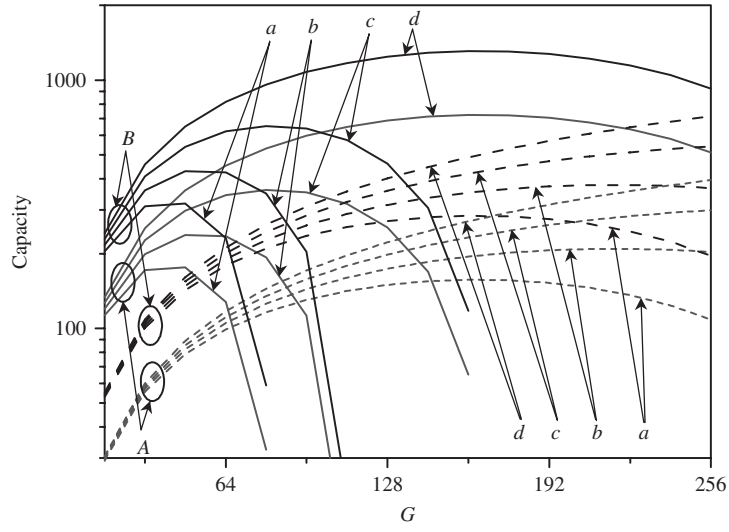

Figure 19.4 Capacity vs processing gain for EGC. a, $v_{rec} = 200$ km/h, b, $v_{rec} = 150$ km/h, c, $v_{rec} = 100$ km/h; d, $v_{rec} = 50$ km/h. Solid line: 4×4 rake; dashed line: 4×1 rake; A real antenna pattern of circular array at base station; B, 3 dB aproximation ($\psi_{3\,dB} = 30^\circ$) of the real antenna pattern; $\rho_c = 1$; $N = 4$, $\lambda_s = \lambda_t = 0$, $Y_0 = 2$, $L = 4$, SNR $= (20^*\alpha_0/\text{alpha\_mean})^{-1}$.

profile. It was shown that for the receiver velocity 100–200 km/h as much as 70–90 % of the system capacity can be lost due to the imperfections of the three-dimensional rake receiver and interference cancellation operation. variety of results are presented for different channel decay factor, fading rate and number of rake fingers. In general, under ideal conditions, the system capacity is increased if the number of fingers is increased. At the same time one should be aware that the system sensitivity is also increased if the fading rate and number of rake fingers are higher. The results and methodology presented in this section offer enough tools and data for the careful choice of the system parameters in realistic environments which are characterized by imperfections.

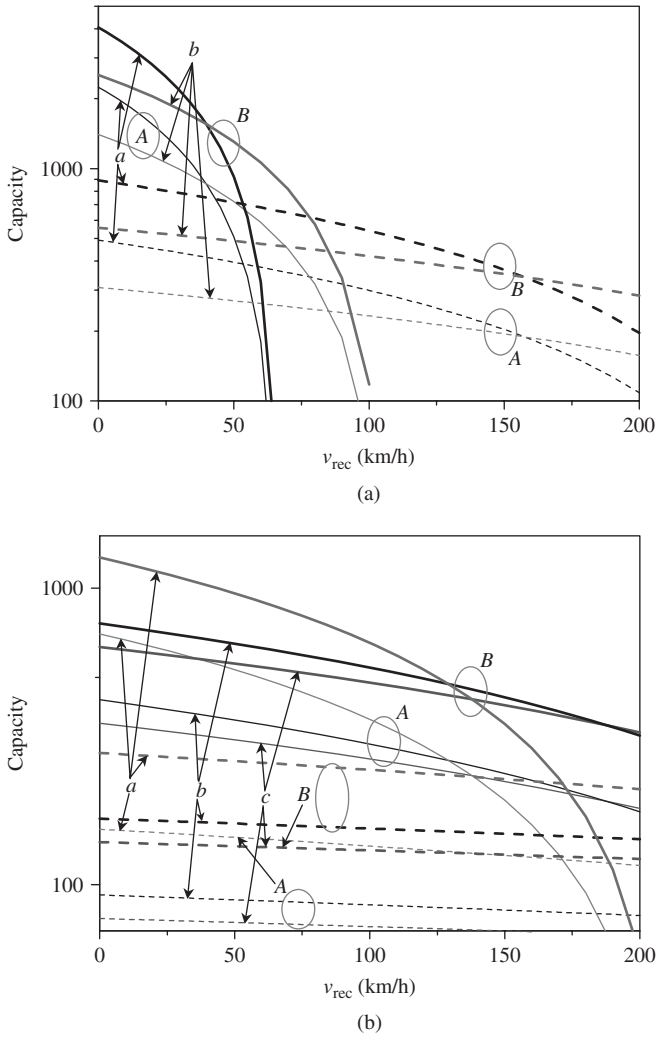

Figure 19.5 Capacity vs the receiver velocity for EGC; solid lines, 4×4 rake; dashed lines, 4×1 rake. A, real antenna; B, 3 dB approximation of the real antenna. $\rho_c = 1; N = 4$, $\lambda_t = \lambda_s = 0, Y_0 = 2, L = 4$, SNR $= (20^*\alpha_0/\text{alpha\_mean})^{-1}$. (a) $a, G = 256; b, G = 160$; (b) $a, G = 80; b, G = 48; c, G = 40$.

19.2 CAPACITY OF *AD HOC* NETWORKS

In this section we now discuss the capacity of wireless networks. The discussion is based on concepts presented in References [32, 33]. In an *ad hoc* network, it is supposed that n nodes are located in a region of area 1 m^2. Each node can transmit at W b/s over a common wireless channel. The channel in general may be broken up into several subchannels of capacity $W_1, W_2, \ldots, W_M$ b/s. This will be immaterial for the final results as long as $\sum_{m=1}^{M} W_m = W$. Packets are sent from node to node in a multihop fashion until they reach their final destination. They can be buffered at intermediate nodes while awaiting transmission. Owing to spatial separation, several nodes

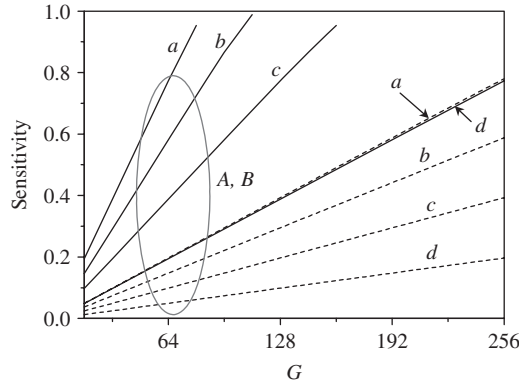

Figure 19.6 Sensitivity vs processing gain for EGC. a, $v_{\text{rec}} = 200\,\text{km/h}$; b, $v_{\text{rec}} = 150\,\text{km/h}$; c, $v_{\text{rec}} = 100\,\text{km/h}$; d, $v_{\text{rec}} = 50\,\text{km/h}$. Solid line, 4×4 Rake; dashed line; 4×1 rake. A, real antenna pattern of circular array at base station; B, 3 dB aproximation ($\psi_{3\,\text{dB}} = 30^\circ$) of the real antenna pattern. $\rho_c = 1$; $N = 4$, $\lambda_s = \lambda_t = 0$, $Y_0 = 2$, $L = 4$, SNR $= (20^*\alpha_0\ /\text{alpha\_mean})^{-1}$.

can make wireless transmissions simultaneously, provided there is no excessive interference from others. In the sequel we will discuss the conditions under which a wireless transmission over a subchannel is received successfully by its intended recipient.

Two types of networks are considered, *Arbitrary networks*, where the node locations, destinations of sources, and traffic demands, are all arbitrary, and *Random Networks*, where the nodes and their destinations are randomly chosen.

19.2.1 Arbitrary networks

In the arbitrary setting we suppose that n nodes are arbitrarily located in a disk of unit area in the plane. Each node chooses an arbitrary destination to which it wishes to send traffic at an arbitrary rate, so that the traffic pattern is arbitrary too. Each node can choose an arbitrary range or power level for each transmission.

To define when a transmission is received successfully by its intended recipient we will allow for two possible models for successful reception of a transmission over one hop, called the *protocol model* and the *physical model*. Let X_i denote the location of a node; we will also use X_i to refer to the node itself.

19.2.1.1 The protocol model

Suppose node X_i transmits over the mth subchannel to a node X_j. In this case transmission is successfully received by node X_j if $|X_k - X_j| \geq (1 + \Delta)|X_i - X_j|$. In this case a guard zone $\Delta > 0$ is specified by the protocol to prevent a neighboring node from transmitting on the same subchannel at the same time.

19.2.1.2 The physical model

Let $\{X_k; k \in T\}$ be the subset of nodes simultaneously transmitting at some time instant over a certain subchannel. Let P_k be the power level chosen by node X_k for $k \in T$. In this case the

transmission from a node X_i, $i \in T$, is successfully received by a node X_j if $S/I \geq \beta$, where

$$S = P/\left|X_i - X_j\right|^{\alpha}$$

and

$$I = N + \sum_{\substack{k \in T \\ k \neq i}} P/\left|X_i - X_j\right|^{\alpha}$$

This models a situation where a minimum signal-to-interference ratio (SIR) of β is necessary for successful receptions, the ambient noise power level is N, and signal power decays with distance r as $1/r^{\alpha}$. For a model outside a small neighborhood of the transmitter, $\alpha > 2$.

19.2.1.3 The transport capacity of arbitrary networks

In this contest we say that the network transports one *bit-meter* (b-m) when 1 b has been transported a distance of 1 m towards its destination. (We do not give multiple credit for the same bit carried from one source to several different destinations as in the multicast or broadcast cases.) This sum of products of bits and the distances over which they are carried is a valuable indicator of a network's *transport capacity* C_{T}. (It should be noted that, when the area of the domain is A square meters rather than the normalized $1\,\mathrm{m}^2$, then all the transport capacity results presented below should be scaled by $\sqrt{A}$.) By using the notation: $f(n) = \Theta[g(n)]$ when $f(n) = O[g(n)]$ as well as $g(n) = O[f(n)]$, we will show later in the section that the transport capacity of an *arbitrary network* under the *protocol model* is $C_{\mathrm{T}} = \Theta(W\sqrt{n})$ b-m/s if the nodes are optimally placed, the traffic pattern is optimally chosen, and if the range of each transmission is chosen optimally. An upper bound is $C_T = \sqrt{(8/\pi)}(W/\Delta)\sqrt{n}$ b-m/s for every arbitrary network for all spatial and temporal scheduling strategies, while $C_T = Wn/[(1+2\Delta)(\sqrt{n} + \sqrt{8\pi})]$ bit-meters per second (for n a multiple of four) can be achieved when the nodes and traffic patterns are appropriately chosen, and the ranges and schedules of transmissions are appropriately chosen.

If this transport capacity were to be equally divided between all the n nodes, then each node would obtain $\Theta(W/\sqrt{n})$ b-m/s. If, further, each source has its destination about the same distance of 1 m away, then each node would obtain a *throughput capacity* of $\Theta(W/\sqrt{n})$ b/s.

The upper bound on transport capacity does not depend on the transmissions being omni-directional, as implied by Equation (19.1), but only on the presence of some dispersion in the neighborhood of the receiver. It will be shown later in the section that, for the physical model, $cW\sqrt{n}$ b-m/s is feasible, while $c'Wn^{\alpha-1/\alpha}$ b-m/s is not, for appropriate c, c'. Specifically,

$$C_{\mathrm{T}} = Wn/\left\{\left(\sqrt{n} + \sqrt{8\pi}\right)\left\{16\beta\left[2^{\frac{\alpha}{2}} + 6^{\alpha-2}/(\alpha-2)\right]\right\}^{1/\alpha}\right\} \text{ b-m/s (for } n \text{ a multiple of 4)}$$

is feasible when the network is appropriately designed, while an upper bound is

$$C_{\mathrm{T}} = \left[(2\beta+2)/\beta\right]^{\frac{1}{\alpha}} Wn^{\frac{\alpha-1}{\alpha}}/\sqrt{\pi} \text{ b-m/s}$$

It is suspected that an upper bound of order $\Theta(W\sqrt{n})$ b-m/s may actually hold. In the special case where the ratio $P_{\max}/P_{\min}$ between the maximum and minimum powers that transmitters can employ is bounded above by β, then an upper bound is in fact

$$C_{\mathrm{T}} = (W\sqrt{8n/\pi})/\left[(\beta P_{\min}/P_{\max})^{\frac{1}{\alpha}} - 1\right] \text{ b-m/s}$$

Both bounds suggest that transport capacity improves when α is larger, i.e. when the signal power decays more rapidly with distance.

19.2.2 Random networks

In this case, n nodes are randomly located, i.e. independently and uniformly distributed, either on the surface S^2 of a three-dimensional sphere of area 1 m^2, or in a disk of area 1 m^2 in the plane. The purpose in studying S^2 is to separate edge effects from other phenomena. Each node has a randomly chosen destination to which it wishes to send $\lambda(n)$ b/s. The destination for each node is independently chosen as the node nearest to a randomly located point, i.e. uniformly and independently distributed. (Thus destinations are on the order of 1 m away on average.) All transmissions employ the same nominal range or power (homogeneous nodes). As for arbitrary networks, both a protocol model and a physical model are considered.

19.2.2.1 The protocol model

All nodes employ a common *range* r for all their transmissions. When node X_i transmits to a node X_j over the mth subchannel, this transmission is successfully received by X_j if $|X_i - X_j| \leq r$ and for every other node X_k simultaneously transmitting over the same subchannel $|X_k - X_j| \geq (1 + \Delta)r$.

19.2.2.2 The physical model

All nodes choose a common power level P for all their transmissions. Let $\{X_k; k \in T\}$ be the subset of nodes simultaneously transmitting at some time instant over a certain subchannel. A transmission from a node X_i, $i \in T$, is successfully received by a node X_j if $S/I \geq \beta$, where

$$S = P/\Big|X_i - X_j|^{\alpha}$$

and

$$I = N + \sum_{\substack{k \in T \\ k \neq i}} P/\Big|X_i - X_j|^{\alpha}$$

19.2.2.3 The throughput capacity of random networks

The throughput is defined in the usual manner as the time average of the number of bits per second that can be transmitted by every node to its destination.

19.2.2.4 Feasible throughput

A throughput of $\lambda(n)$ b/s for each node is *feasible* if there is a spatial and temporal scheme for scheduling transmissions, such that by operating the network in a multihop fashion and buffering at intermediate nodes when awaiting transmission, every node can send $\lambda(n)$ b/s on average to its chosen destination node. That is, there is a $T < \infty$ such that in every time interval $[(i-1)T, iT]$ every node can send $T\lambda(n)$ b to its corresponding destination node.

19.2.2.5 The throughput capacity of random wireless networks

We say that the *throughput capacity* of the class of random networks is of order $\Theta[f(n)]$ b/s if there are deterministic constants $c > 0$ and $c' < +\infty$ such that

$$\lim_{n \to \infty} \text{Prob}\,[\lambda(n) = cf(n) \text{ is feasible}] = 1$$

$$\liminf_{n \to \infty} \text{Prob}\,[\lambda(n) = c'f(n) \text{ is feasible}] < 1$$

It will be shown in the next section that, in the case of both the surface of the sphere and a planar disk, the order of the throughput capacity is $\lambda(n) = \Theta[W/\sqrt{(n \log n)}]$ b/s for the protocol model. For the upper bound for some c',

$$\lim_{n\to\infty} \text{Prob}\left[\lambda(n) = c'W/\sqrt{n \log n} \text{ is feasible 1e}\right] = 0$$

Specifically, there are deterministic constants c'' and c''' not depending on n, Δ or W, such that $\lambda(n) = c''W/\left[(1+\Delta)^2\sqrt{(n \log n)}\right]$ b/s is feasible, and $\lambda(n) = c'''W/\left[\Delta^2\sqrt{(n \log n)}\right]$ b/s is infeasible, both with probability approaching 1 as $n \to \infty$.

It will be also shown that, for the physical model, a throughput of $\lambda(n) = cW/\sqrt{(n \log n)}$ b/s is feasible, while $\lambda(n) = c'W/\sqrt{n}$ bits per second is not, for appropriate c, c', both with probability approaching 1 as $n \to \infty$. Specifically, there are deterministic constants c'' and c''' not depending on n, N, α, β or W, such that

$$\lambda(n) = c''W/\left[\sqrt{n \log n}\left(2\left\{c'''\beta\left[3 + 1/(\alpha-1) + 2/(\alpha-2)\right]\right\}^{\frac{1}{\alpha}} - 1\right)^2\right] \text{ b/s}$$

is feasible with probability approaching one as $n \to \infty$. If $\bar{L}$ is the mean distance between two points independently and uniformly distributed in the domain (either surface of sphere or planar disk of unit area), then there is a deterministic sequence $\varepsilon(n) \to 0$, not depending on N, α, β or W, such that $\left(\sqrt{8/\pi n}\right) W[1+\varepsilon(n)] / \left[\bar{L}(\beta^{\frac{1}{\alpha}} - 1)\right]$ b-m/s is infeasible with probability approaching 1 as $n \to \infty$.

19.2.3 Arbitrary networks: an upper bound on transport capacity

The following assumptions for the setting on a planar disk of unit area are used [32, 33]:

(a1) There are n nodes arbitrarily located in a disk of unit area on the plane.

(a2) The network transports λnT b over T s.

(a3) The average distance between the source and destination of a bit is $\bar{L}$. Together with (a2), this implies that a transport capacity of $\lambda n\bar{L}$ b-m/s is achieved.

(a4) Each node can transmit over any subset of M subchannels with capacities W_m b/s, $1 \le m \le M$, where $\sum_{m=1}^{M} W_m = W$.

(a5) Transmissions are slotted into synchronized slots of length τ s. (This assumption can be eliminated, but makes the exposition easier.)

(a6) Definitions of physical model and protocol model from the previous section are used.

While retaining the restriction for the case of the physical model, we can either retain the restriction in the protocol model or consider an alternate restriction as follows: if a node X_i transmits to another node X_j located at a distance of r units on a certain subchannel in a certain slot, then there can be no other receiver within a radius of Δr around X_j on the same subchannel in the same slot. This alternative restriction addresses situations where the transmissions are not omnidirectional, but there is still some dispersion in the neighborhood of the receiver. Under the above assumptions the following results for the transport capacity have been obtained [32, 33]:

(r1) In the *protocol model*, the transport capacity $\lambda n\bar{L}$ is bounded as: $\lambda n\bar{L} \le W\sqrt{8n/\pi}$ Δ b-m/s.

(r2) In the *physical model*, $\lambda n\bar{L} \le Wn^{\alpha-1/\alpha}\left[(2\beta+2)/\beta\right]^{1/\alpha}/\sqrt{\pi}$ b-m/s.

(r3) If the ratio $P_{\max}/P_{\min}$ between the maximum and minimum powers that transmitters can employ is strictly bounded above by β, then $\lambda n\bar{L} \le W\sqrt{(8n/\pi)}\left[(\beta P_{\min}/P_{\max})^{1/\alpha} - 1\right]^{-1}$ b-m/s.

(r4) When the domain is of A square meters rather than 1 m^2, then all the upper bounds above are scaled by $\sqrt{A}$.

To prove the above results, consider bit b, where $1 \le b \le \lambda nT$. Let us suppose that it moves from its origin to its destination in a sequence of $h(b)$ hops, where the hth hop traverses a distance of r_b^h. Then from (a3) we have

$$\sum_{b=1}^{\lambda nT}\sum_{h=1}^{h(b)} r_b^b \ge \lambda nT\bar{L} \tag{19.39}$$

Having in mind that in any slot at most $n/2$ nodes can transmit for any subchannel m and any slot s we have

$$\sum_{b=1}^{\lambda nT}\sum_{h=1}^{h(b)} 1 \text{ (the } h\text{th hop of bit } b \text{ is over subchannel } m \text{ in slot } s\text{)} \le \frac{W_m\tau n}{2}$$

Summing over the subchannels and the slots, and noting that there can be no more than T/τ slots in T s yields

$$H\colon = \sum_{b=1}^{\lambda nT} h(b) \le \frac{WTn}{2} \tag{19.40}$$

From the triangle inequality and (a6), for the *protocol model*, where X_j is receiving a transmission from X_i over the mth subchannel and at the same time X_ℓ is receiving a transmission from X_k over the same subchannel, we have

$$|X_j - X_\ell| \ge |X_j - X_k| - |X_\ell - X_k| \ge (1+\Delta)|X_i - X_j| - |X_\ell - X_k|$$

Similarly,

$$|X_\ell - X_j| \ge (1+\Delta)|X_k - X_\ell| - |X_j - X_i|$$

Adding the two inequalities, we obtain

$$|X_\ell - X_j| \ge \frac{\Delta}{2}(|X_k - X_\ell| + |X_i - X_j|)$$

This means that disks of radius $\Delta/2$ times the lengths of hops centered at the receivers over the same subchannel in the same slot are essentially disjoint. This conclusion also directly follows from the alternative restriction in (a6). Allowing for edge effects where a node is near the periphery of the domain, and noting that a range greater than the diameter of the domain is unnecessary, we see that at least a quarter of such a disk is within the domain. Having in mind that at most $W_m\tau$ bits can be carried in slot from a receiver to a transmitter over the mth subchannel, we have

$$\sum_{b=1}^{\lambda nT}\sum_{h=1}^{h(b)} 1 \text{ (the } h\text{th hop of bit } b \text{ is over subchannel } m \text{ in slot s)} \times \left(\frac{1}{4}\right)\pi\left(\frac{\Delta}{2}\right)^2 (r_b^h)^2 \le W_m\tau \tag{19.41}$$

Summing over the subchannels and the slots gives

$$\sum_{b=1}^{\lambda nT}\sum_{h=1}^{h(b)} \frac{\pi\Delta^2}{16}(r_b^h)^2 \le WT$$

or equivalently

$$\sum_{b=1}^{\lambda nT}\sum_{h=1}^{h(b)}\frac{1}{H}(r_b^h)^2 \le \frac{16WT}{\pi\Delta^2 H} \tag{19.42}$$

Since the quadratic function is convex we have

$$\left(\sum_{b=1}^{\lambda nT}\sum_{h=1}^{h(b)}\frac{1}{H}r_b^h\right)^2 \le \sum_{b=1}^{\lambda nT}\sum_{h=1}^{h(b)}\frac{1}{H}\left(r_b^h\right)^2 \tag{19.43}$$

Finally combining Equations (19.42) and (19.43) yields

$$\sum_{b=1}^{\lambda nT}\sum_{b=1}^{h(b)} r_b^h \le \sqrt{\frac{16WTH}{\pi\Delta^2}} \tag{19.44}$$

and substituting Equation (19.44) in Equation (19.39) gives

$$\lambda nT\bar{L} \le \sqrt{\frac{16WTH}{\pi\Delta^2}} \tag{19.45}$$

Substituting Equation (19.41) in Equation (19.45) yields the result ($r1$).

For the *physical model* suppose X_i is transmitting to $X_{j(i)}$ over the mth subchannel at power level P_i at some time, and let $\Im$ denote the set of all simultaneous transmitters over the mth subchannel at that time. The initial constraint introduced by (a6) can be represented as

$$\frac{S}{I} = \frac{\frac{P_i}{|X_i - X_j|^\alpha}}{N + \sum\limits_{\substack{k\in\Im\\ k\ne i}}\frac{P_k}{|X_k - X_j|^\alpha}} \ge \beta \tag{19.46}$$

By also including the signal power of X_i in the denominator, the signal-to-interference requirement for $X_{j(i)}$ can be written as

$$\frac{S}{I} = \frac{\frac{P_i}{|X_i - X_{j(i)}|^\alpha}}{N + \sum\limits_{k\in\Im}\frac{P_k}{|X_k - X_{j(i)}|^\alpha}} \ge \frac{\beta}{\beta+1}$$

which results in

$$|X_i - X_{j(i)}|^\alpha \le \frac{\beta+1}{\beta}\frac{P_i}{N + \sum\limits_{k\in\Im}\frac{P_k}{|X_k - X_{j(i)}|^\alpha}} \le \frac{\beta+1}{\beta}\frac{P_i}{N + (\frac{\pi}{4})^{\alpha/2}\sum\limits_{k\in\Im}P_k}$$

(since $|X_k - X_{j(i)}| \le 2/\sqrt{\pi}$).
Summing over all transmitter–receiver pairs,

$$\sum_{i\in\Im}|X_i - X_{j(i)}|^\alpha \le \frac{\beta+1}{\beta}\frac{\sum\limits_{i\in\Im}P_i}{N + (\frac{\pi}{4})^{\alpha/2}\sum\limits_{i\in\Im}P_k} \le 2^\alpha\pi^{-(\alpha/2)}\frac{\beta+1}{\beta}$$

Summing over all slots and subchannels gives

$$\sum_{b=1}^{\lambda nT}\sum_{h=1}^{h(b)} r^\alpha(h,b) \le 2^\alpha \;\; \pi^{-\frac{\alpha}{2}}\frac{\beta+1}{\beta}WT$$

The rest of the proof proceeds along lines similar to the *protocol model*, invoking the convexity of r^α instead of r^2. For the consideration of the special case where $P_{\max}/P_{\min} < \beta$, we start with Equation (19.46). From it, it follows that if X_i is transmitting to X_j at the same time that X_k is transmitting to X_ℓ, both over the same subchannel, then

$$\frac{\dfrac{P_i}{|X_i - X_j|^\alpha}}{\dfrac{P_k}{|X_k - X_j|^\alpha}} \geq \beta$$

Thus

$$|X_k - X_j| \geq (\beta P_{\min}/P_{\max})^{\frac{1}{\alpha}} |X_i - X_j| = (1 + \Delta)|X_i - X_j|$$

where $\Delta := (\beta P_{\min}/P_{\max})^{\frac{1}{\alpha}} - 1$. Thus the same upper bound as for the *protocol model* carries over with Δ defined as above.

19.2.4 Arbitrary networks: lower bound on transport capacity

There is a placement of nodes and an assignment of traffic patterns such that the network can achieve

$$Wn/\left\{(1 + 2\Delta)\left(\sqrt{n} + \sqrt{8\pi}\right)\right\} \text{ b-m/s}$$

under the *protocol model*,

$$Wn/\left\{\left(\sqrt{n} + \sqrt{8\pi}\right)\left[16\beta\left(2^{\frac{\alpha}{2}} + \frac{6^{\alpha-2}}{\alpha - 2}\right)\right]^{-1/\alpha}\right\} \text{ b-m/s}$$

under the *physical model*, both whenever n is a multiple of 4. To prove it, consider the *protocol model* and define

$$r := 1/\left\{(1 + 2\Delta)\left(\sqrt{n/4} + \sqrt{2\pi}\right)\right\}$$

Recall that the domain is a disk of unit area, i.e. of radius $1/\sqrt{\pi}$ in the plane. With the center of the disk located at the origin, place transmitters at locations $[j(1 + 2\Delta)r \pm \Delta r, k(1 + 2\Delta)r]$ and $[j(1 + 2\Delta)r, k(1 + 2\Delta)r \pm \Delta r]$ where $|j + k|$ is even. Also place receivers at $[j(1 + 2\Delta)r \pm \Delta r, k(1 + 2\Delta)r]$ and $[j(1 + 2\Delta)r, k(1 + 2\Delta)r \pm \Delta r]$ where $|j + k|$ is odd. Each transmitter can transmit to its nearest receiver, which is at a distance r away, without interference from any other transmitter–receiver pair. It can be verified that there are at least $n/2$ transmitter–receiver pairs, all located within the domain. This is based on the fact that for a tessellation of the plane by squares of side s, all squares intersecting a disk of radius $R - \sqrt{2}s$ are entirely contained within a larger concentric disk of radius R. The number of such squares is greater than $\pi(R - \sqrt{2}s)^2/s^2$. This proves the above statement for $s = (1 + 2\Delta)r$ and $R = 1/\sqrt{\pi}$. Restricting attention to just these pairs, there are a total of $n/2$ simultaneous transmissions, each of range r, and each at W b/s. This achieves the transport capacity indicated.

For the physical model, a calculation of the SIR shows that it is lower-bounded at all receivers by

$$(1 + 2\Delta)^\alpha \left[16\left(2^{\frac{\alpha}{2}} + \frac{6^{\alpha-2}}{\alpha - 2}\right)\right]^{-1}$$

Choosing Δ to make this lower bound equal to β yields the result.

In the *protocol model*, there is a placement of nodes and an assignment of traffic patterns such that the network can achieve

$2W/\sqrt{\pi}$ *b-m/s for* $n \geq 2$
$4W\left[\sqrt{\pi}(1+\Delta)\right]^{-1}$ *b-m/s, for* $n \geq 8$
$Wn\left[(1+2\Delta)\left(\sqrt{n}+\sqrt{8\pi}\right)\right]^{-1}$ *b-m/s, for* $n = 2, 3, 4, \cdots, 19, 20, 21$ *and*
$4\lfloor n/4 \rfloor W\left\{(1+2\Delta)\left(\sqrt{4\lfloor n/4 \rfloor}+\sqrt{8\pi}\right)\right\}^{-1}$ *b-m/s, for all n*

With at least two nodes, clearly $2W/\sqrt{\pi}$ b-m/s can be achieved by placing two nodes at diametrically opposite locations. This verifies the formula for the bound for $n \leq 8$. With at least eight nodes, four transmitters can be placed at the opposite ends of perpendicular diameters, and each can transmit toward its receiver located at a distance $1/\left[\sqrt{\pi}(2+2\Delta)\right]$ towards the center of the domain. This yields $4W/\left[\sqrt{\pi}(1+\Delta)\right]$ b-m/s, verifying the formula up to $n = 21$.

19.2.5 Random networks: lower bound on throughput capacity

In this section we show that one can spatially and temporally schedule transmissions in a random graph so that, when each randomly located node has a randomly chosen destination, each source–destination pair can indeed be guaranteed a 'virtual channel' of capacity $cW\left[(1+\Delta)^2\sqrt{n\log n}\right]^{-1}$ b/s with probability approaching 1 as $n \to \infty$, for an appropriate constant $c > 0$. We will show how to route traffic efficiently through the random graph so that no node is overloaded.

19.2.5.1 Spatial tessellation

In the following a Voronoi tessellation of the surface S^2 of the sphere is used. For a set of p points $\{a_1, a_2, \cdots, a_p\}$ on S^2 the Voronoi cell $V(a_i)$ is the set of all points which are closer to a_i than to any of the other a_js, i.e. [34],

$$V(a_i) := \{x \in S^2 : |x - a_i| = \min_{1 \leq j \leq p} |x - a_j|\}$$

Above and throughout, distances are measured on the surface S^2 of the sphere by segments of great circles connecting two points. The point a_i is called the generator of the Voronoi cell $V(a_i)$. The surface of the sphere does not allow any regular tessellation where all cells look the same. For our application Voronoi tessellations will also need to be not too eccentrically shaped. Therefore, the properties of Voronoi tessellations needed in this section can be summarized as:

(v1) For every $\varepsilon > 0$, there is a Voronoi tessellation of S^2 with the property that every Voronoi cell contains a disk of radius ε and is contained in a disk of radius 2ε (see illustration in Figure 19.7).

To prove this we denote by $D(x, \varepsilon)$ a disk of radius ε centered at x. Choose a_1 as any point in S^2. Suppose that $a_1, \cdots, a_p$ have already been chosen such that the distance between any two a_js is at least 2ε. There are two cases to consider. Suppose there is a point x such that $D(x, \varepsilon)$ does not intersect any $D(a_i, \varepsilon)$. Then x can be added to the collection: Define $a_{p+1} := x$. Otherwise, we stop. This procedure has to terminate in a finite number of steps since the addition of each a_i removes the area of a disk of radius $\varepsilon > 0$ from S^2. When we stop we will have a set of generators such that they are at least 2ε units apart, and such that all other points on S^2 are within a distance

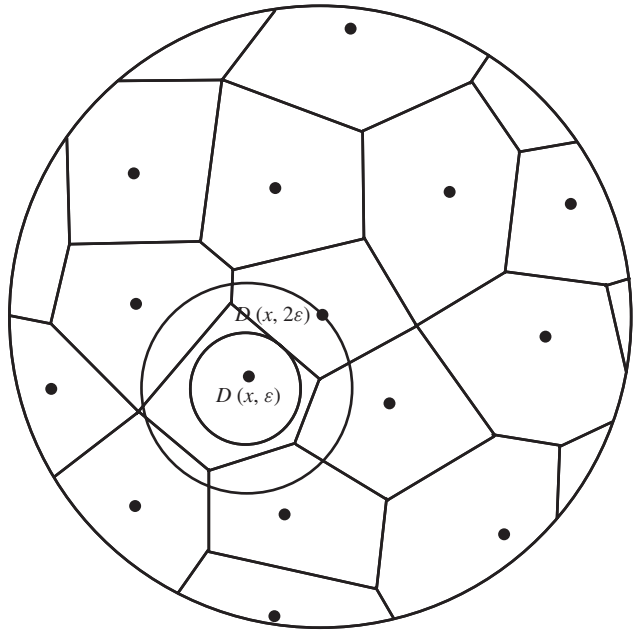

Figure 19.7 A tessellation of the surface S^2 of the sphere.

of 2ε from one of the generators. The Voronoi tessellation obtained in this way has the desired properties.

In the sequel we will use a Voronoi tessellation V_n for which

(v2) Every Voronoi cell contains a disk of area $100 \log n/n$.

Let $\rho(n) :=$ radius of a disk of area $(100 \log n)/n$ on S^2.

(v3) Every Voronoi cell is contained in a disk of radius $2\rho(n)$.

We will refer to each Voronoi cell $V \in V_n$ as simply a 'cell'.

19.2.5.2 Adjacency and interference

By definition, two cells are *adjacent*, if they share a common point. If we choose the range $r(n)$ of each transmission so that $r(n) = 8\rho(n)$, this range will allow direct communication within a cell and between adjacent cells.

(v4) Every node in a cell is within a distance $r(n)$ from every node in its own cell or adjacent cell.

To prove it let we notice that the diameter of cells is bounded by $4\rho(n)$, see (v3). The range of a transmission is $8\rho(n)$. Thus the area covered by the transmission of a node includes adjacent cells.

19.2.5.3 Interfering neighbors

By definition we say that two cells are *interfering neighbors* if there is a point in one cell which is within a distance $(2 + \Delta)r(n)$ of some point in the other cell. In other words if two cells are not

interfering neighbors, then in the protocol model a transmission from one cell cannot collide with a transmission from the other cell.

19.2.5.4 Bound on the number of interfering neighbors of a cell

An important property of the constructed Voronoi tessellation V_n is that the number of interfering neighbors of a cell is uniformly bounded. This will be exploited in the next section in constructing a spatial transmission schedule which allows for a high degree of spatial concurrency and thus frequency reuse.

(v5) Every cell in V_n has no more than c_1 interfering neighbors were c_1 depends only on Δ and grows no faster than linearly in $(1+\Delta)^2$.

To prove it, Let V be a Voronoi cell. If V' is an interfering neighboring Voronoi cell, there must be two points, one in V and the other in V', which are no more than $(2+\Delta)r(n)$ units apart. From (v3), the diameter of a cell is bounded by $4\rho(n)$. Hence V', and similarly every other interfering neighbor in the protocol model, must be contained within a common large disk D of radius $6\rho(n)+(2+\Delta)r(n)$. Such a disk D cannot contain more than $c_2\{[6\rho(n)+(2+\Delta^2)r(n)]^2/\rho^2(n)\}$ disks of radius $\rho(n)$. From (v2), there can therefore be no more than this number of cells within D. This then is an upper bound on the number of interfering neighbors of the cell V. The result follows from the chosen magnitudes of $\rho(n)$ and $r(n)$.

19.2.5.5 A bound on the length of an all-cell inclusive transmission schedule

The bounded number of interfering neighbors for each cell allows the construction of a schedule of bounded length which allows one opportunity for each cell in the tessellation V_n to transmit.

(v6) In the Protocol Model there is a schedule for transmitting packets such that in every $(1+c_1)$ slots, each cell in the tessellation V_n gets one slot in which to transmit, and such that all transmissions are successfully received within a distance $r(n)$ from their transmitters.

(v7) There is a deterministic constant c not depending on n, N, α, β, or W such that if Δ is chosen to satisfy

$$(1+\Delta)^2 > \left(2\left\{c\beta\left[3+(\alpha-1)^{-1}+2(\alpha-2)^{-1}\right]\right\}^{\frac{1}{\alpha}}-1\right)^2$$

then for a large enough common power level P, the above result (v6) holds even for the physical model.

To prove it we show first the result for the protocol model. This follows from a well-known fact about vertex coloring of graphs of bounded degree. A graph of degree no more than c_1 can have its vertices colored by using no more than $(1+c_1)$ colors, with no two neighboring vertices having the same color [35]. One can therefore color the cells with no more than $(1+c_1)$ colors such that no two interfering neighbors have the same color. This gives a schedule of length at most $(1+c_1)$, where one can transmit one packet from each cell of the same color in a slot.

For the physical model one can show that, under the same schedule as above, the required SIR of β is obtained if each transmitter chooses an identical power level P that is high enough, and Δ is large enough. From the previous discussion we know that any two nodes transmitting simultaneously are separated by a distance of at least $(2+\Delta)r(n)$ and disks of radius $(1+\Delta/2)r(n)$ around each transmitter are disjoint. The area of each such disk is at least $c_3\pi(1+\Delta/2)^2r^2(n)$. (In the case of disks on the plane $c_3=1$, but it is smaller for disks on the surface of the sphere.)

Consider a node X_i transmitting to a node X_j at a distance less than $r(n)$. The signal power received at X_j is at least $Pr^{-\alpha}(n)$. Now we look at the interference power due to all the other simultaneous transmissions. Consider the annulus of all points lying within a distance between a and b from X_j. A transmitter within this annulus has the disk centered at itself and of radius $(1+\Delta/2)r(n)$ entirely contained within a larger annulus of all points lying between a distance $a-(1+\Delta/2)r(n)$ and $b+(1+\Delta/2)r(n)$. The area of this larger annulus is no more than

$$c_4\pi\left\{\left[b+(1+\Delta/2)\,r(n)\right]^2-\left[a-(1+\Delta/2)\,r(n)\right]^2\right\}$$

Each transmitter above 'consumes' an area of at least $c_3\pi\,(1+\Delta/2)^2\,r^2(n)$, as noted earlier. Hence the annulus of points at a distance between a and b from the receiver X_j cannot contain more than

$$c_4\pi\left\{\left[b+\left(1+\frac{\Delta}{2}\right)r(n)\right]^2-\left[a-\left(1+\frac{\Delta}{2}\right)r(n)\right]^2\right\}\left[c_3\pi\left(1+\frac{\Delta}{2}\right)^2 r^2(n)\right]^{-1}$$

transmitters. Also, the received power at X_j from each such transmission is at most P/a^α. Noting that there can be no other simultaneous transmitter within a distance $(1+\Delta)r(n)$ of X_j, and taking $a=k(1+\Delta/2)r(n)$ and $b=(k+1)(1+\frac{\Delta}{2})r(n)$ for $k=1\ ,\ 2\ ,\ 3,\ \cdots$, we see that the SIR at X_j is lower-bounded by

$$\begin{aligned}&\mathrm{Pr}^{-\alpha}(n)\left\{N+\sum_{k=1}^{+\infty}c_4P\left[(k+2)^2-(k-1)^2\right]\left[c_3k^\alpha\left(1+\frac{\Delta}{2}\right)^\alpha r^\alpha(n)\right]^{-1}\right\}^{-1}\\&\quad=\frac{P}{N}\left\{r^\alpha(n)+\frac{c_4}{c_3(1+\Delta/2)^\alpha}\frac{P}{N}\sum_{k=1}^{+\infty}\frac{6k+3}{k^\alpha}\right\}^{-1}\end{aligned}$$

Since $\alpha>2$, the sum in the denominator converges, and is smaller than $9+3\,(\alpha-1)^{-1}+6\,(\alpha-2)^{-1}$. When Δ is as specified and $P\to\infty$, the lower bound on the SIR converges to a value greater than β. Using similar arguments one can show that [32]

(v8) Each cell contains at least one node.

(v9) The mean number of routes served by each cell $\leq c_{10}\sqrt{(n\log n)}$.

(v10) The actual traffic served by each cell $\leq c_5\lambda(n)\sqrt{(n\log n\ \mathrm{whp})}$.

19.2.5.6 Lower bound on throughput capacity of random networks

From (v6) we know that there exists a schedule for transmitting packets such that in every $(1+c_1)$ slots, each cell in the tessellation V_n gets one slot to transmit, and such that each transmission is received within a range $r(n)$ of the transmitter. Thus the rate at which each cell gets to transmit is $W/(1+c_1)$ b/s. On the other hand, the rate at which each cell *needs* to transmit is with high probability (*whp*) less than $c_5\lambda(n)\sqrt{n\log n}$ [see (v10)]. With high probability, this rate can be accommodated by all cells if it is less than the rate available, i.e. if $c_5\lambda(n)\sqrt{(n\log n)}\leq W\,(1+c_1)^{-1}$. Moreover, within a cell, the traffic to be handled by the entire cell can be handled by any one node in the cell, since each node can transmit at rate W b/s whenever necessary. In fact, one can even designate one node in each cell as a 'relay' node. This node can handle all the traffic needing to be relayed. The other nodes can simply serve as sources or sinks.

We have proved the following theorem, noting the linear growth of c_1 in $(1+\Delta)^2$ in (v5), and the choice of Δ in (v6) for the physical model.

(v11) For random networks on S^2 in the protocol model, there is a deterministic constant $c > 0$ not depending on n, Δ, or W, such that $\lambda(n) = cW\left\{(1+\Delta)^2\sqrt{(n\log n)}\right\}^{-1}$ b/s is feasible whp.

(v12) For random networks on S^2 in the physical model, there are deterministic constants c' and c'' not depending on n, N, α, β, or W, such that

$$\lambda(n) = c'W\left\{\left(2\left\{c''\beta\left[3+(\alpha-1)^{-1}+2(\alpha-2)^{-1}\right]\right\}^{\frac{1}{\alpha}}-1\right)^2\sqrt{n\log n}\right\}\ \text{b/s}$$

is feasible whp. These throughput levels have been attained without subdividing the wireless channel into subchannels of smaller capacity.

19.3 INFORMATION THEORY AND NETWORK ARCHITECTURES

19.3.1 Network architecture

For the optimization of *ad hoc* and sensor networks we will discuss some performance measure for the architectures shown in Figures 19.8–19.11. We will mainly focus on transport capacity $C_{\mathrm{T}} := \sup\sum_{l=1}^{m} R_l\rho_l$, where the supremum is taken over m, and vectors $(R_1, R_2, \ldots, R_m)$ of feasible rates for m source-destination pairs, and ρ_l is the distance between the lth source and its destination. For the planar network from Figure 19.8 we assume [33]:

(1) There is a finite set N of n nodes located on a plane.

(2) There is a minimum positive separation distance $\rho_{\min}$ between nodes, i.e. $\rho_{\min} := \min_{i\neq j}\rho_{ij} > 0$, where ρ_{ij} is the distance between nodes $i, j \in N$.

(3) Every node has a receiver and a transmitter. At time instants $t = 1, 2, \ldots$, node $i \in N$ sends $X_i(t)$, and receives $Y_i(t)$ with

$$Y_i(t) = \sum_{j\neq i}\frac{\mathrm{e}^{\gamma\rho_{ij}}X_j(t)}{\rho_{ij}^{\delta}} + Z_i(t)$$

where $Z_i(t), i \in N, t = 1, 2, \ldots$ are Gaussian independent and identically distributed (i.i.d.) random variables with mean zero and variance σ^2. The constant $\delta > 0$ is referred to as the path loss exponent, while $\gamma \geq 0$ will be called the absorption constant. A positive γ generally prevails except for transmission in a vacuum, and corresponds to a loss of $20\gamma\log_{10}\mathrm{e}$ decibel per meter.

(4) Denote by $P_i \geq 0$ the power used by node i. Two separate constraints on $\{P_1, P_2, \ldots, P_n\}$ are studied: total power constraint $P_{\text{total}} : \sum_{i=1}^{n} P_i \leq P_{\text{total}}$ or individual power constraint $P_{\text{ind}} : P_i \leq P_{\text{ind}}$, for $i = 1, 2, \ldots, n$.

(5) The network can have several source–destination pairs (s_ℓ, d_ℓ), $\ell = 1, \ldots, m$, where s_ℓ, d_ℓ are nodes in N with $s_\ell \neq d_\ell$, and $(s_\ell, d_\ell) \neq (s_j, d_j)$ for $\ell \neq j$. If $m = 1$, then there is only a single source–destination pair, which we will simply denote (s, d).

A special case is a regular planar network where the n nodes are located at the points (i, j) for $1 \leq i, j \leq \sqrt{n}$; see Figure 19.9. This setting will be used mainly to exhibit achievability of some capacities, i.e. inner bounds. Another special case is a *linear network* where the n nodes are located on a straight line, again with minimum separation distance $\rho_{\min}$; see Figure 19.10. The main reason for considering linear networks is that the proofs are easier to state and comprehend than in the planar case, and can be generalized to the planar case. Also, the linear case may have some utility for, say, networks of cars on a highway, since its scaling laws are different.

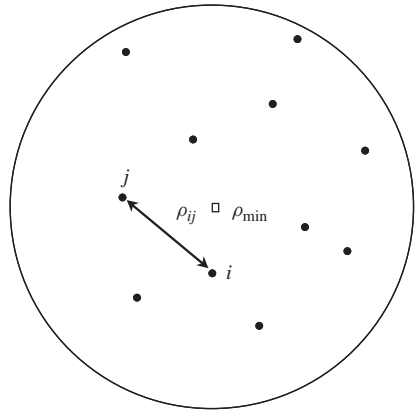

Figure 19.8 A planar network: n nodes located on a two-dimensional plane, with minimum separation distance $\rho_{\min}$.

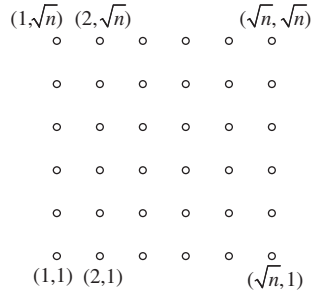

Figure 19.9 A regular planar network: n nodes located on a plane at (i, j) with $1 \leq i, j \leq \sqrt{n}$. (Reproduced by permission of IEEE [33].)

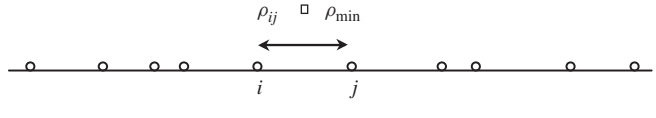

Figure 19.10 A linear network: n nodes located on a line, with minimum separation distance $\rho_{\min}$. (Reproduced by permission of IEEE [33].)

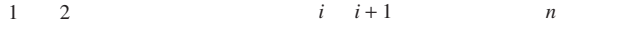

Figure 19.11 A regular linear network: n nodes located on a line at $1, 2, \ldots, n$. (Reproduced by permission of IEEE [33].)

A special case of a linear network is a regular linear network where the n nodes are located at the positions $1, 2, \ldots, n$; see Figure 19.11. This setting will also be used mainly to exhibit achievability results.

19.3.2 Definition of feasible rate vectors

Definition 1
Consider a wireless network with multiple source–destination pairs (s_ℓ, d_ℓ), $\ell = 1, \ldots, m$, with $s_\ell \neq d_\ell$, and $(s_\ell, d_\ell) \neq (s_j, d_j)$ for $\ell \neq j$. Let $S := \{s_\ell, \ell = 1, \ldots, m\}$ denote the set of source nodes. The number of nodes in S may be less than m, since we allow a node to have originating traffic for several destinations. Then a $[(2^{TR_1}, \ldots, 2^{TR_m}), T, P_e^{(T)}]$ code with total power constraint P_{total} consists of the following:

(1) m independent random variables W_ℓ (transmitted words TR_l bits long) with $P(W_l = k_l) = 1/2^{TR_l}$, for any $k_\ell \in \{1, 2, \ldots, 2^{TR_\ell}\}$, $\ell = 1, \ldots, m$. For any $i \in S$, let $\bar{W}_i := \{W_\ell : s_\ell = i\}$ and $\bar{R}_i := \sum_{\{\ell : s_\ell = i\}} R_\ell$

(2) Functions $f_{i,t} : \mathbb{R}^{t-1} \times \{1, 2, \ldots, 2^{T\bar{R}_i}\} \to \mathbb{R}, \quad t = 1, 2, \ldots, T$, for the source nodes $i \in S$ and $f_{j,t} : \mathbb{R}^{t-1} \to \mathbb{R}, t = 2, \ldots, T$, for all the other nodes $j \notin S$, such that

$$X_i(t) = f_{i,t}(Y_i(1), \ldots, Y_i(t-1), \bar{W}_i), \quad t = 1, 2, \ldots, T$$
$$X_j(1) = 0, \qquad X_j(t) = f_{j,t}(Y_j(1), \ldots, Y_j(t-1)), \quad t = 2, 3, \ldots, T$$

such that the following total power constraint holds:

$$\frac{1}{T} \sum_{t=1}^{T} \sum_{i \in N} X_i^2(t) \leq P_{\text{total}} \tag{19.47}$$

(3) m decoding functions

$$g_\ell : \mathbb{R}^T \times \{1, 2, \ldots, |\bar{W}_{d_\ell}|\} \to \{1, 2, \ldots, 2^{TR_\ell}\}$$

for the destination nodes of the m source-destination pairs $\{(s_\ell, d_\ell), \ell = 1, \ldots, m\}$, where $|\bar{W}_{d_\ell}|$ is the number of different values $\bar{W}_{d_\ell}$ can take. Note that W_{d_ℓ} may be empty.

(4) The average probability of error:

$$P_e^{(T)} := \text{Prob}\left[(\hat{W}_1, \hat{W}_2, \ldots, \hat{W}_m) \neq (W_1, W_2, \ldots, W_m)\right] \tag{19.48}$$

where $\hat{W}_\ell := g_\ell(Y_{d_\ell}^T, \bar{W}_{d_\ell})$, with $Y_{d_\ell}^T := \left[Y_{d_\ell}(1), Y_{d_\ell}(2), \ldots, Y_{d_\ell}(T)\right]$.

Definition 2
A rate vector $(R_1, \ldots, R_m)$ is said to be *feasible* for the m source-destination pairs (s_ℓ, d_ℓ), $\ell = 1, \ldots, m$, with total power constraint P_{total}, if there exists a sequence of $[(2^{TR_1}, \ldots, 2^{TR_m}), T, P_e^{(T)}]$ codes satisfying the total power constraint P_{total}, such that $P_e^{(T)} \to 0$ as $T \to \infty$.

The preceding definitions are presented with total power constraint P_{total}. If an individual power constraint P_{ind} is placed on each node, then Equation (19.47) should be modified:

$$\frac{1}{T} \sum_{t=1}^{T} X_i^2(t) \leq P_{\text{ind}}, \quad \text{for } i \in N \tag{19.49}$$

and correspondingly modify the rest of the definitions to define the set of feasible rate vectors under an individual power constraint.

19.3.3 The transport capacity

The capacity *region*, is the closure of the set of all such feasible vector rates. As in Section 19.2 we will, focus mainly on the distance-weighted sum of rates.

Definition 3
As in Section 19.2, the network's *transport capacity* C_{T} is

$$C_{\mathrm{T}} := \sup_{(R_1,\ldots,R_m)\ \text{feasible}} \sum_{\ell=1}^{m} R_\ell \cdot \rho_\ell$$

where $\rho_\ell := \rho_{s_\ell d_\ell}$ is the distance between s_ℓ and d_ℓ, and $R_\ell := R_{s_\ell d_\ell}$. In the following, due to limited space, a number of results from information theory will be presented without the formal proof. For more details the reader is referred to Xie and Kumar [33].

19.3.4 Upper bounds under high attenuation

(r1) The transport capacity is bounded by the network's total transmission power in media with $\gamma > 0$ or $\delta > 3$.

For a single link (s, d), the *rate* R is bounded by the *received* power at d. In wireless networks, owing to mutual interference, the transport capacity is upper-bounded by the total transmitted power P_{total} used by the entire network.

In any planar network, with either positive absorption, i.e. $\gamma > 0$, or with path loss exponent $\delta > 3$

$$C_{\mathrm{T}} \le \frac{c_1(\gamma, \delta, \rho_{\min})}{\sigma^2} \cdot P_{\mathrm{total}} \tag{19.50}$$

where

$$c_1(\gamma, \delta, \rho_{\min}) := \begin{cases} \dfrac{2^{2\delta+7} \log \mathrm{e}\, \mathrm{e}^{-\gamma\rho_{\min}/2}(2 - \mathrm{e}^{-\gamma\rho_{\min}/2})}{\delta^2 {\rho_{\min}}^{2\delta+1} \quad (1 - \mathrm{e}^{-\gamma\rho_{\min}/2})}, & \text{if } \gamma > 0 \\ \dfrac{2^{2\delta+5}(3\delta - 8)\log \mathrm{e}}{(\delta - 2)^2(\delta - 3){\rho_{\min}}^{2\delta-1}}, & \text{if } \gamma = 0 \text{ and } \delta > 3 \end{cases} \tag{19.51}$$

(r2) The transport capacity follows an $O(n)$ scaling law under the individual power constraint, in media with $\gamma > 0$ or $\delta > 3$.

Consider any planar network under the individual power constraint P_{ind}. Suppose that either there is some absorption in the medium, i.e. $\gamma > 0$, or there is no absorption at all but the path loss exponent $\delta > 3$. Then its transport capacity is upper-bounded as follows:

$$C_{\mathrm{T}} \le \frac{c_1(\gamma, \delta, \rho_{\min}) P_{\mathrm{ind}}}{\sigma^2} \cdot n \tag{19.52}$$

where $c_1(\gamma, \delta, \rho_{\min})$ is given by Equation (19.51).

As in the previous section we use notation:

$$f = O(g) \text{ if } \limsup_{n\to+\infty} \left[f(n)/g(n) \right] < +\infty$$

$f = \Omega(g)$ if $g = O(f)$; $f = \Theta(g)$ if $f = O(g)$ as well as $g = O(f)$. Thus, all $O(\cdot)$ results are upper bounds, all $\Omega(\cdot)$ results are lower bounds, and all $\Theta(\cdot)$ results are sharp order estimates for the transport capacity. For n nodes located in an area of A square meters, it is shown in

Section 19.2 that the transport capacity is of order $O[\sqrt{(An)}]$ under a noninformation theoretic protocol model. If A itself grows like n, i.e. $A = \Theta(n)$, then the scaling law is $O[\sqrt{(An)}] = O(n)$, which coincides with the information-theoretic scaling law here. In fact, A must grow at least this rate since nodes are separated by a minimum distance $\rho_{\min} > 0$, i.e. $A = \Omega(n)$, and so the $O(n)$ result here is slightly stronger than the $O[\sqrt{(An)}]$ result in the previous section.

(r3) If either $\gamma > 0$ or $\delta > 2$ in any linear network, then

$$C_{\mathrm{T}} \leq \frac{c_2(\gamma, \delta, \rho_{\min})}{\sigma^2} \cdot P_{\text{total}} \tag{19.53}$$

where

$$c_2(\gamma, \delta, \rho_{\min}) := \begin{cases} \dfrac{2\mathrm{e}^{-\gamma\rho\,\min} \log \mathrm{e}}{(1-\mathrm{e}^{-\gamma\rho\,\min})^2(1-\mathrm{e}^{-2\gamma\rho\,\min})\rho_{\min}^{2\delta-1}}, & \text{if } \gamma > 0 \\ \dfrac{2\delta(\delta^2-\delta-1)\log \mathrm{e}}{(\delta-1)^2(\delta-2)\rho_{\min}^{2\delta-1}}, & \text{if } \gamma = 0 \text{ and } \delta > 2 \end{cases} \tag{19.54}$$

(r4) For any linear network, if either $\gamma > 0$ or $\delta > 2$, then the transport capacity is upper-bounded as follows:

$$C_{\mathrm{T}} \leq \frac{c_2(\gamma, \delta, \rho_{\min}) P_{\text{ind}}}{\sigma^2} \cdot n$$

where $c_2(\gamma, \delta, \rho_{\min})$ is as in Equation (19.44).

19.3.5 Multihop and feasible lower bounds under high attenuation

The $O(n)$ upper bound on transport capacity is tight for regular planar networks in media with $\gamma > 0$ or $\delta > 3$, and it is achieved by multihop. The 'multihop strategy' is defined as the following. Let Π_ℓ denote the set of all paths from source s_ℓ to destination d_ℓ, where by such a path π we mean a sequence $(s_\ell = j_0, j_1, \ldots, \ldots, j_z = d_\ell)$ with $j_q \neq j_r$ for $q \neq r$. The total traffic rate R_ℓ to be provided to the source destination pair (s_ℓ, d_ℓ) is split over the paths in Π_ℓ in such a way that if traffic rate $\lambda_\pi \geq 0$ is to be carried over path π, then $\sum_{\pi \in P_\ell} \lambda_\pi = R_\ell$. On each path π, packets are relayed from node to next node. On each such hop, each packet is fully decoded, treating all interference as noise. Thus, only point-to-point coding is used, and no network coding or multiuser estimation is employed. Such a strategy is of great interest and it is currently the object of much protocol development activity.

The following result implies that, when $\gamma > 0$ or $\delta > 3$, the sharp order of the transport capacity for a regular planar network is $\Theta(n)$, and that it can be attained by multihop.

(r5) In a regular planar network with either $\gamma > 0$ or $\delta > 1$, and individual power constraint P_{ind}

$$C_{\mathrm{T}} \geq S\left(\frac{\mathrm{e}^{-2\gamma} P_{\text{ind}}}{c_3(\gamma, \delta) P_{\text{ind}} + \sigma^2}\right) \cdot n$$

where

$$c_3(\gamma, \delta) := \begin{cases} \dfrac{4(1+4\gamma)\mathrm{e}^{-2\gamma} - 4\mathrm{e}^{-4\gamma}}{2\gamma(1-\mathrm{e}^{-2\gamma})}, & \text{if } \gamma > 0; \\ \dfrac{16\delta^2 + (2\pi - 16)\delta - \pi}{(\delta-1)(2\delta-1)}, & \text{if } \gamma = 0 \text{ and } \delta > 1 \end{cases}$$

and $S(x)$ denotes the Shannon function $S(x) := \big[\log(1+x)\big]/2$.

This order of distance weighted sum of rates is achievable by multihop. Multihop is order-optimal in a random scenario over a regular planar network in media with $\gamma > 0$ or $\delta > 3$, providing some theoretical justification for its use in situations where traffic is diffused over the network.

Consider a regular planar network with either $\gamma > 0$ or $\delta > 1$, and individual power constraint P_{ind}. The n source–destination pairs are randomly chosen as follows: every source s_ℓ is chosen as the node nearest to a randomly (uniformly i.i.d.) chosen point in the domain, and similarly for every destination d_ℓ. Then $\lim_{n\to\infty} \text{Prob}\,[R_\ell = c/\sqrt{(n \log n)}$ is feasible for every $\ell \in \{1, 2, \ldots, n\}] = 1$ for some $c > 0$. Consequently, a distance weighted sum of rates $C_{\text{T}} = \Omega[n/\sqrt{(\log n)}]$ is supported with probability approaching one as $\eta \to \infty$. This is within a factor $l/\sqrt{\log n}$ of the transport capacity $\Theta(n)$ possible when $\delta > 3$.

(r6) A vector of rates $(R_1, R_2, \ldots, R_m)$ can be supported by multihop in a planar network in media with $\gamma > 0$ or $\delta > 1$, if the traffic can be load balanced such that no node is overloaded and no hop is too long.

This is a fairly straightforward result saying nothing about order optimality, and is provided only in support of the above theme that multihop is an appropriate architecture for balanceable scenarios.

(r7) A set of rates $(R_1, R_2, \ldots R_m)$ for a planar network can be supported by multihop if no hop is longer than a distance $\bar{\rho}$, and for every $1 \le i \le n$, the traffic to be relayed by node i

$$\sum_{\ell=1}^{m} \sum_{\{\pi \in \Pi_\ell:\ \text{node } i \text{ belongs to } \pi\}} \lambda_\pi < S\left\{\frac{\mathrm{e}^{-2\gamma\bar{\rho}} P_{\text{ind}}}{\bar{\rho}^{2\delta}[c_4(\gamma, \delta, \rho_{\min}) P_{\text{ind}} + \sigma^2]}\right\}$$

where

$$c_4(\gamma, \delta, \rho_{\min}) := \begin{cases} \dfrac{2^{3+2\delta}\mathrm{e}^{-\gamma\rho_{\min}}}{\gamma \rho_{\min}^{1+2\delta}}, & \text{if } \gamma > 0 \\ \dfrac{2^{2+2\delta}}{\rho_{\min}^{2\delta}(\delta - 1)}, & \text{if } \gamma = 0 \text{ and } \delta > 1 \end{cases}$$

19.3.6 The low-attenuation regime

In this scenario no absorption, i.e. $\gamma = 0$, and small path loss exponent are assumed. In this case coherent relaying with interference subtraction (CRIS) is considered an interesting strategy for information transmission in the following scenarios. For a source–destination pair (s, d), the nodes are divided into groups, with the first group containing only the source, and the last group containing only the destination d. Call the higher numbered groups 'downstream' groups, although they need not actually be closer to the destination. Nodes in group i, for $1 \le i \le k - 1$, dedicate a portion P_{ik} of their power to coherently transmit for the benefit of node k and its downstream nodes. Each node k employs interference subtraction during decoding to subtract out the known portion of its received signal being transmitted by its downstream nodes.

(r8i) If there is no absorption, i.e. $\gamma = 0$, and the path loss exponent $\delta < 3/2$, then even with a fixed total power P_{total}, any arbitrarily large transport capacity can be supported by CRIS in a regular planar network with a large enough number of nodes n.

(r8ii) If $\gamma = 0$ and $\delta < 1$, then even with a fixed total power P_{total}, CRIS can support a fixed rate $R_{\min} > 0$ for any single source–destination pair in any regular planar network, irrespective of the distance between them.

A similar result exists for the regular linear networks.

(r9i) If $\gamma = 0$ and $\delta < 1$, then even with a fixed total power P_{total}, any arbitrarily large transport capacity can be supported by CRIS in a regular linear network with a large enough number of nodes n.

(r9ii) If $\gamma = 0$ and $\delta < 1/2$, then even with a fixed total power P_{total}, CRIS can support a fixed rate $R_{\min} > 0$ for any single source–destination pair in any regular linear network, irrespective of the distance between them.

A superlinear $\Theta(n^\theta)$ scaling law with $1 < \theta < 2$ is feasible for some linear networks when $\gamma = 0$ and $\delta < 1$.

(r10) For $\gamma = 0$ and individual power constraint P_{ind} for every $0.5 < \delta < 1$, and $1 < \theta < 1/\delta$, there is a family of linear networks for which the transport capacity is $C_T = \Theta(n^\theta)$. This order optimal transport capacity is attained in these networks by CRIS.

19.3.7 The Gaussian multiple-relay channel

The results for the low-attenuation regime rely on the following results for the Gaussian multiple-relay channel. An example of a four-node network with two parallel relays as shown in Figure 19.12. Consider a network of n nodes with α_{ij} the attenuation from node i to node j and i.i.d. additive $N(0, \sigma^2)$ noise at each receiver. Each node has an upper bound on the power available to it, which may differ from node to node. Suppose there is a single source-destination pair (s, d). We call this the Gaussian multiple relay channel.

The first result addresses the case where each relaying group consists of only one node. The strategy used is CRIS. Consider the Gaussian multiple-relay channel with coherent multistage relaying and interference subtraction. Consider $M + 1$ nodes, sequentially denoted by $0, 1, \ldots, M$, with 0 as the source, M as the destination, and the other $M - 1$ nodes serving as $M - 1$ stages of relaying.

(r11) Any rate R satisfying the following inequality is achievable from 0 to M:

$$R < \min_{1 \le j \le M} S \left[\frac{1}{\sigma^2} \sum_{k=1}^{j} \left(\sum_{i=0}^{k-1} \alpha_{ij} \sqrt{P_{ik}} \right)^2 \right]$$

where $P_{ik} \ge 0$ satisfies $\sum_{k=i+1}^{M} P_{ik} \le P_i$.

For the network setting in (r11), Theorem 3.1 in Gupta and Kumar [36] shows that a rate R_0 is achievable if there exist some $\{R_1, R_2, \ldots, R_{M-1}\}$ such that

$$R_{M-1} < S \left[P^R_{M,M-1} \left(\sigma^2 + \sum_{\ell=0}^{M-2} P^R_{M,\ell} \right)^{-1} \right]$$

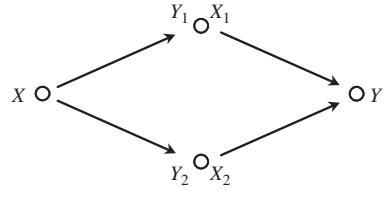

Figure 19.12 A four-node network with two parallel relays [33].

and

$$R_m < \min\left\{ S\left(\frac{P^R_{m+1,m}}{\sigma^2 + \sum_{\ell=0}^{m-1} P^R_{m+1,\ell}}\right), \quad R_{m+1} + \min_{m+2\le k\le M} S\left(\frac{P^R_{k,m}}{\sigma^2 + \sum_{\ell=0}^{m-1} P^R_{k,\ell}}\right)\right\}$$

for each $m = 0, 1, \ldots, M-2$, where

$$P^R_{k,\ell} := \left(\sum_{i=0}^{\ell} \alpha_{ik}\sqrt{P_{i,\ell+1}}\right)^2, \quad 0 \le \ell < k \le M.$$

From the above, recursively for $m = M-2, M-1, \ldots, 0$, it is easy to prove that

$$R_m < \min_{m+1\le j\le M} S\left[\left(\sigma^2 + \sum_{\ell=0}^{m-1} P^R_{j,\ell}\right)^{-1} \sum_{k=m}^{j-1} P^R_{j,k}\right]$$

For $m = 0$, this inequality is exactly (r11), showing a higher achievable rate. The right-hand side (RHS) in (r11) can be maximized over the choice of order of the $M-1$ intermediate nodes. The relaying can also be done by groups, and the next result addresses this. As above, maximization can be done over the assignment of nodes to the groups.

Consider again the Gaussian multiple-relay channel using coherent multistage relaying with interference subtraction. Consider any $M+1$ groups of nodes sequentially denoted by $N_0, N_1, \ldots N_M$ with $N_0 = \{s\}$ as the source, $N_M = \{d\}$ as the destination, and the other $M-1$ groups as $M-1$ stages of relay. Let n_i be the number of nodes in group $N_i, i \in \{0, 1, \ldots, M\}$. Let the power constraint for each node in group N_i be $P_i/n_i \ge 0$.

(r12) Any rate R satisfying the following inequality is achievable from s to d:

$$R < \min_{1\le j\le M} S\left[\frac{1}{\sigma^2}\sum_{k=1}^{j}\left(\sum_{i=0}^{k-1} \alpha_{N_iN_j}\sqrt{P_{ik}/n_i}\cdot n_i\right)^2\right]$$

where $P_{ik} \ge 0$ satisfies $\sum_{k=i+1}^{M} P_{ik} \le P_i$, and $\alpha N_{\dot{x}} N_j := \min\{\alpha_{k\ell} : k \in Ni, \ell \in Nj\}$, $i, j \in \{0, 1, \ldots, M\}$.

As pointed out earlier, more on the results (r1)–(r12) can be found in Xie and Kumar [33].

19.4 COOPERATIVE TRANSMISSION IN WIRELESS MULTIHOP *AD HOC* NETWORKS

The technique discussed in this section allows us to transmit reliably to far destinations that the individual nodes are not able to reach without rapidly consuming their own battery resources, even when using multihop links discussed so far. The results are of interest in both *ad hoc* and sensor networks. The key idea is to have the nodes simply echo the source's (leader) transmission operating as active scatterers while using adaptive receivers that acquire the equivalent network signatures corresponding to the echoed symbols. The active nodes in the network operate either as regenerative or nonregenerative relays. The intuition is that each of the waveforms will be enhanced by the accumulation of power due to the aggregate transmission of all the nodes while, if kept properly under control, the random errors or the receiver noise that propagate together with the useful signals will cause limited deterioration in the performance. The avalanche of signals triggered by the network leaders forms the so-called opportunistic large array (OLA).

In contrast to Sections 19.2 and 19.3, we are interested in this section in a method that utilizes the network as a *distributed modem*, where one or few sources are effectively transmitting data and all the other users are operating as repeaters. A fresh look into the concept of repeaters as a form of cooperative transmission came recently from References [37–40].

We will assume that, in a network of N nodes transmitting over a shared medium, each node is part of a multiple stage relay of a single source transmitting toward a remote receiver whose position is unknown to all the nodes. If no node in the network is powerful enough to communicate reliably with the remote receiver, the problem is referred to as the *reach-back problem*. Coordination among nodes in a large network is an extremely difficult task. In a cooperative transmission mechanism for which cooperation is obtained in a distributed fashion the source (*leader)* transmits a pulse with complex envelope $p_m(t)$ out of an M-ary set of waveforms. The resulting signal at the ith receiver is $r_i(t) = s_{i,m}(t) + n_i(t)$ where $s_{i,m}(t)$ is the network-generated signature of the mth symbol. If N nodes echo *exactly the same symbol*,

$$s_{i,m}(t) = \sum_{n=1}^{N} A_{i,n}(t)\, p_m\left[t - \tau_{i,n}(t)\right], m = 0, \ldots, M-1$$

where $n_i(t)$ is the ith receiver AWGN with variance N_0, $\tau_{i,n}(t)$ is the delay of the link between the ith and the nth node, including the asynchronism of the beginning of transmission for each node n, and $A_{i,n}(t)$ is the product of a complex fading coefficient $\omega_{i,n}(t)$, the transmit power P_t and the channel average gain, e.g. $\propto (1 + d_{i,n})^{-\alpha_{i,n}}$ (log–normal fading), where $d_{i,n}$ is the distance, and $\alpha_{i,n}$ the decay constant between the ith and nth nodes.

The following assumptions are used:

(a1) $A_{i,n}(t)$ and $\tau_{i,n}(t)$ are constant over multiple symbol durations T_s; the nodes are quasi-stationary for a time much greater than T_s.

(a2) The delays are $\tau_{i,1} < \tau_{i,2} \leq \cdots \leq \tau_{i,N}$, where the minimum delay $\tau_{i,1}$ corresponds to the leader. To avoid ISI, the upper bound for the effective symbol rate is $R_s = 1/T_s \leq 1/\Delta\tau$, where $\Delta\tau$ is the maximum *delay spread* of $s_{i,m}(t)$ for all i. The delay spread for node i is defined as

$$\sigma_{\tau i} = \sqrt{\frac{\displaystyle\int_{-\infty}^{\infty} (t - \bar{\tau}_i)^2 \cdot \left|S_{i,m}(t)\right|^2 \mathrm{d}t}{\displaystyle\int_{-\infty}^{\infty} \left|S_{i,m}(t)\right|^2 \mathrm{d}t}}$$

where the average delay

$$\bar{\tau}_i = \frac{\displaystyle\int_{-\infty}^{\infty} t \cdot \left|S_{i,m}(t)\right|^2 \mathrm{d}t}{\displaystyle\int_{-\infty}^{\infty} \left|S_{i,m}(t)\right|^2 \mathrm{d}t}$$

and thus, $\Delta\tau = \max_i \sigma_{\tau_i}$. Echoes that come from farther away are strongly attenuated (by $\approx d^{-\alpha}$); therefore, the echoes received at node i are nonnegligible only for those coming from nodes within a certain distance Δd, which essentially depends on the transmit power and path loss. Hence, R_s can be increased by lowering the transmit power, capitalizing on spatial bandwidth reuse. In the reach back problem, however, the delay spread is $\Delta\tau \approx \sup_i[\tau_{i,N} - \tau_{i,1}]$ because the receiver is roughly at the same distance from all nodes.

(a3) T_s is fixed for all nodes to $c_1\Delta\tau$, where c_1 is a constant taken to satisfy the ISI constraint. With (a3), we guarantee that no ambiguity will occur at the nodes in timing their responses. The transmission activity of the node is solely dependent on the signal that the node

receives. Based on the evolution of $s_{i,m}(t)$, we can distinguish two phases: (1) the earlier *receive phase*, when the upstream waves of signals approach the node, and (2) the period after the *firing instant*, which we call the *rest phase*, where the node hears the echoes of the downstream wave of signals fading away (for the regenerative case, the firing instant occurs shortly after the time when the node has accumulated enough energy to detect the signal). The switching between the two modes can be viewed as a very elementary form of time-division duplex (TDD).

(a4) The leader (and also the nodes in the regenerative case) transmits pulses with complex envelope $p_m(t)$ having limited double-sided bandwidth W and, approximately, duration T_p. By sampling at the Nyquist rate, $N_p = T_p W$ is the approximate length of the sequence $\{p_m(k/W)\}$ of samples. Multipath propagation can be simply included in the model by increasing the number of terms in the summation in $s_{i,m}(t)$; therefore, it does not require special attention. In fact, when we neglect the propagation of errors and noise that occurs in the case of regenerative and nonregenerative repeaters, respectively, the OLA itself is equivalent to a multipath channel, created by a set of active scatterers. In the regenerative case, the ideal OLA response is

$$g_i(\tau) = \sum_{n=1}^{N} A_{i,n}\delta(\tau - \tau_{i,n}) \tag{19.55}$$

The nonregenerative OLA scattering model is more complex due to the feedback effect, which implies that not one but several signal contributions are scattered by each source. The received OLA response is

$$g_i(\tau) = \sum_{n=1}^{N'} A_{i,n'}\delta(\tau - \tau_{i,n'}) \tag{19.55a}$$

For every possible path in the network, there is a contribution to the summation in Equation (19.55a) that has an amplitude equal to the product of all the path link gains traveled so far and a delay equal to the sum of all the path delays. Theoretically, the number of reflections $N' \to \infty$ because the signals and their amplified versions keep cycling in the network and adding up. If properly controlled, the contributions will keep adding up and then opportunistically serve the purpose of enhancing the signal. Hence, the key for the nonregenerative design is to control the noise that accompanies the useful signal. In both regenerative and nonregenerative cases, the received signal can be rewritten as the following convolution:

$$r_i(t) = g_i(t)^* p_m(t) + n_i(t) \tag{19.56}$$

where $g_i(t)$ is the network impulse response, which is analogous to that of a multipath channel. Based on Equation (19.46), the idea is to let the nodes operate as regenerative and nonregenerative repeaters and avoid any complex coordination procedure to forward their signals at the network layer and share the bandwidth at the MAC layer. In addition, no channel state information is used. The information flow is carried forward using receivers that are capable of tracking the *unknown* network response $g_i(t)$ or, directly, the signature waveforms $s_{i,m}(t) \triangleq g_i(t)^* p_m(t)$. We should expect that the OLA behaves as a frequency-selective channel. Nodes' mobility causes changes of the response $g_i(t)$ over time. If most of the network is stationary and N is large, the inertia of the system will be such that mobile nodes will cause small changes in $g_i(t)$.

Since the transmission channel is bandlimited with passband bandwidth W, the signature waveform $p_m(t)$ will have to be bandlimited and, therefore, uniquely expressible through its samples taken at the Nyquist rate $1/T_c$, where $T_c = 1/W$. In general, $p_m(t)$ corresponds to a finite number of samples N_p and is approximately time limited with duration $T_p \approx N_p/W$. Introducing the

vectors $\mathbf{p}_m$, $\mathbf{g}_i$ and $\mathbf{r_i}$ such that

$$\{\mathbf{p}_m\}_k = p_m(kT_c), k = 0, \ldots N_p - 1$$
$$\{\mathbf{g}_i\}_k = \int \text{sinc}(\pi W\tau) g_i(kT_c + l_i T_C - \tau) d\tau, \quad k = 0, \ldots N_i - 1$$
$$\{\mathbf{r}_i\}_k = r_i(kT_c + l_i T_c), k = 0, \ldots, N_i + N_p - 2$$
$$\{\mathbf{n}_i\}_k = n_i(kT_c + l_i T_c), k = 0, \ldots, N_i + N_p - 2$$

where N_i is the number of samples needed to represent $g_i(t)$, we have

$$\{\mathbf{r}_i\}_k = \sum_{n=0}^{N_p-1} \{\mathbf{p}_m\}_n \{\mathbf{g}_i\}_{k-n} + \{\mathbf{n}_i\}_k$$

By using the following Toeplitz convolution matrix:

$$\{\mathbf{G}_i\}_{k,n} = \{\mathbf{g}_i\}_{k-n}, \quad n = 0, \ldots, N_p - 1; k = 0, \ldots, N_i + N_p - 2$$

we obtain

$$\mathbf{r}_i = \mathbf{G}_i \mathbf{p}_m + \mathbf{n}_i \tag{19.57}$$

19.4.1 Transmission strategy and error propagation

The transmission of the OLA is led by a predetermined source node in the network. All the other nodes form multiple stages of relays to either flood the network with the information from the source, or just to pass the information to a remote receiver. The intermediate nodes in OLA have a choice of whether to relay or not, depending on the performance at that node. In the *regenerative scheme*, the OLA nodes has the choice of retransmitting its detected symbol or staying silent. Only nodes that are *connected* actively reply, where connectivity is defined as follows.

Definition 1
The *i*th regenerative node is connected if, based on its estimates of all possible signatures $G_i p_m$ and receiver noise variance, the pairwise symbol error probability of the *i*th receiver not considering error propagation) is below *a* fixed upper-bound ε, i.e. $\max_m Pr\{m \to \mu\} \leq \varepsilon, \forall \mu \neq m, m = 0, \ldots, M - 1$.

In the N_s samples contained in each symbol period, the time instant selected for the detection and subsequent echo is the first sample $\bar{N}_i \leq N_s$ at which the node is connected. If there is no such sample, the node will never echo the signal (but it may obviously detect the information at his own risk.)

In the *nonregenerative scheme*, every node that achieves the SNR constraint amplifies the signal coming from the other nodes as well as their receiver noise. Hence, the noise n_i has a rather complex structure since it includes the noise that comes from every node that has transmitted previously and all its subsequent amplifications along with the signal. Since the geographical area in an *ad hoc* or sensor network is limited, the delay spread of each node response will also be limited, as far as the signal-to-noise contribution is concerned. Considerations on the SNR can be deduced by considering the inherent recursive structure of the signal composition. Details can found in Scaglione and Hong [40].

Definition 2
The *i*th nonregenerative node is said to be connected if the signal to noise ratio at the node ξ_i is above *a* fixed threshold $\xi_i > \bar{\xi}$.

19.4.2 OLA flooding algorithm

In this section, we compare numerically OLA with the more traditional ways of flooding the network described in Chapter 13. The flooding algorithm in Royer and Toh [41] is commonly indicated as one of the simplest ways of distributing information in the network or of searching for a path to the desired destination to initialize table-driven protocols. Some interesting alternatives are the probabilistic scheme [42] and the scalable broadcast algorithm [43]. Most of these methods require the MAC and physical layer to provide virtual transmission pipes (obtained typically with contention) that connect each pair of nodes, which imitates wired networks. The approach is legitimate but obviously inefficient. In fact, in solving the network broadcast problem, it is natural to utilize and integrate in the design the fact that wireless devices are physically broadcasting. This is precisely what happens in the OLA, where, contrary to the networking approaches, the transmission protocol and cooperation strategy operate at the physical layer. In OLA framework, the receiver has to solve an equivalent point-to-point communication problem without requiring higher layers' interventions (MAC or network layer). The benefits from eliminating two layers are higher connectivity and faster flooding. However, the OLA flooding algorithm cannot be used for some broadcasting applications such as route discovery due to the fact that the higher layer information is eliminated.

Each node in the OLA is assumed to have identical transmission resources; therefore, any node has the ability of assuming the role of a leader. The leader can be chosen to be the leader of a troop, the clusterheads in clustering algorithms, or simply some node that has information to send.

19.4.3 Simulation environment

Various network broadcasting methods were analyzed using the ns2 network simulator. The simulation parameters are specified in Table 19.1 [40, 44]. Physical layer resources of the IEEE 802.11 DSSS PHY specifications [45] for the 2.4 GHz carrier were used. Each node-to-node transmission is assumed to experience independent small-scale fading with Rayleigh coefficients of variance 1. The large-scale fading is deterministic, and the path loss model is based on the model used in *ns2* [46], where the *free space model* is used for distance $d < d_c$ (the *cross-over distance*) and the *two-ray ground reflection model* is used for $d > d_c$, where $d_c = 4\pi/\lambda$. The position of the 'leader' is randomly selected, and the OLA is regenerative.

There are three parameters that define the simulation setting. The first is the *point-to-point average SNR* (averaged over the small scale fading), which is defined as $SNR_{p2p}(d) \triangleq P_t/(N_0 d^\alpha)$ where d^α is the path loss. The second is the *transmission radius* $d_{p2p} \triangleq \left[P_t/(N_0\xi)\right]^{-\alpha}$, which is equal to the distance at which the $SNR_{p2p}(d) = \xi$ using the specified path loss model. The exact *SNR* at each node is different due to the accumulation of signals. Therefore, we define a third parameter, which is *the node SNR at the detection level* $\mathrm{SNR}_{\mathrm{det}} \triangleq ||g_i||^2/E\{||n_i||^2\}$. The value of SNR_{det} can be mapped one-to-one into the node error rate if error propagation is neglected and provides a criterion equivalent to the one in definition 1 to establish whether a node is connected

Table 19.1 Simulation parameters

Simulation Paramaters	Values
Network area	350×350 m
Radius of TX	100 m
Payload	64 bytes/packet
Number of trials	100
Modulation	BPSK
Bandwidth (IEEE 802.11)	83.5 Mbs

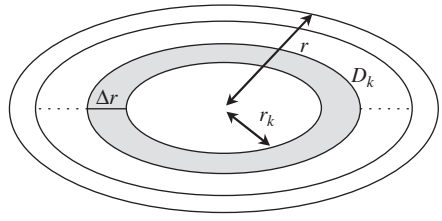

Figure 19.13 Nodes in the ring Δr transmit approximately simultaneously.

or not. In all cases, the threshold on SNR_{det} is the same as the required point-to-point $\text{SNR}_{p2p}(d)$ used to define network links in conventional networks, and let this value be ξ.

To simplify the network simulations, it is assumed that the transmission propagates through the network approximately in a multiple ring structure shown in Figure 19.13. In each ring, we prune away the nodes that do not have strong enough SNR_{det}, but we do not detect and retransmit at the exact time when the SNR_{det} reaches the threshold. Because we just partition the network geographically, we can expect, in general, nonuniform and lower error rates than the ones prescribed by the threshold on SNR_{det}. In the experiments, it was assumed that the signal space is perfectly estimated at each relaying node. This assumption is practical, because the network is static, and when the number of training symbols is sufficiently large, the noise variance caused by the contribution of the estimation error can be neglected. Figure 19.14 shows to what degree the network is connected according to definition 1 when the threshold for $(\text{SNR}_{\text{det}})_{\text{dB}}$ is 10 dB. Specifically, the *connectivity ratio* (CR) is shown, which is defined as *the number of nodes that are* '*connected*', *over the total number of nodes in the network*. The nodes' transmit power and thermal noise are constant and are fixed so that $(\text{SNR}_{p2p})_{\text{dB}} = 10$ at the distances $d_{p2p} = 100, 80$ and 60 m, representing the transmission radii.

For $d_{p2p} = 100$ m, the CR is 100 % even at very low node density. As we shorten the radius of transmission, the connectivity of the network will decrease. Figure 19.15 plots the *delivery ratio* (DR), which is defined as the ratio between the average number of nodes that receive packets using a specific flooding algorithm over the number of nodes that are *connected in multiple hops*, i.e. nodes for which there exists a path from the leader that is formed with point-to-point links having SNR_{p2p} above a fixed threshold. The only cause of packet loss considered in Williams and Camp [44] is the fact that the packet is not delivered because it is dropped by the intermediate

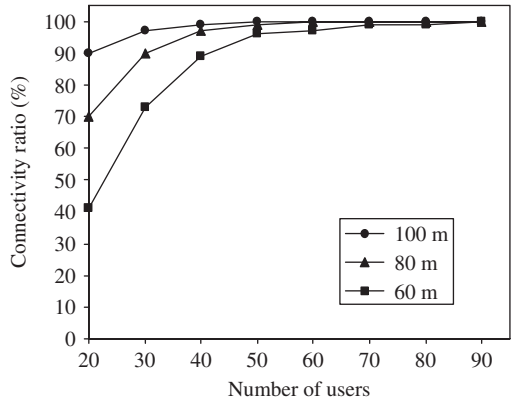

Figure 19.14 Connectivity ratio vs number of nodes in the network.

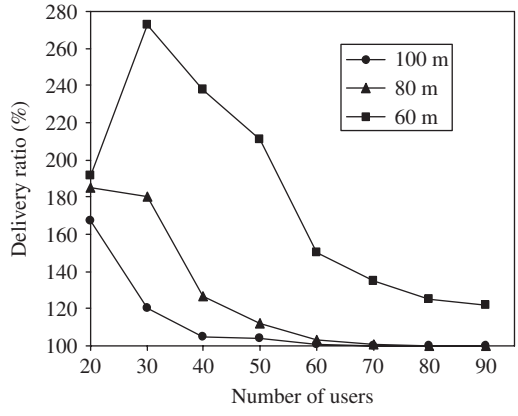

Figure 19.15 Delivery ratio vs number of nodes in the network.

relays' queues to reduce the nodes congestion. *Routing, MAC and physical layer errors and their possible propagation are ignored* in the definition of DR. DR essentially shows how routing and MAC problems can reduce the probability of successfully reaching the nodes. Hence, according to Williams and Camp [44], the simple flooding algorithm achieves 100 % DR, even if it might create longer delays and instability due to the increased level of traffic. In the OLA, the accumulation of signal energy may still allow extra nodes (besides the ones that have a multihop route) to receive the broadcasted packets reliably. Therefore, if we calculate the ratio between the number of nodes connected in the OLA according to definition 1 and the number of nodes that are connected through multihop point-to-point links, we must be able to achieve more than 100 % DR. Using the parameters in Table 19.1, Figure 19.15 plots the DR vs the number of nodes. It is shown that there can be remarkable gains in connectivity over any scheme operating solely on point-to-point links.

The *end-to-end delay* is the time required to broadcast the packet to the entire network. In the OLA flooding algorithm, there is no channel contention, and therefore, the overhead necessary for

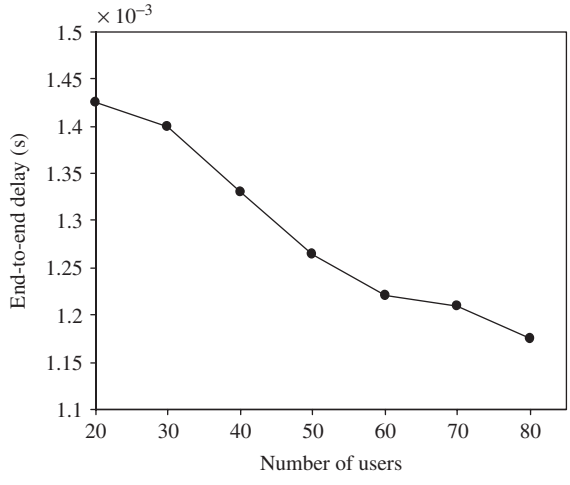

Figure 19.16 End-to-end delay vs number of nodes in the network.

carrier sensing and collision avoidance used in IEEE 802.11 is eliminated. With the reduction of overheads and the time saved by avoiding channel contention, it is clear that the speed of flooding will be much higher than the traditional broadcasting methods. Figure 19.16 shows the end-to-end delay vs the number of nodes in the network. The end-to-end delay is only in the order of milliseconds for a packet payload of 64 bytes, which coincides with the symbol period T_s times the number of bits in a packet.

19.5 NETWORK CODING

In this section we consider a communication network in which certain source nodes multicast information to other nodes on the network in multihops where every node can pass on any of its received data to others. The question is how the data should be sent and how fast *each* node can receive the complete information. Allowing a node to encode its received data before passing it on, the question involves optimization of the multicast mechanisms at the nodes. Among the simplest coding schemes is linear coding, which regards a block of data as a vector over a certain base field and allows a node to apply a linear transformation to a vector before passing it on.

As in Chapter 7, we define a *communication network* as a pair (G, S), where G is a finite *directed* multigraph and S (source) is the unique node in G without any incoming edges. A directed edge in G is called a *channel* in the communication network (G, S). A channel in graph G represents a noiseless communication link on which one unit of information (e.g. a bit) can be transmitted per unit time. The multiplicity of the channels from a node X to another node Y represents the *capacity* of direct transmission from X to Y. We assume that, every single channel has unit capacity.

At the source S, information is generated and multicast to other nodes on the network in the multihop fashion where every node can pass on any of its received data to other nodes. At each nonsource node which serves as a sink, the complete information generated at S is recovered. Now the question is how fast each sink node can receive the complete information. As an example, consider the multicast of two data bits, b_1 and b_2, from the source S in the communication network depicted by Figure 19.17(a) as both nodes Y and Z. One solution is to let the channels ST, TY, TW and WZ carry the bit b_1 and channels SU, UZ, UW and WY carry the bit b_2. Note that, in this scheme, an intermediate node sends out a data bit only if it receives the same bit from another node. For example, the node T receives the bit b_1 and sends a copy on each of the two channels TY and TW. Similarly, the node U receives the bit b_2 and sends a copy into each of the two channels UW and UZ. We assume that there is no processing delay at the intermediate nodes.

Unlike a conserved physical commodity, information can be replicated or coded. The notion of network coding refers to coding at the intermediate nodes when information is multicast in a

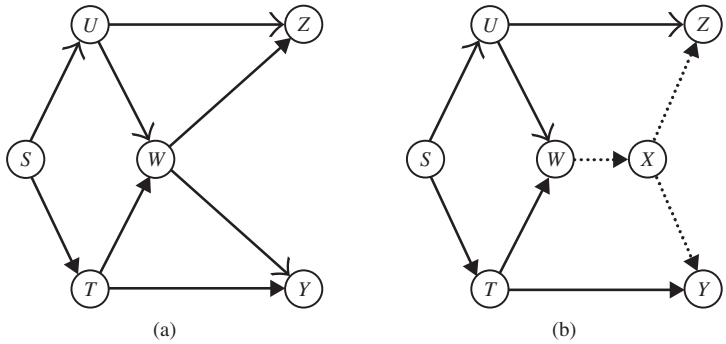

Figure 19.17 Illustration of network coding.

network. Let us now illustrate network coding by considering the communication network depicted in Figure 19.17(b). Again, we want to multicast two bits b_1 and b_2 from the source S to both the nodes Y and Z. A solution is to let the channels ST, TW and TY carry the bit b_1, channels SU, UW and UZ carry the bit b_2, and channels WX, XY and XZ carry the exclusive-OR $b_1 \oplus b_2$. Then, the node Y receives b_1 and $b_1 \oplus b_2$, from which the bit $b_2 = b_1 \oplus (b_1 \oplus b_2)$ can be decoded. Similarly, the node Z can decode the bit b_1 from b_2 and $b_1 \oplus b_2$ as $b_1 = b_2 \oplus (b_1 \oplus b_2)$. The coding/decoding scheme is assumed to have been agreed upon beforehand. In order to discuss this issue in more detail, in this section we first introduce the notion of a *linear-code multicast* (LCM). Then we show that, with a 'generic' LCM, every node can simultaneously receive information from the source at rate equal to its max-flow bound. After that, we describe the physical implementation of an LCM, first when the network is acyclic and then when the network is cyclic followed by a presentation of a greedy algorithm for constructing a generic LCM for an acyclic network. The same algorithm can be applied to a cyclic network by expanding the network into an acyclic network. This results in a 'time-varying' LCM, which, however, requires high complexity in implementation. After that, we introduce the time-invariant LCM (TILCM).

Definition 1
Over a communication network a *flow* from the source to a nonsource node T is a collection of channels, to be called the *busy* channels in the flow, such that: (1) the subnetwork defined by the busy channels is acyclic, i.e. the busy channels do not form directed cycles; (2) for any node other than S and T, the number of incoming busy channels equals the number of outgoing busy channels; (3) the number of outgoing busy channels from S equals the number of incoming busy channels to T. The number of outgoing busy channels from S will be called the *volume* of the flow. The node T is called the *sink* of the flow. All the channels on the communication network that are not busy channels of the flow are called the *idle* channels with respect to the flow.

Definition 2
For every nonsource node T on a network (G, S), the maximum volume of a flow from the source to T is denoted $max\ flow_G(T)$, or simply *mf(T)* when there is no ambiguity.

Definition 3
A *cut* on a communication network (G, S) between the source and a nonsource node T means a collection C of nodes which includes S but not T. A channel XY is said to be *in* the cut C if $X \in C$ and $Y \notin C$. The number of channels in a cut is called the *value* of the cut.

19.5.1 Max-flow min-cut theorem (mfmcT)

For every nonsource node T, the minimum value of a cut between the source and a node T is equal to *mf (T)*. Let d be the maximum of *mf (T)* over all T. In the sequel, the symbol Ω will denote a fixed d-dimensional vector space over a sufficiently large base field. The information unit is taken as a symbol in the base field. In other words, one symbol in the base field can be transmitted on a channel every unit time.

Definition 4
An LCM v on a communication network *(G, S)* is an assignment of a vector *space* $v(X)$ to every node X and a vector $v(XY)$ to every channel XY such that (1) $v(S) = \Omega$; (2) $v(XY) \in v(X)$ for every channel XY; and (3) for any collection $\wp$ of nonsource nodes in the network $\langle\{v(T) : T \in \wp\}\rangle = \langle\{v(XY) : X \notin \wp Y \in \wp\}\rangle$. The notation $\langle\cdot\rangle$ is for *linear span*. Condition (3) says that the vector

spaces $v(T)$ on all nodes T inside $\wp$ together have the same linear span as the vectors $v(XY)$ on all channels XY to nodes in $\wp$ from outside $\wp$.

LCM v data transmission: *The information to be transmitted from S is encoded as a d-dimensional row vector, referred to as an information vector. Under the transmission mechanism prescribed by the LCM v, the data flowing on a channel XY is the matrix product of the information (row) vector with the (column) vector v(XY). In this way, the vector v(XY) acts as the kernel in the linear encoder for the channel XY. As a direct consequence of the definition of an LCM, the vector assigned to an outgoing channel from a node X is a linear combination of the vectors assigned to the incoming channels to X. Consequently, the data sent on an outgoing channel from a node X is a linear combination of the data sent on the incoming channels to X. Under this mechanism, the amount of information reaching a node T is given by the dimension of the vector space v(T) when the LCM v is used.*

Coding in Figure 19.17(b) is achieved with the LCM v specified by

$$\begin{aligned} v(ST) = v(TW) = v(TY) &= (1\ 0)^{\mathrm{T}} \\ v(SU) = v(UW) = v(UZ) &= (0\ 1)^{\mathrm{T}} \end{aligned} \tag{19.58}$$

and

$$v(WX) = v(XY) = v(XZ) = (1\ 1)^{\mathrm{T}}$$

where $(\,)^{\mathrm{T}}$ stands for transposed vector. The data sent on a channel is the matrix product of the *row* vector $(b_1\ b_2)$ with the *column* vector assigned to that channel by v. For instance, the data sent on the channel WX is

$$(b_1, b_2)v(WX) = (b_1, b_2)\,(1\ 1)^{\mathrm{T}} = b_1 + b_2$$

Note that, in the special case when the base field of Ω is $GF(2)$, the vector $b_1 + b_2$ reduces to the exclusive-OR $b_1 \oplus b_2$ in an earlier example.

Proposition P1
For every LCM v *on a network, for all nodes* T $\dim[v(T)] \leq mf\ (T)$. *To prove it fix a nonsource node* T *and any cut* C *between the source and* T $v(T) \subset \langle v(Z) : Z \notin C\rangle = \langle v(YZ) : Y \in C \text{ and } Z \notin C\rangle$. *Hence,* $\dim[v(T)] \leq \dim(\langle v(YZ) : Y \in C \text{ and } Z \notin C\rangle)$, *which is at most equal to the value of the cut. In particular,* $\dim[v(T)]$ *is upper-bounded by the minimum value of a cut between S and T, which by the max-flow min-cut theorem is equal to mf(T).*

This means that *mf (T)* is an upper bound on the amount of information received by T when an LCM v is used.

19.5.2 Achieving the max-flow bound through a generic LCM

In this section, we derive a sufficient condition for an LCM v to achieve the max-flow bound on $\dim[v(T)]$ in Proposition 1.

Definition
An LCM v on a communication network is said to be generic if the following condition holds for any collection of channels $X_1Y_1, X_2Y_2, \ldots, X_mY_m$ for $1 \leq m \leq d : (*)v(X_k) \not\subset$

$\langle\{v(X_jY_j) : j \neq k\}\rangle$ for $1 \leq k \leq m$ if and only if the vectors $v(X_1Y_1), v(X_2Y_2), \ldots, v(X_mY_m)$ are linearly independent. If $v(X_1Y_1), v(X_2Y_2), \ldots, v(X_mY_m)$ are linearly independent, then $v(X_k) \not\subset \langle\{v(X_jY_j) : j \neq k\}\rangle$ since $v(X_kY_k) \in v(X_k)$. A generic LCM requires that the converse is also true. In this sense, a generic LCM assigns vectors which are as linearly independent as possible to the channels.

With respect to the communication network in Figure 19.17(b), the LCM v defined by Equation (19.58) is a generic *LCM*. However, the *LCM* u defined by

$$\begin{aligned} u(ST) = u(TW) = u(TY) &= (1\ 0)^{\mathrm{T}} \\ u(SU) = u(UW) = u(UZ) &= (0\ 1)^{\mathrm{T}} \end{aligned} \tag{19.59}$$

and

$$u(WX) = u(XY) = u(XZ) = (1\ 0)^{\mathrm{T}}$$

is not generic. This is seen by considering the set of channels $\{ST, WX\}$ where

$$u(S) = u(W) = \left\langle \begin{pmatrix} 1 \\ 0 \end{pmatrix}, \begin{pmatrix} 0 \\ 1 \end{pmatrix} \right\rangle$$

Then $u(S) \not\subset \langle u(WX)\rangle$ and $u(W) \not\subset \langle u(ST)\rangle$, but $u(ST)$ and $u(WX)$ are not linearly independent. Therefore, u is not generic. Therefore, in a generic LCM v any collection of channels $XY_1, XY_2, \ldots, XY_m$ from a node X with $m \leq \dim[v(X)]$ must be assigned linearly independent vectors by v.

Theorem T1

If v is a generic LCM on a communication network, then for all nodes T, $\dim[v(T)] = mf(T)$. To prove it, consider a node T not equal to S. Let f be the common value of $mf(T)$ and the minimum value of a cut between S and T. The inequality $\dim[v(T)] \leq f$ follows from Proposition 1. So, we only have to show that $\dim[v(T)] \geq f$. To do so, let $\dim(C) = \dim(\langle v(X, Y) : X \in C \text{ and } Y \notin C\rangle)$ for any cut C between S and T. We will show that $\dim[v(T)] \geq f$ by contradiction. Assume $\dim[v(T)] < f$ and let A be the collection of cuts U between S and T such that $\dim(U) < f$. Since $\dim[v(T)] < f$ implies $V\backslash\{T\} \in A$, where v is the set of all the nodes in G, A is nonempty.

By the assumption that v is a generic LCM, the number of edges out of S is at least d, and $\dim(\{S\}) = d \geq f$. Therefore, $\{S\} \notin$ A. Then there must exist a minimal member $U \in A$ in the sense that for any $Z \in U\backslash\{S\} \neq \phi$, $U\backslash\{Z\} \notin$ A. Clearly, $U \neq \{S\}$ because $\{S\} \notin A$. Let K be the set of channels in cut U and B be the set of boundary nodes of U, i.e. $Z \in B$ if and only if $Z \in U$ and there is a channel (Z, Y) such that $Y \notin U$. Then for all $W \in B$, $v(W) \not\subset \langle v(X, Y) : (X, Y) \in K\rangle$ which can be seen as follows. The set of channels in cut $U\backslash\{W\}$ but not in K is given by $\{(X, W) : X \in U\backslash\{W\}\}$. Since v is an LCM $\langle v(X, W) : X \in U\backslash\{W\}\rangle \subset v(W)$. If $v(W) \subset \langle v(X, Y) : (X, Y) \in K\rangle$, then $\langle v(X', Y') : X' \in U\backslash\{W\}, Y' \notin U\backslash\{W\}\rangle$ the subspace spanned by the channels in cut $U\backslash\{W\}$, is contained by $\langle v(X, Y) : (X, Y) \in K\rangle$. This implies that $\dim(U\backslash\{W\}) \leq \dim(U) < f$ is a contradiction. Therefore, for all $W \in B$, $v(W) \not\subset \langle v(X, Y) : (X, Y) \in K\rangle$. For all $(W, Y) \in K$, since $\langle v(X, Z) : (X, Z) \in K\backslash\{(W, Y)\}\rangle \subset \langle v(X, Y) : (X, Y) \in K\rangle$, $v(W) \not\subset \langle v(X, Y) : (X, Y) \in K\rangle$ implies that $v(W) \not\subset \langle v(X, Z) : (X, Z) \in K\backslash\{(W, Y)\}\rangle$.

Then, by the definition of a generic LCM $\{v(XY) : (X, Y) \in K\}$ is a collection of vectors such that $\dim(U) = \min(|K|, d)$. Finally, by the max-flow min-cut theorem, $|K| \geq f$, and since $d \geq f$, $\dim(U) \geq f$. This is a contradiction to the assumption that $U \in A$. The theorem is proved.

An LCM for which $\dim[v(T)] = mf(T)$ for all T provides a way for broadcasting a message generated at the source S for which every nonsource node T receives the message at rate equal to $mf(T)$. This is illustrated by the next example, which is based upon the assumption that the

base field of Ω is an infinite field or a sufficiently large finite field. In this example, we employ a technique which is justified by the following arguments.

Lemma 1
Let X, Y and Z be nodes such that mf(X) = i, mf(Y) = j, and mf(Z) = k, where $i \leq j$ and $i > k$. By removing any edge UX in the graph, mf(X) and mf(Y) are reduced by at most 1, and mf(Z) remains unchanged.

To prove it we note that, by removing an edge UX, the value of a cut C between the source S and node X (respectively, node Y) is reduced by 1 if edge UX is in C, otherwise, the value of C is unchanged. By the *mfmcT*, we see that *mf(X)* and *mf(Y)* are reduced by at most 1 when edge UX is removed from the graph. Now consider the value of a cut C between the source S and node Z. If C contains node X, then edge UX is not in C, and, therefore, the value of C remains unchanged upon the removal of edge UX. If C does not contain node X, then C is a cut between the source S and node X. By the *mfmcT*, the value of C is at least i. Then, upon the removal of edge UX, the value of C is lower-bounded by $i - 1 \geq k$. Hence, by the *mfmcT*, *mf(Z)* remains to be k upon the removal of edge UX.

Example E1
Consider a communication network for which $mf(T) = 4, 3$ or 1 for nodes T in the network. The source S is to broadcast 12 symbols $a_1, \ldots, a_{12}$ taken from a sufficiently large base field F. (Note that 12 is the least common multiple of 4, 3 and 1.) Define the set $\mathbf{T}_i = \{T : mf(T) = i\}$, for $i =$ 4, 3, 1. For simplicity, we use the second as the time unit. We now describe how $a_1, \ldots, a_{12}$ can be broadcast to the nodes in $\mathbf{T}_4$,$\mathbf{T}_3$, $\mathbf{T}_1$, in 3, 4 and 12 s, respectively, assuming the existence of an LCM on the network for $d = 4, 3, 1$.

(1) Let v_1 be an *LCM* on the network with d = *4*. Let $\alpha_1 = (a_1\ a_2\ a_3\ a_4), \alpha_2 = (a_5\ a_6\ a_7\ a_8)$ and $\alpha_3 = (a_9\ a_{10}\ a_{11}\ a_{12})$. In the first second, transmit α_1 as the information vector using v_1, in the second second, transmit α_2, and in the third second, transmit α_3. After 3 s, after neglecting delay in transmissions and computations all the nodes in $\mathbf{T}_4$ can recover α_1, α_2 and α_3.

(2) Let r be a vector in F^4 such that $\langle\{r\}\rangle$ intersects trivially with $v_1(T)$ for all T in $\mathbf{T}_3$, *i.e.*$\langle\{r, v_1(T)\}\rangle = F^4$ for all T in $\mathbf{T}_3$. Such a vector r can be found when F is sufficiently large because there are a finite number of nodes in $\mathbf{T}_3$. Define $b_i = \alpha_i r$ for $i =$ *1, 2, 3*. Now remove incoming edges of nodes in $\mathbf{T}_4$, if necessary, so that $mf(T)$ becomes 3 if T is in $\mathbf{T}_4$, otherwise, $mf(T)$ remains unchanged. This is based on Lemma 1). Let v_2 be an *LCM* on the resulting network with $d = 3$. Let $\beta = (b_1\ b_2\ b_3)$ and transmit β as the information vector using v_2 in the fourth second. Then all the nodes in $\mathbf{T}_3$ can recover β and hence α_1, α_2 *and* α_3.

(3) Let s_1 and s_2 be two vectors in F^3 such that $\langle\{s_1, s_2\}\rangle$ intersects with $v_2(T)$ trivially for all T in $\mathbf{T}_1$, *i.e.*$\langle\{s_1, s_2, v_2(T)\}\rangle = F^3$ for all T in $\mathbf{T}_1$. Define $\gamma_i = \beta s_i$ for $i = 1, 2$. Now remove incoming edges of nodes in $\mathbf{T}_4$ and $\mathbf{T}_3$, if necessary, so that $mf(T)$ becomes 1 if T is in $\mathbf{T}_4$ or $\mathbf{T}_3$, otherwise, $mf(T)$ remains unchanged. Again, this is based on Lemma 1). Now let v_3 be an *LCM* on the resulting network with $d = 1$. In the fifth and the sixth seconds, transmit γ_1 and γ_2 as the information vectors using v_3. Then all the nodes in $\mathbf{T}_1$ can recover β.

(4) Let t_1 and t_2 be two vectors in F^4 such that $\langle\{t_1, t_2\}\rangle$ intersects with $\langle\{r, v_1(T)\}\rangle$ trivially for all T in $\mathbf{T}_1$, *i.e.* $\langle\{t_1, t_2, r, v_1(T)\}\rangle = F^4$ for all T in $\mathbf{T}_1$. Define $\delta_1 = \alpha_1 t_1$ and $\delta_2 = \alpha_1 t_2$. In the seventh and eighth seconds, transmit δ_1 and δ_2 as the information vectors using

v_3. Since all the nodes in $\mathbf{T}_1$ already know b_1, upon receiving δ_1 and δ_2, α_1 can then be recovered.

(5) Define $\delta_3 = \alpha_2 t_1$ and $\delta_4 = \alpha_2 t_2$. In the ninth and tenth seconds, transmit δ_3 and δ_4 as the information vectors using v_3. Then α_2 can be recovered by all the nodes in $\mathbf{T}_1$.

(6) Define $\delta_5 = \alpha_3 t_1$ and $\delta_6 = \alpha_0 t_2$. In the eleventh and twelveth seconds, transmit δ_5 and δ_6 as the information vectors using v_3. Then α_3 can be recovered by all the nodes in $\mathbf{T}_1$.

So, in the ith second for $i = 1, 2, 3$, via the generic LCM v_1, each node in $\mathbf{T}_4$ receives all four dimensions of α_i, each node in $\mathbf{T}_3$ receives three dimensions of α_i, and each node in T_1 receives one dimension of α_i. In the fourth second, via the generic LCM v_2, each node in $\mathbf{T}_3$ receives the vector β, which provides the three missing dimensions of α_1, α_2 and α_3 (one dimension for each) during the first 3 s of multicast by v_1. At the same time, each node in $\mathbf{T}_1$ receives one dimension of β. Now, in order to recover β, each node in $\mathbf{T}_1$ needs to receive the two missing dimensions of β during the fourth second. This is achieved by the generic LCM v_3 in the fifth and sixth seconds. So far, each node in $\mathbf{T}_1$ has received one dimension of α_i for $i = 1, 2, 3$ via v_1 during the first 3 s, and one dimension of α_i for $i = 1, 2, 3$ from β via v_2 and v_3 during the fourth to sixth seconds. Thus, it remains to provide the six missing dimensions of α_1, α_2 and α_3 (two dimensions for each) to each node in $\mathbf{T}_1$, and this is achieved in the seventh to the twelfth seconds via the generic LCM v_3. The previous scheme can be generalized to arbitrary sets of max-flow values.

19.5.3 The transmission scheme associated with an LCM

Let v be an LCM on a communication network (G, S), where the vectors $v(SX)$ assigned to outgoing channels SX linearly span a d-dimensional space. As before, the vector $v(XY)$ assigned to a channel XY is identified with a d-dimensional column vector over the base field of Ω by means of the choice of a basis. On the other hand, the total information to be transmitted from the source to the rest of the network is represented by a d-dimensional row vector, called the information vector. Under the transmission scheme prescribed by the LCM v, the data flowing over a channel XY is the matrix product of the information vector with the column vector $v(XY)$. We now consider the physical realization of this transmission scheme associated with an LCM.

A communication network (G, S) is said to be *acyclic* if the directed multigraph G does not contain a directed cycle. The nodes on an acyclic communication network can be sequentially indexed such that every channel is from a smaller indexed node to a larger indexed node. On an acyclic network, a straightforward realization of the above transmission scheme is as follows. Take one node at a time according to the sequential indexing. For each node, 'wait' until data is received from every incoming channel before performing the linear encoding. Then send the appropriate data on each outgoing channel. This physical realization of an LCM over an acyclic network, however, does not apply to a network that contains a directed cycle. This is illustrated by the following example.

Example 2

Let p, q, and r be vectors in Ω, where p and q are linearly independent. Define $v(SX) = p$, $v(SY) = q$ and $v(WX) = v(XY) = v(YW) = r$.

This specifies an *LCM* v on the network illustrated in Figure 19.18 if the vector r is a linear combination of p and q. Otherwise, the function v gives an example in which the law of information flow is observed for every single node but not observed for every set of nodes. Specifically, the law of information flow is observed for each of the nodes X, Y and W, but not for the set of nodes $\{X, Y, W\}$. Now, assume that $p = (1\,0)^T$, $q = (0\,1)^T$ and $r = (1\,1)^T$.

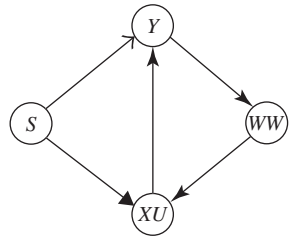

Figure 19.18 An LCM on a cyclic network.

Then, v is an LCM. Write the information vector as $(b_1\ b_2)$, where b_1 and b_2 belong to the base field of Ω. According to the transmission scheme associated with the LCM, all three channels on the directed cycle transmit the same data $b_1 + b_2$. This leads to the logical problem of how any of these cyclic channels acquires the data $b_1 + b_2$ in the first place.

In order to discuss the transmission scheme associated with an LCM over a network containing a directed cycle, we need to introduce the parameter of time into the scheme. Instead of transmitting a single data symbol (i.e. an element of the base field of Ω) through each channel, we shall transmit a time-parameterized stream of symbols. In other words, the channel will be time-slotted. As a consequence, the operation of coding at a node will be time-slotted as well.

19.5.4 Memoryless communication network

Given a communication network $(G,\ S)$ and a positive integer τ, the associated *memoryless* communication network denoted as $(G^{(\tau)},\ S)$ is defined as follows. The set of nodes in $G^{(\tau)}$ includes the node S and all the pairs of the type $[X, t]$, where X is a nonsource node in G and t ranges through integers $1 - \tau$. The channels in the network $(G^{(\tau)},\ S)$ belong to one of the three types listed below. For any nonsource nodes X and Y in $(G,\ S)$:

(1) for $t \leq \tau$, the multiplicity of the channel from S to $[X,\ t]$ is the same as that of the channel SX in the network $(G,\ S)$;

(2) for $t < \tau$, the multiplicity of the channel from $[X,\ t]$ to $[Y,\ t + 1]$ is the same as that of the channel XY in the network $(G,\ S)$;

(3) for $t < \tau$, the multiplicity of the channel from $[X,\ t]$ to $[X,\ \tau]$ is equal to $max\ flow_G(X) = mfG(X)$.

Lemma 2
The memoryless communication network $(G^{(\tau)},\ S)$ is acyclic.

Lemma 3
There exists a fixed number ε, independent of τ, such that for all nonsource nodes X in $(G,\ S)$, the maximum volume of a flow from S to the node $[X,\ \tau]$ in $(G^{(\tau)},\ S)$ is at least $\tau - \varepsilon$ times $mfG(X)$. For proof see Li *et al.* [47].

Transmission of data symbols over the network $(G^{(\tau)},\ S)$ may be interpreted as '*memoryless*' transmission of data *streams* over the network $(G,\ S)$ as follows:

(1) A symbol sent from S to $[X,\ t]$ in $(G^{(\tau)},\ S)$ corresponds to the symbol sent on the channel SX in $(G,\ S)$ during the time slot t.

(2) A symbol sent from $[X, t]$ to $[Y, t+1]$ in $(G^{(\tau)}, S)$ corresponds to the symbol sent on the channel XY in (G, S) during the time slot $t+1$. This symbol is a linear combination of symbols received by X during the time slot t and is unrelated to symbols received earlier by X.

(3) The channels from $[X, t]$ to $[X, t]$ for $t < \tau$ signify the accumulation of received information by the node X in (G, S) over time.

Since this is an acyclic network, the LCM on the network $(G^{(\tau)}, S)$ can be physically realized in the way mentioned above. The physical realization can then be interpreted as a *memoryless* transmission of data streams over the original network (G, S).

19.5.5 Network with memory

In this case we have to slightly modify the associated acyclic network.

Definition 1
Given a communication network (G, S) and a positive integer τ, the associated communication network *with memory*, denoted as $(G^{[\tau]}, S)$, is defined as follows. The set of nodes in $G^{[\tau]}$ includes the node S and all pairs of the type $[X, t]$, where X is a nonsource node in G and t ranges through integers 1 to τ. Channels in the network $(G^{[\tau]}, S)$ belong to one of the three types listed below. For any nonsource nodes X and Y in (G, S);

(1) for $t \leq \tau$, the multiplicity of the channel from S to $[X, t]$ is the same as that of the channel SX in the network (G, S);

(2) for $t < \tau$, the multiplicity of the channel from $[X, t]$ to $[Y, t+1]$ is the same as that of the channel XY in the network (G, S);

(3) for $t < \tau$, the multiplicity of channels from $[X, t]$ to $[X, t+1]$ is equal to $t \times mfG(X)$.

(4) The communication network $(G^{[\tau]}, S)$ is acyclic.

(5) Every flow from the source to the node X in the network $(G^{(\tau)}, S)$ corresponds to a flow with the same volume from the source to the node $[X, t]$ in the network $(G^{[\tau]}, S)$.

(6) Every *LCM* v on the network $(G^{(\tau)}, S)$ corresponds to an *LCM* u on the network $(G^{[\tau]}, S)$ such that for all nodes X in G: $\dim[u([X, \tau])] = \dim[v(X)]$.

19.5.6 Construction of a generic LCM on an acyclic network

Let the nodes in the acyclic network be sequentially indexed as $X_0 = S, X_1, X_2, \ldots, X_n$ such that every channel is from a smaller indexed node to a larger indexed node. The following procedure constructs an LCM by assigning a vector $v(XY)$ to each channel XY, one channel at a time.

```
{
  for all channels XY
    v(XY) = the zero vector; // initialization
  for (j = 0;   j ≤ n;   j++)
{
    arrange all outgoing channels X_j Y from X_j
     in an arbitrary order;
    take one outgoing channel from X_j at a time
```

```
    {
      let the channel taken be X_j Y;
      choose a vector w in the space v(X_j) such
      that w ∉ ⟨v(UZ) : UZ ∈ ξ⟩ for any collection
      ξ of at most d − 1 channels with
        v(X_j) ⊄ ⟨v(UZ) : UZ ∈ ξ⟩;
        v(X_j Y) = w;
      }
       v(X_{j+1}) = the linear span by vectors
       v(XX_{j+1}) on all incoming channels XX_{j+1}
       to  X_{j+1};
    }
}
```

The essence of the above procedure is to construct the generic LCM iteratively and make sure that in each step the partially constructed LCM is generic.

19.5.7 Time-invariant LCM and heuristic construction

In order to handle delays, we can use an element $a(z)$ of $F[(z)]$ to represent the z-transform of a stream of symbols $a_0, a_1, a_2, \ldots, a_t, \ldots$ that are sent on a channel, one symbol at a time. The formal variable z is interpreted as a unit-time shift. In particular, the vector assigned to an outgoing channel from a node is z *times* a linear combination of the vectors assigned to incoming channels to the same node. Hence a TILCM is completely determined by the vectors that it assigns to channels. On the communication network illustrated in Figure 19.18, define the TILCM v as

$$v(SX) = (1\ 0)^{\mathrm{T}},\ v(SY) = (0\ 1)^{\mathrm{T}},\ v(XY) = (z\ z^3)^{\mathrm{T}}$$
$$v(YW) = (z^2\ z)^{\mathrm{T}} \text{ and } v(WX) = (z^3\ z^2)$$

By formal transformation we have for example

$$\begin{aligned} v(XY) = (z\ z^3) &= z(1 - z^3)(1\ 0)^{\mathrm{T}} + z(z^3\ z^2)^{\mathrm{T}} \\ &= z[(1 - z^3)v(SX) + v(WX)] \end{aligned}$$

Thus, $v(XY)$ is equal to z times the linear combination of $v(SX)$ and $v(WX)$ with coefficients $1 - z^3$ and 1, respectively. This specifies an encoding process for the channel XY that does not change with time. It can be seen that the same is true for the encoding process of every other channel in the network. This explains the terminology '*time-invariant*' for an LCM.

To obtain further insight into the physical process write the information vector as $[a(z)\quad b(z)]$, where

$$a(z) = \sum_{j \geq 0} a_j z^j \text{ and } b(z) = \sum_{j \geq 0} b_j z^j$$

belong to $F[(z)]$. The product of the information (row) vector with the (column) vector assigned to that channel represents the data stream transmitted over a channel

$$\begin{aligned} [a(z)\quad b(z)] \cdot v(SX) &= [a(z)\quad b(z)] \cdot (1\ 0)^{\mathrm{T}} \\ &= a(z) \to (a_0, a_1, a_2, a_3, a_4, a_5, \ldots, a_t, \ldots)[a(z)\quad b(z)] \cdot v(SY) \\ &= b(z) \to (b_0, b_1, b_2, b_3, b_4, b_5, \ldots, b_t, \ldots)[a(z)\quad b(z)] \cdot v(XY) \\ &= za(z) + z^3 b(z) \to (0, a_0, a_1, a_2 + b_0, a_3 + b_1, a_4 + b_2, \ldots, \\ &\quad a_{t-1} + b_{t-3}, \ldots)[a(z)\quad b(z)] \cdot v(YW) \end{aligned}$$

$$= z^2a(z) + zb(z) \to (0, b_0, a_0 + b_1, a_1 + b_2, a_2 + b_3, a_3 + b_4, \ldots,$$
$$a_{t-2} + b_{t-1}, \ldots)[a(z) \quad b(z)] \cdot v(WX)$$
$$= z^3a(z) + z^2b(z) \to (0, 0, b_0, a_0 + b_1, a_1 + b_2, a_2 + b_3, \ldots,$$
$$a_{t-3} + b_{t-2}, \ldots)$$

Adopt the convention that $a_t = b_t = 0$ for all $t < 0$. Then the data symbol flowing over the channel XY, for example, at the time slot t is $a_{t-1} + b_{t-3}$ for all $t \geq 0$. If infinite loops are allowed, then the previous definition of TILCM v is modified as follows:

$$v(SX) = (1\ 0)^{\mathrm{T}}, \quad v(SY) = (0\ 1)^{\mathrm{T}}$$
$$v(XY) = (1 - z^3)^{-1}(z\ z^3)^{\mathrm{T}}, \quad v(YW) = (1 - z^3)^{-1}(z^2\ z)^{\mathrm{T}}$$

and

$$v(WX) = (1 - z^3)^{-1}(z^3\ z^2)$$

The data stream transmitted over the channel XY, for instance, is represented by

$$\left(\sum_{j\geq 0} a_j z^j \sum_{j\geq 0} b_j z^j\right) \cdot v(XY) = \sum_{j\geq 0}(a_j z^{j+1} + b_j z^{j+3})/(1 - z^3)$$
$$= \left[\sum_{j\geq 0}\left(a_j z^{j+1} + b_j z^{j+3}\right)\right] \sum_{i\geq 0} z^{3i} = \sum_{j\geq 0}\sum_{j\geq 0}\left(a_j z^{3i+j+1} + b_j z^{3i+j+3}\right)$$
$$= \sum_{t\geq 1} z^t(a_{t-1} + a_{t-4} + a_{t-7} + \cdots + b_{t-3} + b_{t-6} + b_{t-9} + \cdots)$$

That is, the data symbol $a_{t-1} + a_{t-4} + a_{t-7} + \cdots + b_{t-3} + b_{t-6} + b_{t-9} + \cdots$ is sent on the channel XY at the time slot t. This TILCM v, besides being time invariant in nature, is a 'memoryless' one because the following linear equations allows an encoding mechanism that requires no memory:

$$v(XY) = zv(SX) + zv(WX)$$
$$v(YW) = zv(SY) + zv(XY) \tag{19.60}$$

and

$$v(WX) = zv(YW)$$

19.5.7.1 TILCM construction

There are potentially various ways to define a *generic* TILCM and, to establish desirable dimensions of the module assigned to every node. In this section we present a heuristic construction procedure based on graph-theoretical *block decomposition* of the network. For the sake of computational efficiency, the procedure will first remove '*redundant*' channels from the network before identifying the 'blocks' so that the 'blocks' are smaller. A channel in a communication network is said to be *irredundant* if it is on a simple path starting at the source. otherwise, it is said to be *redundant*. Moreover, a communication network is said to be *irredundant* if it contains no redundant channels. In the network illustrated in Figure 19.19, the channels ZX, TX and TZ are redundant.

The deletion of a redundant channel from a network results in a subnetwork with the same set of irredundant channels. Consequently, the irredundant channels in a network define an irredundant subnetwork. It can be also shown that, if v is an LCM (respectively, a TILCM) on a network, then v also defines an LCM (respectively, a TILCM) on the subnetwork that results from the deletion of any redundant channel. In addition we say that two nodes are equivalent if there exists

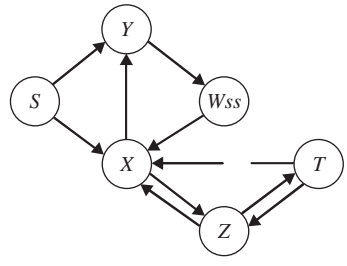

Figure 19.19 Redundant channels in a network.

a directed path leading from one node to the other and vice versa. An equivalence class under this relationship is called a *block* in the graph. The source node by itself always forms a block. When every block '*contracts*' into a single node, the resulting graph is acyclic. In other words, the blocks can be sequentially indexed so that every interblock channel is from a smaller indexed block to a larger indexed block.

For the construction of a 'good' TILCM, smaller sizes of blocks tend to facilitate the computation. The extreme favorable case of the block decomposition of a network is when the network is acyclic, which implies that every block consists of a single node. The opposite extreme is when all nonsource nodes form a single block exemplified by the network illustrated in Figure 19.19. The removal of redundant channels sometimes serves for the purpose of breaking up a block into pieces. For the network illustrated in Figure 19.19, the removal of the three redundant channels breaks the block $\{T, W, X, Y, Z\}$ into the three blocks $\{T\}, \{W, X, Y\}$ and $\{Z\}$.

In the construction of a 'good' LCM on an *acyclic* network, as before, the procedure takes one node at a time according to the acyclic ordering of nodes and assigns vectors to outgoing channels from the taken node. For a general network, we can start with the trivial TILCM v on the network consisting of just the source and then expand it to a 'good' TILCM v that covers one more block at a time.

The sequential choices of blocks are according to the acyclic order in the block decomposition of the network. Thus, the expansion of the 'good' TILCM v at each step involves only *incoming* channels to nodes in the new block. A heuristic algorithm for assigning vectors $v(XY)$ to such channels XY is for $v(XY)$ to be z times an *arbitrary convenient* linear combination of vectors assigned to incoming channels to X. In this way, a system of linear equations of the form of $Ax = b$ is set up, where A is a square matrix with the dimension equal to the total number of channels in the network and x is the unknown column vector whose entries are $v(XY)$ for all channels XY. The elements of A and b are polynomials in z. In particular, the elements of A are either $\pm 1, 0$, or a polynomial in z containing the factor z. Therefore, the determinant of A is a formal power series with the constant term (the zeroth power of z) being ± 1, and, hence is invertible in $F(z)$. According to Cramer's rule, a unique solution exists. This is consistent with the physical intuition because the whole network is completely determined once the encoding process for each channel is specified. If this unique solution does not happen to satisfy the requirement for being a 'good' TILCM, then the heuristic algorithm calls for adjustments on the coefficients of the linear equations on the trial-and-error basis.

After a 'good' TILCM is constructed on the subnetwork formed by irredundant channels in a given network, we may simply assign the zero vectors to all redundant channels.

Example

After the removal of redundant channels, the network depicted by Figure 19.19 consists of four blocks in the order of $\{S\}, \{W, X, Y\}, \{Z\}$ and $\{T\}$. The subnetwork consisting of the first two

blocks is the same as the network in Figure 19.18. When we expand the trivial TILCM on the network consisting of just the source to cover the block $\{W, X, Y\}$, a heuristic trial would be

$$v(SX) = (1\ 0)^T \quad v(SY) = (0\ 1)^T$$

together with the following linear equations:

$$v(XY) = zv(SX) + zv(WX)$$
$$v(YW) = zv(SY) + zv(XY)$$

and

$$v(WX) = zv(YW).$$

The result is the memoryless TILCM v in the preceding example. This TILCM can be further expanded to cover the block $\{Z\}$ and then the block $\{T\}$.

19.6 CAPACITY OF WIRELESS NETWORKS USING MIMO TECHNOLOGY

In this section an information theoretic network objective function is formulated, which takes full advantage of multiple input multiple output (MIMO) channels. The demand for efficient data communications has fueled a tremendous amount of research into maximizing the performance of wireless networks. Much of that work has gone into enhancing the design of the receiver, however considerable gains can be achieved by optimizing the transmitter.

A key tool for optimizing transmitter performance is the use of channel reciprocity. Exploitation of channel reciprocity makes the design of optimal transmit weights far simpler. It has been recognized that network objective functions that can be characterized as functions of the output signal-to-interference noise ratio (SINR) are well suited to the exploitation of reciprocity, since it permits us to relate the uplink and downlink objective functions [48–50]. It is desirable, however, to relate the network objective function to information theory directly, rather than *ad-hoc* SINR formulations, due to the promise of obtaining optimal channel capacity. This section demonstrates a link between the information theoretic, Gaussian interference channel [51] and a practical network objective function that can be optimized in a simple fashion and can exploit channel reciprocity. The formulation of the objective function permits a water filling [52] optimal power control solution, that can exploit multipath modes, MIMO channels and multipoint networks.

Consider the network of transceivers suggested by Figure 19.20. Each transceiver is labeled by a node number. The nodes are divided into two groups. The group 1 nodes transmit in a given time-slot, while the group 2 nodes receive. In alternate time-slots, group 2 nodes transmit, while group 1 nodes receive, according to a time division duplex (TDD) transmission scheme.

The channel is assumed to be channelized into several narrow band frequency channels, whose bandwidth is small enough so that all multipath is assumed to add coherently. This assumption allows the channel between any transmit antenna and any receive antenna to be modeled as a single complex gain and is consistent with an orthogonal frequency division multiplexing (OFDM) modulation scheme. All transceivers are assumed to have either multiple antennas or polarization diversity, for both transmit and receive processing. The link connecting nodes may experience multipath reflections. For this analysis we assume that the receiver synchronizes to a given transmitter and removes any propagation delay offsets. The channel, for a given narrow band, between the transmitter and receiver arrays is therefore modeled as a complex matrix multiply.

Let ℓ_1 be an index into the group 1 transceivers, and ℓ_2 an index into the group 2 transceivers. When node ℓ_2 is transmitting during the uplink, we model the channel between the two nodes as a complex matrix $\mathbf{H}_{12}(\ell_1, \ell_2)$ of dimension $M_1(\ell_1) \times M_2(\ell_2)$, where $M_1(\ell_1)$ is the size of the antenna array at node ℓ_1, and $M_2(\ell_2)$ is the size of the array at node ℓ_2. Polarization diversity is treated

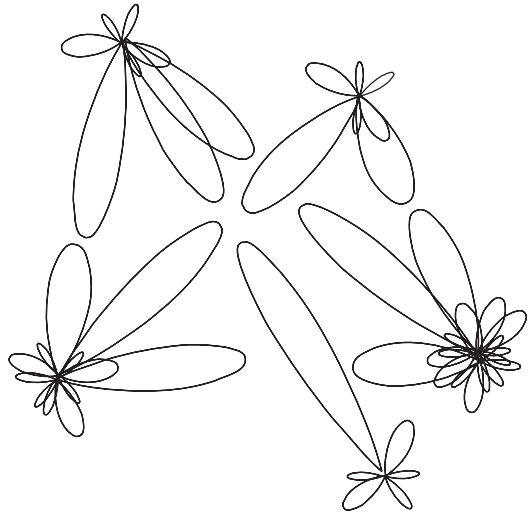

Figure 19.20 Network layout.

like additional antennae. In the next TDD time slot, during the downlink, node ℓ_1 will transmit and the channel from ℓ_1 to ℓ_2 is described by the complex $M_2(\ell_1) \times M_1(\ell_2)$ matrix $\mathbf{H}_{21}(\ell_2, \ell_1)$. For every node pair (ℓ_1, ℓ_2) that forms a communications link in the network, we assign a MIMO channel link number, indexed by k or m, in order to label all such connections established by the network. Obviously not every node pair is necessarily assigned a link number, only those that actually communicate. We also define the mapping from the MIMO link number to the associated group 1 node, $\ell_1(k)$ and the associated group 2 node $\ell_2(k)$ by the association of k with the link $[\ell_1(k), \ell_2(k)]$. Because each channel is MIMO, a given node will transmit multiple symbols over possibly more than one transmission mode. The set of all transmission modes over the entire network is indexed by q and p. This index represents all the symbol streams that are transmitted from one node to another and therefore represents a lower level link number. The low level link numbers will map to its MIMO channel link, via the mapping $k(q)$. Because our network will exploit channel reciprocity, we assume that every uplink symbol stream indexed by q has an associated downlink symbol stream assigned to the same index. The q'th uplink symbol stream is spread by an $M_1(q) \times 1$ complex vector $g_1(q)$, where $M_1(q) \equiv M_1\{\ell_1[k(q)]\}$. Similarly $g_2(q)$ is the associated transmit vector for the downlink.

For each node, we group the transmit vectors into a single matrix,

$$\mathbf{G}_2(k) \equiv \left[g_2(q_1), g_2(q_2), \ldots, g_2(q_{M_c(k)})\right] \tag{19.61}$$

and

$$\mathbf{G}_1(k) \equiv \left[g_1(q_1), g_1(q_2), \ldots, g_1(q_{M_c(k)})\right] \tag{19.62}$$

where $k(q_i) = k$ and there are $M_c(k)$ transmission modes associated with MIMO link k. With these conventions the signal model can be written as:

$$\mathbf{x}_1(n;k) = \mathbf{i}_1(n;k) + \mathbf{H}_{12}(k,k)\mathbf{G}_2(k)\mathbf{d}_2(n;k) \tag{19.63}$$

$$\mathbf{x}_2(n;k) = \mathbf{i}_2(n;k) + \mathbf{H}_{21}(k,k)\mathbf{G}_1(k)\mathbf{d}_1(n;k) \tag{19.64}$$

where $\mathbf{x}_1(n;k)$ is the received complex data vector at sample n, and node $\ell_1(k), \mathbf{H}_{12}(k,m) \equiv \mathrm{H}_{12}[\ell_1(k), \ell_2(m)]$ is the $M_1[\ell_1(k)] \times M_2[\ell_2(m)]$ complex MIMO channel matrix for downlink

transmission, n is a time/frequency index, that represents an independent reuse of the channel, either due to adjacent frequency channels (e.g. adjacent OFDM channels) or due to multiple independent time samples, $\mathbf{i}_1(n;k)$ is the interference vector seen at node $\ell_1(k)$ due to the other transmitting nodes as well as due to background radiation, and $\mathbf{d}_2(n;k)$ is the $M_c(k) \times 1$ downlink information symbol vector, transmitted for sample n. The analogous model for the uplink case is shown in (4). The interference vector can be written as

$$\mathbf{i}_r(n;k) = \sum_{m \neq k} \mathbf{H}_{rt}(k,m) G_t(m) \mathbf{d}_t(n;m) + \varepsilon_r(n,k) \tag{19.65}$$

where $\varepsilon_r(n,k), r = \{1,2\}$, is the background radiation noise vector seen by the receiving node $\ell_r(k)$ and $t = \{2,1\}$ is the transmission timeslot indicator. The convention is adopted that $t = 2$ if $r = 1$, otherwise $t = 1$ when $r = 2$.

19.6.1 Capacity metrics

In this section we will be interested in the asymptotic maximum achievable throughput under certain network constraints:

(1) We will assume that signal energy from all the nodes in the network, other than the one from the link being processed, is treated as interference. This is due to difficulty of synchronizing a node to multiple interference sources and reduces the complexity of the receiver.

(2) The interference $\mathbf{i}_r(n;k)$ is modeled as complex circular Gaussian noise. The superposition of many distant interferers will appear Gaussian by the central limit theorem.

Considering therefore the channel model described by Equations (19.63) and (19.65), we can write the mutual information between the source data vector and the received data vector as [52, 53]:

$$I[\mathbf{x}_r(k); \mathbf{d}_t(k)] = \log_2 \left| \mathbf{I} + \mathbf{R}^{-1}_{i_r i_r}(k) \mathbf{R}_{s_t s_t}(k) \right| \triangleq C_{rt}(k; \mathbf{G}_t) \tag{19.66}$$

where, $\mathbf{G}_t \leftrightarrow \{g_t(q)\}$ represents all transmit weights stacked into a single parameter vector and where we neglect the n dependency for the random vectors $\mathbf{x}_r(n;k)$ and $\mathbf{d}_t(n;k)$. The interference and the signal covariance matrices are defined as:

$$\mathbf{R}_{i_r i_r}(k) \triangleq \sum_{m \neq k} \mathbf{A}_{rt}(k,m) A^H_{rt}(k,m) + \mathbf{R}_{\varepsilon_r \varepsilon_r}(k) \tag{19.67}$$

$$\mathbf{A}_{rt}(k,m) \triangleq \mathbf{H}_{rt}(k,m) \mathbf{G}_t(m) \tag{19.68}$$

$$\mathbf{R}_{s_t s_t}(k) \triangleq \mathbf{A}_{rt}(k,k) \mathbf{A}^H_{rt}(k,k), \tag{19.69}$$

and where $\mathbf{R}_{\varepsilon_r \varepsilon_r}(k)$ is the covariance of the background noise vector $\varepsilon_r(n,k)$. The covariance of the source statistics is assumed governed by the transmit weights $\mathbf{G}_t(k)$, therefore the covariance of $\mathbf{d}_t(k)$ is assumed to be the identity matrix.

Let us now consider the introduction of complex linear beam-forming weights at the receiver. For each low level link q, we assign a receive weight vector $\mathbf{w}_r(q), r \in \{1,2\}$ for use at receiver $\ell_r[\mathbf{k}(q)]$. The weights, in theory, are used to copy the transmitted information symbol,

$$\hat{d}_t(n;q) \triangleq w_r^{\mathrm{H}}(q) x_r(n;k) \tag{19.70}$$

$$= \mathbf{w}_r^{\mathrm{H}}(q) \mathbf{i}_r(n;k) + \mathbf{w}_r^{\mathrm{H}}(q) \mathbf{A}_{rt}(k,k) \mathbf{d}_t(n;k) \tag{19.71}$$

$k(q) = k$ where,

$$\mathbf{d}_t(n;k) \equiv \left[d_t(q_1), d_t(q_2), \ldots d_t(q_{M_c(k)}) \right]^{\mathrm{T}} \tag{19.72}$$

and $k(q_j) = k$. The vector version of this can be written as:

$$\hat{\mathbf{d}}_t(n;k) = \mathbf{W}_r^{\mathrm{H}}(k)\mathbf{i}_r(n;k) \; + \; \mathbf{W}_r^{\mathrm{H}}(k)\mathbf{A}_{rt}(k,k)\mathbf{d}_t(n;k) \tag{19.73}$$

where

$$\mathbf{W}_r(k) \equiv \left[\mathbf{w}_r(q_1), \mathbf{w}_r(q_2), \cdots \mathbf{w}_r(q_{M_c(k)})\right] \tag{19.74}$$

and $k(q_j) = k$. The structure of the transceiver channel model is illustrated in Figure 19.21 for the uplink case, highlighting the first $M_c(k)$ low-level links, all assumed to be associated with the same MIMO-channel link. The MIMO channel link index k and sample index n are omitted for simplicity. The downlink case is the same after the 1 and 2 indices are swapped.

Owing to the additional processing [52], the mutual information either remains the same or is reduced by the application of the linear receive weights,

$$I[\hat{\mathbf{d}}_t(k); \mathbf{d}_t(k)] \leq I[\mathbf{x}_r(k); \mathbf{d}_t(k)] \tag{19.75}$$

In addition to inequality, Equation (19.75), it can be also shown [54, 55] that, if the source symbols $d_t(q)$ are mutually independent then,

$$I\left[\hat{\mathbf{d}}_t(k); \mathbf{d}_t(k)\right] \geq \sum_{q:\, k(q)=k} I\left[\hat{d}_t(q); d_t(q)\right] \tag{19.76}$$

The lower bound of in Equation (19.76) is referred to as the decoupled capacity and can be written as:

$$D_{rt}(k; \mathbf{W}_r, \mathbf{G}_t) \equiv \sum_{q:\, k(q)=k} I[\hat{d}_t(q); d_t(q)] \tag{19.77}$$

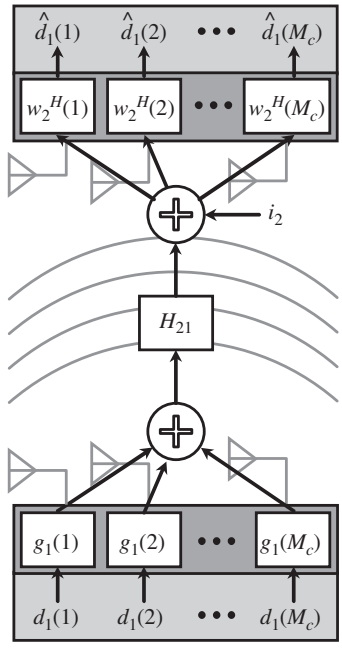

Figure 19.21 Uplink transceiver channel model.

where the collection of all receive weights is stacked into the parameter vector $\mathbf{W}_r \leftrightarrow \{\mathbf{w}_r(q)\}$. Equations (19.75) and (19.76) demonstrate that

$$C_{rt}(k;\mathbf{G}_t) \geq D_{rt}(k;\mathbf{W}_r,\mathbf{G}_t) \tag{19.78}$$

The decoupled capacity is implicitly a function of the *transmit weights* $\mathbf{g}_t(q)$ and the *receive weights* $\mathbf{w}_r(q)$. Optimizing over these weights can always acheive the full capacity of the Gaussian interference channel and hence the upper bounds in Equation (19.78).

First we write $\hat{d}_t(n;q)$ as,

$$\hat{d}_t(n;q) = \mathbf{w}_r^{\mathrm{H}}(q)\mathbf{a}_r(q) + \mathbf{w}_r^{\mathrm{H}}(q)\mathbf{i}_r(q),$$

$$i_r(n;q) \equiv \sum_{p\neq q} \mathbf{H}_{rt}[k,k(p)]\mathbf{g}_t(p)d_t(n;p) + \varepsilon_r(n,k)$$

$$\mathbf{a}_r(q) \equiv \mathbf{H}_{rt}(k,k)\mathbf{g}_t(q), k = k(q) \tag{19.79}$$

Now the mutual information on the right-hand side of Equation (19.55a) can be written as,

$$I\left[\hat{d}_t(q);d_t(q)\right] = \log_2\left(1+\frac{|\mathbf{w}_r^{\mathrm{H}}(q)\mathbf{a}_r(q)|^2}{\mathbf{w}_r^{\mathrm{H}}(q)\mathbf{R}_{i_ri_r}(q)\mathbf{w}_r}\right) \tag{19.80}$$

$$R_{i_ri_r}(q) = R_{i_ri_r}(k) + \cdots \quad H_{rt}(k,k)\left(\sum_{\substack{p:k(p)=k\\ p\neq q}} = g_t(p)g_t^{\mathrm{H}}(p)\right)H_{rt}^{\mathrm{H}}(k,k)$$

$$= \quad R_{i_ri_r}(k) + \sum_{\substack{p:k(p)=k\\ p\neq q}} a_r(p)d_r^{\mathrm{H}}(p) \tag{19.81}$$

where $k = k(q)$. In the following we will also use the fact that scrambling the transmit weights by an orthonormal scrambling matrix does not change the values of the mutual informations for the Gaussian interference channel. In other words, if

$$\tilde{\mathbf{G}}_t(k) \stackrel{\Delta}{=} \mathbf{G}_t(k)\mathbf{V}_t(k) \tag{19.82}$$

$$\mathbf{V}_t(k)\mathbf{V}_t^{\mathrm{H}}(k) = \mathbf{I}$$

then for all k,

$$C_{rt}(k;\tilde{\mathbf{G}}) = C_{rt}(k;\mathbf{G}) \tag{19.83}$$

where $\tilde{\mathbf{G}} \leftrightarrow \{\tilde{\mathbf{g}}_t(q)\}$ is the parameter vector of all stacked, scrambled transmit weights, $\tilde{\mathbf{g}}_t(q)$ drawn from the columns of $\tilde{\mathbf{G}}_\mathbf{t}(k)$. The proof is based on the fact that the mutual information is completely determined by the statistics, $\mathbf{R}_{\mathbf{i_ri_r}}(k)$ and $\mathbf{R}_{\mathbf{s_ts_t}}(k)$. From Equations (19.67) and (19.47), these depend only on the outer products $\mathbf{G}_t(m)\mathbf{G}_t^{\mathrm{H}}(m)$, which are invariant with respect to orthonormal scrambling because $\tilde{\mathbf{G}}_t(m)\,\tilde{\mathbf{G}}_t^{\mathrm{H}}(m) = \mathbf{G}_t(m)\mathbf{G}_t^{\mathrm{H}}(m)$. Therefore replacing $\mathbf{G}_t(m)$ with $\tilde{\mathbf{G}}_t(m)$ does not change the mutual information. Based on this we have the following relation. For any set of network wide transmit weights $\mathbf{G}$, there exists a set of receive weights $\hat{\mathbf{w}}_\mathbf{r}(q)$ and transmit weights $\tilde{\mathbf{g}}_t(q)$ such that for all k,

$$C_{rt}(k;\mathbf{G}_t) = C_{rt}(k;\tilde{\mathbf{G}}_t) = D_{rt}(k;\hat{\mathbf{W}}_r,\tilde{\mathbf{G}}_t) \tag{19.84}$$

where $\hat{\mathbf{W}}_r \leftrightarrow \{\hat{\mathbf{w}}_\mathbf{r}(q)\}$ and $\tilde{\mathbf{G}}_\mathbf{t} \leftrightarrow \{\tilde{\mathbf{g}}_t(q)\}$. Given the transmit weights $\tilde{\mathbf{G}}_t$, the receive weights can be found from

$$\hat{\mathbf{w}}_r(q) = \arg\max_{\mathbf{w}_r(q)} I[\hat{d}_t(q);d_t(q)] = \arg\max_{\mathbf{w}_r(q)} \gamma_r(q) = \mathbf{R}_{\mathbf{i_ri_r}}^{-\mathbf{1}}(q)\mathbf{a}_r(q) \tag{19.85a}$$

where $\gamma_r(q)$ is the output signal to interference noise ratio (SINR) given by,

$$\gamma_r(q) \triangleq \frac{|\mathbf{w}_r^{\mathrm{H}}(q)\mathbf{a}_r(q)|^2}{\mathbf{w}_r^{\mathrm{H}}(q)\mathbf{R}_{\mathbf{i_r i_r}}(q)\mathbf{w}_r(q)} \tag{19.85b}$$

For the formal proof see References [54–57]. Equations (19.84)–(19.85) are significant because they allow us to optimize the Gaussian interference channel using decoupled capacity. The decoupled capacity can be shown to obey the reciprocity theorem [54, 55], which permits us to relate uplink network metrics to downlink network metrics. We can either consider minimizing total power subject to a channel capacity constraint, or maximizing channel capacity subject to a transmit power constraint.

In References [54, 55] a technique called locally enabled global optimization (LEGO) is designed to fully exploit the reciprocity theorem. This technique transforms the optimization over the transmit powers to one over the set of achievable output SINRs in Equation (19.85). The LEGO algorithm can be efficiently implemented using local information, and requires only an estimate of the post beamforming interference power, $y_r(q) \equiv \mathbf{w}_r^{\mathrm{H}}(q)\mathbf{R}_{\mathbf{i_r i_r}}\mathbf{w}_r(q)$, and an estimate of the post-beamforming channel gain, $T_{rt}(q,q) \equiv |\mathbf{w}_r^{\mathrm{H}}(q)\mathbf{H}_{rt}[k(q),k(q)]\mathbf{g}_t(q)|^2$. If a collection of links through which we desire to compute a channel capacity is $Q(m) \triangleq \{q : k(q) = m\}$, then the algorithm can be summarized as below.

Algorithm 1: LEGO

(1) Update the remote receiver weights for every link during downlink transmission:

$$\mathbf{w}'_1(p) = \arg\max_{\mathbf{w}_1(p)} \gamma_1(p)$$

(2) Set the remote transmit weights to a scaled version of the conjugated receive weights,

$$\mathbf{g}_1(p) = \mathbf{w}_1^*(p)\sqrt{\pi_l(p)/[\mathbf{w}_1^H(p)\mathbf{R}_{\varepsilon_r\varepsilon_r}\mathbf{w}_1(p)]}$$

(3) For each link p, estimate the associated post-beamforming interference power $y_1(p)$ and relay this information back to the base station.

(4) Update the base receiver weights for every link during uplink transmission:

$$\mathbf{w}'_2(p) = \arg\max_{\mathbf{w}_2(p)} \gamma_2(p).$$

(5) For each link p, estimate the associated post-beamforming interference power $y_2(p)$.

(6) Update the target SINR for each link, by optimizing the linearized model over each aggregate set m:

$$\gamma(q) = \arg\min_{\gamma(q)} \sum_{q\in Q(m)} \gamma(q)\frac{y_1(q)y_2(q)}{T_{12}(q,q)} s.t.c(m) \quad \leq \quad \sum_{q\in Q(m)} \log[1+\gamma(q)]$$

for $q \in Q(m)$,

$$\gamma(p)' = \alpha[\hat{\gamma}(p) - \gamma(p)] + \gamma(p), \textit{for some } 0 < \alpha \leq 1 (\alpha \textit{ is initially set to 1).}$$

(7) Update the downlink transmit powers $\pi_2(q)$:

$$\pi_2'(q) = \gamma(q)y_1(q)/T_{12}(q,q)$$

(8) Update the uplink transmit powers $\pi_1(q)$ and relay them back to the remote units. $\pi_1'(q) = \gamma(q)y_2(q)/T_{21}(q,q)$.

(9) Set the base transmit weights to a scaled version of the conjugated receive weights,

$$g_2(p) = \mathbf{w}_2^*(p)\sqrt{\pi_2(p)/\left[\mathbf{w}_2^H(p)\mathbf{R}_{\varepsilon_r\varepsilon_r}\mathbf{w}_2(p)\right]}$$

(10) Return to step 1.

References [54, 55] provide a numerical example of a four-cell wireless network as illustrated in Figure 19.22. Each 1 km radius cell contains two remote units (RU), each of which communicates to two base stations. The base stations have eight antennae and the RUs two antennae. There are eight

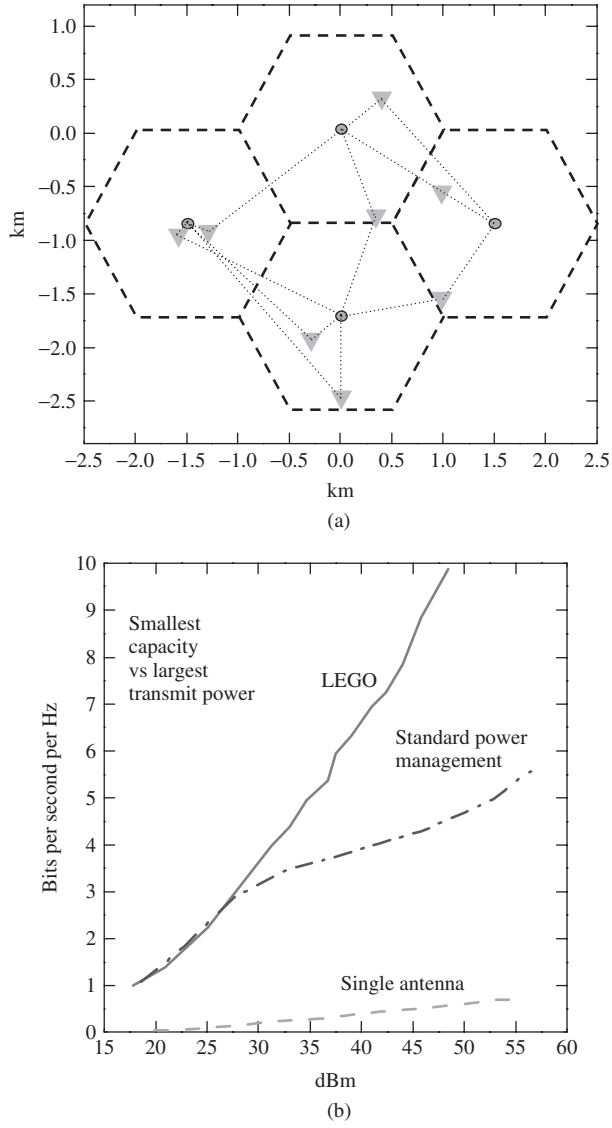

Figure 19.22 (a) Cell network geometry; (b) LEGO performance: worst case capacity vs worst transmit power. (Reproduced by permission of IEEE [55].)

independent 50 kHz channels and thus each RU has 16 transmit modes [i.e. each $Q(m)$ contains 16 links]. The performance of LEGO is compared with a standard power management algorithm, that seeks to transmit a constant power for each link from each base station, and a single antenna network, that uses frequency division multiplexing to isolate each RU into a separate channel. Background radiation is assumed to be thermal white noise at room temperature, with an added 10 dB noise figure. As can be seen from the figure, the performance improvement of the LEGO algorithm is significant.

19.7 CAPACITY OF SENSOR NETWORKS WITH MANY-TO-ONE TRANSMISSIONS

In sensor networks the many-to-one throughput capacity is the *per source data throughput*, when all or many of the sources are transmitting to a single fixed receiver or sink [58–63]. Earlier in this chapter we have shown that the achievable per node throughput in a wireless network is $\theta\left[W/(n\log n)\right]$, where W is the transmission capacity and n is the total number of nodes in the network.

The result was based on the assumption that communications are one-to-one, and that sources and destinations are randomly chosen. It does not apply to scenarios where there are communication hot spots in the network. Since many-to-one communication causes the sink to become a point of traffic concentration, the throughput achievable per source node in this case is reduced. In this section we are only interested in the case where every source gets an equal (on average) amount of original data (not including relayed data) across to the sink. This is because otherwise throughput can be maximized by having only the sensors closest to the destination transmit. Equal share of throughput from every sensor is desired for applications like imaging where each sensor represents a certain region of the whole field and data from each part are equally important. When distributed data compression is used, this is again approximately the case. However, when conditional coding is used this may no longer be true, since the amount of processed data can vary from source to source. In order to achieve the above goal we use the following assumptions about the network architecture.

19.7.1 Network architecture

(1) The network is deployed in a field of circular shape. There are n nodes, sources (we will use nodes, sources and sensors interchangeably in subsequent discussions) deployed in a network. A sink/destination is located at the center of the network/circle. Each node is not only a source of data, but also a relay for some other sources to reach the sink.

(2) A network where the nodes are randomly placed following a uniform distribution will be referred to as a randomly deployed network or a random network. In such a network we have no direct control over the exact location of the nodes. A network where we can determine the exact locations of the nodes will be referred to a as an arbitrary network.

(3) Two network organizational architectures are considered: (a) a flat architecture where nodes communicate with the sink via possibly multi-hop routes by using peer nodes as relays; and (b) hierarchical architecture, where clusters are formed so that sources within a cluster send their data (via a single hop or multihop depending on the size of the cluster) to a designated node known as the clusterhead. The clusterhead can potentially perform data aggregation and processing and then forward data to the sink. In this study, we will assume that the clusterheads serve as simple relays and no data aggregation is performed. We will also assume that the communication between nodes and clusterheads and communication between clusterheads and the sink are on separate frequency channels so that the two layers do not interfere.

(4) Throughout the section we will assume that the sources transmit following a schedule that consists of time slots.

(5) To simplify the resulting expressions, we assume the field has an area of 1. Nodes share a common wireless channel using omnidirectional antennas. We assume nodes use a fixed transmission power and achieve a fixed transmission range. We adopt the commonly used interference model, as earlier in this chapter. Let X_i and X_j be two sources with distance $d_{i,j}$ between them. Then the transmission from X_i to X_j will be successful if and only if

$$d_{i,j} \leq r \text{ and } d_{k,j} > r + \Delta, \Delta \geq 0 \tag{19.76}$$

for any source X_k that is simultaneously transmitting. In the following r will be referred to as the transmission range. There are two interference concepts here. A node may interfere with another node that is transmitting if it is within distance $2r + \Delta$ of that node. To see this consider two transmitting nodes. If one node is within $2r + \Delta$ of the other node there will be an overlap between a circle of radius r around the first transmitting node and a circle of radius $r + \Delta$ around the second transmitting node. If the intended receiver is located within the overlapping area the transmission will fail because of interference. Therefore the two nodes need to be at least $2r + \Delta$ apart. On the other hand a node will interfere with another node that is receiving if it is within distance $r + \Delta$ for obvious reasons. In the following both will be generally referred to as interference range. The distinction will be clear from the context. Also note that this interference model, Equation (19.76), essentially implies that no nodes can receive more than one transmission at a time. We will also assume that no node can transmit and receive at the same time.

(6) The network scenario is depicted in Figure 19.23. The sink is placed at the center of this field. It receives all data generated by sources in the network.

(7) In the following W refers to the transmission capacity of the channel in a flat network. In a hierarchical network W refers to the transmission capacity of the channel used within clusters. W' refers to the transmission capacity of the channel used from the heads to the sink. The capacity is derived as a function of the transmission range, assuming the transmission range can provide connectivity.

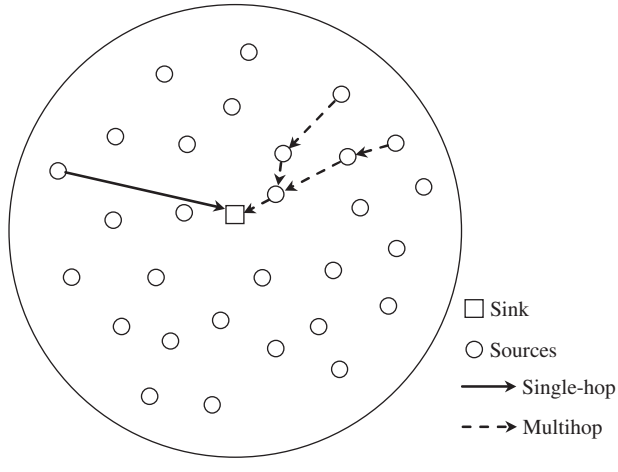

Figure 19.23 Many-to-one network scenario.

19.7.2 Capacity results

In this section we summarize capacity results for the *network defined above*. For formal proofs of the results the reader is referred to References [58–63].

19.7.2.1 Capacity in a flat network

(1) The maximum per node throughput in the network is upper bounded by W/n.

(2) $\lambda = W/n$ can be achieved when every source can directly reach the sink.

(3) $\lambda = W/n$ is not achievable if not every source can directly reach the destination and $\Delta > r$.

(4) $\lambda = W/n$ may be achieved in an arbitrary network when not every source can directly reach the destination and $\Delta < r$.

When the sink cannot directly receive from every source in the network, and assuming that the channel allocation does not take into account difference in traffic load, then $\lambda = W/n$ is not achievable with high probability regardless of the value of Δ. In this case we will use the upper bound on throughput by deriving the maximum number of simultaneous transmissions.

Denote by A_r the area of a circle of radius r, i.e. $A_r = \pi r^2$. Let random variable V_r denote the number of nodes within an area of size A_r and assume a total area of 1. We then have [58–63]:

(5) In a randomly deployed network with n nodes,

$$Pr\left(nA_r - \sqrt{\alpha_n n} \leq V_r \leq nA_r + \sqrt{\alpha_n n}\right) \rightarrow 1 \text{ as } n \rightarrow \infty$$

where the sequence $\{\alpha_n\}$ is such that $\lim_{n\rightarrow\infty} \alpha n/n = \varepsilon$, ε being positive but arbitrarily small.

(6) If a network has randomly deployed sources and the transmission range r is such that not all sources can directly reach the sink, then with high probability the throughput upper bound $\lambda = W/n$ is not achievable.

(7) A randomly deployed network using multihop transmission for many-to-one communication can achieve throughput

$$\lambda \geq W\left(\pi r^2 - \sqrt{\varepsilon}\right) / \left\{n\left(4\pi r^2 + 4\pi r\Delta + \pi\Delta^2 + \sqrt{\varepsilon}\right)\right\}$$

with high probability, when no knowledge of the traffic load is assumed and ε is as given in (1).

In the following we will use a concept of *virtual sources*. As an example consider a simple network consisting of three sources and a sink, shown in Figure 19.24(a). The distance between adjacent nodes is r. Regardless of the value of Δ, when one source transmits, it interferes with all other sources in this network. Therefore only one source can transmit at a time. The number of interfering neighbors for any of the sources is two, which is the highest degree of the graph that represents the interference relationship in this network. Thus a schedule of length 3 allows all sources to transmit once during the schedule. The load on the source closest to the sink, source 3, is 3λ, since it carries the traffic of all three sources. The achievable throughput is then calculated as $3\lambda = W/3$, thus $\lambda = W/9$.

The way the schedule was calculated previously assigned the same share of the resources (time) to all the sources. Since we used the source with the highest need of resource (the one carrying the most traffic) to calculate the amount of resource needed, every other source is wasting resource. In our example we are giving every source the possibility of making three transmissions. Source 3 does indeed need all three transmissions, but source 2 only needs two and source 1 only needs one,

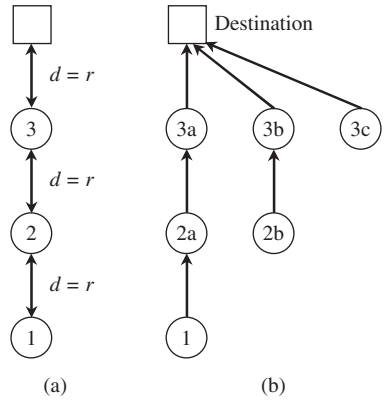

Figure 19.24 (a) Chain network (b) virtual sources.

hence a total of six transmissions. Now consider a similar network, only this time we have three sources that can reach the sink, shown in Figure 19.24(b). We create a schedule where each one of the sources gets to transmit once and once only. However this time not all sources generate data. Using labels shown in Figure 19.24(b), source 1 generates a packet and transmits it to source $2a$. Source $2a$ relays the packet to source $3a$, which then relays it to the sink. Then source $2b$ generates a packet and transmits it to source $3b$, which relays it to the sink. Finally source $3c$ generates and transmits a packet to the destination. We can view each raw of sources in this network as an equivalent of a single source in the previous example, i.e. $2a$ and $2b$ combined are equivalent to 2 in Figure 19.24(a); $3a$, $3b$ and $3c$ combined are equivalent to 3, in terms of interference and traffic load. We will define sources $2a, 2b$ and $3a, 3c$ as *virtual sources* in the sense that they each represent one actual source in the network but they are co-located in one physical source. Adopting this concept, in this network the highest number of interfering neighbors is five (with a total of six virtual sources all in one interference area) and therefore there exists a schedule of length 6 that enables every virtual source to transmit once. Since the traffic load is the same for all virtual sources, the resources will be shared equally and no source will be wasting its share. In this case we get $\lambda = W/6$. Note that this is the largest λ that could be obtained for the example in Figure 19.24(a). This concept allows us to define a 'traffic load-aware' schedule in the following way.

(1) For each source node, create one virtual source for every source node whose traffic goes through this node, including itself.

(2) Counting all the virtual sources we can determine the number of interfering neighbors (virtual sources) k. The new maximum degree of the interference graph is then $k - 1$.

(3) A schedule of length $s \leq k$ exists which is equally shared among virtual sources.

(4) The achievable throughput per node is simply the share obtained by any virtual source in the network, i.e. $\lambda = W/s \geq W/k$.

The concept of virtual source is used in References [58–63] to prove the following theorems:

(8) A randomly deployed network using multi-hop transmission for many-to-one communication can achieve $\lambda \geq W/\Sigma_{h=1}^{h=\left\lceil 2+\frac{\Delta}{r}\right\rceil} l_h^+ n_h^+$ with high probability, when knowledge of the traffic load is assumed. l_h^+ and n_h^+ are the upper bounds on the number of virtual sources per actual source and the number of actual sources respectively, that are h hops away from the sink with high probability.

(9) A randomly deployed network using multihop transmission for many-to-one communication can achieve a throughput arbitrarily close to $W/\{n(2-\pi r^2)\}$, when knowledge of the traffic load is assumed and $\Delta = 0$.

In a *hierarchical network* with H clusters (heads) we assume that each cluster head creates a cluster containing the sources closest to it. Within each cluster the communication is either via a single hop or via multihop, while the communication from clusterheads to the sink is assumed to be done via a single hop on a different channel. We assume that cluster heads cannot transmit and receive simultaneously. In order to avoid boundary problems, we will assume there is at least a distance of $2(2r+\Delta)$ between any two clusterheads. We will also assume that each cluster covers an area of same size, as though not necessarily the same shape. Following these two assumptions and using result (5), we have with high probability that the number of nodes in each cluster is within $(\alpha_n n)$ of n/H, where α_n is such that $\lim_{n\to\infty} \alpha_n/n = \varepsilon$. Therefore the clusters essentially form a Voronoi tessellation of the field, where every cluster (or Voronoi cell) contains a circle of radius $2r+\Delta$. Consequently sources located near the boundary between two clusters will not have a higher number of interfering neighbors (in terms of virtual sources), due to low traffic load, than the ones closer to the clusterheads. Thus previous results are directly applicable and we do not have to be concerned with the boundary.

The question of interest is whether there exists an appropriate number of clusters H that would allow the network to achieve $\lambda = W/n$ with high probability using clustering, when clusterheads have the same transmission capacity W as the sources. That W/n remains to be the upper bound is again obvious considering the fact that the sink cannot receive from more than one node (at rate W), and that there are n sources in the network. In References [58–63] the following results are proven:

(10) In a network using clustering, where cluster heads have the same transmission capacity W as the sources, there exists an appropriate number of clusters H and an appropriate range of transmission r that would allow the network to achieve $\lambda = W/n$ with high probability as $n \to \infty$. The range of transmission r must satisfy

$$\frac{20r^4 + 36\Delta r^3 + 25\Delta^2 r^2 + 8\Delta^3 r + \Delta^4}{r^2 - \sqrt{\in}\left(4r^2 + 4r\Delta + \Delta^2 - \frac{1}{\pi}\right)} \leq \frac{1}{\pi} \text{ and } H \geq 3 - \pi r^2$$

In the case of $\Delta = 0$ and letting $\sqrt{\varepsilon} \approx 0$, we need $r < \sqrt{1/20\pi}$.

(11) In a network using clustering, where cluster heads have transmission capacity W', there exists an appropriate number of clusters H and an appropriate range of transmission r, as $n \to \infty$, that allows the network to achieve $\lambda = W'/n$ with high probability. W'/n is also the upper bound on throughput in this scenario. The condition is $H \geq \left(3 - \pi r^2\right) W'/W$.

REFERENCES

[1] A. Ephremides and B. Hajek, Information theory and communication networks: an unconsummated union, *IEEE Trans. Inform. Theory*, vol. 44, no. 6, 1998, pp. 2416–2434.

[2] S. Glisic, *Adaptive WCDMA, Theory and Practice*. Wiley: Chichester 2003.

[3] A. Baiocchi *et al*., Effects of user mobility on the capacity of a CDMA cellular network, *Eur. Trans. Telecommun.*, vol. 7, no. 4, 1996, pp. 305–314.

[4] A.M. Viterbi and A.J. Viterbi, Erlang capacity of a power controlled CDMA system, *IEEE J. Select. Areas Commun.*, vol. 11, no. 6, 1993, pp. 892–899.

[5] M.A. Landolsi, V.V. Veeravalli and N. Jain, New results on the reverse link capacity of CDMA cellular networks, *Proc. IEEE VTC'96*, 1996, pp. 1462–1466.

[6] J.C. Liberti Jr and T.S. Rappaport, Analytical results for capacity improvements in CDMA, *IEEE Trans. Vehicular Technol.*, vol. 43, no. 3, 1994, pp. 680–690.

[7] A.F. Naguib, A. Paulraj and T. Kailath, Capacity improvement with base-station antenna arrays in cellular CDMA, *IEEE Trans. Vehicular Technol.*, vol. 43, no. 3, 1994, pp. 691–698.

[8] L. Tomba, Outage probability in CDMA cellular systems with discontinuous transmission, *Proc. IEEE ISSSTA'96*, 1996, pp. 481–485.

[9] S. Hämäläinen, H. Holma and A. Toskala, Capacity evaluation of a cellular CDMA uplink with multiuser detection, *Proc. IEEE ISSSTA'96*, 1996, pp. 339–343.

[10] H. Holma, A. Toskala and T. Ojanperä, Cellular coverage analysis of wideband MUD-CDMA system, *Proc. IEEE PIMRC'97*, 1997, pp. 549–553.

[11] J. Blanz, A. Klein, M. Naβhan and A. Steil, Capacity of a cellular mobile radio system applying joint detection, COST 231 TD94 002, 1994.

[12] J. Blanz, A. Klein, M. Naβhan and A. Steil, Performance of a cellular hybrid C/TDMA mobile radio system applying Joint detection and coherent receiver antenna diversity, *IEEE J. Select. Areas Commun.*, vol. 12, no. 4, 1994, pp. 568–579.

[13] S. Manji and N.B. Mandayam, Outage probability for a zero forcing multiuser detector with random signature sequences, *Proc. IEEE VTC'98*, 1998, pp. 174–178.

[14] W. Huang and V.K. Bhargava, Performance evaluation of a DS/CDMA cellular system with voice and data services, *Proc. IEEE PIMRC'96*, 1996, pp. 588–592.

[15] V.H. MacDonald, The cellular concept, *Bell Syst. Tech. J.*, vol., 58, 1979, pp. 15–41.

[16] G.K. Chan, Effects of sectorization on the spectrum efficiency of cellular radio systems, *IEEE Trans. Vehicular Technol.*, vol. 41, 1992, 217–225.

[17] S.G. Glisic and P. Pirinen, Co-channel interference in digital cellular TDMA networks, in *Encyclopedia of Telecommunications*, J. Proakis (ed.). Wiley: Chichester, 2003.

[18] S.C. Swales, M. A. Beach, D.J. Edwards and J.P. McGeehan, The performance enhancement of multibeam adaptive base station antennas for cellular land mobile radio systems, *IEEE Trans. Vehicular Technol.*, vol. 39, 1990, pp. 56–67.

[19] J.H. Winters, Smart antennas for wireless systems, *IEEE Person. Commun.*, vol. 5, 1998, pp. 23–27.

[20] P. Petrus, R.B. Ertel and J.H. Reed, Capacity enhancement using adaptive arrays in an AMPS system, *IEEE Trans. Vehicular Technol.*, vol. 47, 1998, pp. 717–727.

[21] P.E. Mogensen, P.L. Espensen, P. Zetterberg, K.I. Pedersen and F. Frederiksen, Performance of adaptive antennas in FH-GSM using conventional beamforming, *Wireless Person. Commun.*, vol. 14, 2000, pp. 255–274.

[22] E. Kudoh and T. Matsumoto, Effect of transmitter power control imperfections on capacity in DS/CDMA cellular mobile radios, *Proc. IEEE ICC'92*, 1992, pp. 237–242.

[23] A.J. Paulraj and C.B. Papadias, Space–time processing for wireless communications, *IEEE Signal Process. Mag.*, vol. 14, 1997, pp. 49–83.

[24] L.C. Godara, Applications of antenna arrays to mobile communications, part I: performance improvement, feasibility, and system considerations, *Proc. IEEE*, vol. 85, 1997, pp. 1031–1060.

[25] J. Litva and T. K.-Y. Lo, *Digital Beamforming in Wireless Communications*. Artech House: Boston, MA, 1996.

[26] J.H. Winters, Optimum combining in digital mobile radio with cochannel interference, *IEEE Trans. Vehicular Technol.*, vol. VT-33, 1984, pp. 144–155.

[27] P. Zetterberg, A comparison of two systems for downlink communication with base station antenna arrays, *IEEE Trans. Vehicular Technol.*, vol. 48, 1999, pp. 1356–1370.

[28] P. Zetterberg and B. Ottersten, The spectrum efficiency of a base station antenna array system for spatially selective transmission, *IEEE Trans. Vehicular Technol.*, vol. 44, 1995, pp. 651–660.

[29] W.S. Au, R.D. Murch and C.T. Lea, Comparison between the spectral efficiency of SDMA systems and sectorized systems, *Wireless Personal Commun.*, vol. 16, 2001, pp. 15–67.
[30] L.-C. Wang, K. Chawla and L.J. Greenstein, Performance studies of narrow-beam trisector cellular systems, *Int. J. Wireless Inform. Networks*, vol. 5, 1998, pp. 89–102.
[31] S. Glisic *et al*. Effective capacity of advanced wireless cellular networks (invited paper), in *PIMRC2005*, Berlin, 11–14 September 2005.
[32] P. Gupta and P.R. Kumar, The capacity of wireless networks, *IEEE Trans. Inform. Theory*, vol. 46, no. 2, 2000, pp. 388–404.
[33] L.-L. Xie and P.R. Kumar, A network information theory for wireless communication: scaling laws and optimal operation, *IEEE Trans. Inform. Theory*, vol. 50, no. 5, 2004, pp. 748–767.
[34] A. Okabe, B. Boots and K. Sugihara, *Spatial Tessellations Concepts and Applications of Voronoi Diagrams*. Wiley: New York, 1992.
[35] J.A. Bondy and U. Murthy, *Graph Theory with Applications*. Elsevier: New York, 1976.
[36] P. Gupta and P.R. Kumar, Toward an information theory of large networks: an achievable rate region, *IEEE Trans. Inform. Theory*, vol. 49, 2003, pp. 1877–1894.
[37] A. Sendonaris, E. Erkip and B. Aazhang, Increasing uplink capacity via user cooperation diversity, *Proc. IEEE Int. Symp. Inform. Theory*, 2001, p. 156.
[38] J. Laneman and G. Wornell, Energy-efficient antenna sharing and relaying for wireless networks, *Proc. IEEE Wireless Commun. Networking Conf.*, 2000, p. 294.
[39] J. Laneman, G. Wornell and D. Tse, An efficient protocol for realizing cooperative diversity in wireless networks, *Proc. IEEE Int. Symp. Inform. Theory*, 2001, p. 294.
[40] A. Scaglione and Y.W. Hong, Opportunistic large arrays: cooperative transmission in wireless multihop *ad hoc* networks to reach far distances, *IEEE Trans. on Signal Process.*, vol. 51, no. 8, 2003, pp. 2082–2093.
[41] E.M. Royer and C.K. Toh, A review of current routing protocols for *ad hoc* mobile wireless networks, *IEEE Person. Commun. Mag.*, vol. 6, 1999, pp. 46–55.
[42] Y.-C. Tseng, S.-Y. Ni, Y.-S. Chen and J.-P. Sheu, The broadcast storm problem in a mobile *ad hoc* network, *ACM Wireless Networks*, vol. 8, 2002, pp. 153–167.
[43] W. Peng and X.-C. Lu, On the reduction of broadcast redundancy in mobile *ad hoc* networks, in *Proc. IEEE/ACM Mobile Ad Hoc Networking Computing*, November 2000, pp. 129–130.
[44] B. Williams and T. Camp, Comparison of broadcasting techniques for mobile *ad hoc* networks, in *Proc. ACM Int. Symp. Mobile Ad Hoc Networking Computing*, June 2002.
[45] ANSI/IEEE Std 802.11, 1999 ed., Available at: http://standards.ieee.org/getieee802/download/802.11–1999.pdf, 1999.
[46] Network Simulator – ns2. Available at: http://isi.edu/nsnam/ns/
[47] S.-Y. R. Li, R.W. Yeung and N. Cai, Linear network coding, *IEEE Trans. Inform. Theory*, vol. 49, no. 2, February 2003, pp. 371–381.
[48] J.-H Chang, L. Tassiulas and F Rashid-Farrokhi, Joint transmitter receiver diversity for efficient space division multiaccess, *IEEE Trans. Wireless Commun.*, vol. 1, 2002, pp. 16–27.
[49] F. Rashid-Fwrokhi, K.J.R. Liu, and L. Tassiulas, Transmit beamforming and power control for cellulw wireless systems, *IEEE J. Select. Areas Commun.*, vol. 16, 1988, pp. 1437–1450.
[50] F. Rashid-Farrokhi, L. Tassiulas and K.J.R. Liu, Joint optimal power control and beamforming in wireless networks using antenna wrays, *IEEE Trans. Commun.*, vol. 46, 1998, pp. 1313–1324.
[51] A. Cwleial, A case where interference does not reduce capacity, *IEEE Trans. Inform. Theory*, vol. IT-21, 1975, pp. 569–570.
[52] T. Cover and J. Thomas, *Elements of Information Theory*. Wiley: New York, 1991.
[53] G.G. Raleigh and VK. Jones, Multivariate modulation and coding for wireless communication, *IEEE J. Select. Areas Commun.*, vol. 17, no. 5, 1999, pp. 851–866.
[54] M.C. Bromberg, Optimizing MIMO multipoint wireless networks assuming Gaussian other-user interference, *IEEE Trans. Inform. Theory*, vol. 49, no. 10, 2003, pp. 2352–2362.

[55] M.C. Bromberg and B.G. Agee, Optimization of spatially adaptive reciprocal multipoint communication networks, *IEEE Trans. Commun.*, vol. 51, no. 8, 2003, pp. 1254–1257.

[56] J.-H Chang, L. Tassiulas and F Rashid-Farrokhi, Joint transmitter receiver diversity for efficient space division multiaccess, *IEEE Trans. Wireless Commun.*, vol. 1, 2002, pp. 16–27.

[57] F. Rashid-Farrokhi, L. Tassiulas and K.J.R. Liu, Joint optimal power control and beamforming in wireless networks using antenna wrays, *IEEE Trans. Commun.*, vol. 46, 1998, pp. 1313–1324.

[58] H.E. Gamal, On the transport capacity of the many-to-one dense wireless network, *IEEE Vehicular Technol. Conf., VTC 2003*, vol. 5, 6–9 October 2003, pp. 2881–2885.

[59] A.D. Murugan, P.K. Gopala and H.E. Gamal, Correlated sources over wireless channels: cooperative source-channel coding, *IEEE J. Select. Areas Commun.*, vol. 22, no. 6, 2004, pp. 988–998.

[60] T. J. Kwon, M. Gerla, V.K. Varma, M. Barton and T.R. Hsing. Efficient flooding with passive clustering-an overhead-free selective forward mechanism for *ad hoc*/sensor networks *Proc. IEEE*, vol. 91, no. 8, 2003, pp. 1210–1220.

[61] A. Sabharwal, On capacity of relay-assisted communication, in *IEEE GLOBECOM'02*, vol. 2, 17–21 November 2002, pp. 1244–1248.

[62] H.E. Gamal, On the scaling laws of dense wireless sensor networks: the data gathering channel, *IEEE Trans. Inform. Theory*, vol. 51, no. 3, 2005, pp. 1229–1234.

[63] D. Marco, E.J. Duarte-Melo, M. Liu and D.L. Neuhoff, On the many-to-one transport capacity of a dense wireless sensor network and the compressibility of its data, in *Int. Workshop on Information Processing in Sensor Networks*, Berkeley, CA, April 2003, pp. 104–109.

[64] L. Tomba, Computation of the outage probability in rice fading radio channels, *Eur. Trans. Telecommun.*, vol. 8, no. 2, 1997, pp. 127–134.

[65] I. Howitt and Y.M. Hawwar, Evaluation of outage probability due to cochannel interference in fading for a TDMA system with a beamformer, *Proc. IEEE Vehicular Technology Conf.*, 1998, pp. 520–524.

20

Energy-efficient Wireless Networks

20.1 ENERGY COST FUNCTION

In Chapter 5 we discussed the impact of MAC layer protocols on energy efficiency, including TCP controlled retransmissions. In this chapter, we extend this analysis to the network layer and focus on routing algorithms. We discuss how the error rate associated with a link affects the overall probability of reliable delivery, and consequently the energy associated with the reliable transmission of a single packet. For any particular link $\langle i, j \rangle$ between a transmitting node i and a receiving node j, let $T_{i,j}$ denote the transmission power and $p_{i,j}$ represent the packet error probability. Assuming that all packets are of a constant size, the energy involved in a packet transmission, $E_{i,j}$, is simply a fixed multiple of $T_{i,j}$.

Any signal transmitted is affected by two different factors: attenuation due to the medium, and interference with ambient noise at the receiver. The attenuation is proportional to D^K, where D is the distance between the receiver and the transmitter. The bit error rate associated with a particular link is essentially a function of the ratio of the received signal power to the ambient noise. In the constant-power scenario, $T_{i,j}$ is independent of the characteristics of the link $\langle i, j \rangle$ and is a constant. In this case, a receiver located further away from a transmitter will suffer greater signal attenuation (proportional to D^K) and will, accordingly, be subject to a larger bit-error rate. In the variable-power scenario, a transmitter node adjusts $T_{i,j}$ to ensure that the strength of the (attenuated) signal received by the receiver is *independent of* D and is above a certain threshold level Th. The minimum transmission power associated with a link of distance D in the variable-power scenario is $T_m = Th \times \gamma \times D^K$, where γ is a constant and K is the coefficient of channel attenuation ($K \geq 2$). Since Th is typically a technology-specific constant, we can see that the minimum transmission energy over such a link varies as $E_m(D) \propto D^K$.

If links are considered error-free, then minimum hop paths are the most energy-efficient for the fixed-power case. Similarly, in the absence of transmission errors, paths with a large number of small hops are typically more energy efficient in the variable power case. However in the

Advanced Wireless Technologies: Cognitive, Cooperative & Opportunistic 4G Technology Second Edition Savo G. Glisic

presence of link errors, none of the above choices may give optimal energy efficient paths. We now analyze the consequences of this behavior for the variable-power scenario and end-to-end (EER) and hop-by-hop (HHR) packet retransmission techniques. The analysis for the fixed-power scenario is simpler, and is a special case of the variable-power scenario. Energy consumption for additional signal processing in the transmitter/receiver (modulation/demodulation) will be neglected. Modification of the models to include these losses is straightforward.

In the EER case, a transmission error on any link leads to an end-to-end retransmission over the path. Given the variable-power formulation of E_m, it is easy to see why breaking up a link of distance D into two shorter links of distance D_1 and D_2 such that $D_1 + D_2 = D$ always reduces the total E_m. To elaborate on this, let us consider communication between a sender (S) and a receiver (R) separated by a distance D. Let N represent the total number of hops between S and R, so that $N - 1$ represents the number of forwarding nodes i: $i = \{2, \ldots, N\}$, with node i referring to the $(i - 1)$th intermediate hop in the forwarding path. Node 1 refers to S and node $N + 1$ refers to R. In this case, the total energy spent in simply transmitting a packet once (without considering whether or not the packet was reliably received) from the sender to the receiver over the $N - 1$ forwarding nodes is:

$$E_{\mathrm{t}} = \sum_{i=1}^{N} E_m^{i,i+1} = \sum_{i=1}^{N} \alpha D_{i,i+1}^{K} \tag{20.1}$$

where $D_{i,j}$ refers to the distance between nodes i and j and α is a proportionality constant. To understand the tradeoffs associated with the choice of $N - 1$, we compute the lowest possible value of E_{t} for any given layout of $N - 1$. Using very simple symmetry arguments, it is easy to see that the minimum transmission energy case occurs when each of the hops are of equal length D/N. In that case, E_{t} is given by

$$E_{\mathrm{t}} = \sum_{i=1}^{N} \alpha D^K / N^K = \alpha D^K / N^{K-1}$$

We now consider how the choice of N affects the probability of transmission errors and the consequent need for retransmissions. Clearly, increasing the number of intermediate hops increases the likelihood of transmission errors over the entire path. Assuming that each of the N links has an independent packet error rate of p_{link}, the probability of a transmission error over the entire path, denoted by p, is given by $p = 1 - (1 - p_{\mathrm{link}})^N$.

The number of transmissions (including retransmissions) necessary to ensure the successful transfer of a packet between S and D is then a geometrically distributed random variable X, such that $\Pr\{X = k\} = p^{k-1} \times (1 - p)$, $\forall k$. The *mean* number of individual packet transmissions for the successful transfer of a single packet is thus $1/(1 - p)$. Since each such transmission uses total energy E_{t} given above, the total expected energy required in the reliable transmission of a single packet is given by:

$$E_{\mathrm{t}}(EER) = \alpha \frac{D^K}{N^{K-1}} \cdot \frac{1}{1-p} = \frac{\alpha D^K}{N^{K-1}(1 - p_{\mathrm{link}})^N} \tag{20.2}$$

By treating N as a continuous variable and differentiating, it follows that the optimal value of the number of hops, N_{opt} is given by:

$$N_{\mathrm{opt}} = -(K - 1)/\log(1 - p_{\mathrm{link}}) \tag{20.3}$$

The existence of the optimum value is demonstrated in Figure 20.1.

In the case of the HHR model, the number of transmissions on each link is *independent of the other links* and is geometrically distributed. The total energy cost for the HHR case with N

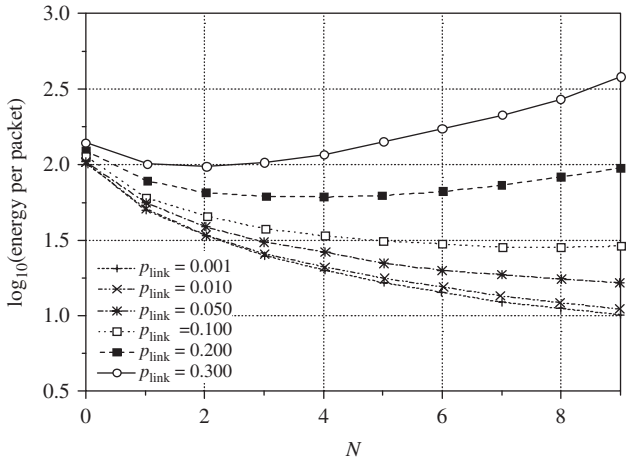

Figure 20.1 Total energy costs (K = 2, EER).

intermediate nodes, with each hop being of distance D/N and having a link packet error rate of p_{link}, is

$$E_{\text{t}}(HHR) = \sum_{i=1}^{N} \alpha \frac{D_{i,i+1}^{k}}{1 - p_{i,i+1}} = \alpha \frac{D^{K}}{N^{K-1} \cdot (1 - p_{\text{link}})} \tag{20.4}$$

In this case, it is easy to see that the total energy required always decreases with increasing N. One should be aware that in a practical system at some point when N is sufficiently large, the signal processing energy will become comparable with the energy spent for transmissions.

20.2 MINIMUM ENERGY ROUTING

Energy-aware routing protocols typically compute the shortest-cost path, where the cost associated with each link is some function of the transmission (and/or reception) energy associated with the corresponding nodes. To adapt such minimum cost route determination algorithms (such as Dijkstra's or the Bellman–Ford algorithm) for energy-efficient reliable routing, the link cost must now be a function of not just the associated transmission energy, but the link error rates as well. A link is assumed to exist between node pair $\{i, j\}$ as long as node j lies within the transmission range of node i. This transmission range is uniquely defined for the constant-power case. For the variable-power case, this range is really the *maximum permissible range* corresponding to the maximum transmission power of a sender. Let $E_{i,j}$ be the energy associated with the transmission of a packet over link $l_{i,j}$, and $p_{i,j}$ be the link packet error probability associated with that link. In the fixed-power scenario, $E_{i,j}$ is independent of the link characteristics; in the variable-power scenario, $E_{i,j}$ is a function of the distance between nodes i and j. Now, the routing algorithm's job is to compute the shortest path from a source to the destination that minimizes the sum of the energy costs over each constituent link.

Choosing path P for communication between S and D implies that the total energy cost for HHR is

$$E_P = \sum_{i=1}^{N} \frac{E_{i,i+1}}{1 - p_{i,i+1}} \tag{20.5}$$

Choosing a minimum-cost path from node 1 to node $N+1$ is thus equivalent to choosing the path P that minimizes Equation (20.5). It is thus easy to see that the corresponding link cost for link $L_{i,j}$, denoted $C_{i,j}$, is given by $C_{i,j} = E_{i,j}/(1 - p_{i,j})$. *Ad-hoc* routing protocols, discussed in Chapter 13, such as AODV, DSR and TORA, can use this link cost to compute the appropriate energy-efficient routes. Some of the existing energy-efficient routing techniques, e.g. PARO, can also be easily adapted to use this new link cost formulation to compute minimum-energy routes. Thus, in such a modified version of the PARO algorithm, an intermediate node C would offer to interject itself between two nodes A and B if the sum of the link cost $C_{A,C} + C_{C,B}$ was less than the 'direct' link cost $C_{A,B}$.

In *end-to-end retransmissions*, the total energy cost along a path contains a multiplicative term involving the packet error probabilities of the individual constituent links. In fact, assuming that transmission errors on a link do not stop downstream nodes from relaying the packet, the total energy cost can be now expressed as:

$$E_P = \frac{\sum_{i=1}^{N} E_{i,i+1}}{\prod_{i=1}^{N}(1 - p_{i,i+1})} \tag{20.5a}$$

Given this form, the total cost of the path cannot be expressed as a linear sum of individual link costs, thereby making the exact formulation inappropriate for traditional minimum-cost path computation algorithms. In [1] a heuristic cost function for a link, was suggested as

$$C_{i,j} = \frac{E_{i,j}}{(1 - p_{i,j})^L} \tag{20.6}$$

where $L = 2, 3, \ldots$, and is chosen to be identical for all links. Clearly, if the exact path length is known and all nodes on the path have identical link error rates and transmission costs, L should be chosen equal to that path length. However, in accordance with current routing schemes, we require that a link should associate only a single link cost with itself, irrespective of the lengths of specific routing paths that pass through it. Therefore, we need to fix the value of L independent of the different paths that cross a given link. If better knowledge of the network paths is available, then L *should be chosen to be the average path length of this network*. Higher values of L impose progressively stiffer penalties on links with non-zero error probabilities. Given this formulation of the link cost, the minimum-cost path computation effectively computes the path with the minimum "approximate" energy cost given by:

$$E_P \sim \sum_{i=1}^{N} \frac{E_{i,i+1}}{(1 - p_{i,i+1})^L} \tag{20.7}$$

As before, protocols like AODV, DSR, TORA and PARO can use this new link cost function to make their routing decisions.

20.3 MAXIMIZING NETWORK LIFETIME

We now discuss how we can include the retransmission-aware formulation of the link cost in an algorithm, that attempts to increase the operational lifetime of multihop wireless networks. Unlike previous protocols, *maximum reliable packet carrying capacity* (MRPC) considers both the node characteristics (residual battery energy at the transmitting node) and the link characteristics (link distance and link error rates), while evaluating the suitability of alternative paths. Given the current battery power levels at the different nodes, MRPC selects a route that has the *maximum reliable packet carrying capacity* among all possible paths, assuming no other cross-traffic passes through the nodes on that path.

To formalize the algorithm, let us assume that the residual battery power at a certain instance of time at node i is B_i. As before, let the transmission energy required by node i to transmit a packet over link $\langle i, j \rangle$ to node j be $E_{i,j}$. Let the source and destination nodes for a specific session (route) be S and D respectively. If the route-selection algorithm then selects a path P from S to D that includes the link $\langle i, j \rangle$, then the maximum number of packets that node i can forward over this link is clearly $B_i/E_{i,j}$. Accordingly, we can define a node-link metric, $M_{i,j}$ for the link $\langle i, j \rangle$ as:

$$M_{i,j} = \frac{B_i}{E_{i,j}} \tag{20.8}$$

The key point in this formulation is that the cost metric includes both a node-specific parameter (the battery power) and a link-specific parameter (the packet transmission energy for reliable communication across the link). Clearly, the 'lifetime' of the chosen path P, defined by the maximum number of packets that may be potentially forwarded between S and D using path P, is determined by the *weakest intermediate node* – one with the smallest value of $M_{i,j}$. Accordingly, the 'lifetime' $\Im$ associated with route P is:

$$\Im_P = \min_{(i,j) \in P} \{M_{i,j}\} \tag{20.9}$$

The MRPC algorithm then selects the candidate route P_c that maximizes the 'lifetime' of communication between S and D. Formally, the chosen route is such that:

$$P_c = \arg\max\{\Im_P \,|\, P \in \textit{all possible routes}\} \tag{20.10}$$

Given the cost and lifetime formulations for MRPC it is then easy to use a modified version of Dijkstra's minimum cost algorithm for decentralized route computation.

To apply Dijkstra's algorithm for determining the minimum-cost path, the distance metric from any node to the given destination should be defined as the value of $\Im_P$ over the optimal path from that node to D. Now consider a node A that sees advertisements from its neighbors, $\{X, Y, Z, \ldots\}$, with corresponding distance metrics $\Im_X$, $\Im_Y$, $\Im_Z$, ... for a given destination D. Node A can then compute the best path to D (using its optimal neighbor) by using the following simple algorithm:

(1) For each of the neighboring nodes ($j \in \{X, Y, Z, \ldots\}$), compute the link cost $M_{A,j}$ using Equation (20.8).

(2) For each of the neighboring nodes ($j \in \{X, Y, Z, \ldots\}$) compute the potential new value of $\Im_{\text{pot}}$ using $\Im_{\text{pot}}(A, j) = \min\{M_{A,j}, \Im_j\}$.

(3) Select as the next-hop neighbor towards D the node which results in the maximum value of $\Im_{\text{pot}}$, i.e. choose node k such that $k = \arg\max_{j \varepsilon \{X,Y,Z\}}\{\Im_{\text{pot}}(A, j)\}$ and assign $\Im_A = \Im_{\text{pot}}(A, k)$.

Using this recursive formulation allows all nodes in the *ad hoc* network to iteratively build their optimal route towards a specific destination D. The distance-vector formulation presented here can easily be incorporated in protocols, such as AODV, DSR and TORA, that are specifically designed for *ad hoc* mobile environments.

The basic MRPC formulation for power-aware routing does not need to specify the value of the transmission energy cost associated with a specific link. Note that Equation (20.8) is expressed as a function of a generic link cost $M_{i,j}$. Accordingly, by specifying different forms of $M_{i,j}$ it is possible to tailor the MRPC mechanism for specific technologies and/or scenarios.

For the fixed-power scenario, the energy involved in a single packet transmission attempt, $E_{i,j}$, is a constant for all $\langle i, j \rangle$ and is independent of the distance between neighboring nodes i and j. For the variable-power scenario, $E_{i,j}$ will typically be $\propto D_{i,j}^K$, where $D_{i,j}$ is the distance between nodes i and j. A routing algorithm for reliable packet transfer should include the link's packet error probability in formulating the transmission energy cost. By ignoring the packet error probability,

the link cost concentrates (wrongly) only on the energy spent in transmitting a single packet. The correct metric is the *effective* packet transmission energy for reliable transmission, which includes the energy spent in one or more re-transmissions that might be necessary in the face of link errors. A transmission energy metric of the form $C_{i,j} = E_{i,j}/(1 - p_{i,j})^L$ was suggested, where $p_{i,j}$ is the link's packet error probability, $L \geq 1$. For hop-by-hop re-transmissions L should be chosen to be 1. In the absence of hop-by-hop re-transmissions (i.e. re-transmissions are only performed end-to-end), the transmission cost is well approximated by $L \in [3, 5]$. Power-aware routing has been studied in a number of papers [1–42].

The *conditional MRPC* (CMRPC) algorithm is the MRPC equivalent of the *conditional min–max minimum battery cost routing* (CMMBCR) algorithm presented in Toh *et al.* [2]. The CMMBCR algorithm is based on the observation that using residual battery energy as the sole metric throughout the lifetime of the *ad hoc* network can actually lower the overall lifetime, since it never attempts to minimize the total energy consumption. Accordingly, the CMMBCR algorithm uses regular minimum-energy routing as long as there is even one candidate path, where the remaining battery power level in all the constituent nodes lies above a specified threshold γ. When no such path exists, CMMBCR switches to MMBCR, i.e. it picks the path with the maximum residual capacity on the 'critical node'.

The CMRPC algorithm differs from CMMBCR in that the cost-functions at all times include the link-specific parameters (e.g. error rates) as defined earlier in this chapter. The algorithm can thus be specified as follows. Let Ψ be the set of all possible paths between the source S and destination D and let Ω represent the set of paths such that: for any route $Q \in \Omega$, $\Im_Q \geq \gamma$. In other words Ω represents the set of paths whose most critical nodes have a lifetime greater than a specified threshold. The routing scheme thus consists of the following actions:

(1) If $\Omega \neq \emptyset$ (there are one or more paths with $\Im > \gamma$, the algorithm selects a path $\bar{Q} \in \Omega$ that minimizes the total transmission energy for reliable transfer, i.e.

$$\bar{Q} = \arg\min_{Q \in \Omega} \left\{ \sum_{(i,j) \in Q} M_{i,j} \right\} \tag{20.11}$$

(2) Otherwise, switch to the MRPC algorithm, i.e. select $\bar{Q}$ such that

$$\bar{Q} = \arg\max_{Q \in \Omega} \{\Im_Q | Q \in \Psi\}$$

The threshold γ is a parameter of the CMRPC algorithm. A lower value of γ implies a smaller protection margin for nodes nearing battery power exhaustion. Accordingly, the performance of the CMRPC algorithm will be a function of γ.

The *performance example* is based on network topology shown in Figure 20.2. The corner nodes and the mid-points of each side of the rectangular grid were chosen as traffic sources and destinations; the bold lines in the figure show the session end-points [1].

Each (source, destination) pair had two simultaneous sessions activated in the opposite direction, giving rise to a total of 16 different sessions. For the results reported here, each session consisted of a UDP traffic generated by a CBR source whose inter-packet gap was distributed uniformly between 0.1 and 0.2 s. The error rate on each link was independently distributed uniformly between $(0.05, p_{\max})$. Varying values of $p_{\max}$ were used. Routes were recomputed at 2 s intervals in these simulations to capture the effect of changes in the residual packet capacity on the link metrics.

Whenever nodes died (when its battery power gets completely drained) during the course of a simulation, the simulation code would check whether the graph became partitioned. The simulations were run until each of the 16 sessions failed to find any route from their source to the corresponding destination. To avoid the termination of a simulation due to battery power exhaustion at source or

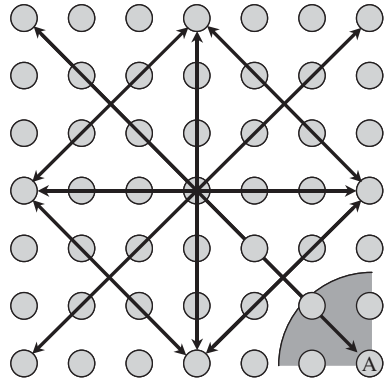

Figure 20.2 Simulation scenario.

destination nodes, all source and sink nodes were configured to have 'infinite' power resources. All the other 'intermediate' nodes were configured with identical initial battery power levels.

To study the performance of the various algorithms, experiments were performed where the maximum transmission radius, R, of each node was varied. Figure 20.2 shows the set of neighboring nodes for a corner node when the transmission radius is set to 1.5. The expiration sequence, as well as the node expiry times were noted, for each simulation. The *expiration sequence* (sorted in ascending order of the expiration times) provides a useful indicator of how each algorithm affects the lifetime of the individual nodes, and the entire network. In addition to the expiration sequence, the *total packet throughput* was also calculated by counting the total number of packets successfully received at the destination nodes, and the *energy costs per packet* by dividing the total energy expenditure by the total packet throughput. Except for the expiration sequences, all other metrics were obtained by averaging over multiple runs. The results are shown in Figures 20.3–20.5. From these results one can see that CMRPC/MRPC outperforms other options.

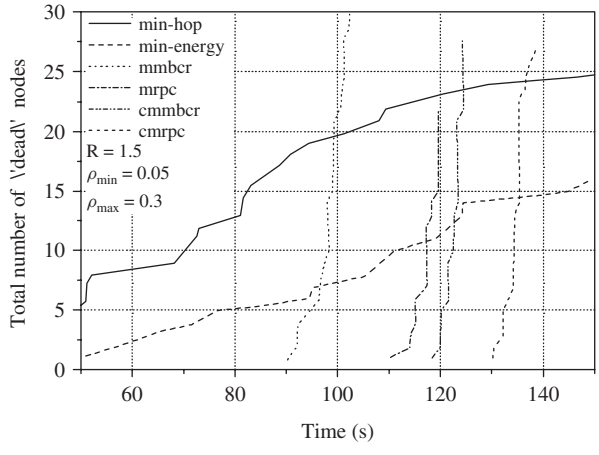

Figure 20.3 Expiration sequence for different algorithms, $R = 1.5$. (Reproduced by permission of IEEE [1].)

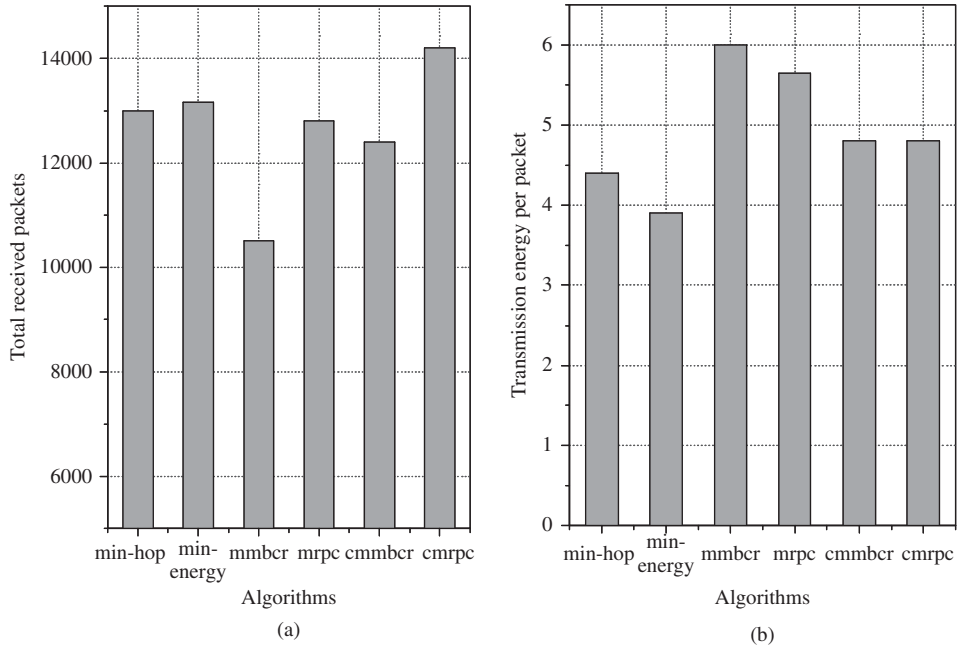

Figure 20.4 (a) Total packet throughput; (b) average transmission energy per received packet (UDP sources), $R = 1.5$. (Reproduced by permission of IEEE [1].)

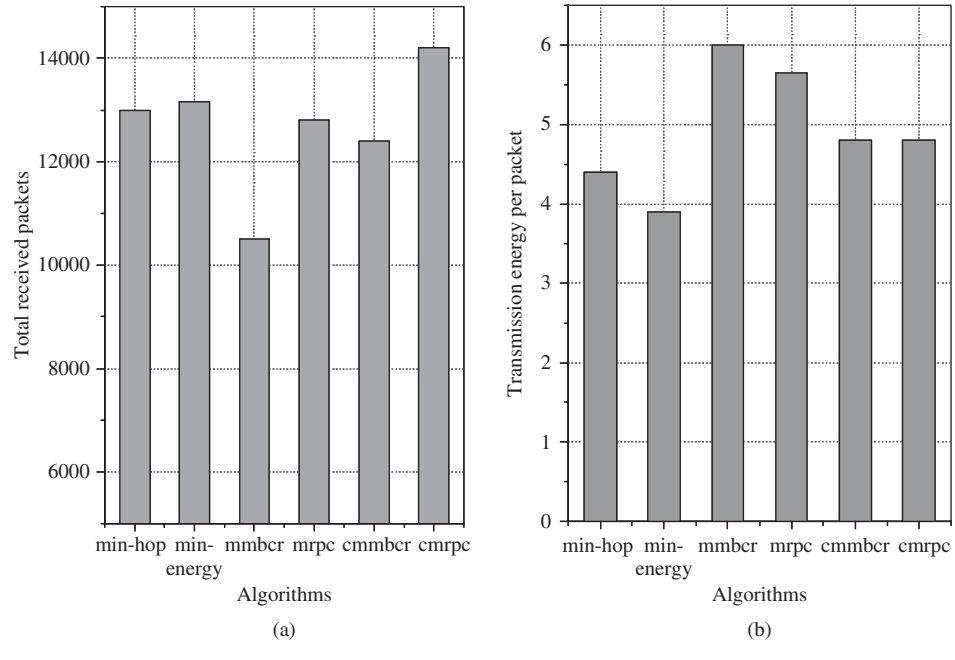

Figure 20.5 CMRPC: (a) total packet throughput; (b) average. transmission energy per received packet vs the protection threshold. (Reproduced by permission of IEEE [1].)

20.4 ENERGY-EFFICIENT MAC IN SENSOR NETWORKS

Among the requirements for MACs in wireless sensor networks, energy efficiency is typically the primary goal. In these systems, idle listening is identified as a major source of energy wastage. Measurements show that idle listening consumes nearly the same power as receiving. Since in sensor network applications traffic load is very light most of the time, it is often desirable to turn off the radio when a node does not participate in any data delivery. Some schemes put (scheduled) idle nodes in power-saving mode (SMAC) and switch nodes to full active mode when a communication event happens. Although a low duty cycle MAC is energy-efficient, it has three side-effects.

(1) It increases the packet delivery latency. At a source node, a sampling reading may occur during the sleep period and has to be queued until the active period. An intermediate node may have to wait until the receiver wakes up before it can forward a packet received from its previous hop. This is called *sleep latency* in SMAC, and it increases proportionally with hop length by a slope of schedule length (active period plus sleep period).

(2) A fixed duty cycle does not adapt to the varying traffic rate in sensor network. A fixed duty cycle for the highest traffic load results in significant energy wastage when traffic is low while a duty cycle for low traffic load results in low message data delivery and long queuing delay. Therefore it is desirable to adapt the duty cycle under variant traffic load.

(3) A fixed synchronous duty cycle may increase the possibility of collision. If neighboring nodes turn to active state at the same time, all may contend for the channel, making a collision very likely. There are several possibilities to reduce sleep delay and adjust duty cycle to the traffic load. Those mechanisms are either implicit, in which nodes remain active on overhearing an ongoing transmission or explicit, in which there are direct duty cycle adjusting messages. In adaptive listening, a node that overhears its neighbor's transmission wakes up for a short period of time at the end of the transmission, so that if it is the next hop of its neighbor, it can receive the message without waiting for its scheduled active time. A node also can keep listening and potentially transmitting as long as it is in an active period. An active period ends when no activation event has occurred for a certain time. The activation time events include reception of any data, the sensing of communication on the radio, the end-of-transmission of a node's own data packet or acknowledgement, etc.

If the number of buffered packets for an intended receiver exceeds a threshold L, the sender can signal the receiver to remain on for the next slot. A node requested to stay awake sends an acknowledgement to the sender, indicating its willingness to remain awake in the next slot. The sender can then send a packet to the receiver in the following slot. The request is renewed on a slot-by-slot basis.

However, in previous mechanisms (whether explicit or implicit), not all nodes beyond one hop away from the receiver can overhear the data communication, and therefore packet forwarding will stop after a few hops. This *data forwarding interruption problem* causes sleep latency for packet delivery.

DMAC employs a *staggered active/sleep schedule* to solve this problem and enable continuous data forwarding on the multihop path. In DMAC, *data prediction* is used to enable active slot request when multiple children of a node have packets to send in a same sending slot, while the *more to send packet* is used when nodes on the same level of the data gathering tree with different parents compete for channel access.

20.4.1 Staggered wakeup schedule

For a sensor network application with multiple sources and one sink, the data delivery paths from sources to sink are in a tree structure, a *data gathering tree*. Flows in the data gathering tree are

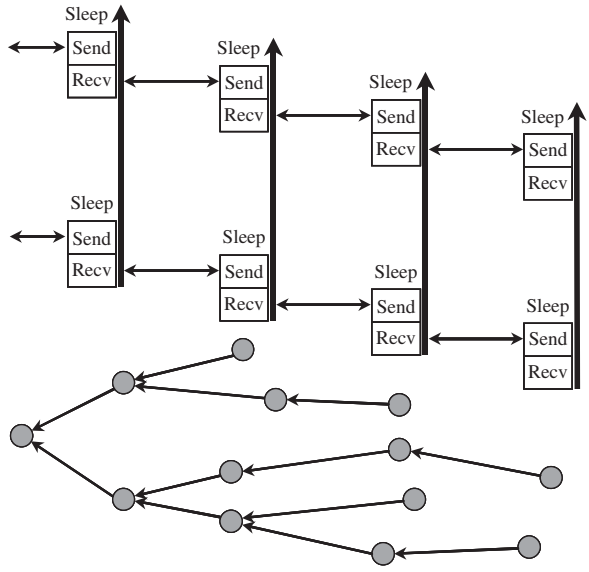

Figure 20.6 DMAC in a data gathering tree.

unidirectional from sensor nodes to sink. There is only one destination, the sink. All nodes except the sink will forward any packets they receive to the next hop. The key insight in designing a MAC for such a tree is that it is feasible to stagger the wake-up scheme so that packets flow continuously from sensor nodes to the sink. *DMAC is designed to deliver data along the data gathering tree*, aiming at both energy efficiency and low latency.

In DMAC, the activity schedule of nodes on the multihop path is staggered to wake up sequentially like a chain reaction. Figure 20.6 shows a data gathering tree and the staggered wake-up scheme. An interval is divided into receiving, sending and sleep periods. In receiving state, a node is expected to receive a packet and send an ACK packet back to the sender. In the sending state, a node will try to send a packet to its next hop and receive an ACK packet. In sleep state, nodes will turn off radio to save energy. The receiving and sending periods have the same length of μ, which is enough for one packet transmission and reception. Depending on its depth d in the data gathering tree, a node skews its wake-up scheme $d\mu$ ahead from the schedule of the sink. In this structure, data delivery can only be done in one direction towards the root. Intermediate nodes have a sending slot immediately after the receiving slot.

A staggered wake-up schedule has four advantages: (1) since nodes on the path wake up sequentially to forward a packet to next hop, sleep delay is eliminated if there is no packet loss due to channel error or collision; (2) a request for longer active period can be propagated all the way down to the sink, so that all nodes on the multihop path can increase their duty cycle promptly to avoid data stuck in intermediate nodes; (3) since the active periods are now separated, contention is reduced; and (4) only nodes on the multihop path need to increase their duty cycle, while the other nodes can still operate on the basic low duty cycle to save energy. The simulation results for the three different protocols are shown in Figure 20.7. DMAC demonstrates good performance. In the simulation the following parameters were used, as in Lu *et al.* [43]: Radio bandwidth 100 kbps, radio transmission range 250 m, radio interference range 550 m, packet length 100 bytes, transmit power 0.66 W, receive power 0.395 W and idle power 0.35 W. The sleeping power consumption is set to 0. An MTS (more to send) packet is 3 bytes long. According to the parameters of the radio and packet length, the receiving and sending slot μ is set to 10 ms for DMAC and 11 ms for

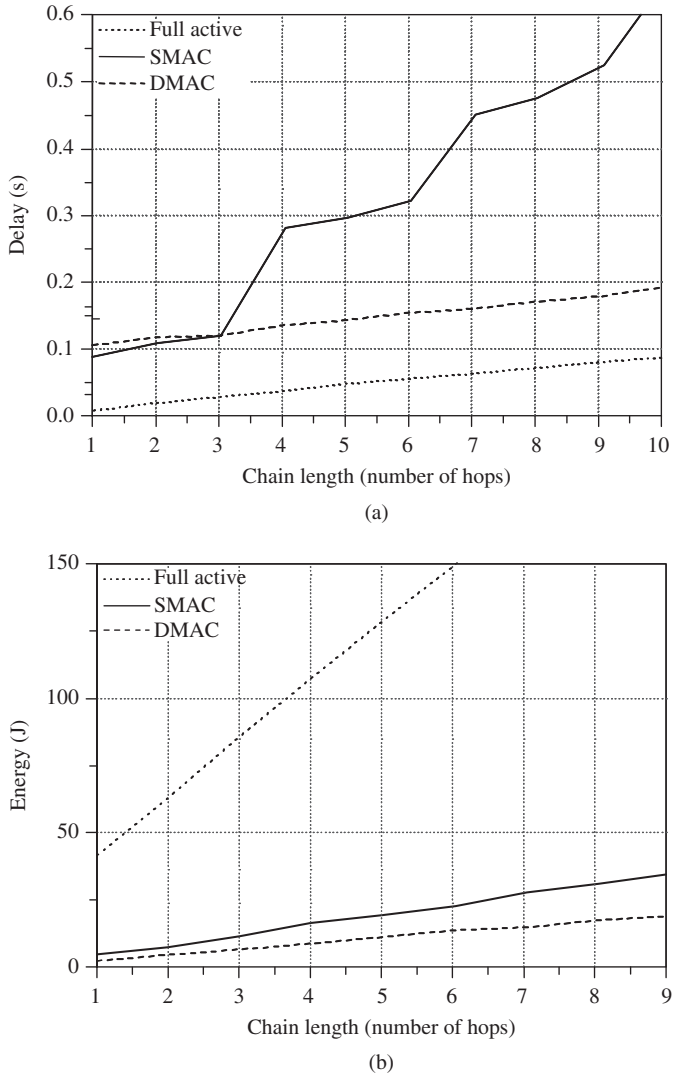

Figure 20.7 (a) Mean packet latency on each hop under low traffic load; (b) total energy consumption on each hop under low traffic load.

DMAC/MTS. The active period is set to 20 ms for SMAC with adaptive listening. All schemes have the basic duty cycle of 10 %. This means a sleep period of 180 ms for DMAC and SMAC, 198 ms for DMAC/MTS.

REFERENCES

[1] A. Misra and S. Banerjee, MRPC: maximizing network lifetime for reliable routing in wireless environments, in *Wireless Communications and Networking Conf., WCNC 2002* , vol. 2, 17–21 March 2002. IEEE: New York, pp. 800–806.

[2] C.-K., Toh, H. Cobb and D.A. Scott, Performance evaluation of battery-life-aware routing schemes for wireless *ad hoc* networks, in *IEEE Int. Conf. Communications, ICC 2001*, Helsinki, vol. 9, 11–14 June 2001, pp. 2824–2829.

[3] I. Stojmenovic and X. Lin, Power-aware localized routing in wireless networks, *IEEE Trans. Parallel and Distributed Systems*, vol. 12, no. 11, November 2001, pp. 1122–1133.

[4] J.-C. Cano and D. Kim, Investigating performance of power-aware routing protocols for mobile ad-hoc networks, in *International Mobility and Wireless Access Workshop, MobiWac 2002*, 12 October 2002, pp. 80–86.

[5] C.-K. Toh, Maximum battery life routing to support ubiquitous mobile computing in wireless *ad hoc* networks, *IEEE Commun. Mag.*, vol. 39, no. 6, 2001, pp. 138–147.

[6] J.-H. Chang and L. Tassiulas, Maximum lifetime routing in wireless sensor networks, *IEEE/ACM Trans. Networking*, vol. 12, no. 4, 2004, pp. 609–619.

[7] M. Tarique, K.E. Tepe and M. Naserian, Energy saving dynamic source routing for *ad hoc* wireless networks, in *Third Int. Symp. Modeling and Optimization in Mobile, Ad Hoc, and Wireless Networks, WIOPT 2005*, 4–6 April 2005, pp. 305–310.

[8] J. Gomez, A.T. Campbell, M. Naghshineh and C. Bisdikian, Power-aware routing in wireless packet networks, in *IEEE Int. Workshop on Mobile Multimedia Communications (MoMuC '99)*, 15–17 November 1999, pp. 380–383.

[9] Y. Xue and B. Li, A location-aided power-aware routing protocol in mobile *ad hoc* networks, in *IEEE Global Telecommun. Conf., GLOBECOM '01*, vol. 5, 25–29 November 2001, pp. 2837–2841.

[10] A. Avudainayagam, Y. Fang and W. Lou, DEAR: a device and energy aware routing protocol for mobile *ad hoc* networks, in *Proc. MILCOM 2002*, vol. 1, 7–10 October 2002, pp. 483–488.

[11] R. Ranjan and A. Saad, Generic architecture for power aware routing in wireless sensor networks, *29th Annual IEEE Int. Conf. Local Computer Networks*, 16–18 November 2004, pp. 575–576.

[12] B. Zhang and H.T. Mouftah, Localized power-aware routing for wireless *ad hoc* networks, in *IEEE Int. Conf. Communications*, vol. 6, 20–24 June 2004, pp. 3754–3758.

[13] J. Shen and J. Harms, Position-based routing with a power-aware weighted forwarding function in MANETs, in *IEEE Int. Conf. Performance, Computing, and Communications*, 2004, pp. 347–355.

[14] A. Safwat, H. Hassanein and H. Moufta, A MAC-based performance study of energy-aware routing schemes in wireless *ad hoc* networks, in *IEEE Global Telecommunications Conf., GLOBECOM '02*. vol. 1, 17–21 November 2002, pp. 47–51.

[15] L. De Nardis, G. Giancola and M.-G. Di Benedetto, A position based routing strategy for UWB networks, in *IEEE Conf. Ultra Wideband Systems and Technologies*, 16–19 November 2003, pp. 200–204.

[16] J. Nie and Z. Zhou, An energy based power-aware routing protocol in *ad hoc* networks, *IEEE Int. Symp. Communications and Information Technology, ISCIT*, vol. 1, 26–29 October 2004, pp. 280–285.

[17] J.-P. Sheu, C.-W. Lai and C.-M. Chao, Power-aware routing for energy conserving and balance in *ad hoc* networks, in *IEEE Int. Conf. Networking, Sensing and Control*, vol. 1, 21–23 March 2004, pp. 468–473.

[18] S.-H. Lee, E. Choi and D.-H. Cho, Timer-based broadcasting for power-aware routing in power-controlled wireless *ad hoc* networks, *IEEE Commun. Lett.*, vol. 9, no. 3, 2005, pp. 222–224.

[19] A. Helmy, Contact-extended zone-based transactions routing for energy-constrained wireless *ad hoc* networks, *IEEE Trans. Vehicular Technol.*, vol. 54, no. 1, 2005, pp. 307–319.

[20] M. Maleki, K. Dantu and M. Pedram, Power-aware source routing protocol for mobile *ad hoc* networks, in *Proc. Int. Symp. Low Power Electronics and Design, ISLPED '02*, 2002, pp. 72–75.

[21] R.K. Guha, C.A. Gunter and S. Sarkar, Fair coalitions for power-aware routing in wireless networks, *43rd IEEE Conf. Decision and Control, CDC*, vol. 3, 14–17 December 2004, pp. 3271–3276.

[22] L. De Nardis, G. Giancola and M.-G. Di Benedetto, Power-aware design of MAC and routing for UWB networks, in *IEEE Global Telecommunications Conf. Workshops*, 29 November to 3 December 2004, pp. 235–239.

[23] Q. Li, J. Aslam and D. Rus, Distributed energy-conserving routing protocols, in *Proc. 36th Annual Hawaii Int. Conf. System Sciences*, 6–9 January 2003, p. 10.

[24] J. Gomez, A.T. Campbell, M. Naghshineh and C. Bisdikian, Conserving transmission power in wireless *ad hoc* networks, in *Ninth Int. Conf. Network Protocols*, 11–14 November 2001, pp. 24–34.

[25] J.-E. Garcia, A. Kallel, K. Kyamakya, K. Jobmann, J.C. Cano and P. Manzoni, A novel DSR-based energy-efficient routing algorithm for mobile *ad-hoc* networks, *IEEE Vehicular Technol. Conf., VTC 2003*, vol. 5, 6–9 October, pp. 2849–2854.

[26] N. Gemelli, P. LaMonica, P. Petzke and J. Spina, Capabilities aware routing for dynamic *ad hoc* networks, *Int. Conf. Integration of Knowledge Intensive Multi-Agent Systems*, 30 September to 4 October 2003, pp. 585–590.

[27] M. Krunz, A. Muqattash and S.-J. Lee, Transmission power control in wireless *ad hoc* networks: challenges, solutions and open issues, *IEEE Networks*, vol. 18, no. 5, 2004, pp. 8–14.

[28] J. Schiller, A. Liers, H. Ritter, R. Winter and T. Voigt, ScatterWeb – low power sensor nodes and energy aware routing, in *Proc. 38th Annual Hawaii Int. Conf. System Sciences*, 3–6 January 2005, p. 286c.

[29] B. Zhang and H. Mouftah, Adaptive energy-aware routing protocols for wireless *ad hoc* networks, in *First Int. Conf. Quality of Service in Heterogeneous Wired/Wireless Networks, QSHINE*, 18–20 October 2004, pp. 252–259.

[30] Y. Zhou, D.I. Laurenson and S. McLaughlin, High survival probability routing in power-aware mobile *ad hoc* networks, *Electron. Lett.*, vol. 40, no. 22, 2004, pp. 1424–1426.

[31] S. Agarwal, A. Ahuja, J.P. Singh and R. Shorey, Route-lifetime assessment based routing (RABR) protocol for mobile *ad-hoc* networks, in *IEEE Int. Conf. Commun., ICC*, vol. 3, 18–22 June 2000, pp. 1697–1701.

[32] A. Safwat, H. Hassanein and H. Mouftah, Power-aware fair infrastructure formation for wireless mobile *ad hoc* communications, in *IEEE Global Telecommun. Conf., GLOBECOM '01*, vol. 5, 25–29 November 2001, pp. 2832–2836.

[33] S. Guo and O. Yang, An optimal TDMA-based MAC scheduling for the minimum energy multicast in wireless *ad hoc* networks, *IEEE Int. Conf. Mobile Ad-hoc and Sensor Systems*, 25–27 October 2004, pp. 552–554.

[34] K. Wang, Y.-L. Xu, G.-L. Chen and Y.-F. Wu, Power-aware on-demand routing protocol for MANET, in *Proc. 24th Int. Conf. Distributed Computing Systems Workshops*, 23–24 March 2004, pp. 723–728.

[35] R. Min and A. Chandrakasan, A framework for energy-scalable communication in high-density wireless networks, in *Proc. Int. Symp. Low Power Electronics and Design, ISLPED '02*, 2002, pp. 36–41.

[36] D. Shin and J. Kim, Power-aware communication optimization for networks-on-chips with voltage scalable links, in *Int. Conf. Hardware/Software Codesign and System Synthesis, CODES + ISSS*, 8–10 September 2004, pp. 170–175.

[37] L. Hughes and Y. Zhang, Self-limiting, adaptive protocols for controlled flooding in *ad hoc* networks, in *Proc. Second Annual Conf. Communication Networks and Services Research*, 19–21 May 2004, pp. 33–38.

[38] Y. Liu and P.X. Liu, A two-hop energy-efficient mesh protocol for wireless sensor networks, in *Proc. of IEEE/RSJ Int. Conf. Intelligent Robots and Systems (IROS 2004)*, vol. 2, 28 September to 2 October 2004, pp. 1786–1791.

[39] A. Safwat, H. Hassanein and H. Mouftah, Energy-efficient infrastructure formation in MANETs, in *Proc. IEEE Conf. Local Computer Networks*, 14–16 November 2001, pp. 542–549.

[40] G. Dimitroulakos, A. Milidonis, M.D. Galaris, G. Theodoridis, C.E. Gontis and F. Catthoor, Power aware data type refinement on the HIPERLAN/2, in *IEEE Int. Conf. Electronics, Circuits and Systems, ICECS*, vol. 1, 14–17 December 2003, pp. 216–219.

[41] S. Jayashree, B.S. Manoj and C.S.R. Murthy, Next step in MAC evolution: battery awareness?, in *IEEE Global Telecommunications Conf., GLOBECOM '04*, vol. 5, 29 November to 3 December 2004, pp. 2786–2790.

[42] L. Zhao, X. Hong and Q. Liang, Energy-efficient self-organization for wireless sensor networks: a fully distributed approach, in *IEEE Global Telecommunications Conf., GLOBECOM '04*, vol. 5, 29 November to 3 December 2004, pp. 2728–2732.

[43] G. Lu, B. Krishnamachari and C.S. Raghavendra, An adaptive energy-efficient and low-latency MAC for data gathering in wireless sensor networks, in *Proc. Int. Parallel and Distributed Processing Symp.*, 26–30 April 2004, p. 224.

21

Quality-of-Service Management

QoS has been the main criterion in the analysis of the schemes presented so far in the book. However, in the last chapter we present some additional solutions that will be of interest in 4G networks.

21.1 BLIND QoS ASSESSMENT SYSTEM

In this section we present a method to blindly estimate the quality of a multimedia communication link using digital fragile watermarking. Data hiding by digital watermarking is usually employed for multimedia copyright protection, authenticity verification or similar purposes. However, watermarking is here adopted as a technique to provide a blind measure of the quality of service in multimedia communications [1–28]. The watermark embedding procedure is sketched in Figure 21.1. It consists of embedding a watermark sequence, which is usually binary, into host data by means of a key. In the detection phase, the key is used to verify the presence of the embedded sequence. With regard to the domain where the watermark embedding occurs, we can distinguish methods operating in the spatial domain [15], in the discrete cosine transform DCT domain [16–19], in the Fourier transform domain [20], and in the wavelet transform domain [1– 5].

When unwanted modifications of the watermarked data affect even the extracted watermark, the embedding scheme is known as fragile. Fragile watermarking [6–8] can be used to obtain information about the tampering process. In fact, it indicates whether or not the data has been altered and supplies localization information as to where the data was altered.

Here, an unconventional use of a fragile watermark to evaluate the QoS in multimedia mobile communications is presented. Specifically, a known watermark is superimposed onto the host data. The rationale behind this approach is that, by transmitting the watermarked data onto a channel, the mark undergoes the same alterations as suffered by the data. At the receiving side, the watermark is estimated and compared with the original. Since the alterations endured by the watermark are

Advanced Wireless Technologies: Cognitive, Cooperative & Opportunistic 4G Technology Second Edition Savo G. Glisic

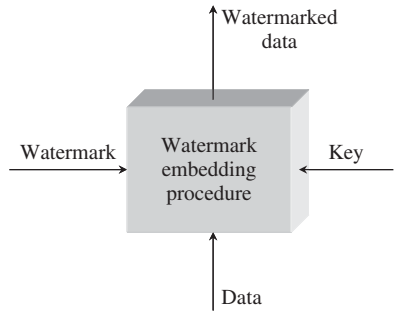

Figure 21.1 Watermark embedding process.

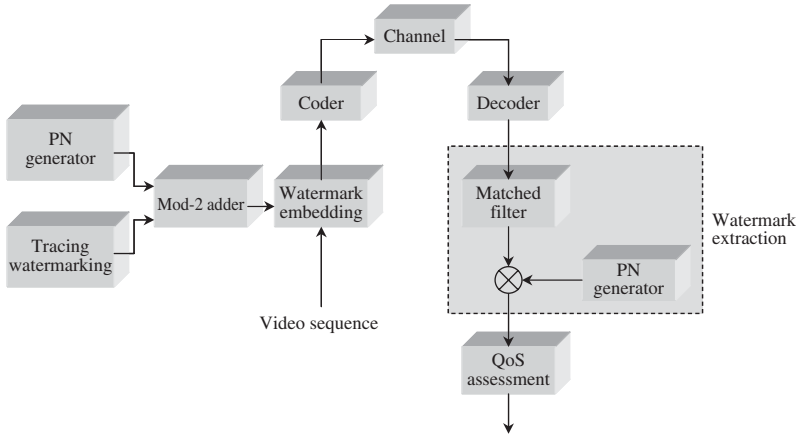

Figure 21.2 Principle scheme of tracing watermarking for coder-channel quality assessment in multimedia communications.

also likely to be suffered by the entire data, as they follow the same communication link, the watermark degradation can be used to estimate the overall alterations endured by the data.

The tracing watermarking procedure for coder-channel quality assessment is given in Figure 21.2. The watermark embedding is performed by resorting to the spread-spectrum technique proposed in Cox *et al*. [17] for still images and applied to video sequences in Hartung and Girod [18]. The watermark is a narrowband low-energy signal. It is then spread so that it has a larger bandwidth. Consequently, the watermark energy contribution for each host frequency bin is negligible, which makes the watermark imperceptible.

In the application addressed here, a system embedded into the data stream that is able to *trace* the degradations introduced by the transmission system composed by the coder-channel cascade and not perceptually affecting the data themselves is described.

A set of uncorrelated pseudorandom noise (PN) matrices is multiplied by the reference watermark. Both the PN matrices and the embedded watermark are known at the receiving side. The watermark is the same for each video sequence frame, whereas the PN matrices are different for each frame. This insures that the spatial localization of the mark is different frame-by-frame so that the watermark visual persistency is negligible.

After the randomization of the watermark by the PN matrices, the embedding of the tracing marks is performed in the DCT domain. The watermark is embedded in the DCT middle-band

frequencies of the whole image. After the inverse DCT (IDCT) has been performed on each frame, the whole sequence is coded by a video coder and, finally, transmitted.

At the receiving side, the video is first decoded; then, from the DCT of each received frame of the sequence, a matched filter extracts the spread watermark, which is finally despread using the known PN matrices. After having extracted the received watermark, it is matched to the reference one, which is known at the receiving side, and the mean-square error (MSE), between the original mark and the received one, is used as an index of the degradation affecting the received watermark.

21.1.1 System modeling

A two-dimensional video sequence will be represented as $\{f_i[n_1, n_2], i = 1, 2, \ldots M\}$. The sequence is composed of M frames $f_i[n_1, n_2]$ of $N_1 \times N_2$ pixels. Let $\omega[k_1, k_2]$ be the employed watermark, having dimensions $K_1 \times K_2$ and $\{p_i[k_1, k_2], i = 1, 2, \ldots M\}$ the M PN matrices of dimensions $K_1 \times K_2$. The watermark $\omega[k_1, k_2]$ is a visual pattern, like a logo, consisting of binary pixels.

The PN matrices $\{p_i[k_1, k_2], i = 1, 2, \ldots M\}$ are employed to spread a narrowband signal (watermark) over a much larger bandwidth signal (host frame) in such a way that the watermark energy is undetectable in any single frequency of the host image. This can be expressed as follows: $\omega_i^{(s)}[k_1, k_2] = \omega[k_1, k_2] \cdot p_i[k_1, k_2], i = 1, 2, \ldots, M$, where $\omega_i^{(s)}[k_1, k_2]$ is the spread version of the watermark to be embedded in the ith frame. Let $F_i[k_1, k_2] = \mathrm{DCT}\{f_i[n_1, n_2]\}$ be the DCT transform of the ith frame $f_i[n_1, n_2]$. The spread watermark is embedded, in the DCT domain, in the middle-high frequency region S of $F_i[k_1, k_2]$.

The embedding is performed in the DCT domain according to the following rule:

$$F_i^{(\omega)}[k_1, k_2] = \begin{cases} F[k_1, k_2] + \alpha\omega_i^{(s)}[k_1, k_2], & (k_1, k_2) \in S \\ F[k_1, k_2], & (k_1, k_2) \notin S \end{cases} \tag{21.1}$$

where $F_i^{(\omega)}[k_1, k_2]$ represents the DCT of the ith watermarked frame $f_i[n_1, n_2]$, and α is a scaling factor that determines the watermark strength. Parameter α must be chosen in such a way as to compromise between not degrading the picture on one side and being detectable by the tracing algorithm on another.

The ith watermarked frame is then obtained by performing the IDCT transform $f_i^{(\omega)}[n_1, n_2] = \mathrm{IDCT}\{F_i^{(\omega)}[k_1, k_2]\}$. Finally, the whole sequence is coded and then transmitted through a noisy channel. If $\{\hat{f}_i^{(\omega)}[n_1, n_2], i = 1, 2, \ldots M\}$ is the received video sequence then the DCT transform in the receiver gives $\hat{F}_i^{(\omega)}[k_1, k_2] = \mathrm{DCT}\{\hat{f}_i^{(\omega)}[n_1, n_2]\}$.

The middle–high frequency region of embedding S is selected. Then, the corresponding portion of $\hat{F}_i^{(\omega)}[k_1, k_2]$ is multiplied by the watermark $\omega[k_1, k_2]$, which is known at the receiving side, giving an estimation $\hat{\omega}_i^{(s)}[k_1, k_2]$ of the spread version of the watermark embedded in the ith frame, $\hat{\omega}_i^{(s)}[k_1, k_2] = \hat{F}_i^{(\omega)}[k_1, k_2] \cdot \omega[k_1, k_2]$. The dispreading operation, for the generic ith frame gives $\hat{\omega}_i[k_1, k_2] = \hat{\omega}_i^{(s)}[k_1, k_2] \cdot p_i[k_1, k_2]$. Finally, the watermark is estimated by averaging the dispread watermark over the M transmitted frames

$$\hat{\omega}[k_1, k_2] = \frac{1}{M} \sum_{i=1}^{M} \hat{\omega}_i[k_1, k_2] \tag{21.2}$$

The QoS is evaluated by comparing the extracted watermark with the original one. Formally this can be represented as

$$\mathrm{MSE}_i = \frac{1}{K_1 K_2} \sum_{K_1=1}^{K_1} \sum_{k_2=1}^{K_2} (\omega_i[k_1, k_2] - \hat{\omega}_i[k_1, k_2])^2 \tag{21.3}$$

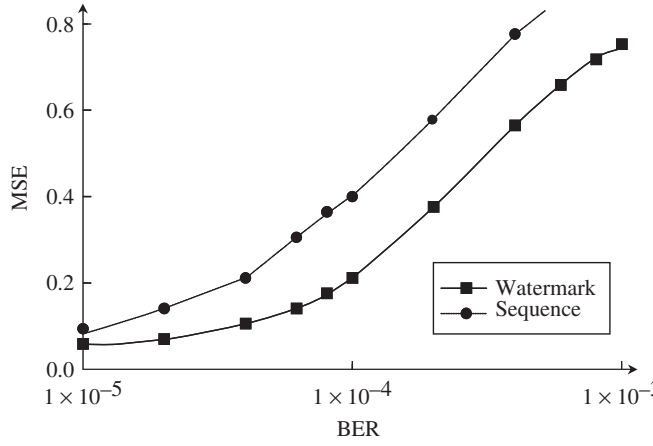

Figure 21.3 Watermark MSE and video sequence MSE (normalized to 1) vs the BER for the sequence 'Akiyo' MPEG-2 coded at 600 kb/s.

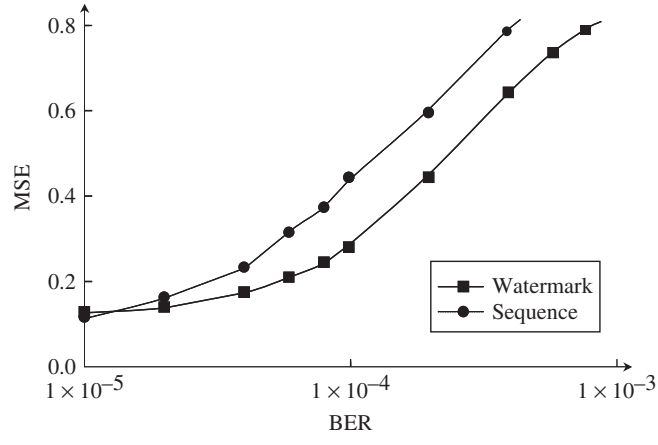

Figure 21.4 Watermark MSE and video sequence MSE (normalized to 1) vs the BER for the sequence 'Akiyo' MPEG-2 coded at 200 kb/s.

and

$$\mathrm{MSE} = \frac{1}{M}\sum_{i=1}^{M}\mathrm{MSE}_i \tag{21.4}$$

In experiments presented in References [26, 28], the dimensions of the video sequences employed have been properly chosen in order to simulate a multimedia service in a UMTS scenario. Therefore, QCIF (144 × 176) video sequences, which well match the limited dimensions of a mobile terminal's display, have been employed. Sample results are shown in Figures 21.3 and 21.4. As shown in the figures, the quality degradation of the watermark embedded into the host video has the same behavior as the one affecting the video.

21.2 QoS PROVISIONING IN WLAN

As an example system, the 802.11 WLAN consists of *basic service sets* (BSS), each of which is composed of wireless stations (STA). The WLAN can be configured as an *ad hoc* network (an independent BSS) or an infrastructure network (composed of an access point and the associated STAs).

The channel access for the STAs in a BSS is under the control of a coordination function. The 802.11 MAC protocol provides two coordination functions: *distributed coordination function* (DCF) and *point coordination function* (PCF). The DFC is a contention-based access scheme using *carrier sense multiple access with collision avoidance* (CSMA/CA).

Priority levels for access to the channel are provided through the use of *interframe spaces* such as short interframe space (SIFS) and distributed interframe space (DIFS). The backoff procedure is used for collision avoidance, where each STA waits for a *backoff time* (a random time interval in units of slot times) before each frame transmission. The PCF provides contention-free frame transmission in an infrastructure network using the *point coordinator* (PC), operating at the access point (AP), to determine which STA currently gets the channel access. The DCF and the PCF can coexist by alternating the *contention period* (CP), during which the DCF is performed, and the *contention-free period* (CFP), during which the PCF is performed. A CFP and a CP are together referred to as a *repetition interval* or a *superframe*. Different aspects of 802.11 WLAN are discussed in References [29–40]. The performance analysis of the DCF was studied in References [29, 30, 35]. The performance of DCF degrades in high traffic loads due to serious collisions. The CSMA/CA is not suitable for data traffic at higher channel speeds [29] due to the large waste on the backoff time. The influence of various sizes of the backoff time on the channel throughput and the optimal setting of the backoff time was studied in Cali *et al.* [31]. A common technique is to adjust the backoff time according to the traffic priority. The PCF based on a polling scheme is suitable for time-bounded real-time traffic. The simple polling schedules for voice traffic and video traffic are presented in Crow *et al.* [35]. Some complex polling schedules are proposed in References [32–34, 36, 39].

To expand support for applications with QoS requirements, the IEEE 802.11E task group [37] is proceeding to build the QoS enhancements of the 802.11 MAC. The techniques for providing prioritized and parameterized QoS data deliveries have been discussed in the task group. An enhanced DCF was proposed, where each traffic flow is assigned with a different backoff time whose value decreases with increasing traffic priority, to achieve the prioritized QoS data delivery. To guarantee the bounded delay requirements in the parameterized QoS data delivery, the hybrid coordination function (HCF) was proposed [42]. In the HCF, an STA can be guaranteed to issue the frame transmission even during the CP using the contention-free burst (CFB). The CFB can be considered a temporary CFP during which the transmissions of STAs are coordinated by the polling scheme as the PCF. Moreover, a multipolling mechanism (called contention-free multipoll, CF-multipoll) was proposed [41] to reduce the polling overhead that the traditional PCF suffers from. In the multipoll, the PC can poll more than one STA simultaneously using a single polling frame.

In this section, we consider how to efficiently serve real-time traffic in the IEEE 802.11 WLAN by using the multipolling mechanism. The multipolling mechanism can increase the channel utilization and is robust in mobile and error-prone environments. The mechanism can be used in the PCF and the HCF. Moreover, a polling schedule is provided to guarantee the bounded delay requirements of real-time flows.

21.2.1 Contention-based multipolling

In the PCF or the HCF, each STA in the polling list takes a polling frame when polled. This polling scheme is called *SinglePoll*. The number of polling frames for a polling list can be reduced

if a multipolling mechanism is used. Here, we discuss an efficient multipolling mechanism that has the advantages of high channel utilization and low implementation overhead. This multipolling mechanism, referred to as *contention period multipoll (CP-Multipoll)*, incorporates the DCF access scheme into the polling scheme.

In the DCF, any contending STA for the channel will select a backoff time in units of slot times and execute the backoff procedure as follows: if the channel is sensed idle for a DIFS period, an STA starts the transmission immediately. Otherwise, an STA should defer until the channel becomes idle for a DIFS period and then the backoff time is decreased. If the channel is idle for a slot time, an STA decreases the backoff time by one or else freezes the backoff time. When the backoff time becomes zero, an STA begins the frame transmission. If a collision occurs, the STA duplicates the backoff time used in the last transmission and executes the backoff procedure again. In the DCF, the virtual carrier sensing using the *Network Allocation Vector* (NAV) is performed at the MAC sublayer. The information on the duration of a frame exchange sequence for one STA is included in the frame header (duration field) and is announced to other STAs. Other contending STAs will wait for the completion of the current frame exchange by updating their NAVs according to the announced duration information. For a communication the RTS (*request to send*) and CTS (*clear to send*) frames are exchanged before the data frame transmission. Other STAs defer their channel access by setting their NAVs according to the duration field in the RTS, the RTS, or the data frame. The exchange of RTS/CTS frames can also avoid the hidden terminal problem [35].

The basic idea of CP-Multipoll is to transform the polling order into the contending order which indicates the order of winning the channel contention. Different backoff time values are assigned to the flows in the polling group and the corresponding STAs execute the backoff procedures after receiving the CP-Multipoll frame. The contending order of these STAs is the same as the ascending order of the assigned backoff time values. Therefore, to maintain the polling order in a polling group, we can assign the backoff time value incrementally according to the expected polling order.

The CP-Multipoll has the following advantages: a polled STA can hold the channel access flexibly depending on the size of local buffered data, so it becomes easy to deal with the data burst; if a polled STA makes no response to the CP-Multipoll, other STAs in the same polling group will detect the channel idle right away and advance the starting of channel contention. Therefore, the CP-Multipoll can decrease the waste of channel space and can afford any polling error.

21.2.2 Polling efficiency

We consider the environment with overlapping BSSs. In the overlapping BSS, we distinguish the STAs associated with one BSS from the STAs associated with neighboring BSSs by using the terms ‘internal STAs’ and ‘external STAs’, respectively. Moreover, a STA that will cause an internal collision is called a nonbehaved STA; otherwise, the STA is called a behaved one.
The following terminology is used in the performance analysis:

- *frame_num*, maximum number of data frames allowed to be transmitted in a TXOP (transmission opportunity);
- l_{type}, number of bits in a ‘type’ frame;
- t_{type}, transmission time on the channel for a ‘type’ frame;
- *single-poll*, the single polling frame in the single poll (i.e. CF-Poll frame);
- n, poll size (i.e. the number of poll records in a multipolling frame);
- n-poll, the multipolling frame with n poll records;
- ERR_{type}, probability that a ‘type’ frame is dropped due to bit errors;
- α, probability that an STA has no data to send when polled;

- β, probability that an STA becomes a nonbehaved STA;
- h, number of PCs operating in the overlapping space;
- *InitBT*, initial backoff time;
- E, polling efficiency.

The following assumptions will be used in the analysis:

(1) The PC (point coordinator) always performs the initial backoff before sending any polling frame.

(2) The data frame is transmitted without any acknowledgment. When an STA is polled, the STA either sends a half of *frame_num* data frames on average or sends a null data frame if there is no data to send.

(3) There is an equal probability BER for a bit error to occur due to the channel noise (interference, fading or multipath). Hence, ERR_{type} can be expressed as $1-(1-BER)^{l_{\text{type}}}$.

(4) An STA becomes a nonbehaved one if the STA fails to receive the CTS frame from the PC. That is, $\beta = ERR_{\text{CTS}}$.

If $AvgD$ and $AvgT$ denote the total number of bits in the data frames successfully sent from the polled STAs and the average complete time in time units for a poll, respectively, then the polling efficiency is defined as $E = AvgD/AvgT$. This represents the average uplink data rate during a poll.

In the single poll, a polled STA contributes data frames if the STA successfully receives a CF-Poll frame and has pending data frames to be successfully transmitted. The polled STA may suffer frame error due to interference from external STAs. Therefore,

$$\begin{aligned} AvgD = {} & (1-\alpha)\cdot frame\_num/2 \cdot l_{\text{data\_frame}} \\ & (1-ERR_{\text{data\_frame}})\cdot(1-ERR_{\text{single\_poll}}) \end{aligned} \tag{21.5}$$

The polled STA will give a response to the PC after an SIFS period for a successful CF-Poll. If a polled STA does not respond to the PC after a PIFS period for a failed CF-Poll, the PC takes over the channel control and may send the next CF-Poll frame. In the HCF, the RTS/CTS frames should be exchanged before the data transmission to prevent the interference from other STAs. Since the HCF is being substituted for the PCF in the 802.11E, we consider the single poll of the HCF in our analysis. Therefore,

$$\begin{aligned} AvgT = {} & InitBT + (t_{\text{single-poll}} + PIFS)\cdot ERR_{\text{single-poll}} + [t_{\text{single-poll}} + SIFS \\ & + t_{\text{RTS}} + t_{\text{CTS}} + 2SIFS + (1-\alpha)frame\_num/2 \cdot (t_{\text{data\_frame}} + SIFS) \\ & + \alpha(t_{\text{null\_frame}} + SIFS)]\cdot(1-ERR_{\text{single-poll}}) \end{aligned} \tag{21.6}$$

Next, we use a state diagram to represent the situation after sending a multipolling frame with poll size n. In Figure 21.5, the state $m : fail (0 \le m \le n)$ represents the event that there are m STAs in

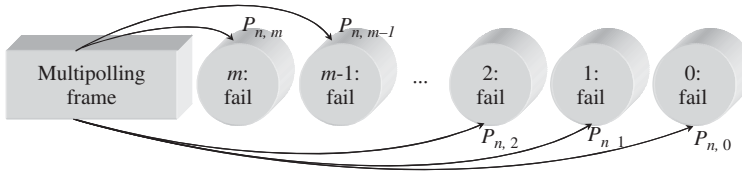

Figure 21.5 The state diagram of the multipolling mechanism. (Reproduced by permission of IEEE [43].)

the polling group which failed to receive the multipolling frame. Let $P_{n,m}$ denote the probability of the state $m : fail$. Let $D_{n,m}$ and $T_{n,m}$ denote the amount of uplink data frames in bits and the total time duration in time units under the state $m : fail$, respectively. Generally, we have the following values:

$$\begin{aligned} P_{n,m} &= \binom{n}{m} \cdot (ERR_{n-\text{poll}})^m \cdot (1 - ERR_{n-\text{poll}})^{n-m} \\ AvgD &= \sum_{m=0}^{n} P_{n,m} \cdot D_{n,m} \\ AvgT &= InitBT + \sum_{m=0}^{n} P_{n,m} \cdot T_{n,m} \end{aligned} \tag{21.7}$$

For the CF-Multipoll, the external STAs in the overlapping BSS will have their TXOPs overlap the ones allocated to the internal STAs. We assume that the interference from external STAs has been included in the parameter BER. Hence,

$$D_{n,m} = (n - m) \cdot (1 - \alpha) \cdot frame\_num/2 \cdot l_{\text{data\_frame}} \cdot (1 - ERR_{\text{data\_frame}})$$

Also, each successive TXOP starts an SIFS period after the predecessor's TXOP limit expires in the CF-Multipoll. Note that the time spent by a polled STA is fixed regardless of the number of pending data frames. Hence,

$$T_{n,m} = t_{n-\text{poll}} + n \cdot SIFS + n \cdot frame\_num \cdot (t_{\text{data\_frame}} + SIFS) \tag{21.8}$$

In the CP-Multipoll, there are two processing phases: one is for the normal multipoll and the other is for the error recovery. In the normal phase, there are $(n - m)$ STAs successfully receiving the multipolling frame under the state $m : fail$. Among these STAs, $(1 - \beta)(n - m)$ STAs are behaved STAs and $\beta(n - m)$ STAs are nonbehaved ones. Each nonbehaved STA is assumed to destroy one data frame transmitted by a behaved one. In the recovery phase, m STAs failed to receive the multipolling frame and $(n - m)$ nonbehaved STAs will be served individually using the CP-Multipoll with poll size one. The analysis of this phase is similar to the one in the single poll. Hence, $D_{n,m}$ has the following value:

$$\begin{aligned} D_{n,m} &= D_{n,m}^{\text{normal}} + D_{n,m}^{\text{recovery}} \\ D_{n,m}^{\text{normal}} &= [(1 - \beta) \cdot (n - m) \cdot frame\_num/2 - \beta(n - m)] \\ &\quad (1 - \alpha) \cdot l_{\text{data\_frame}} \cdot (1 - ERR_{\text{data\_frame}}) \\ D_{n,m}^{\text{recovery}} &= [m + \beta(n - m)] \cdot (1 - \alpha) \cdot frame\_num/2 \\ &\quad l_{\text{data\_frame}} \cdot (1 - ERR_{\text{data\_frame}}) \cdot (1 - ERR_{1-\text{poll}}) \end{aligned} \tag{21.9}$$

The length of the time of the normal phase is dominated by the transmission time of those $(1 - \beta)(n - m)$ behaved STAs. The total backoff time consumed in the normal phase is $h \times n + 1$, regardless of the value m. Hence,

$$\begin{aligned} T_{n,m} &= T_{n,m}^{\text{normal}} + T_{n,m}^{\text{recovery}} \\ T_{n,m}^{\text{normal}} &= t_{n-\text{poll}} + (h \cdot n + 1) \cdot Slot + (1 - \beta) \cdot (n - m) \\ &\quad (t_{\text{RTS}} + t_{\text{CTS}} + 2\,SIFS + (1 - \alpha) \cdot frame\_num/2 \cdot (t_{\text{data\_frame}} + SIFS) \\ &\quad + \alpha \cdot t_{\text{null\_frame}}) T_{n,m}^{\text{recovery}} = [m + \beta(n - m)] \cdot [(t_{1-\text{poll}} \\ &\quad + 2\,Slot) \cdot ERR_{1-\text{poll}} + (t_{1-\text{poll}} + 2\,Slot + t_{\text{RTS}} + t_{\text{CTS}} + 2\,SIFS + (1 - \alpha) \\ &\quad frame\_num/2 \cdot (t_{\text{data\_frame}} + SIFS) + \alpha \cdot t_{\text{null\_frame}}) \\ &\quad (1 - ERR_{1-\text{poll}})]. \end{aligned} \tag{21.10}$$

Table 21.1 System and poll-related parameters. (Reproduced by permission of IEEE [43])

Parameter	Value
Channel rate	11 Mbs
PHYheader	192 b
MAC header	272 b
Slot	20 μs
SIFS	10 μs
DIFS	50 μs
PIFS	30 μs
Superframe	25 μs
CFP_Max_Duration	20 μs
frame_num	3
ldata_frame(*octets)*	200(default), 400, 600, 800
lnull_frame(*octets*)	34
lsingle_poll(*octets*)	34
ln_poll(*octets*)	$16 + 8n$
n	1–20
BER	10^{-3}, 10^{-4}, 10^{-5}(default), 10^{-6}
α	0.2 (default), 0.4, 0.6, 0.8
h, the number of PCs operating in the overlapping space	1, 2 (default), 3, 4
InitBT(μs)	90(default), 110, 130, 150

The superpoll can poll a group of STAs together as the CF-Multipoll and the CP-Multipoll. In the superpoll, the polled STA will attach the poll records of those polled ones whose polling orders are after it to its current transmitted data frame. This scheme can be considered as one with replicated poll records. To keep the correct polling order, each polled STA in the polling group should monitor the channel and check whether the previous STA has finished sending a data frame. If a polled STA fails to receive its poll record, the next following STA in the polling group will wait for a timeout before its own frame transmission. However, the situation where some STAs cannot listen to other STAs' channel activities is not considered. This may cause inconsistent setting of timers among polled STAs and may cause internal collisions.

21.2.2.1 Performance example

The parameter settings related to system and the polling schemes are listed in Table 21.1 [43]. The performance improvement of CP-Multipoll in percentage over other schemes is shown in Figure 21.6.

21.3 DYNAMIC SCHEDULING ON RLC/MAC LAYER

In wireless networks, the fading characteristics of the wireless physical channel may introduce location-dependent channel errors. A scheduling algorithm, referred to as *channel-condition independent packet fair queueing* (CIF-Q), is presented in Ng *et al.* [44] to solve the problem of location-dependent channel errors in wireless networks by suspending transmission service of a connection of a mobile station (MS) when the MS is in a high BER region. *To compensate for the*

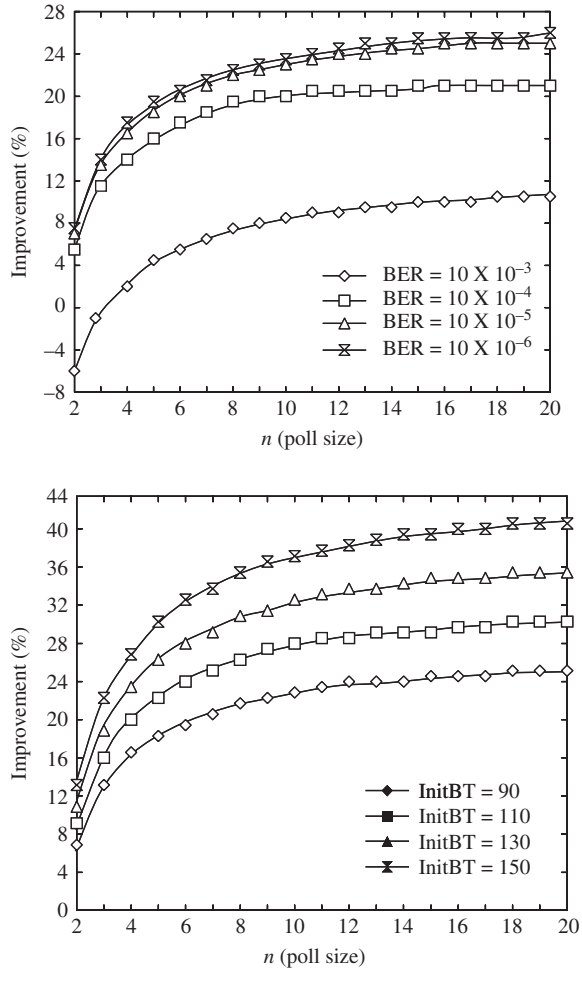

Figure 21.6 Comparison between single poll and CP-Multipoll.

service loss of the MS in a high BER region, the CIF-Q scheduling algorithm increases the service priority after the MS returns to a low BER region to fulfill its QoS specification. However, this suspension may cause long delays for the connection of the MS, because the duration that an MS resides within a high interference region may be unpredictably long. In many services, such as video transmissions, minor errors are acceptable to the receiver-side applications, but a long delay is not.

In Yars *et al*. [45], a scheduling scheme at the RLC/MAC layer is proposed, referred to as a dynamic scheduling mechanism for mobile communication (DSMC). The scheme is discussed in the context of GPRS applications. DSMC is a dynamic scheduling architecture that can conform to a variety of QoS requirements in the networks without changing the coding rate on RLC layer. The DSMC scheduling scheme, which is based on the self-clocked fair queuing (SCFQ) algorithm [46], can dynamically adjust the service rate (weight) for a particular connection in accordance with the channel quality. It will use the low service rate when an MS is within a high interference

(*high-IF*) region to reduce bandwidth waste due to retransmissions, and use the high service rate when the MS is within a low interference (*low-IF*) region to fulfill the QoS requirements (e.g. delay bound and loss ratio) of the MS. The high and low service rates are both determined at connection setup time. Thus, the complexity of scheduling algorithm in wireless networks can be reduced.

21.3.1 DSMC functional blocks

An MS issues a connection request to the CAC controller by specifying its QoS requirements $(D_{e,k}, R_p, R_m)$, its priority level e, as well as the number of blocks m to be transmitted. $D_{e,k}$ is the delay bound required for the requested session k with a priority of e on air interface, U_m. R_p and R_m, respectively, denote the peak and the minimum data rates requested by the session k. In other words, the MS requests that m blocks of the session k should be scheduled in a queue of priority level e, and transmitted at a minimum rate higher than R_m or a peak rate not higher than R_p before the delay bound $D_{e,k}$ is reached. The minimum data rate R_m is used as the low service rate when the MS is within a high interference region. On the other side, the peak data rate R_p is not taken for granted as the high service rate when the MS is within a low interference region. Instead, the high service rate is determined by a simple calculation performed by the service rate (SR) calculator inside the radio resource manager. The SR calculator determines the admissible peak data rate (high service rate) R'_p that can be supported by the BSS according to the delay bound $D_{e,k}$, and the minimum data rate R_m under a hypothetical interference model of the MS.

As in many examples throughout the book, the interference model is based on a two-state Markov chain with transition probabilities α and β. These parameters α and β can be collected from a user behavior profile and can be updated dynamically. After receiving the R'_p from the SR calculator, the CAC controller can optionally accept, reject or renegotiate with the MS. If the connection request is accepted, the CAC controller stores the parameters (R'_p, R_m, m, e) to a parameter database. The rate selector can then select and send the current data rate R to the CCU (channel codec unit) associated with the MS according to the interference level measured by the interference monitor.

The *DSMC scheduling architecture* can be situated in a BSS of the GPRS networks and applied to either uplink or downlink transmission. The system will adopt a certain number of priority levels. As an example, in GPRS, block transmission is classified into five scheduling priority levels, including four data priority levels and a signal priority level, which is the highest priority level [47]. The DSMC scheduling architecture follows the specification but includes a new data priority level for the retransmission blocks. The DSMC scheduling architecture [45] consists of five scheduling servers for data block transmission, one server for each priority level. Each server is responsible for scheduling data blocks transmitting through a single packet data channel (PDCH). The highest priority level, $P1$, is for the retransmission blocks and the lowest priority level, $P5$, is for the best-effort data blocks. Both $P1$ and $P5$ schedule data blocks in a first-come-first-served order. However, the scheduling servers of priority levels $P2$–$P4$ adopt the SCFQ scheduling algorithm in scheduling data blocks of QoS specific connections. In other words, multiple queues may exist in each priority of $P2$–$P4$. The queues with the same priority will be served in accordance with the SCFQ scheduling algorithm, to be explained in below.

The block requests of a particular priority can not be served until all the blocks of the higher priority have been served. The transmission of a block is nonpreemptive.

The *SCFQ scheduling algorithm* is basically a packet-based general processor sharing scheme [48, 49] without the complex virtual clock tracking mechanism. The elimination of the virtual clock tracking mechanism makes SCFQ easier to implement on a high-speed network. In SCFQ, an arrival block request is tagged with a service finish time (FT) before it is placed in a queue. The service FT tag of a block request is computed from the service time and the service starting

time of the block as

$$\text{FT} = \frac{\text{block length}}{\text{service rate}} + \max(\text{FT of the tail block, FT of the serving block})$$

The service starting time of the block can be the FT of the tail block of the queue if the queue is nonempty, or it is the FT of the serving block. The block requests among the heads of the queues will be picked up to be served one by one in accordance with the increasing order of FT tags, and in a round-robin fashion if more than two heading blocks have the same FT tags.

21.3.2 Calculating the high service rate

In order to determine the service rate, we need to first obtain the total delay of a block. The total delay depends on the service discipline and the input traffic. Owing to the bursty nature of multimedia traffic streams, a leaky-bucket regulator, as discussed in Chapter 8, is assumed at the network interface of the sender site to regulate the block request flow of each session.

In the DSMC scheduling scheme, a block of a connection will experience queueing delay, block transmission delay, and retransmission delay. A block at the head of a queue (henceforth referred to as a 'heading block') may experience a priority delay, which, in turn, consists of an *interpriority delay* caused by all block transmissions in the higher priority levels and an *intrapriority delay* resulted from the SCFQ scheduling.

Each preceding block of the newly arrived block will experience a priority delay and a block transmission delay when the preceding block becomes a heading block. In addition, the newly arrived block will experience an intrapriority delay when it becomes the heading block of the queue itself. Hence, the queueing delay of a block is, thus, the summation that the priority delay and the block transmission delay experienced by all preceding blocks, plus the intrapriority delay experienced by the block. In analytical modeling the following notation will be used:

- sj, session j
- L, block length (b);
- $P_{\text{hi}}^{\text{be}}$, block error probability when the block is transmitting within a high-interference region;
- $P_{\text{li}}^{\text{be}}$, block error probability when the block is transmitting within a low-interference region;
- P_{hi}, stationary probability that the MS is within a high-interference region;
- P_{li}, stationary probability that the MS is within a low-interference region;
- $(r_{e,k})^{\text{hi}}$, low service rate of session k of priority e;
- $(r_{e,k})^{\text{li}}$, high service rate of session k of priority e;
- $(HD_{e,k})^{\text{hi}}$, heading-block delay of session k of priority e within a high-interference region;
- $(HD_{e,k})^{\text{li}}$, heading-block delay of session k of priority e within a low-interference region;
- $\overline{b}_{e,k}$, mean queue length of the session k of priority e;
- $\overline{w}_{e,k}$, mean queueing delay with the session k of priority e;
- dp, data priorities.

The *interpriority delay* is the time that the selected heading block waits for the blocks from higher priority levels to be served. In the following, we refer to the priority level under discussion as the priority e. Let $A_{p,s}[t_1, t_2]$ denote the amount of blocks arrived to a session with a priority p during a time interval (t_1, t_2) and $W_{p,s}[t_1, t_2]$, is the number of blocks served for a session with

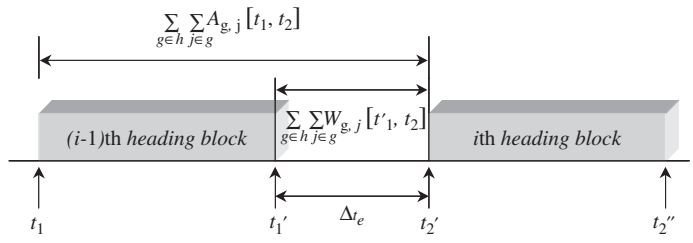

Figure 21.7 Dealy caused by higher priority session to the particular priority. (Reproduced by permission of IEEE [45].)

a priority p during a time interval (t_1, t_2). As shown in Figure 21.7, after the $(i-1)$th selected heading block has been served, the ith heading block selected by the server of the priority e may encounter an interpriority delay, which is the time period (t_1', t_2). Each session j with a priority g higher than e must be served up within the time period (t_1', t_2). Thus, the amount of traffic served during the time period (t_1', t_2), $W_{g,g}[t_1', t_2]$, is equal to the amount of arrival traffic to the session during the time period (t_1, t_2), $A_{g,j}[t_1, t_2] = A_{g,g}[t_1, t_1' + \Delta t_e]$, as in Equation (21.11). Here, t_1' is the epoch of the final time of serving the $(i-1)$th heading block selected from the priority e and Δt_e the interpriority delay encountered by each heading block selected from the priority e

$$W_{g,j}[t_1', t_2] = A_{g,j}[t_1, t_2], \forall t_2 > t_1' > t_1, t_1 \geq 0 \tag{21.11}$$

Let H represent the set of all priority levels higher than e. Summing up Equation (21.11) for all sessions of the priorities in H, we have the following inequality:

$$\sum_{g\in H}\left[\sum_{sj\in g} W_{g,j}[t_1', t_2]\right] = \sum_{g\in H}\left[\sum_{sj\in g} A_{g,j}[t_1, t_2]\right] \forall t_2 > t_1' > t_1, t_1 \geq 0 \tag{21.12}$$

where sj stands for session j. The traffic $A_{g,j}[t, t+\tau]$ during a time period $(t, t+\tau)$ has an upper bound since the DSMC scheduling architecture uses a leaky bucket to regulate the flow of each session [8]. Let $A^*_{g,j}(\tau)$ denote the upper bound of $A_{g,j}[t, t+\tau]$. From Chapter 8 and also Cruz [50], we have the following inequality according to the *leaky-bucket constrained* envelope function:

$$A_{g,j}[t, t+\tau] \leq A^*_{g,j}(\tau) = \sigma_{g,g} + \rho_{g,j} \cdot t \quad \forall t \geq 0, \quad \forall \tau \geq 0 \tag{21.13}$$

where $\sigma_{g,g}$ is the leaky-bucket size and $\rho_{g,j}$ is the token arrival rate for the session j of the priority g. Therefore, from the above leaky-bucket constraint, we can derive the following inequality:

$$\sum_{g\in H}\left[\sum_{sj\in g} A_{g,j}[t_1, t_2]\right] \leq \sum_{g\in H}\left[\sum_{sj\in g} A^*_{g,j}(t_2 - t_1)\right] \quad \forall t_2 > t_1' > t_1, t_1 \geq 0 \tag{21.14}$$

Since the retransmission of data blocks has the highest priority and there is only one retransmission queue, we can denote the arrival traffic to the retransmission queue during the period (t_1, t_2) as $A_{1,1}[t_1, t_2]$. The retransmission traffic is the aggregated traffic of the retransmission of all sessions. By observing the system over a substantially long period of time, we can find that $A_{1,1}[t_1, t_2]$ also conforms to the leaky-bucket constraint, and we rewrite the above inequality Equation (21.1) as

$$A_{1,1}[t_1, t_2] + \sum_{g\in h, g\neq 1}\left[\sum_{sj\in g} A_{g,j}[t_1, t_2]\right] \leq A^*_{1,1}(t_2 - t_1) + \sum_{g\in h, g\neq 1}\left[\sum_{sj\in g} A^*_{g,j}(t_2 - t_1)\right]$$

$$\forall t_2 > t_1' > t_1, t_1 \geq 0 \tag{21.15}$$

By using notation specified earlier we can derive the equation for $A^*_{1,1}(t_2 - t_1)$ as

$$A_{1,1}[t_1, t_2] \le A^*_{1,1}(t_2 - t_1) = L \times \sum_{s \in \{dp\}} \left\{ \lceil \frac{\sum_{sj \in s} \sigma_{s,j} + \rho_{s,j} \cdot (t_2 - t_1)}{L} \rceil \times P^{\text{be}}_{\text{hi}} \times P_{\text{hi}} + \lceil \frac{\sum_{sj \in s} \sigma_{s,j} + \rho_{s,j} \cdot (t_2 - t_1)}{L} \rceil \times P^{\text{be}}_{\text{li}} \times P_{\text{li}} \right\} \quad (21.15a)$$

By combining Equation (21.12) and inequality Equation (21.15), we have

$$\sum_{g \in h} \left[\sum_{sj \in g} W_{g,j}[t'_1, t_2] \right] \le A^*_{1,1}(t_2 - t_1) + \sum_{g \in h, g \ne 1} \left[\sum_{sj \in g} A^*_{g,j}(t_2 - t_1) \right]$$

$$\forall t_2 > t'_1 > t_1, t_1 \ge 0$$

Finally, if C_i is the link capacity of the radio band (channel) i, by applying the inequality Equation (21.13) we have

$$C_i \times \Delta t_e \le A^*_{1,1}(\Delta t_e + t'_1 - t_1) + \sum_{g \in h, g \ne 1} \left[\sum_{sj \in g} \sigma_{i,j} + \rho_{i,j} \times (\Delta t_e + t'_1 - t_1) \right]$$

$$\forall t_2 > t'_1 > t_1, t_1 \ge 0 \quad (21.16)$$

From the above inequality, we calculate the maximum value of Δt_e.

The *intrapriority delay* is delay contributed from the SCFQ scheduling delay. It is the delay during which a heading block of a session waits for the heading blocks of some other sessions with the same priority to be served. Following the results presented by Golestani [51], we can derive the maximum intrapriority delay of the heading block of a session k with priority e as $(|\kappa_e| - 1) \cdot (L/C_i)$, where C_i represents the capacity (b/s) of link (band) i, κ_e represents the set of backlog sessions for priority e, and $|\kappa_e|$ represents the number of backlog sessions in the priority e.

21.3.3 Heading-block delay

A heading block will encounter an intrapriority delay, an interpriority delay, and a block transmission delay of its own. The heading-block delay, denoted HD, for an MS depends on the transmission rates and can be derived as

$$(HD_{e,k})^{\text{li}} = |\kappa_e| \cdot \Delta t_e + (|\kappa_e| - 1) \cdot \frac{L}{C_i} + \frac{L}{(r_{e,k})^{\text{li}}} \quad (21.17)$$

$$(HD_{e,k})^{\text{hi}} = |\kappa_e| \cdot \Delta t_e + (|\kappa_e| - 1) \cdot \frac{L}{C_i} + \frac{L}{(r_{e,k})^{\text{hi}}} \quad (21.18)$$

where $(r_{e,k})^{\text{li}}$ and $(r_{e,k})^{\text{hi}}$ are the service rate (b/s) of session k of priority e, i.e. the high and low service rate, within low-IF region and high-IF region, respectively. The item on the further right-hand side in each of the above equations represents the transmission delay of the heading block of the session k with the priority e. Since Δt_e is likely to be short under the control of the leaky-bucket regulator, HD is relatively small compared with the mean duration that an MS will stay in an interference region. Therefore, it was assumed that the interference condition will not change during a heading-block delay.

The *queueing delay* of a data block is the time during which the block waits until the block is selected for transmission. Clearly, a data block newly arrived in a queue cannot be served by the corresponding SCFQ server until all the proceeding data blocks in the same queue have been

served. Therefore, the queueing delay of a data block includes the time that the block waits for it to become a heading block itself, plus the interpriority and intrapriority delays that the block encounters when it becomes a heading block.

If $\overline{b}_{e,k}$ represent the mean queue length of a session k with a priority e then from Little's result, from Chapter 6, the mean queue length encountered by a newly arrived data block is equal to the block arrival rate multiplied by the mean heading-block delay time. Parameter $\overline{b}_{e,k}$ is given as

$$\overline{b}_{e,k} = \lceil \frac{\rho_{e,k}}{L} \rceil \cdot \left[(HD_{e,k})^{\text{li}} \cdot P_{\text{li}} + (HD_{e,k})^{\text{hi}} \cdot P_{\text{hi}} \right] \tag{21.19}$$

Now, the mean queueing delay $\bar{w}_{e,k}$ for the session k with a priority e can be calculated as

$$\overline{w}_{e,k} = \lceil \frac{\rho_{e,k}}{L} \rceil \cdot \left[(HD_{e,k})^{\text{li}} \cdot P_{\text{li}} + (HD_{e,k})^{\text{hi}} \cdot F_{\text{hi}} \right]^2 + |\kappa_e| \cdot \Delta t_e + (|\kappa_e| - 1) \frac{L}{C_i} \tag{21.20}$$

21.3.4 Interference model

We assume that the general interference model is an interrupted poisson process with transition probabilities of α and β. Hence, the duration that an MS is within the low- region or the high-interferece region can be represented, respectively, by an exponential distribution $1 - \mathrm{e}^{-\alpha \cdot t}$, denoted $L(t)$, or $1 - \mathrm{e}^{-\beta \cdot t}$, denoted $H(t)$.

The interference state in which a block is served is determined by the starting state and the waiting time of the block. Therefore, we use an alternating renewal process to calculate the probability of the interference state in which a block is served. In this alternating renewal process, the block waiting time can be divided into several renewal intervals. A renewal interval consists of two exponential distributions, $L(t)$ and $H(t)$. Let $F(t)$ be the convolution sum of $L(t)$ and $H(t)$. We use the notation $P_{\text{ls}}^{\text{hi}}(W)$ to represent the probability that a block with a waiting time W arrives when an MS is within a low-interference (IF) region and is served when the MS is within a high-IF region. Following the same convention, the notations of probabilities $P_{\text{ls}}^{\text{li}}(W)$, $F_{\text{hs}}^{\text{hi}}(W)$, and $F_{\text{hs}}^{\text{li}}(W)$ should be self-explanatory. These probabilities can be derived as [52]:

$$\begin{aligned}
P_{\text{ls}}^{\text{li}}(W) &= [1 - L(W)] + \int_0^w [1 - L(W - y)] \mathrm{d} \left[\sum_{n=1}^{\infty} F_n(y) \right] \\
P_{\text{ls}}^{\text{hi}}(W) &= 1 - P_{\text{ls}}^{\text{li}}(W) P_{\text{hs}}^{\text{hi}}(W) = [1 - H(W)] + \int_0^w [1 - H(W - y)] \mathrm{d} \left[\sum_{n=1}^{\infty} F_n(y) \right] \\
P_{\text{hs}}^{\text{li}}(W) &= 1 - P_{\text{hs}}^{\text{hi}}(W)
\end{aligned} \tag{21.21}$$

21.3.5 Normal delay of a newly arrived block

Both the MS-terminated downlink data block and the MS-originated uplink block transmission requests may arrive at an SCFQ queue when the MS is within either a low-IF region with a probability P_{li} or a high-IF region with a probability P_{hi}. A block may be served when the MS is within a high-IF region or a low-IF region. So, the normal delay (without retransmissions) of a newly arrived data block, is equal to $(\overline{b}_{e,k} + 1) \cdot HD_{e,k}$, where $HD_{e,k}$ can be $(HD_{e,k})^{\text{li}}$ or $(HD_{e,k})^{\text{hi}}$. By using the above Equation (21.21), we can obtain the normal delay $(ND_{e,k})$ of a block with a mean waiting time of $\bar{w}_{e,k}$ as

$$\begin{aligned}
ND_{e,k} = \; & P_{\text{li}} \cdot [(\overline{b}_{e,k} + 1) \cdot (HD_{e,k})^{\text{li}} \cdot P_{\text{ls}}^{\text{li}}(\bar{w}_{e,k}) \\
& + (\overline{b}_{e,k} + 1) \cdot (HD_{e,k})^{\text{hi}} \cdot F_{\text{ls}}^{\text{hi}}(\bar{w}_{e,k})] + P_{\text{hi}} \cdot [(\overline{b}_{e,k} + 1) \cdot (HD_{e,k})^{\text{hi}} \cdot P_{\text{hs}}^{\text{hi}}(\bar{w}_{e,k}) \\
& + (\overline{b}_{e,k} + 1) \cdot (HD_{e,k})^{\text{li}} \cdot P_{\text{hs}}^{\text{li}}(\bar{w}_{e,k})]
\end{aligned} \tag{21.22}$$

The *retransmission delay of* each retransmission consists of two delays, the waiting time T_a of a selective ARQ request, and the retransmission time T_r. The transmission of a data block and the retransmission of this block may occur in either interference condition. In other words, a retransmission cycle may start and end in either interference region. Let A denote the mean retransmission delay starting from a low-IF region, whereas B denotes the mean retransmission delay starting from a high-IF region. Hence, we can describe the mean retransmission delays A and B by two cross recursive equations, as shown below. As a consequence, the retransmission delay ($RD_{e,k}$) of a block can be obtained as

$$\begin{aligned}
A &= P_{\text{li}}^{\text{be}}\{(T_a + T_r) + A \cdot P_{\text{ls}}^{\text{li}}(T_a + T_r) + B \cdot P_{\text{ls}}^{\text{hi}}(T_a + T_r)\} \\
B &= P_{\text{hi}}^{\text{be}}\{(T_a + T_r) + B \cdot P_{\text{hs}}^{\text{hi}}(T_a + T_r) + A \cdot P_{\text{HS}}^{\text{low-if}}(T_a + T_r)\} \\
RD_{e,k} &= P_{\text{li}} \cdot \left\{ A \cdot P_{\text{ls}}^{\text{li}} \left(\bar{w}_{e,k} + \frac{L}{(r_{e,k})^{\text{li}}} \right) + B \cdot P_{\text{ls}}^{\text{hi}} \left(\bar{w}_{e,k} + \frac{L}{(r_{e,k})^{\text{hi}}} \right) \right\} \\
&\quad + P_{\text{hi}} \cdot \left\{ B \cdot P_{\text{hs}}^{\text{hi}} \left(\bar{w}_{e,k} + \frac{L}{(r_{e,k})^{\text{hi}}} \right) + A \cdot P_{\text{hs}}^{\text{li}} \left(\bar{w}_{e,k} + \frac{L}{(r_{e,k})^{\text{li}}} \right) \right\}
\end{aligned} \tag{21.23}$$

21.3.6 High service rate of a session

By summing up the normal delay, Equation (21.22), and the retransmission delay, Equation (21.23), of a newly arrived block, the SR calculator can calculate the total delay ($TD_{e,k}$) for a newly arrived block in a session k with a priority e. For simplicity it is assumed that the low service rate of a session when the MS is within a high-IF region is a predefined value. The value of this low service rate can be chosen by a user application in accordance with the required characteristics of the media stream used in the application. For example, the low service rate can be assigned as the minimum tolerable decoding rate of a Motion Pictures Expert Group (MPEG) video stream.

If we assume that a session k with a priority e has a QoS specification for m block transmissions with air-interface delay bound $D_{e,k}$, then the SR calculator can calculate the high service rate of the session k with a priority e under the constraint of the inequality $TD_{e,k} \leq D_{e,k}/m$.

21.3.6.1 Performance example

The three algorithms are compared by simulation with the same parameters as in Yang *et al.* [45]. The results are shown in Figure 21.8.

21.4 QoS IN OFDMA-BASED BROADBAND WIRELESS ACCESS SYSTEMS

Vector orthogonal frequency division multiplexing (VOFDM) is considered as a base for BWA systems by the Broadband Wireless Internet Forum (BWIF) [1]. The BWA system is used with existing wireless LAN technologies such as IEEE802.11 (a, b) and IEEE 802.16 Group aims to unify the BWA solutions [56]. 802.16 Group issued standards in the 10–66 GHz bands and IEEE802.16a Group was formed to develop standards to operate in the 2–11 GHz bands in which channel impairments, multipath fading and path loss become more significant with the increase in the number of subscribers.

System performance at high transmission rates depends on the ability of BWA system to provide efficient and flexible resource allocation. Recent studies [55,57] on resource allocation demonstrate that significant performance gains can be obtained if frequency hopping and adaptive modulation are used in subcarrier allocation, assuming knowledge of the channel gain in the transmitter.

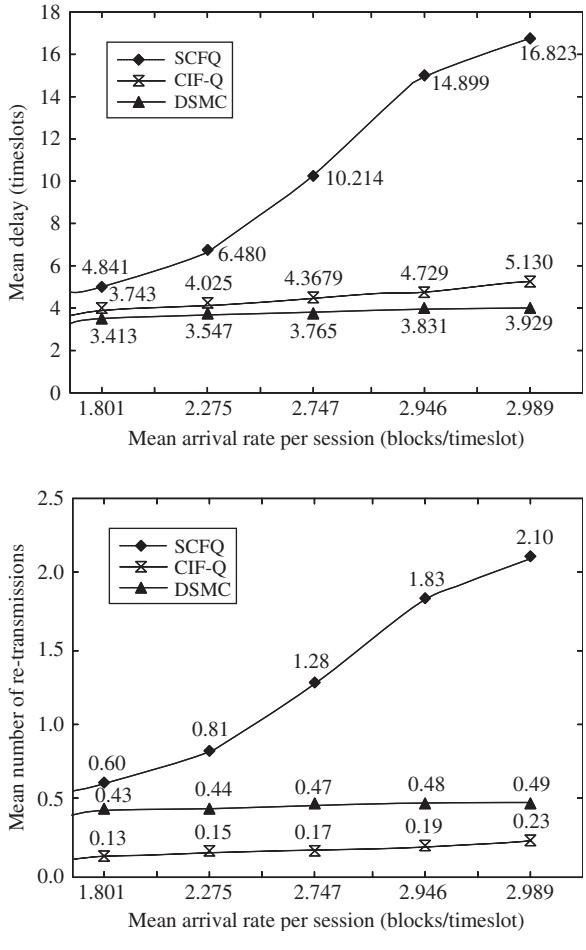

Figure 21.8 System performance. (Reproduced by permission of IEEE [45].)

The resource allocation problem has been considered in many studies. Almost all of them define the problem as a real-time resource allocation problem in which QoS requirements are fixed by the application. QoS requirement is defined as achieving a specified data transmission rate and BER of each user in each transmission. In this regard, the problem differs from the water-feeling schemes wherein the aim is to achieve Shannon capacity under the power constraint [57].

Therefore, in this section we consider the problem where K users are involved in the OFDMA system to share N subcarriers. Each user allocates nonoverlapping set of subcarriers S_k where the number of subcarriers per user is $J(k)$. In the following, $X_k(l)$ represents the lth subcarrier of the FFT block belonging to the kth user. $X_k(l)$ is obtained by coding the assigned c bits with the corresponding modulation scheme. In the downlink the $X_k(l)$ are multiplexed to form the OFDM symbol of length $(N + L)$ with the appended guard prefix L in order to eliminate ISI. At the uplink, the equivalent overall OFDM symbol (with a synchronization error) has the form

$$x(l) = \sum_{k=0}^{K-1} \sum_{n=0}^{j(k)-1} X_k(n) \mathrm{e}^{j(2\pi/N)[I_k(n)]l} \tag{21.24}$$

where $n = -L, \ldots, N-1$, and $I_k(n)$ denotes the subcarrier assigned to the kth user. Resource allocation mechanism associates the set of subcarriers to the users with different bits loaded into them. The received signal from the jth user can be represented as

$$y_j(l) = x(l) \otimes h_j(l) + w(l) \tag{21.25}$$

where $h_j(t)$ is the baseband impulse response of the channel between BS and the jth user. $y_j(l)$ is the received signal $y_j(t)$ sampled at rate $1/T$. The first L samples are discarded and the N-point FFT is computed. The data of the jth user is

$$Y_j(n) = \begin{cases} X_j(n)H_j(i_j(n)) + W(n), & \text{if } i_j(n) \in S_j \\ 0, & \text{otherwise} \end{cases} \tag{21.26}$$

where $H_j(n) := \sum_i h_j(i) \exp[j2(\pi/N)ni]$ is the frequency response of the channel of the kth user.

The allocation module of the transmitter assigns subcarriers to each user according to some QoS criteria. QoS metrics in the system are rate and BER. Each user's bit stream is transmitted using the assigned subcarriers and adaptively modulated for the number of bits assigned to the subcarrier. The power level of the modulation is adjusted to meet QoS for given fading of the channel. The transmission power for the AWGN channel can be predicted. In addition the channel gain of subcarrier n to the corresponding user k should be known. The channel gain of the subcarrier is defined as $\alpha_{k,n} = H_k(n) * PL_k$,where PL is the path loss, defined by $PL_k = PL(d_o) + 10\alpha \log_{10}(d_k/d_o) + X_\sigma$. Parameter d_o is the reference distance, d_k is the distance between transmitter and receiver, α is the path loss component and X_σ is a Gaussian random variable for shadowing with a standard deviation σ[58, 59].

With the known channel information, the objective of resource allocation problem can be defined as maximizing the throughput subject to a given total power constraint regarding the user's QoS requirements.

If $\gamma_{k,n}$ is the indicator of allocating the nth subcarrier to the kth user, the transmission power allocated to the nth subcarrier of kth user can be expressed as $P_{k,n} = f_k(c_{k,n}, BER_k)/\alpha_{k,n}^2$, where $f_k(c_k, n)$ is the required received power with unity channel gain for reliable reception of $c_{k,n}$ bits per symbol. Therefore, the resource allocation problem with an imposed power constraint can be formulated as

$$\max_{C_{k,n},\gamma_{k,n}} R_k = \sum_{n=1}^{N} c_{k,n}\gamma_{k,n} \quad \text{for all } k$$

$$\text{subject to } P_T = \sum_{k=1}^{K}\sum_{n=1}^{N} \frac{f_k(c_{k,n}, BER_k)}{\alpha_{k,n}^2}\gamma_{k,n} \le P_{max} \tag{21.27}$$

The limit on the total transmission power is expressed as $P_{\max}$ for all $n \in \{1, \ldots, N\}, k \in \{1, \ldots, K\}$ and $c_{k,n} \in \{1, \ldots, M\}$. If there is no power constraint, Equation (21.27) is changed in order to minimize P_T subject to allocating R_k bits for all k. In other words problem is to find the values of the $\gamma_{k,n}$ and the corresponding $c_{k,n}$ while minimizing P_T.

The *optimal solution* in a multiuser environment with multiple modulation techniques is complicated since it needs to pick the subcarriers in balance. The problem can be classified according to each set of bits assigned to a subcarrier. For a user k, $f_k(c_{k,n}) \in \{f_k(1, BER_k), \ldots, f_k(M, BER_k)\}$and M times $[K * N]$ power matrices $\{P^c\}$ can be constructed for each c. For a constant c, $\{f(c)\}$ can be computed and the transmission power requirement can be found. The dimension of the indicator function is incremented and represented now by $\gamma_{k,n,c}$ and defined as

$$\gamma_{k,n,c} = \begin{cases} 1, & if\ c_{k,n} = c \\ 0, & \text{otherwise} \end{cases} \tag{21.28}$$

The above problem can be solved with integer programming (IP). We refer to the IP approach as the optimal solution to the resource allocation problem. There are $K \cdot N \cdot M$ indicator variables and M power matrices where the entries of each matrix for a given c can be found from

$$P_{k,n}^{c} = \frac{f_k(c, BER_k)}{\alpha_{k,n}^2} \tag{21.29}$$

Using Equation (21.29) as an input, the cost function now can be written as

$$P_T = \sum_{k=1}^{K} \sum_{n=1}^{N} \sum_{c=1}^{M} P_{k,n}^{c} \gamma_{k,n,c} \tag{21.30}$$

and the description of the IP problem is

$$\min_{\gamma_{k,n,c}} P_T, \quad \text{for } \gamma_{k,n,c} \in \{0, 1\} \tag{21.31}$$

subject to

$$R_k = \sum_{n=1}^{N} \sum_{c=1}^{M} c \cdot \gamma_{k,n,c}, \quad \text{for all } k, \text{ and } 0 \leq \sum_{k=1}^{K} \sum_{c=1}^{M} \gamma_{k,n,c}, \leq 1, \quad \text{for all } n$$

Although the optimal solution gives the exact results, from an implementation point of view, it is too complex. This leads to searching suboptimal solutions that are fast and close to the optimal solution. *Suboptimal solutions*, in most attempts to simplify the resource allocation, decompose the problem into two procedures, a subcarrier allocation with fixed modulation, and bit loading. Subcarrier allocation with fixed modulation deals with one P^c matrix with fixed c and then, by using bit loading scheme, the number of bits is incremented.

Subcarrier allocation is based on the fact that $f_k(x, y)$ is a convex function [57]. We can start with $P_{k,n}^{1}$ and we can define new $\bar{R}_k$ with $\sum_{k=1}^{K} \bar{R}_k \leq N$, which can be obtained by decrementing R_k properly. Then the solution to this problem can be solved with Linear Programming or Hungarian problem.

Linear programming

For simplicity, we briefly restate the problem description,

$$P_T = \min \sum_{k=1}^{K} \sum_{n=1}^{N} P_{k,n}^{1} \rho_{k,n} \quad \rho_{k,n} \in [0, 1] \tag{21.32}$$

subject to

$$\sum_{n=1}^{N} \rho_{k,n} = \overline{R}_k \forall k \in \{1, \ldots, K\} \quad \text{and} \quad \sum_{k=1}^{K} \rho_{k,n} = 1 \quad \forall n \in \{1, \ldots, N\}$$

After linear programming, the $[K \cdot N]$ allocation matrix has entries ranging between 0 and 1. The entries are converted to integers by selecting the highest $\bar{R}_k$ nonzero values from N columns for each k and assigning them to the kth user.

Hungarian algorithm

The problem described above can also be solved by an assignment method such as the Hungarian algorithm [58]. The Hungarian algorithm works with square matrices. Entries of the square matrix can be formed by adding $\bar{R}_k$ times the row of each k. The problem formulation is as

$$P_T = \min \sum_{k=1}^{N} \sum_{n=1}^{N} P_{k,n}^{1} \rho_{k,n} \quad \rho_{k,n} \in \{0, 1\} \tag{21.33}$$

and the constraints become

$$\sum_{n=1}^{N} \rho_{k,n} = 1 \quad \forall n \in \{1, \ldots, N\} \quad \text{and} \quad \sum_{k=1}^{N} \rho_{k,n} = 1 \quad \forall k \in \{1, \ldots, N\}$$

Although the Hungarian method has computation complexity $O(n^4)$ in the allocation problem with fixed modulation, it may serve as a base for adaptive modulation.

The *Bit loading algorithm* (BLA) is used after the subcarriers are assigned to users that have at least $\bar{R}_k$ bits assigned. The bit loading procedure is as simple as incrementing bits of the assigned subcarriers of the users until $P_T \leq P_{\max}$. If $\Delta P_{k,n}(c)$ is the additional power needed to increment one bit of the nth subcarrier of kth user $\Delta P_{k,n}(c_{k,n}) = [f(c_{k,n}+1) - f(c_{k,n})]/\alpha_{k,n}^2$, then the bit loading algorithm assigns one bit at a time with a greedy approach to the subcarrier as $\{\arg\min_{k,n} \Delta P_{k,n}(c_{k,n})\}$.

BL algorithm

(1) *For all n, Set* $c_{k,n} = 0$, $\Delta P_{k,n}(c_{k,n})$, *and* $P_T = 0$;

(2) *Select* $\bar{n} = arg\ min_n \Delta P_{k,n}(0)$;

(3) *Set* $c_{k,\bar{n}} = c_{k,\bar{n}} + 1$ *and* $P_T = P_T + \Delta P_{k,n}(c_{k,n})$;

(4) *Set* $\Delta P_{k,n}(c_{k,\bar{n}})$;

(5) *Check* $P_T \leq P_{max}$ *and* R_k *for* $\forall k$, *if not satisfied GOTO STEP 2*.

(6) *Finish*.

The Hungarian approach and LP approach with bit loading appear as two different suboptimal solutions to the resource allocation with adaptive modulation. In the sequel they will be referred to as GreedyHungarian (GH) and GreedyLP (GLP).

21.4.1 Iterative solution

The GreedyLP and GreedyHungarian methods both first determine the subcarriers and then increment the number of bits on them according to the rate requirements of users. This may not be a good schedule in some cases, like a user with only one good subcarrier and low rate requirement. The best solution for that user is allocating its good carrier with high number of bits. However, if GreedyLP or GreedyHungarian is used, the user may have allocated more than one subcarrier with lower number of bits and, in some cases, its good subcarrier is never selected. Consider another scenario where a user does not have any good subcarrier (i.e. it may have a bad channel or be at the edge of the cell). In this case, rather than pushing more bits and allocating fewer subcarriers, as in GreedyLP and GreedyHungarian, the opposite strategy is preferred since fewer bits in higher number of subcarriers give a better result. Another difficulty arises in providing fairness. Since GreedyLP and GreedyHungarian are based on a greedy approach, the user in the worst condition usually suffers. In any event, these are complex schemes and simpler schemes are needed to finish the allocation within the coherence time. To cope with these challenges, in the following a simple, efficient and fair subcarrier allocation scheme is introduced with iterative improvement [53].

The scheme is composed of two modules, referred to as *scheduling* and *improvement modules*. In the scheduling section, bits and subcarriers are distributed to the users and passed to the improvement module where the allocation is improved iteratively by bit swapping and subcarrier swapping algorithms.

The *fair scheduling algorithm* starts the allocation procedure with the highest level of modulation scheme. In this way, it tries to find the best subcarrier of a user to allocate the highest number

of bits. In Koutsopoulos and Tassiulas [55] the strategy is described by an analogy: "The best strategy to fill a case with stone, pebble and sand is as follows. First filling the case with the stones and then filling the gap left from the stones with pebbles and in the same way, filling the gap left from pebbles with sand. Since filling in opposite direction may leave the stones or pebbles outside". With this strategy more bits can be allocated and the scheme becomes immune to uneven QoS requirements. The fair scheduling algorithm (FSA) runs greedy release algorithm (GRA) if there are nonallocated subcarriers after the lowest modulation turn and the rate requirement is not satisfied. GRA decrements one bit of a subcarrier to gain power reduction, which is used to assign higher number of bits to the users on the whole. FSA is described as follows.

FS algorithm

(1) *Set* $c = M$, *Select a* k, *and* $P_T = 0$;

(2) *Find* $\bar{n} = arg\ min_n P^c_{k,n}$;

(3) *Set* $R_k = R_k - c$ *and* $\rho_{k,\bar{n}} = 1$, *update* P_T, *shift to the next* k;

(4) *If* $P_T > P_{\max}$, *step out and set* $c = c - 1$, *GOTO STEP 2*.

(5) *If* $\forall k$, $R_k < c$, *set* $c = c - 1$, *GOTO STEP 2*.

(6) *If* $\{c == 1\}, \sum_{k=1}^{K} \sum_{n=1}^{N} \rho_{k,n} < N$, $P_T > P_{\max}$, *run "greedy release" and GOTO STEP 2*.

(7) *Finish*.

The *greedy releasing algorithm* tends to fill the unallocated subcarriers. It releases one of the bits of the most expensive subcarrier to gain power reduction in order to drive the process. GRA works in the opposite direction to BLA. GRA is described as follows.

GR algorithm

(1) *Find* $\{\bar{k}, \bar{n}, \bar{c}_{\bar{k},\bar{n}}\} = arg\ max_{k,n,c} P^c_{k,n} \rho_{k,n} \forall c$;

(2) *Set* $\bar{c}_{k,n} = \bar{c}_{k,n} - 1$, $P_T = P_T - \Delta P_{\bar{k},\bar{n}}(c_{\bar{k},\bar{n}})$;

(3) *Set* $c = c_{\bar{k},\bar{n}} - 1$;

(4) *Finish*.

The *horizontal swapping algorithm* (HSA) aims to smooth the bit distribution of a user. When the subcarriers are distributed, the bit weight per subcarrier can be adjusted to reduce power. One bit of a subcarrier may be shifted to the other subcarrier of the same user if there is a power reduction gain. Therefore, variation of the power allocation per subcarrier is reduced and a smoother transmission is performed. HSA is described as follows.

HS algorithm

(1) *Set* $P_C = \infty$;

(1a) *Find* $\{\bar{k}, \bar{n}, \bar{c}_{\bar{k},\bar{n}}\} = arg\ max_{k,n,c}(P^c_{k,n} \rho_{k,n}) < P_C \forall c$;

(2) *Define* $n \in S_k$, *where* $\{\rho_{k,n} == 1\}$ *for* $\forall n_i$;

(3) *Set* $\Delta_{\dot{n}} = max_n \Delta P_{\bar{k},\bar{n}}(c_{\bar{k},\bar{n}} - 1) - \Delta P_{\bar{k},\dot{n}}(c_{\bar{k},\dot{n}}), \dot{n} \in S_k$;

(4) *Set* $P_C = P^{\bar{c}}_{\bar{k},\bar{n}}$;

(4a) *If* $\Delta_{\hat{n}} > 0$, *set* $P_T = P_T - \Delta_{\hat{n}}$
(4b) *Set* $c_{\bar{k},\bar{n}} = c_{\bar{k},\bar{n}} - 1, c_{\bar{k},\dot{n}} = c_{\bar{k},\dot{n}} + 1$ *GOTO Step (1a)*

(5) *If* $\{P_C = min_{k,n,c}(P^c_{k,n}\rho_{k,n})\}$, *finish.*

The *vertical swapping algorithm* (VSA) does vertical swapping for every pair of users. In each iteration, users try to swap their subcarriers such that the power allocation is reduced. There are different types of vertical swapping. For instance, in triple swapping, user i gives its subcarrier to user j and in the same way user j to user k and user k to user i. In Koutsopoulos ad Tassiulas [55], pairwise swapping is modified to cope with the adaptive modulation case. In this case, there is more than one class where each class is defined with its modulation (i.e number of bits loaded to a subcarrier) and swapping is only within the class. Each pair of user swap their subcarriers that belong to the same class if there is a power reduction. In this way, adjustment of subcarrier is done across users, to try to approximate the optimal solution. VSA is described as follows.

VS algorithm

(1) $\forall$ *pair of user* $\{i, j\}$;
(1a) *Find* $\partial P_{i,j}(n) = P^{\dot{c}}_{i,n} - P^{\dot{c}}_{j,n}$ *and* $\Delta^{\hat{n}} P_{i,j} = max\partial P_{i,j}(n), \forall n \in S_i$;
(1b) *Find* $\partial Pj, i(n) = P^{\dot{c}}_{j,n} - P^{\dot{c}}_{i,n}\Delta^{\breve{n}} P_{j,i} = max\partial P_{j,i}(n), \forall n \in S_j$;
(1c) *Set* $\Omega^{\hat{n},\breve{n}} P_{i,j} = \Delta^{\hat{n}} P_{i,j} + \Delta^{\hat{n}} P_{j,i}$;
(1d) *Add* $\Omega^{\hat{n},\breve{n}} P_{i,j}$ *to the* $\{\Lambda\}$ *list*;

(2) *Select* $\Omega = max_{(i,\hat{n}),(j,\breve{n})}\Lambda$;

(3) *If* $\Omega > 0$, *Switch subcarriers and* $P_T = P_T - \Omega$ *GOTO STEP (1a)*;

(4) *If* $\Omega \leq 0$, *finish.*

21.4.2 Resource allocation to maximize capacity

Suppose there is no fixed requirements per symbol and the aim is to maximize capacity. It has been shown in Viswanath *et al.* [60] that, for point-to-point links, a fair allocation strategy maximizes total capacity and the throughput of each user in the long run, when the user's channel statistics are the same. This idea underlying the proposed fair scheduling algorithm is exploiting the multiuser diversity gain.

With a slight modification, the fair scheduling algorithm for point-to-point communication was extended to an algorithm for point-to-multipoint communication [53]. Suppose the user time varying data rate requirement $R_k(t)$ is sent by the user to the base station as feedback of the channel condition. We treat symbol time as the time slot, so t is discrete, representing the number of symbols. We keep track of average throughput $t_{k,n}$ of each user for a subcarrier in a past window of length t_c. The scheduling algorithm will schedule a subcarrier $\bar{n}$ to a user $\bar{k}$ according to the criterion

$$\{\bar{k}, \bar{n}\} = \arg\max_{k,n}(r_{k,n}/t_{k,n})$$

where $t_{k,n}$ can be updated using an exponentially weighted low-pass filter described in Viswanath *et al.* [60]. Here, we are confronted with determining the $r_{k,n}$ values. We can set $r_{k,n}$ to R_k/N, where N is the number of carriers. With this setting, the peaks of the channel for a given subcarrier can be tracked. The algorithm schedules a user to a subcarrier when the channel quality

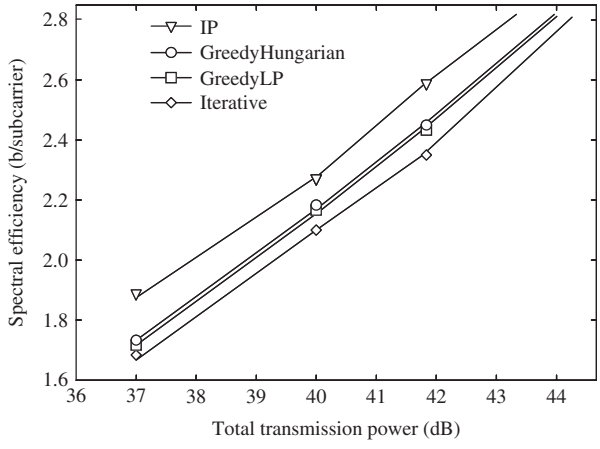

Figure 21.9 Spectral efficiency vs total transmission power.

in that subcarrier is high relative to its average condition in that subcarrier over the time scale t_c. When we consider all subcarriers the fairness criterion matches with the point-to-point case as

$$\bar{k} = \max_k R_k/T_k, \text{ where} T_k = \sum_{n=1}^{N} t_{k,n}$$

The theoretical analysis of fairness property of the above relation for point-to-point communication is derived in Viswanath *et al*. [60]. Those derivations can be apply for point-to-multipoint communication.

21.4.2.1 Performance example

The required transmission power for c bits/subcarrier at a given BER with unity channel gain is [57]:

$$f(c, BER) = \frac{N_0}{3}\left[Q^{-1}\left(\frac{BER}{4}\right)\right]^2 (2^c - 1)$$

where $Q^{-1}(x)$ is the inverse function of $Q(x) = \frac{1}{\sqrt{2\pi}} \int_x^\infty e - t^2/2 \mathrm{d}t$

Figure 21.9 shows the average data rates per subcarrier vs total power constraint when there are four users. Each user has a rate requirement of 192 b/symbo1 (maximum rate) and BER requirement of 10^{-4}. The performance of the iterative approach is close to that of the optimal and difference between suboptimal and iterative approaches decreases as the total transmit power increases.

21.5 PREDICTIVE FLOW CONTROL AND QoS

Even if the dimensioning of network resources has been done correctly and the admission control mechanism is good, the network may go into periods of congestion due to the transient oscillations in the network traffic. For this reason it is necessary to develop a mechanism to quickly reduce the congestion or pre-empt it, so as to cause the least possible degradation of QoS to the underlying applications [61–81]. 4G networks will carry a mixture of *real-time* (RT) traffic, like video or voice traffic, and *nonreal-time* (NRT) traffic, like data. One approach to controlling the NRT traffic is to be able to predict the RT traffic (at the link of interest) at some time in the future, then, based on this prediction, control the NRT traffic.

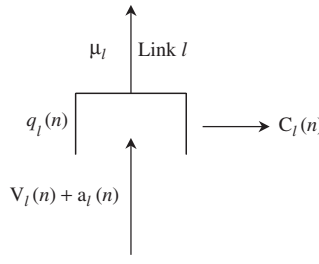

Figure 21.10 Individual link-level model.

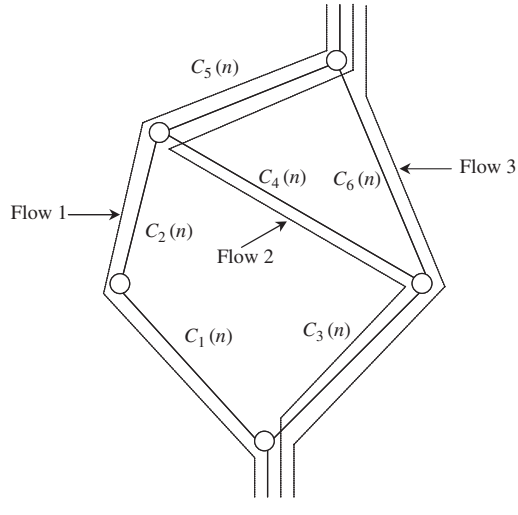

Figure 21.11 Network-level model.

In Figure 21.10, $V_l(n)$ and $\alpha_l(n)$ correspond to the aggregate RT traffic and NRT traffic, respectively, arriving at a link of interest (link l having capacity μ_l), at time n. One can then estimate $C_l(n)$, the available link capacity for NRT traffic, at some time in the future. This information would then be used at the *network-level* to distribute the available link capacities to the NRT flows.

On the network level the available link capacities for the NRT flows is then distributed to maximize throughput (or more generally some utility function), based on appropriate fairness requirements. An example network is shown in Figure 21.11, where flows traverse links with available capacities for the NRT flows calculated at the individual link level. In Chapter 7, the network-level problem has been investigated in the case when the available link capacity for NRT flows at each node is a constant. The problem remains open in the case when the available capacity is time-varying.

21.5.1 Predictive flow control model

In this section we focus on the individual link-level problem, a single multiplexing point in the network which consists of a link and an associated buffer that serve both RT and NRT traffic. The multiplexing point in the network could be an output port of a router/switch or a multiplexer. The system diagram is shown in Figure 21.12.

In the following $V(n)$ will represent the aggregate amount of RT traffic that arrives at the queue of interest at time n. $V_{\max} := \sup_{n>0}\{V(n)\}$ will be assumed finite and $V(n)$ stationary in the mean,

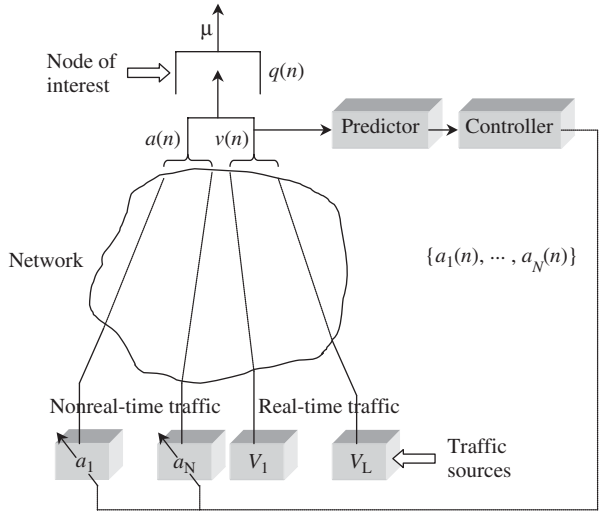

Figure 21.12 System diagram of predictive flow control.

i.e. $\bar{V} := \mathrm{E}\{V(n)\}$. The goal is to control the NRT traffic based on predicting the aggregate RT traffic arrival rate at the queue. $a_i(n)$ will refer to the available link capacity for the ith NRT traffic computed at time n based on the predicted value of the RT traffic rate. This explicit rate information is sent back to the ith NRT traffic source.

If N is the number of NRT traffic sources and $n_i, \imath = 1, \ldots, N$ is the round-trip delay between the ith NRT source and the destination, then $a(n) = \Sigma_{i=1}^{N} a_i(n - n_i)$ is the aggregate NRT traffic arrival to the queue at time n. A control message is propagated from the queue of interest to the destination and back to the source. $\hat{V}_i(n)$ will represent the predicted value of $V(n)$ based on the history of V before time $n - n_i$. We assume that the predictor is linear. A simple example can be represented as $\hat{V}_i(n + n_i) = \Sigma_k h_k V_i(n - k)$. If $V(z)$ is the Z-transform of $V(n) - \bar{V}$ and $\hat{V}_i(z)$ the Z-transform of $\hat{V}_i(n) - \bar{V}$ then $\hat{V}_i(z) = z^{-n_i} H_i(z) V(z)$ where $H_i(z)$, for NRT traffic source i, is a causal, stable, linear, time-invariant system [74]. It should be noted that $H_i(z)$ will be the same for all sources with the same RTT n_i. For example, if there is only one NRT flow with round-trip delay 5, a possible predictor (in time domain) could be $\hat{V}_1(n + 5) = (1/2)V(n) + (1/2)V(n - 1)$. In this case, we will have $H_1(z) = (1/2)(1 + z^{-1})$.

The queue-length, $q(n)$, at time n at the queue of interest will be determined by $a(n)$, $V(n)$, and the service rate (link rate) of the queue μ. We assume that the queue process begins at time $n = 0$ and $q(0) = 0$. For stability, we also require that $\bar{V} < \mu$. The feedback control scheme is as follows. We predict the aggregate RT traffic rate and use the predicted value to compute $a_i(n)$, $1 \leq n \leq N$.

21.5.1.1 Predictive flow control algorithm for single NRT traffic model

To start with, we assume that there is only one NRT traffic source $a_1(n)$ (or a group of NRT traffic loops with the same round-trip delay n_1). So, by definition, $a(n) = a_1(n - n_1)$. Ideally, what we want to achieve is $a(n) + V(n) = \mu$ at all time n. However, there are two difficulties in achieving this. First, since we do not know $V(n)$ in advance, we need to estimate its value through prediction, resulting in a certain possibility of error. Second, $V(n)$ could be greater than μ but since $a(n)$ cannot be negative, the sum $a(n) + V(n)$ cannot be made equal to μ. Having in mind the possibility of prediction error and the possibility that $V(n) > \mu$, the NRT traffic $a_1(n)$ will be controlled as

$$a_1(n) = [p\mu - \hat{V}_1(n + n_1)]^{+} \tag{21.34}$$

where p is the percentage of output link capacity that we would like to utilize $[p > (\bar{V}/\mu)]$ and $[x]^+ = x$, if $x \geq 0$, and $[x]^+ = 0$, otherwise. Consider now the situation of perfect prediction, and let $V(n)$ have exceeded μ for some time. During the period that $V(\cdot)$ has exceeded μ, the above equation correctly sets $a_1(\cdot)$ to zero, but even after $V(\cdot)$ is no longer larger than μ, there could still be a substantial backlog in the queue, during which time $a_1(\cdot)$ should be set to zero. However, according to Equation (21.34), the moment $V(n)$ is less than μ, the NRT source is allowed to transmit, thus potentially causing unnecessary congestion at the queue. So, what we will attempt to do is to keep the queue length at the node of interest small, while maintaining a certain level of throughput given by

$$\lim_{n\to\infty} \frac{\sum_{j=1}^{n}[a(j) + V(j)]}{n} = p\mu \tag{21.35}$$

For this reason we define the control algorithm [81] as follows.

Control algorithm ($N = 1$ case)

(1) *Define a virtual queueing process $q_1(n)$ and set $q_1(0) = 0$.*

(2) $q_1(n) = [q_1(n-1) + \hat{V}_1(n) - p\mu]^+$. *For $n \leq 0$, we let $V(n) = 0$.*

(3) $a_1(n) = [p\mu - \hat{V}_1(n + n_1) - q_1(n + n_1 - 1)]^+$. *For $n \leq 0$, we let $a_1(n) = 0$.*

For N NRT traffic sources the algorithm is modified as follows.

Control algorithm ($N > 1$ case)

(1) *Set $q_i(0) = 0$, $1 \leq i \leq N$.*

(2) $q_i(n) = [q_i(n-1) + \hat{V}_i(n) - p\mu]^+$. *For $n \leq 0$, we let $V(n) = 0$.*

(3) $a_i(n) = [p\mu - \hat{V}_i(n + n_i) - q_i(n + n_i - 1)]^+/N$.

(4) *For $n \leq 0$, we let $a_i(n) = 0$.*

21.5.1.2 Performance example

Three different alternatives for predictor are used [81]. In A1, the fixed low-pass filter is chosen as $H_{\text{LPF}}(z) = (1/4)(1 + z^{-1} + z^{-2} + z^{-3})$. The MMSE predictor is designed as follows. First, a low-pass filter A1 is applied to the high-priority RT traffic. Next, a standard minimizing mean square error linear predictor $H_{\text{MMSE}}(z)$ with the form $\sum_{m=0}^{M_i} B_m^{(i)} z^{-n_i - m}$ is calculated based on the low-frequency part of the RT traffic. The final MMSE predictor is $z^{-n_i} H_i(z) = H_{\text{LPF}}(z) H_{\text{MMSE}}(z)$. Note that $H_{\text{MMSE}}(z)$ will require explicit knowledge of the round-trip delays per-flow information n_i. In A3 that information is approximated by an average value n_0 for all flows. The prediction error is defined as $\Delta(j) = V(j) - \hat{V}_1(j)$.

The queue length at the node of interest is bounded by [79]

$$q(n) \leq q_0(n) + \sup_{0\leq n_0\leq n} \sum_{j=n_0+1}^{n} \Delta(j) - \inf_{0\leq n_0\leq n} \sum_{j=n_0+1}^{n} \Delta(j)$$

Under the definitions and predictive flow control algorithm defined above, if $V_{\max} < \infty$ and $[(p\mu - \bar{V})/(\mu - \bar{V})] \leq H_1(1) \leq 1$, we have [81] $q(n) - q_0(n) \leq 2C_1$, where C_1 is a constant that does not depend on n.

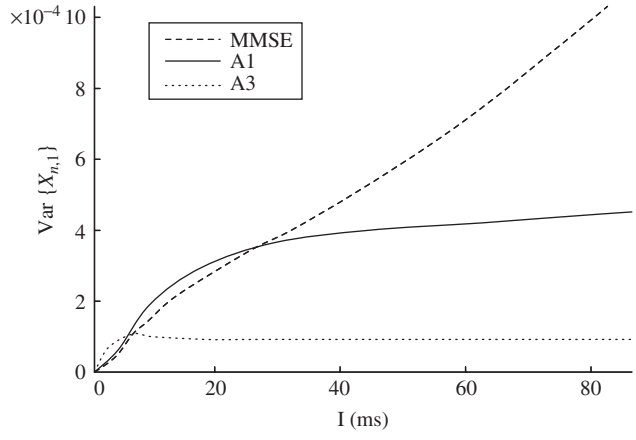

Figure 21.13 Var$\{X_{n,l}\}$ with different predictors. (Reproduced by permission of IEEE [81].)

For $l = n - n_0$ we define the accumulated error as

$$X_{n,l} \triangleq \sum_{j=n-l+1}^{n} \Delta(j) = \sum_{j=n_0+1}^{n} \Delta(j)$$

where $\mathrm{E}\{X_{n,l}\} = 0$ (because the predictor is unbiased) and

$$\begin{aligned} \mathrm{Var}\{X_{n,l\}} &= \mathrm{Var}\left\{\sum_{j=n-l+1}^{n} \Delta(j)\right\} \\ &= \sum_{j1=n-l+1}^{n} \sum_{j2=n-l+1}^{n} C_{\Delta}(j1 - j2) = \sum_{j1=-l+1}^{0} \sum_{j2=-l+1}^{0} C_{\Delta}(j1 - j2) \end{aligned} \tag{21.36}$$

For the results shown below, $V(n)$ is a generated Gaussian process which is multitimescale-correlated with $C_v(k) = 479.599 \times 0.999^{|k|} + 161.787 \times 0.99^{|k|} + 498.033 \times 0.9^{|k|}$ and $\bar{V} =$ 100 kb/s. This type of source has often been used to represent the multiple time-scale correlation in network traffic [71, 80]. The link capacity is 200 kb/s, and the utilization is set to 98 %. The time unit is 1 ms and the unit of the queue length is 1 bit [81]. Var$\{X_{n,l}\}$ is shown in Figure 21.13. We can see that, for A1 and A3 predictors, Var$\{X_{n,l}\}$ converges to some constant when l is large enough. The asymptotic variance of A3 is also smaller than that of Al. In Figure 21.14, we compare the above control algorithm with the control algorithm that uses Equation (21.34). As we mentioned before, when $\hat{V}_1(n) \leq p\mu$ for all n, the control algorithms reduce to the same linear equation. However, when this condition is not true, the two algorithms are quite different. We can see this difference in performance in Figure 21.14. In this simulation, there is only one NRT source with round-trip delay of 5 ms. The RT source and the link capacity are still the same as in Figure 21.13. To see the difference when the condition $\hat{V}_1(n) \leq p\mu$ is violated, we use the same A3 predictor in both control algorithms. In the figure, the control algorithm is marked C1, and the one that uses Equation (21.34) is marked C2. The utilization is set to $p = 98$ %. Note that when using control algorithm C2, given p, the utilization is not equal to p. In this simulation, we set p such that the measured utilization for C2 is 98 %, which is the same as in C1. From this figure, using the same predictor, we can see that the improved control algorithm outperforms the one that uses Equation (21.34).

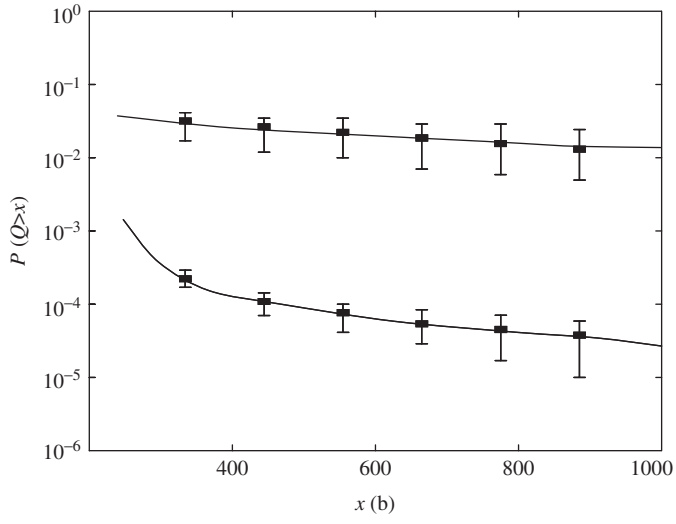

Figure 21.14 Tail (cumulative queue length) probabilities with different control algorithms. (Reproduced by permission of IEEE [81].)

REFERENCES

[1] R. Dugad, K. Ratakonda and N. Ahuja, A new wavelet-based scheme for watermarking images, in *Proc. IEEE Int. Conf. Image Processing*, Chicago, IL, 4–7 October 1998, pp. 419–423.

[2] D. Kundur and D. Hatzinakos, Digital watermarking using multiresolution wavelet decomposition, in *Proc. IEEE Int. Conf. Acoustics, Speech, Signal Processing*, vol. 5, 1998, pp. 2969–2972.

[3] H. Inoue, A. Miyazaki and T. Katsura, An image watermarking method based on the wavelet transform, in *Proc. IEEE Int. Conf. Image Processing*, Kobe, 25–28 October, 1999, pp. 296–300.

[4] H.J.M. Wang, P.C. Su and C.C.J. Kuo, Wavelet-based blind watermark retrieval technique, in *Proc. SPIE, Conf. Multimedia System Applications*, vol. 3528, Boston, MA, November 1998.

[5] P. Campisi, A. Neri and M. Visconti, A wavelet based method for high frequency subbands watermark embedding, in *Proc. SPIE Multimedia System Applications III*, Boston, MA, November 2000.

[6] M.M. Yeung and F. Mintzer, An invisible watermarking technique for image verification, in *Proc. IEEE Int. Conf. Image Processing*, Santa Barbara, CA, 1997, pp. 680–683.

[7] D. Kundur and D. Hatzinakos, Toward a telltale watermarking tech- nique for tamper-proofing, in *Proc. IEEE Int. Conf. Image Processing*, Chicago, IL, 4–7, October 1998, pp. 409–413.

[8] R.H. Wolfgang and E.J. Delp, Fragile watermarking using the *VW2D* watermark, in *Proc. SPIE*, *Security Watermarking Multimedia Contents*, vol. 3657, San Jose, CA, January 1999.

[9] P.D.F. Correira, S.M.M. Faria, and P.A.A. Assunqão, Matching MPEG-1/2 coded video to mobile applications, in *Proc. Fourth Int. IEEE Symp. Wireless Personal Multimedia Communications*, Aalborg, 9–12, September 2001.

[10] Information technology – coding of moving pictures and associated audio for digital storage media at up to about 15 *Mb/s* – Part 2: Video. ISO, ISO/IECII I72–2, 1993.

[11] F. Yong Li, N. Stol, T.T. Pham and S. Andresen, A priority-oriented QoS management framework for multimedia services in IJMTS, in *Proc. Fourth Int IEEE Symp. Wireless Personal Multimedia Communication*, Aalborg, 9–12, September 2001.
[12] L. Hanzo, P.J. Cherriman and J. Streit, *Wireless Video Mommunication. Second to Third Generation Systems and Beyond*, IEEE Series on Digital and Mobile Communication. IEEE: New York, 2001.
[13] Hanjalic, G.C. Langelaar, P.M.B. van Roosmalen, J. Biemond and R.L. Lagendijk, *Image and Video Databases. Restoration, Watermarking and Retrieval*. Elsevier: New York, 2000.
[14] I.J. Cox, M.L. Miller and J.A. Bloom, *Digital Watermarking*. Morgan Kaufmann: San Francisco, CA, 2002.
[15] N. Nikolaidis and I. Pitas, Robust image watermarking in the spatial domain, *Signal Process.*, vol. 66, no. 3, 1998, pp. 385–403.
[16] M. Bami, F. Bartolini, V. Cappellini and A. Piva, A DCT-domain system for robust image watermarking, *Signal Process.*, vol. 66, no. 3, 1998, pp. 357–372.
[17] I. Cox, J. Kilian, F. Leighton and T. Shamoon, Secure spread spectrum watermarking for multimedia, *IEEE Trans. Image Processing*, vol. 6, 1997, pp. 1673–1687.
[18] H. Hartung and B. Girod, Watermarking of uncompressed and compressed video, *Signal Process.*, vol. 66, 1998, pp. 283–301.
[19] M.D. Swanson, B. Zhu and A.H. Tewfik, Transparent robust image watermarking transform, in *Proc. IEEE Int. Conf. Image Processing*, Lausanne, 16–19, September 1996, pp. 211–214.
[20] R.M. Wolfgang and E.J. Delp, A watermark for digital images, in *Proc. IEEE Int. Conf. Image Processing*, Lausanne, 16–19, September 1996, pp. 219–222.
[21] T. Ebrahimi, MPEG-4 video verification model: A video encoding/de coding algorithm based on content representation, perceived quality: Toward comprehen- sive metrics, *Proc. SPIE*, vol. 4299, 2001.
[22] R. Gold, Optimal binary sequences for spread spectrum multiplexing, *IEEE Trans. Inform. Theory*, vol. IT-13, 1967, pp. 619–621.
[23] K.T. Tan, M. Ghanbari and D.E. Pearson, An objective measurement tool for MPEG video quality, *Signal Process.*, vol. 70, no. 3, 1998, pp. 279–294.
[24] S. Winkler, Visual fidelity and perceived quality: toward comprehensive metrics, *Proc. SPIE*, vol. 4299, 2001.
[25] P. Campisi, M. Carli, G. Giunta and A. Neri, Tracing watermarking for multimedia communication quality assessment, in *Proc. IEEE Int. Conf. Communications*, New York, 28 April to 2 May 2002.
[26] P. Campisi, G. Giunta and A. Neri, Object based quality of service assessment for MPEG-4 videos using tracing watermarking, in *Proc. IEEE Int. Conf. Image Processing*, Rochester, NY, 22–25 September, 2002.
[27] H. Liu, *Signal Processing Applications in CDMA Communications*. Artech House: Norwell, MA, 2000.
[28] P. Campisi, M. Carli, G. Giunta and A. Neri, Blind quality assessment system for multimedia communications using tracing watermarking, *IEEE Trans. Signal Processing*, vol. 51, no. 4, April 2003, pp. 996–1002.
[29] G. Anastasi and L. Lenzini, QoS provided by the IEEE 802.11 wireless LAN to advanced data applications: a simulation analysis, *Wireless networks*, vol. 6, no. 2, 2000, pp. 99–108.
[30] G. Bianchi, Performance analysis of the IEEE 802.11 distributed coordination function, *IEEE J. Select. Areas Commun*, vol. 18, no. 3, 2000, pp. 535–587.
[31] F. Cali, M. Conti and E. Gregori, Dynamic tuning of the IEEE 802.11 protocol to achieve a theoretical throughput limit, *IEEE/ACM Trans. Networking*, vol. 8, no. 6, 2000, pp. 785–799.
[32] C. Coutras, S. Gupta and N.B. Shroff, Scheduling of real-time traffic in IEEE 802.11 wireless lAN, *Wireless Networks*, vol. 6, no. 6, 2000, pp. 457–466.

[33] S. Choi and K.G. Shin, A cellular wireless local area network with QoS guarantee for heterogeneous traffic, *ACM Mobile Networks Applic.*, vol. 3, no. 1, 1998, pp. 89–100.
[34] S. Choi and K.G. Shin, A unified wireless LAN architecture for real-time and non-real-time communication services, *IEEE/ACM Trans. Networking*, vol. 8, no. 1, 2000, pp. 44–59.
[35] B.P. Crow, I. Widjaja, J.G. Kim and P.T. Sakai, IEEE 802.11 wireless local area networks, *IEEE Commun. Mag.*, vol. 35, no. 9, 1997, pp. 116–126.
[36] A. Ganz and A. Phonphoem, Robust superpoll with chaining protocol for IEEE 802.11 wireless LANs in support of multimedia applications, *Wireless Networks*, vol. 7, no. 1, 2001, pp. 65–73.
[37] IEEE 802.11 Task Group, http://grouper.ieee.org/groups/802/11/, 2000.
[38] R.C. Meier, An integrated 802.11 QoS model with point-controlled contention arbitration, IEEE Document 802.11-00/448, November 2000.
[39] O. Sharon and E. Altman, An efficient polling MAC for wireless LANs, *IEEE/ACM Trans. Networking*, vol. 9, no. 4, 2001, pp. 439–451.
[40] S.T. Sheu and T.F. Sheu, A bandwidth allocation/sharing/extension protocol for multimedia over IEEE 802.11 ad hoc wireless LANs, *IEEE J. Select. Areas Commun.*, vol. 19, no. 10, 2001, pp. 2065–2080.
[41] M. Fischer, QoS baseline proposal for the IEEE 802.11E, IEEE Document 802.11-00/360, November 2000.
[42] M. Fischer, EHCF normative text, IEEE Document 802.11-01/110, March 2001.
[43] S.-C. Lo, G. Lee and W.–T. Chen, An efficient multipolling mechanism for IEEE 802.11 wireless LANs, *IEEE Trans. Comput.*, vol. 52, no. 6, 2003, pp. 764–778.
[44] T.S.E. Ng, I. Stoica and H. Zhang, Packet fair queueing algorithms for wireless networks with location-dependent errors, in *Proc. INFOCOM' 98*, vol. 3, 1998, pp. 1103–1111.
[45] J. -S. Yang, C. -C. Tseng and R. -G. Cheng, Dynamic scheduling framework on an RLC/MAC layer for general packet radio service, *IEEE Trans. Wireless Commun.*, vol. 2, no. 5, 2003, pp. 1008–1016.
[46] S.J. Golestani, A self-clocked fair queuing scheme for broadband applications, in *Proc. IEEE INFOCOM'94*, April 1994, pp. 636–646.
[47] *GSM 03.60 General Packet Radio Service (GPRS); Service Description;Stage 2*, ETSI Standard v. 7.0.0, 1999.
[48] W. Stallings, *High-Speed Networks: TCP/IP and ATM Design Principles*. Prentice-Hall: Englewood Cliffs, NJ, 1998, pp. 325–330.
[49] A. Demers, S. Keshav and S. Shenkar, Analysis and simulation of a fair queuing algorithm, in *Proc. SIGCOMM'89*, Austin, TX, September 1989, pp. 1–12.
[50] R.L. Cruz, A calculus for network delay–Part I: Network elements in isolation, *IEEE Trans. Inform. Theory*, vol. 37, 1991, pp. 114–131.
[51] S.J. Golestani, Network delay analysis of a class of fair queuing algorithms, *IEEE J. Select. Areas Commun.*, vol. 13, 1995, pp. 1057–1070.
[52] S. Ross, *Stochastic Processes*, 2nd edn. Wiley: New York, 1980, pp. 114–115.
[53] M. Ergen, S. Coleri and P. Varaiya, QoS aware adaptive resource allocation techniques for fair scheduling in OFDMA based broadband wireless access systems, *IEEE Trans. Broadcasting*, vol. 49, no. 4, 2003, pp. 362–370.
[54] I. Koffman and V. Roman, Broadband wireless access solutions based on OFDM access in IEEE 802.16, *IEEE Commun. Mag.*, April 2002.
[55] I. Koutsopoulos and L. Tassiulas, Channel state-adaptive techniques for throughput enhancement in wireless broadband networks, in *INFOCOM 2001*, vol. 2, 2001, pp. 757–766.
[56] *IEEE Standard for Local and Metropolitan Area Networks Part 16: Air Interface*, IEEE Std 802.16-2001.
[57] C.Y. Wong, R.S. Cheng, K.B. Letaief and R.D. Murch, Multiuser OFDM with adaptive subcarrier, bit, and power allocation, *IEEE J. Select. Areas Commun.*, vol. 17, no. 10, 1999, pp. 1747–1758.

[58] S.G. Glisic, *Adaptive WCDMA, Theory and Practice*. Wiley: Chichester, 2003.
[59] S.G. Glisic, *Advanced Wireless Communications, 4G Technology.*, Wiley: Chichester, 2004.
[60] P. Viswanath, D.N.C. Tse and R. Laroia, Opportunistic beamforming using dumb antennas, *IEEE Trans. Inform. Theory*, vol. 48, no. 6, 2002, pp. 1277–1294.
[61] J. Bolot and A. Shankar, Dynamic behavior of rate-based flow control mechanisms, *ACM Comput. Commun. Rev.*, vol. 20, no. 2, 1992, pp. 35–49.
[62] M. Hluchyj and N. Yin, On closed-loop rate control for ATM networks, in *Proc. IEEE INFOCOM*, 1994, pp. 99–108.
[63] E. Altman, T. Basar and R. Srikant, Congestion control as a stochastic control problem with action delays, *Automatica*, vol. 35, no. 12, 1999, pp. 1937–1950.
[64] L. Benmohamed and S. Meerkov, Feedback control of congestion in store-and-forward networks: the case of single congestion node, *IEEE/ACM Trans. Networking*, vol. 1, 1993, pp. 693–798.
[65] S.Q. Li, S. Chong and C. Hwang, Link capacity allocation and network control by filtered input rate in high speed networks, *IEEE/ACM Trans. Networking*, vol. 3, 1995, pp. 10–15.
[66] D. Bertsekas and R. Gallager, *Data Networks*. Prentice-Hall: Englewood Cliffs, NJ, 1992.
[67] S.H. Low and D.E. Lapsley, Optimization flow control, I: basic algorithm and convergence, *IEEE/ACM Trans. Networking*, vol. 7, 1999, pp. 861–874.
[68] F.P. Kelly, A. Maulloo and D. Tan, Rate control for communication networks: Shadow prices, proportional fairness and stability, *J. Opns. Res. Soc.*, 1998, pp. 237–252.
[69] H. Yaiche, R. R. Mazumdar and C. Rosenberg, A game theoretic framework for bandwidth allocation and pricing in broadband networks, *IEEE/ACM Trans. Networking*, vol. 8, 2000, pp. 667–678.
[70] O. Ait-Hellal, E. Altman and T. Basar, Rate based flow control with bandwidth information, *Eur. Trans. Telecommun.*, vol. 8, no. 1, 1997, pp. 55–65.
[71] H.S. Kim and N.B. Shroff, Loss probability calculations at a finite buffer multiplexer, *IEEE/ACM Trans. Networking*, vol. 9, 2001, pp. 765–768.
[72] H.S. Kim and N.B. Shroff, On the asymptotic relationship between the overflow probability and the loss ratio, *Adv. Appl. Prob.*, vol. 33, no. 4, 2001, pp. 810–835.
[73] A.P. Zwart, A fluid queue with a finite buffer and subexponential input, *Adv. Appl. Probabil.*, vol. 32, 2000, pp. 221–243.
[74] A.V. Oppenheim, A.S. Willsky and S.H. Nawab, *Signals and Systems*. Prentice-Hall: Englewood Cliffs, NJ, 1997.
[75] P.W. Glynn and W. Whitt, Logarithmic asymptotics for steady-state tail probabilities in a single-server queue, *J. Appl. Prob.*, 1994, pp. 131–155.
[76] R.M. Loynes, The stability of a queue with nonindependent inter-arrival and service times, in *Proc. Cambridge Phil. Soc.*, vol. 58, pp. 497–520, 1962.
[77] J. Choe and N.B. Shroff, Use of the supremum distribution of Gaussian processes in queueing analysis with long-range dependence and selfsimilarity, *Stochast. Models*, vol. 16, no. 2, 2000.
[78] N.B. Likhanov and R. Mazumdar, Cell loss asymptotics in buffers fed by heterogeneous longtailed sources, in *Proc. IEEE INFOCOM*, 2000, pp. 173–180.
[79] D. Qiu and N.B. Shroff, Study of predictive flow control, Purdue University, Technical Report Available at: http://min.ecn.purdue.edu/∼dongyu/paper/techrep.ps, May 2001.
[80] J. Choe and N.B. Shroff, A central limit theorem based approach for analyzing queue behavior in high-speed networks, *IEEE/ACM Trans. Networking*, vol. 6, 1998, pp. 659–671.
[81] D. Qiu and N.B. Shroff, A predictive flow control scheme for efficient network utilization and QoS, *IEEE/ACM Trans. Networking*, vol. 12, no. 1, 2004, pp. 161–172.

Index